United States
Environmental Protection
Agency

EPA/600/R-08/060
January 2008

Mine Waste Technology Program

Linking Waterfowl with Contaminant Speciation in Riparian Soils

Bull Run Lake Test Site

Black Rock Slough Test Site

EPA/600/R-08/060
January 2008

MINE WASTE TECHNOLOGY PROGRAM

LINKING WATERFOWL WITH CONTAMINANT SPECIATION IN RIPARIAN SOILS

By:

Suzzann Nordwick
MSE Technology Applications, Inc.
Mike Mansfield Advanced Technology Center
Butte, Montana 59702

Under Contract No. DE-AC09-96EW96405
Through EPA IAG No. DW89939550-010-0

Norma Lewis, EPA Project Officer
Systems Analysis Branch
National Risk Management Research Laboratory
Cincinnati, Ohio 45268

This study was conducted in cooperation with
U.S. Department of Energy
Environmental Management Consolidated Business Center
Cincinnati, Ohio 45268

National Risk Management Research Laboratory
Office of Research and Development
U.S. Environmental Protection Agency
Cincinnati, Ohio 45268

Notice

The U.S. Environmental Protection Agency (EPA) through its Office of Research and Development funded the research described here under IAG DW89939550-010-0 through the U.S. Department of Energy (DOE) Contract DE-AC09-96EW96405. It has been subjected to the Agency's peer and administrative review and has been cleared for publication as an EPA document. Reference herein to any specific commercial product, process, or service by trade name, trademark, manufacturer, or otherwise, does not necessarily constitute or imply its endorsement or recommendation. The views and opinions of authors expressed herein do not necessarily state or reflect those of EPA or DOE, or any agency thereof.

Foreword

The U.S. Environmental Protection Agency is charged by Congress with protecting the Nation's land, air, and water resources. Under a mandate of national environmental laws, the Agency strives to formulate and implement actions leading to a compatible balance between human activities and the ability of natural systems to support and nurture life. To meet this mandate, EPA's research program is providing data and technical support for solving environmental problems today and building a science knowledge base necessary to manage our ecological resources wisely, understand how pollutants affect our health, and prevent or reduce environmental risks in the future.

The National Risk Management Research Laboratory is the Agency's center for investigation of technological and management approaches for preventing and reducing risks from pollution that threaten human health and the environment. The focus of the Laboratory's research program is on methods and their cost effectiveness for prevention and control of pollution to air, land, water, and subsurface resources; protection of water quality in public water systems; remediation of contaminated sites, sediments, and groundwater; prevention and control of indoor air pollution; and restoration of ecosystems. The NRMRL collaborates with both public and private sector partners to foster technologies that reduce the cost of compliance and to anticipate emerging problems. NRMRL's research provides solutions to environmental problems by developing and promoting technologies that protect and improve the environment; advancing scientific and engineering information to support regulatory and policy decisions; and providing the technical support and information transfer to ensure implementation of environmental regulations and strategies at the national, state, and community levels.

This publication has been produced as part of the Laboratory's strategic long-term research plan. It is published and made available by EPA's Office of Research and Development to assist the user community and to link researchers with their clients.

Sally Gutierrez, Director
National Risk Management Research Laboratory

Abstract

This report summarizes the results of Mine Waste Technology Program (MWTP) Activity III, Project 38, *Linking Waterfowl with Contaminant Speciation in Riparian Soils*, implemented and funded by the U.S. Environmental Protection Agency (EPA) and jointly administered by EPA and the U.S. Department of Energy (DOE). This project addressed EPA's technical issue of Mobile Toxic Constituents – Water and Acid Generation.

Soil samples were collected from the Coeur d'Alene River Basin and were analyzed for mineralogy and metal contaminant speciation. Both phosphorus (P)-treated soils and untreated soils were examined to determine the effect of P-amendment on metal speciation. Previous studies suggested P-amendments result in precipitation of poorly soluble lead phosphate minerals. In this study, P appears to associate with iron bearing minerals in the soil, whereas lead associates predominantly with manganese bearing phases.

The research conducted on site mineralogy and speciation generated no irrefutable evidence that P-amendments promoted formation of poorly soluble lead (Pb)-P mineral phases. In theory, such phases would lower Pb bioavailability in waterfowl exposed to Pb-contaminated soils and sediments. Thus, development of a screening-level method for assessing P-treatment effectiveness (and subsequent reduction in Pb bioavailability) becomes a critical issue.

This need is addressed by the two-step sequential extraction procedure that simulates the gizzard and intestinal phases of a typical waterfowl's gastrointestinal tract. Dr. Strawn's approach is a modified version of the physiologically based extraction test (PBET) for estimating Pb bioaccessibility in humans, and is subsequently called W-PBET. The gizzard phase of this test demonstrated high Pb extraction reproducibility and accuracy. The Pb bioaccessibility results were positively correlated with those from waterfowl fed contaminated and in situ-treated soils from the lower Coeur d'Alene River Basin. Therefore, W-PBET is a promising, cost-effective method for initial assessment of site-specific Pb bioavailability in waterfowl.

Contents

Contents (Cont'd)

Figures

Figures (Cont'd)

Page

Tables

Acronyms and Abbreviations

ABA	absolute bioavailability
Al	aluminum
ANOVA	analysis of variances
AOD	ammonium oxalate
As	arsenic
C	carbon
Ca	calcium
CBD	citrate-bicarbonate-dithionite
Cd	cadmium
CERCLA	Comprehensive Environmental Response, Compensation, and Liability Act
Cl	chlorine
DOE	U.S. Department of Energy
DTPA	diethylene triamine pentaacetic acid
EDS	energy dispersive spectrum
E_H	oxidation reduction potential
EMPA	electron microprobe analysis
EPA	U.S. Environmental Protection Agency
Fe	iron
FTIR	Fourier transform infrared spectrometer
GI	gastrointestinal
HCl	hydrochloric acid
ICP-AES	inductively coupled plasma atomic emission spectrometer
IVB	in vitro bioaccessibility
Mn	manganese
MSE	MSE Technology Applications, Inc.
MWTP	Mine Waste Technology Program
N	normal
N_2	nitrogen
NaCl	sodium chloride
NIST	National Institute of Standards and Technology
NRMRL	National Risk Management Research Laboratory
ORP	oxidation-reduction potential
P	phosphorus
p	probability
Pb	lead
PBET	physiologically based extraction test
PbB	blood lead
pe	negative $\log_{10}$ of electron activity
pH	negative $\log_{10}$ of hydrogen ion concentration
QA	quality assurance
QAPP	quality assurance project plan
rpm	revolutions per minute
RSD	relative standard deviation
S	sulfur
Si	silicon

Acronyms and Abbreviations (Cont'd)

WDS	wavelength dispersive spectrum
W-PBET	waterfowl physiologically based extraction test
XRD	X-ray diffraction
Zn	zinc

Acknowledgments

This document was prepared by MSE Technology Applications, Inc. (MSE) for the U.S. Environmental Protection Agency's (EPA) Mine Waste Technology Program (MWTP) and the U.S. Department of Energy's (DOE) Environmental Management Consolidated Business Center. Ms. Diana Bless is EPA's MWTP Project Officer, while Mr. Dave Hicks is DOE's Technical Program Officer. Ms. Helen Joyce is MSE's MWTP Program Manager. Ms. Norma Lewis was the EPA Project Manager for this project. Ms. Suzzann Nordwick was the MSE MWTP Project Manager. Dr. Daniel G. Strawn was the Project Director from the University of Idaho, Department of Plant, Soil and Entomological Sciences.

Executive Summary

The Mine Waste Technology Program (MWTP), Activity III, Project 38, *Linking Waterfowl with Contaminant Speciation in Riparian Soils* was implemented by the U.S. Environmental Protection Agency (EPA) and jointly administered by EPA and the U.S. Department of Energy (DOE).

The two major components of this project were to:

- evaluate mineralology and contaminant speciation in phosphorus (P)-treated and untreated soils; and
- evaluate a physiologically based extraction test for determining lead (Pb) bioaccessibility in P-treated and untreated soils.

Soil samples from the Coeur d'Alene River Basin were analyzed for mineralogy and metal contaminant speciation. Both P-treated soils and untreated soils were examined to determine the effect of P-amendment on metal speciation. Other studies have suggested P-amendments lead to precipitation of poorly soluble Pb phosphate minerals. No evidence was found for this behavior in this study. Instead, P appears to associate with iron (Fe)-bearing minerals in the soil, whereas Pb associates predominantly with manganese (Mn)-bearing phases.

Due to variations in soil physicochemical properties, species physiology, and contaminant speciation, Pb toxicity is difficult to evaluate without conducting in vivo dose-response studies. However, such tests are expensive and time consuming, making them unrealistic to use in assessment and management of contaminated environments. One possible alternative is to develop a physiologically based extraction test (PBET) that can be used to measure relative bioaccessibility. The development and correlation of a PBET test designed to measure the bioaccessibility of Pb to waterfowl (W-PBET) is discussed in this report. The W-PBET results showed a positive correlation with tissue Pb levels from a bird feeding study. The W-PBET test was applied to investigate remediation success in contaminated soils from the Coeur d'Alene River Basin, Idaho. The W-PBET Pb concentrations were positively correlated with the bird feeding study results, exhibiting a logarithmic relationship. W-PBET concentrations for cadmium, zinc, and Mn contaminants present in the soils were evaluated. W-PBET results for these contaminants varied, depending on site conditions, soil amendment, and element. Results from this study indicate that a W-PBET extraction test can be used to assess relative changes in bioaccessibility and, therefore, is a valuable test to manage and remediate contaminated wetland soils.

1. Introduction

1.1 Project Description

This report summarizes the results of Mine Waste Technology Program (MWTP) Activity III, Project 38, *Linking Waterfowl with Contaminant Speciation in Riparian Soils*, implemented and funded by the U.S. Environmental Protection Agency (EPA) and jointly administered by EPA and the U.S. Department of Energy (DOE). This report encompasses the following four areas.

- Mineral and Contaminant Characterization in Soils from the Coeur d'Alene River Basin
- Lead Bioaccessibility to Waterfowl in the Lower Coeur d'Alene Basin Part 1: Development of a Physiologically Based Extraction Test for Waterfowl
- Lead Bioaccessibility to Water in the Lower Coeur d'Alene Basin Part 2: Seasonal Effect on Metal Bioaccessibility
- Geochemical Modeling using PHREEQCi software from the U.S. Geological Survey

This report is summarized from a document prepared by the University of Idaho's Department of Plant, Soil, and Entomological Sciences that was submitted to MSE Technology Applications, Inc. (MSE) as the University of Idaho's final deliverable for this project (Strawn, 2006; see Appendix A). The University of Idaho's role on this project was to perform laboratory and field testing and report on results. MSE's role was to provide project direction, oversight of the University of Idaho, reporting, and interface with EPA.

This project was a follow-on to a previous study completed by University of Idaho. In the previous study, the ability of phosphate amendments to reduce the bioavailability of lead (Pb) to waterfowl was investigated by the Idaho Department of Environmental Quality and the U.S. Fish and Wildlife Service. The Coeur d'Alene Basin Commission and EPA Region 10 jointly funded this investigation.

1.2 Background

The Coeur d'Alene mining district is rich in economically viable minerals and has yielded significant quantities of silver, Pb, zinc (Zn), and other metals. This mining region has produced in excess of one billion ounces of silver, eight and one-half million tons of Pb and three million tons of Zn (Bennett 1989). However, because of mining and mineral processing operations, soils, sediments, and waters of the Coeur d'Alene River Basin have been heavily contaminated. Subsequently, the Coeur d'Alene Basin (Figure 1-1) was placed on the Superfund National Priority List in 1984. Mill tailings from more than 90 mines, including America's largest underground mine (Bunker Hill) and deepest mine (Star-Morning), were released into the South Fork of the Coeur d'Alene River and its tributaries (Bennett 1989). It is estimated that 56 million metric tons of mill tailings have been deposited in the river (Long 1998a). Dumping into the river was discontinued in 1968 when mandates required tailing storage or return of tailings to the mines.

Dredged tailings were commonly used for local construction fill materials, brick manufacturing, and railroad ballast, which led to the spread of the contamination into populated areas (Davis 1993). Precipitation and flooding events have moved tailings into lakes and wetlands along the river.

Recovery efforts since 1900 have reclaimed approximately 6 million metric tons of deposited tailings from creeks and dumps (Mitchell and Bennett 1983). In the 1930s, the Mine Owners Association dredged a portion of the Coeur d'Alene River near Cataldo Mission Flats and deposited the collected tailings on the nearby floodplain (Cassner 1991). However, unknown amounts of tailings still reside in the Coeur d'Alene River (Mitchell and Bennett 1983).

Wildlife habitats and recreational facilities common along the river and its wetlands increase the environmental significance of mining contaminants present. Animal communities use the river basin's lakes, wetlands, and riparian corridors as breeding areas, feeding areas, and migratory flight path stopovers.

Studies have shown that fish and fowl caught in these areas for the purpose of consumption have high levels of trace metals. Many camping locations, bike trails, and other recreation sites occur in contaminated areas. A prime concern for human exposure is ingestion of soils within these recreation sites, especially during dry and dusty conditions, as well as contamination from drinking contaminated waters.

1.3 Scope of Work

Project 38 was an investigation to determine contaminant reaction processes in previously treated soils. The project focused on gaining insight into phosphorous (P)-Pb interactions in riparian soils using spectroscopic and microscopic techniques. The reactions involving Pb and other metals of regulatory concern, P-containing soil amendments, and solid-phase soil components were evaluated.

1.4 Goals and Objectives

The project objectives were to determine the reaction mechanisms of Pb in P-amended soils and relate this information to the bioavailability of Pb as indicated by the waterfowl study results.

The goal of this study was to characterize the mineralogy and contaminant speciation in soil samples from field sites in the Coeur d'Alene River Basin. Elemental concentration in the soils was measured as a function of particle size, and elements were mapped using an electron microprobe. Bulk mineralogy was characterized using x-ray diffraction, Fourier transform infrared spectrometry (FTIR), and selective extraction. Assessment of P-amendments on Pb partitioning was evaluated to determine if P-enhanced *in situ* Pb immobilization in the soils was occurring.

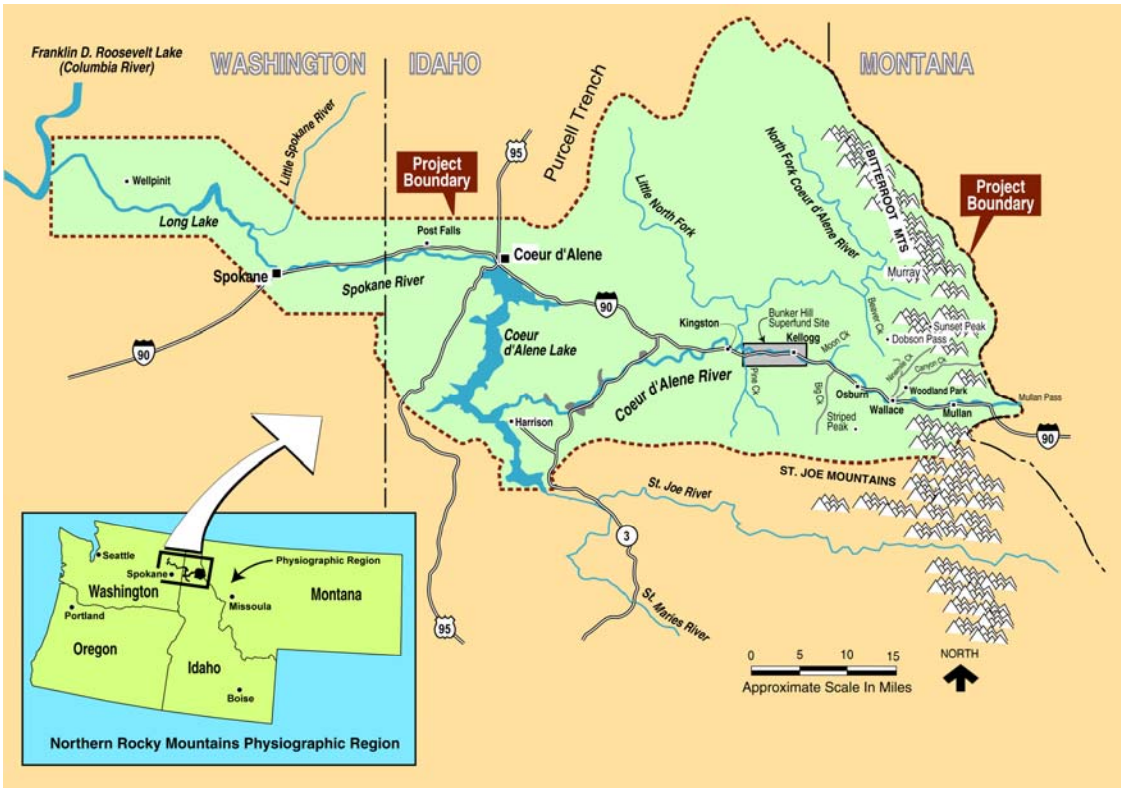

Figure 1-1. Coeur d'Alene Basin location map.

2. Technologies

The University of Idaho's role on this project was to perform laboratory and field testing and report on results. MSE's role was to provide project direction, oversight of the University of Idaho, reporting, and interface with EPA.

2.1 Physicochemical Characterization Tools

This study characterized the mineralogy and contaminant speciation in soil samples from field sites. Elemental concentration in the soils was measured as a function of particle size, and elements were mapped using an electron microprobe. Bulk mineralogy was characterized using x-ray diffraction, FTIR, and selective extraction. An assessment of P-amendments on Pb in soils was evaluated.

2.1.1 Mineralogical Analysis

Experiments using advanced spectroscopic and microscopic techniques were conducted. Soil samples were collected and analyzed using redox preservation techniques with spectroscopic and microscopic analytical instrumentation.

2.1.2 Chemical Cycling Analysis

Mechanistic data (i.e., pH and E_h) were collected to determine how seasonal changes affected soil mineralogy, Pb and P speciation, and bioavailability characteristics.

2.1.3 Thermodynamic Database

The experimental and mechanistic data were used along with a thermodynamic database to generate aqueous phase stability diagrams and to develop the model of Pb behavior at the waterfowl plots.

2.2 Lead Bioavailability versus Bioaccessibility Assessment Tools

Contaminant bioavailability is the ratio of absorbed dose to ingested dose. For example, 30 micrograms (μg) of Pb measured in the bloodstream following ingestion of 100 μg Pb in soil represents an absolute bioavailability (ABA) of 30%. Contaminant in vitro bioaccessibility (IVB) indicates the potential for a substance to be taken up into the bloodstream. For example, 525 μg Pb measured in simulated gastric fluid contacting soils containing 2,250 μg Pb represents an IVB of about 23%.

Because of its relative simplicity and lower cost, the IVB method was considered ideal for site-specific screening of contaminant bioavailability. However, a generally acceptable correlation between the ABA and IVB results must be demonstrated before this approach can occur. In the present case, this involved:

- a waterfowl feeding study to estimate Pb bioavailability in floodplain soils (along the Coeur d'Alene River); versus
- development of an in vitro method that simulates Pb bioaccessibility in the gastrointestinal tract of waterfowl.

MWTP Activity III, Project 38 focused on the latter effort. However, interpretation of the IVB results required some background on the waterfowl feeding study performed by the U.S. Geological Survey's Patuxent Wildlife Research Center. The respective methodologies are summarized below.

2.2.1 Waterfowl Feeding Study

The general study design is shown in Table 2-1 (Heinz et al, 2004). Male, 2-week old mallard ducks were kept outdoors in 1-square meter pens and given feed and fresh water *ad libitum* over an 8-week period. Venous blood samples were collected at the end of the feeding period, prior to humane euthanasia. Samples of blood, liver, and kidney from each bird were prepared and analyzed for their respective Pb levels. ABAs were calculated by dividing in vivo tissue concentrations by normalized Pb levels in diet, for each of the eight groups.

2.2.2 Lead Bioaccessibility Estimation

Dr. D. G. Strawn developed a physiologically based extraction test (PBET) that simulates Pb behavior in the gastrointestinal tract of waterfowl (W-PBET). Development and application of the W-PBET to Coeur d'Alene floodplain soils are discussed in Sections 4 and 5, respectively, of this report. Additional details are presented in his final report (Strawn, 2006), which is attached in CD-form to this report as Appendix A.

2.2.3 Data Correlation

The physicochemical and biological-related information were correlated with each other so as to produce preliminary assessments regarding:

- how P-treatment of Pb-contaminated soils affected Pb speciation and bioavailability under varying environmental conditions; and
- the credibility of the W-PBET results being used as surrogates for waterfowl feeding studies.

The first issue is addressed in Sections 3 and 6, while the latter is addressed in Sections 4 and 5, of this report.

Table 2-1. General Study Design for the Waterfowl Feeding Study

Group	Number of Animals	Sediment Source	Phosphate Amendment	Where Aged [a]	Average Concentration in Feed (ppm, dry weight basis)	
					Pb	P
1	10	Round Lake	No	Lab	2.9	87
2	10	Harrison Slough	No	Lab	507	75
3	10	Harrison Slough	Yes	Lab	488	1,248
4	10	Black Rock Slough	No	Lab	535	85
5	10	Black Rock Slough	Yes	Field	458	2,232
6	10	Bull Run Lake	No	Lab	791	53
7	10	Bull Run Lake	Yes	Lab	757	1,224
8	10	Bull Run Lake	No	Field	683	2,556

Note: [a] Water-saturated soils were allowed to react for 5 months (i.e., to form pyromorphite) prior to use in the feeding study.
Source: Heinz et al. 2004.

3. Mineral and Contaminant Characterization in Soils from the Coeur d'Alene River Basin

3.1 Sampling

Soil samples were collected from two sites located in the Coeur d'Alene River Basin: the northwest shore of Bull Run Lake and the northeast site of the Black Rock Slough. These sites are located near Rose Lake within Operable Unit-3 of the Bunker Hill Superfund site (Figure 1-1). Figures 3-1a and 3-1b present photographs (2003) of the test sites. As part of a previous effort by the University of Idaho (see Introduction for more details), different soil amendments were used to treat the three plots from each site. These were:

- liquid phosphorus fertilizer with lime;
- ground fishbone apatite; and
- lime.

The fourth plot was untreated. A schematic of the plots is shown in Figure 3-2.

Four of the eight plots were selected, measured, and staked in the spring of 2003 to the following specifications.

- Plots 2, 4, and 6 measured 20 feet by 20 feet with a buffer of 1 foot on all sides. These plots consisted of 15 subplots (3 rows with 5 plots each).
- Plot 8 measured 20 feet by 25 feet with a buffer of 1 foot on the north, west, and south side that consisted of 21 subplots (3 rows with 7 plots each).

Samples were collected randomly from the subplots specified above using a 20-centimeter (cm) long, 5-cm diameter stainless steel sampler with a plastic sleeve insert. Core samples were submerged in liquid nitrogen (N_2), sealed, placed on ice and transported to the laboratory. Soils were air-dried and crushed to passing pore size of 1 millimeter (mm).

3.2 Analysis

Total metal concentrations were determined using EPA method 3052. An electron microprobe analysis (EMPA) was used to provide the energy dispersive spectrum (EDS) and wavelength dispersive spectrum (WDS) images and graphs with a high degree of spatial precision and sensitivity that corresponds to the soil particle elemental concentration. Analytical results are summarized in Section 3.3 and the complete data package can be found in Appendix A, the University of Idaho's final deliverable for this project (Strawn, 2006).

3.2.1 Electron Microprobe Analysis

Three samples each from the amended Plots 2 and 6 and unamended Plots 4 and 8 were taken in August 2003. Thin sections were made using soil from the top 5 cm of each of the triplicate cores and dried in the oven at 100 degrees Celsius (ºC). The soil, approximately 5 cm^3, was vacuum impregnated with an acrylic resin, cut into thin sections, and mounted on petrographic slides. The thin sections were ground to a thickness between 250 micrometers (µm) and 1 mm, and polished using 6-µm, 3-µm, and 0.05-µm grits to achieve an acceptable finish.

The 12 thin sections were randomly scanned using a Cameca Camebax electron microprobe, located at the Washington State University Geology Department. During the scanning, in-depth analysis of three to six areas was carried out using a 4-micron beam, accelerating voltage of 15 kilo electron volt (keV), and beam current of 12 nanoamperes (nA). The detailed analysis involved taking an electron backscatter image of the thin section, creating a single WDS element map of the same region for five elements [iron (Fe), manganese (Mn), Pb, P, and silicon (Si)], and generating an EDS portrait of six to twelve distinct points within the area. The EDS portrait provides a relative measure of elemental

concentrations within the analysis area. The size of the EDS peaks is a qualitative indication of what elements are present.

3.2.2 X-Ray Diffraction

X-ray diffraction (XRD) was done on composite samples to determine the dominant mineralogy and crystalline structure of the soil samples. Citrate-bicarbonate-dithionite (CBD) and ammonium oxalate (AOD) treatments were used to remove amorphous coatings and free Fe oxides that act as cementing agents. Both untreated and AOD and CBD treated samples were run on the XRD using EVA software to collect data and identify samples. The clay-sized fraction from Plots 2, 4, 6, and 8 were also analyzed on XRD.

Particle size analysis was performed on soil composites from Plots 2, 4, 6, and 8. Approximately 14 grams (g) of soil were added to 60 milliliters (mL) of triple distilled water in four 100-mL plastic centrifuge tubes. The four soil-water mixtures were homogenized then centrifuged at 750 revolutions per minute (rpm) for approximately 2 minutes and 54 seconds to separate clay-sized particles from silt and sand-sized particles. The clay-containing supernatant was decanted into a 500-mL graduated cylinder. This procedure was repeated until the suspensions in the 100-mL centrifuge tubes were visibly free of clay-sized particles. The soil-clay percentage was determined by massing two oven-dried 10-mL aliquots sampled from the thoroughly mixed clay-water solutions.

The remaining soil-water mixture was passed through a 325-mesh sieve to separate the silt and sand-sized particles. The sand-sized material remaining in the 325-mesh was dried in an oven at 70 °C. The dried sand-sized particles were screened in a nest of sieves. Silt passing through the nest of sieves was collected and added to the total silt mass of the composite sample. The silt-sized material that passed through the 325-mesh sieve was allowed to settle and the silt-free water was poured off. The remaining material was dried in the oven at 70 °C and then weighed.

Iron and Mn were extracted using AOD and sodium CBD procedures. AOD is used to remove Fe and Mn oxides while CBD is used to reduce and extract Fe and Mn oxides. For AOD extraction, triplicate 0.05-g subsamples from composites 2, 4, 6, and 8 were placed in separate 100-mL plastic centrifuge tubes to which 60 mL of 0.2 molar (*M)* ammonium oxalate [$(NH_4)_2$ C_2O_4] was added. The samples were covered to exclude light and placed on a shaking table at 280 rpm, and allowed to mix thoroughly for 4 hours. After shaking, the samples were centrifuged at 1,200 rpm for 15 minutes and 30 mL of extractant was collected. The extractant was diluted with deionized water and stored in polypropylene containers in preparation for inductively coupled plasma atomic emission spectrometer (ICP-AES) analysis.

For CBD extraction, triplicate 0.05-g subsamples of composites 2, 4, 6, and 8 were placed into 12 separate 100-mL centrifuge tubes along with 45 mL of 0.3-*M* sodium citrate ($C_6H_5Na_3O_4 \cdot 2H_2O$) and 5 mL of 1-*M* sodium bicarbonate. The samples were agitated at 15 rpm in a water bath of 80 °C for a 5-minute temperature equilibration, after which 1 g of reagent-grade sodium dithionite ($Na_2S_2O_4$) was stirred into the samples. Stirring of the samples was performed continuously for 1 minute and then intermittently approximately every 5 minutes for a total of 15 minutes. After 15 minutes, 1 g of sodium dithionite was added to the samples. The samples were stirred intermittently for 10 minutes, removed from the water bath, allowed to cool to room temperature, and centrifuged at 1,200 rpm for approximately 15 minutes. After centrifuging, 30 mL of the extractant was collected, diluted 1:10 in deionized water, and stored in polypropylene containers in preparation for ICP-AES analysis.

3.3 Results Summary

Total elemental composition is shown in Table 3-1. Raw data can be found in the University of

Idaho's final deliverable for this project (Strawn 2006; Appendix A). Plots 2 and 4 on Bull Run Lake have higher concentrations of contaminants than the plots near Black Rock Slough (Plots 6 and 8). There are two possibilities for this difference as follows.

- The elevation difference between the two sites allows for variable sediment deposition. The Bull Run Lake sites are at a lower elevation thus receiving more contaminated sediment.
- The difference in elevation also creates different water table inundation periods, creating variable biogeochemistry, which affects the mobility of the contaminants.

Particle size for Plots 6 and 8 were silt loam. Plots 2 and 4 had very fine sandy loam particles. Size classifications are shown in Table 3-2. The very fine sand fraction provided 67.8% or greater of total sands in all samples and is not shown in the table. Raw data can be found in Appendix A, University of Idaho's final deliverable for this project (Strawn, 2006).

Particle size differences were due to water velocity and sedimentation rate, which are impacted by elevation. Thus, fine particles will preferentially settle at the high elevation sites near Black Rock Slough and coarser particles will settle at the lower elevation sites near Bull Run Lake.

3.3.1 Electron Microprobe Analysis

Electron microprobe analysis was done on all plots. The results are summarized in Table 3-3. The WDS images and EDS plots are shown in Appendix A, University of Idaho's final deliverable for this project (Strawn, 2006).

Associations between elements in soil samples were determined by visually estimating the percentage of common elemental coverage between WDS images. A high correlation was defined as 75% to 100% mutual elemental coverage in the WDS image, moderate correlation had 50% to 74% mutual coverage, and weak correlation had 25% to 49% mutual coverage. Mutual coverage of less than 25% was considered not visually correlated.

Qualitative analyses of the WDS images revealed that greater than 50% of the scans contained moderate to high correlations between Fe/Mn and Fe/P. However, there was a poor correlation between Mn/P, indicating that the P preferentially associates with Fe not associated with Mn. Closer examination of the EMPA element maps suggests that Fe and P are most strongly associated to the exterior surfaces of larger mineral particles such as quartz. These results are shown in Appendix A, University of Idaho's final deliverable for this project (Strawn, 2006).

High correlations were observed between Pb and Mn in 11% of the images, and moderate correlations were observed in 30% of the images. This suggests that the Pb has a preferential association with Mn minerals over Fe containing minerals, even if the Fe-bearing mineral contained Mn. Only a small fraction of the images showed correlation between Pb/P. It is concluded that Pb is primarily associated with Mn oxides, while P is associated with Fe oxides.

The bulk of the Si in the soil samples is not associated with the other elements analyzed. The overlap between Si and other elements most likely occurs because Si is present in clay minerals, which also have the other elements associated with their structure or absorbed on their surfaces.

3.3.2 AOD and CBD Extractable Iron and Manganese Results

AOD extractable Fe comprised 54.3% to 76.8% of the total Fe, indicating that most of the Fe in the soils is poorly crystalline. Plots 2 and 4 show the total Fe and amount of extractable Fe is greater than in Plots 6 and 8. This is because of the higher rate of sediment deposition on these plots compared to Plots 6 and 8. AOD extractable Fe and Mn from Plot 4 are

significantly greater than CBD extractable Fe and Mn. This suggests that there is a significant fraction of nonreducible Fe and Mn in the soil from Plot 4. Fe(II) or Mn(II) adsorbed on poorly crystalline minerals such as ferrihydrite would be a possible reason for this observation. Minerals such as Fe(II) and Mn(II) carbonates may also be extracted with AOD but not CBD.

3.3.3 FTIR Analysis

FTIR spectra were collected from the clay-size fractions of the four soils before and after treatment with AOD and CBD. Results are presented in Figures 3-3 through 3-5 and Table 3-4. The FTIR spectra have distinct bands for kaolinite, quartz, and soil organic matter as shown in Table 3-5. Distinct changes in the spectra were observed when the soils were extracted with AOD and CBD that appear to correspond to the soil organic matter fraction.

3.3.4 XRD Analysis

To determine the mineral phases, XRD was run on the less than 2-μm fractions of P-treated and untreated soils. The soils were extracted with a solution of CBD, a common extractant that selectively removes the reducible free Fe and Mn minerals. To enhance the detection capabilities of Fe minerals, the XRD data from the extracted sample was subtracted from the non-extracted sample XRD data (differential XRD). The resulting peaks are from the minerals extracted by CBD. XRD from the clay-size fraction of the four plots are presented in Figures 3-6 through 3-9 and the results are summarized in Table 3-6. Results from the differential XRD are shown in Figures 3-10 and 3-11.

XRD analysis suggests that the minerals present in the soils are quartz, mica, chlorite (clinochlore), siderite, lepidocrocite, and poorly crystalline goethite and ferrihydrite. No P or Pb minerals were detected. The lack of detection of these minerals indicates that:

- they are too poorly crystalline; and/or
- their concentration is below the detection limit of the instrument.

Mica is a common primary mineral that weathers to secondary layer silicates such as chlorite and vermiculite. The secondary clay minerals can have a significant contribution to cation adsorption in the soils. Poorly crystalline Fe oxides have large surface areas that correspond to large sorption capacities for metals and anions. Sorption capacity on oxides is pH dependent. Siderite is a ferrous carbonate that is not stable in oxidizing environments. The redox status of the soils varies from oxic to anoxic, depending on the level of the water table, which is dependent on seasonal runoff and flooding conditions. The presence of siderite in the soils is most likely detrital because siderite is a common mineral in the ore containing rocks, and would require long periods of reducing conditions to be diagenetic. The soils from Bull Run Lake had much stronger XRD peaks for siderite than the soil at Black Rock Slough, which corresponds to the frequency of inundation. Lepidocrocite is an Fe oxide commonly observed in soils in which ferrous Fe is oxidized. Plots 2 and 4 did not have XRD peaks for lepidocrocite. The lack of lepidocrocite on these plots may be a result of the more dynamic redox environment that does not allow for stable Fe oxides such as goethite and lepidocrocite to form, but instead favors meta-stable poorly crystalline oxides such as ferrihydrite.

3.4 Conclusions

The research conducted on site mineralogy and speciation has found no conclusive evidence that P-amendments promoted the formation of poorly soluble Pb-P mineral phases. However, the results show that P is preferentially absorbed to Fe oxide minerals and Pb is preferentially associated with Mn oxide minerals. The fate of P is important when considering amendment rates to form poorly soluble Pb-P minerals. Additional information regarding soil organic carbon types and distribution would enhance the understanding of this process.

The selective extraction results and the XRD analysis showed that highly reactive Fe and Mn oxide phases and siderite were present in the soils. Such information is important for predicting reaction processes in the soil because temporal and ecosystem processes impact the stability of the Fe and Mn minerals, which will impact contaminant release and P availability for reacting with Pb or other metals, or leaching into the surface water.

Based on the results of this research, a conceptual model was developed for Pb speciation and reactivity in the wetlands. This model can be used to predict Pb bioavailability, transport availability, temporal fluxes as a function of water table and inundation, and impacts of remediation. A generalized system model is presented in Figure 3-12. Information on mineral and contaminant speciation can be input into this model to predict processes for reactions between the various phases. This type of predictive model is needed to develop improved management and remediation strategies, and develop new experiments that will allow for quantitative analysis of contaminant availability.

Figure 3-1a. 2003 photograph of Bull Run Lake test site near Rose Lake, Idaho.

Figure 3-1b. 2003 photograph of Black Rock Slough test site near Rose Lake, Idaho.

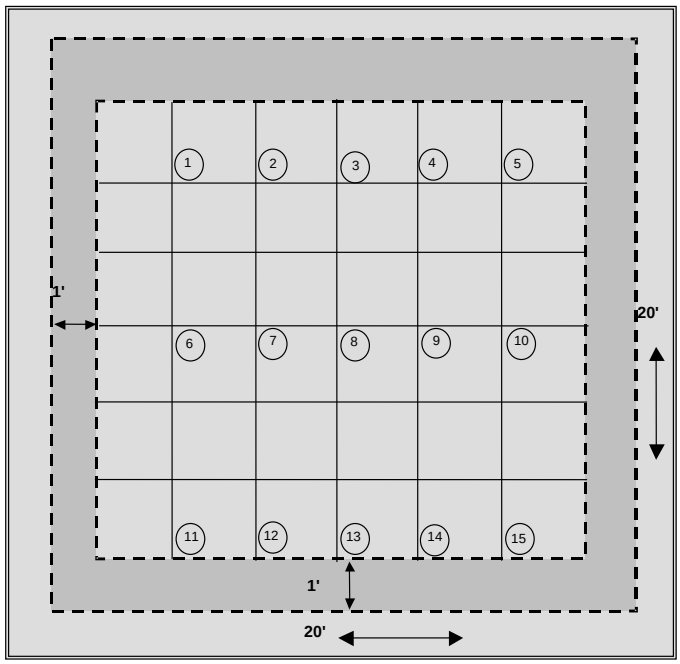

Figure 3-2. Plot schematic.

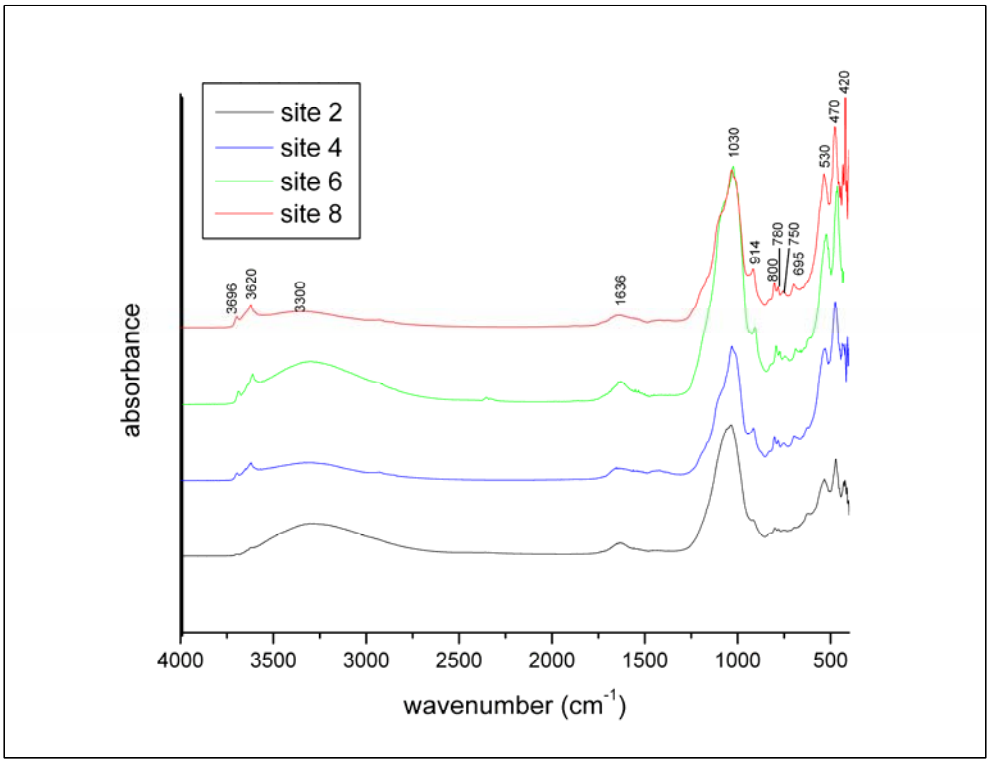

Figure 3-3. FTIR spectra of clay-size fraction of soils from Plot 2, 4, 6, and 8.

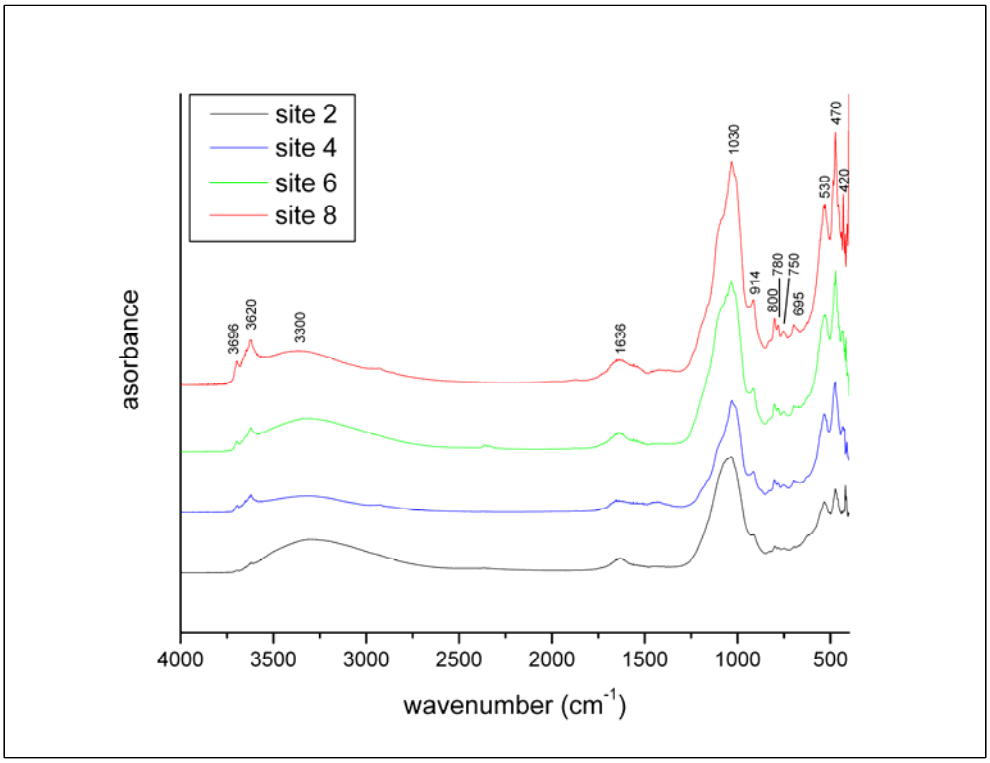

Figure 3-4. FTIR spectra of AOD-treated soil samples (clay-size fraction).

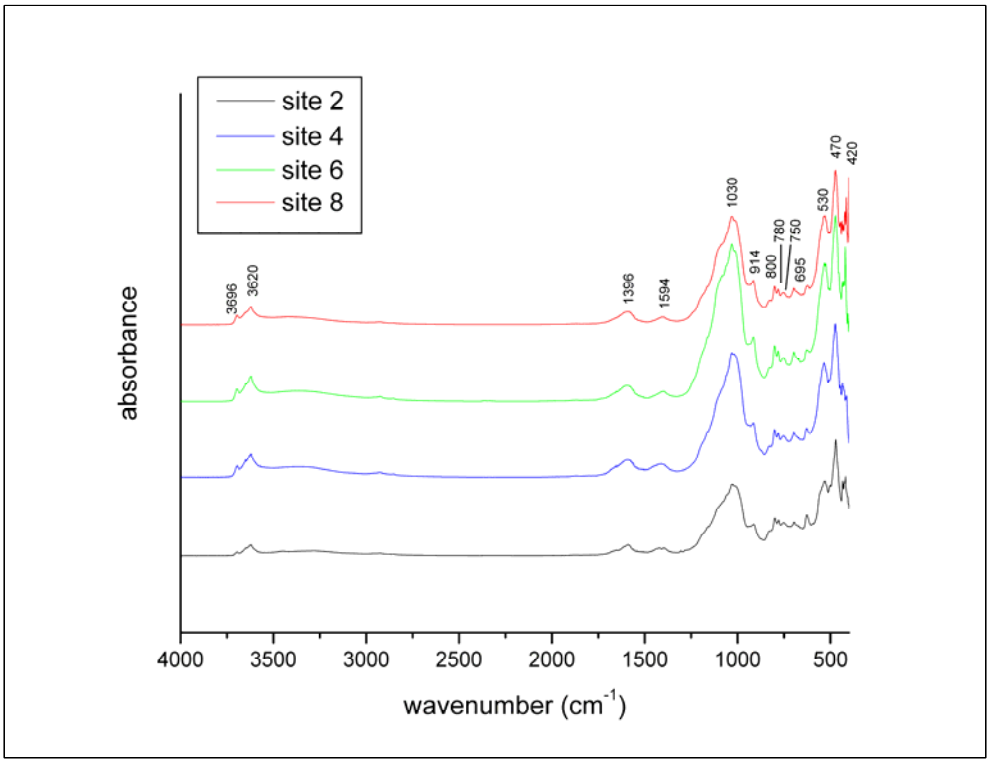

Figure 3-5. FTIR spectra of CBD-treated soil samples (clay-size fraction).

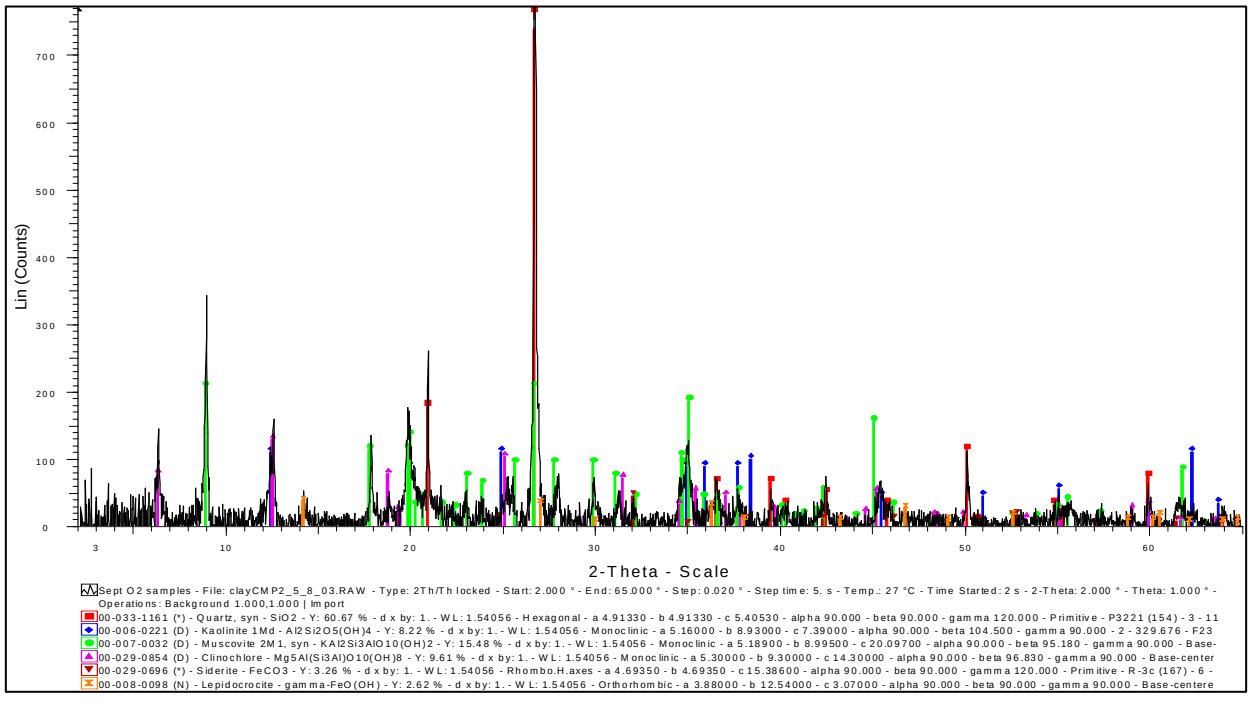

Figure 3-6. XRD analysis of clay sample from site 2, showing stick patterns of the mineral set (kaolinite, muscovite, quartz, siderite, clinochlore, and lepidocrocite).

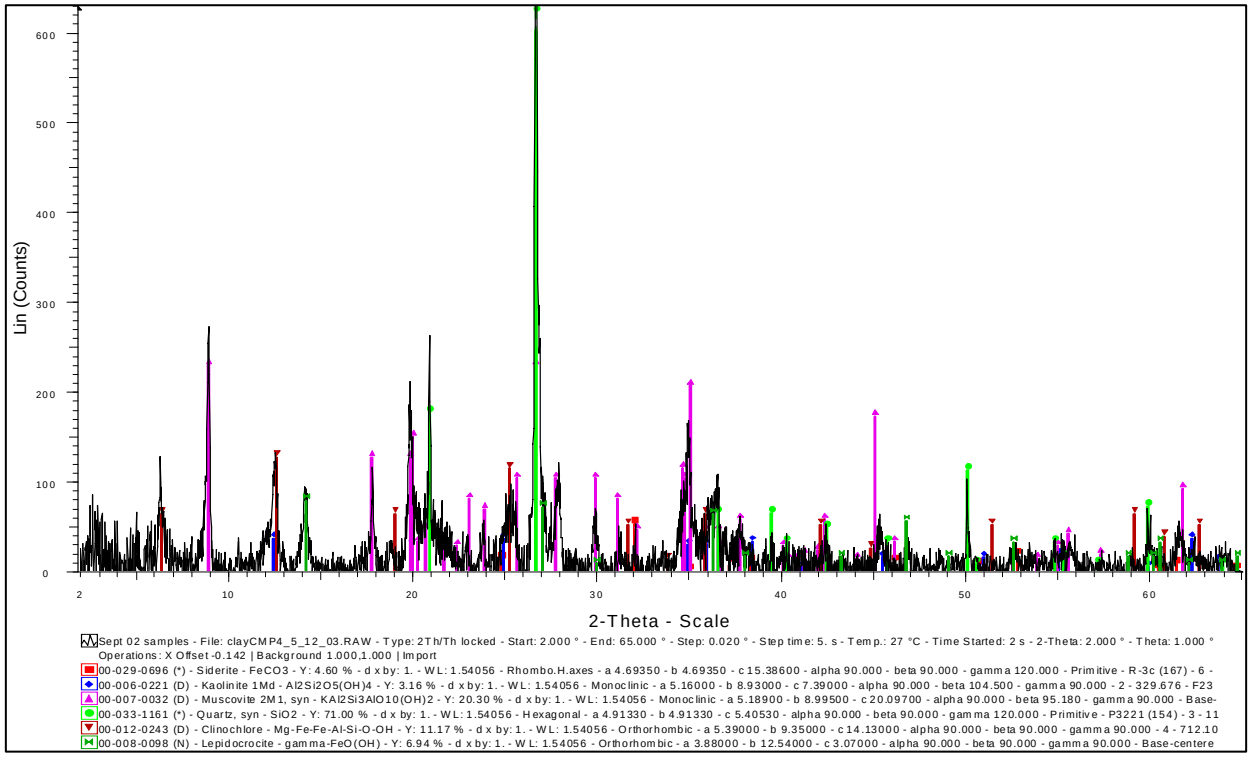

Figure 3-7. XRD analysis of clay sample from site 4, showing stick patterns of the mineral set (kaolinite, muscovite, quartz, siderite, clinochlore, and lepidocrocite).

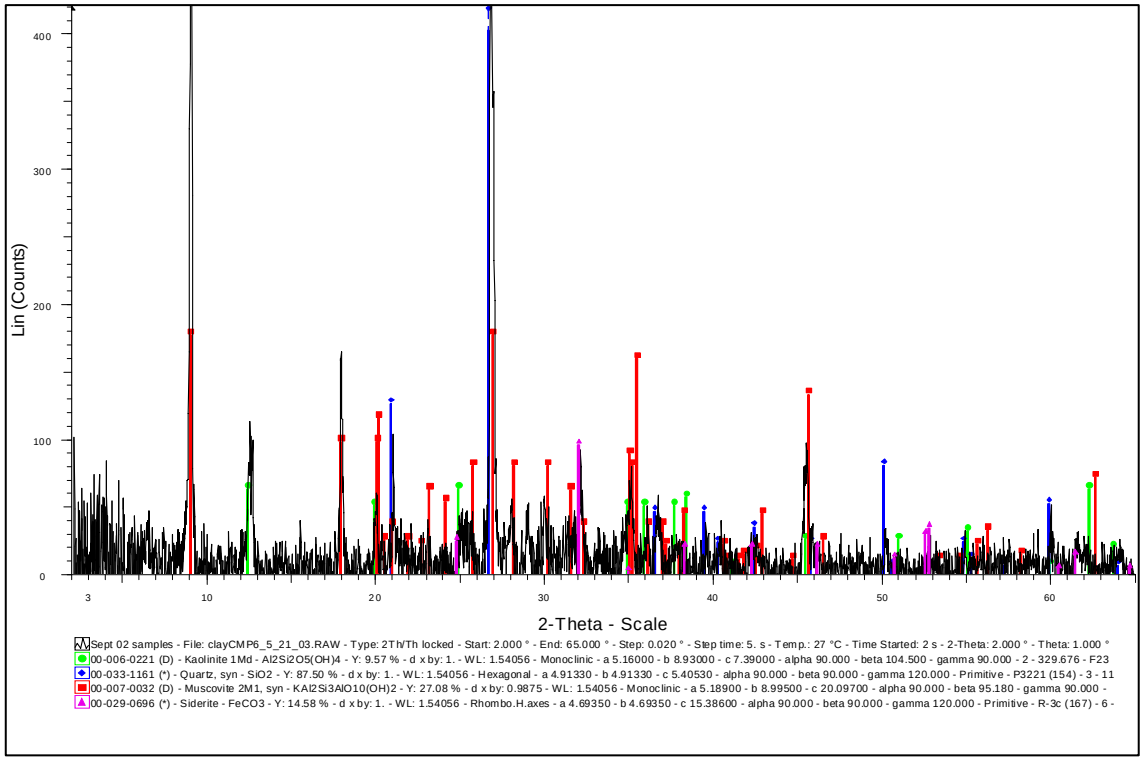

Figure 3-8. XRD analysis of clay sample from site 6, showing stick patterns of the mineral set (kaolinite, muscovite, quartz, and siderite).

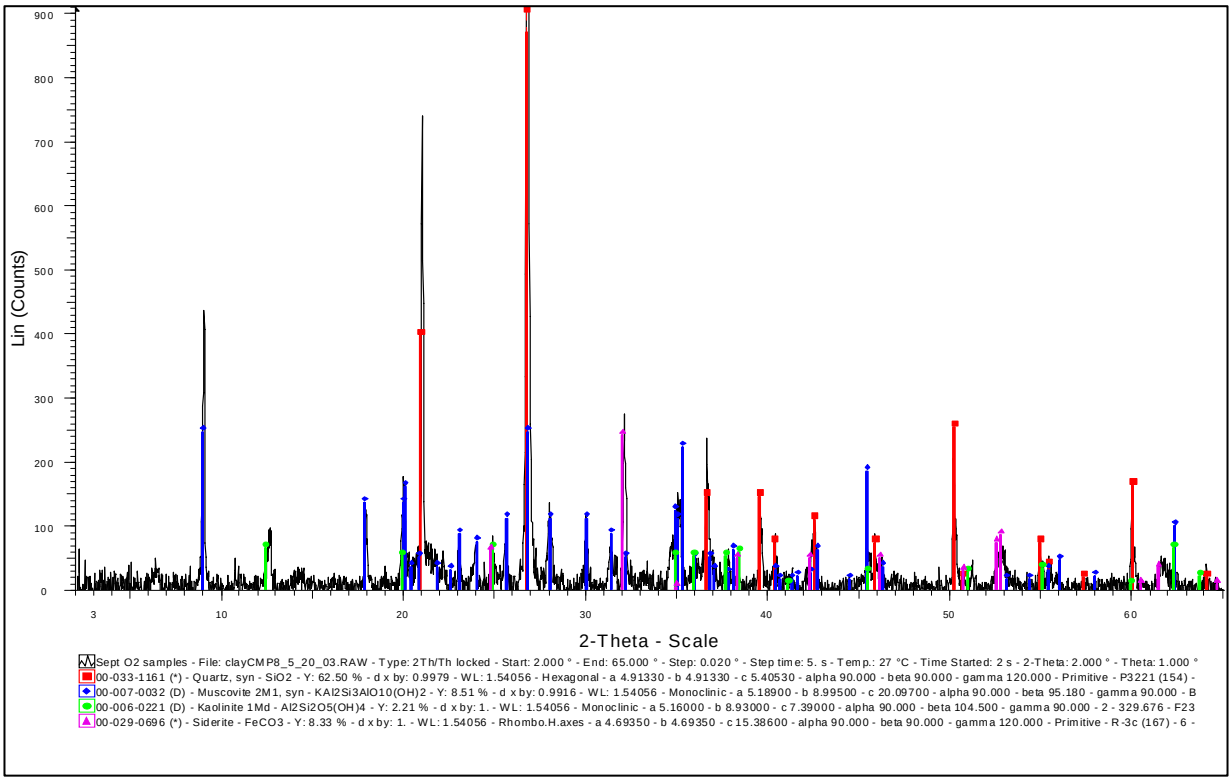

Figure 3-9. XRD analysis of clay sample from site 8, showing stick patterns of the mineral set (kaolinite, muscovite, quartz, and siderite).

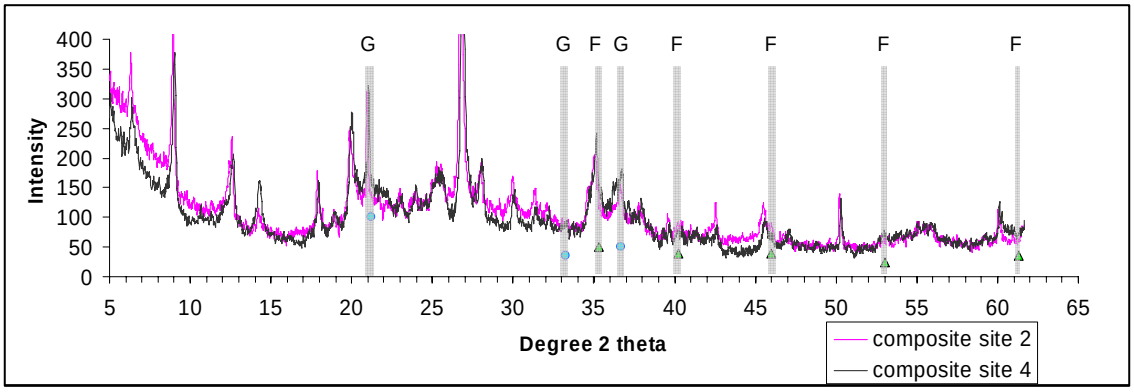

Figure 3-10. XRD data with peaks for goethite (G) and ferrihydrite (F) indicated.

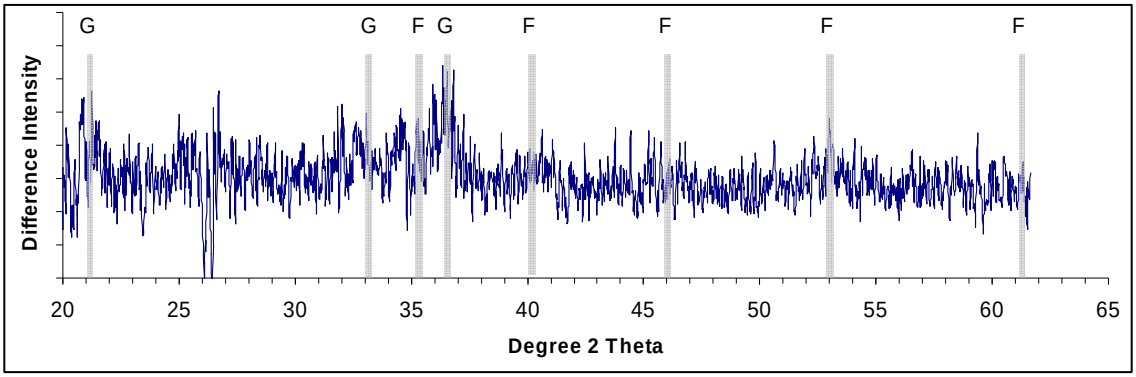

Figure 3-11. Differential XRD for composite sample 4. Peaks for goethite (G) and ferrihydrite (F) indicated.

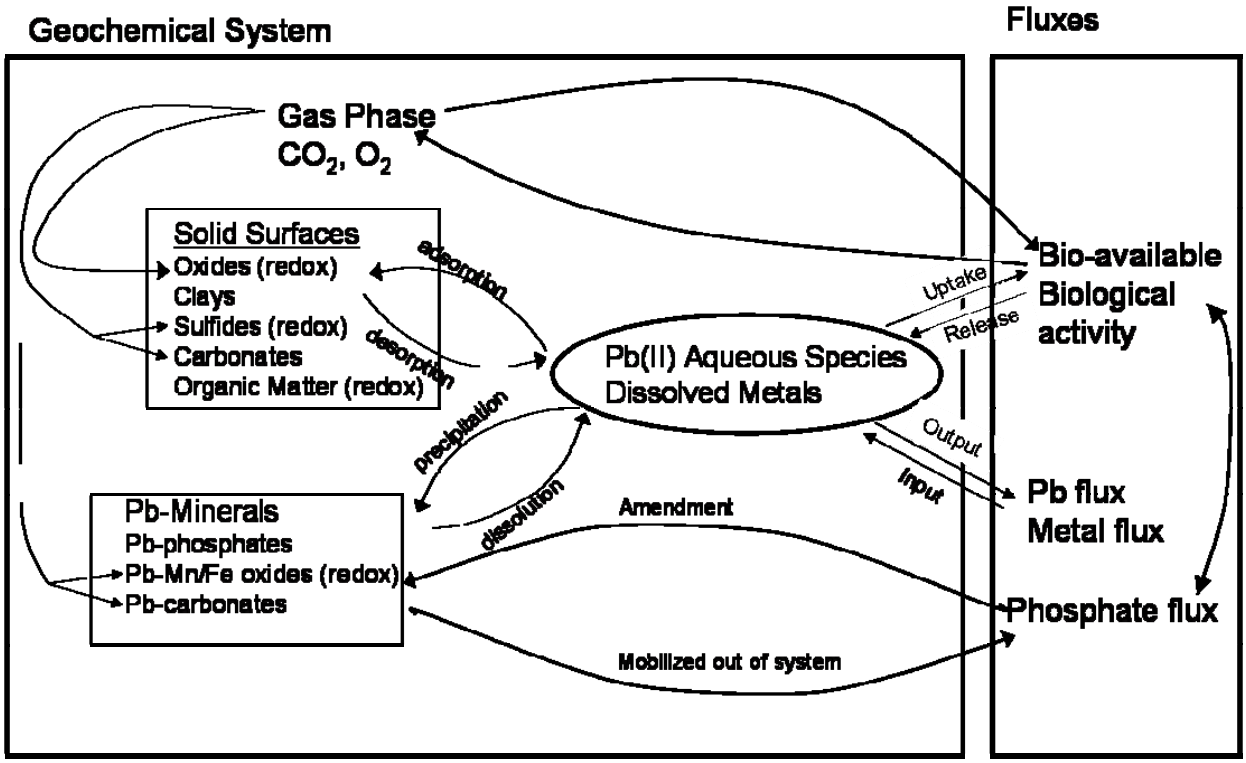

Figure 3-12. Diagram illustrating biogeochemical cycling of Pb in the environment.

Table 3-1. Elemental Analysis Results of Composite Soils from Study Plots 2, 4, 6, and 8 (values in parenthesis are standard deviation of 3 replicates)

Plot	As	Cd	Fe	Mn	P	Pb	Sulfur (S)	Zn
	milligrams per kilogram (mg/kg)							
2	80.7 (4.4)	30.2 (1.9)	78,600 (742)	5,738.7 (161)	24,800 (1,070)	5,180 (191)	1,738.6 (74.3)	2,350 (60.0)
4	136 (8.3)	16.4 (0.4)	84,800 (1,060)	7,312.2 (165)	597 (59.6)	4,500 (56.9)	1,841.2 (54.9)	2,840 (39.9)
6	37.9 (2.6)	11.2 (0.1)	40,200 (138)	1,440 (47.6)	16,400 (234)	3,560 (37.4)	432.1 (18.7)	769 (5.4)
8	55.9 (0.8)	9.40 (0.4)	47,800 (1,350)	2,750 (113)	1,320 (10.1)	3,780 (110)	457.2 (8.1)	1,090 (22.9)

Table 3-2. Particle Size Analyses for Composite Sample from Plots 2, 4, 6 and 8

	Sand	Silt	Clay	Texture Classification
Plot 2 Composite	58.3%	35.0%	6.64%	Very Fine Sandy Loam
Plot 4 Composite	59.7%	35.3%	5.06%	Very Fine Sandy Loam
Plot 6 Composite	35.6%	55.3%	9.14%	Silt Loam
Plot 8 Composite	26.6%	63.6%	9.82%	Silt Loam

Table 3-3. Associations between Elements in Soil Samples Analyzed by Electron Microprobe

Association	Sample Count[1] (High correlation)	Percentage Scans (High correlation)	Sample Count[1] (Moderate correlation)	Percentage Scans (Moderate correlation)
Mn-Fe	23	28.4 %	34	42.0 %
P-Fe	20	24.7 %	22	27.2 %
Pb-Mn	10	12.3 %	24	29.6 %
Pb-Fe	5	6.2 %	15	18.5 %
Fe-Si	2	2.5 %	17	21.0 %
Pb-P	1	1.25 %	9	11.1 %
P-Mn	0	0 %	5	6.2 %

[1] Total of 81 analyses on 12 thin sections.

Table 3-4. AOD and CBD Extraction Results for Plot 2, 4, 6, and 8 Composite Soils (values in parenthesis are standard deviations for 3 replicates)

Plot	AOD Fe (mg/kg)	AOD Mn (mg/kg)	CBD Fe (mg/kg)	CBD Mn (mg/kg)
2	60,400 (2,740)	4,070 (153)	57,100 (3,650)	3,570 (464)
4	50,000 (1,440)	4,364 (141)	29,100 (740)	2,170 (72.4)
6	24,000 (1,130)	1,130 (155)	31,000 (1,920)	1,220 (63.6)
8	26,000 (491)	2,410 (122)	34,000 (337)	2,510 (46.6)

Table 3-5. FTIR Peaks in Clay Fractions from Plots 2, 4, 6, and 8

Peak Location	Mineral
3696	Kaolinite
3620	Kaolinite
3300	Water adsorbed on soil organic matter
1636 (not in CBD treated)	Water adsorbed on soil organic matter
1594 (CBD treated only)	Soil organic matter
1396 (CBD treated only)	Soil organic matter
1030	Kaolinite
914	Kaolinite
800	Quartz
780	Quartz
750	Kaolinite
695	Quartz
530	Kaolinite
470	Kaolinite
420	Kaolinite

Table 3-6. XRD Analysis Results

Minerals Present Based on Fit (plots)	Other Minerals Queried
Quartz (2, 4, 6, 8)	Pyromorphite [$Pb_5(PO_4)_3Cl$]
Muscovite (2, 4, 6, 8)	Vivianite [$Fe_3(PO_4)_2 \cdot 8(H_2O)$]
Clinochlore (6, 8)	Chloropyromorphite [$Pb_5(PO_4)_3Cl$]
Siderite (2, 4, 6, 8)	Goethite [α-FeO(OH)]
Kaolinite (2, 4, 6, 8)	Hematite [Fe_2O_3]
Lepidocrocite (6, 8)	Siderite [$FeCO_3$]
	Akaganeite [$Fe^{3+}O(OH,Cl)$]
	Maghemite [γ-Fe_2O_3]
	Ferrihydrite [$5Fe_2O_3 \cdot 9H_2O$]
	Tenorite [CuO]
	Corkite [$PbFe_3(OH)_6SO_4PO_4$]
	Anglesite [$PbSO_4$]
	Galena [PbS]
	Beudantite [$PbFe_3AsO_4SO_4(OH)_6$]
	Plumbojarosite [$PbFe_6((OH)_3SO_4)_4$]

4. Lead Bioaccessibility to Waterfowl in the Lower Coeur d'Alene Basin Part 1: Development of a Physiologically Based Extraction Test for Waterfowl

4.1 Introduction

Mining and smelting activities in the Silver Valley Region of Idaho from the latter part of the 19th and through much of the 20th century have caused extensive heavy metal contamination in the Coeur d'Alene River basin. Metals in mining and milling wastes were carried downstream and deposited in the floodplains on approximately 18,000 acres in the Lower Coeur d'Alene River Basin. About 280 migratory and nesting bird species, mammals, reptiles (snakes, turtles), and amphibians inhabit the Lower Coeur d'Alene Basin (Ridolfi 1993). Heavy metals cause harm to humans and wildlife. One alarmingly apparent example is the lead poisoning of migrating waterfowl that stop over in the Coeur d'Alene River Basin. The majority of Pb poisoned waterfowl in the Coeur d'Alene Basin are tundra swans, Canada geese, and 14 other species (Sileo, Creekmore et al. 2001).

The Lower Coeur d'Alene River Basin provides feeding, resting and reproductive habitat. Contamination of the Coeur d'Alene River sediments from mine tailings has been identified as the main source of waterfowl Pb poisoning (Blus, Henny et al. 1991; Sileo, Creekmore et al. 2001). After soil ingestion, contaminants can be partially or totally released from the soil matrix during digestion and absorbed in the bloodstream (Oomen, Hack et al. 2002). Lead affects gastrointestinal epithelium, kidney, red blood cells, bone marrow, and nervous and reproductive systems. Clinical signs of Pb poisoning in waterfowl include severe pectoral muscle atrophy and bile stained feces, greenish diarrhea, excessive amount of bile present in the gall bladder, impaction of gastrointestinal tract with food leading to starvation, up to 40% loss in original body weight, erosion of the gizzard lining, loss of vision, convulsions, coma and death (Kendall and Driver 1982).

Due to the risks of Pb poisoning to wildlife and humans in the Lower Coeur d'Alene River Basin, and the vast area that needs to be remediated, addition of P to the soils has been proposed as an in situ remediation strategy. Application of P-amendments changes the Pb chemistry through formation of sparingly soluble Pb phosphates (Davis, Drexler et al. 1993; Ruby, Davis et al. 1994; Zhang, Ryan et al. 1997; Yang, Mosby et al. 2001). Several studies have demonstrated decreased (bio)availability of Pb minerals in the P-treated (abundant) soils (Davis, Drexler et al. 1993; Ruby, Davis et al. 1994; Zhang, Ryan et al. 1997; Yang, Mosby et al. 2001). However, due to the variable environmental conditions and dynamic nature of soil biogeochemistry an assessment of the in-situ remediation strategy must be done on a case-by-case basis, and must take into account the environmental factors controlling contaminant speciation (e.g., reduction and oxidation cycling).

There are several different approaches for measuring bioavailability. An in vivo (in living organism) test uses an animal to measure absolute bioavailability and toxicity. An in vitro (outside living organism) test can be used as a PBET that incorporates gastrointestinal tract parameters representative of a particular species. Initially, the PBET model was designed to simulate the human gastrointestinal tract, which includes stomach and intestinal phases (Ruby, Davis et al. 1993; Ruby, Davis et al. 1996; Medlin 1997; Rodriguez and Basta 1999; Basta and Gradwohl 2000; Oomen, Hack et al. 2002; Schroder, Basta et al. 2003). Absolute bioavailability is the amount of a substance absorbed into the organism's tissue via a particular route of exposure (gastrointestinal) divided by the total amount administered (U.S. EPA 1999). In vitro bioavailability (bioaccessibility) is defined as the solubility of

soil Pb in simulated stomach and intestinal solutions over total Pb in the soil (Berti and Cunningham 1997). The PBET differs from other soil extraction tests {e.g., toxicity characteristic leaching procedure (TCLP), Mehlich, etc.] because it incorporates physiological parameters from the target species, therefore making it a more representative test for bioavailability.

Soil particle size, mineralogy, Pb speciation, and food are among factors that influence Pb bioavailability (Steele, Beck et al. 1990). Processes regulating interactions between different metal species and their bioavailability values include solubility, adsorption, complexation, redox reactions, and biological uptake (Samiullah 1990). Thus it is critical to know Pb speciation to evaluate Pb bioavailability. Traina and Laperche (1999) reported that the toxicity of a metal is directly proportional to the activity of the free ion, and the most toxic solid will be that which supports the largest equilibrium activity of the metal. This indicates that the Pb minerals with the lowest solubility will be the least poisonous to waterfowl. Bioavailability of Pb minerals has been assessed by PBET in several studies to determine which minerals contribute to higher metal bioavailability and pose the greatest toxicity potential (Davis, Drexler et al. 1993; Ruby, Davis et al. 1994; Ruby, Schoof et al. 1999; Yang, Mosby et al. 2001). For example, Ruby et al. (1999) reported that Pb bioaccessibility increases in minerals in the order: galena<pyromorphite<Fe-Pb oxides<Pb jarosite<Mn-Pb oxides<Pb oxides<cerussite.

This study focused on developing an in vitro method that can be used to measure relative changes in bioavailability with various treatments and under specific conditions. Previous studies demonstrate strong linear relationships between bioaccessible Pb in the stomach and intestine phases and bioavailable Pb determined by animal studies (Ruby, Davis et al. 1996; Ruby, Schoof et al. 1999). The purpose of this study was to correlate the W-PBET extractable Pb with the results obtained from a bird-feeding study (Heinz et al. 2004), thus ensuring that observed trends are correct. Such an in vitro test for waterfowl will be useful because it is less expensive, simpler, and more easily reproduced than a bird feeding study, making it more feasible for use by regulators and scientists to assess the effectiveness of a particular remediation strategy on a site-specific basis.

4.1 Waterfowl Physiologically Based Extraction Test Design

The PBET method for the mammalian gastrointestinal (GI) system was modified for waterfowl; therefore, it is referred to in this report as W-PBET. In this study, PBET models for humans were modified to take into account waterfowl parameters based on bird physiology. Levengood and Skowron (2001) studied metal bioavailability in the waterfowl gizzard by taking gizzard contents from waterfowl and immersing them into a simulated gastric juice (gizzard phase). This research was used as a basis to develop gizzard phase extraction in the W-PBET. The parameters pH, temperature, mixing, soil solution ratio, and presence of enzymes in the simulated gastrointestinal tract are simulated in the PBET model (Ruby, et al. 1996). These parameters are discussed with respect to bird physiology and experimental design in the following sections.

4.2 Gastric and Small Intestine pH

Oomen et al. (2002) compared five in vitro digestion models for humans and concluded that the main difference in test results of bioaccessibility was the gastric-phase pH. The pH of the gizzard in birds ranges from 2.0 to 3.2, depending on the presence of food (Kimball and Munir 1971). The pH of pure gastric secretions is approximately 2, but the pH of gastric content is usually higher because the secretions are diluted by ingesta (Sturkie 1976). Intestinal pH ranges from about 5.2 to 7.2, and increases later due to the pancreatic secretions and buffers secreted by the intestinal epithelium (Klasing 1998). The average pH values 2.6 (stomach

phase) and 6.2 (intestine phase) are used in the W-PBET model. The effect of pH on metal extractability in the simulated gizzard for pH values of 2.0, 2.6, and 3.2 were measured.

4.3 Soil Mass and Fluid Volume

In this study the solid to solution ratio was chosen based on the waterfowl's daily ingestion of soil, which was derived from in vivo studies (Heinz, Hoffman, et al 2004) and 50 mL of gastric solution, which was the estimate used by Levengood and Skowron (2001). A non-breeding mallard eats between 70-100 g of food on a dry-weight basis per day and sediments constitute 12% of the diet (Heinz, Hoffman, et al 2004). Therefore, the ducks ate approximately 8.4 g of soil per day, and the estimated soil to solution ratio was 8.4 g to 50 mL = 0.168 g mL^{-1} (1:5.95). In this study, the effect of soil to solution ratio (1:6, 1:8.3, 1:100 and 1:200) on W-PBET metal bioaccessibility was tested.

4.4. Stomach Mixing

The gizzard exhibits regular rhythmic contractions. Peristaltic and segmenting movements comprise the mixing behavior in the bird's intestine (Sturkie 1976). An oscillating water bath at 250 rpm was used to simulate mixing for this test.

4.5 Soil Particle Size

Development of PBET models for humans considered soil particle sizes of < 250 μm because particles of this size and smaller would adhere to a child's hands, and could be ingested (Duggan, et al. 1985; Ruby, et al. 1996; Rodriguez and Basta 1999). Several ongoing studies use soils with particle size < 500 μm to measure bioavailability to ecological receptors such as the shrew and American Robin (Ruby 2003). In this study soil particles less than 1 mm were used because this is the size fraction used by Heinz, et al. (2004) in a waterfowl feeding study. Smaller particles have greater ratios of surface area to volume, hence, are more soluble, which may result in greater Pb bioavailability (Sparks 1989; Ruby, et al. 1992). Waterfowl can contain grit at an average of 45 g in the gizzard Klasing 1998), increasing the grinding effect. Grinding is not simulated in the centrifuge tubes when mixing in the water bath in the W-PBET test. Therefore, the effect of particle size on bioaccessibility was tested.

4.6 Stomach Emptying Rate and Small Intestinal Transit Time

In 1999, Rodriguez and Basta concluded that the length of time to perform the stomach phase and intestinal phase for humans was not clearly described in literature. In their study, they found that arsenic (As) concentrations in samples taken every 60 minutes remained constant over 3 hours.

The length of time that food materials spend in the gizzard depends on particle size. Small particles and liquid components pass through in minutes, whereas hard grains may remain in the gizzard for several hours. According to Klasing (1998), the mean retention time required for digesta to move through the GI tract in herbivorous birds is 50-300 minutes. In chickens, turkeys, and geese, food spends about 50% of the time in the stomach, which means that stomach incubation time is about 25-150 minutes. In this study the effect of incubation times of 30, 60, and 150 minutes on metal extractable concentrations in the simulated gizzard were tested.

4.7 Temperature

Because dissolution reactions are dependent on temperature, a significant temperature influence on the rate and equilibrium status of the reactions occurring in the extraction test was expected. In the PBET, the temperature is set to mimic a human (37 °C). Waterfowl body temperature is 42 °C and was used in the W-PBET test (Levengood and Skowron 2001).

4.8 Gastrointestinal Fluids

In 2001, Levengood and Skowron examined concentrations of heavy metals in the gizzard contents of 18 mallards. Gizzard contents were

transferred into 50 mL of simulated gastric juice containing 1 normal (N) sodium chloride (NaCl), 10 grams per liter (g/L) of pepsin, and hydrochloric acid (HCl) to adjust the pH to 2.0. These are the gizzard fluid parameters used in the W-PBET model, except pH is adjusted to 2.6. The same intestinal solution containing bile salts and pancreatin as in the in vitro model by Rodriguez and Basta (1999) was used. Across species, the small intestine is considerably less variable than other organs because the diverse physical constitution of different foods is reduced to a relatively uniform fluid suspension, or chyme, by the action of the proventriculus and gizzard (Klasing 1998). However, different bile concentrations and bile salts from either porcine or bovine origin may induce different bioaccessibility values for the different models (Oomen, et al. 2002). A summary of the physiologically based extraction test parameters for humans and waterfowl are presented in Table 4-1 along with the model developed for this study.

4.9 Soils

Soil samples used in measuring method reproducibility, accuracy, and sensitivity analysis were collected from a soil remediation test located on the northwest shore of Bull Run Lake in the Lower Coeur d'Alene Basin (Figure 3-1). This site includes a control plot (unamended) and P-amended plot to test the immobilization of Pb. Soils collected from the control plot were used in method validation. Samples were collected using a random sampling from a grid overlaid on the plots using a 20-cm long 5-cm diameter stainless steel sampler with a plastic sleeve insert. Core samples were submerged in liquid N_2, sealed, placed on ice, and transported to the laboratory where they were kept at –5 °C. Soils were air-dried and gently crushed and sieved to passing 1-mm pore size. Total metal concentration was measured on the soils using a hydrofluoric acid/*aqua regia* digest as outlined in EPA Method 3052.

Soils fed to mallards in the bird feeding study were used in the W-PBET model to investigate relations between in vitro Pb and in vivo Pb. Lead-contaminated soil samples from the Coeur d'Alene River Basin (Harrison Slough, Black Rock Slough, and Bull Run lake soils) in Idaho were P-amended in either laboratory incubations or field trials (Heinz, et al. 2004; Table 4-1). The soils from the Bull Run Lake site were amended in both the laboratory and field. A reference soil sample from Round Lake in the St. Joe River in Idaho that had relatively low Pb concentrations was compared to the three Pb-contaminated sites in the Coeur d'Alene River Basin in Idaho. The amendments consisted of phosphoric acid, lime to raise the pH of the soils, and potassium chloride to enhance chloropyromorphite [$Pb_5(PO_4)_3Cl$] formation.

The soils aged in the laboratory were thoroughly mixed under water in a commercial stainless steel mixing bowl and remained under the water continuously (Heinz, et al., 2004). The soils in the field were amended to a depth of 12 inches and rototilled. After aging the soils in the laboratory and field for 5 months, they were homogenized, dried, and screened through a 1-mm sieve. Unamended and amended soils were combined with the duck maintenance diet and pelletized (Heinz, et al., 2004). All of the experimental diets contained 12% soil. Table 4-2 summarizes the results of Pb concentrations in the tissues of mallards fed experimental diets. Raw data on W-PBET extractable gizzard Pb are shown in Appendix A, the University of Idaho's final deliverable for this project (Strawn, 2006).

Soil particle size analysis was conducted on the soils by first dispersing the soil aggregates and separating them using sedimentation (Gee and Bauder 1986). The W-PBET test was conducted on eight soil samples from the bird feeding study four separate times. These results are shown in Table 4-2. Ten percent of filtrates were run as duplicates on ICP-AES. Blanks and standard soils were run through the experiment.

4.10 W-PBET Procedure

A two-step sequential extraction consisting of the gastric and intestinal phases, as two separate measurements of gastrointestinal availability was used for the W-PBET. This approach is a modified version of the PBET model developed by Ruby et al. (1996).

4.10.1 Gizzard Phase

The gizzard solution was made up of 1 N NaCl and 10 g/L pepsin (from porcine stomach mucosa) and acidified to a pH 2.6 with HCl (Kimball and Munir 1971). Thirty mL of the gizzard solution was combined with 3.6 g of contaminated soil in a 50-mL polycarbonate centrifuge tube. The tube was degassed with high purity N_2, sealed, and placed in a water bath at 42 °C. Samples were mixed in the water bath at 250 rpm. Temperature and pH for all solutions was taken prior to adding the soil. Following incubation of one hour, the samples were removed centrifuged and filtered. Measurements of pH taken before and after centrifuging did not appear to be that different, therefore, pH was measured only after centrifuging. Samples were centrifuged for 24 minutes at 12,000 rpm and the supernatant was filtered through a 25-mm syringe filter with a 0.2-μm membrane following pH measurement. Because the proteins and salts may cause a high background effect and filter clogging during analysis, the samples were diluted 1:10 in deionized water. The filtrate was analyzed for calcium (Ca), cadmium (Cd), P, Pb, Zn and Mn using ICP-AES. Detection limits for the gizzard and intestine phase Pb on the ICP-AES were 0.01 milligrams per liter (mg/L).

4.10.2 Intestinal Phase

Following the gizzard phase, a separate set of un-centrifuged samples was adjusted to a pH of 6.2 by the addition of sodium bicarbonate. Bile salts and pancreatin (from porcine pancreas) were added in the amount of 0.35% and 0.035%, respectively (Rodriguez and Basta, 1999). Samples were mixed in the water bath at 250 rpm. Following incubation for two hours, the samples were removed, centrifuged, filtered, and the pH was measured. All other aspects of the sample treatment and analysis were the same as the gizzard phase.

4.11 Effect of W-PBET Parameters on Metal Extractability

Sensitivity analysis was conducted on the gizzard phase to determine the effect of pH, grinding, soil to solution ratio, and incubation time on Pb extractability in the simulated gizzard. Bull Run unamended soil samples were run at pH of 2.0, 2.6, and 3.2 through the W-PBET gizzard phase. Another W-PBET experiment was conducted on soils to test incubation time of 30, 60, and 150 minutes. All other parameters are shown in Table 4-1. Grinding effect was tested on soils with particle sizes of < 1 mm and < 0.25 mm. Soil-to-solution effect on W-PBET metal bioaccessibility was investigated at 1:6, 1:8.3, 1:100, and 1:200 (g/mL). All samples were run in triplicates. Details of the analytical results are provided in Appendix A, the University of Idaho's final deliverable for this project (Strawn, 2006).

4.12 Data Analysis

Note: The reported statistical analyses for this work were performed using Statistical Analysis Software (SAS) Version 8.2. However, details about the specific code and model used were not fully documented. An EPA review of the following section found that the information provided was insufficient to verify the statistical analysis. With this understanding, specific results should be interpreted and used with caution.

W-PBET metal bioaccessibility was calculated as the ratio of metal concentration in the extracted phase (mg/kg) over total Pb concentration in the soil (mg/kg). In vivo Pb bioavailability was calculated as a ratio of Pb concentration in the tissue (mg/kg, wet weight) over total Pb concentration in the diet (mg/kg).

Statistical analyses were performed using Statistical Analysis System Version 8.2. Least significant difference t-tests were used to separate means. Pearson and Spearman correlation coefficients were used to determine if W-PBET Pb results were correlated with bird feeding results, and to determine if extractability of the different soil metals were correlated with each other. Linear regression was performed for metal gizzard extractabilities and W-PBET parameters.

4.13 Results and Discussion

Reproducibility of Pb extractability in the W-PBET gizzard phase was high [relative standard deviation (RSD) = 4.3%]. However, reproducibility of Pb extractability in the intestine extractions was lower (RSD = 17%). The low precision in the Pb concentrations in the simulated intestine extractions were most likely due to the concentrations being near the ICP-AES detection limit (0.01 mg/L). Results from spiked solutions carried through the extraction experiments indicated that the gizzard phase recovered an average of 90% ± 8% of the spiked Pb, while the intestine phase recovered an average of 73% ± 7% of the spiked Pb. The low recovery for the intestine phase suggests that a fraction of the soluble Pb is lost in this extraction, possibly due to precipitation of Pb carbonate minerals. Although such a process may be indicative of processes occurring in the digestion system of waterfowl, the exact reason for the low recovery is unclear and, therefore, adds uncertainty to the intestine-phase extraction results. Because of this observation, and the fact that the intestine extraction concentrations are near or below the detection limit, the results and discussion presented below focus on the gizzard phase.

4.13.1 Sensitivity Analyses

One of the governing factors of Pb extractability in the simulated gizzard is pH. Results for Pb extractability in the simulated gizzard at different pH values indicate linear relations between pH and Pb concentration in the gizzard phase (Figure 4-1). The concentration of Pb in the gizzard extraction doubles as pH decreases from 3.0 to 2.0. Because conditions in a bird stomach vary depending on food presence and bird speciation, an average pH value of 2.6 was used in the W-PBET experiments. The linear relationship between pH and extractable Pb indicates that pH should not affect the correlation between W-PBET Pb and in vivo Pb.

Incubation time (30, 60, and 150 minutes) did not create a significant difference in Pb concentrations in the gizzard as shown in Figure 4-2. This is consistent with the findings of other PBET experiments (Rodriguez and Basta, 1999; Hettiarachchi, et al. 2000). Since incubation time (kinetics) does not control Pb extractability in the gizzard, the dissolution or desorption of Pb must reach equilibrium within the 60-minute time frame of the experiment.

Pb concentrations in the gizzard extractions from soils with particle sizes < 1 mm and < 0.250 mm are significantly different as shown in Figure 4.3. However, the difference is small: 1501.4 ± 53.6 mg/kg Pb in the simulated gizzard from particle size soil less than 1 mm, and 1669.5 ± 31.7 mg/kg Pb in the simulated gizzard from particle size soil less than 0.250 mm (i.e., 10% difference). Bull Run Lake soils are very fine sandy loam soils. Previous studies conducted in the laboratory indicated that Pb was predominantly associated with the clay minerals with size < 0.002 mm. This is significantly smaller than the tested particle size of < 0.250 mm and < 1 mm, explaining the small difference in particle size effect on Pb extractability. Because the gizzard mainly grinds larger particles, the relative differences in bioaccessible Pb were minimally impacted by grinding effects.

Soil to solution ratio in the simulated gizzard was investigated due to uncertainty about its true value in the waterfowl digestion system. In general, an increase in soil-solution ratio causes a decrease in Pb extractability as shown in Figure 4-4.

There was not a notable difference in Pb bioaccessibility for soil to solution ratios 1:100 and 1:200; however, there were differences noted between Pb bioaccessibility for soil to solution ratios 1:6 and 1:8.3.

The relationship between Pb extractability and soil to solution ratio in the simulated gizzard was linear (R^2=0.96) as shown in Figure 4-4. Strong linear relations between Pb extractability and soil-to-solution ratios indicate that different soil-to-solution ratio values used in W-PBET and PBET models should not affect metal bioaccessibility results in comparative studies. However, differences are significant in studies that are designed to calculate absolute bioavailability.

4.13.2 W-PBET Lead and In Vivo Lead Comparison

W-PBET and bird feeding results indicating that P-amendments significantly reduce Pb bioavailability are shown in Table 4-2. However, previous studies have suggested that reduced Pb concentrations in amended soils with 1% P present hazards to waterfowl (Heinz et al. 2004). The relationship between Pb concentrations in the W-PBET gizzard extraction and Pb concentrations in the tissues is logarithmic as shown in Figure 4-5. Correlations of the W-PBET Pb concentrations and Pb concentrations in the different tissues (blood, kidney and liver) were similar. Both Pearson and Spearman coefficients show the highest correlation between log Pb in the W-PBET gizzard and Pb concentrations in the tissues, and the lowest correlations between Pb bioaccessibility and Pb bioavailability. The statistical results are shown in Table 4-3. When the in vitro tissue and W-PBET gizzard Pb concentrations were normalized by the total concentration of Pb in the diet and in the soil, respectively, the correlations were similar to the non-normalized, except for the blood Pb data, which had no significant correlation according to the Pearson correlation test. Both bioavailability and bioaccessibility have the same trend for Pb in the amended and unamended soil samples.

The most significant difference between W-PBET and bird feeding tests is that the Harrison Slough soil had greater bioaccessible Pb values compared to other soils, while the in vivo test did not have as large a difference for Pb bioavailability in Harrison Slough soils versus other soils. This difference between the two tests is likely a result of discrepancies between the in vivo and W-PBET gastrointestinal physical parameters and biochemistry that are affected differently by the varying soil characteristics. All soils had similar particle size distributions and total Pb concentrations, eliminating the possibility of surface area differences as the reason for the differences in the W-PBET and in vivo results. Thus, it is concluded that the differences are due to differences in Pb speciation or soil mineralogy, and that this difference does not impact in vivo bioavailability. Soil mineralogy can impact the amount of Pb in solution because different minerals will maintain varying solution concentrations of Pb in the simulated digest solution. This difference highlights the importance of understanding how soil variability can impact bioavailability, and the need for tests that can measure such variation.

4.13.3 W-PBET Results for Lead, Zinc, Cadmium, and Manganese

Concentrations of Pb, Zn, Cd, and Mn in the W-PBET gizzard extractions from the Lower Coeur d'Alene Basin amended and unamended soils were analyzed. In the Lower Coeur d'Alene River, Pb, Zn, and Cd are present at elevated levels and threaten wildlife (LeJeune, et al. 2000). High concentrations of Mn were present, which can be toxic because of the trace metals that readily absorb on Mn oxides (McKenzie, 1980; Hettiarachchi, et al, 2002). W-PBET results for Cd, Zn, and Pb gizzard extractability were correlated to each other in the unamended Harrison Slough, Black Rock, and Bull Run Lake soils using Pearson correlation coefficients: $R_{Pb/Cd}$ = 0.82, $R_{Pb/Zn}$ = 0.96, $R_{Cd/Zn}$

= 0.93, probability (p) < 0.01. Soils from different locations in the Lower Coeur d'Alene Basin had different metal bioaccessibility, indicating that the speciation is different and metal bioaccessibility is site-specific as shown in Figure 4-6. Different reduction values were observed in metals bioavailability to earthworms in the P-amended soils from different locations reported by Maenpaa et al. (2002). This study concluded that soil characteristics other than P-amendments affect metals bioavailability to earthworms.

According to W-PBET results, only Pb showed a significant reduction in bioaccessibility in all P-amended soils. This indicates that P-amendments immobilized Pb species. Many studies have investigated the decrease in Pb bioavailability in P-amended soils through formation of Pb phosphates, such as pyromorphite (Ruby et al, 1994; Laperche et al, 1997; Hettiarachchi et al 2000; Melamed et al 2003). In solutions with several metals present, the phase with the lowest solubility precipitates from solution before the more soluble metals such as Cd, Zn, and Mn least soluble metals (Cao et al 2003). Reaction kinetics also plays a role. In 2003, Oomen et al. reported that pyromorphite formation is a rapid process and the reactions between available Pb and phosphate can take place in the acidic conditions of the simulated gastrointestinal fluid and result in formation of pyromorphite in vivo. Lead phosphates are considered to be insoluble. However, Oomen et al. (2003) used voltammetry to measure Pb species in solution and observed that lead phosphate complexes are soluble in the simulated chyme of the human digestive system, and could therefore be a source of Pb^{2+} that is available for transport across the intestinal epithelium. This suggests that poorly soluble lead phosphate minerals may not be completely non-reactive in the digestive system.

Phosphate amendments are primarily used to immobilize Pb, but they can also stabilize other metals (Chen et al. 1997; Maenpaa, et al. 2002). The availability of Cd and Zn has been studied in apatite-treated soils and solutions and it was determined that the aqueous Cd and Zn concentrations decreased in the presence of apatite (Chen et al. 1997; Cao et al. 2003). Cao et al. reported in 2003 that different mechanisms are responsible for decreased Zn and Cd solubility in the presence of apatite: ion exchange at the surface of hydroxyapatite; surface complexation; precipitation of amorphous to poorly crystalline mixed-metal phosphate; and, metal substitution for Ca in hydroxyapatite during recrystallization.

The W-PBET gizzard extraction phase showed no significant difference between P-amended and unamended soils in Harrison Slough and Black Rock soils for Cd and Zn. However, there was a significant reduction in Cd and Zn gizzard extractability in the Bull Run Lake soils P-amended in the field as shown in Figure 4-6. Maenpaa et al. (2002) did not observe significant Pb, Zn, and Cd bioavailability reductions to earthworms in the soils with lower P rate amendments (600 mg P/kg dry weight). However, at higher P-amendment rates (5,000 mg/kg dry weight) there was significant reduction in Pb, Cd, and Zn earthworm bioavailability. The field-amended soils had significantly higher P-amendments; however, the Black Rock Slough field-amended soils did not show a significant difference in Cd and Zn bioaccessibility, discounting this as the sole reason for the decreased bioaccessibility in the Bull Run Lake field-amended soils. It is hypothesized that the differences are due to the dramatically different environments that are present between the two sites. P-amendment application, incubation, water inundation, mixing, and soil characteristics could account for the different metal availabilities between the field- and lab-aged samples (Heinz et al. 2004). Although they are only separated by approximately 100 meters, the Bull Run Lake soils are located on a lateral lake shore and subjected to different flooding cycles than the Black Rock Slough soils, which are located at a slightly higher elevation and subjected to flooding for only short times.

The bioaccessibility of Cd and Zn behaved similarly in all soils as shown in Figure 4-6. This is likely due to these elements lying in the same group on the periodic table, which means they have similar chemical properties. There was a linear correlation between Cd and Zn in the P-amended and unamended soils as shown in Figure 4-7. The similarities in release in the gizzard extract indicate that Cd and Zn exist as the same species in the soils, and react similarly with P-amendments.

4.14 Discussion and Conclusions

W-PBET gizzard phase demonstrated high Pb extraction reproducibility and accuracy. The intestine phase has been excluded as Pb concentrations in this phase were near the ICP-AES detection limit (0.01 mg/L), which leads to low reproducibility. The W-PBET parameters on Pb extractability in the simulated waterfowl gastrointestinal tract showed that pH had the most significant impact on Pb bioaccessibility. Results showed linear relations between pH and Pb extractability in the gizzard phase (R^2 = 0.97). In the gizzard phase, incubation time did not affect Pb extractability, indicating that Pb is at equilibrium and that soil grinding had only a small effect on Pb extractability. There was a negative linear relationship between soil to solution ratio and Pb extractability in the simulated gizzard.

Although W-PBET was designed to simulate the waterfowl digestive tract, it must be emphasized that extractable Pb should be viewed in a relative context. The use of the predicted Pb bioaccessibility for absolute bioavailability predictions is weakened by the many assumptions within W-PBET model and the difficulty in precisely simulating bio-uptake in the GI system. Despite these limitations, the W-PBET Pb bioaccessibility model developed during this project was positively correlated with bird feeding results for contaminated and *in situ* remediated soils from the Lower Coeur d'Alene River Basin.

There was a significant decrease in Pb bioavailability/bioaccessibility in all of the P-amended soils. These results show that phosphate has a different effect on Cd, Zn, and Mn than on Pb. Cd and Zn showed a significant decrease in gizzard extractability only in the Bull Run Lake soils that were P-amended in the field. Similarities were noted between the behavior of Zn and Cd extractability in the unamended and amended soils, suggesting that they have similar speciation and their availability is governed by the same mechanisms in the P-amended soils. Mn bioaccessibility was variable between the different soils and treatments. W-PBET gizzard phase results showed that metal extractability in the soils was site-specific.

Because the geochemistry of Pb and other metals in the soils is dynamic, it is critical to have an assessment tool that will allow scientists, managers, and engineers to evaluate how environmental variables, and remediation and management strategies might impact the Pb bioavailability. The W-PBET model is a cost effective method to accomplish this.

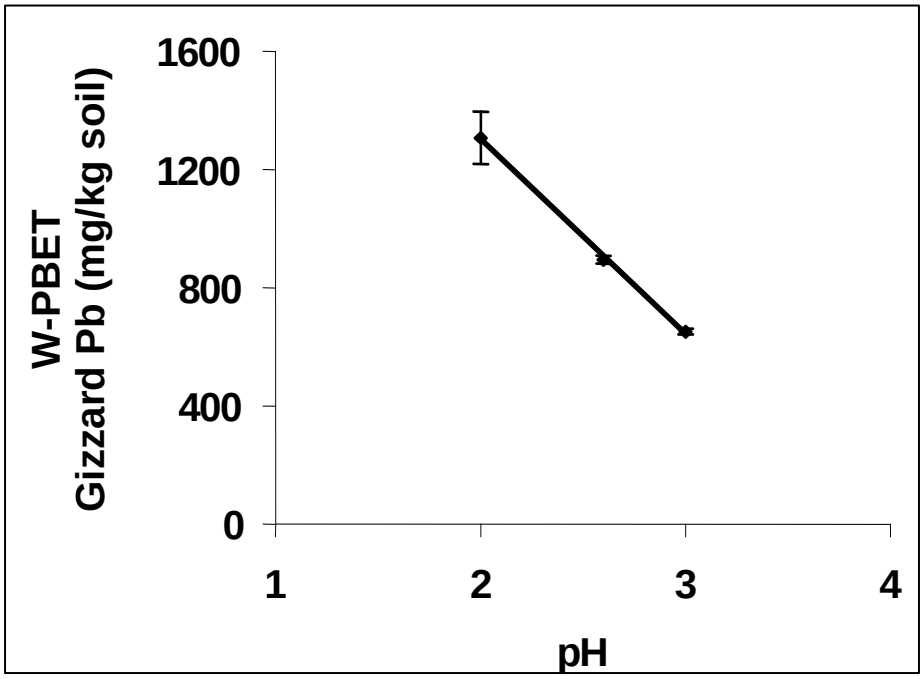

Figure 4-1. pH effect on Pb extractability in the gizzard. Error bars represent one standard deviation of triplicates (R^2 = 0.97).

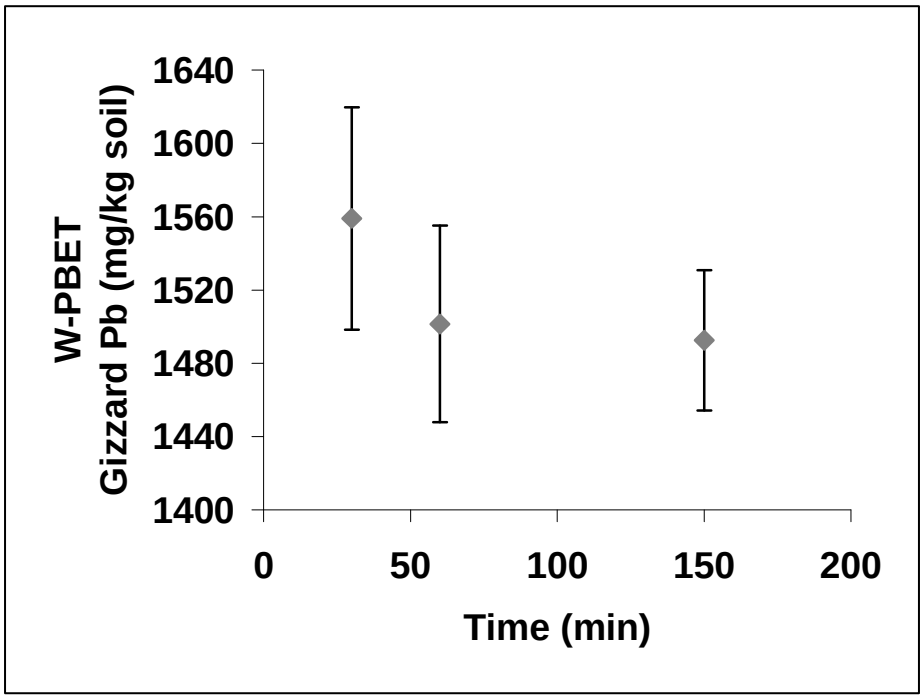

Figure 4-2. Incubation time effect on Pb solubility in the gizzard phase. Error bars represent one standard deviation of triplicates.

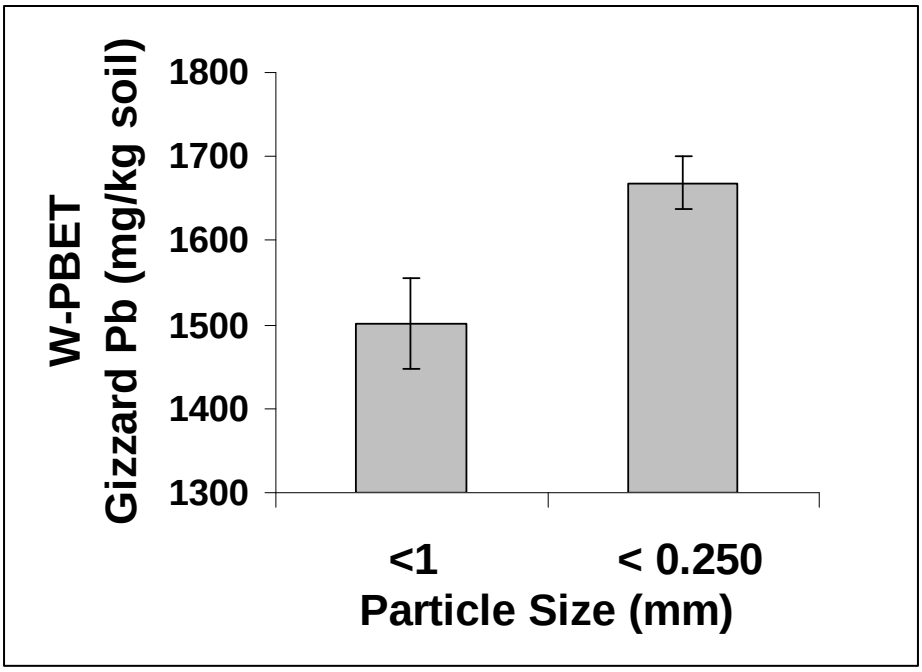

Figure 4-3. Effect of grinding on extractable Pb in the simulated gizzard. Error bars represent one standard deviation of triplicates.

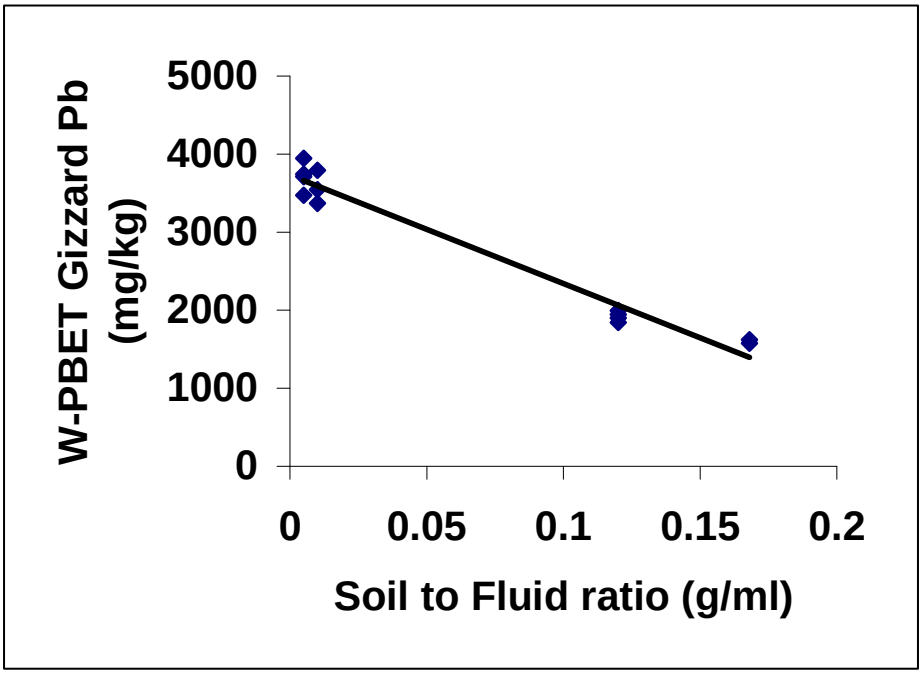

Figure 4-4. Relationship between extractable metal in the simulated gizzard and soil to fluid ratio in the simulated gizzard solution (R^2 = 0.96).

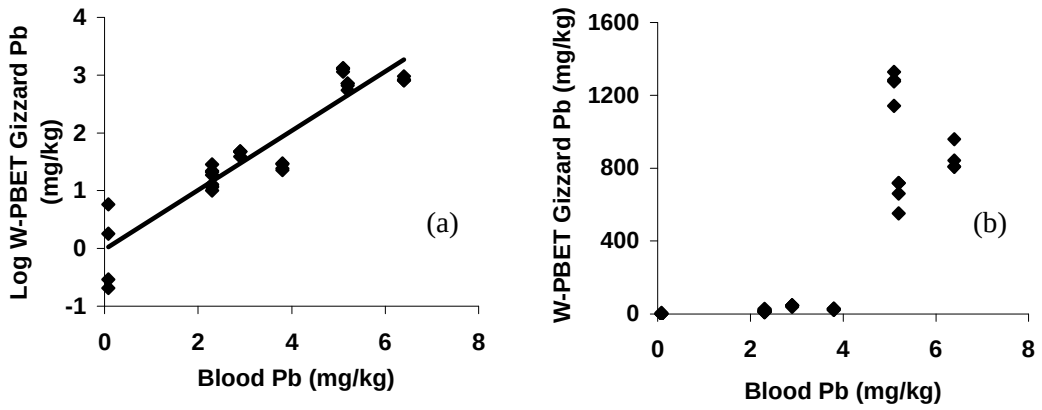

Figure 4-5. Log (a) and linear (b) correlations between Pb concentrations in the simulated gizzard and Pb concentrations in the blood.

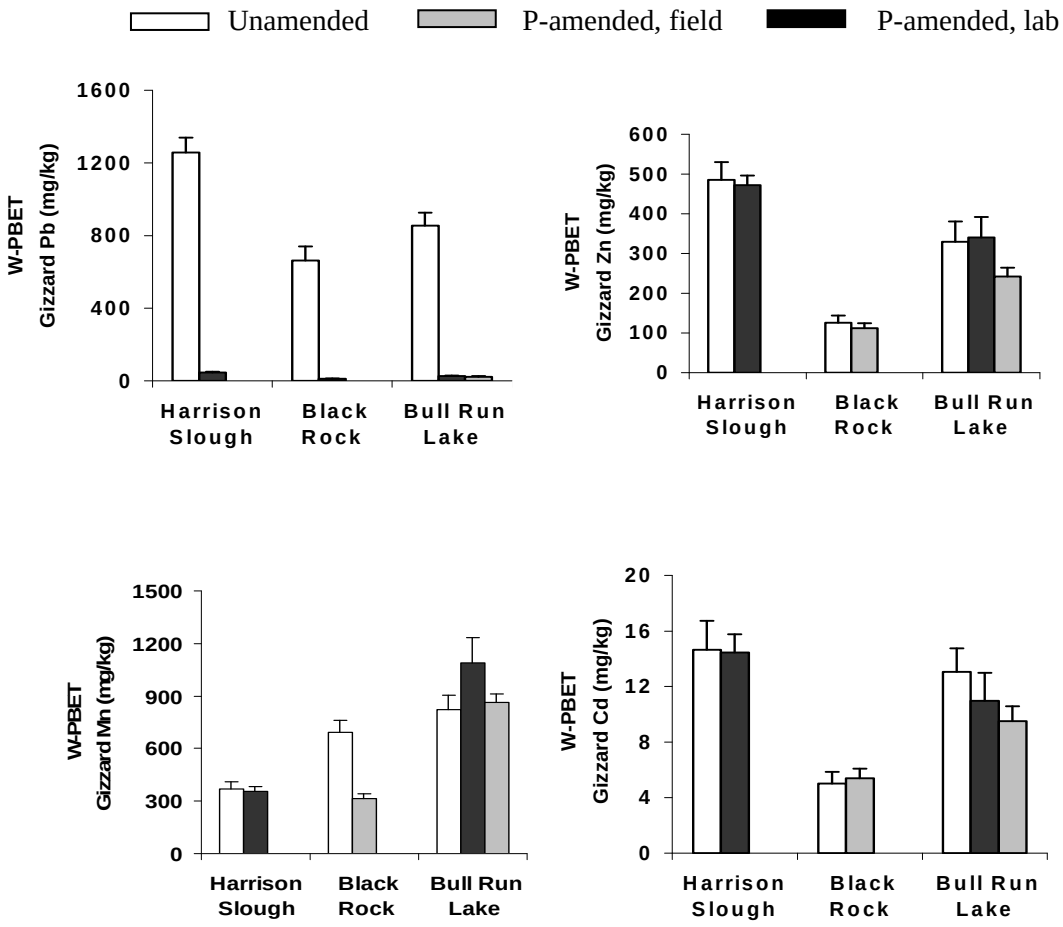

Figure 4-6. Lead, Zn, Mn, and Cd release in the W-PBET gizzard extractions from the Lower Coeur d'Alene Basin soils. Error bars represent one standard deviation (N = 4).

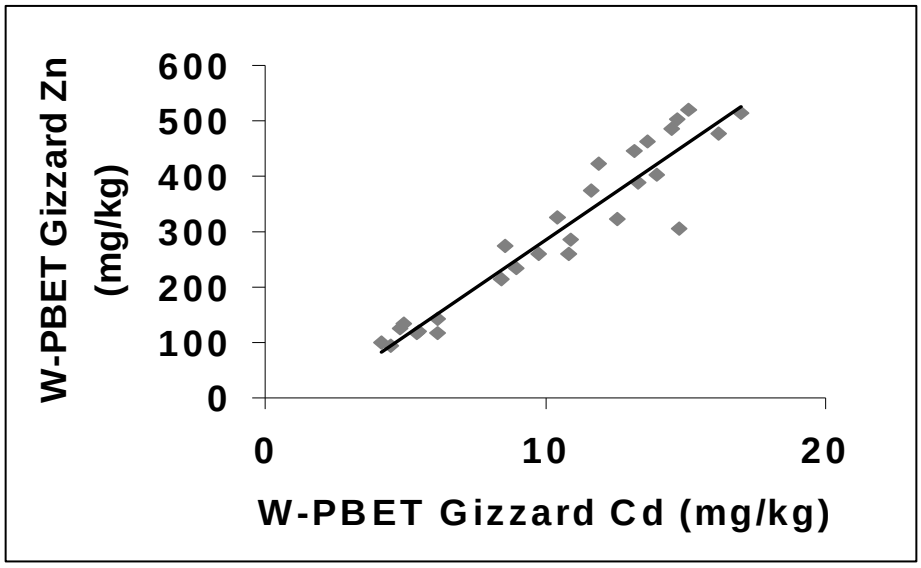

Figure 4-7. Correlation between Zn and Cd extractability in the W-PBET gizzard phase from the P-amended and unamended Lower Coeur d'Alene River soils (R^2 = 0.96).

Table 4-1. Summary of In Vitro Parameters Used in Different Models and Proposed W-PBET

Parameter	PBET Model (Ruby et. al., 1996)	IVG Model (Rodriguez and Basta, 1999)	Gizzard Simulation (Levengood and Skowron, 2001)	W-PBET Experiment Design (this study)
Gastric Solution				
Target Organism	Human	Human	Waterfowl	Waterfowl
pH	1.3; 2.5; 4.0	1.8	2.0	2.0-3.2
NaCl	None	0.15 *M*	1 N	1 N
Pepsin	1.0% (1.25 g)	0.10%	10 g/l	10 g/l
Citrate	0.05%	None	None	None
Malate	0.05%	None	None	None
Lactic Acid	0.5%	None	None	None
Acetic Acid	0.5%	None	None	None
Fluid Solution	40 mL	600 mL	50 mL	30 mL
Amount of Soil Added	0.4 g	4 g	Gizzard Content	3.6 g
Temperature	37 °C	37 ºC	42 ºC	42 ºC
Food Added	No	Yes	Yes	No
Incubation Time	1 hour	1 hour	1 hour	1 hour (or until equilibrium is established)
Soil:Solution Ratio	1:160 (assuming density of 1.6 g/cm^3 for the test soil)	1:150 (assuming density of 1.0 g/cm^3 for the test soil)	Gizzard content:50 mL of simulated gastric juice	6 g:50 mL (based on waterfowl bird feeding study)
Intestinal Solution				
pH	5.5	7.0	-	5.2-7.2
Pancreatin	0.018% (20 mg)	0.035% (0.21g)	-	0.035%
Bile Extract	0.05% (70 mg)	0.35% (2.10 g)	-	0.35%
Incubation Time	4 hour	1 hour	-	2 hour

Table 4-2. Lead Bioaccessibility and Bioavailability Values Based on W-PBET and Bird Feeding Studies; Pb and P Concentrations in the Soils and Blood Pb Values are from Heinz et al. (2004)

Samples	Treatments	Pb	P	W-PBET Gizzard-Pb	Bioaccess-ibility	Blood Pb	In Vivo Bioavailability (blood)
		mg/kg dry weight		mg/kg	%[††]	mg/kg wet weight	%[§]
Round Lake	None	21 ± 1.9	723 ± 5	BDL	-	0.08	-
Harrison Slough	None	4,520 ± 68	628 ± 21	1,258 ± 81[†]	28	5.1 ± 0.30	1.0
Harrison Slough	Amend, Lab	4,370±21	10,400 ± 20	45.5 ± 4	1.04	2.9 ± 0.32	0.6
Black Rock Slough	None	5,390±40	708 ± 10	662 ± 79	13	5.2 ± 0.46	0.97
Black Rock Slough	Amend, Field	4,070 ± 164	18,600 ± 440	12 ± 1	0.3	2.3 ± 0.28	0.5
Bull Run Lake	None	6,990 ± 125	440 ± 15	854 ± 71	12.2	6.4 ± 0.56	0.8
Bull Run Lake	Amend, Lab	6,910 ± 61	10,200 ± 66	26 ± 3	0.4	3.8 ± 0.33	0.5
Bull Run Lake	Amend, Field	6,100 ± 68	21,300 ± 209	22 ± 4	0.4	2.3 ± 0.26	0.34

[†] Standard deviations for N = 4
[††] Percentage is W-PBET gizzard extractable Pb normalized by soil Pb (mg/kg)
[§] Percentage is in vivo tissue Pb normalized by diet Pb (mg/kg)
BDL – below detection limit

Table 4-3. Correlation Coefficients between W-PBET Pb and In Vivo Pb (N = 32, p < 0.05)

Parameter	W-PBET Gizzard Pb (mg/kg)	W-PBET Log Gizzard Pb (mg/kg)	Parameter	W-PBET Gizzard Pb Soil Pb (%)
Blood Pb (mg/kg)	0.88[†] 0.78[††]	0.88 0.93	Blood Pb/diet Pb (%)	0.78 0.31[§]
Liver Pb (mg/kg)	0.93 0.78	0.94 0.95	Liver Pb/diet Pb (%)	0.81 0.59
Kidney Pb (mg/kg)	0.94 0.82	0.94 0.88	Kidney Pb/diet Pb (%)	0.81 0.69

† Spearman correlation coefficient
†† Pearson correlation coefficient
§ Correlation is not significant (p > 0.05)

5. Lead Bioaccessibility to Waterfowl in the Lower Coeur d'Alene River Basin Part 2: Seasonal Effect on Metal Bioaccessibility

5.1 Introduction

To assess a potential remediation strategy for Pb poisoning to wildlife and humans in the Lower Coeur d'Alene River Basin, P-amendment trials were conducted (TerraGraphics Environmental Engineering 2003; Heinz, Hoffman et al. 2004). Several studies have demonstrated decreased availability of Pb minerals in P-treated soils (Davis, Drexler et al. 1993; Ruby, Davis et al. 1994; Zhang, Ryan et al. 1997; Yang, Mosby et al. 2001). An in vitro, physiologically based extraction test that incorporates gastrointestinal tract parameters representative of waterfowl was developed and calibrated to measure Pb bioavailability to waterfowl. PBET models for humans (Medlin 1997; Rodriguez and Basta 1999; Basta and Gradwohl 2000; Oomen, Hack et al. 2002; Schroder, Basta et al. 2003) were modified to take into account waterfowl parameters, based on bird physiology (Sturkie 1976; King and McLelland 1979; Sturkie 1986; Klasing 1998; Levengood and Skowron 2001). The W-PBET model was positively correlated with bird feeding studies described by Heinz et al. (2004), and both investigations (in vivo and W-PBET) showed that Pb bioavailability was significantly reduced in the P-amended soils. Thus, we concluded that the developed W-PBET model can be used to measure relative changes in bioavailability with various treatments and under specific conditions. Such an in vitro test for waterfowl is useful because it is less expensive, simpler, and more easily reproduced than a bird feeding study. As a result of these benefits, the W-PBET model can be used to assess site-specific remediation strategies and relative bioavailability, and has potential to be used as a regulatory tool to assess the effectiveness of a particular remediation strategy.

In this study, Pb bioaccessibility was examined in soils from the Coeur d'Alene River Basin as a function of seasonal changes using the W-PBET model. Soils in contaminated wetlands undergo temporal fluctuations in water inundation, resulting in fluctuations in the redox potential. Changes in redox status of the soils can affect the availability and mobility of metals, and consequently their bioavailability. Thus, to account for influences of reduction and oxidation on metal bioavailability, it is important to investigate soils collected during different times of the year. Iron and Mn geochemistry in wetlands is particularly interesting because these elements are redox reactive and have high surface areas for interactions with both P and Pb and, therefore, dynamic changes in the Fe and Mn speciation will impact Pb bioavailability. Manganese-lead oxide and Fe-Pb oxide can be formed in soils by a combination of geochemical or bacterially-mediated reactions (Davis et al. 1993). Oxygen depletion in flooded soils may cause a successive reduction of Mn oxides and Fe oxides, thereby releasing contaminants associated with them (Hem 1978; Matsunga et al. 1993), and increasing heavy metal bioavailability. Beyer and Day (2004) estimated exposure of mute swans to metals from contaminated sediments in Chesapeake Bay, USA. Exposure to Pb at the reference site was found to be correlated with Mn and Fe. Although Pb is the main element of focus in many studies on waterfowl toxicity, in this study we also report on trends in extractability of Zn, Cd, Mn, and Fe as well.

5.1 Soil Sampling

Soils were sampled from two field sites. One site is located on the northwest shore of Bull Run Lake, and the other one is on the northwest side of Black Rock Slough (Figure 3-1). Each site contained an unamended (control) plot (25 feet by 30 feet) and a plot amended with phosphoric acid, lime, and potassium chloride (Heinz et al 2004). Amendments were applied and tilled to a depth of 1 foot in April 2001. The two sites are approximately 200 feet apart.

Black Rock Slough soils are water saturated for shorter periods compared to Bull Run Lake soils.

Samples from the P-fertilizer amended soils and the control plots were collected on May 14, August 7 and October 30, 2003 using a random sampling from a grid overlaid on the plots as shown in Figure 3-2. Three cells from each plot were sampled using a 20-cm long 5-cm diameter split core stainless steel sampler with a plastic sleeve insert. Core samples were immediately submerged in liquid N_2, sealed in airtight nitrogen purged bags, placed on ice, and transported back to the laboratory where they were kept at –5 °C. A combination reference electrode was used to measure redox state. The measured potentials of the samples were corrected to the standard H-electrode using theoretical redox potential of potassium ferric-ferrocyanide and the measured potential of potassium ferric-ferrocyanide solution relative to the reference electrode. The pH was measured using a combination pH electrode. Prior to extraction, the frozen soil cores were freeze-dried and gently crushed and sieved to passing 1-mm pore size. Total elemental concentrations in the soils were determined using EPA Method 3050. The complete results are shown in Appendix A, the University of Idaho's final deliverable for this project (Strawn, 2006).

5.2 W-PBET Experiment

To measure Pb bioaccessibility, W-PBET gizzard phase extraction was conducted on the soil samples. Each soil sample was run in duplicate, and 10% of the samples were run in triplicate. Blanks and a standard soil (soil used in all extractions) were run in all extractions.

The gizzard solution consisted of 1 N NaCl and 10 g/L pepsin from porcine stomach mucosa acidified to pH 2.6 with HCl (Kimball and Munir 1971). Thirty mL of the gizzard solution was combined with 3.6 g of contaminated soil in a 50-mL polycarbonate centrifuge tube. The tube was degassed with high purity N_2, sealed, and placed in a water bath at 42 °C. Samples were mixed in the water bath at 250 rpm. All solutions were analyzed for pH and temperature prior to adding to the soil. Following incubation of 1 hour, the samples were removed, centrifuged, the pH measured, and the mixture was filtered. A test was conducted on pH stability; results indicated that the final pH ranged from 3 to 3.5. The samples were diluted 1:10 in deionized water and centrifuged for 24 minutes at 12,000 rpm, through a 25-mm syringe filter with a 0.2 μm membrane filter. The filtrate was analyzed for Cd, Pb, Zn, Fe, and Mn using ICP-AES. National Institute of Standards and Technology (NIST) traceable multi-element standards were used to assure accuracy in measuring metal concentrations. Ten percent of the extracts were run in duplicate on ICP-AES. All analytical results are provided in Appendix A, the University of Idaho's final deliverable for this project (Strawn, 2006).

5.3 Data Analysis

Note: The reported statistical analyses for this work were performed using Statistical Analysis Software (SAS) Version 8.2. However, details about the specific code and model used were not fully documented. An EPA review of the following section found that the information provided was insufficient to verify the statistical analysis. With this understanding, specific results should be interpreted and used with caution.

Element bioaccessibility values were calculated by normalizing the W-PBET extracted Pb using the total Pb concentration in the soil. Data analysis was conducted using Statistical Analysis System Version 8.2. Least significant difference was applied to separate means. Each sample site contains unamended and amended plots and within each site, there was a completely randomized design with three replicates within two plots, sampled across time. Pooled–repeated measures analysis of variances (ANOVA) was used and the model was run separately for each element. Correlation analysis was run between Pb, Cd, Zn, and Mn bioaccessibility values in the P-amended and

unamended soils, between metal bioaccessibility values and soil pH, and between total metal concentrations in the soils and soil pH. The results from an inferential test were identified as statistically significant if the p-value of the test statistic was less than 0.05.

5.4 Results and Discussion

Lead, Zn, Mn, Cd, and Fe concentrations in the Lower Coeur d'Alene Basin exceed common ranges of metal concentrations for soils as shown in Table 5-1. Phosphorus concentrations in the unamended soils were low, suggesting that P may be a limiting element for precipitation of poorly soluble metal P minerals in the soils. The average pH value for amended soil samples was 3.6 ± 0.4 (standard deviation) at the 0-5 cm depth. The pH for unamended soil samples was 4.9 ± 0.7 at the 0 to 5-cm depth. The P treatment decreased the average pH of the soils by 1.3 units, and the lime added to the soils was not sufficient to neutralize the pH.

Soil pH can have a significant affect on metal mobility and bioavailability. Generally, the highest concentrations of available metals are found in soils with low pH (Iskandar and Kirkham 2001). However, Ruby et al. (1996) observed that acidic pH decreased Pb bioavailability due to formation of the Pb minerals anglesite and Pb jarosite, which are stable in acidic soils. These phases should be stable in the simulated gastrointestinal conditions as well (Ruby, Schoof et al. 1999). Chen et al. (1997) investigated pH effects on metal removal by apatite. They found that effects of pH on aqueous Pb sorption by the apatite were not significant, but formation of solid reaction products (pyromorphite) were pH dependent. There were no correlations between metal (Pb, Zn, Cd, and Mn) bioaccessibility and pH in either unamended or P-amended soils, or between total elemental concentrations in the soils and soil pH. The lack of any correlation within treated and untreated soils indicates that a pH decrease of ~1 unit did not affect metal bioaccessibility or total soil concentrations. Small seasonal changes in pH values also did not affect metal bioaccessibility. The small range of soil pH and the fact that effects of pH change may have been superceded by reactions with the phosphate are possible reasons for the lack of correlations between pH and heavy metal bioaccessibility in the soils.

Redox state of soils collected in August and October 2003 was oxic. Redox conditions of soils collected in May 2003 ranged from suboxic to oxic conditions as shown in Appendix A, the University of Idaho's final deliverable for this project (Strawn, 2006). The pH and Eh conditions shown in Figure 5-1 were favorable for dissolution of Pb sulfides and carbonates, as well as desorption of Pb from mineral surfaces, making it available for pyromorphite formation in the P-amended soils.

Pb concentrations in the W-PBET gizzard and total Pb concentration in the unamended and amended soils were not correlated. However, in vivo studies on waterfowl have shown high correlation between Pb in the blood and Pb in the soils (Wixson and Davies 1993; Beyer, Conner et al. 1994).The lack of correlation between total and bioaccessible Pb in this study, and the variable Pb bioaccessibility between the two sites suggests that Pb speciation, not total Pb concentration in the soils, controls Pb bioaccessibility. Other items that might influence bioaccessibility were not part of this study.

Metal bioaccessibility of the control and P-amended soils collected at different times are shown in Figure 5-2. Iron and As extractability in the simulated gizzard from freeze-dried soils collected at different times were below the detection limit (approximately 0.01 mg/L) and are thus not reported. Lead, Cd, and Zn bioaccessibility decreased in the P-amended soils. Other investigations have observed a reduction in Pb, Cd, and Zn aqueous concentrations and bioavailability in P-amended soils (e.g., Maenpaa et al. 2002). Different binding mechanisms of Pb, Cd, and Zn to P or other minerals control their solubility in the

simulated gastrointestinal tract. Previous studies determined that the disappearance of Zn and Cd from aqueous solutions with apatite addition was due to sorption reactions rather than precipitation reactions, and that the speciation of the Zn and Cd was distinct from Pb. This hypothesis is a possible explanation for the greater decrease in Pb bioaccessibility compared to Cd and Zn bioaccessibility in the P-amended soils.

Phosphorus-amendments increased Mn bioaccessibility. This increase could be due to Mn phosphate minerals ($MnHPO_4$, $Mn_3(PO_4)_2$) formed in the P-amended soils that have increased solubility in the acidic conditions of the simulated gizzard compared to the Mn oxides, causing higher Mn bioaccessibility (Lindsay 1979). In 2000, Hettiarachchi et al. reported the effects of P and Mn oxide on bioavailable Pb in five contaminated soils. That study concluded that Mn oxides are strong sorbents of both Pb and P, and that both soil characteristics and Mn and P speciation affect Mn solubility in the gizzard and Mn redox state. Surface precipitation of comparatively insoluble Pb phosphate on Mn minerals (encapsulation) restricts dissolution of Mn oxides because Pb phosphate is more stable in a reduced acidic environment. The increased solubility from P amendment in this study does not support that hypothesis. Seaman et al. (2001) observed a decrease in Mn solubility in contaminated soils when hydroxyapatite was added. However, similar to our soils, there was an increase in Mn bioaccessibility in P-amended soils, suggesting that P amendments do not restrict Mn solubility in the acidic gizzard.

Statistical analyses indicated that the Pb, Zn, and Mn bioaccessibility was not significantly different at the three sampling times ($p > 0.05$), but there was a significant difference between P-amended and unamended sites as shown in Figure 5-2. This suggests that seasonal influences on Pb, Zn, and Mn bioavailability in these soils are minimal. However, the redox state of samples collected in May was not low enough to represent reducing conditions, and only the Bull Run unamended plot showed suboxic conditions. The 2003 spring runoff was below average, minimizing soil saturation duration, therefore limiting the onset of reducing conditions. Additionally, although the soils were purged with N_2 and preserved in cold temperatures, redox state may not have been completely preserved.

Another explanation for the lack of seasonal difference in heavy metal bioaccessibility is that reductive mineral dissolution and subsequent heavy metal release may be followed by precipitation with P, carbonates, or sulfides. This process would be highly likely in the P-amended soils where phosphate is present in excess. Silviera and Sommers (1977) found that diethylene triamine pentaacetic acid (DTPA) extractable Pb, which simulates plant available Pb, remained constant with time in a water-saturated soil-sludge system during 28 days of incubation. Bostick et al. reported in 2001 that Zn speciation in contaminated seasonal wetlands near the Coeur d'Alene River in northern Idaho is dictated by water depth and redox potential. The data show that Zn is associated with the hydroxide phases in dry, oxidized soils, and with sulfides and carbonates in flooded systems. This indicates that Zn sorption is a dynamic process influenced by environmental changes. As indicated above, the conditions on wetland sites this sampling season were not reducing, and therefore may not have created enough phase transformation for significant temporal changes in Zn, Mn, or Pb bioaccessibility.

Cadmium bioaccessibility was significantly lower in the P-amended plots compared to the unamended plots, as shown in Figure 5-2. There was no seasonal Cd bioaccessibility variability within the two P-treated sites, and the trends in Cd bioaccessibility were similar between the two sites. However, the unamended plot from Black Rock Slough had significantly lower Cd bioaccessibility in August than in May and October. Additionally, using data from both sites in ANOVA suggested that the August

sampling event had significantly lower Cd bioaccessibility than October or May samples. The decrease in Cd bioaccessibility in August indicates that the least bioavailable Cd phases are formed in summer in the unamended soils. The redox state of the soils did not change significantly between the three sampling periods. Thus, factors other than redox state are responsible for lower Cd bioaccessibility in August, such as biological activity, temperature, or other undetermined fluxes.

Bioaccessibility was positively correlated for Cd and Pb ($R_{Pearson}$=0.67, $p < 0.01$), and Cd and Zn ($R_{Pearson}$=0.73, $p < 0.01$) in the P-amended and unamended soils. Cd is more bioaccessible in the plots compared to Pb bioaccessibility as shown in Figure 5-2. Pb solubility is controlled by poorly soluble mineral phases that include phosphate, sulfate, carbonate, and chloride anions. Cadmium forms fewer poorly soluble complexes in soils, and is more mobile than the other metals.

These results did not show a temporal effect on metal bioaccessibility. One possible reason for this lack of change in bioaccessibility is that the soils were not sufficiently reduced. Another limitation is that purging soils with N_2, storing them frozen, and freeze-drying the soil samples may not have fully preserved the redox state. Previous studies have demonstrated oxygenation and drying of the soils can affect contaminant chemistry (e.g., Bostick et al. 2001).

5.5 Conclusions

Findings from this study showed that there were no seasonal effects on Pb, Mn, and Zn bioaccessibility in the test plot soils. Only Cd showed lower bioaccessibility in August compared to May and October. The lack of any seasonal differences can be explained by the minimal seasonal change observed in soil redox potential. Pb, Cd and Zn bioaccessibility values significantly decreased in the P-amended soils compared to the unamended soils. Bioaccessibility reduction was the highest for Pb, possibly through formation of sparingly soluble Pb PO_4^-, such as pyromorphite-like minerals. Cd and Zn either precipitated or formed surface complexes with P minerals. Mn bioaccessibility increased in the P-amended soils. This indicates that Pb phosphate, formed in P-amended soils, did not restrict Mn solubility in acid solution of the simulated gizzard. There were significant differences between the two sites' Pb, Mn. and Zn bioaccessibility values. This observation can be explained by site-specific differences in metal speciation, flooding time, water depth, microbial activity, and vegetation.

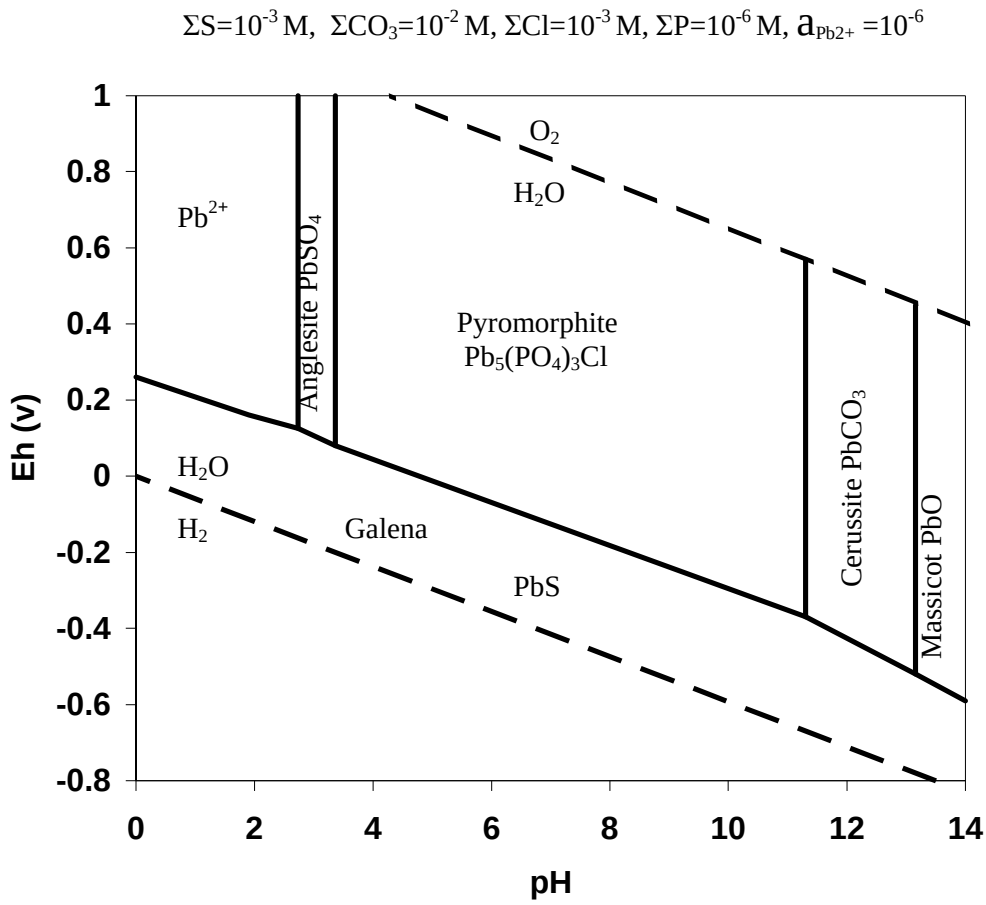

Figure 5-1. Hypothesized Eh-pH stability diagram for Pb at the test plots. Assumed aqueous concentrations are listed at top.

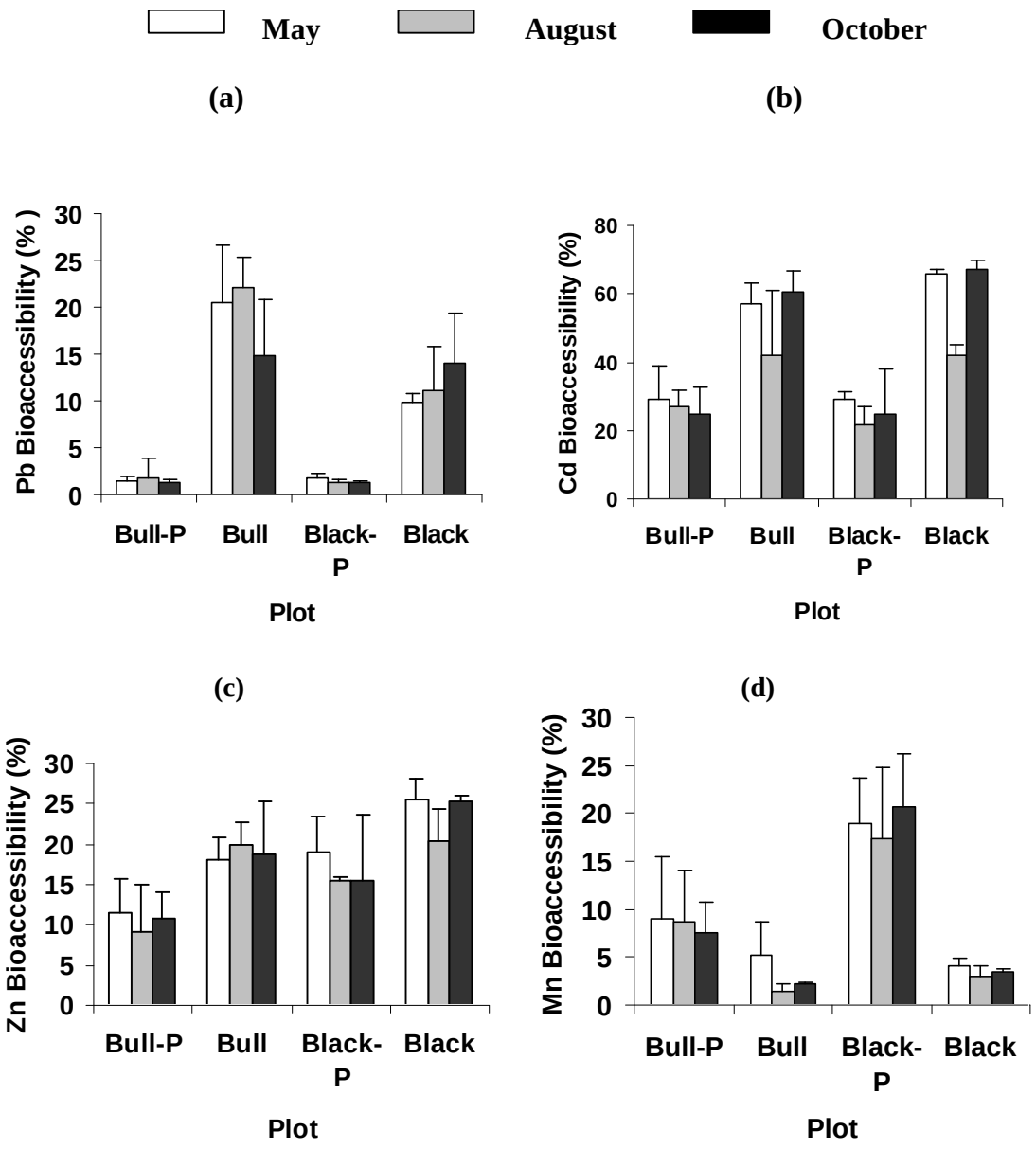

Figure 5-2. W-PBET bioaccessibility of Pb (a), Cd (b), Zn (c) and Mn(d) in the soils collected from Bull Run Lake and Black Rock Slough soils at different times. Plots Bull-P and Black-P are P-amended; Plots Bull and Black are unamended. Error bars represent one standard deviation from discrete samples within a plot (N = 3).

Table 5-1. Metal Concentrations (Means and Ranges) in the Lower Coeur d'Alene Basin Study Area

	Pb	Cd	Zn	Ca	Mn	Fe	P	As	S
Common ranges for soils* (mg/kg)	10 (2-200)	0.06 (0.01-0.7)	50 (10-300)	13,700 (7,000-500,000)	600 (20-3,000)	38,000 (7,000-550,000)	600 (200-5,000)	5 (1-50)	700 (30-10,000)
Unamended (mg/kg)	6,035 (4,100-12,000)	16 (5-29)	2041 (570-3,800)	1,405 (448-2,100)	5,731 (2,000-9,700)	73,557 (29,000-100,339)	849 (380-1,500)	87 (19-143)	1,532 (392-3,200)
P-amended (mg/kg)	4,958 (3,200-6,800)	25 (12-51)	1793 (580-5,000)	1,326 (671-1,900)	4,053 (500-9,900)	64,084 (31,000-103,301)	21,062 (14,000-30,000)	67 (15-126)	1,309 (297-2,800)

* Data from Lindsay 1979

6. Geochemical Modeling

6.1 Introduction

Soils in the Coeur d'Alene River Basin are located in seasonal wetlands. The cycling of flooding and drying makes the biogeochemical processes occurring in these soils dynamic. The soils in these wetlands contain high concentrations of the Pb, Fe, Mn, Zn, Cd, and As. Because speciation controls availability for transport and biouptake in the environment, a clear understanding of how seasonal cycling impacts speciation is required. Geochemical modeling is one approach that can be used to make predictions of speciation and aqueous concentrations.

The objective of the geochemical modeling is to use aqueous concentrations and mineralogy of elements and species of interest for the Coeur d'Alene Basin to model the system so that prediction of Pb solubility can be determined. Results from the following tasks will be presented:

- Predict speciation of Pb and Fe in soils.
- Predict speciation of Pb and Fe in P-amended soils.
- Develop redox diagrams for Pb and Fe species using input parameters relevant to Coeur d'Alene system.
- Evaluate Cd and Zn geochemical reactions relevant to Coeur d'Alene soils.

6.2 Methods

The general approach for geochemical modeling assumes that the system is at equilibrium and that the solid phase controlling speciation is the species that has the lowest solubility, unless information is known regarding formation of other solid phases. In dynamic systems such as seasonal wetlands, the assumption of equilibrium may not be accurate, particularly for solid phases and redox reactions. However, modeling the equilibrium phases in systems is still valuable because it allows for prediction of the lowest energy state of the system with respect to characterized pure mineral species; such results serve as a basis to better understand the processes that control aqueous concentrations. For aqueous reactions the assumption of equilibrium is likely accurate because reactions are generally rapid.

Modeling geochemical reactions uses a systematic approach. Summarized below is the approach as applied to the soils in the Lower Coeur d'Alene River Basin.

- *System* – Soils in the Lower Coeur d'Alene River Basin.
- *Phases* – Solid, liquid, gas.
- *Inputs* – Solid phases, aqueous concentration of ions, redox potential, total inorganic carbon (C), temperature. The inputs are listed in Table 6-1. Data were taken from several sources to create a typical pore water composition for the geochemical modeling.
- *Species* – Species are defined by the inputs; the geochemical program uses a database to search all forms of the input species. The database is based on the MINTEQ database developed by the EPA.
- *Reactions* – Reactions define species transformations and are used together with equilibrium constants to model the system. Reactions and equilibrium constants for all species presented in graphs in this report are listed in Tables 6-2 and 6-3.
- *Output* – Output is determined by the modeler. Output was generated as aqueous speciation, saturation index, and stability diagrams for solid phases. Output is defined by dependent and independent variables; dependent variables are controlled by inputs. For this system, independent variables were pH, temperature, redox potential, and P concentration.

The above are easily managed by a computer program. Modeling in this report was done using the U.S. Geological Survey program PHREEQCi, Version 2. PHREEQCi is an iterative model that mathematically distributes aqueous constituent data, [i.e., pH, electron potential (pe) plus major and element of interest ion concentrations], among thermodynamic mass action expressions. Geochemist's Workbench was used to develop stability diagrams. MINEQL+ was used to develop solubility diagrams.

6.3 Results of Geochemical Modeling for Pb and Fe in Soils

Data from Table 6-1 was input into the program PHREEQCi to predict aqueous speciation and solubility of Pb as a function of pH and redox potential. Figure 6-1 shows the aqueous concentration as a function of pH at 14.3 °C in oxic soils. The predominant species below pH 6.5 is Pb^{2+}; if pH increases past 6.5, Pb carbonate aqueous will become the dominant species in solution. Total Pb concentration was controlled by input and no solids were allowed to precipitate. Modeling did not include complexation with dissolved organic acids, which can be significant.

Saturation indices for the system as a function of pH and redox potential are reported in Figures 6-2 through 6-4. A saturation index above zero indicates that the mineral is oversaturated with respect to the system conditions. In this system control precipitation was not allowed, thus each mineral species can be evaluated based on aqueous species and concentrations independent of each other. This is an advantage as kinetic controls on mineral formation are not known, and often the least soluble mineral will not be the mineral controlling the aqueous concentration. Under oxidizing conditions, plumbogummite and chloropyromorphite are saturated in the system, while hydroxypyromorphite is not as shown in Figure 6-2. As the system becomes reducing, aqueous Pb^{2+} species concentration decreases due to the formation of Pb-sulfide complexes. This causes the saturation index for plumbogummite and hydroxypyromorphite to be less than zero below pH 6 in the most reducing conditions, while galena is saturated in this pH range. The saturation index (SI) is defined as the logarithm of the ion activity product divided by the reaction equilibrium constant. Negative values indicate undersaturation with respect to a particular solid phase, positive values indicate oversaturation, and a value of zero indicates equilibrium. Analysis of the Pb in the soil pore waters suggests that under most conditions the soil pore water is saturated with respect to lead phosphate minerals. When the soils become reduced, the soil pore water becomes under saturated with respect to lead phosphate; however, and total dissolved Pb will be controlled by Pb-sulfides. Expected aqueous concentrations controlled by the Pb phosphate minerals are shown in Figure 6-5. The systems shown on the graph are defined as follows.

- HPM – aqueous Pb and phosphate concentration controlled by hydroxypyromorphite.
- CPM – aqueous Pb, chlorine (Cl) and phosphate concentration controlled by chloropyromorphite.
- CPM (strengite, ferrihydrite) – aqueous Pb and Cl concentration controlled by chloropyromorphite, and phosphate concentration controlled by solubility of strengite and soil ferrihydrite
- CPM (field) – aqueous Pb concentration controlled by chloropyromorphite.
- Cl^- and phosphate $^-$ concentrations are given in Table 6-1 and based on typical field concentrations.
- PGM (strengite, gibbsite, ferrihydrite) – aqueous Pb concentration controlled by plumbogummite, and phosphate concentration controlled by solubility of strengite and soil ferrihydrite, and aluminum (Al) concentration controlled by gibbsite.

- In all systems solid phases were set as fixed, temperature = 25 °C.

Monitoring of the pore water indicated that the aqueous Pb concentrations in the P-amended and untreated plots at the two sites ranged from below detection limits (0.002 mg/L) to 0.04 mg/L. The complete data set for the soil pore waters collected from the experimental plots is presented in Figure 6-5. Soil solutions appear to fall within the expected range for solutions in equilibrium with poorly soluble Pb phosphate minerals. Therefore, it is expected that the dissolved Pb concentration in the soils will be relatively low because the concentration is controlled by minerals that have relatively low solubility. The effects of adding phosphate are further discussed below.

The soil water temperatures ranged from 5 to 22 °C. Temperature can increase or decrease mineral solubility, and thus impacts aqueous concentrations of metals. Chloropyromorphite solubility as a function of temperature is shown in Figure 6-6. For every 1 °C change in solubility there is an absolute 0.02 change in log Pb_T concentration. Chloropyromorphite has a retrograde solubility indicating that at the lowest soil water temperatures solubility is increased. The geochemical modeling analysis presented in this study was done at 14.3 °C; deviations due to temperature fluctuations are expected to be minimal.

Iron minerals are important solid phases in the Coeur d'Alene soils because they provide reactive surfaces for the adsorption of Pb and other contaminants. Below pH 6, the oxidized system is only slightly saturated with respect to hematite and magnetite as shown in Figure 6-7. However, the kinetics in the soils are not favorable for the formation of these minerals. Analysis by selective extraction and differential XRD suggests that goethite and ferrihydrite are the dominant Fe minerals in the system. The fact that the soil waters are unsaturated with respect to these minerals suggests that the soil minerals have variable solubility and/or the conditions used for the model are not at equilibrium; most likely both scenarios are true.

The Fe oxides in the soil are dominated by ferrihydrite. Ferrihydrite is a poorly crystalline metastable mineral. Given time it will convert to crystalline goethite or hematite minerals. However, because the soils in this study are dynamic with respect to fluxes of ions and redox conditions, equilibrium is not expected, and thus ferrihydrite minerals can persist. The lack of saturation in the soil pore-water system is consistent with this condition.

Under reducing conditions, the soil pore waters are saturated with respect to pyrite below pH 6 as shown in Figure 6-8 and Figure 6-9. However, the transitory nature of redox in these systems may inhibit the formation of slowly precipitating Fe sulfide minerals, and instead favor formation of poorly crystalline Fe sulfide phases, such as mackinawite. It is suspected, that the addition of P to soils will promote the formation of strengite in oxidizing conditions and vivianite under reducing. This is illustrated in the stability diagram (Figure 6-10).

Figure 6-11 shows the effect of phosphate concentration on mineral stability for two aqueous Pb activities. At pH values below 6 and hydrogen phosphate (HPO_4^{2-}) activities above 10^{-7} chloropyromorphite is the stable mineral phase. The log pKa_2 for phosphate is 6.79, thus HPO_4^{2-} concentrations are much lower than the dihydrogen phosphate ($H_2PO_4^-$) concentrations. The different phosphate speciation will affect the magnitude of the Y-axis variables in Figure 6-11, but not the relative stability field relationships. From Figure 6-11 it is apparent that with a pH below 6, phosphate concentrations promotes the formation of chloropyromorphite. A more quantitative analysis is presented in Figure 6-12. The red box represents the minimum and maximum field of aqueous Pb and phosphate concentrations observed in the soil water sampling study at pH = 5.5 by Terra Graphics Environmental Engineering Inc. 2003a. The arrow on the

bottom of the figure indicates that increasing phosphate in the soil solution will cause the soil to become increasingly saturated with respect to poorly soluble Pb phosphate minerals. Based on the model, the lower left hand region is undersaturated with respect to Pb phosphate minerals, suggesting that adding P will increase stability of Pb in the soils. However, this model assumes that dissolved phosphate is controlled by Ca phosphate minerals. If Ca is limiting, or Fe concentrations are high (i.e., low pH), then adsorption to Fe oxides or dissolution/precipitation of Fe phosphate minerals will control aqueous P concentrations. Figure 6-13 shows a full soil stability diagram for lead phosphate minerals. The box represents observed aqueous concentrations of Pb and pH observed in the field plots. This diagram shows similar trends as Figure 6-12 with respect to Pb speciation and mineral stability. For the solubility lines to be lowered, the available phosphate and Cl^- must be increased. In a soil with excess concentrations of Fe-oxide, this will take large quantities of phosphate amendment, which may pose additional unwanted impacts (e.g., decreased soil pH, excessive soil aggregation and cementation, and increased risk of nutrient loading into the surface waters).

A general redox stability diagram for Pb minerals is shown in Figure 6-14. This diagram shows the stability fields for Pb minerals as a function of pH and Eh. Based on the redox potentials observed in the field trials, chloropyromorphite is the most stable mineral. However, in soils that have longer saturation times, redox potentials have been observed that are suboxic and anoxic; these redox potentials would favor the formation of galena in the soils. Galena is a poorly soluble Pb-sulfide mineral. A redox stability diagram specific to the soil pore water system described in Table 6-1 is shown in Figure 6-15. This diagram indicates there are three Pb minerals present in pH range of 3.5 to 6; galena, chloropyromorphite, and plumbogummite depending on the redox conditions. Transformation from galena to either plumbogummite or chloropyromorphite is a function of redox potential, while transformation between the two $PbPO_4^-$ minerals is pH dependent. All three minerals have low solubility.

6.4 Evaluation Cd and Zn Solubility

Saturation indices for Cd and Zn minerals in the systems are shown in Table 6-1 and Table 6-2 and Figure 6-16 and Figure 6-17, respectively. Zinc silicates and phosphates are the only minerals saturated in the models. Under reducing conditions, sphalerite becomes saturated. Bostick et al. (2001) investigated speciation of Zn in Coeur d'Alene wetland soils and confirmed that under reducing conditions sphalerite was present, as well as carbonate minerals. All Cd minerals tested were unsaturated under oxidizing conditions; however, under reducing conditions the Cd-sulfide mineral greenockite is saturated. From this it is concluded that dissolved Cd and Zn under oxidizing conditions are prevalent in the soil plots for most of the year and are primarily controlled by adsorption reactions on mineral surfaces. However, under reducing conditions Cd and Zn solubility is dramatically reduced by precipitation of sulfide phases.

6.5 Summary

This modeling has provided results that predict speciation in soil pore water from the soils studied in this project. Additionally, an analysis of the effect of P and redox on Pb solubility was conducted. The modeling suggests that in the soils, the aqueous speciation is dominated by Pb^{2+} ions. However, aqueous organic acids were not included in the model, which would have a significant impact on partitioning in the aqueous phase. The models predicted that under all field conditions Pb solubility is controlled by the minerals plumbogummite, chloropyromorphite, or galena. Because these minerals have low solubility, aqueous Pb concentrations will be maintained at low levels, regardless of redox potential. However, Fe minerals are dissolving in the soils, and may provide a new flux of Pb to the soil water that can be transported out of the

soil into surface and ground waters before equilibrium with the Pb-solid phases is possible.

Another important factor for modeling Pb availability is the quantification of interactions of mineral surfaces with aqueous species. Sorption of aqueous anions and cations often control dissolved concentrations. For example, adsorption of P on mineral surfaces may limit its availability for reaction with Pb to form poorly soluble minerals. This example is particularly relevant in the soils studied as they have high Fe contents and a low pH, which are favorable conditions for anion adsorption.

Additionally, although the aqueous phase is predicted to be controlled by a poorly soluble phase, equilibrium is rare in soils, particularly wetland soils, where fluxes are dramatic. It is recommended that additional research be done to characterize kinetics, adsorption, and interaction of metals with organic acids to allow for a more thorough analysis of the solubility and speciation of Pb and other contaminant minerals. Improved understanding of biogeochemical reactions will allow for development of more accurate models for predicting availability for transport and bio-uptake.

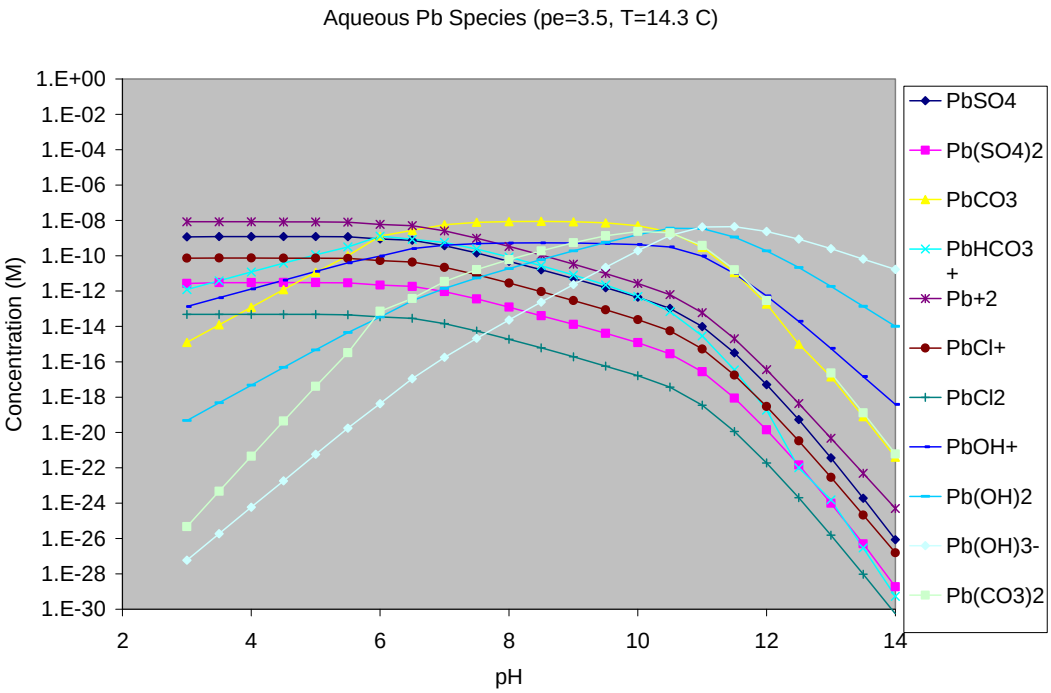

Figure 6-1. Aqueous Pb speciation as a function of pH. Input data are listed in Table 6.1. No solids were allowed to precipitate.

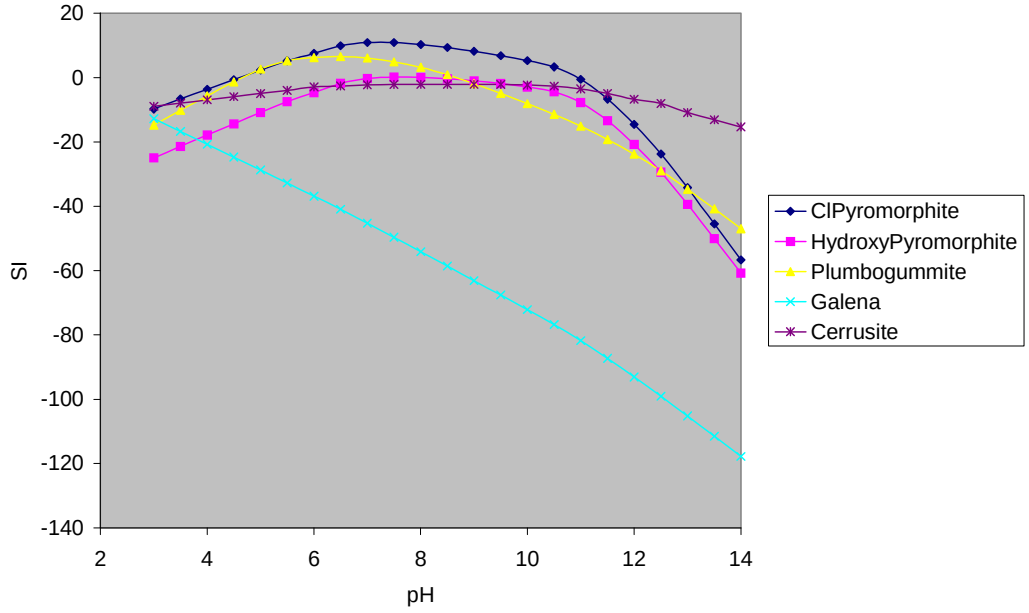

Figure 6-2. Saturation index for Pb minerals as a function of pH. System parameters are defined in Tables 6-1 and 6-2 (pe = 3.5).

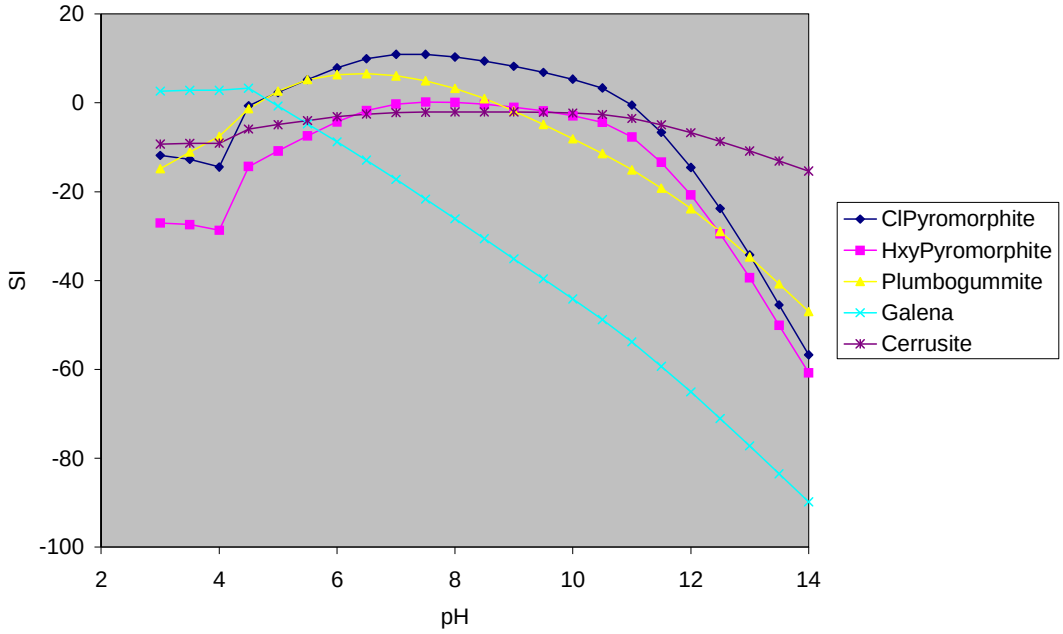

Figure 6-3. Saturation index for Pb minerals as a function of pH. System parameters are defined in Tables 6-1 and 6-2 (pe = 0).

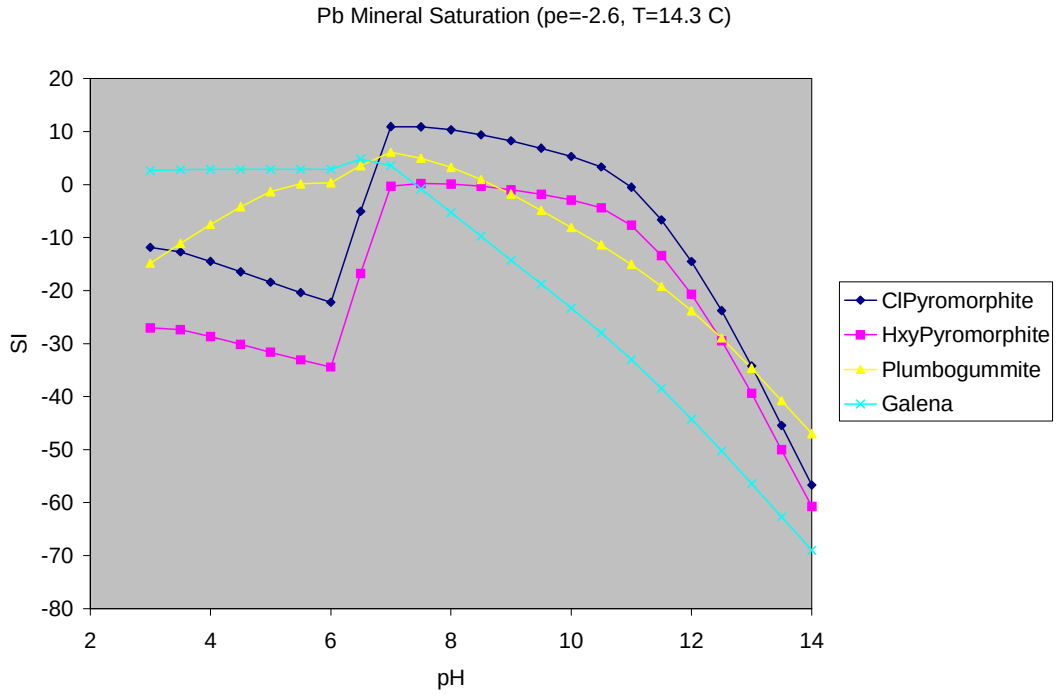

Figure 6-4. Saturation index for Pb minerals as a function of pH. System parameters are defined in Tables 6-1 and 6-2 (pe = -2.6).

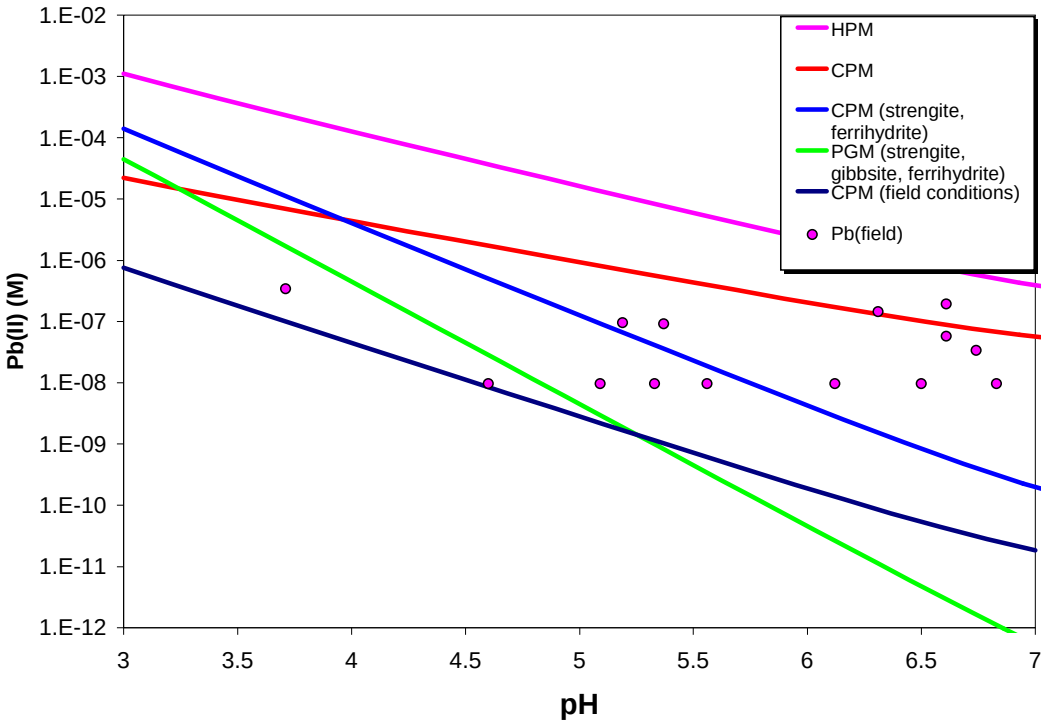

Figure 6-5. Aqueous Pb concentrations as a function of pH controlled by several Pb-phosphate minerals and observed Pb concentrations in P-amended and non-amended field sites.

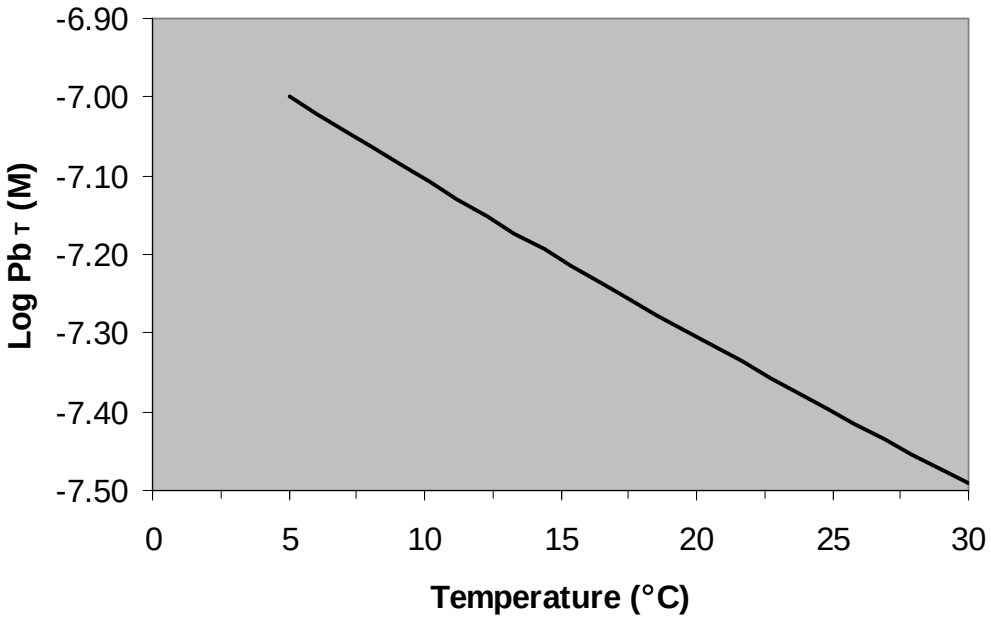

Figure 6-6. Total dissolved Pb concentrations as a function of temperature controlled by chloropyromorphite dissolution.

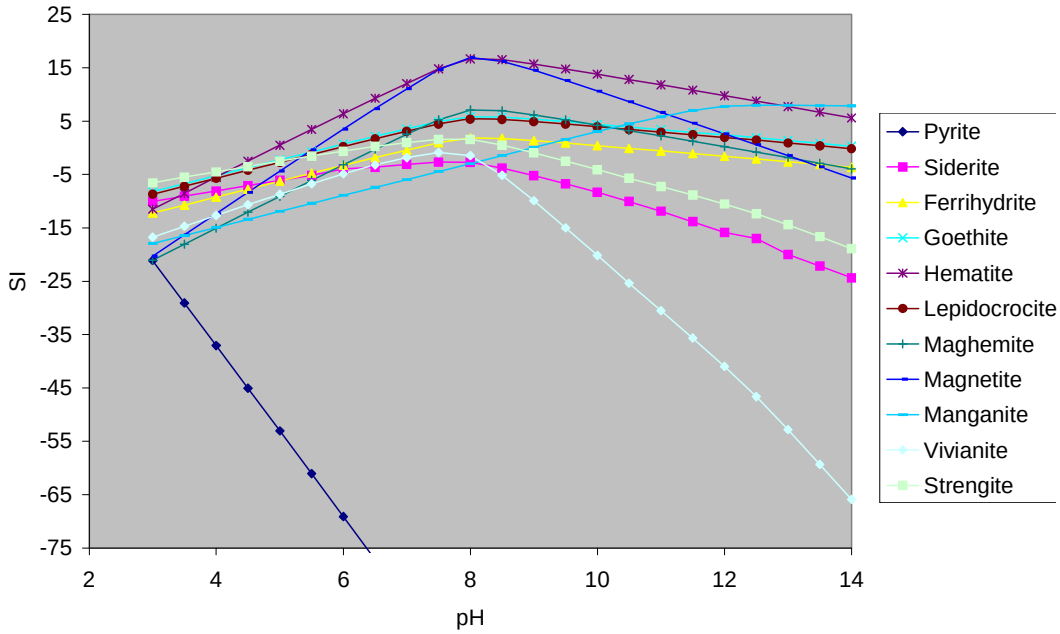

Figure 6-7. Saturation index for Fe minerals as a function of pH. System parameters are defined in Table 6-1 and Table 6-2 (pe = 3.5).

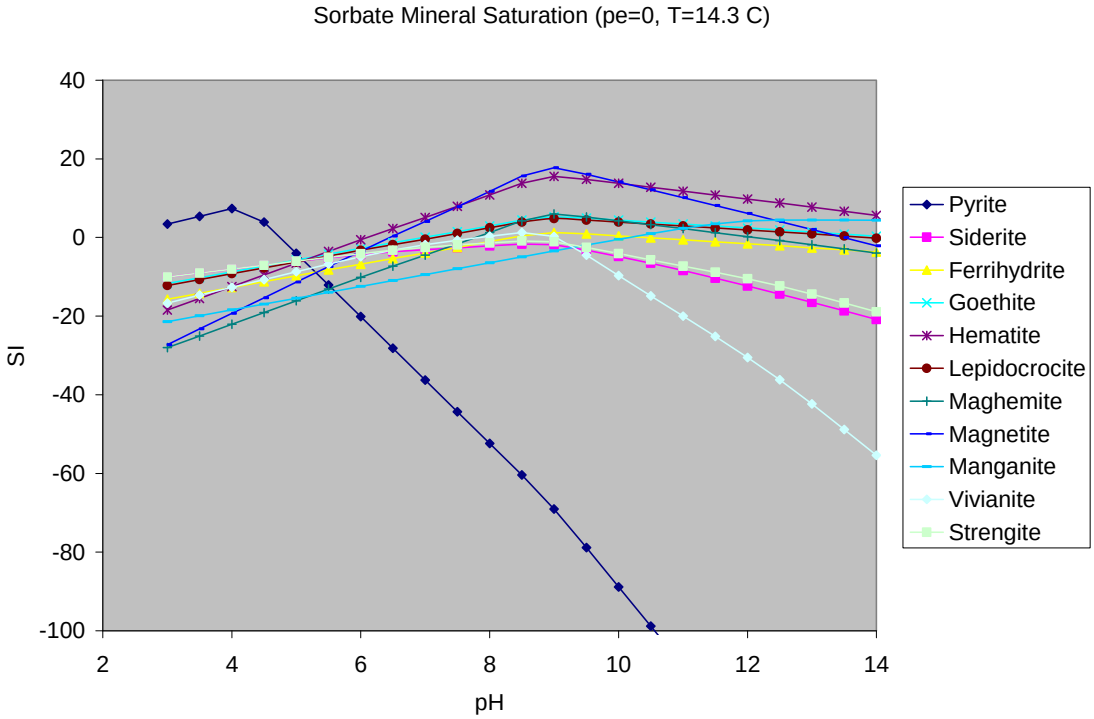

Figure 6-8. Saturation index for Fe minerals as a function of pH. System parameters are defined in Table 6-1 and Table 6-2 (pe = 0).

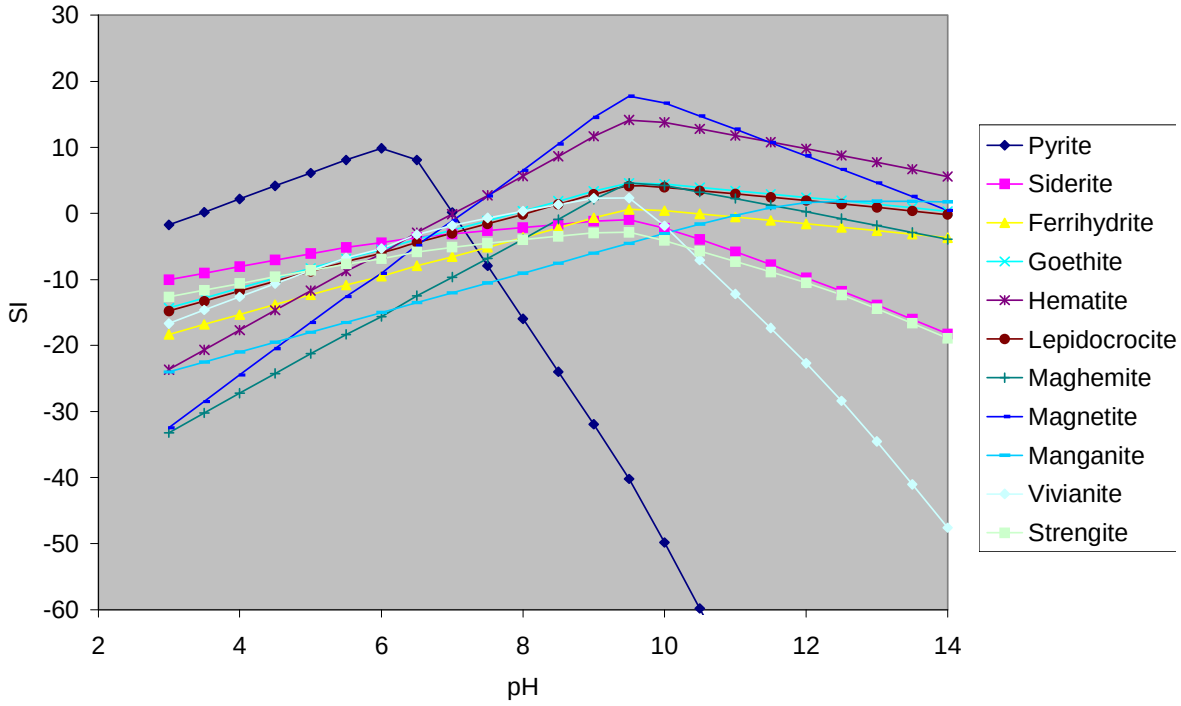

Figure 6-9. Saturation index for Fe minerals as a function of pH. System parameters are defined in Table 6-1 and Table 6-2 (pe = -2.6).

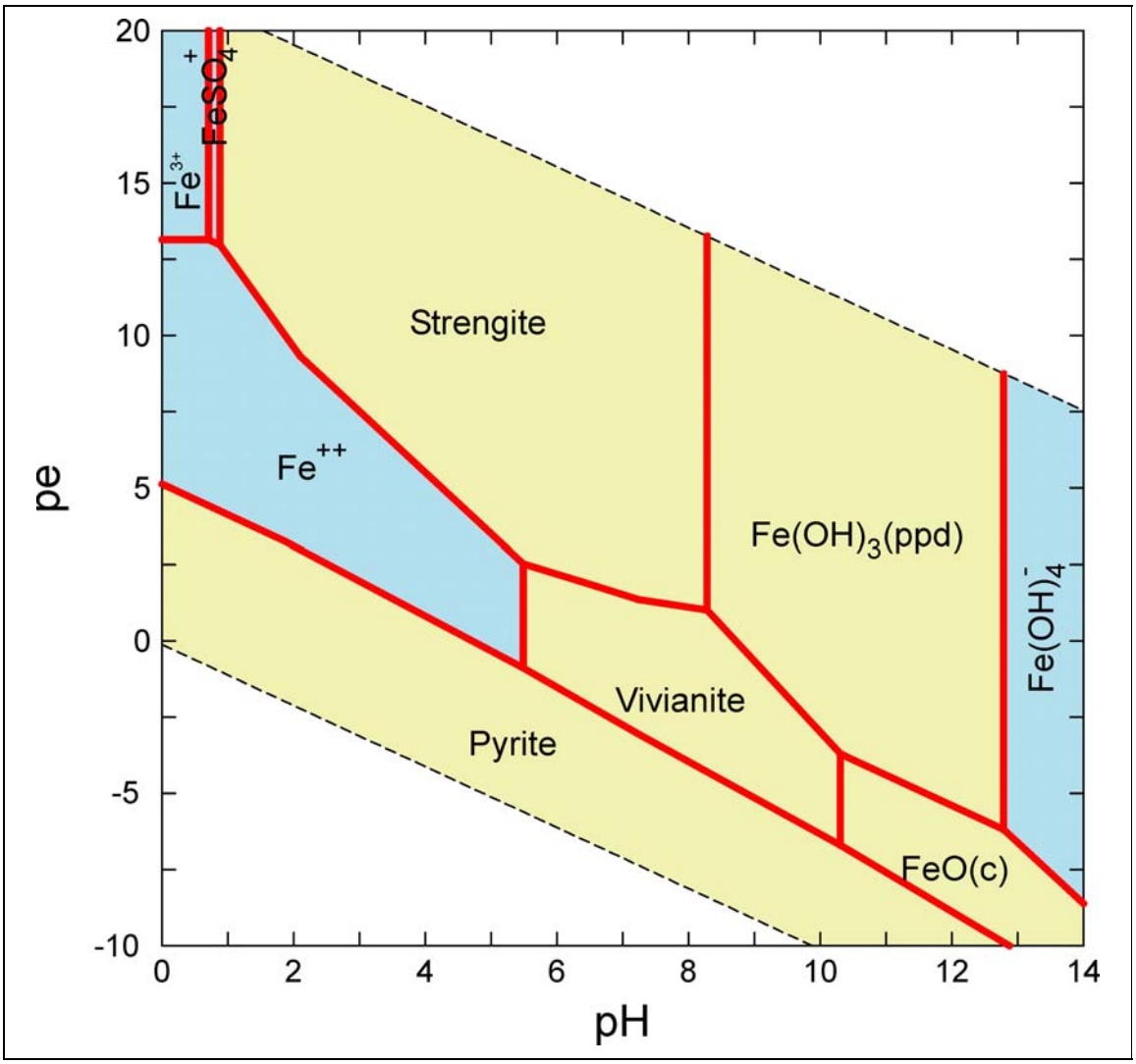

Figure 6-10. Redox stability diagram for Fe, T = 15 °C, P = 1.013 bars, $a_{Fe} = 10^{-4.301}$, $a_{Cl} = 10^{-3.405}$, $a_{HCO3-} = 10^{-2.499}$, $a_{HPO4--} = 10^{-2.824}$, $a_{SO4--} = 10^{-2.807}$; Suppressed: goethite, hematite, magnetite.

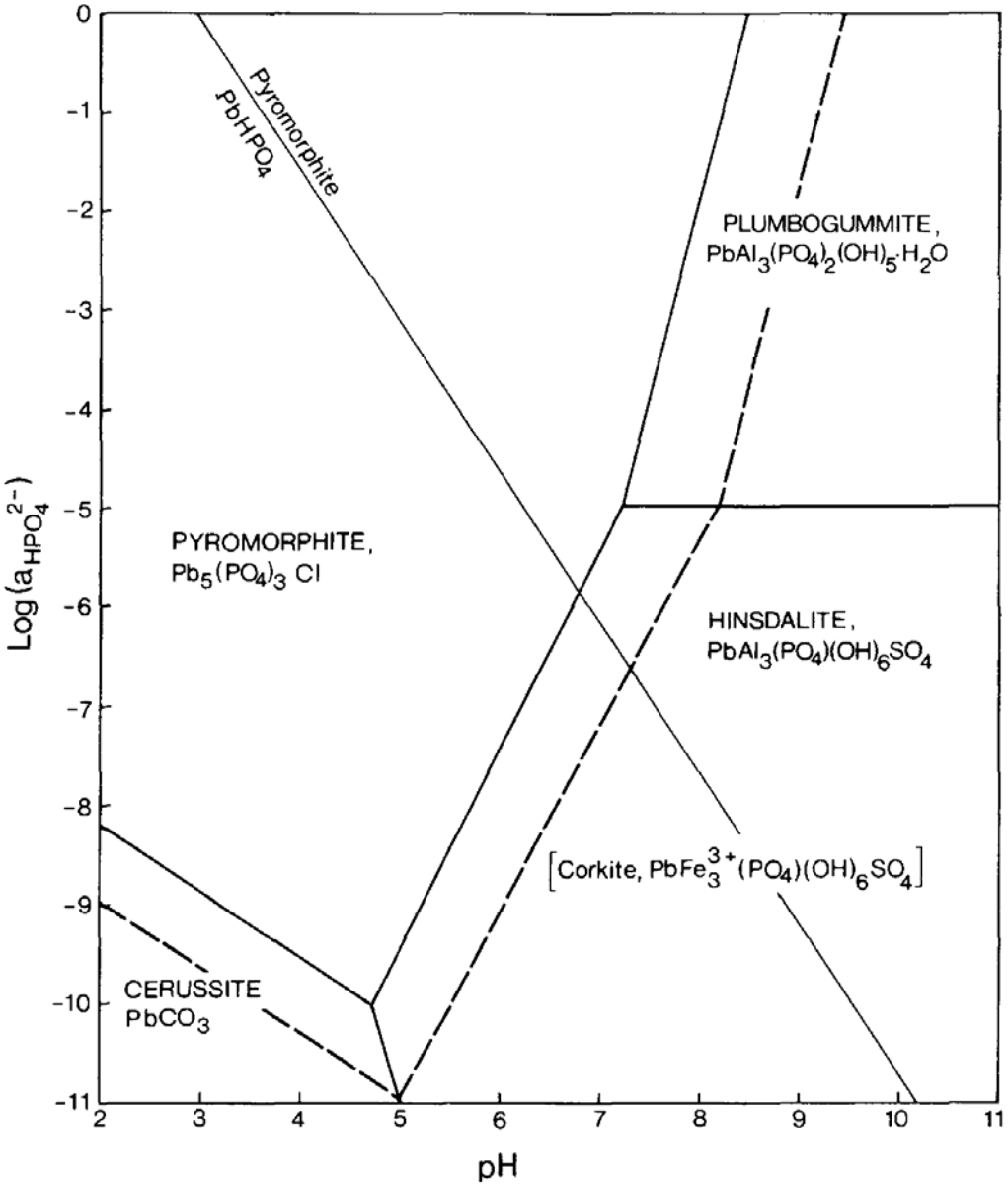

Figure 6-11. Stability diagram for Pb minerals as a function of HPO_4^{2-} concentration and pH (Nriagu, 1984). Calculated for $a_{SO42-} = a_{HCO3-} = 10^{-3}$, $a_{Al3+} = 10^{-6}$. Solid lines are for $a_{Pb2+} = 10^{-6}$; dashed lines are for $a_{Pb2+} = 10^{-5}$.

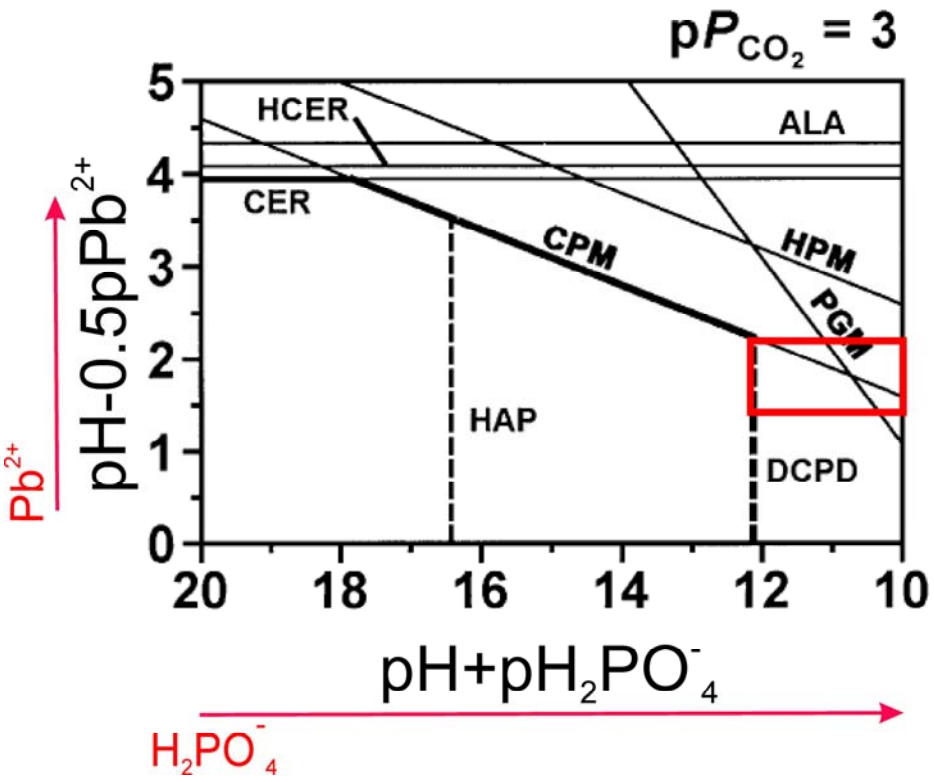

Figure 6-12. Activity ratio/product diagram showing the relative stability of Pb bearing minerals as a function of pH, H_2PO4- activity, and Pb activity. HAP is hydroxyl apatite, CPM is chloropyromorphite, HPM is hydroxypyromorphite, PGM is plumbogummite, CER is cerussite, HCER is hydrocerussite, ALA is alamosite, and DCPD is di-calcium phosphate dehydrate. Chloride is fixed at 10^{-3} *M* at pH 8, Ca is controlled by calcite mineral, and Al is controlled by gibbsite mineral. Figure is from Essington et al. (2004).

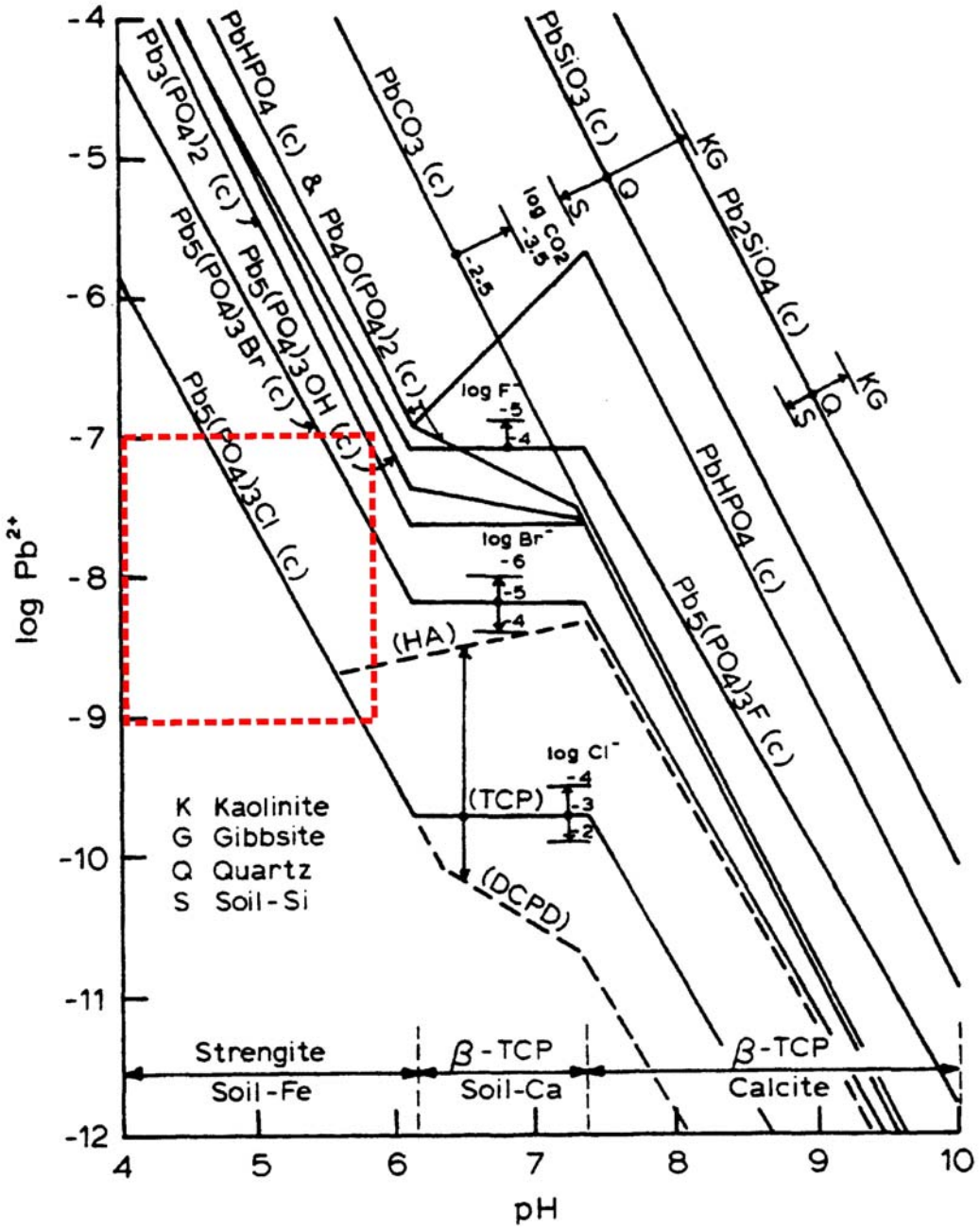

Figure 6-13. The solubility of various Pb silicates and phosphates compared to cerussite when phosphate is controlled by various solid phases, as indicated above x-axis, and CO_2(g) is 0.003 atm. From Lindsay (1979).

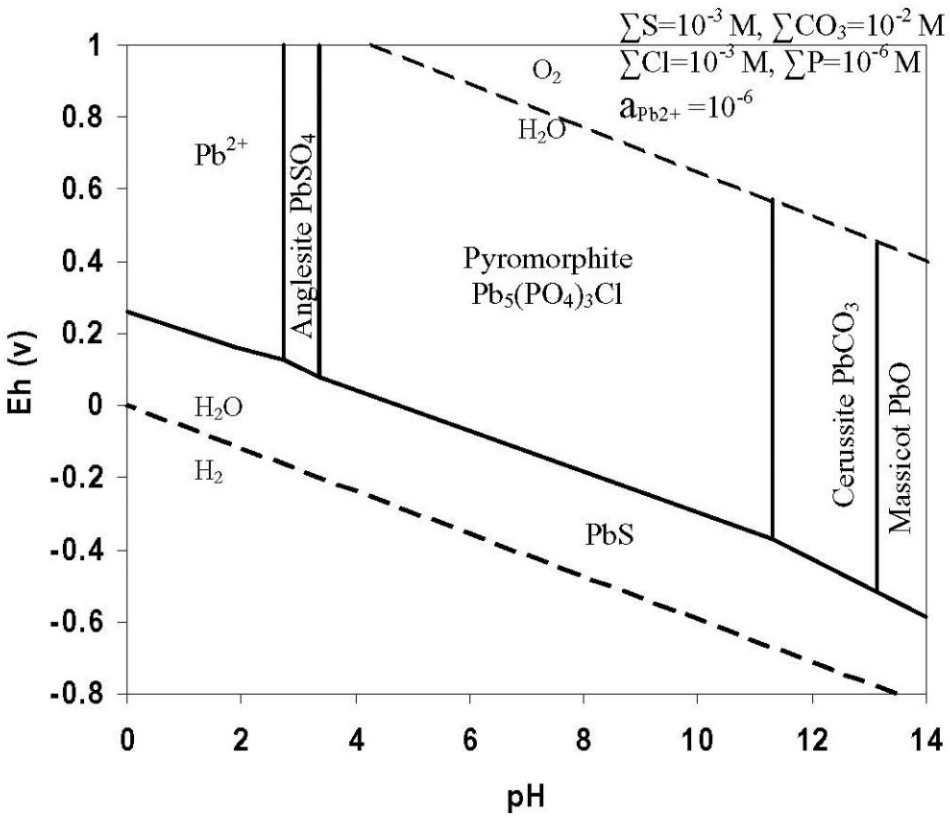

Figure 6-14. Stability diagram for Pb minerals as a function of redox potential and pH, adapted from Nriagu (1984).

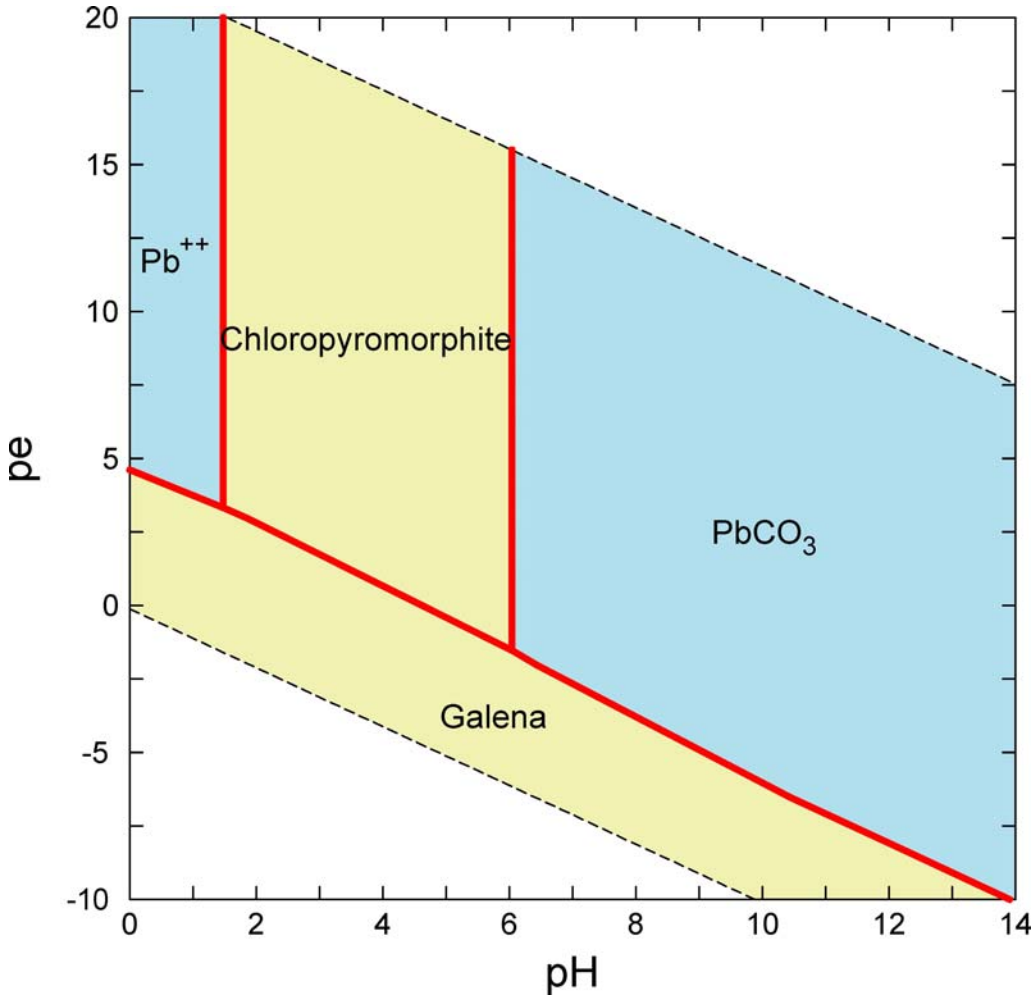

Figure 6-15. Redox stability diagram specific to soil pore water conditions given in Table 6-1.

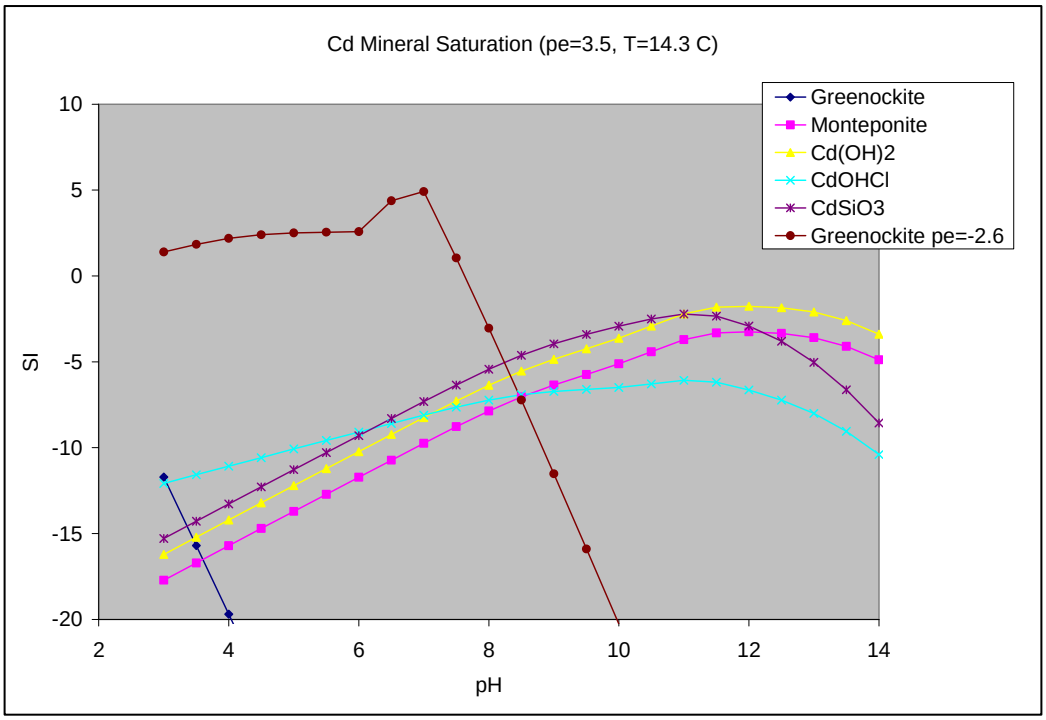

Figure 6-16. Saturation index for Cd minerals as a function of pH. System parameters are defined in Table 1 and Table 2 (pe = 3.5, except as noted).

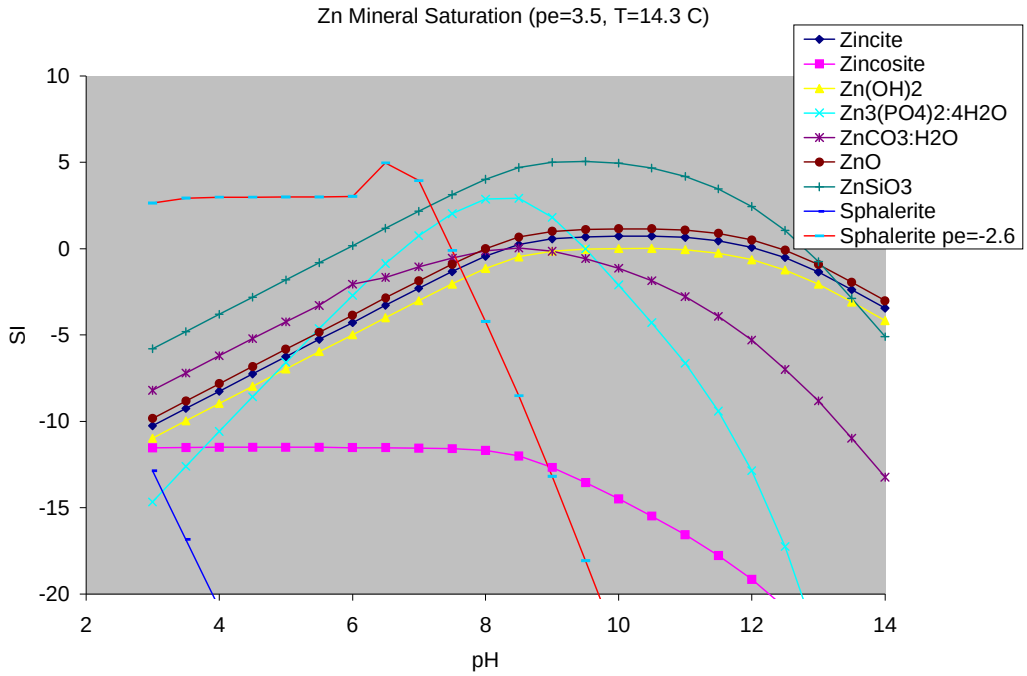

Figure 6-17. Saturation index for Zn minerals as a function of pH. System parameters are defined in Table 6-1 and Table 6-2 (pe = 3.5, except as noted).

Table 6-1. Simulated Pore Water Concentrations Used as Inputs for Aqueous Speciation and Solubility Modeling in Soils

Input	Value	Reference
Temperature	14.3 C	1
pH	5.6, varied	1
pe	varied	
Ca	0.274 millimole per liter (mmol/L)	1
Sodium	0.648 mmol/L	1
Magnesium	0.852 mmol/L	1
Mn	1.89 µmol/L	2
Fe	0.56 µmol/L	2
Copper	0.01 µmol/L	2
As	0.214 µmol/L	1
Pb	$9.65*10^{-3}$ µmol/L	1
Cd	0.018 µmol/L	1
Zn	42.2 µmol/L	1
Al	0.19 µmol/L	2
Si	140.0 µmol/L	3
Cl	389 µmol/L	1
P	1530 µmol/L	1
S	1560 µmol/L	1
C	3160 µmol/L	1

1 Terra Graphics Environmental Engineering Inc., 2003
2 Paulson, 2001
3 Balistrieri et al., 2003a, b

Table 6-2. Reactions and Equilibrium Constants for All Aqueous Species Considered (Complete Thermodynamic Database Used Was from Schecher, 1998)

Aqueous Species	Reaction	log K
$PbSO_4$	$Pb^{+2} + SO_4^{-2} = PbSO_4$	2.75
$Pb(SO4)_2^{-2}$	$Pb^{+2} + 2SO_4^{-2} = Pb(SO_4)_2^{-2}$	3.47
$PbCO_3$	$Pb^{+2} + CO_3^{-2} = PbCO_3$	7.24
$PbHCO_3^{+}$	$Pb^{+2} + CO_3^{-2} + H^{+} = PbHCO_3+$	13.2
$Pb(CO3)2^{-2}$	$Pb^{+2} + 2CO_3^{-2} = Pb(CO_3)_2^{-2}$	10.64
$PbCl^{+}$	$Pb^{+2} + Cl^{-} = PbCl^{+}$	1.6
$PbCl_2$	$Pb^{+2} + 2C^{l-} = PbCl_2$	1.8
$PbOH^{+}$	$Pb^{+2} + H_2O = PbOH^{+} + H^{+}$	-7.71
$Pb(OH)_2$	$Pb^{+2} + 2H_2O = Pb(OH)_2 + 2H^{+}$	-17.12
$Pb(OH)_3^{-}$	$Pb^{+2} + 3H_2O = Pb(OH)_3^{-} + 3H^{+}$	-28.06
$Pb(OH)_4^{-2}$	$Pb^{+2} + 4H_2O = Pb(OH)_4^{-2} + 4H^{+}$	-36.99
$Pb(HS)_2$	$Pb^{+2} + 2HS^{-} = Pb(HS)_2$	15.27
$ZnSO_4$	$Zn^{+2} + SO_4^{-2} = ZnSO_4$	2.37
$Zn(SO4)_2^{-2}$	$Zn^{+2} + 2SO_4^{-2} = Zn(SO_4)_2^{-2}$	3.28
$ZnCO_3$	$Zn^{+2} + CO_3^{-2} = ZnCO_3$	5.3
$Zn(CO3)_2^{-2}$	$Zn^{+2} + 2CO_3^{-2} = Zn(CO_3)_2^{-2}$	9.63
$ZnHCO_3^{+}$	$Zn^{+2} + CO_3^{-2} + H+ = ZnHCO_3^{+}$	12.4
$ZnCl^{+}$	$Zn^{+2} + Cl^{-} = ZnCl^{+}$	0.43
$ZnCl_2$	$Zn^{+2} + 2Cl^{-} = ZnCl_2$	0.45
$ZnOH^{+}$	$Zn^{+2} + H_2O = ZnOH^{+} + H^{+}$	-8.96
$Zn(OH)_2$	$Zn^{+2} + 2H_2O = Zn(OH)_2 + 2H^{+}$	-16.90
$Zn(OH)_3^{-}$	$Zn^{+2} + 3H2O = Zn(OH)3^{-} + 3H^{+}$	-28.20
$Zn(OH)_4^{-2}$	$Zn^{+2} + 4H_2O = Zn(OH)_4^{-2} + 4H^{+}$	-41.99
$Zn(HS)_2$	$Zn^{+2} + 2HS^{-} = Zn(HS)_2$	14.94
$CdSO_4$	$Cd^{+2} + SO_4^{-2} = CdSO_4$	2.46
$Cd(SO4)_2^{-2}$	$Cd^{+2} + 2SO_4^{-2} = Cd(SO_4)_2^{-2}$	3.5
$CdCO_3$	$Cd^{+2} + CO_3^{-2} = CdCO_3$	5.399
$CdHCO_3^{+}$	$Cd^{+2} + CO_3^{-2} + H^{+} = CdHCO_3^{+}$	12.4
$CdCl^{+}$	$Cd^{+2} + Cl^{-} = CdCl^{+}$	1.98
$CdCl_2$	$Cd^{+2} + 2Cl^{-} = CdCl_2$	2.6
$CdOH^{+}$	$Cd^{+2} + H_2O = CdOH^{+} + H^{+}$	-10.08
$Cd(OH)_2$	$Cd^{+2} + 2H_2O = Cd(OH)_2 + 2H^{+}$	-20.35
$Cd(OH)_3^{-}$	$Cd^{+2} + 3H_2O = Cd(OH)_3^{-} + 3H^{+}$	-33.3
$Cd(OH)_4^{-2}$	$Cd^{+2} + 4H_2O = Cd(OH)_4^{-2} + 4H^{+}$	-47.35
$Cd(HS)_2$	$Cd^{+2} + 2HS^{-} = Cd(HS)_2$	16.53

Table 6-3. Reactions and Equilibrium Constants for All Minerals Considered (Complete Thermodynamic Database Used Was from Schecher, 1998)

Minerals	Reaction	log K
Pyrite	$FeS_2 + 2H^+ + 2e^- = Fe^{+2} + 2HS^-$	-18.48
Siderite	$FeCO_3 = Fe^{+2} + CO_3^{-2}$	-10.55
Ferrihydrite	$Fe(OH)_3 + 3H^+ = Fe^{+3} + 3H_2O$	4.891
Goethite	$FeOOH + 3H^+ = Fe^{+3} + 2H_2O$	-14.48
Strengite	$FePO_4{:}2H_2O = Fe^{+3} + PO_4^{-3} + 2H_2O$	-26.4
Hematite	$Fe_2O_3 + 6H^+ = 2Fe^{+3} + 3H_2O$	-30.84
Lepidocrocite	$FeOOH + 3H^+ = Fe^{+3} + 2H_2O$	1.371
Maghemite	$Fe_2O_3 + 6H^+ = 2Fe^{+3} + 3H_2O$	6.386
Magnetite	$Fe_3O_4 + 8H^+ = 2Fe^{+3} + Fe^{+2} + 4H_2O$	3.737
Manganite	$MnOOH + 3H^+ = Mn^{+3} + 2H_2O$	-0.24
Vivianite	$Fe_3(PO_4)_2{:}8H_2O = 3Fe^{+2} + 2PO_4^{-3} + 8H_2O$	-36
Chloropyromorphite	$Pb_5(PO_4)3Cl = 5Pb^{+2} + 3PO_4^{-3} + Cl^-$	-84.43
Hydroxylpyromorphite	$Pb_5(PO_4)3OH + H^+ = 5Pb^{+2} + 3PO_4^{-3} + H_2O$	-62.79
Galena	$PbS + H^+ = Pb^{+2} + HS^-$	-15.13
Cerussite	$PbCO_3 = Pb^{+2} + CO_3^{-2}$	-13.13
Plumbogummite	$PbAl_3(PO4)_2(OH)_5{:}H_2O + 5H^+ = Pb^{+2} + 3Al^{+3} + 2PO_4^{-3} + 6H_2O$	-32.79
Zincite	$ZnO + 2H^+ = Zn^{+2} + H_2O$	11.14
Zincosite	$ZnSO_4 = Zn^{+2} + SO_4^{-2}$	3.01
$Zn(OH)_2$	$Zn(OH)_2 + 2H^+ = Zn^{+2} + 2H_2O$	12.2
$Zn_3(PO4)_2{:}4H_2O$	$Zn_3(PO_4)_2{:}4H_2O = 3Zn^{+2} + 2PO_4^{-3} + 4H_2O$	-32.04
$ZnCO_3{:}H_2O$	$ZnCO_3{:}H_2O = Zn^{+2} + CO3^{-2} + H_2O$	-10.26
ZnO	$ZnO + 2H^+ = Zn^{+2} + H_2O$	11.31
ZnSiO3	$ZnSiO_3 + 2H^+ + H_2O = Zn^{+2} + H_4SiO_4$	2.93
Sphalerite	$ZnS + H^+ = Zn^{+2} + HS^-$	-11.62
Greenockite	$CdS + H^+ = Cd^{+2} + HS^-$	-15.93
Monteponite	$CdO + 2H^+ = Cd^{+2} + H_2O$	15.12
$Cd(OH)_2$	$Cd(OH)_2 + 2H^+ = Cd^{+2} + 2H_2O$	13.73
CdOHCl	$CdOHCl + H^+ = Cd^{+2} + H_2O + Cl^-$	3.52
$CdSiO_3$	$CdSiO_3 + H_2O + 2H^+ = Cd^{+2} + H_4SiO_4$	9.06

7. Summary of Quality Assurance Activities

7.1 Introduction

The specific details of the quality assurance (QA) aspects for this project were addressed in a previously prepared and EPA-endorsed document entitled *Quality Assurance Project Plan – Geochemical Modeling for Linking Waterfowl Contaminant Speciation in Riparian Soils* for Mine Waste Technology Program Activity III, Project 38. The portion of the project that the MWTP focused on was the geochemical modeling. Analytical data presented for other portions of the project was part of a larger effort for EPA Region 10, the Idaho Department of Environmental Quality, and the U.S. Fish and Wildlife Service. MSE included additional information and results from early portion of the project in this report to present the broader context of the project and the ultimate "big picture" objective of reducing the bioavailability of lead to reduce impacts of waterfowl in the region.

The main purpose of the quality assurance project plan (QAPP) was to assure that the model developed to evaluate P-Pb soil interactions used appropriate thermodynamic data with respect to mineralogical stability. The objective of the geochemical modeling effort was to find reaction mechanisms of Pb in P-amended soils in environments resembling the specific aqueous elemental concentrations and mineral species found in the Lower Coeur d'Alene River Basin.

The QAPP stated that PHREEQCI and Geochemist's Workbench software packages would be utilized to perform the modeling. PHREEQCI is publicly available from the U.S. Geological Survey, while Geochemist's Workbench is commercially available from RockWare USA, Inc.

7.2 Quality Assurance Assessment

Quality assurance assessment activities for geochemical modeling were performed by MSE and were documented in a memo dated January 12, 2006, as required in the QAPP.

In part, MSE's assessment included telephone conversations and email exchanges with the principal investigator. It was determined that most of the modeling was conducted before the QAPP was finalized. However, MSE personnel did review the modeling inputs prior to the modeling effort to help ensure that the modeling effort was congruent with project objectives outlined in the EPA-approved project work plan. In addition to the two software packages identified in the QAPP, the MINEQL+ commercially available software produced by Environmental Research Software, Inc. was also used, mainly to develop solubility curves. This software also used the MINTEQ thermodynamic database that was specified in the QAPP.

To simulate the specific aqueous elemental concentrations characteristic of the Lower Coeur d'Alene River Basin for modeling purposes, a representative pore water composition was assembled from several separate documented sources and presented in the QAPP. As part of the QA assessment, it was noted that this composition had a charge imbalance with a relative percent difference of 275% as the ratio of cations to anions was about 3:11 milliequivalents per liter. The QA assessment findings noted that an equal charge balance is not a requirement for theoretical modeling as it would be carried through all the calculations; however, the charge imbalance could have been an indication to question the validity of the input chemistry.

The QAPP required that supporting documentation be maintained as to the data inputs for each model output. The QA assessment findings noted that although specific input files were not saved, there was essentially only one input file that represented the single pore water composition characteristic of the Lower Coeur d'Alene River Basin.

In the summary of the QA assessment documentation, it was noted that the original reason for preparing a QAPP was to ensure that any new modifications to the thermodynamic databases were tracked and could be associated with the model results. At the start of the project, it had been anticipated that thermodynamic data for additional Pb species would be obtained from the literature and added to the database. It was further anticipated that modification of the values contained with the default databases might be performed in an attempt to calibrate the model to field results. However, these potential changes to the thermodynamic databases did not become necessary. The QA assessment concluded that since no data was added to the databases and no data was modified in an attempt to calibrate the model results, the project was essentially reduced to a standard geochemical modeling effort, for which, typically, no QAPP would be needed or prepared.

8. Conclusions and Recommendations

8.1 Conclusions

8.1.1 Mineralogical Analyses

The EMPA/XRD investigations conducted on test sites(s) and element speciation found no conclusive evidence that phosphoric acid/lime (P)-treatments enhanced formation of poorly soluble Pb-P mineral phases. However, the results indicate that P is preferentially absorbed to Fe-oxide minerals, while Pb is preferentially associated with Mn-oxide minerals. Thus, these highly reactive Fe/Mn-oxide phases will affect Pb contaminant release as leachable species; they will also influence P availability for reaching with Pb or other metallic contaminants of concern.

8.1.2 Metals Bioaccessibility to Waterfowl

The W-PBET gizzard phase results demonstrated high Pb extraction accuracy (90% ± 8% spike recovery) and precision (4.3% relative standard deviation). Data from the intestinal phase were near the ICP-AES method detection limit of 0.01 mg/L, which led to low reproducibility of the results. Despite limitations posed by model assumptions and its implementation, the gizzard phase results were positively correlated with bird feeding results for contaminated and *in situ* remediated soils from the Lower Coeur d'Alene River Basin. The Spearman and Pearson correlation coefficients for log-scale gizzard Pb versus blood Pb were 0.88 and 0.93, respectively.

The addition of 1.0 to 2.0 weight percent phosphoric acid to the test site soils resulted in statistically significant ($p < 0.05$) reductions in Pb levels in blood, liver, and kidney. Such P-treatment also lowers bioavailable- and bioaccessible-Pb levels, although such reductions are probably affected by site-specific differences in Pb speciation or mineralogy. The lack of any seasonal differences in bioaccessibility of Pb, Mn, or Zn may be due to minimal changes observed in soil redox potential. Only Cd showed lower bioaccessibility in August (2003) compared to May and October. Thus, factors other than oxidation-reduction potential (ORP) (e.g., temperature, biological activity) must exert seasonal influences on Cd bioaccessibility. Finally, the P-treatment induced reductions in tissue-Pb levels observed during this study may not be completely protective to many waterfowl species. The lowering of blood lead (PbB) levels from 5.0 to 2.5 μg/L is indeed environmentally significant; however, severe chemical signs of Pb toxicity can occur at PbB levels ≤ 2.0 μg/L (Beyer, 2000; Pain, 1996).

8.1.3 Geochemical Modeling

The PHREEQCi and other modeling results suggest that P treatment removes Pb^{+2} ions via formation of poorly soluble Pb-phosphate species, including chloropyromorphite. However, the effects of organo-lead complex formation, plus PO_4^{-3} absorption to mineral (e.g., Fe-oxide) surfaces, on the above reaction were not addressed in this study. Furthermore, long-term seasonal variability in ORP and/or pH conditions probably exerts more intense and transient effects on Pb speciation and Pb bioavailability than indicated by these modeling efforts.

8.2 Recommendations

Follow-on work should include:

- periodic assessment of the long-term effectiveness of phosphoric acid treatment of Pb-contaminated soils; and
- refinements to the geochemical model.

Annual screening of composite samples (from the untreated and P-treated plots) for Pb bioaccessibility (using W-PBET) would provide cost-effective insight into potential changes in contaminant bioavailability to waterfowl over time. This effort could be supplemented every 4 years with another waterfowl feeding study, so

as to recalibrate the W-PBET results. These combined data sets would coincide with the 5-year Comprehensive Environmental Response, Compensation, and Liability Act (CERCLA) remedy review process assumed to occur at such sites within the Coeur d'Alene River Basin.

Finally, additional research to characterize kinetics, adsorption, and interaction of metals with organic (humic/fulvic) acids would allow a more thorough analysis of the solubility and speciation of Pb and other metallic contaminants of concern. This activity, along with better quantitation of interactions between mineral surfaces with aqueous metal and P-species, would result in more accurate models for predicting contaminant availability for transport and uptake into environmental receptors.

9. References

Balistrieri, L. S., S. E. Box, et al. 2003. Modeling Precipitation and Sorption of Elements during Mixing of River Water and Porewater in the Coeur d'Alene River Basin. Environmental Science and Technology 37: 4694-4701.

Berti, W.R., and S.D. Cunningham. 1997. In-place inactivation of Pb in Pb-contaminated soils. Environmental Science and Technology 31:1359-1364

Bennett, E.H., Siems, P. L., Constantopoulos, J. T. 1989. The geology and history of the Coeur d'Alene mining district, Idaho, p. 137-156, In V. E. Chamberlain, Breckenridge, R. M., Bonnichsen, B., ed. Guidebook to the geology of northern and western Idaho and surrounding area, Vol. 28, Bulletin 28 ed. Idaho Geological Survey, Moscow, ID

Beyer, W. N., D. K. Audet, et al. 2000. "Relation of Waterfowl Poisoning to Sediment Lead Concentrations in the Coeur d'Alene River Basin", Ecotoxicology 9:207-218

Beyer, W.N., E.E. Conner, and S. Gerould. 1994. Estimates of soil ingestion by wildlife. Journal of Wildlife Management 58:375-382.

Blus, J.L., C.J. Henny, D.J. Hoffman, and R.A. Grove. 1991. Lead toxicosis in tundra swans near a mining and smelting complex in Northern Idaho. Archives of Environmental Contamination and Toxicology. 21:549-555

Bostick, B.C., C.M. Hansel, M.J. La Force, and S. Fendorf. 2001. Seasonal fluctuations in Zinc speciation within a contaminated wetland. Environmental Science and Technology 35:3823-3829.

Cao, R.X., L.Q. Ma, M. Chen, S.P. Singh, and W.G. Harris. 2003. Phosphate-induced metal immobilization in a contaminated site. Environmental Pollution 122:19-28.

Cassner, N.A. 1991 Toxic River: politics and Coeur d'Alene mining pollution in the 1930's Idaho Yesterdays 35:2-19.

Chen, X. B., J. V. Wright, et al. 1997. Effects of pH on heavy metal sorption on the mineralapatite. Environmental Science and Technology 31: 624-631.

Davis, A., J.W. Drexler, R. M.V., and A. Nicholson. 1993. Micromineralogy of mine wastes in relation to lead bioavailability, Butte, Montana. Environmental Science and Technology 27:1415-1425.

Duggan, M.J., M.J. Inkskip, S.A. Rundle, and J.S. Moorcroft. 1985. Pb in playground dust and on the hands of schoolchildren. Science of the Total Environment 44:65-79.

Essington, M.E., J.E. Foss, and Y. Roh. 2004. The soil mineralogy of lead at Horaces Villa. Soil Science Society of America Journal 68:979-993.

Gee, G.W., and J.W. Bauder. 1986. Particle-size analysis., In A. Klute, ed. Methods of soil analysis., 2nd. ed. SSSA, Maddison, Wisconsin

Heinz, G.H., D.J. Hoffman, and D.J. Audet. 2004. Phosphorus amendment reduces bioavailability of lead to mallards ingesting contaminated sediments. Archives of Environmental Contamination and Toxicology. 46:534-541.

Hettiarachchi, G.M., G.M. Pierzynski, and M.D. Ransom. 2000. In situ stabilization of soil lead using phosphorus and manganese oxide. Environmental Science and Technology 34:4614-4619.

Iskandar, I. K., and M. B. Kirkham. Trace Elements in Soil Bioavailability, Flux, and Transfer. Boca Raton, Fla: Lewis Publishers, 2001.

Kendall, R.J., and C.J. Driver. 1982. Lead poisoning in swans in Washington State. Journal of Wildlife Diseases 18:385-387.

Kimball, W.H., and Z.A. Munir. 1971. The corrosion of lead in a simulated waterfowl gizzard. Journal of Wildlife Management 35:360-365.

Klasing, K.C. 1998. Comparative avian nutrition. Cab International, New York

Laperche, V., T.J. Logan, P. Gaddam, and S.J. Traina. 1997. Effect of apatite amendments on plant uptake of lead from contaminated soil. Environmental Science and Technology 31:2745-2753.

LeJeune, K., T. Podrabsky, J. Lipton, D. Cacela, and a. et. 2000. Report of injury assessment and injury determination: Coeur d'Alene Basin natural resource damage assessment. Prepared by Status Consulting Inc. for United States Department of the Interior, Fish and Wildlife Service, United States Department of Agriculture, Forest Service Coeur d'Alene Tribe, Boulder, Colorado.

Levengood, J.M., and L.M. Skowron. 2001. Use of a simulated gizzard to measure bioavailability of metals and other elements to waterfowl. Ecotoxicology 10:299-304.

Lindsay, W.L. 1979. Chemical equilibria in soils. John Wiley and Sons, New York.

Long, K.R. 1998a. Grade and tonnage models for Coeur d' Alene-type polymetallic veins. Open File Report 98-583. U.S. Geological Survey, Tucson

Maenpaa, K.A., J.V.K. Kukkonen, and M.J. Lydy. 2002. Remediation of heavy metal-contaminated soils using phosphorus: evaluation of bioavailability using an earthworm assay. Archives of Environmental Contamination and Toxicology. 43:389-398.

McKenzie, R.M. 1980. The adsorption of lead and other heavy metals on oxides of manganese and iron. Australian Journal of Soil Research 18:61-73.

Melamed, R., X. Cao, M. Chen, and L.Q. Ma. 2003. Field assessment of lead immobilization in a contaminated soil after phosphate application. Science of the Total Environment 305:117-127

Mitchell, V.E., Bennett, E.H. 1983 Production statistics for the Coeur d'Alene mining district, Shoshone County, Idaho; 1884-1890. Technical Report 83-3. Idaho Geological Survey.

Nriagu, J. O. 1984. Formation and stability of base metal phosphates in soils and sediments. Phosphate Minerals. J. O. Nriagu and P. B. Moore. New York, Springer-Verlag: 318-329.

Oomen, A.G., A. Hack, M. Minekus, E. Zeijdner, C. Cornelis, G. Schoeters, W. Verstraete, T. Van De Wiele, J. Wragg, C.J. Rompelberg, A. Sips, and J. Van Wijnen. 2002. Comparison of five in vitro digestion models to study the bioaccessibility of soil contaminants. Environmental Science and Technology 36:3326-3334.

Oomen, A.G., J. Tolls, A.J.A.M. Sips, and M.A.G.T. Van den Hoop. 2003. Lead speciation in artificial human digestive fluid. Archives of Environmental Contamination and Toxicology. 44:107-115.

Pain, D.J. 1996. "Lead in Waterfowl", Chapter 10 (pp. 251-264) In Beyer, W.N. et al. (Eds.), Environmental Contaminants in Wildlife: Interpreting Tissue Concentrations, Lewis Publishers, Boca Raton, Florida.

Paulson, A. J. 2001. Biogeochemical removal of Zn and Cd in the Coeur d'Alene river Idaho, USA, downstream of a mining district. The Science of the Total Environment 278: 31-44.

Ridolfi. 1993. Confirmation of exposure of natural resources to hazardous substances in the Coeur d'Alene Basin of northern Idaho. Ridolfi Engineers and Associates, Inc., Seattle, WA

Rodriguez, R.R., and N.T. Basta. 1999. An in vitro gastrointestinal method to estimate bioavailable arsenic in contaminated soils and solid media. Environmental Science and Technology 33:642-649.

Ruby, M.V., A. Davis, J.H. Kempton, J.W. Drexler, and P.D. Bergstrom. 1992. Lead bioavailability: dissolution kinetics under simulated gastric conditions. Environmental Science and Technology 26:1242.

Ruby, M.V., A. Davis, R. Schoof, S. Eberle, and C.M. Sellstone. 1996. Estimation of lead and arsenic bioavailability using a physiologically based extraction test. Environmental Science and Technology 30:422-430.

Ruby, M. V., R. Schoof, et al. 1999. Advances in evaluating the oral bioavailability of inorganics in soil for use in human health risk assessment. Environmental Science and Technology 33: 3697-3705.

Ruby, M.V. 2003. Application of in vitro extraction tests to estimate lead bioavailability from soil. EPA Bioavailable Workshop, Tampa, Florida

Ruby, M.V., Davis, A., Nicholson, A. 1994. In situ formation of lead phosphate in soils as a method to immobilize lead. Environmental Science and Technology 28:646-654

Schecher, W. 1998. MINEQL+ version 4.5. Hallowell, ME, Environmental Research Software.

Seaman, J.C., J.S. Arey, and P.M. Bertsch. 2001. Immobilization of nickel and other metals in contaminated sediments by hydroxylapatite addition. J. Environ. Qual. 30:460–469.

Sileo, L., L.H. Creekmore, D.J. Audet, M.R. Snyder, C.U. Meteyer, J.C. Franson, L.N. Locke, M.R. Smith, and D.L. Finley. 2001. Lead poisoning of waterfowl by contaminated sediment in the Coeur d'Alene River. Archives of Environmental Contamination and Toxicology. 41:364-368.

Silviera, D.J., and L.E. Sommers. 1977. Extractability of copper, zinc, cadmium and lead in soils incubated with sewage sludge. Journal of Environmental Quality 6:47-52.

Sparks, D.S. 1989. Kinetics of soil chemical processes. Academic Press Inc, San Diego

Strawn, D.G. 2005. University of Idaho, Final Report Contaminant Speciation in Riparian Soils, for Mine Waste Technology Program, Activity III, Project 38. Complete copy in Appendix A.

Sturkie, P.D. 1986. Avian physiology. 4th ed. Springer-Verlag, New York, Herdelberg, Berlin

TerraGraphics Environmental Engineering Inc. 2003a. Soil amendment studies at Bull Run and Black Rock Slough Coeur d'Alene basin. Final Data Summary Memorandum, Moscow, ID.

TerraGraphics Environmental Engineering, Inc. 2003b. Data summary memorandum: Soil amendment studies at Bull Run and Black Rock Slough, Coeur d'Alene basin. Final Report, Moscow, ID.

Wixson, G.W., and B.E. Davies, (eds.) 1993. Lead in soil: recommended guidelines. Science Reviews, Northwood.

Yang, J., D.E. Mosby, S.W. Casteel, and R.W. Blanchar. 2001. Lead immobilization using phosphoric acid in a smelter-contaminated urban soil. Environmental Science and Technology 35:3553-3559

Zhang, P.C., J.A. Ryan, and L.T. Bryndzia. 1997. Pyromorphite formation from goethite adsorbed lead. Environmental Science and Technology 31:2673-2678

Appendix A: D.G. Strawn's Final Report to MSE, Dated January 26, 2006

Table A.1. Raw elemental composition data (mg kg^{-1}) for soils in Table 1.1, showing three replicates of each soil composite and the wavelength used for each element.

Sample	**As**	**Cd**	**Fe**	**Mn**	**P**	**Pb**	**S**	**Si**	**Zn**
ID	**189.042**	**228.802**	**239.562**	**257.61**	**178.768**	**220.353**	**182.034**	**251.612**	**202.548**
2(a) Avg	77.129	28.093	77,986.074	5,626.674	23,256.561	4,959.829	1,656.133	237,680.771	2,279.861
Stddev	0.0156	0.0014	1.0940	0.1128	0.5787	0.0526	0.0527	3.7510	0.0729
2(b) Avg	79.348	30.832	79,427.359	5,922.587	24,257.688	5,318.134	1,800.371	247,348.887	2,395.281
Stddev	0.0212	0.0016	3.0370	0.2667	1.3990	0.2264	0.0318	12.4400	0.1389
2(c) Avg	85.591	31.668	78,399.582	5,666.841	24,837.866	5,253.661	1,759.414	242,913.180	2,366.109
Stddev	0.0110	0.0038	2.5390	0.1861	1.4090	0.1705	0.1015	5.8130	0.0942
2 Avg.	**80.6893**	**30.1980**	**78,604.3383**	**5,738.7008**	**24,117.3719**	**5,177.2078**	**1,738.6394**	**242,647.6126**	**2,347.0835**
StDev	**4.3876**	**1.8701**	**742.1388**	**160.5120**	**799.9361**	**190.9960**	**74.3295**	**4,839.5256**	**60.0161**
4(a) Avg	126.027	16.199	85,933.437	7,332.293	252,522.101	4,568.383	1,894.696	262,350.494	2,831.513
Stddev	0.0245	0.0018	1.2190	0.0909	7.3380	0.0853	0.0313	0.7848	0.0483
4(b) Avg	139.433	16.101	84,538.376	7,466.630	280,033.370	4,468.854	1,843.993	261,401.557	2,811.457
Stddev	0.0178	0.0014	1.6960	0.1803	12.5000	0.1002	0.0623	4.3520	0.1260
4(c) Avg	141.241	16.814	83,863.399	7,137.643	288,581.856	4,470.803	1,784.932	263,555.787	2,888.425
Stddev	0.0074	0.0003	0.7681	0.0692	0.6260	0.0430	0.0766	2.2400	0.0050
4 Avg.	**135.5669**	**16.3714**	**84,778.4042**	**7,312.1888**	**273,712.4425**	**4,502.6800**	**1,841.2071**	**262,435.9462**	**2,843.7986**
StDev	**8.3111**	**0.3867**	**1,055.6867**	**165.4120**	**18,842.5604**	**56.9086**	**54.9348**	**1,079.6542**	**39.9278**
6(a) Avg	40.650	11.220	40,103.567	1,482.451	17,079.977	3,550.058	453.682	290,851.554	764.384
Stddev	0.0308	0.0015	1.7420	0.0654	0.7613	0.1943	0.0912	10.8900	0.0331
6(b) Avg	37.252	11.065	40,066.225	1,388.245	16,846.026	3,526.490	420.530	300,496.689	767.936
Stddev	0.0164	0.0015	0.5197	0.0212	0.2928	0.0142	0.0224	2.2880	0.0178
6(c) Avg	35.654	11.208	40,321.730	1,446.994	16,977.848	3,599.684	421.941	296,677.215	775.053
Stddev	0.0197	0.0002	0.7011	0.0293	0.6114	0.0100	0.0318	3.3270	0.0067
6 Avg.	**37.8519**	**11.1642**	**40,163.8408**	**1,439.2299**	**16,967.9505**	**3,558.7437**	**432.0510**	**296,008.4858**	**769.1244**
StDev	**2.5516**	**0.0860**	**138.0049**	**47.5805**	**117.2889**	**37.3619**	**18.7466**	**4,857.2171**	**5.4326**

Table A.1. Continued

Sample ID	As 189.042	Cd 228.802	Fe 239.562	Mn 257.61	P 178.768	Pb 220.353	S 182.034	Si 251.612	Zn 202.548
8(a) Avg	55.330	9.560	48,873.626	2,840.659	543.681	3,862.637	459.066	298,076.923	1,096.703
Stddev	0.0113	0.0012	1.8260	0.1207	0.1347	0.1850	0.0330	9.0440	0.0450
8(b) Avg	56.764	9.629	48,328.912	2,790.451	705.570	3,832.891	464.191	301,326.260	1,102.387
Stddev	0.0164	0.0013	1.0290	0.0691	0.0839	0.1394	0.0475	4.9840	0.0170
8(c) Avg	55.553	8.965	46,316.360	2,625.677	454.767	3,659.263	448.267	293,607.801	1,060.130
Stddev	0.0052	0.0013	1.1270	0.0723	0.0898	0.0450	0.0294	4.4390	0.0285
8 Avg.	**55.8820**	**9.3848**	**47,839.6328**	**2,752.2625**	**568.0062**	**3,784.9306**	**457.1745**	**297,670.3279**	**1,086.4069**
StDev	**0.7718**	**0.3649**	**1,347.0149**	**112.4638**	**127.1587**	**109.8427**	**8.1290**	**3,875.2604**	**22.9332**

Table A.2. Raw data from particle size analysis of composite soil samples reported in Table 1.2.

	Units	Very Coarse Sand	Coarse Sand	Medium Sand	Fine Sand	Very Fine Sand	Sand Total	Silt Total	Clay Total	Total	Original Total
Comp 2	g	0.039	0.043	0.039	1.478	6.821	8.420	5.059	0.958	14.437	14.632
Very Fine Sandy Loam	%	0.27	0.30	0.27	10.24	47.25	58.32	35.04	6.64	98.67	
Comp 4	g	0.021	0.007	0.012	2.683	5.750	8.473	5.012	0.718	14.202	14.319
Very Fine Sandy Loam	%	0.15	0.05	0.09	18.89	40.48	59.66	35.29	5.06	99.18	
Comp 6	g	0.049	0.109	0.086	0.899	3.905	5.049	7.847	1.298	14.194	14.364
Silt Loam	%	0.34	0.77	0.61	6.34	27.51	35.57	55.29	9.14	98.82	
Comp 8	g	0.009	0.002	0.020	0.959	2.790	3.780	9.017	1.393	14.190	14.305
Silt Loam	%	0.06	0.01	0.14	6.76	19.66	26.64	63.55	9.82	99.19	

Table A.3. Electron Microprobe Elemental Associations:

Strongly associated = 4
Moderately associated = 3
Weakly associated = 2
No visual association = 1

Plot 2 Associations								
Sample	Area of Interest (x,y)	Fe-Pb	Mn-Pb	P-Pb	Fe-P	Mn-P	Mn-Fe	Fe-Si
P2C7	308,231	2	4	3	4	2	2	1
P2C7	346,230	2	2	2	2	2	2	2
P2C7	360,310	2	2	2	3	2	4	2
P2C7	369,291	2	2	2	4	2	3	2
P2C7	441,181	3	3	2	4	3	3	3
P2C7	447,145	2	1	2	4	1	4	1
P2C8	303,178	1	1	2	2	1	4	1
P2C8	314,272	2	1	2	4	3	4	2
P2C8	376,249	2	2	2	4	2	4	2
P2C8	427,161	3	4	2	3	3	4	1
P2C8	439,161	2	4	2	4	2	3	2
P2C8	482,255	1	1	2	3	2	4	1
P2C9	312,123	3	2	2	4	2	3	2
P2C9	320,109	2	1	2	3	2	3	2
P2C9	348,105	2	2	2	4	3	3	2
P2C9	372,114	2	2	2	4	2	4	1
P2C9	394,083	2	2	2	4	2	2	2
P2C9	428,243	2	2	2	4	2	3	2

Table A.3. Continued

Plot 4 Associations								
Sample	Area of Interest (x,y)	Fe-Pb	Mn-Pb	P-Pb	Fe-P	Mn-P	Mn-Fe	Fe-Si
P4C7	333, 151	2	2	1	1	1	4	2
P4C7	403, 199	1	1	1	1	1	4	1
P4C7	428, 198	1	2	1	1	1	3	3
P4C7	456, 153	1	2	1	1	1	4	1
P4C7	485, 208	1	1	1	1	1	4	1
P4C7	486, 202	1	4	1	1	1	3	2
P4C8	354, 306	1	1	1	1	1	2	2
P4C8	370, 216	3	2	3	3	2	2	2
P4C8	391, 328	4	1	1	1	1	4	2
P4C8	408, 221	1	1	1	1	1	4	3
P4C8	424, 202	1	2	1	2	1	4	4
P4C8	424, 217	2	4	2	1	1	2	2
P4C8	470, 208	1	3	1	1	1	3	3
P4C8	473, 203	2	2	2	2	2	3	2
P4C9	319, 289	3	2	3	2	1	4	2
P4C9	338, 313	4	3	4	3	2	4	3
P4C9	443, 152	4	3	3	2	2	4	3
P4C9	452, 298	4	2	3	2	2	3	2
P4C9	459, 210	3	3	2	2	2	3	3
P4C9	487, 204	4	2	3	3	2	3	2

Table A.3. Continued

Plot 6 Associations								
Sample	Area of Interest (x,y)	Fe-Pb	Mn-Pb	P-Pb	Fe-P	Mn-P	Mn-Fe	Fe-Si
P6C7	312, 242	2	2	3	4	2	2	2
P6C7	344, 248	1	1	1	3	1	1	3
P6C7	356, 231	2	3	2	3	2	3	2
P6C7	358, 261	2	3	2	4	2	4	3
P6C7	371, 216	3	2	3	4	2	2	3
P6C7	378, 276	1	3	2	2	2	2	2
P6C7	398, 208	3	3	2	3	2	3	2
P6C7	402, 315	2	2	2	4	3	2	2
P6C7	434, 278	2	2	2	3	2	4	2
P6C7	465, 249	2	3	2	4	2	2	2
P6C7	498, 110	3	2	2	4	2	2	2
P6C8	354, 256	2	3	2	3	2	3	2
P6C8	361, 147	1	1	1	1	1	4	1
P6C8	399, 228	2	4	2	3	2	4	2
P6C8	400, 208	3	2	3	4	2	2	2
P6C8	454, 290	1	1	1	3	1	2	2
P6C9	331, 212	2	2	2	3	2	3	3
P6C9	357, 180	1	2	1	2	1	4	2
P6C9	395, 183	2	2	2	4	2	3	3
P6C9	452, 188	1	1	1	3	1	2	2
P6C9	482, 224	3	2	2	3	2	3	2

Table A.3. Continued

Plot 8 Associations								
Sample	Area of Interest (x,y)	Fe-Pb	Mn-Pb	P-Pb	Fe-P	Mn-P	Mn-Fe	Fe-Si
P8C7	312, 164	3	3	2	1	2	3	2
P8C7	325, 245	2	3	1	1	1	2	----
P8C7	380, 269	3	2	1	2	1	3	2
P8C7	398, 323	1	3	1	1	1	2	2
P8C7	456, 196	3	2	1	1	1	2	2
P8C7	490, 265	1	4	1	1	1	2	----
P8C8	302, 323	1	4	1	2	1	3	2
P8C8	328, 376	2	3	2	2	1	3	3
P8C8	333, 340	1	3	1	1	1	2	2
P8C8	354, 225	1	4	1	2	1	3	2
P8C8	361, 241	2	3	2	2	2	3	3
P8C8	395, 203	2	2	2	3	2	3	3
P8C8	399, 204	2	3	1	2	1	3	4
P8C8	413, 208	2	3	1	1	2	3	3
P8C8	429, 346	2	3	2	3	1	2	2
P8C8	442, 252	3	2	1	3	1	3	2
P8C8	472, 213	2	3	2	3	2	3	2
P8C9	413, 154	2	4	1	1	1	2	3
P8C9	448, 239	2	2	1	3	1	3	2
P8C9	451, 293	2	3	1	2	2	2	2
P8C9	456, 227	2	3	2	2	1	3	1
P8C9	484, 269	1	3	1	1	1	3	2

Table A.4. Raw data from ICP-AES analysis of AOD- and CBD-extracted soils shown in Table 1.4, showing three replicates of each soil composite and the wavelength used for each element.

Sample ID	**AOD Fe 240.488**	**AOD Mn 257.610**	**CBD Fe 238.204**	**CBD Mn 259.373**
2(a) Avg	57,260.8696	4,033.9130	58,904.5936	4,064.4876
Stddev	0.4666	0.0302	0.1752	0.0124
2(b) Avg	62,269.0058	3,937.3099	59,547.9204	3,503.6166
Stddev	0.1050	0.0059	0.2211	0.0130
2(c) Avg	61,688.8889	4,236.8889	52,934.7826	3,143.1159
Stddev	0.2408	0.0127	0.2085	0.0120
2 Avg.	**60,406.2548**	**4,069.3706**	**57,129.0989**	**3,570.4067**
StDev	**2,739.3831**	**152.9046**	**3,646.5990**	**464.3028**
4(a) Avg	48,382.4701	4,276.4940	29,774.3682	2,103.7906
Stddev	0.0350	0.0034	0.1359	0.0094
4(b) Avg	50,382.6715	4,527.0758	28,297.0297	2,151.4851
Stddev	0.0482	0.0078	0.0952	0.0071
4(c) Avg	51,185.4545	4,288.1455	29,103.6907	2,246.0457
Stddev	0.1292	0.0087	0.1285	0.0092
4 Avg.	**49,983.5320**	**4,363.9051**	**29,058.3629**	**2,167.1072**
StDev	**1,443.4904**	**141.4300**	**739.7116**	**72.4028**
6 (a) Avg	24,338.2550	1,074.3624	32,686.0254	1,155.1724
Stddev	0.1200	0.0027	0.0725	0.0025
6 (b) Avg	22,719.7183	1,014.0845	28,892.1569	1,282.3529
Stddev	0.0024	0.0003	0.0342	0.0015
6 (c) Avg	24,883.7545	1,307.4368	31,320.5645	1,221.7742
Stddev	0.0669	0.0026	0.0784	0.0026
6 Avg.	**23,980.5760**	**1,131.9612**	**30,966.2489**	**1,219.7665**
StDev	**1,125.4839**	**154.9262**	**1,921.5916**	**63.6140**
8(a) Avg	25,385.9779	2,268.4871	34,396.0396	2,538.6139
Stddev	0.1012	0.0063	0.0832	0.0052
8(b) Avg	26,225.6055	2,485.9516	33,916.9675	2,454.8736
Stddev	0.2325	0.0204	0.1066	0.0077
8(c) Avg	26,248.3271	2,473.6059	33,745.2471	2,532.3194
Stddev	0.0276	0.0018	0.0906	0.0064
8 Avg.	**25,953.3035**	**2,409.3482**	**34,019.4181**	**2,508.6023**
StDev	**491.4498**	**122.1454**	**337.2755**	**46.6367**

Appendix Images for Microprobe Analysis of Plots, 2, 4, 6, 8

Organized by plot, cell, and location on thin section. Each WDS image is 512 x 512 μm.

Plot 2

2C7 – 308, 231
BSE Image

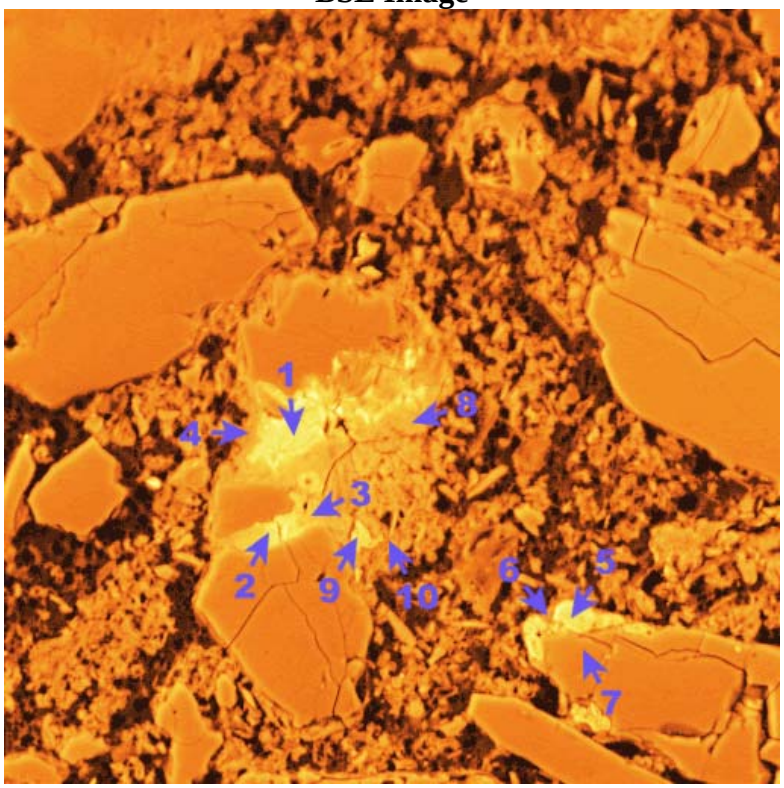

Iron (Fe)

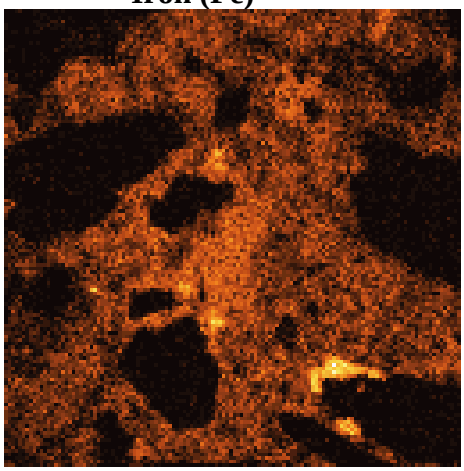

Manganese (Mn)

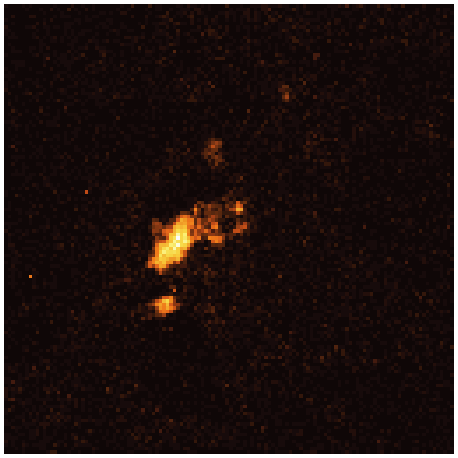

Phosphorous (P)

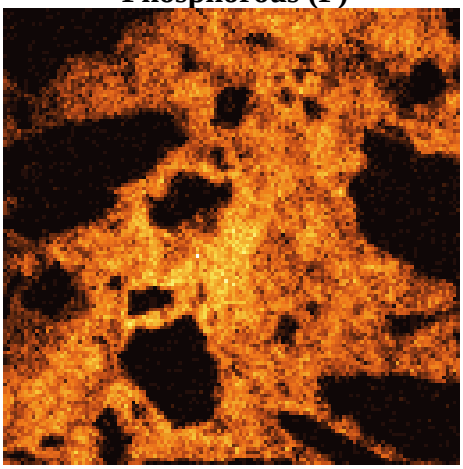

Lead (Pb)

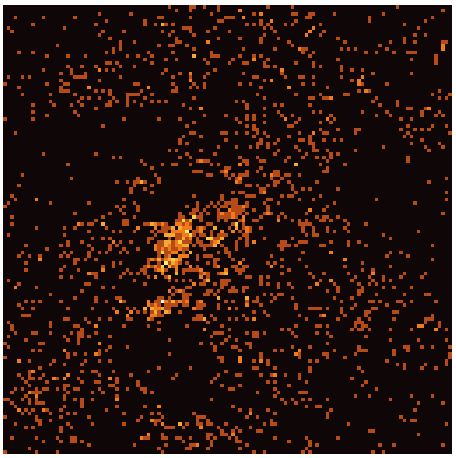

Silicon (Si)

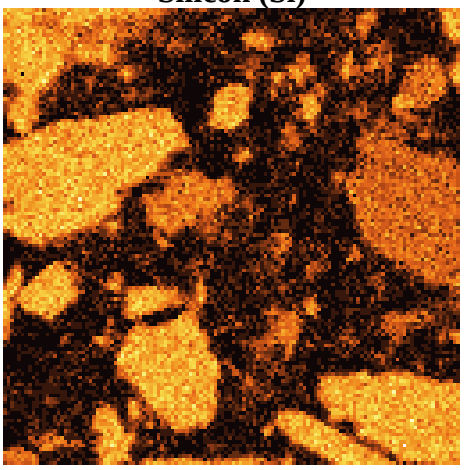

EDS Profiles by Analysis Point
Point 1

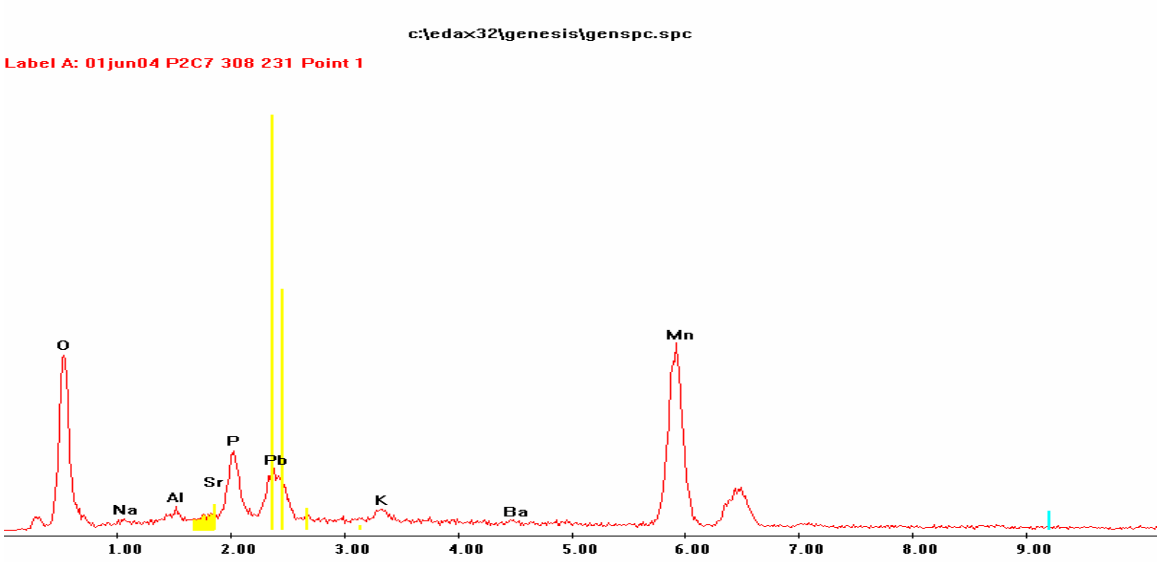

Point 2

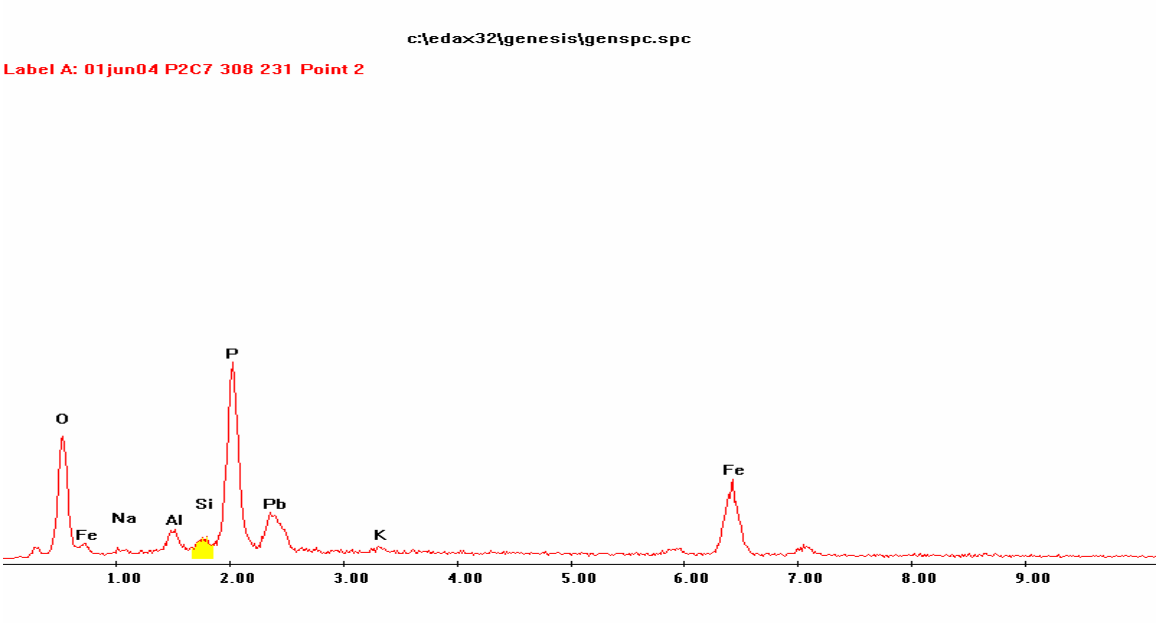

Point 3

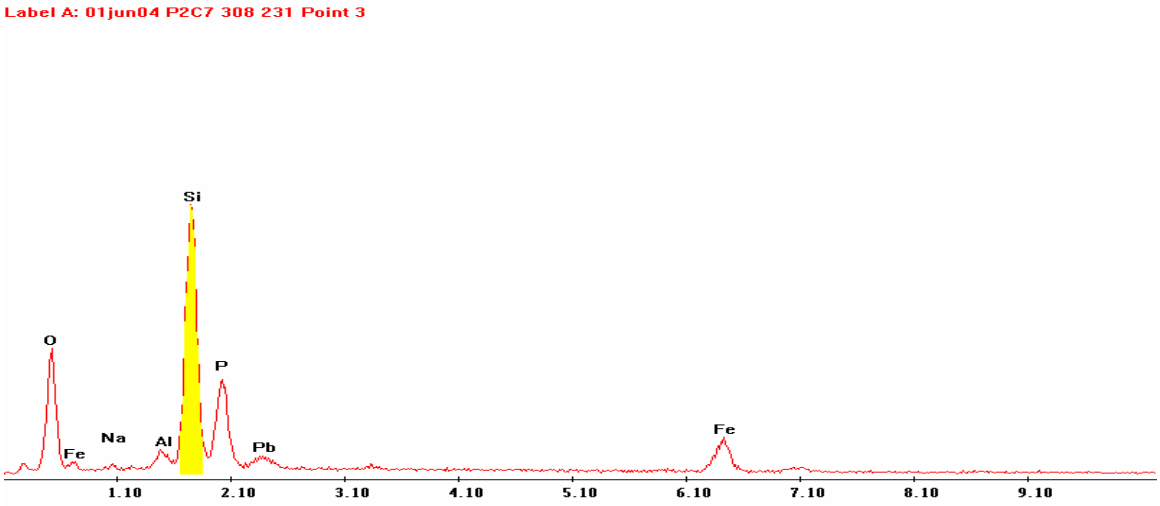

Point 4

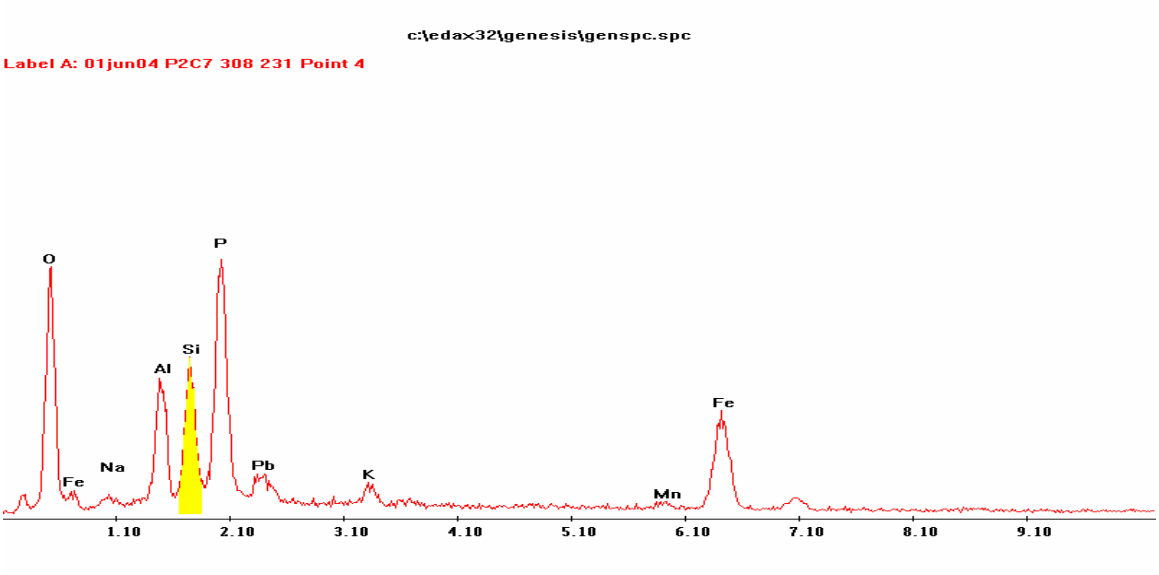

Point 5

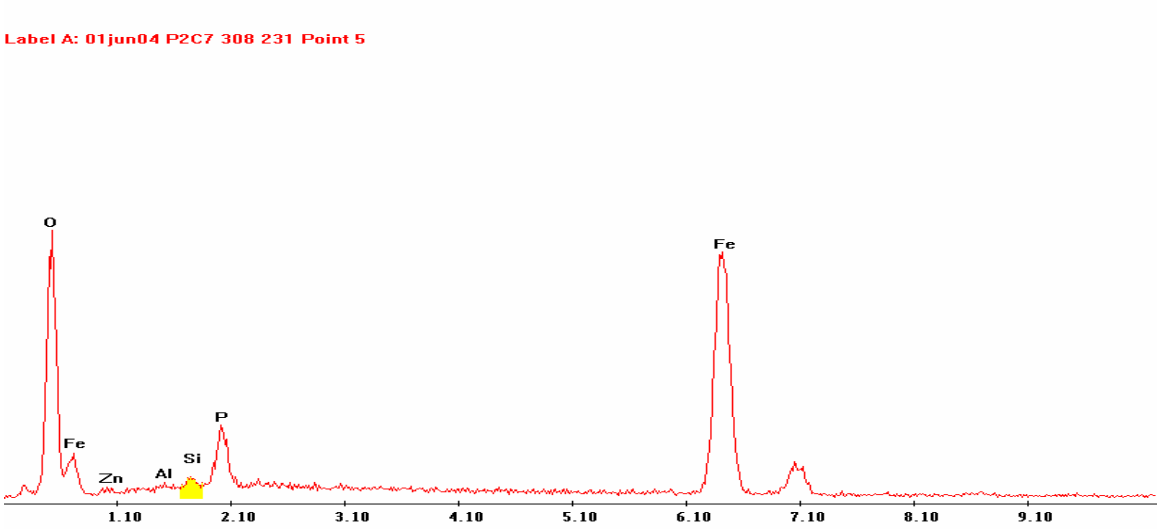

Point 6

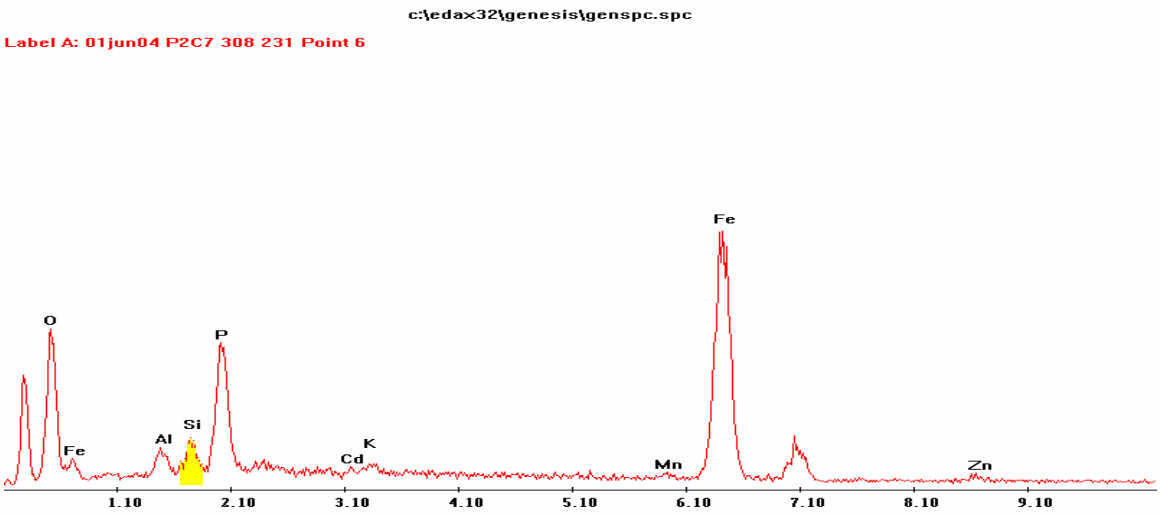

Point 7

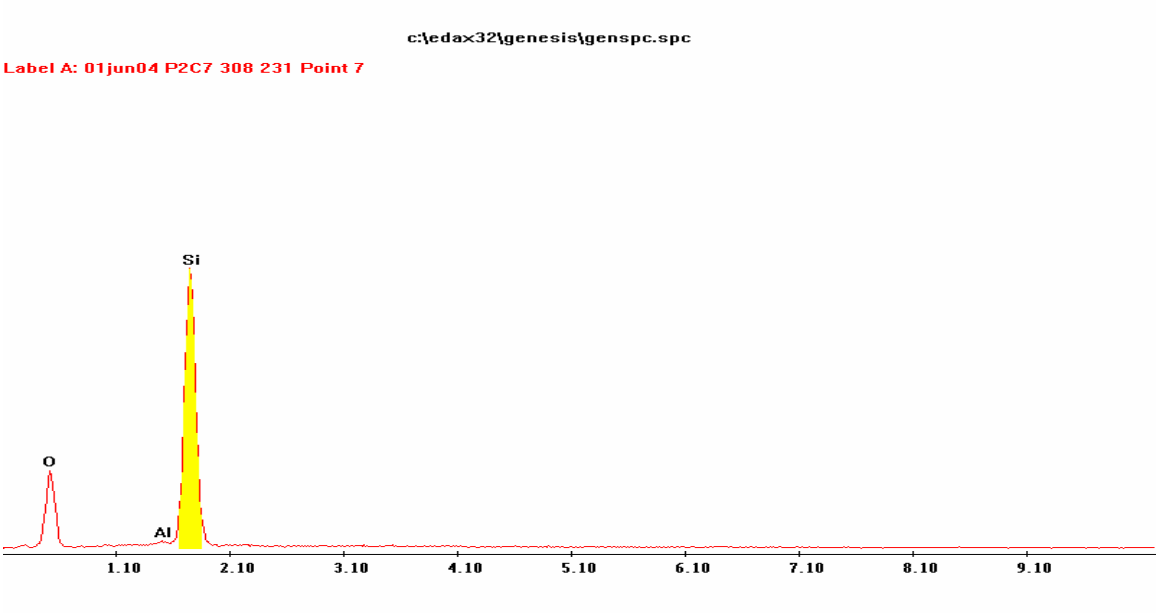

Point 8

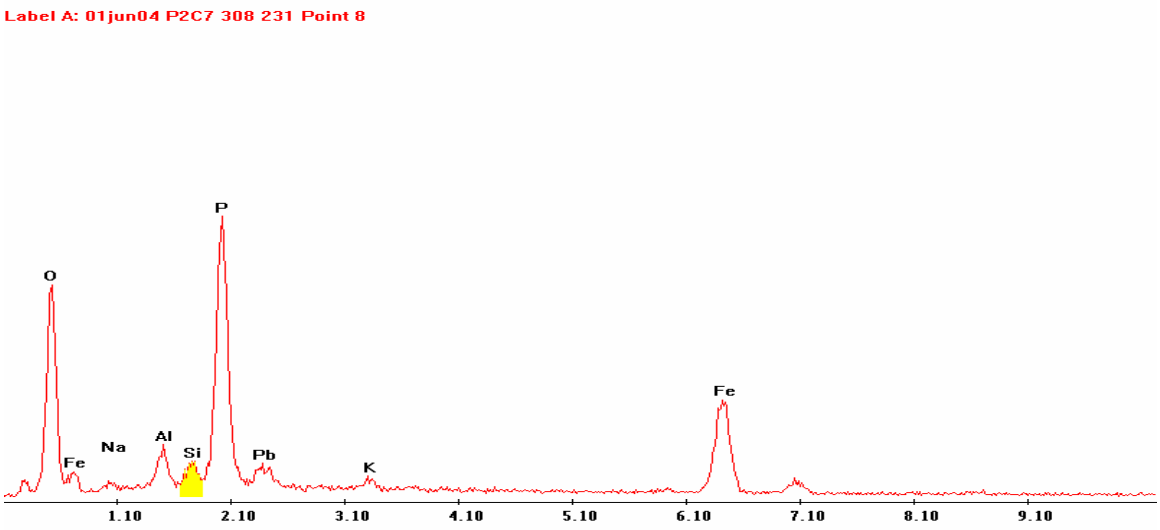

Point 9

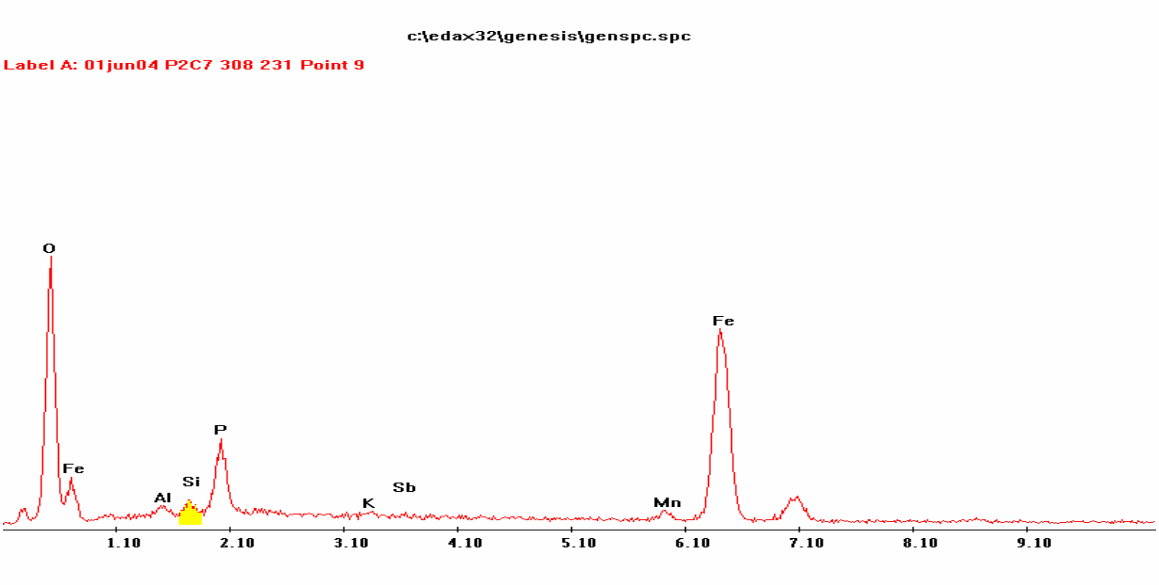

Point 10

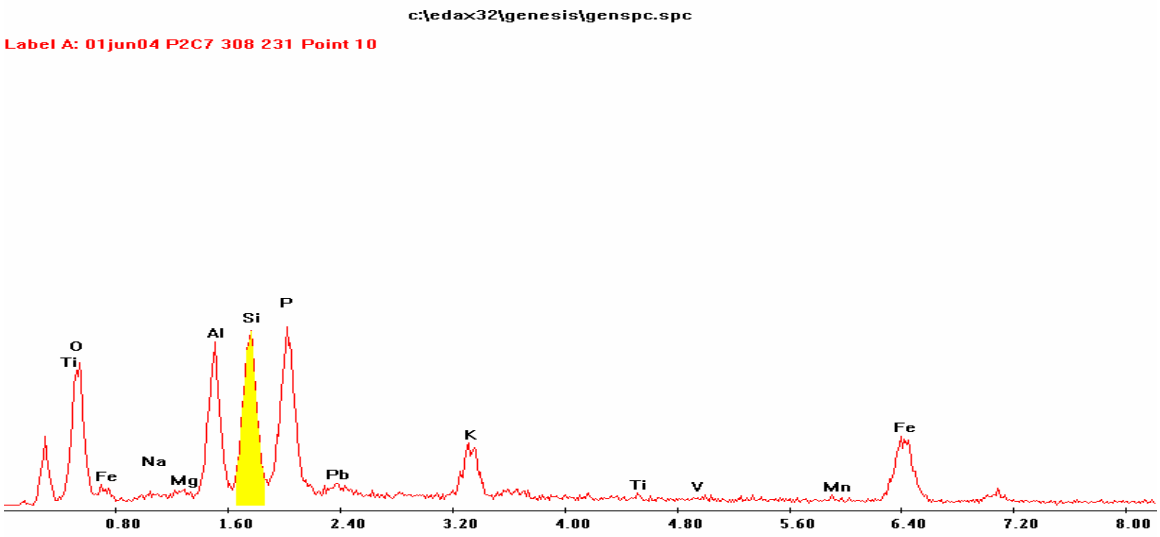

P2C7 – 346, 230

BSE Image

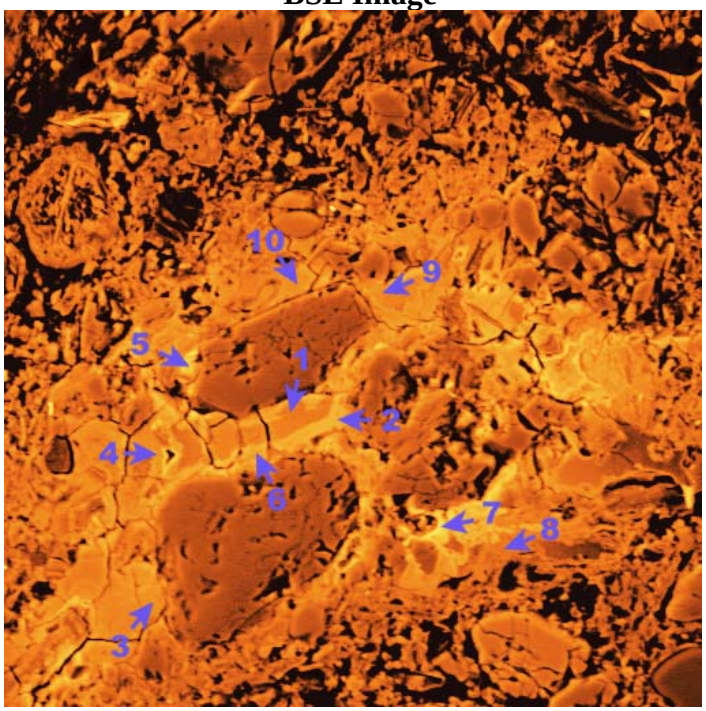

Iron (Fe)

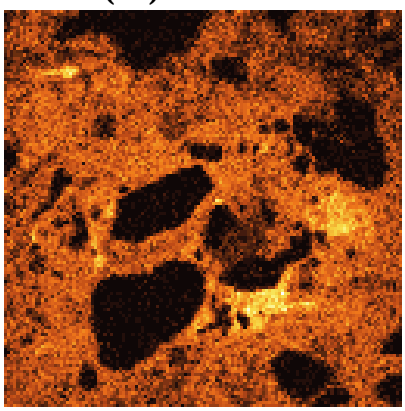

Manganese (Mn)

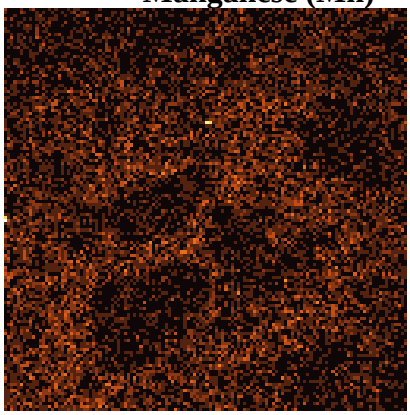

Phosphorous (P)

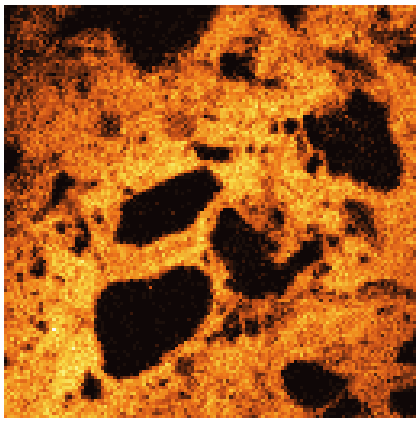

Lead (Pb)

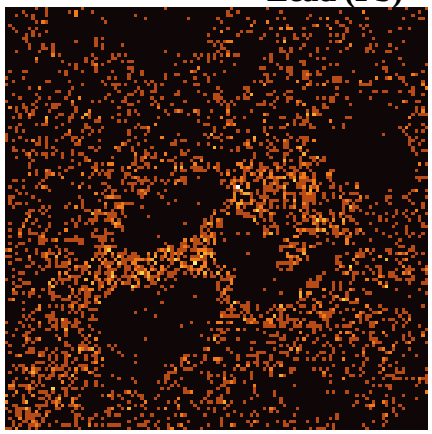

Silicon (Si)

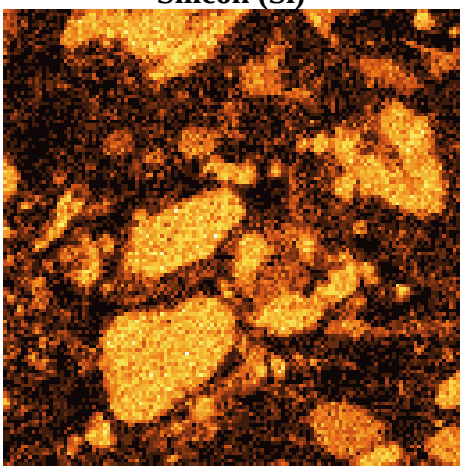

EDS Scan Images by Point

Point 1

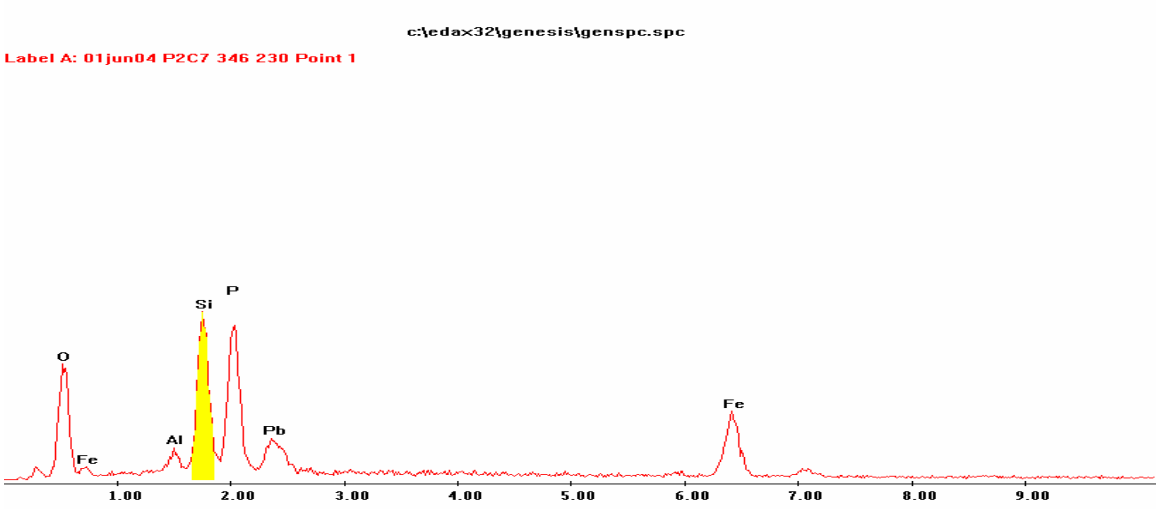

Point 2

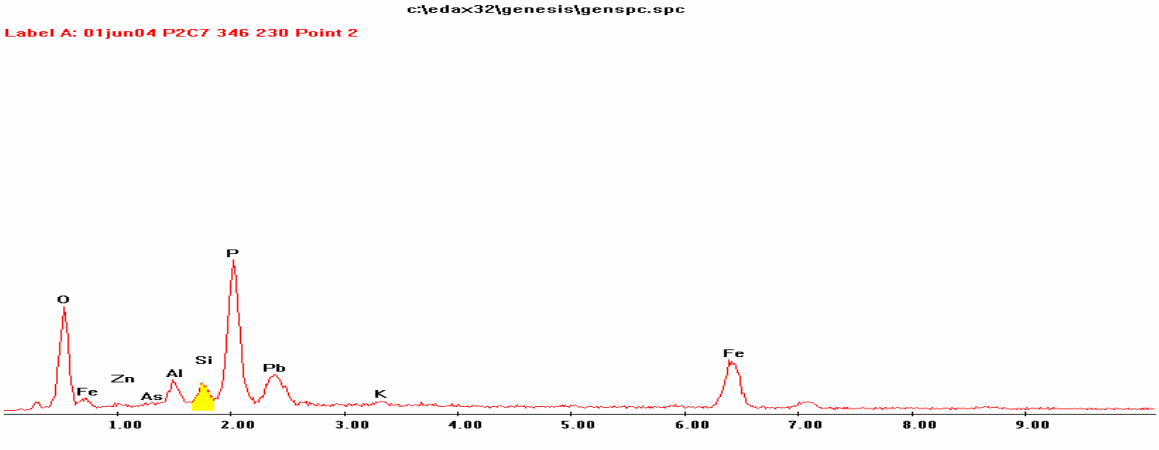

Point 3

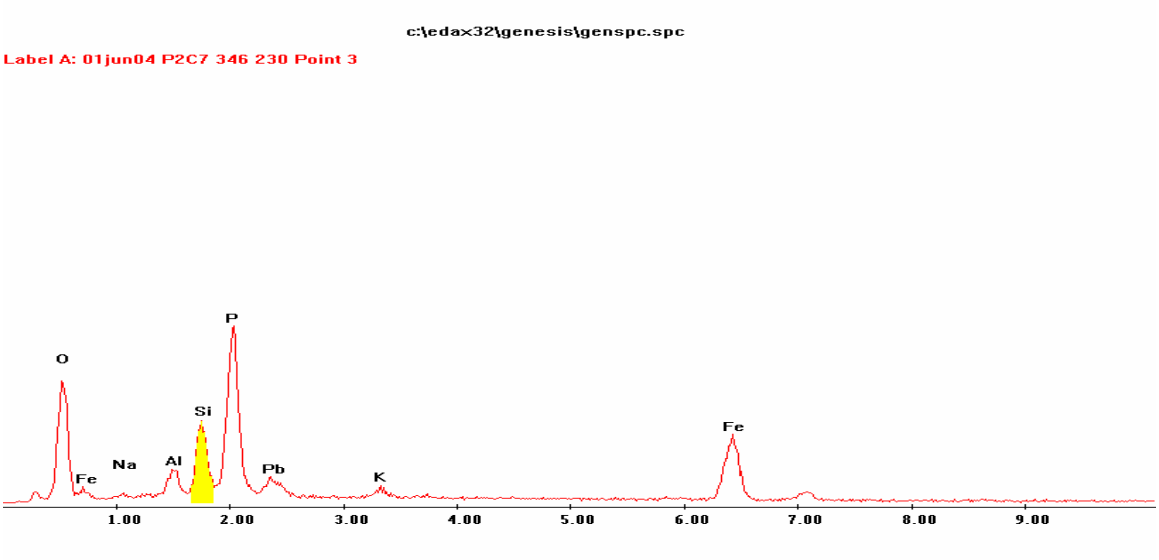

Point 4

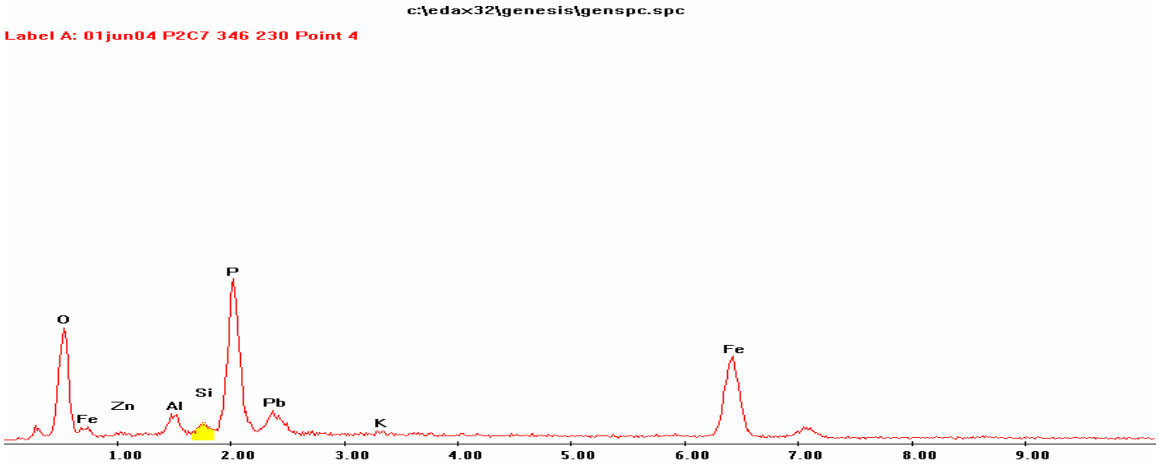

Point 5

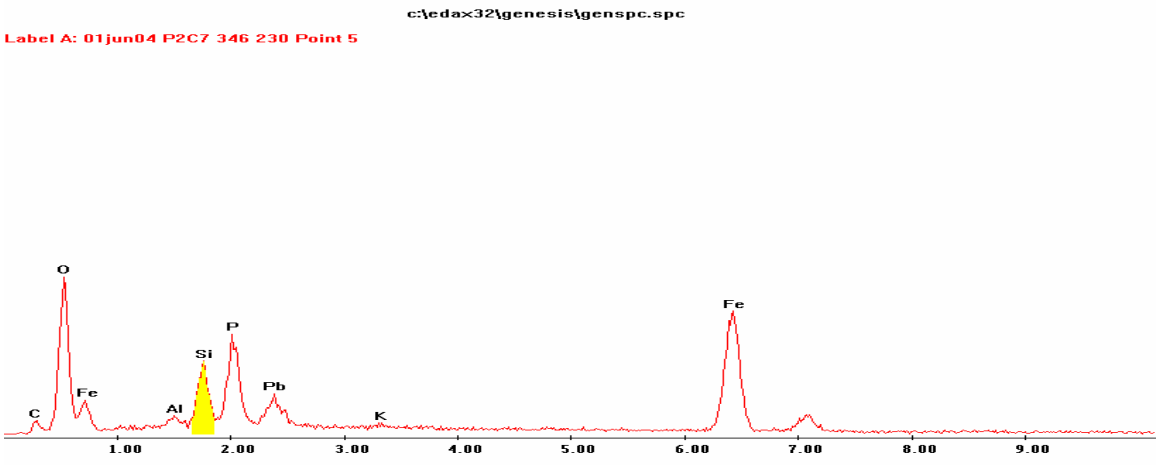

Point 6

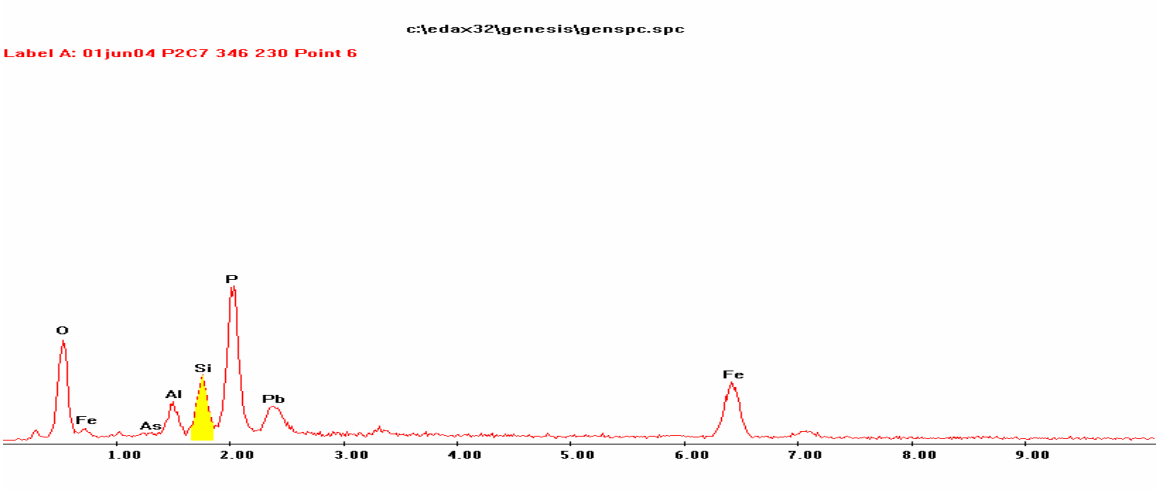

Point 7

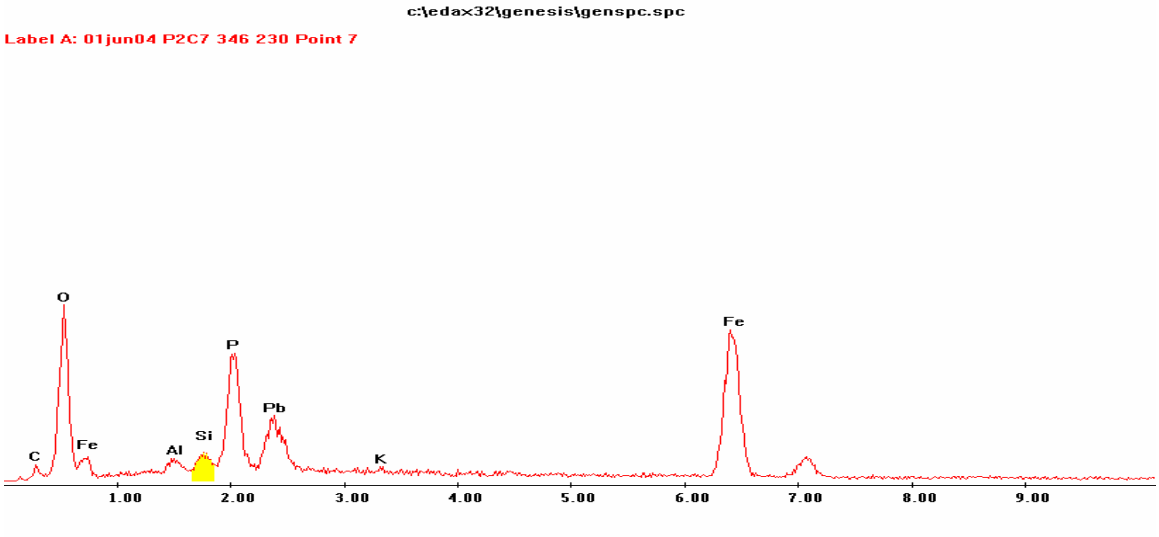

Point 8

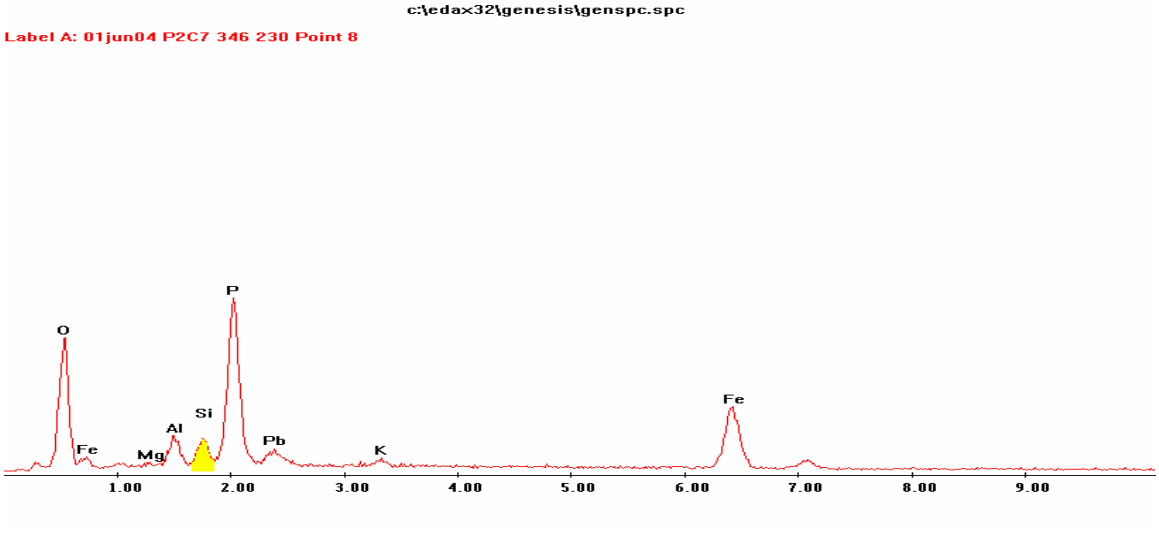

Point 9

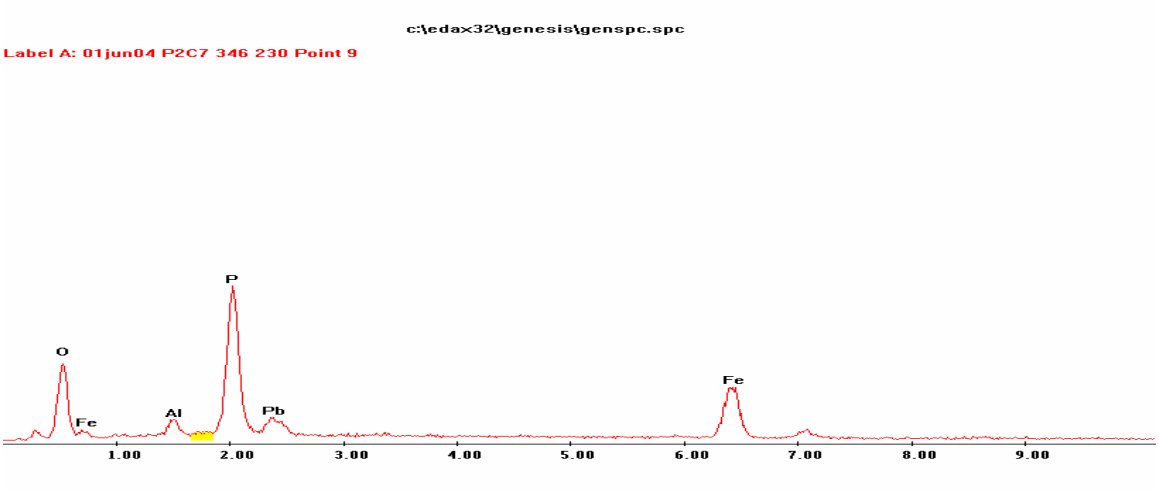

Point 10

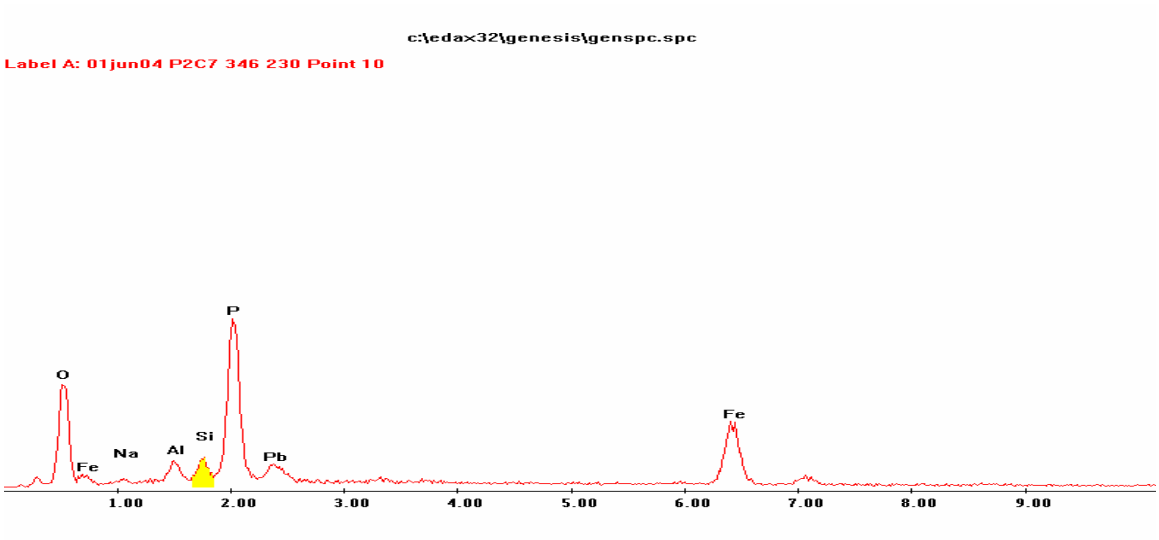

P2C7 – 360, 310

BSE Image

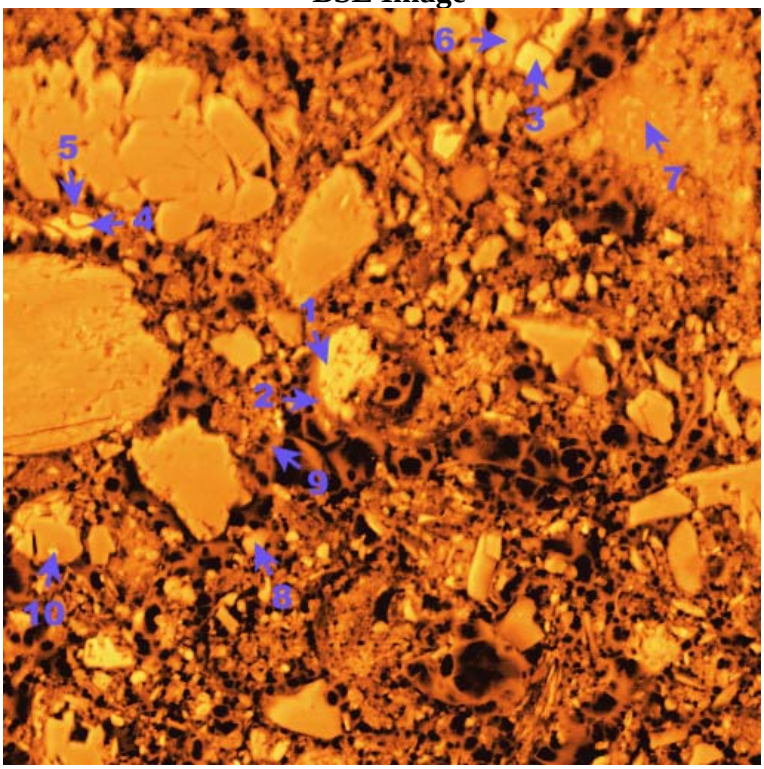

Iron (Fe)

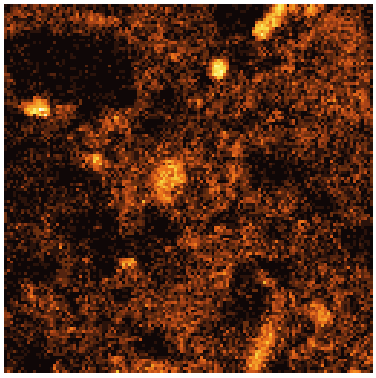

Manganese (Mn)

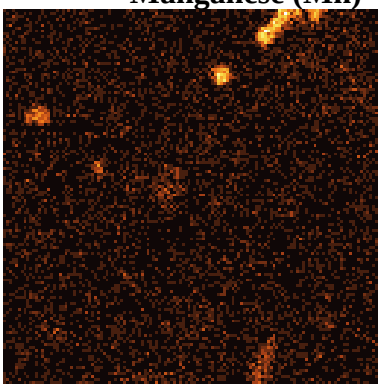

Phosphorous (P)

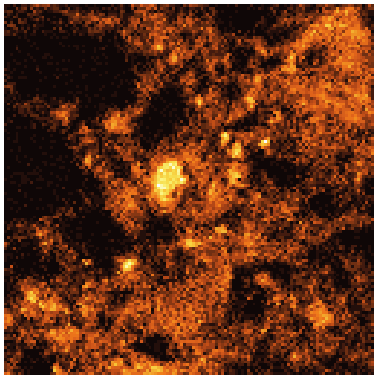

Lead (Pb)

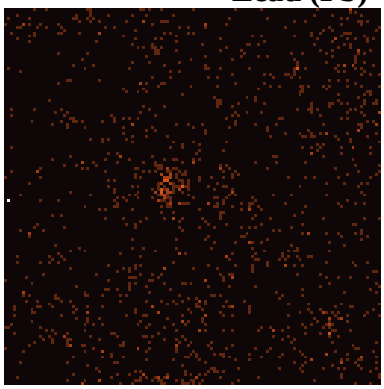

Silicon (Si)

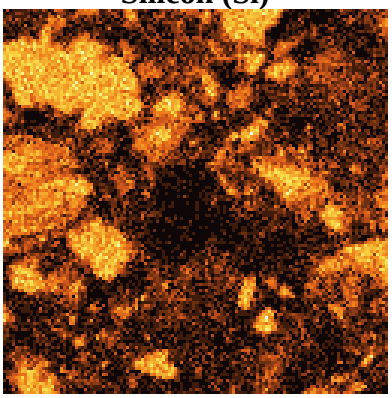

EDS Scan Images by Point

Point 1

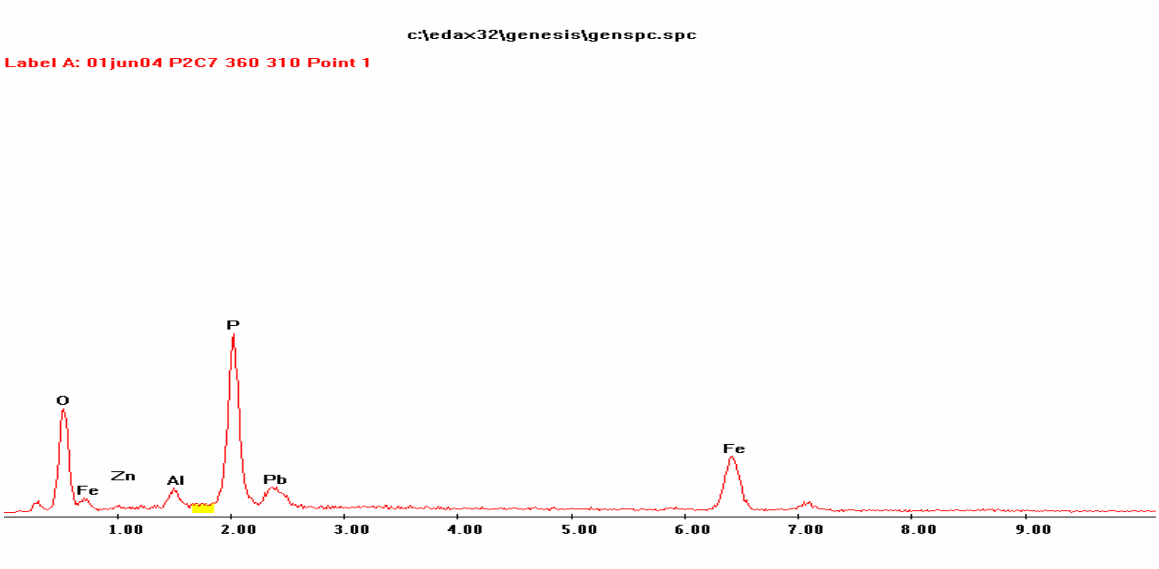

Point 2

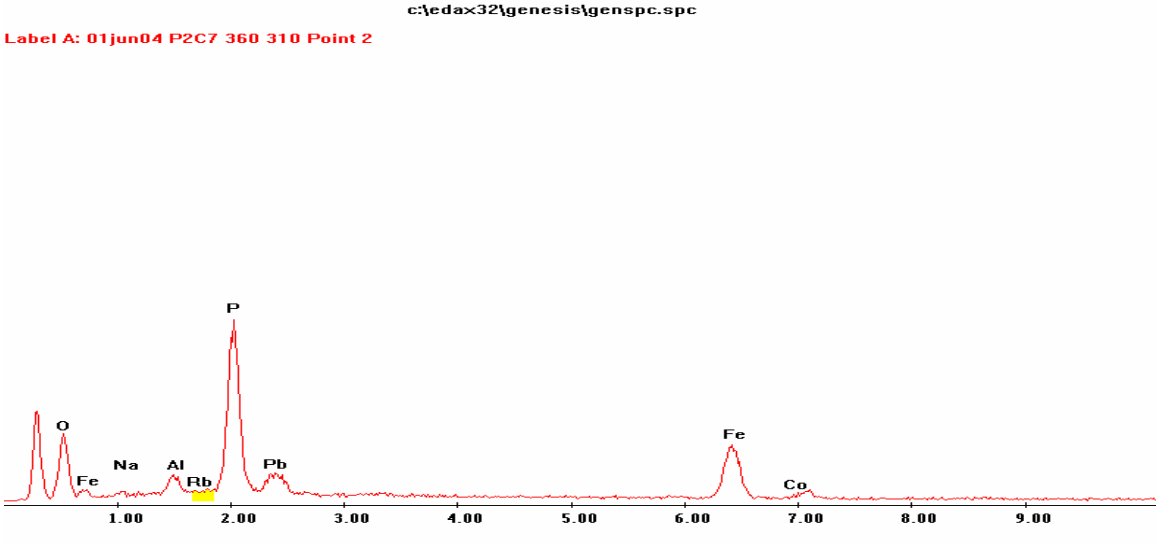

Point 3

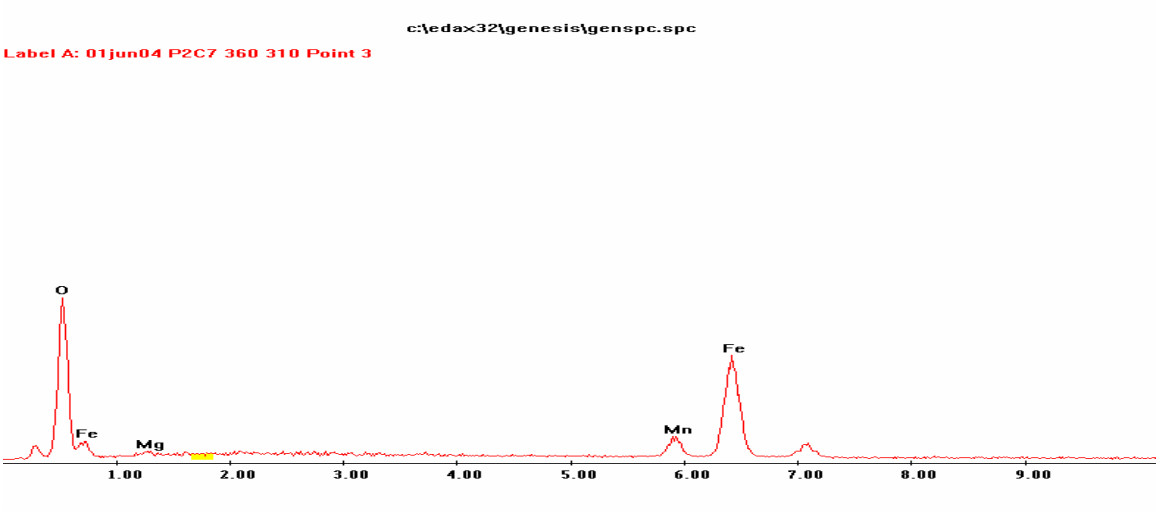

Point 4

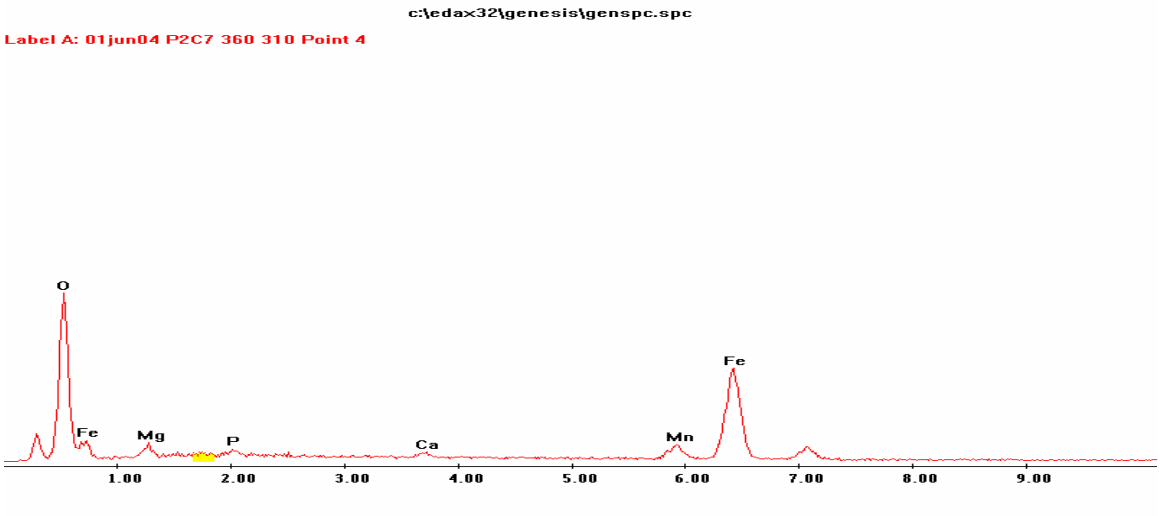

Point 5

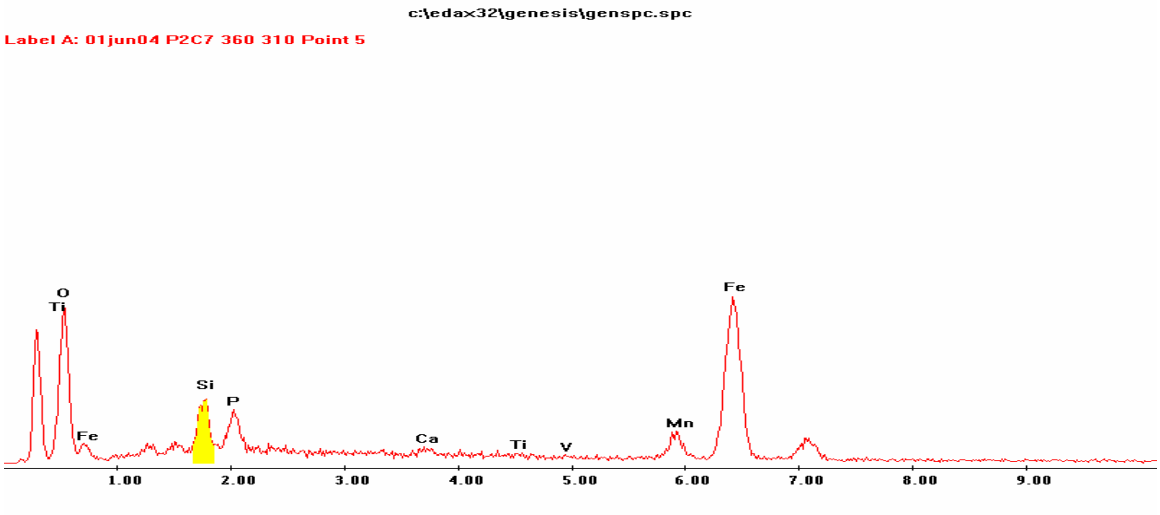

Point 6

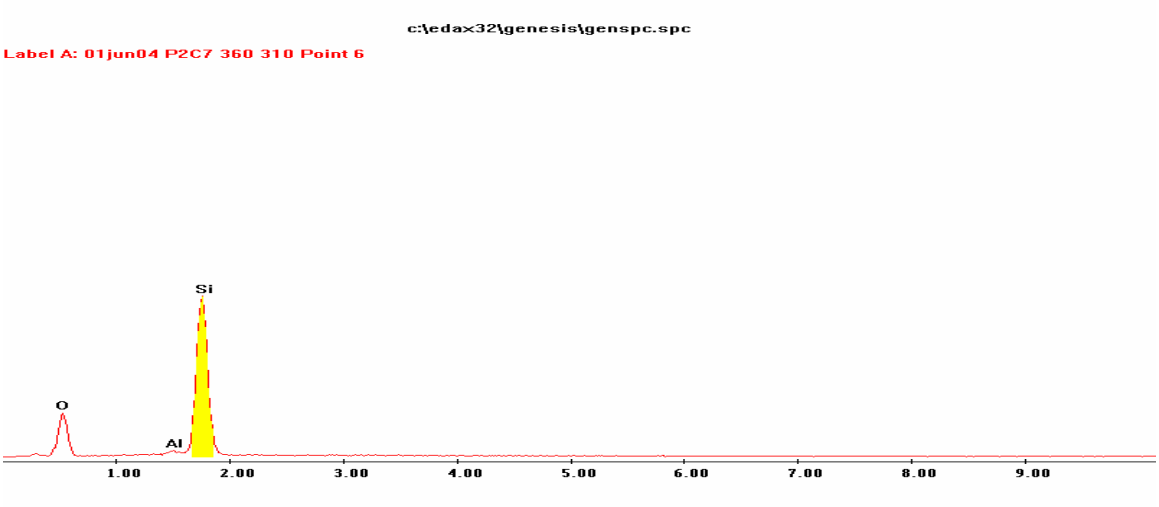

Point 7

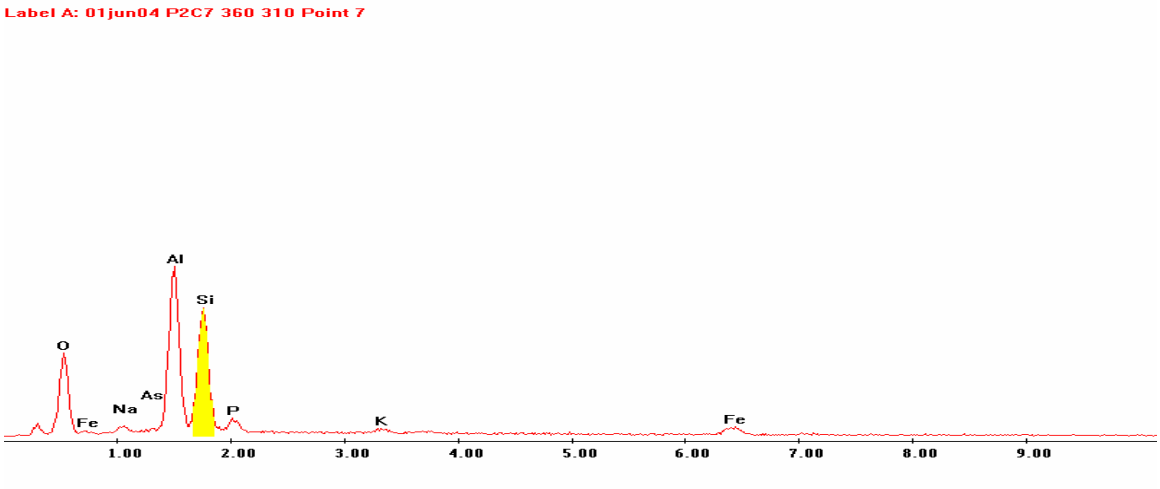

Point 8

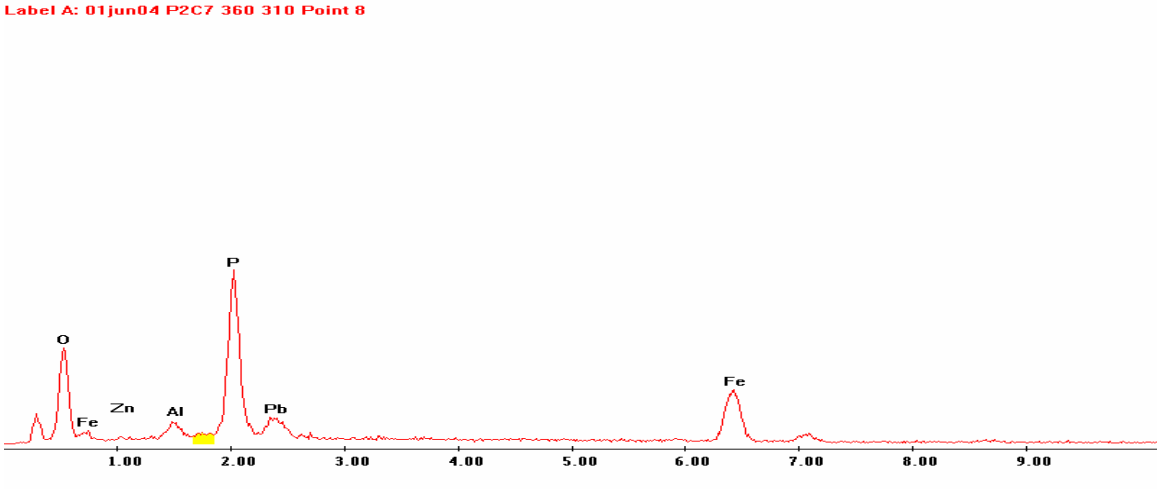

Point 9

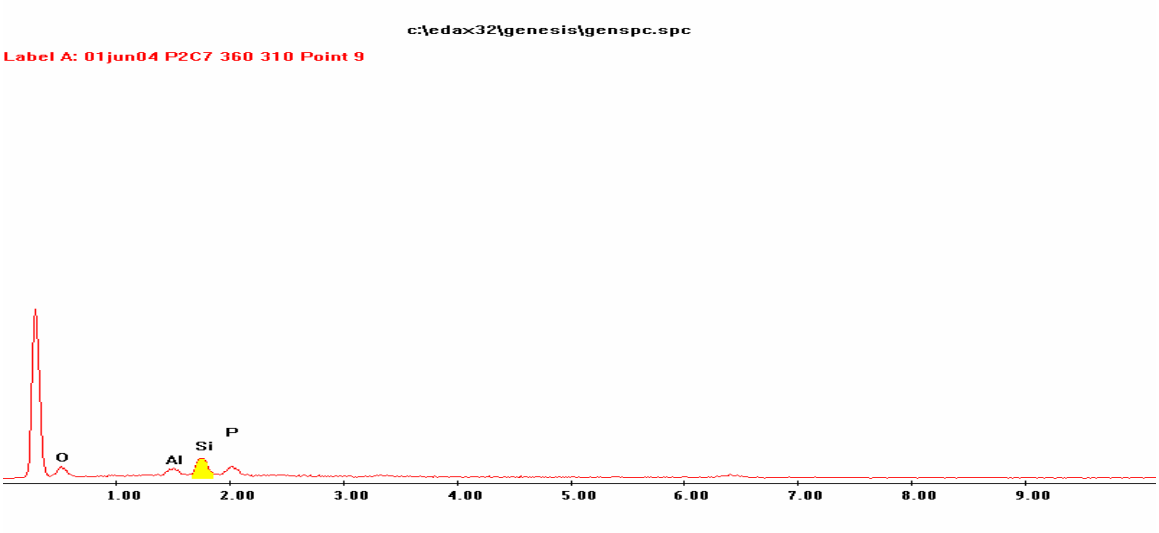

Point 10

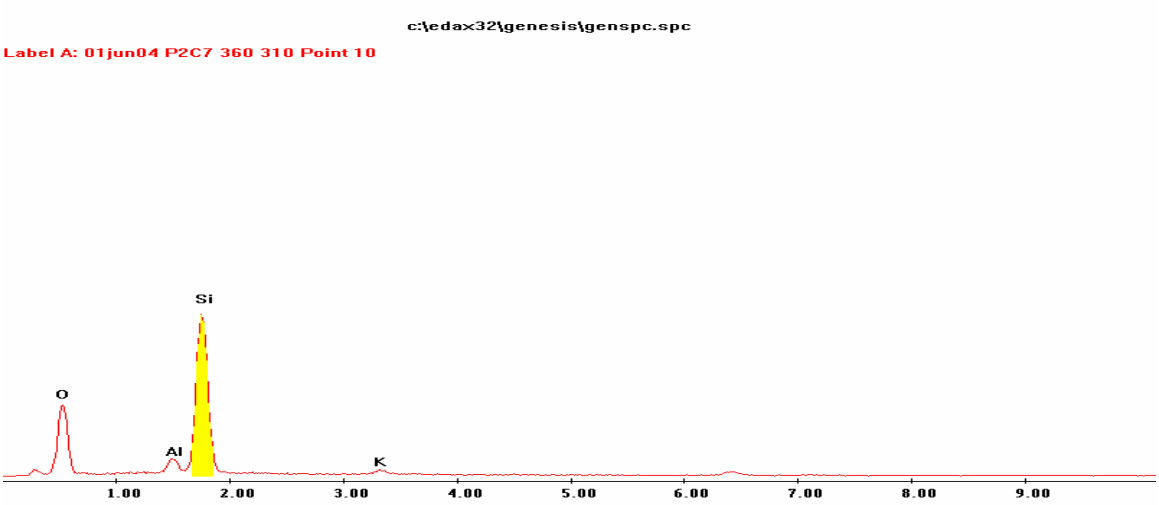

P2C7 – 441, 181

BSE Image

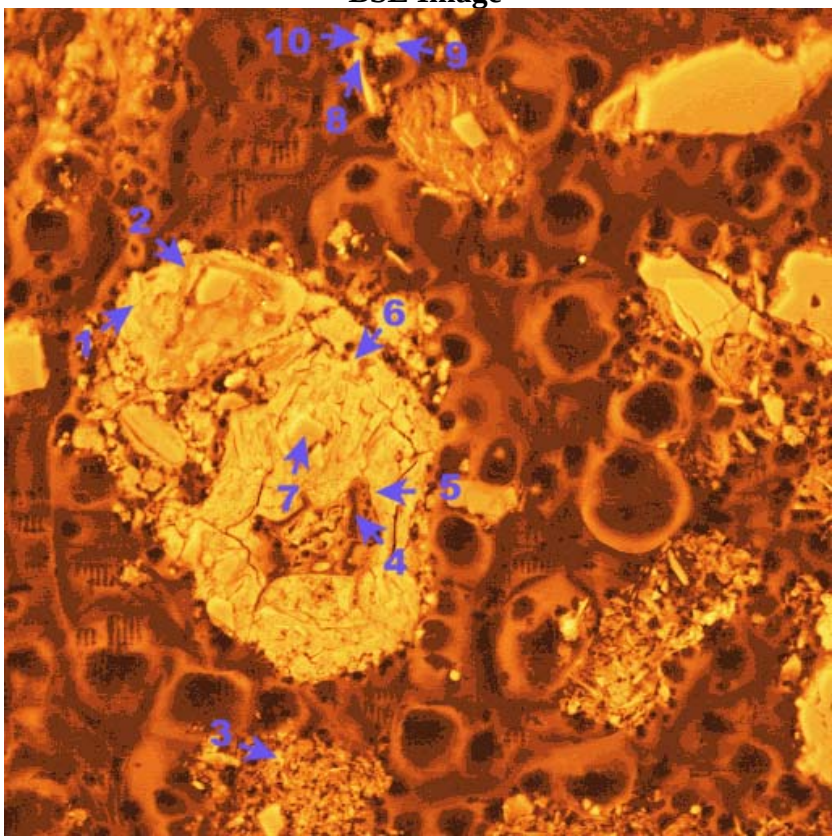

Iron (Fe)

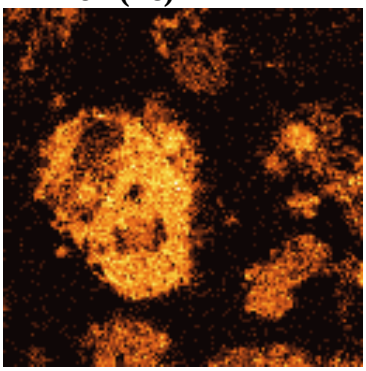

Manganese (Mn)

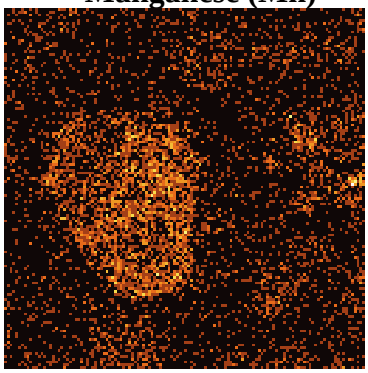

Phosphorous (P)

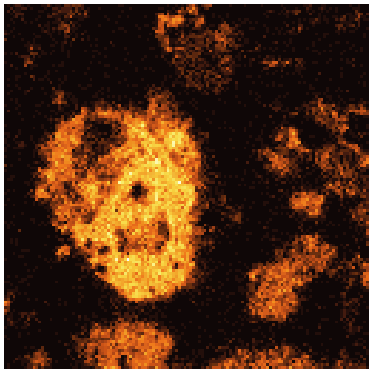

Lead (Pb)

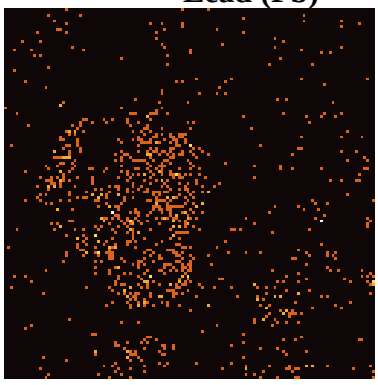

Silicon (Si)

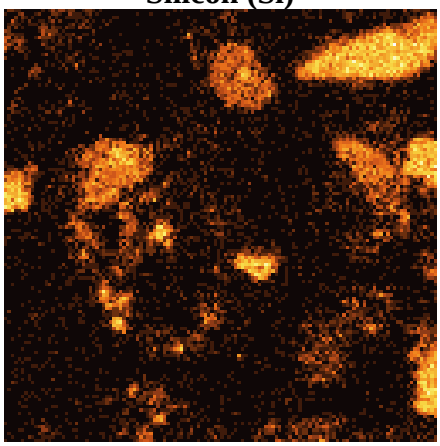

EDS Scan Images by Point

Point 1

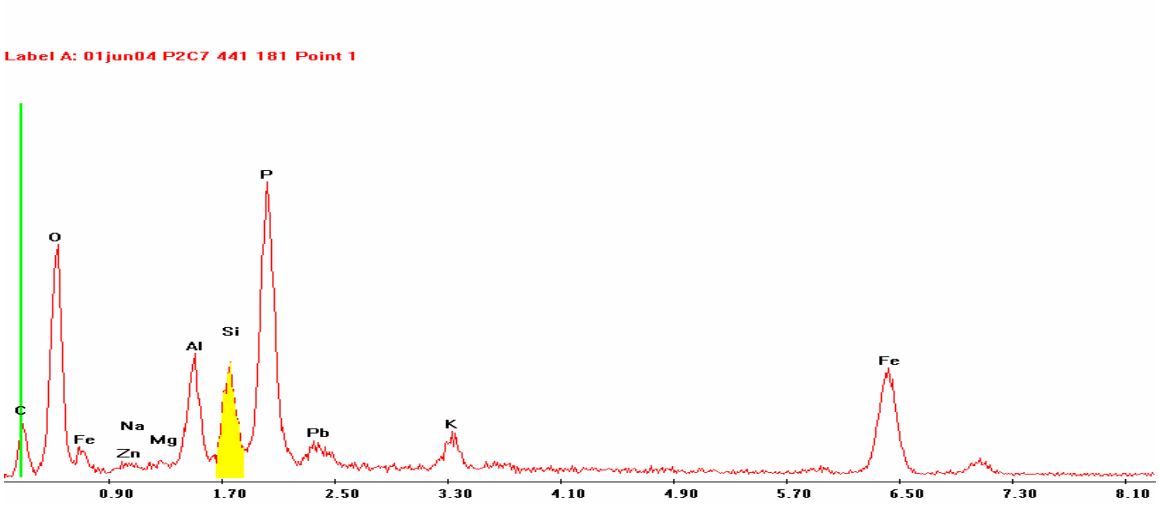

Point 2

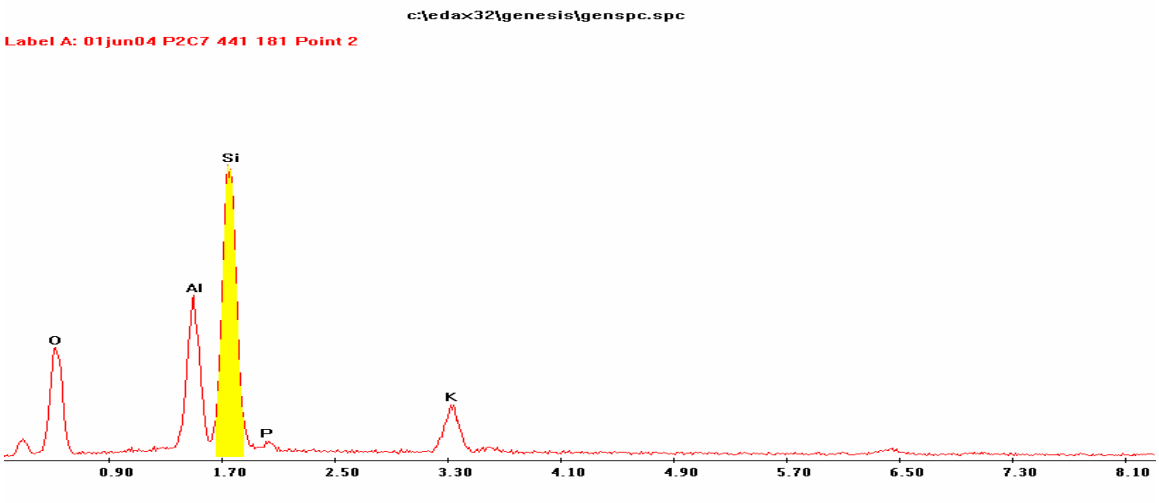

Point 3

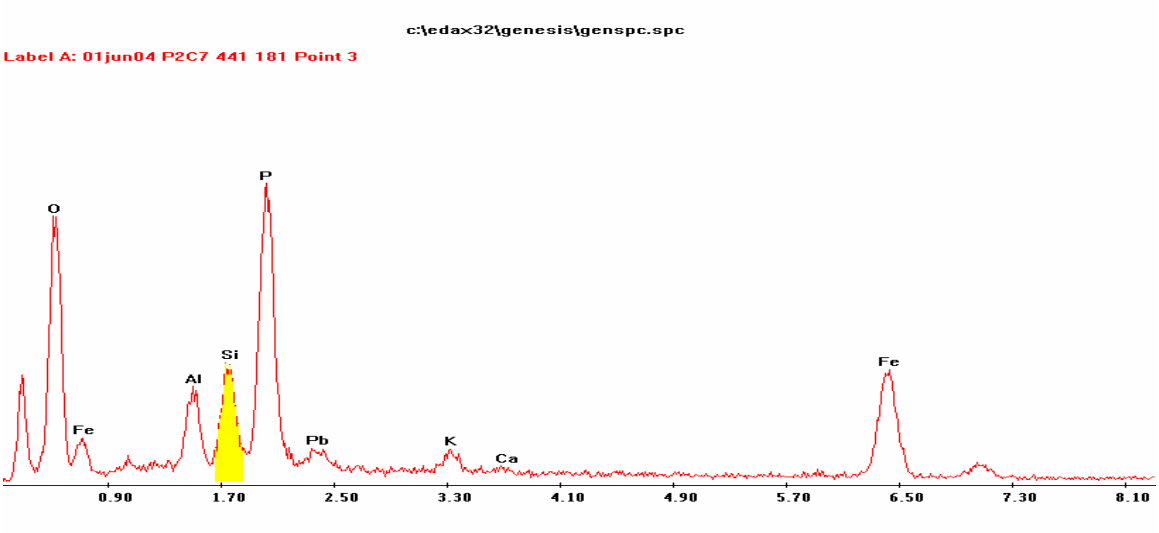

Point 4

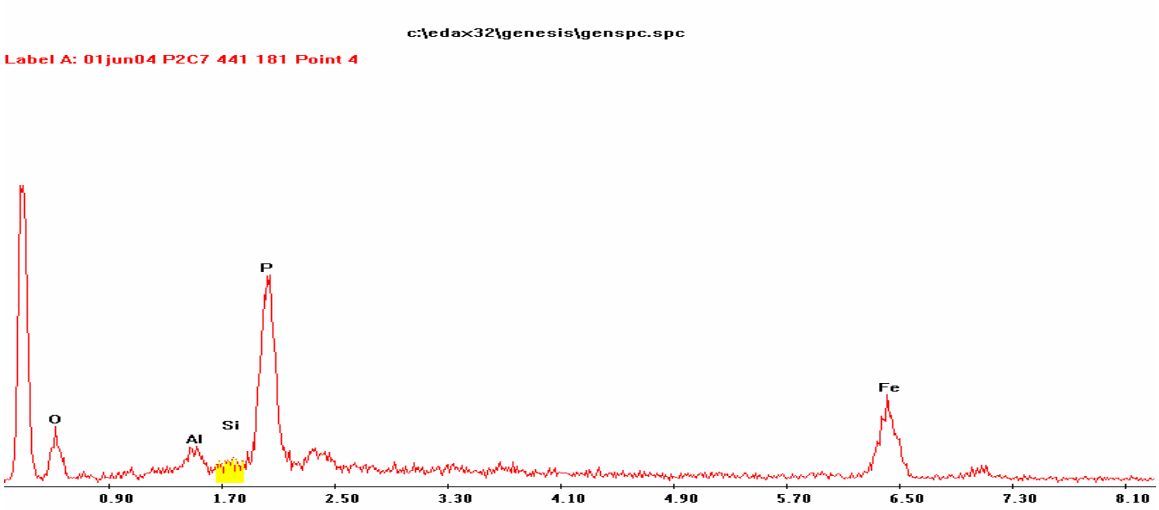

Point 5

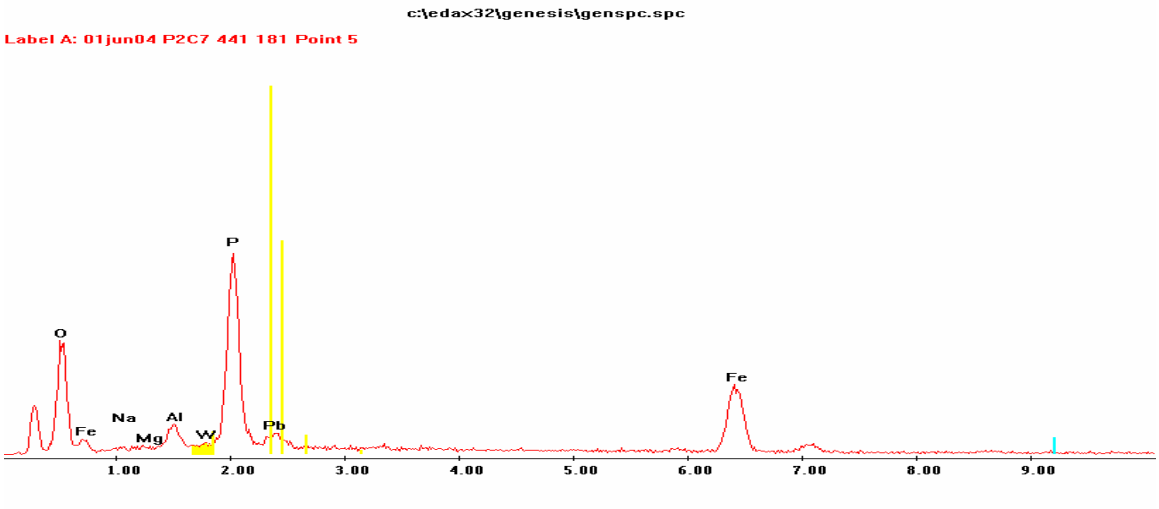

Point 6

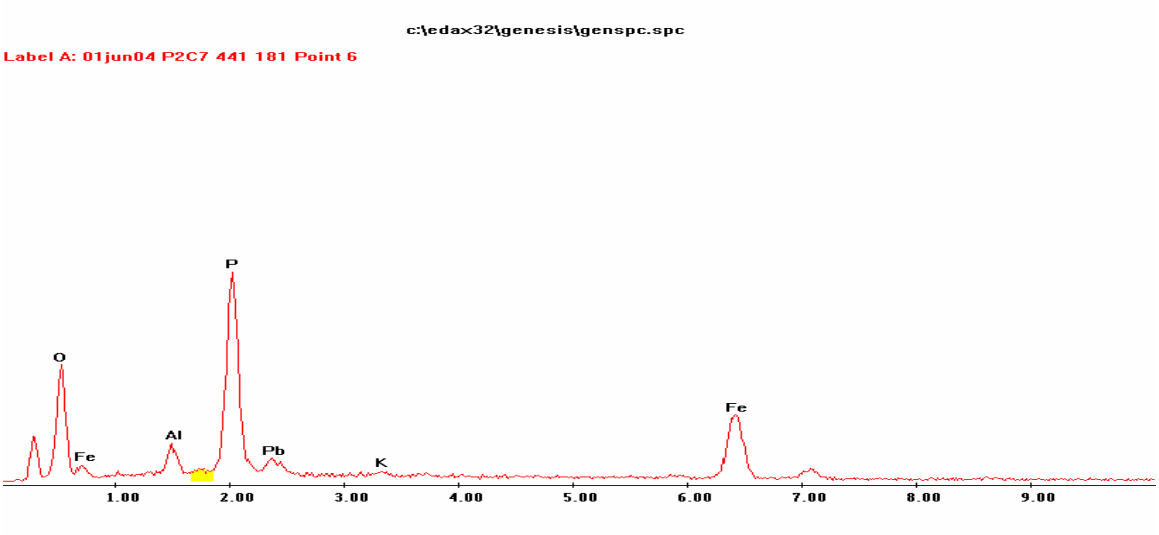

Point 7

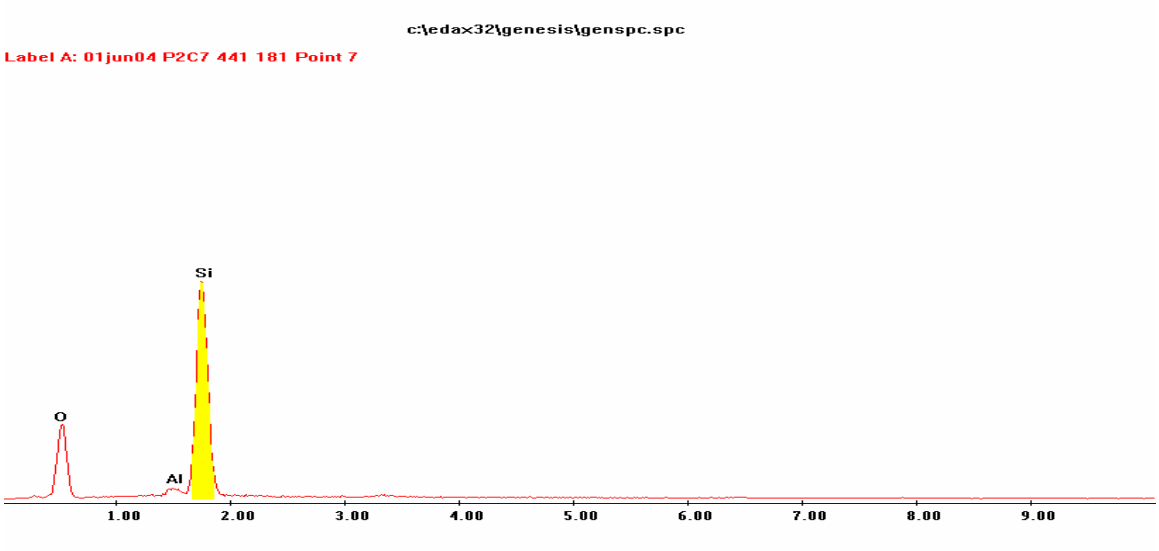

Point 8

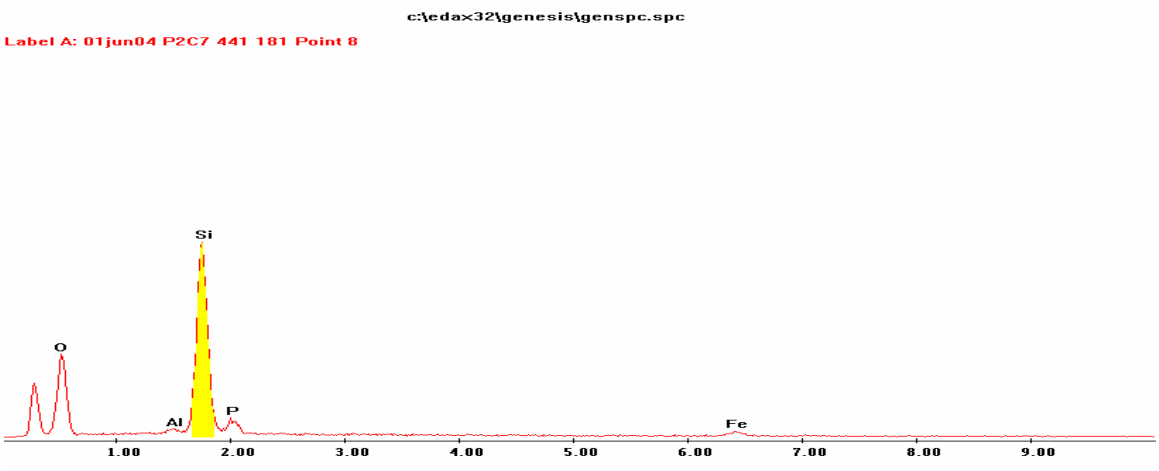

Point 9

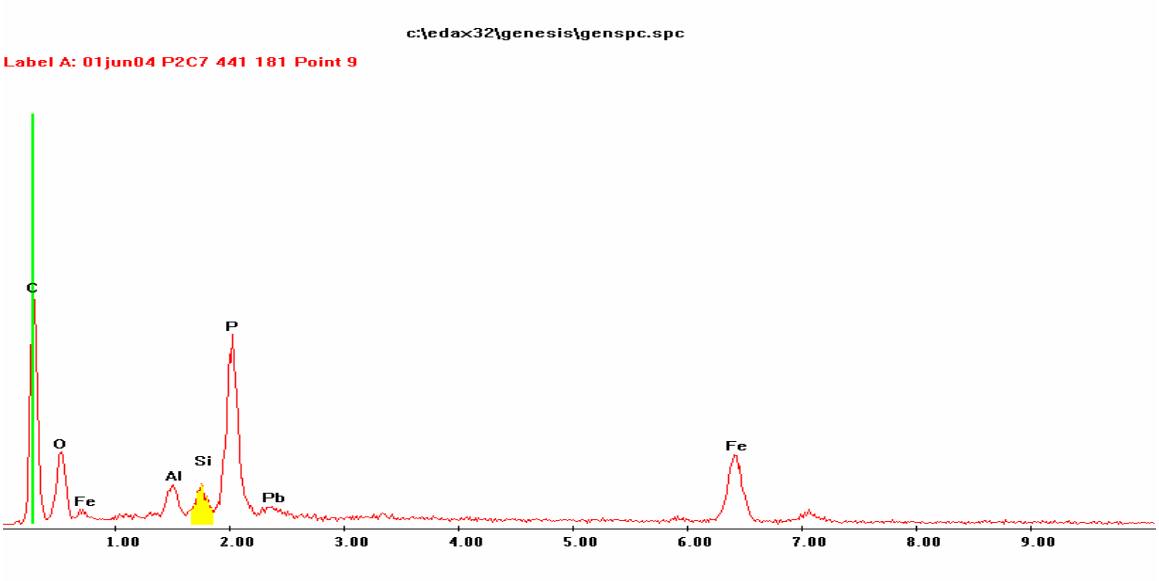

Point 10

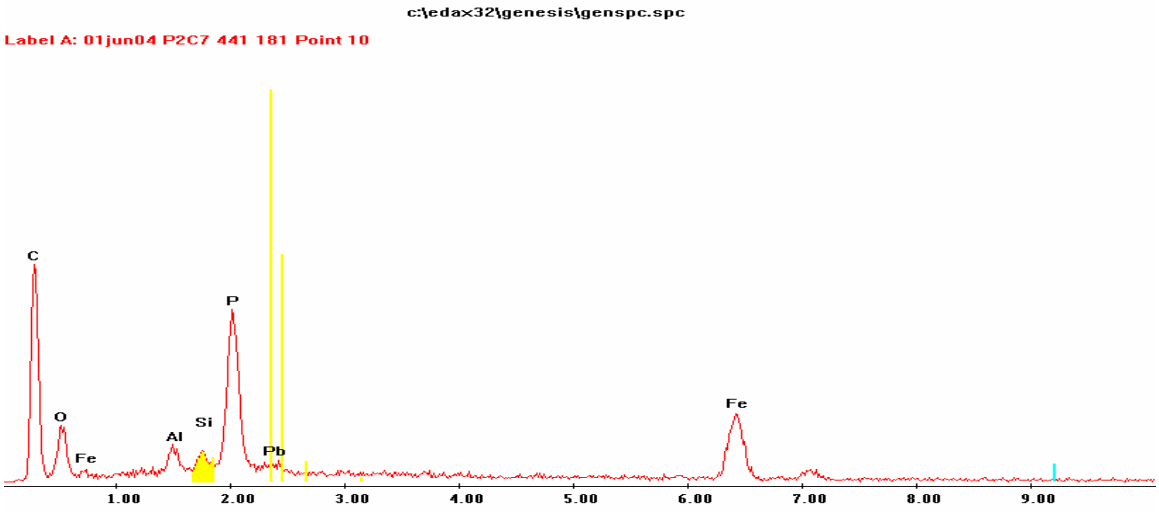

P2C7 – 447, 145

BSE Image

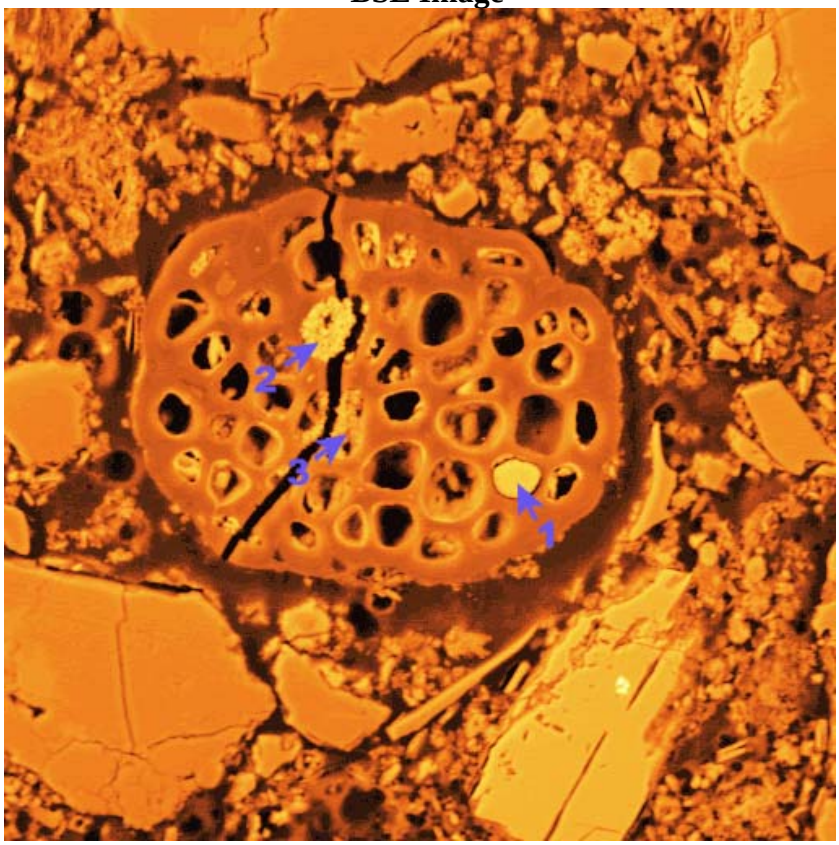

Iron (Fe)

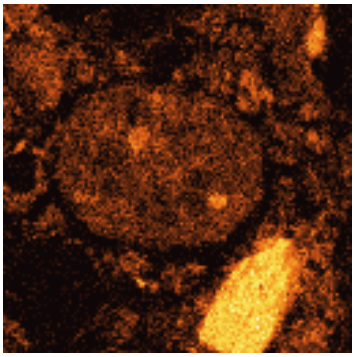

Manganese (Mn)

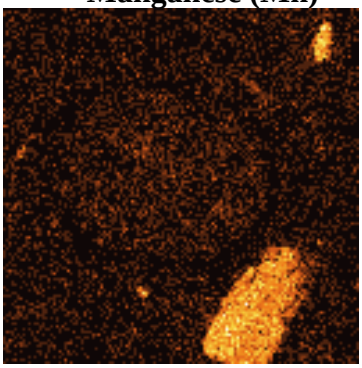

Phosphorous (P)

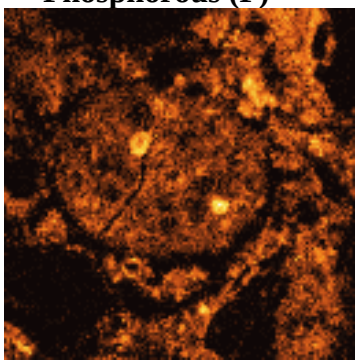

Lead (Pb)

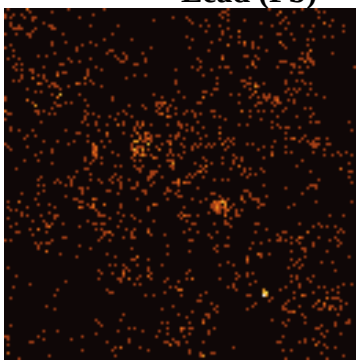

Silicon (Si)

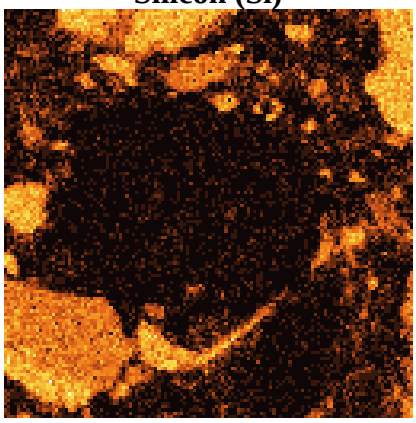

EDS Scan Images by Point

Point 1

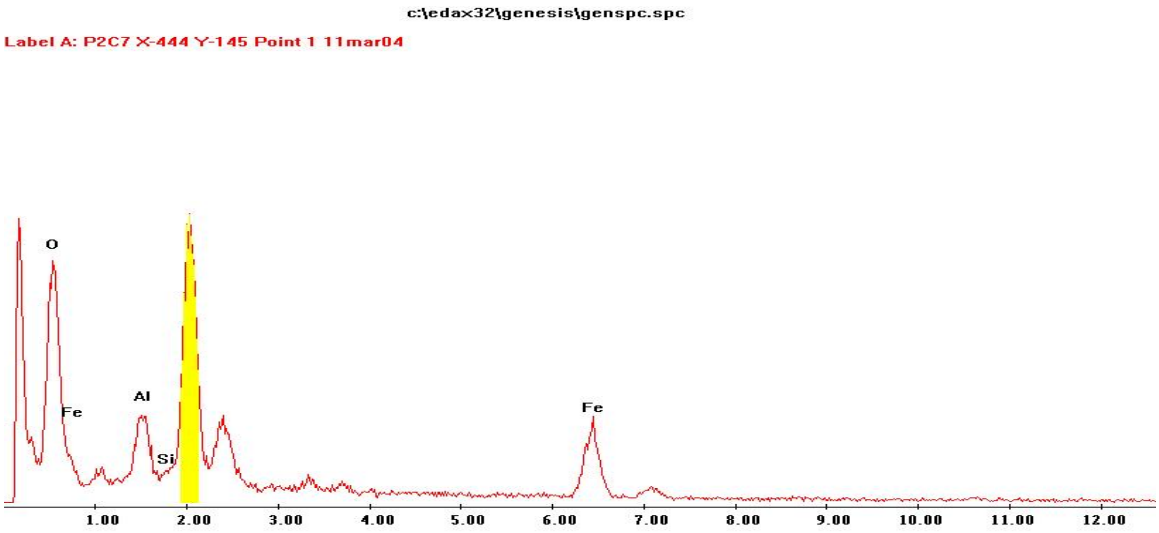

Point 2

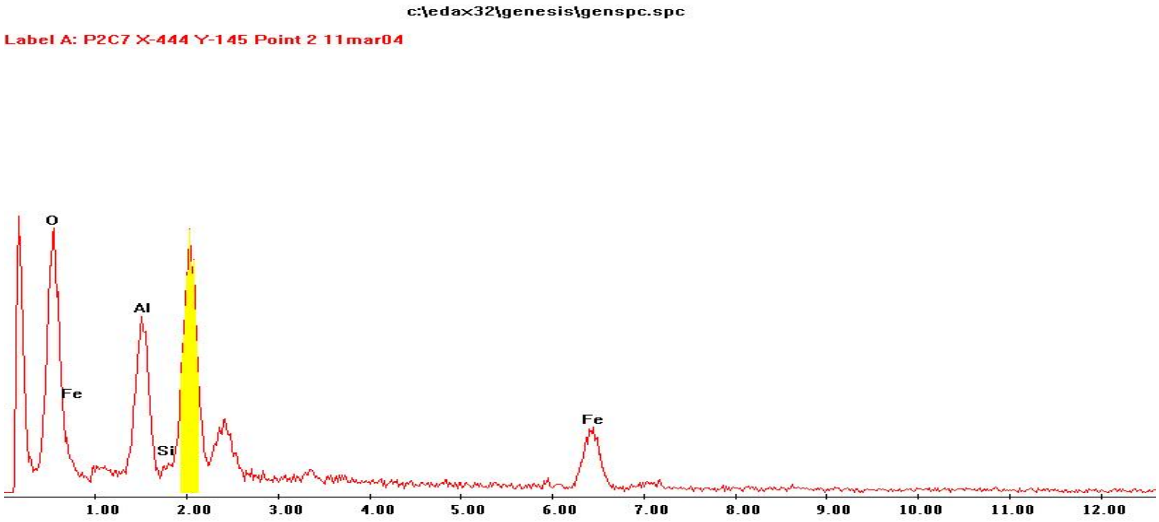

Point 3

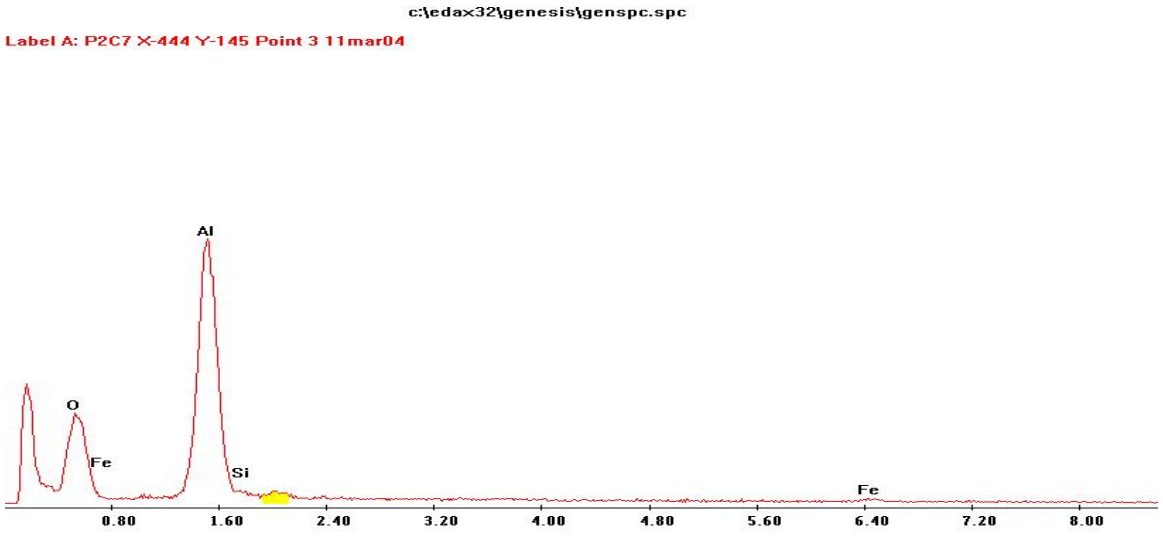
c:\edax32\genesis\genspc.spc
Label A: P2C7 X-444 Y-145 Point 3 11mar04
Al
O
Fe
Si
Fe
0.80
1.60
2.40
3.20
4.00
4.80
5.60
6.40
7.20
8.00

P2C7 – 369, 291

BSE Image

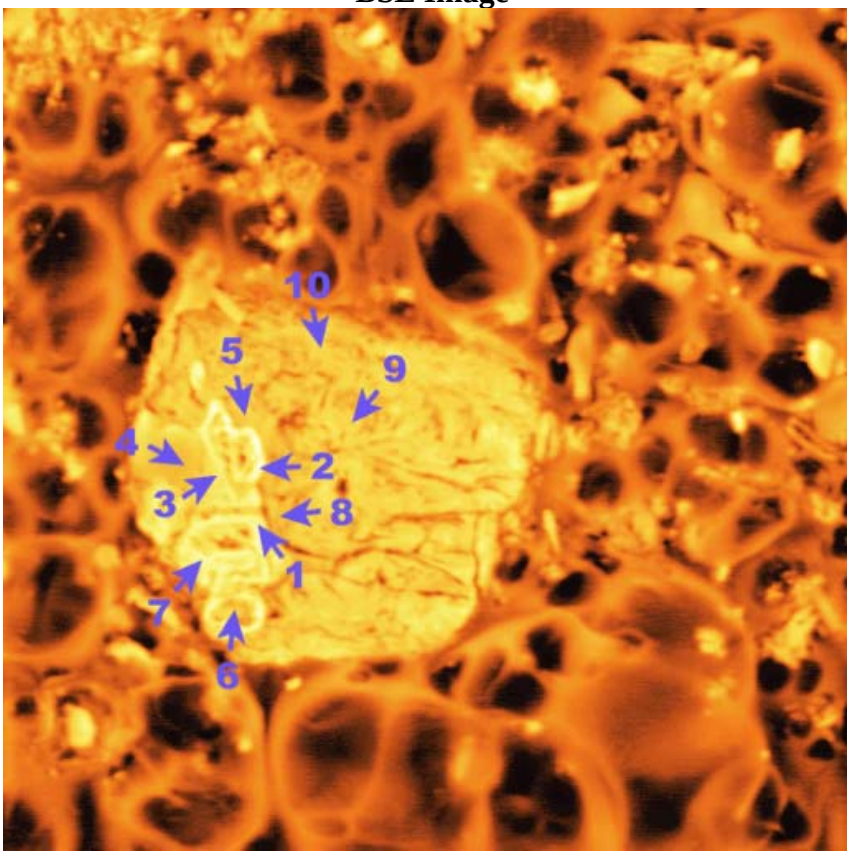

Iron (Fe)

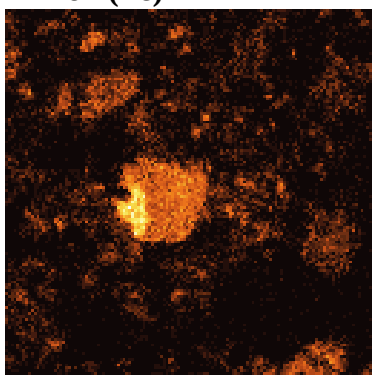

Manganese (Mn)

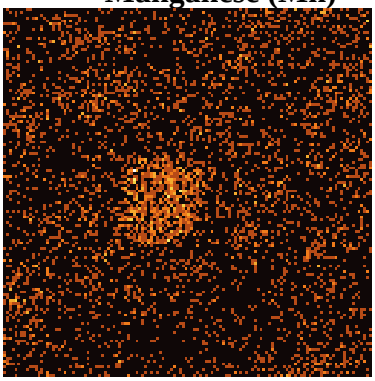

Phosphorous (P)

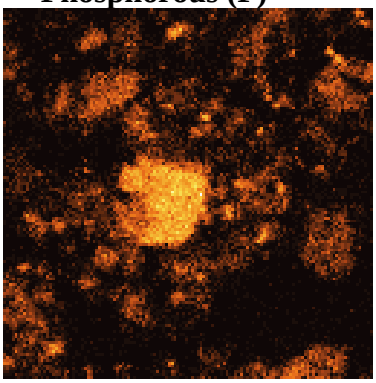

Lead (Pb)

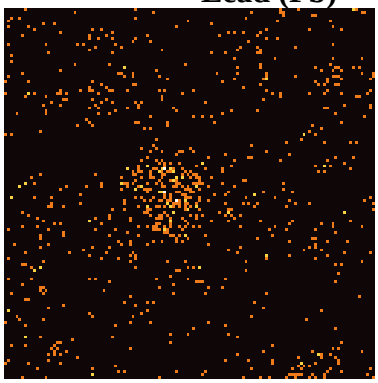

Silicon (Si)

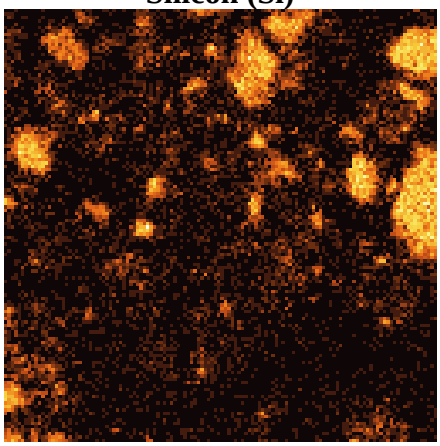

EDS Scan Images by Point

Point 1

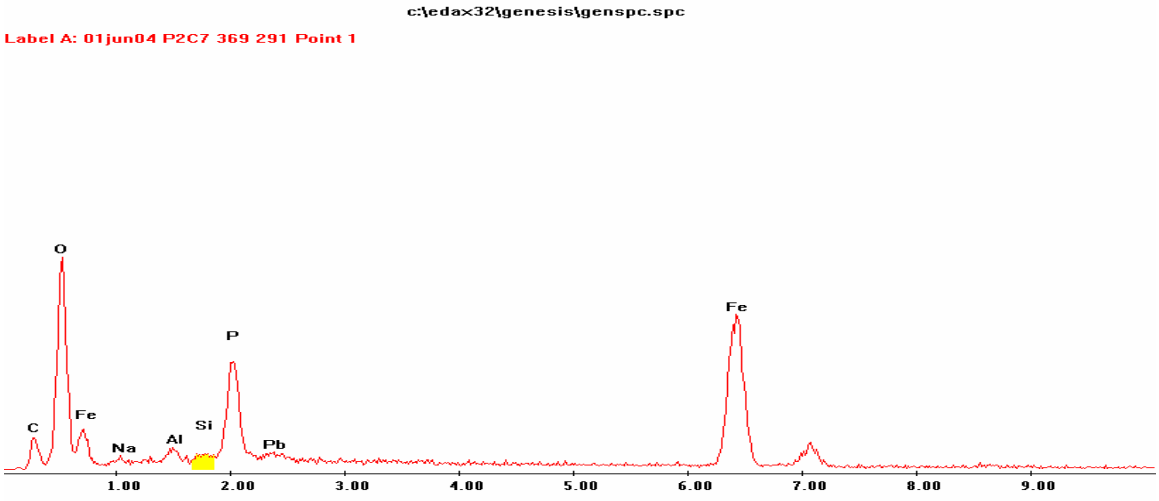

Point 2

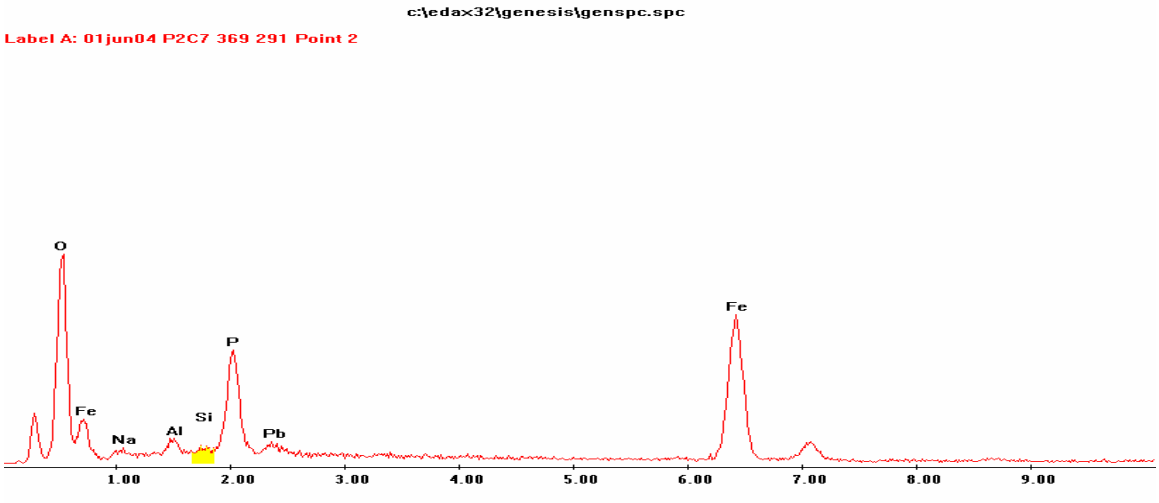

Point 3

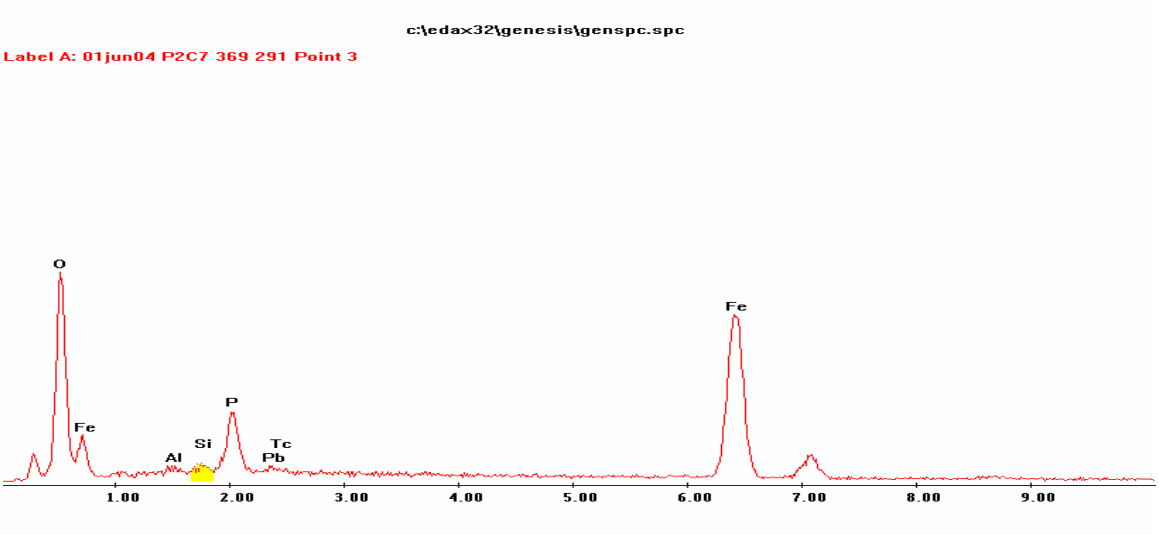

Point 4

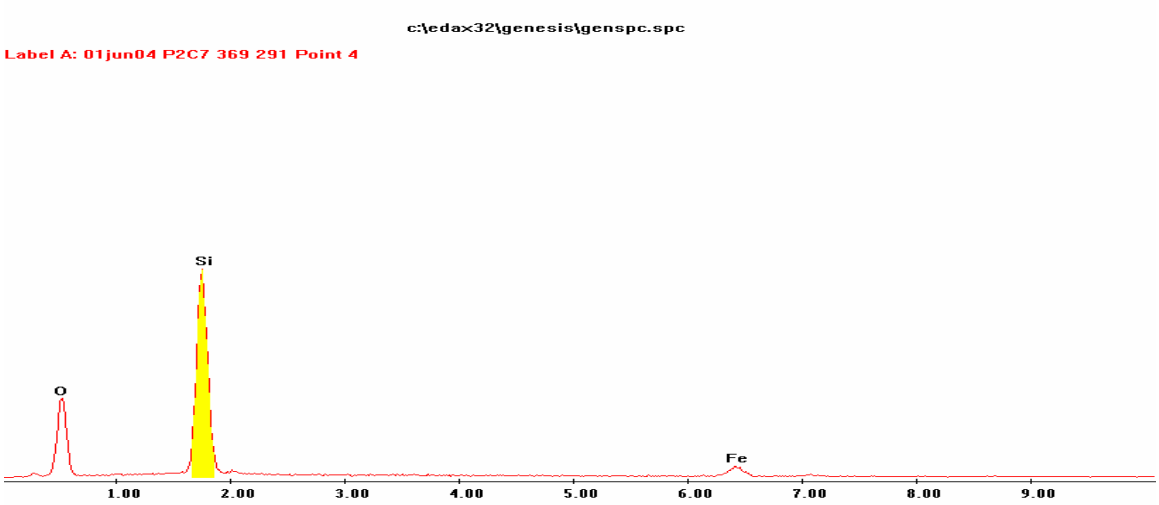

Point 5

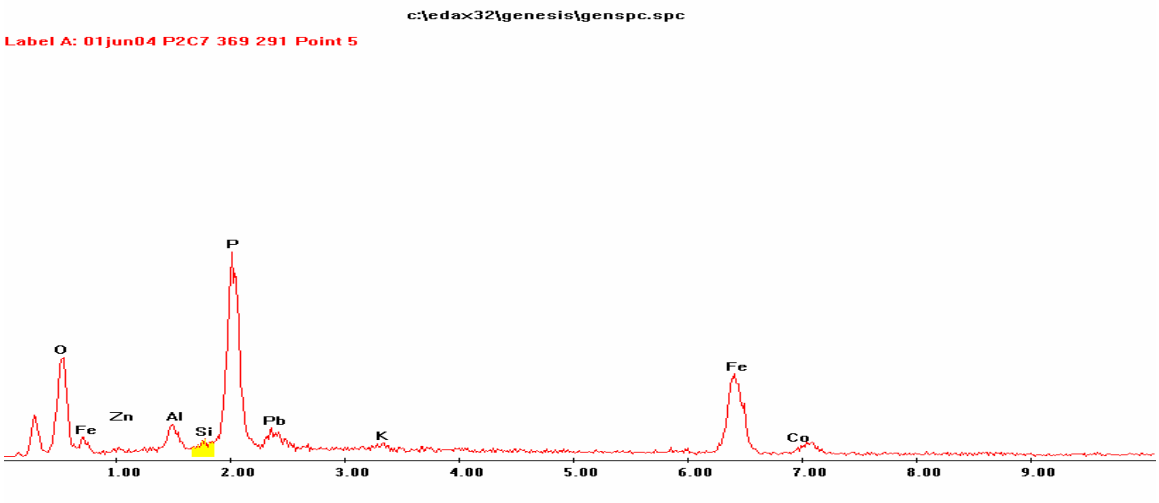

Point 6

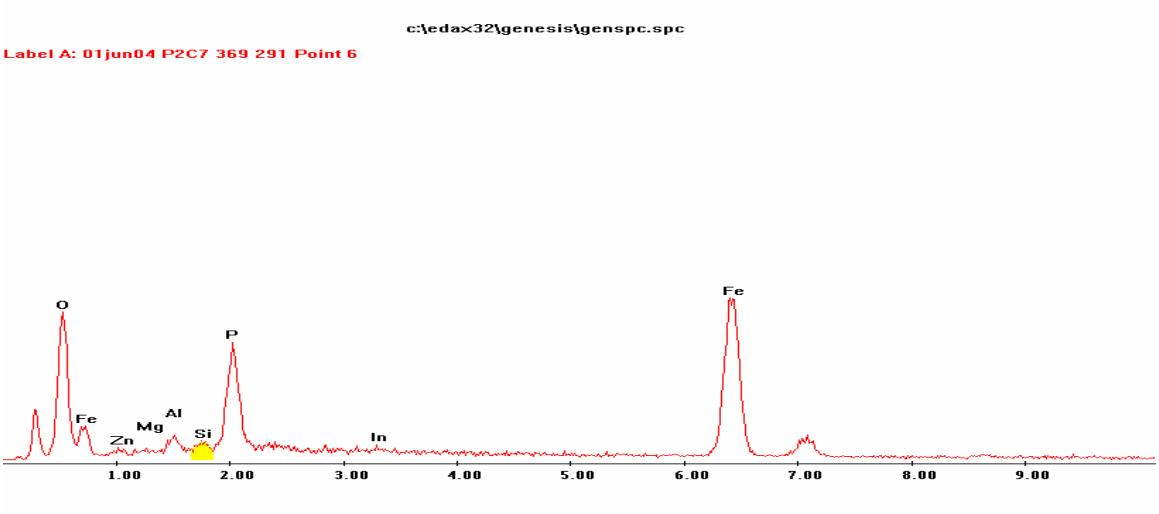

Point 7

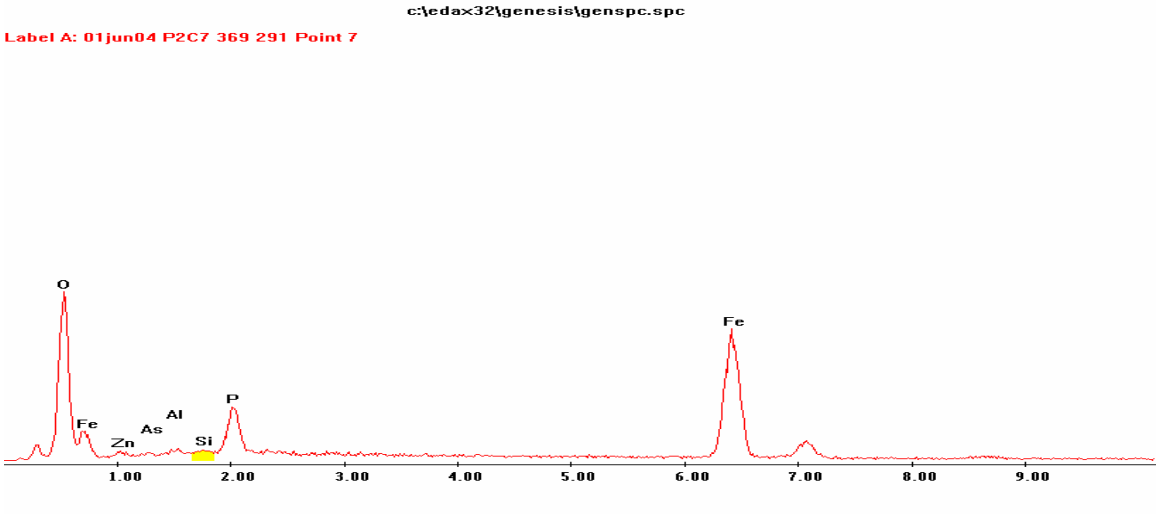

Point 8

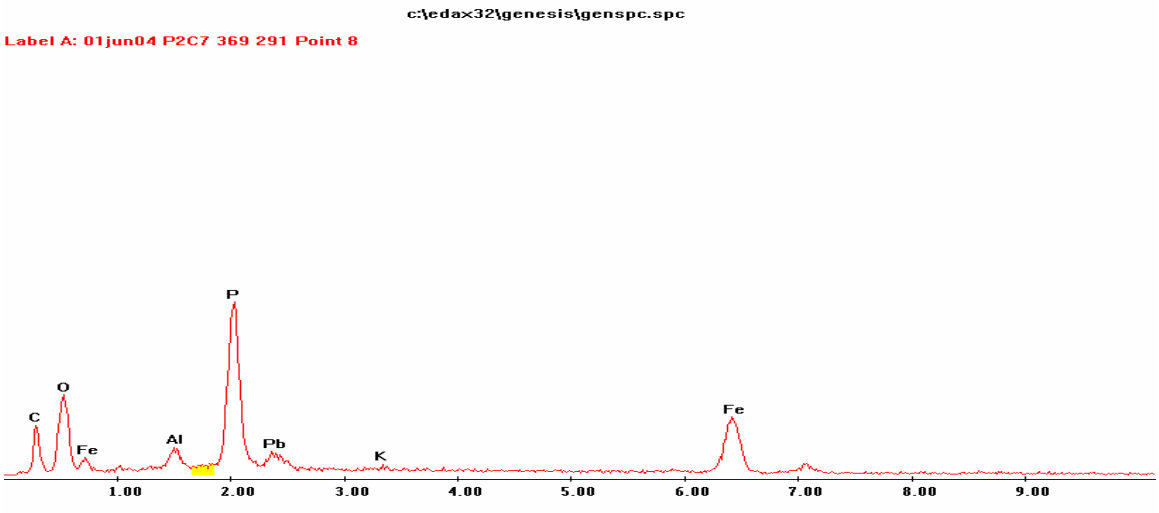

Point 9

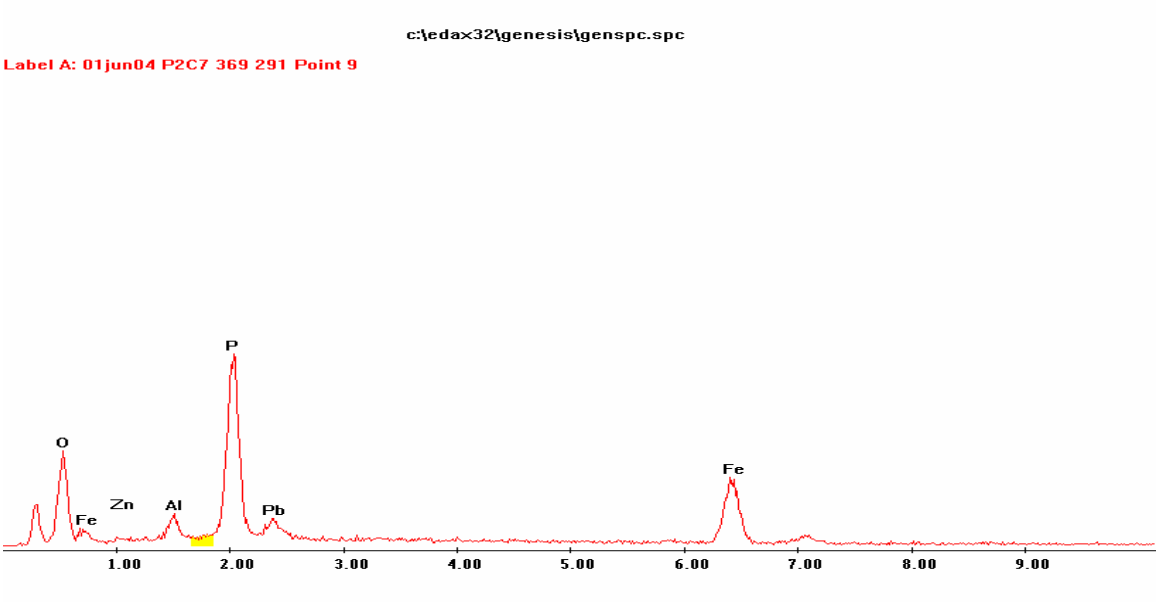

Point 10

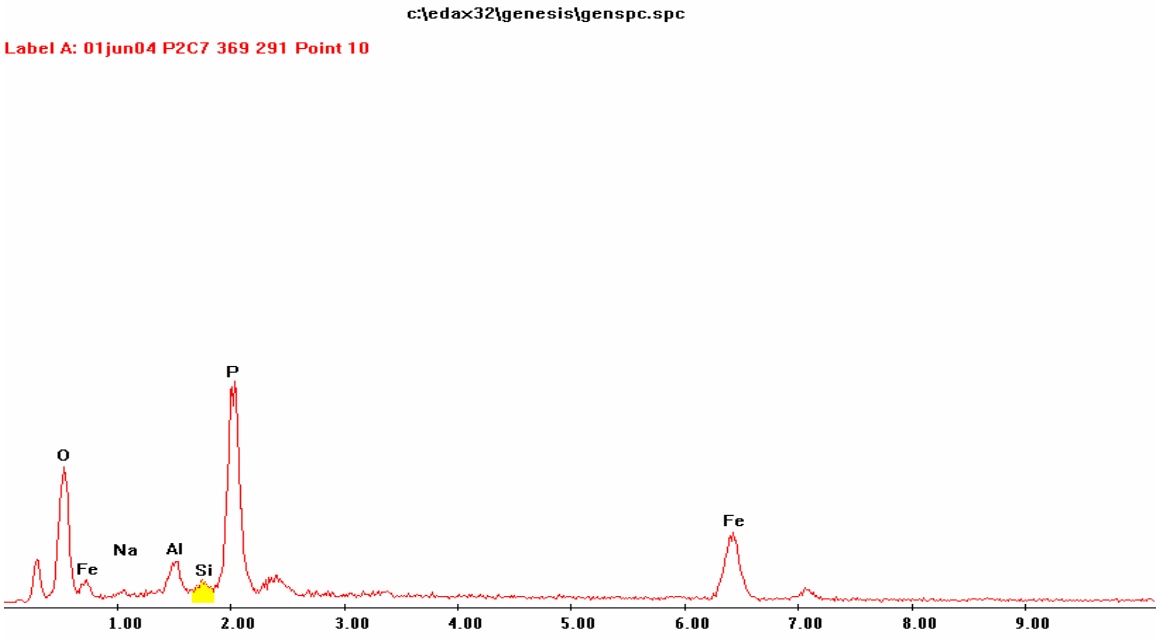

P2C8 – 303, 178

BSE Image

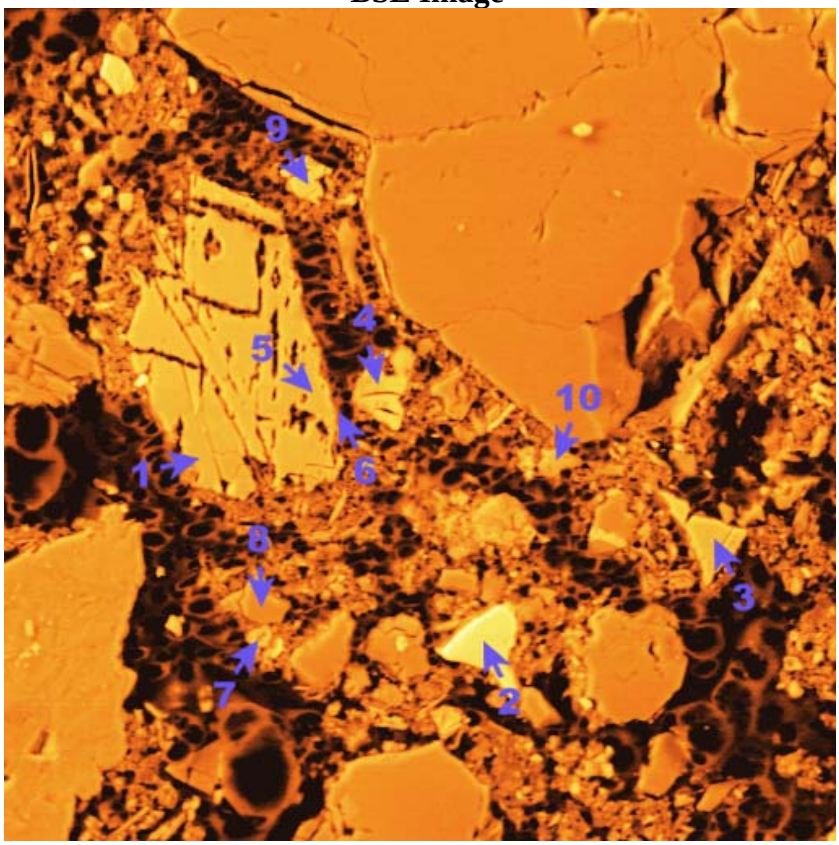

Iron (Fe)

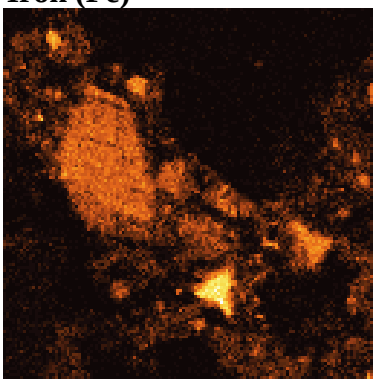

Manganese (Mn)

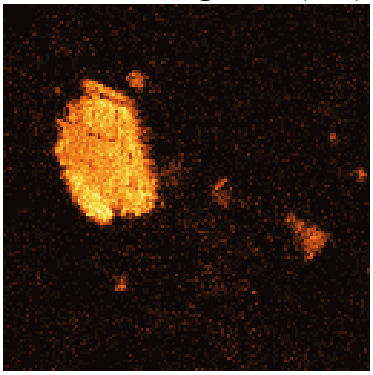

Phosphorous (P)

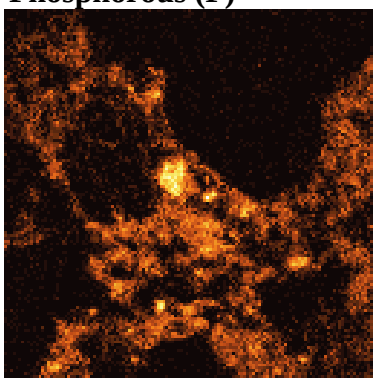

Lead (Pb)

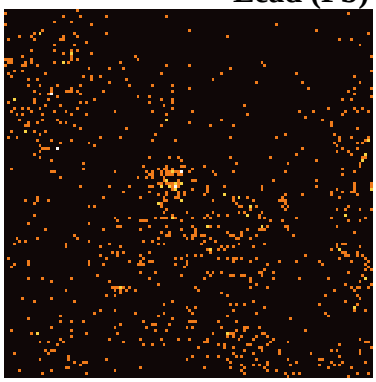

Silicon (Si)

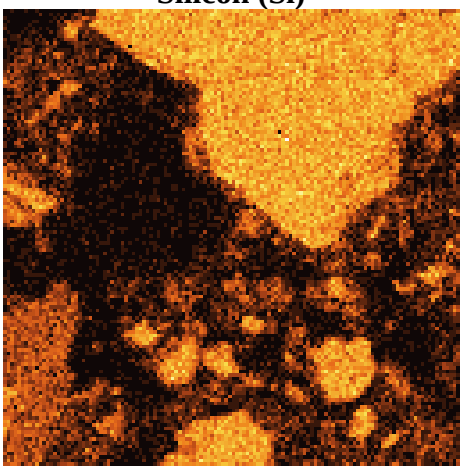

EDS Scan Images by Point

Point 1

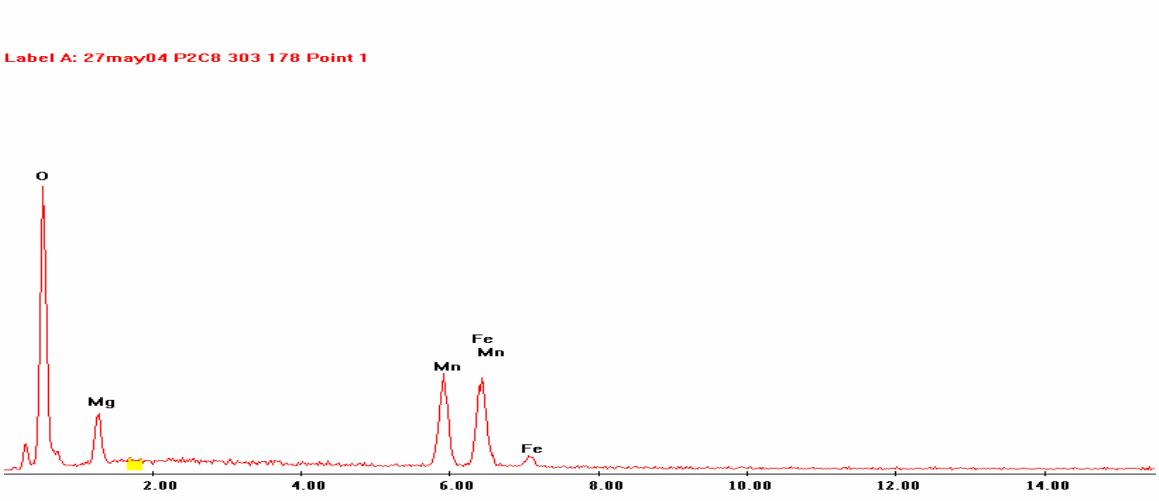

Point 2

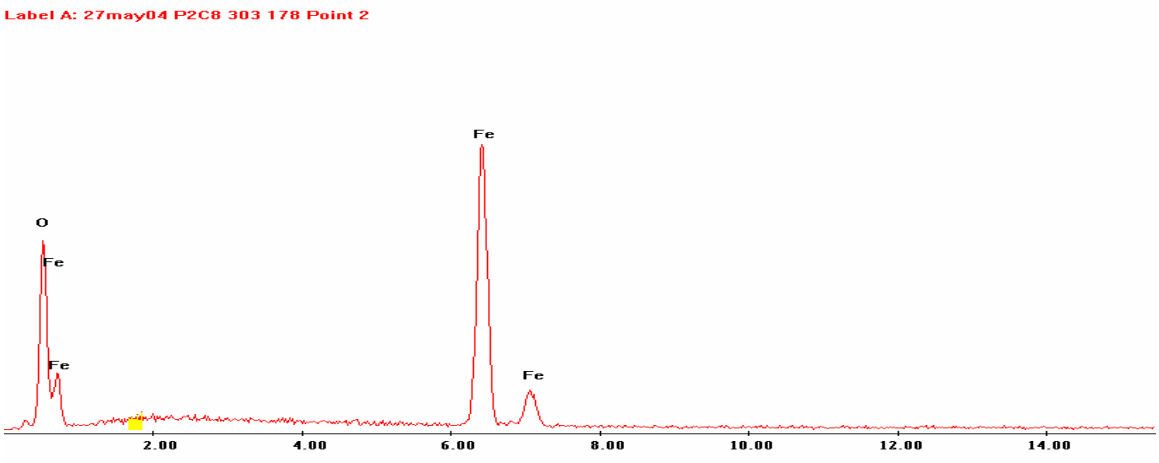

Point 3

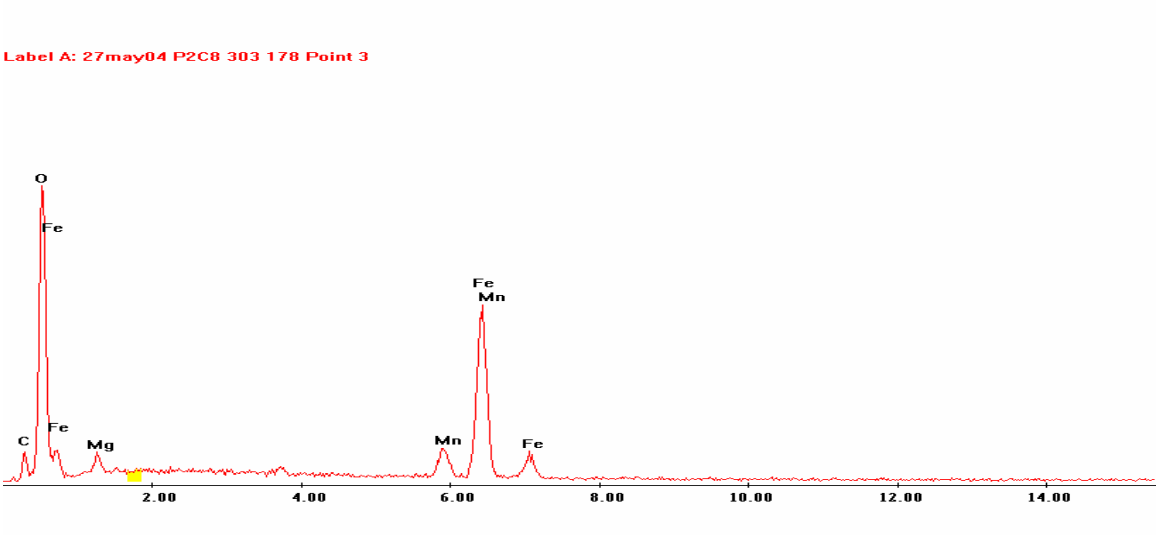

Point 4

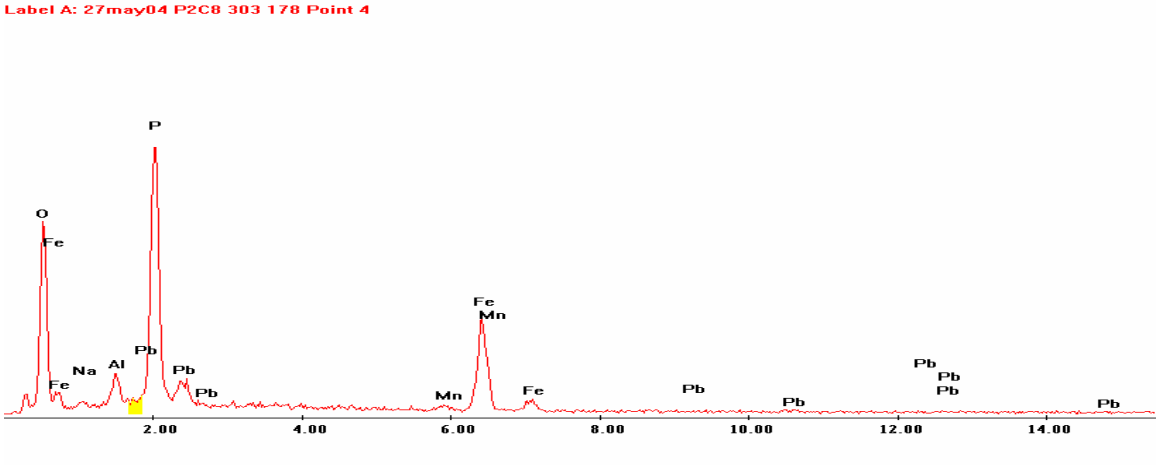

Point 5

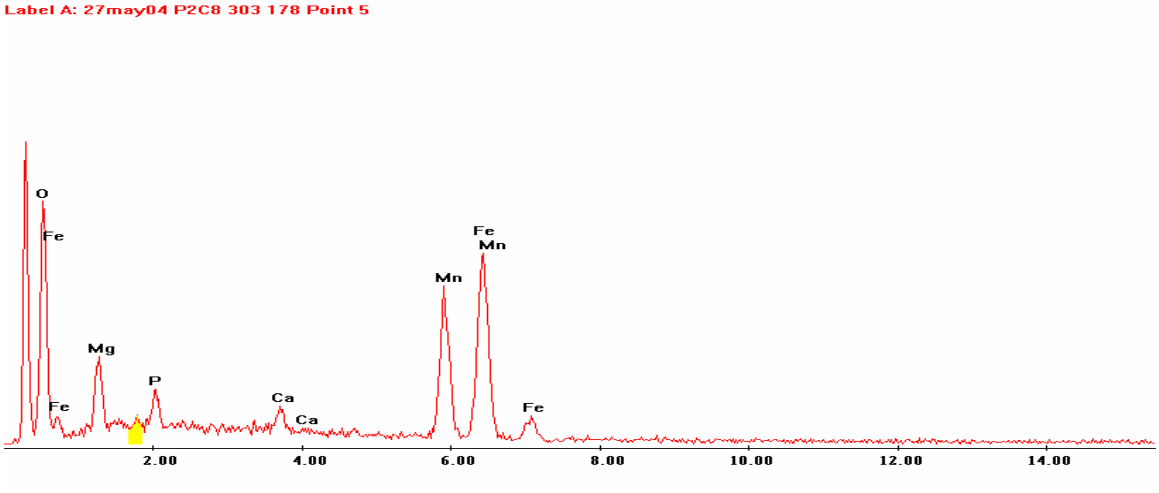

Point 6

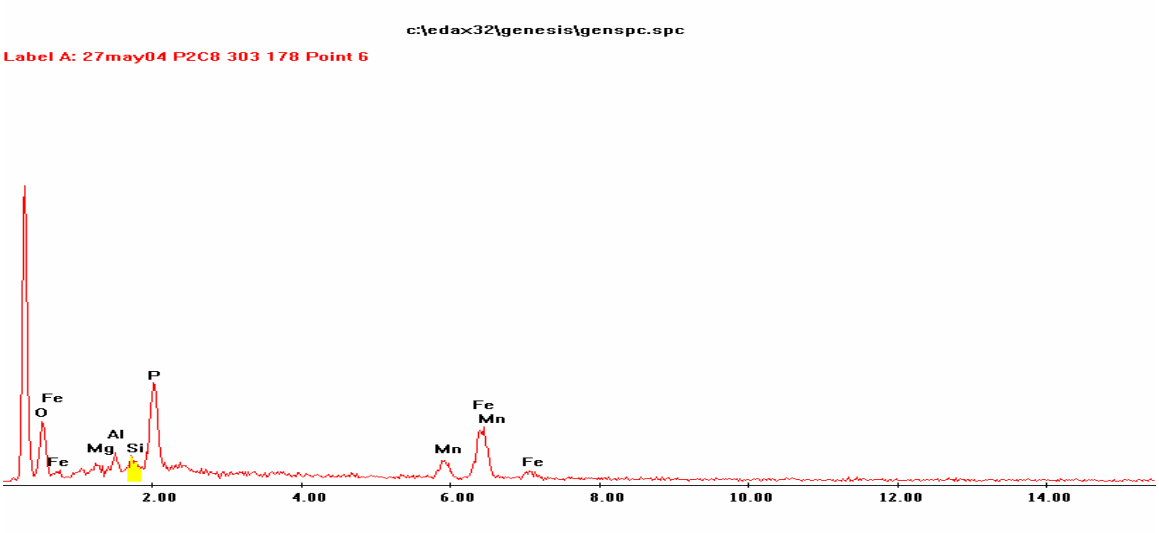

Point 7

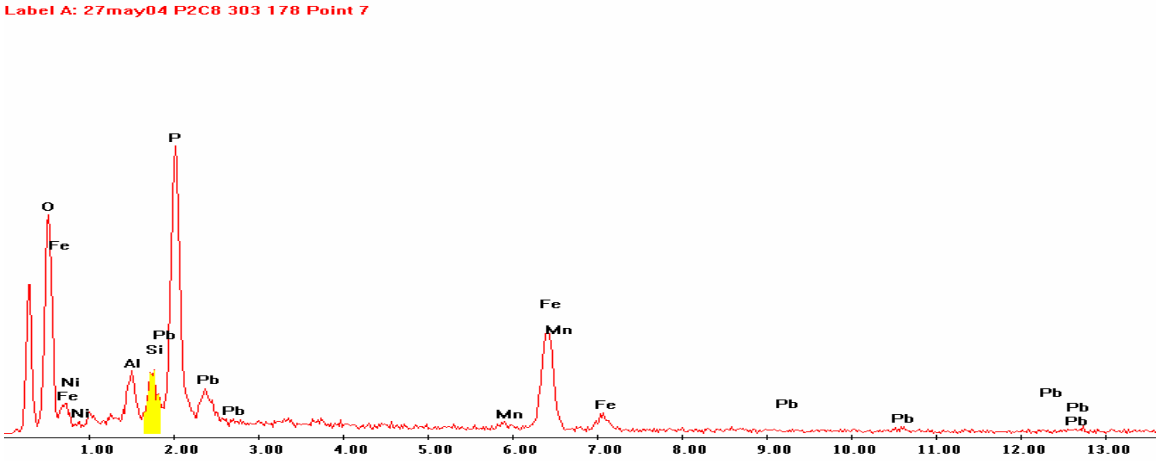

Point 8

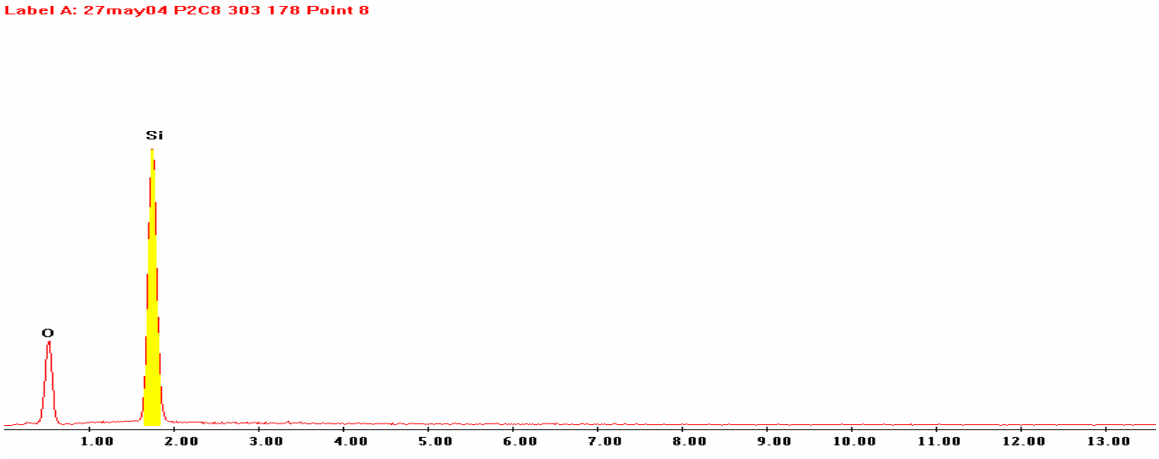

Point 9

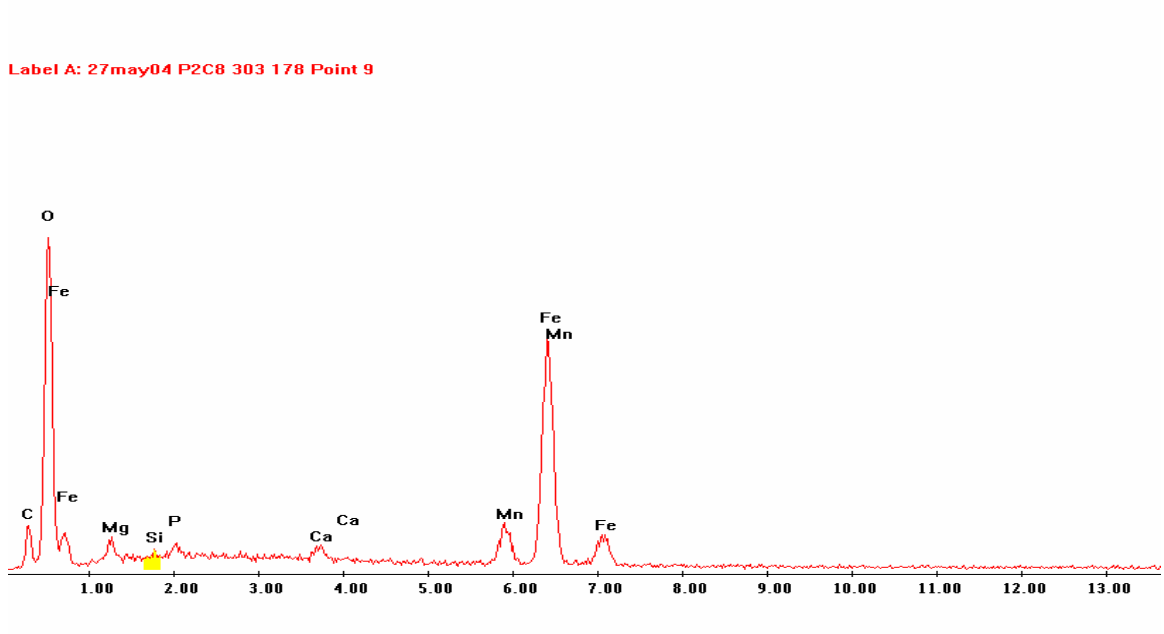

Point 10

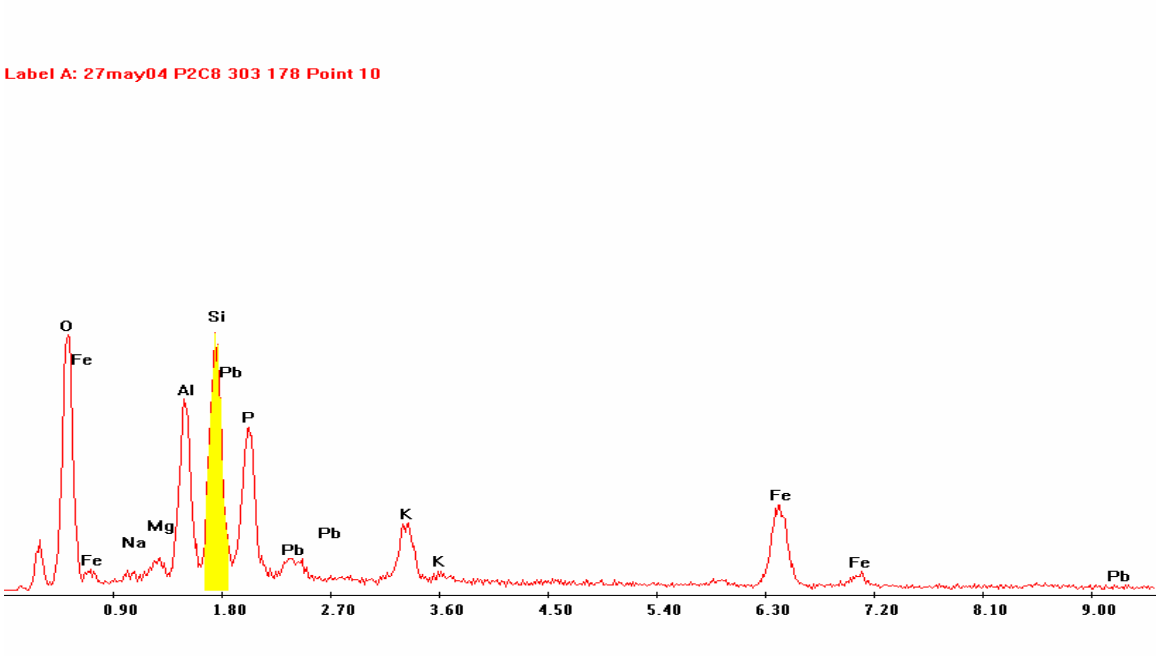

P2C8 – 314, 272

BSE Image

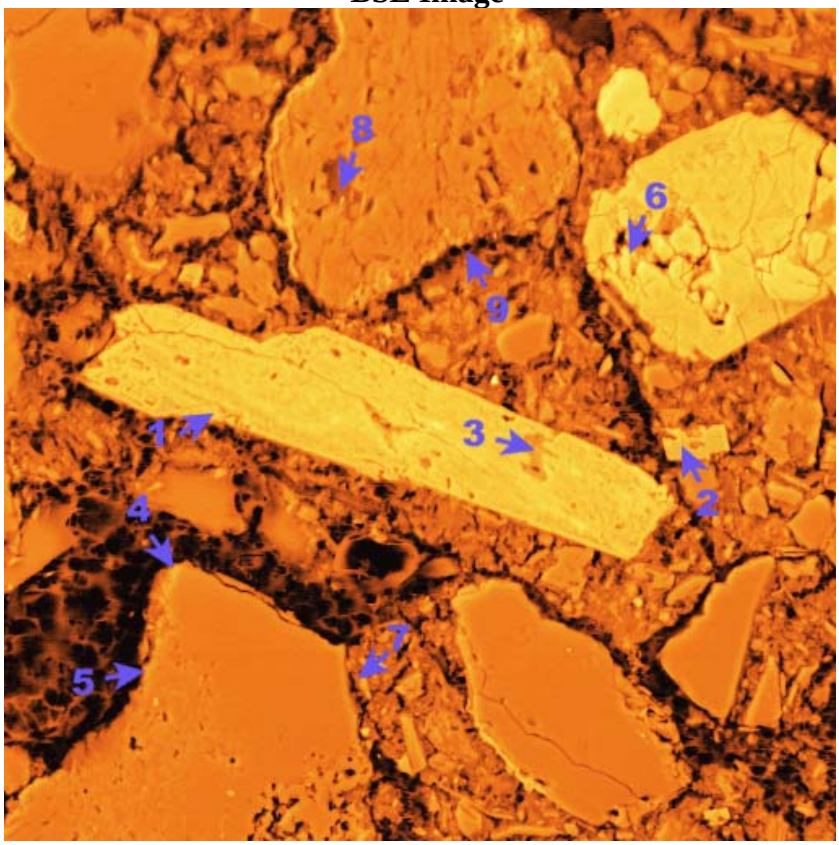

Iron (Fe)

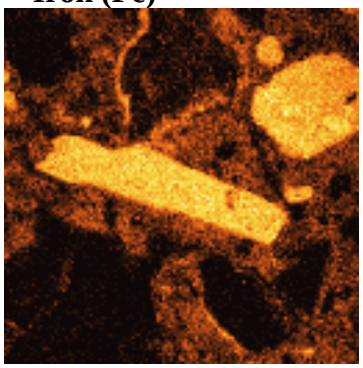

Manganese (Mn)

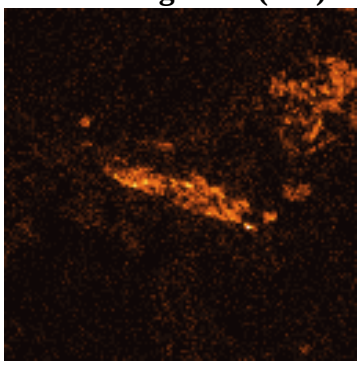

Phosphorous (P)

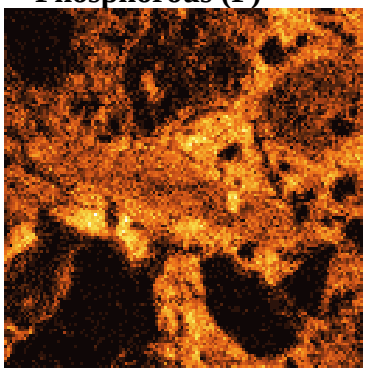

Lead (Pb)

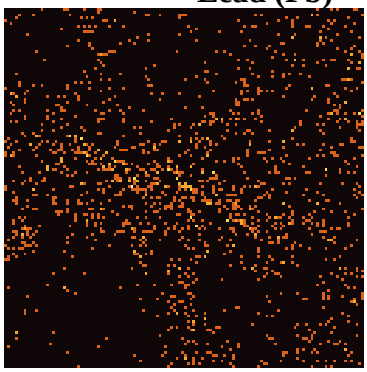

Silicon (Si)

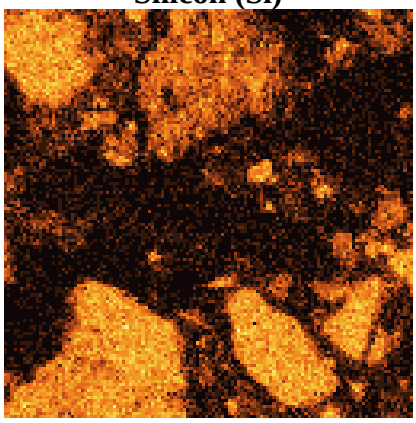

EDS Scan Images by Point

Point 1

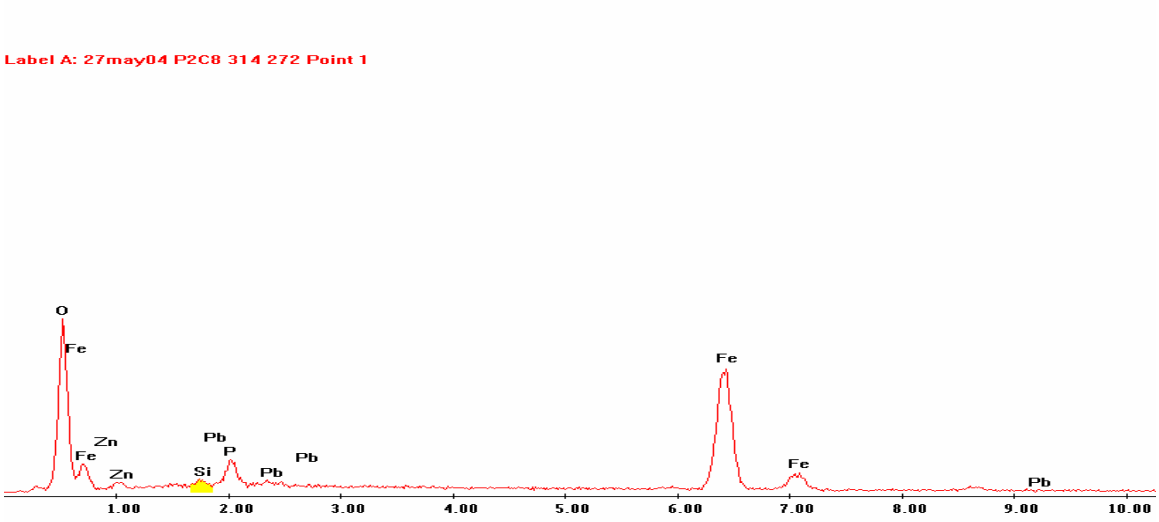

Point 2

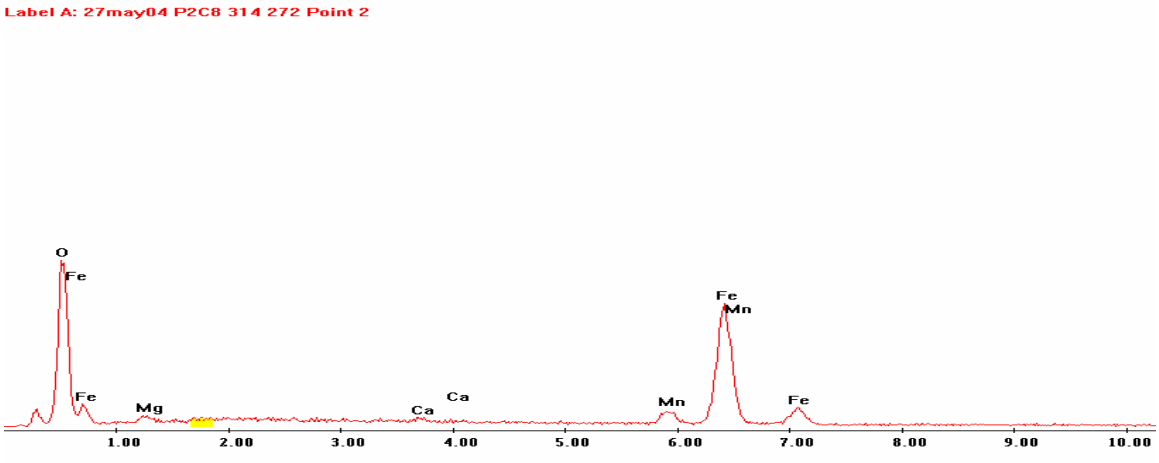

Point 3

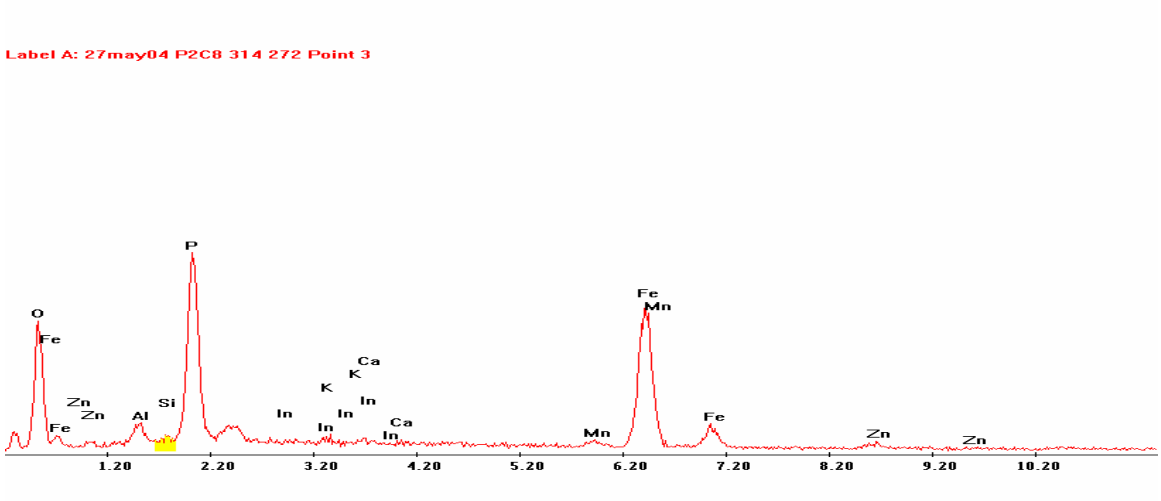

Point 4

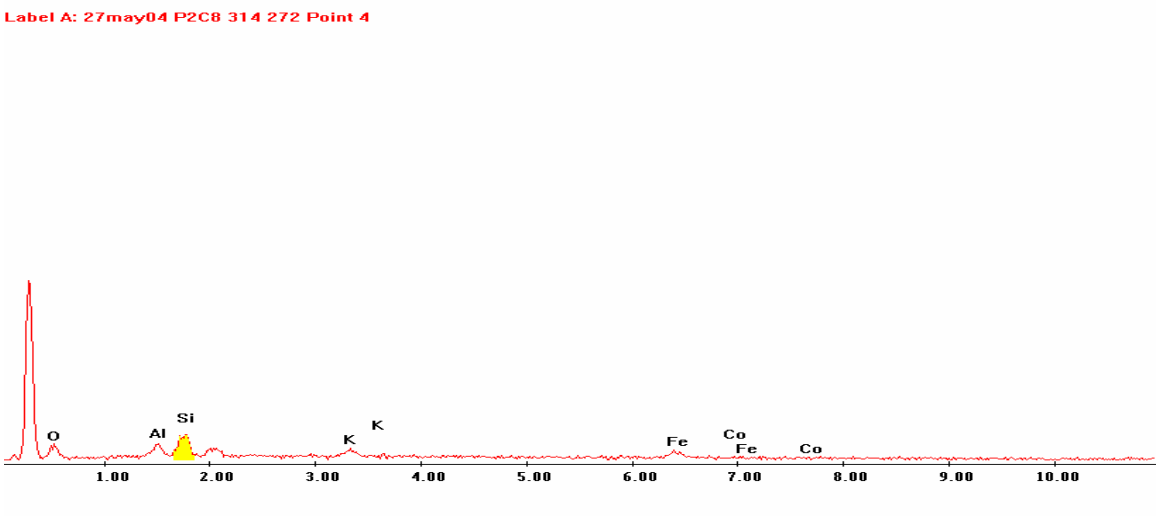

Point 5

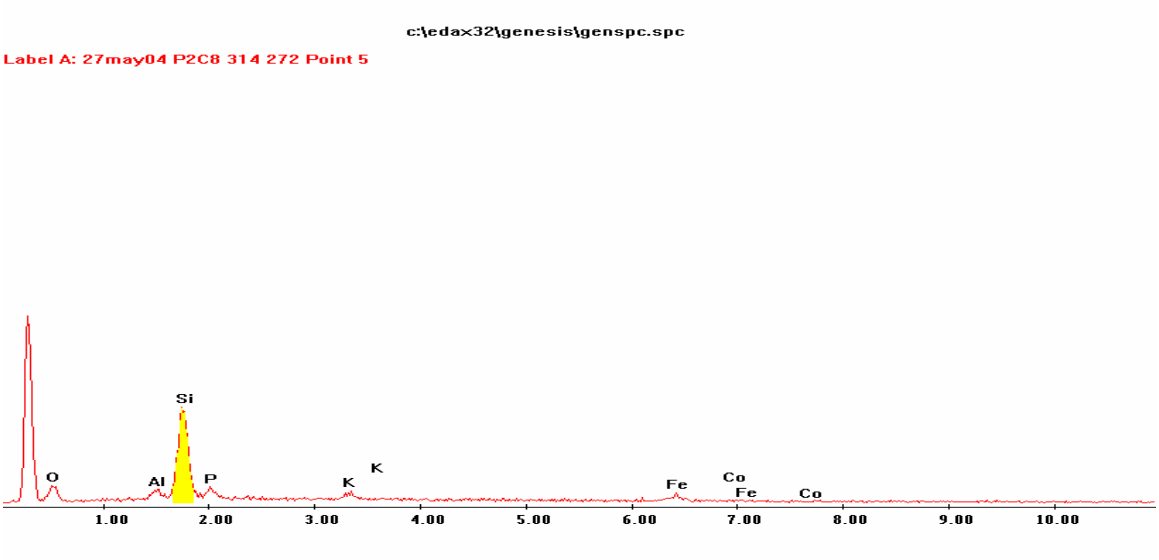

Point 6

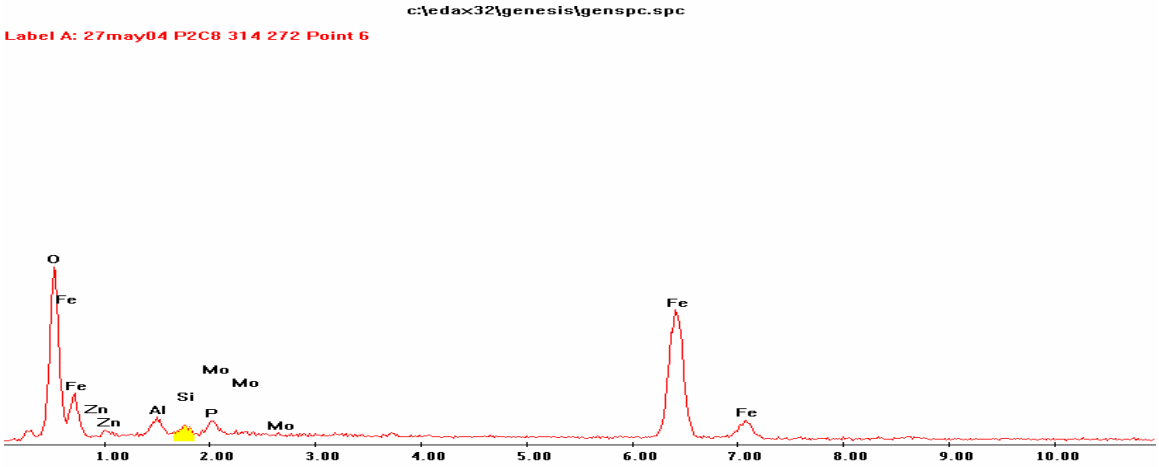

Point 7

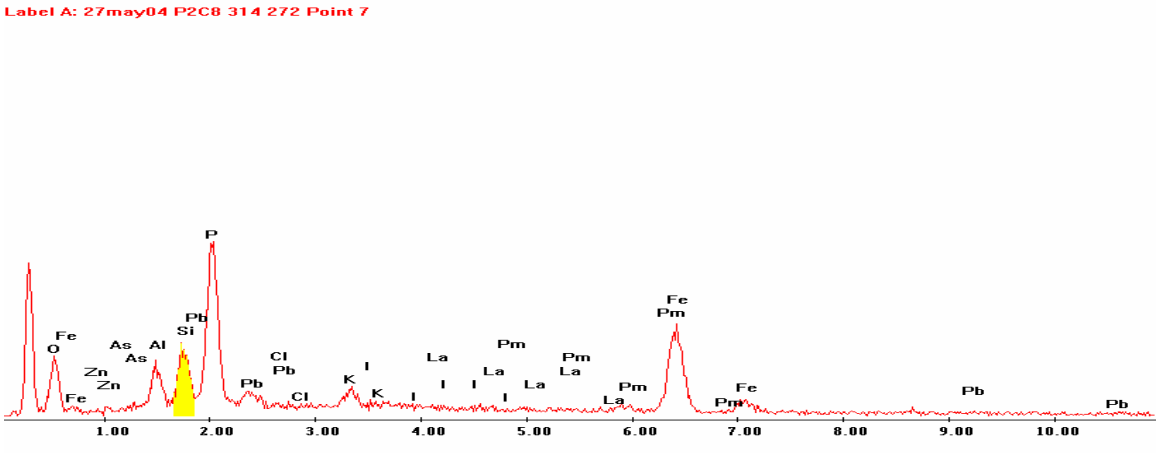

Point 8

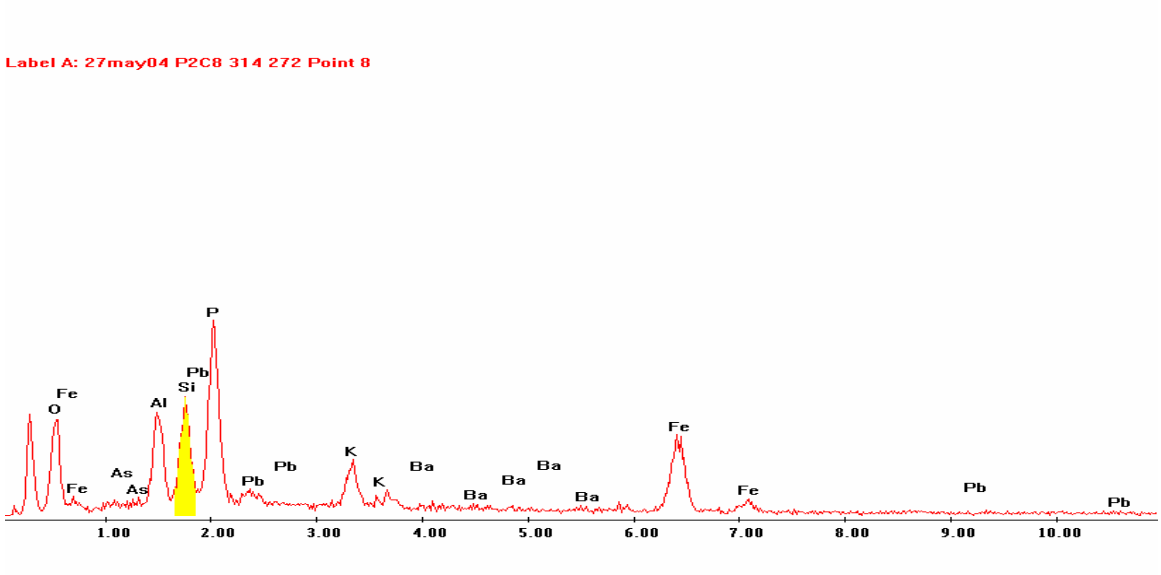
Label A: 27may04 P2C8 314 272 Point 8
O
Fe
Fe
As
As
Al
Si
Pb
P
Pb
Pb
K
K
Ba
Ba
Ba
Ba
Ba
Fe
Fe
Pb
Pb
1.00
2.00
3.00
4.00
5.00
6.00
7.00
8.00
9.00
10.00

P2C8 – 376, 249

BSE Image

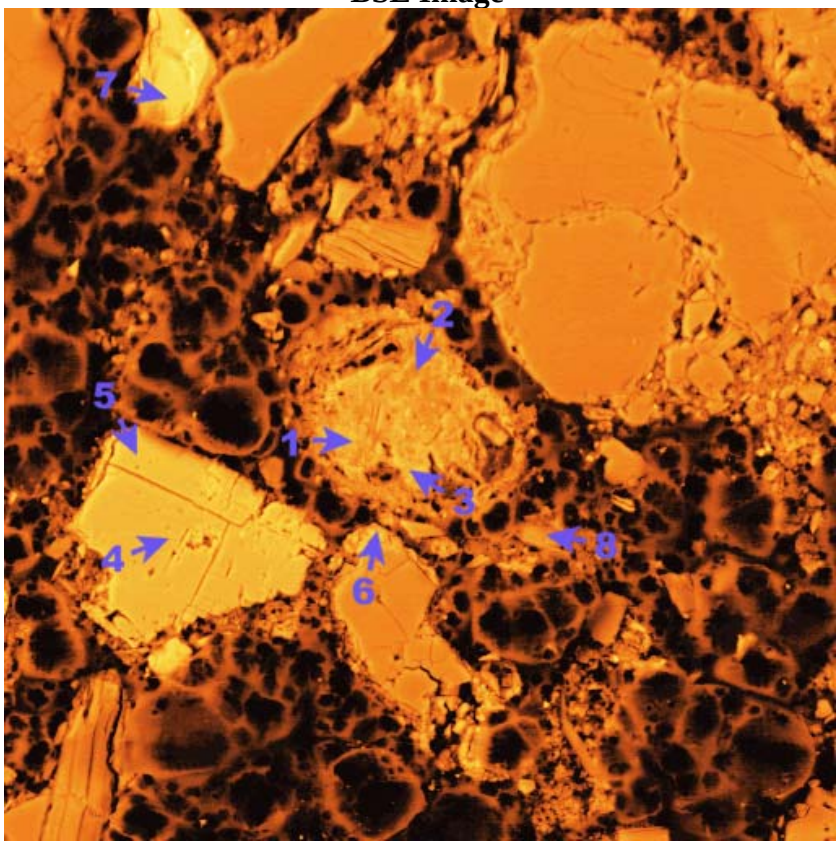

Iron (Fe)

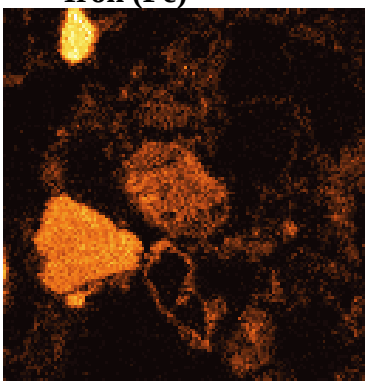

Manganese (Mn)

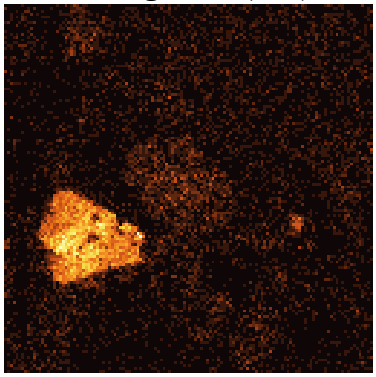

Phosphorous (P)

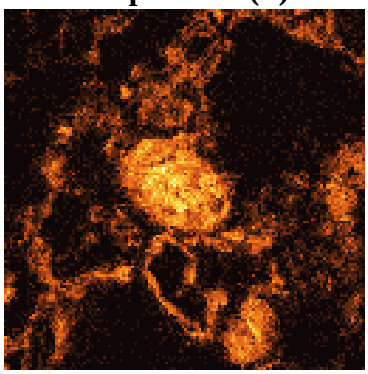

Lead (Pb)

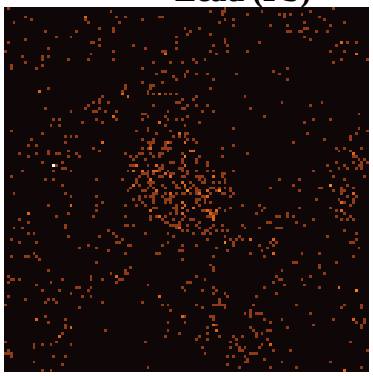

Silicon (Si)

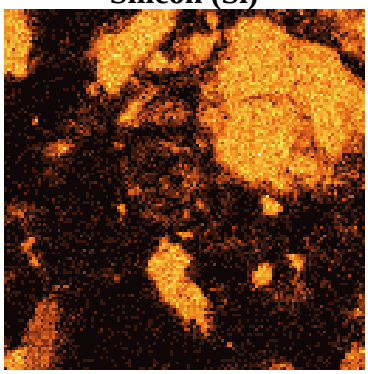

EDS Scan Images by Point

Point 1

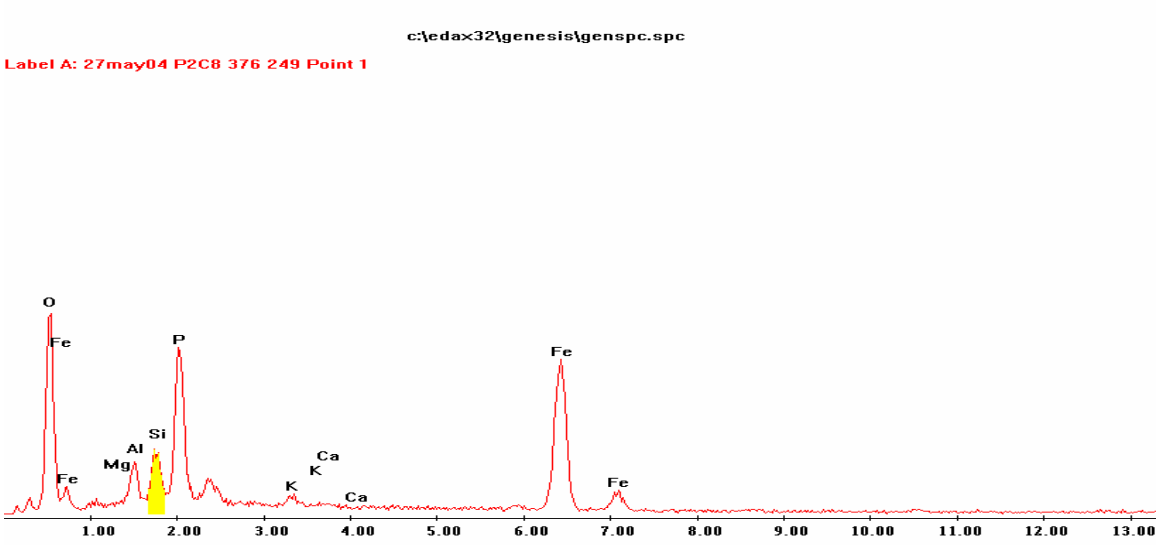

Point 2

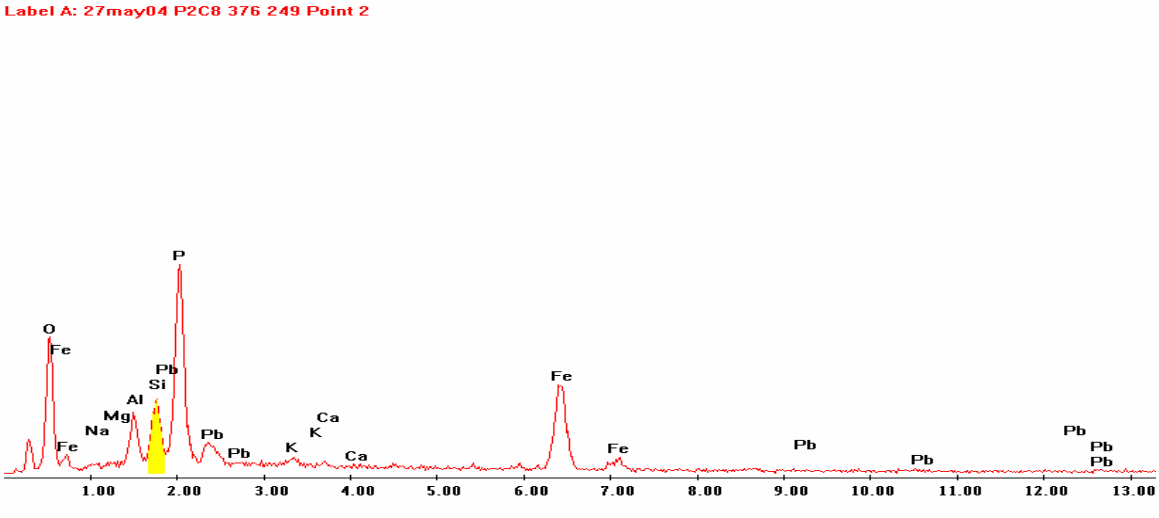

Point 3

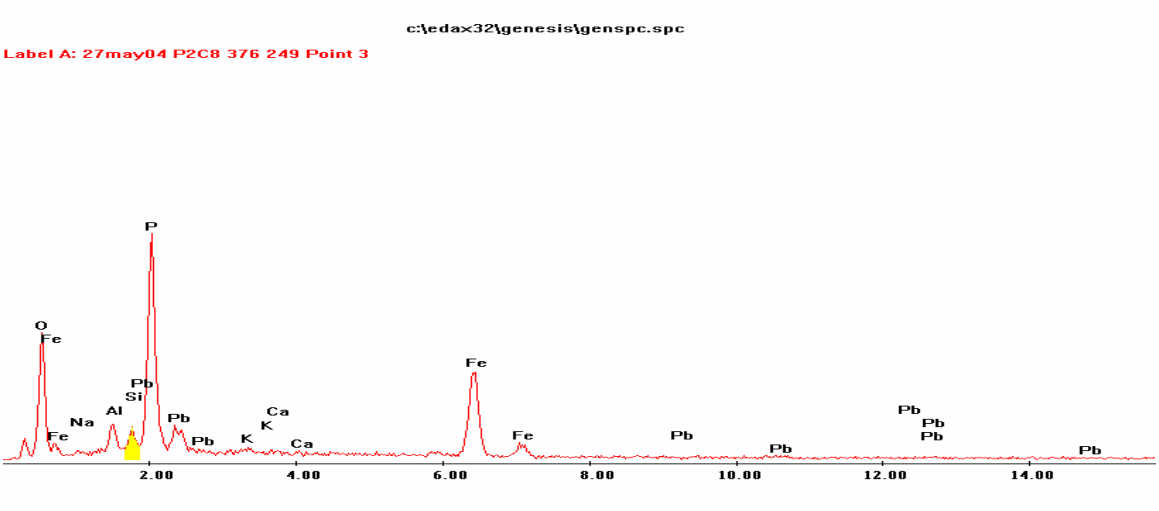

Point 4

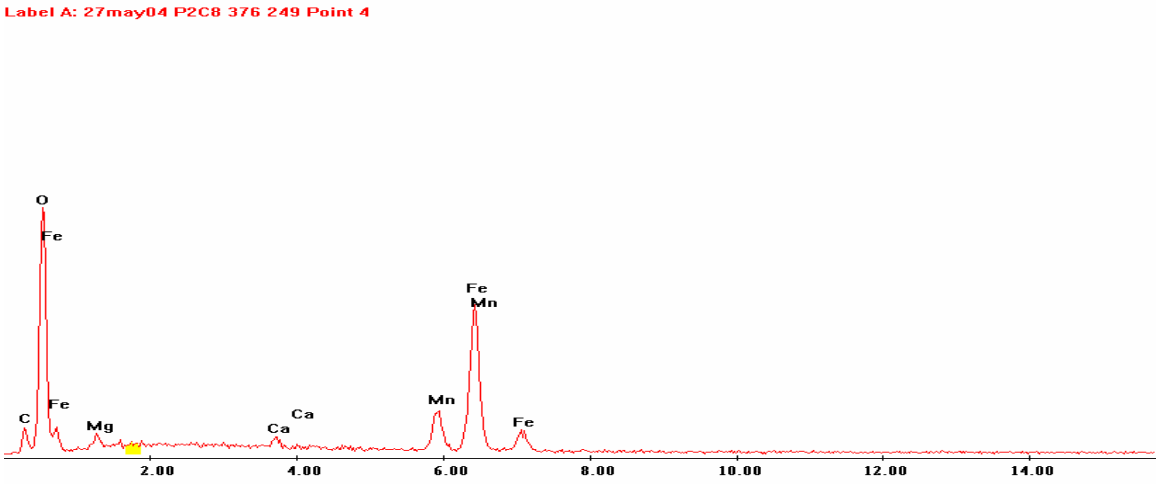

Point 5

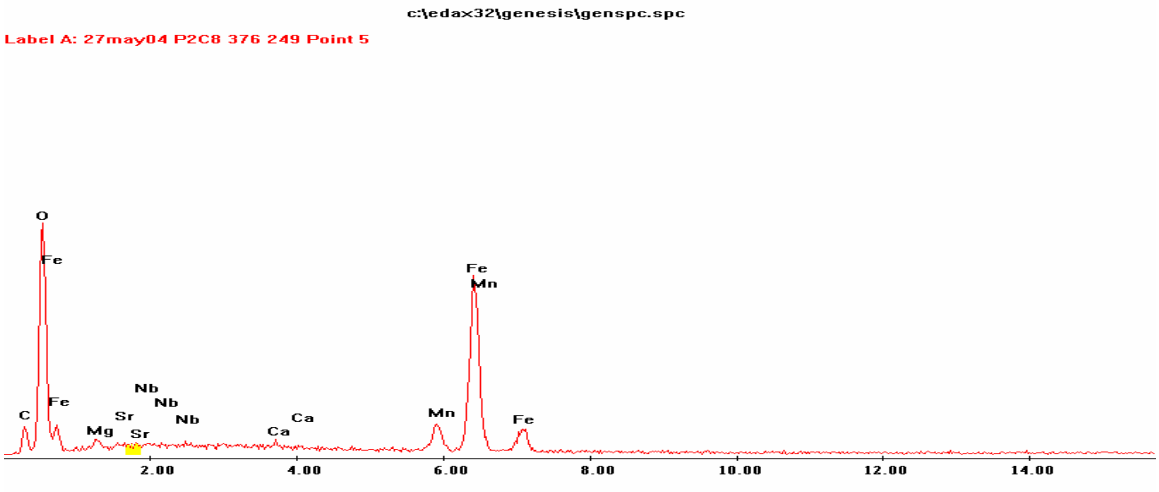

Point 6

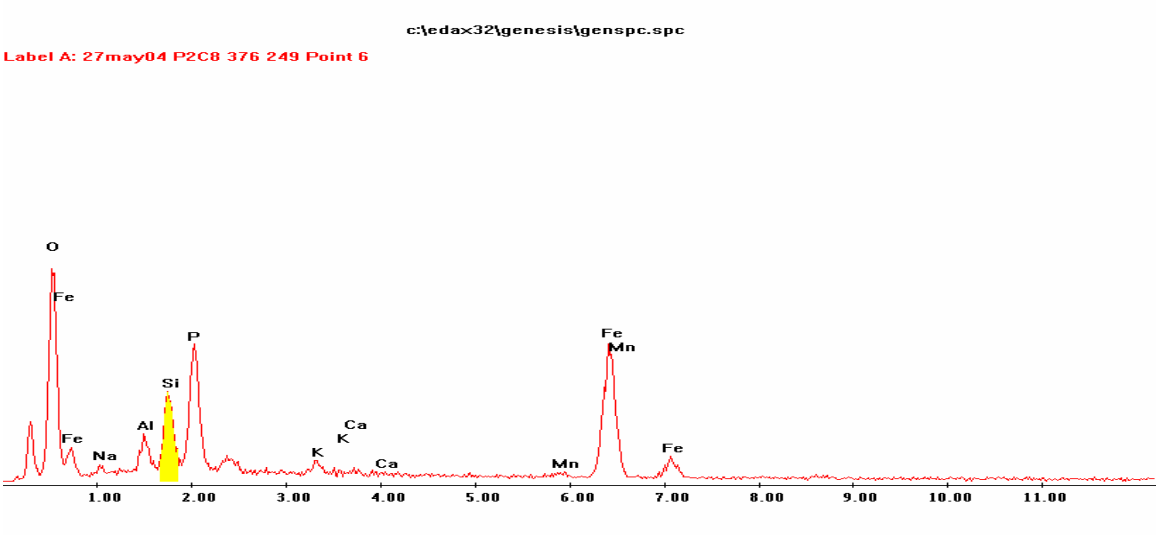

Point 7

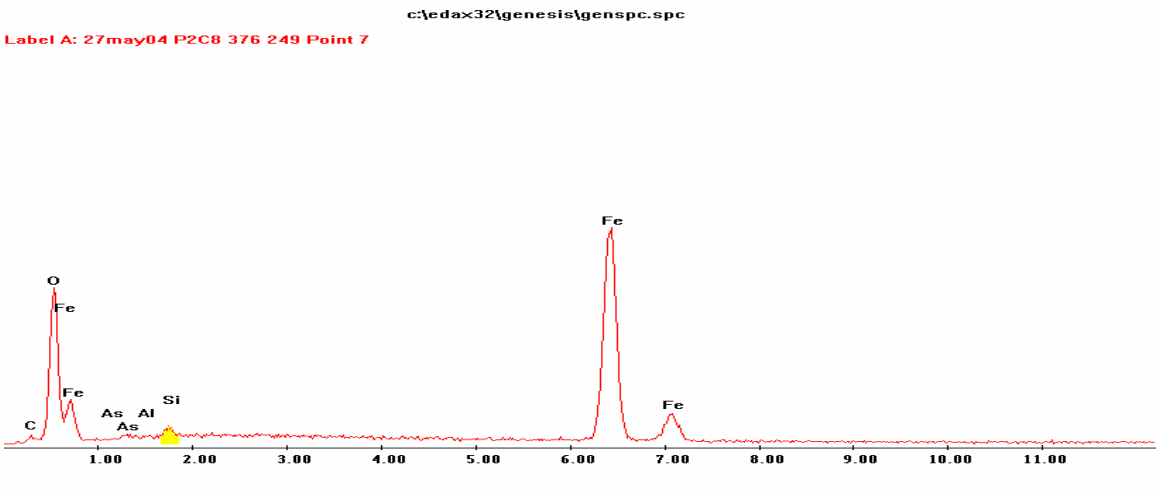

Point 8

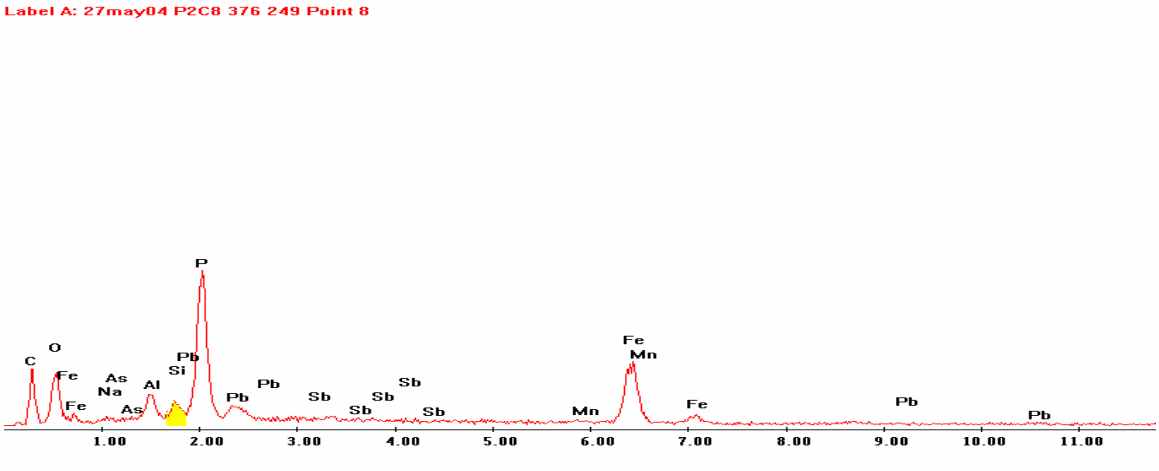

P2C8 – 427, 161

BSE Image

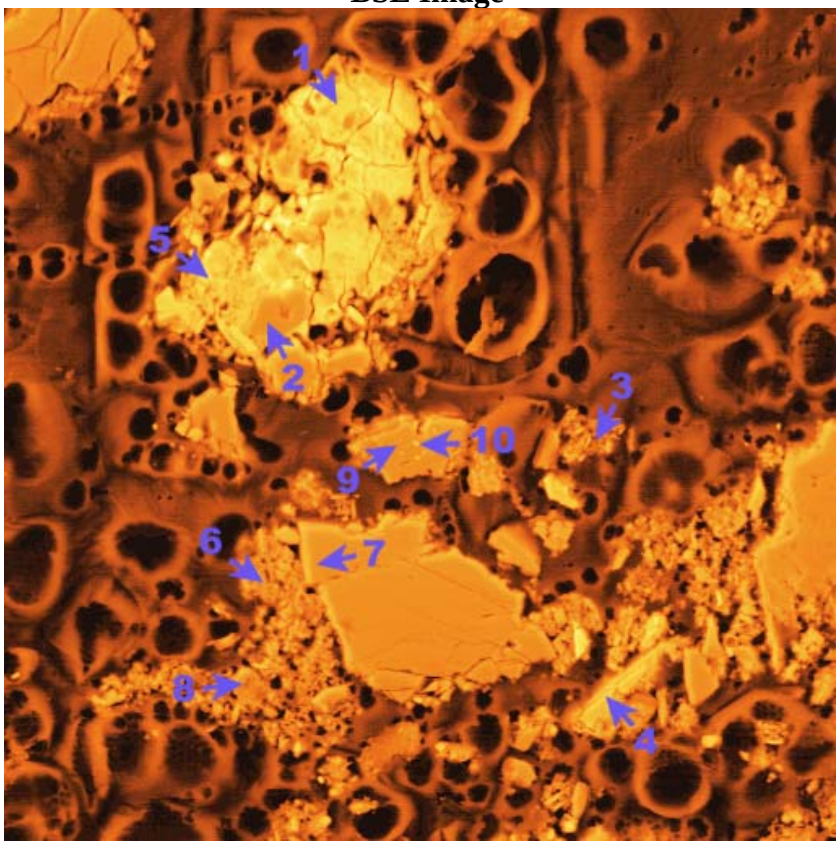

Iron (Fe)

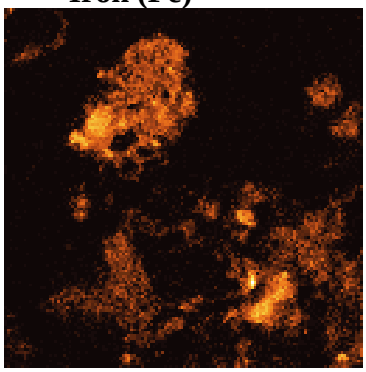

Manganese (Mn)

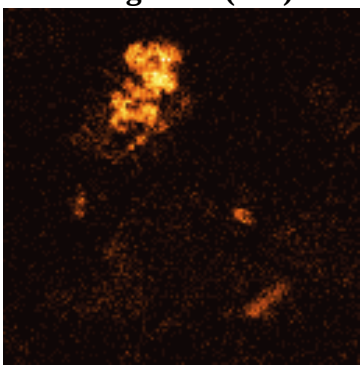

Phosphorous (P)

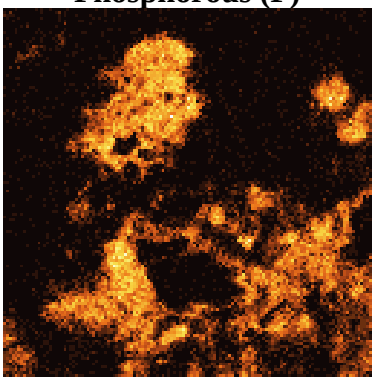

Lead (Pb)

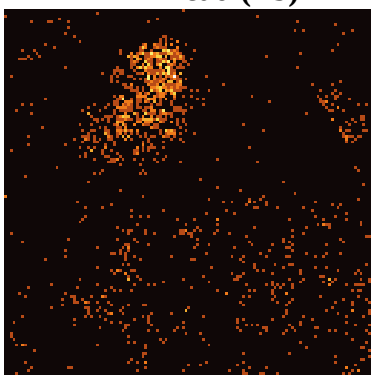

Silicon (Si)

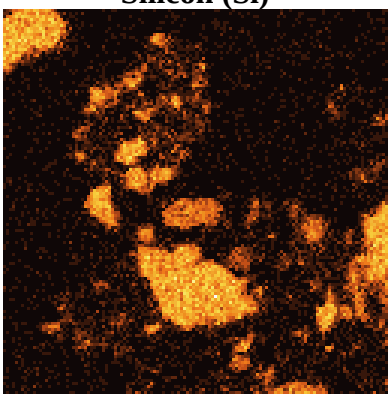

EDS Scan Images by Point

Point 1

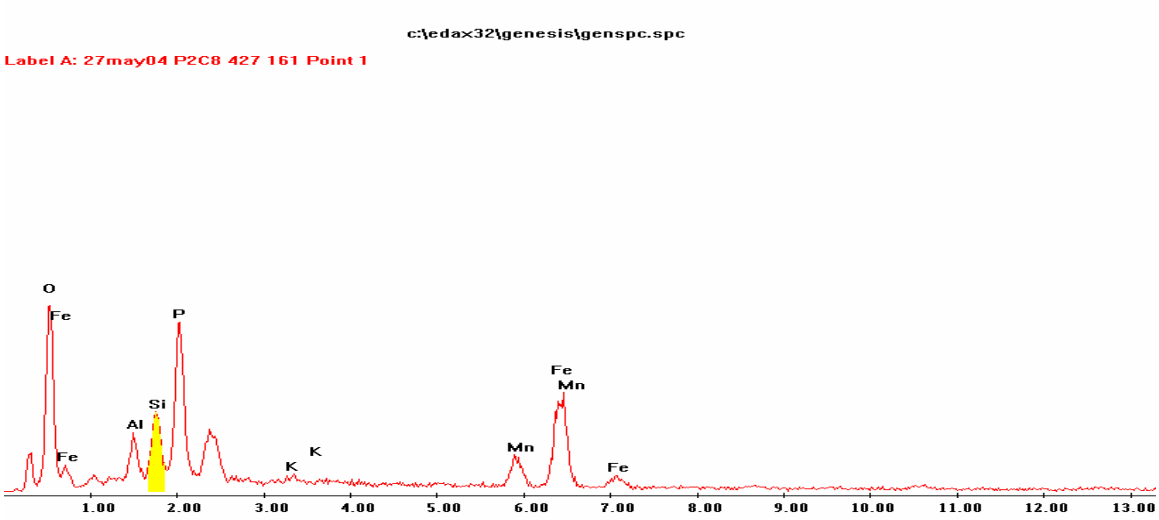

Point 2

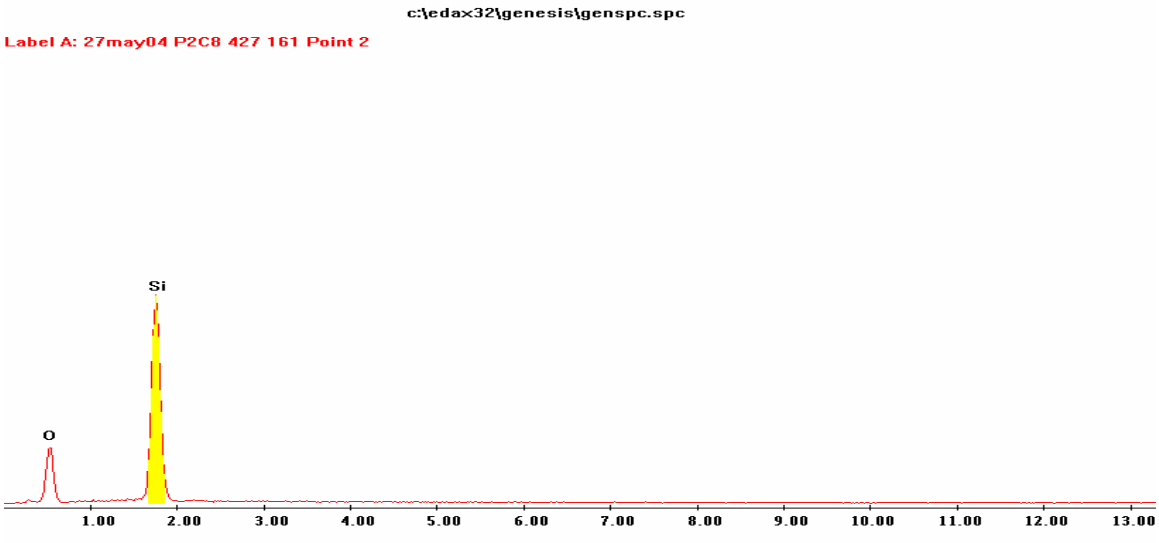

Point 3

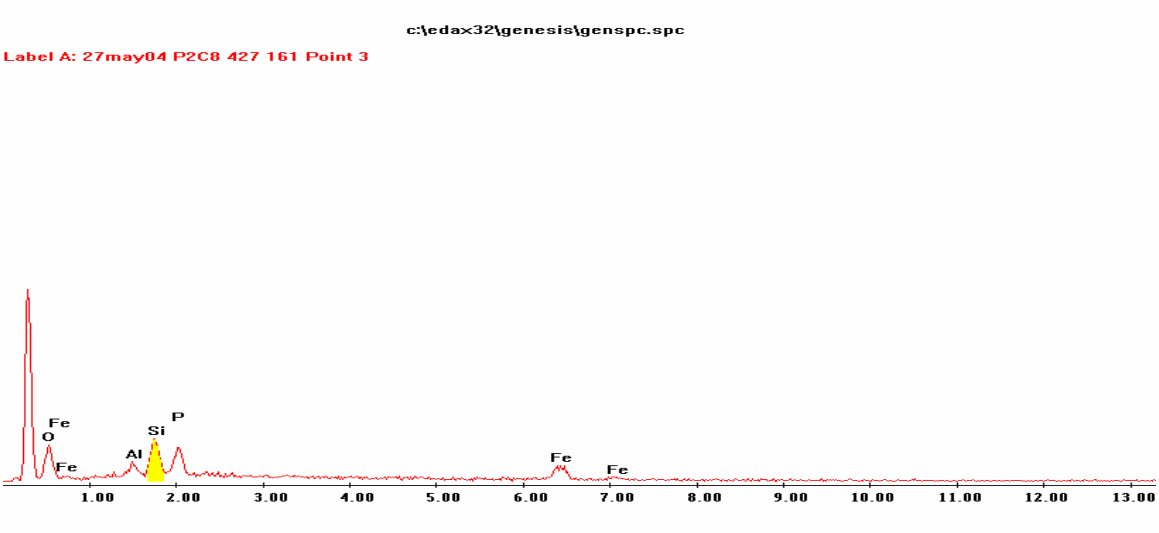

Point 4

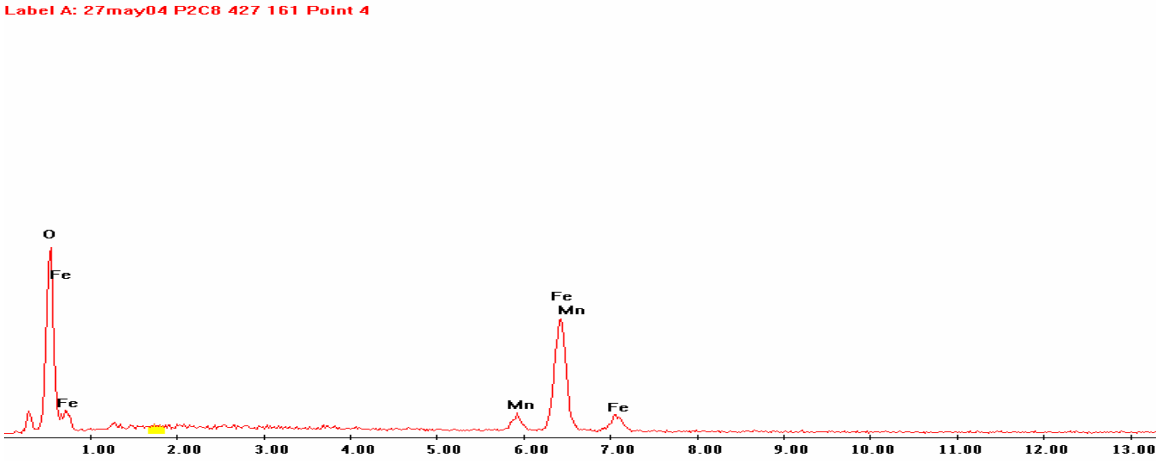

Point 5

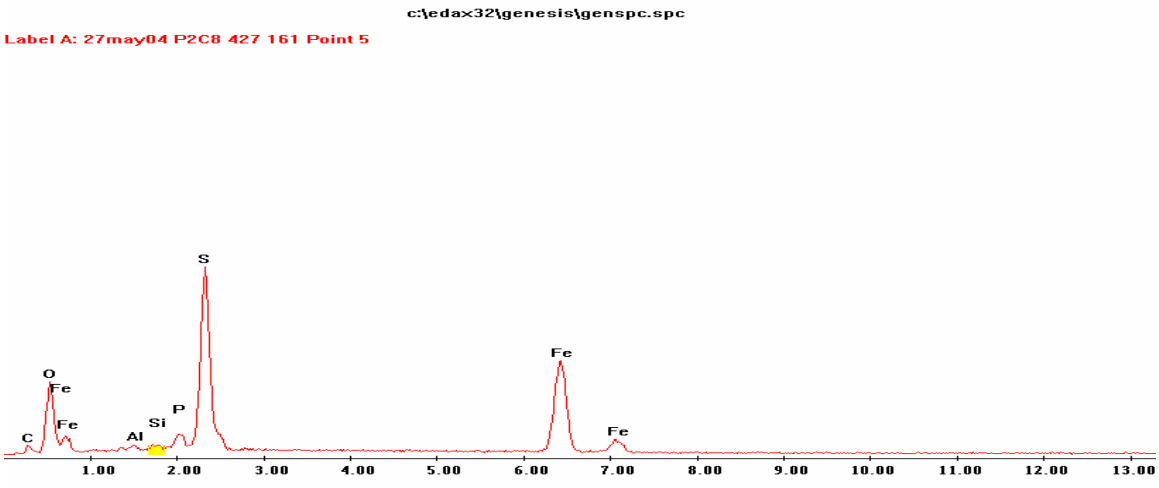

Point 6

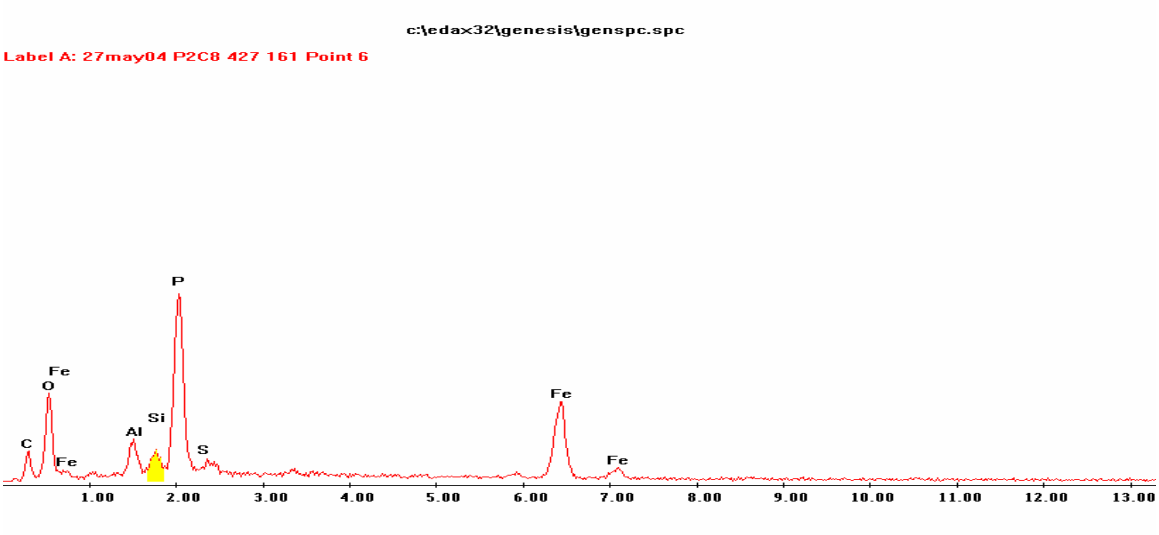

Point 7

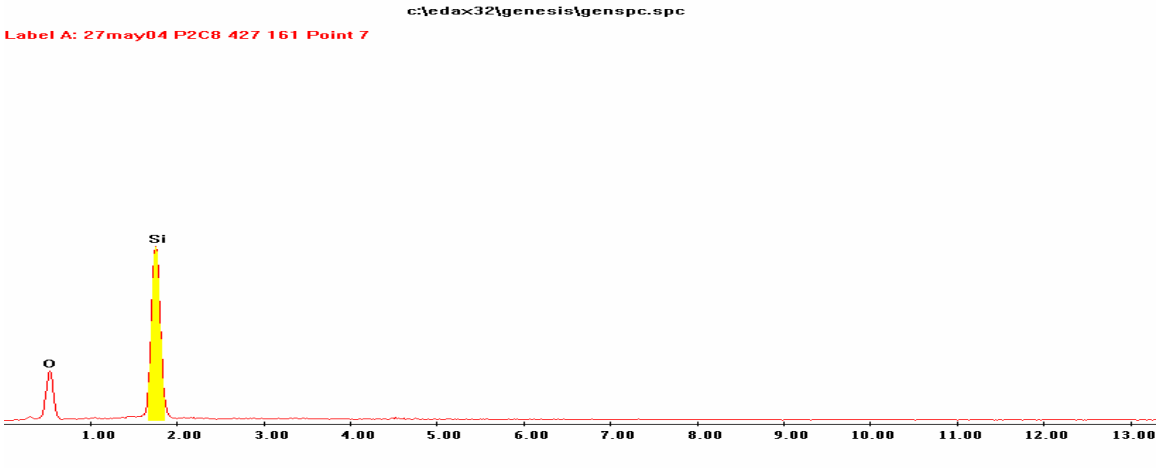

Point 8

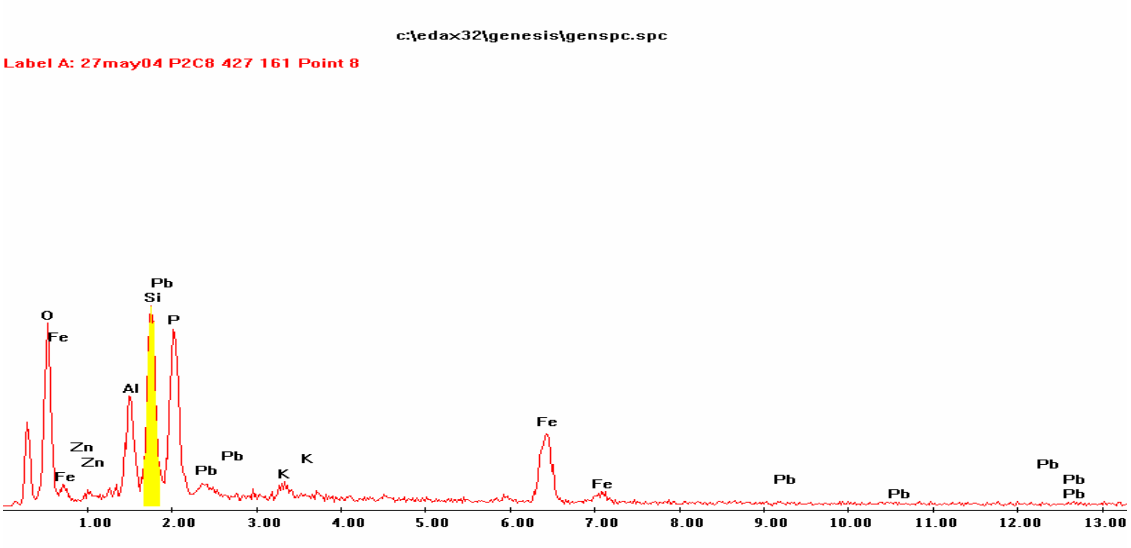

Point 9

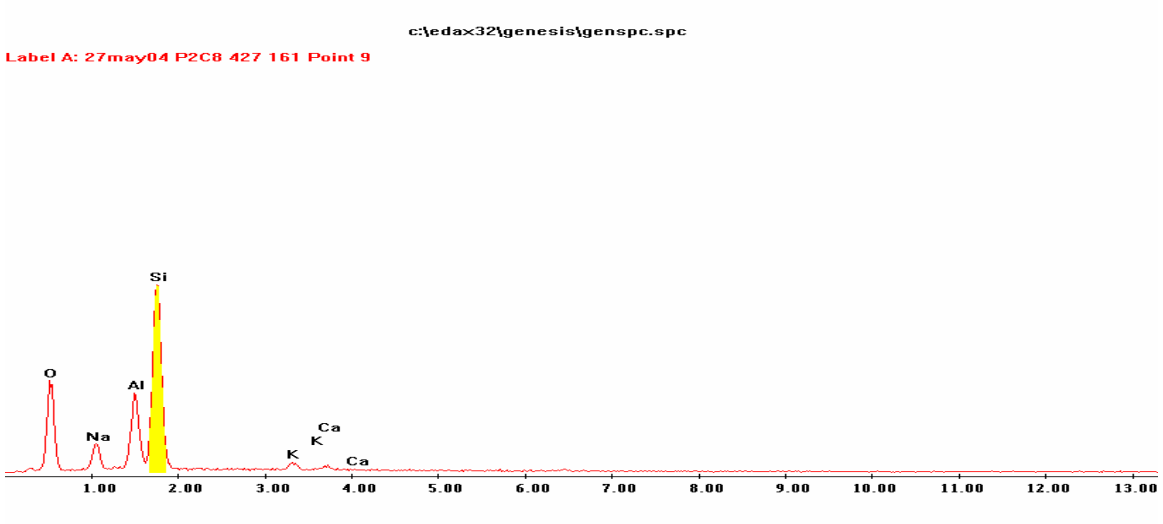

Point 10

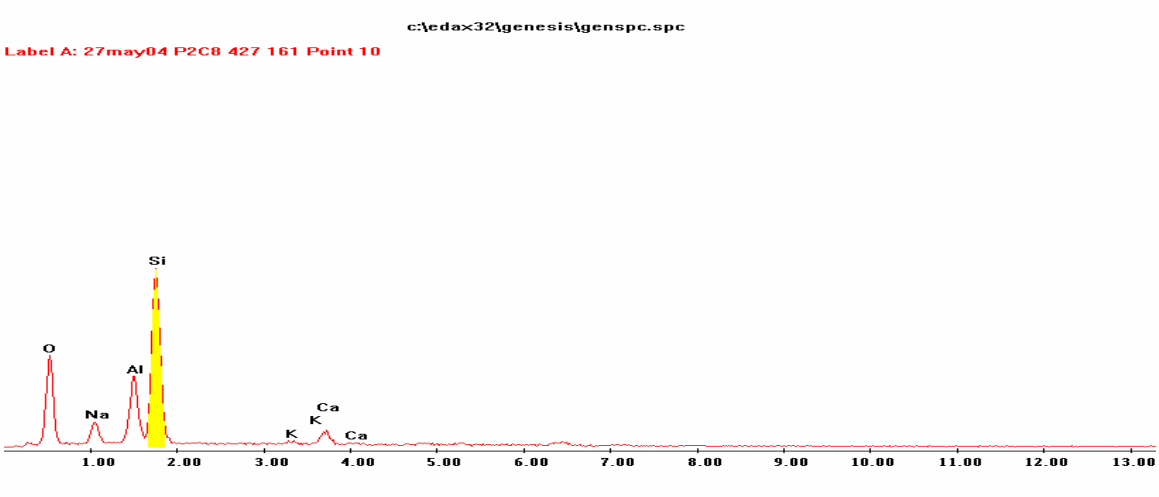

P2C8 – 439, 136

BSE Image

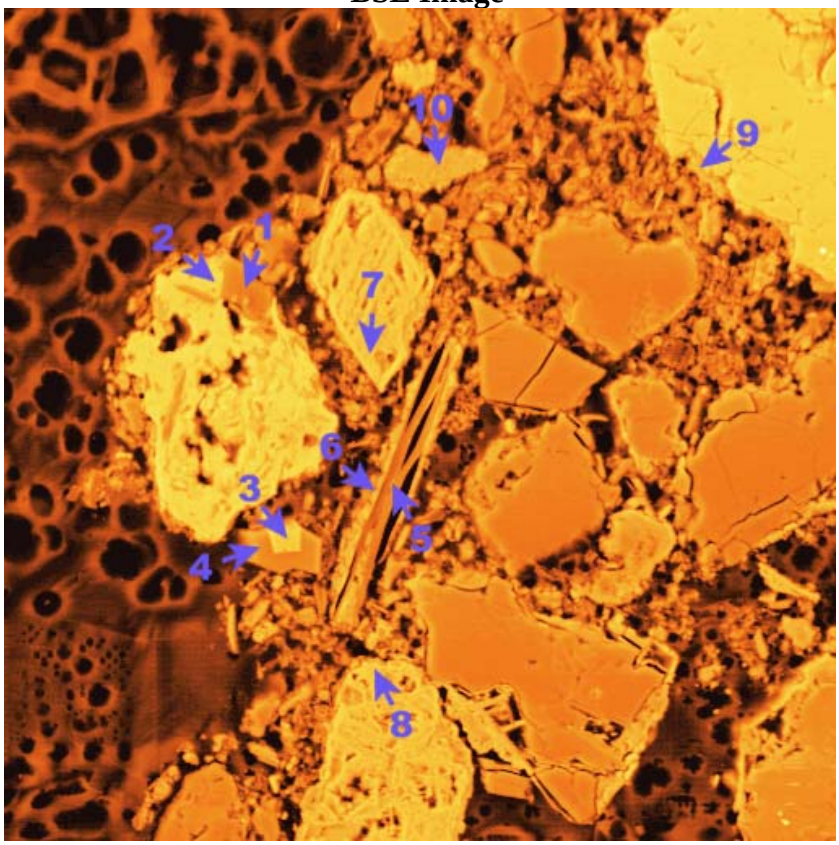

Iron (Fe)

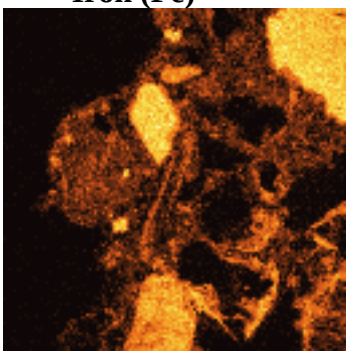

Manganese (Mn)

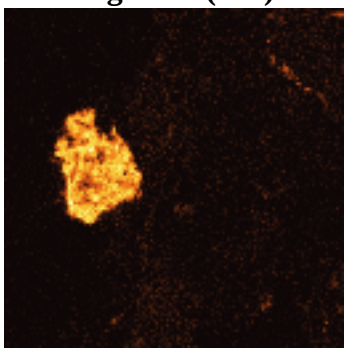

Phosphorous (P)

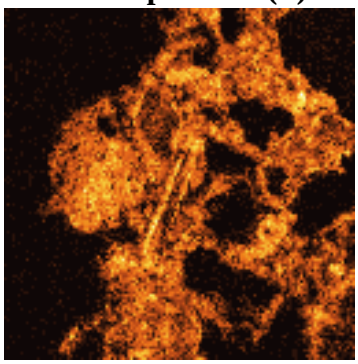

Lead (Pb)

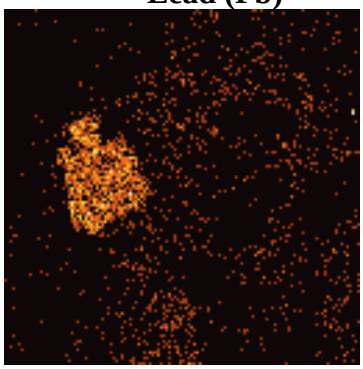

Silicon (Si)

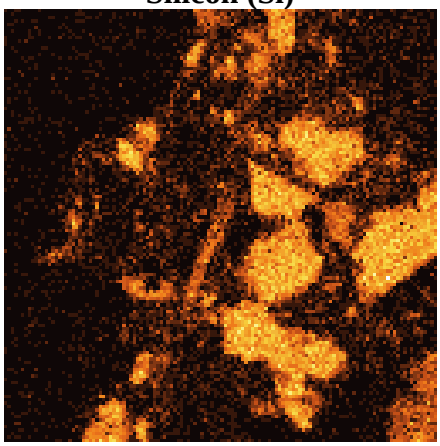

EDS Scan Images by Point

Point 1

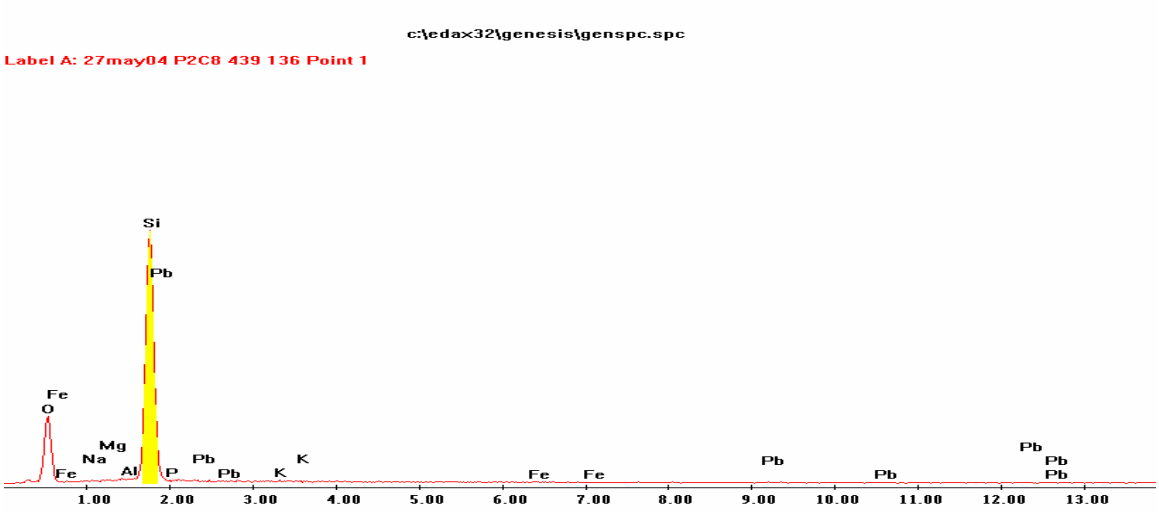

Point 2

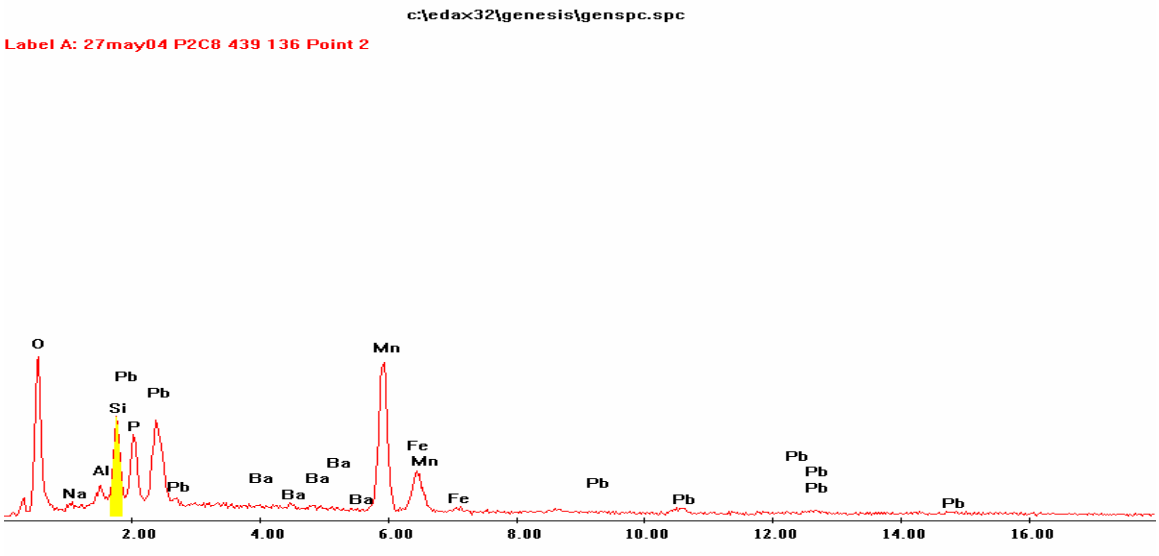

Point 3

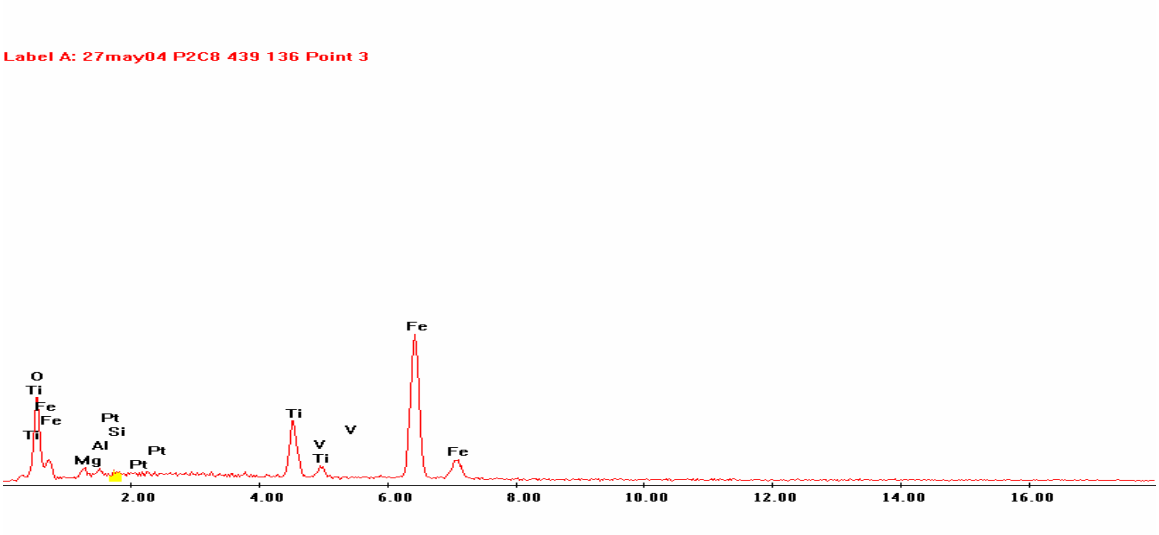

Point 4

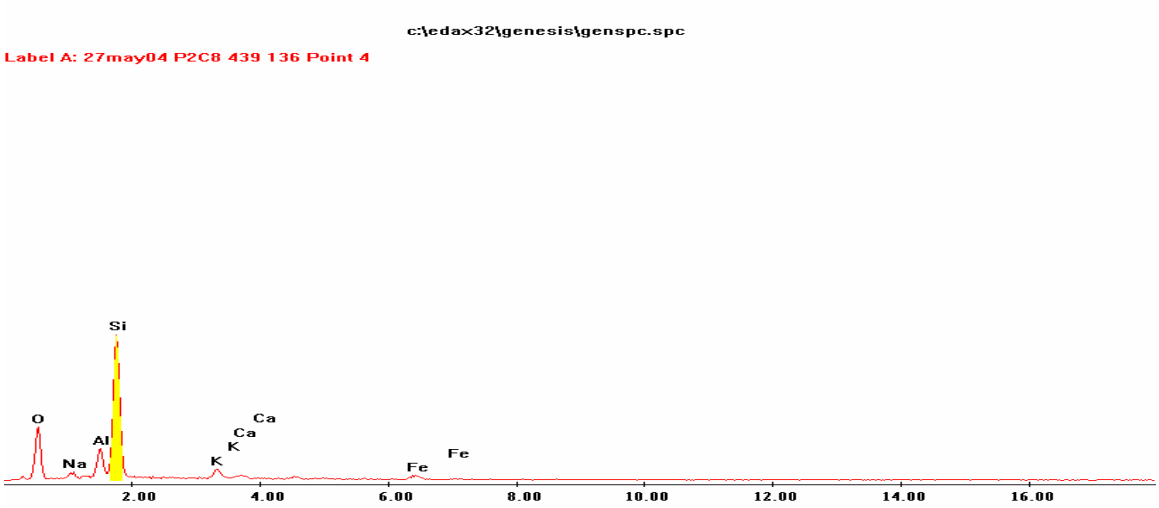

Point 5

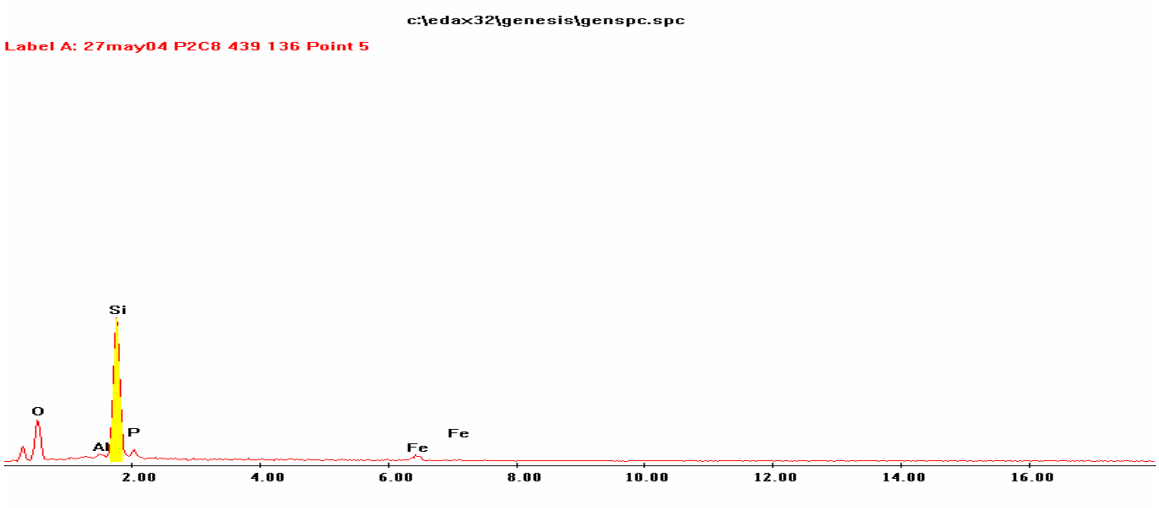

Point 6

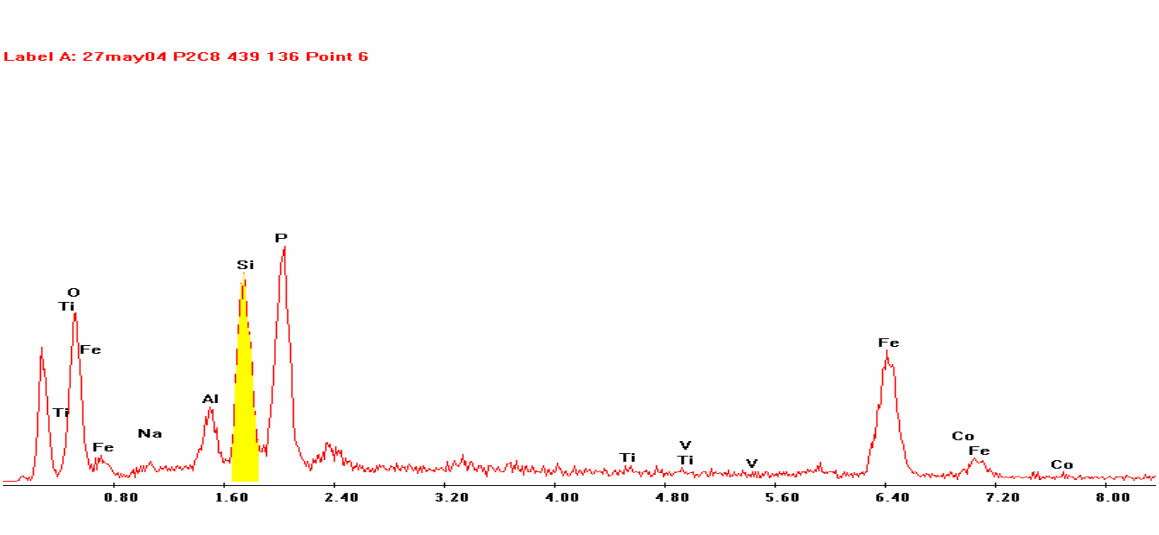

Point 7

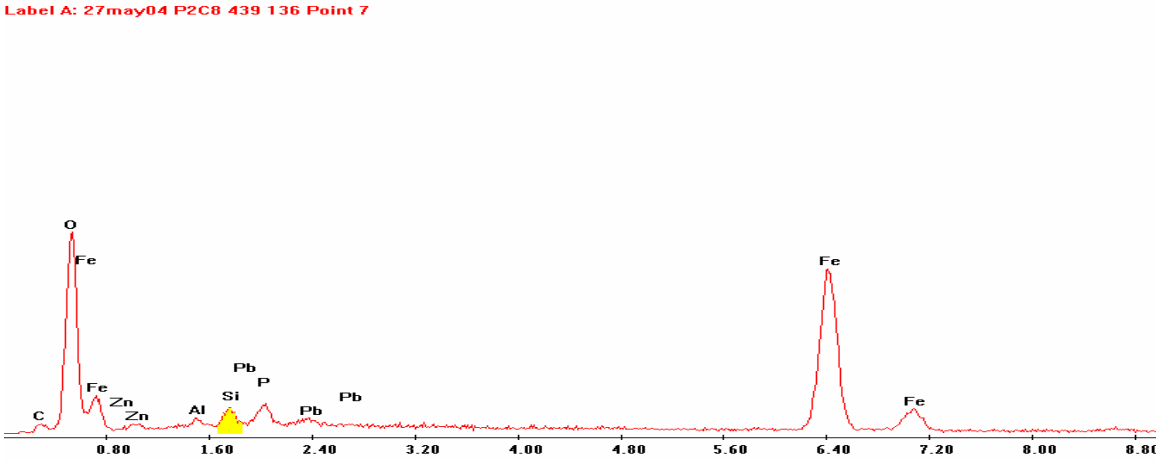

Point 8

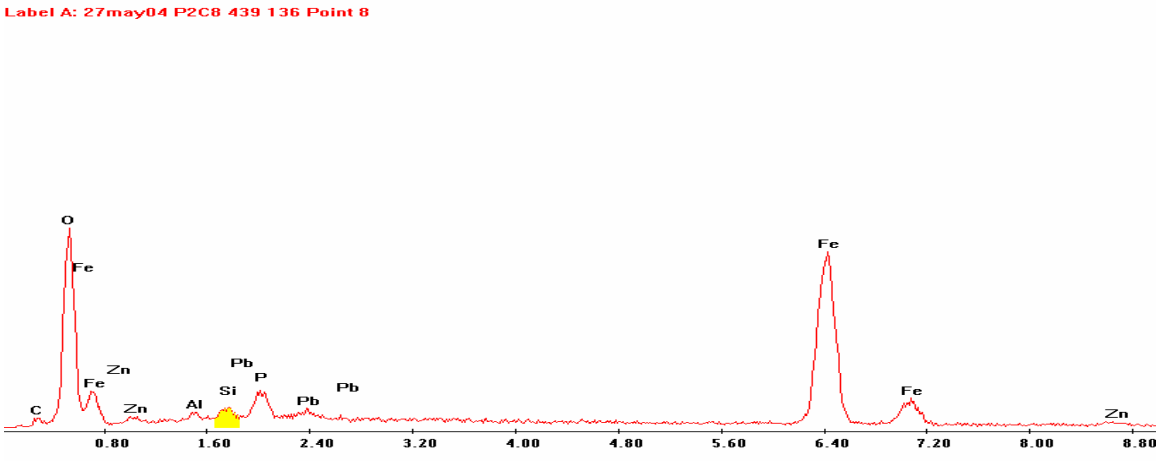

Point 9

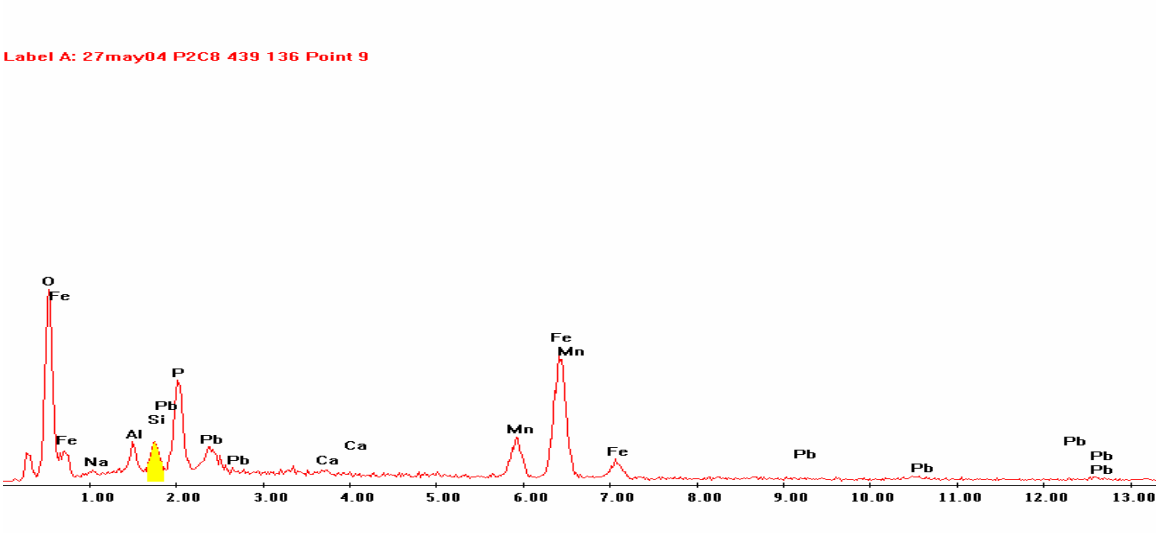

Point 10

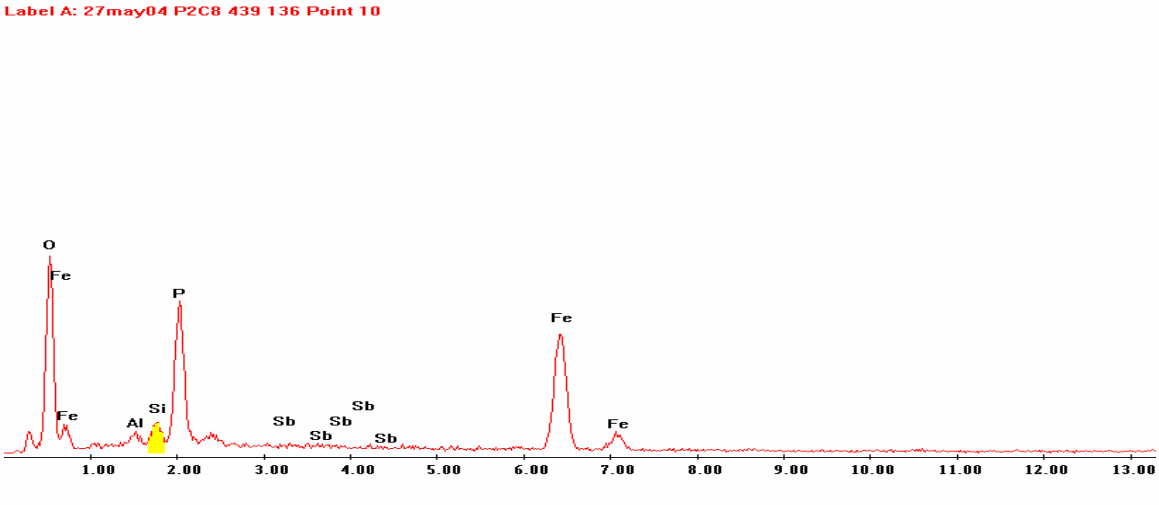

P2C8 – 482, 255

BSE Image

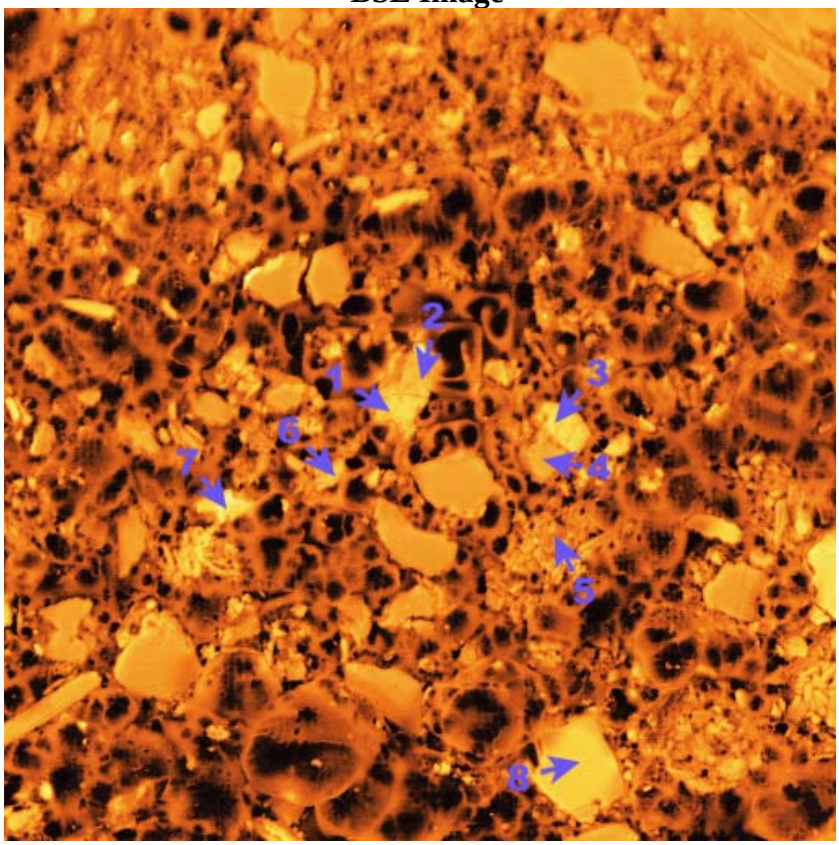

Iron (Fe)

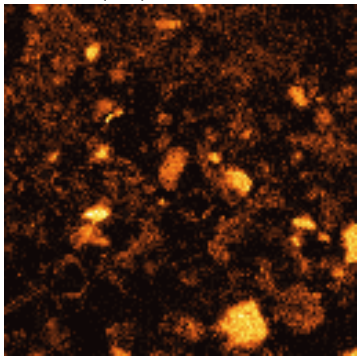

Manganese (Mn)

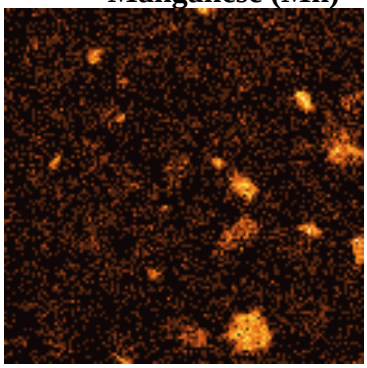

Phosphorous (P)

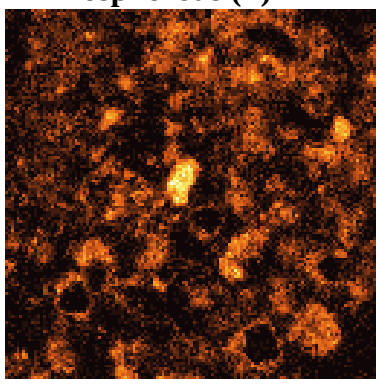

Lead (Pb)

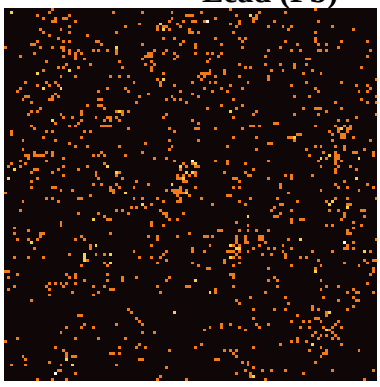

Silicon (Si)

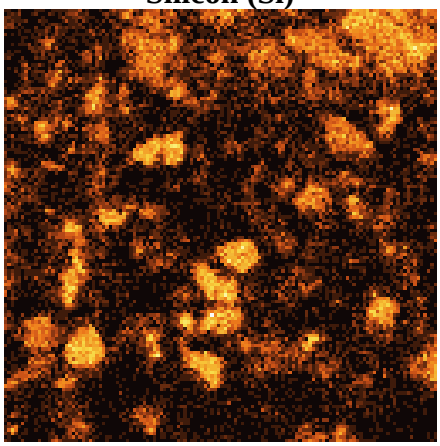

EDS Scan Images by Point

Point 1

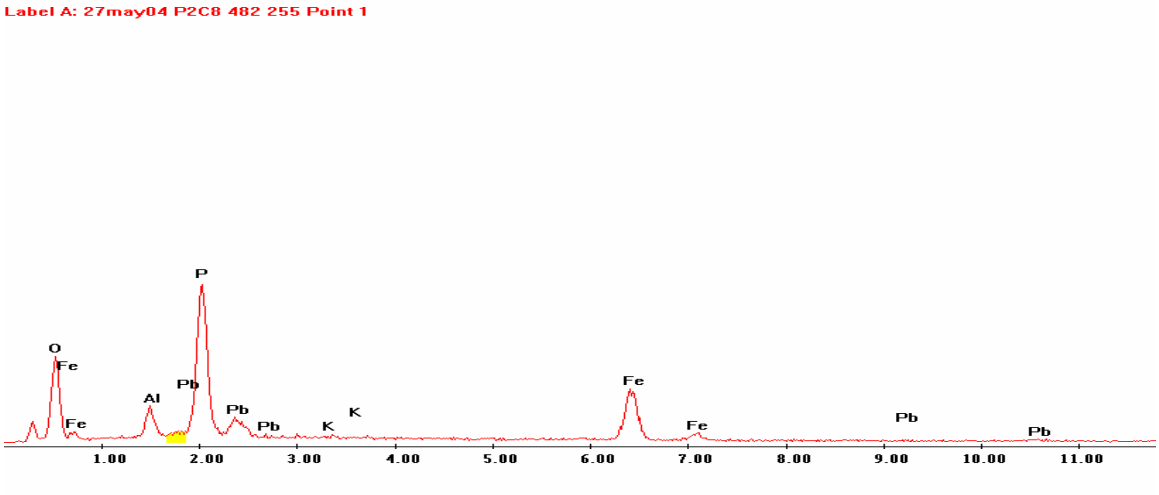

Point 2

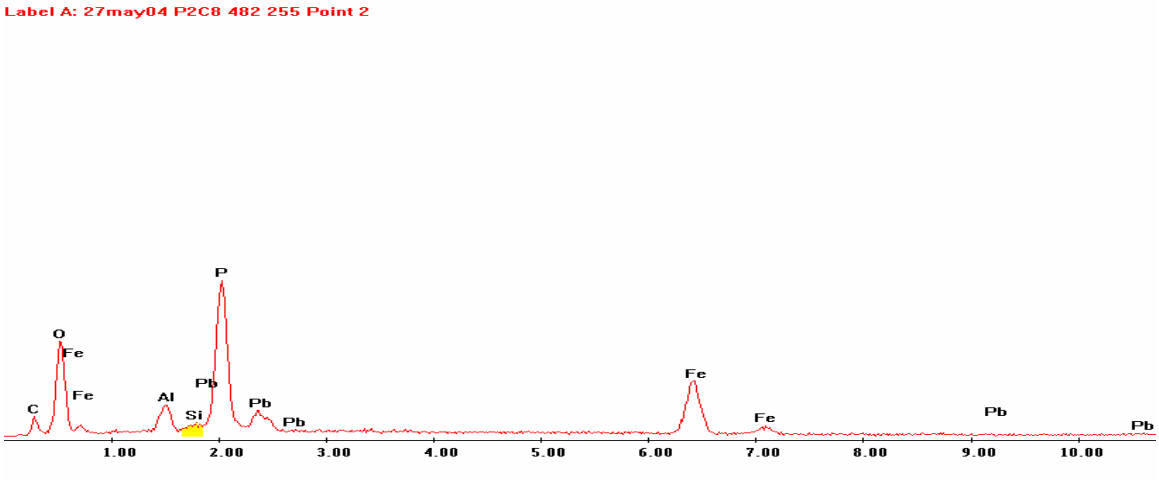

Point 3

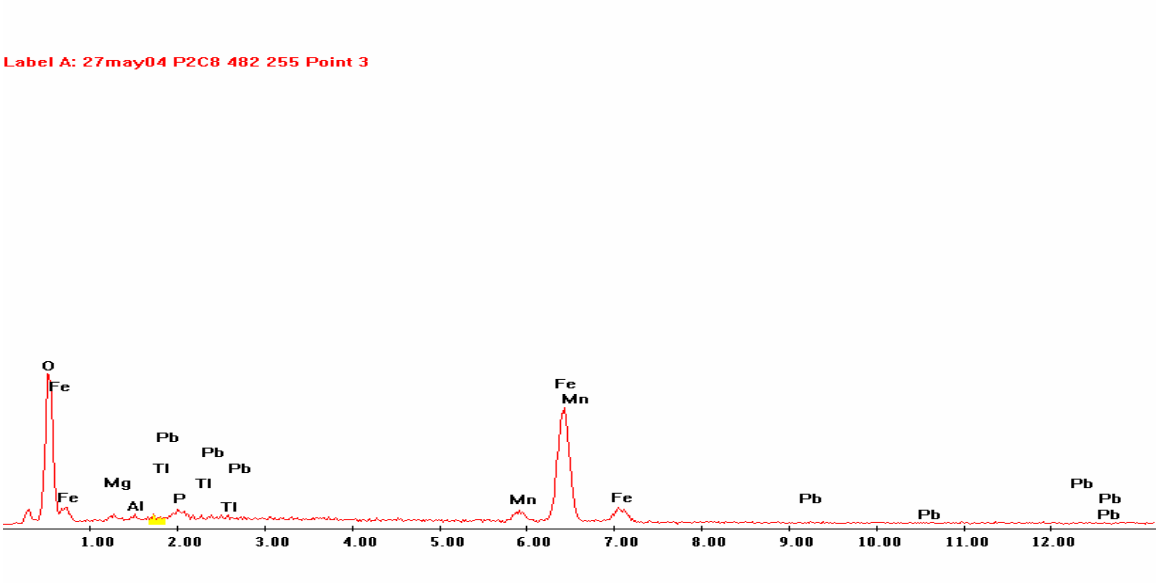

Point 4

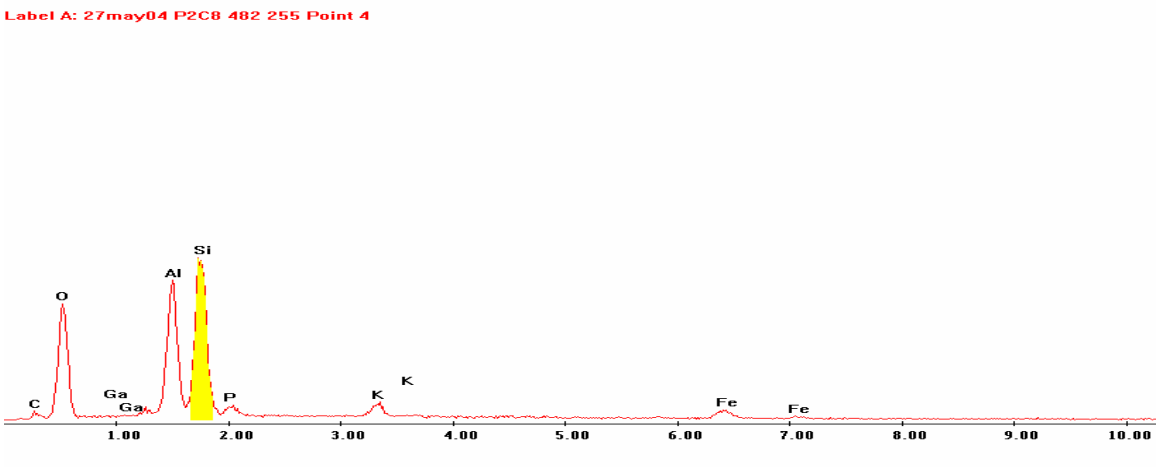

Point 5

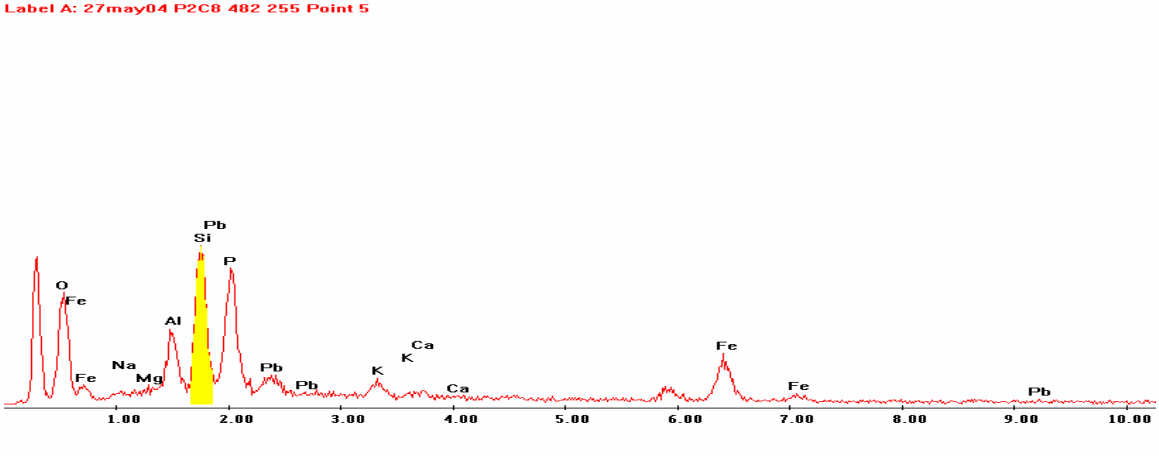

Point 6

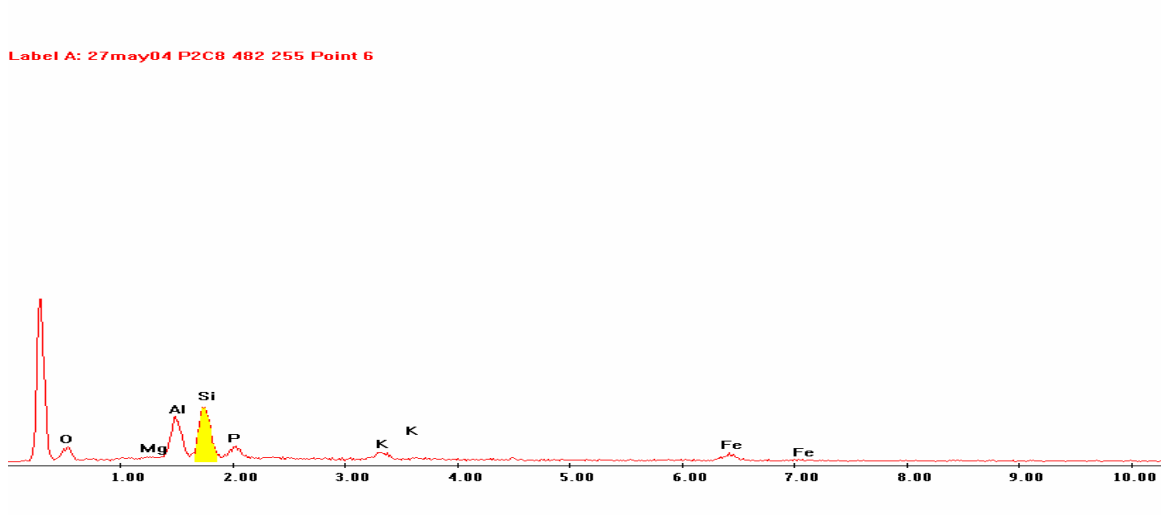

Point 7

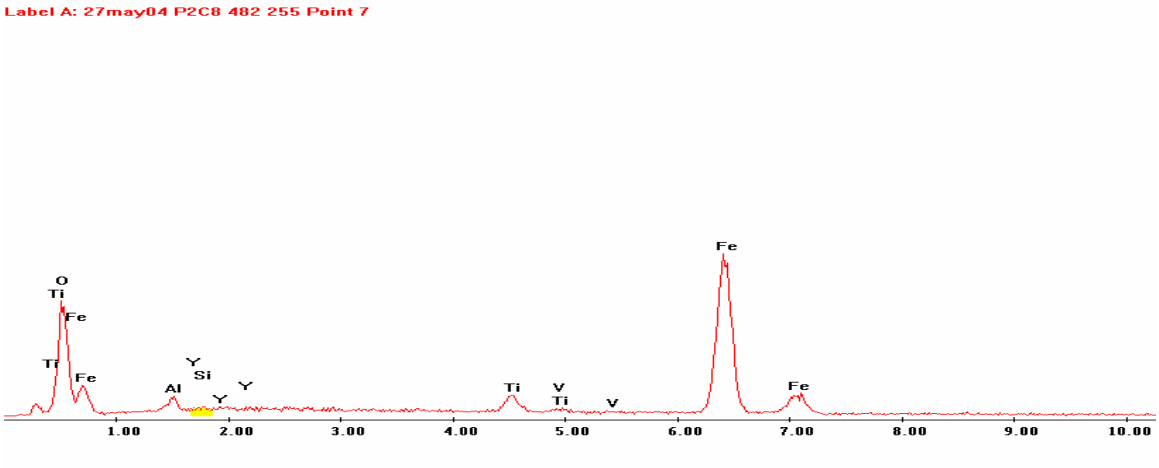

Point 8

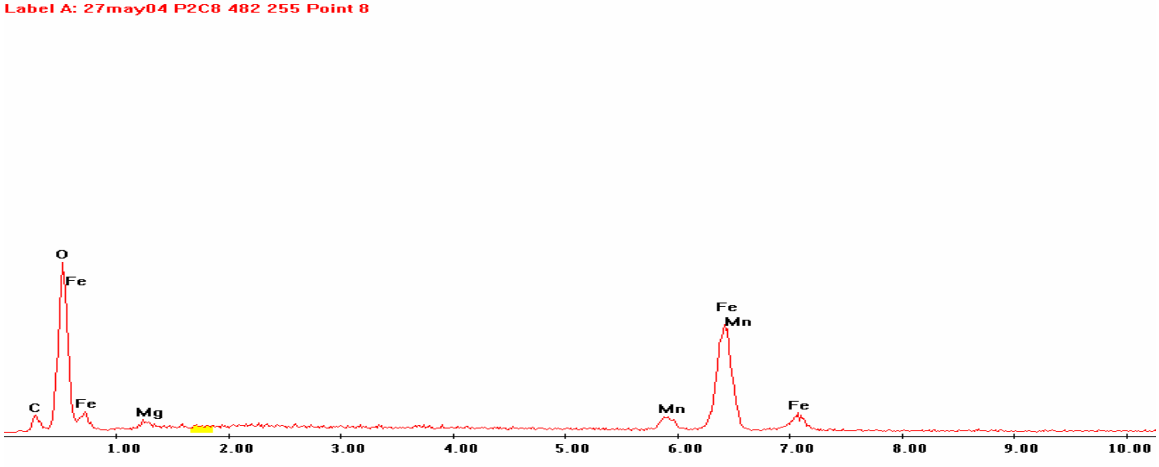

P2C9 – 312, 123

BSE Image

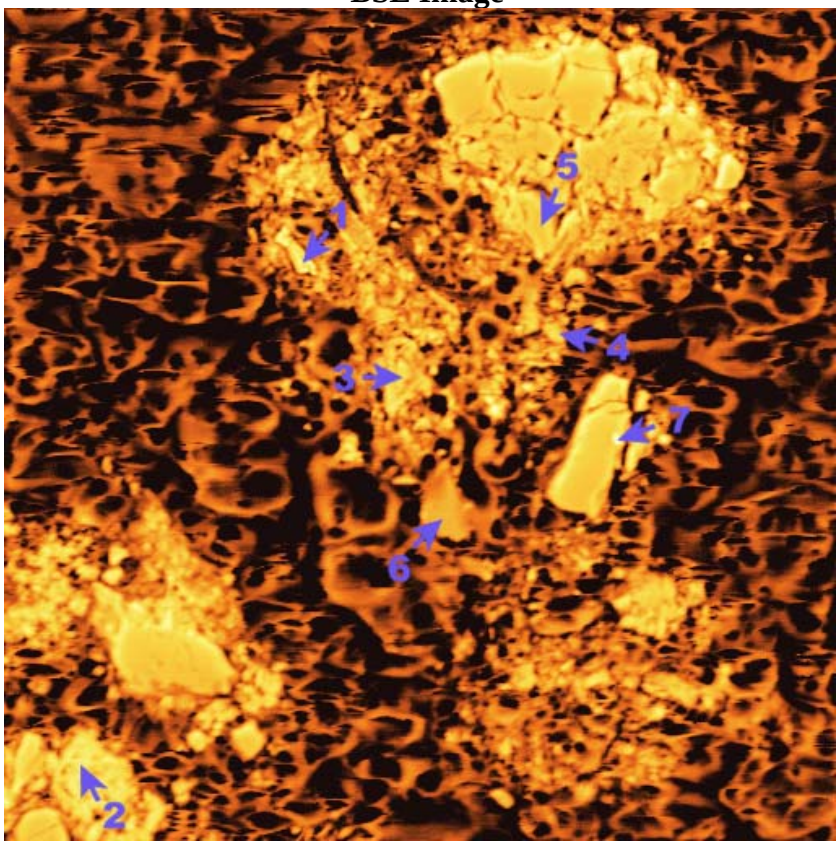

Iron (Fe)

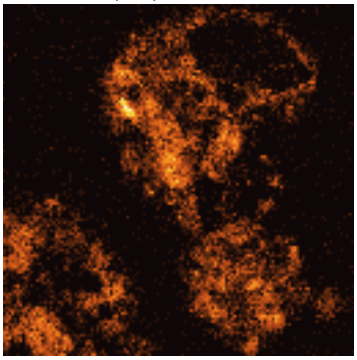

Manganese (Mn)

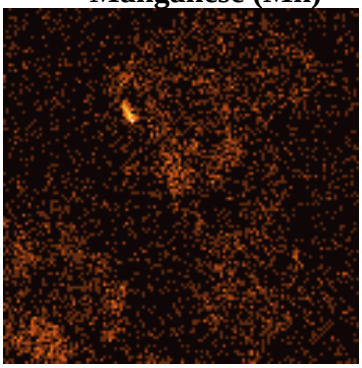

Phosphorous (P)

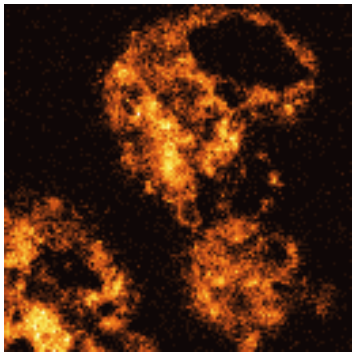

Lead (Pb)

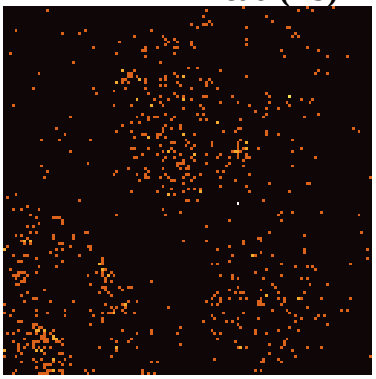

Silicon (Si)

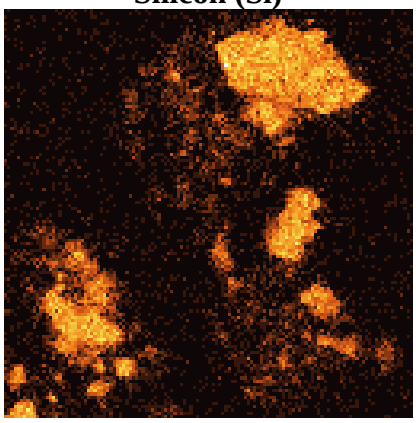

EDS Scan Images by Point

Point 1

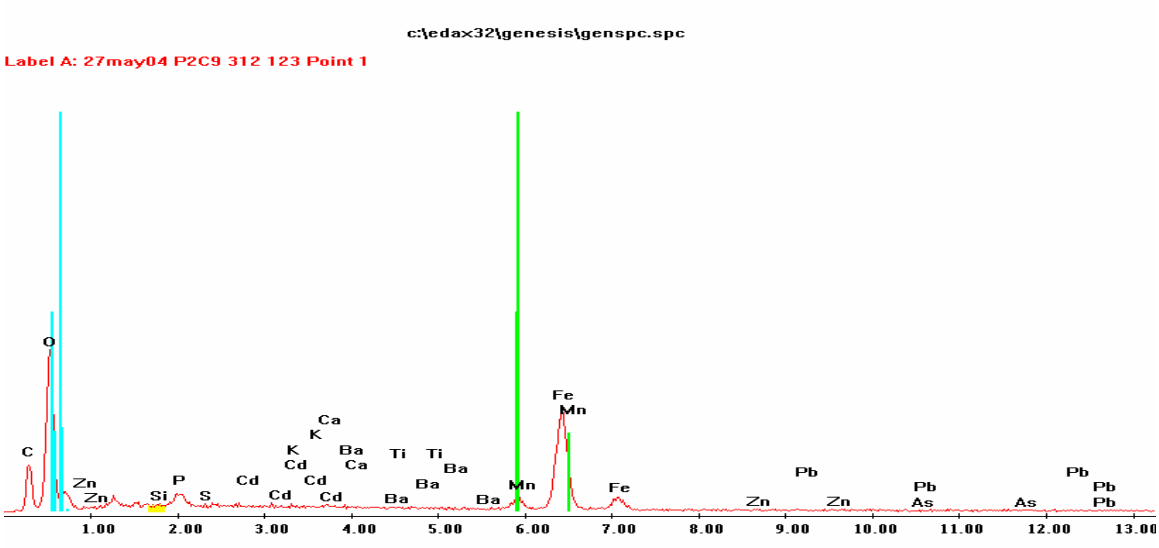

Point 2

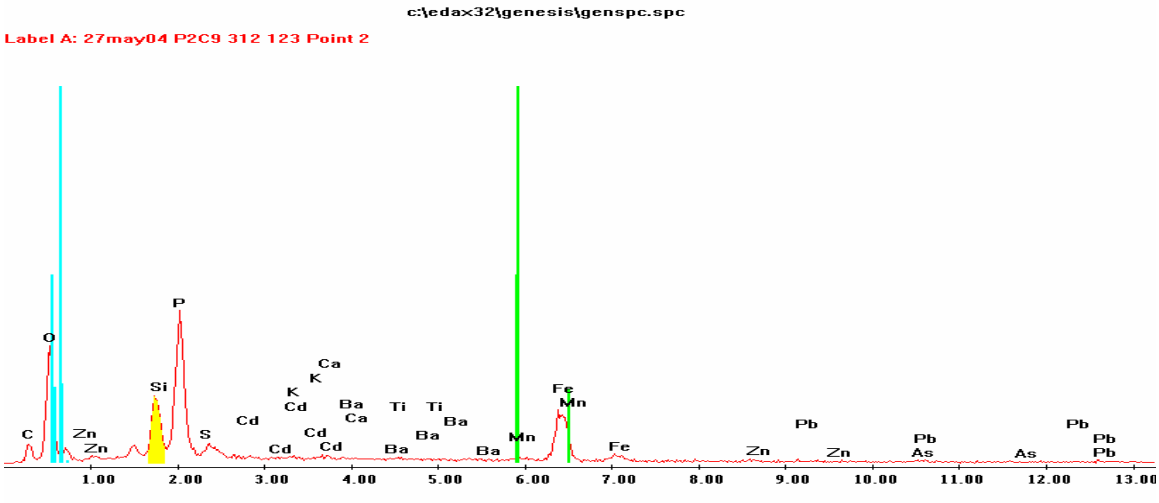

Point 3

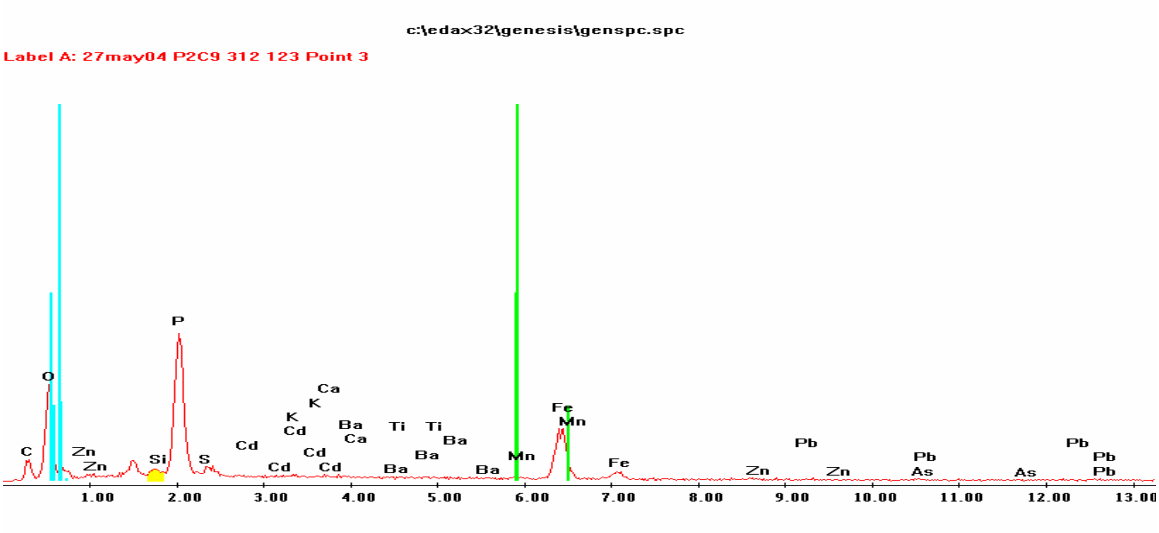

Point 4

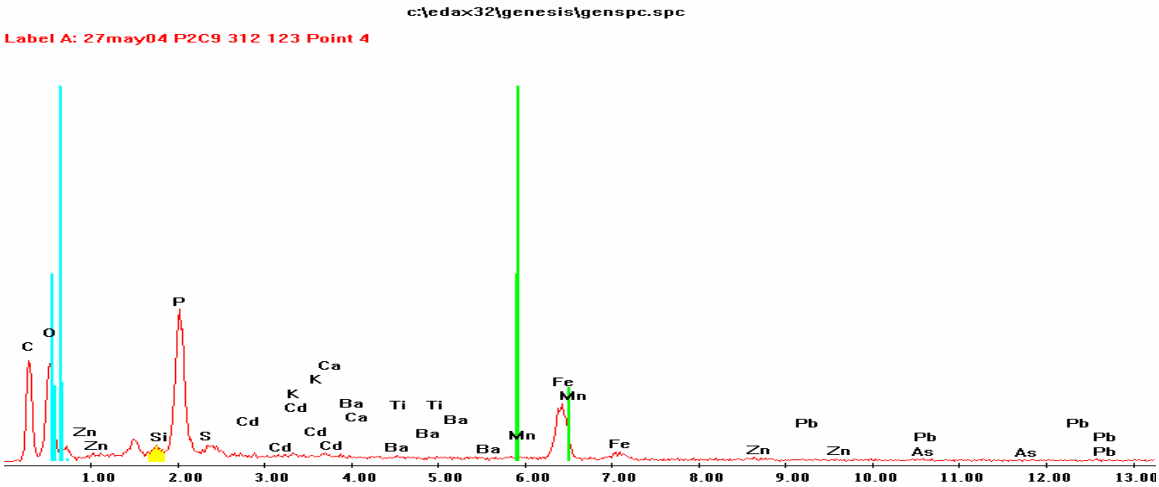

Point 5

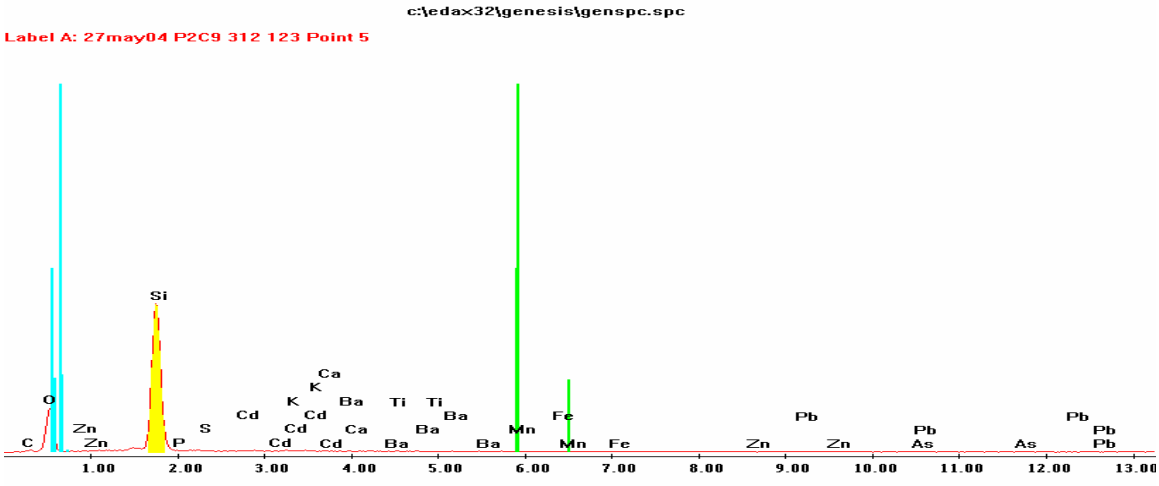

Point 6

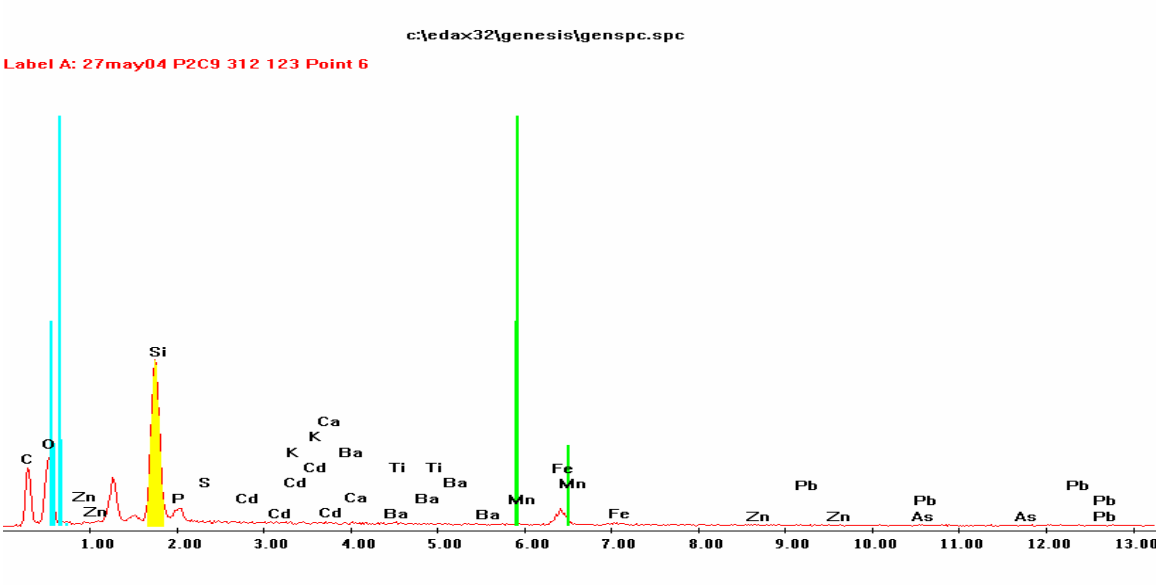

Point 7

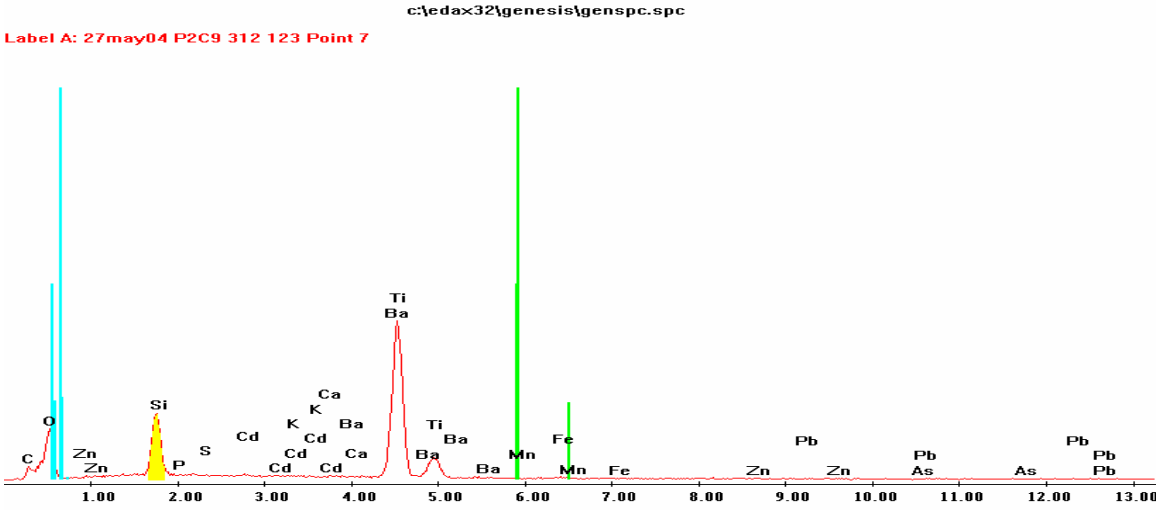

P2C9 – 320, 109

BSE Image

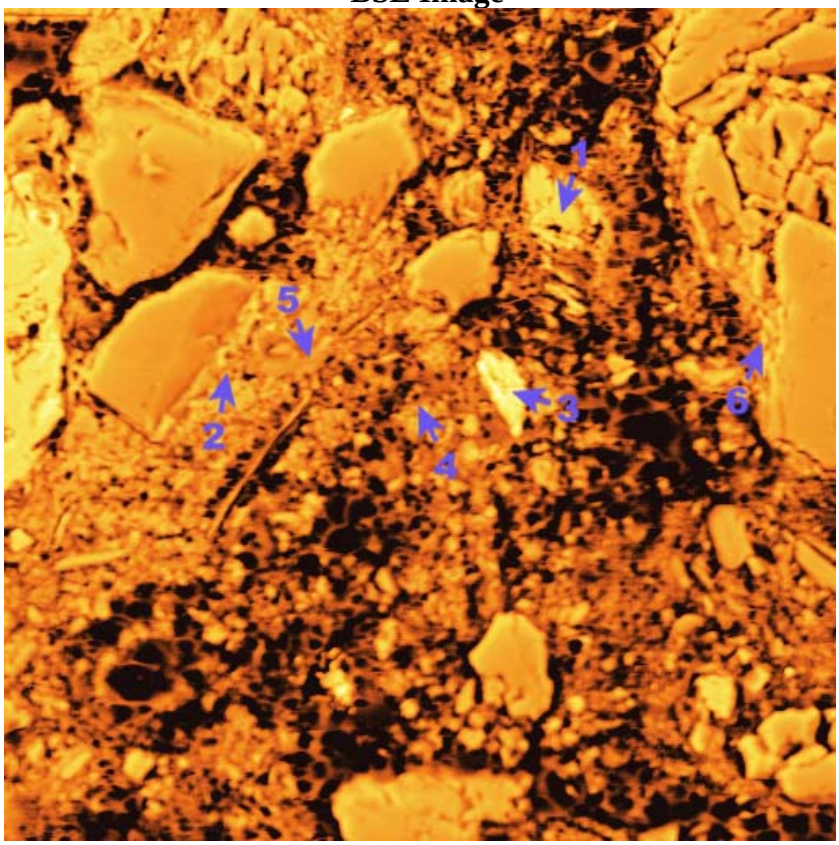

Iron (Fe)

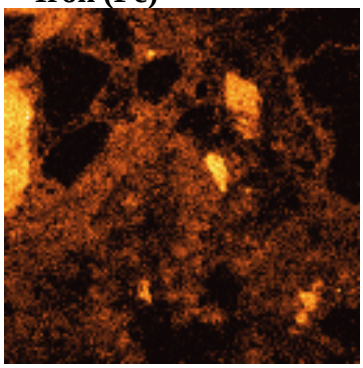

Manganese (Mn)

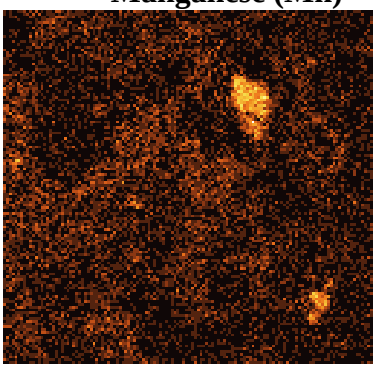

Phosphorous (P)

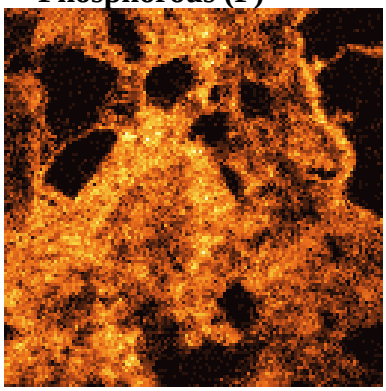

Lead (Pb)

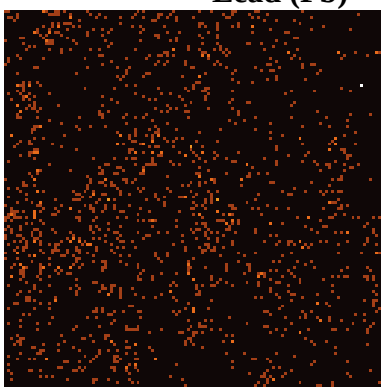

Silicon (Si)

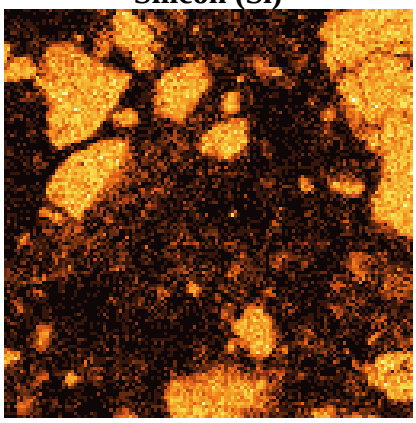

EDS Scan Images by Point

Point 1

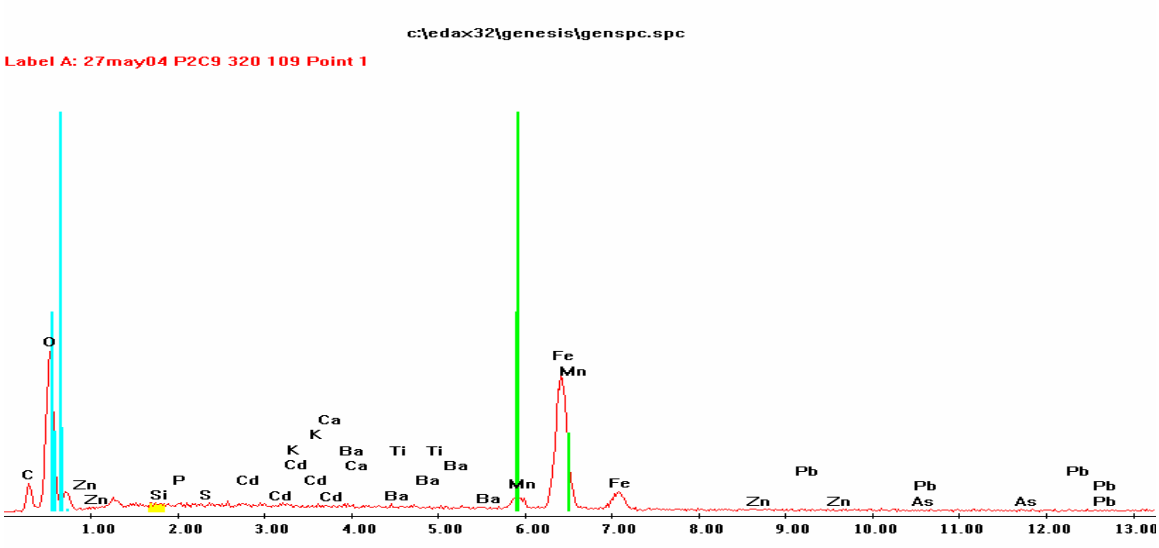

Point 2

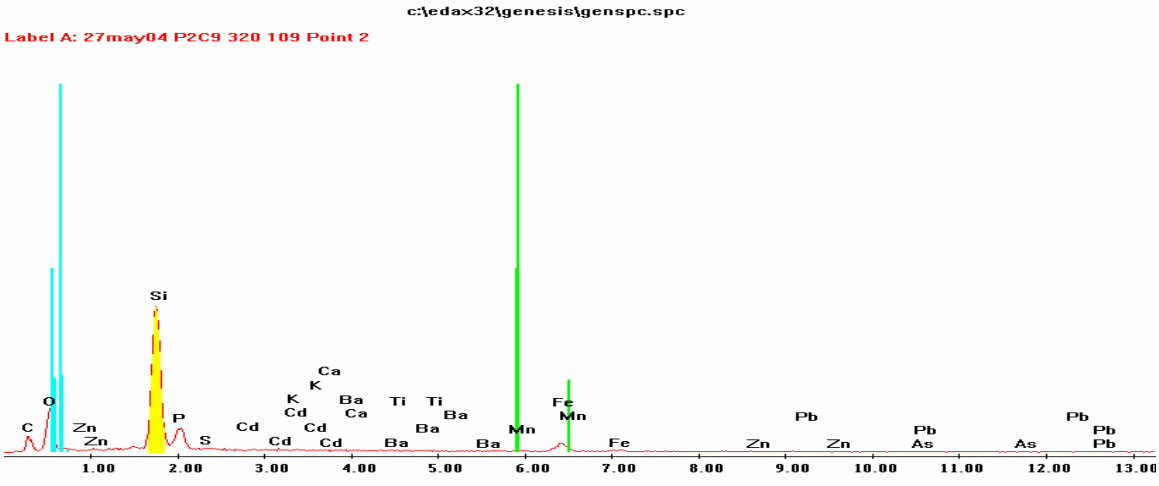

Point 3

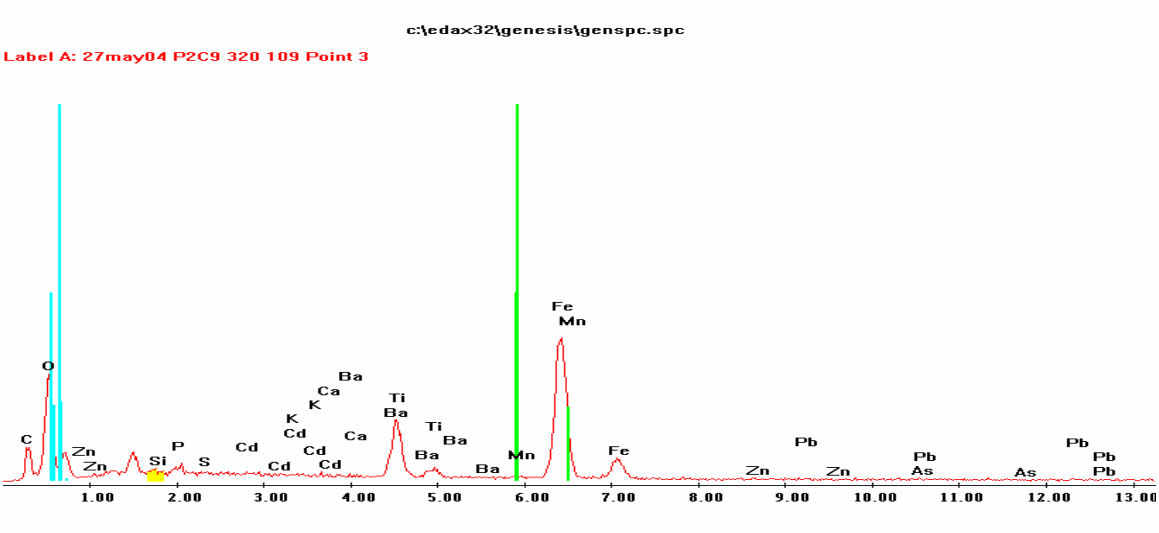

Point 4

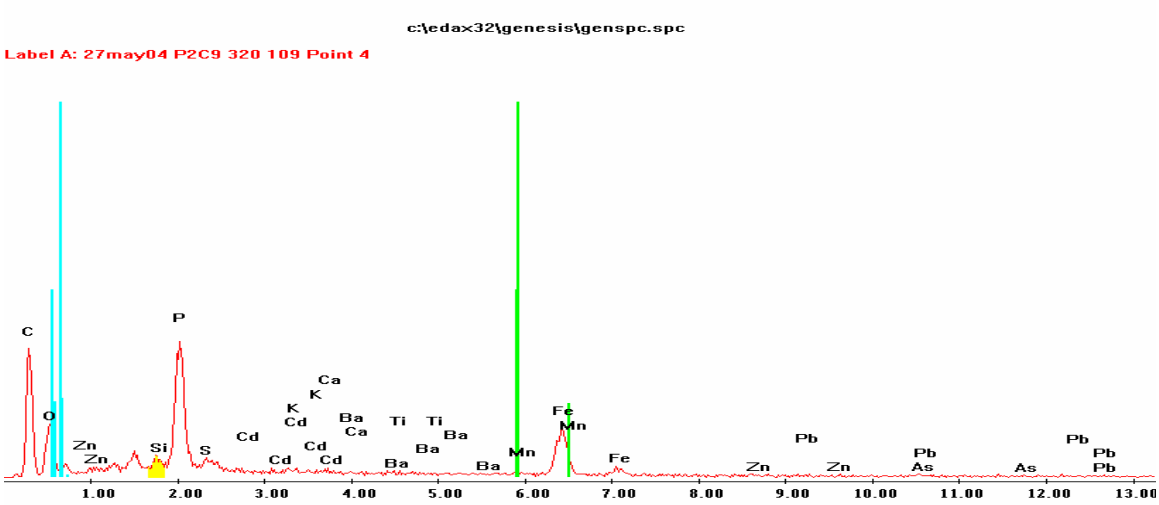

Point 5

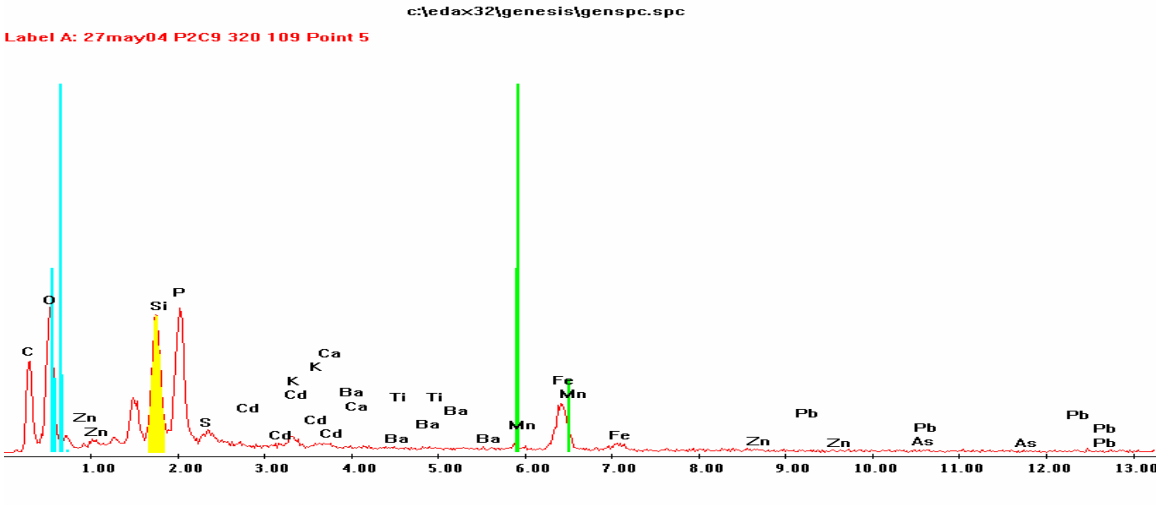

Point 6

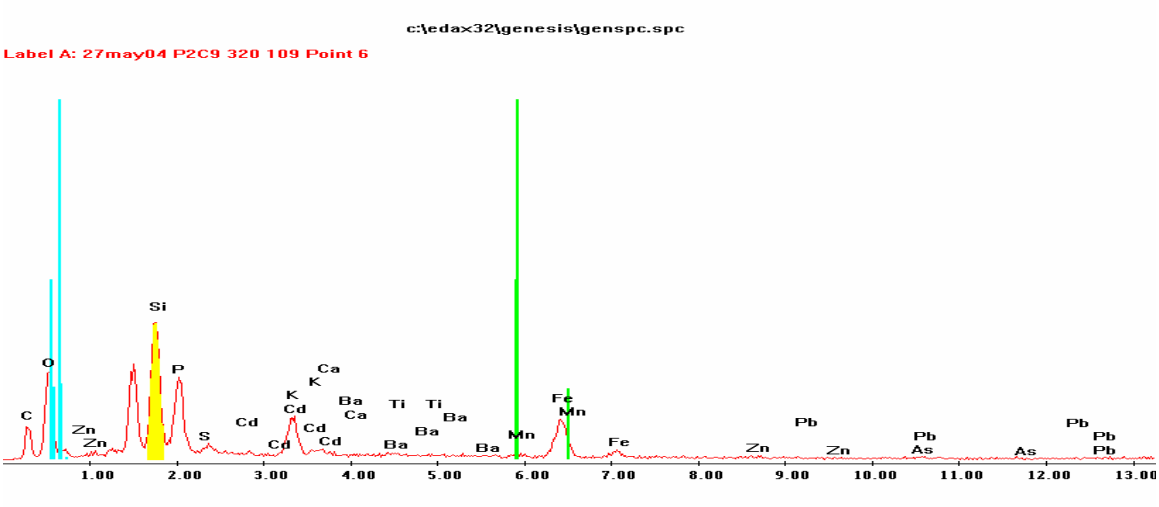
c:\edax32\genesis\genspc.spc
Label A: 27may04 P2C9 320 109 Point 6
C
O
Zn
Zn
Si
P
S
Cd
Cd
K
Cd
Ca
K
Cd
Cd
Ba
Ca
Ba
Ti
Ba
Ti
Ba
Mn
Fe
Mn
Fe
Zn
Pb
Zn
Pb
As
As
Pb
Pb
Pb
1.00
2.00
3.00
4.00
5.00
6.00
7.00
8.00
9.00
10.00
11.00
12.00
13.00

P2C9 – 348, 105

BSE Image

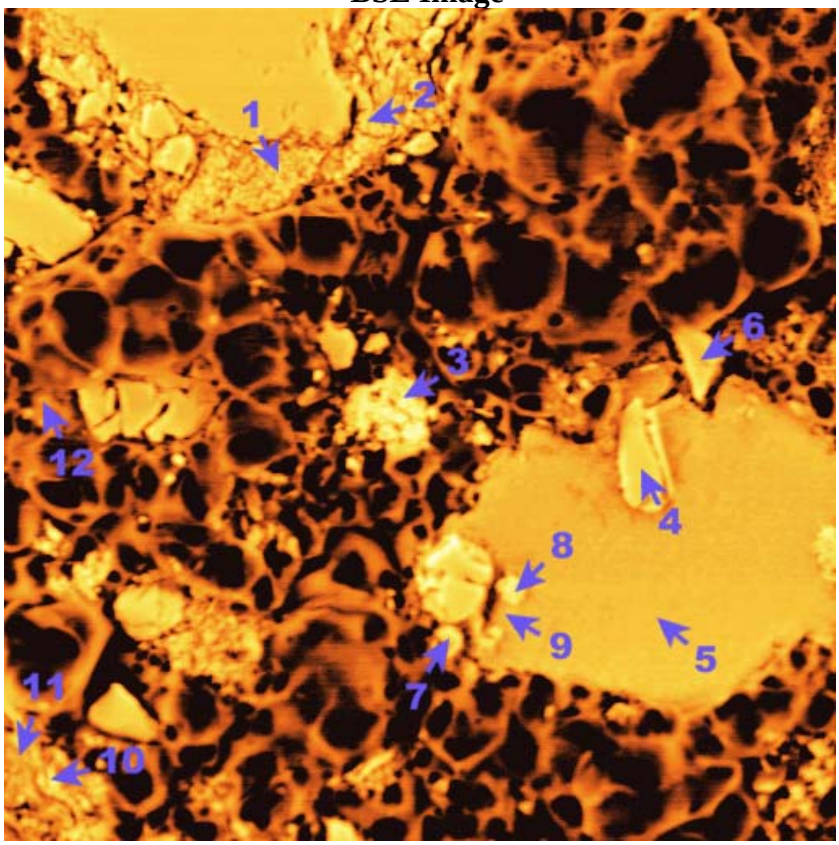

Iron (Fe)

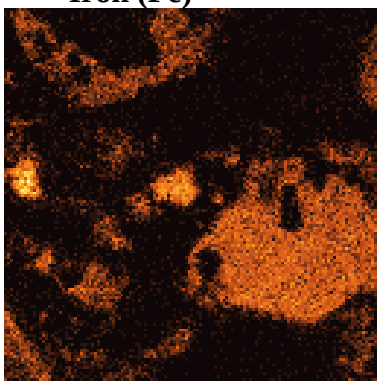

Manganese (Mn)

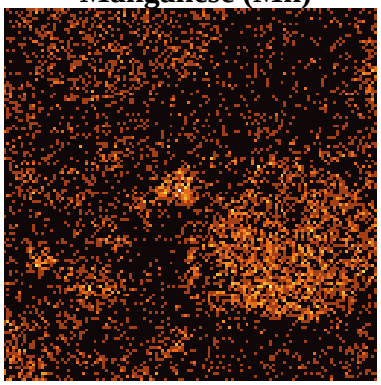

Phosphorous (P)

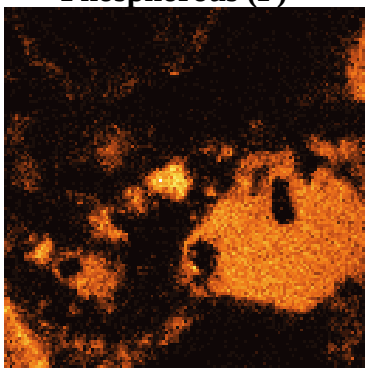

Lead (Pb)

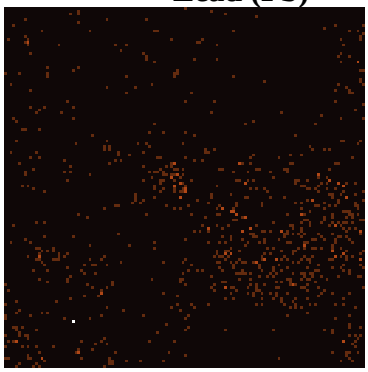

Silicon (Si)

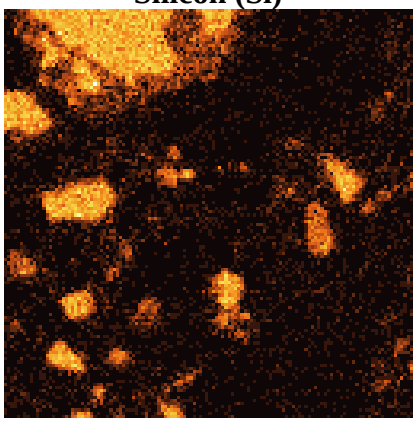

EDS Scan Images by Point

Point 1

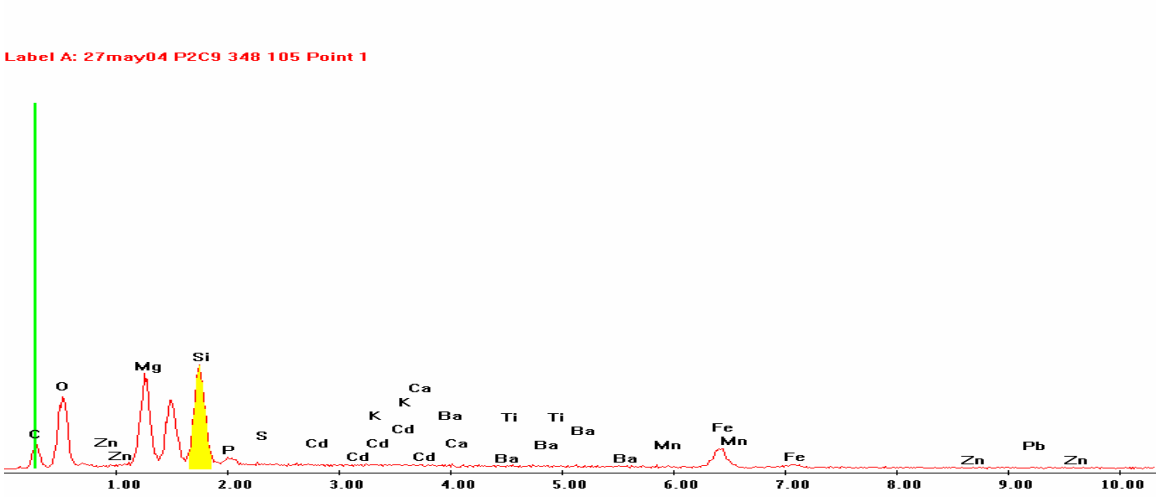

Point 2

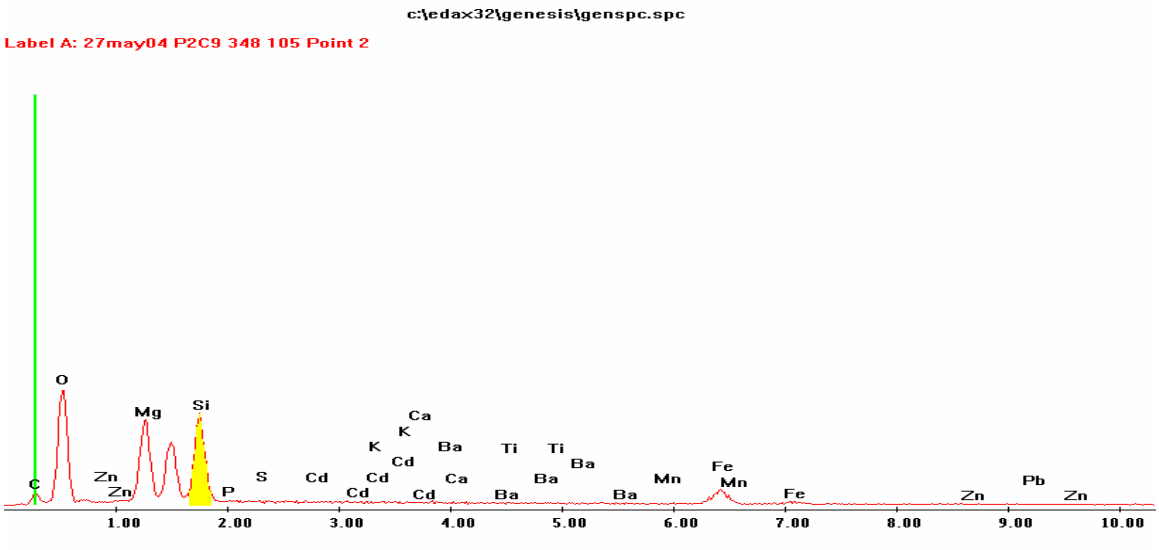

Point 3

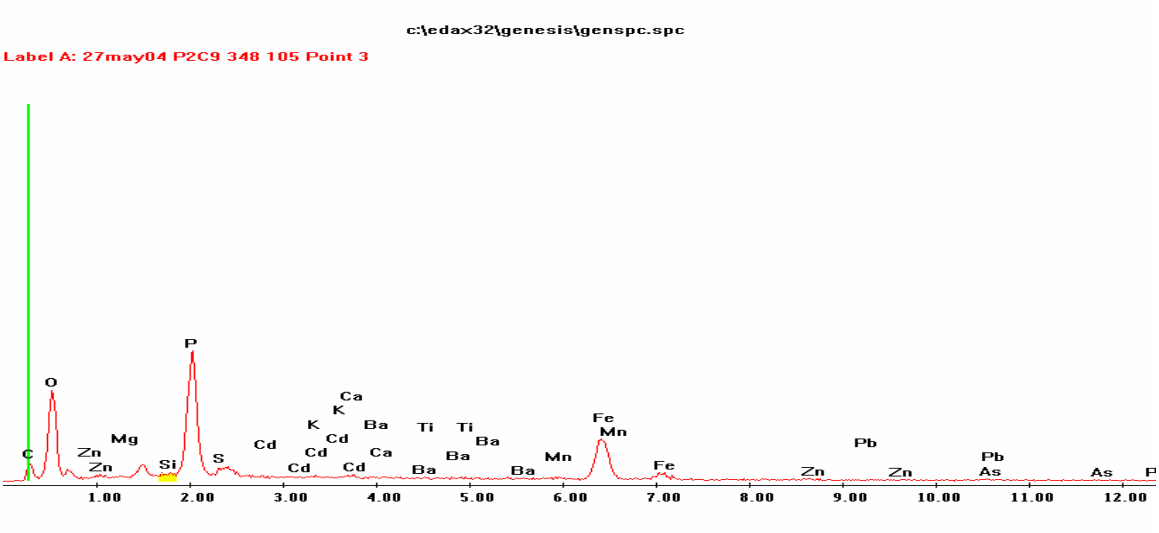

Point 4

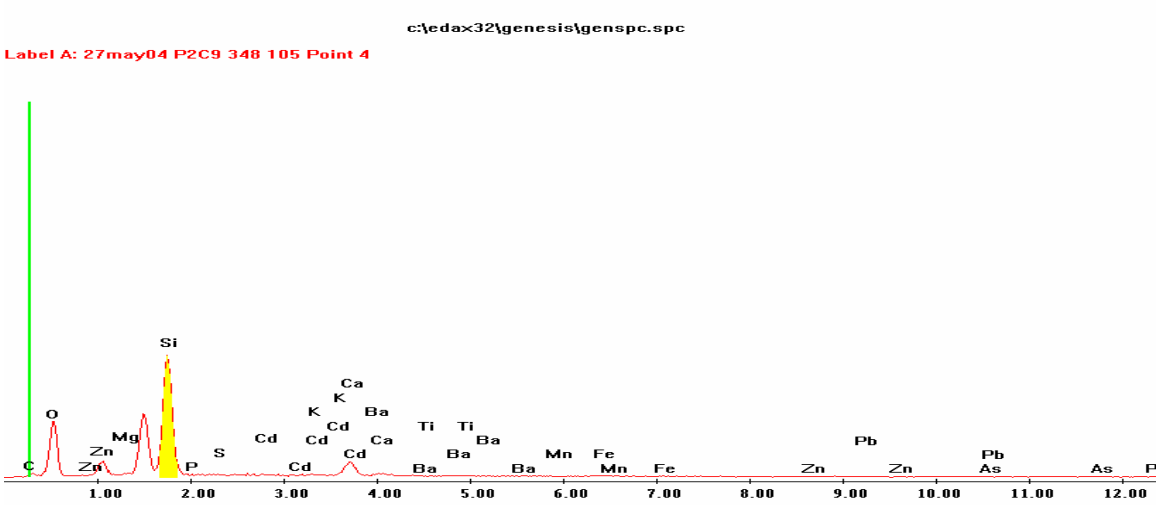

Point 5

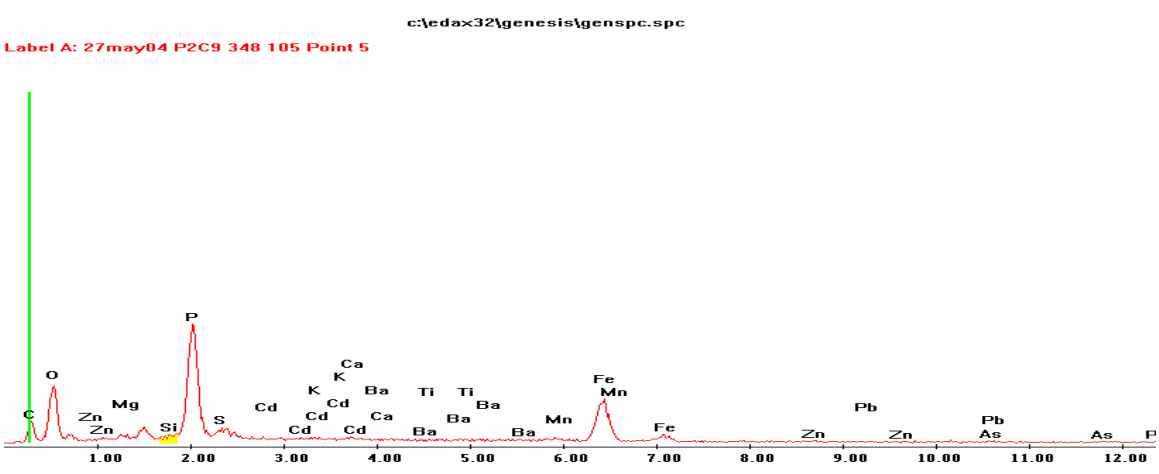

Point 6

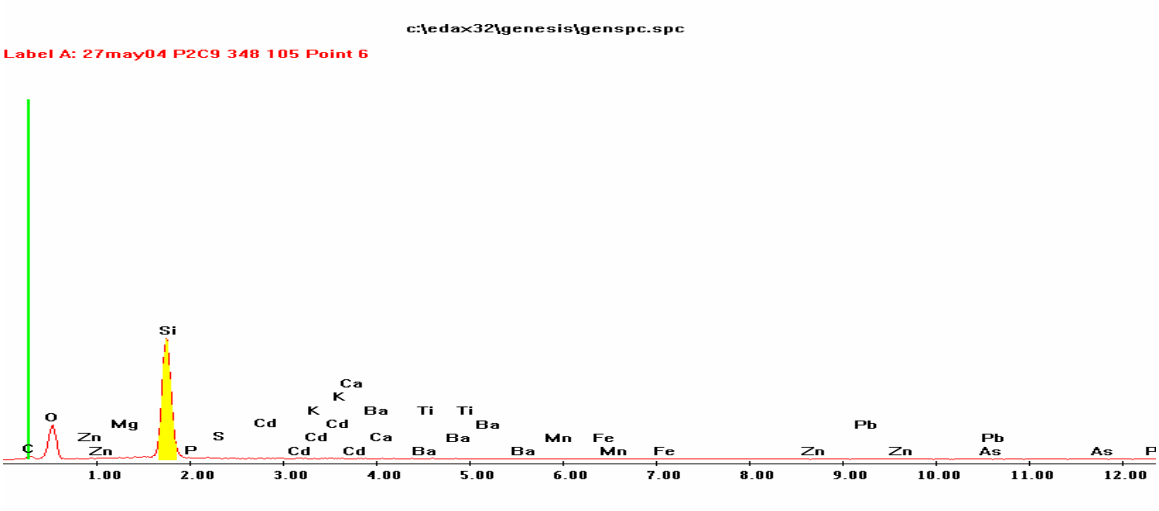

Point 7

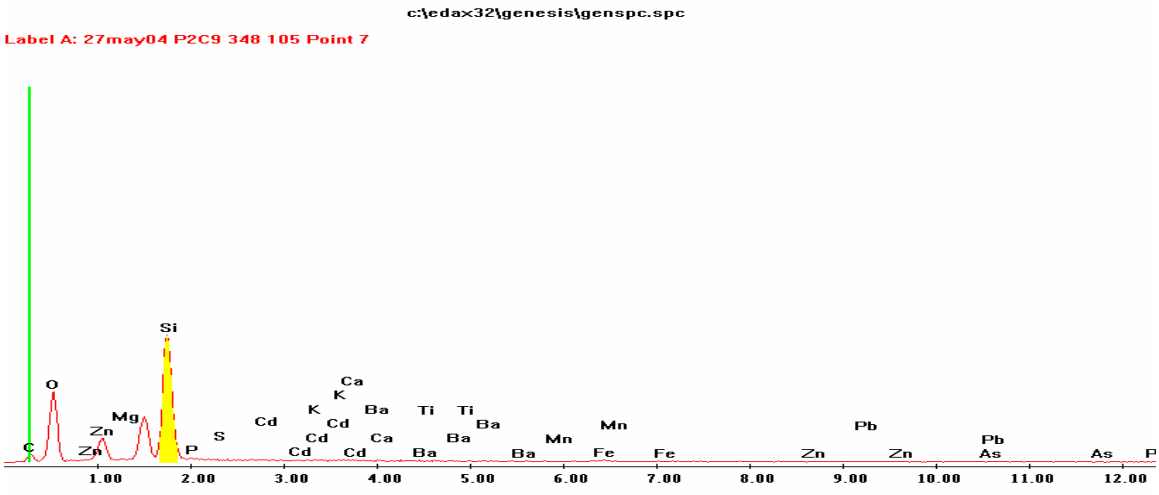

Point 8

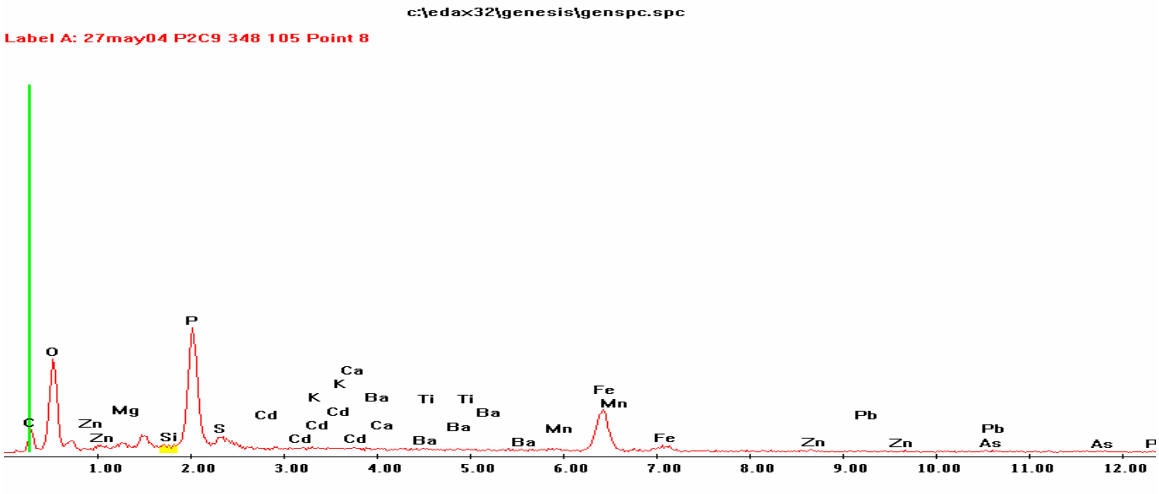

Point 9

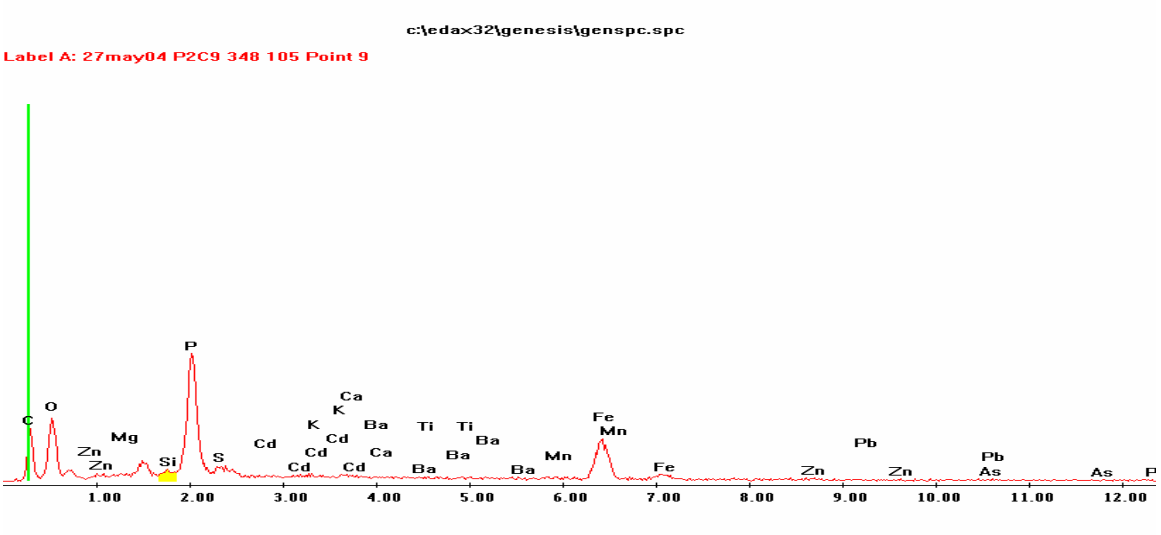

Point 10

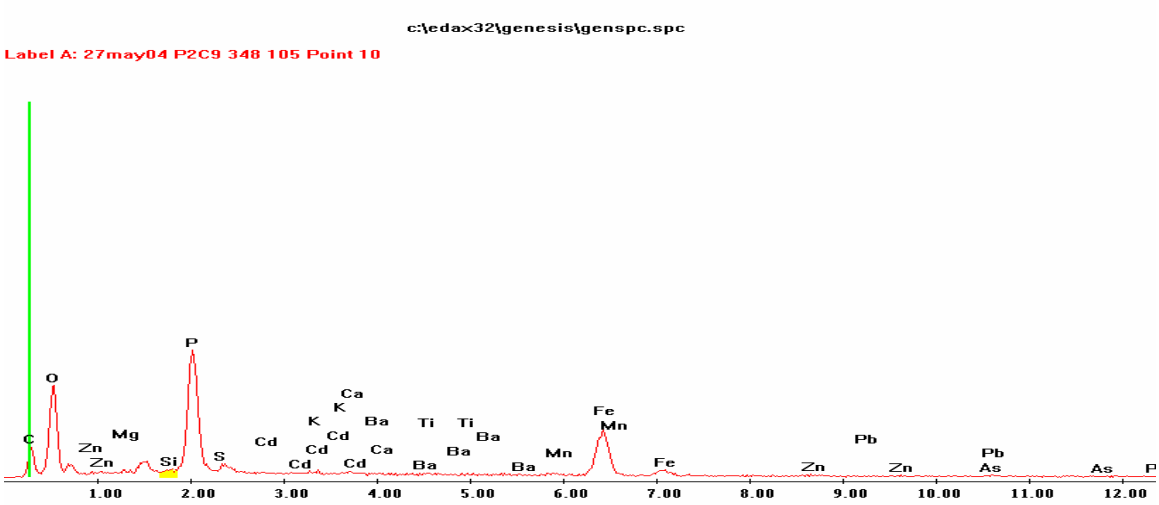

Point 11

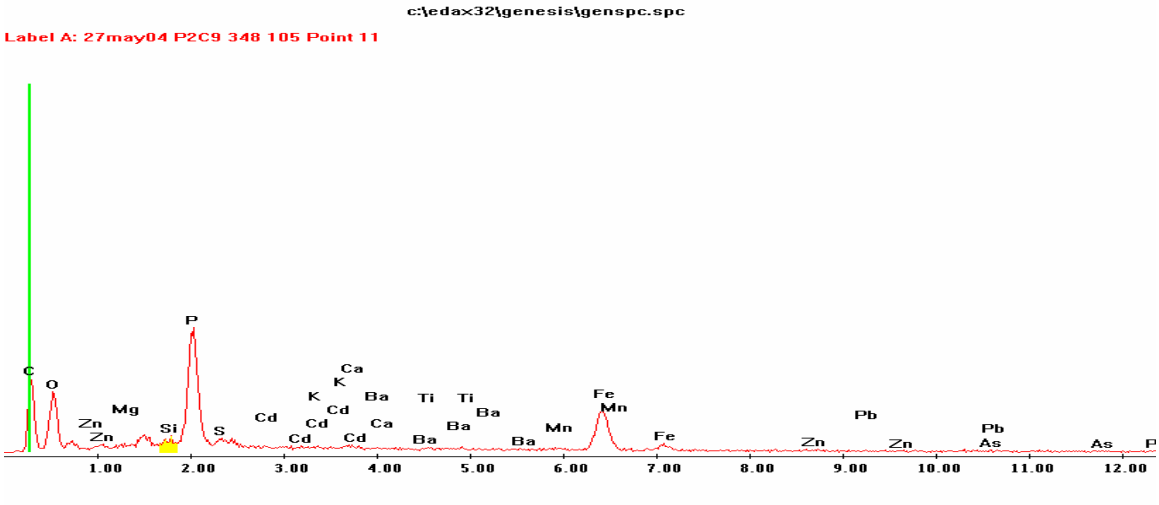

Point 12

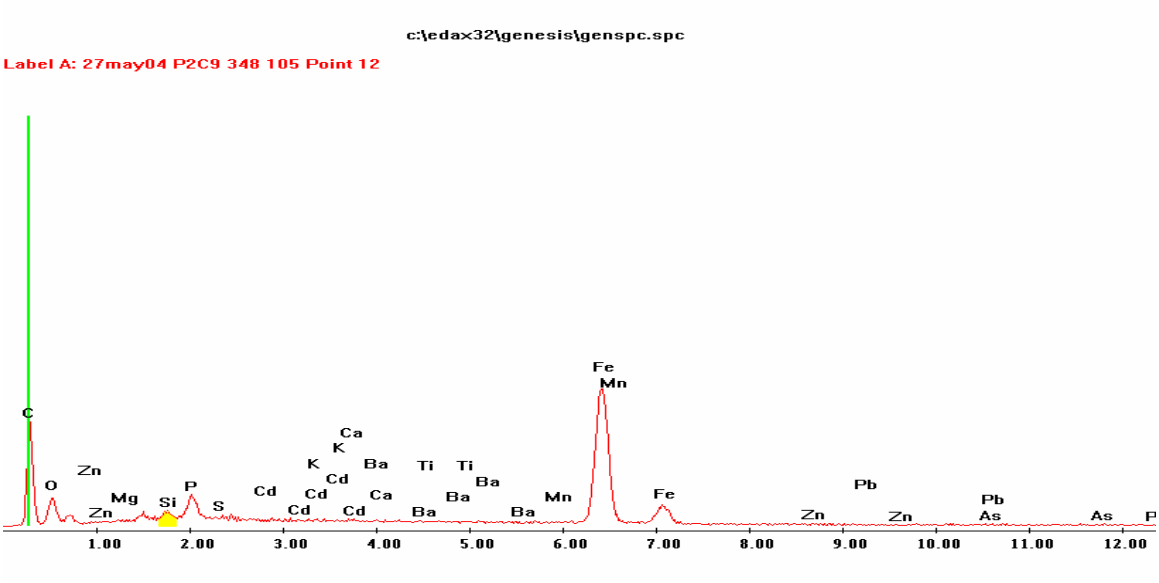
c:\edax32\genesis\genspc.spc
Label A: 27may04 P2C9 348 105 Point 12
C
O
Zn
Mg
Zn
Si
P
S
Cd
Cd
Cd
Cd
Ca
K
Ca
K
Cd
Ba
Ba
Ti
Ti
Ba
Ba
Ba
Mn
Fe
Mn
Fe
Zn
Pb
Zn
Pb
As
As
1.00
2.00
3.00
4.00
5.00
6.00
7.00
8.00
9.00
10.00
11.00
12.00

P2C9 – 372, 114

BSE Image

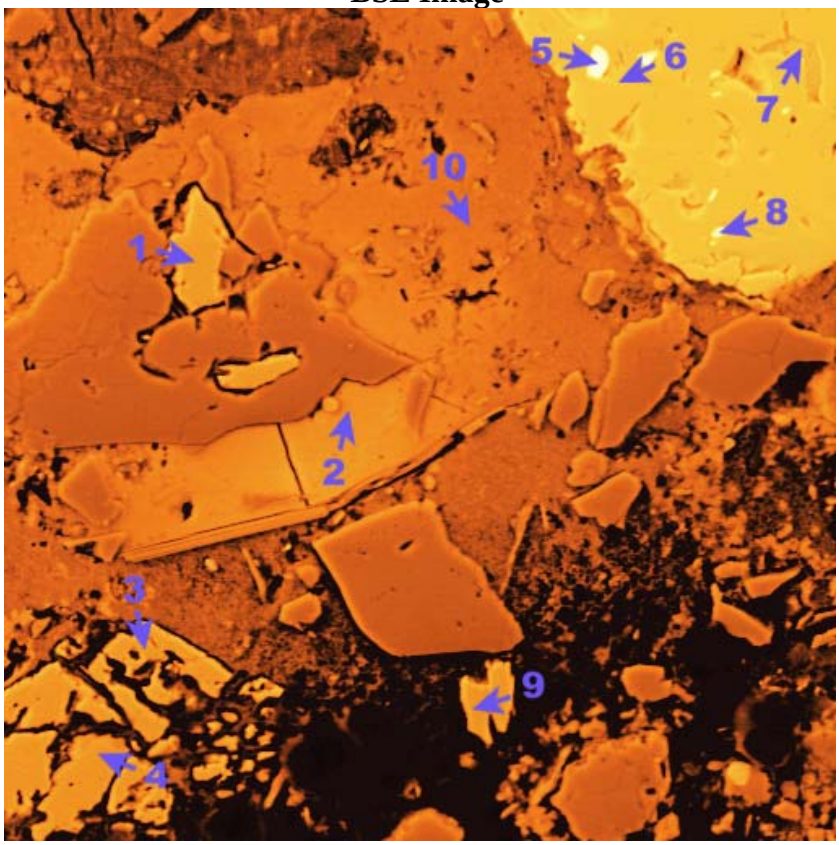

Iron (Fe)

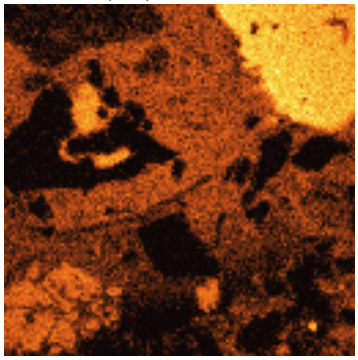

Manganese (Mn)

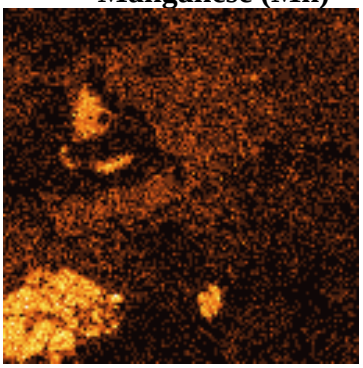

Phosphorous (P)

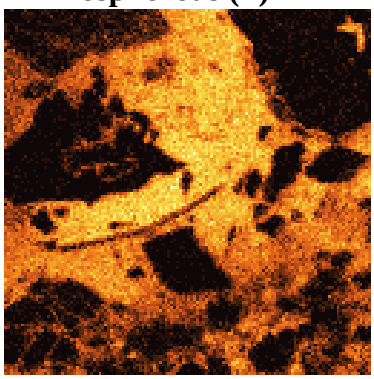

Lead (Pb)

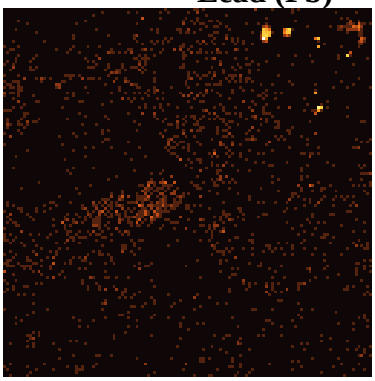

Silicon (Si)

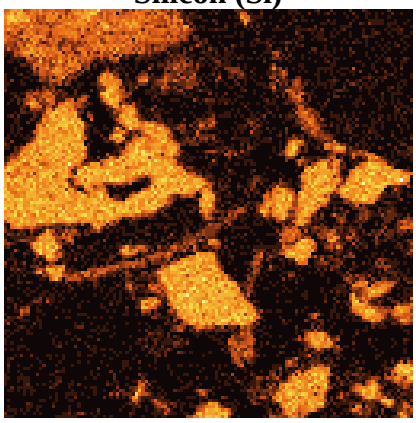

EDS Scan Images by Point

Point 1

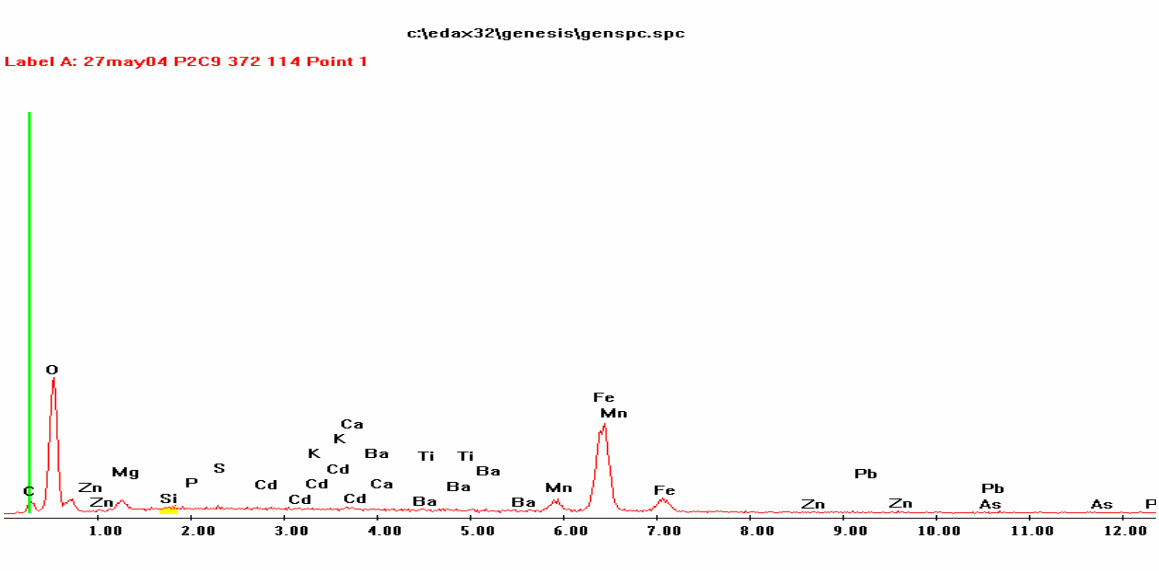

Point 2

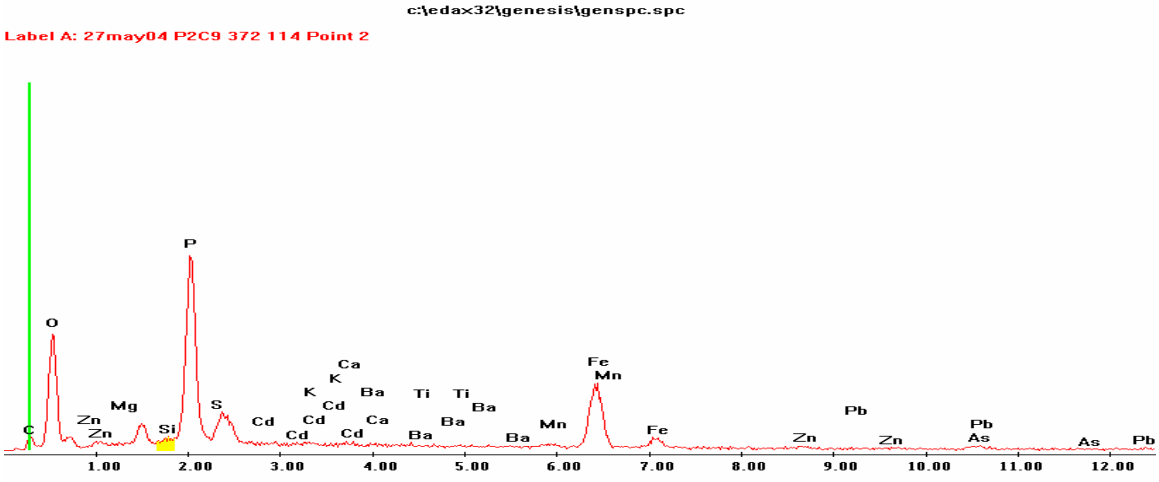

Point 3

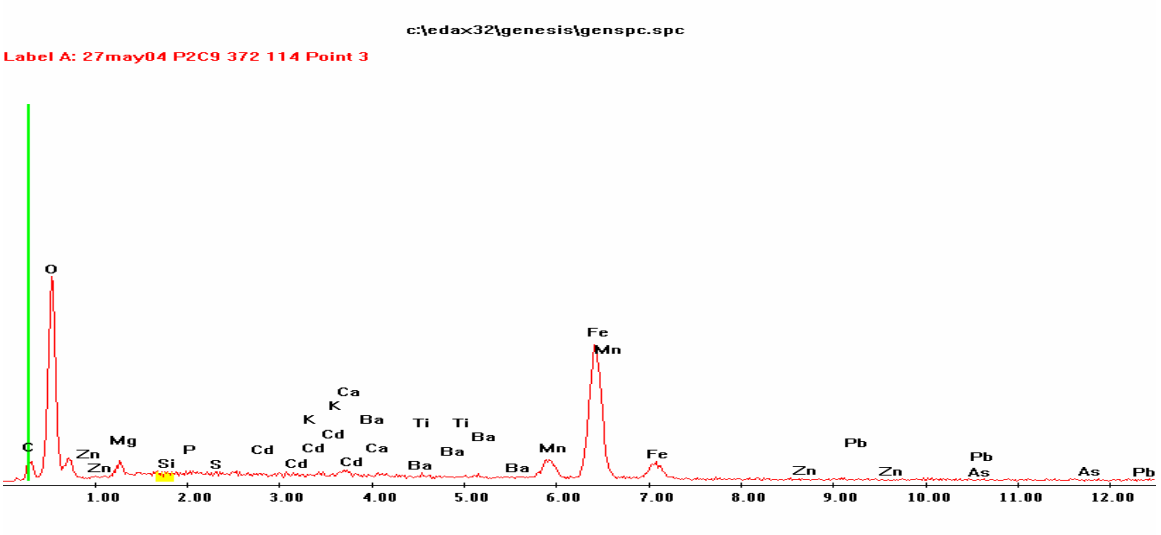

Point 4

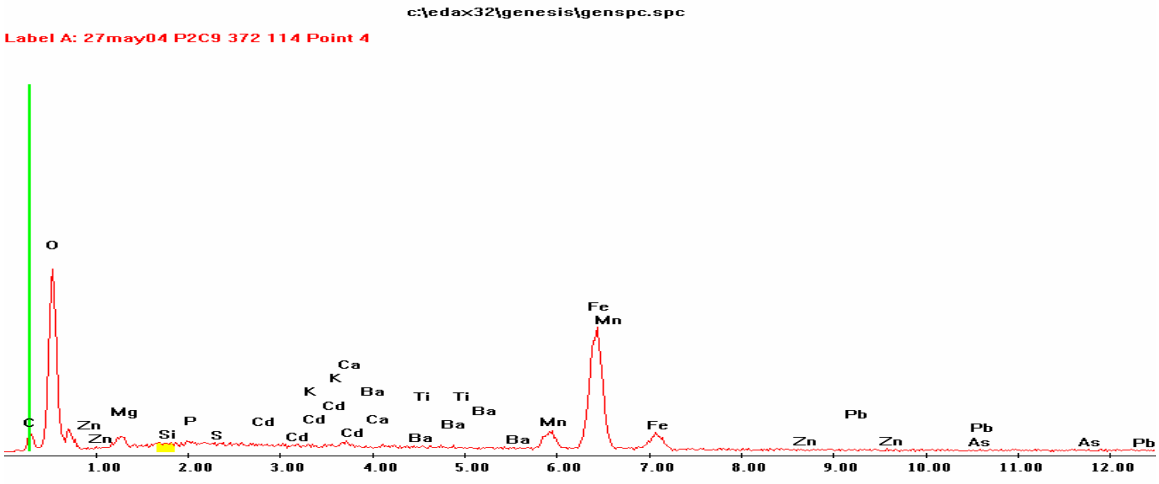

Point 5

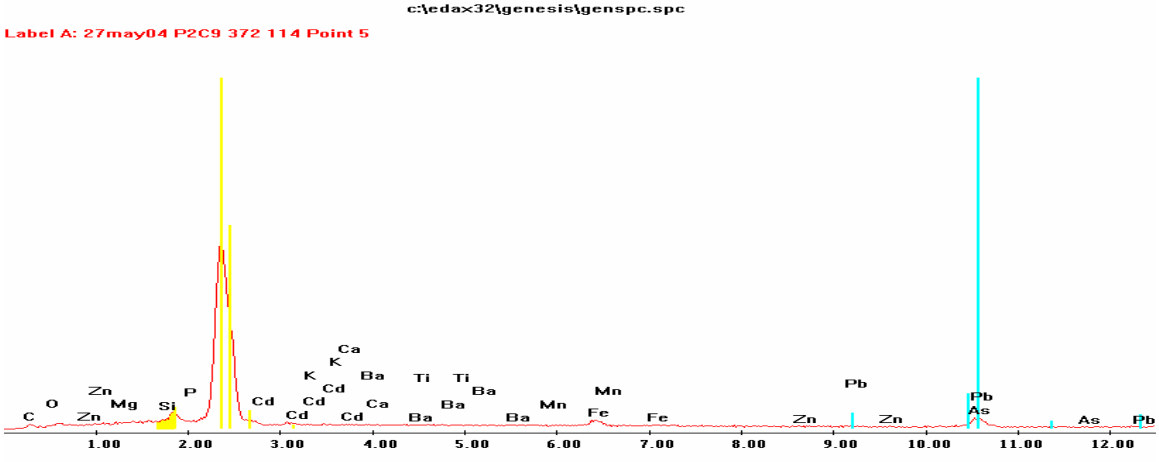

Point 6

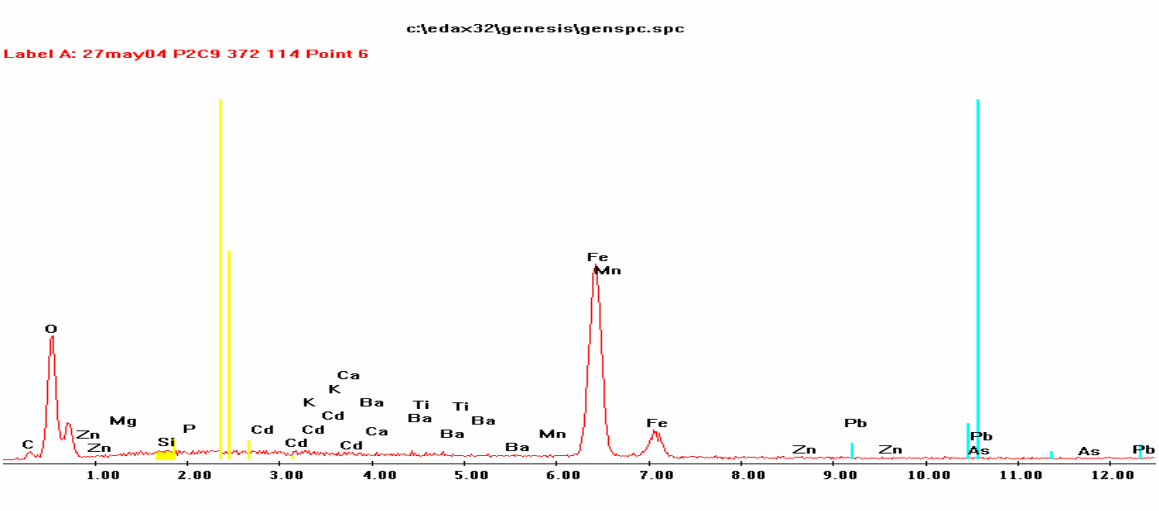

Point 7

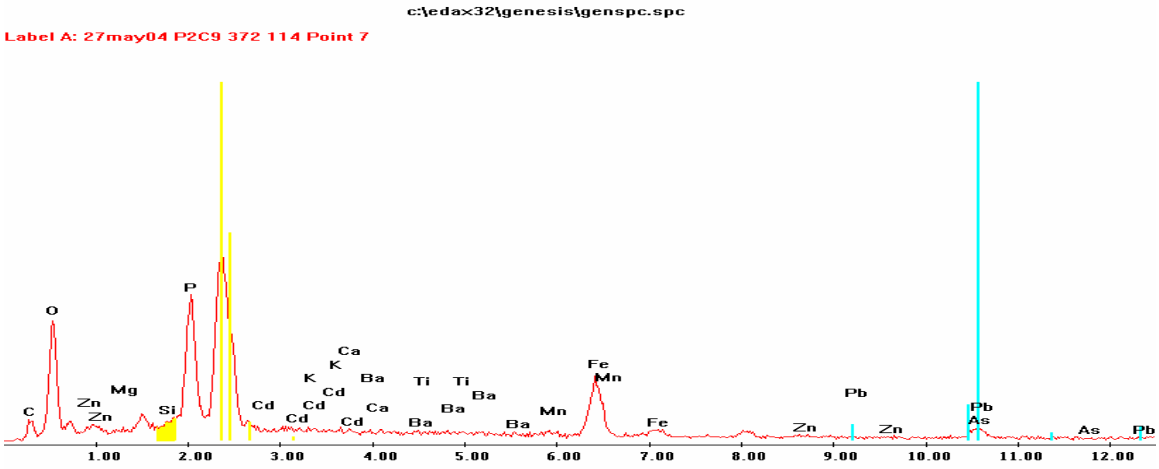

Point 8

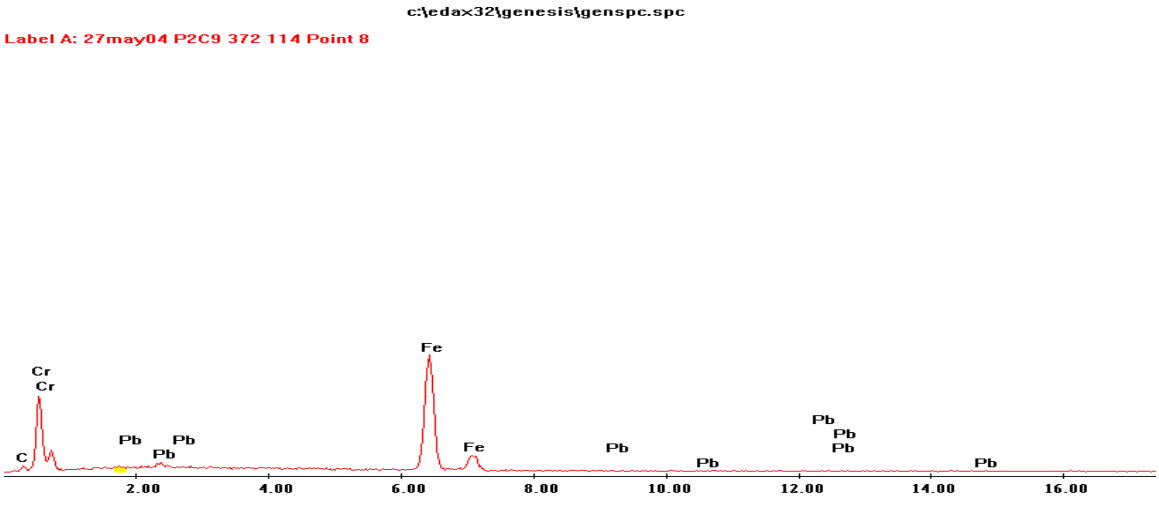

Point 9

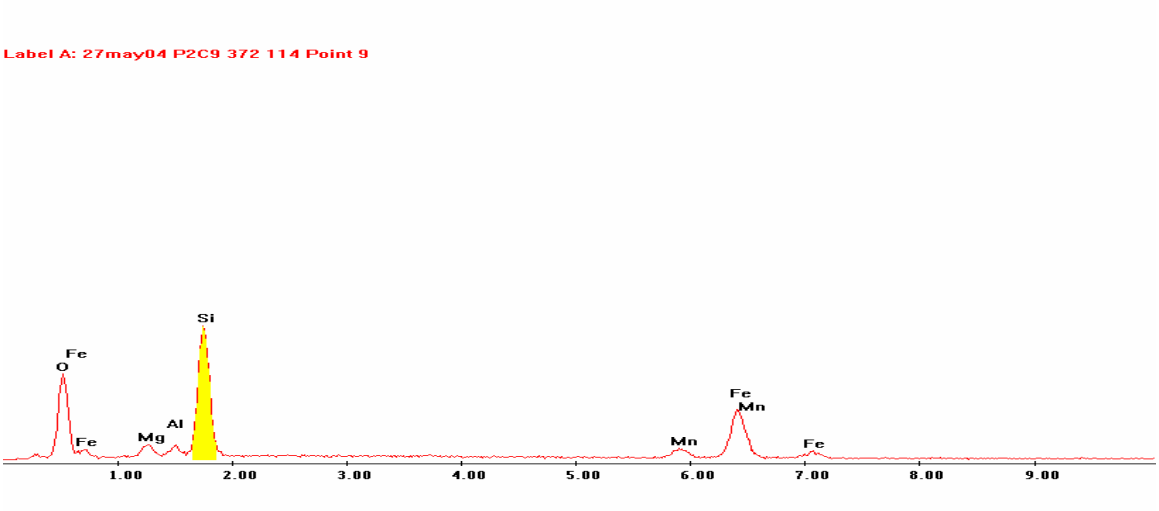

Point 10

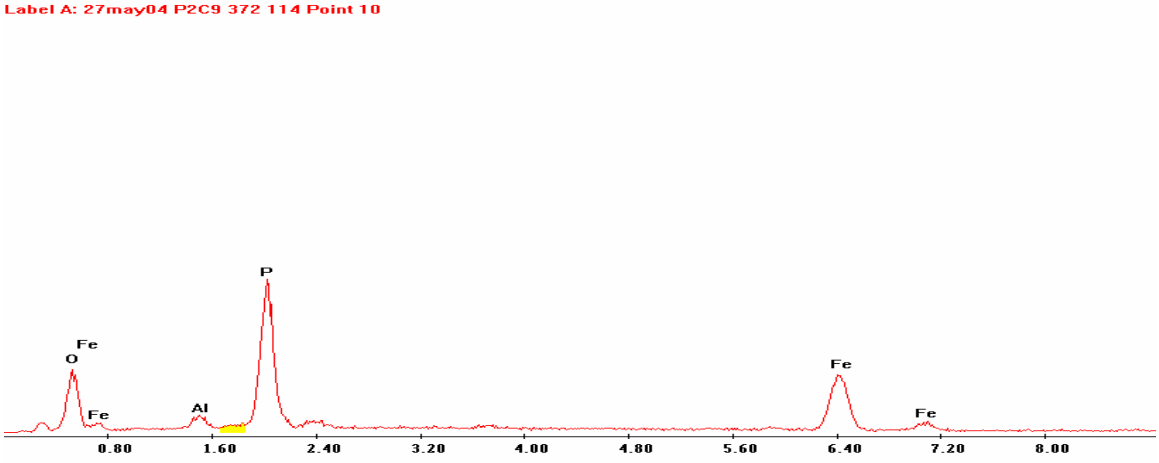

P2C9 – 394, 083

BSE Image

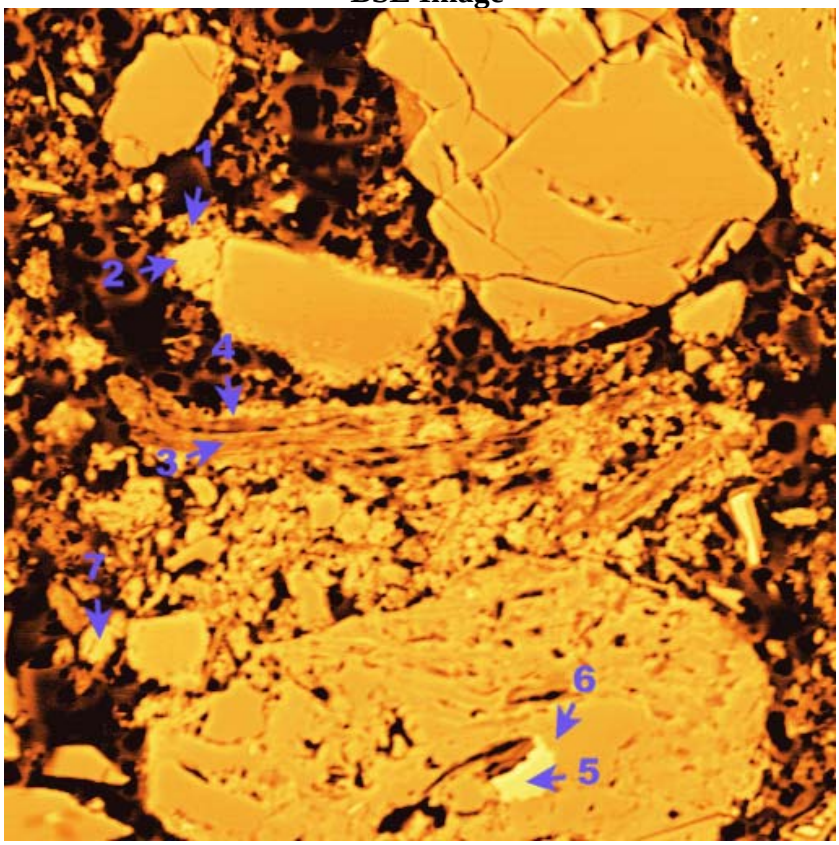

Iron (Fe)

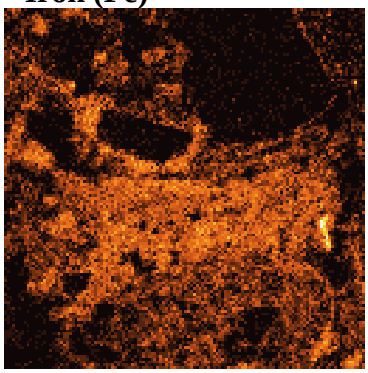

Manganese (Mn)

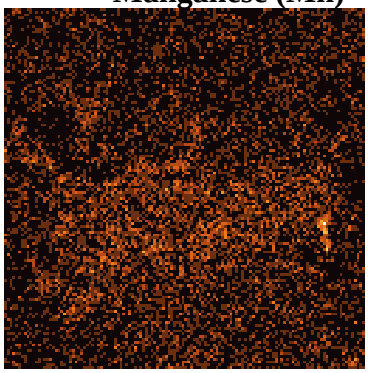

Phosphorous (P)

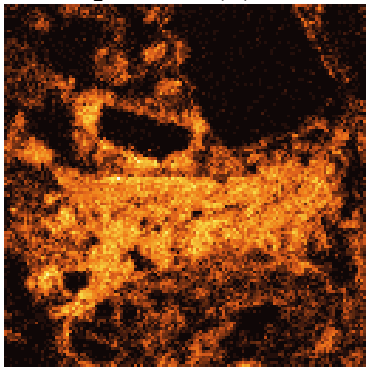

Lead (Pb)

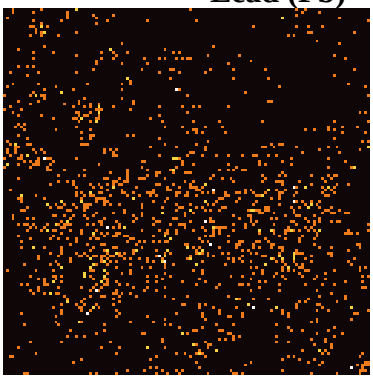

Silicon (Si)

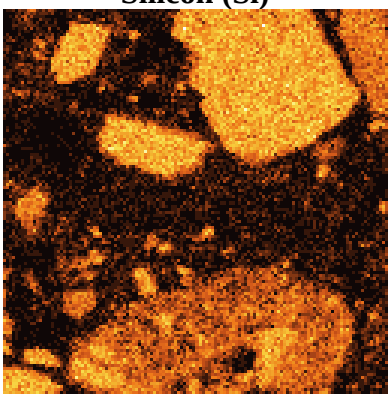

EDS Scan Images by Point

Point 1

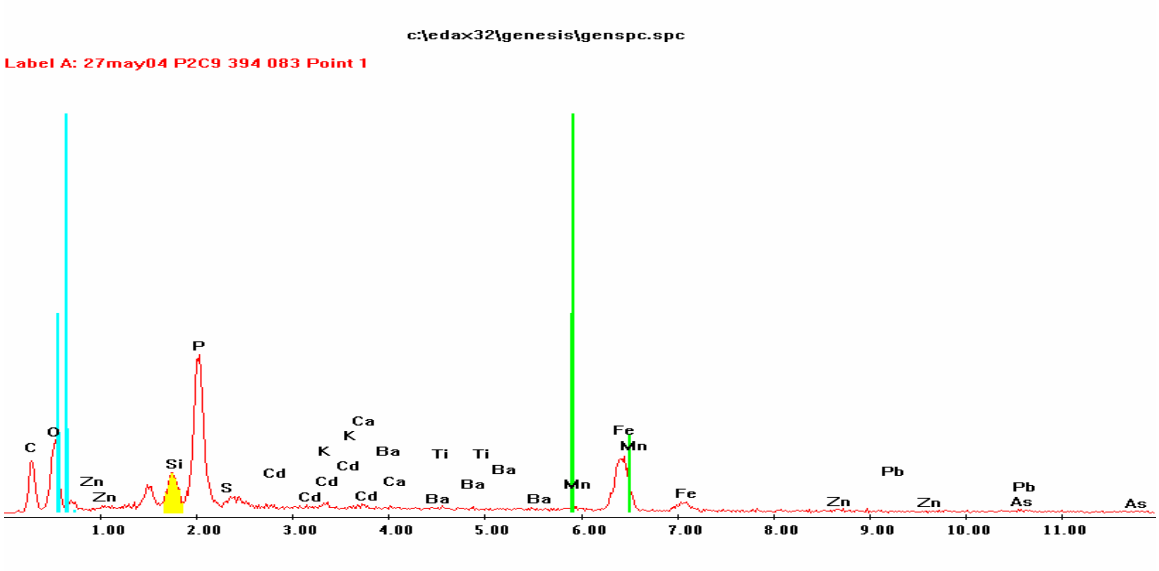

Point 2

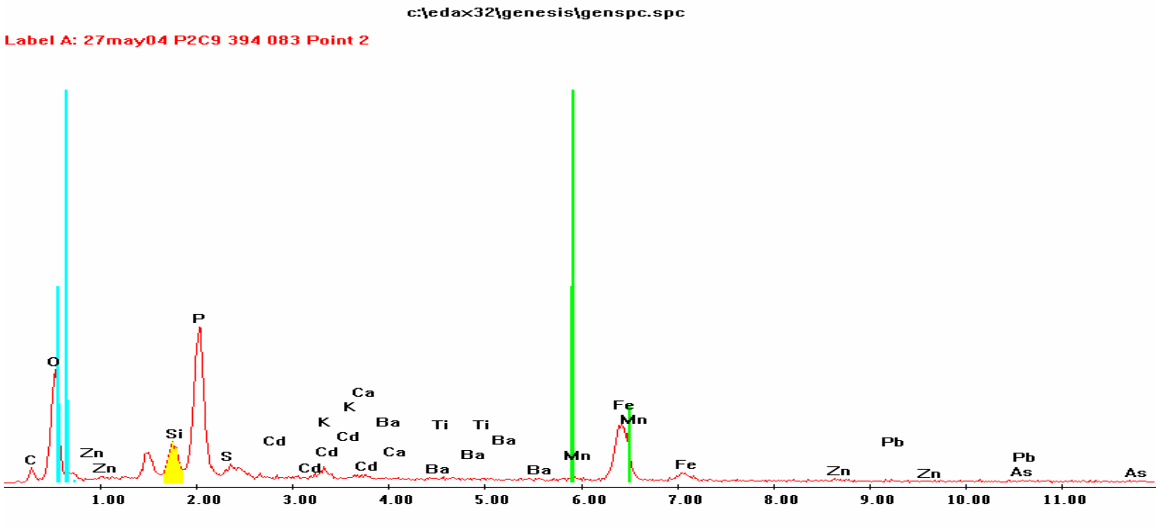

Point 3

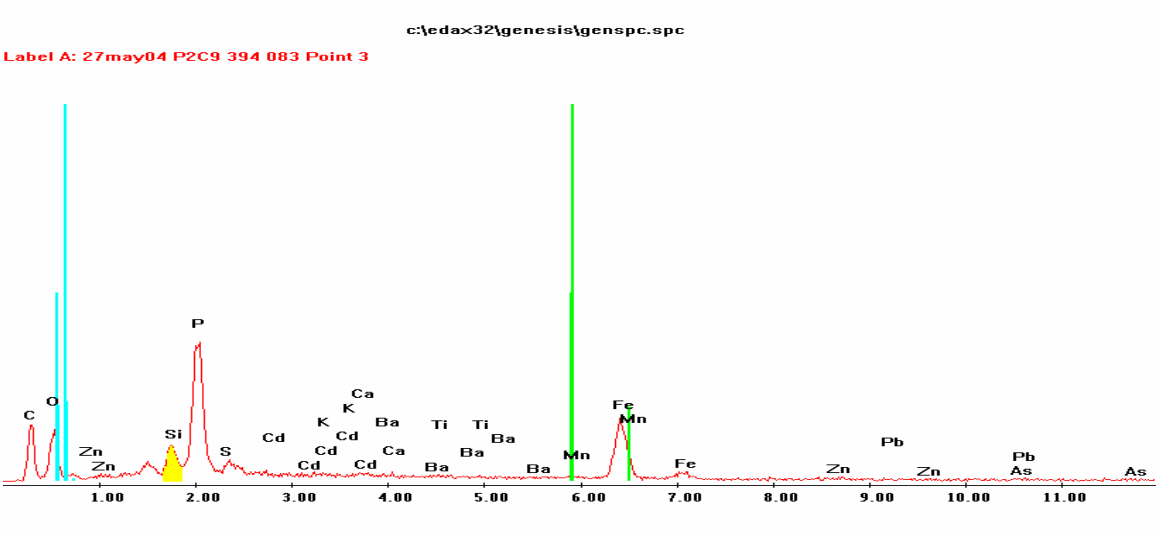

Point 4

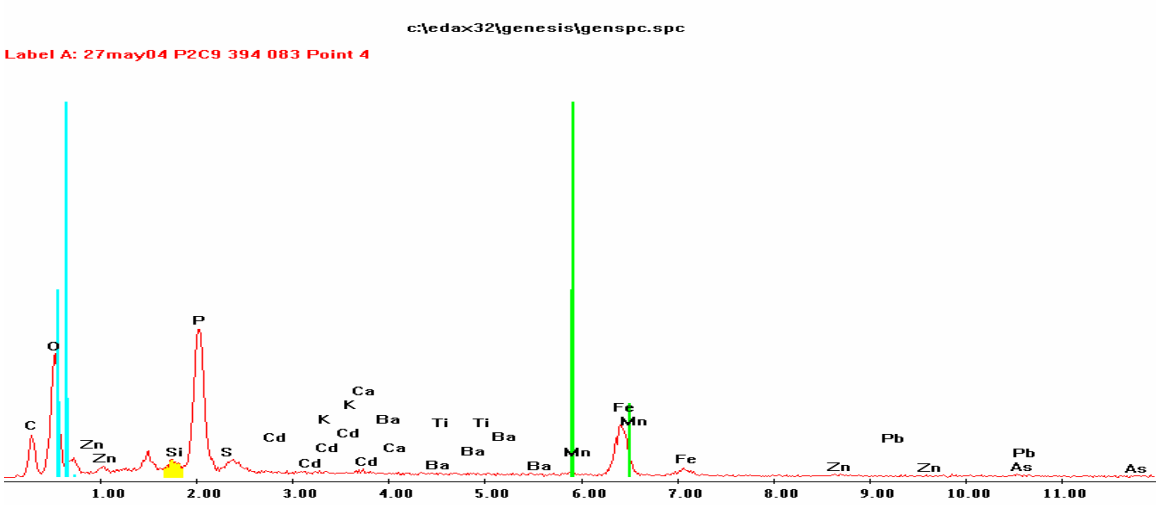

Point 5

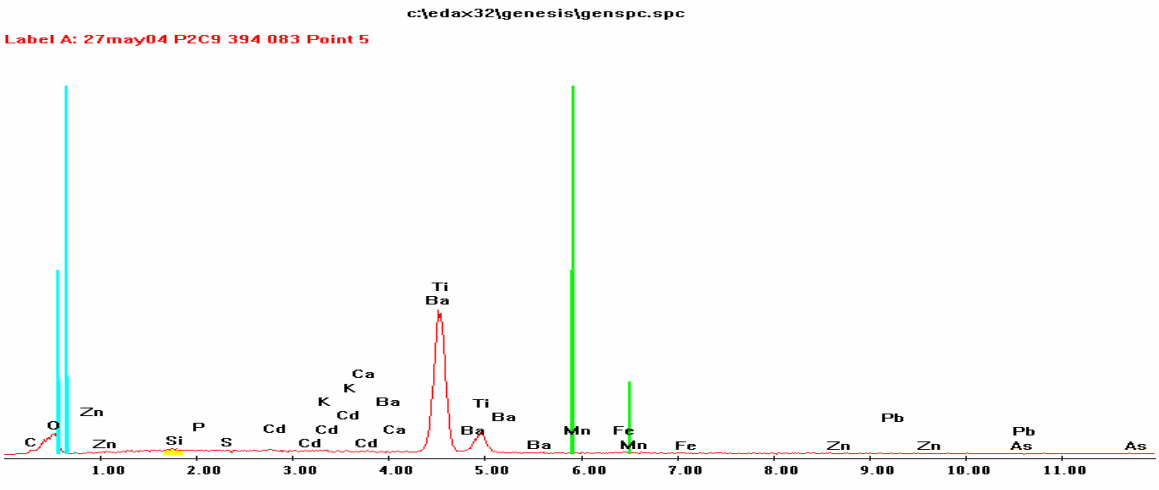

Point 6

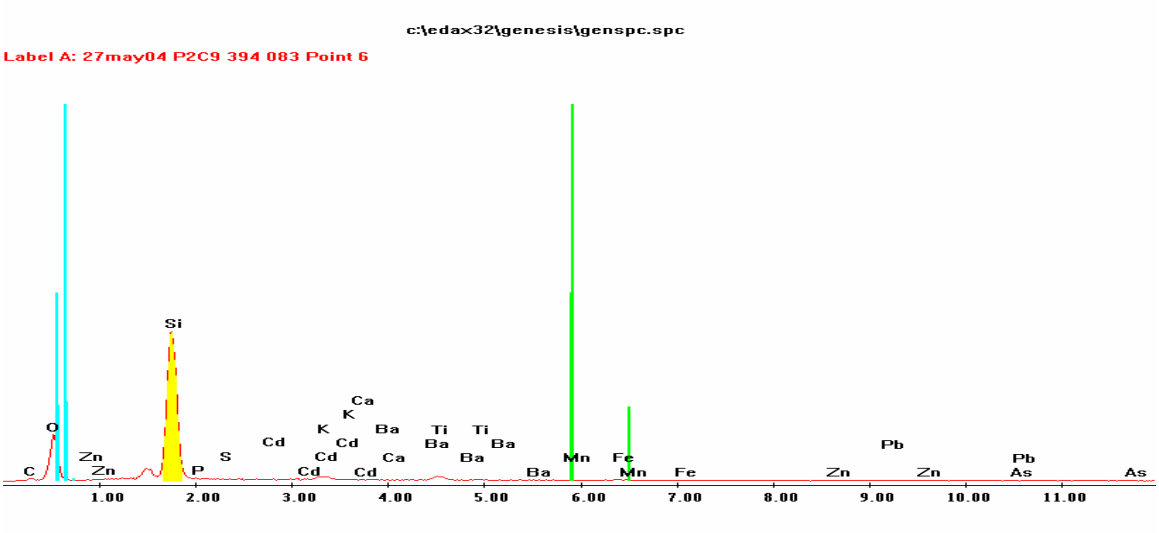

Point 7

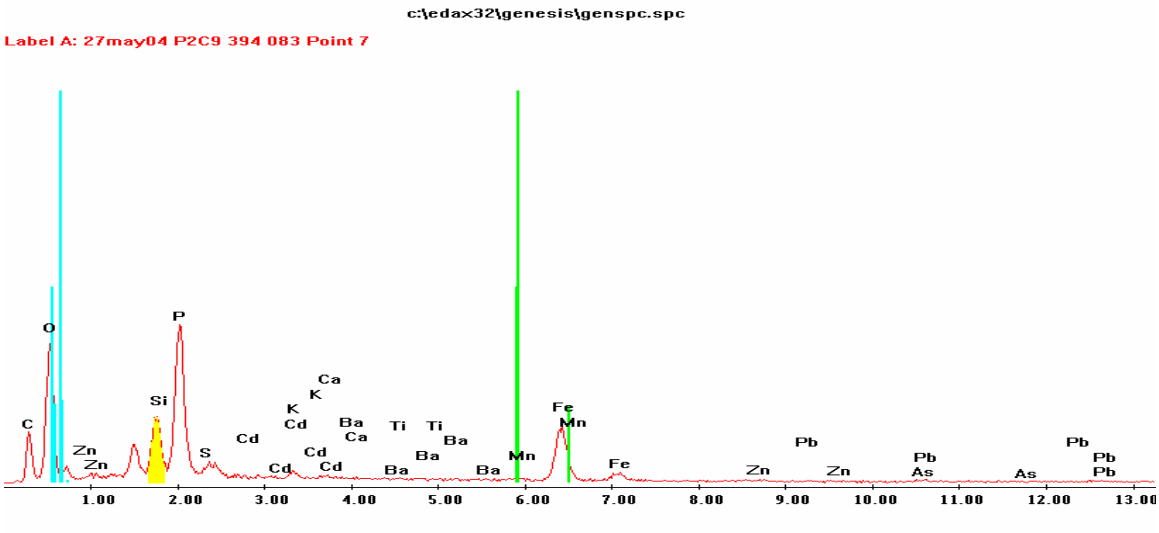

P2C9 – 428, 243

BSE Image

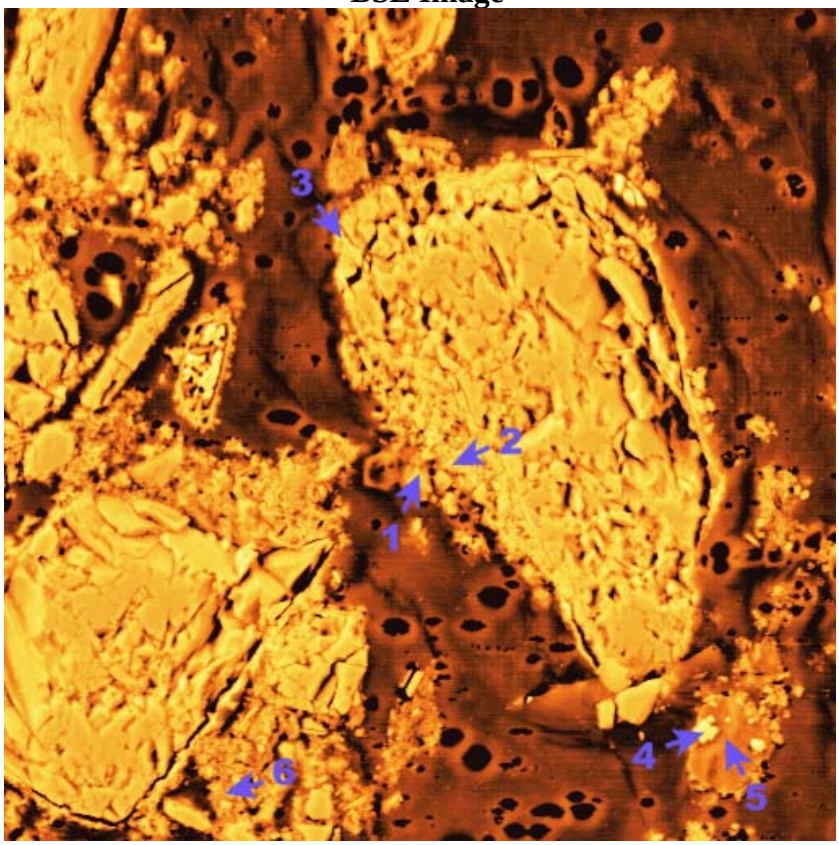

Iron (Fe)

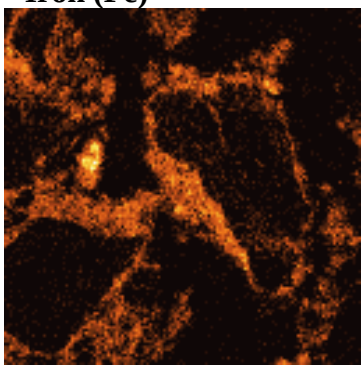

Manganese (Mn)

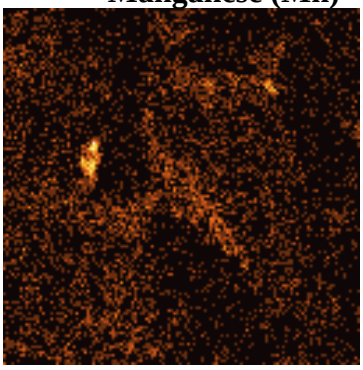

Phosphorous (P)

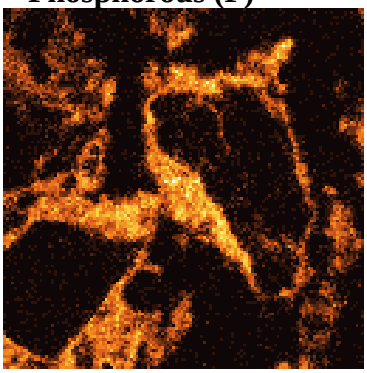

Lead (Pb)

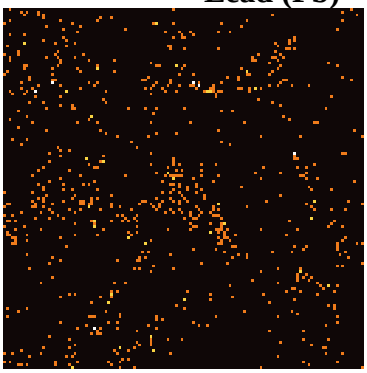

Silicon (Si)

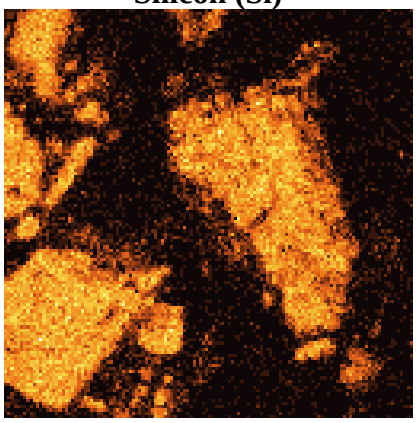

EDS Scan Images by Point

Point 1

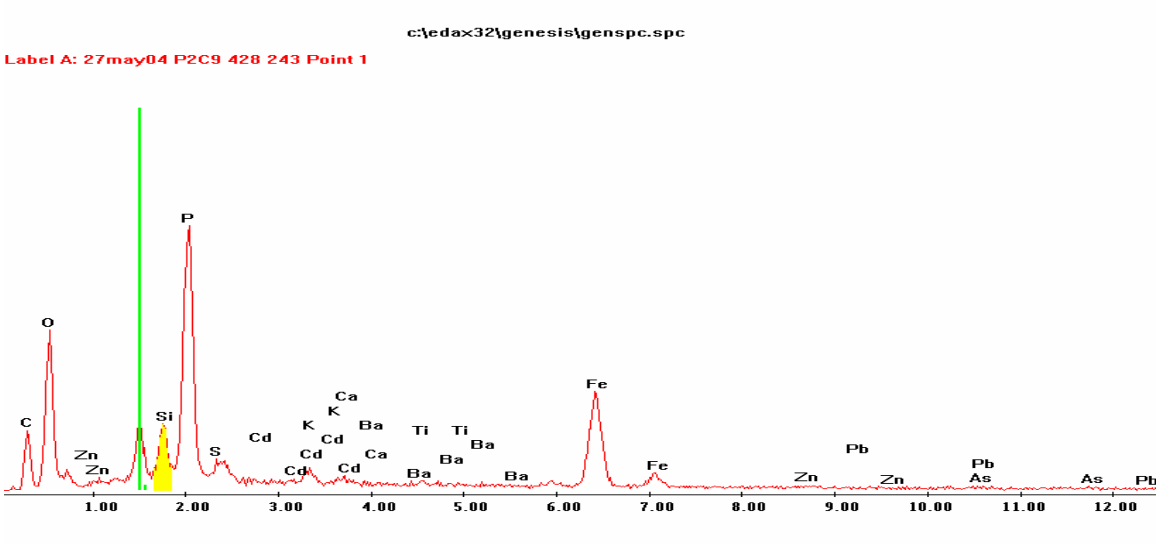

Point 2

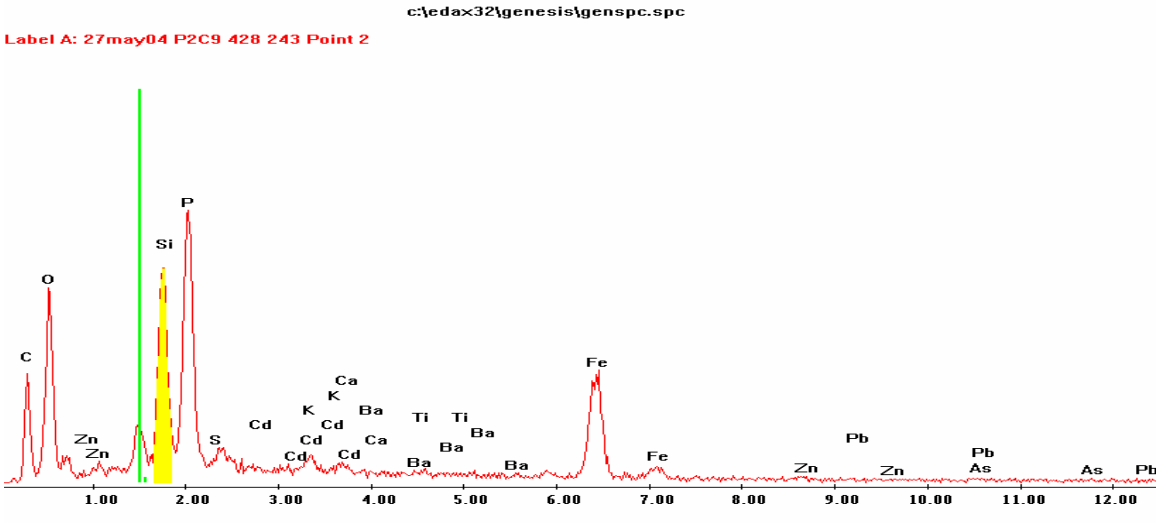

Point 3

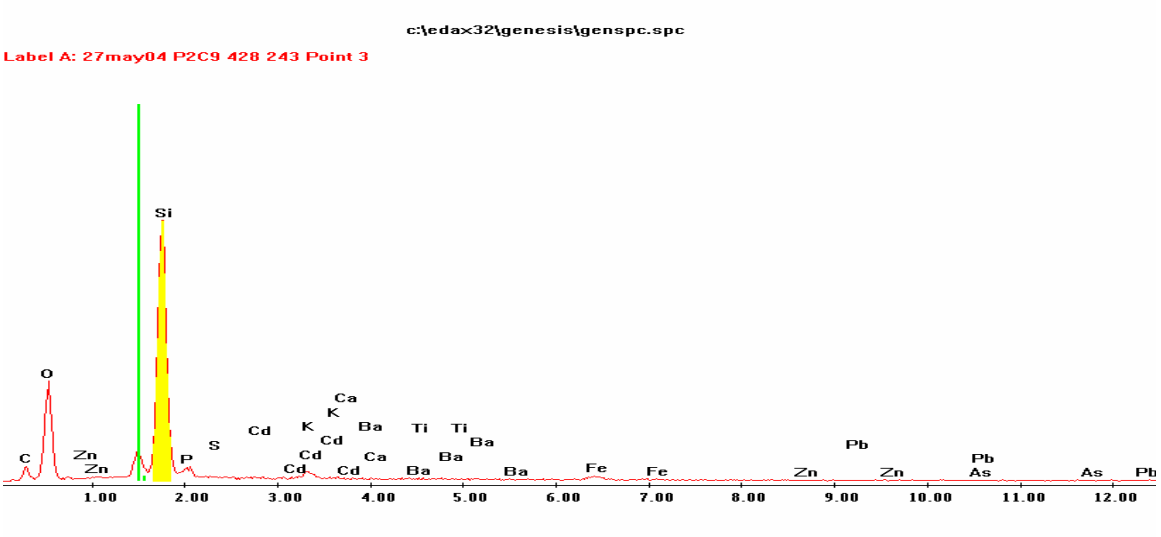

Point 4

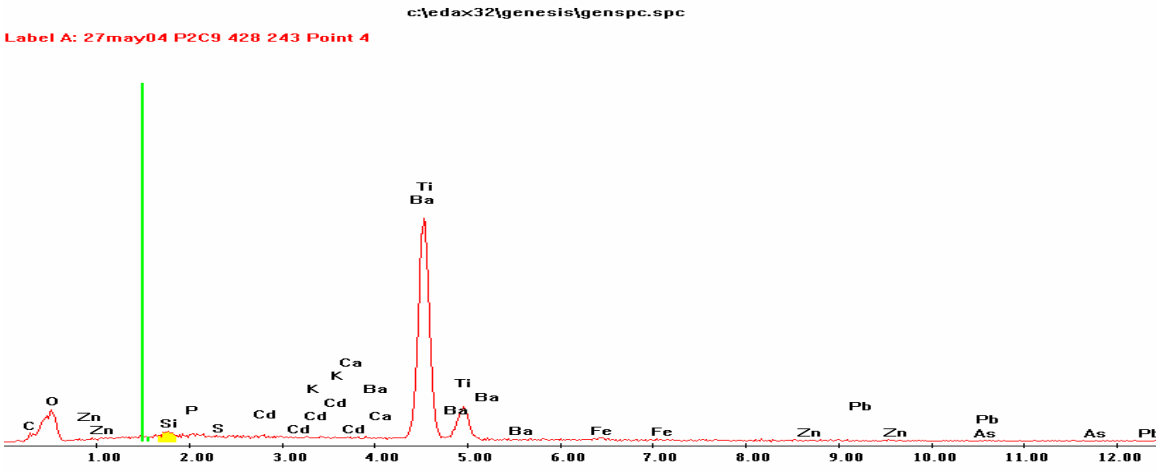

Point 5

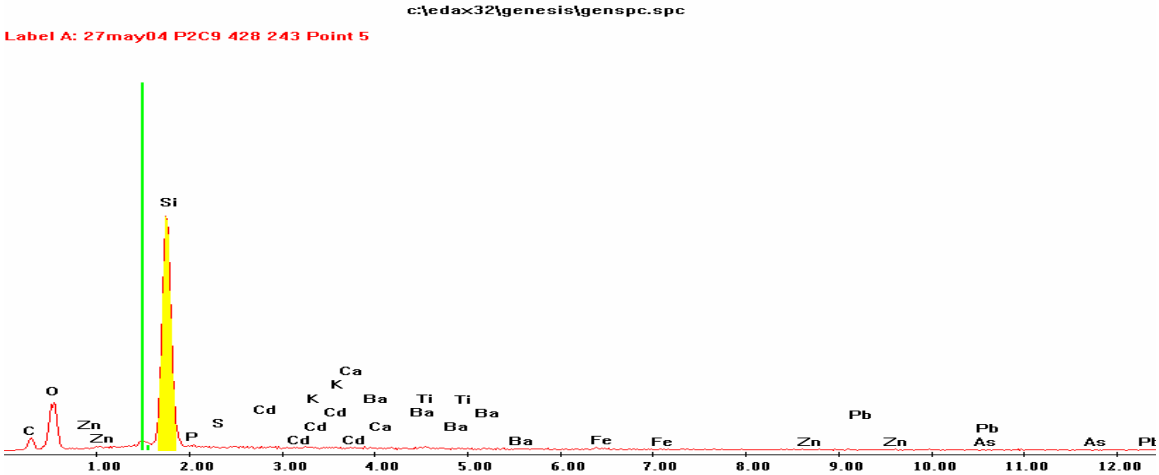

Point 6

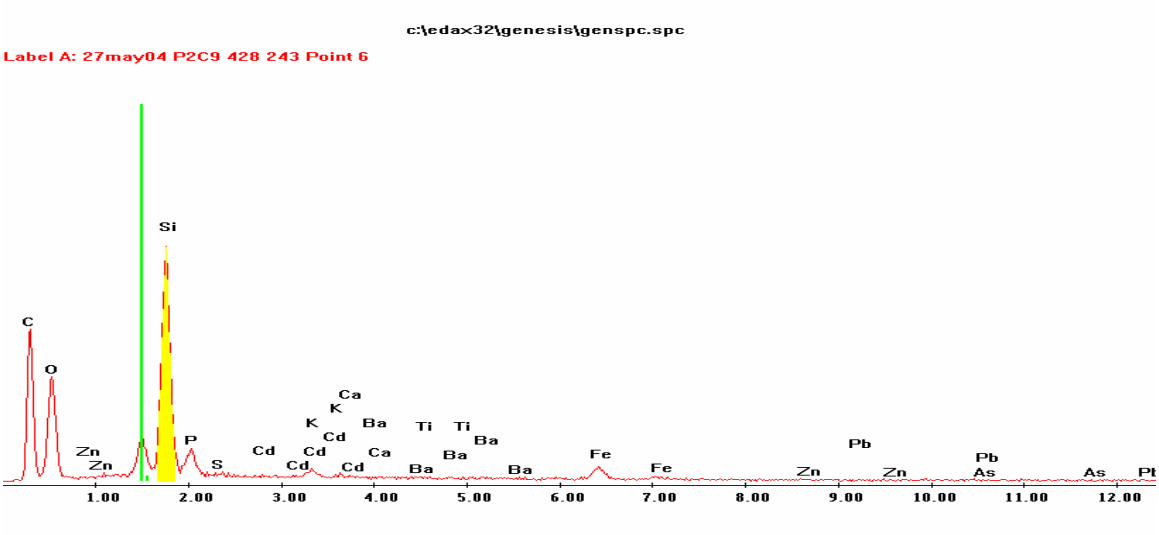

Point 7

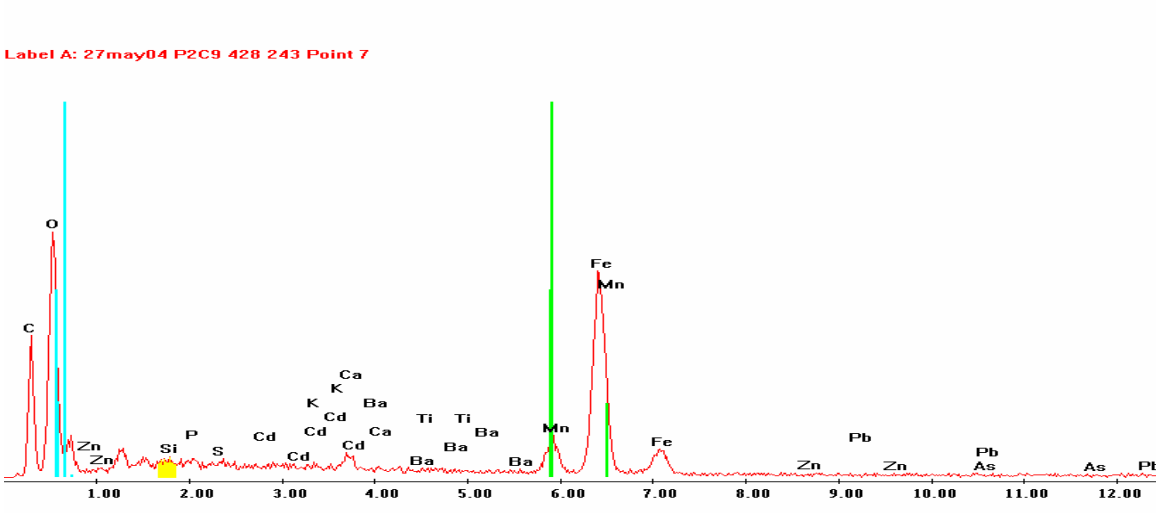

Plot 4

P4C7 – 333, 151

BSE Image

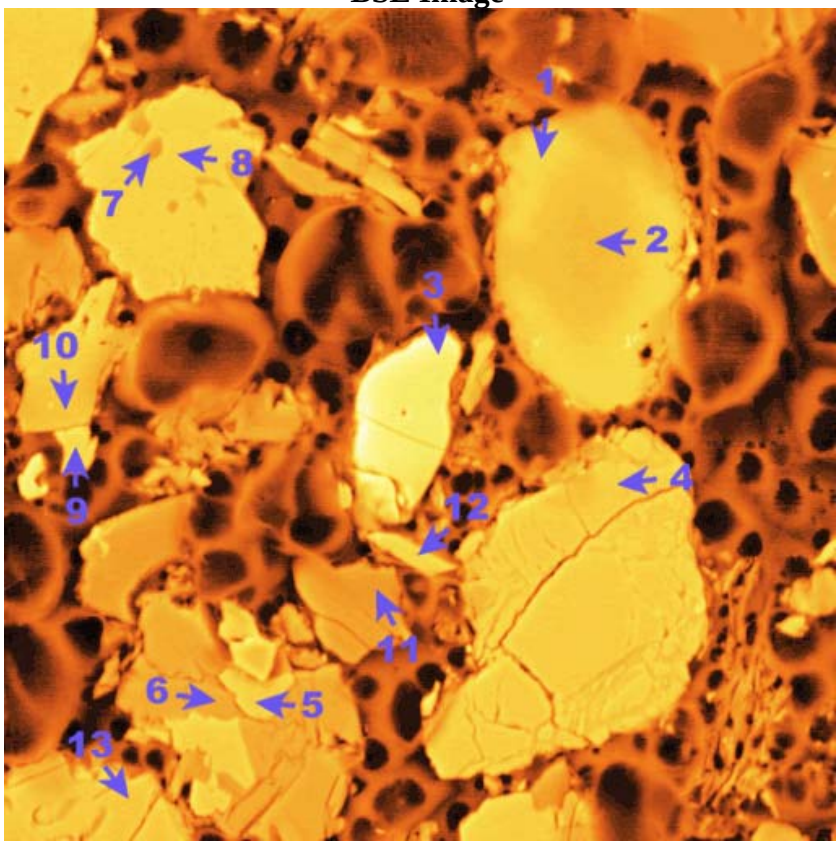

Iron (Fe)

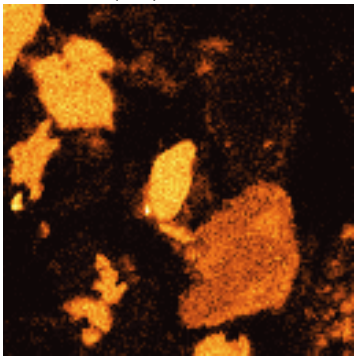

Manganese (Mn)

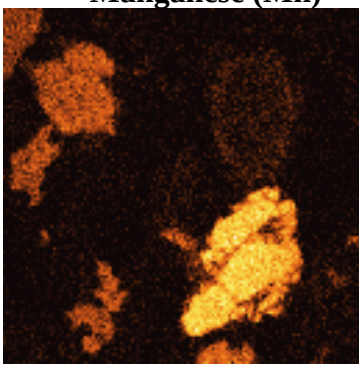

Phosphorous (P)

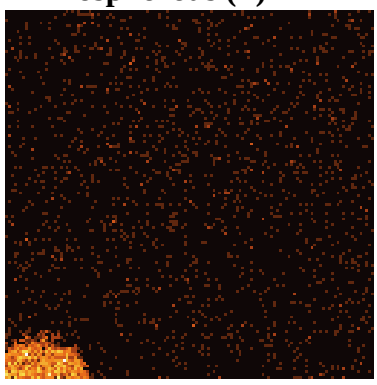

Lead (Pb)

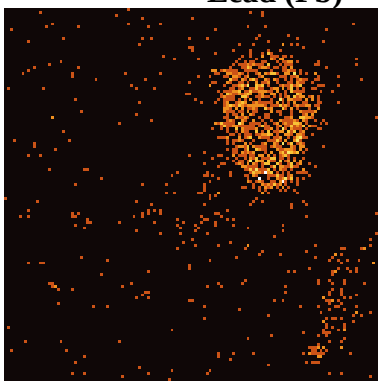

Silicon (Si)

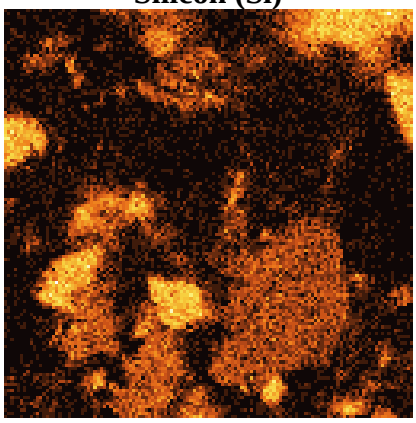

EDS Scan Images by Point

Point 1

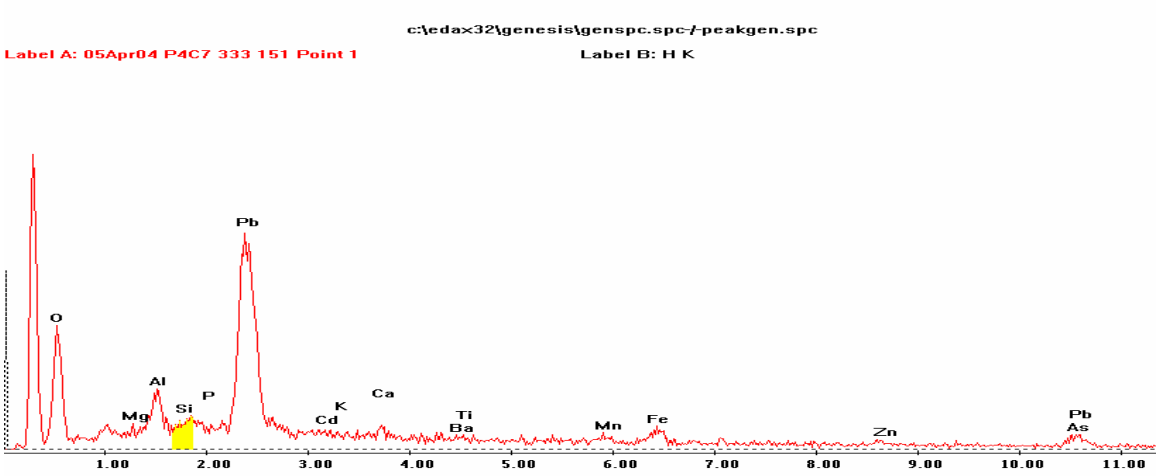

Point 2

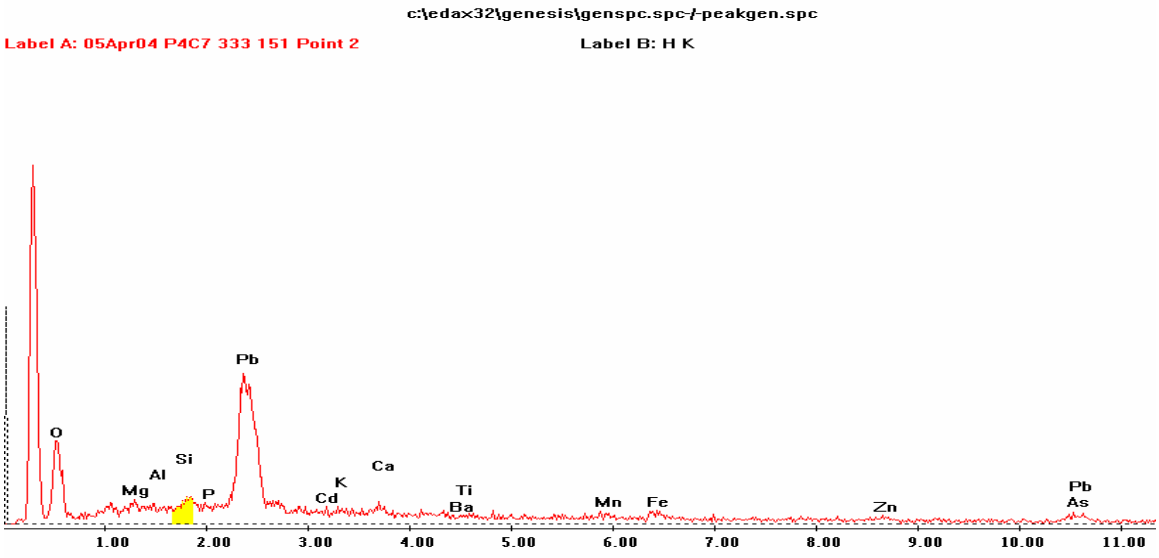

Point 3

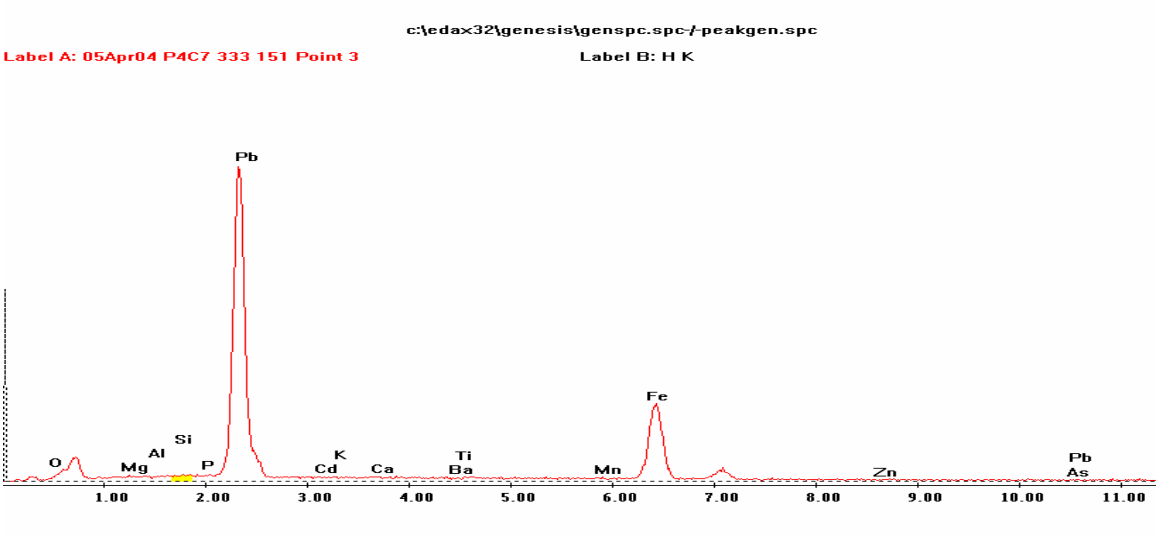

Point 4

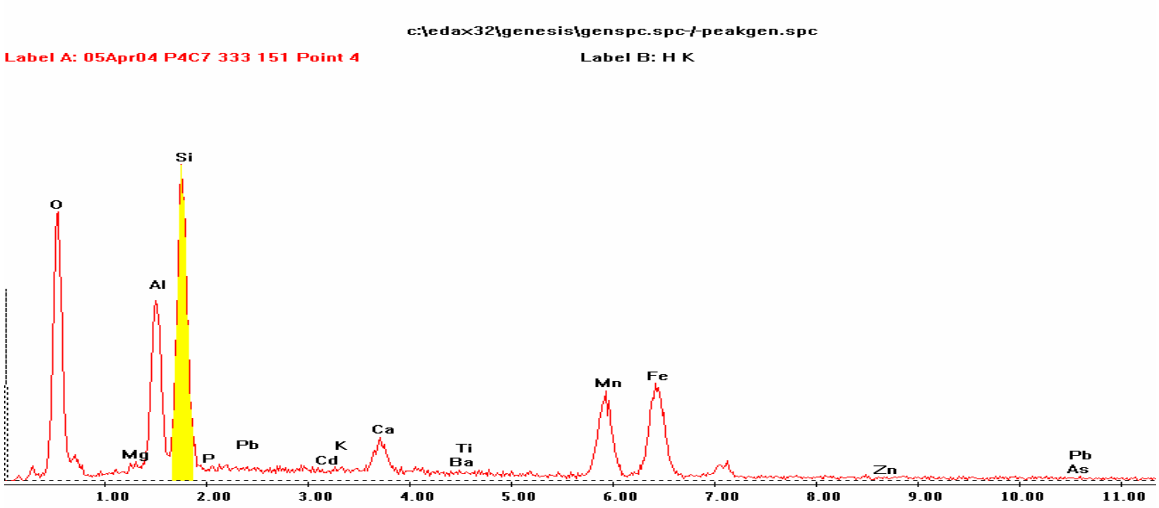

Point 5

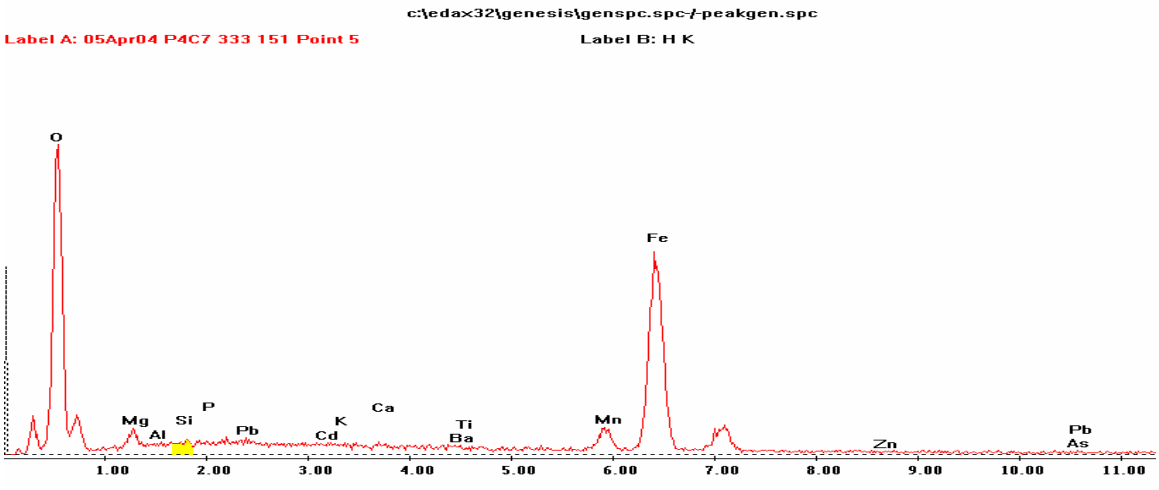

Point 6

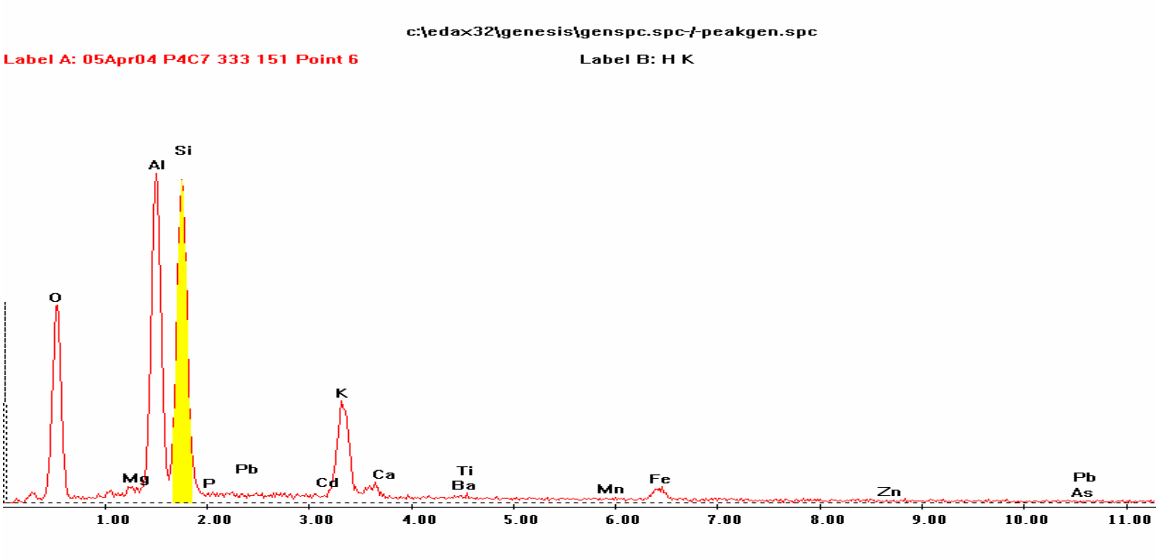

Point 7

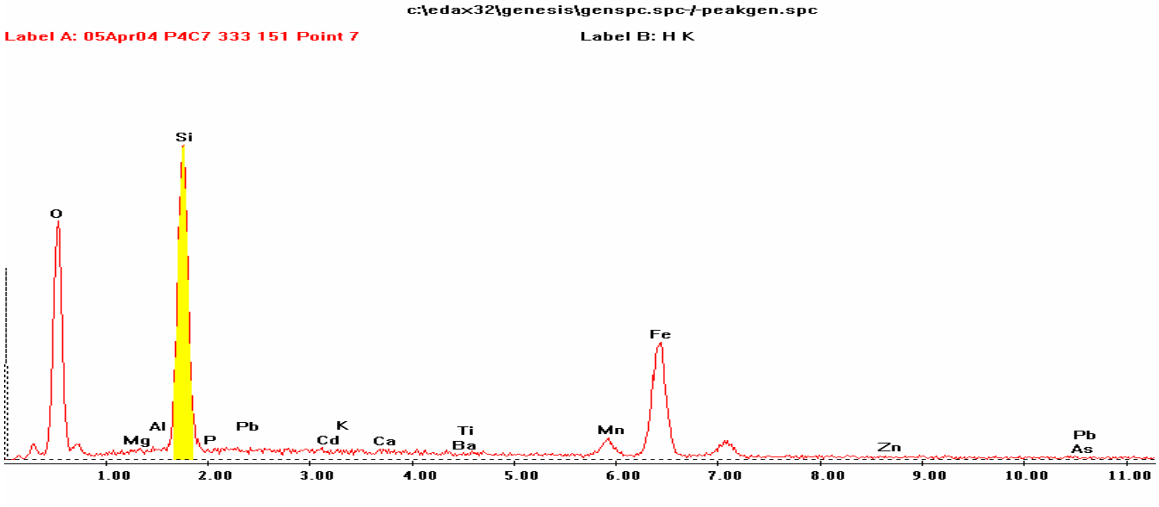

Point 8

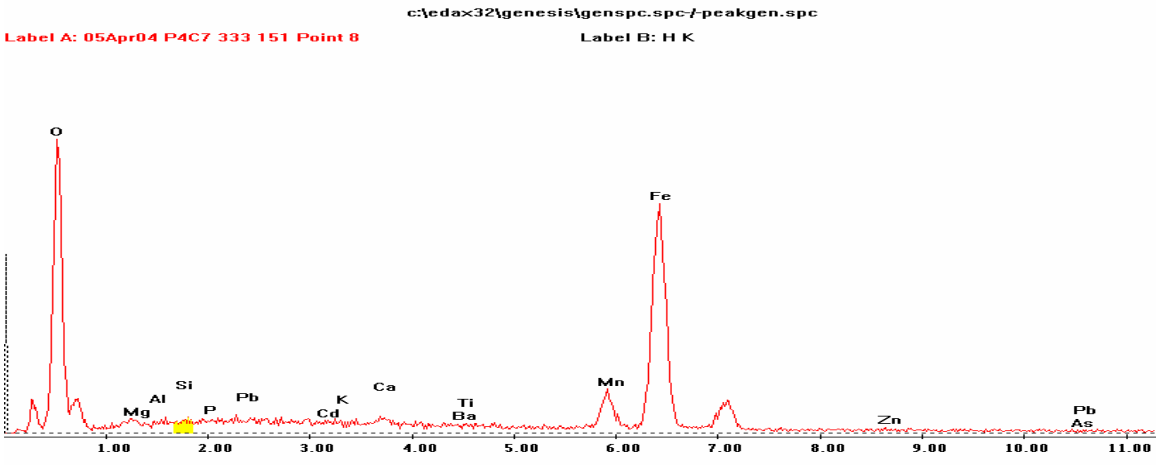

Point 9

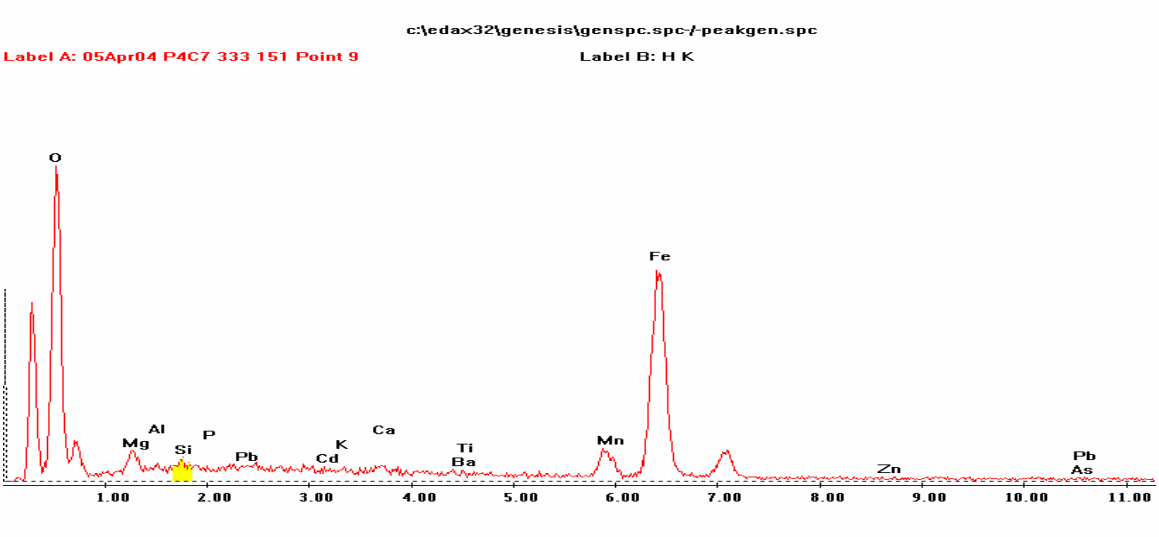

Point 10

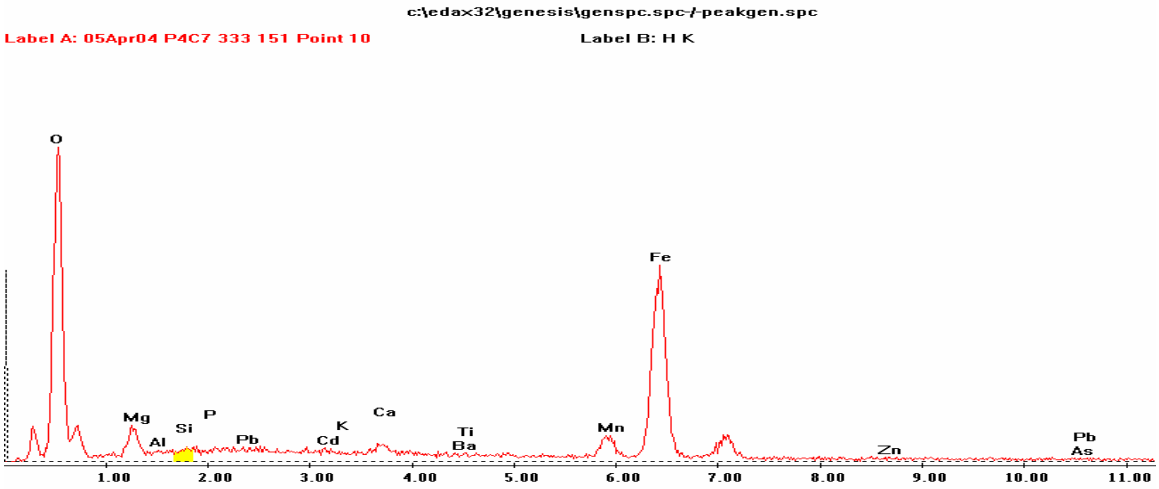

Point 11

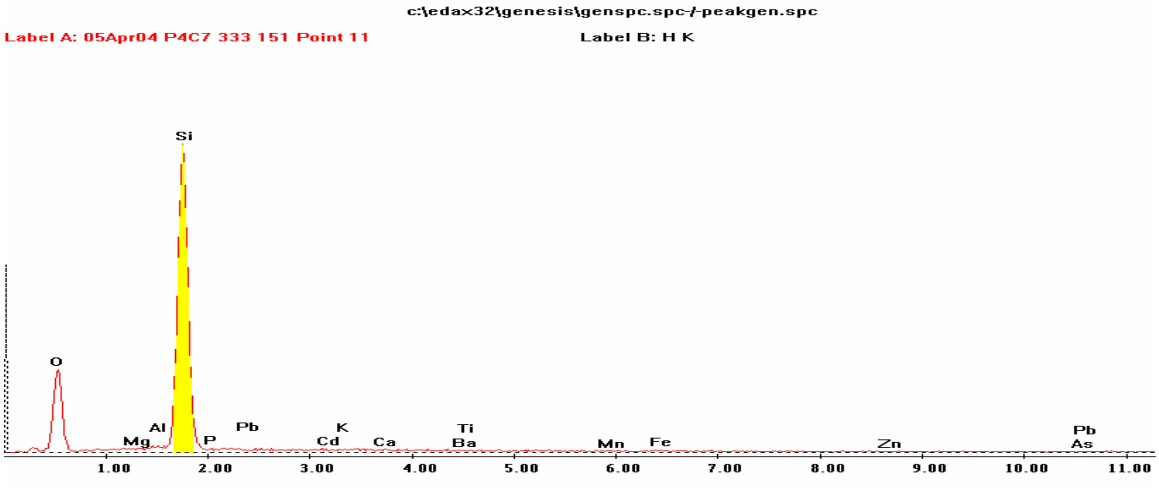

Point 12

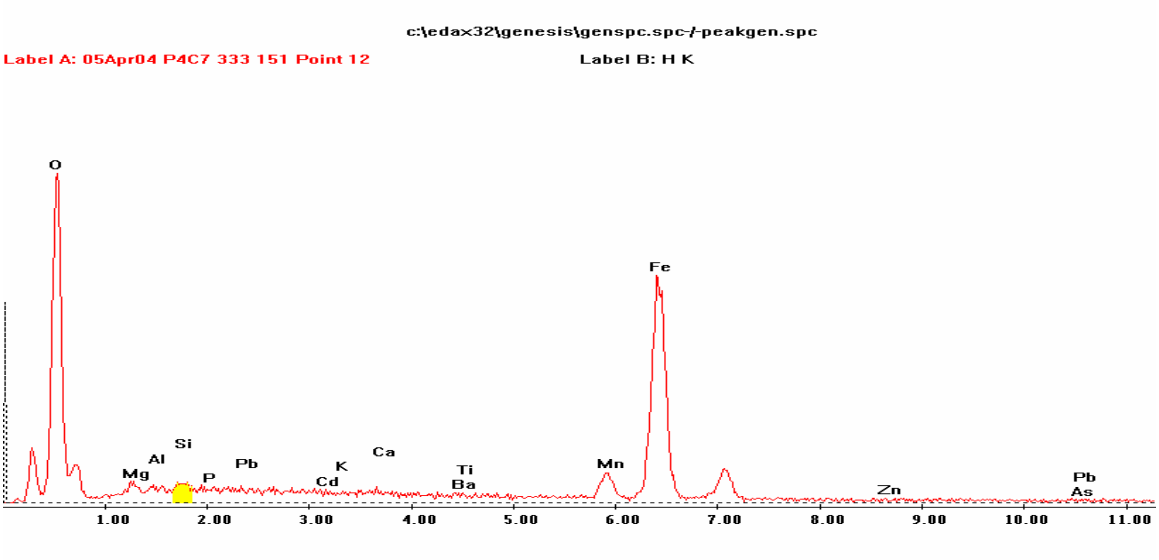

Point 13

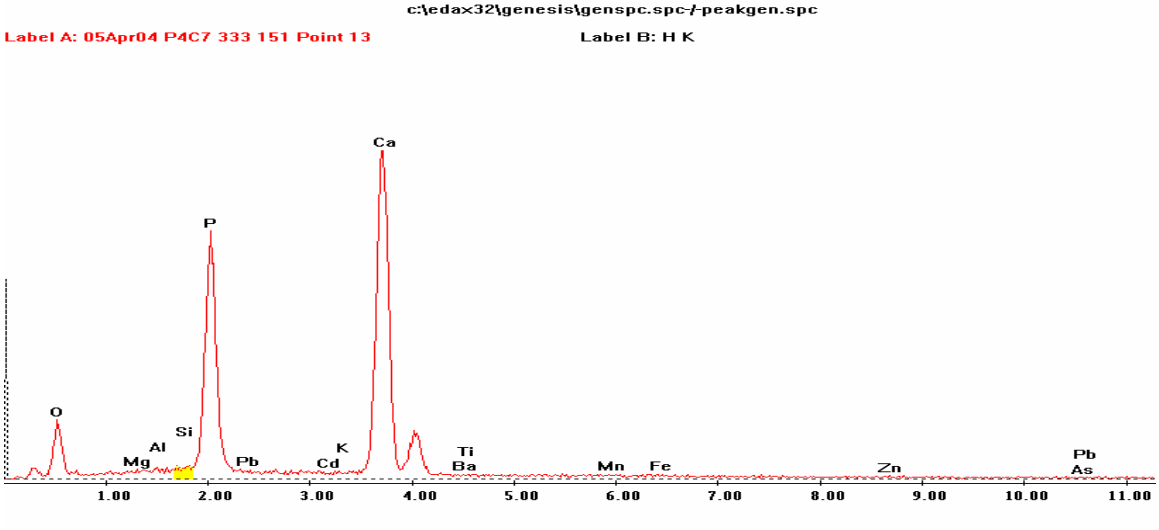

P4C7 – 403, 199

BSE Image

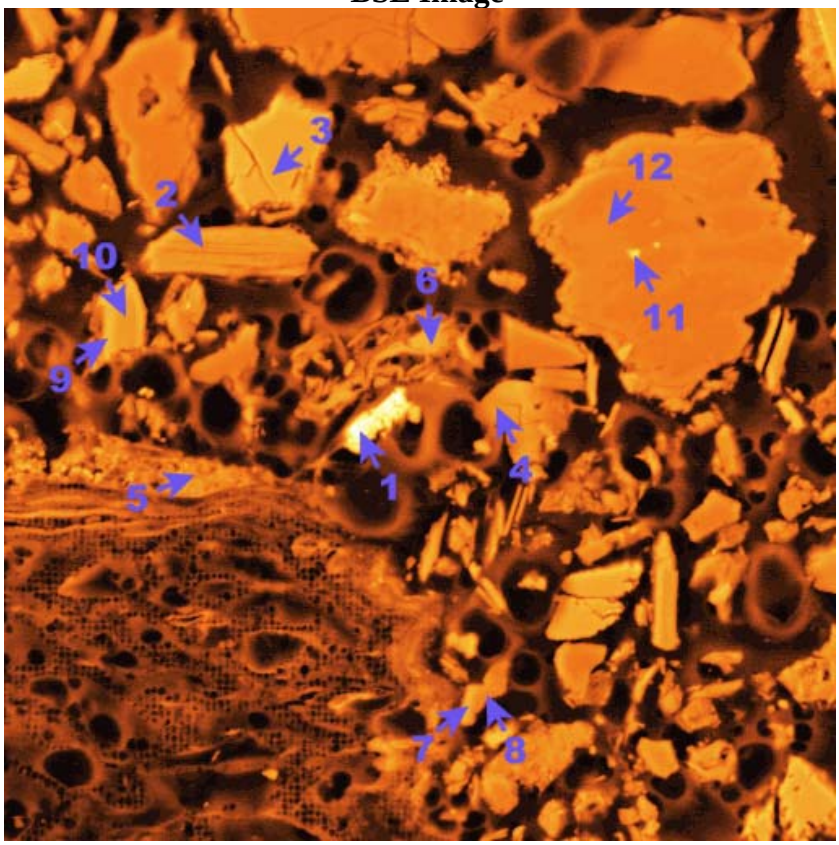

Iron (Fe)

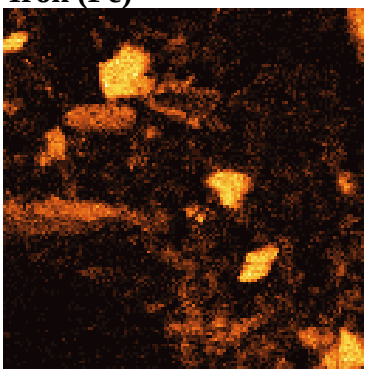

Manganese (Mn)

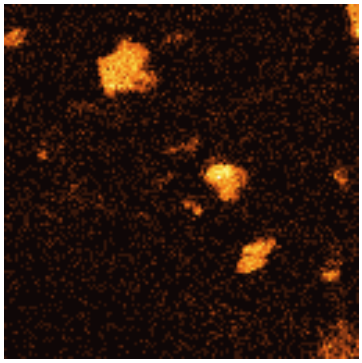

Phosphorous (P)

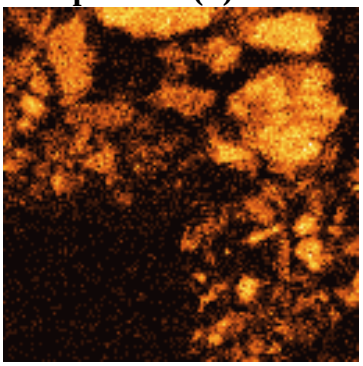

Lead (Pb)

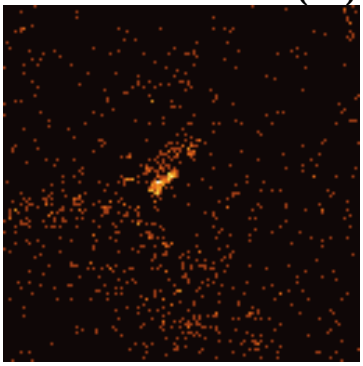

Silicon (Si)

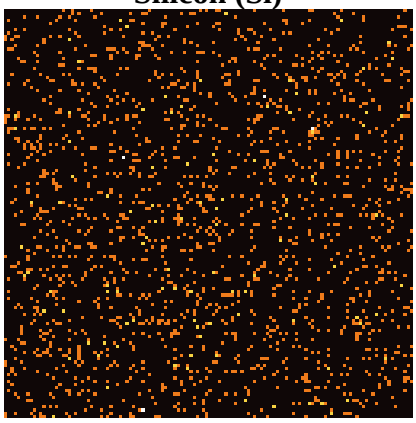

EDS Scan Images by Point

Point 1

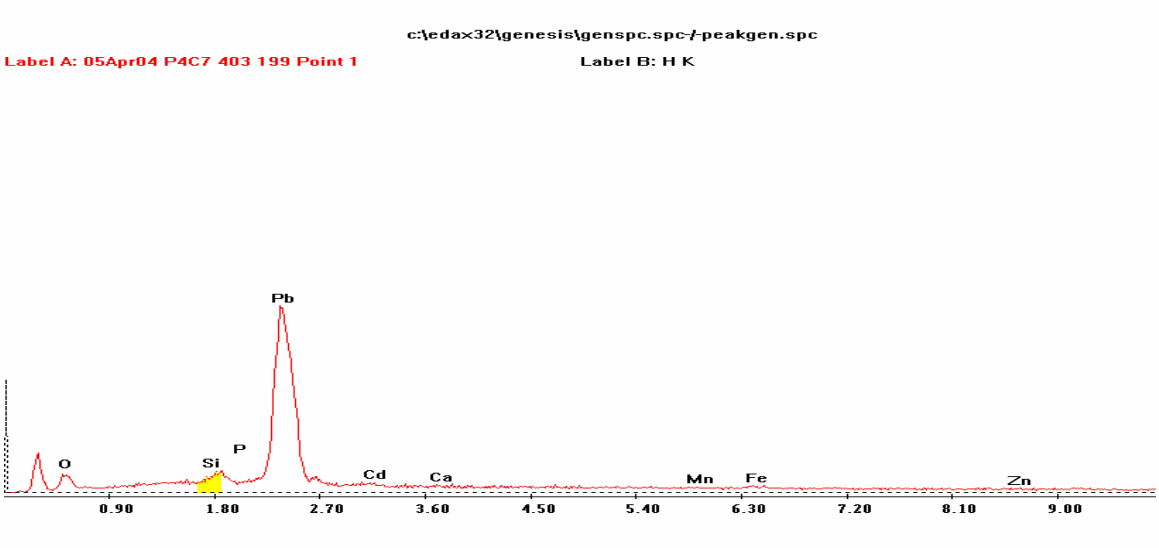

Point 2

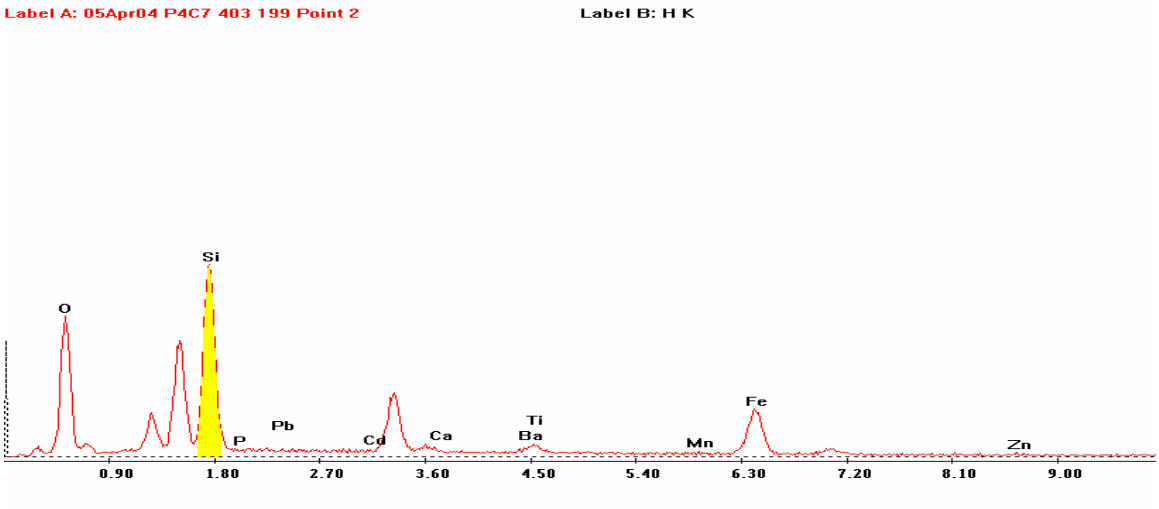

Point 3

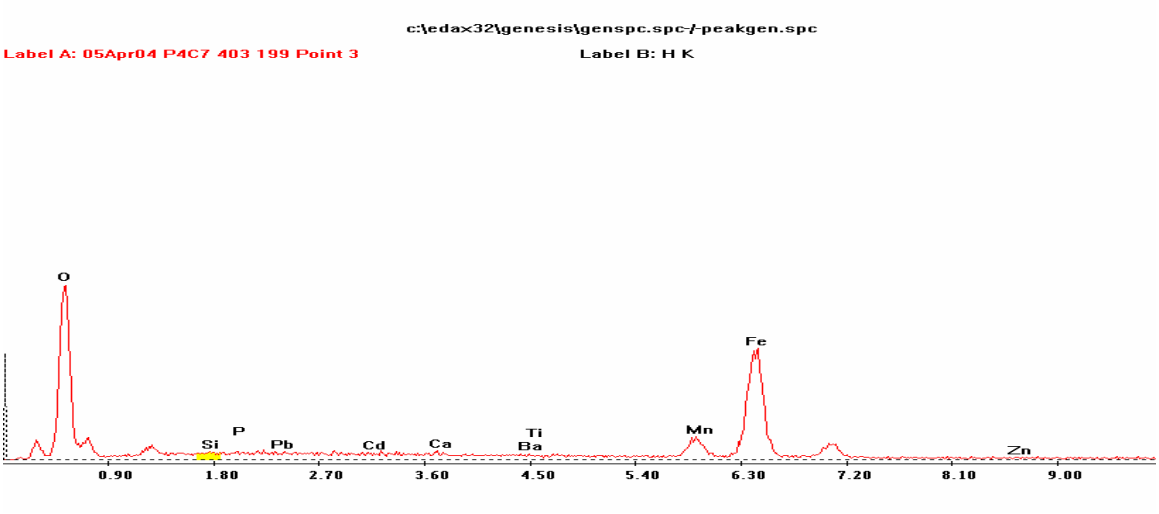

Point 4

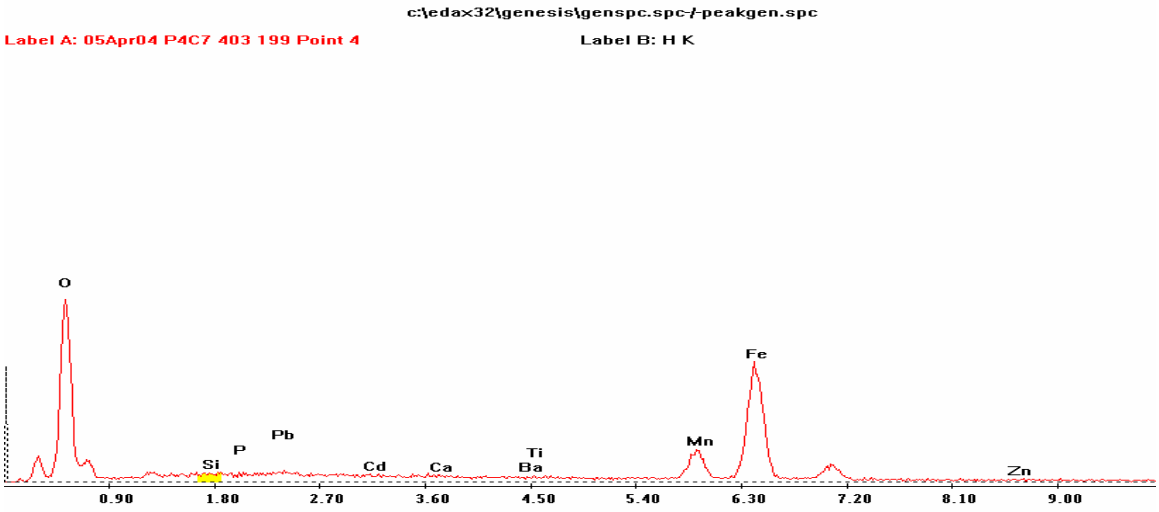

Point 5

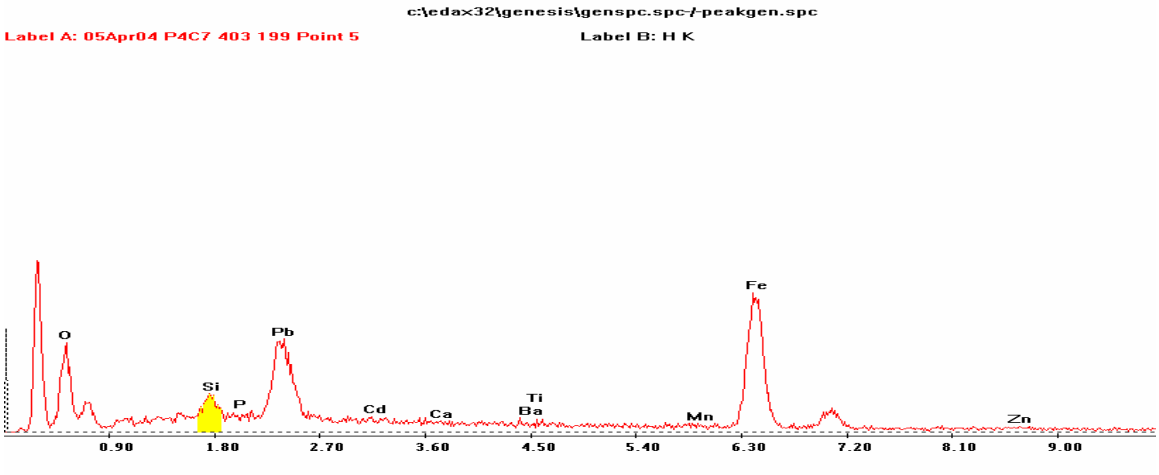

Point 6

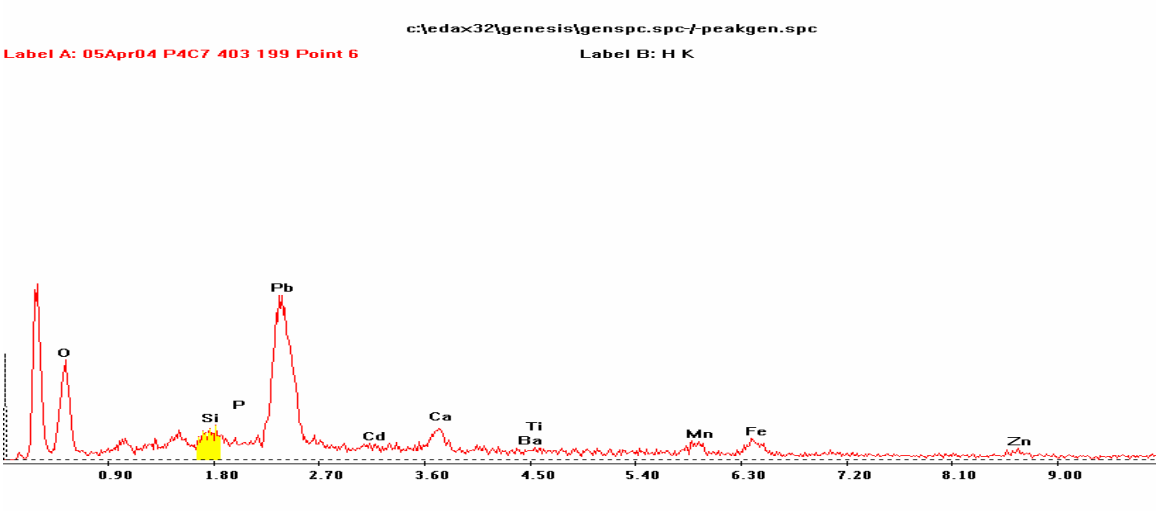

Point 7

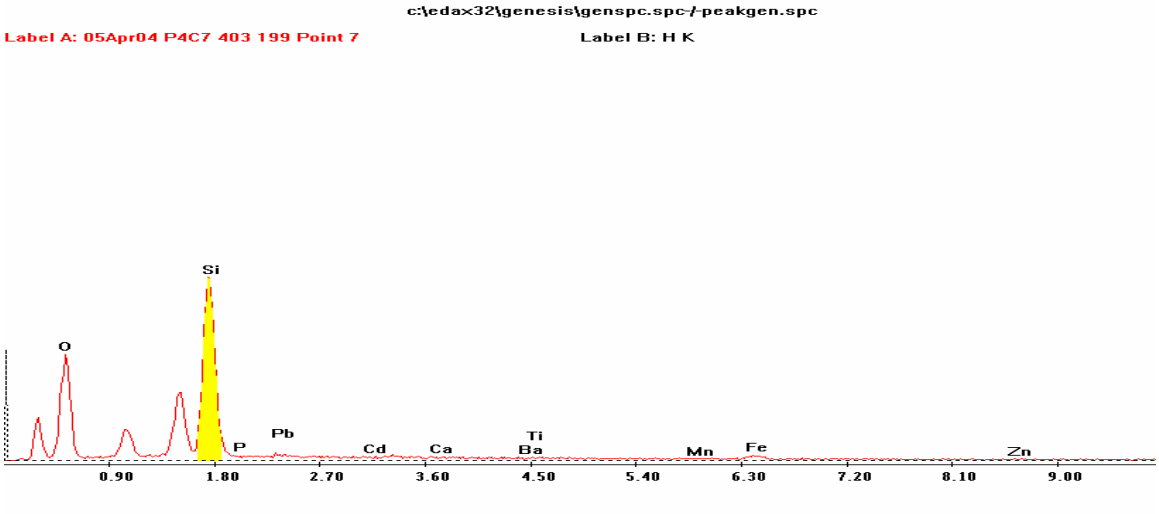

Point 8

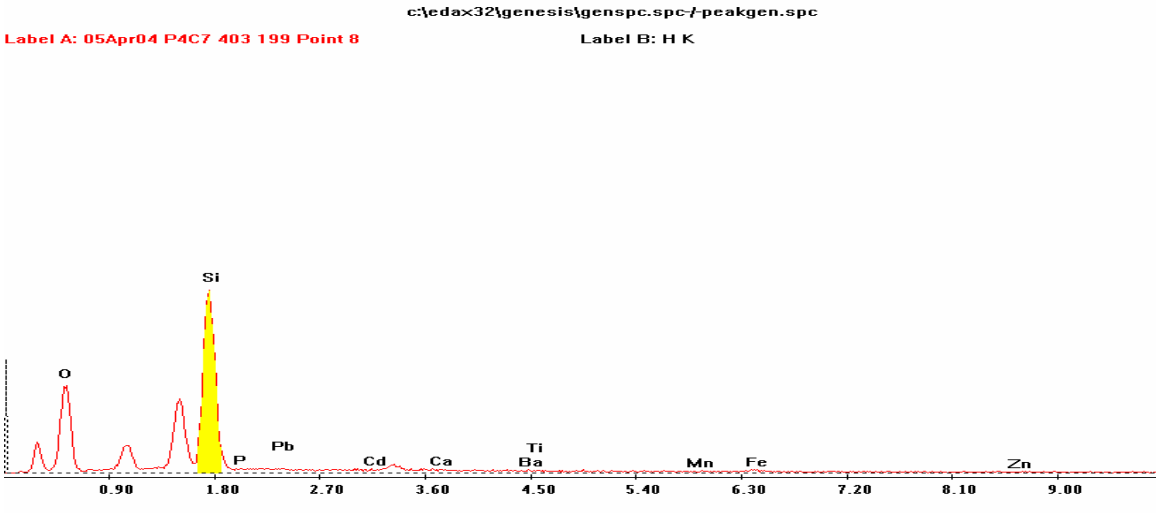

Point 9

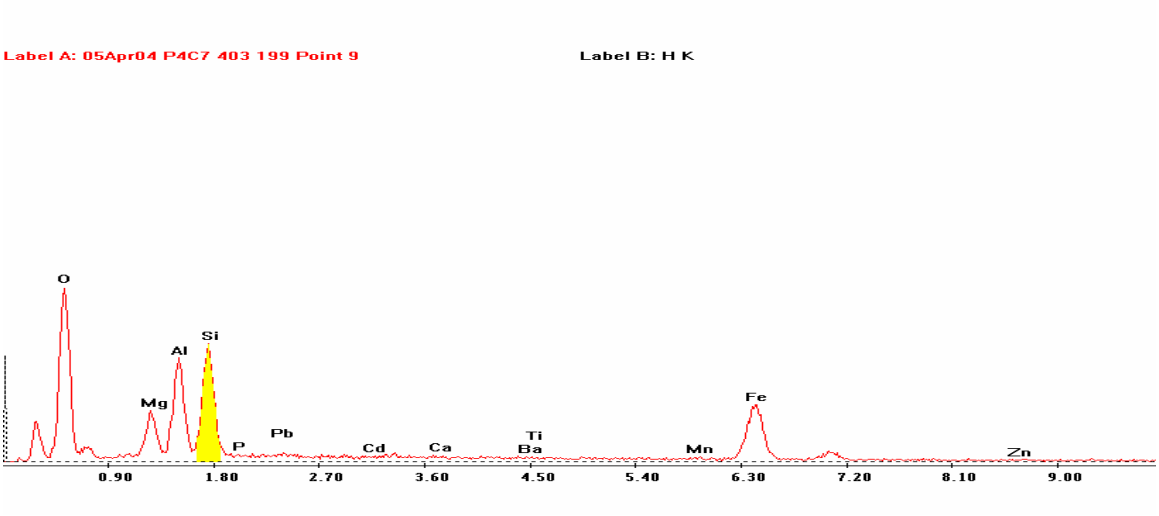

Point 10

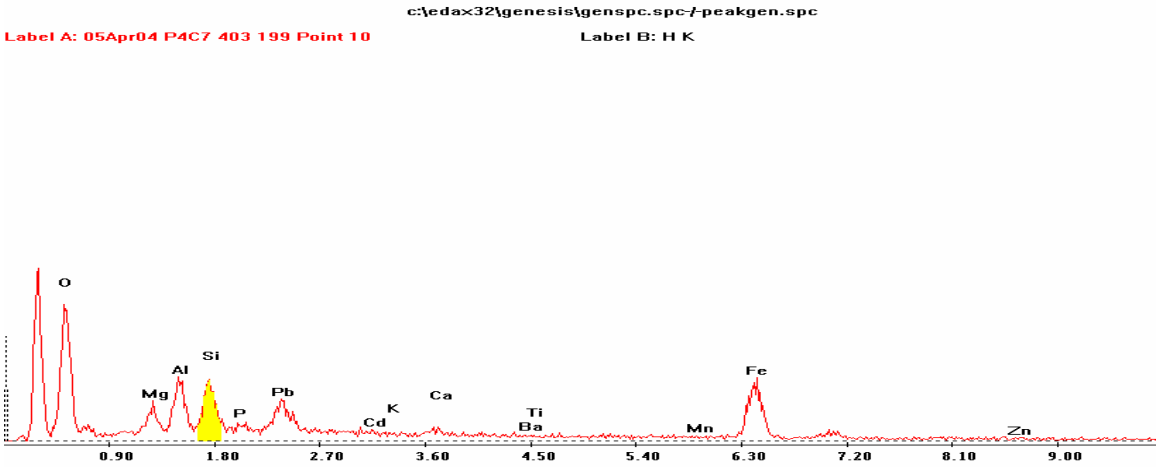

Point 11

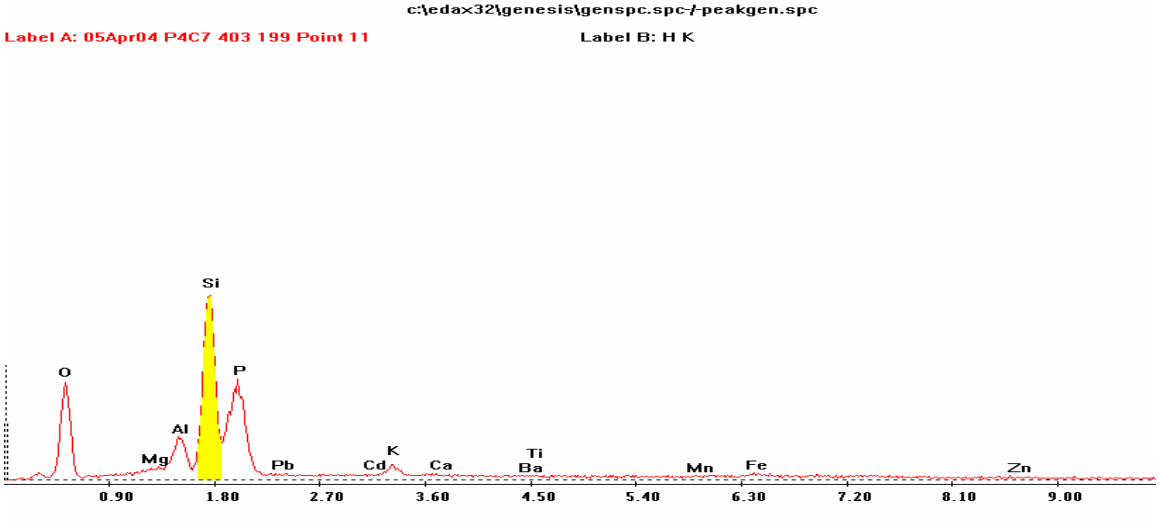

Point 12

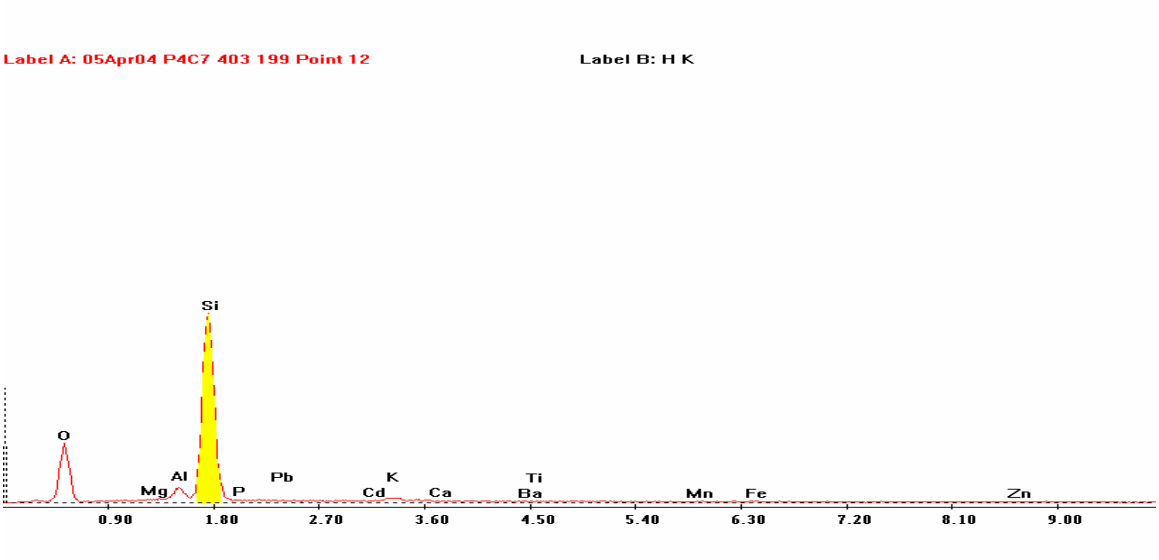
Label A: 05Apr04 P4C7 403 199 Point 12
Label B: H K
O
Mg
Al
Si
P
Pb
Cd
K
Ca
Ti
Ba
Mn
Fe
Zn
0.90
1.80
2.70
3.60
4.50
5.40
6.30
7.20
8.10
9.00

P4C7 – 456, 153

BSE Image

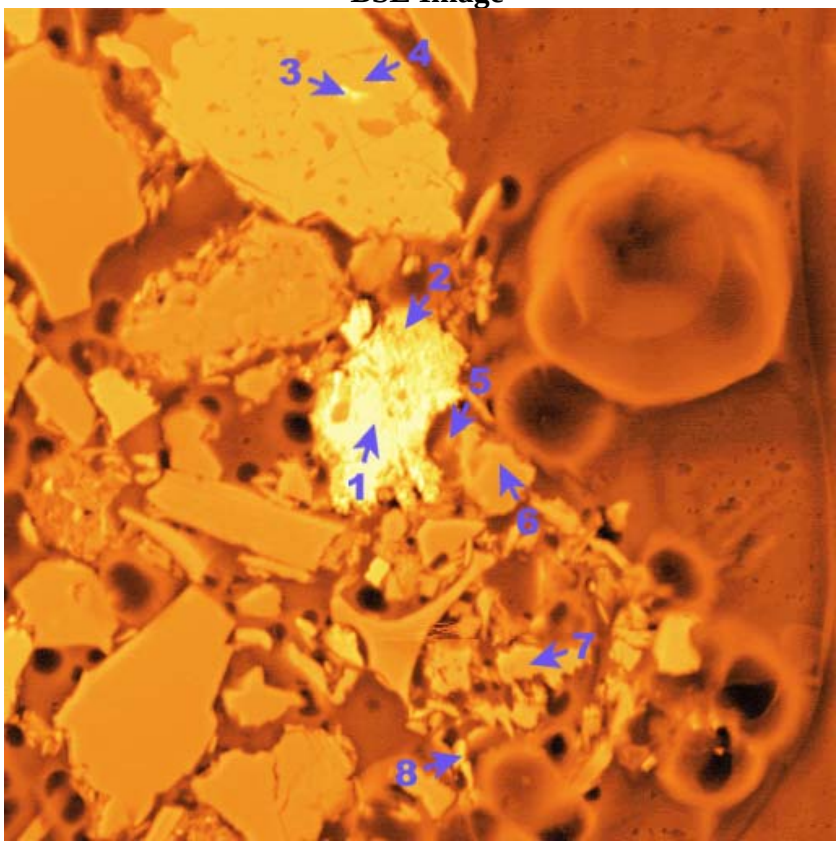

Iron (Fe)

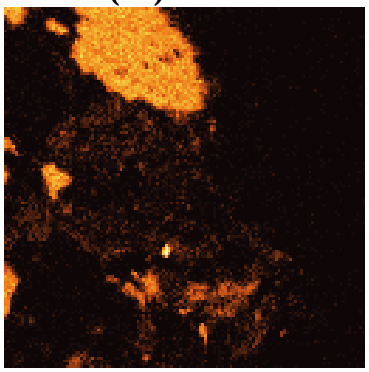

Manganese (Mn)

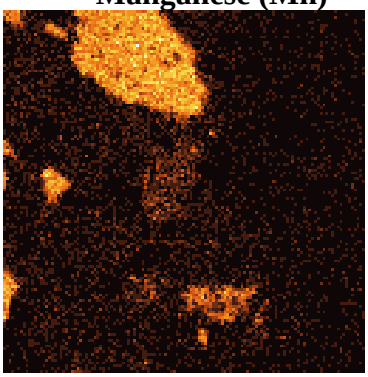

Phosphorous (P)

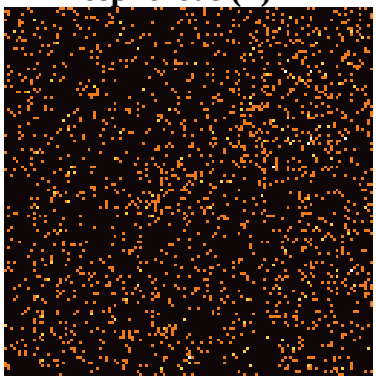

Lead (Pb)

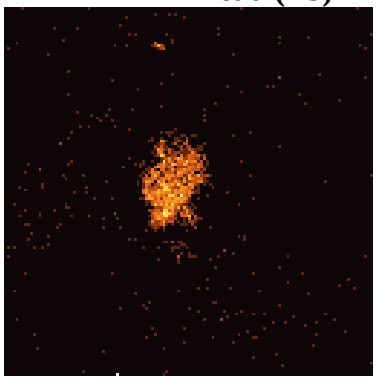

Silicon (Si)

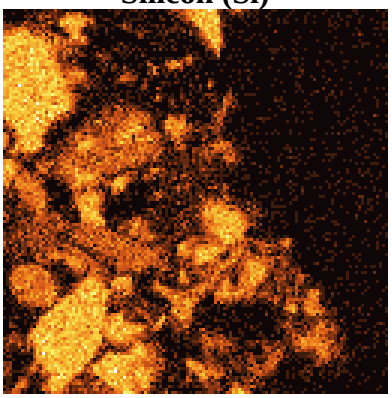

EDS Scan Images by Point

Point 1

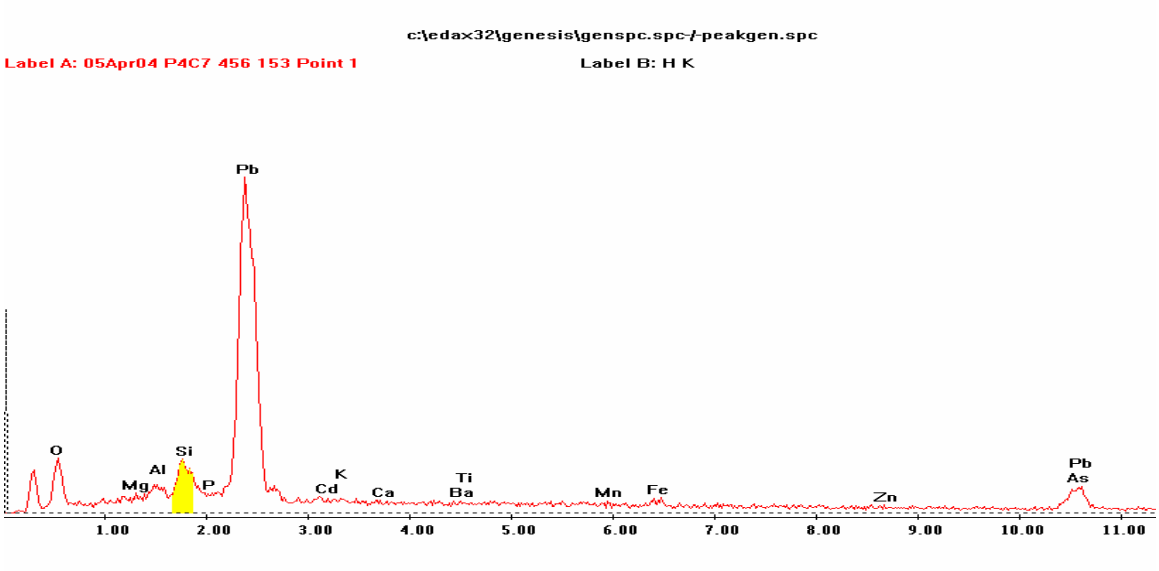

Point 2

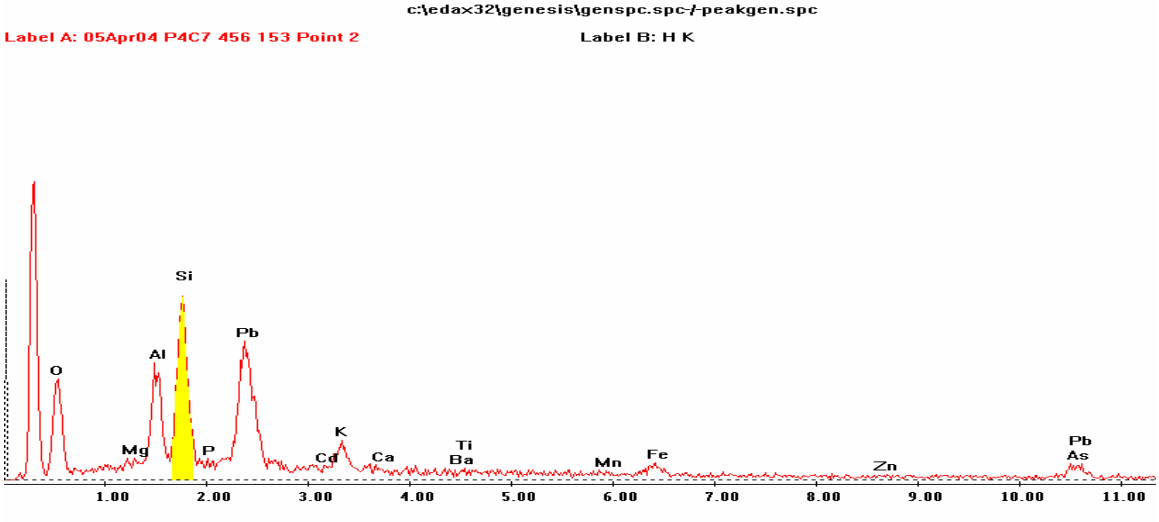

Point 3

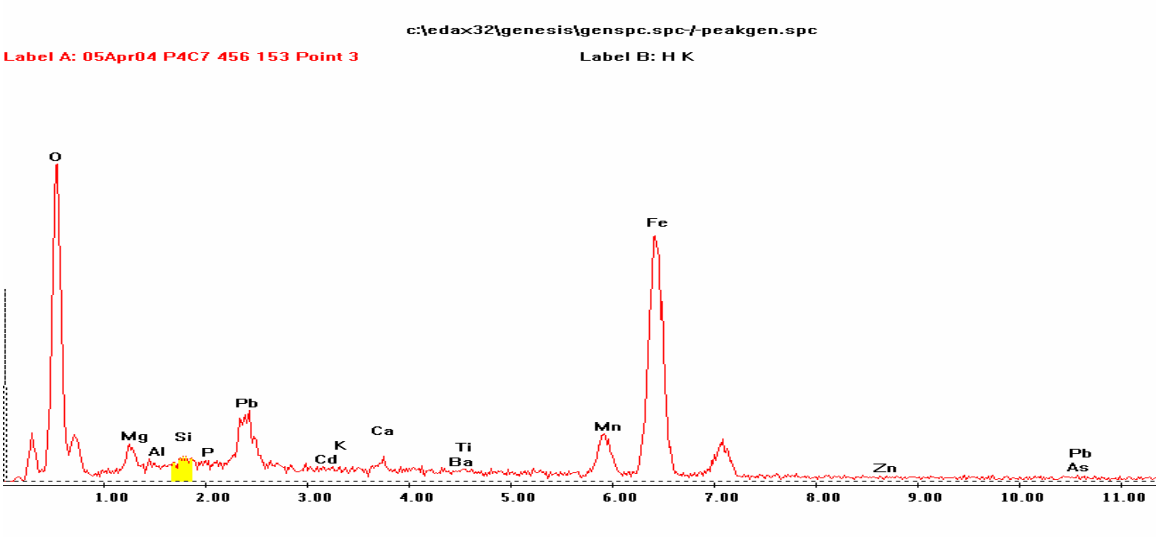

Point 4

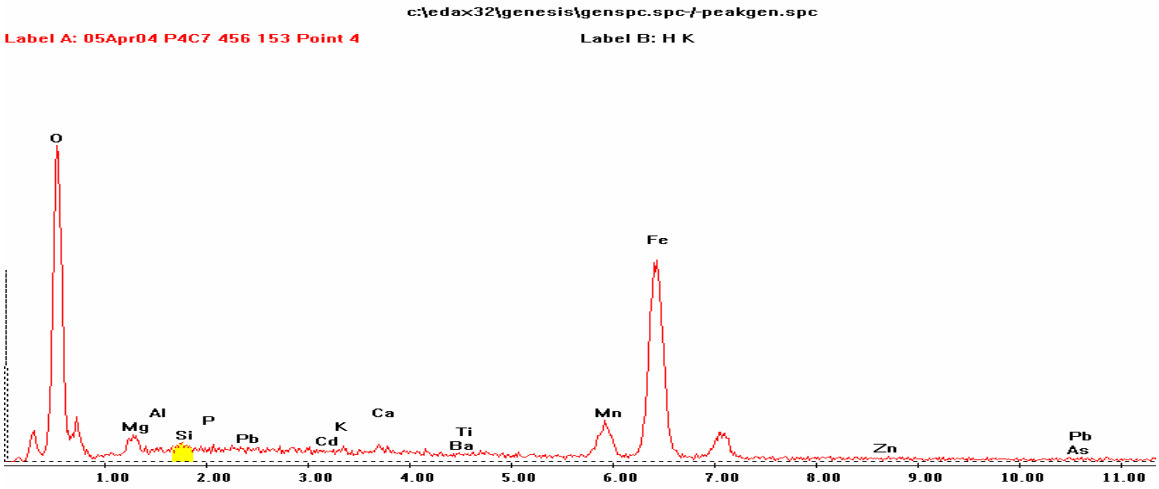

Point 5

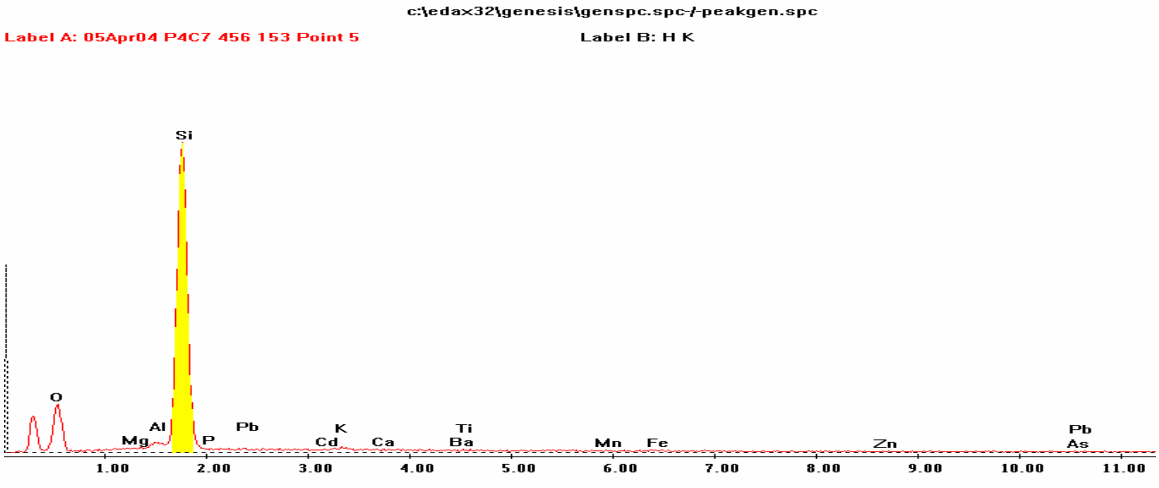

Point 6

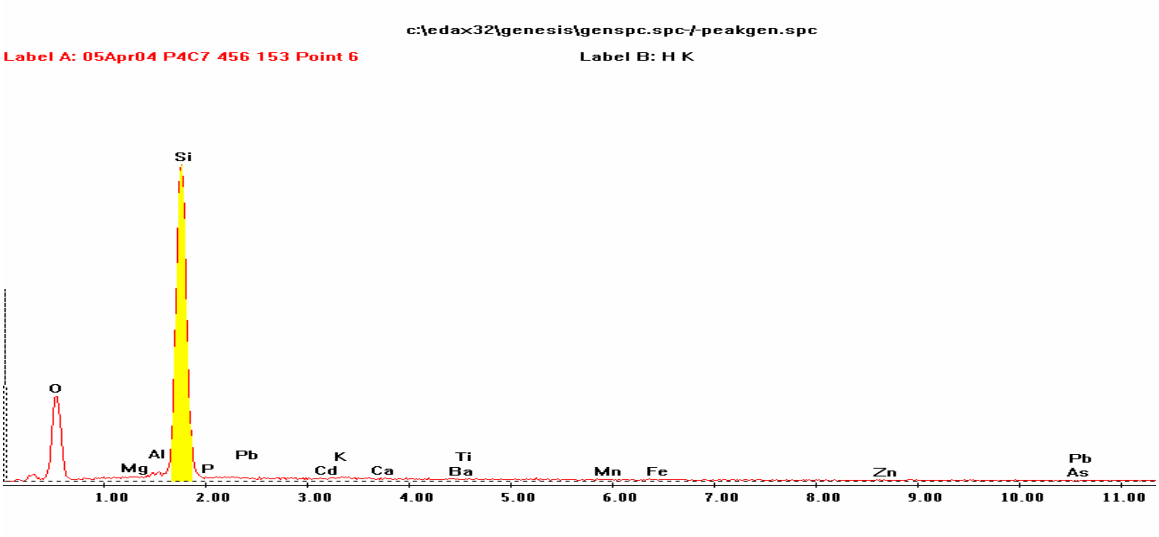

Point 7

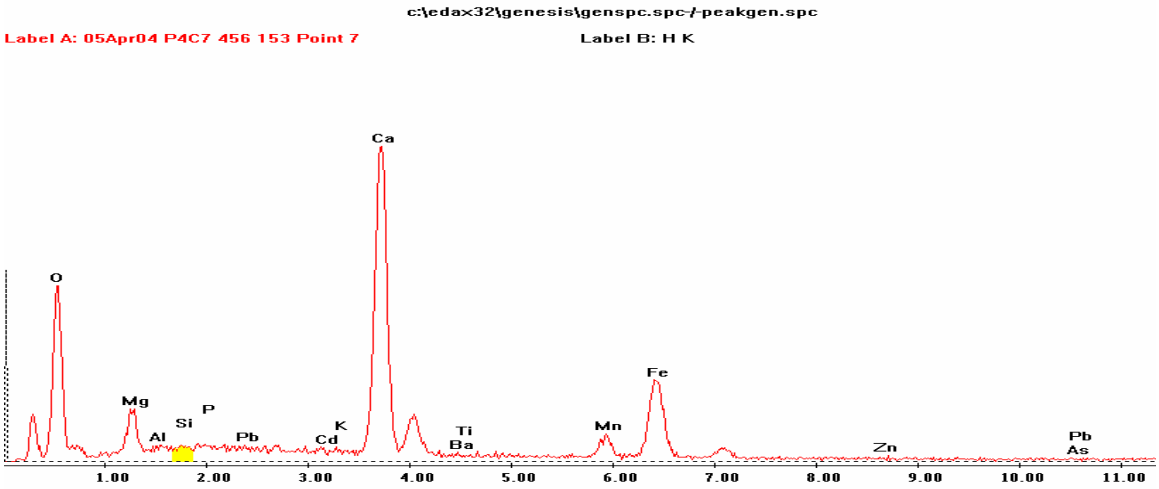

Point 8

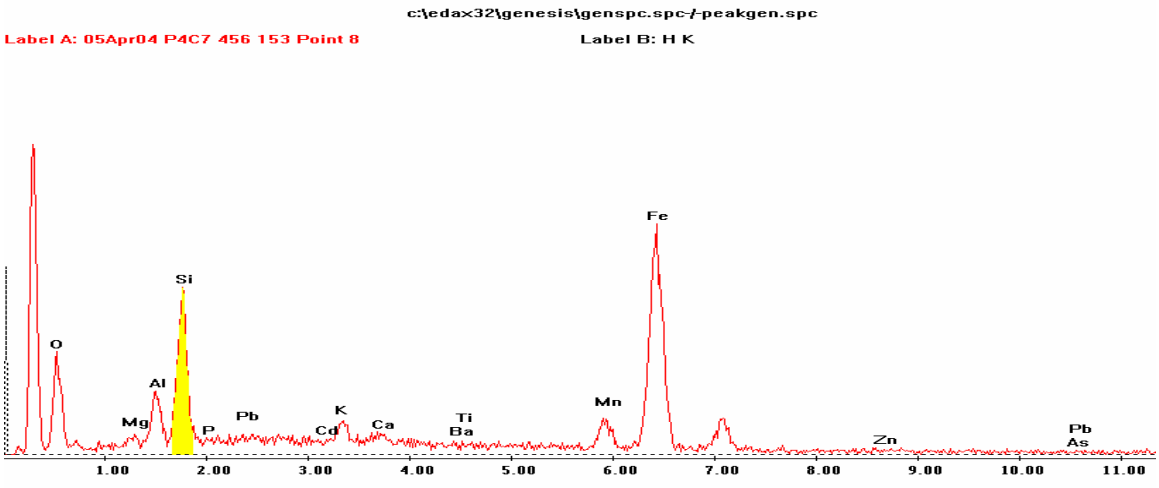

P4C7 – 485, 208

BSE Image

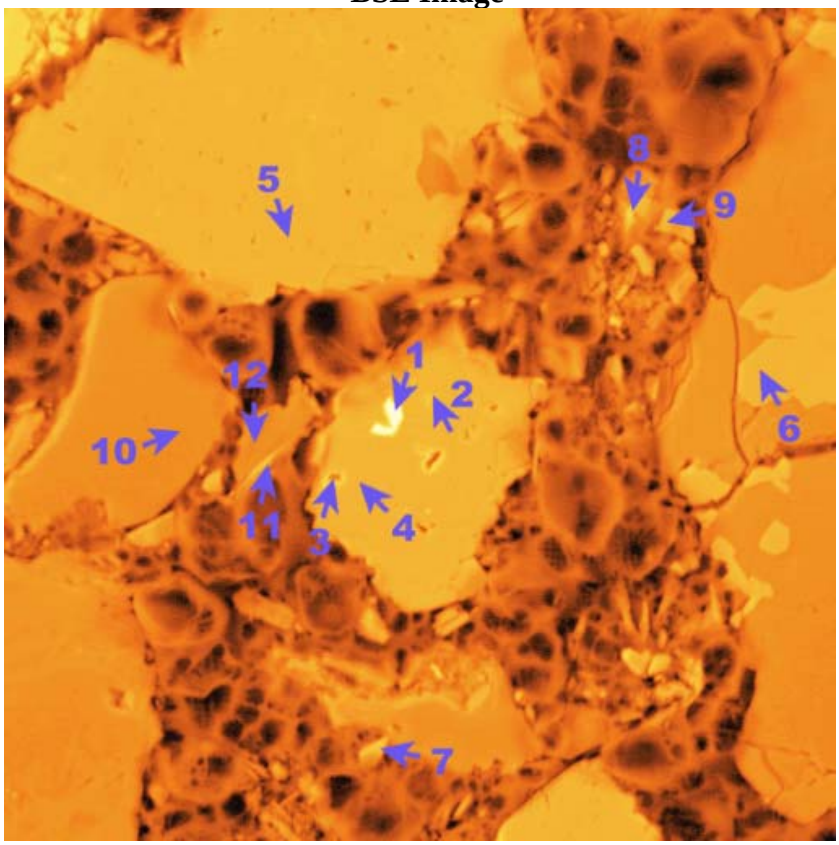

Iron (Fe)

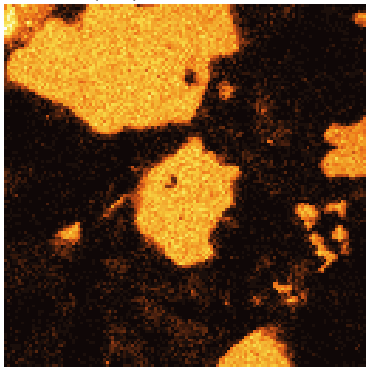

Manganese (Mn)

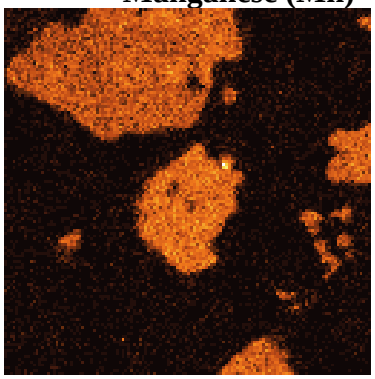

Phosphorous (P)

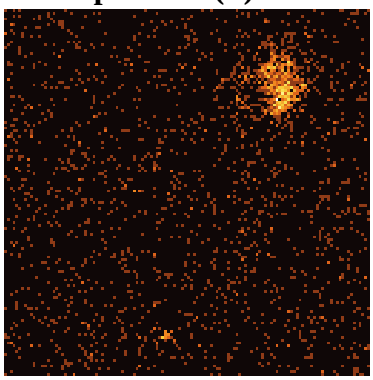

Lead (Pb)

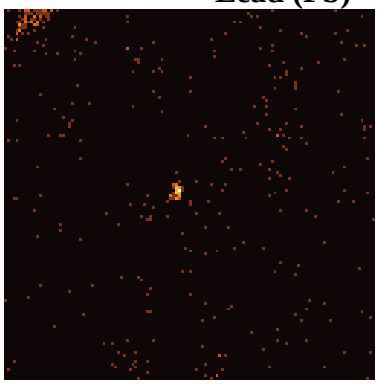

Silicon (Si)

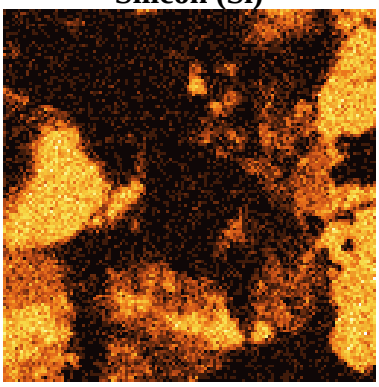

EDS Scan Images by Point

Point 1

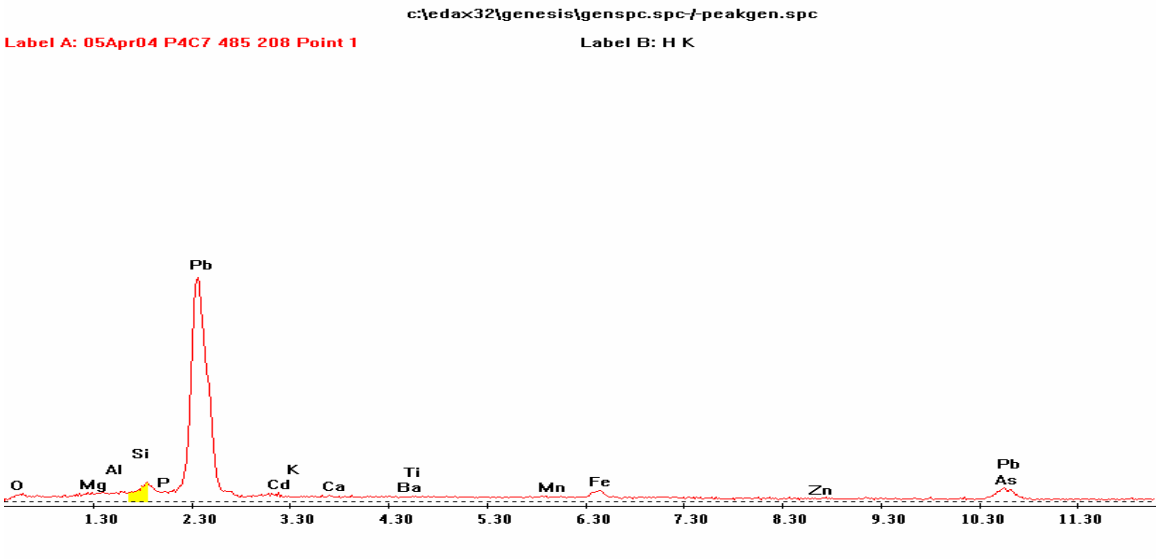

Point 2

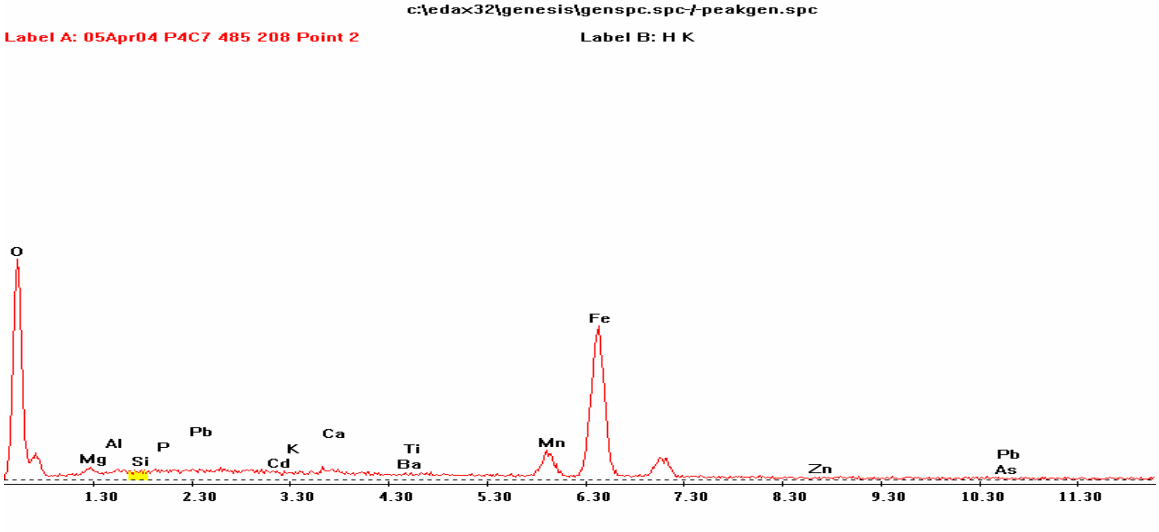

Point 3

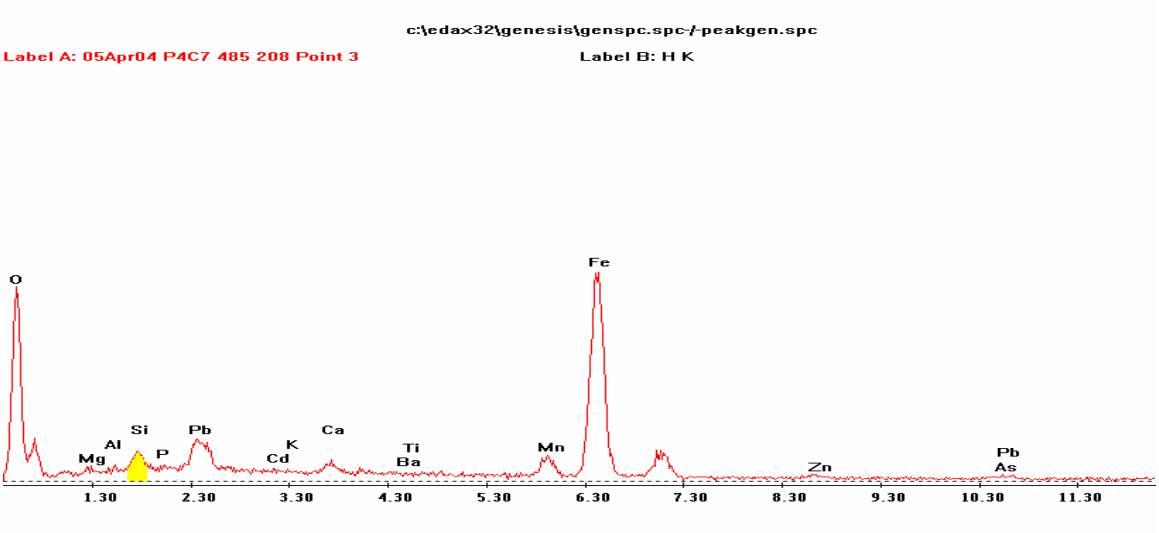

Point 4

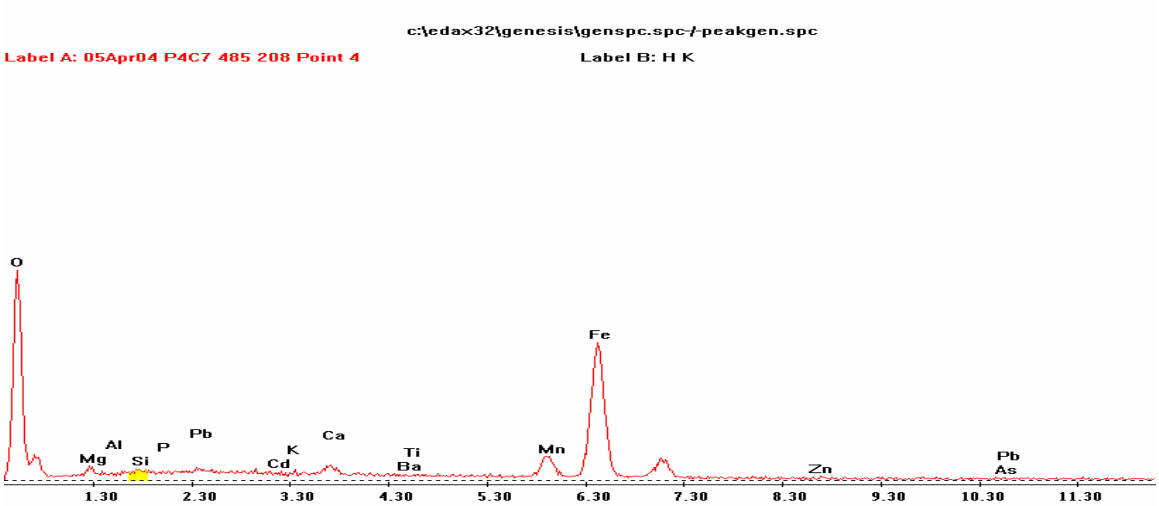

Point 5

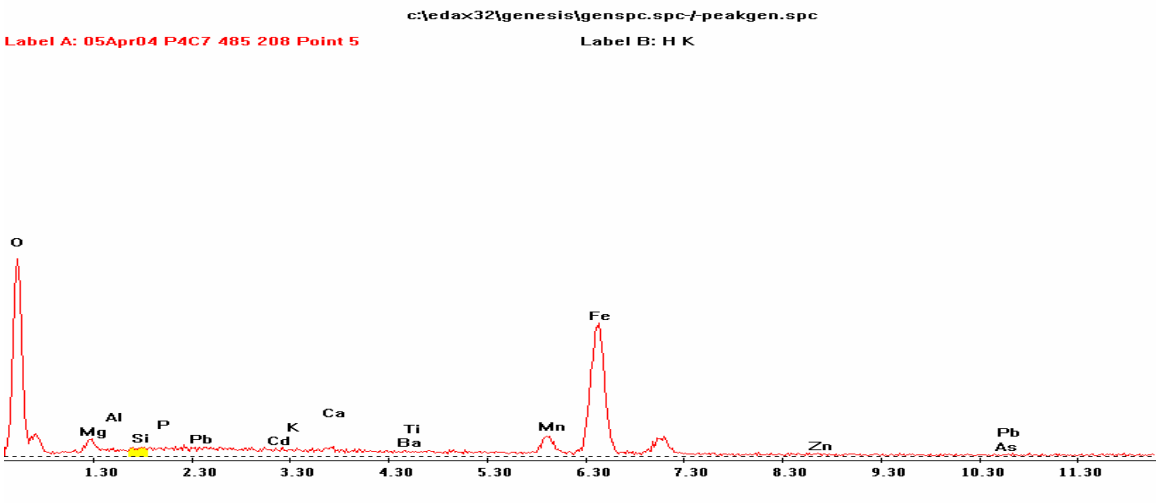

Point 6

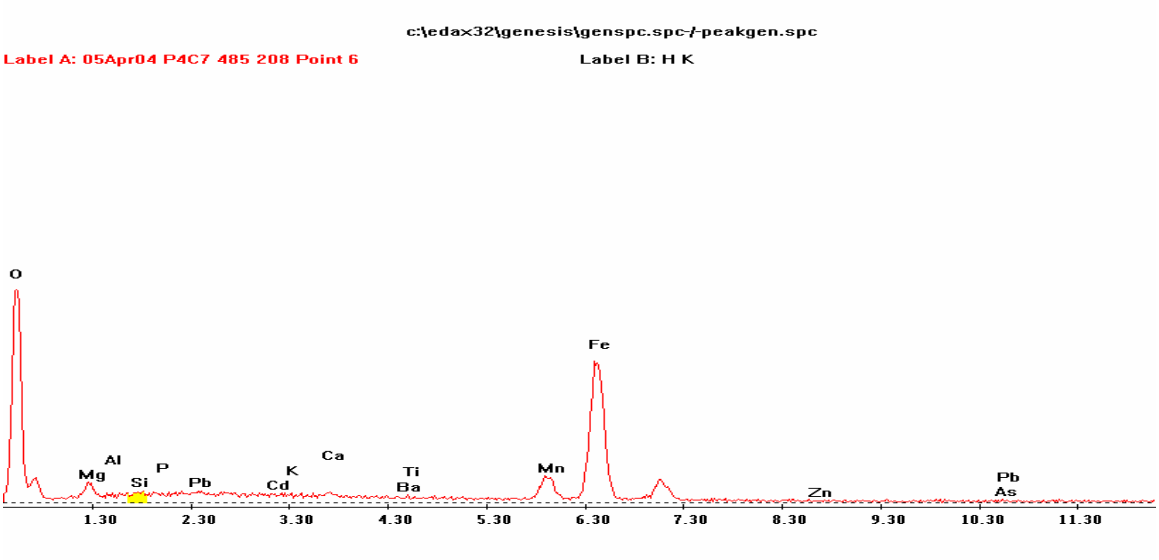

Point 7

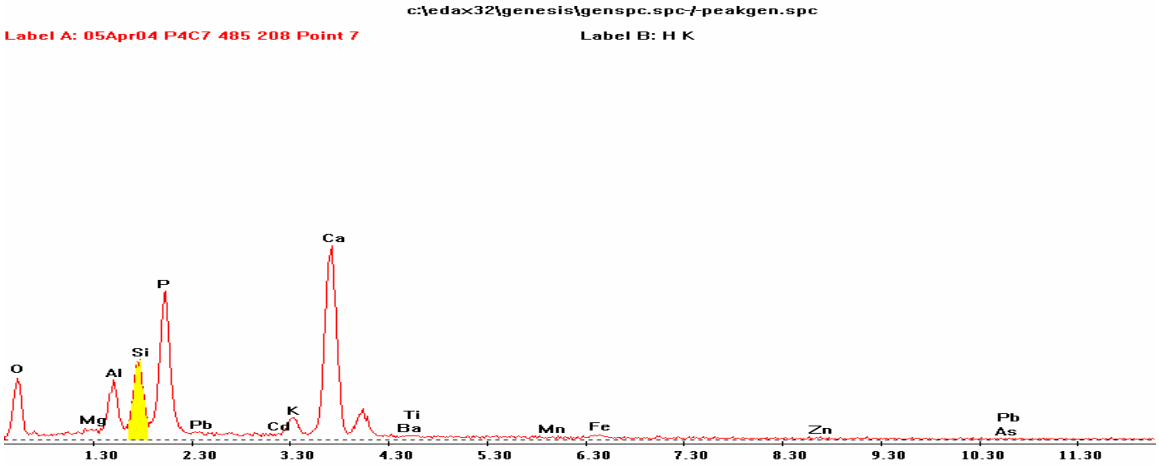

Point 8

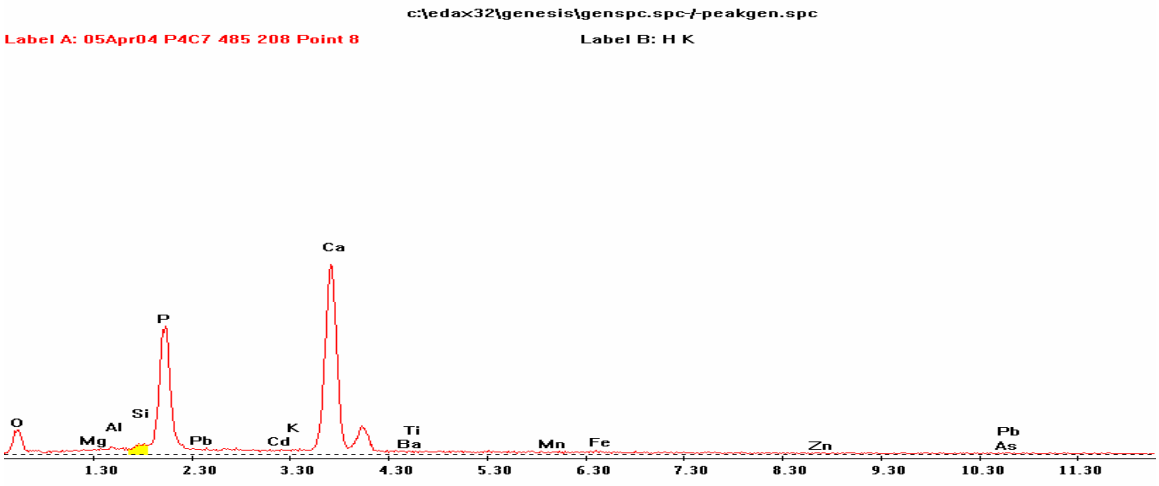

Point 9

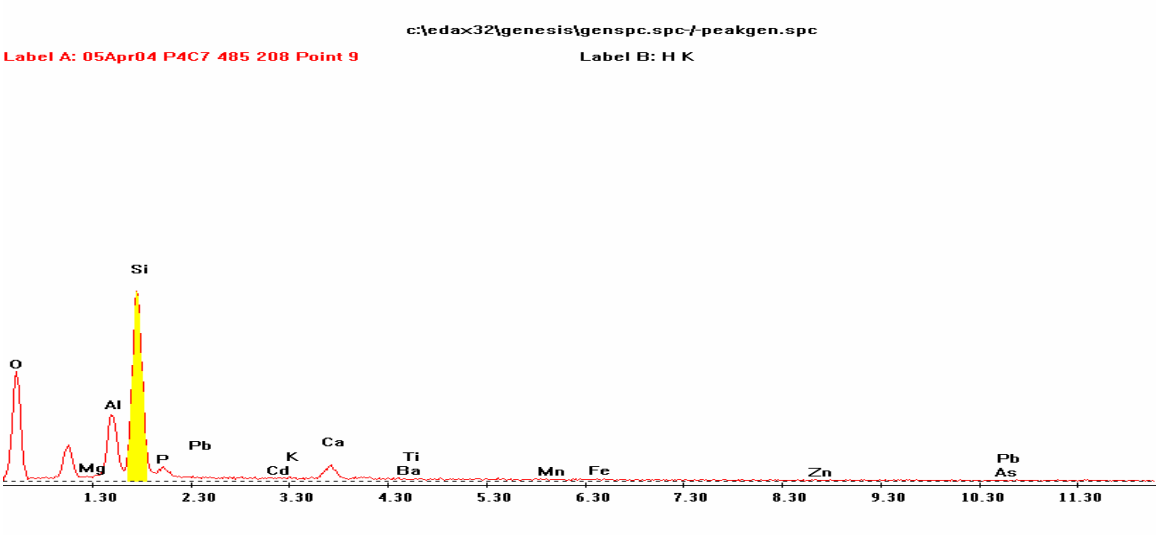

Point 10

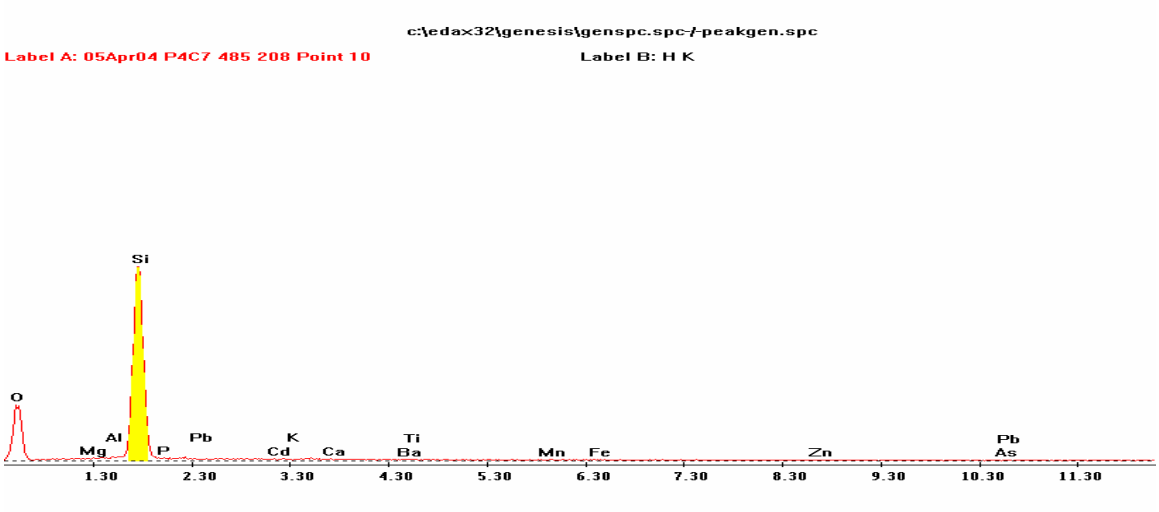

Point 11

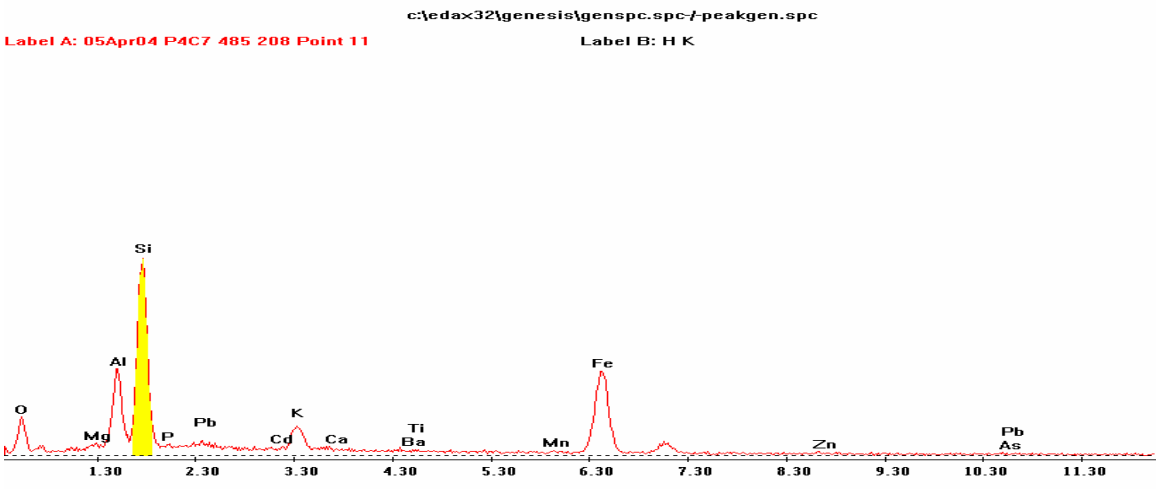

Point 12

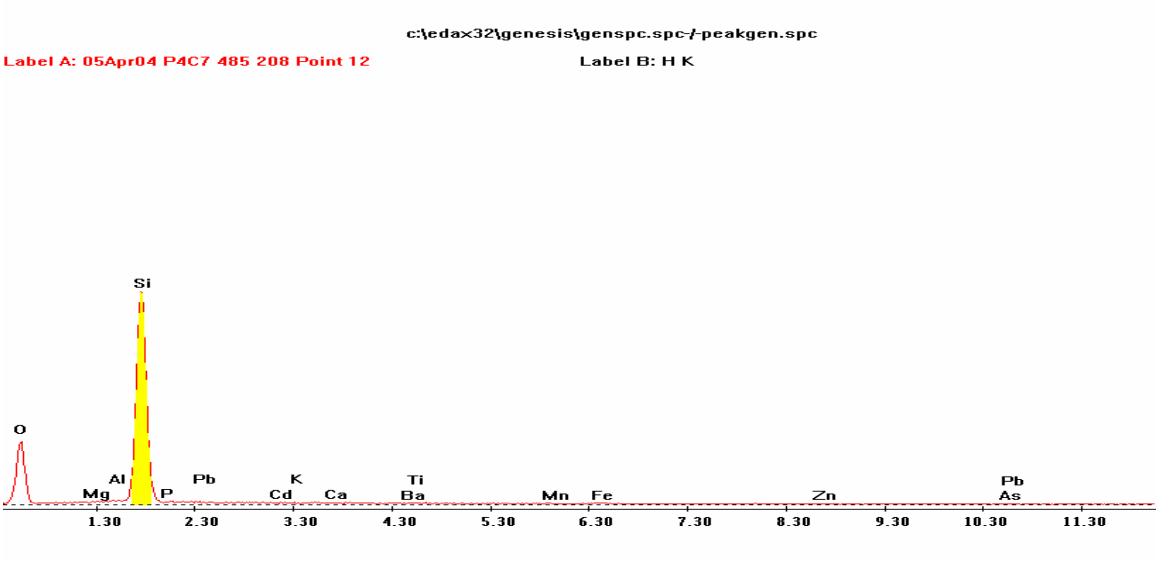
c:\edax32\genesis\genspc.spc-/-peakgen.spc
Label A: 05Apr04 P4C7 485 208 Point 12
Label B: H K
O
Si
Mg
Al
P
Pb
Cd
K
Ca
Ti
Ba
Mn
Fe
Zn
Pb
As
1.30
2.30
3.30
4.30
5.30
6.30
7.30
8.30
9.30
10.30
11.30

P4C7 – 486, 202

BSE Image

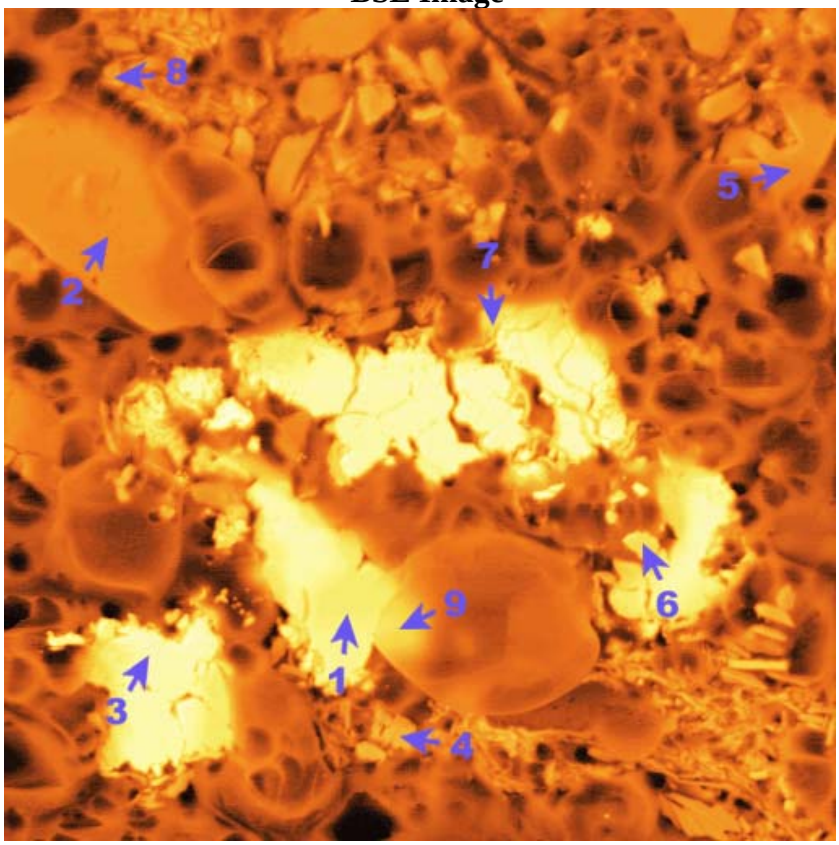

Iron (Fe)

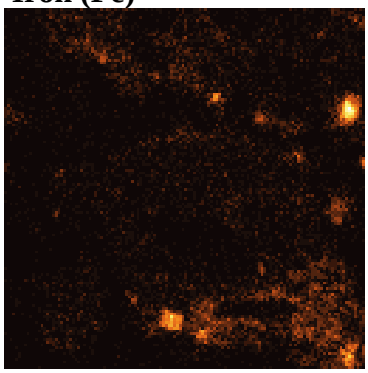

Manganese (Mn)

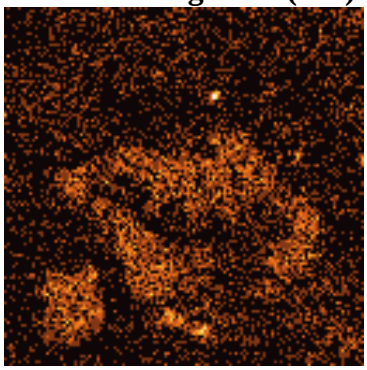

Phosphorous (P)

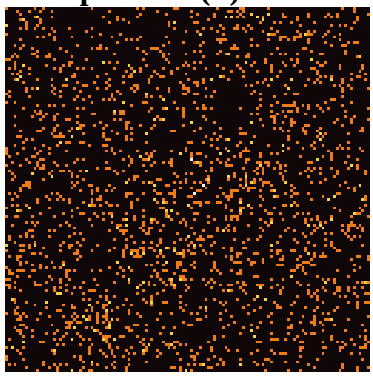

Lead (Pb)

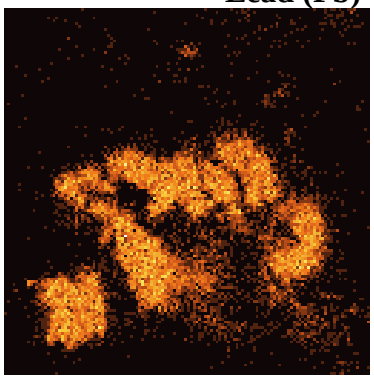

Silicon (Si)

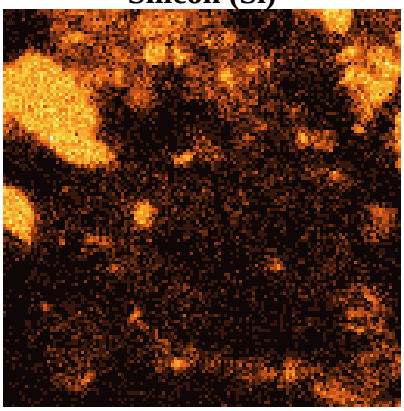

EDS Scan Images by Point

Point 1

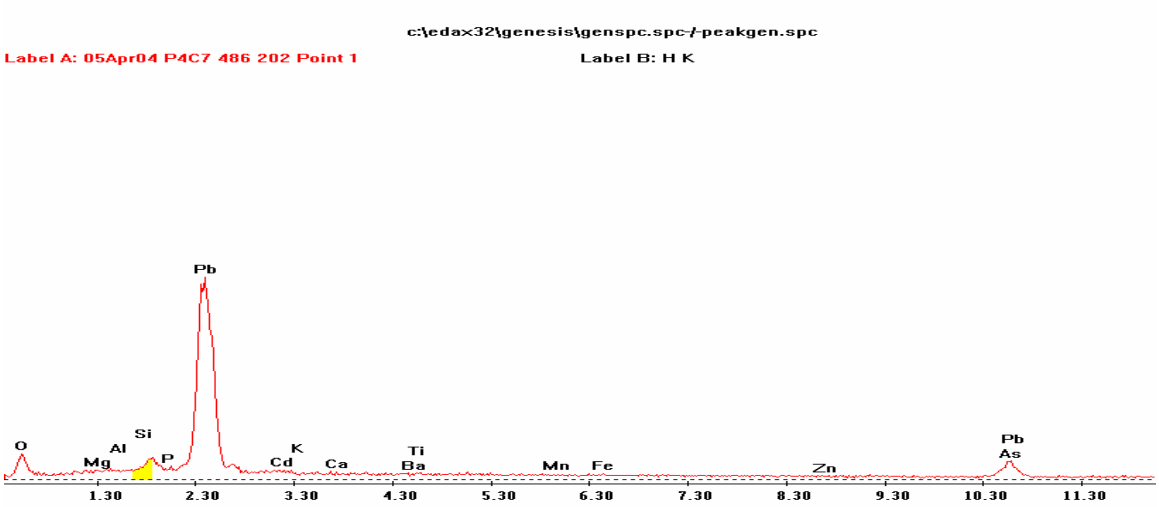

Point 2

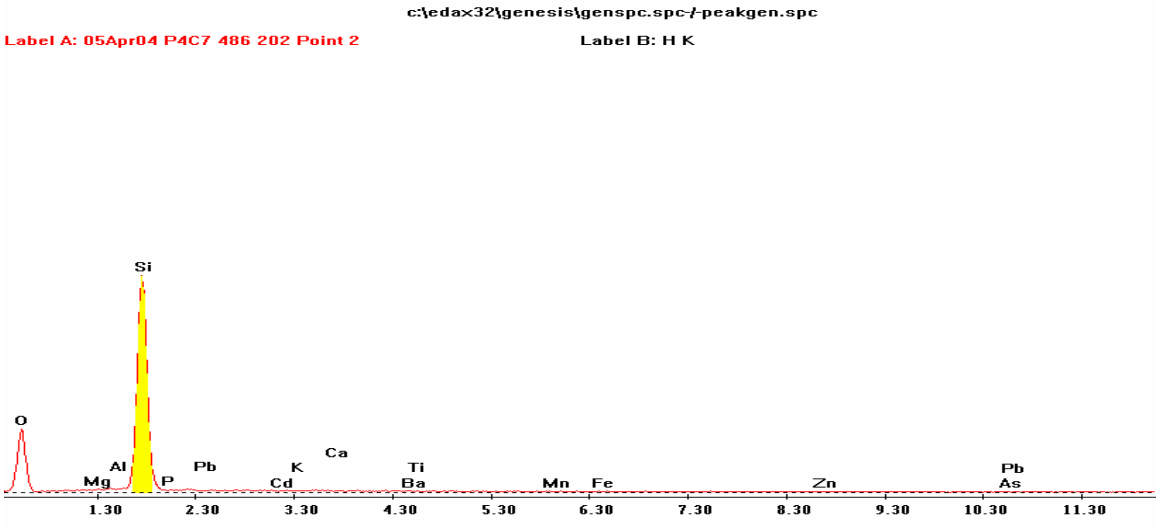

Point 3

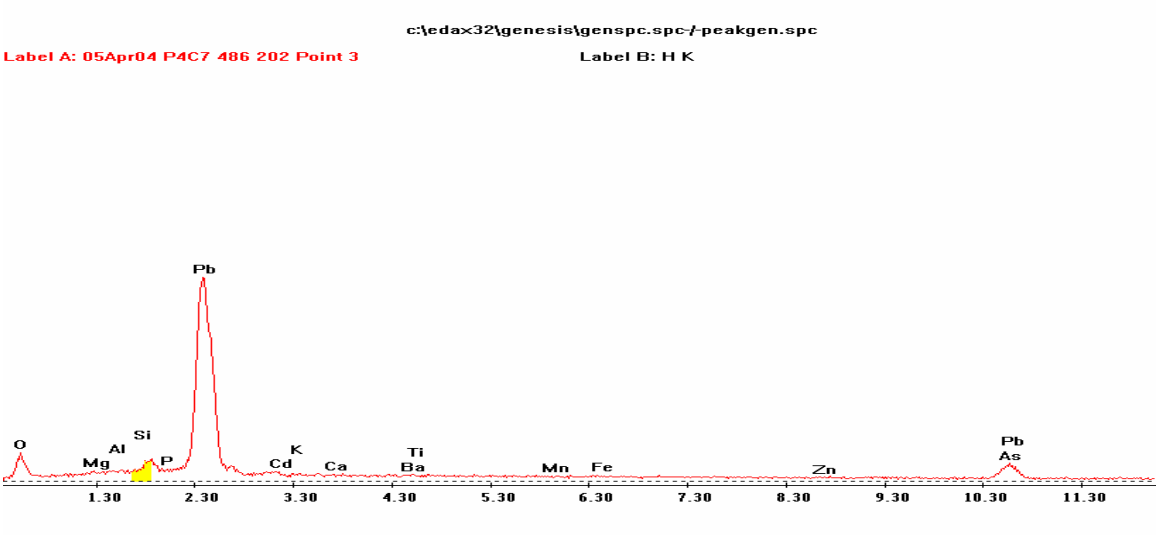

Point 4

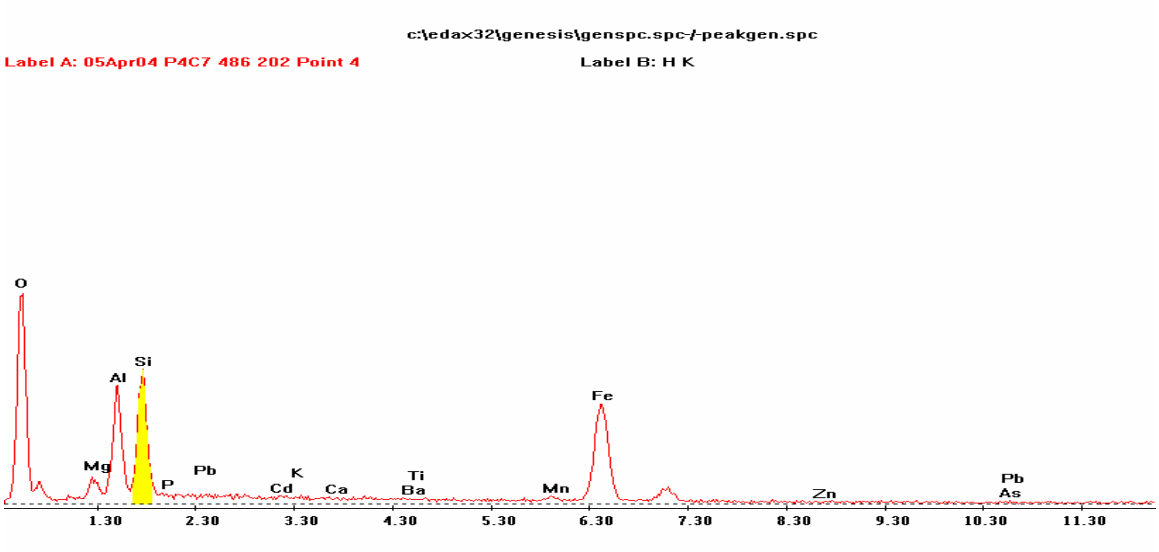

Point 5

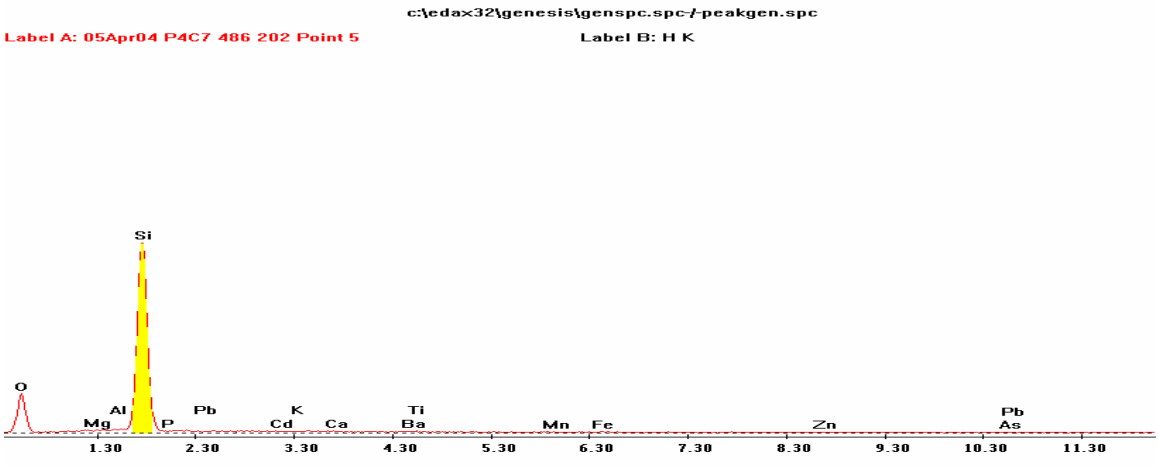

Point 6

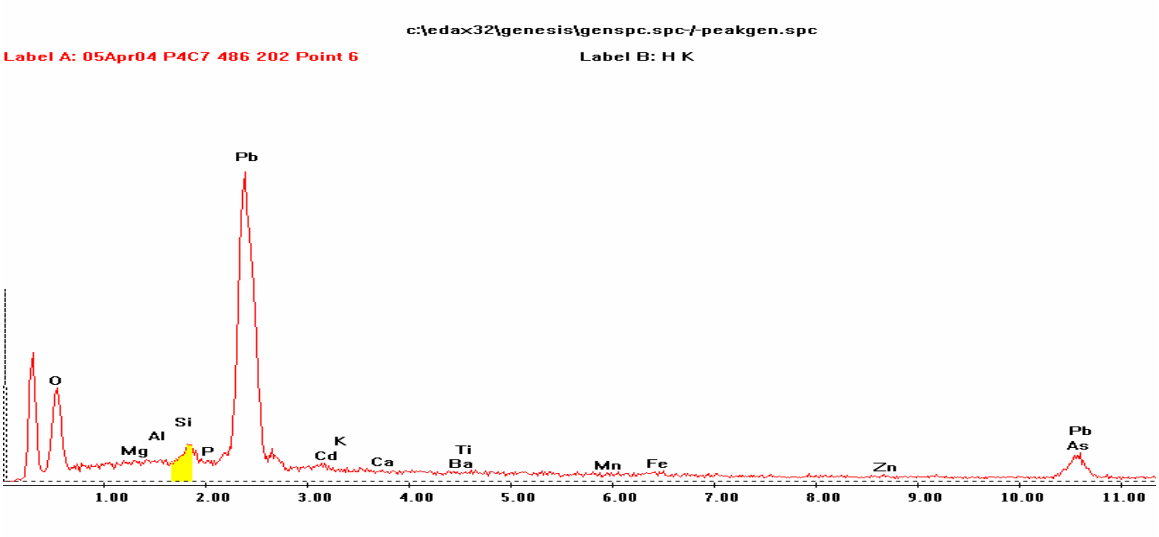

Point 7

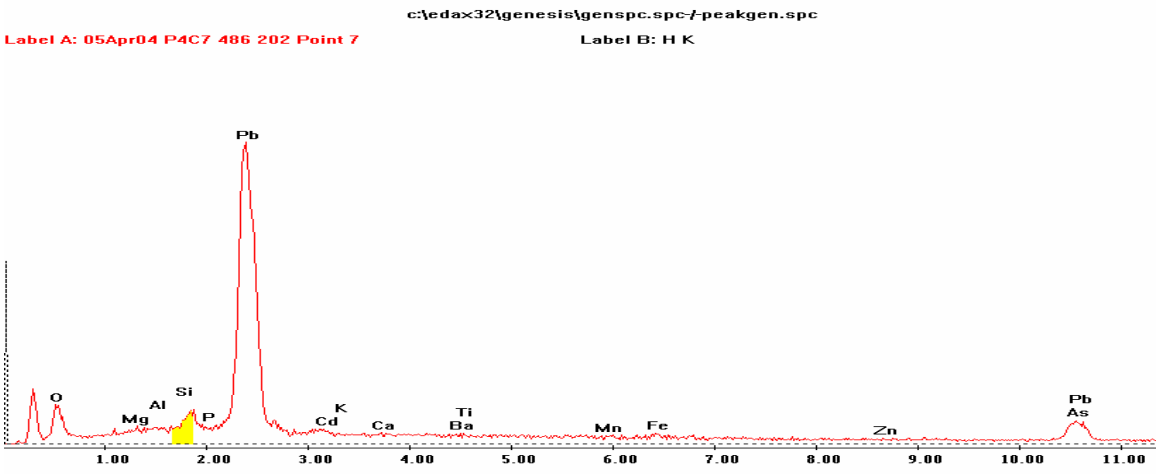

Point 8

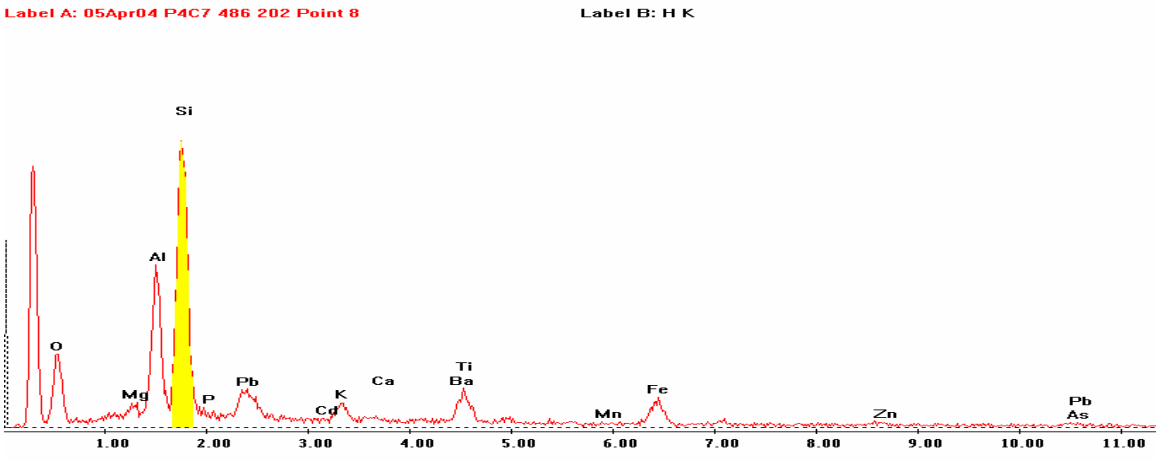

Point 9

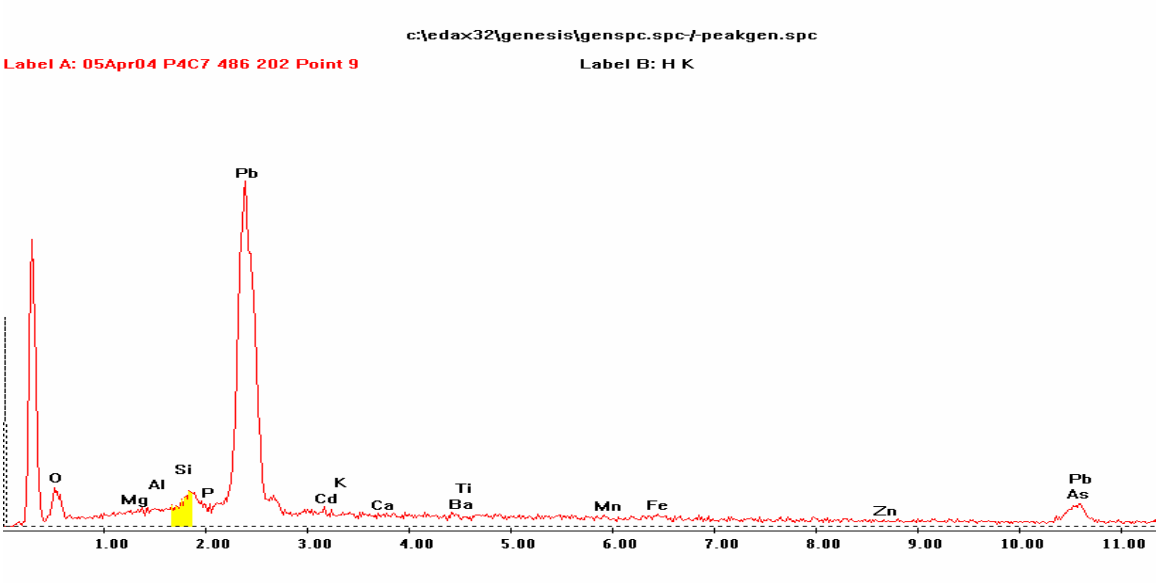
c:\edax32\genesis\genspc.spc-/-peakgen.spc
Label A: 05Apr04 P4C7 486 202 Point 9
Label B: H K
Pb
O
Mg
Al
Si
P
K
Cd
Ca
Ti
Ba
Mn
Fe
Zn
Pb
As
1.00
2.00
3.00
4.00
5.00
6.00
7.00
8.00
9.00
10.00
11.00

P4C8 – 354, 306

BSE Image

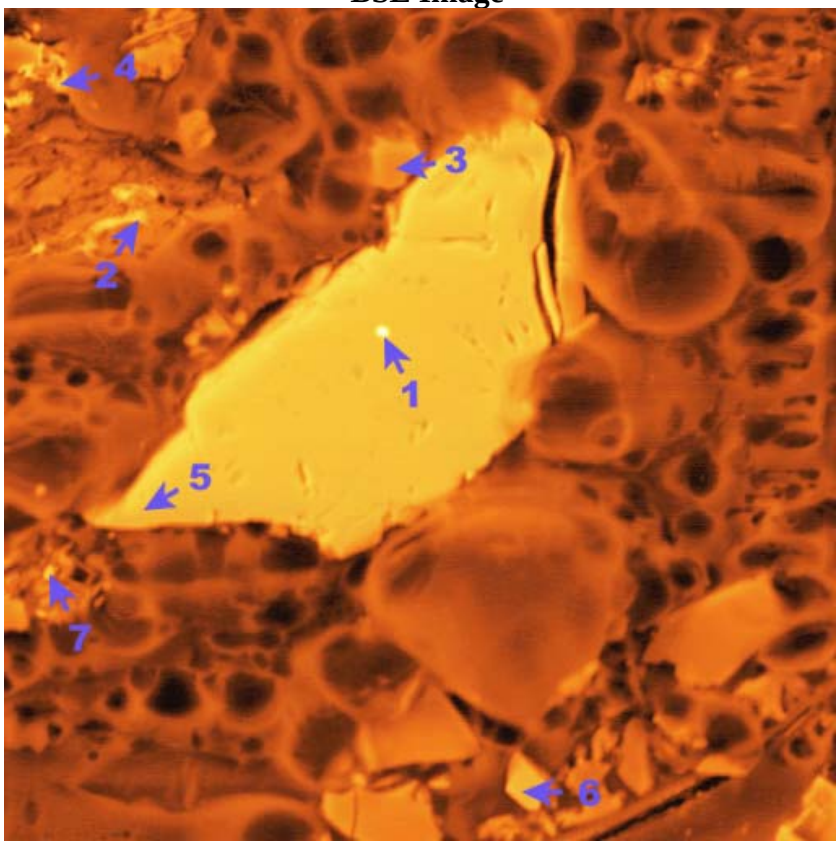

Iron (Fe)

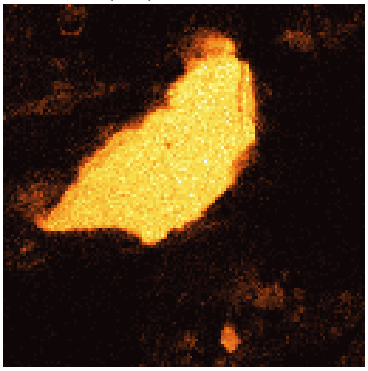

Manganese (Mn)

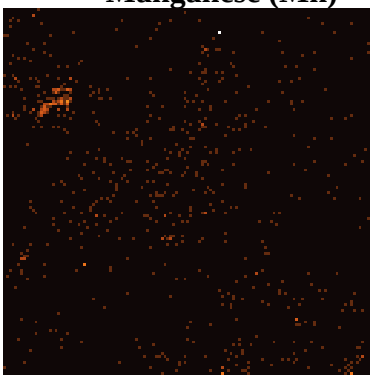

Phosphorous (P)

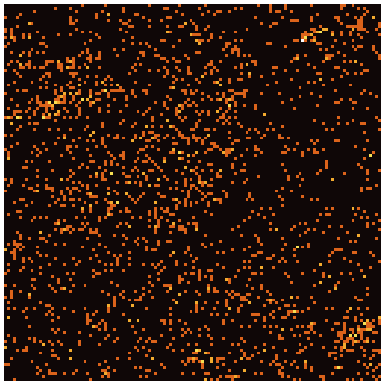

Lead (Pb)

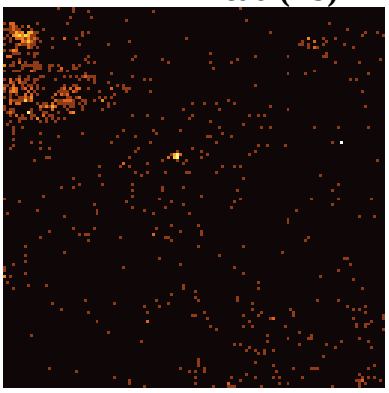

Silicon (Si)

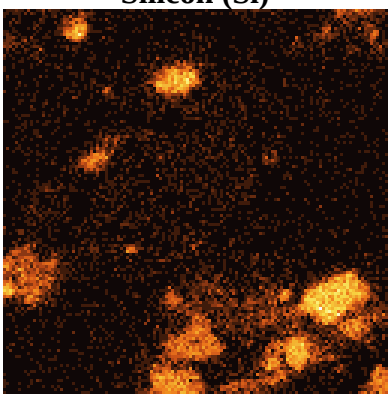

EDS Scan Images by Point

Point 1

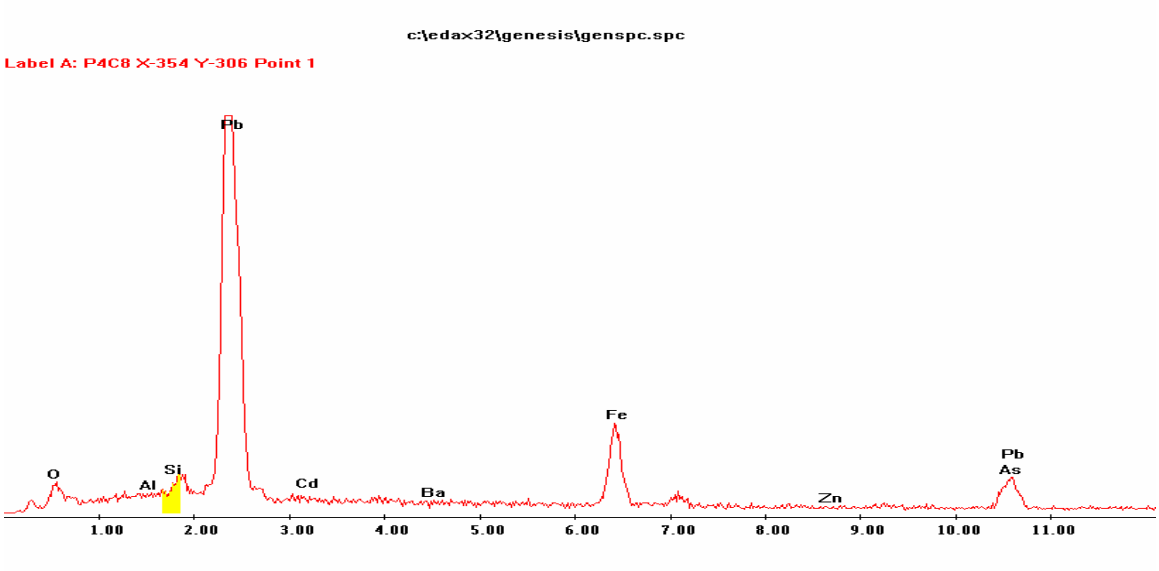

Point 2

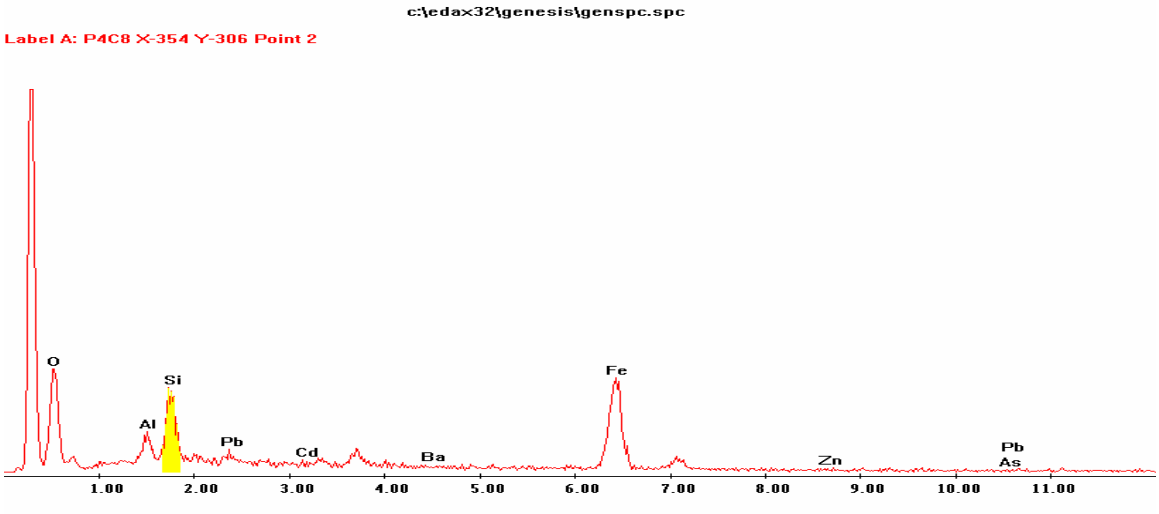

Point 3

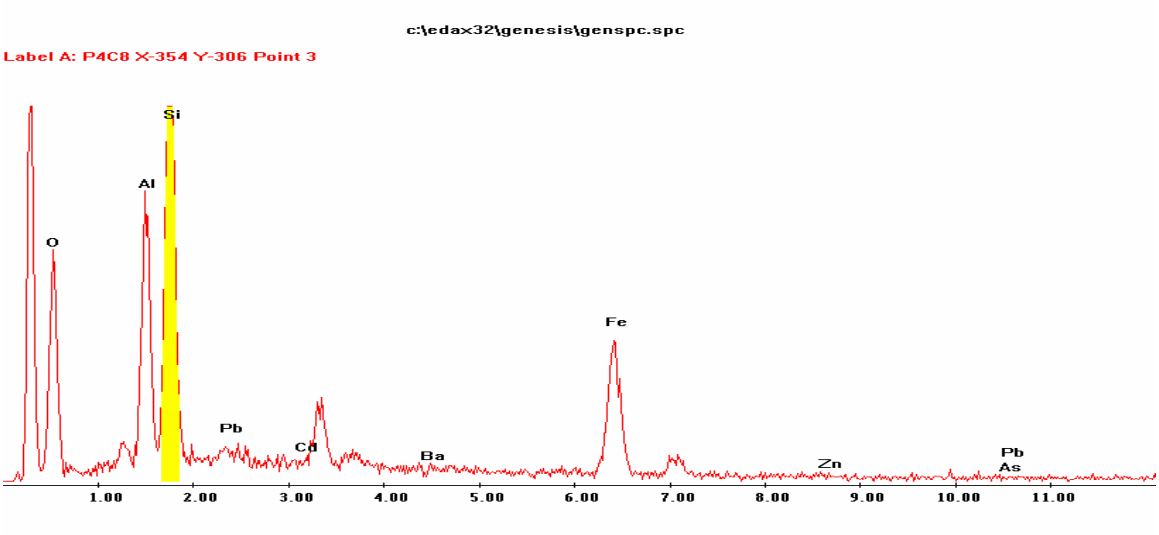

Point 4

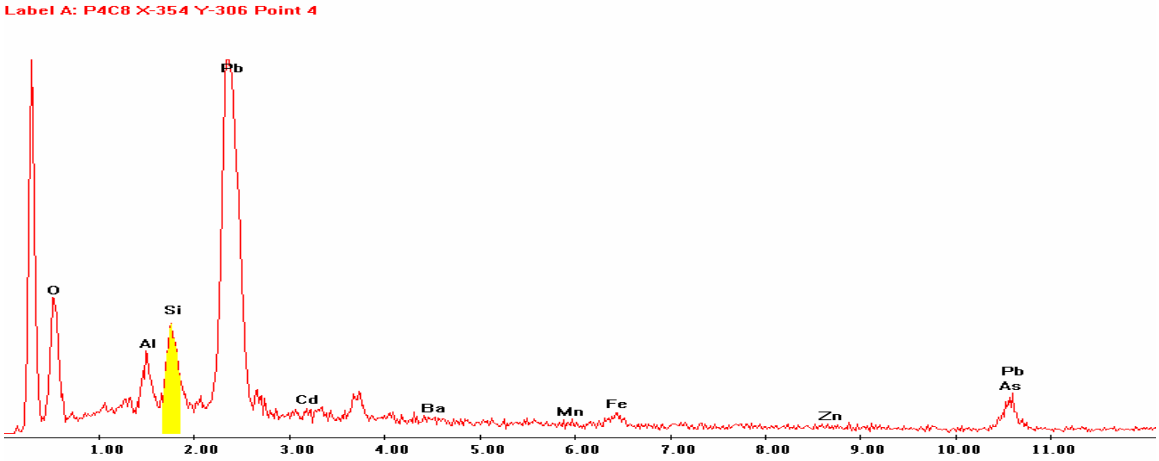

Point 5

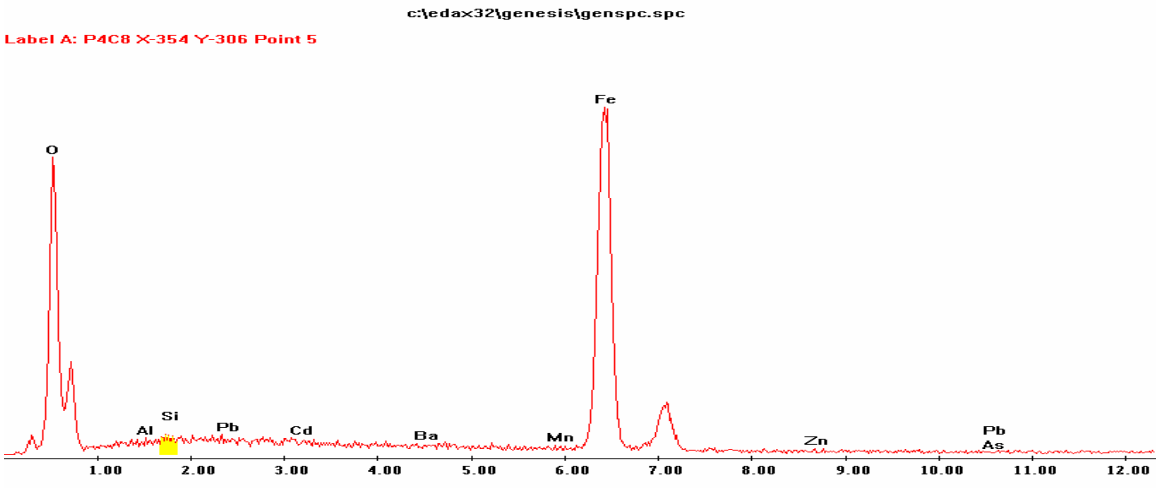

Point 6

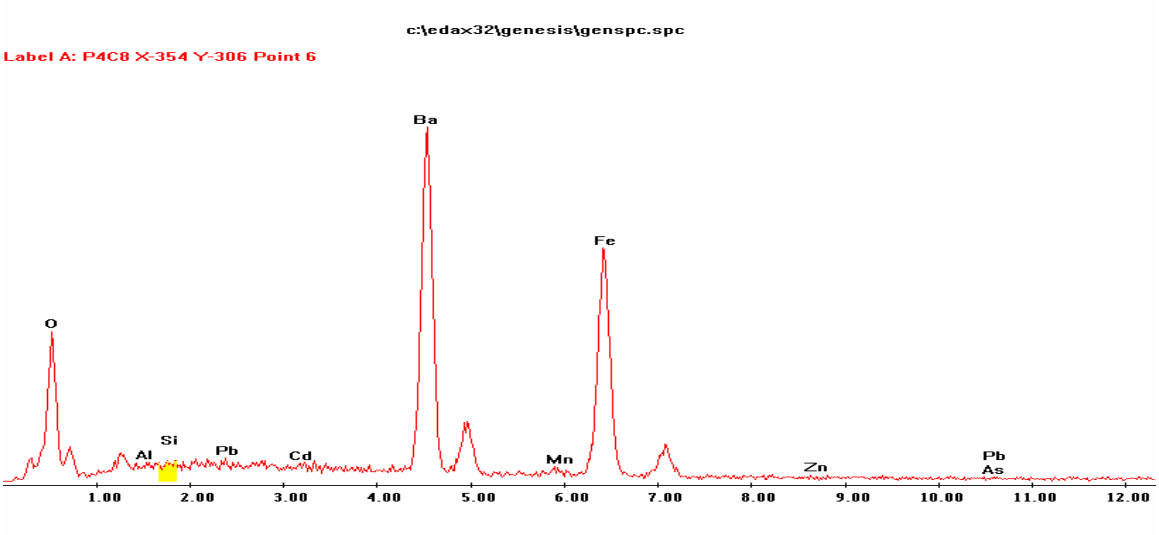

Point 7

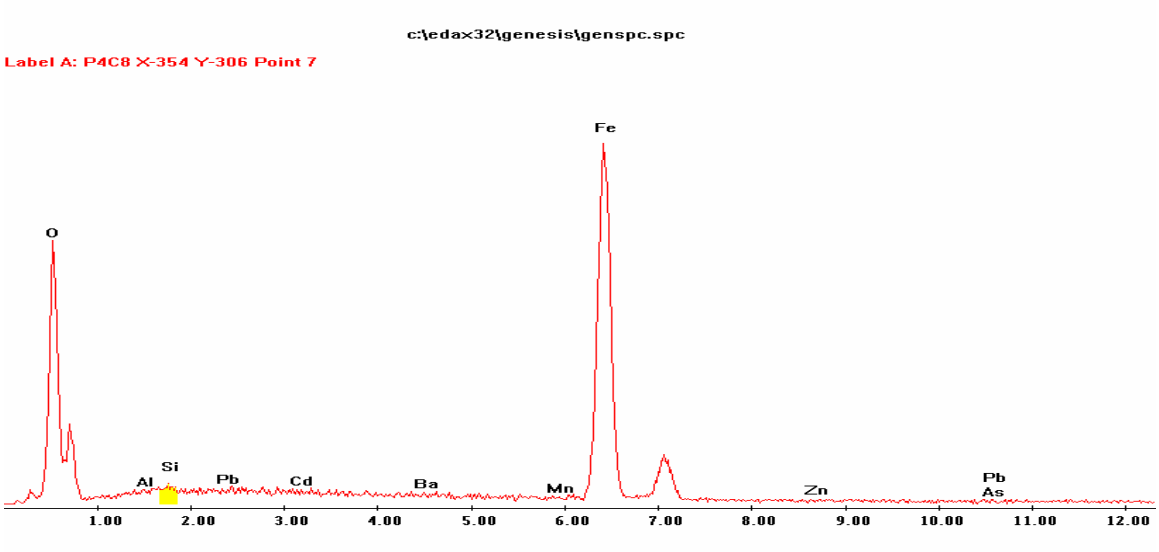

P4C8 – 370, 216

BSE Image

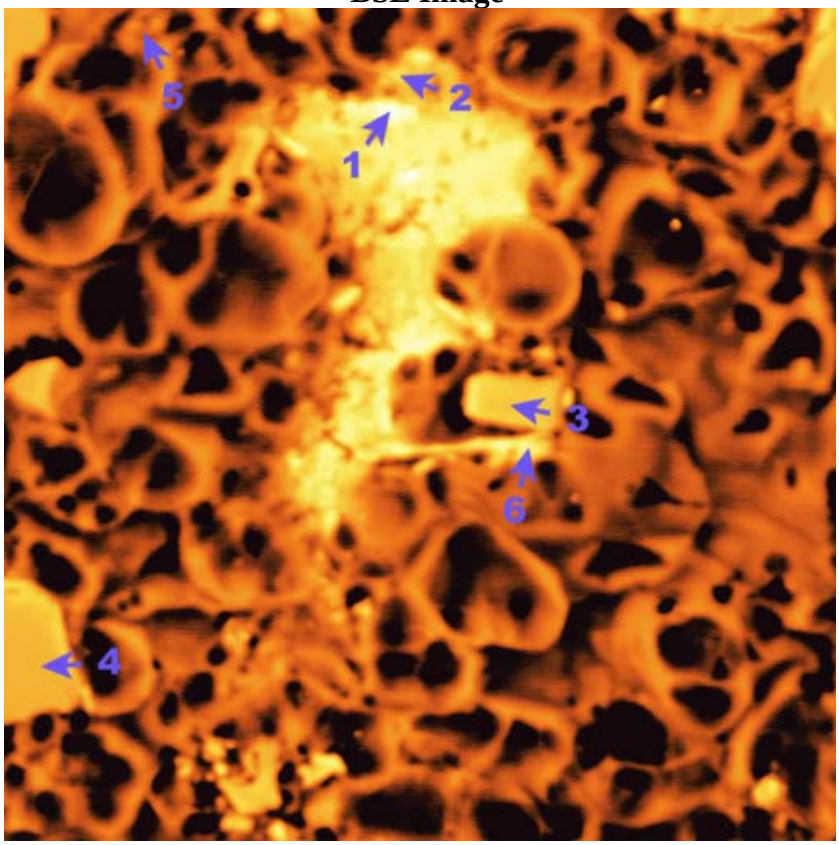

Iron (Fe)

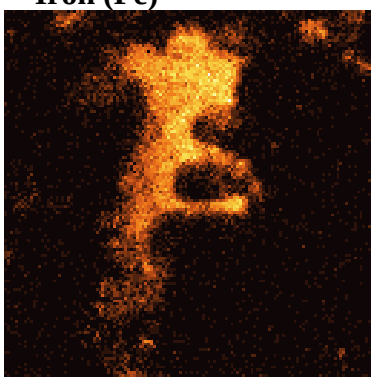

Manganese (Mn)

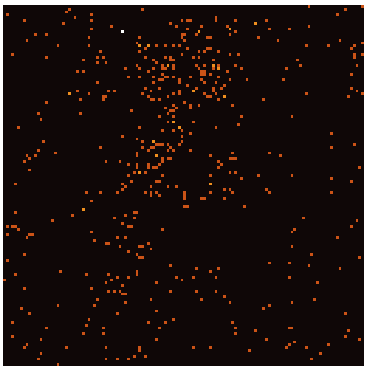

Phosphorous (P)

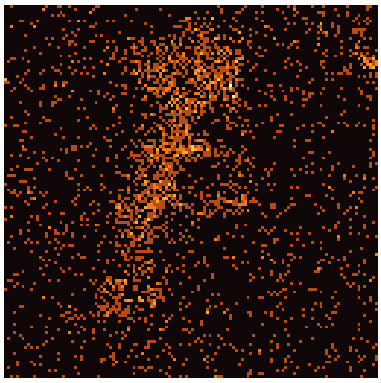

Lead (Pb)

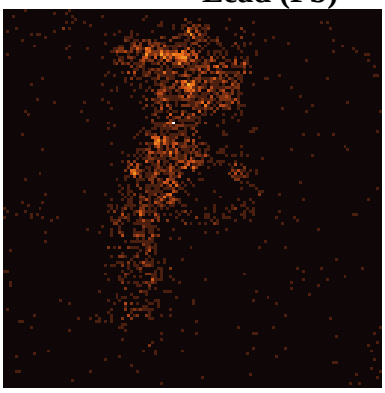

Silicon (Si)

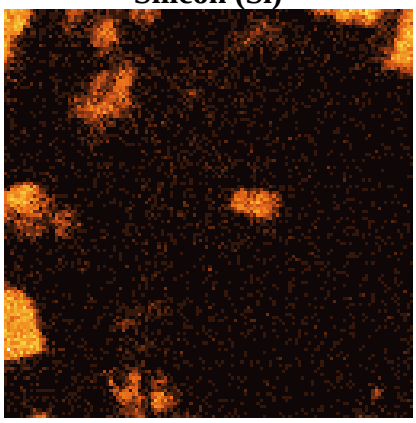

EDS Scan Images by Point

Point 1

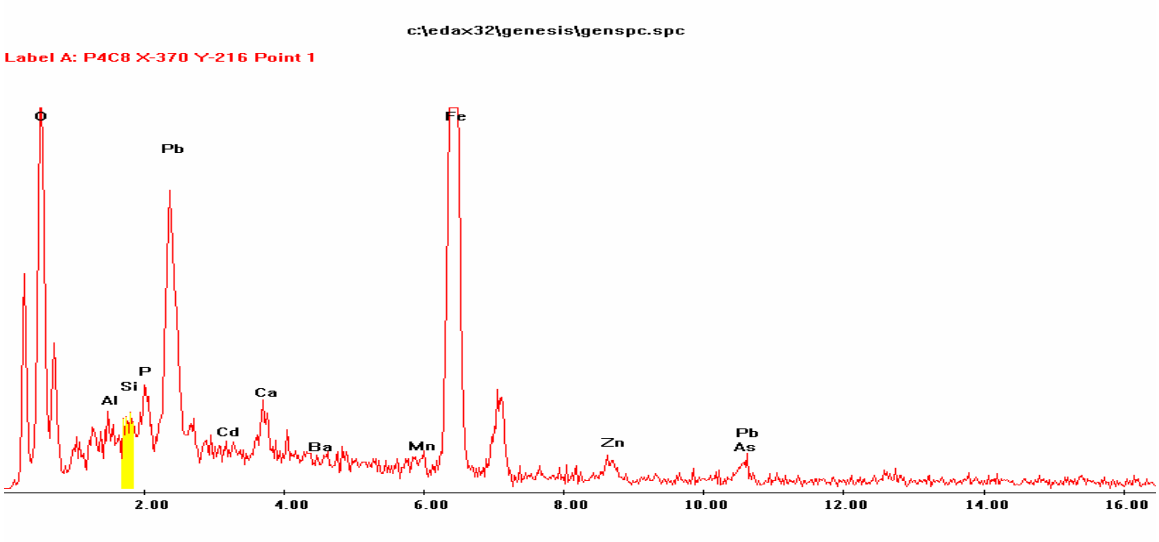

Point 2

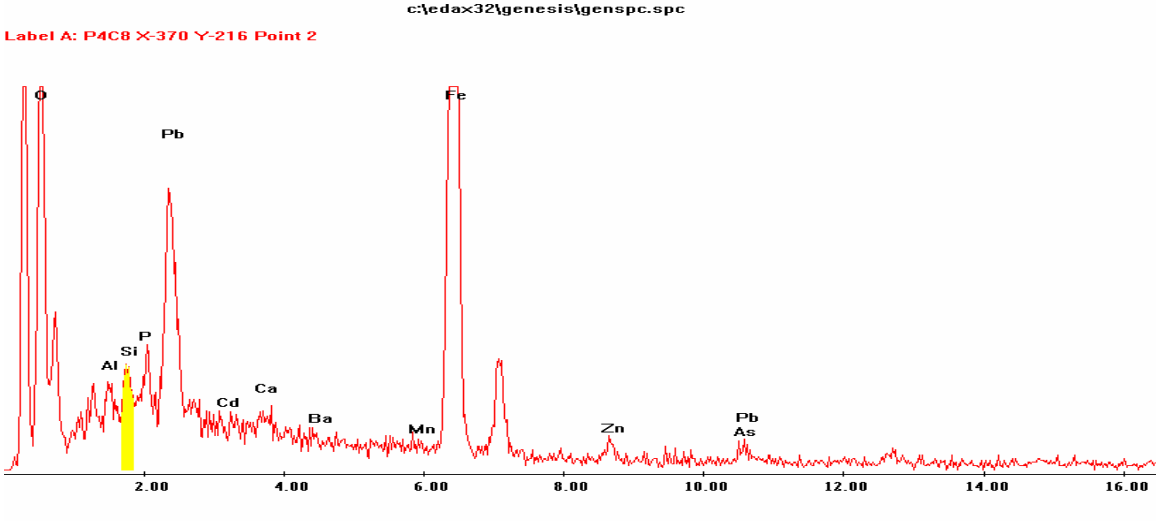

Point 3

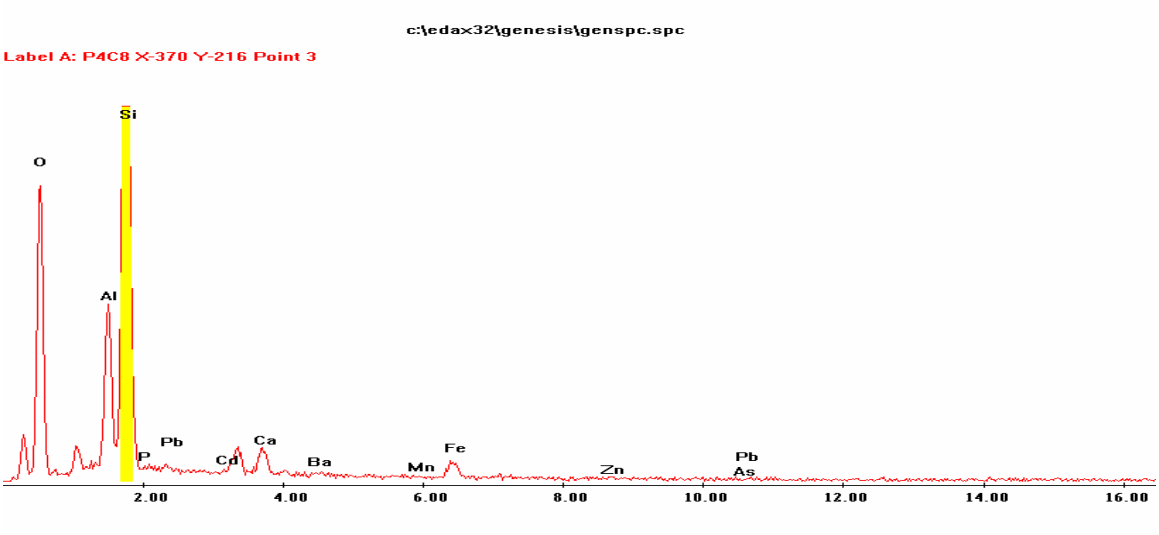

Point 4

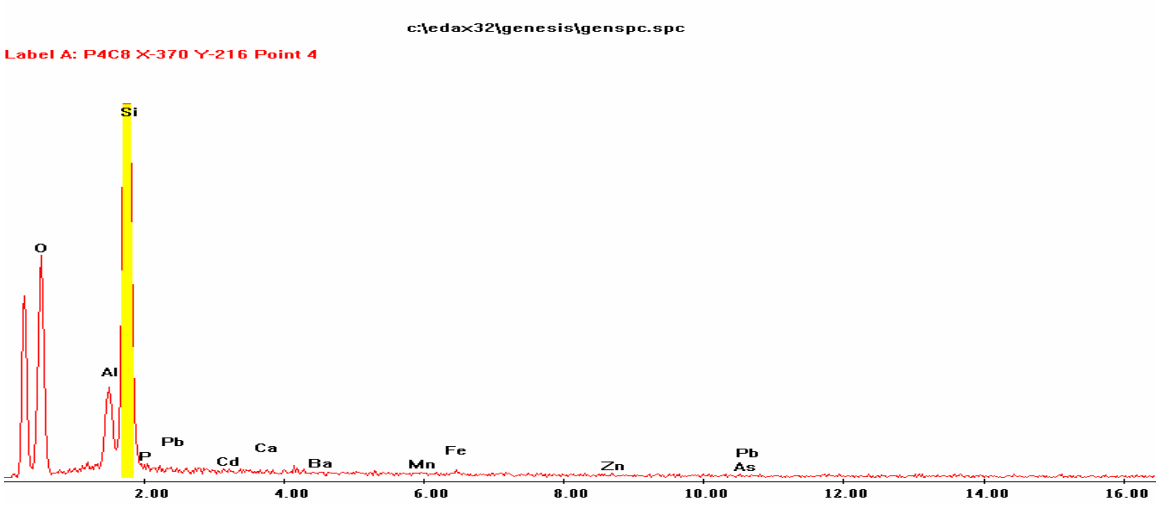

Point 5

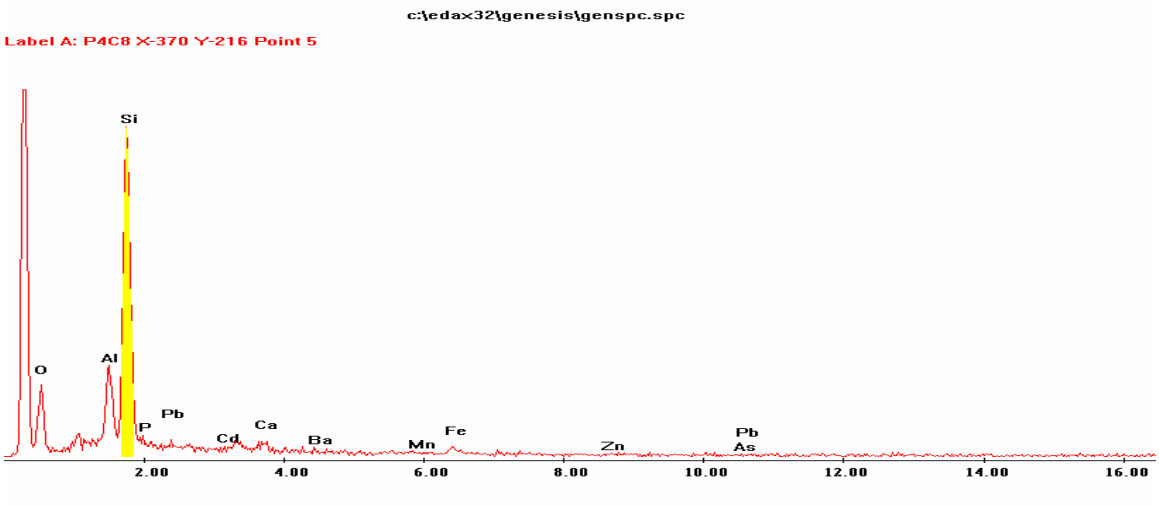

Point 6

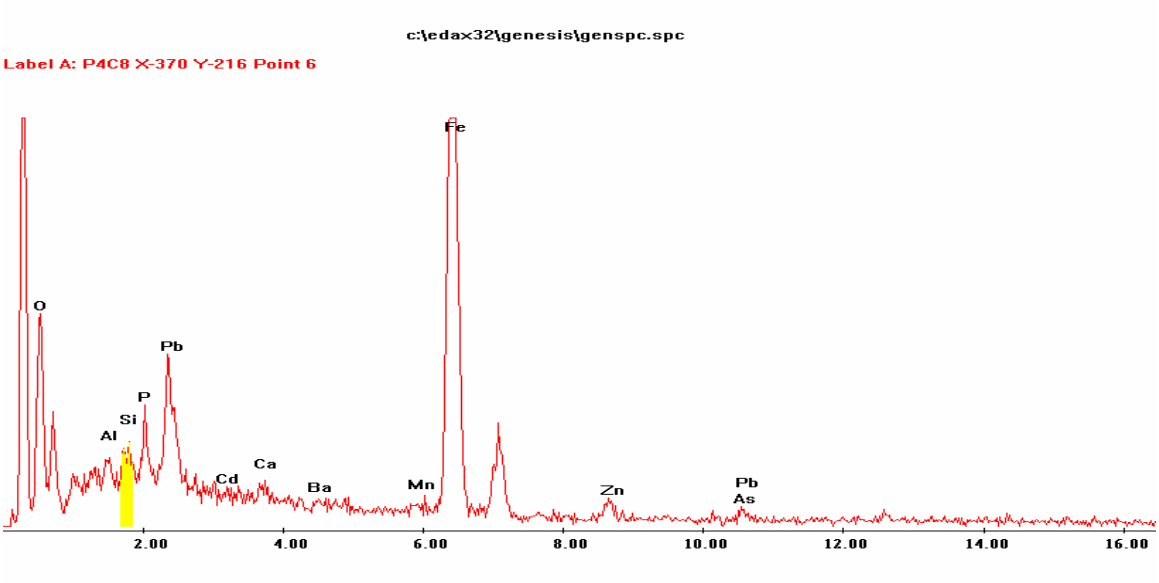
c:\edax32\genesis\genspc.spc
Label A: P4C8 X-370 Y-216 Point 6
O
Al
Si
P
Pb
Cd
Ca
Ba
Mn
Fe
Zn
Pb
As
2.00
4.00
6.00
8.00
10.00
12.00
14.00
16.00

P4C8 – 391, 328

BSE Image

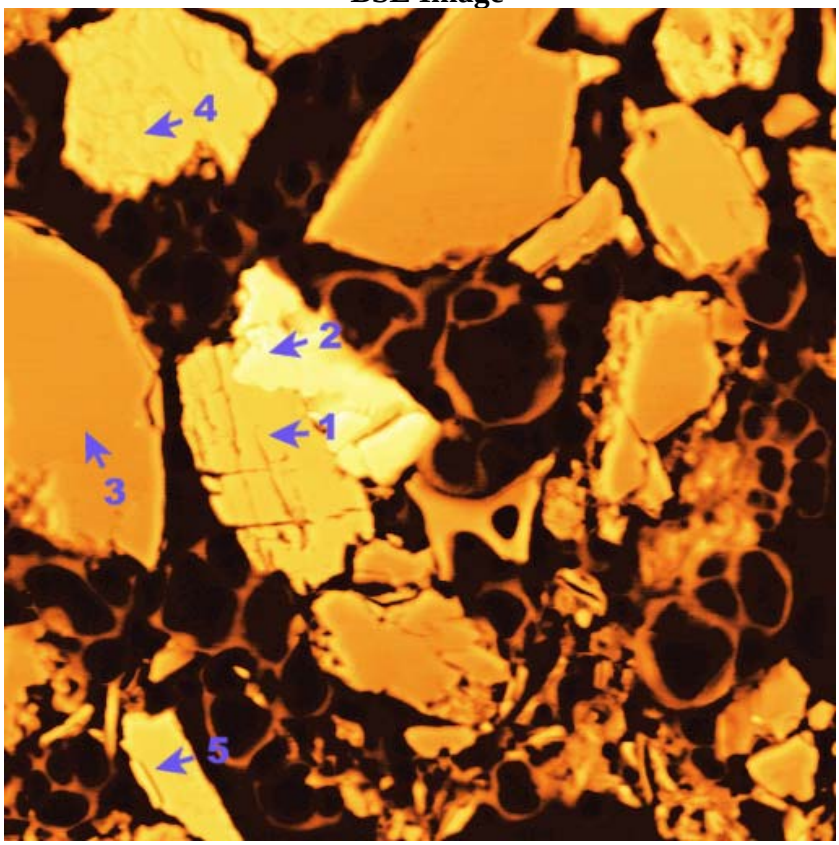

Iron (Fe)

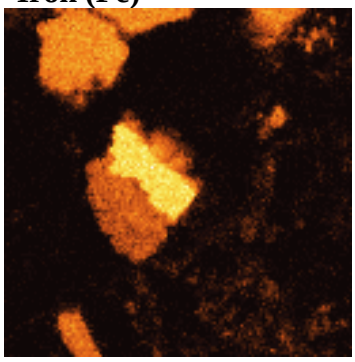

Manganese (Mn)

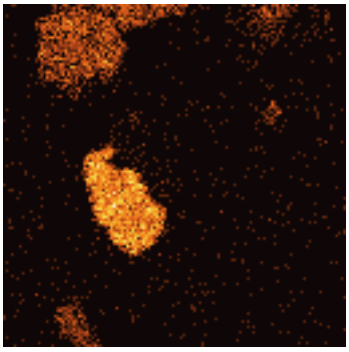

Phosphorous (P)

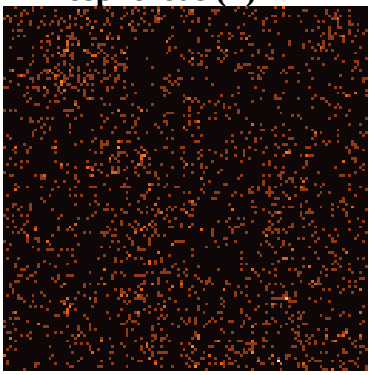

Lead (Pb)

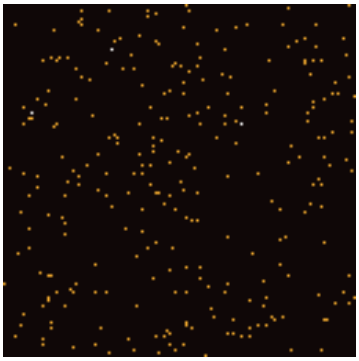

Silicon (Si)

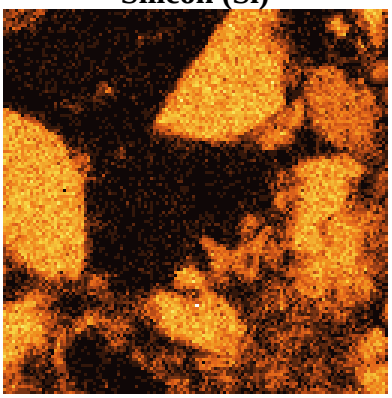

EDS Scan Images by Point

Point 1

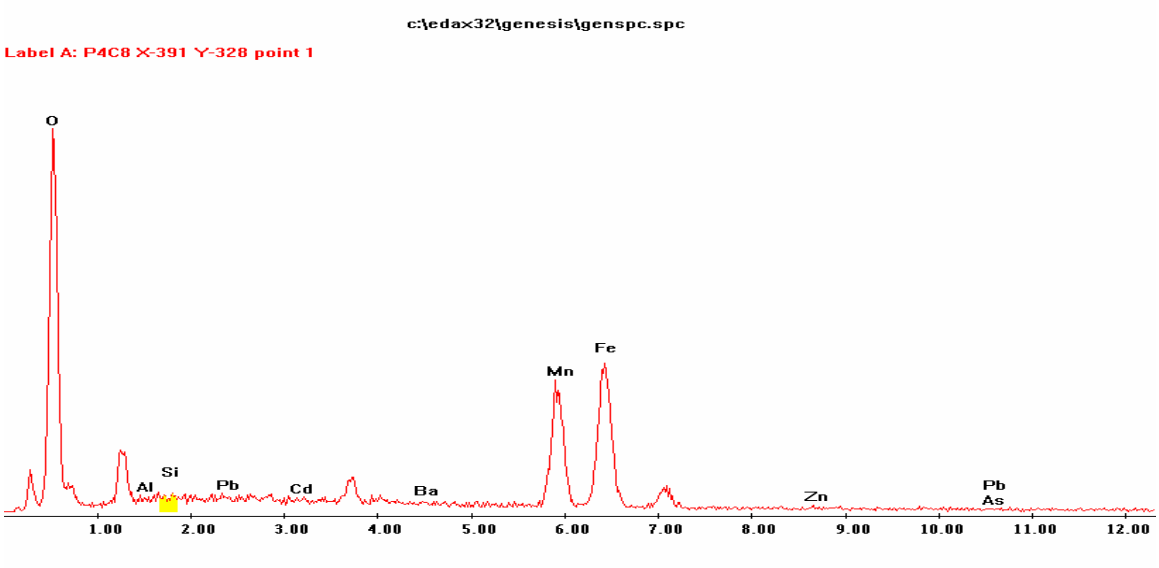

Point 2

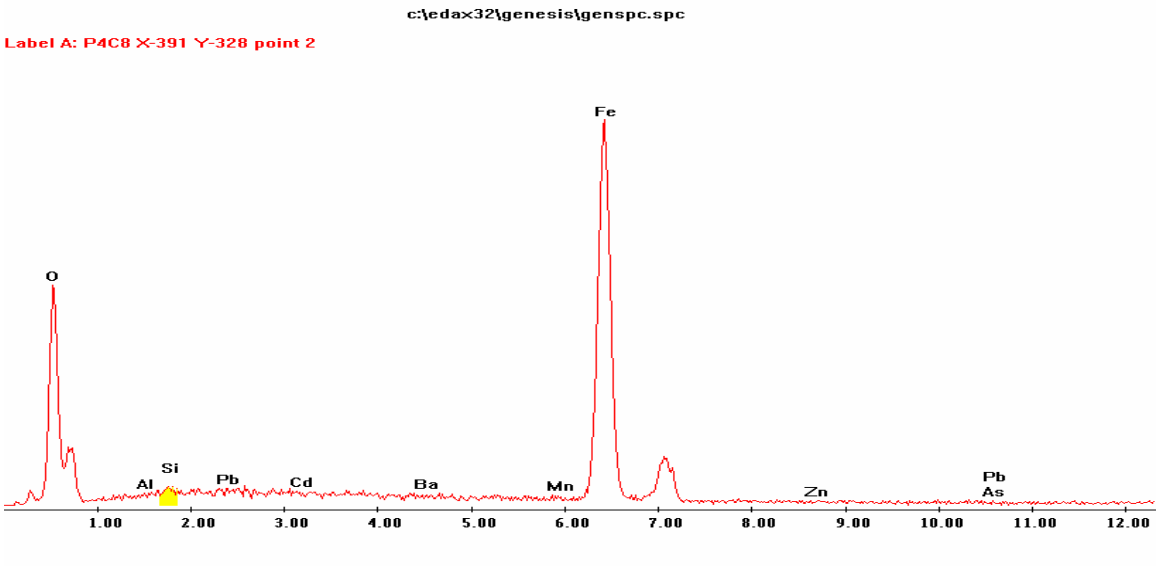

Point 3

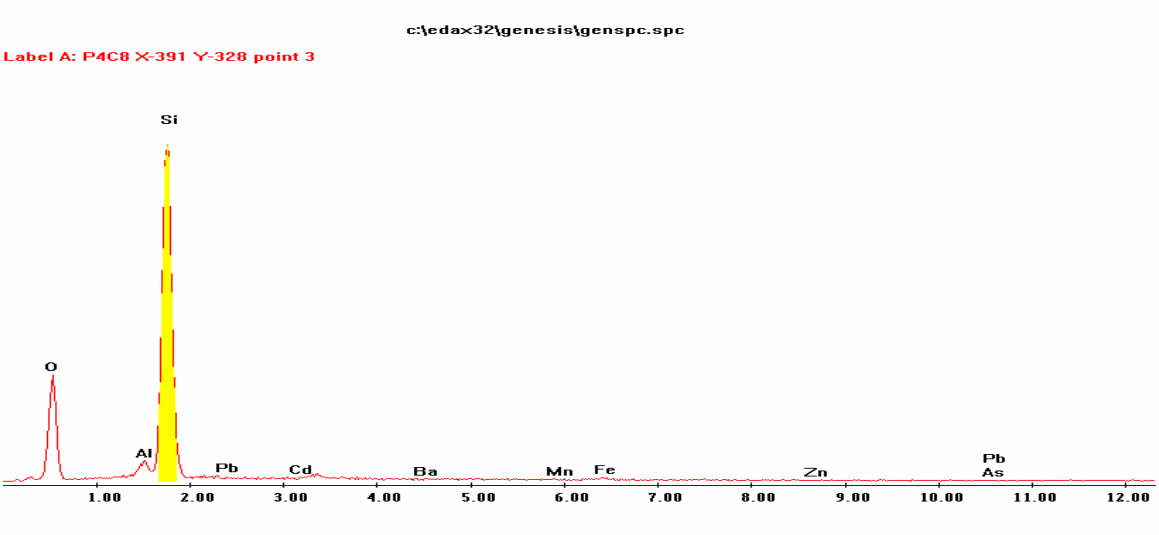

Point 4

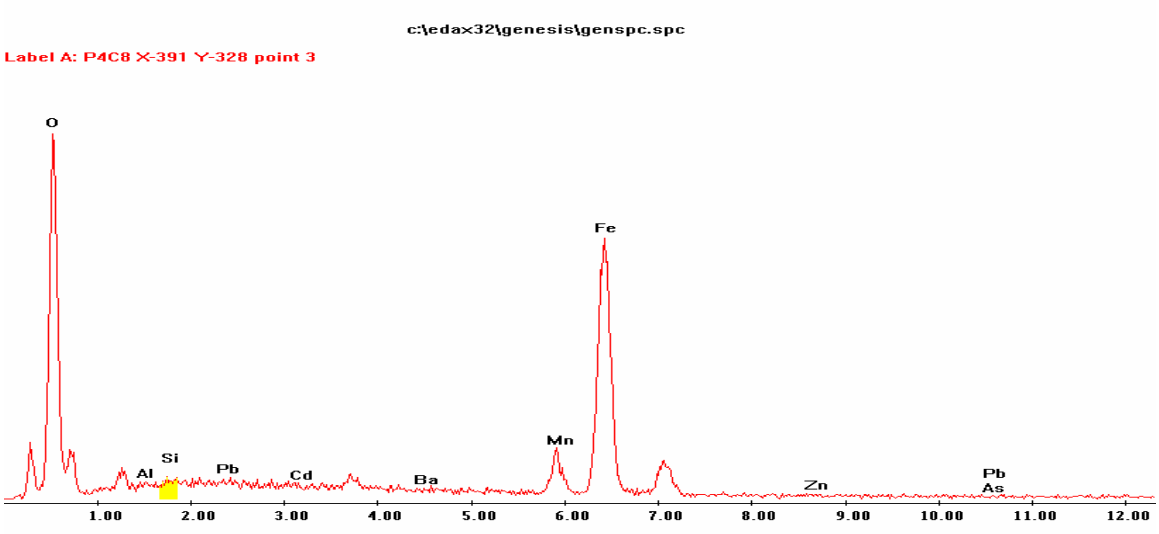

Point 5

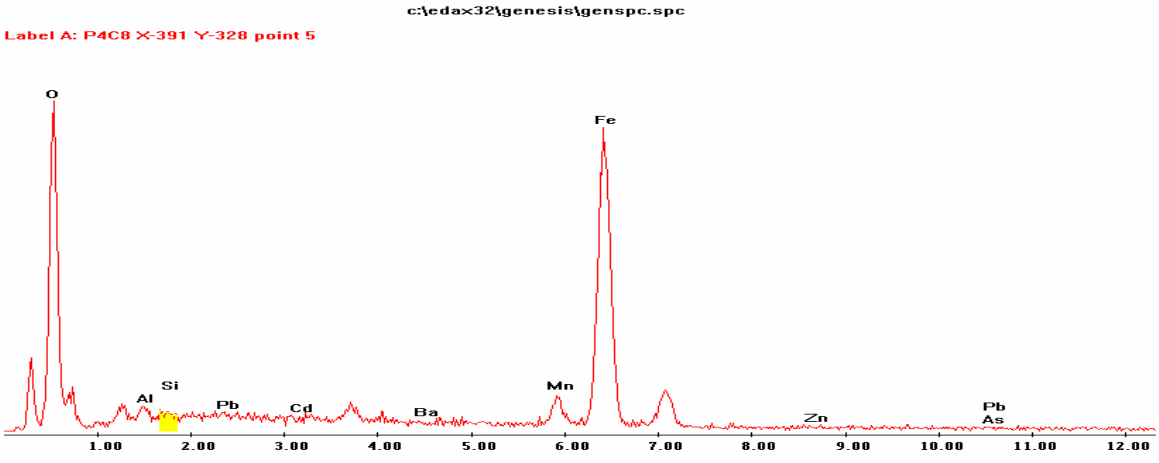

P4C8 – 408, 221

BSE Image

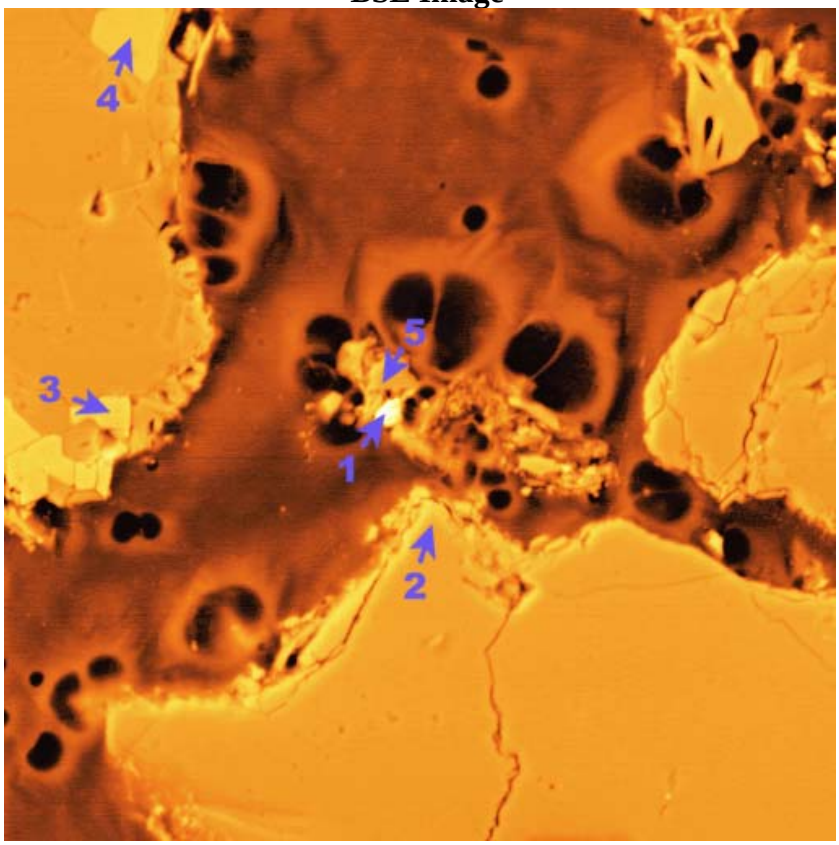

Iron (Fe)

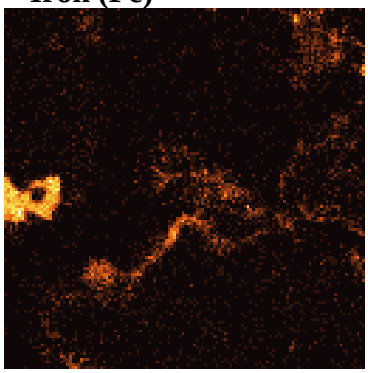

Manganese (Mn)

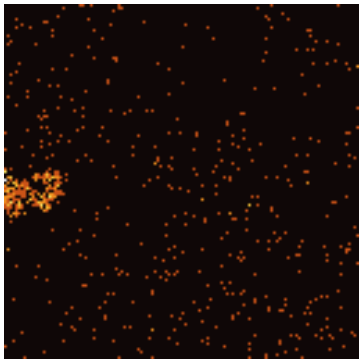

Phosphorous (P)

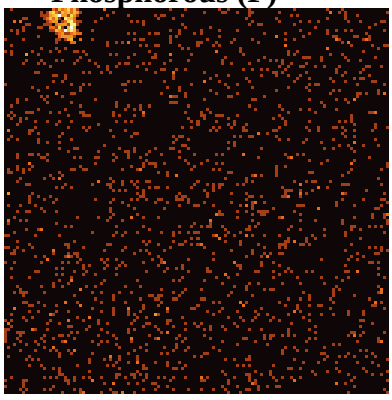

Lead (Pb)

Silicon (Si)

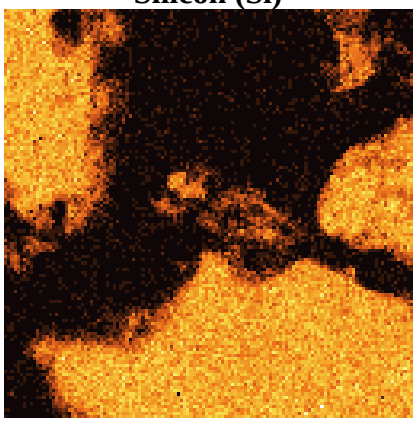

EDS Scan Images by Point

Point 1

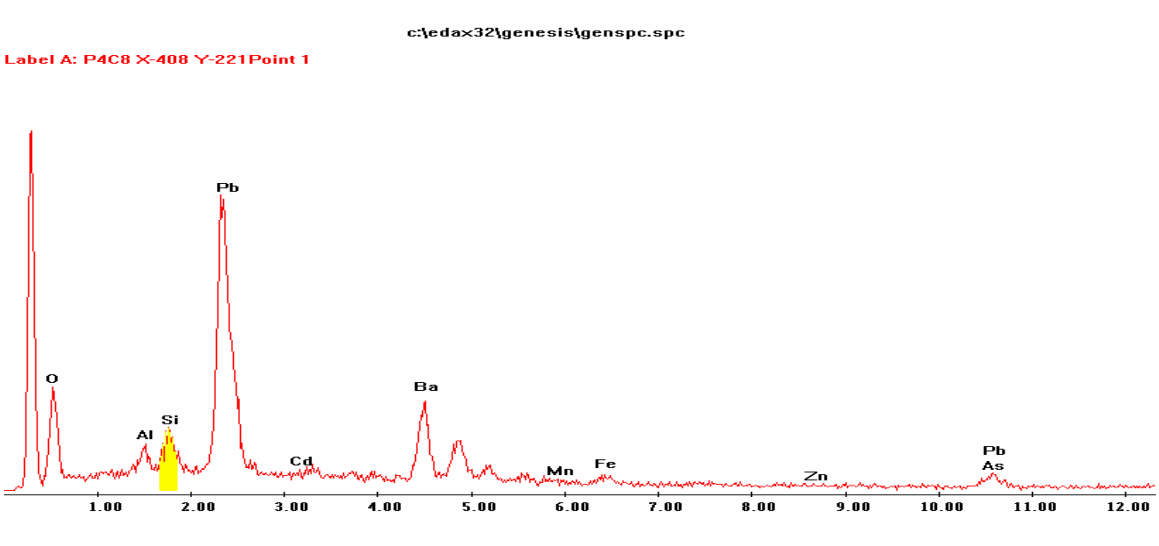

Point 2

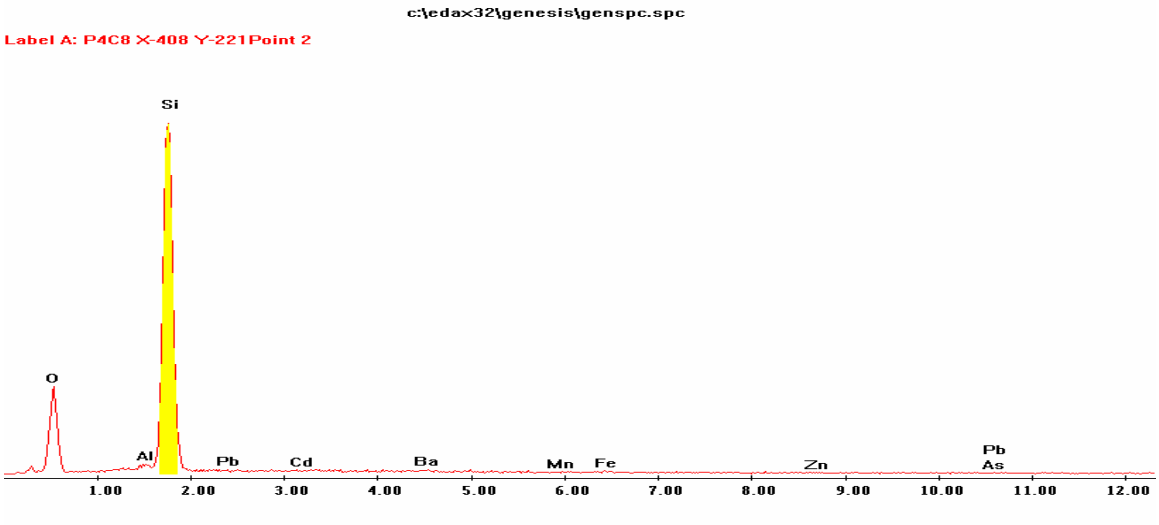

Point 3

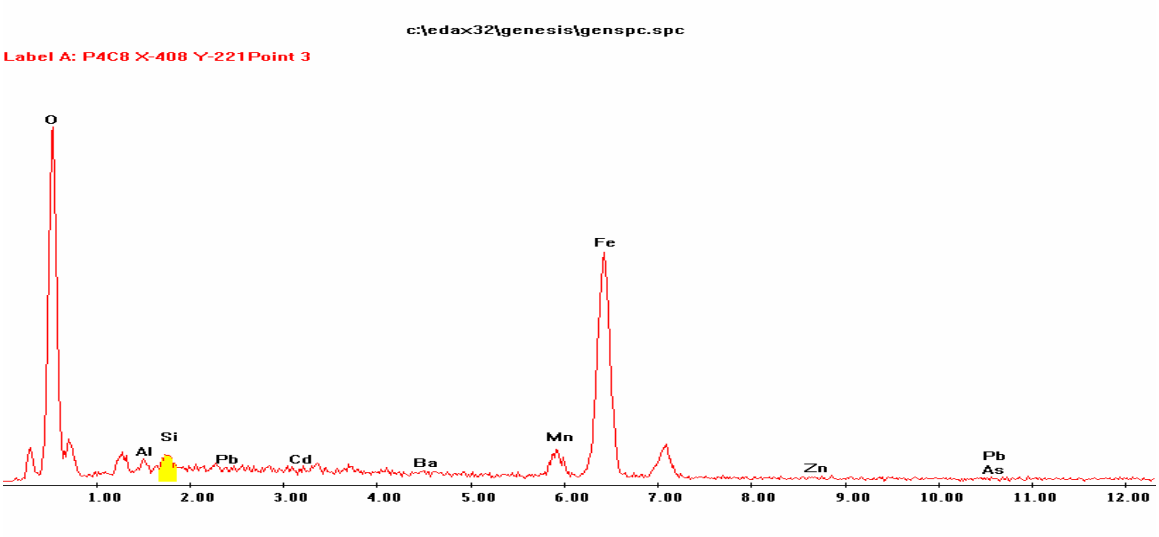

Point 4

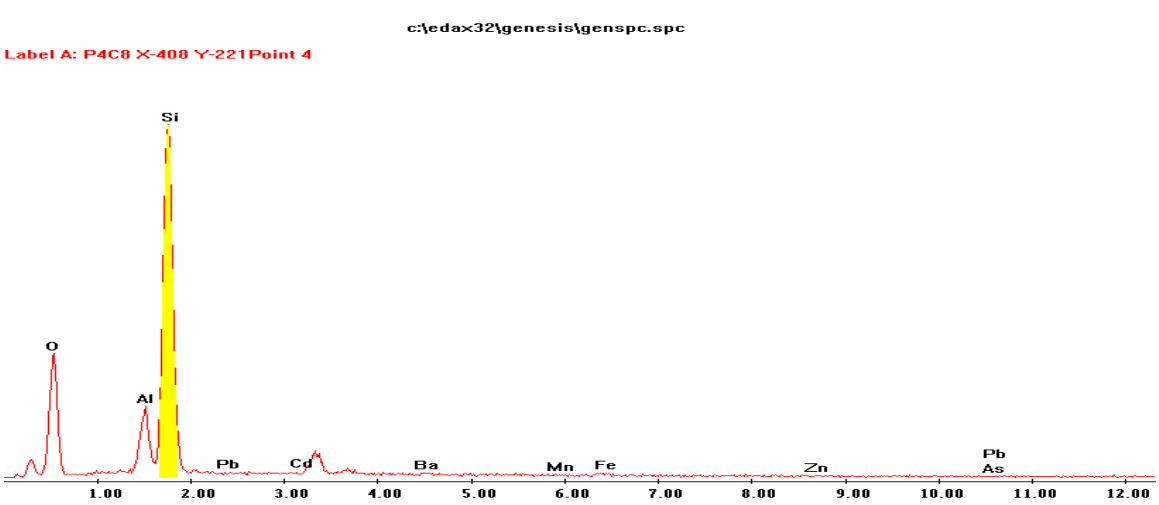

Point 5

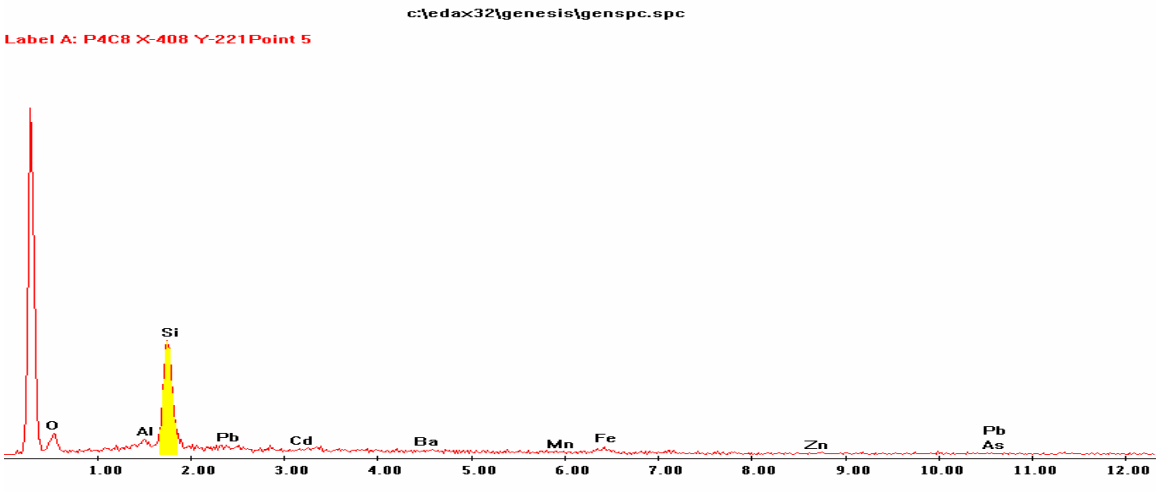

P4C8 – 424, 202

BSE Image

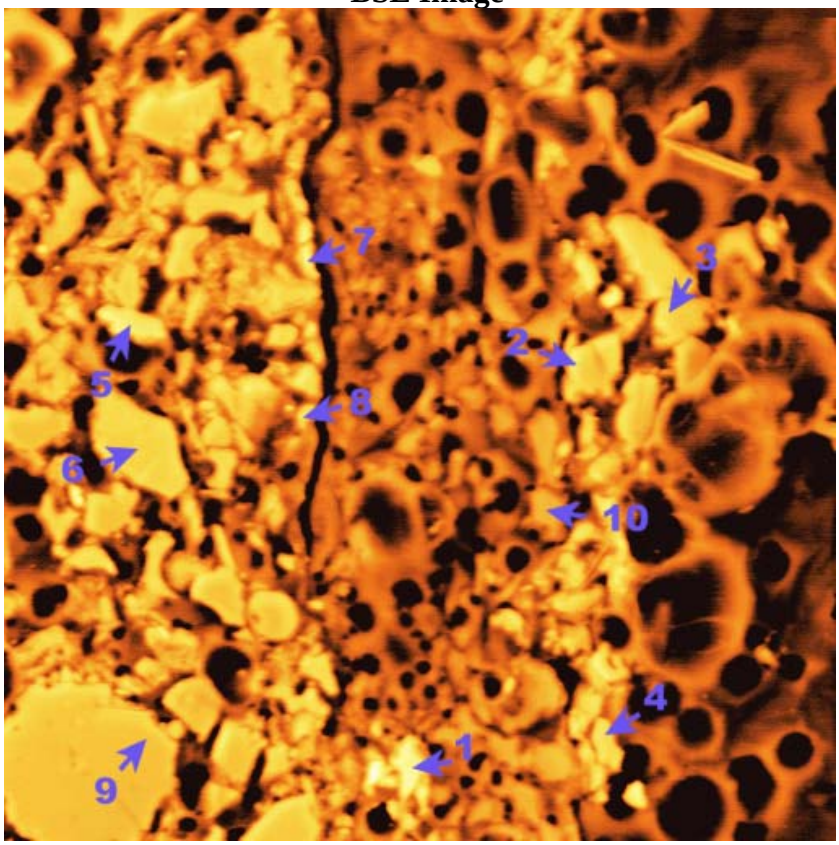

Iron (Fe)

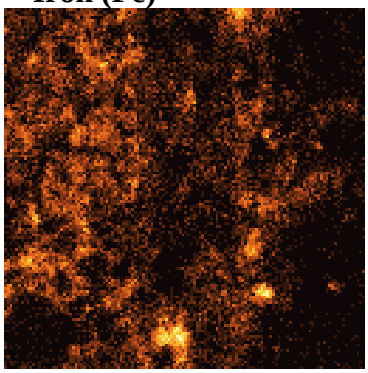

Manganese (Mn)

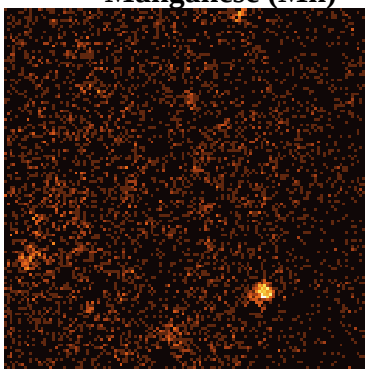

Phosphorous (P)

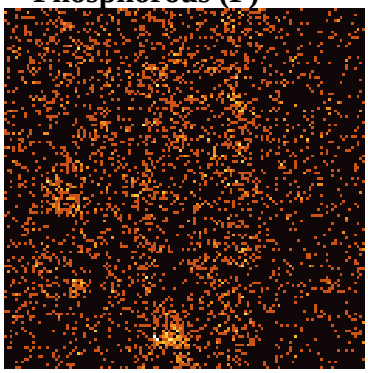

Lead (Pb)

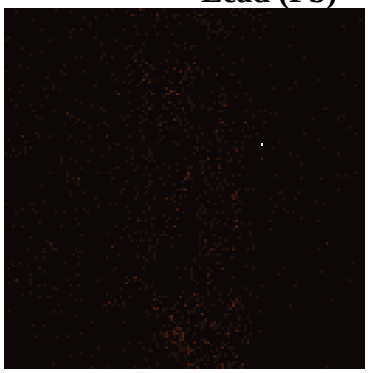

Silicon (Si)

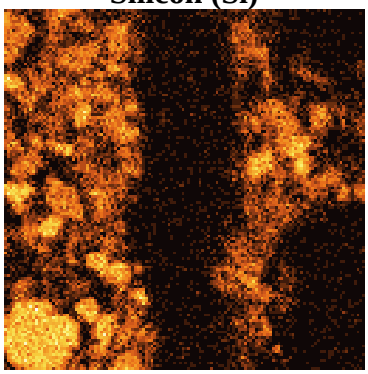

EDS Scan Images by Point

Point 1

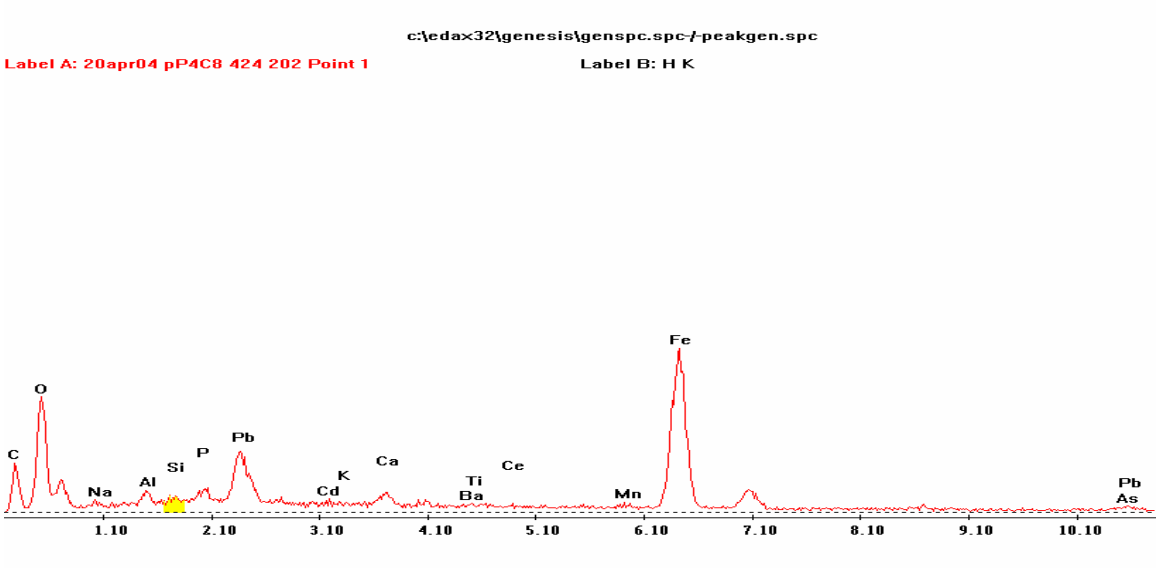

Point 2

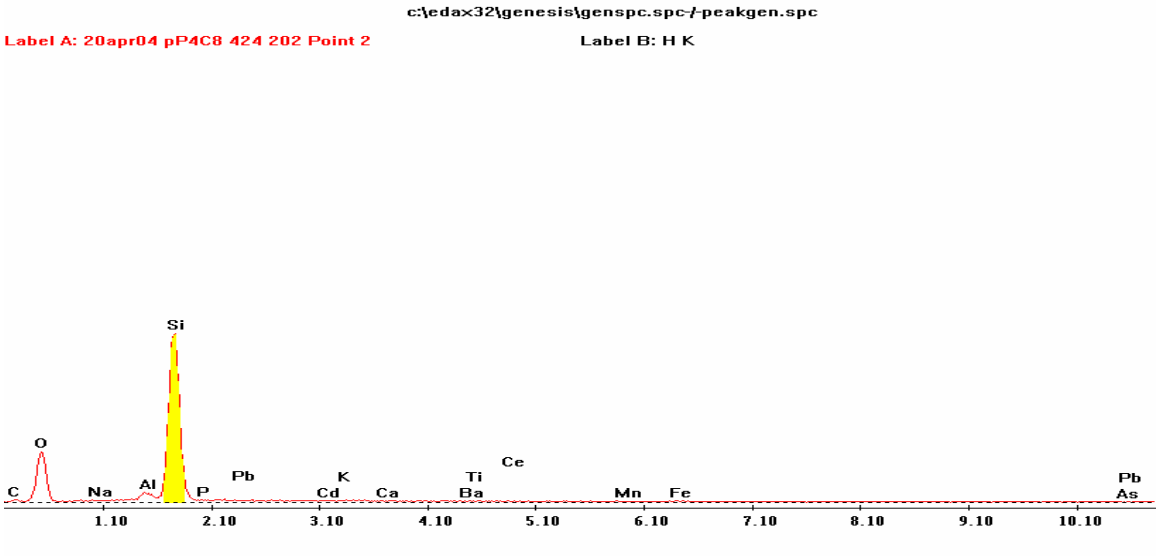

Point 3

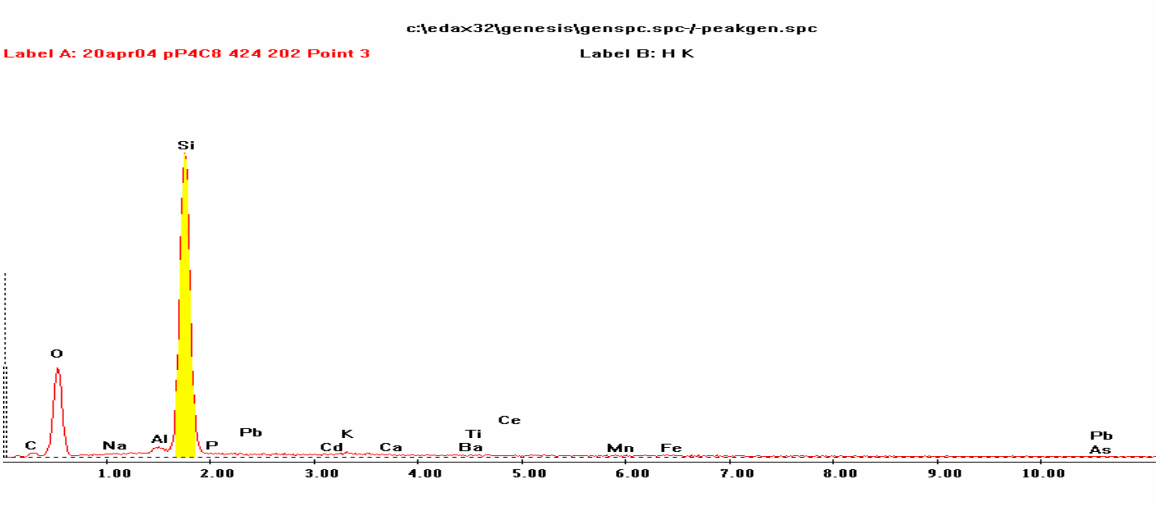

Point 4

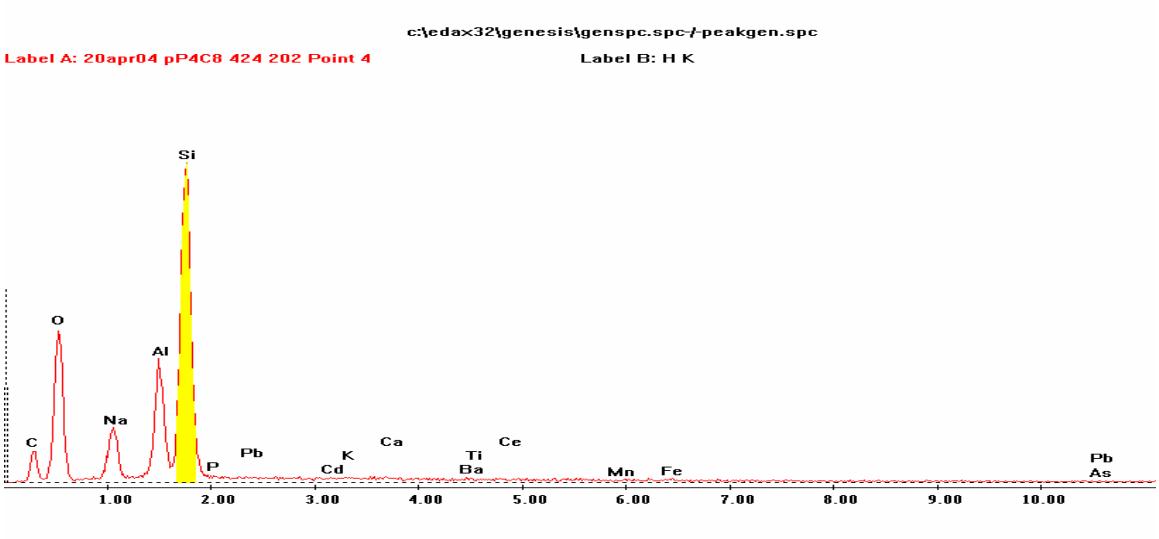

Point 5

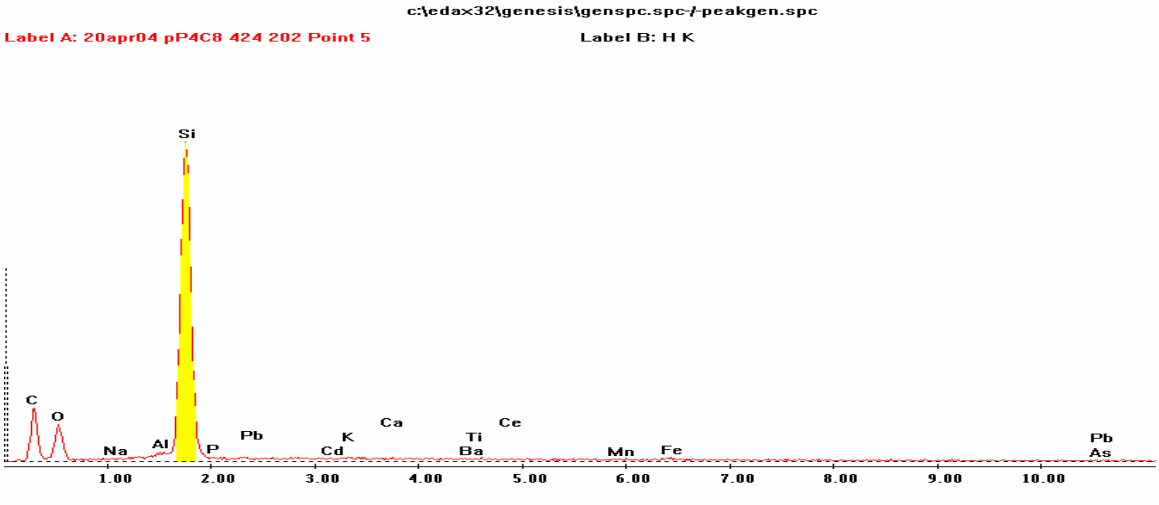

Point 6

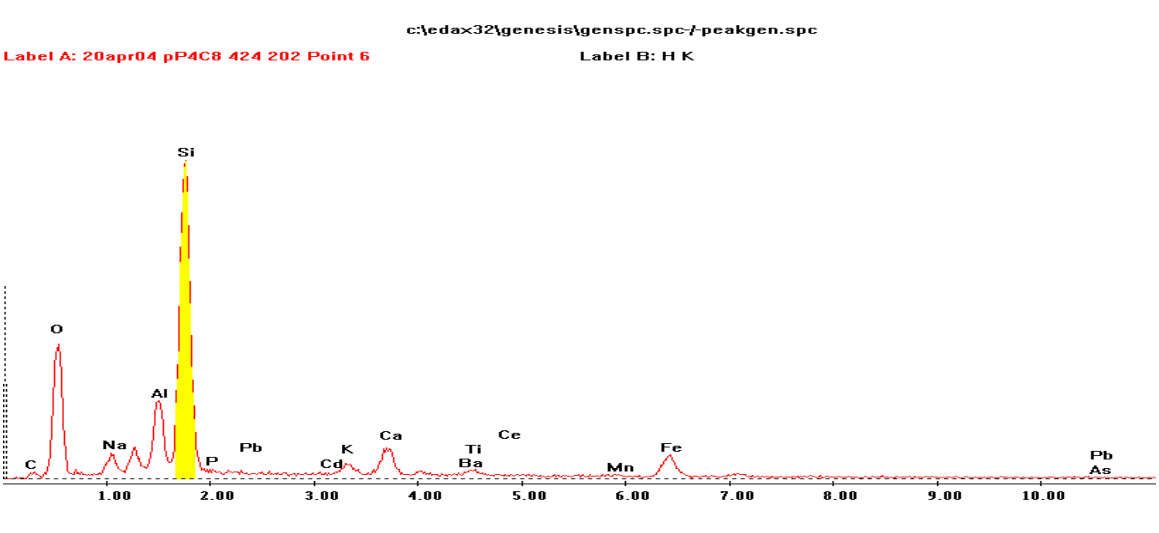

Point 7

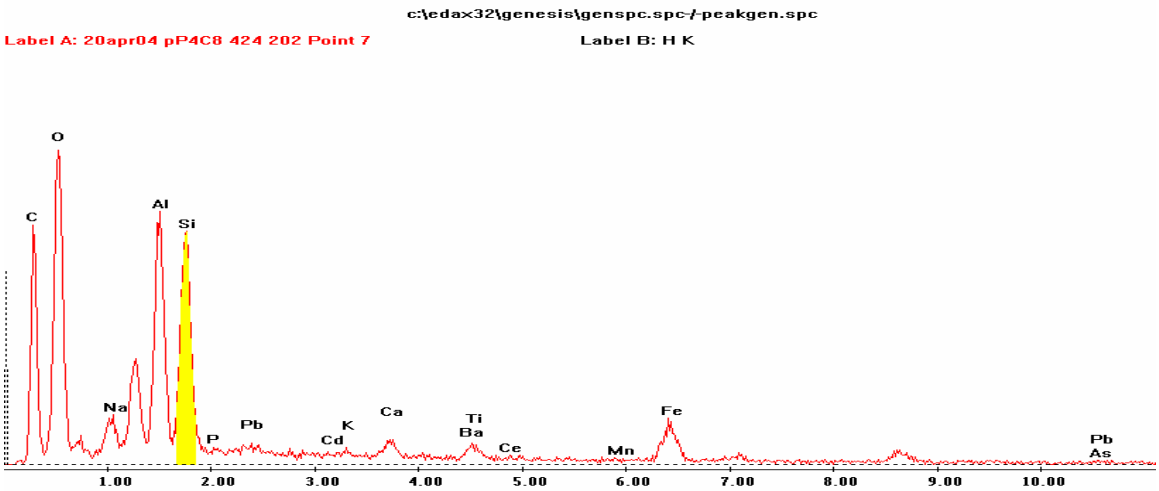

Point 8

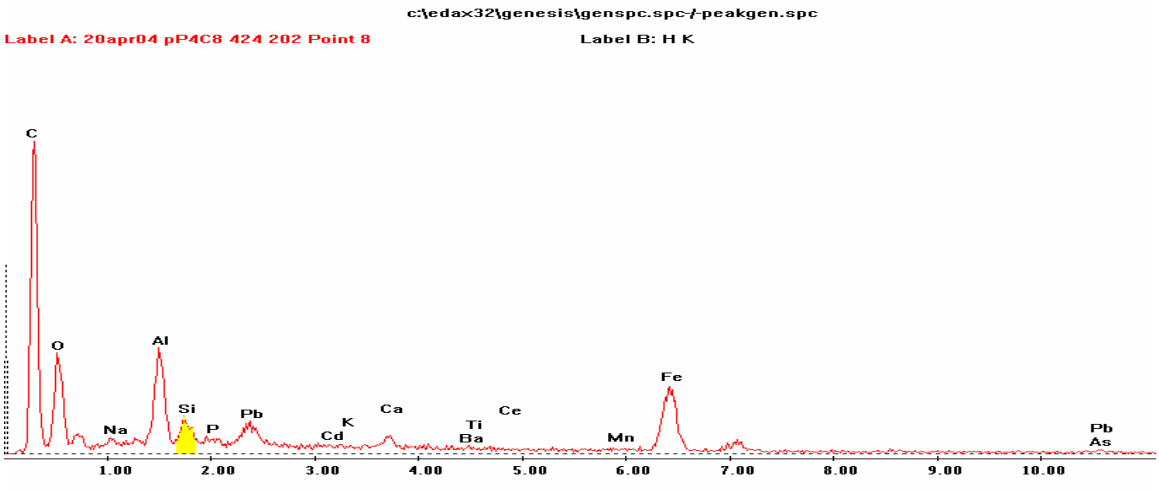

Point 9

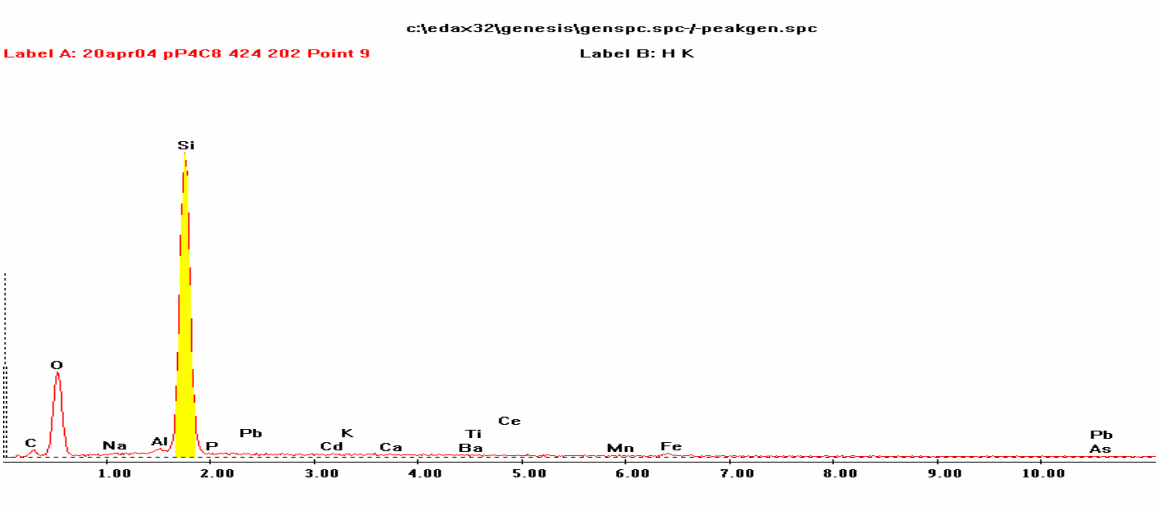

Point 10

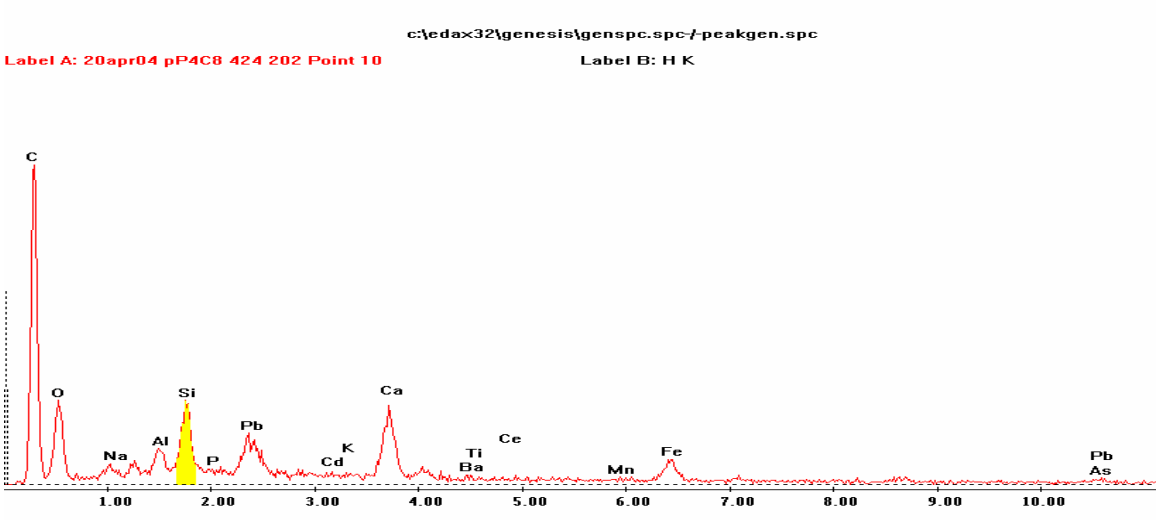

P4C8 – 424, 217

BSE Image

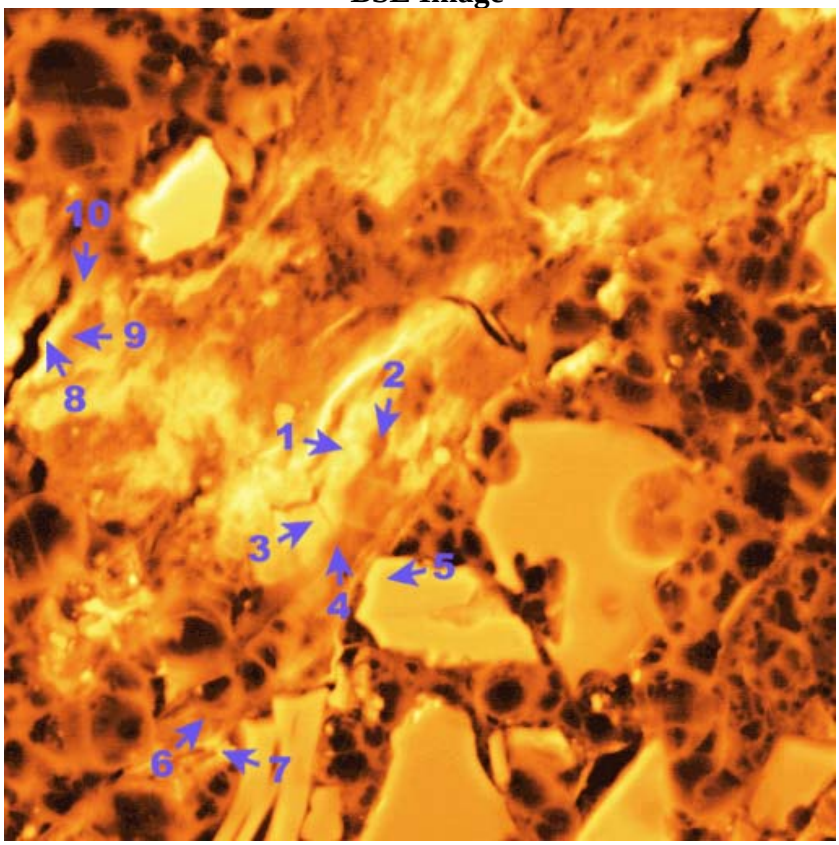

Iron (Fe)

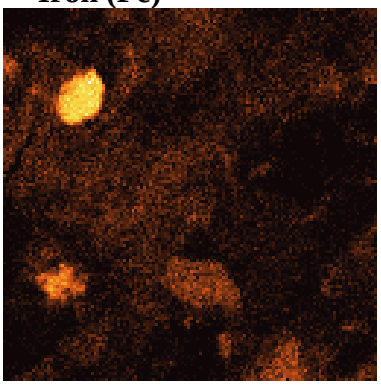

Manganese (Mn)

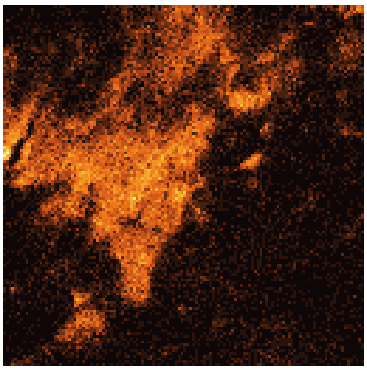

Phosphorous (P)

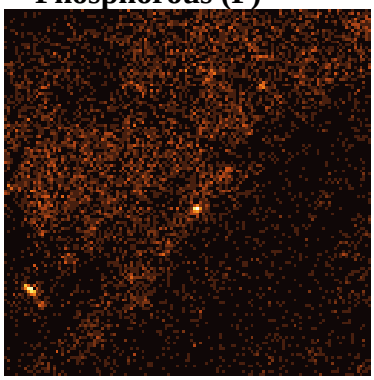

Lead (Pb)

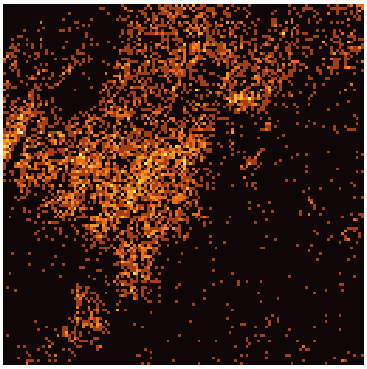

Silicon (Si)

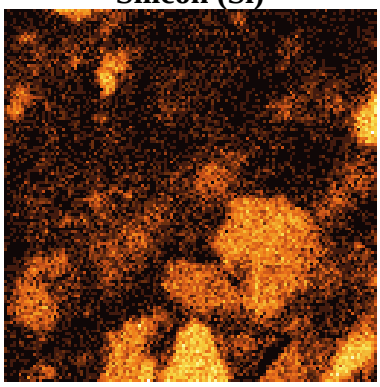

EDS Scan Images by Point

Point 1

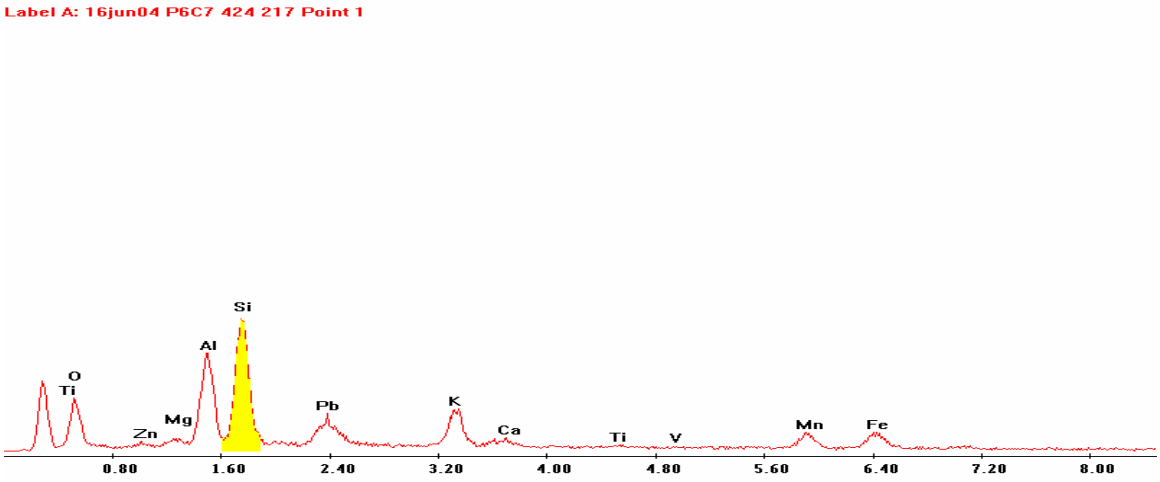

Point 2

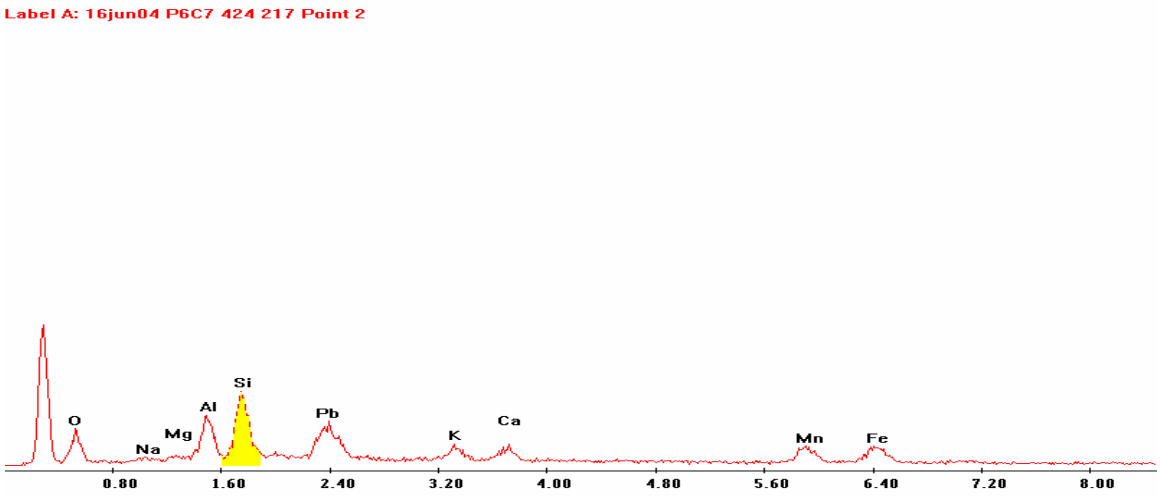

Point 3

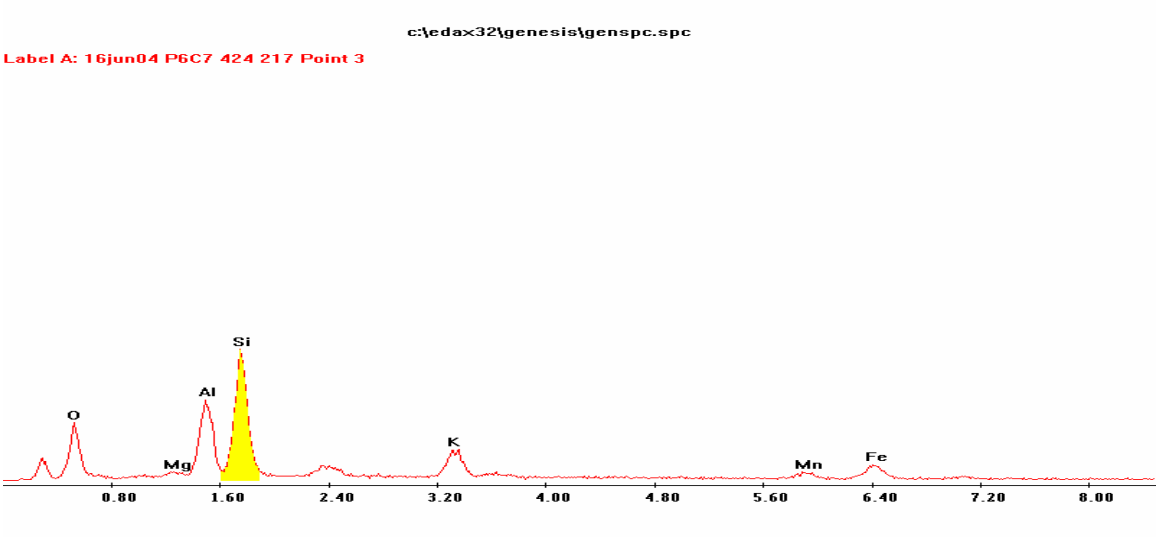

Point 4

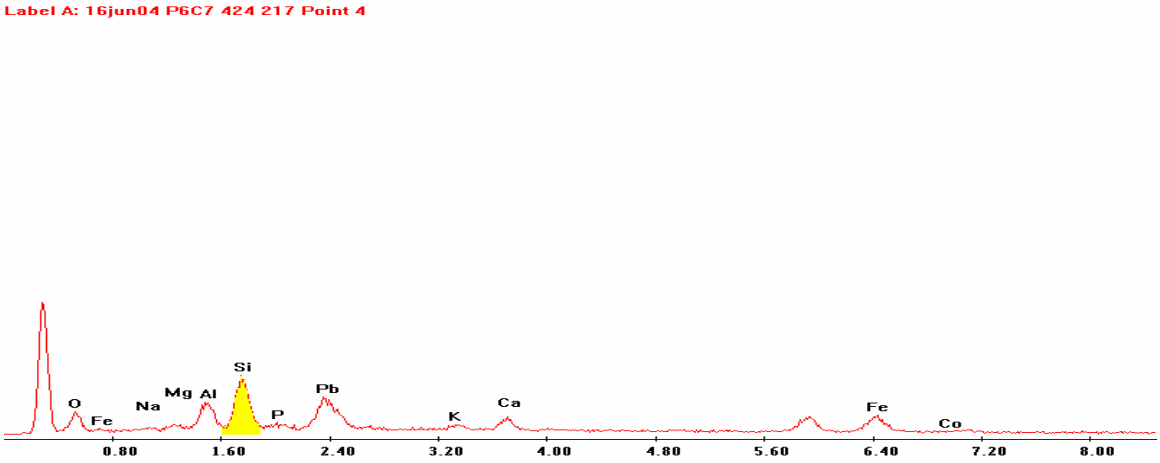

Point 5

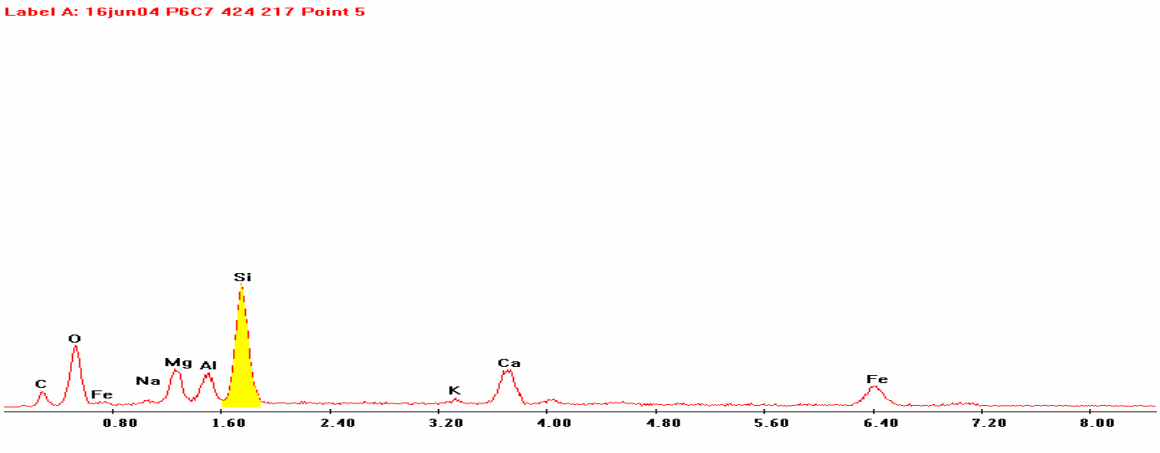

Point 6

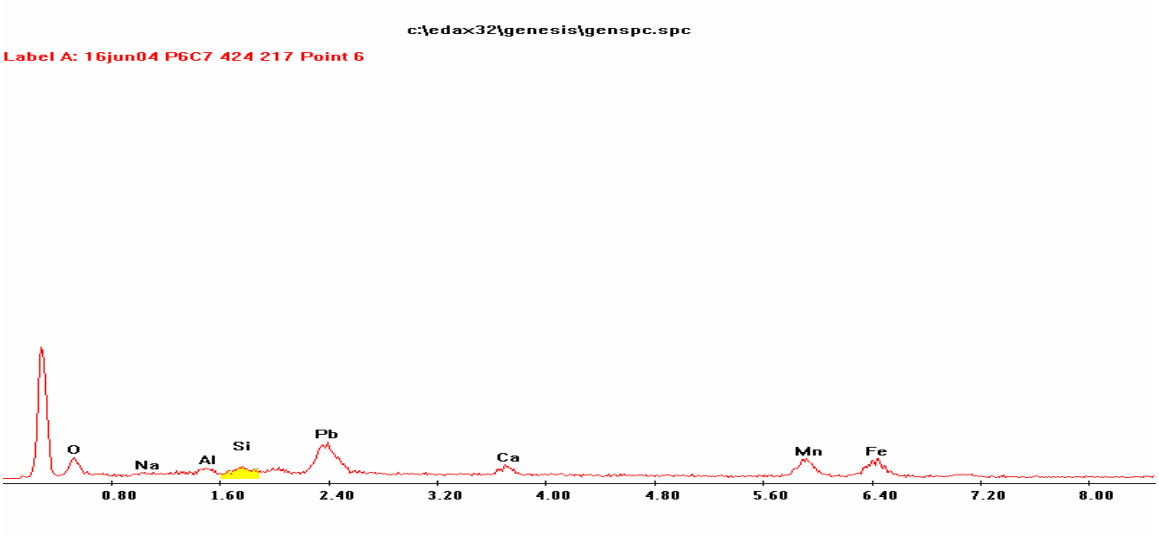

Point 7

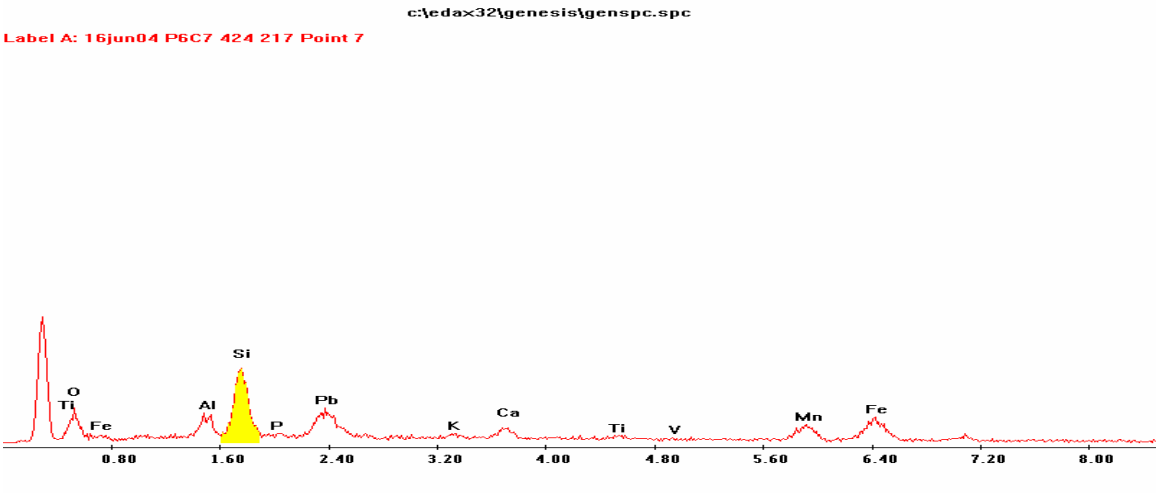

Point 8

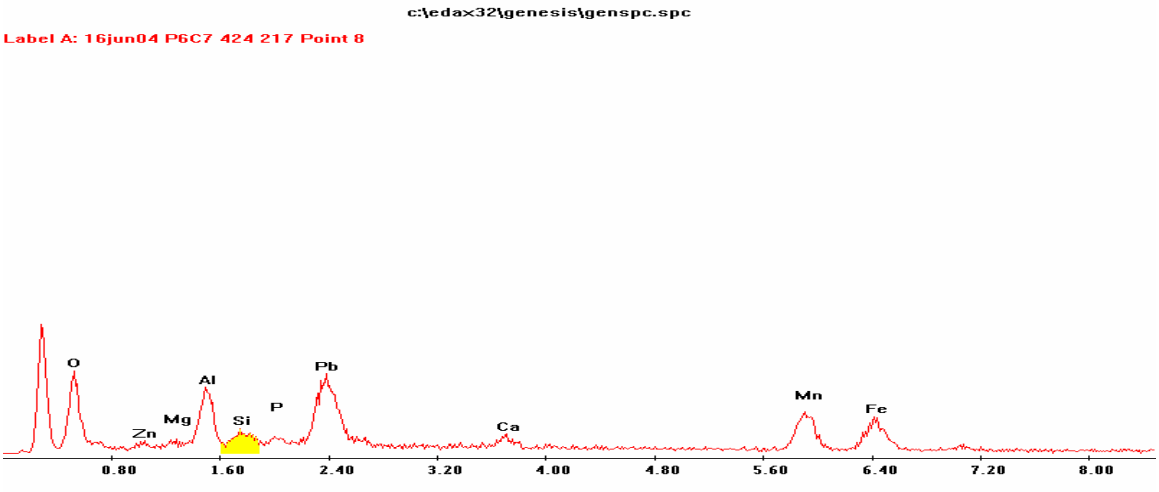

Point 9

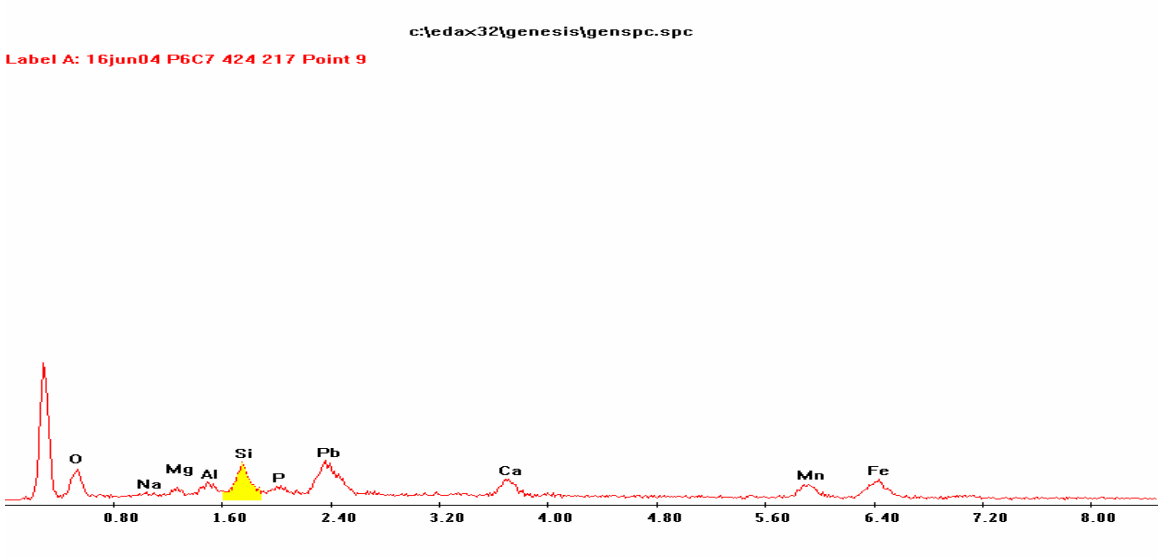

Point 10

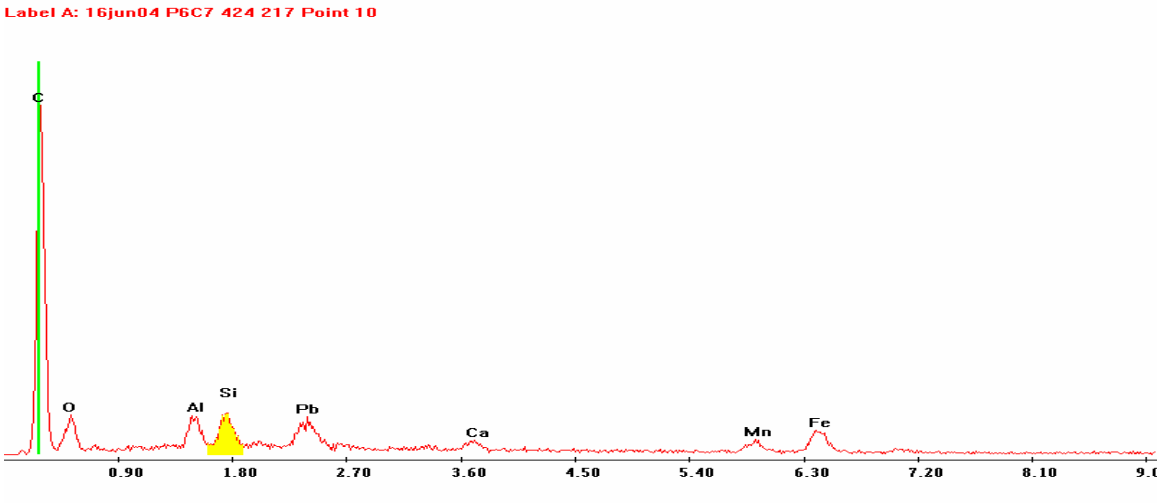

P4C8 – 470, 208

BSE Image

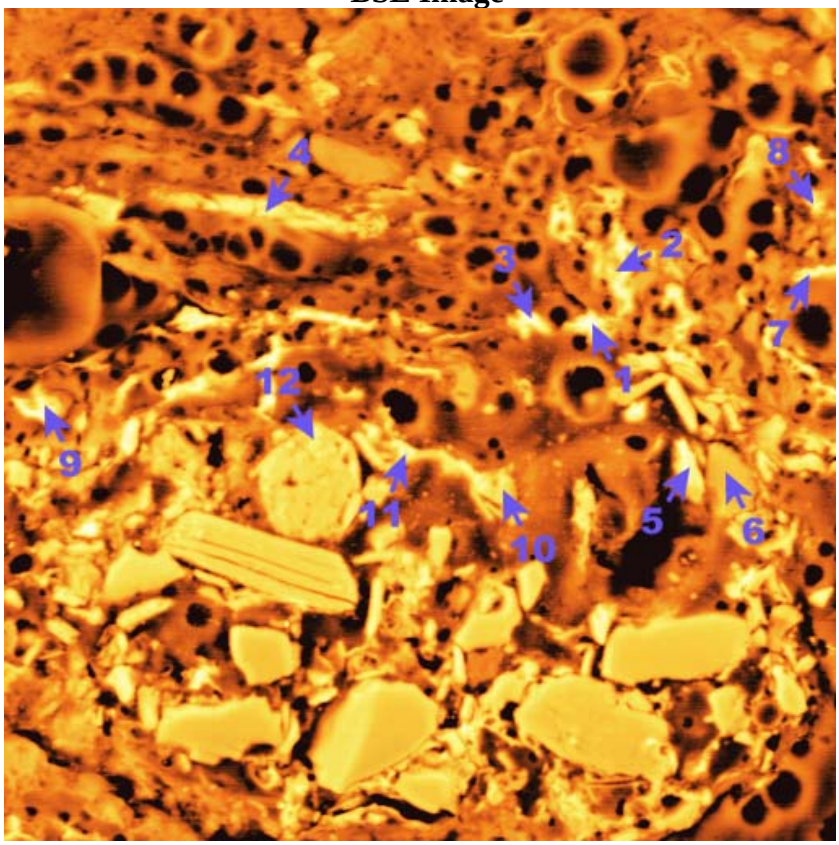

Iron (Fe)

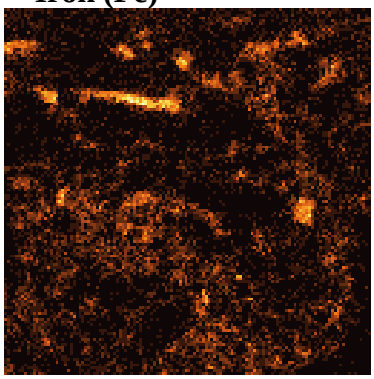

Manganese (Mn)

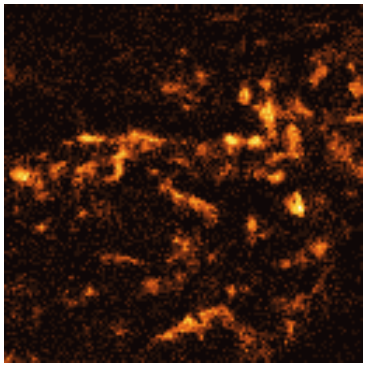

Phosphorous (P)

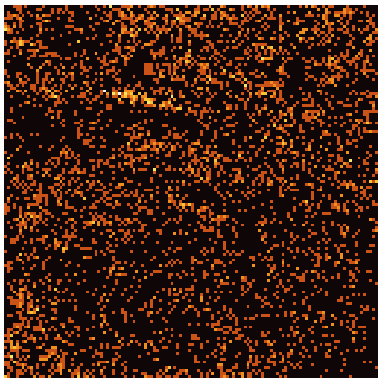

Lead (Pb)

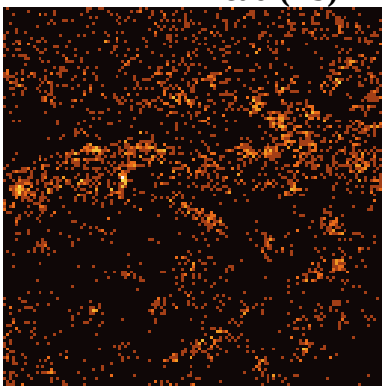

Silicon (Si)

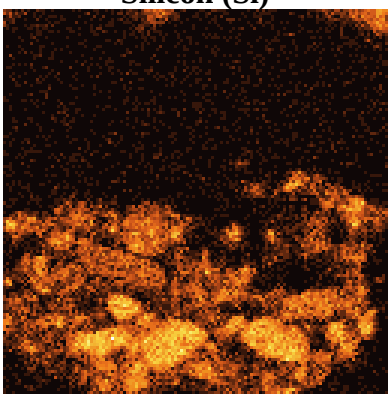

EDS Scan Images by Point

Point 1

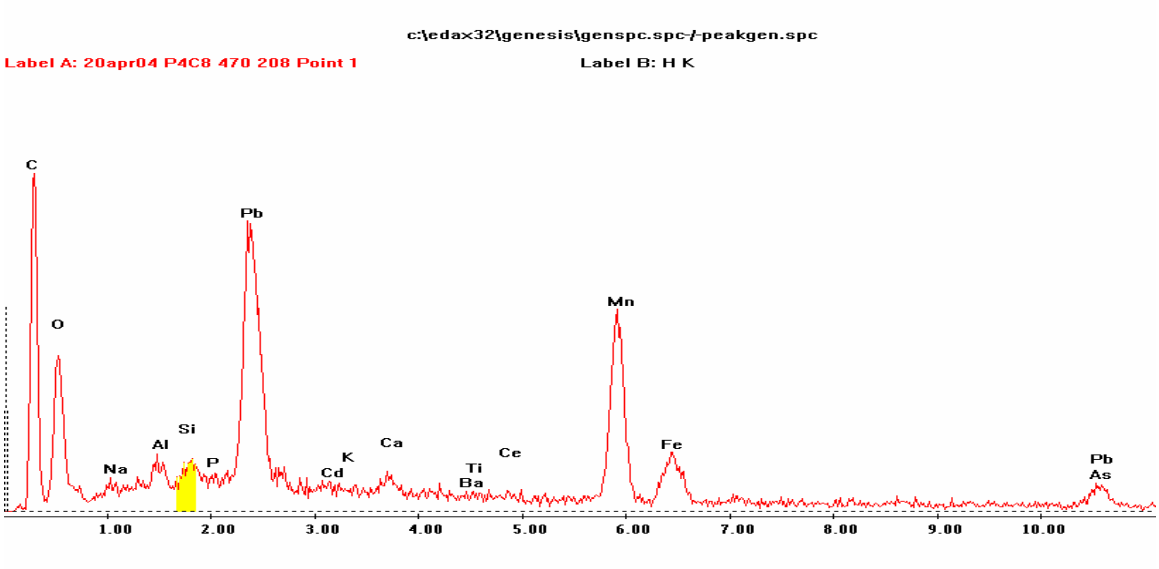

Point 2

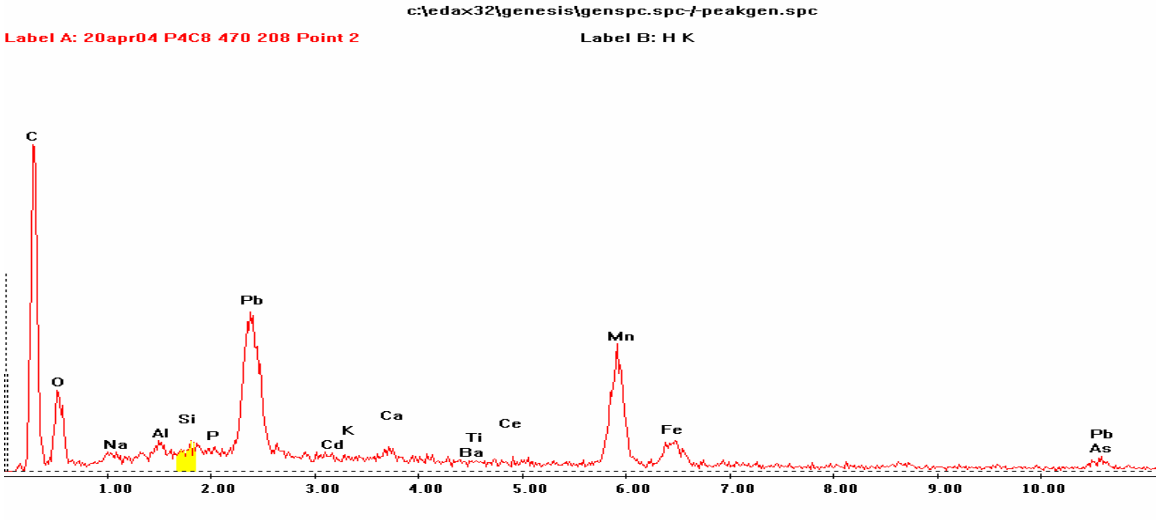

Point 3

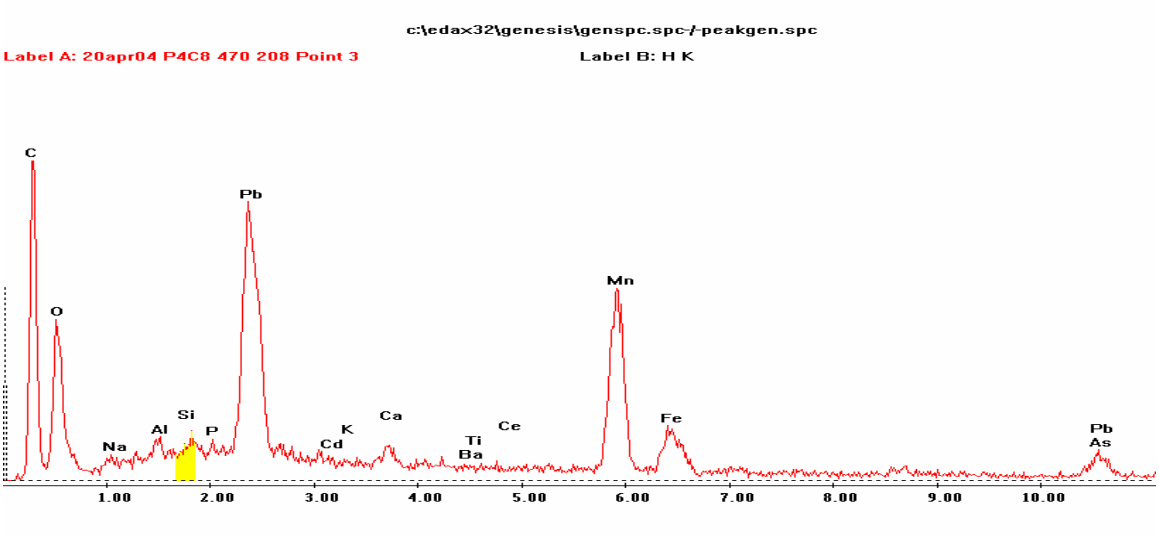

Point 4

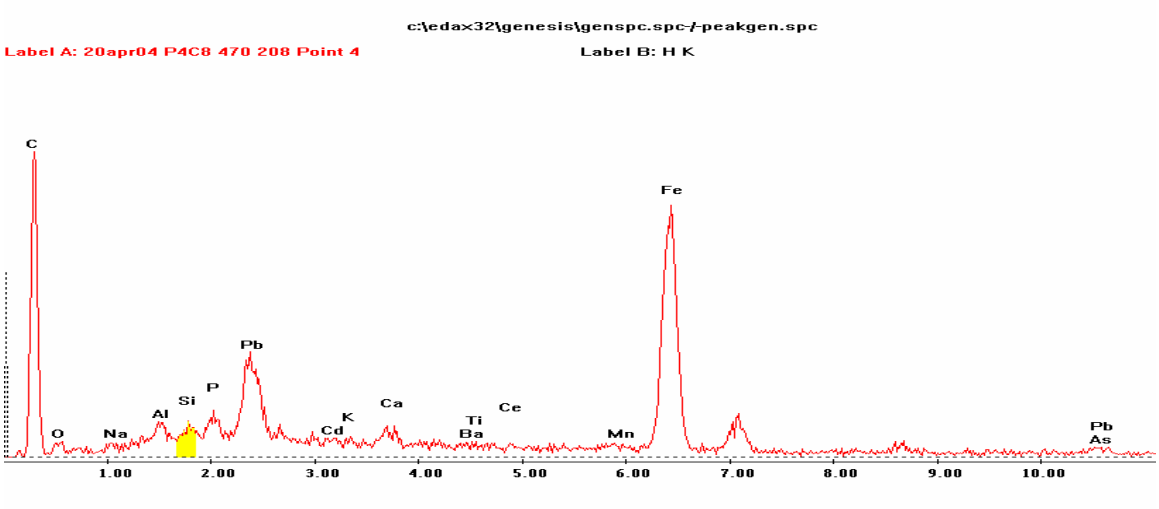

Point 5

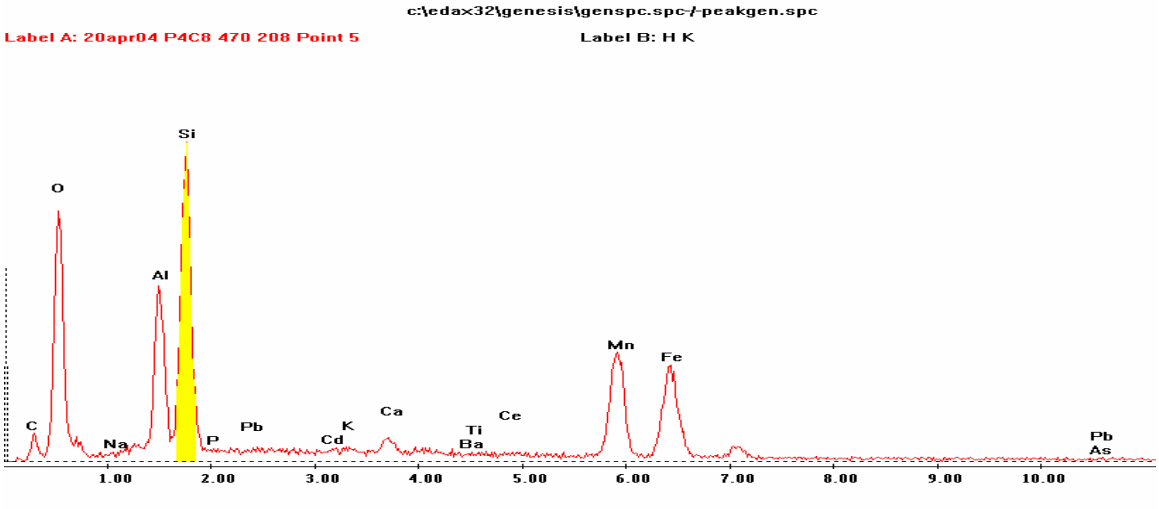

Point 6

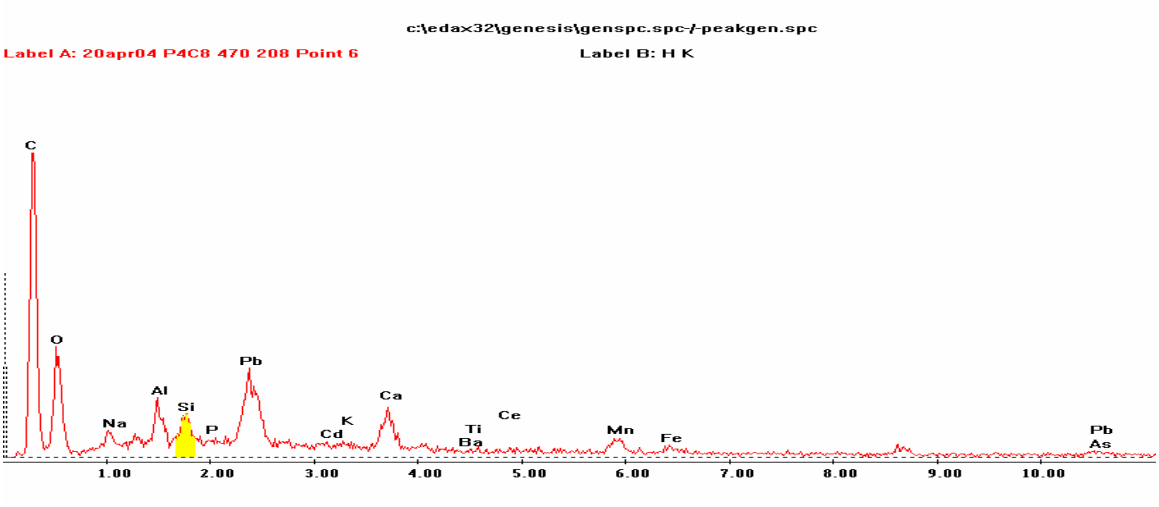

Point 7

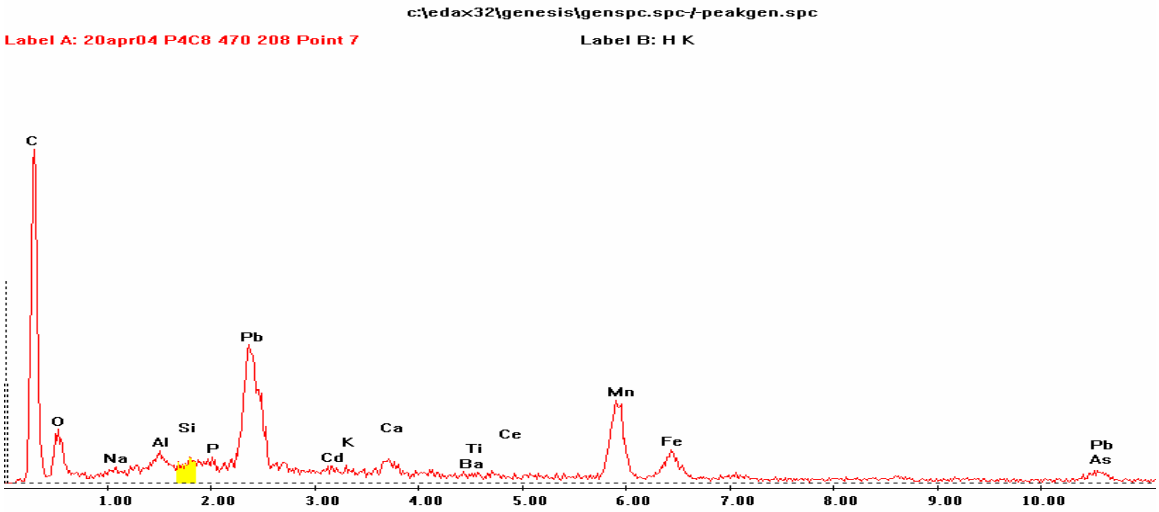

Point 8

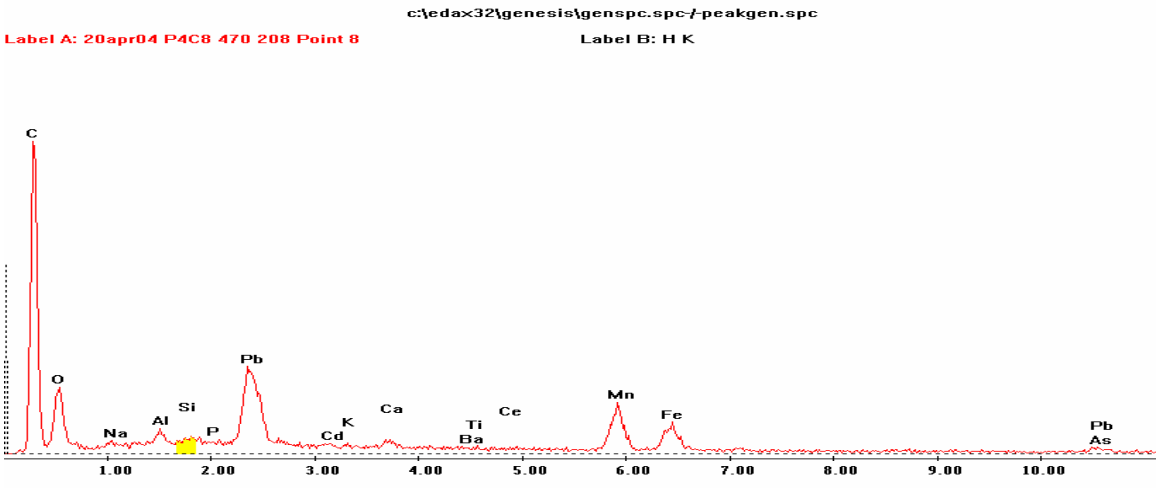

Point 9

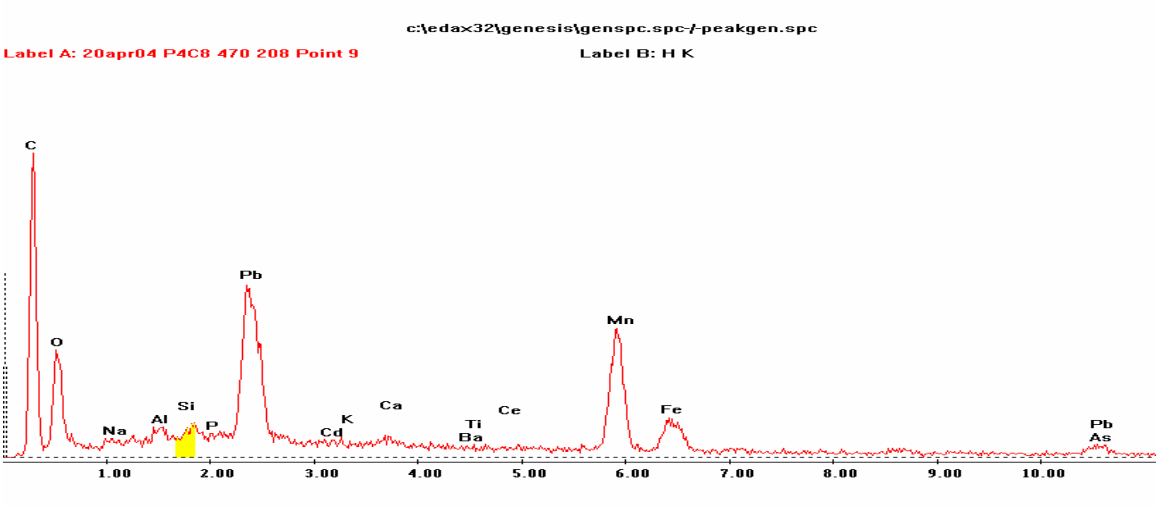

Point 10

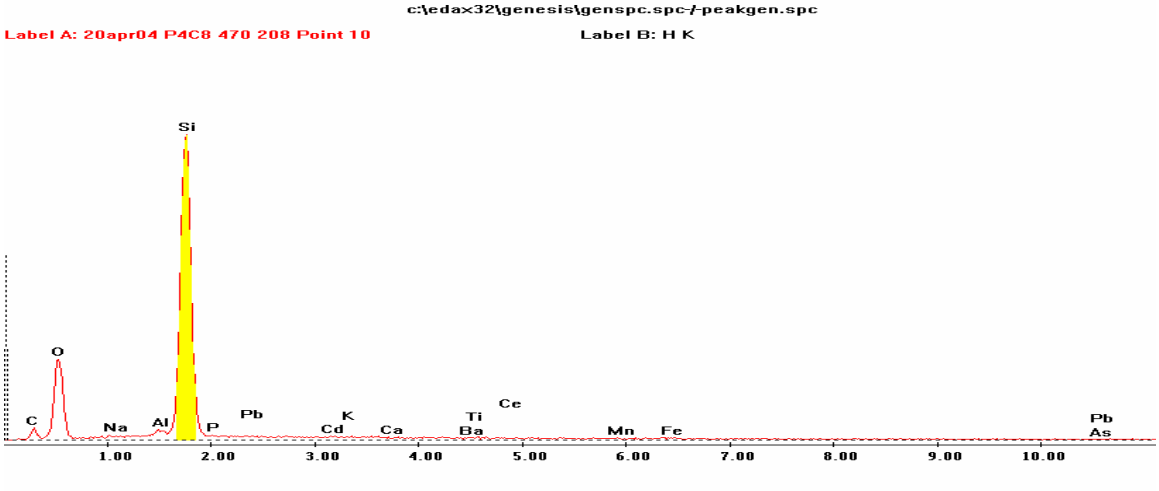

Point 11

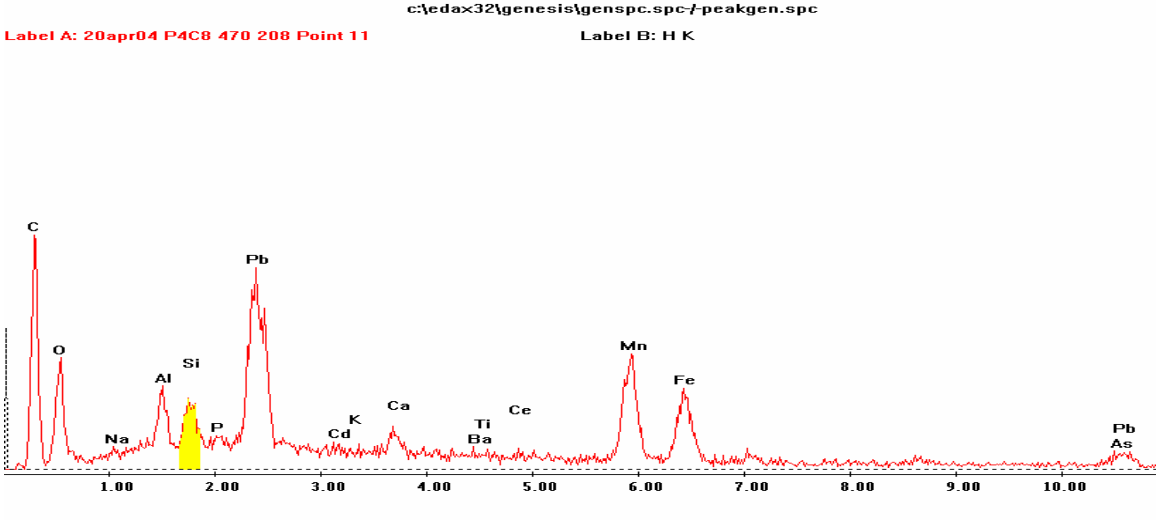

Point 12

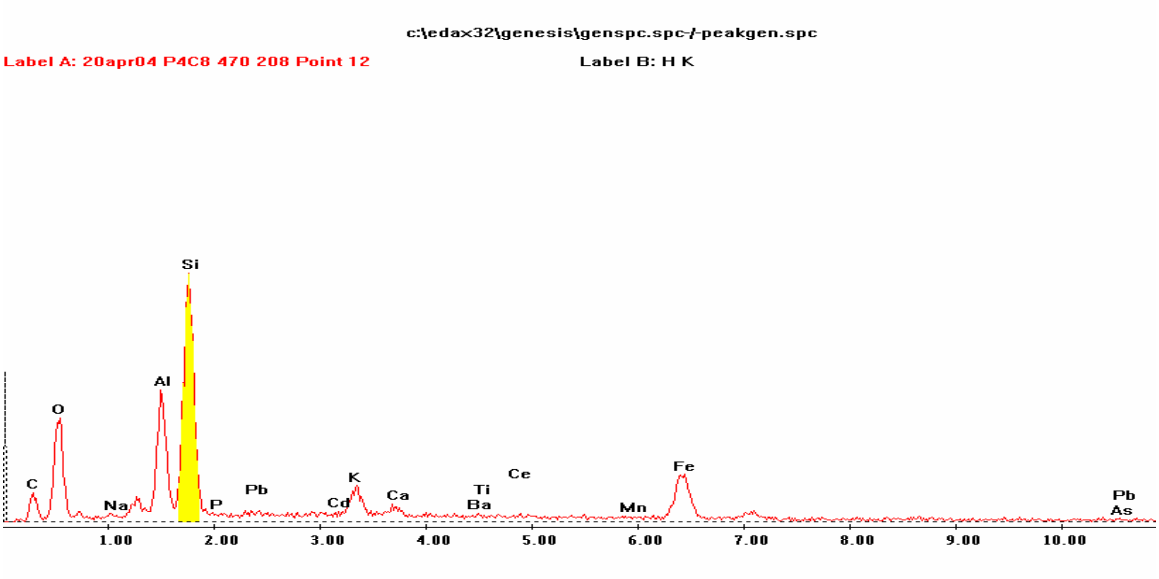
c:\edax32\genesis\genspc.spc-/-peakgen.spc
Label A: 20apr04 P4C8 470 208 Point 12
Label B: H K
Si
Al
O
C
Na
P
Pb
Cd
K
Ca
Ti
Ba
Ce
Mn
Fe
Pb
As
1.00
2.00
3.00
4.00
5.00
6.00
7.00
8.00
9.00
10.00

P4C8 – 473, 203

BSE Image

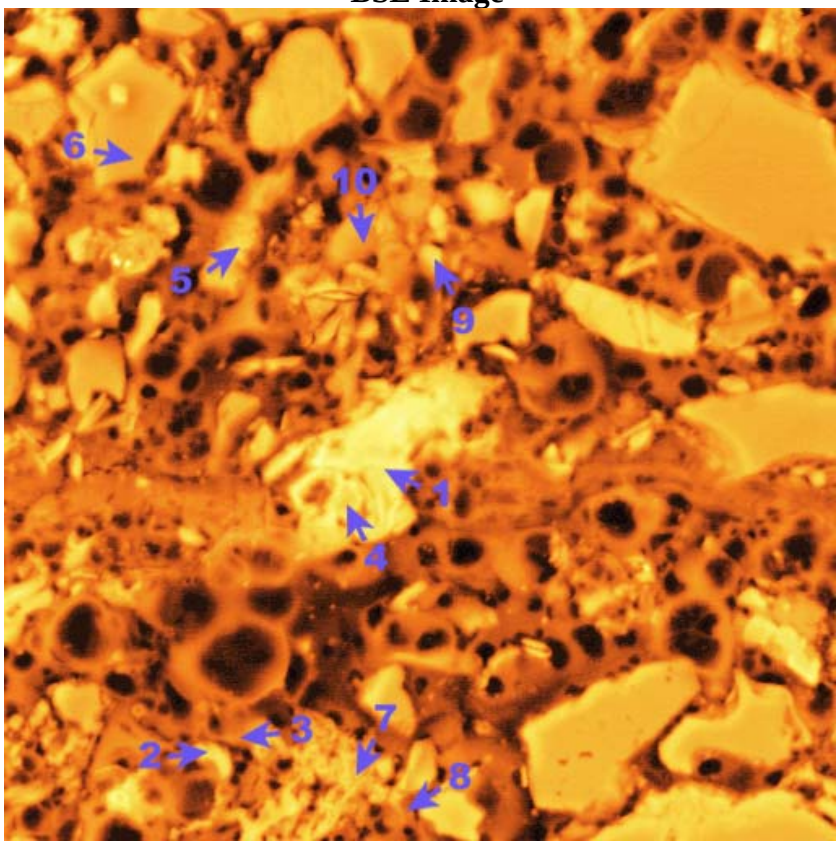

Iron (Fe)

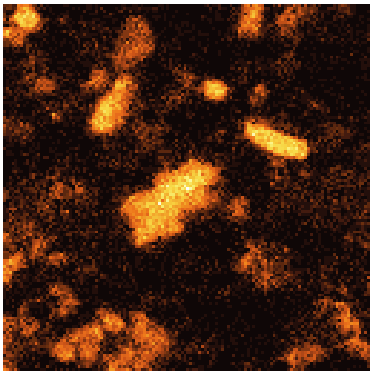

Manganese (Mn)

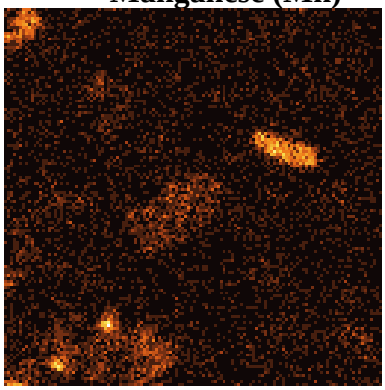

Phosphorous (P)

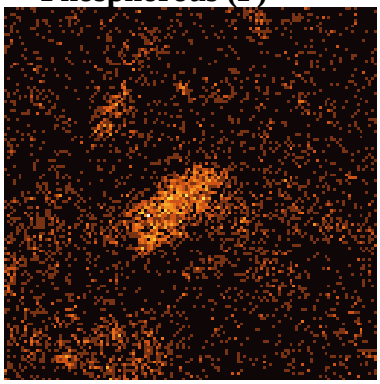

Lead (Pb)

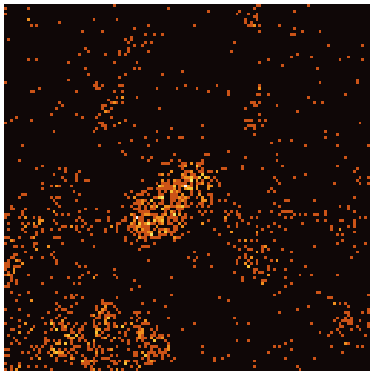

Silicon (Si)

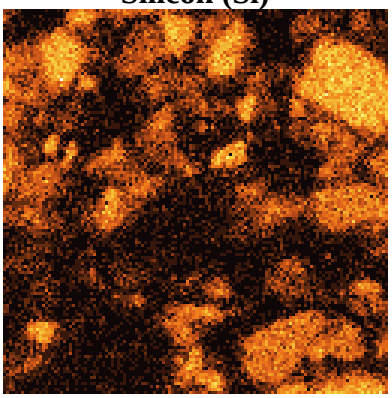

EDS Scan Images by Point

Point 1

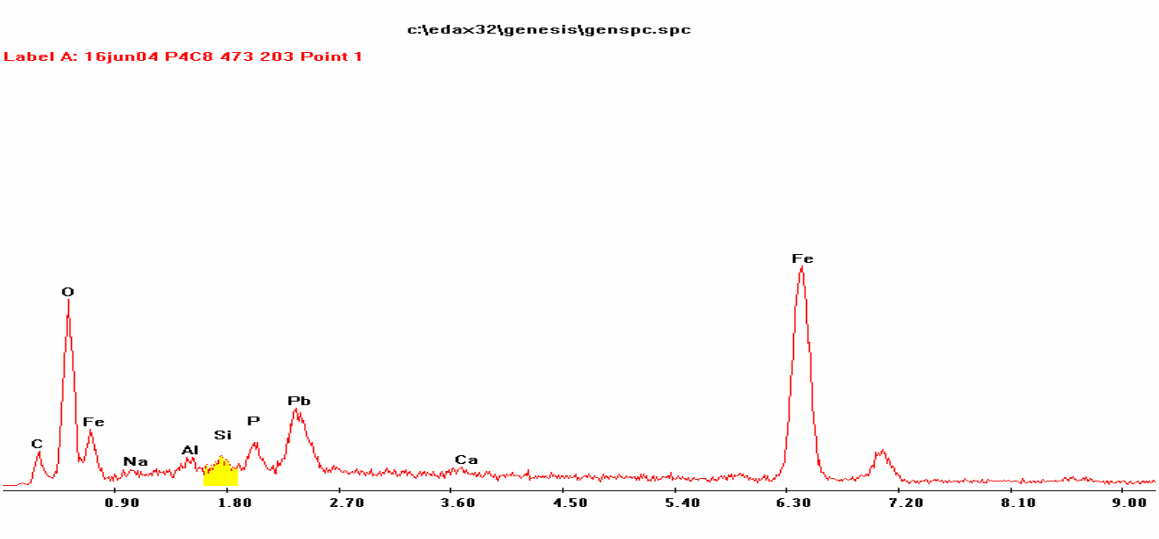

Point 2

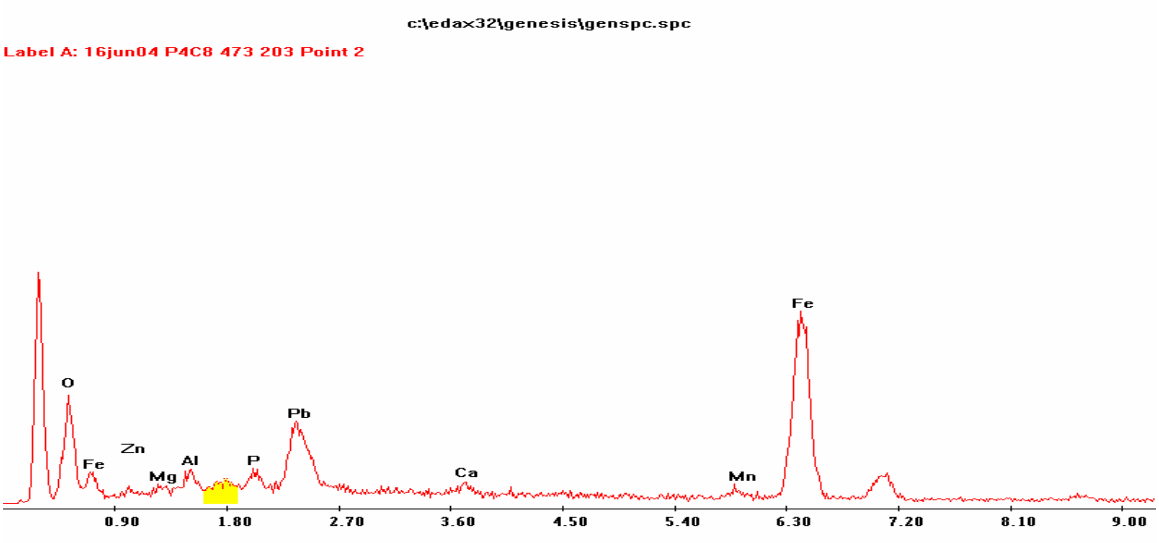

Point 3

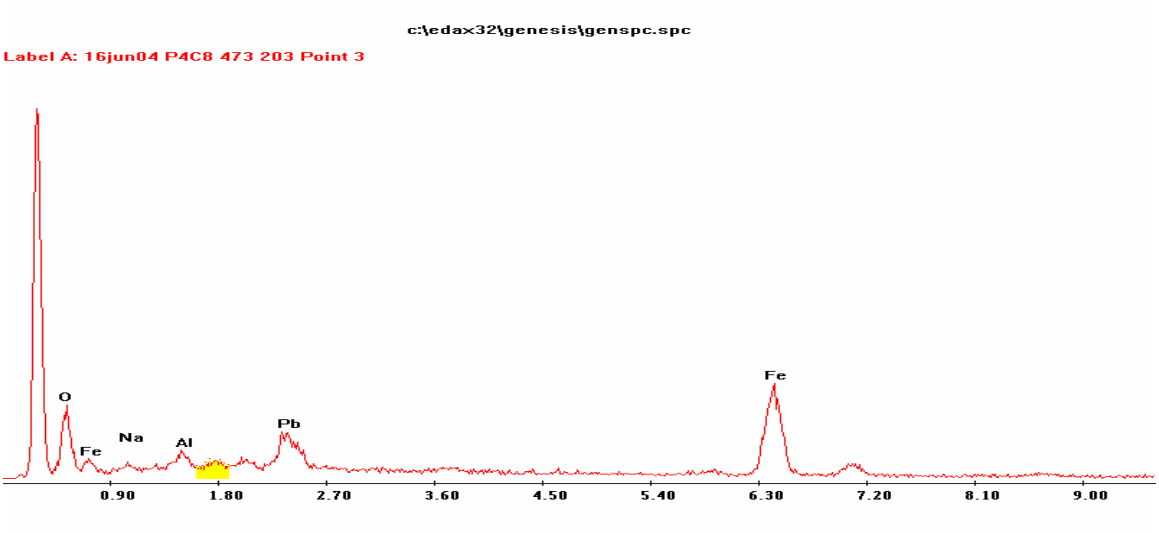

Point 4

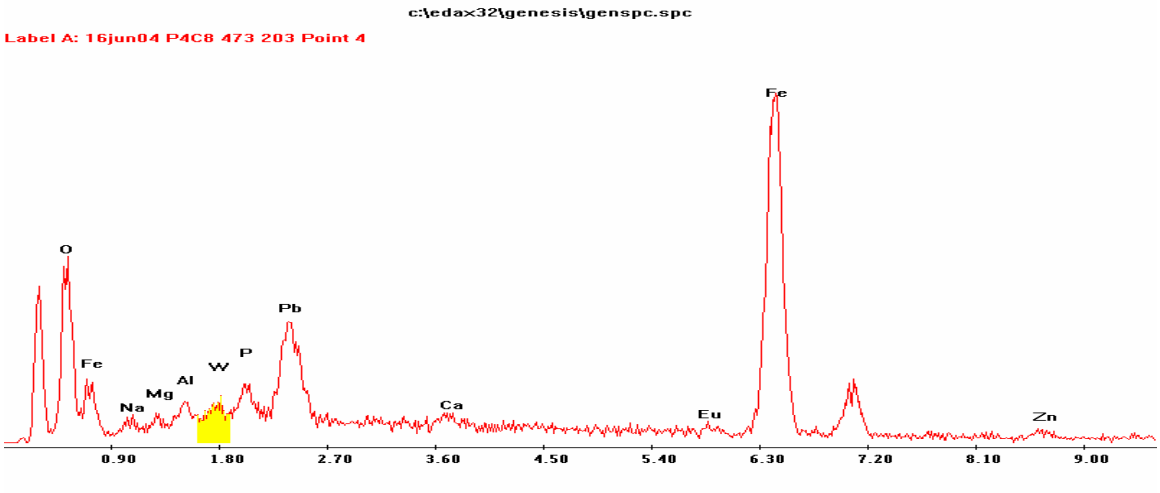

Point 5

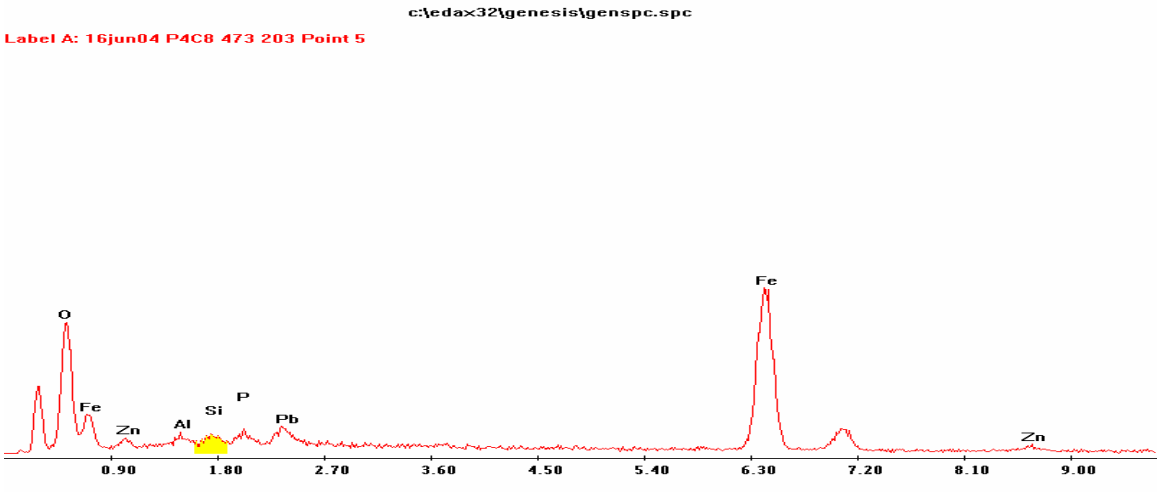

Point 6

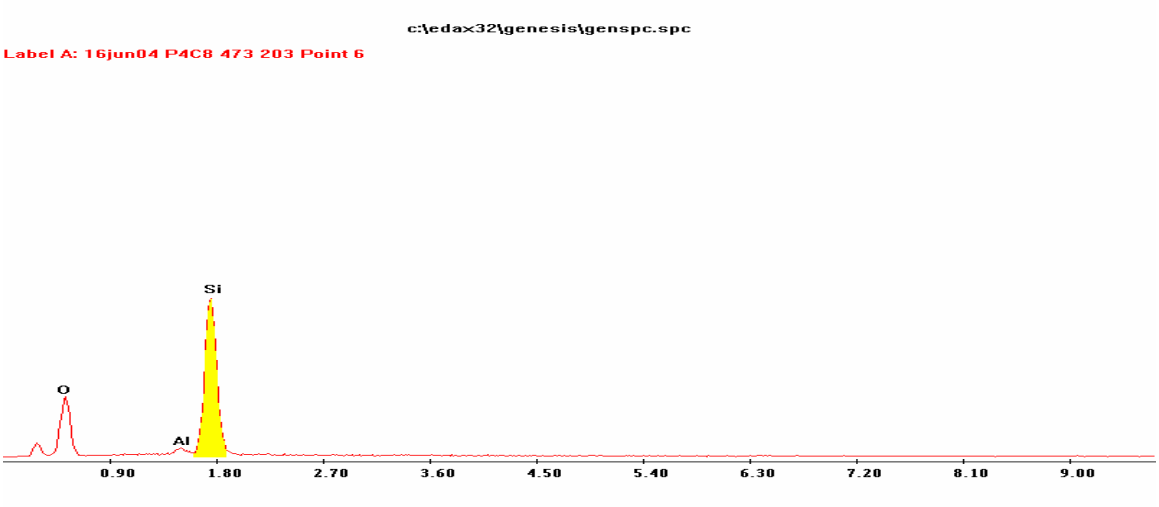

Point 7

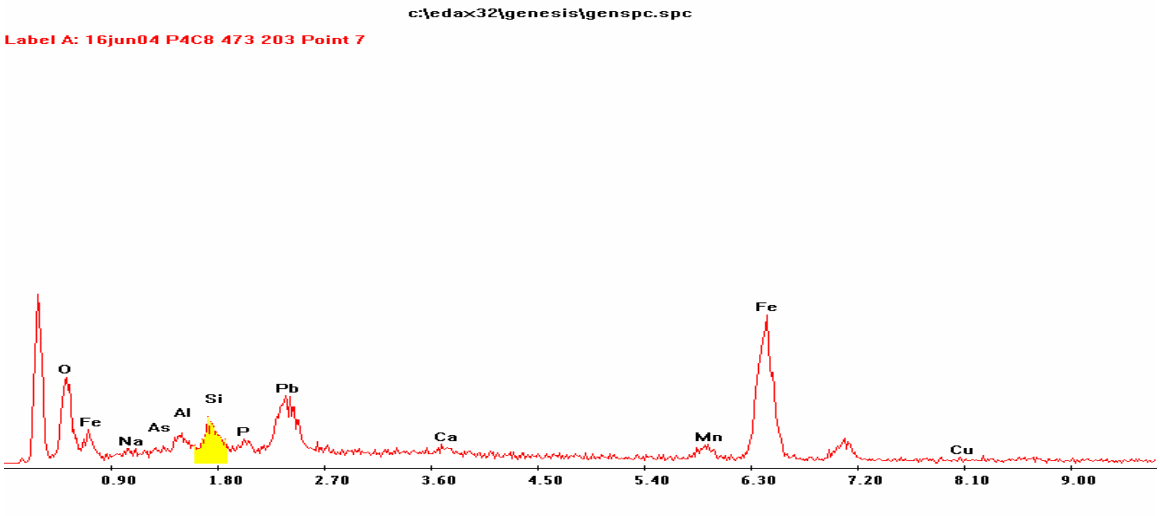

Point 8

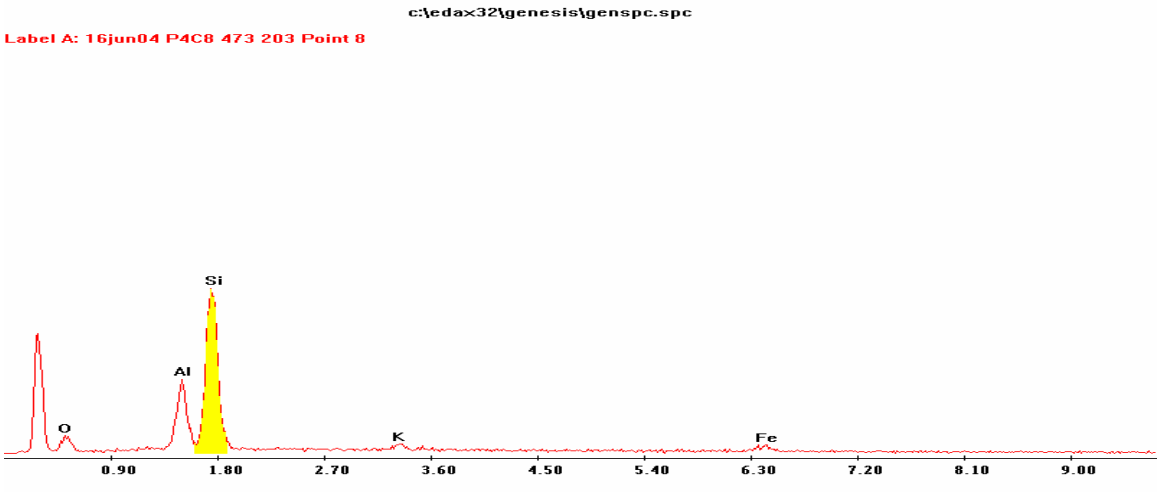

Point 9

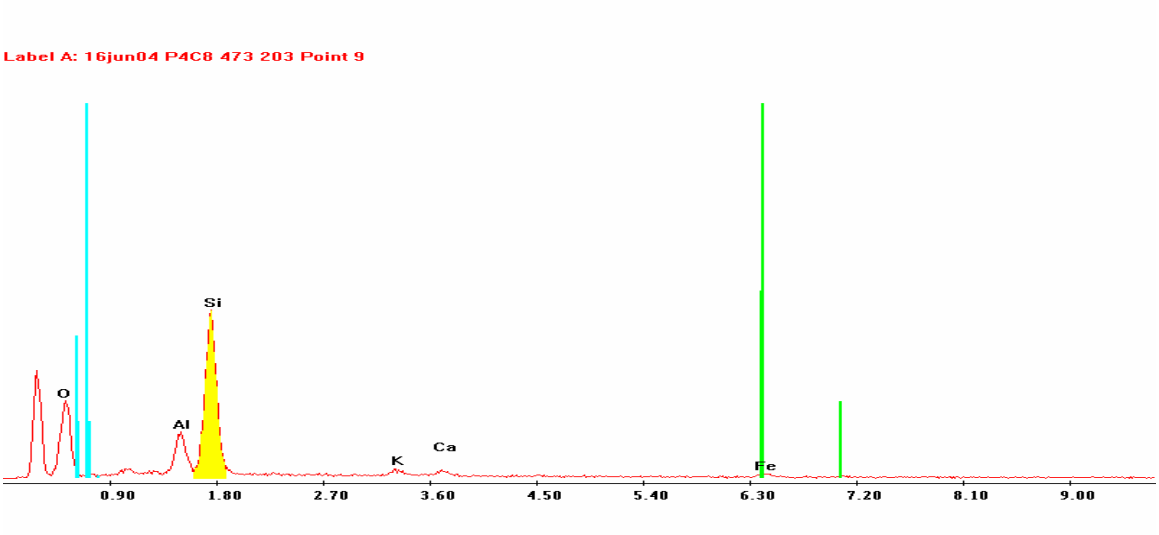

Point 10

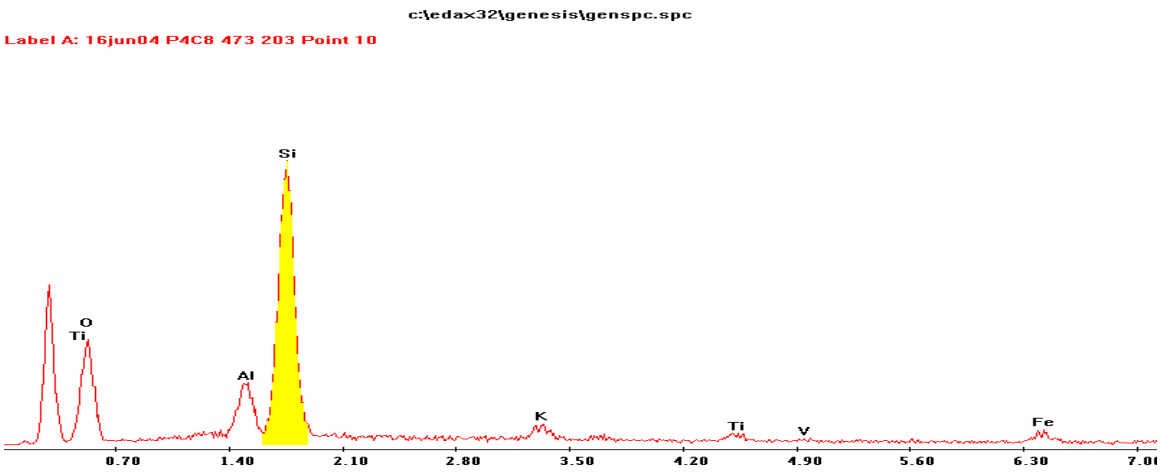

P4C9 – 319, 289

BSE Image

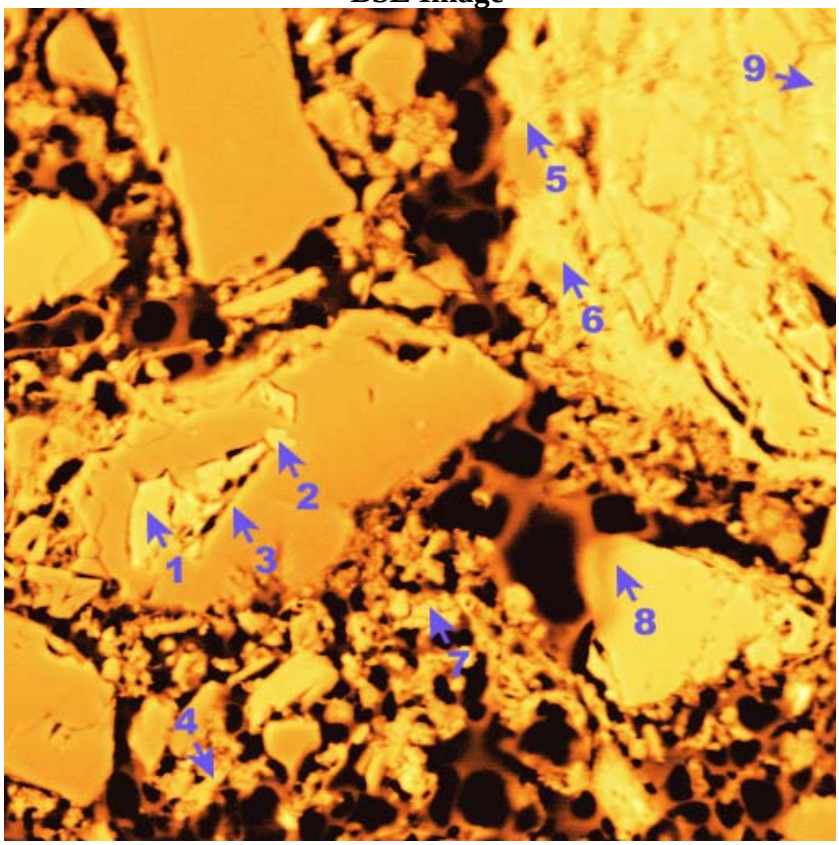

Iron (Fe)

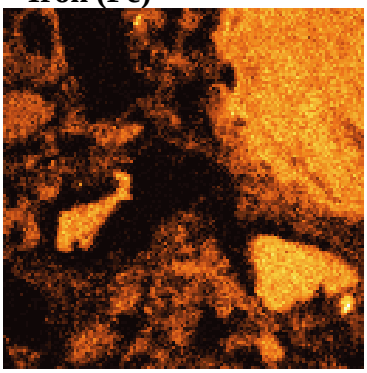

Manganese (Mn)

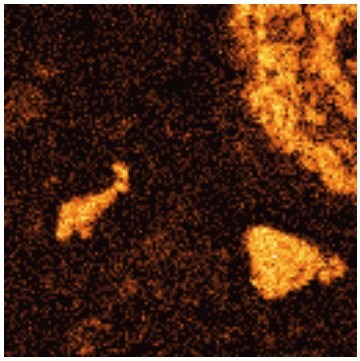

Phosphorous (P)

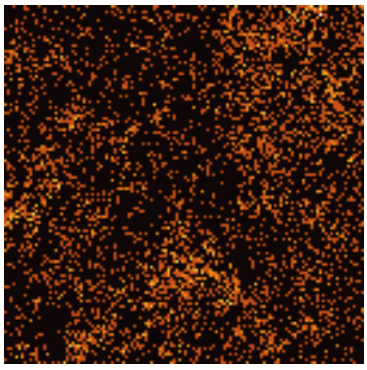

Lead (Pb)

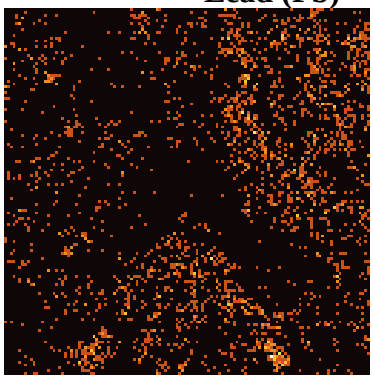

Silicon (Si)

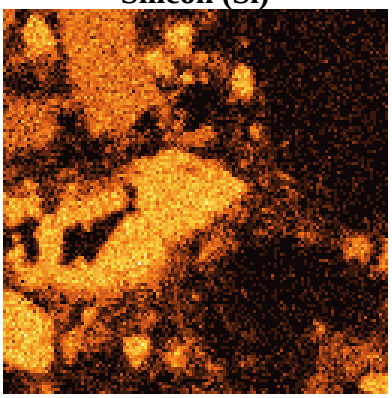

EDS Scan Images by Point

Point 1

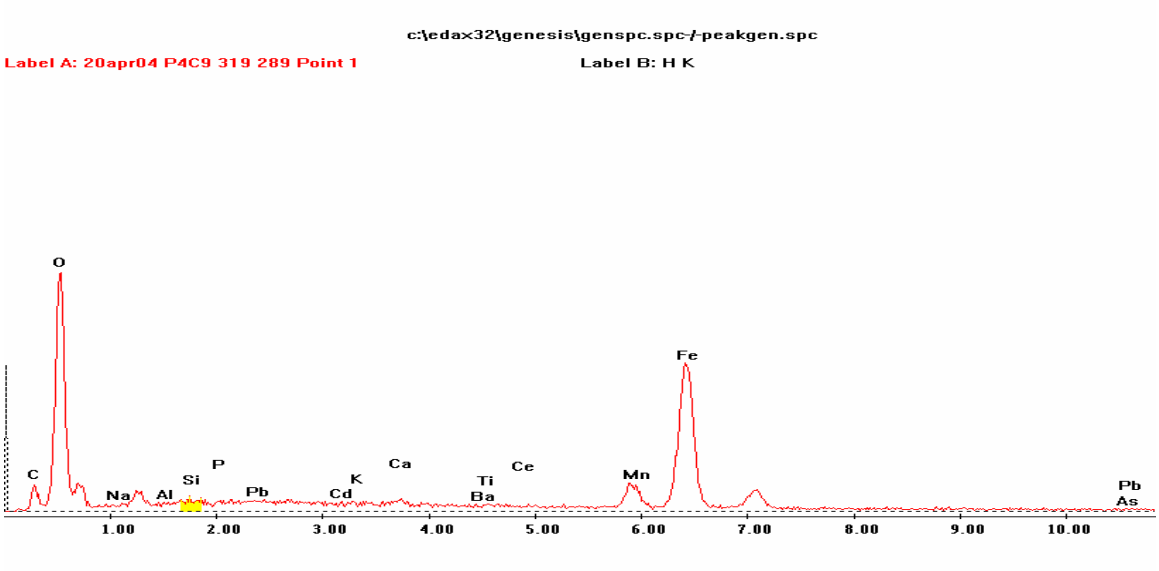

Point 2

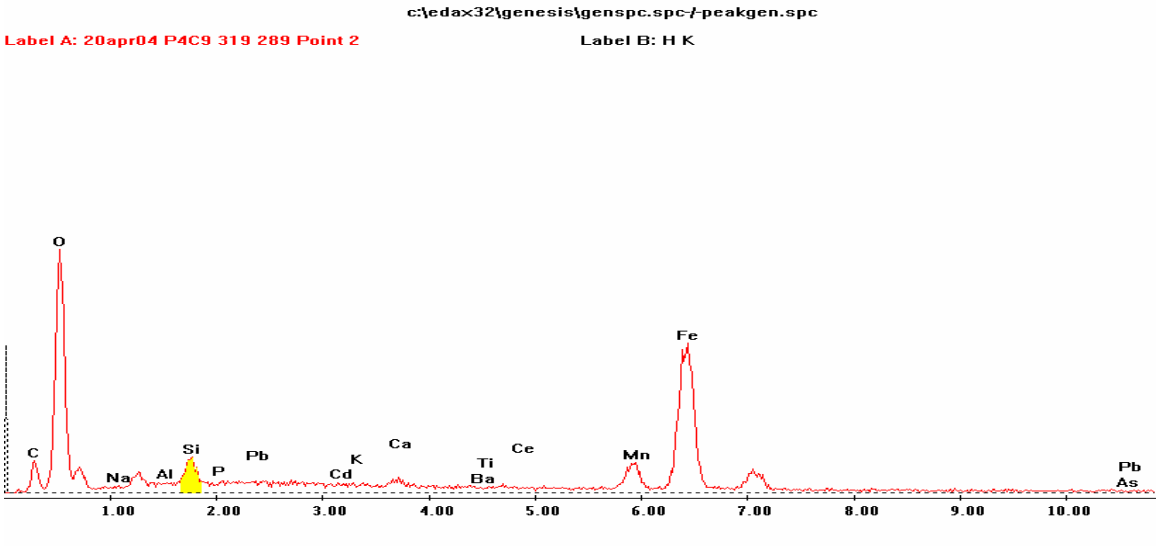

Point 3

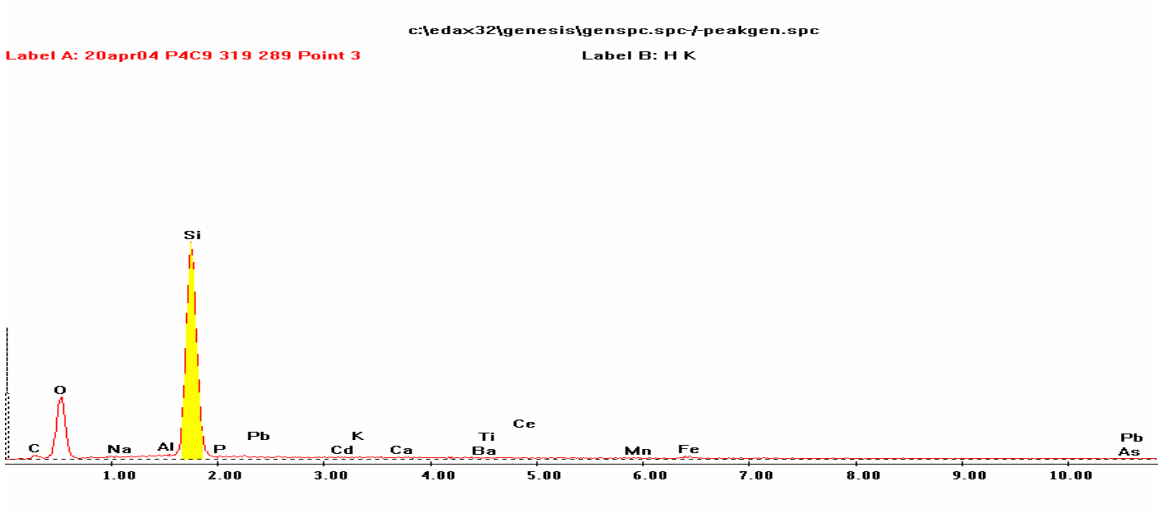

Point 4

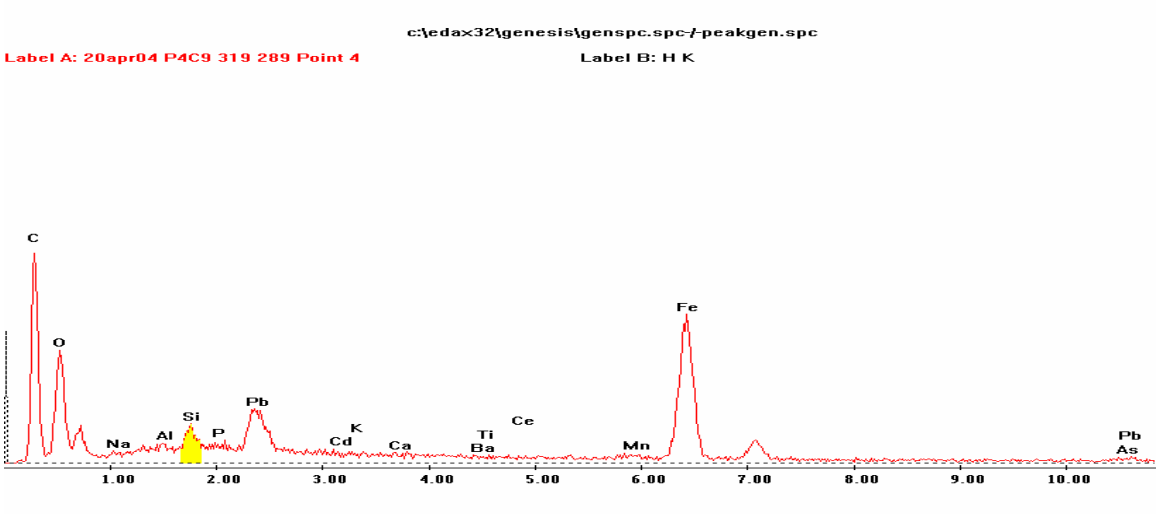

Point 5

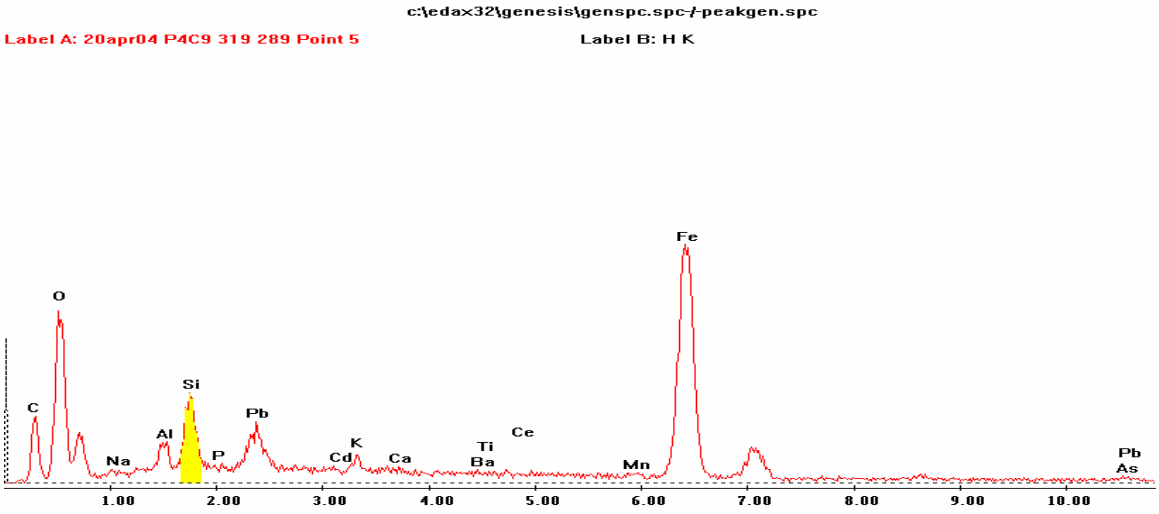

Point 6

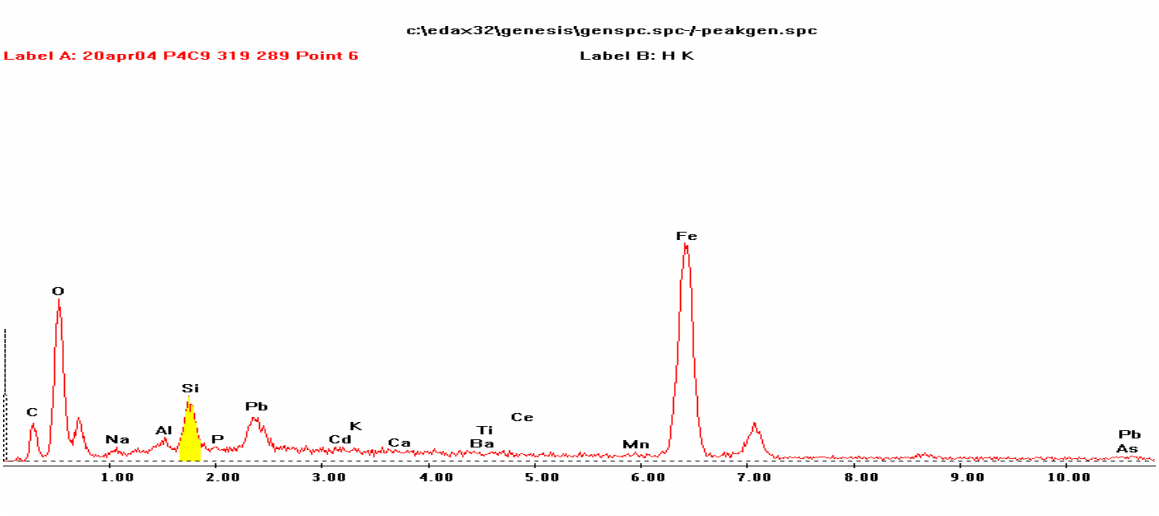

Point 7

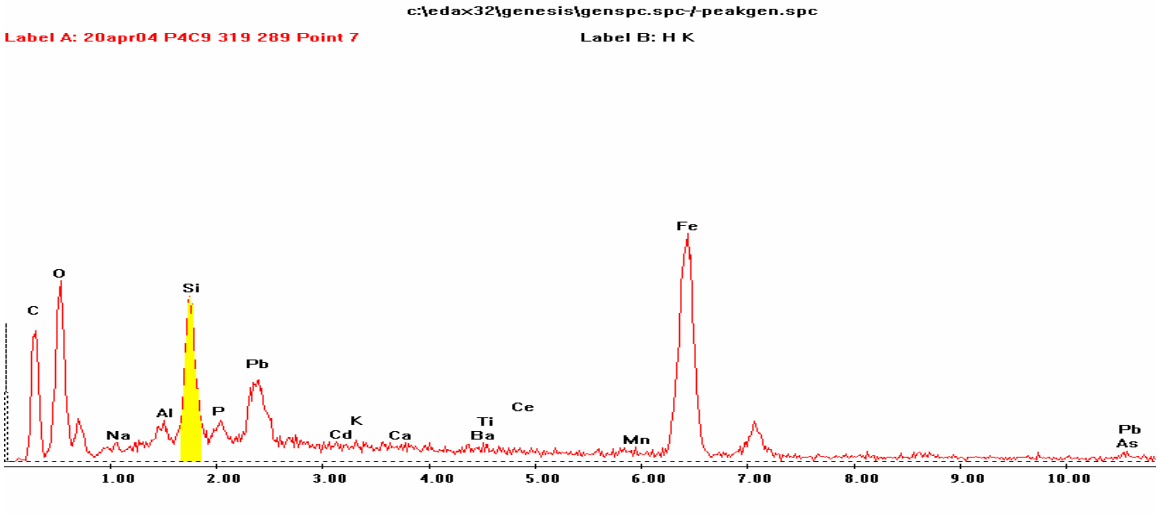

Point 8

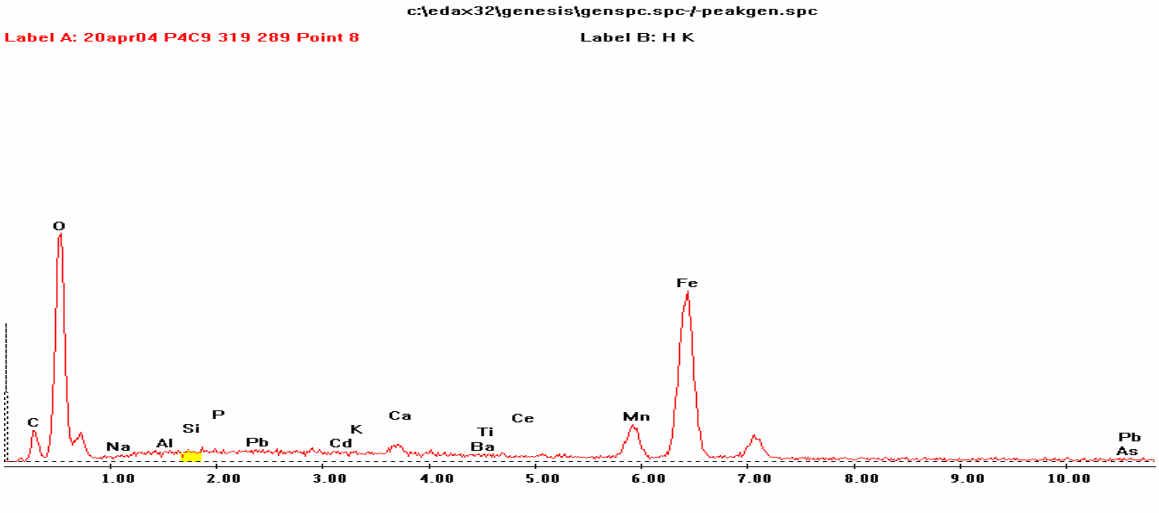

Point 9

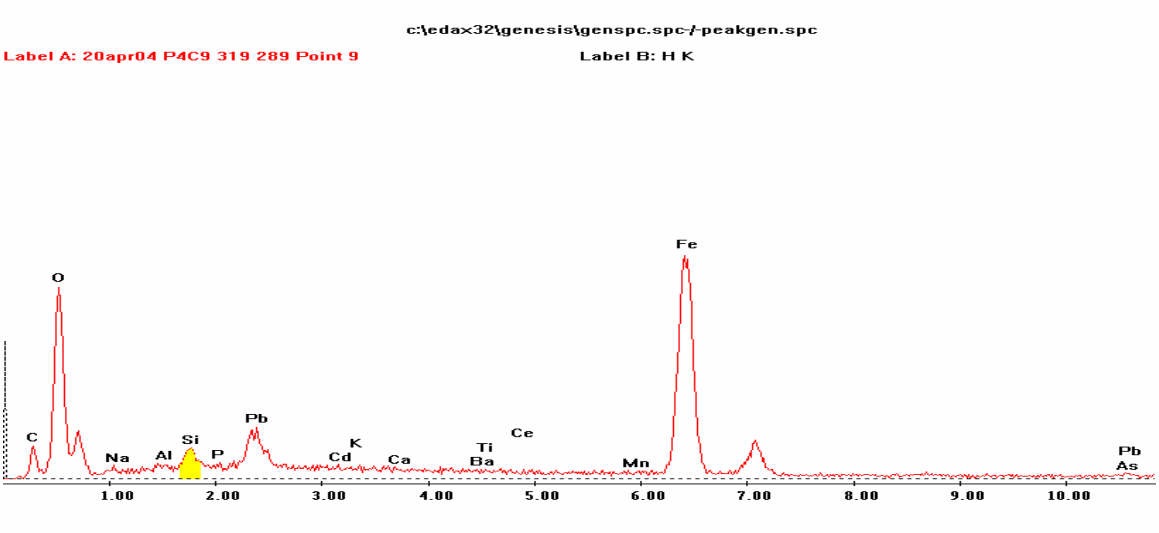
c:\edax32\genesis\genspc.spc-/-peakgen.spc
Label A: 20apr04 P4C9 319 289 Point 9
Label B: H K
O
Fe
C
Na
Al
Si
P
Pb
Cd
K
Ca
Ti
Ba
Ce
Mn
Pb
As
1.00
2.00
3.00
4.00
5.00
6.00
7.00
8.00
9.00
10.00

P4C9 – 338, 318

BSE Image

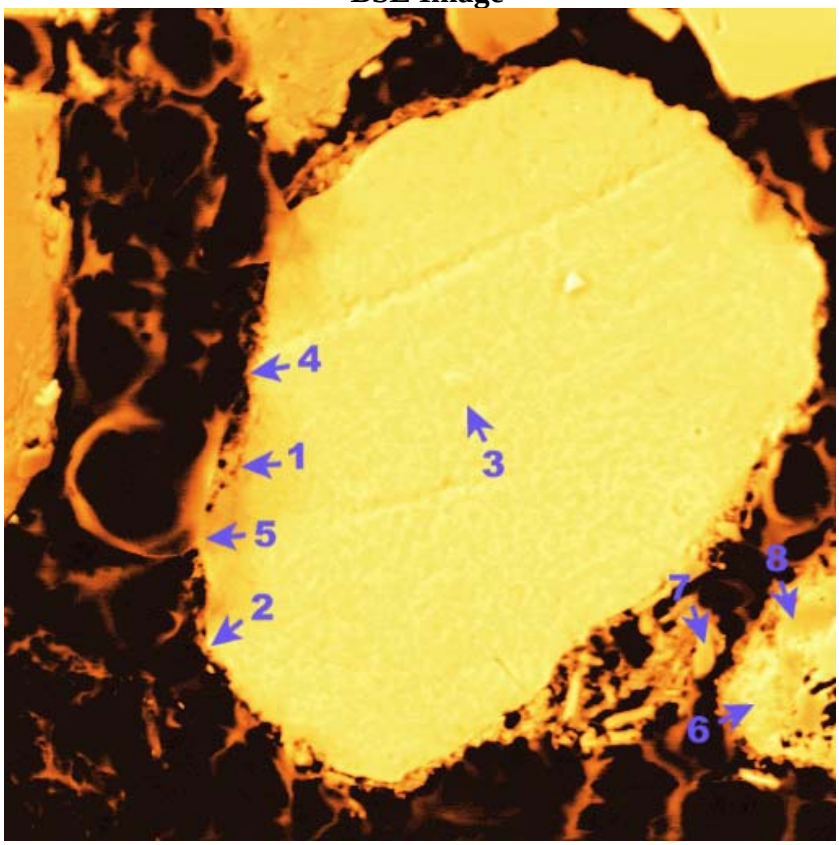

Iron (Fe)

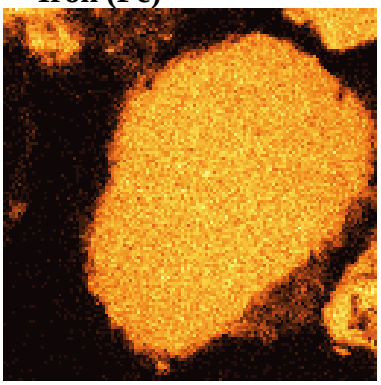

Manganese (Mn)

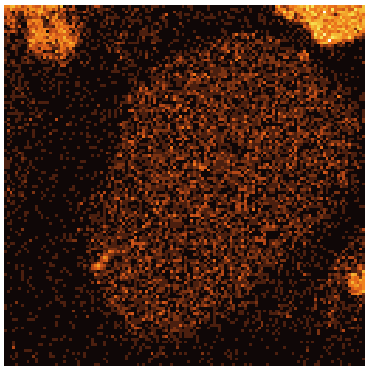

Phosphorous (P)

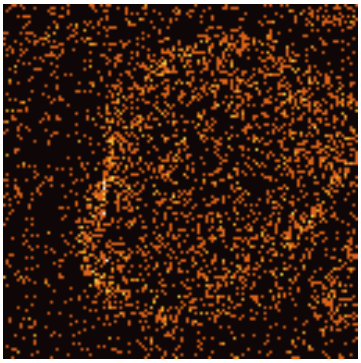

Lead (Pb)

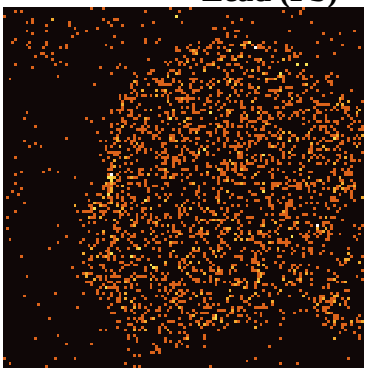

Silicon (Si)

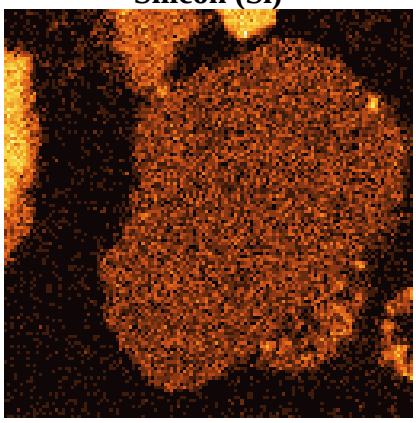

EDS Scan Images by Point

Point 1

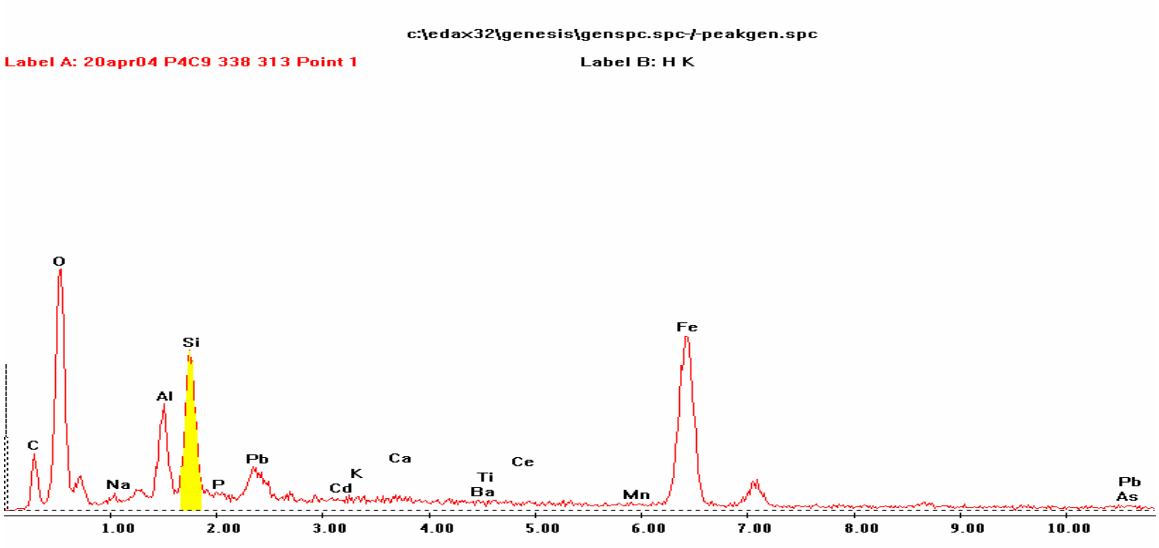

Point 2

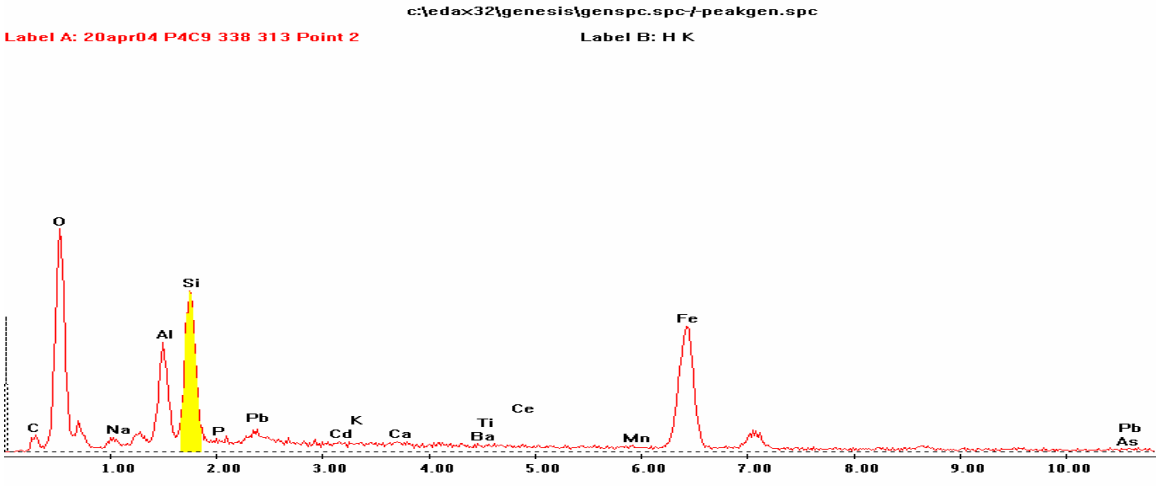

Point 3

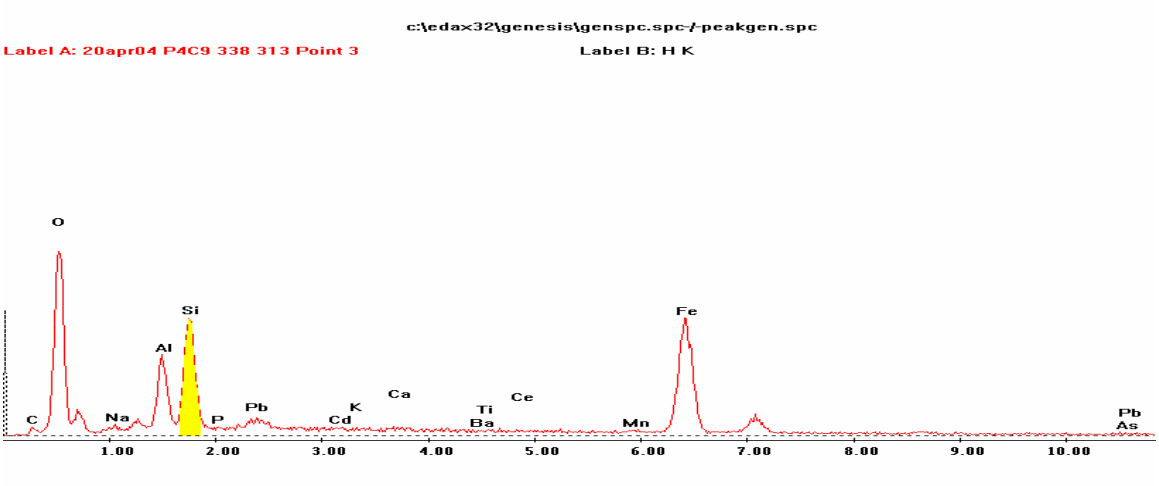

Point 4

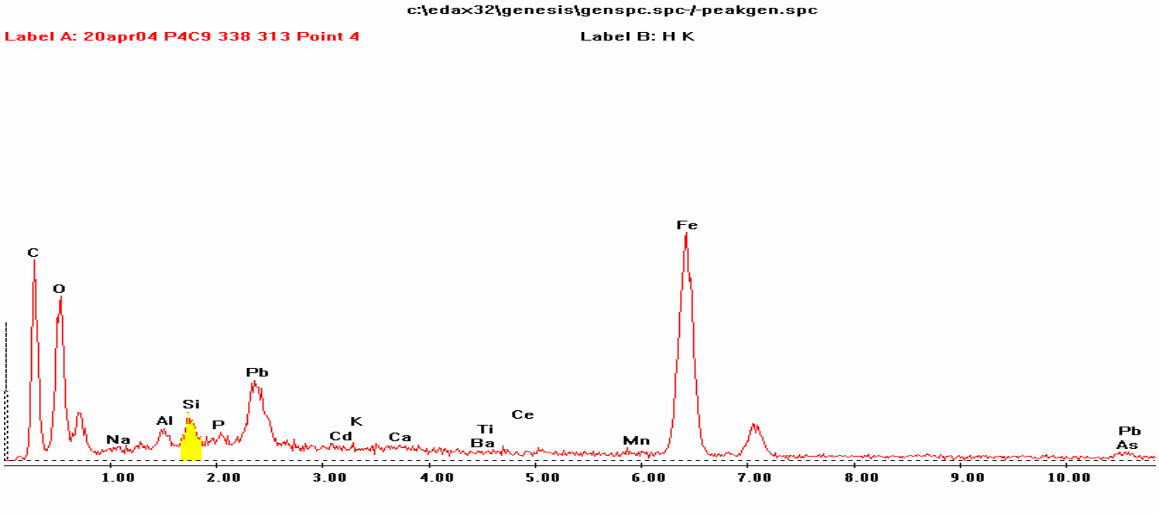

Point 5

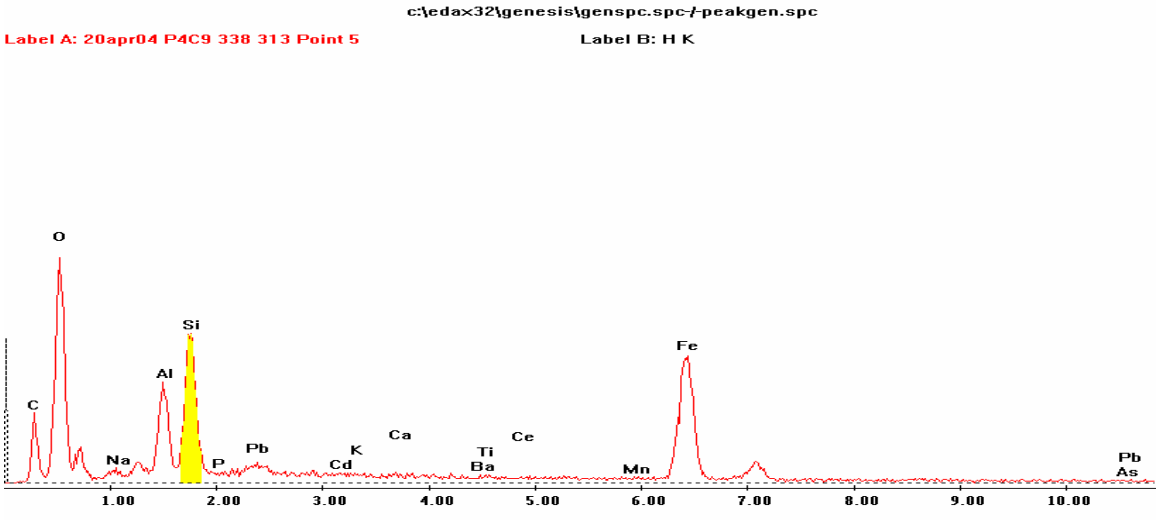

Point 6

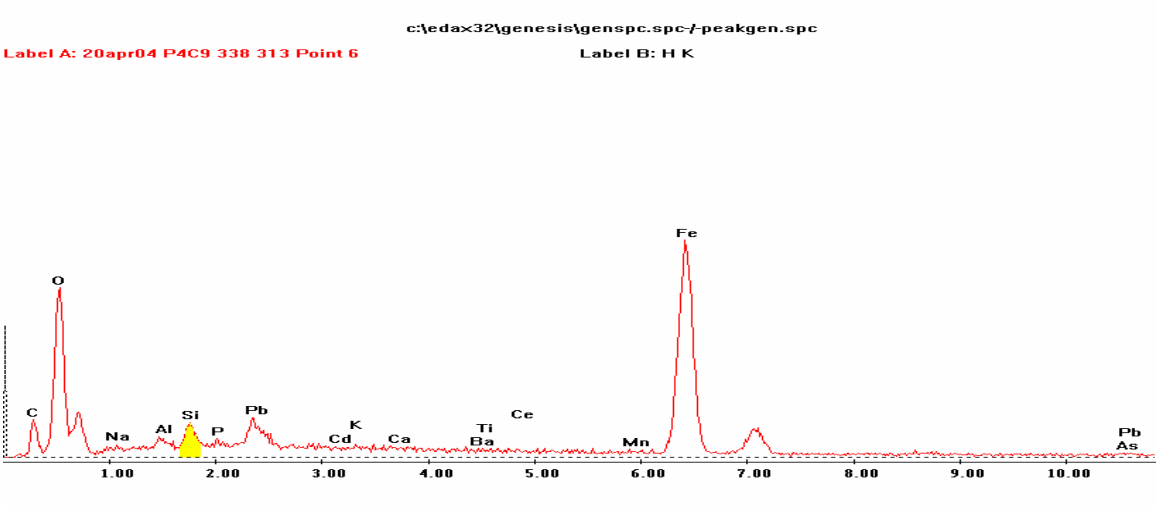

Point 7

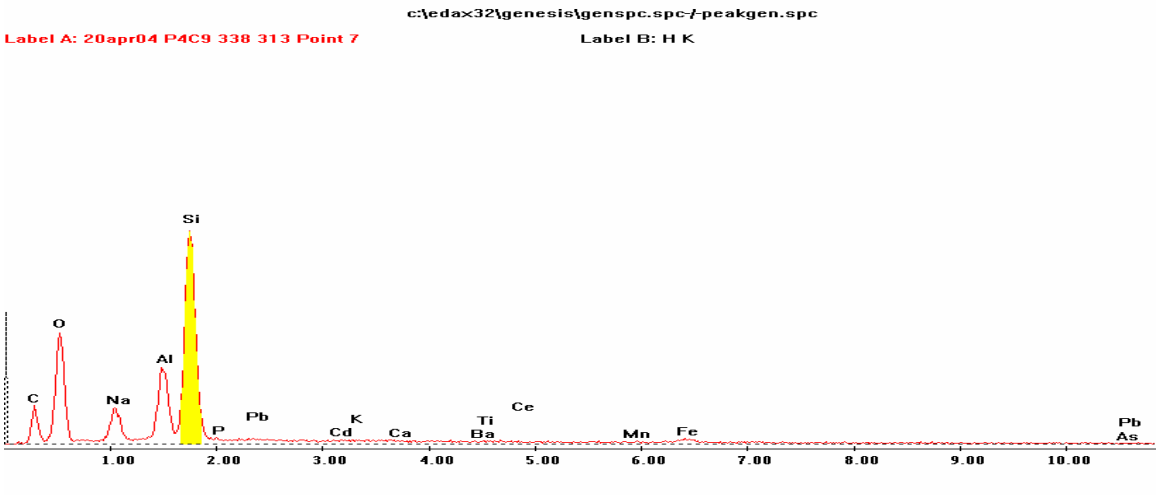

Point 8

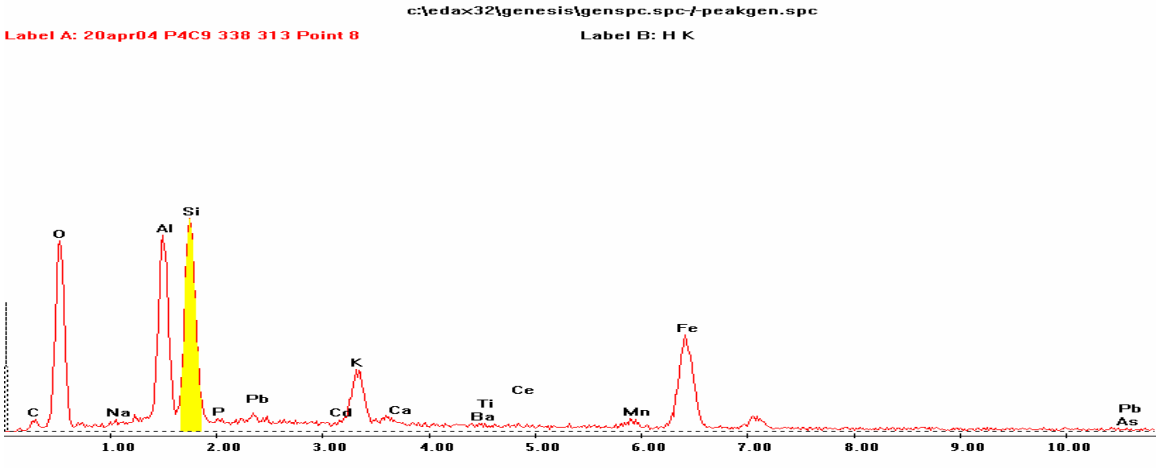

P4C9 – 443, 152

BSE Image

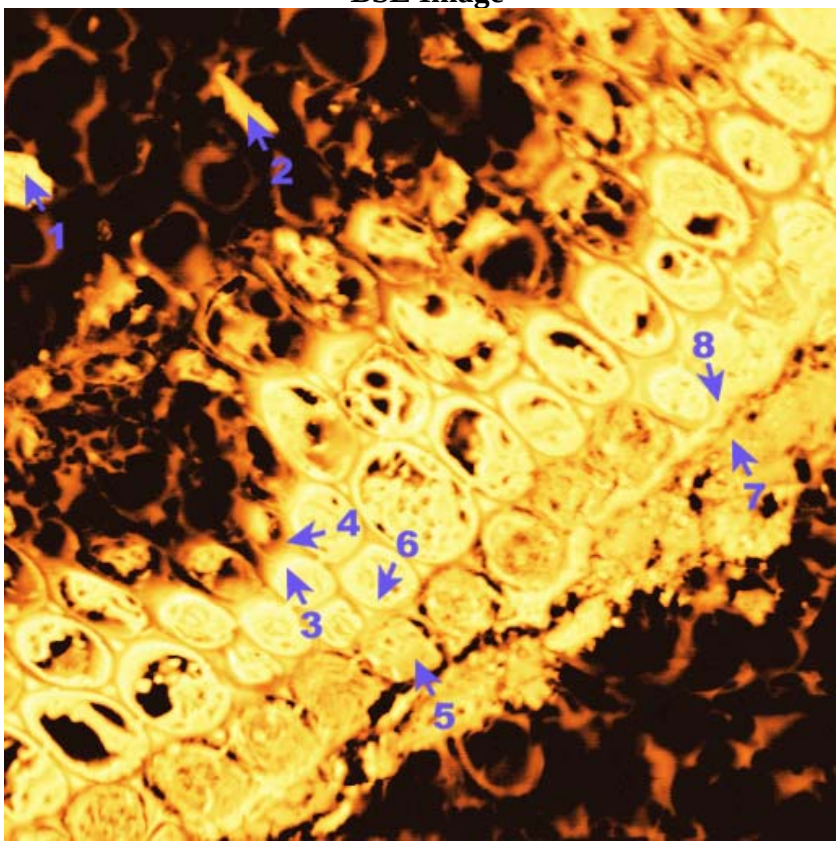

Iron (Fe)

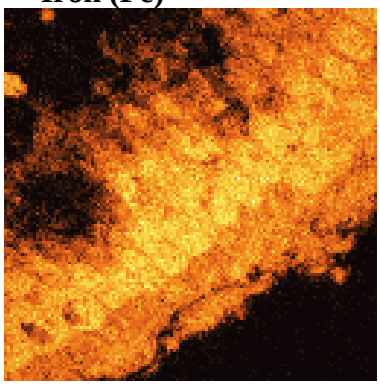

Manganese (Mn)

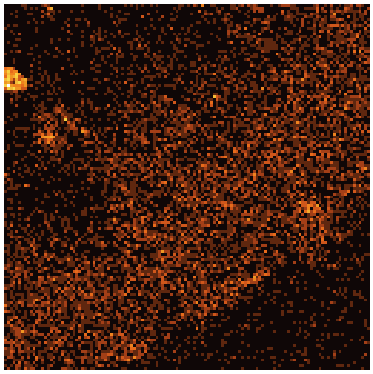

Phosphorous (P)

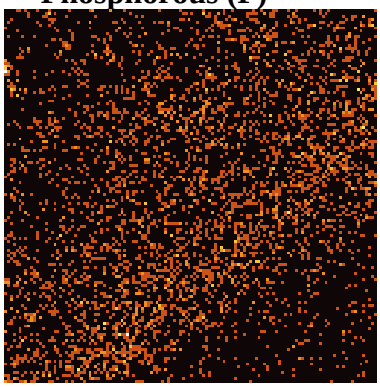

Lead (Pb)

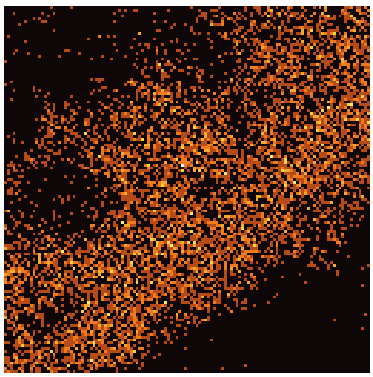

Silicon (Si)

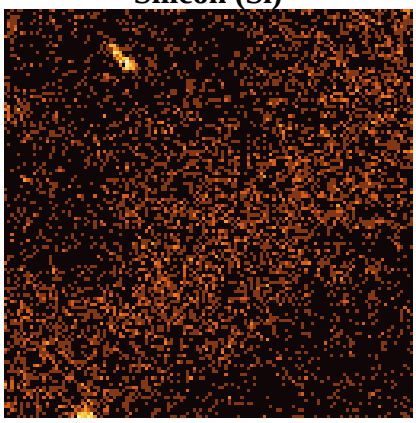

EDS Scan Images by Point

Point 1

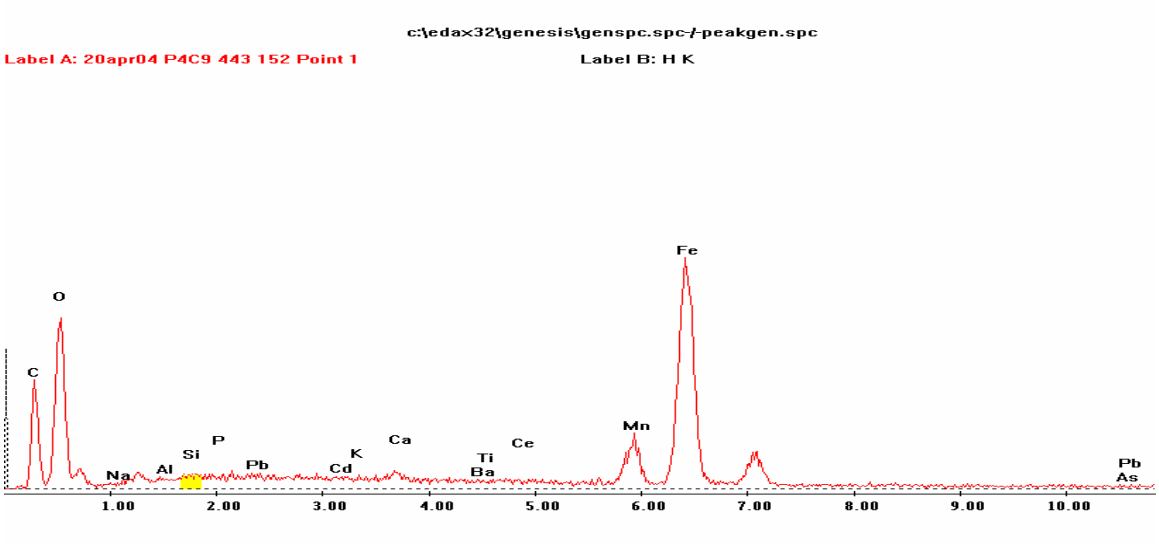

Point 2

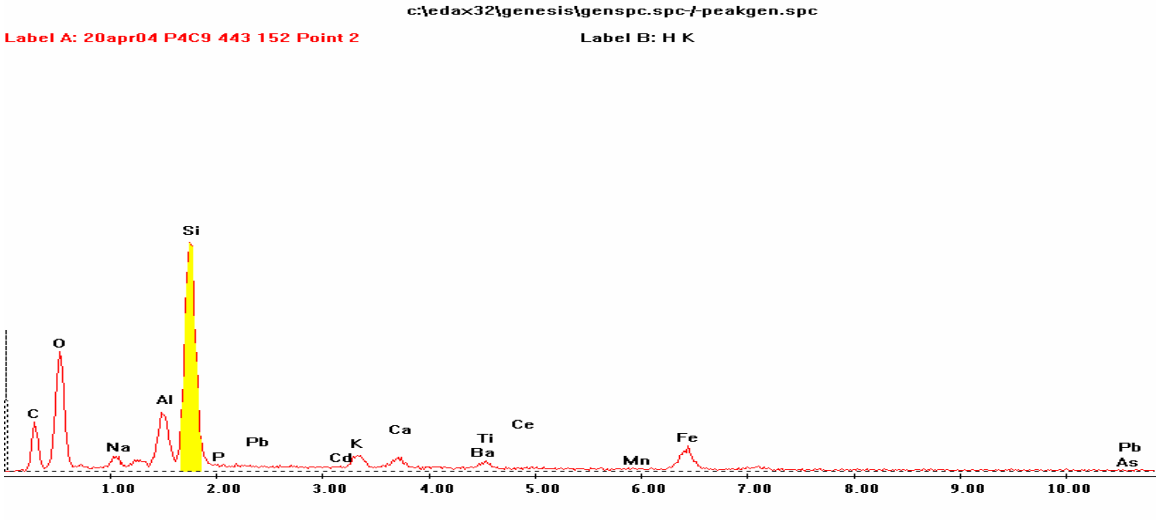

Point 3

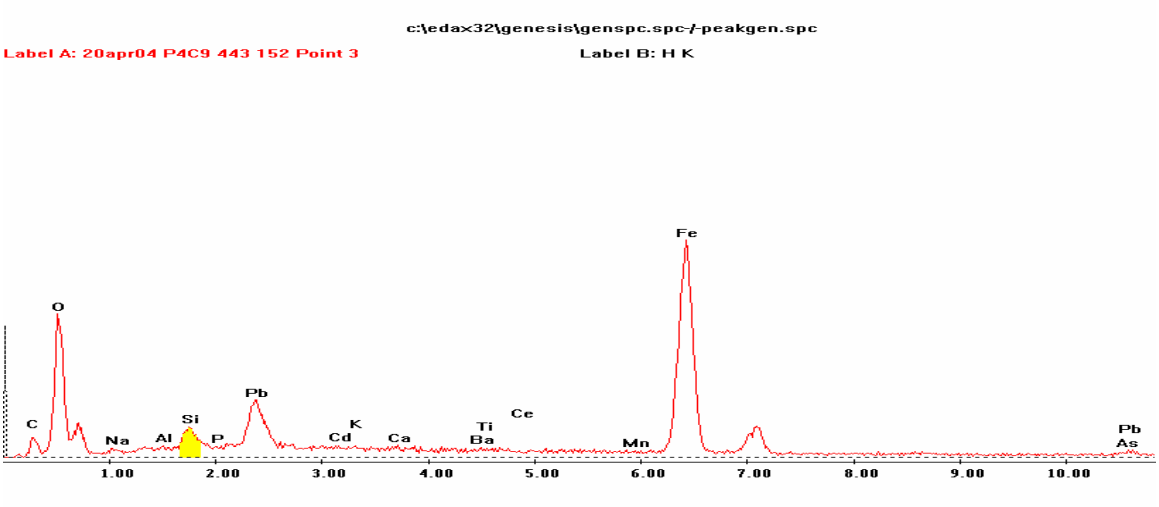

Point 4

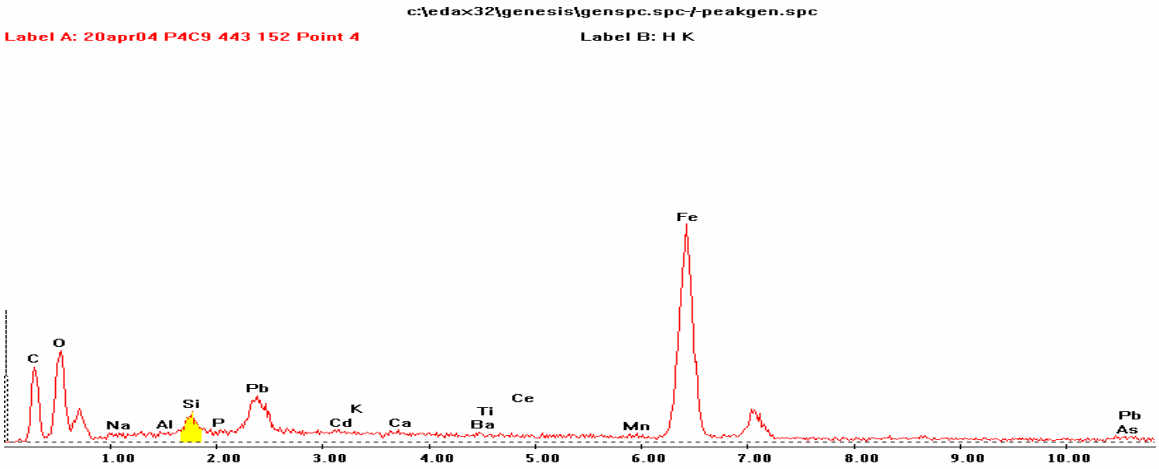

Point 5

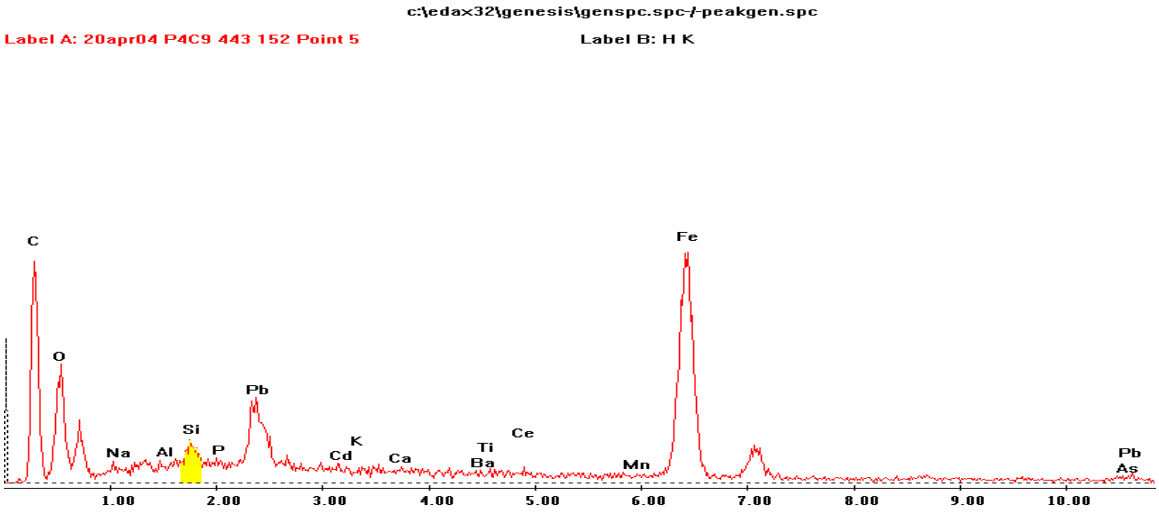

Point 6

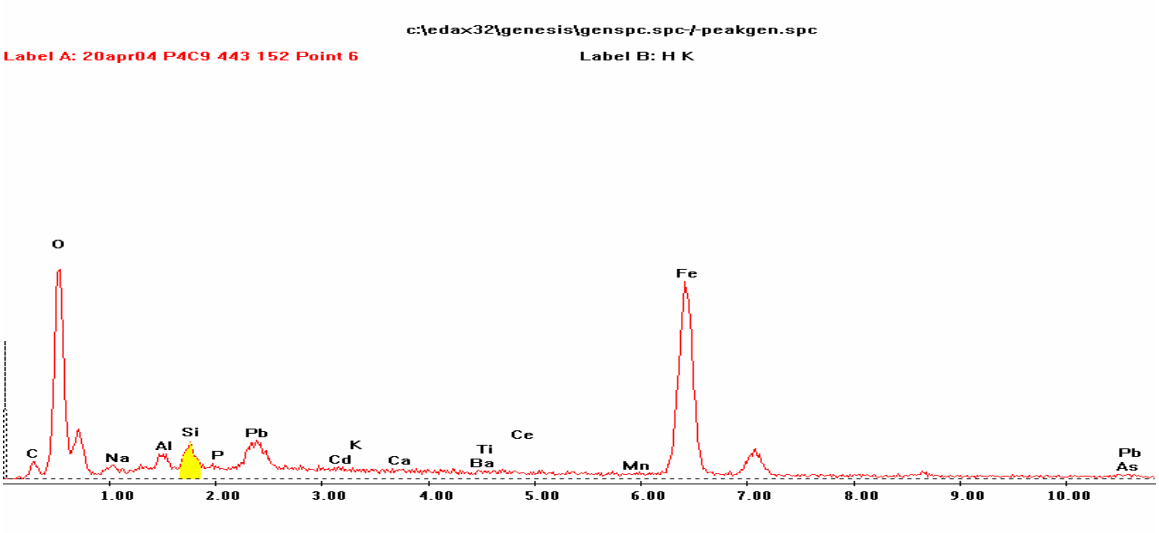

Point 7

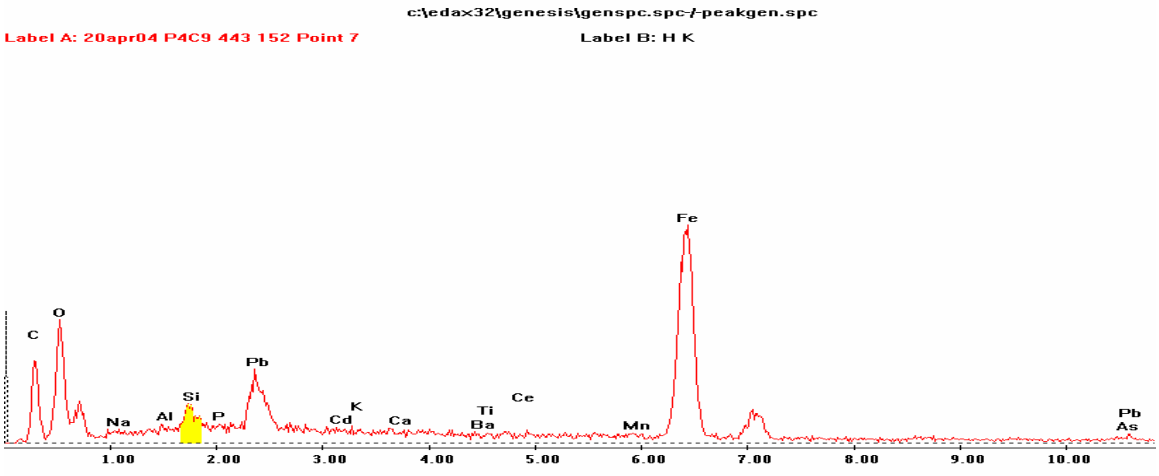

Point 8

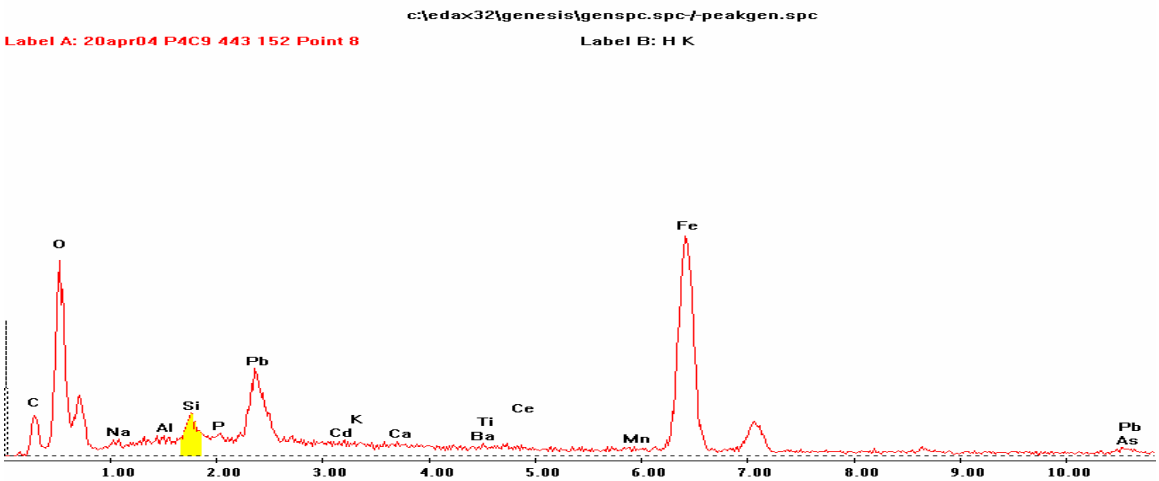

P4C9 – 452, 298

BSE Image

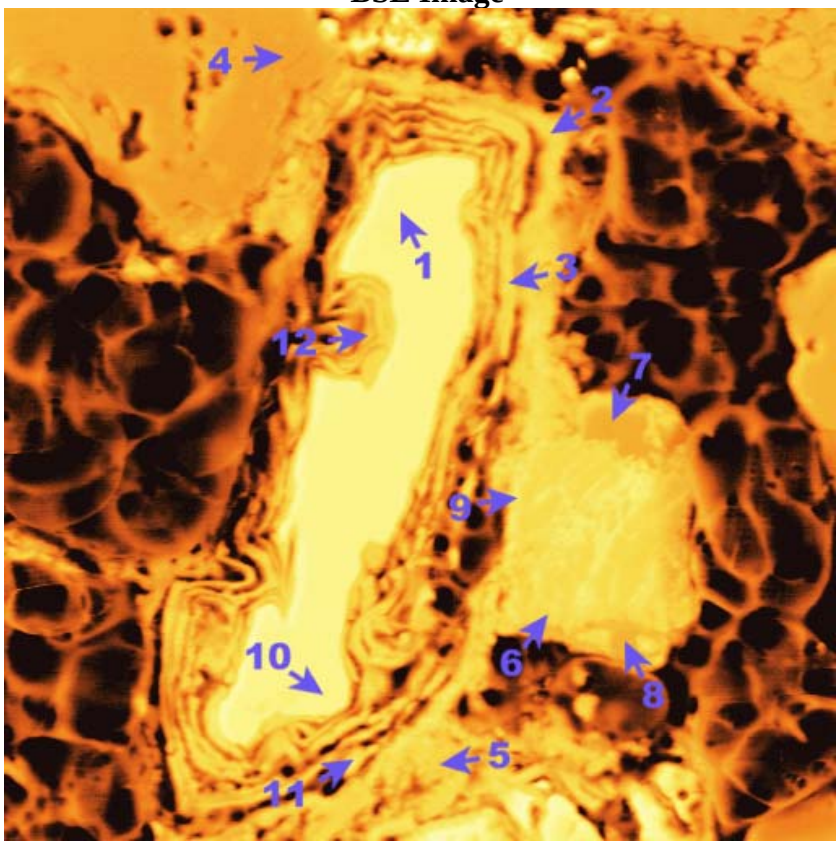

Iron (Fe)

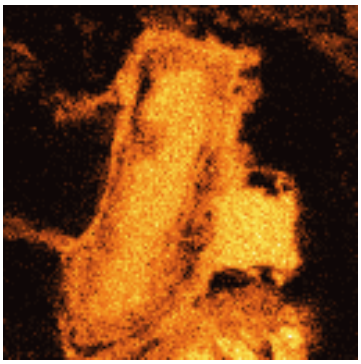

Manganese (Mn)

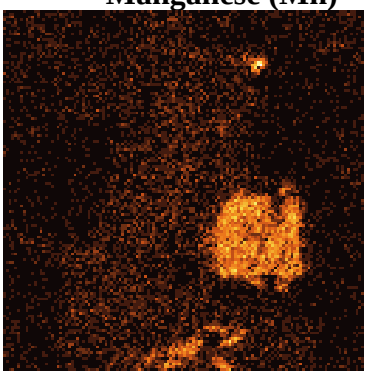

Phosphorous (P)

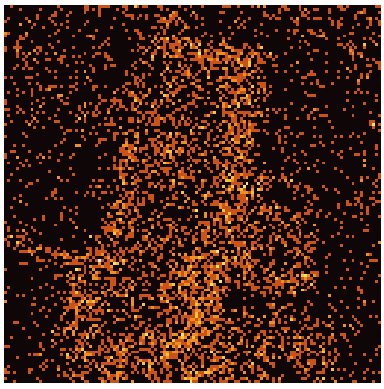

Lead (Pb)

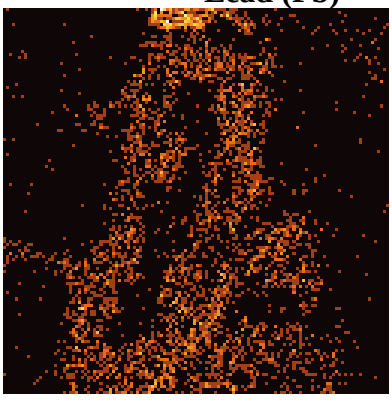

Silicon (Si)

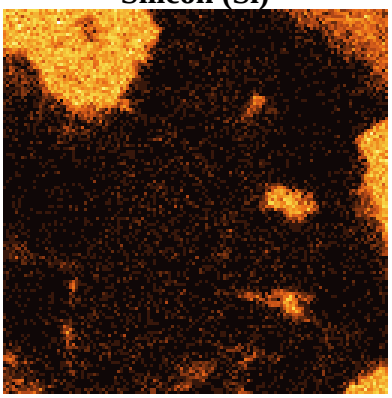

EDS Scan Images by Point

Point 1

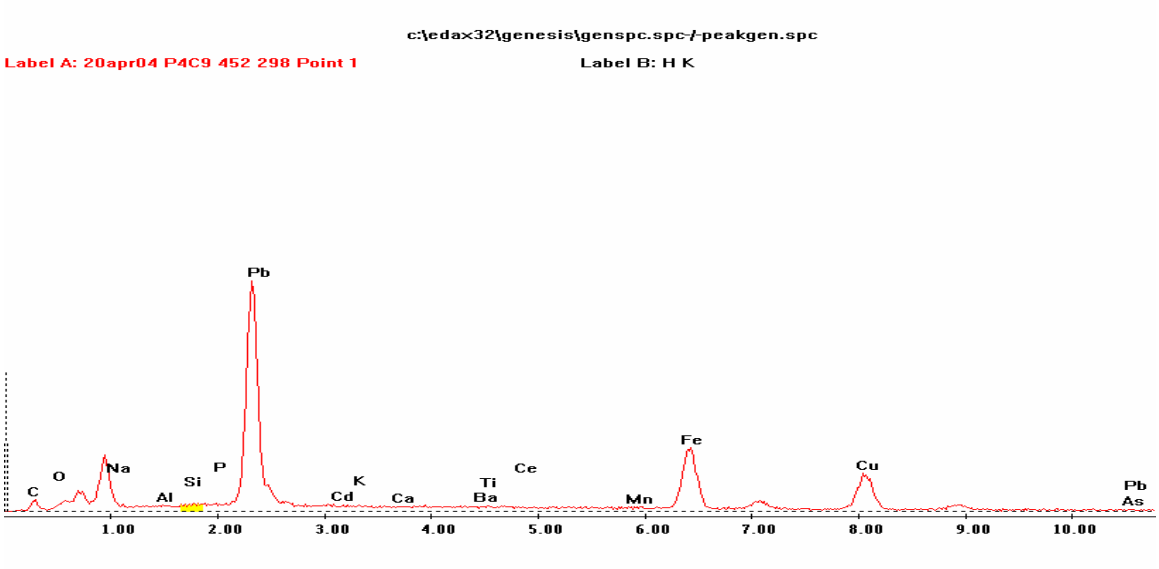

Point 2

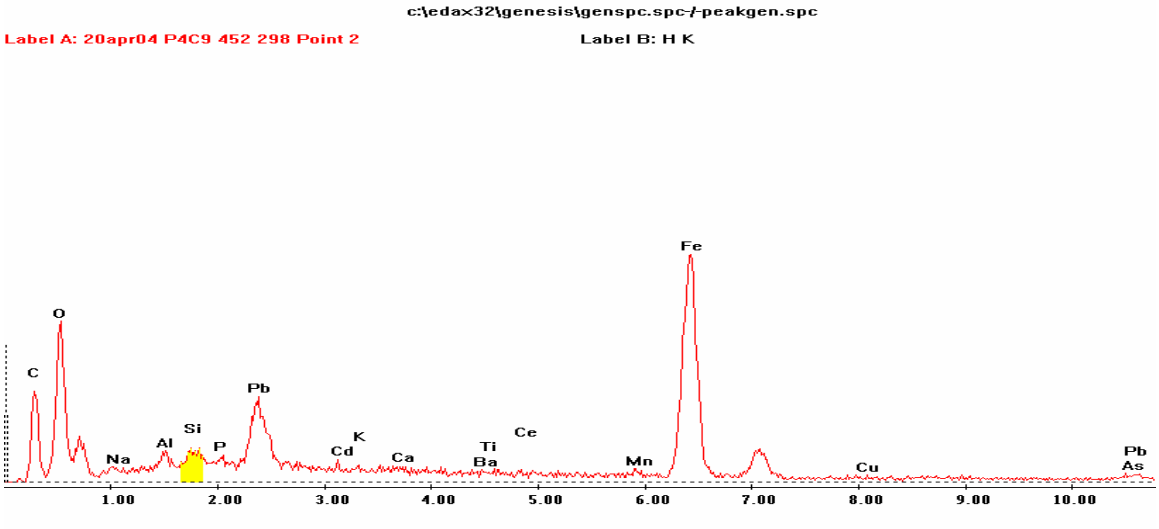

Point 3

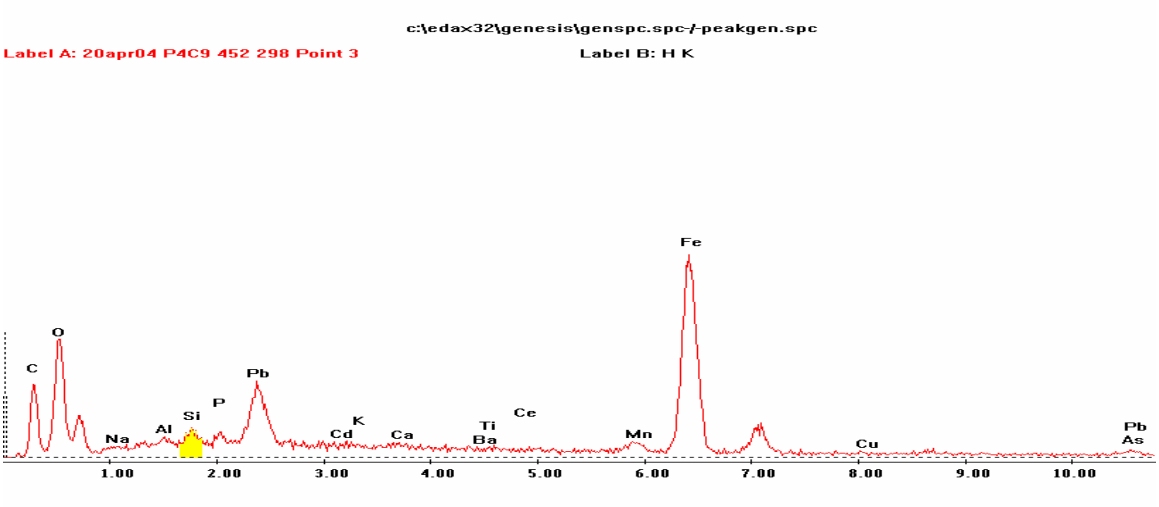

Point 4

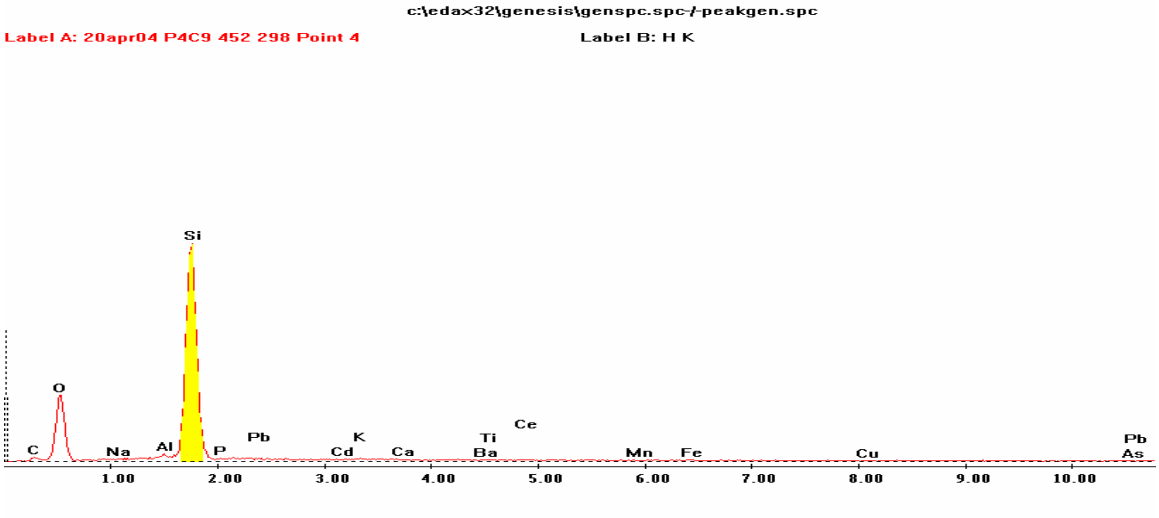

Point 5

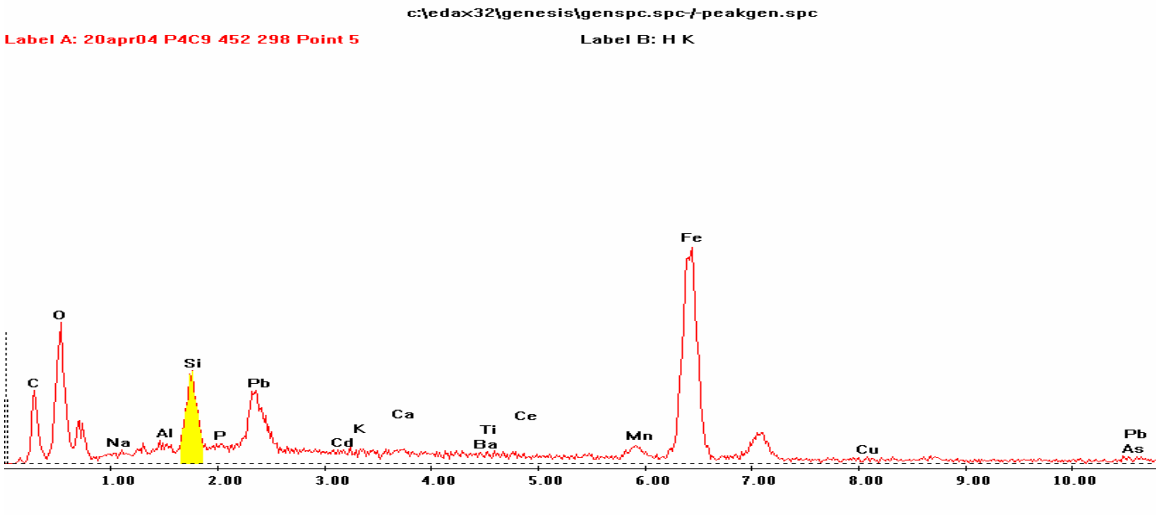

Point 6

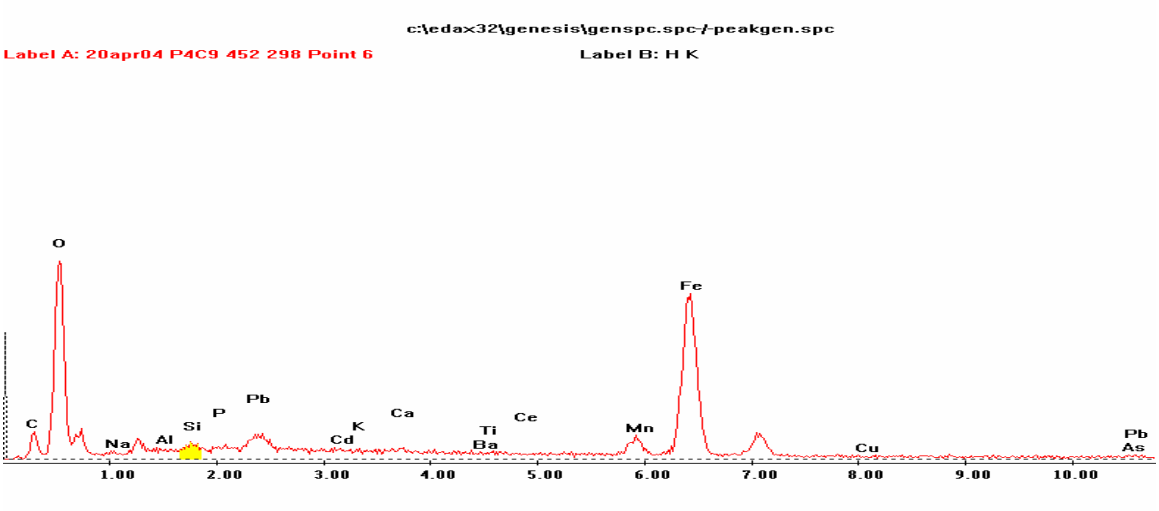

Point 7

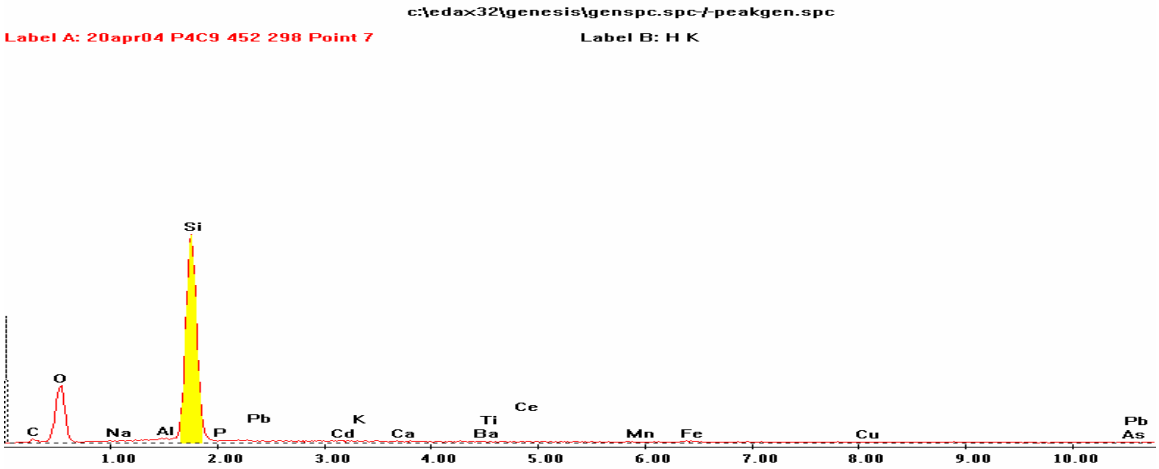

Point 8

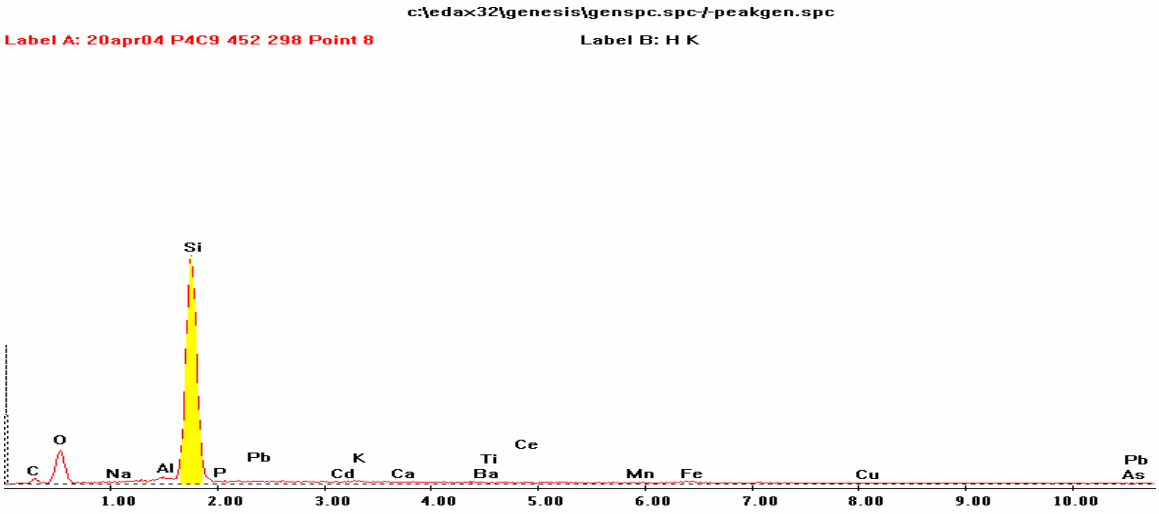

Point 9

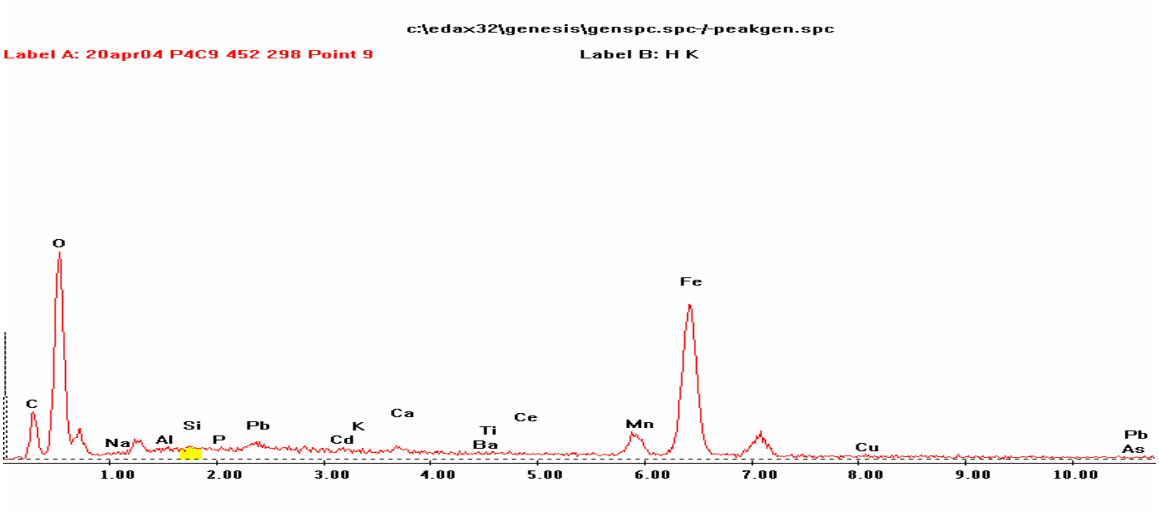

Point 10

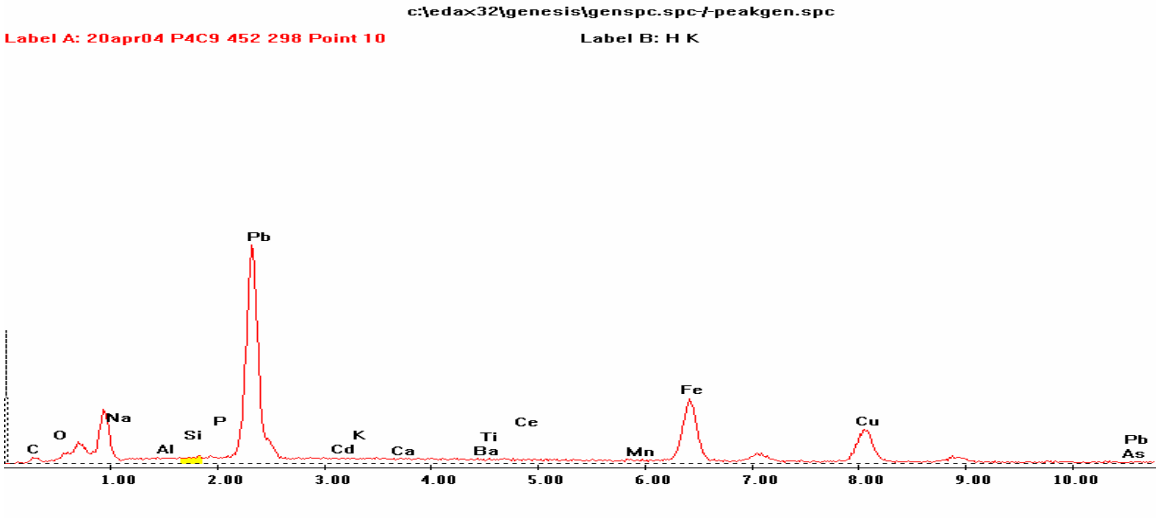

Point 11

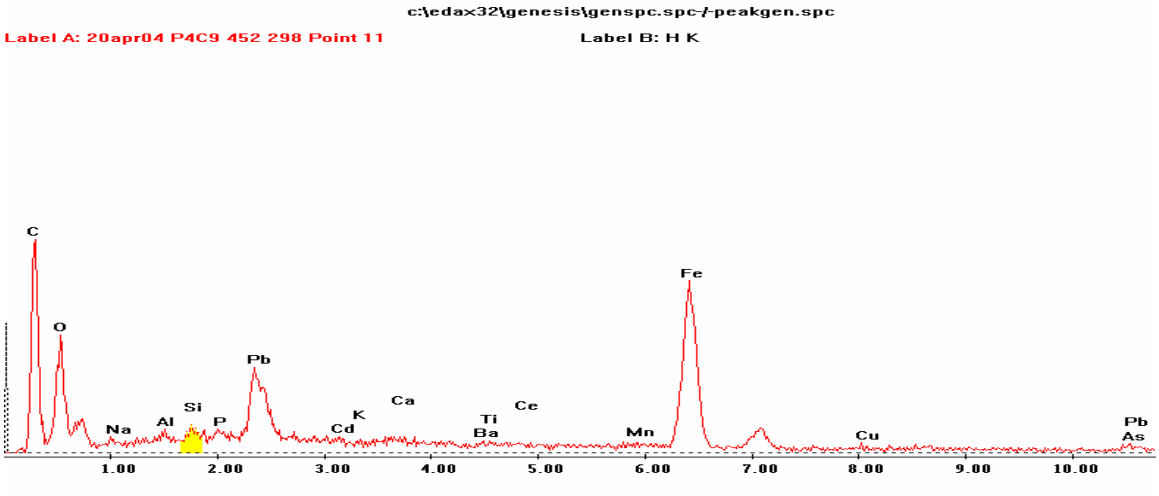

Point 12

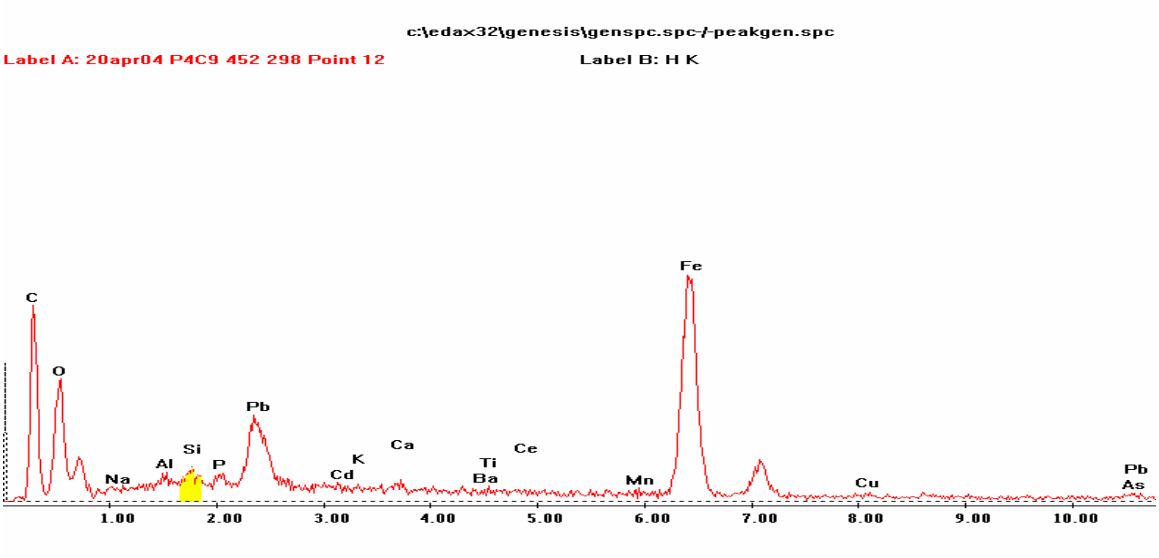
c:\edax32\genesis\genspc.spc-/-peakgen.spc
Label A: 20apr04 P4C9 452 298 Point 12
Label B: H K
C
O
Na
Al
Si
P
Pb
Cd
K
Ca
Ti
Ba
Ce
Mn
Fe
Cu
Pb
As
1.00
2.00
3.00
4.00
5.00
6.00
7.00
8.00
9.00
10.00

P4C9 – 459, 210

BSE Image

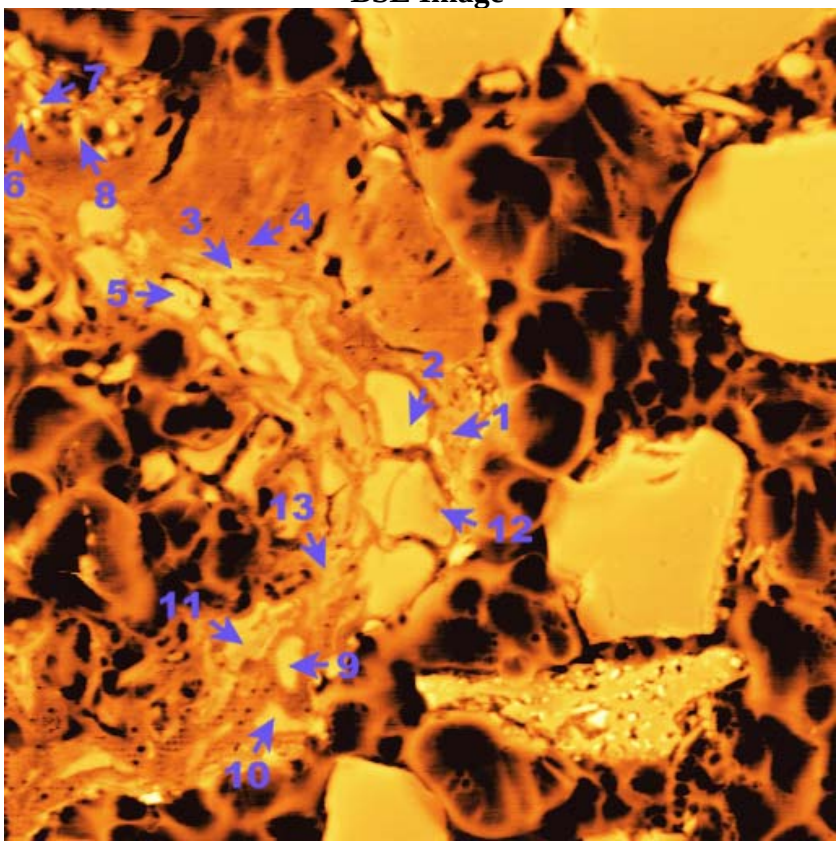

Iron (Fe)

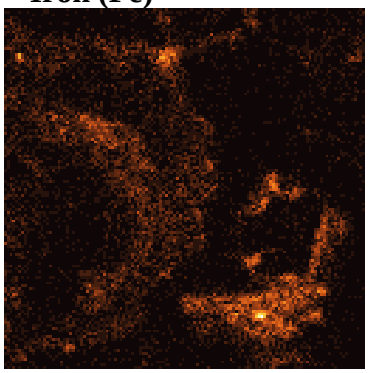

Manganese (Mn)

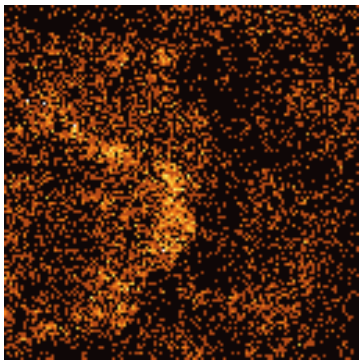

Phosphorous (P)

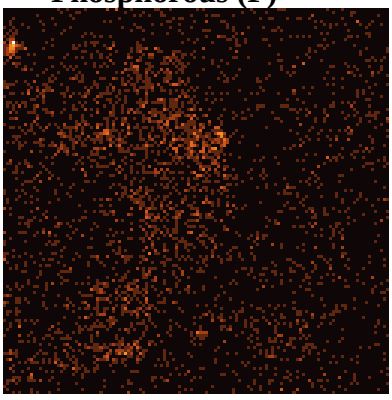

Lead (Pb)

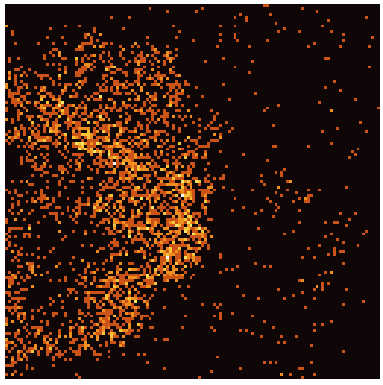

Silicon (Si)

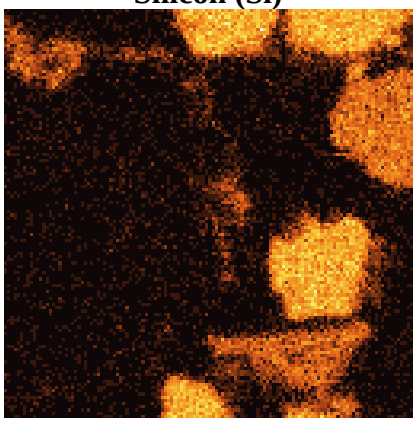

EDS Scan Images by Point

Point 1

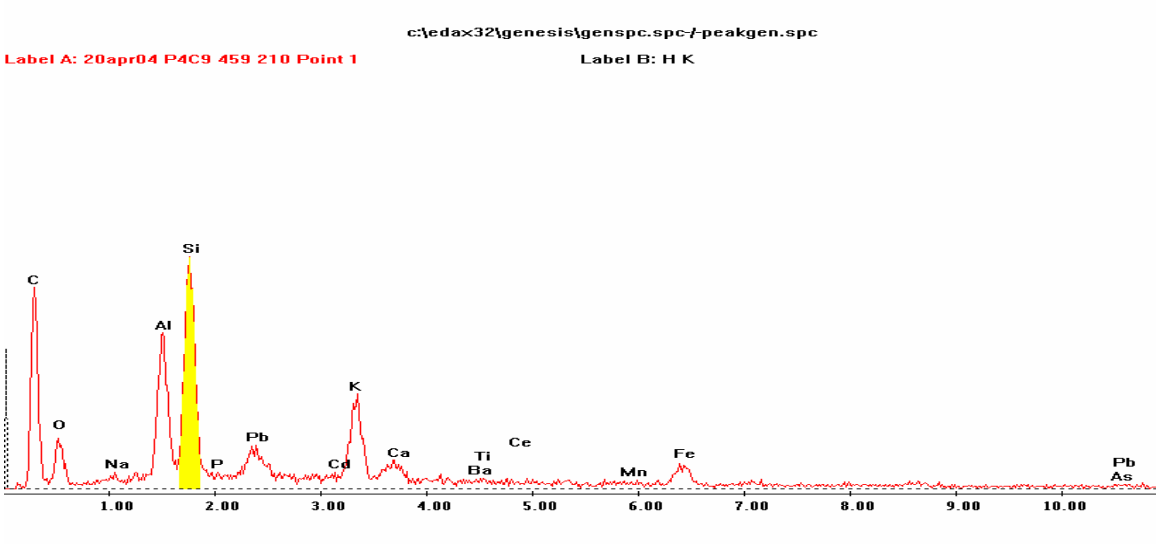

Point 2

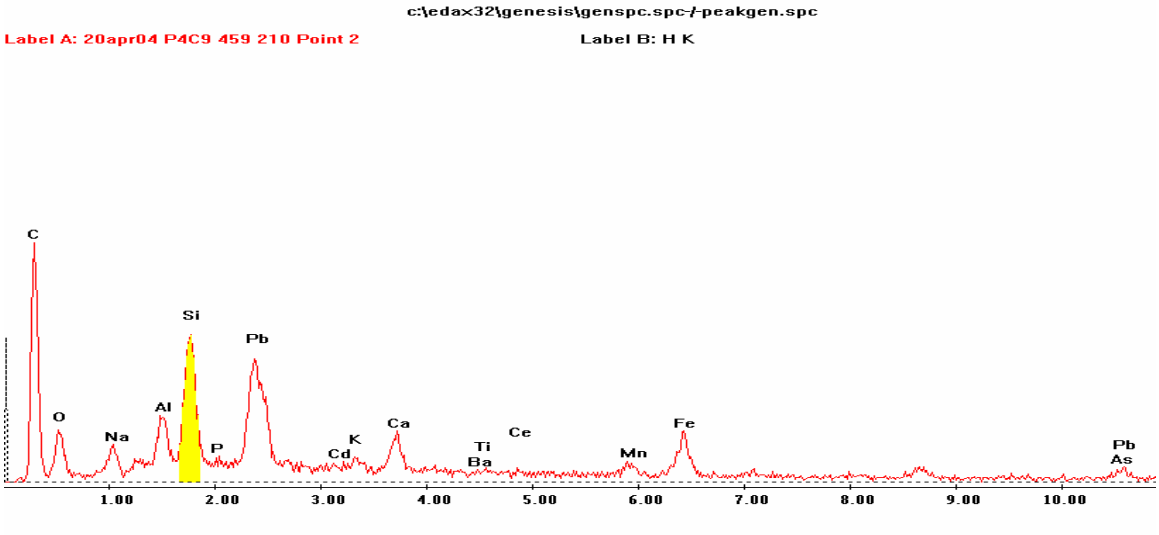

Point 3

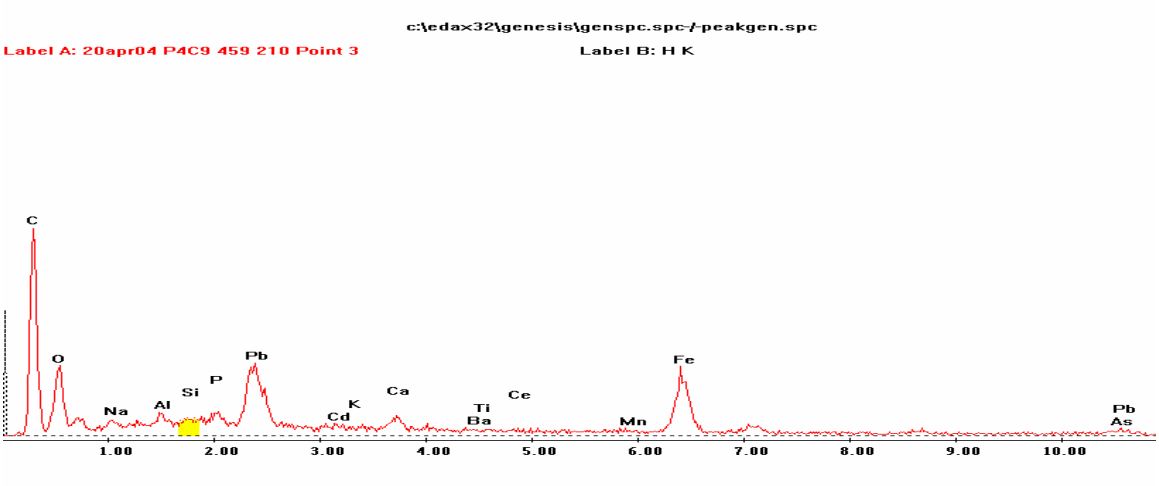

Point 4

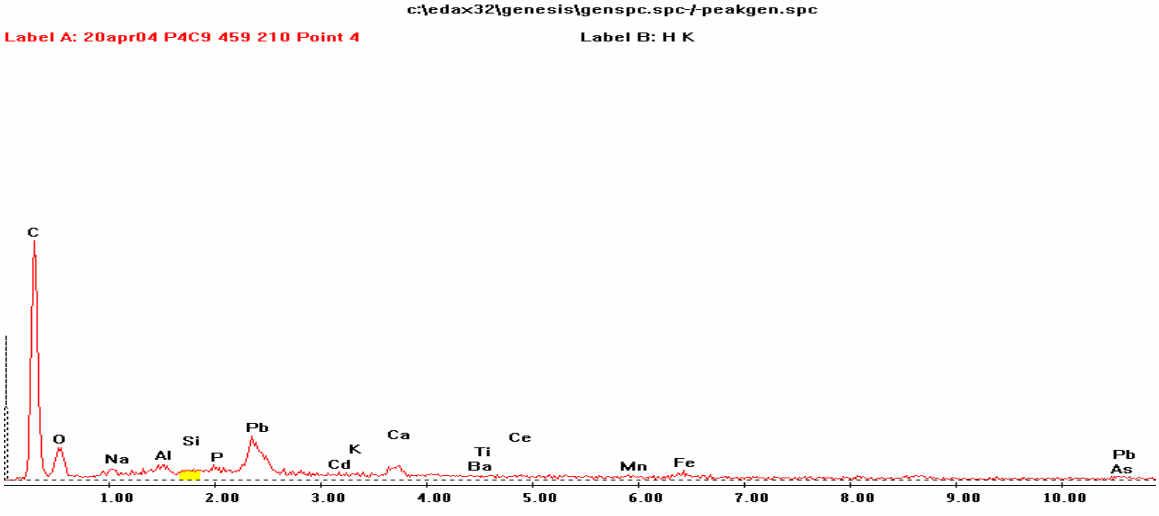

Point 5

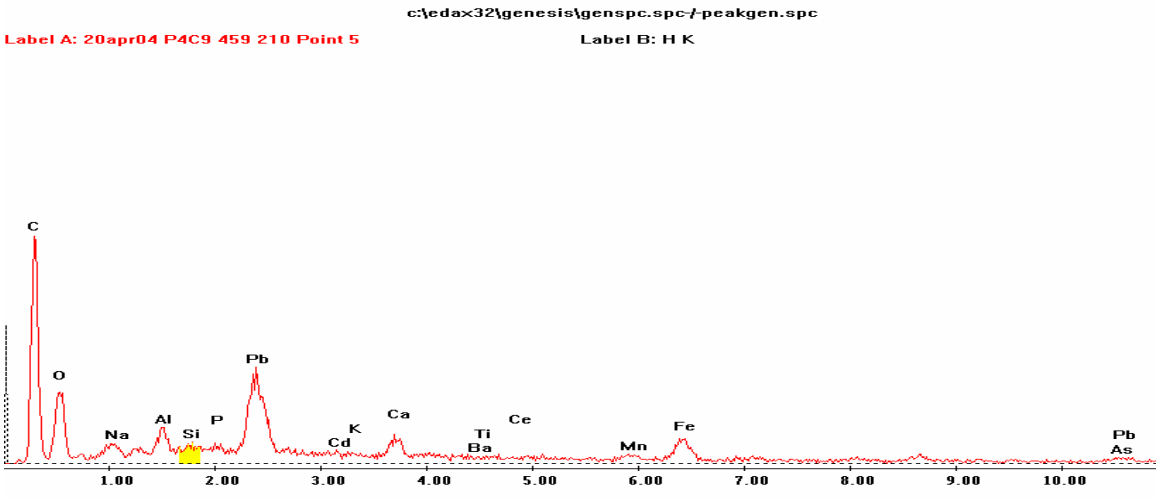

Point 6

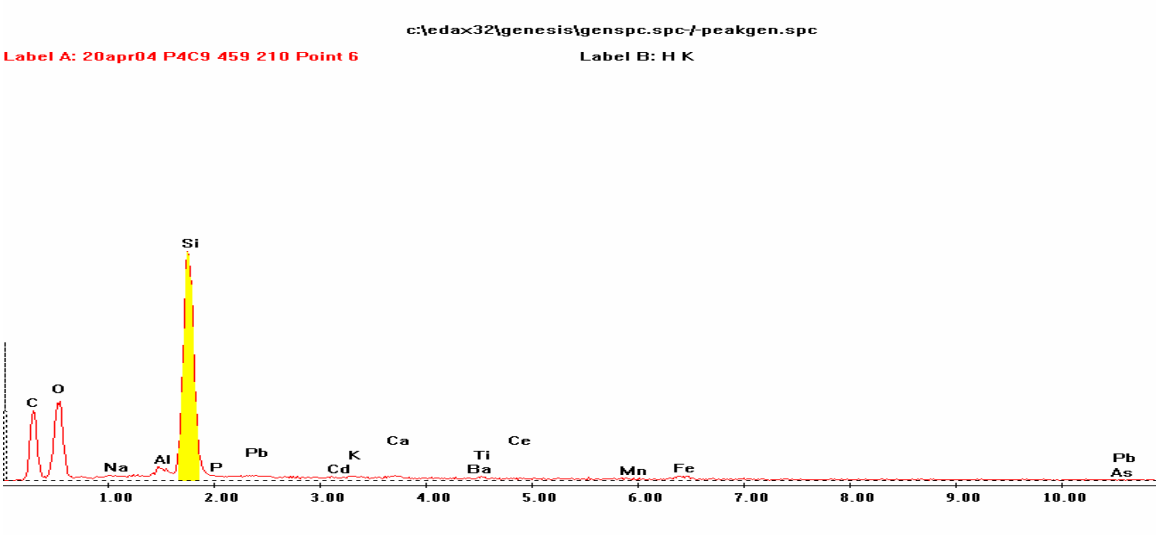

Point 7

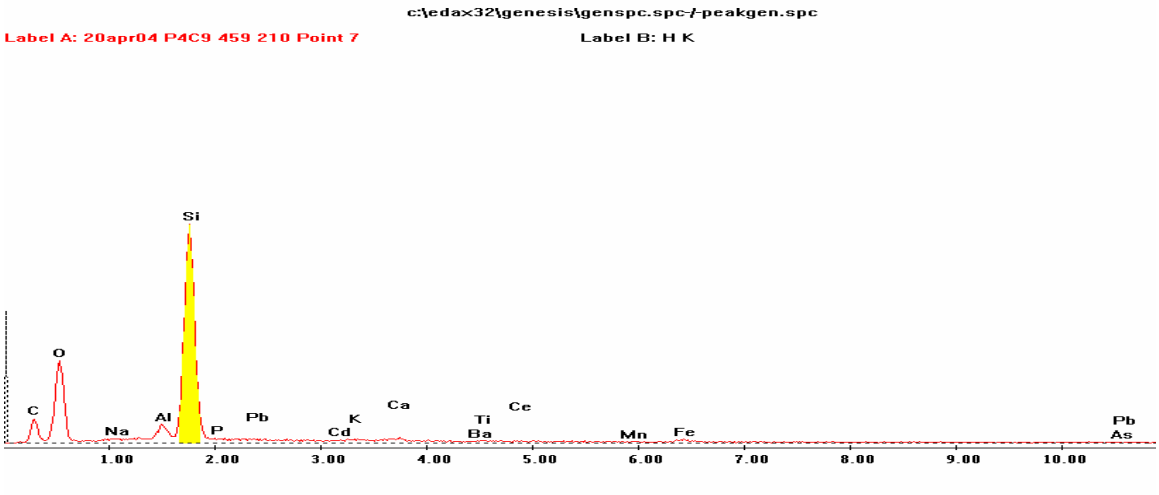

Point 8

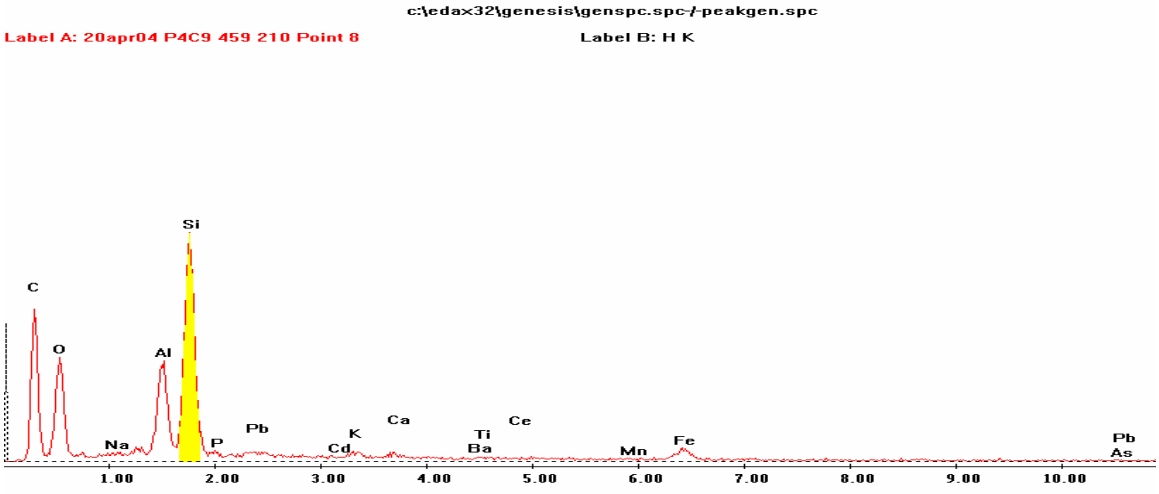

Point 9

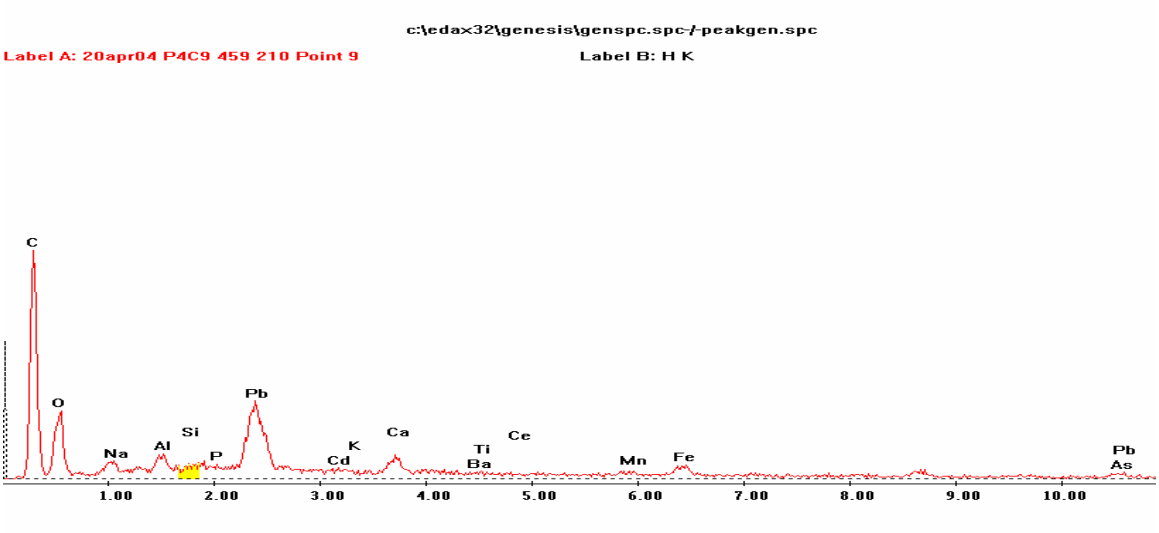

Point 10

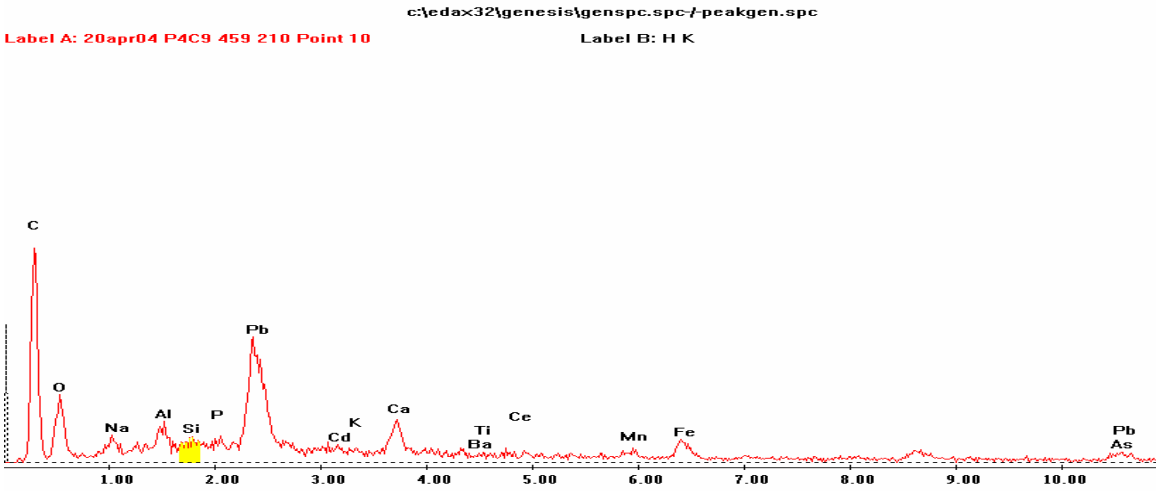

Point 11

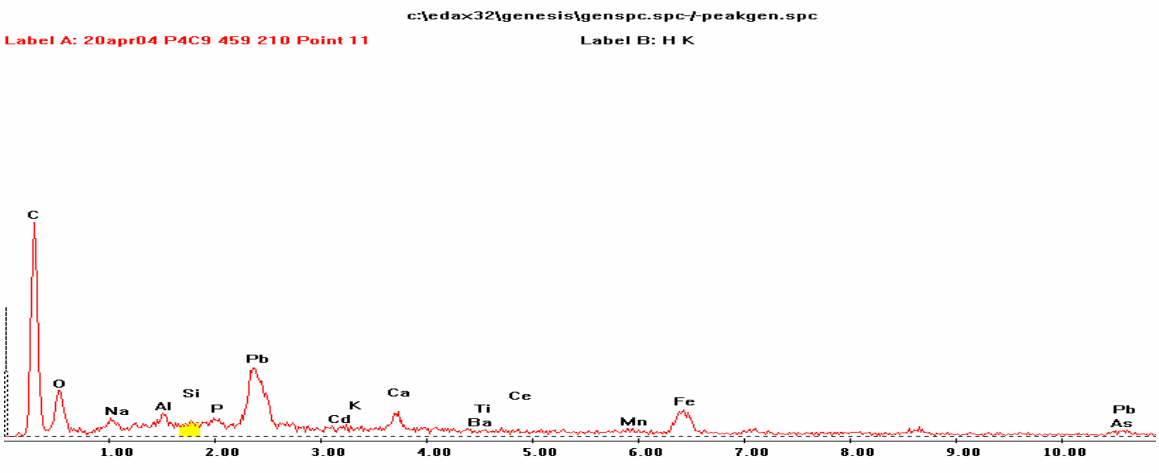

Point 12

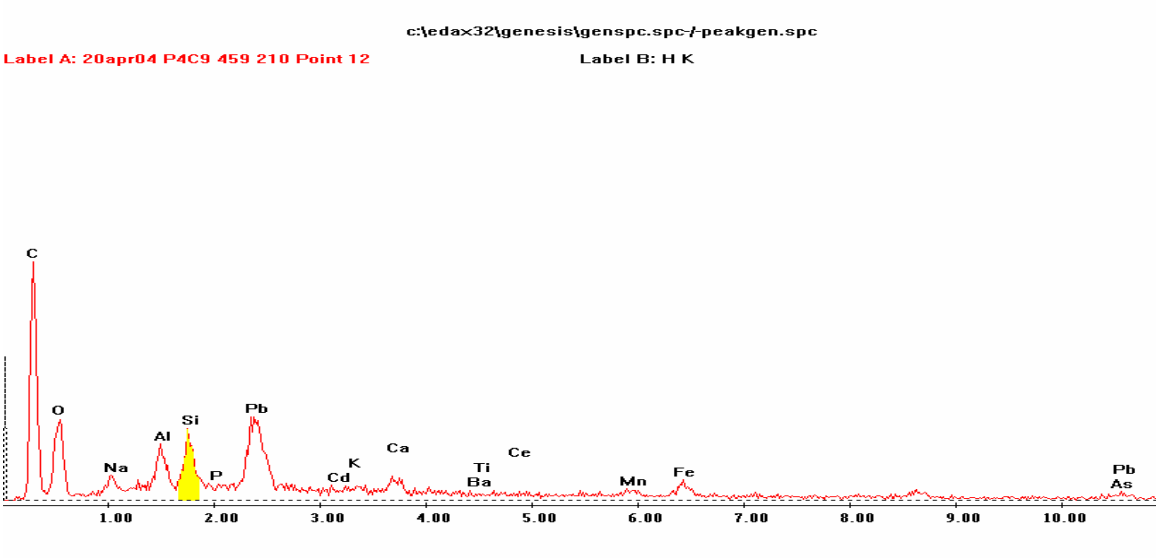

Point 13

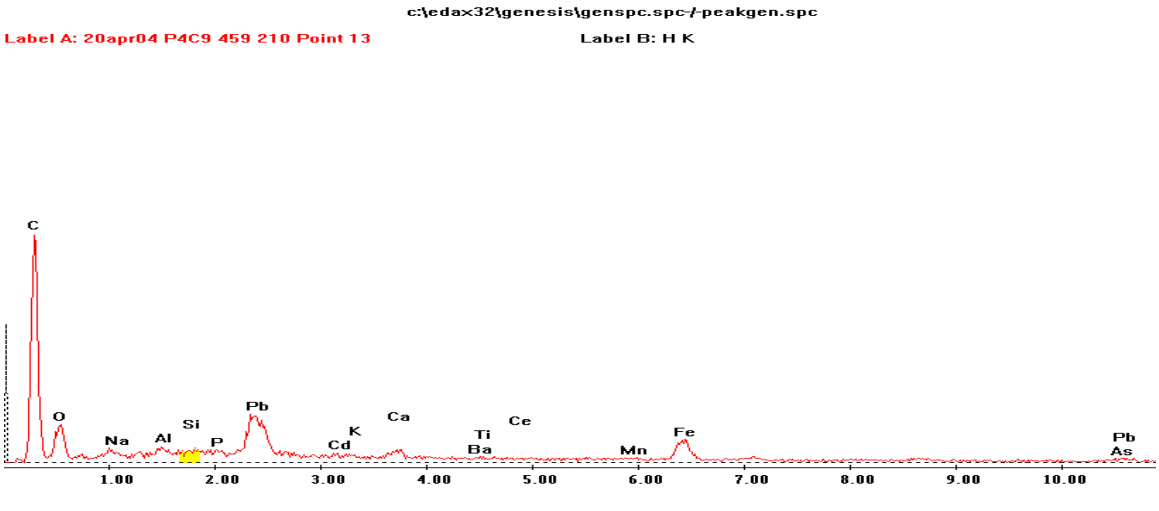

P4C9 – 487, 204

BSE Image

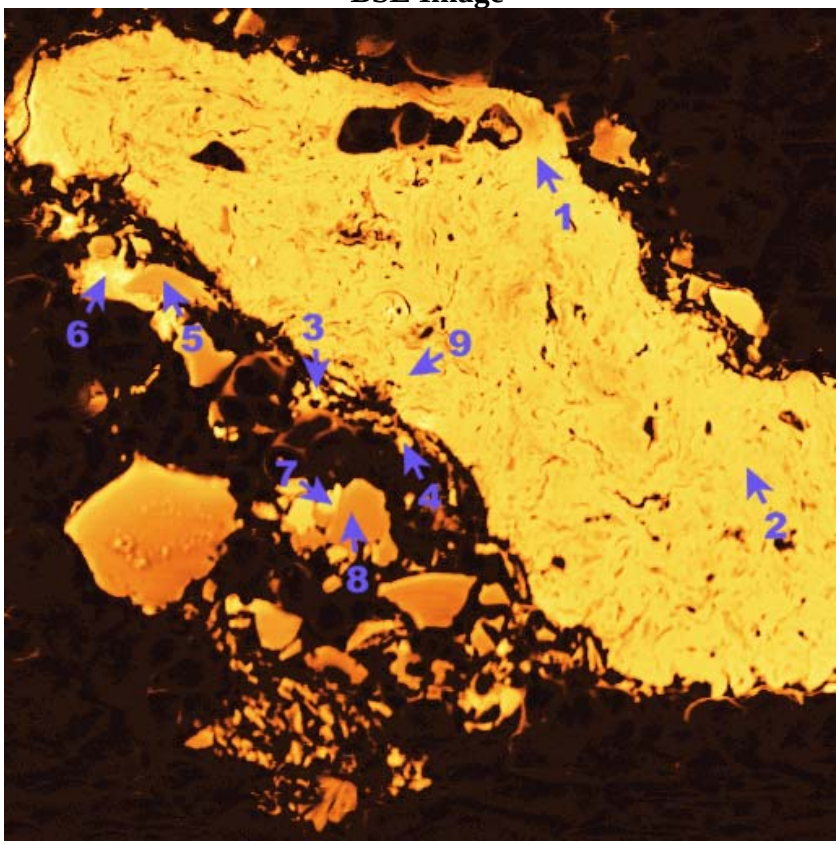

Iron (Fe)

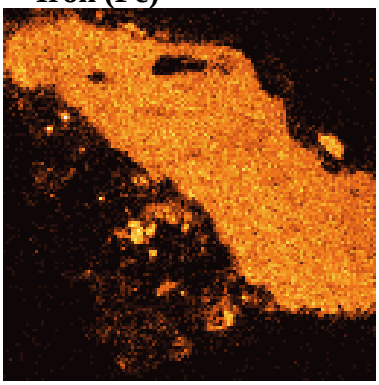

Manganese (Mn)

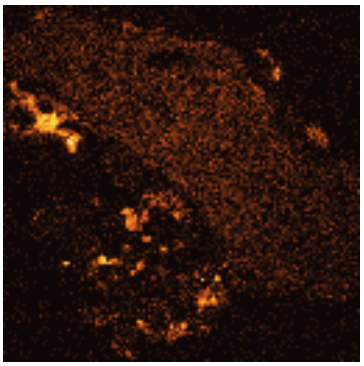

Phosphorous (P)

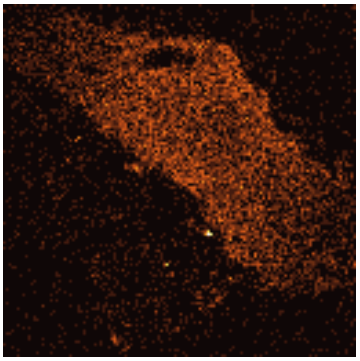

Lead (Pb)

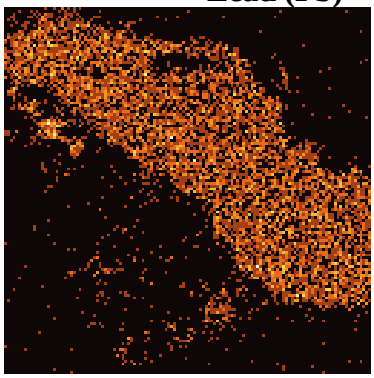

Silicon (Si)

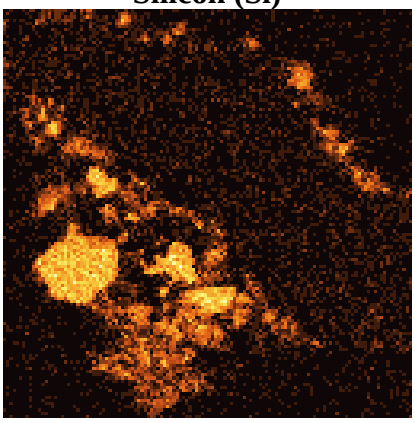

EDS Scan Images by Point

Point 1

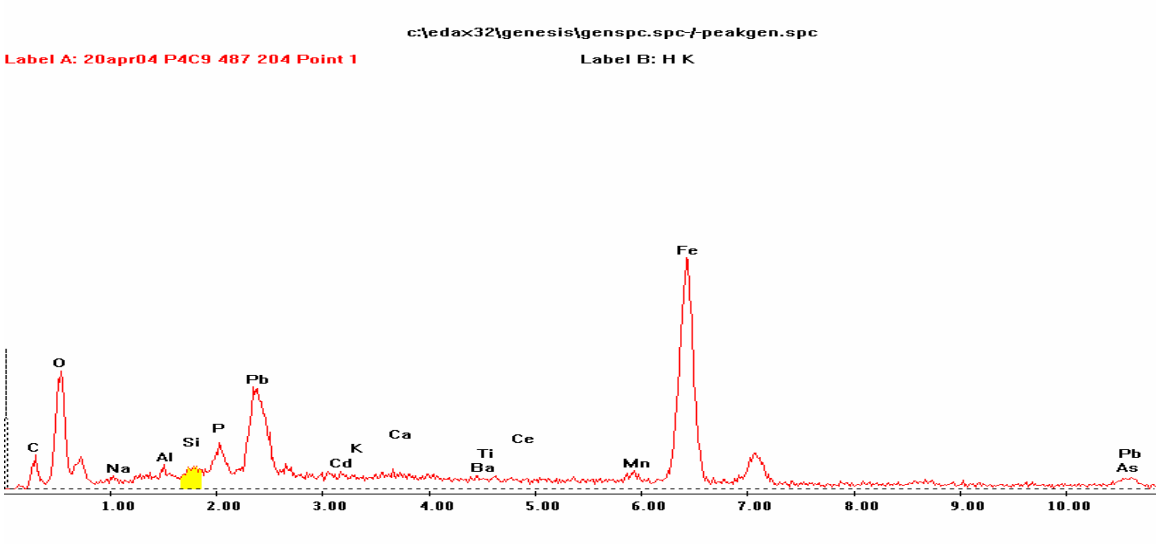

Point 2

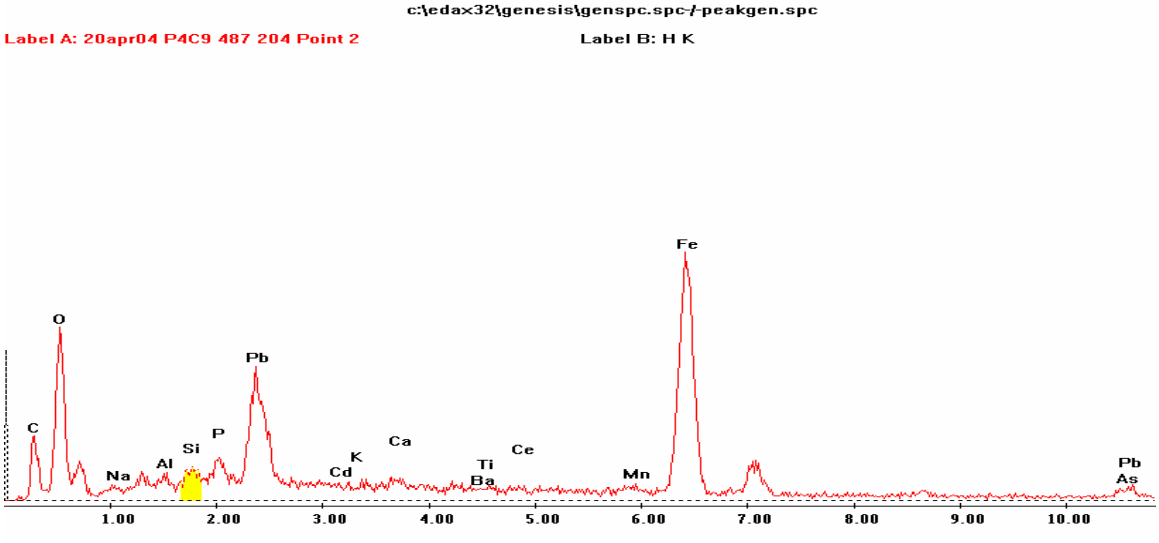

Point 3

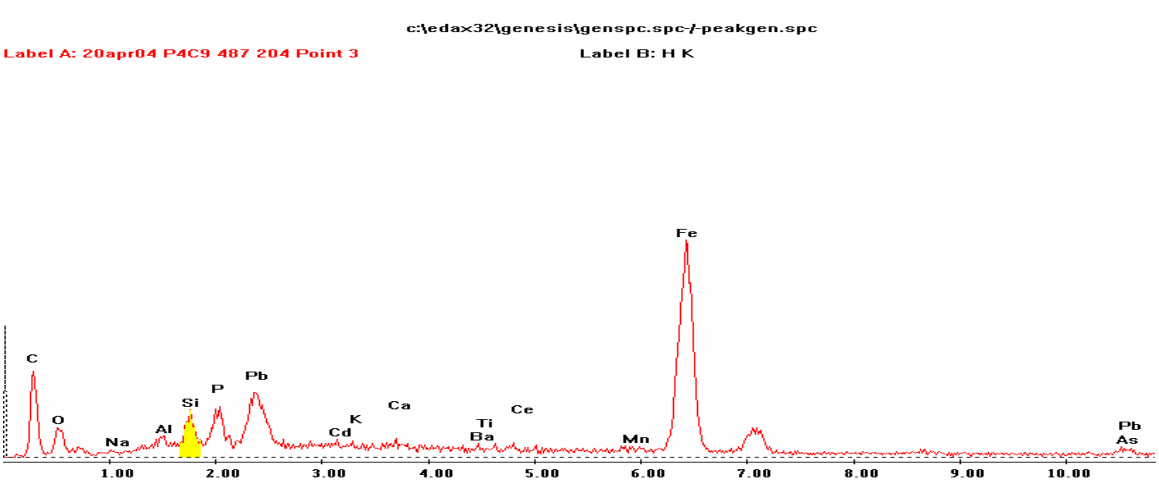

Point 4

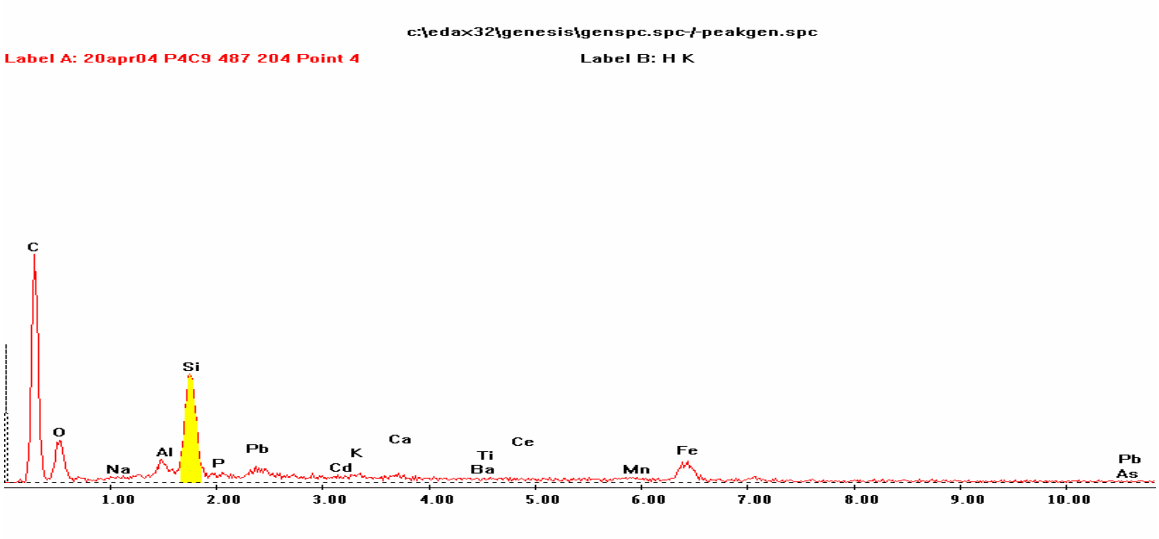

Point 5

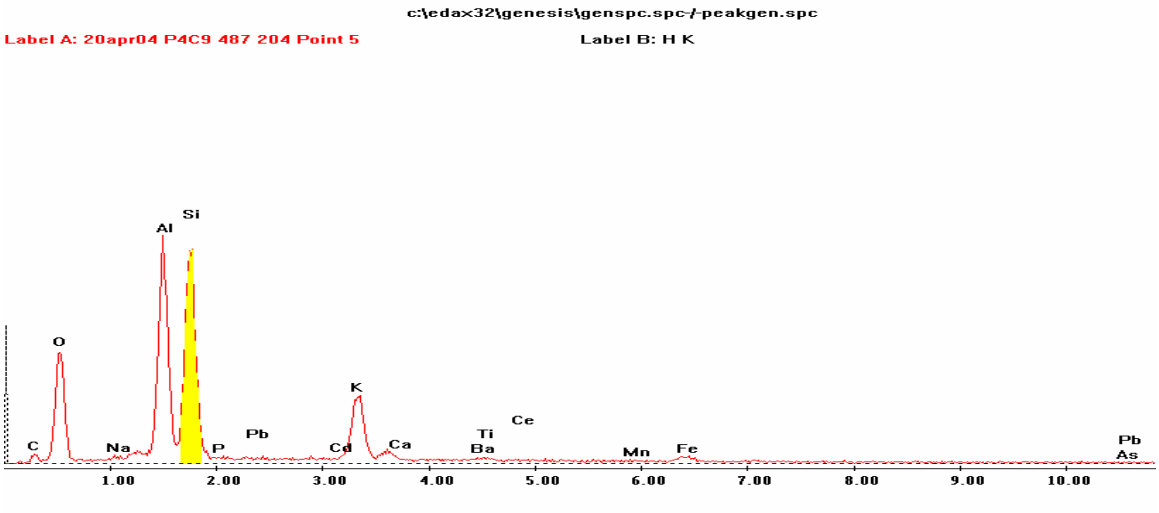

Point 6

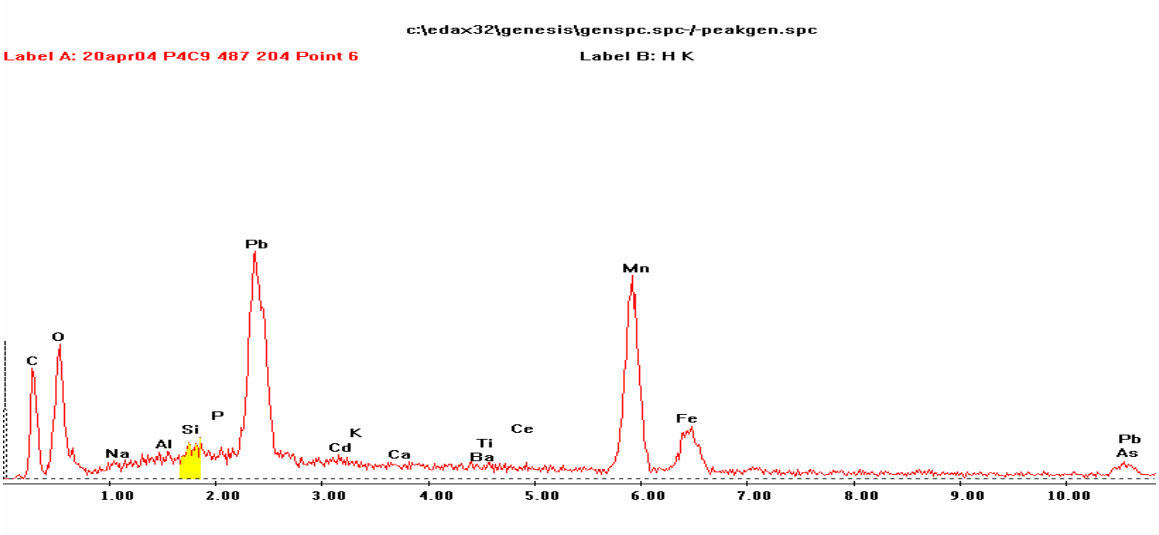

Point 7

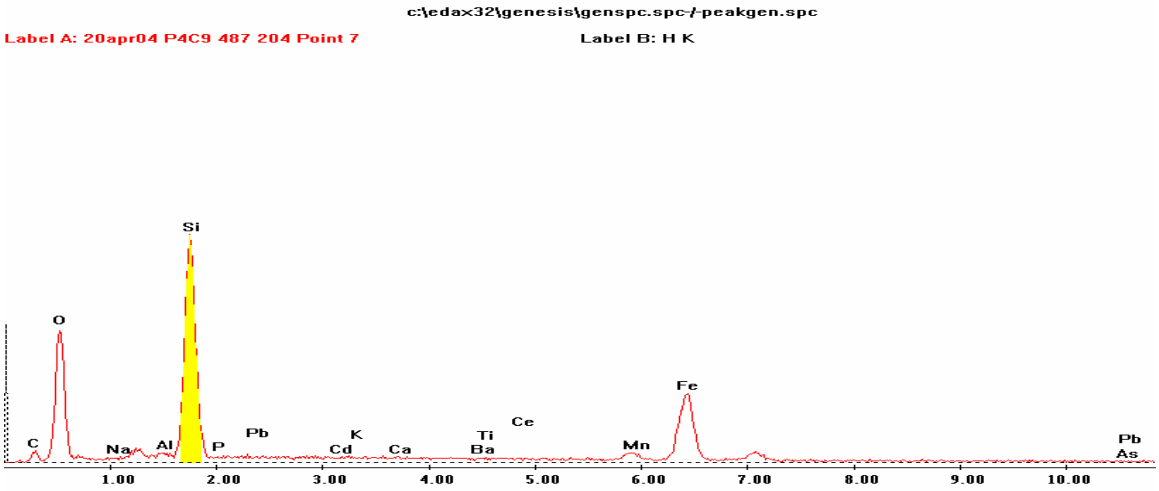

Point 8

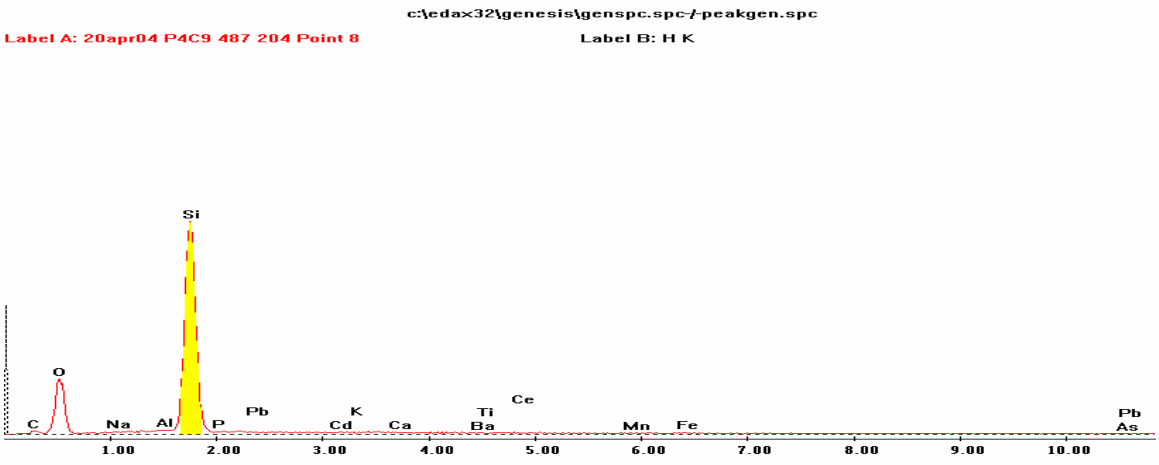

Point 9

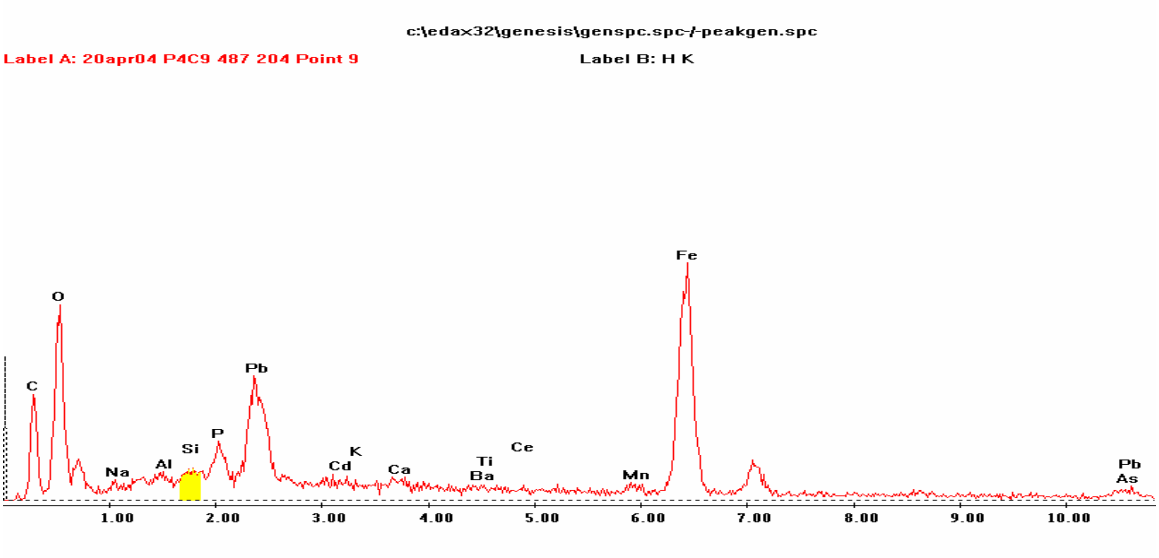

Plot 6

P6C7 – 312, 242

BSE Image

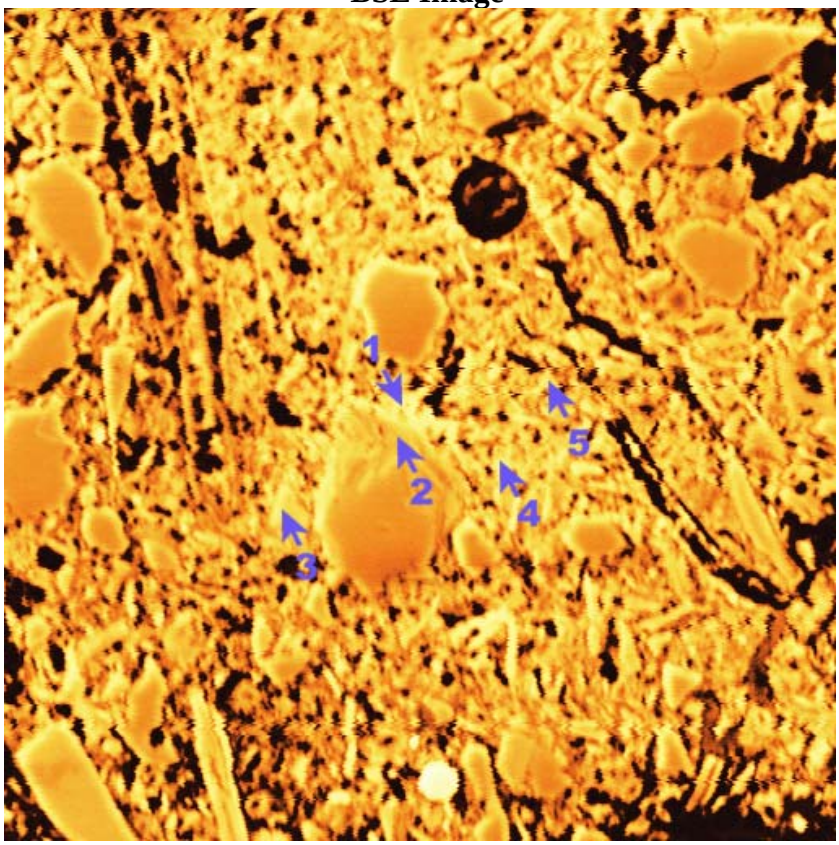

Iron (Fe)

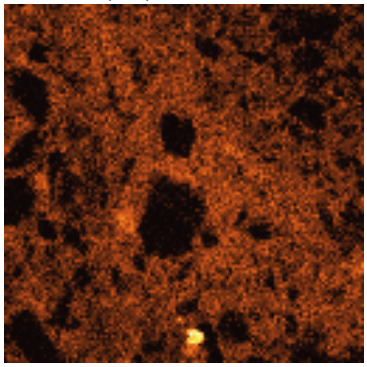

Manganese (Mn)

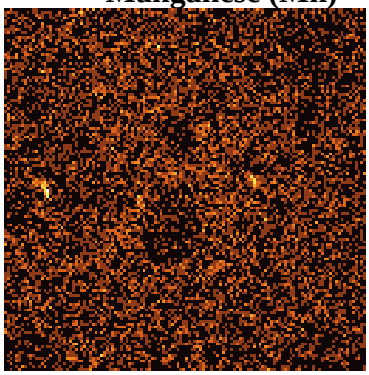

Phosphorous (P)

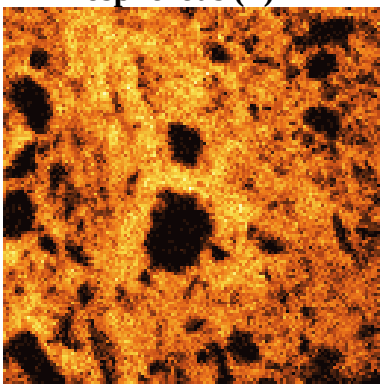

Lead (Pb)

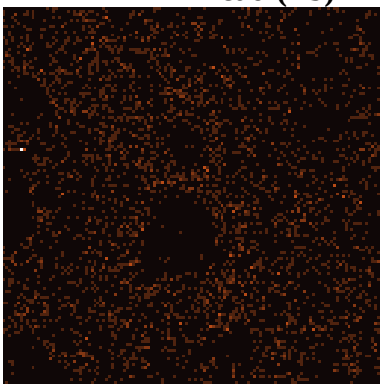

Silicon (Si)

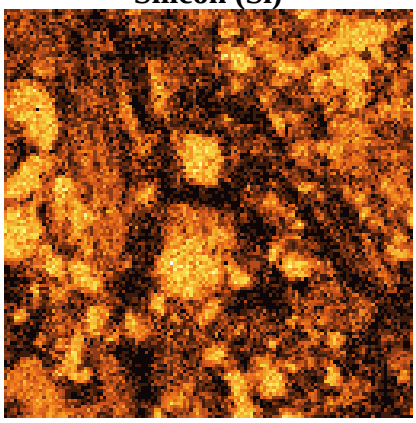

EDS Scan Images by Point

Point 1

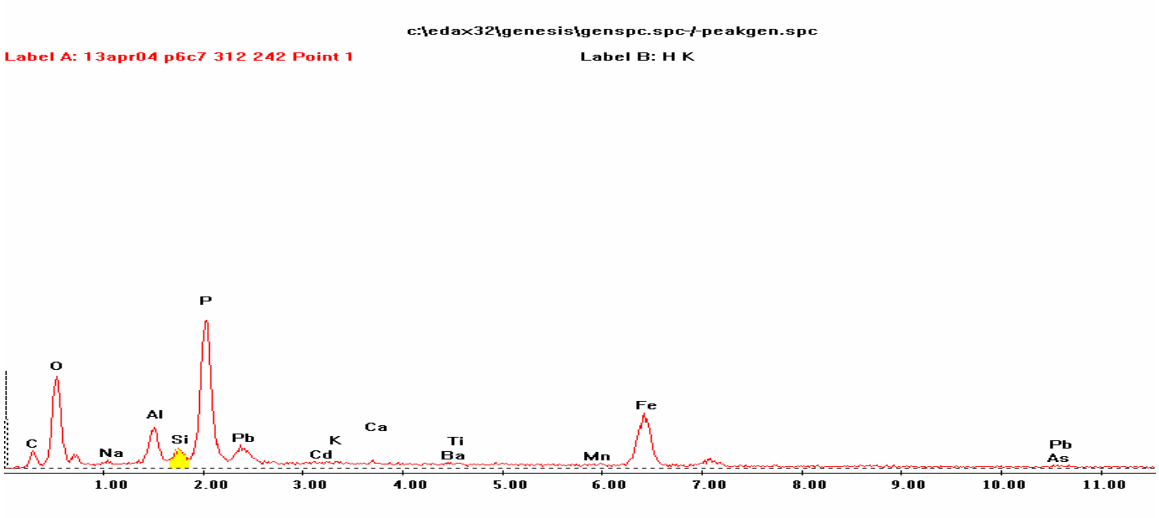

Point 2

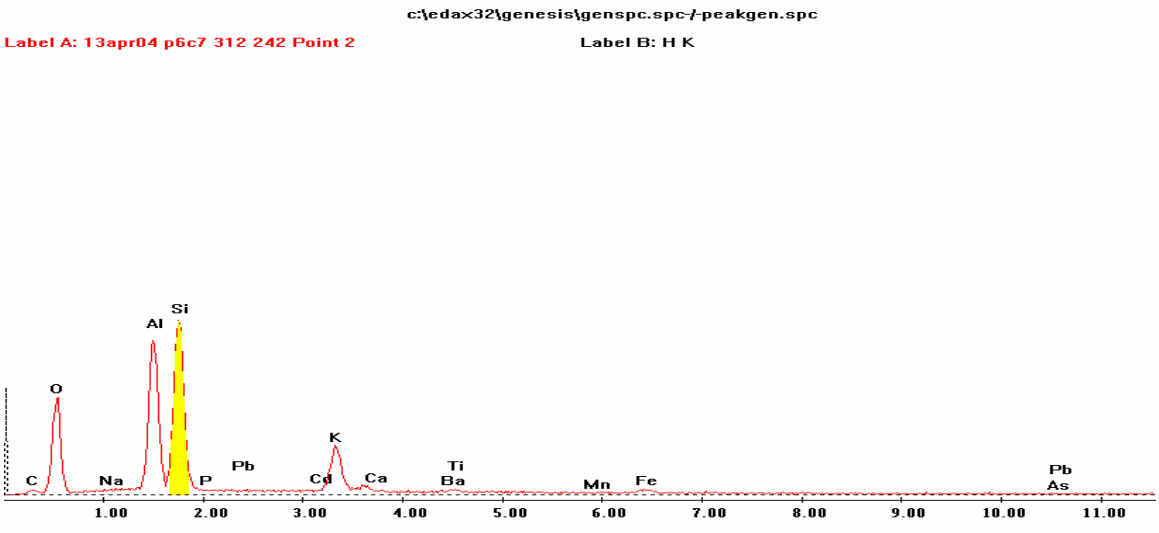

Point 3

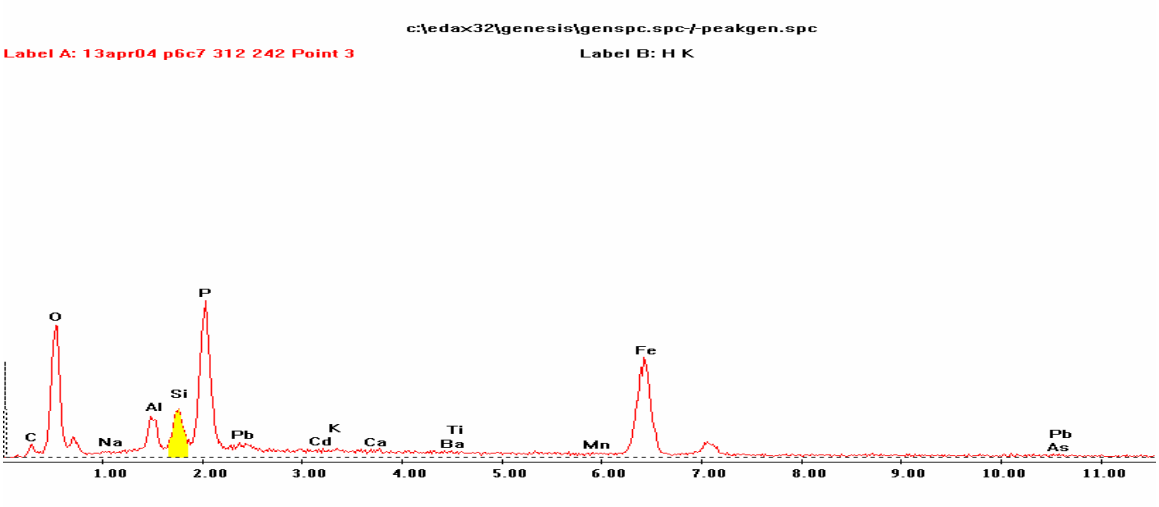

Point 4

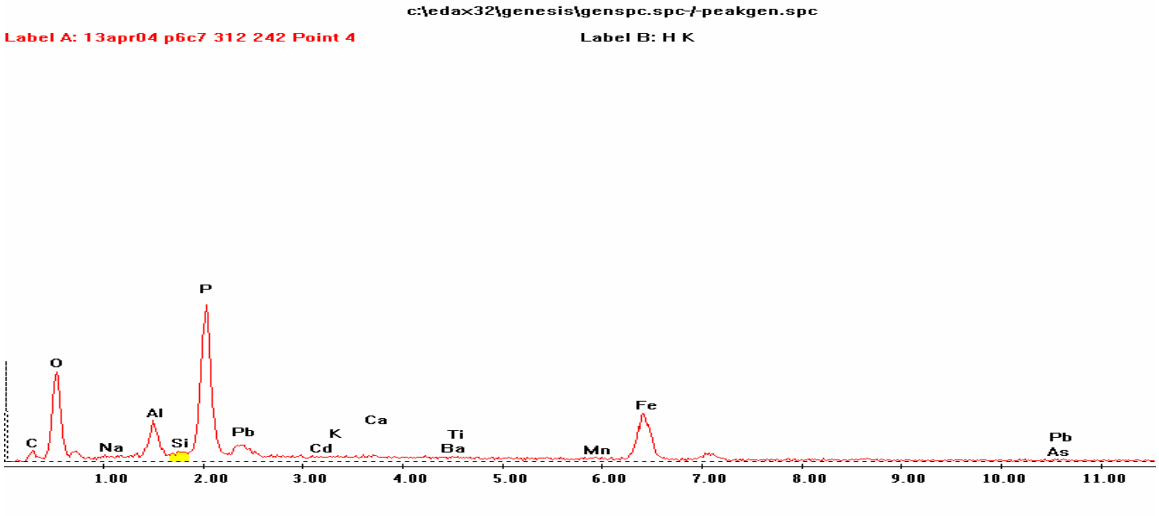

Point 5

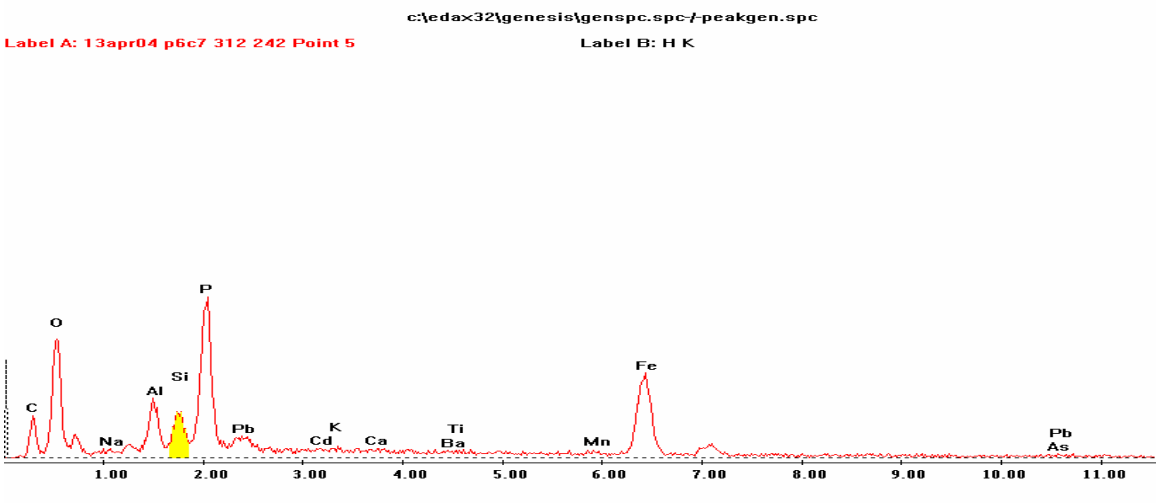

Point 6

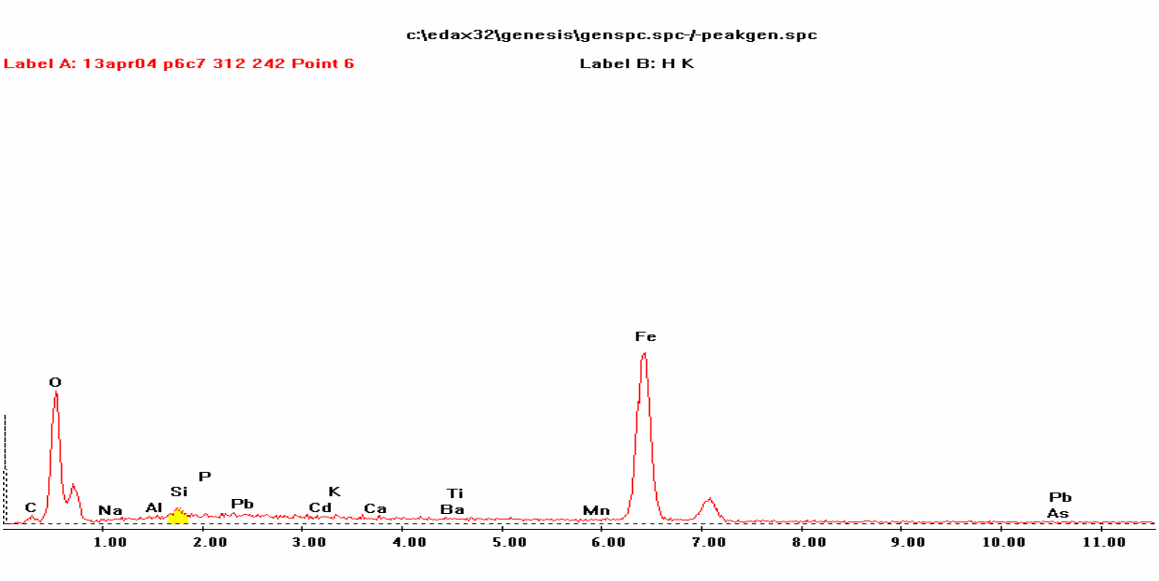
c:\edax32\genesis\genspc.spc-/-peakgen.spc
Label A: 13apr04 p6c7 312 242 Point 6
Label B: H K
O
C
Na
Al
Si
P
Pb
K
Cd
Ca
Ti
Ba
Mn
Fe
Pb
As
1.00
2.00
3.00
4.00
5.00
6.00
7.00
8.00
9.00
10.00
11.00

P6C7 – 344, 248

BSE Image

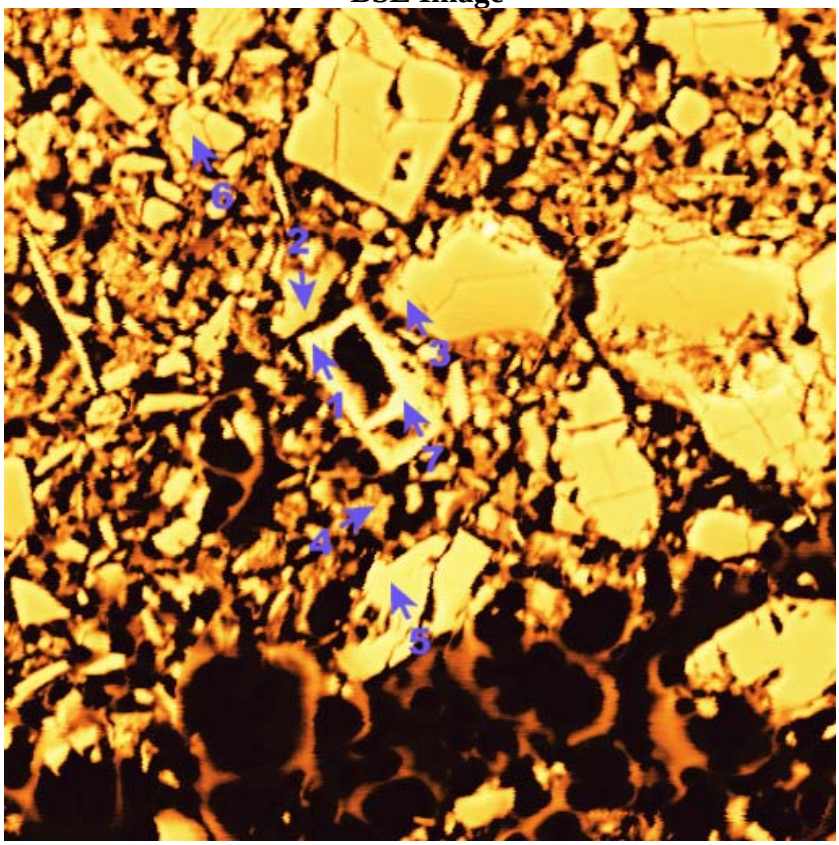

Iron (Fe)

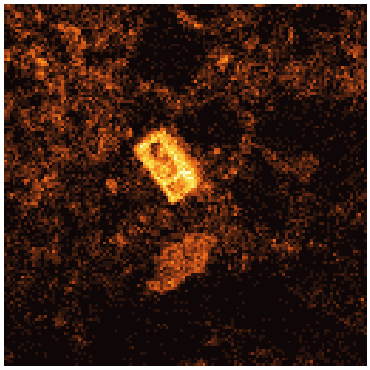

Manganese (Mn)

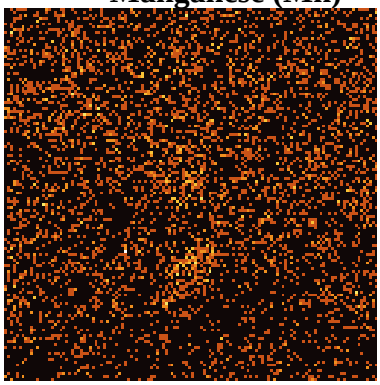

Phosphorous (P)

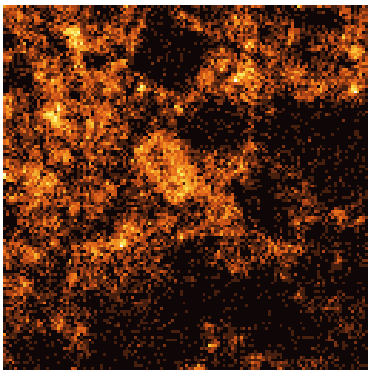

Lead (Pb)

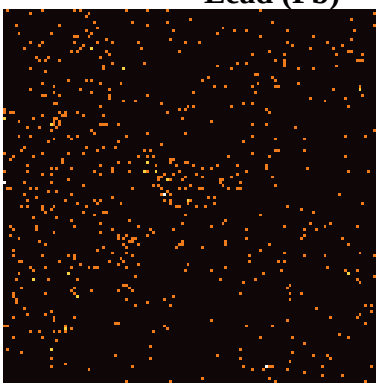

Silicon (Si)

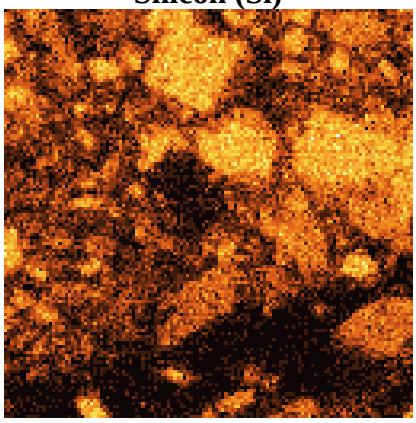

EDS Scan Images by Point

Point 1

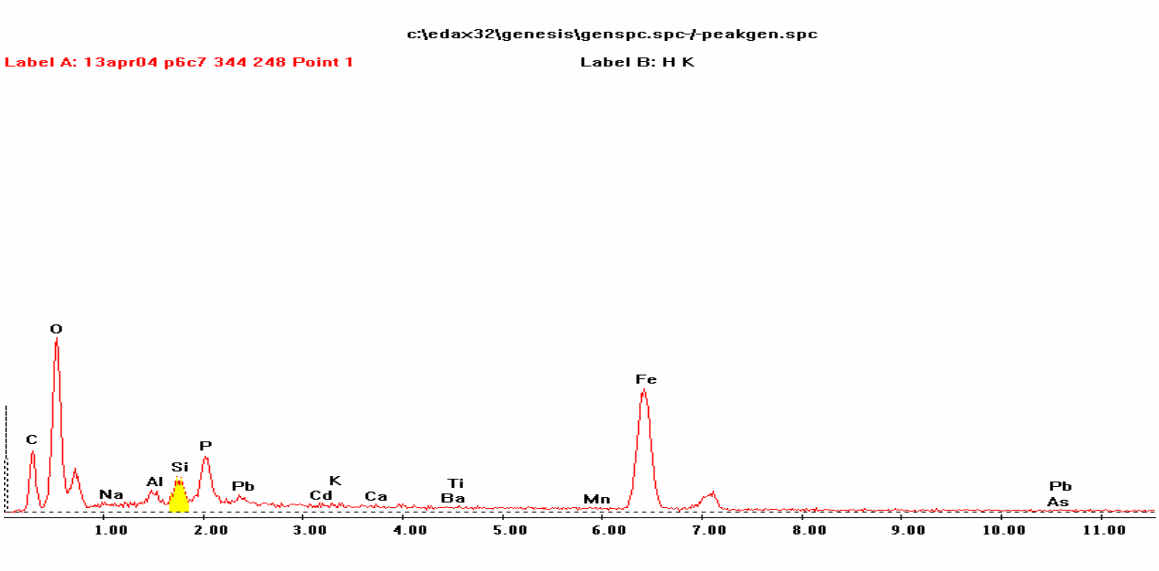

Point 2

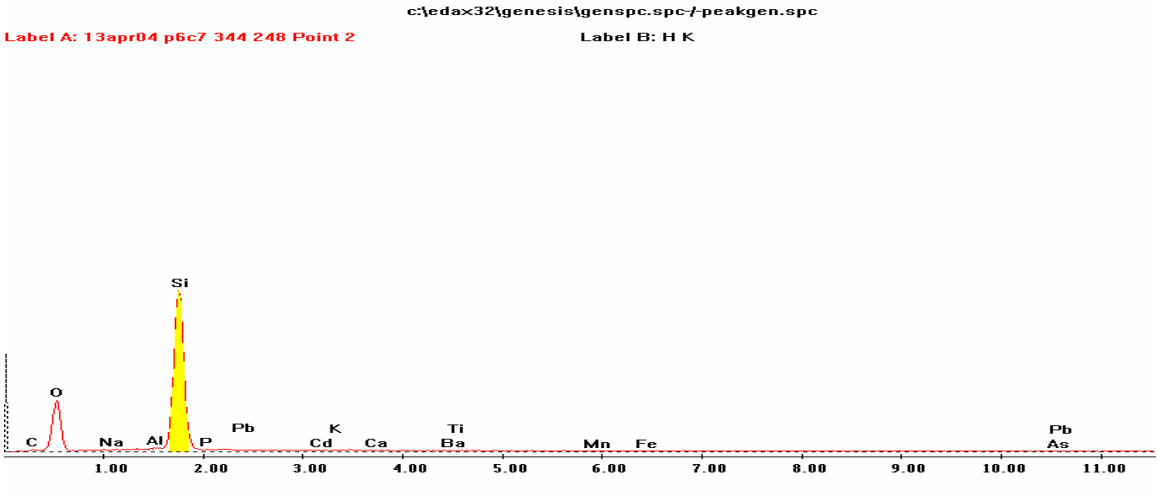

Point 3

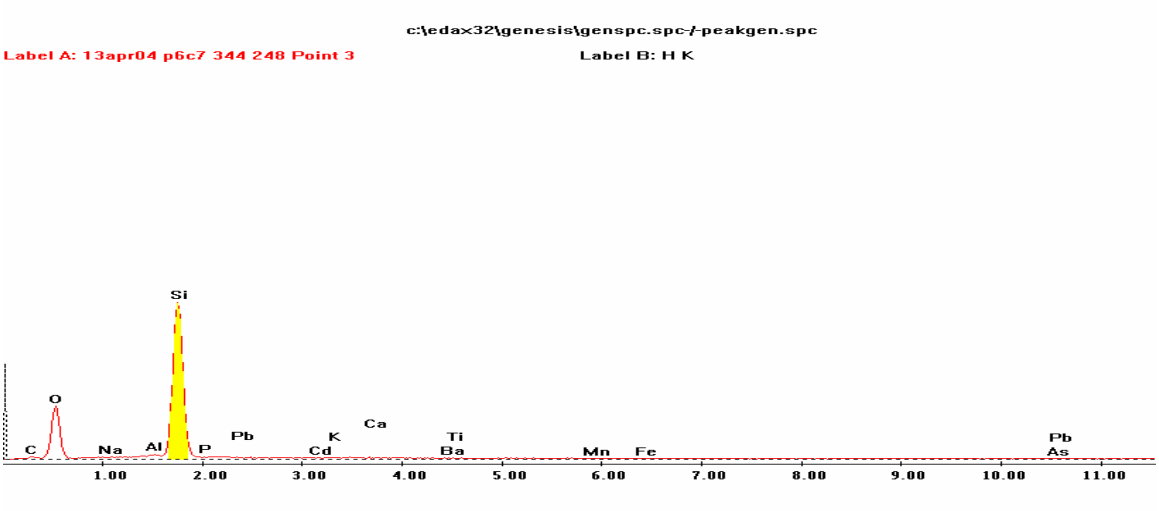

Point 4

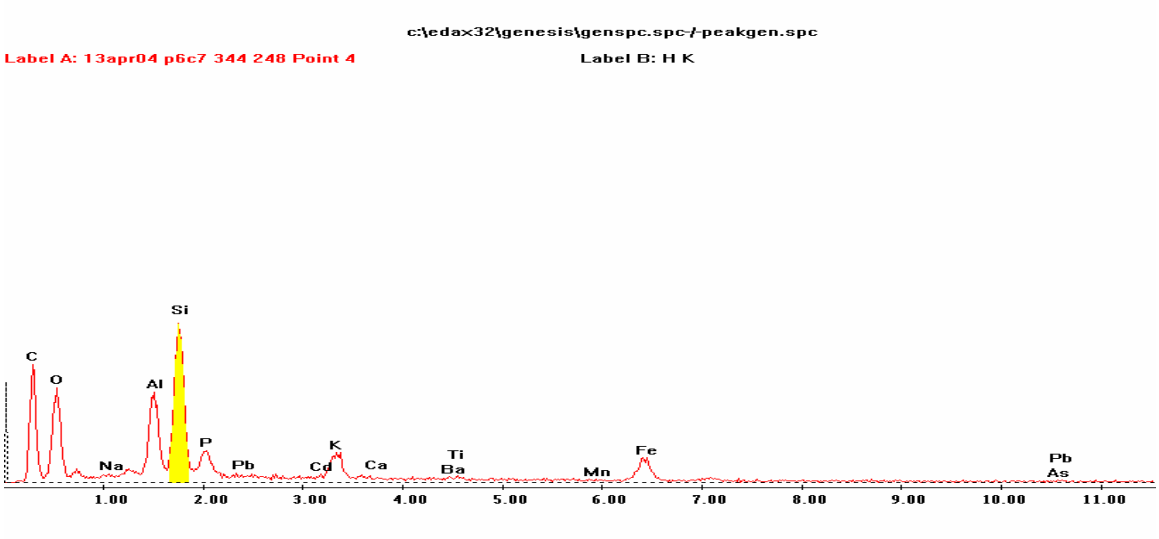

Point 5

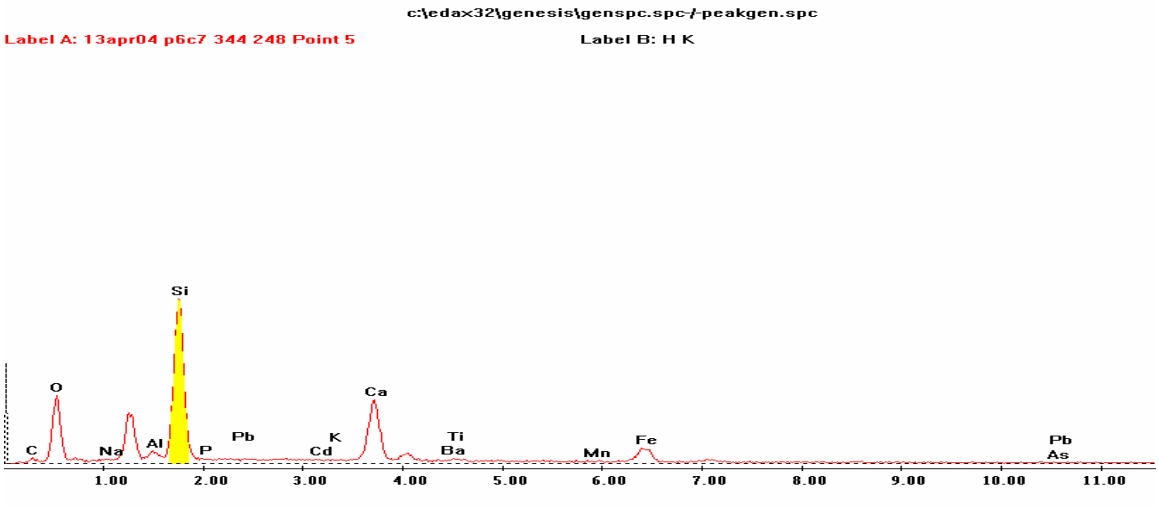

Point 6

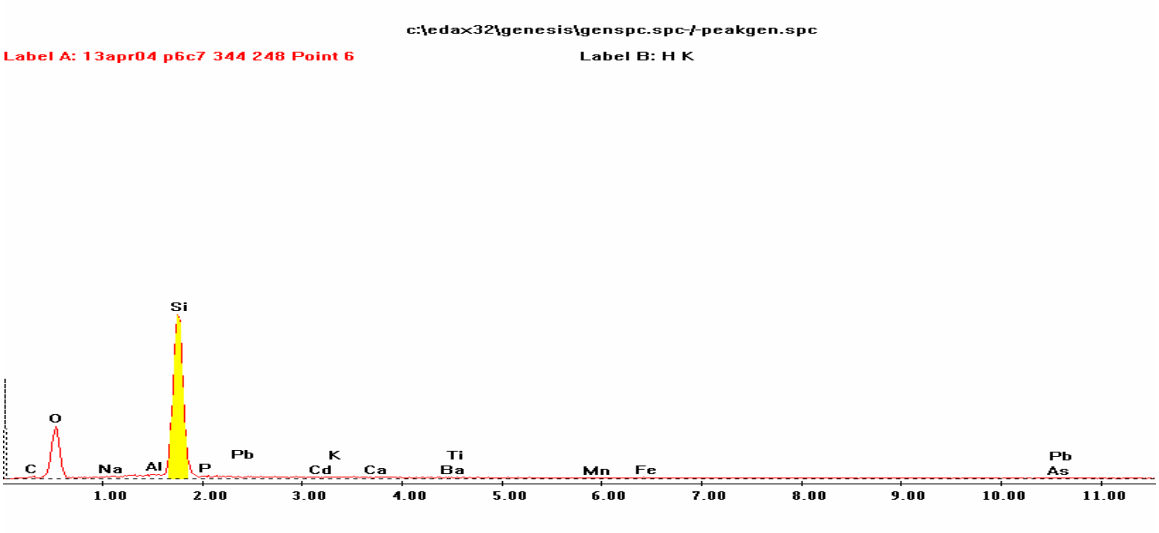

Point 7

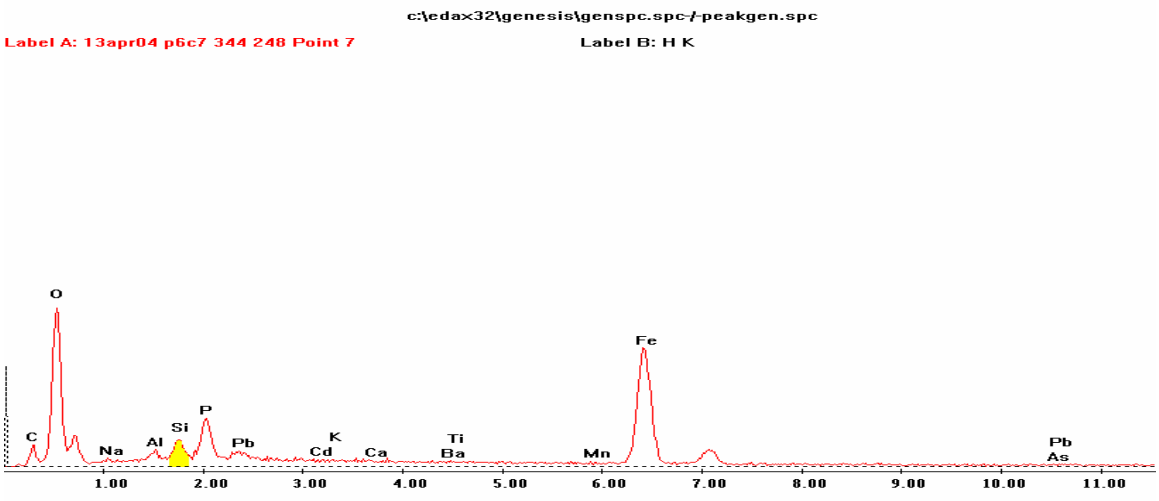

P6C7 – 356, 231

BSE Image

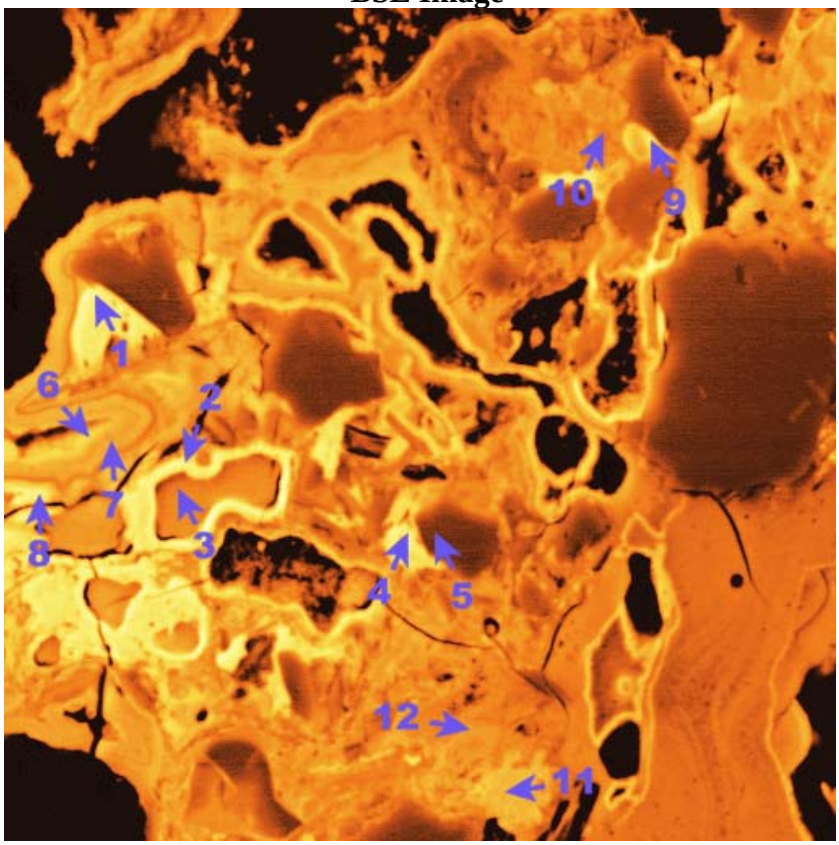

Iron (Fe)

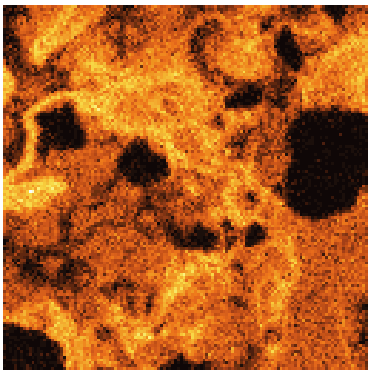

Manganese (Mn)

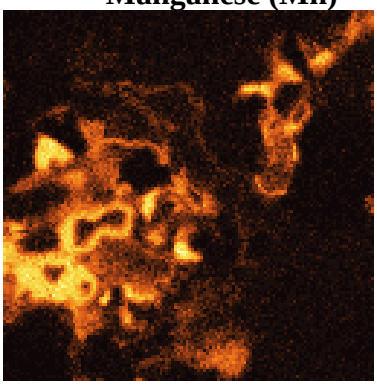

Phosphorous (P)

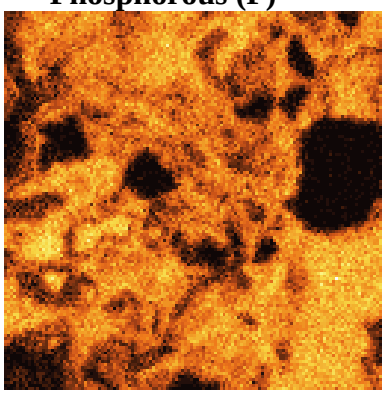

Lead (Pb)

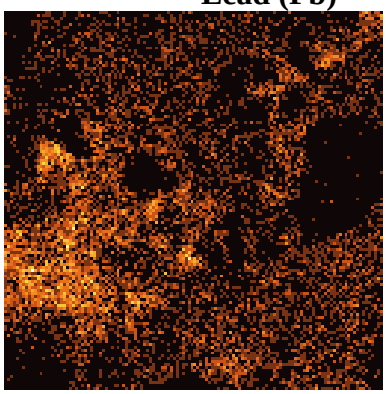

Silicon (Si)

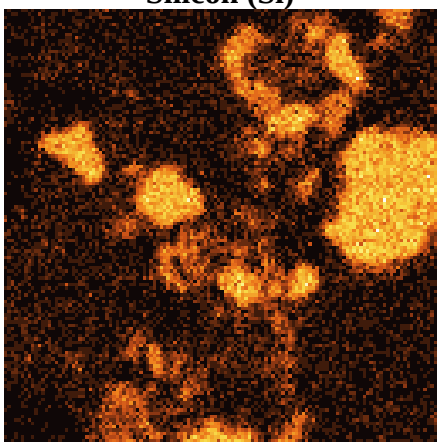

EDS Scan Images by Point

Point 1

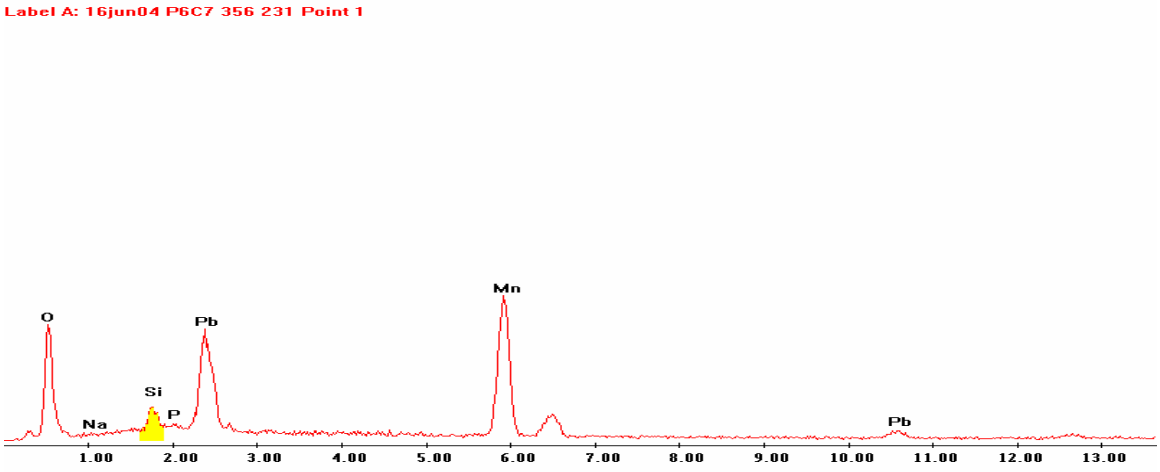

Point 2

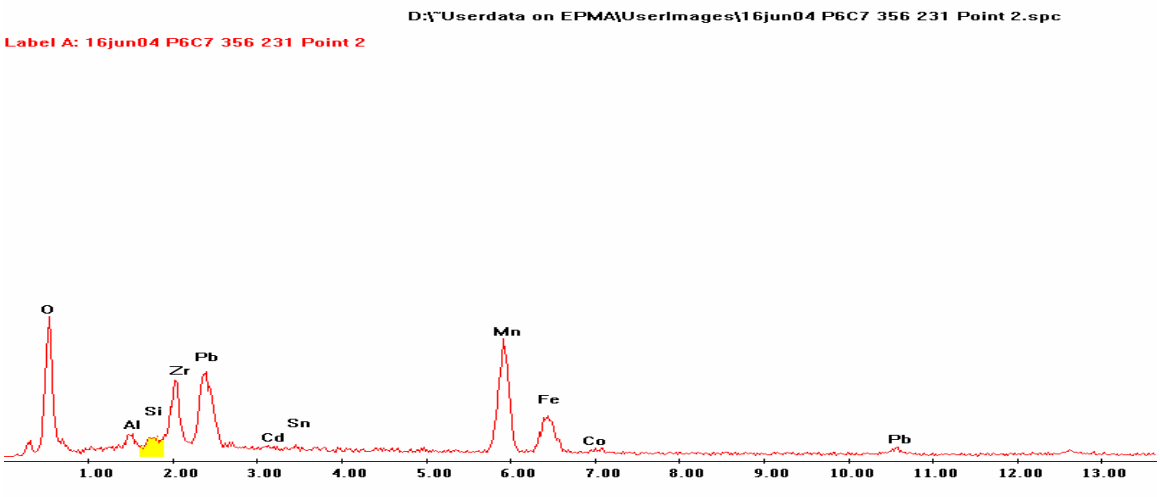

Point 3

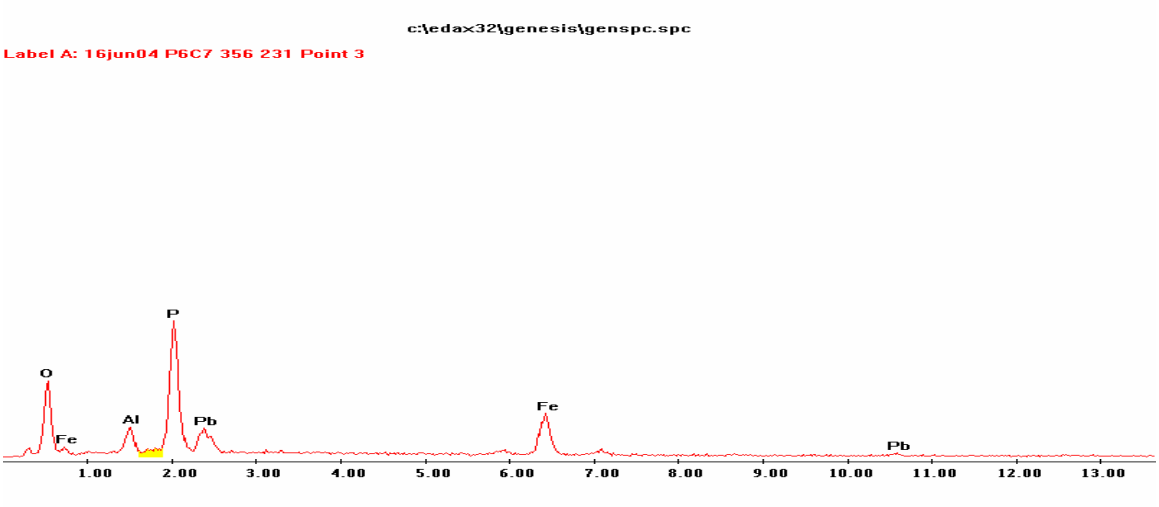

Point 4

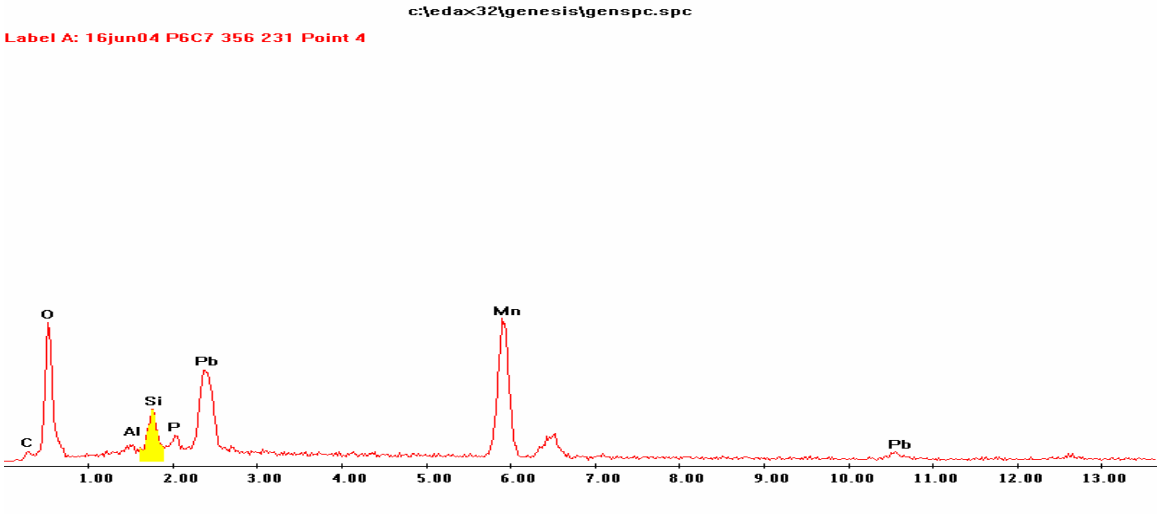

Point 5

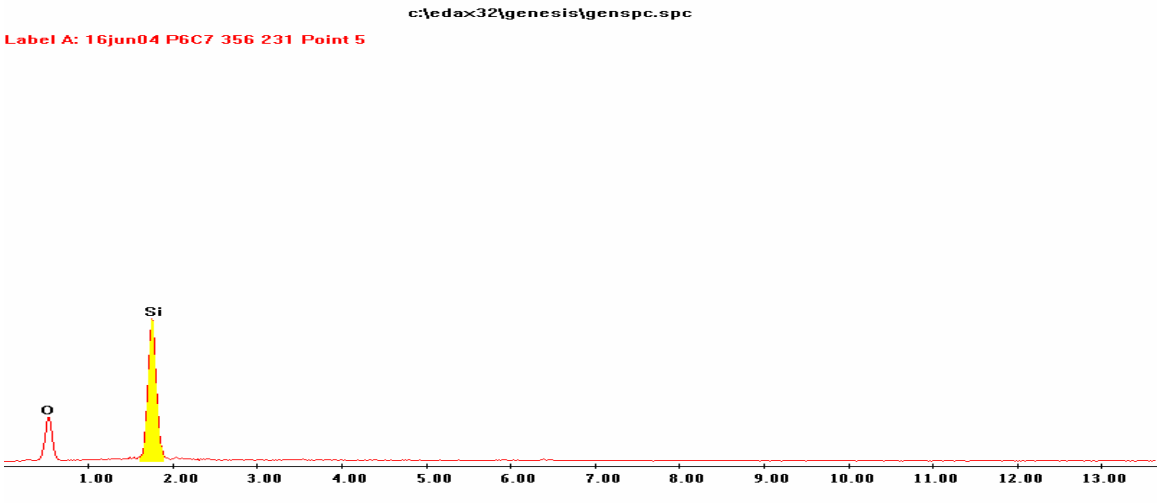

Point 6

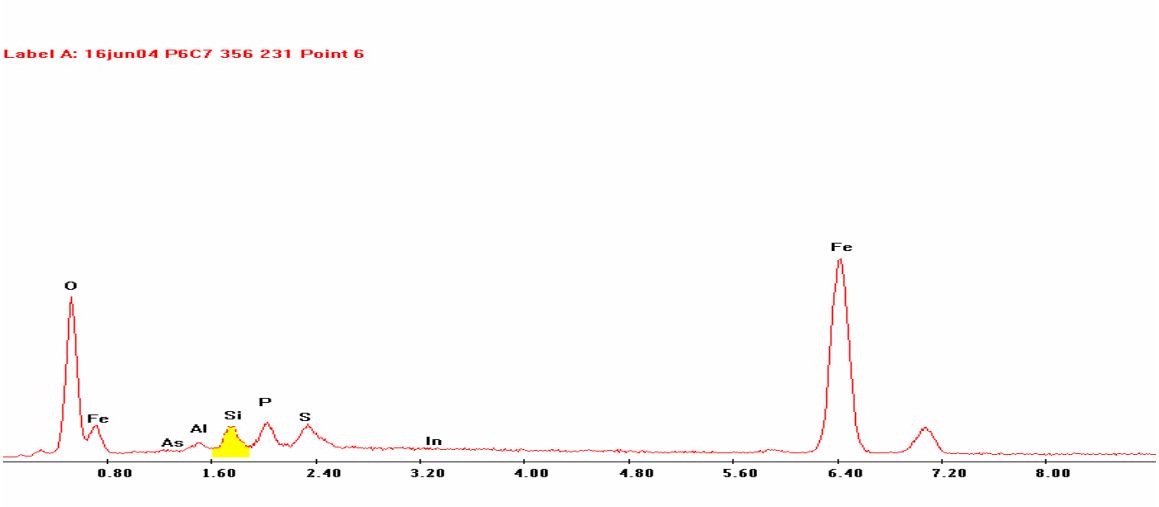

Point 7

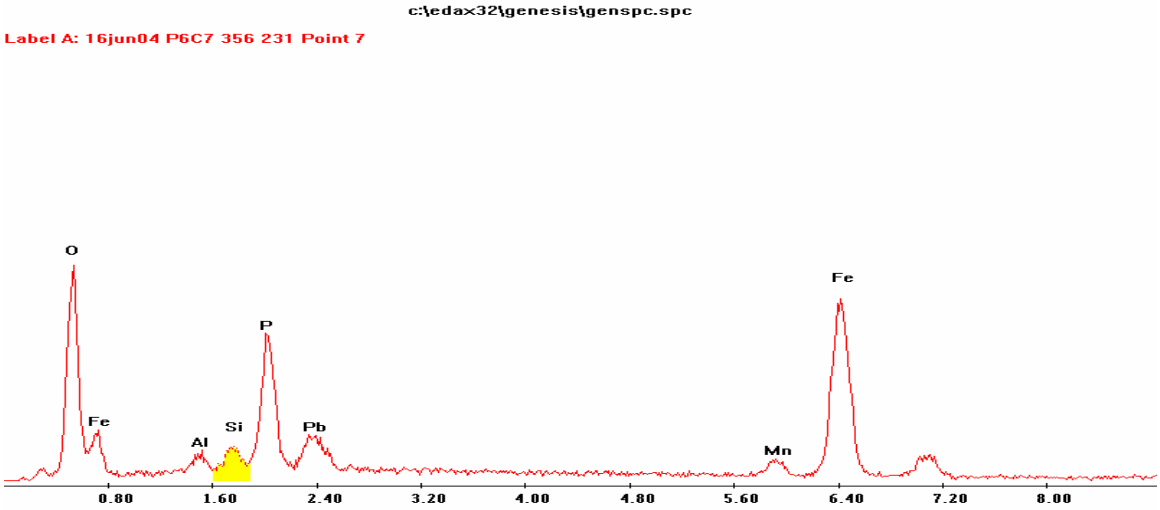

Point 8

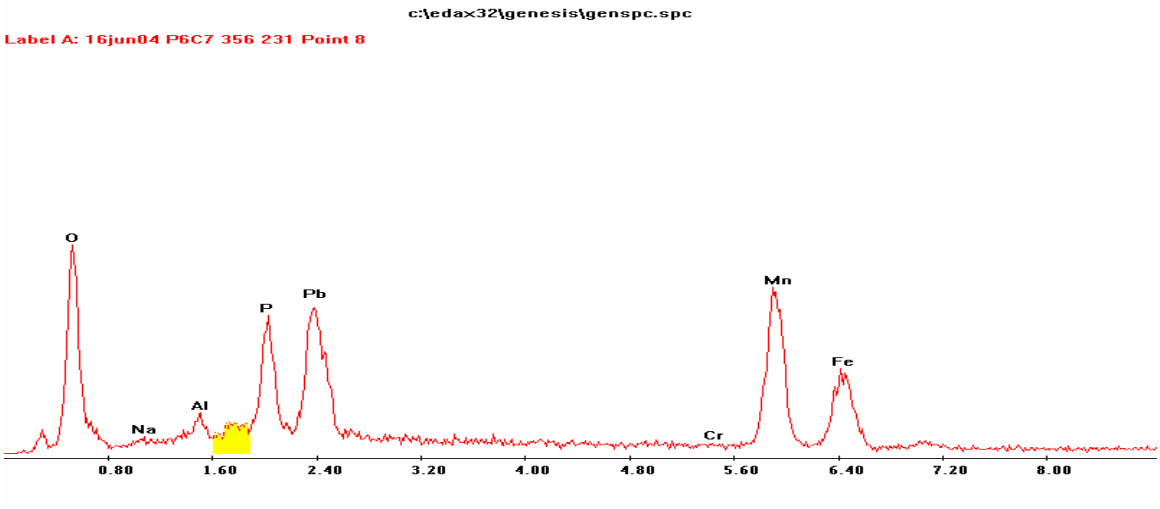

Point 9

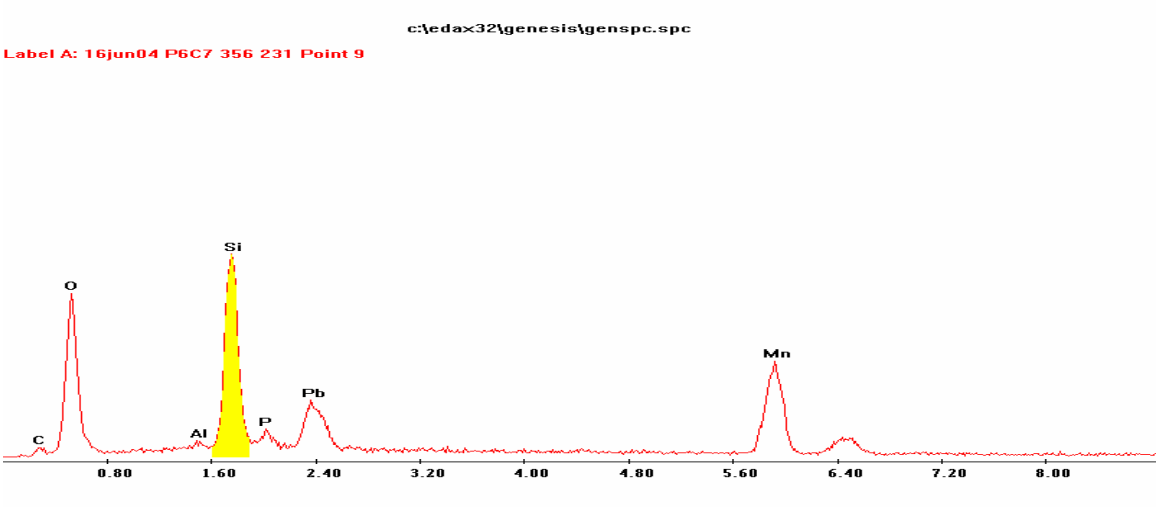

Point 10

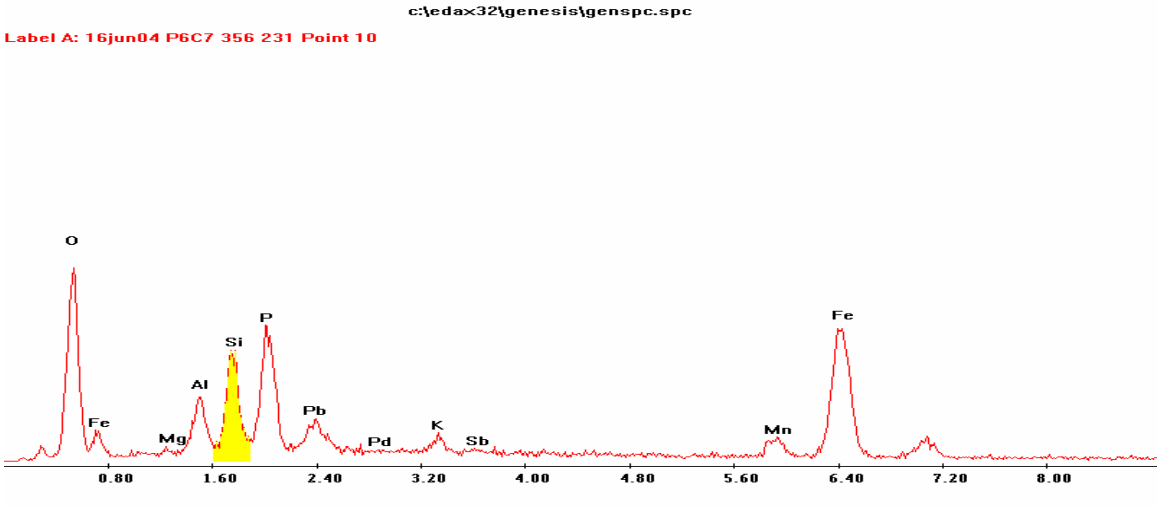

Point 11

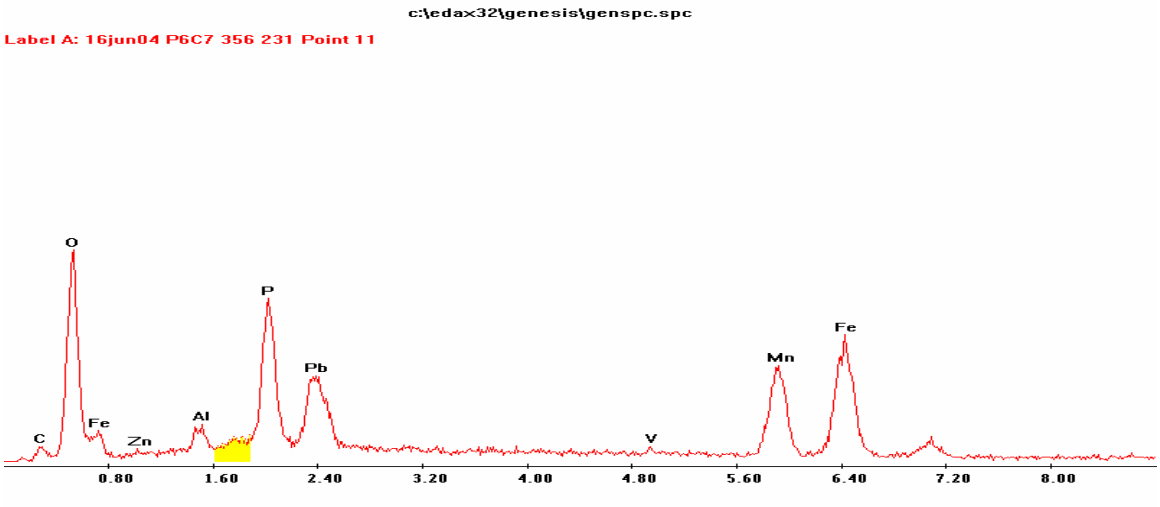

Point 12

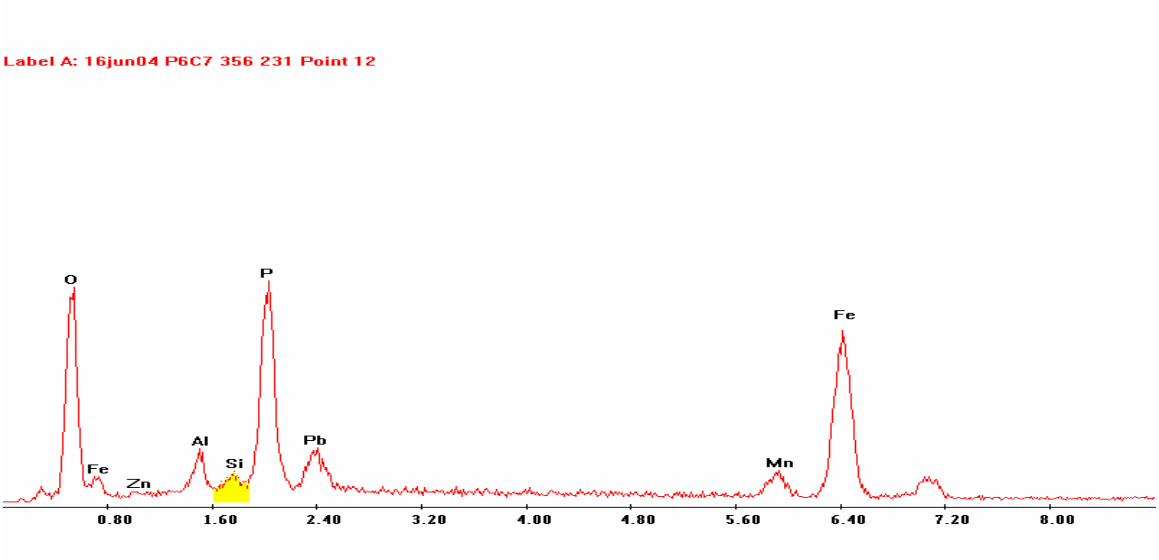
Label A: 16jun04 P6C7 356 231 Point 12
O
Fe
Zn
Al
Si
P
Pb
Mn
Fe
0.80
1.60
2.40
3.20
4.00
4.80
5.60
6.40
7.20
8.00

P6C7 – 358, 261

BSE Image

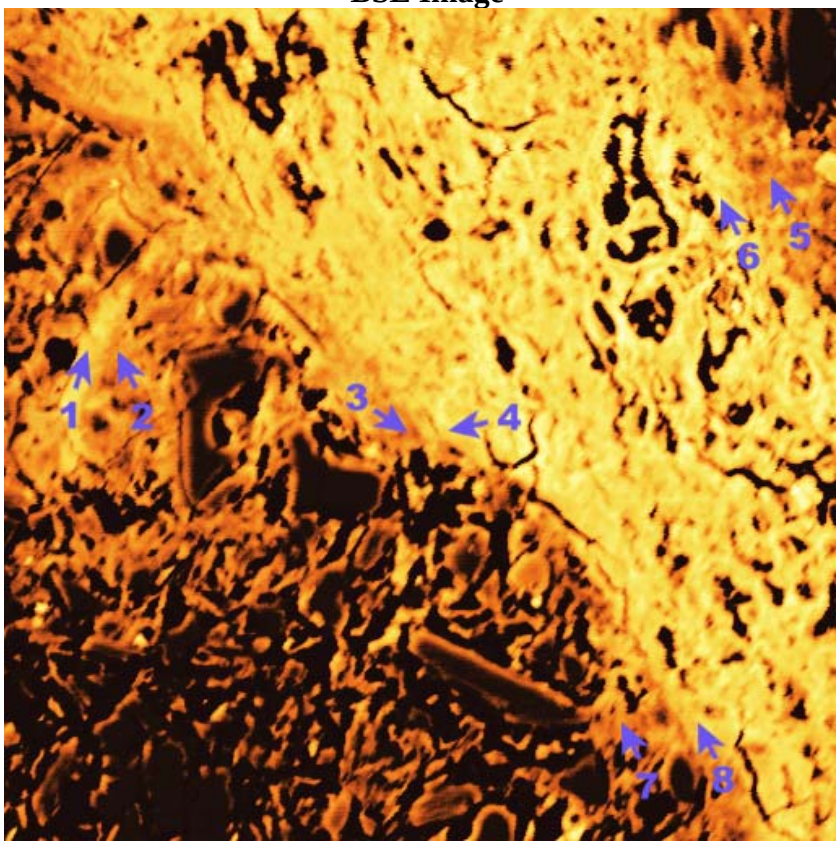

Iron (Fe)

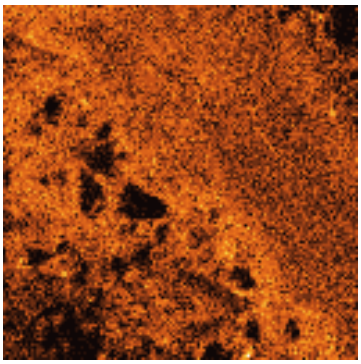

Manganese (Mn)

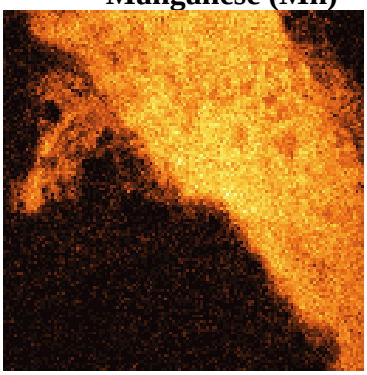

Phosphorous (P)

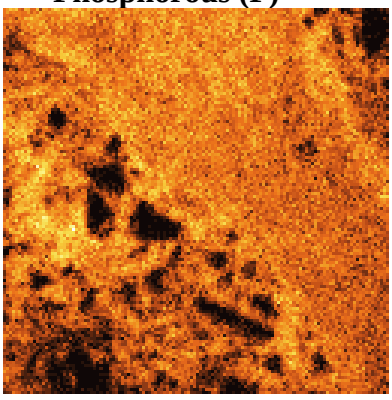

Lead (Pb)

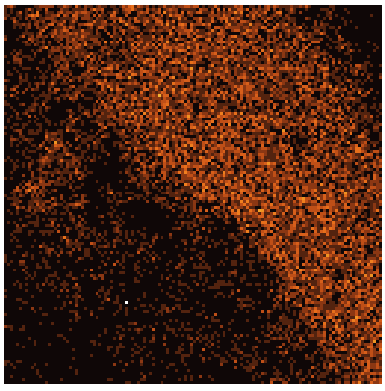

Silicon (Si)

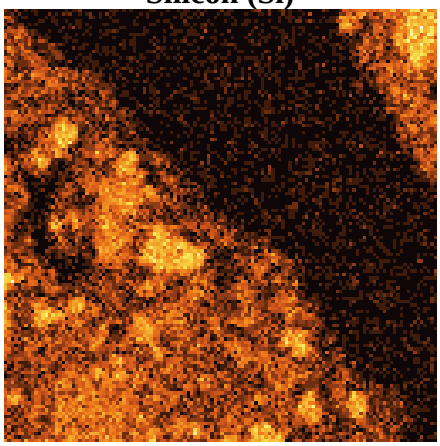

EDS Scan Images by Point

Point 1

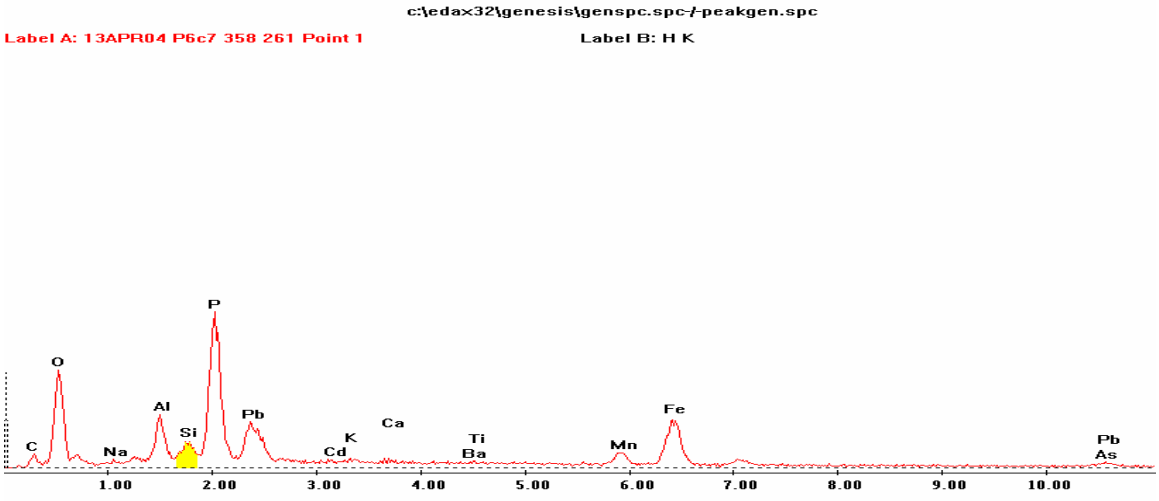

Point 2

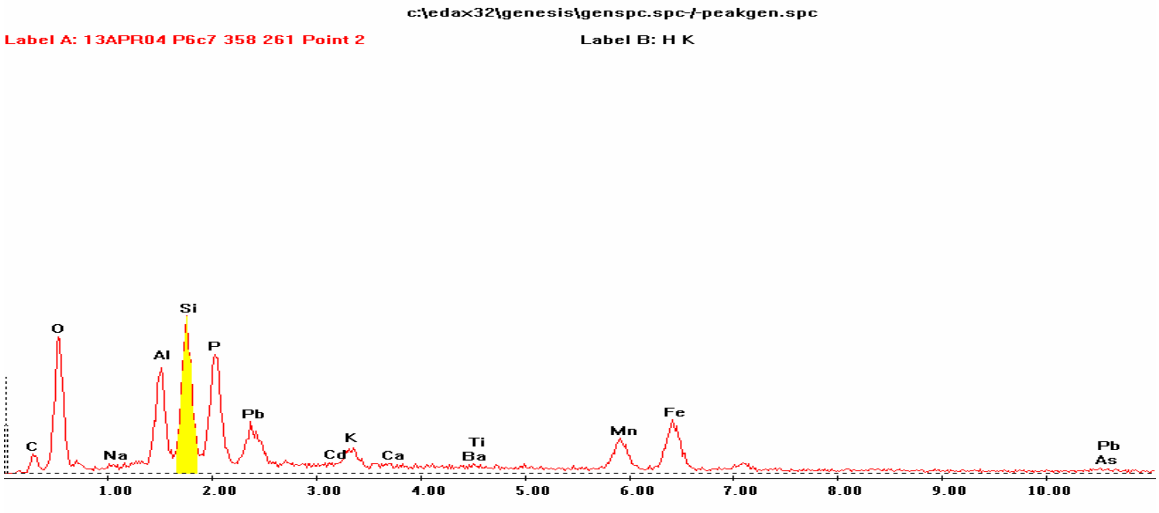

Point 3

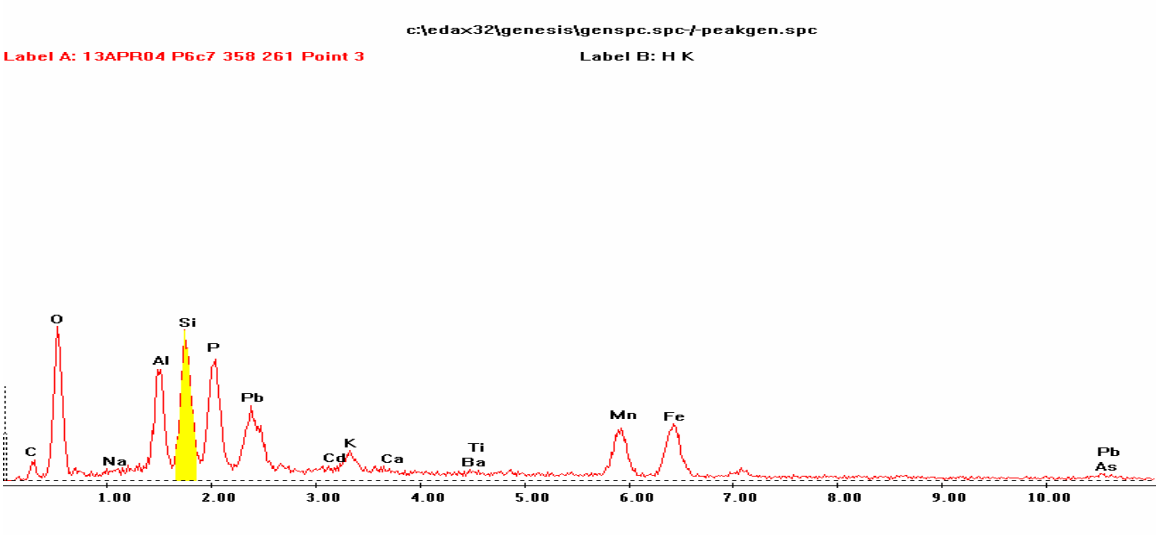

Point 4

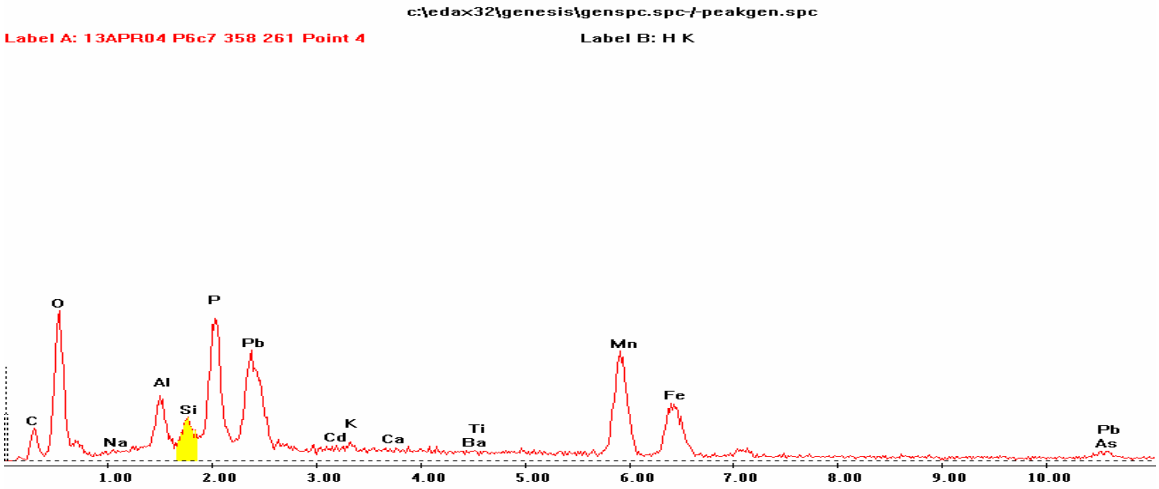

Point 5

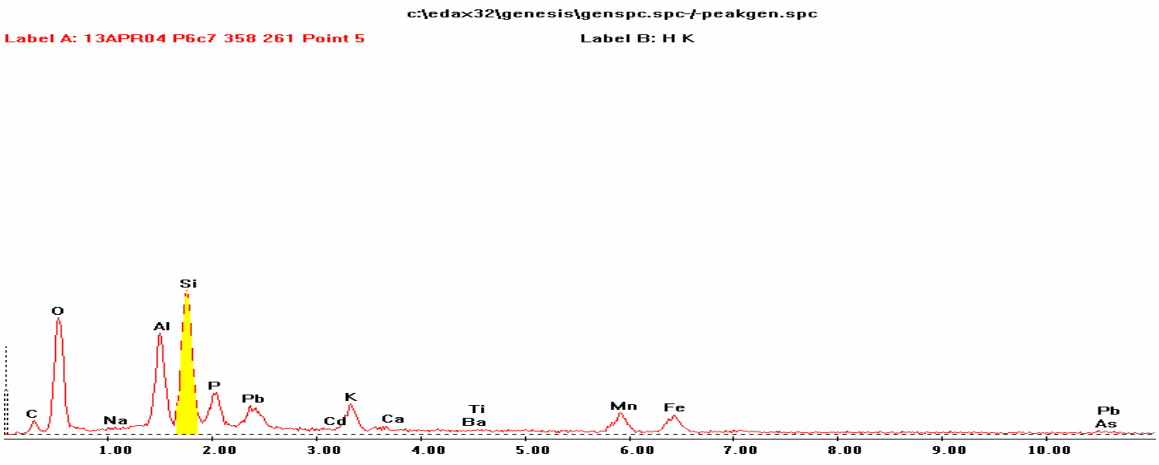

Point 6

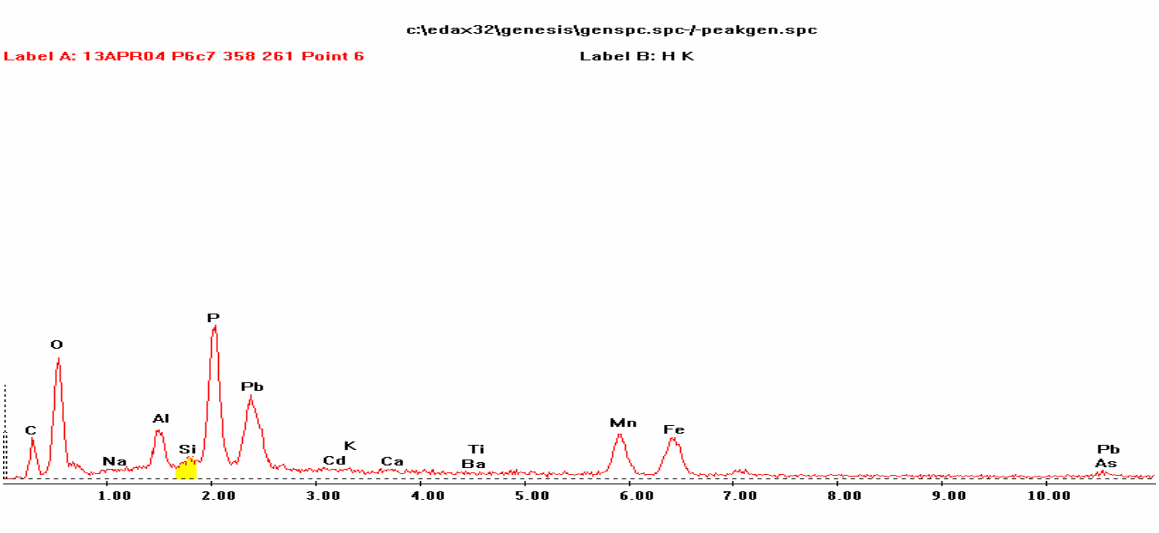

Point 7

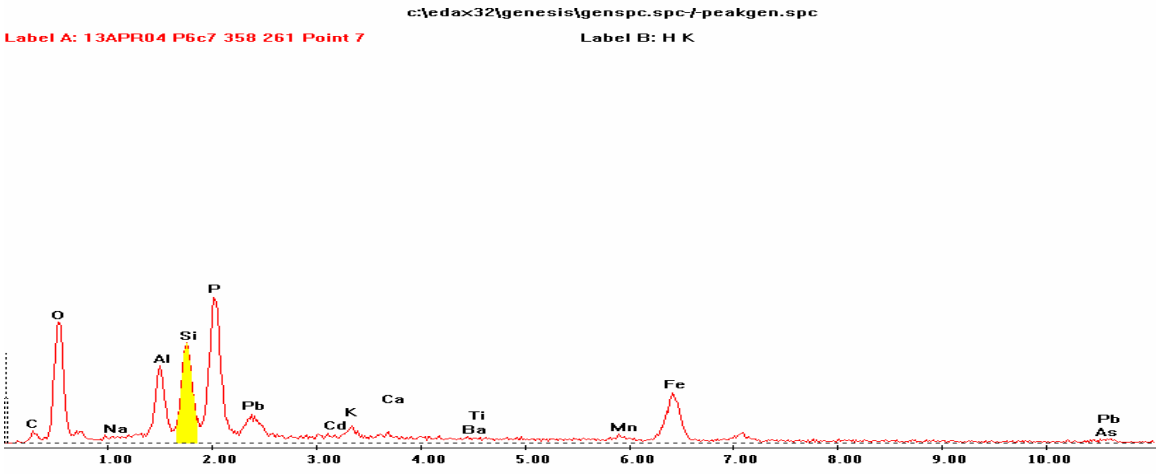

Point 8

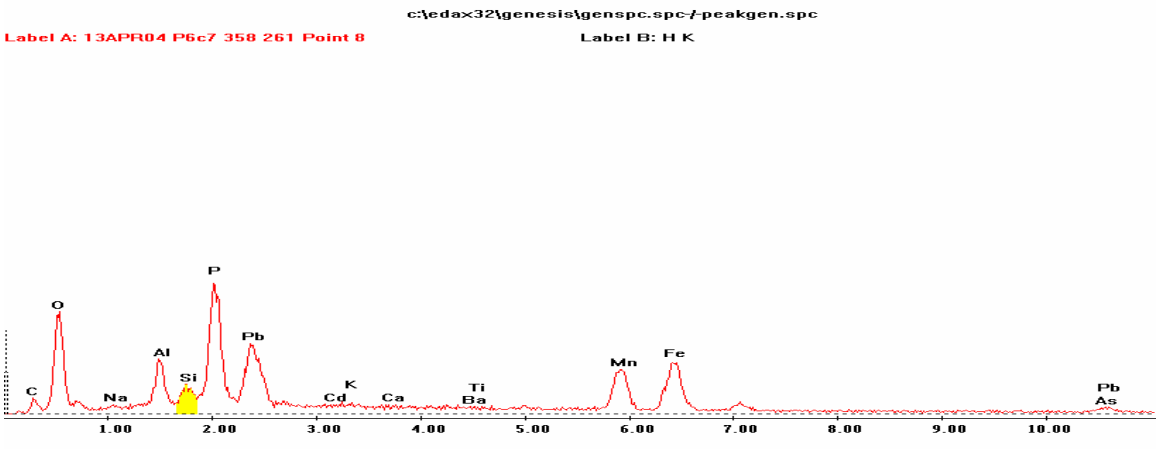

P6C7 – 371, 216

BSE Image

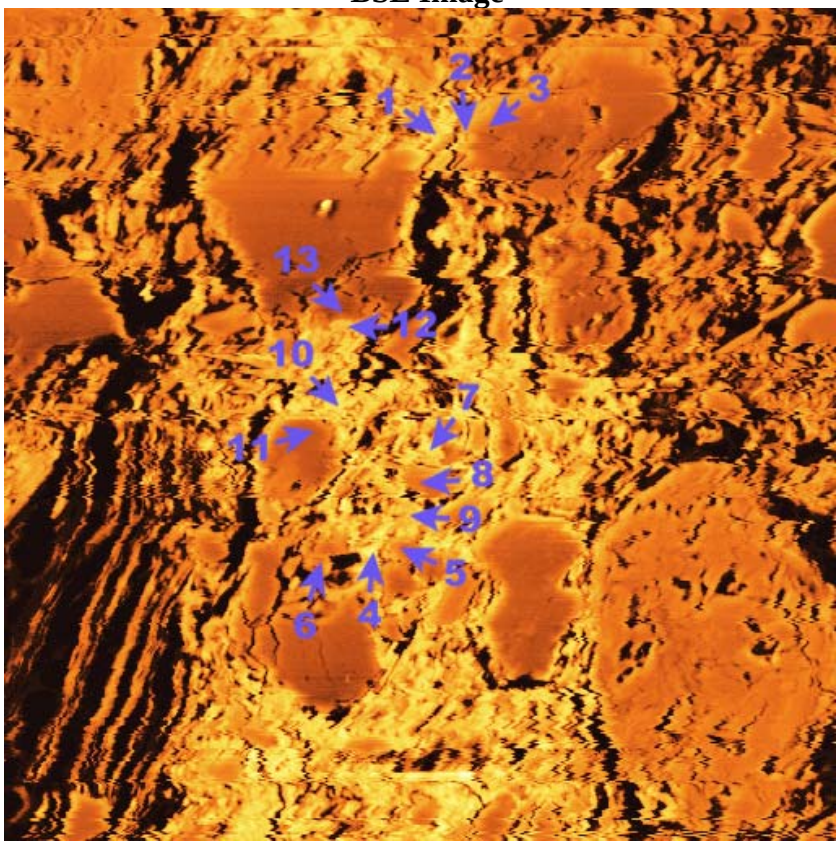

Iron (Fe)

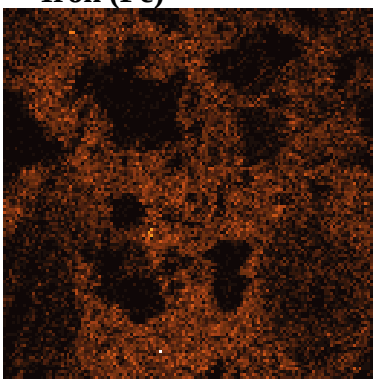

Manganese (Mn)

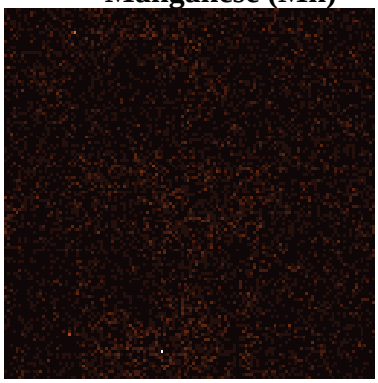

Phosphorous (P)

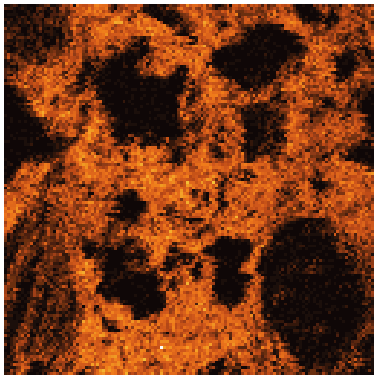

Lead (Pb)

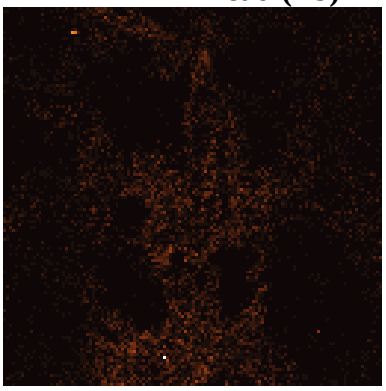

Silicon (Si)

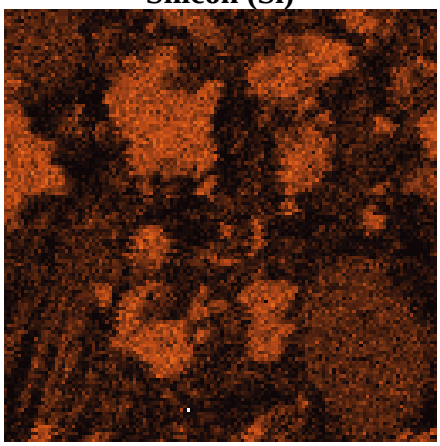

EDS Scan Images by Point

Point 1

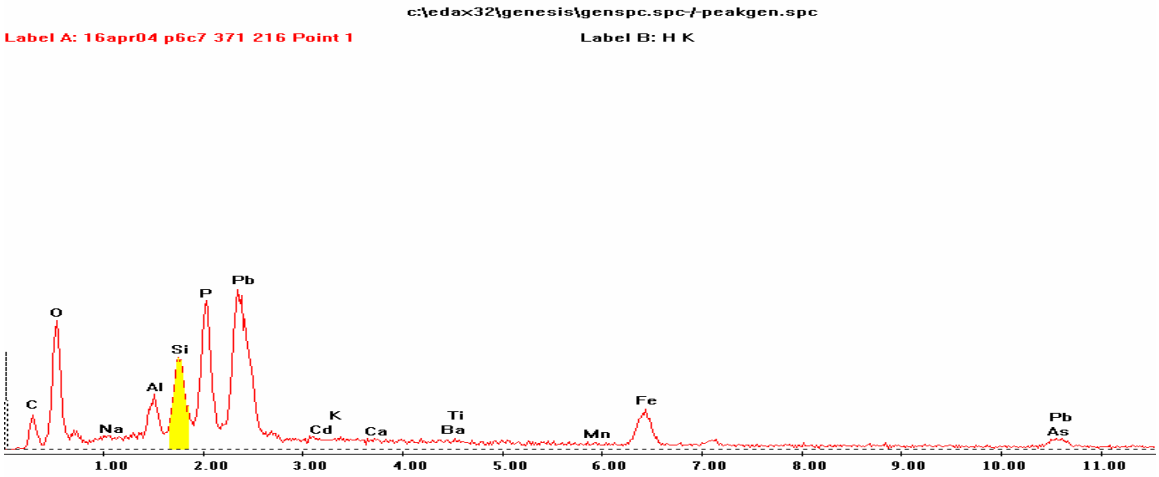

Point 2

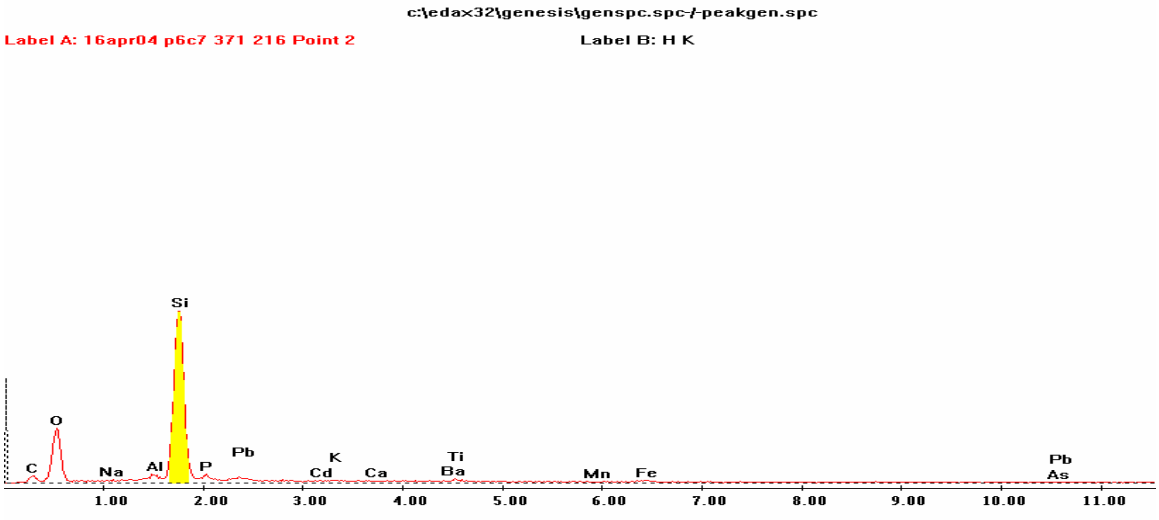

Point 3

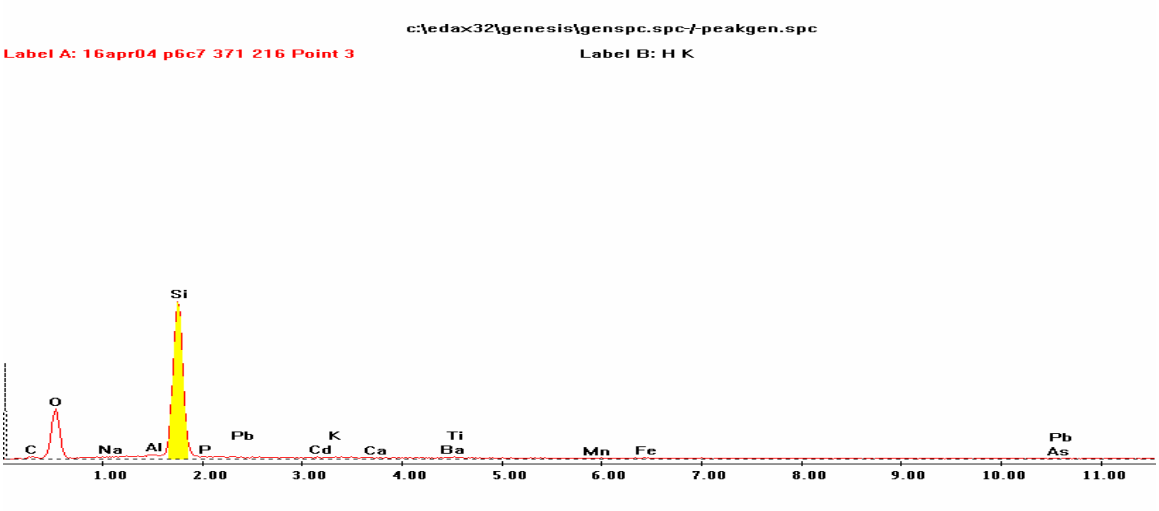

Point 4

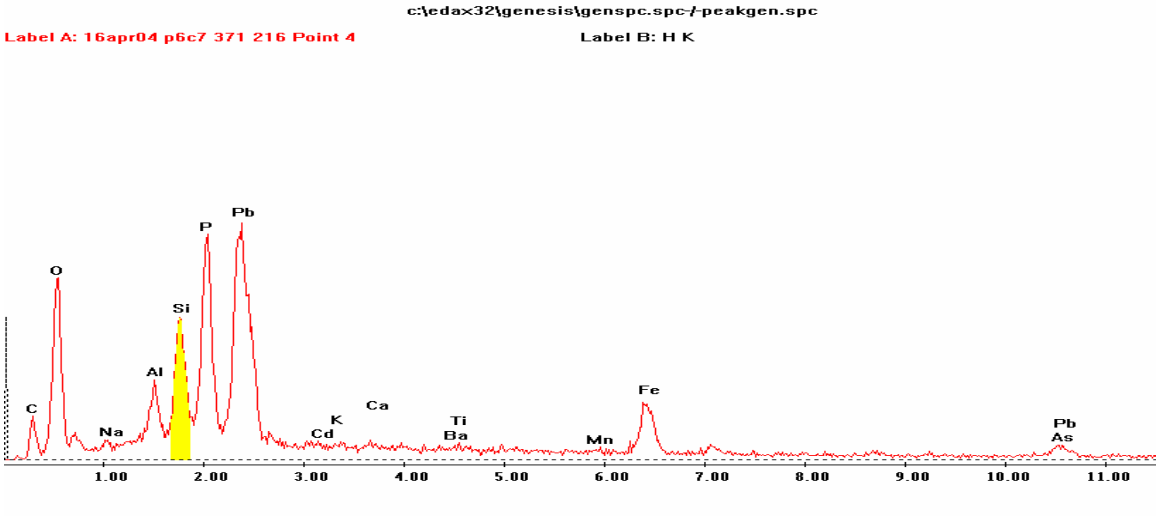

Point 5

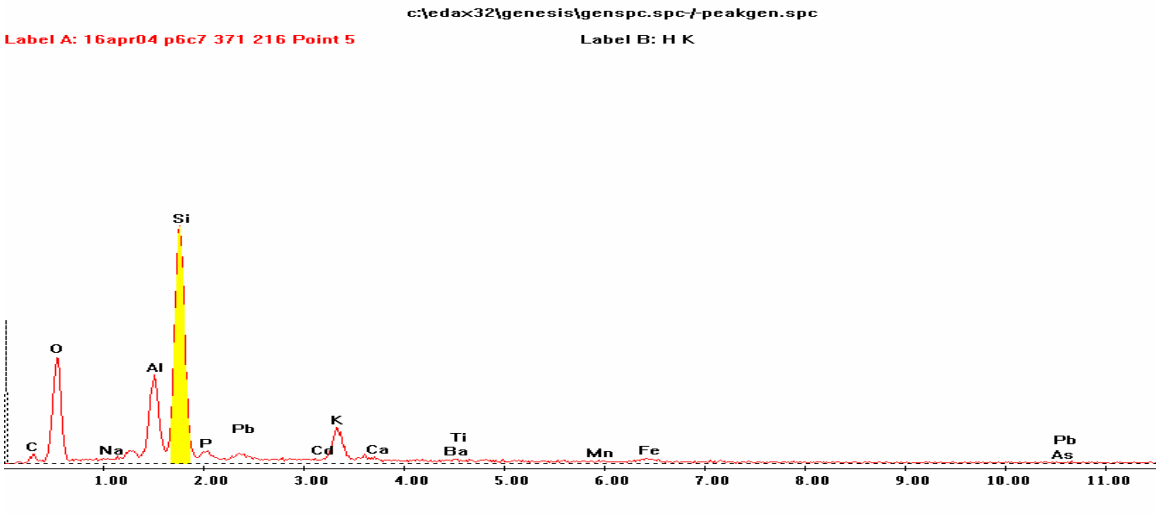

Point 6

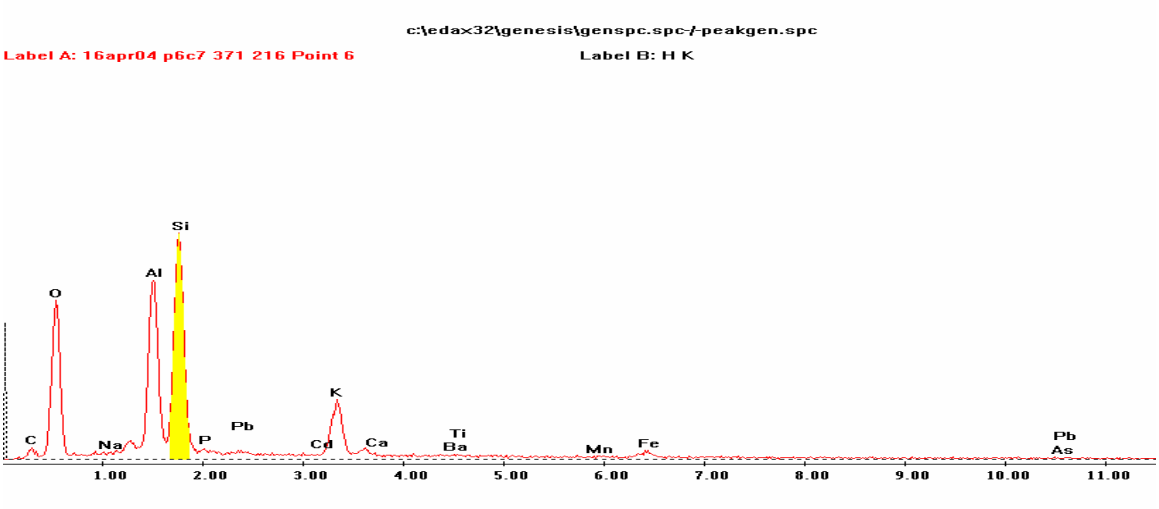

Point 7

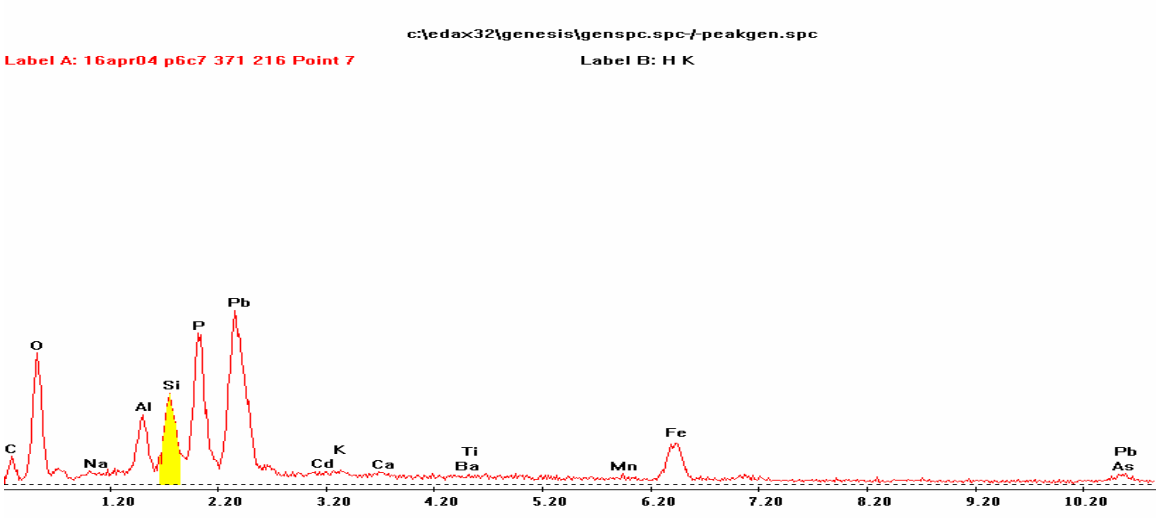

Point 8

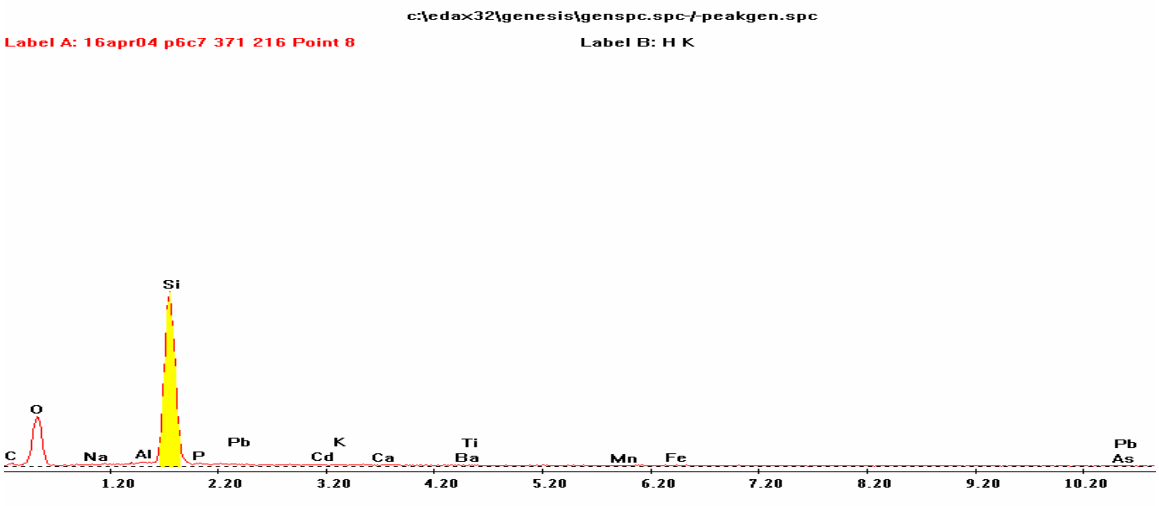

Point 9

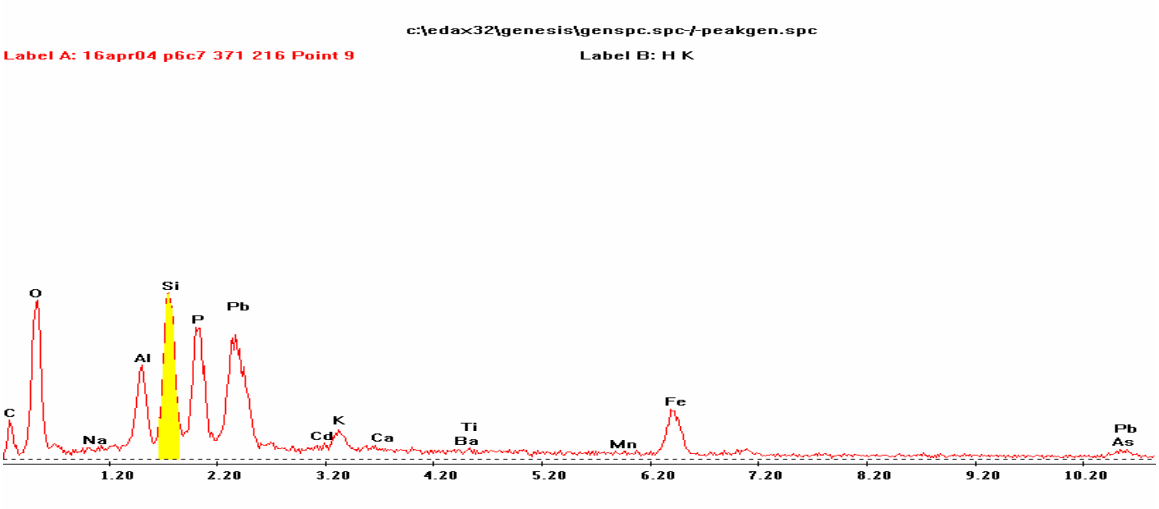

Point 10

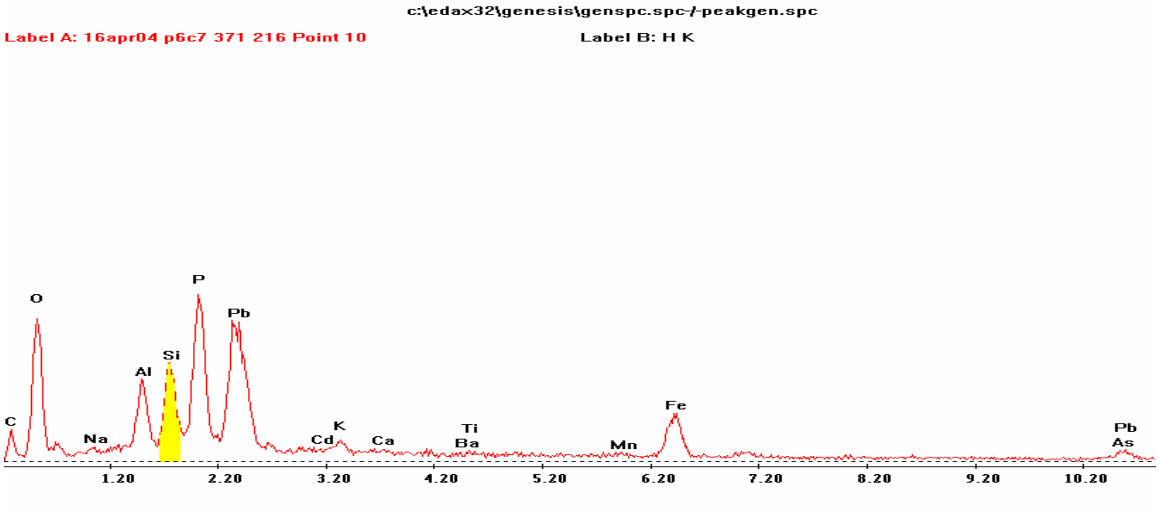

Point 11

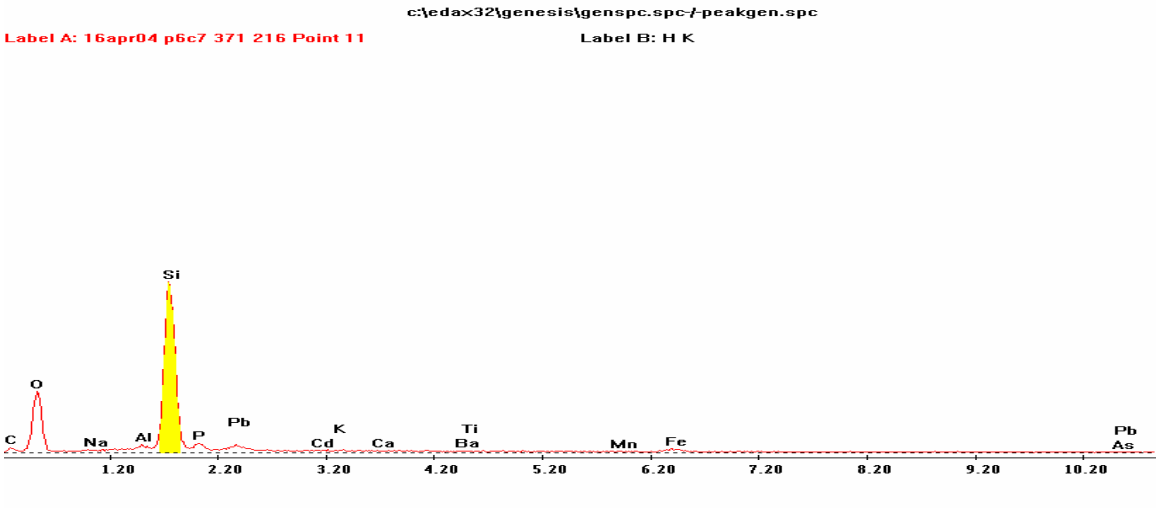

Point 12

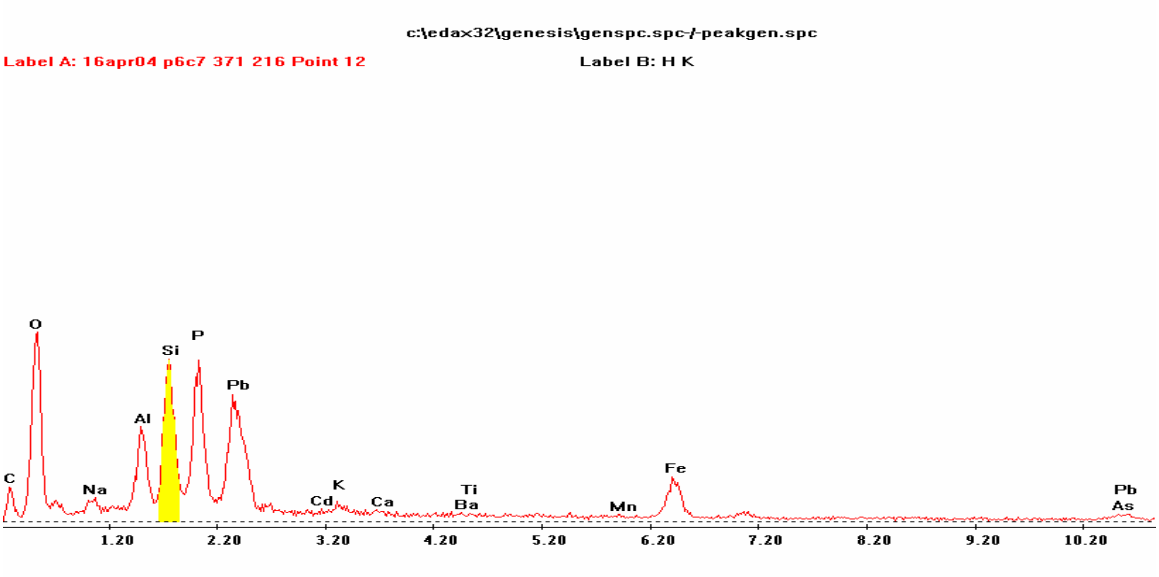

Point 13

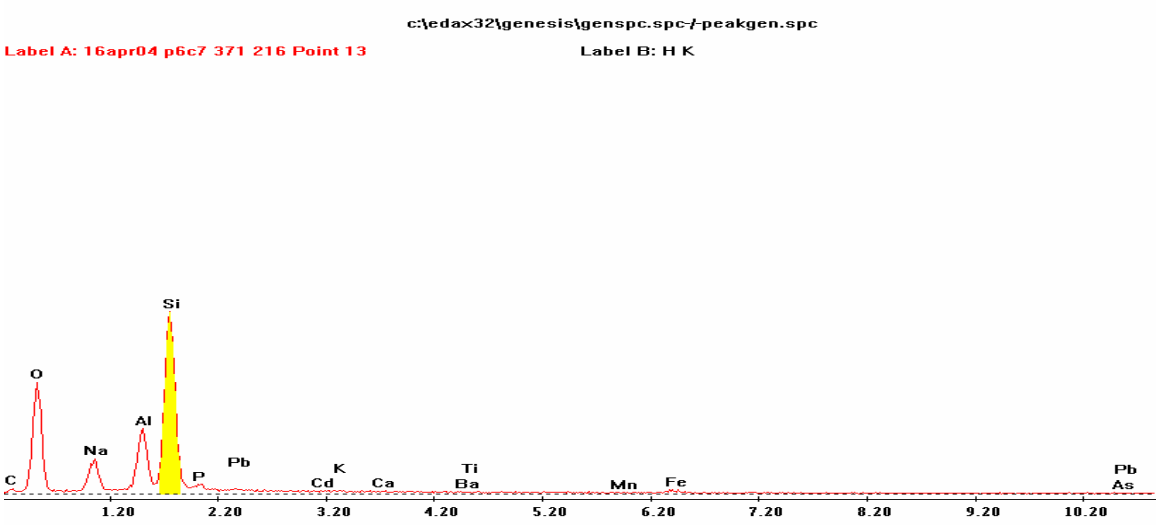

P6C7 – 378, 276

BSE Image

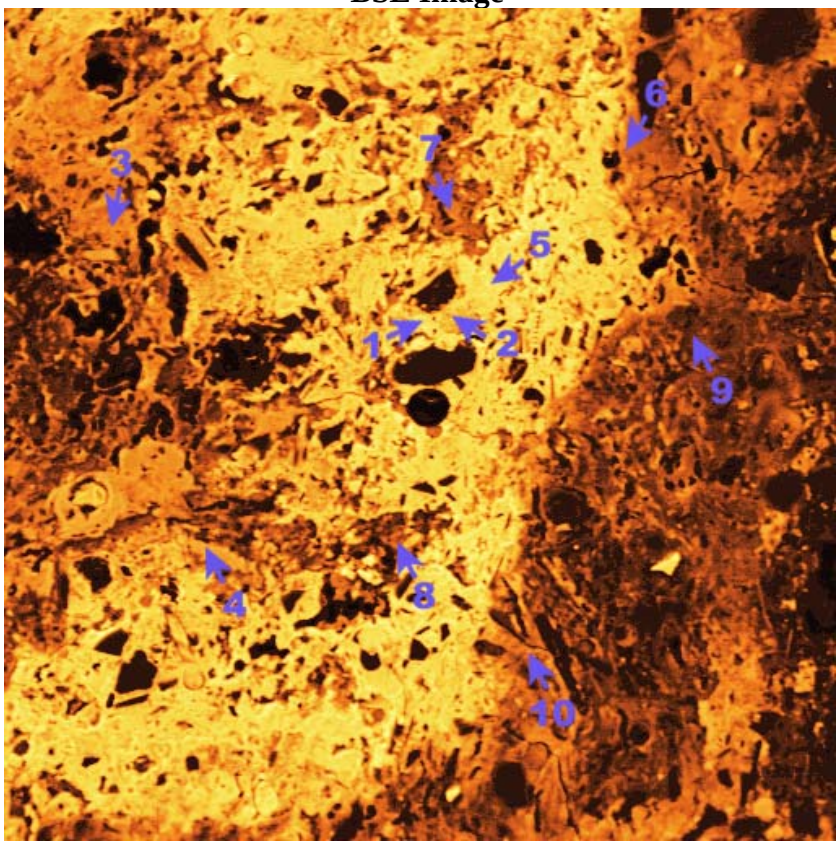

Iron (Fe)

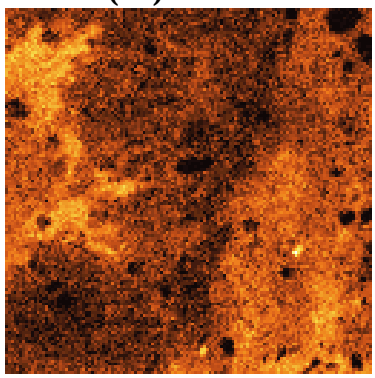

Manganese (Mn)

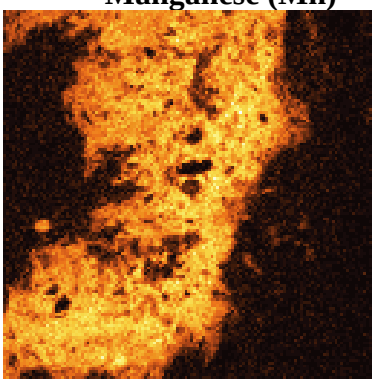

Phosphorous (P)

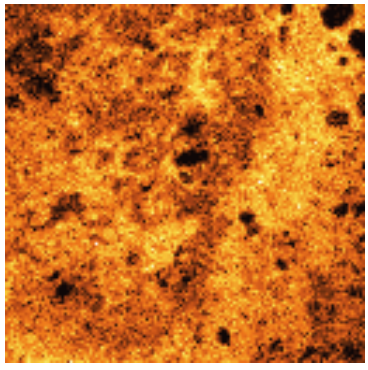

Lead (Pb)

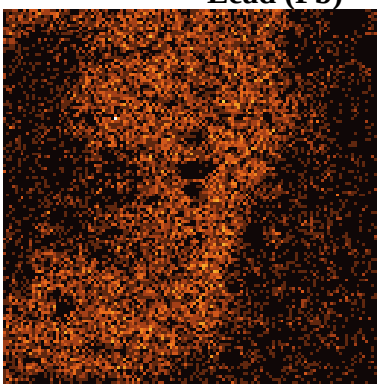

Silicon (Si)

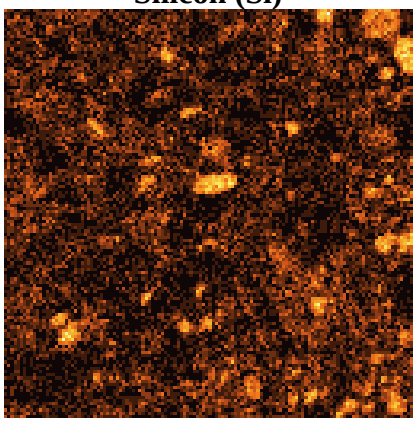

EDS Scan Images by Point

Point 1

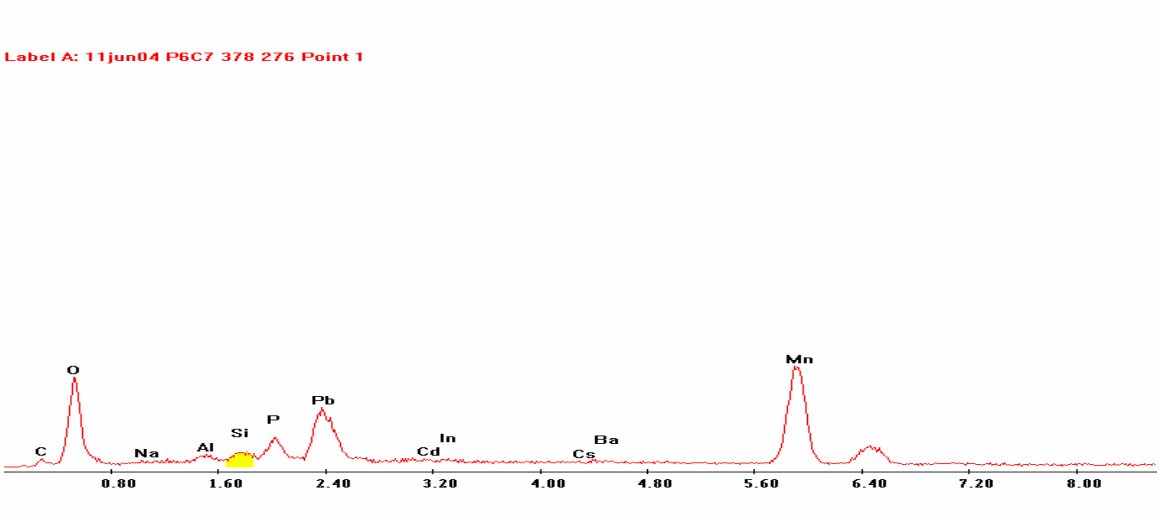

Point 2

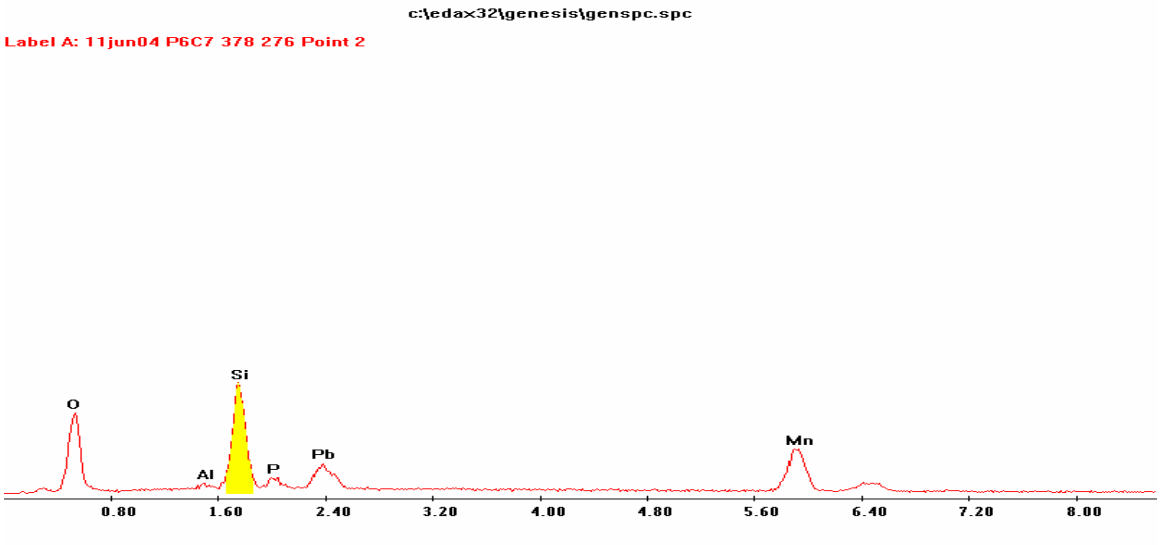

Point 3

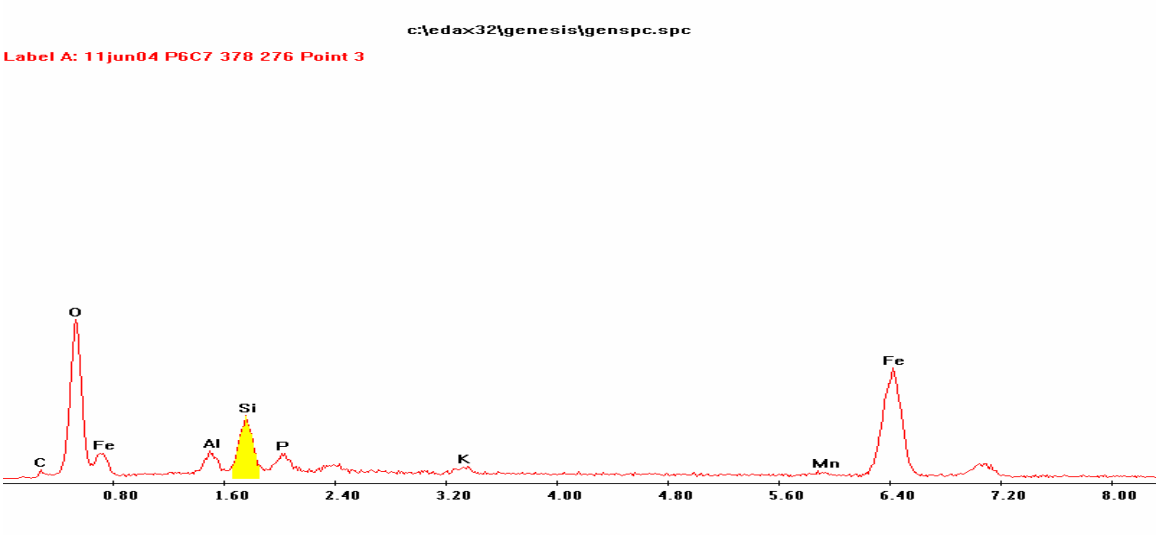

Point 4

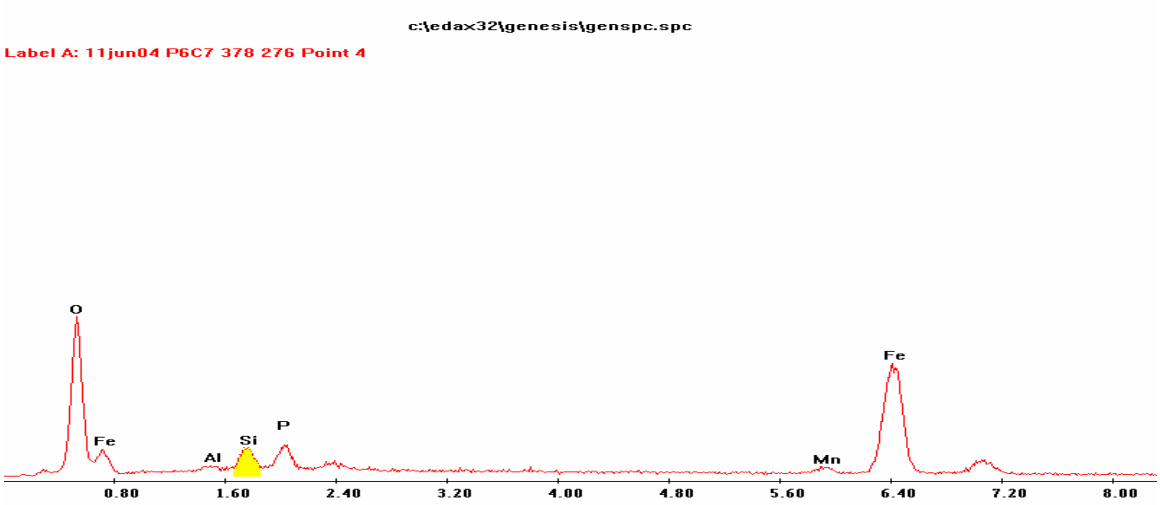

Point 5

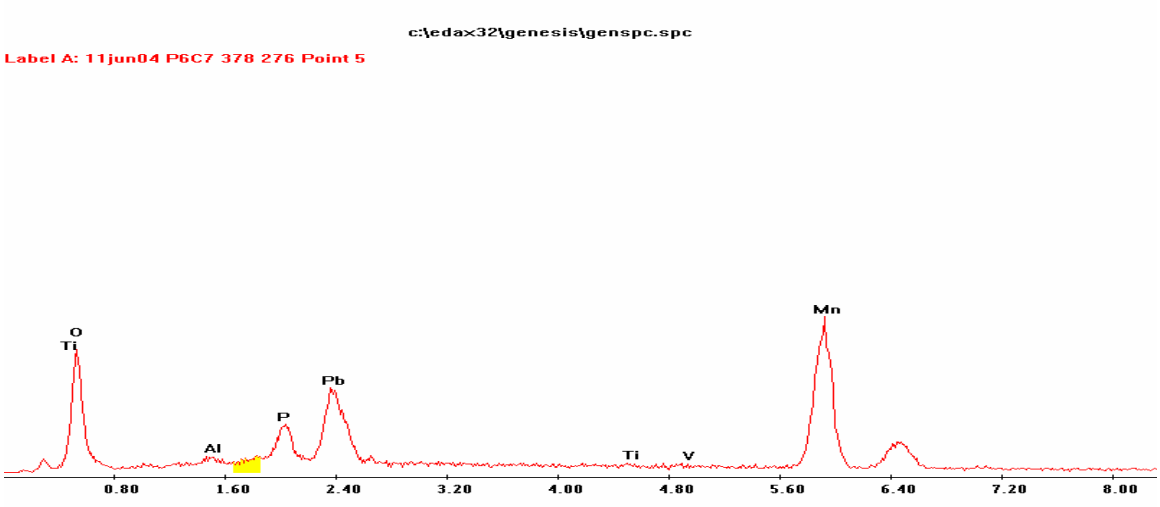

Point 6

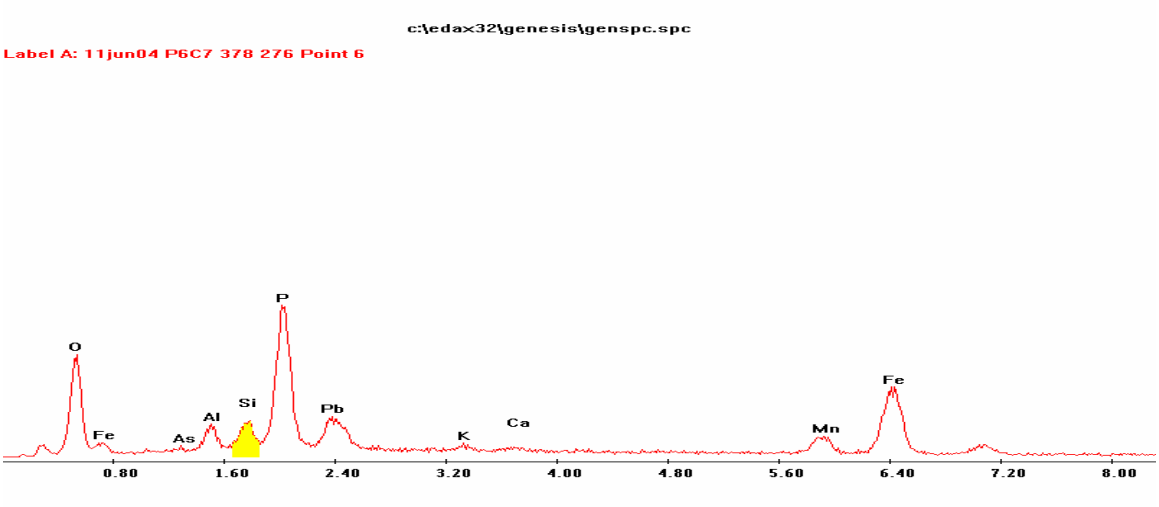

Point 7

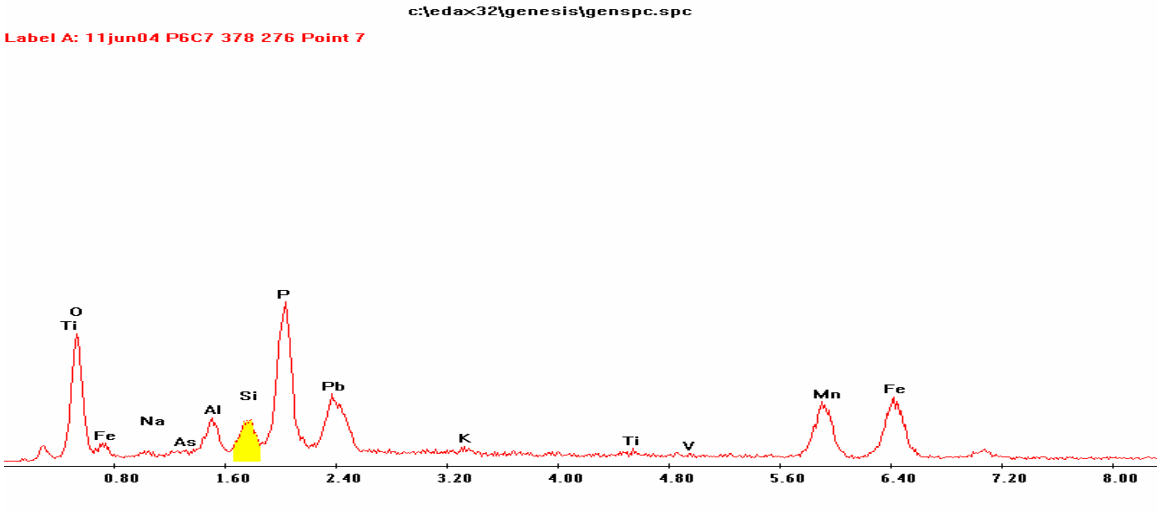

Point 8

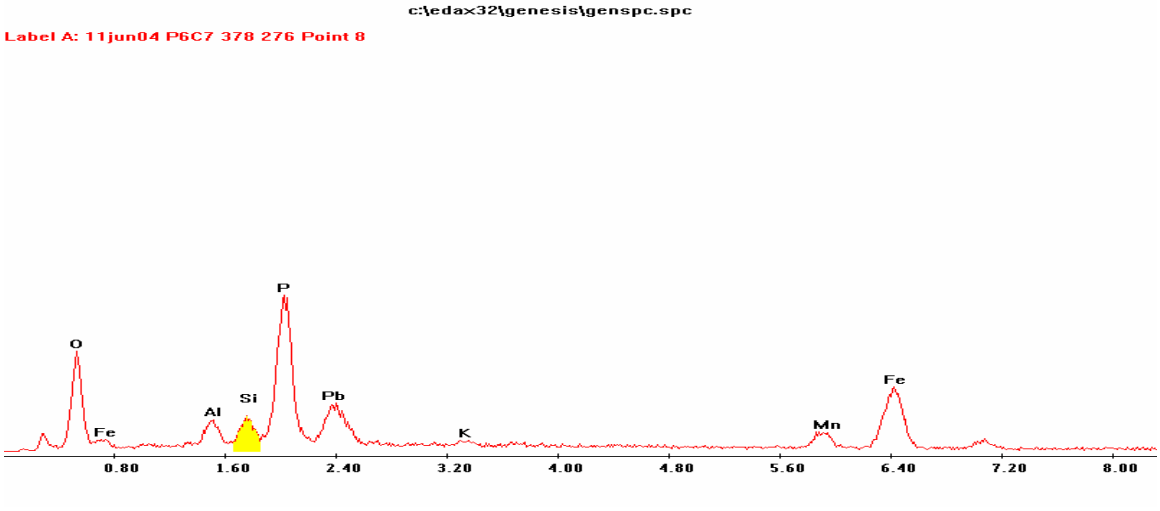

Point 9

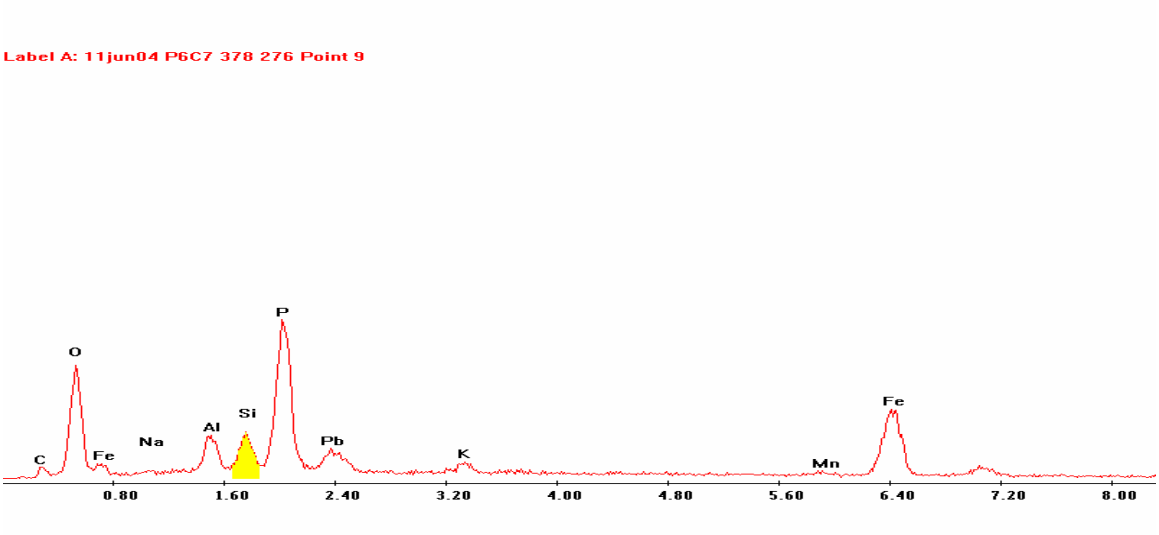

Point 10

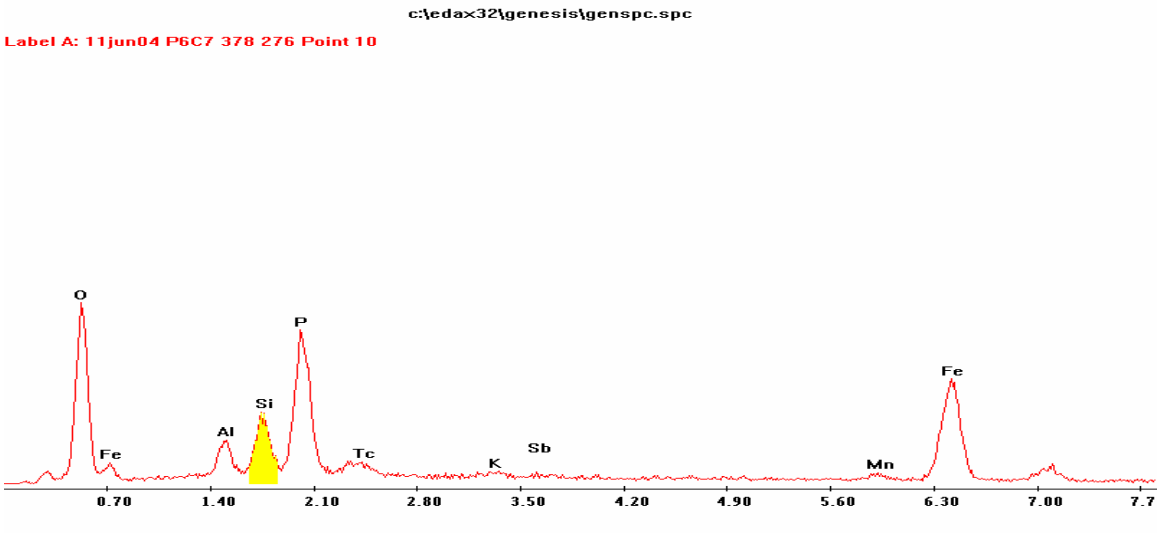

P6C7 – 398, 208

BSE Image

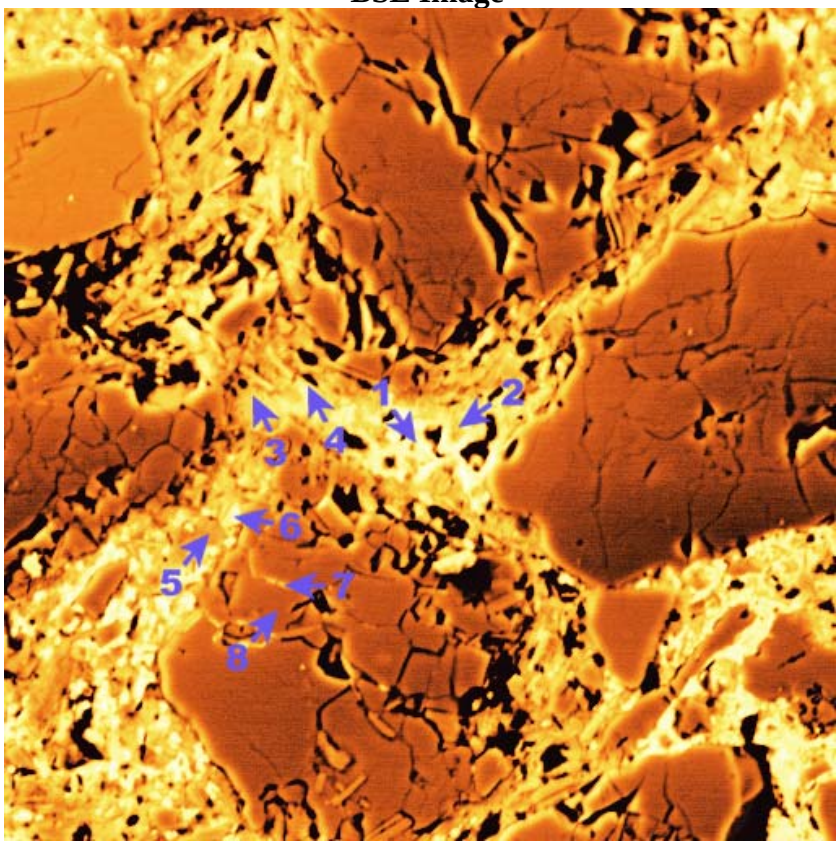

Iron (Fe)

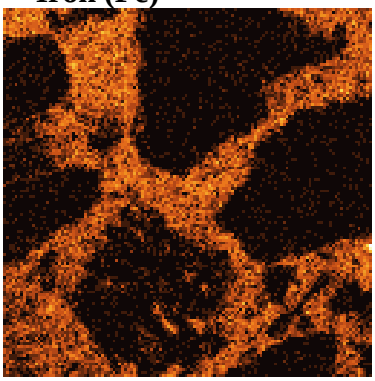

Manganese (Mn)

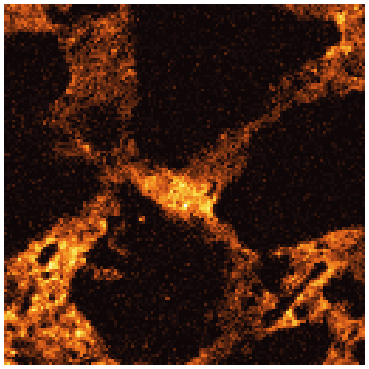

Phosphorous (P)

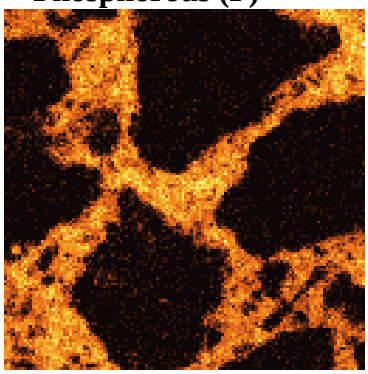

Lead (Pb)

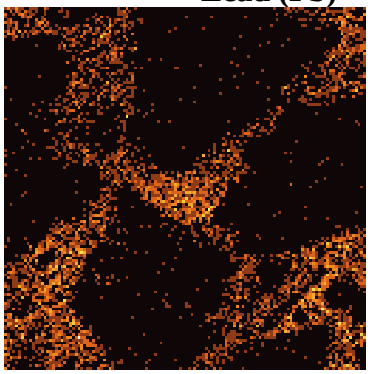

Silicon (Si)

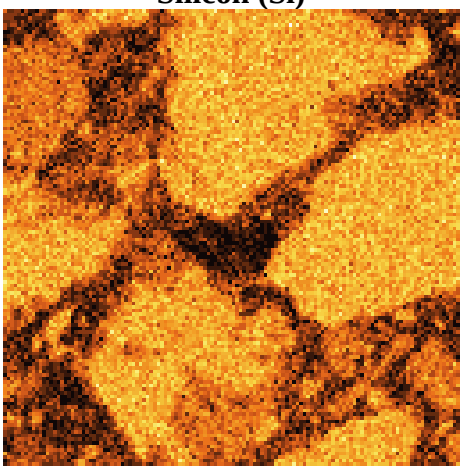

EDS Scan Images by Point

Point 1

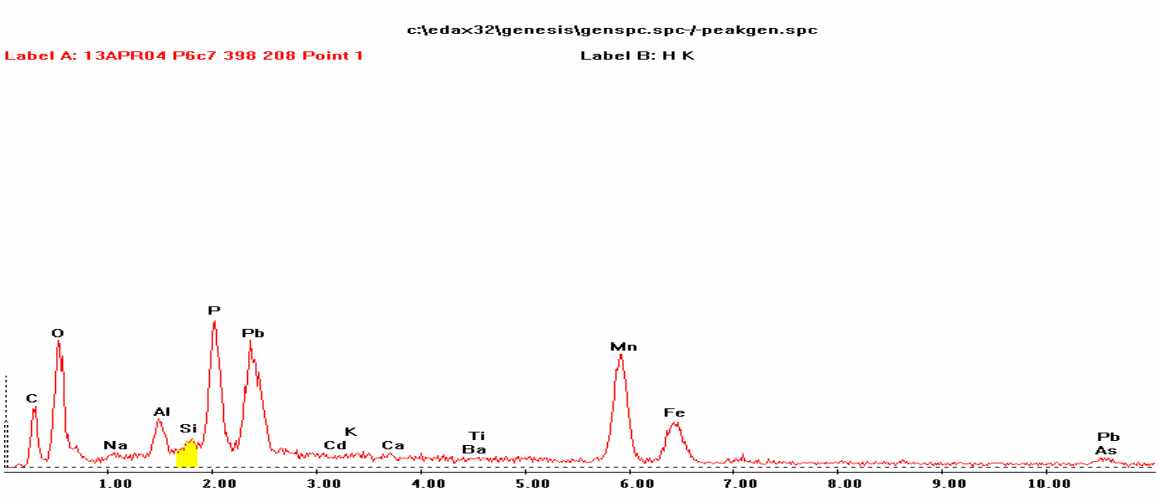

Point 2

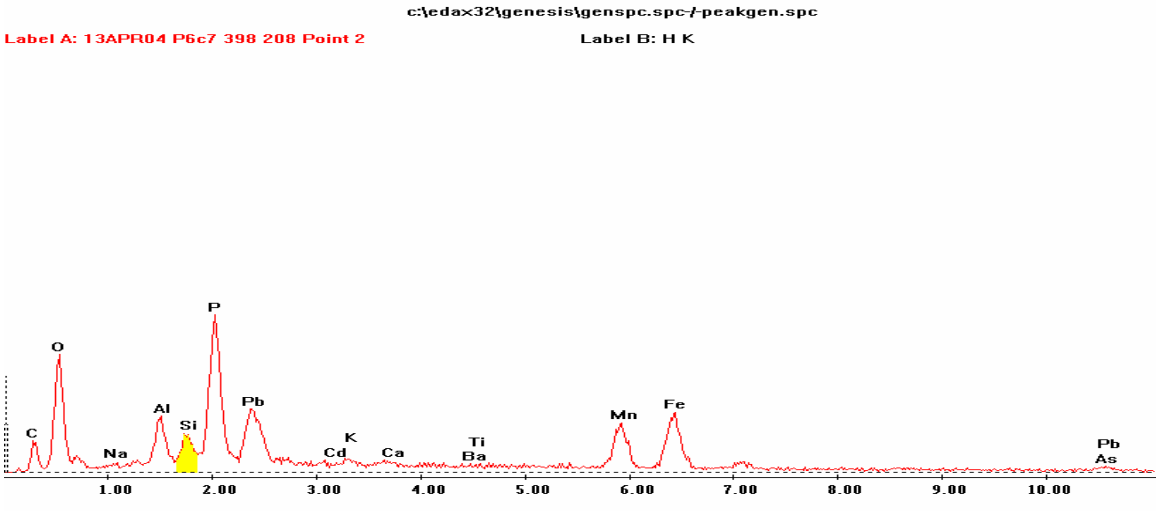

Point 3

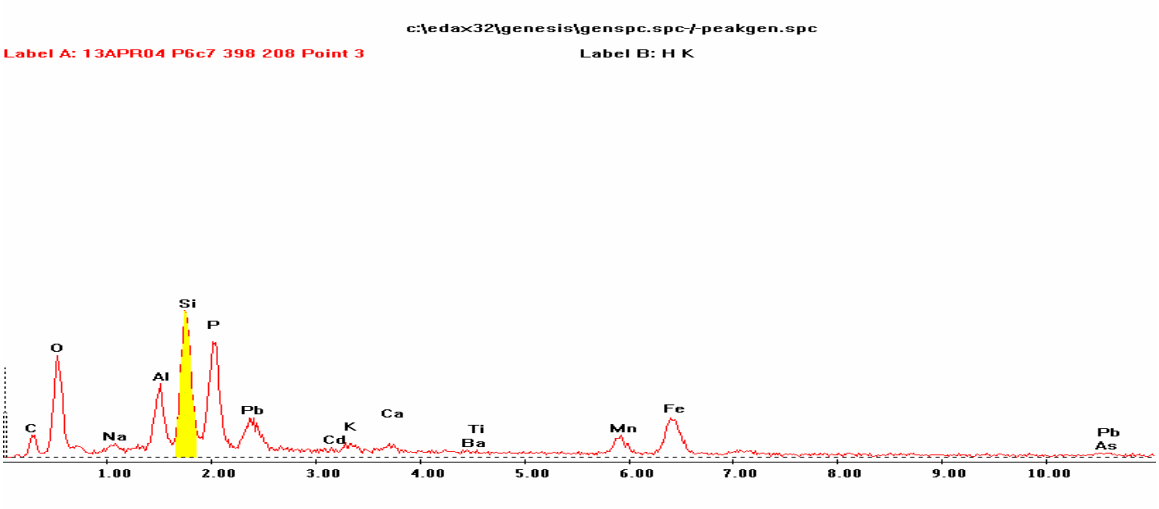

Point 4

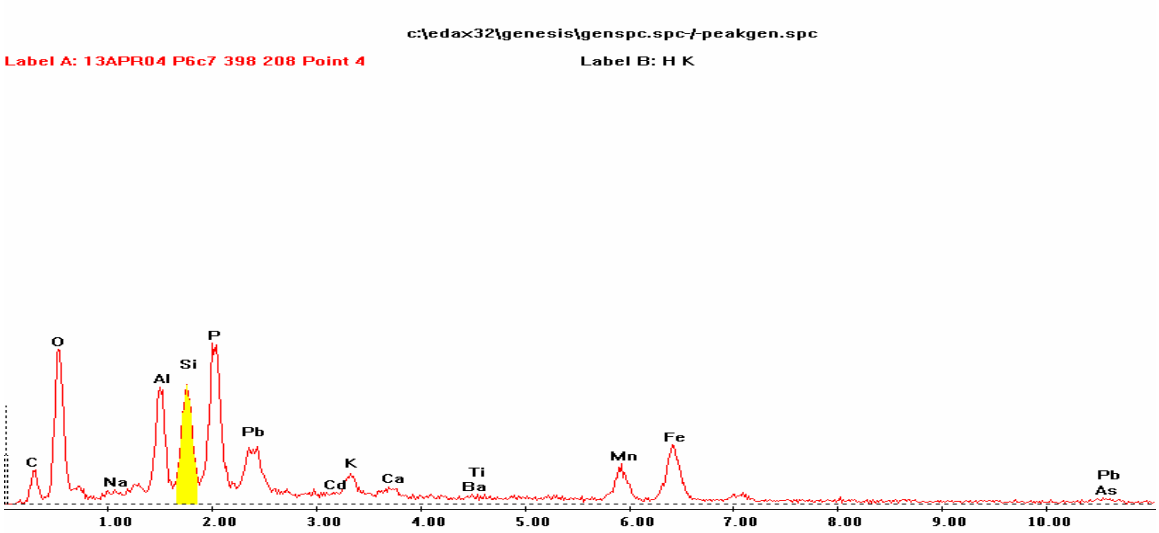

Point 5

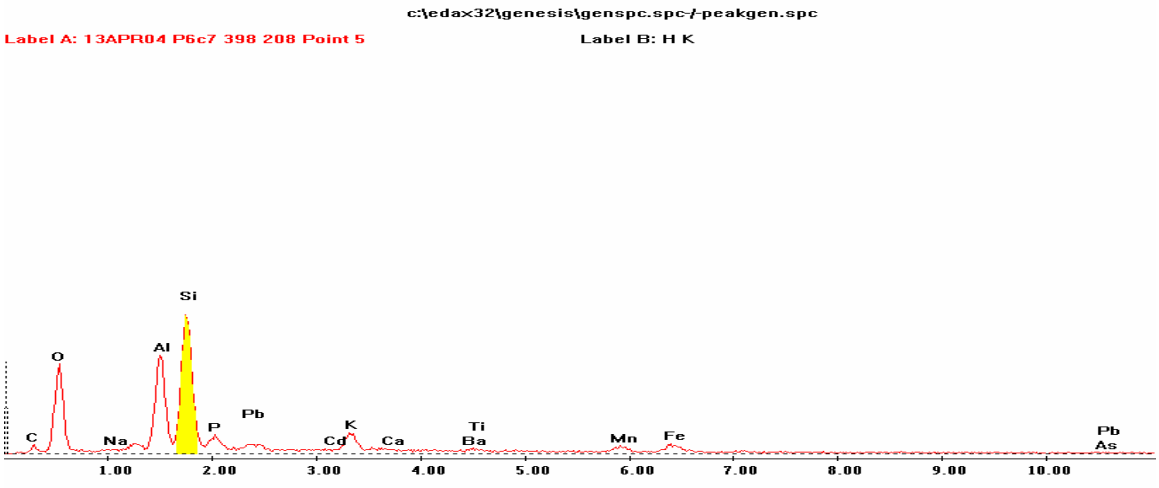

Point 6

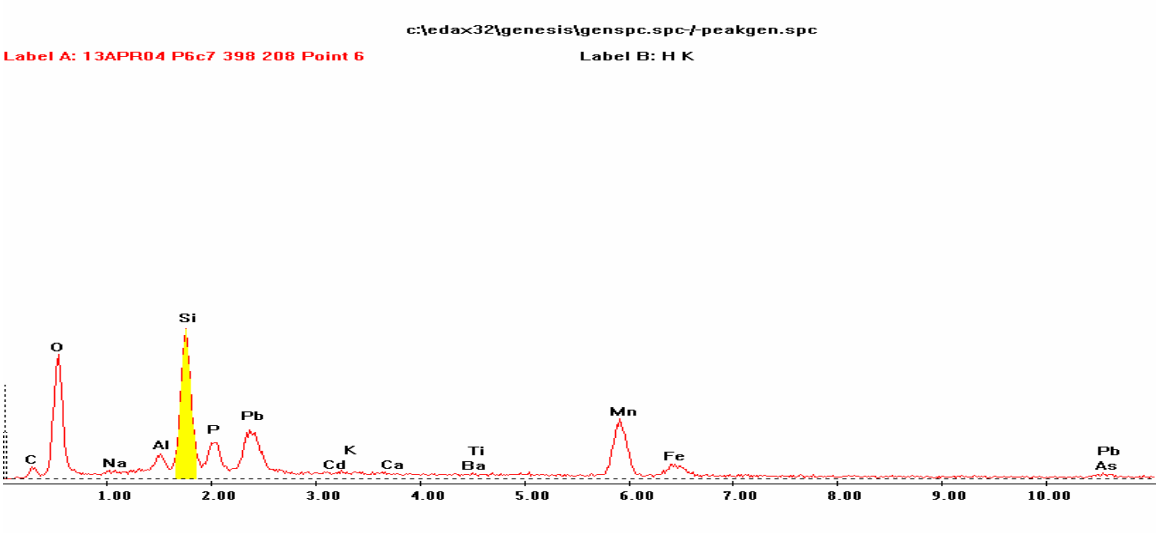

Point 7

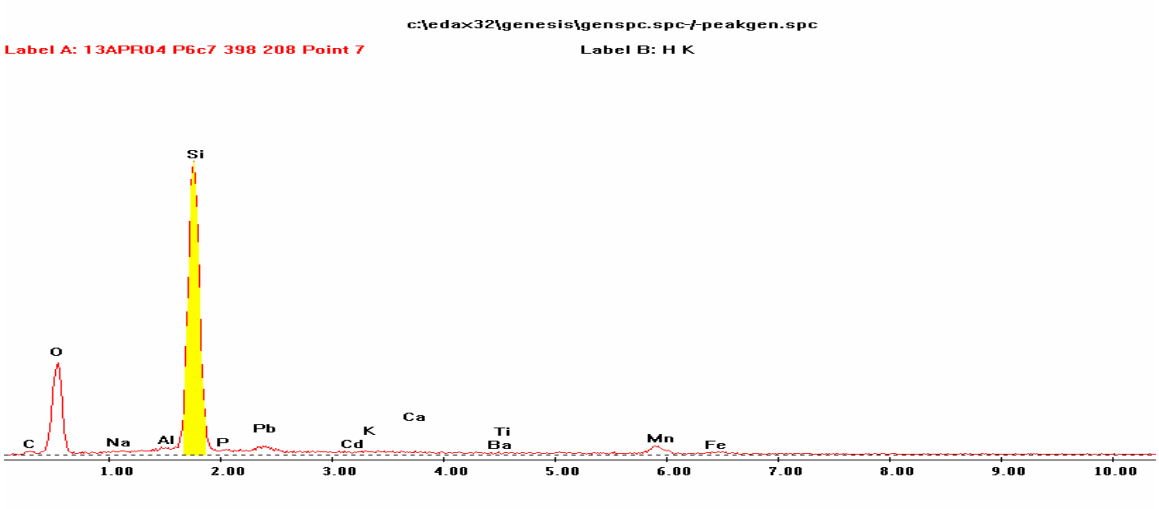

Point 8

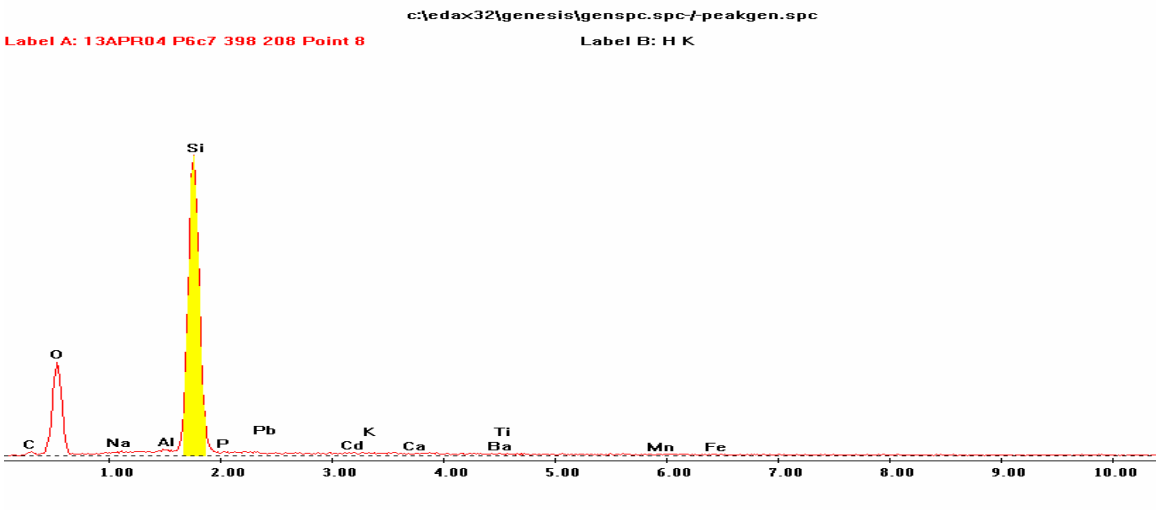

Point 9

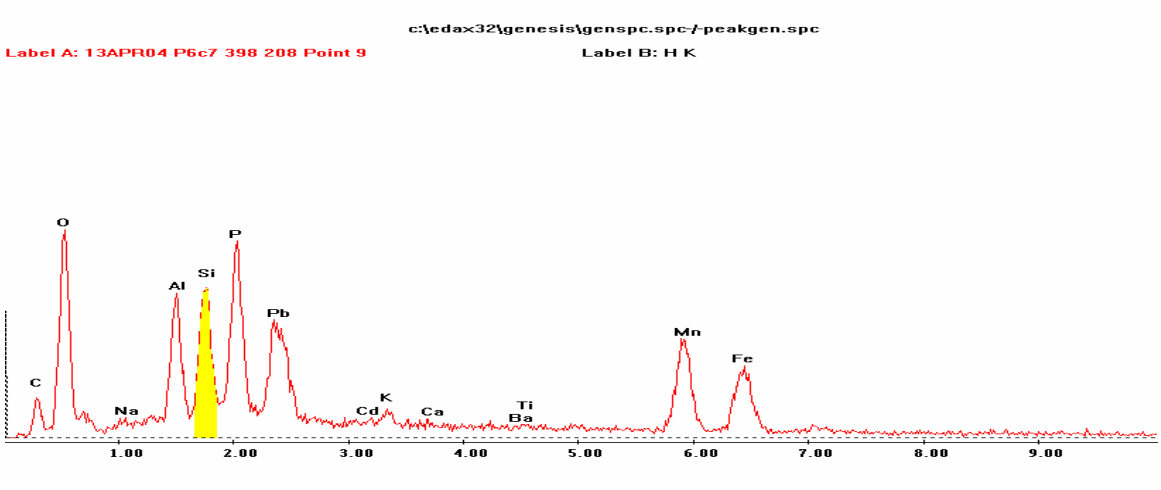

Point 10

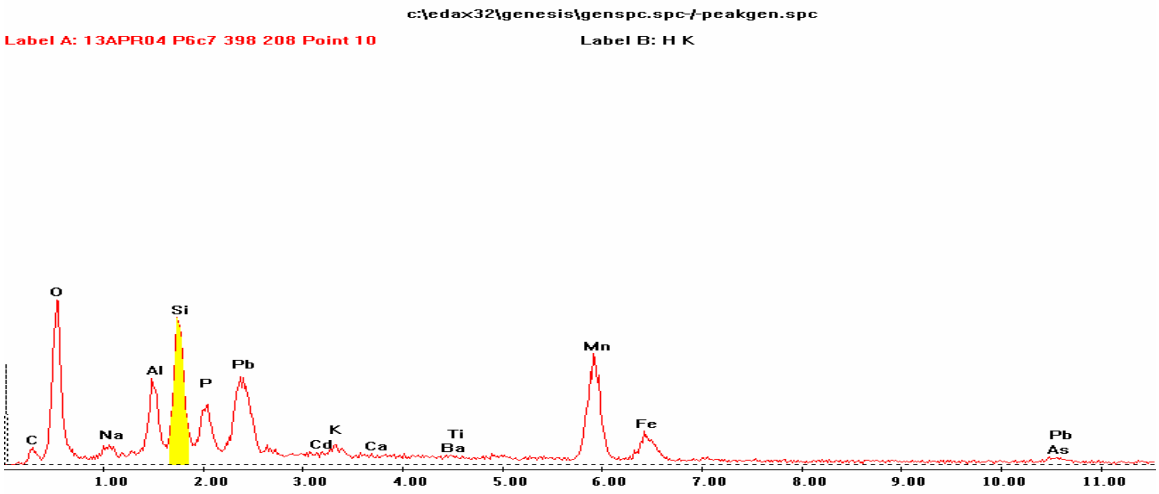

P6C7 – 402, 315

BSE Image

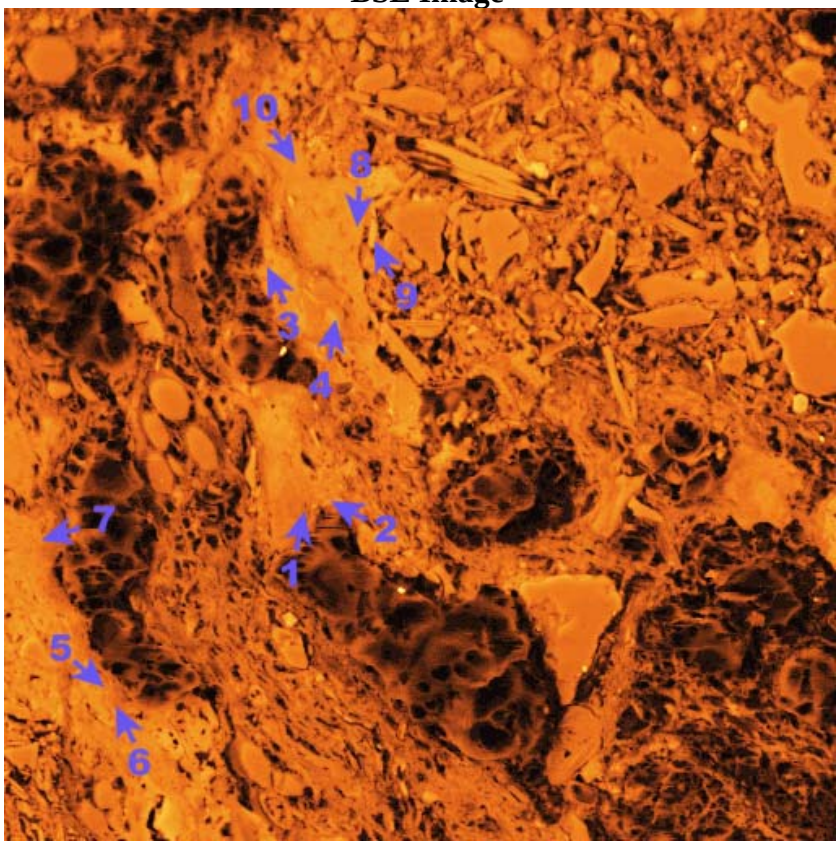

Iron (Fe)

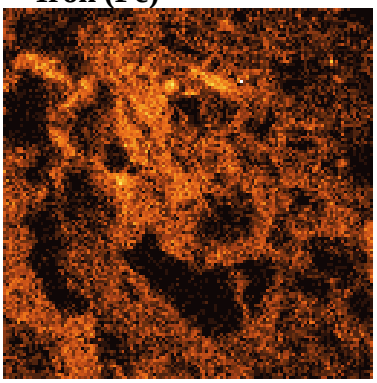

Manganese (Mn)

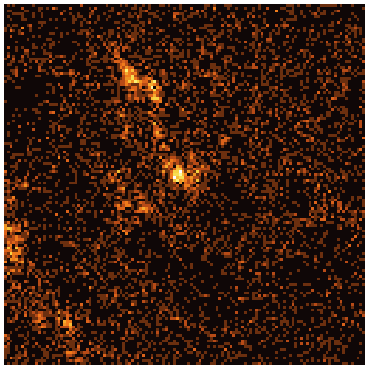

Phosphorous (P)

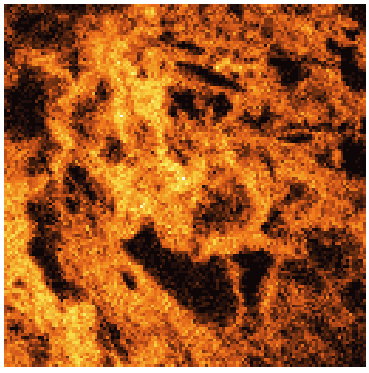

Lead (Pb)

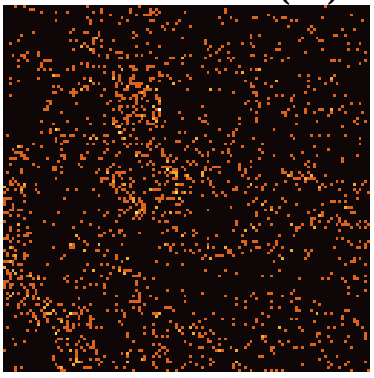

Silicon (Si)

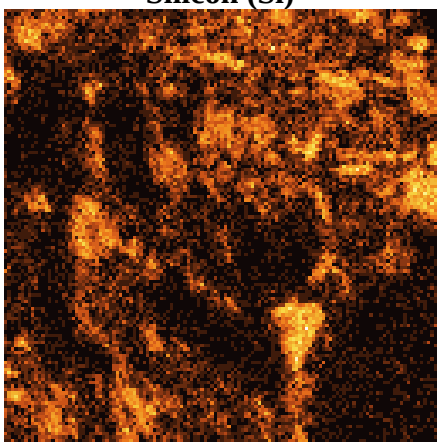

EDS Scan Images by Point

Point 1

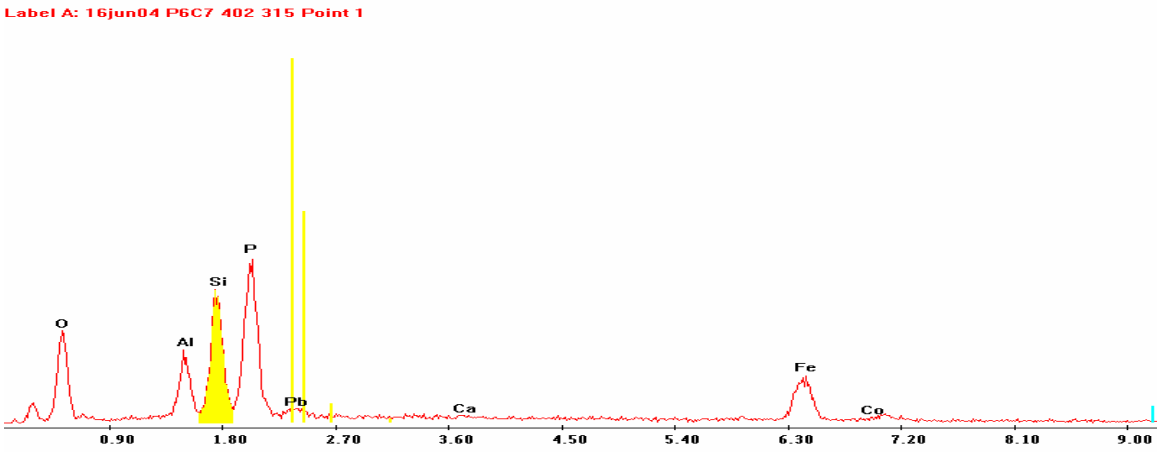

Point 2

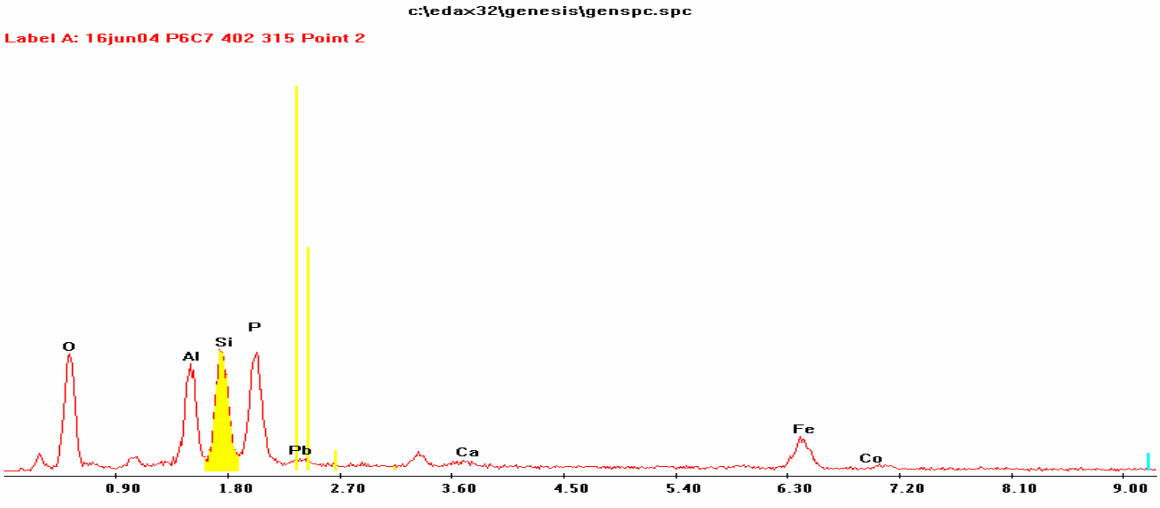

Point 3

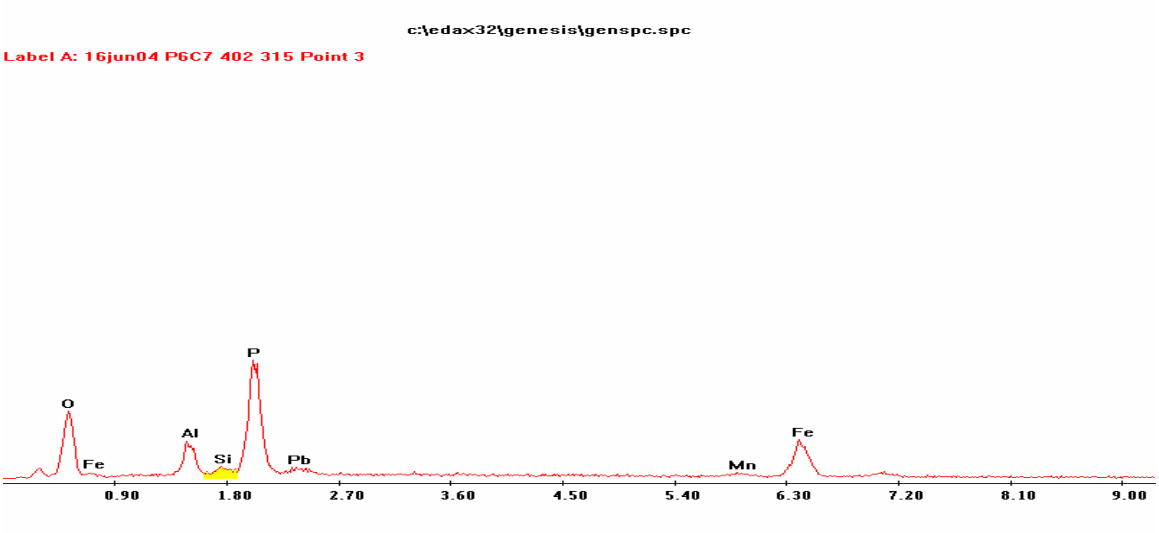

Point 4

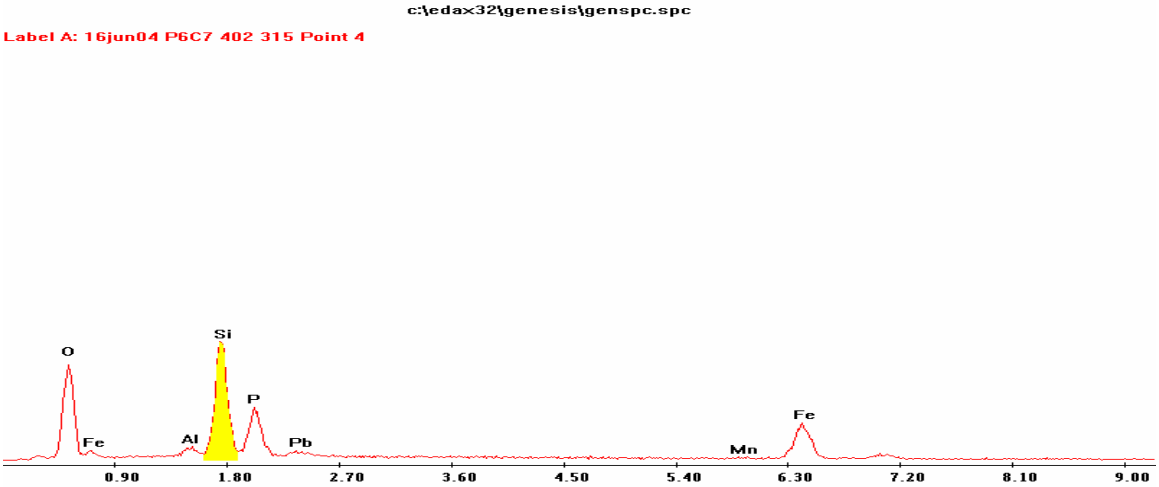

Point 5

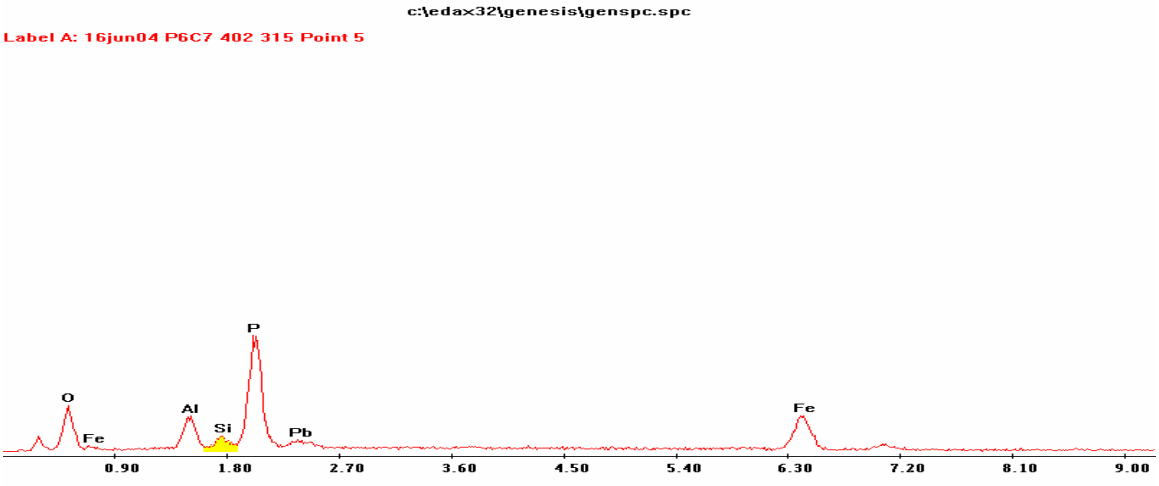

Point 6

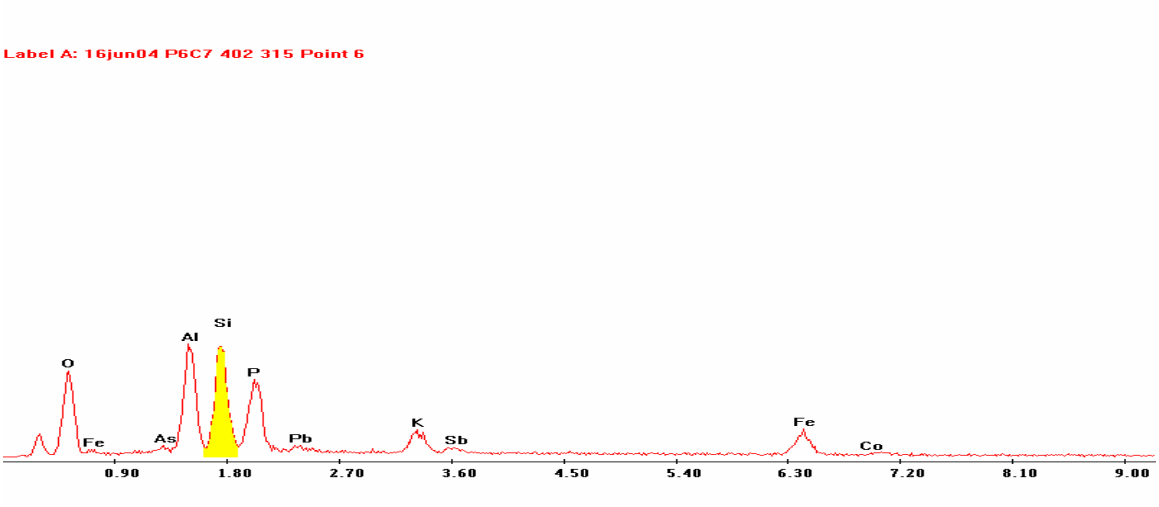

Point 7

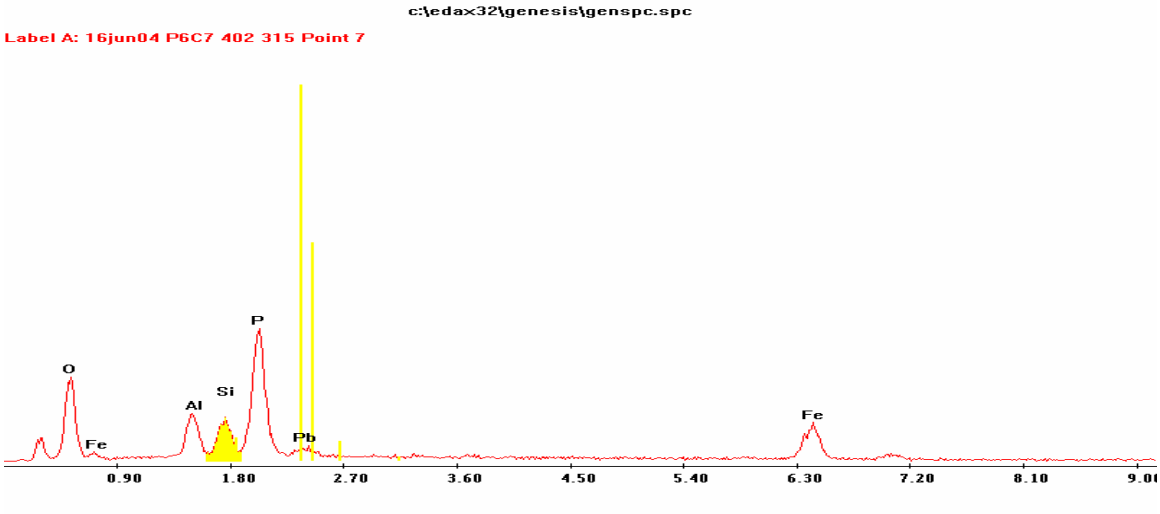

Point 8

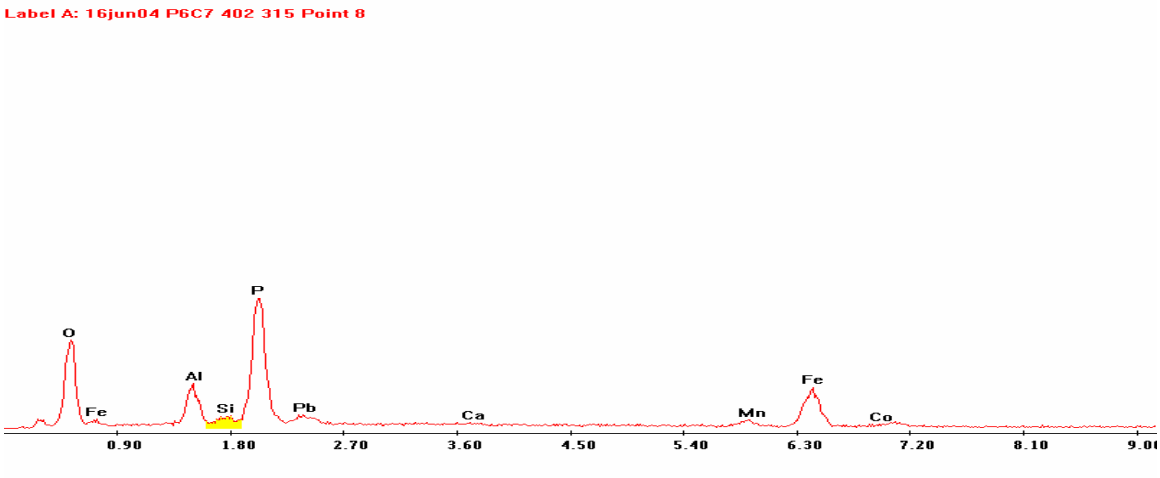

Point 9

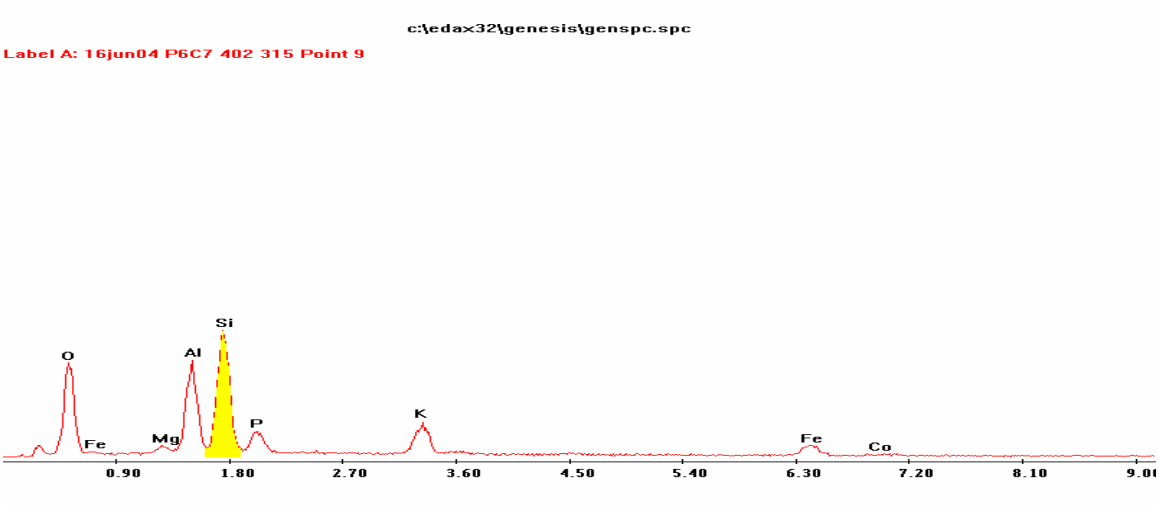

Point 10

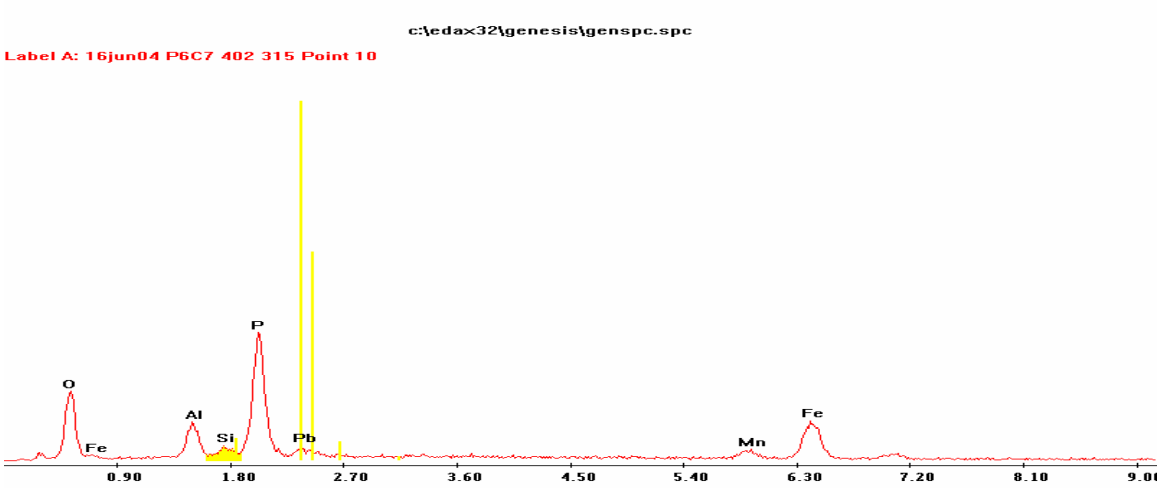

P6C7 – 434, 278

BSE Image

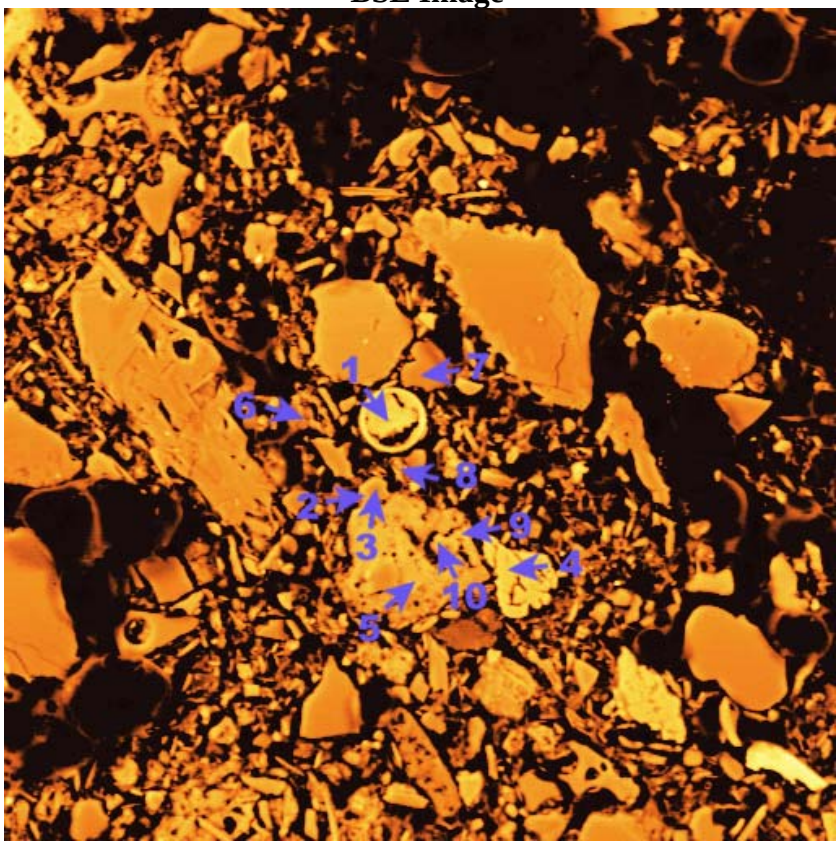

Iron (Fe)

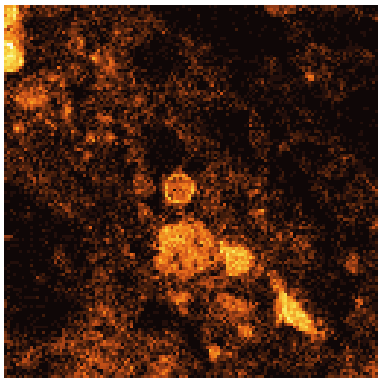

Manganese (Mn)

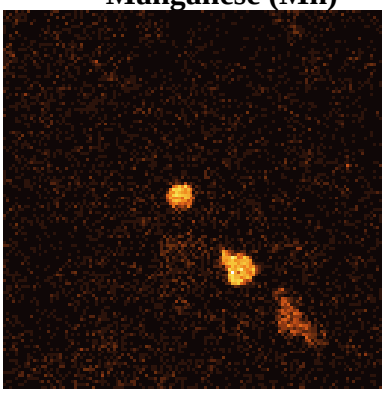

Phosphorous (P)

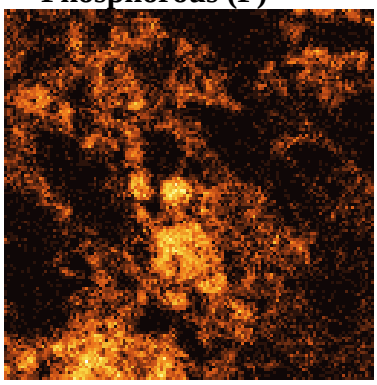

Lead (Pb)

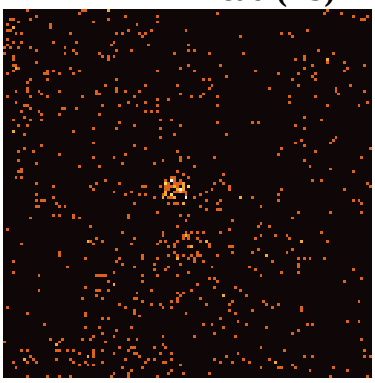

Silicon (Si)

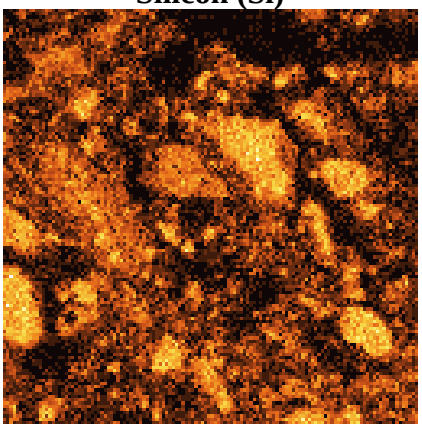

EDS Scan Images by Point

Point 1

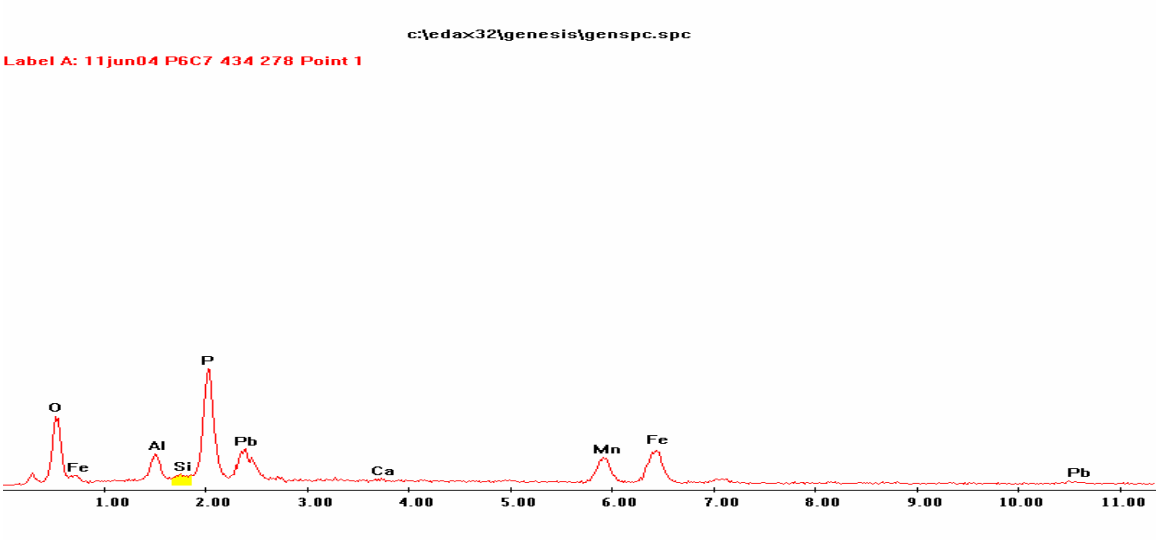

Point 2

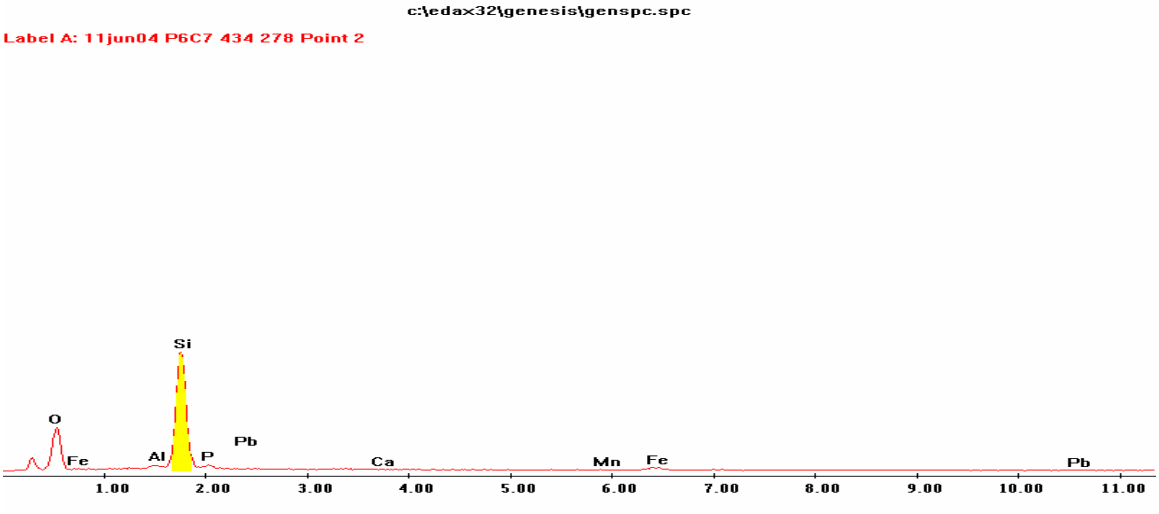

Point 3

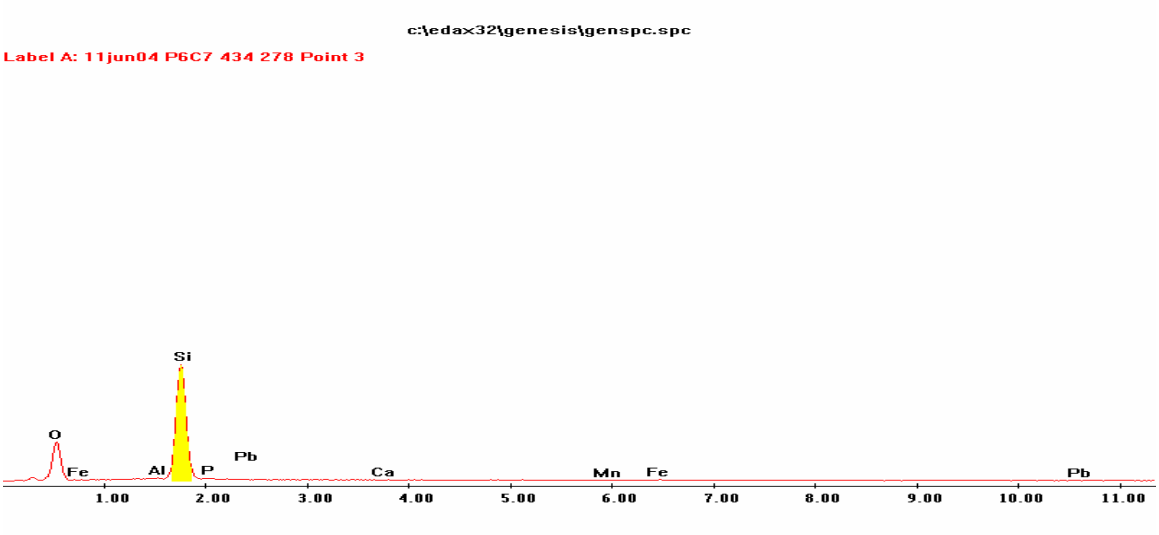

Point 4

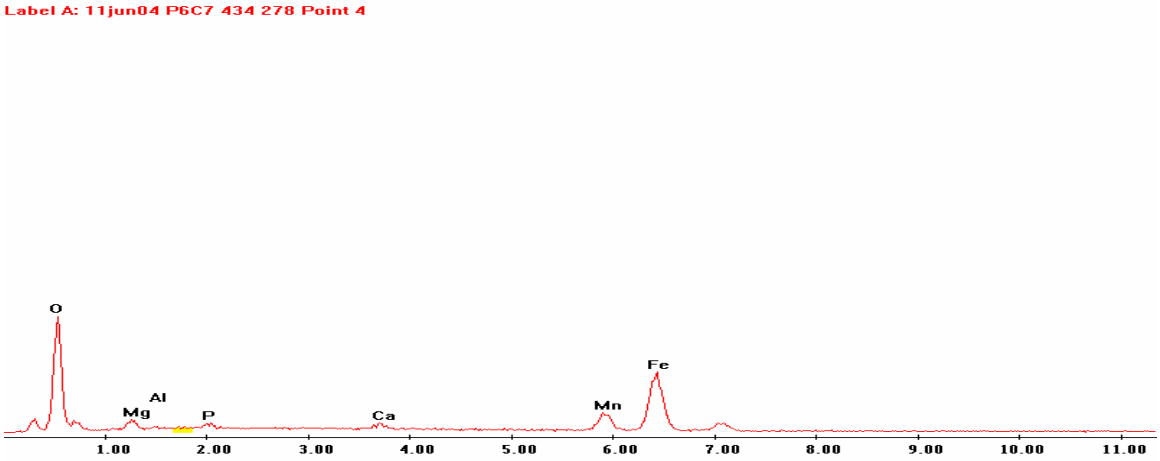

Point 5

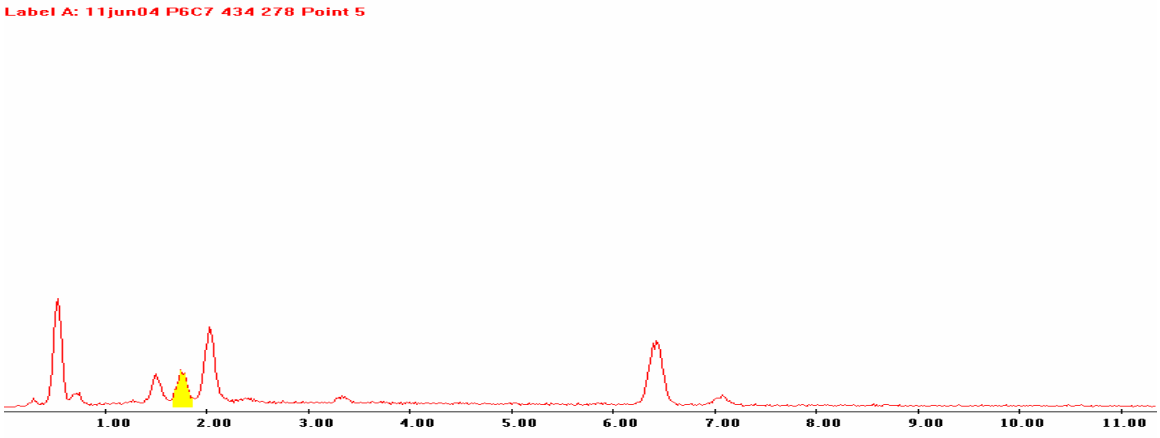

Point 6

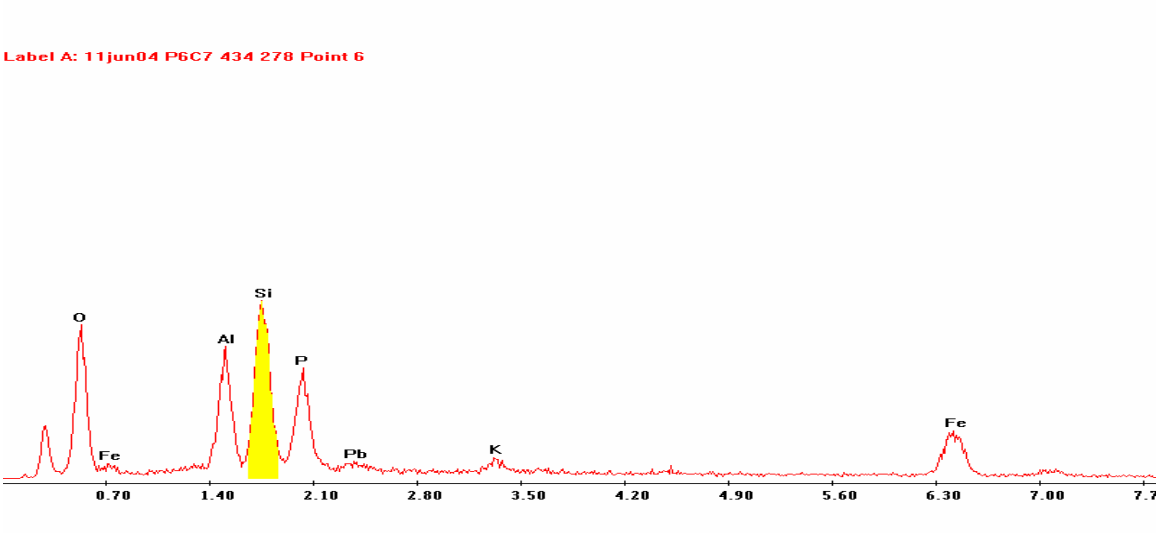

Point 7

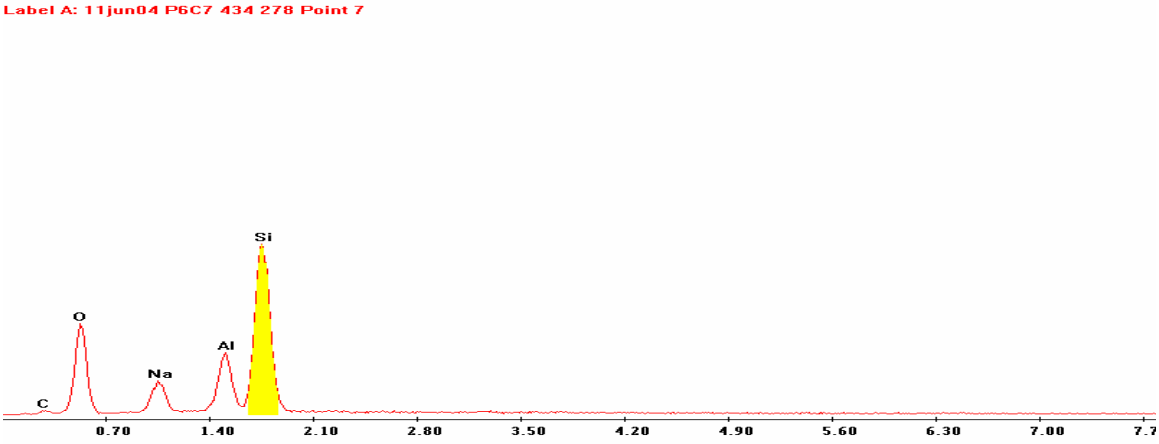

Point 8

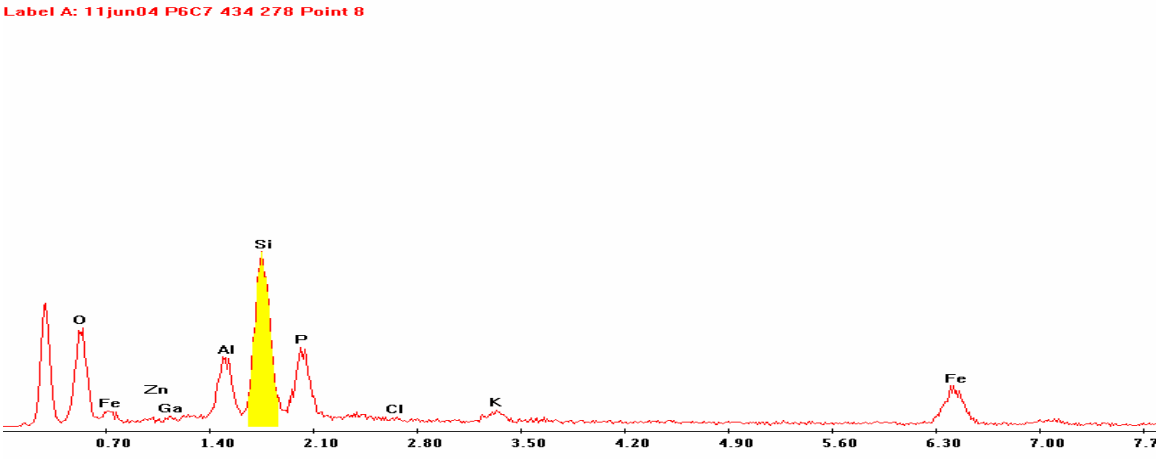

Point 9

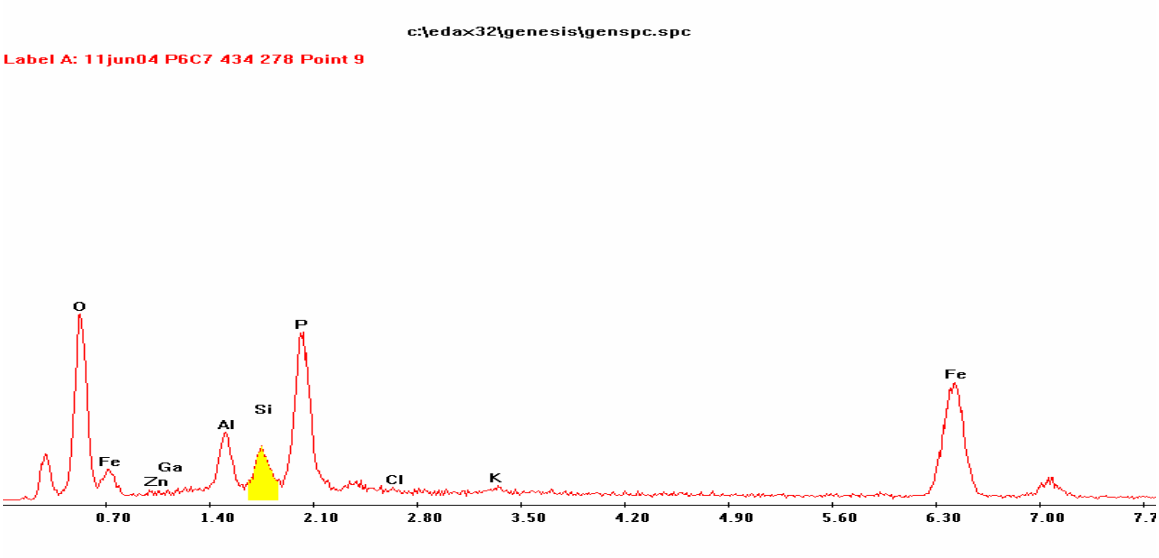

Point 10

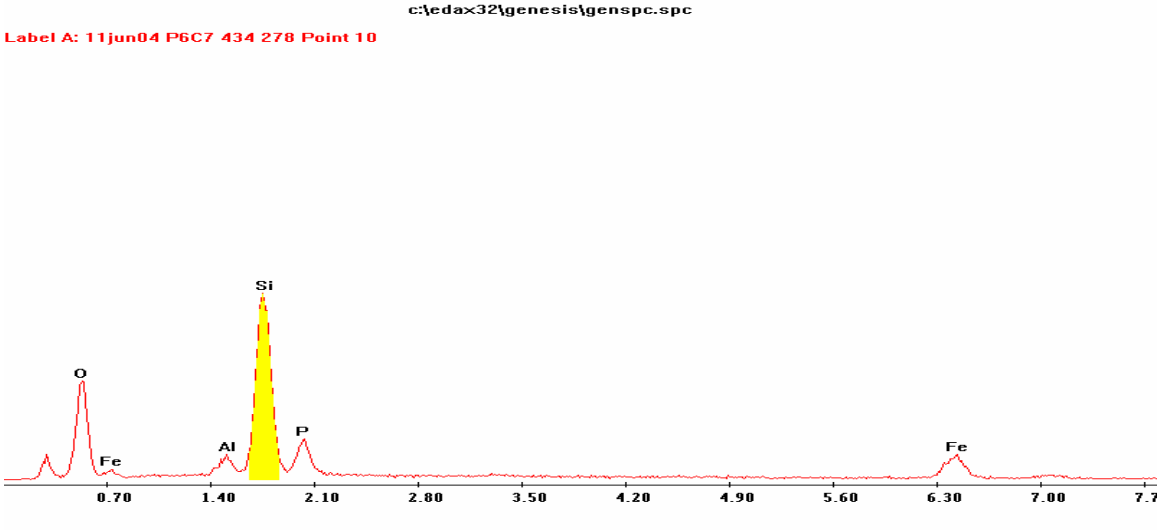

P6C7 – 465, 249

BSE Image

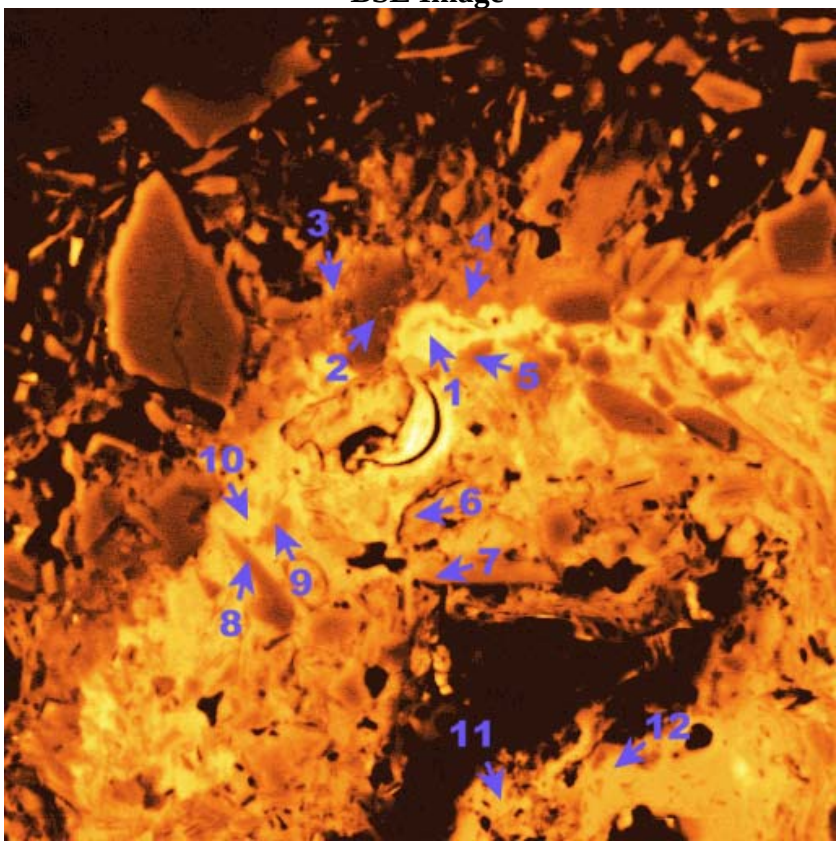

Iron (Fe)

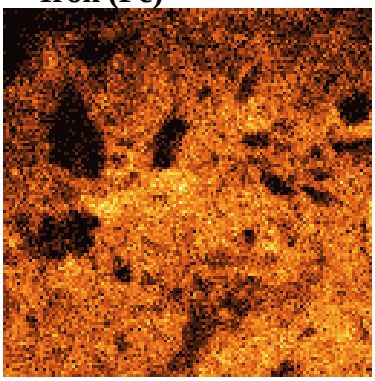

Manganese (Mn)

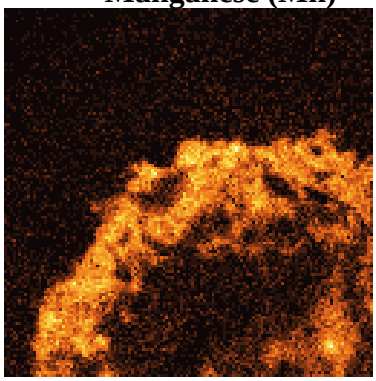

Phosphorous (P)

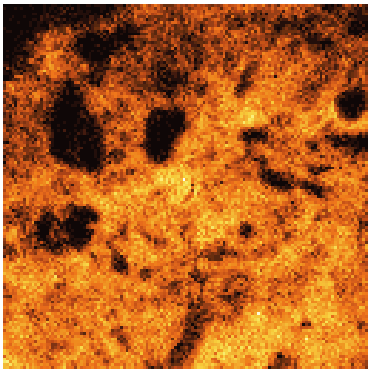

Lead (Pb)

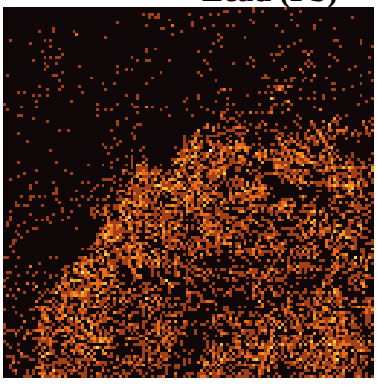

Silicon (Si)

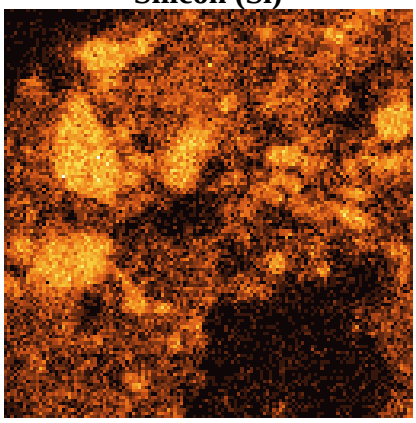

EDS Scan Images by Point

Point 1

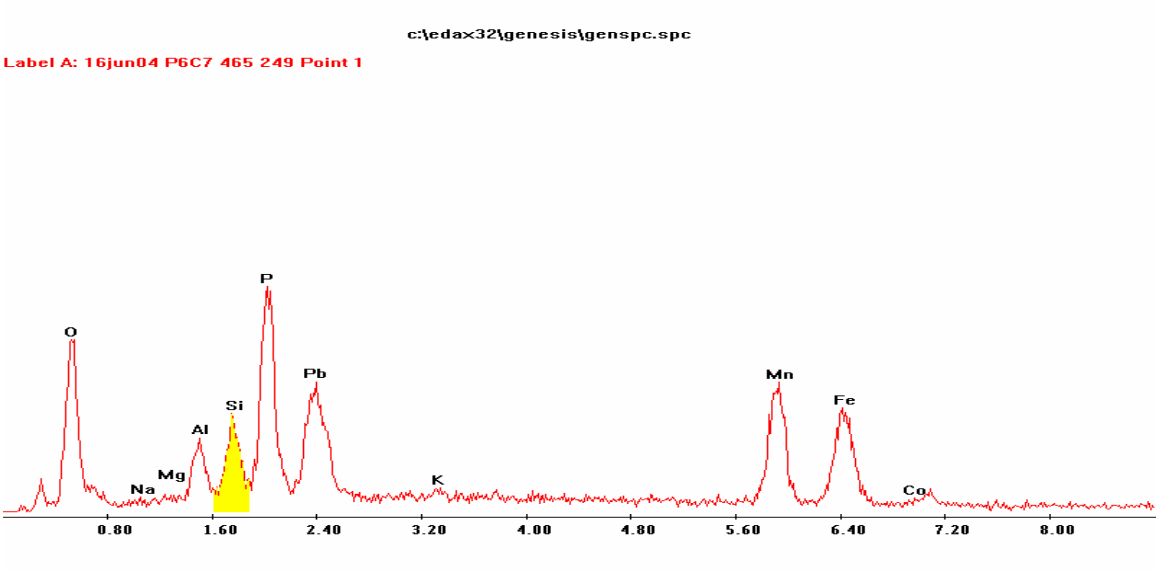

Point 2

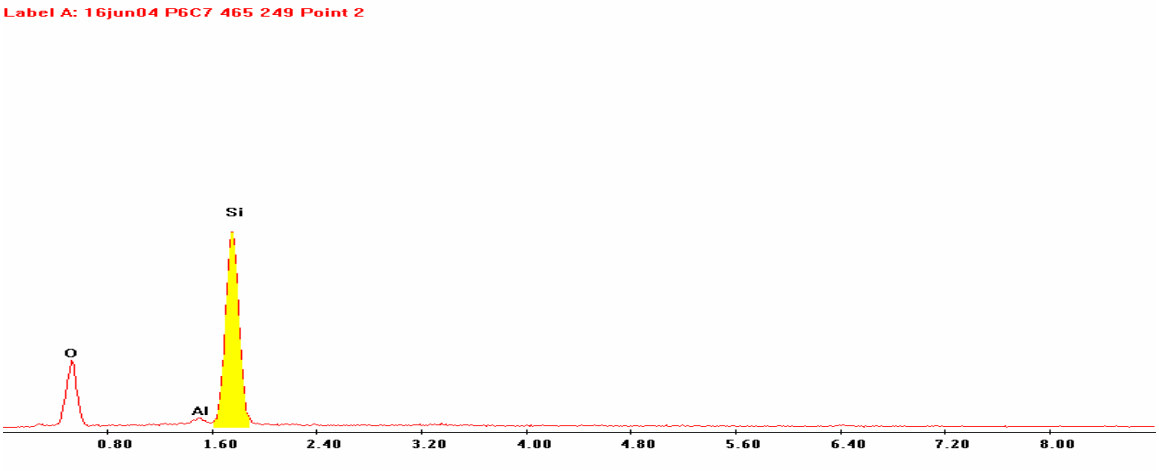

Point 3

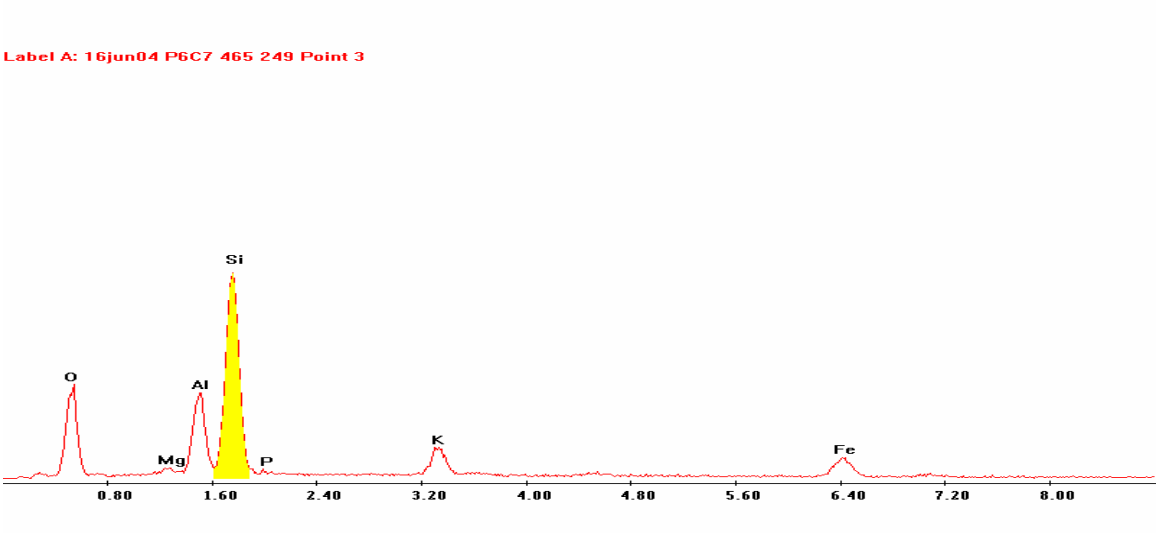

Point 4

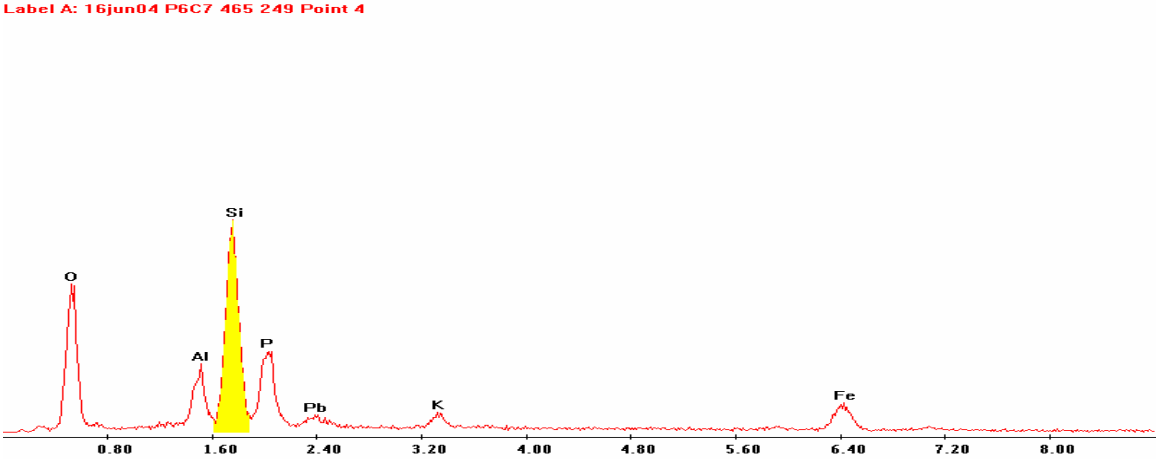

Point 5

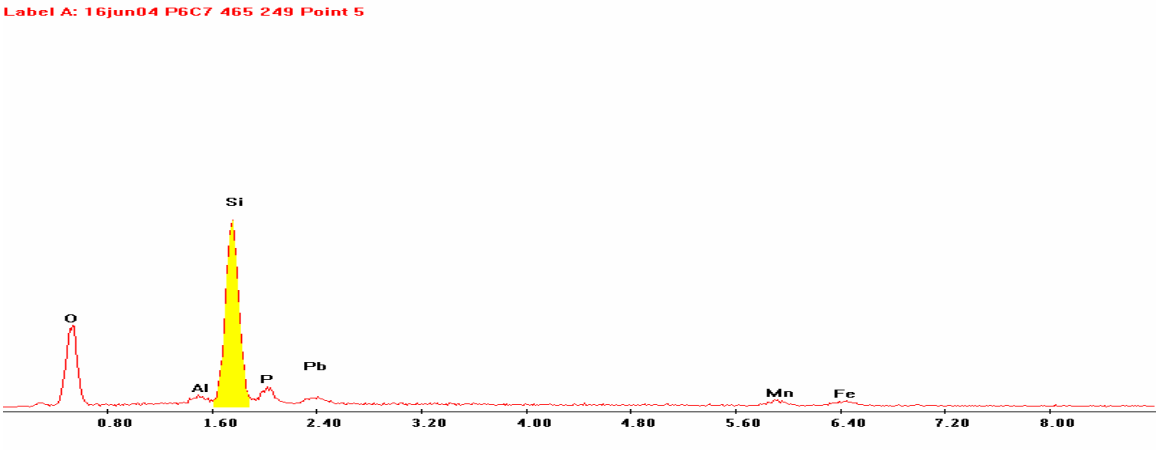

Point 6

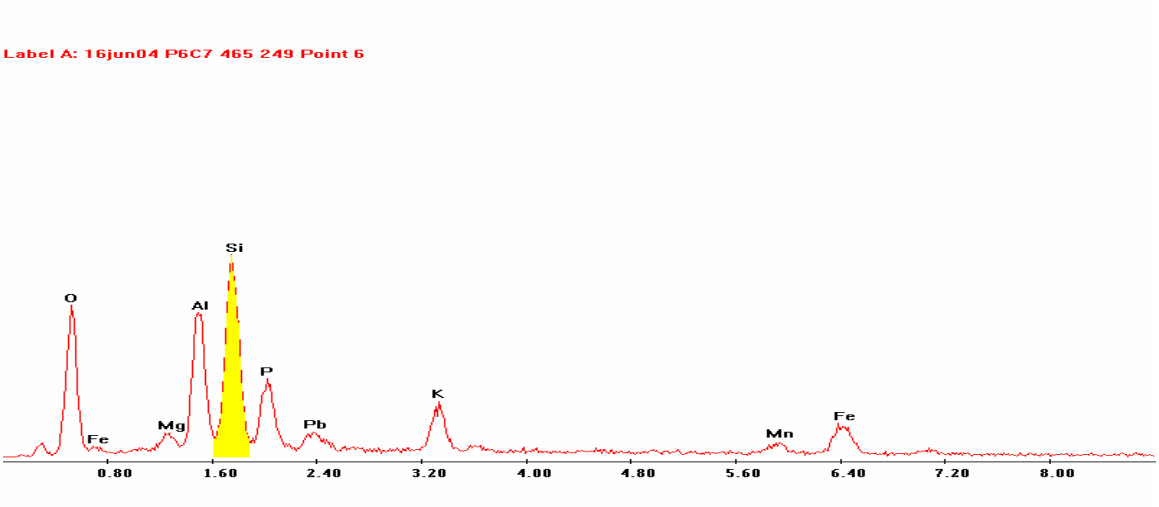

Point 7

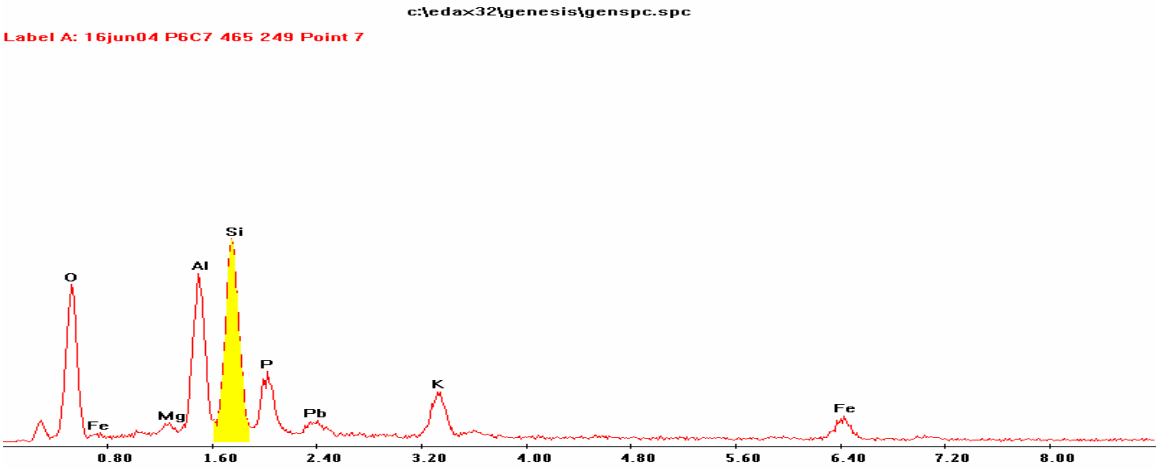

Point 8

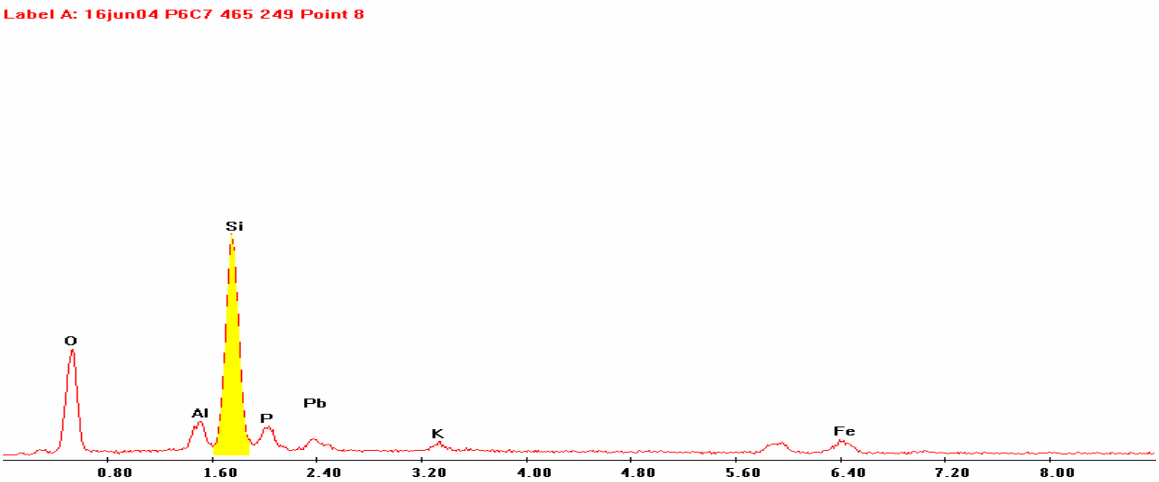

Point 9

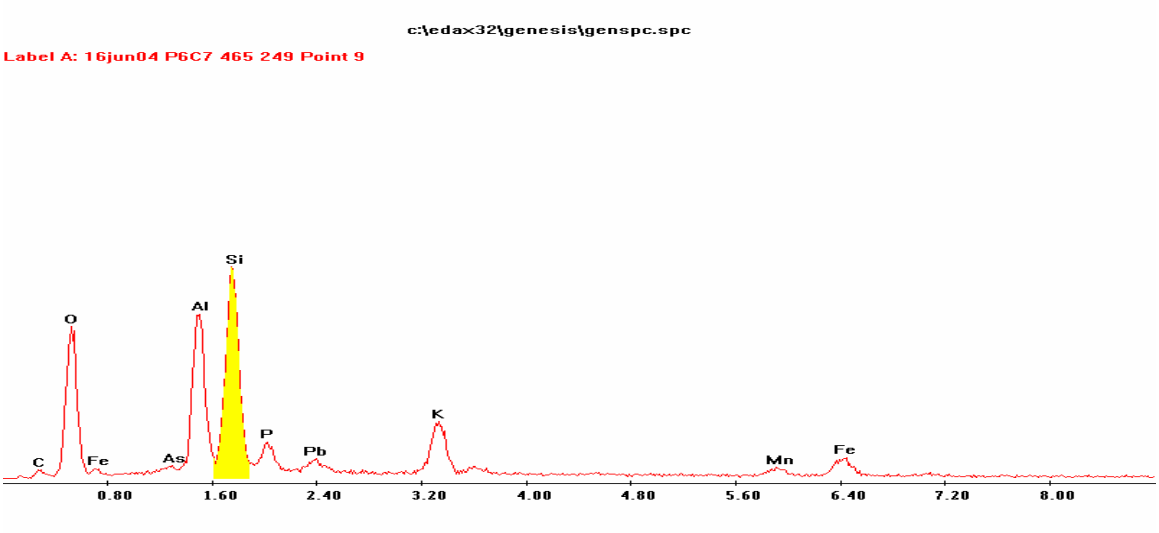

Point 10

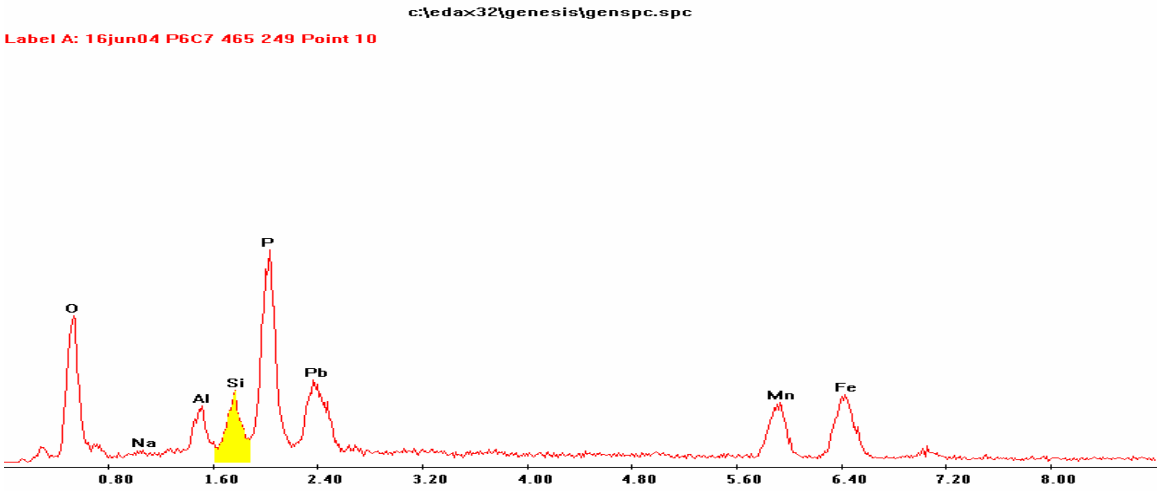

Point 11

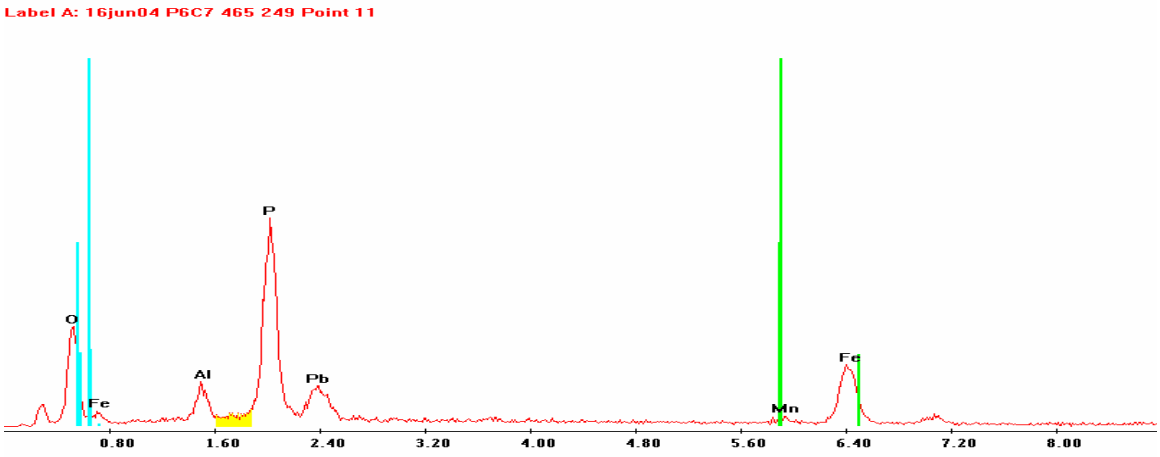

Point 12

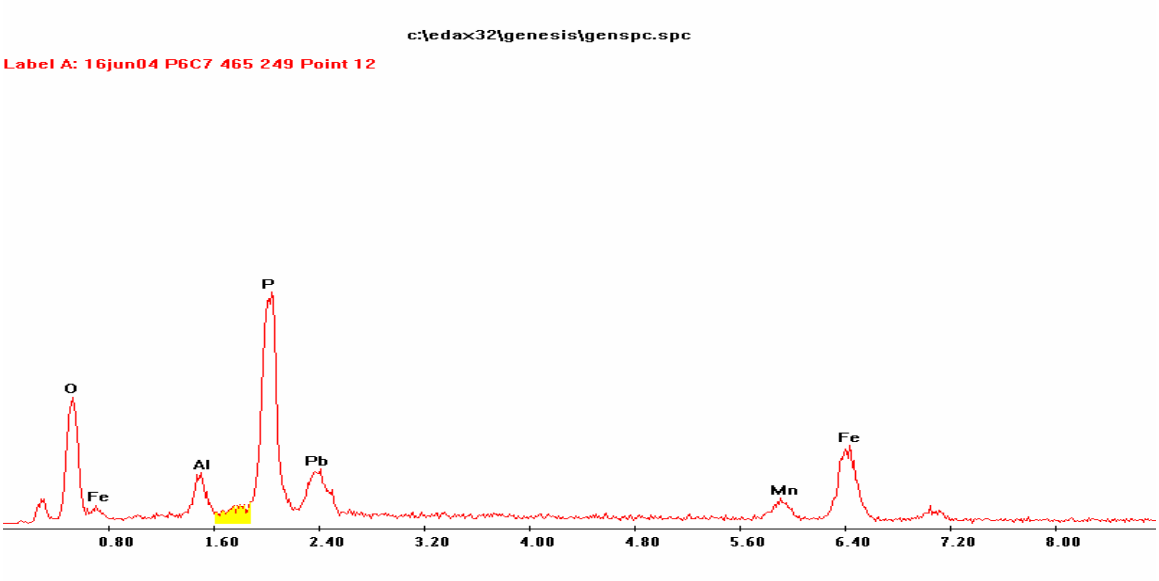
c:\edax32\genesis\genspc.spc
Label A: 16jun04 P6C7 465 249 Point 12
O
Fe
Al
P
Pb
Mn
Fe
0.80
1.60
2.40
3.20
4.00
4.80
5.60
6.40
7.20
8.00

P6C7 – 498, 110

BSE Image

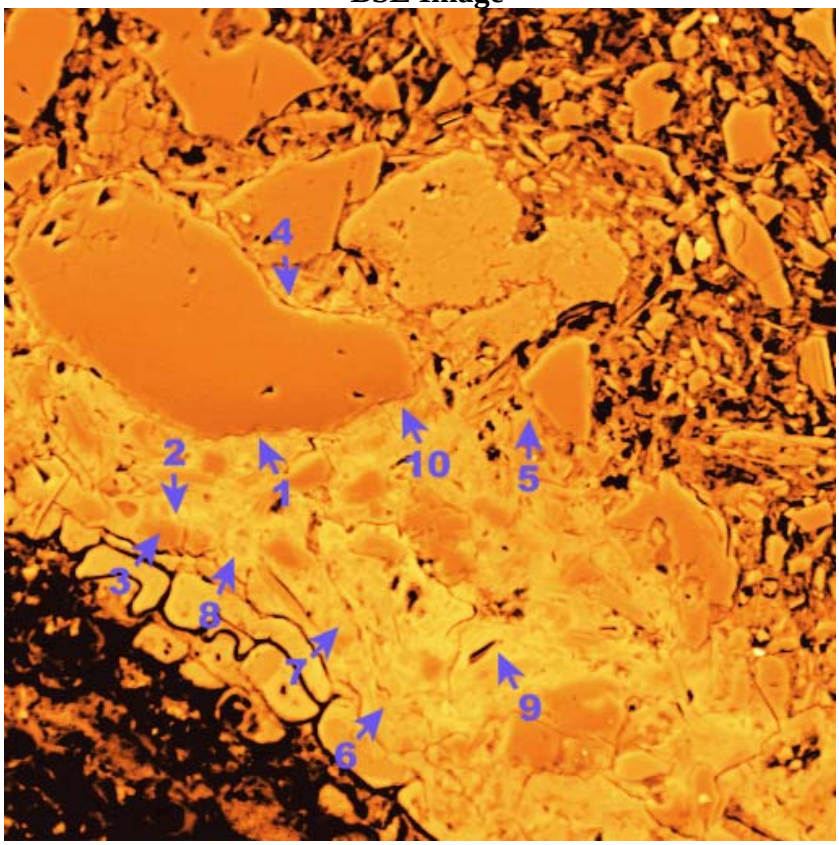

Iron (Fe)

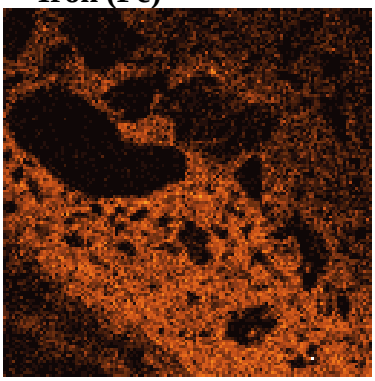

Manganese (Mn)

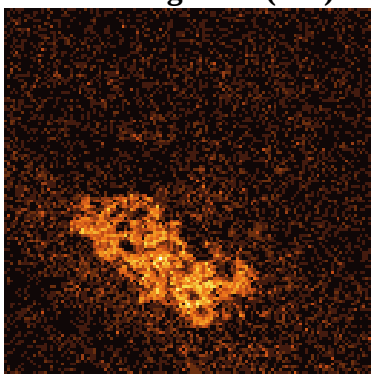

Phosphorous (P)

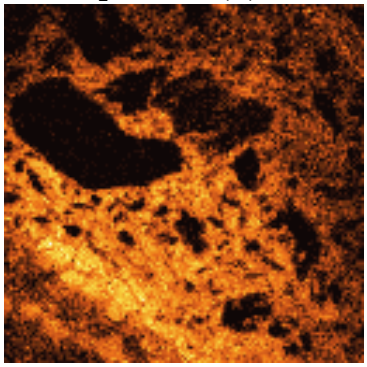

Lead (Pb)

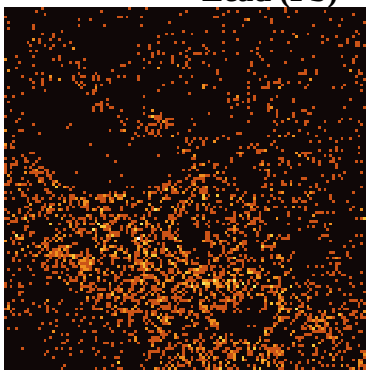

Silicon (Si)

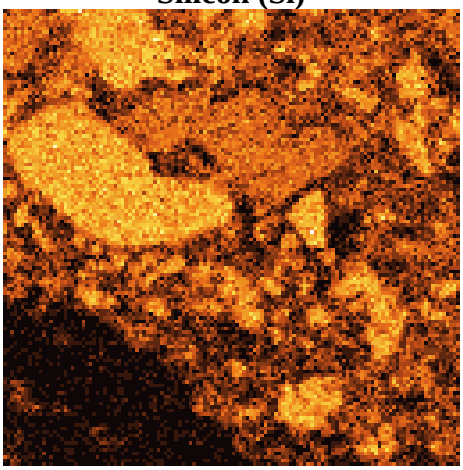

EDS Scan Images by Point

Point 1

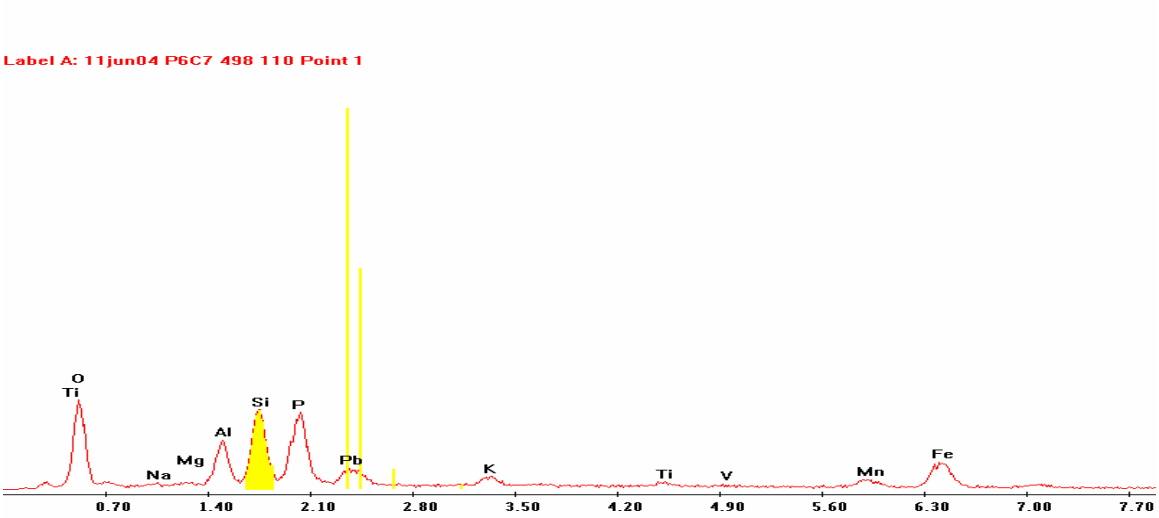

Point 2

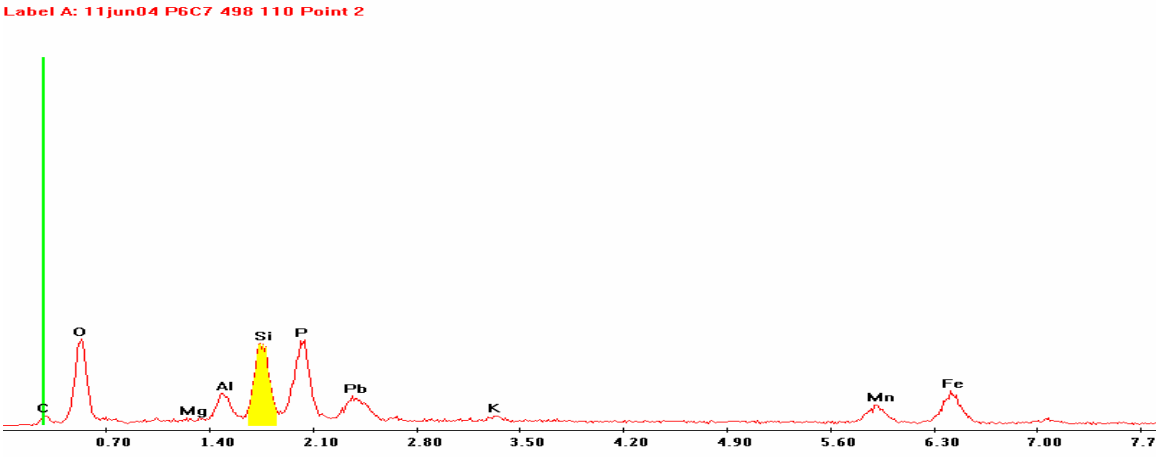

Point 3

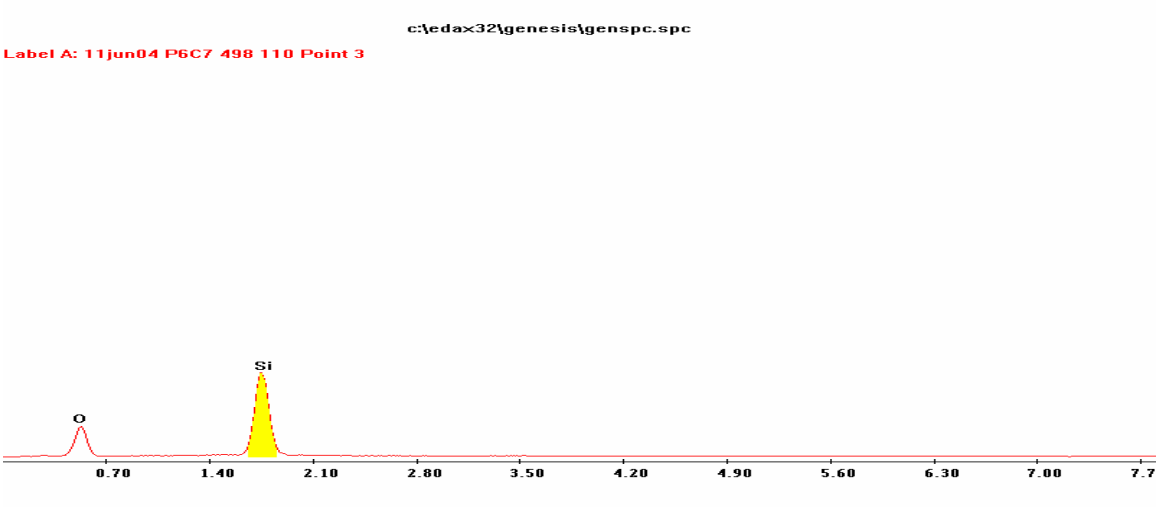

Point 4

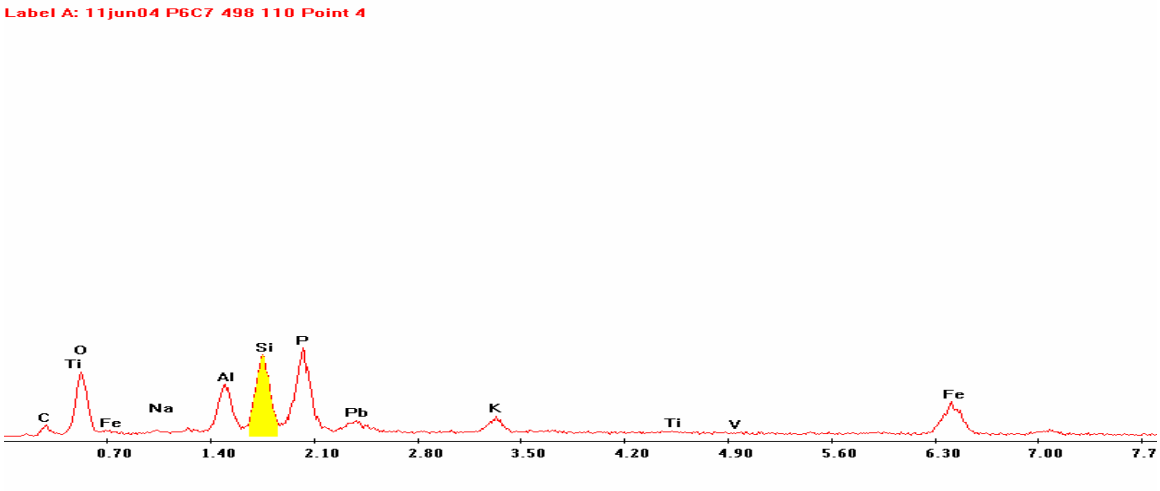

Point 5

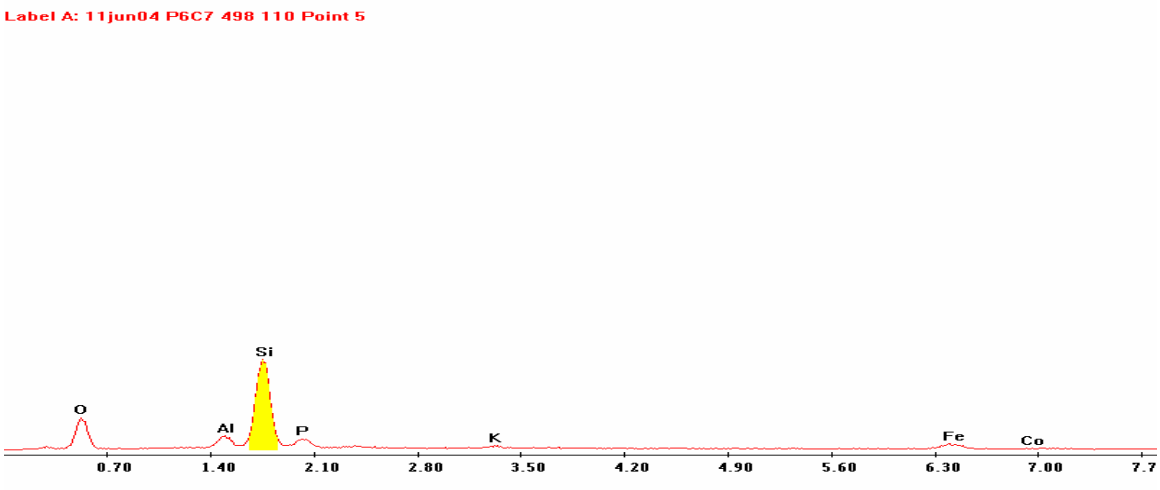

Point 6

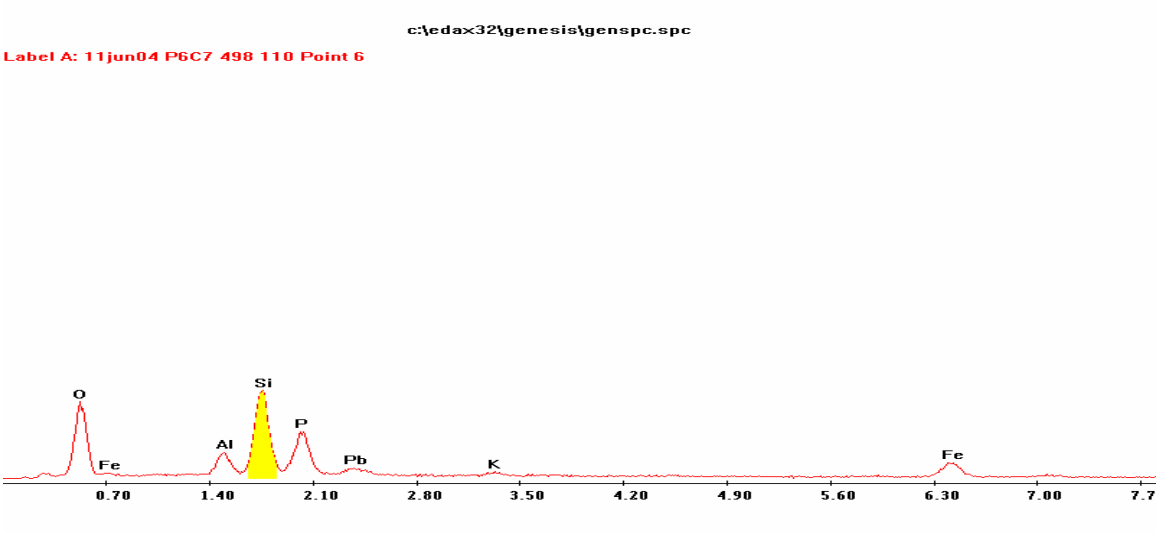

Point 7

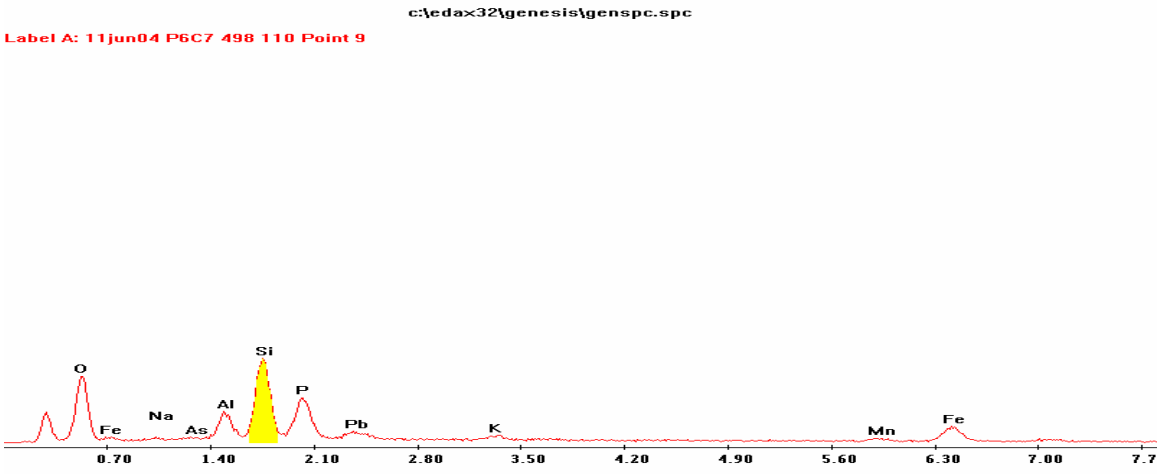

Point 8

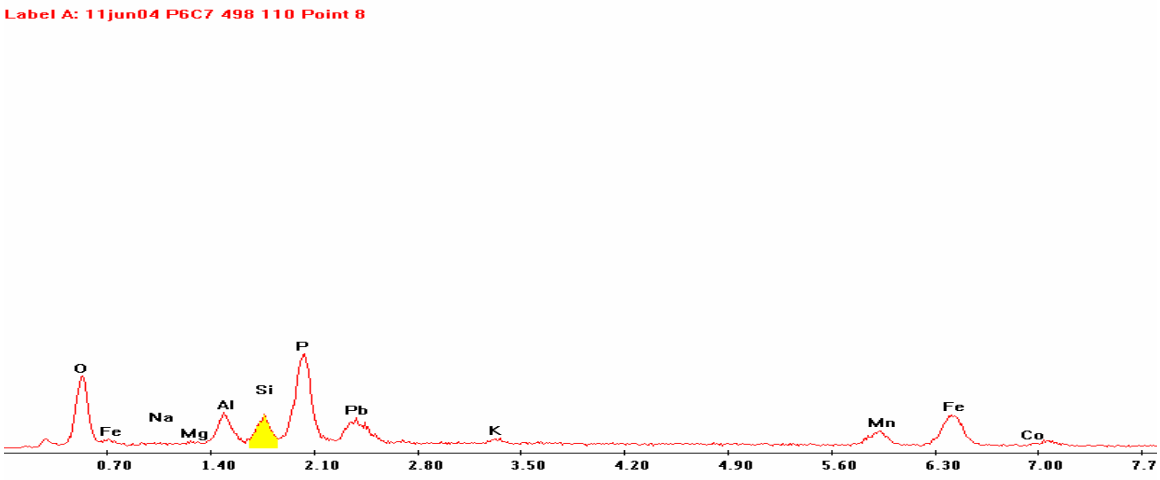

Point 9

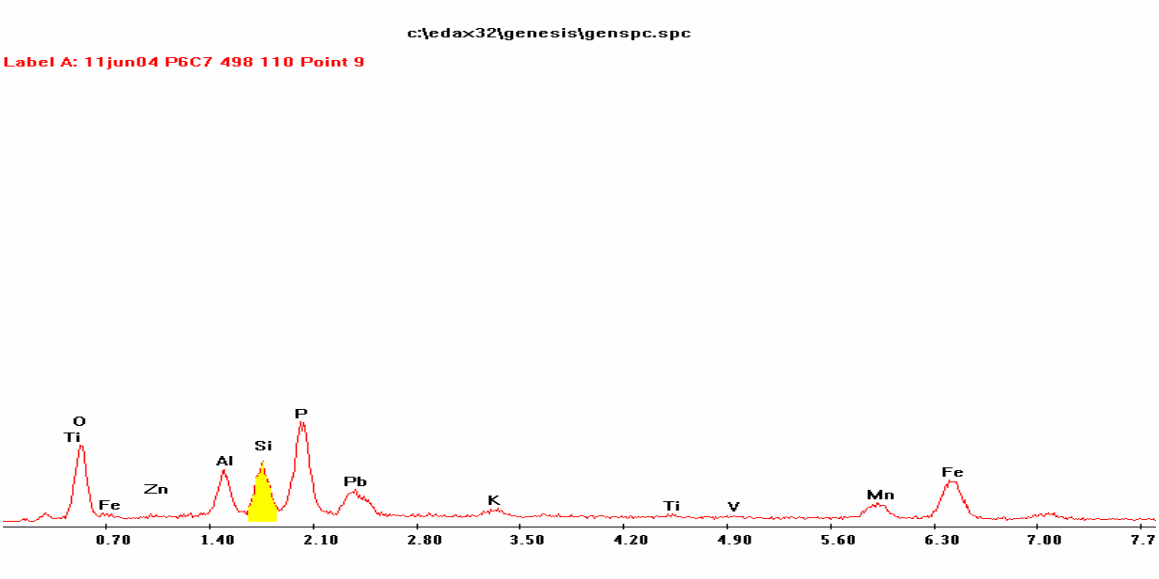

Point 10

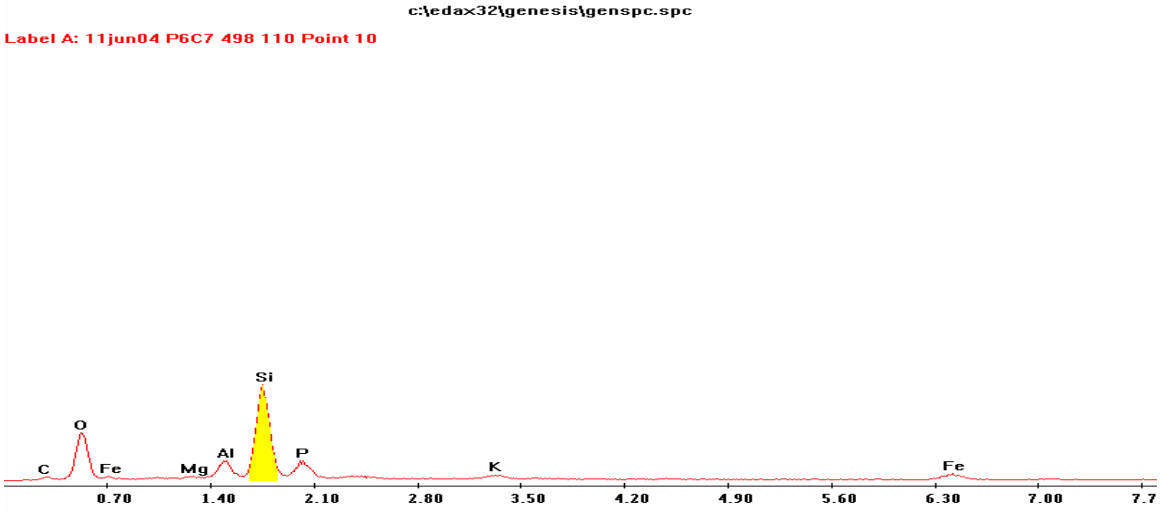

P6C8 – 345, 256

BSE Image

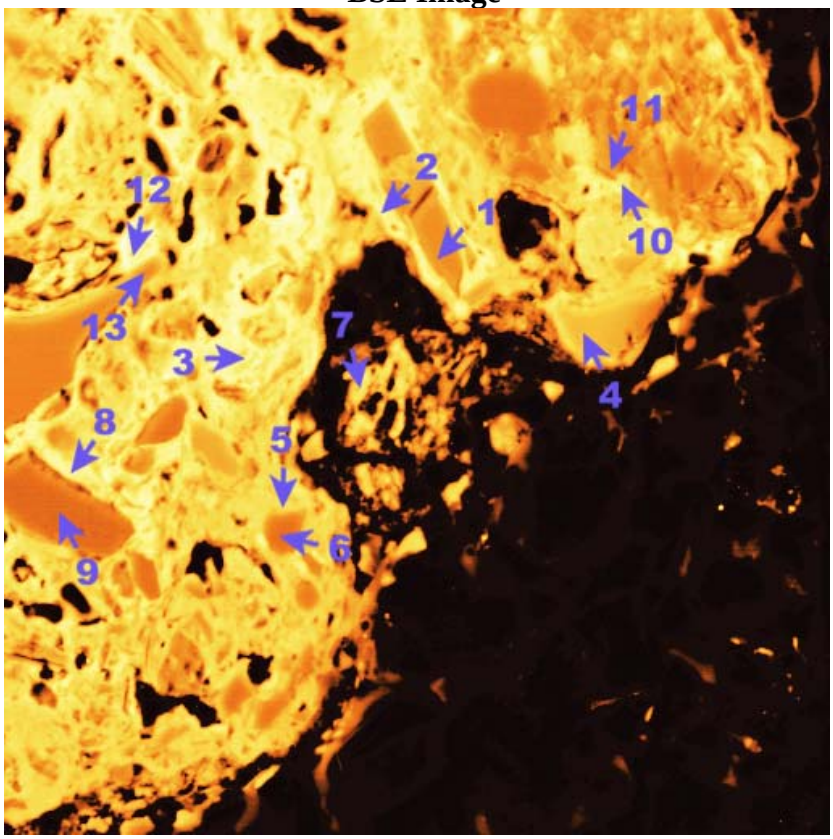

Iron (Fe)

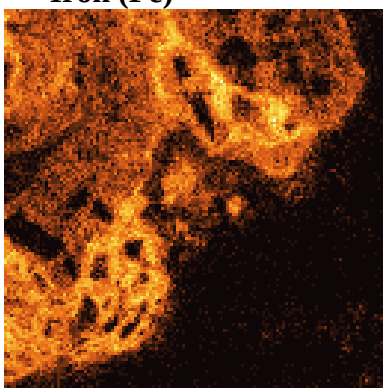

Manganese (Mn)

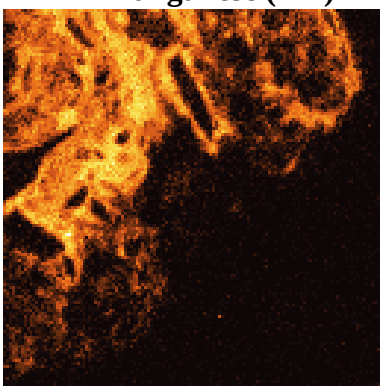

Phosphorous (P)

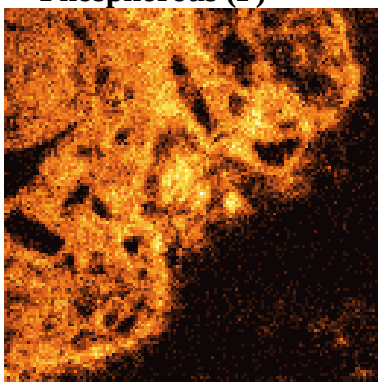

Lead (Pb)

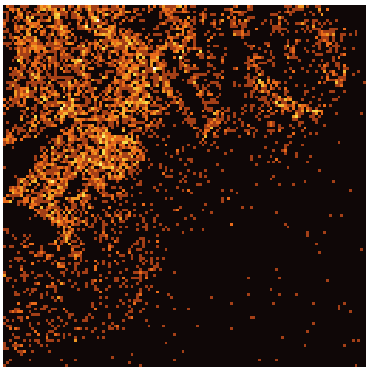

Silicon (Si)

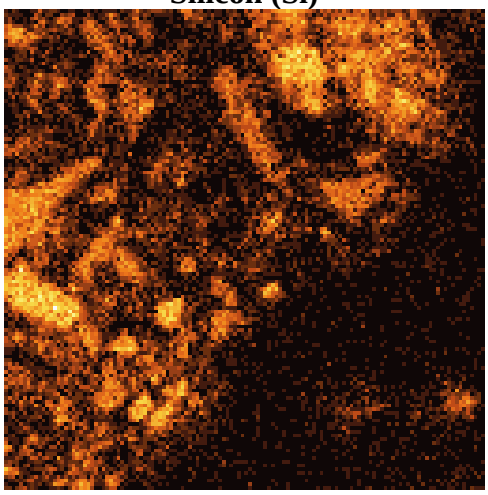

EDS Scan Images by Point

Point 1

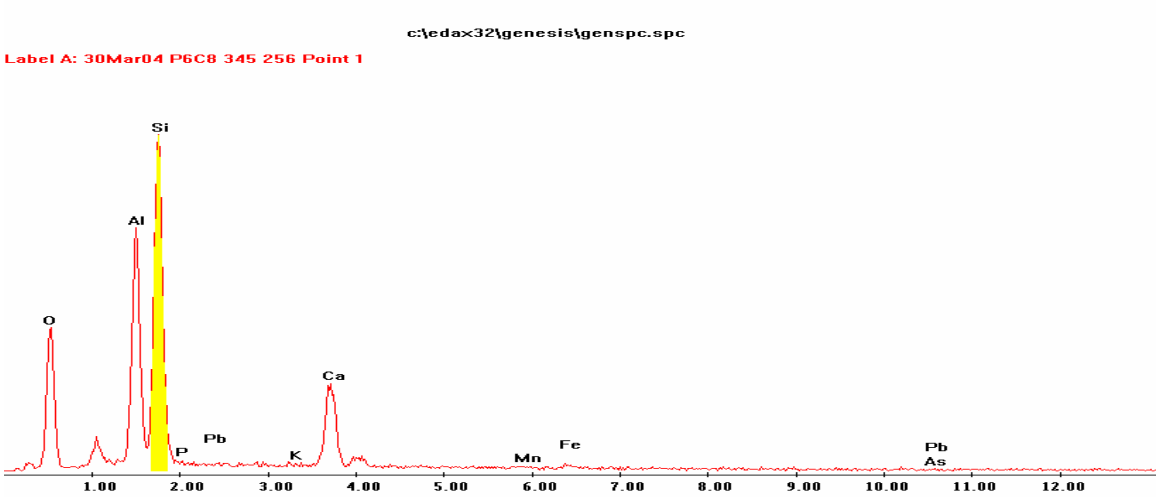

Point 2

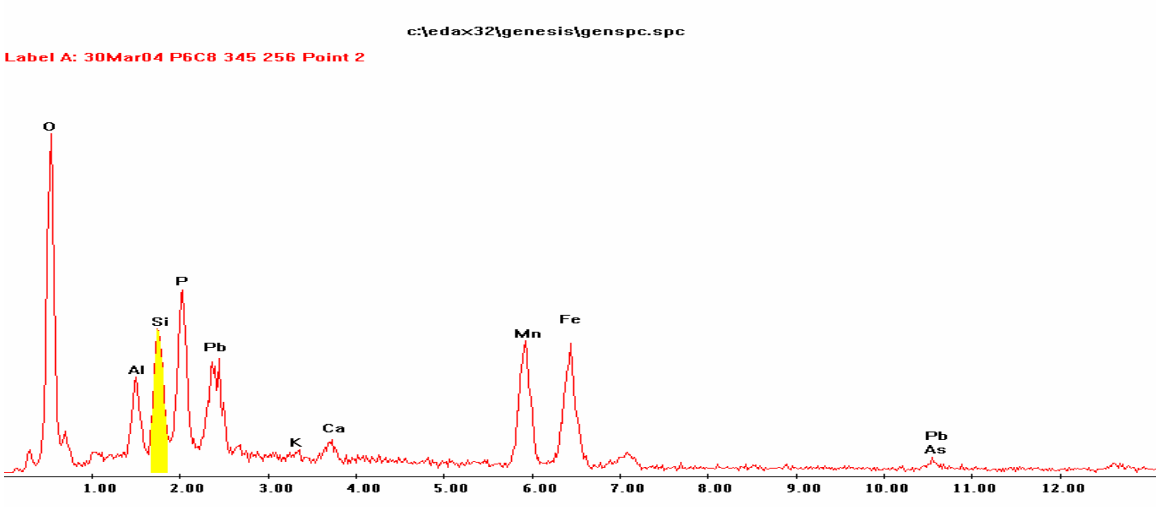

Point 3

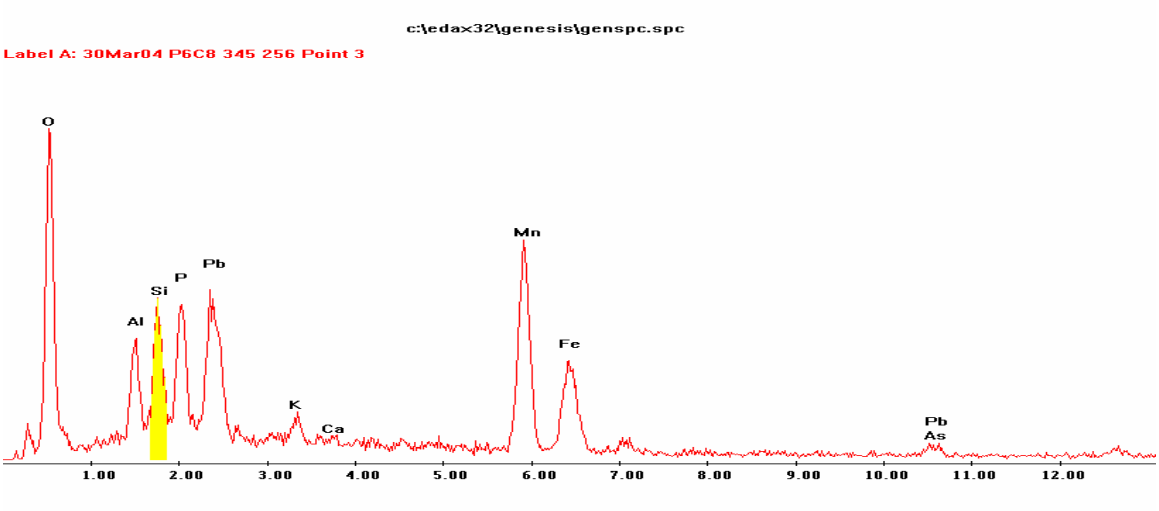

Point 4

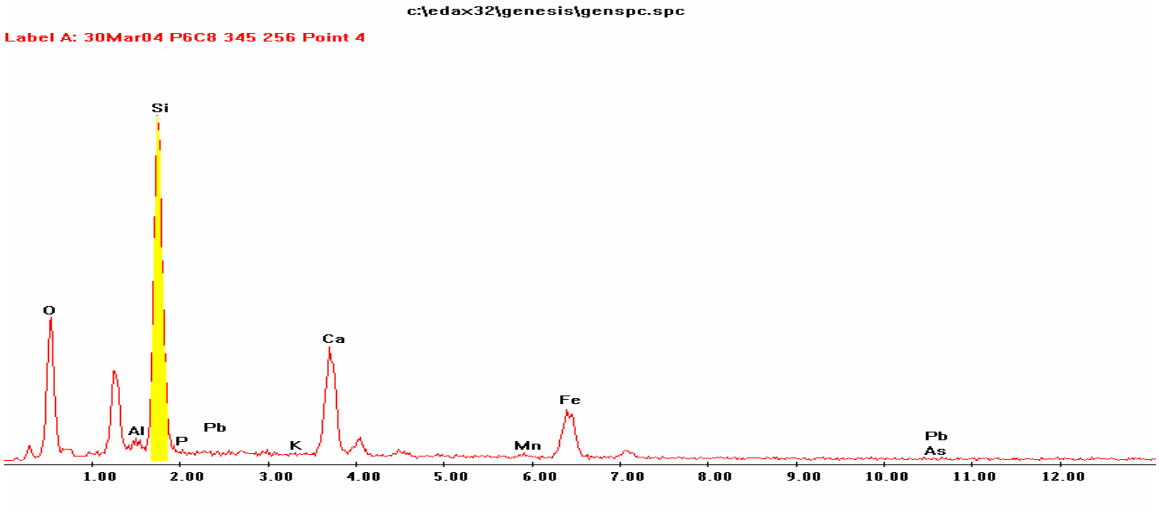

Point 5

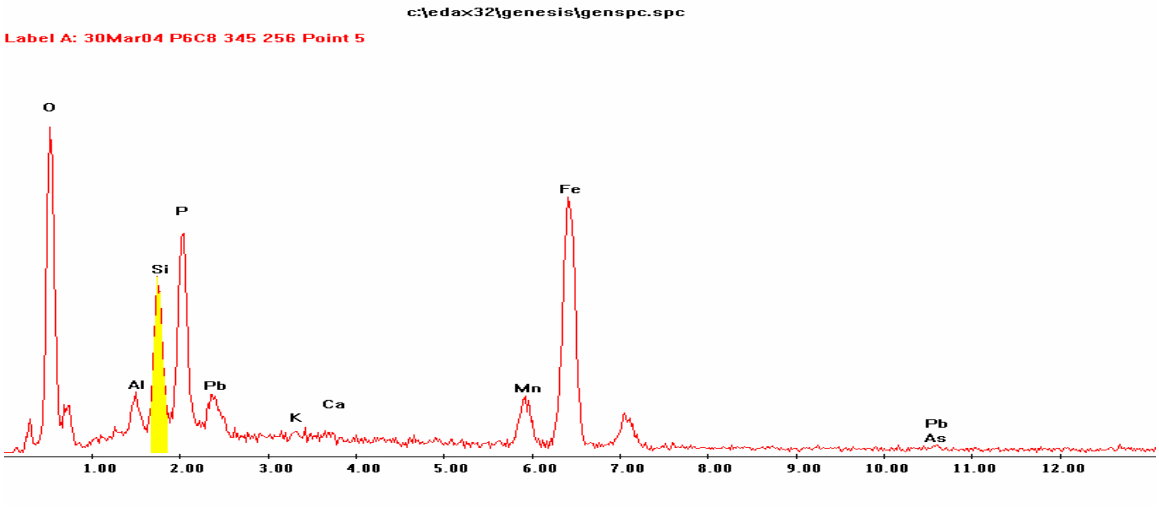

Point 6

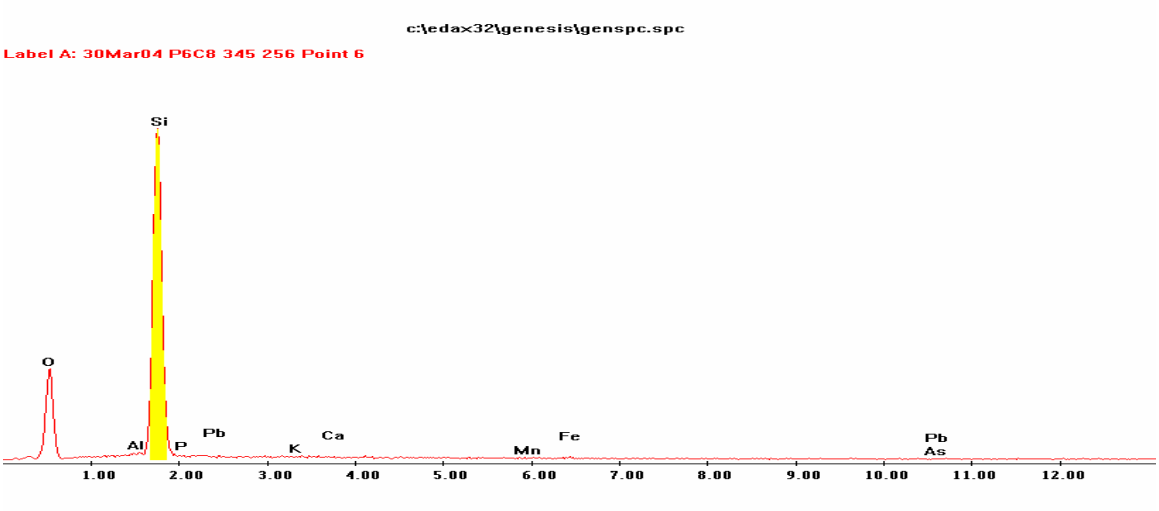

Point 7

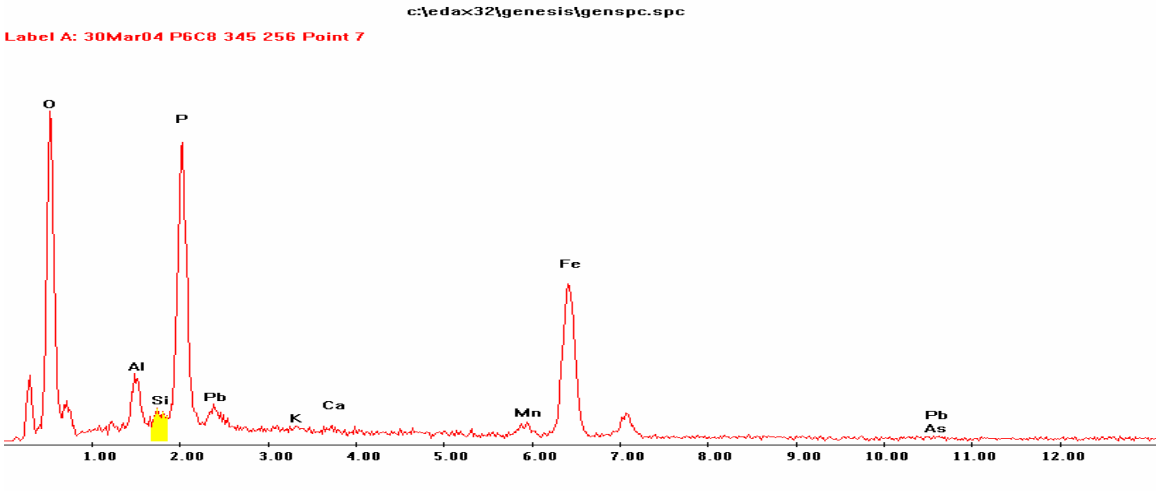

Point 8

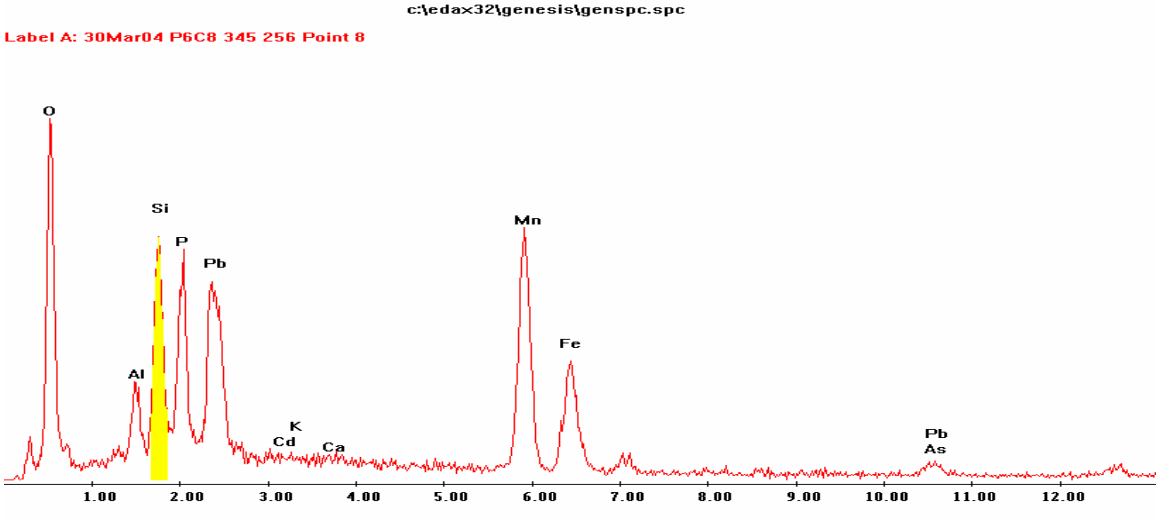

Point 9

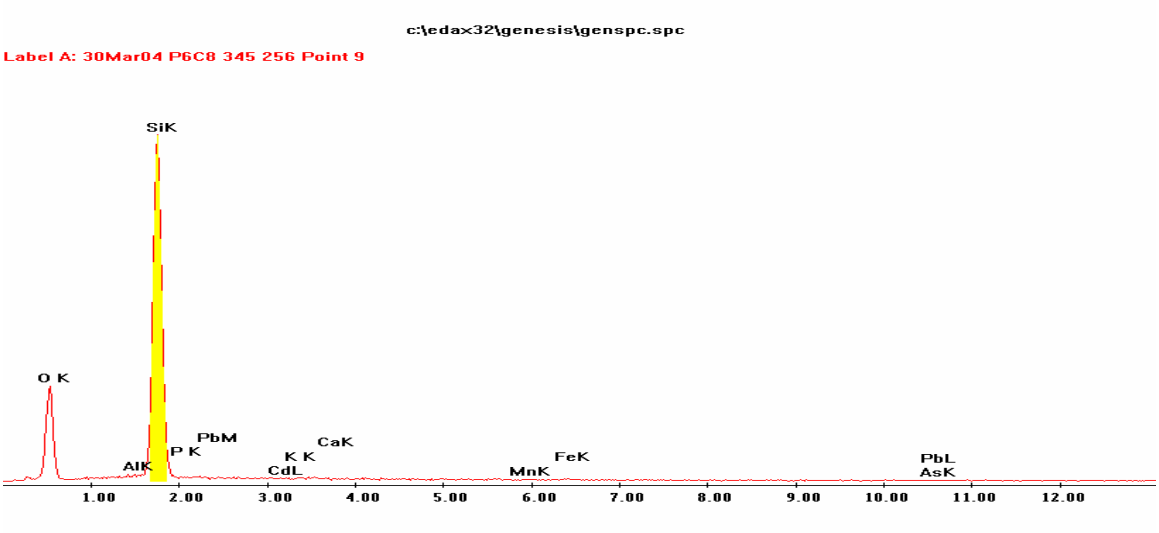

Point 10

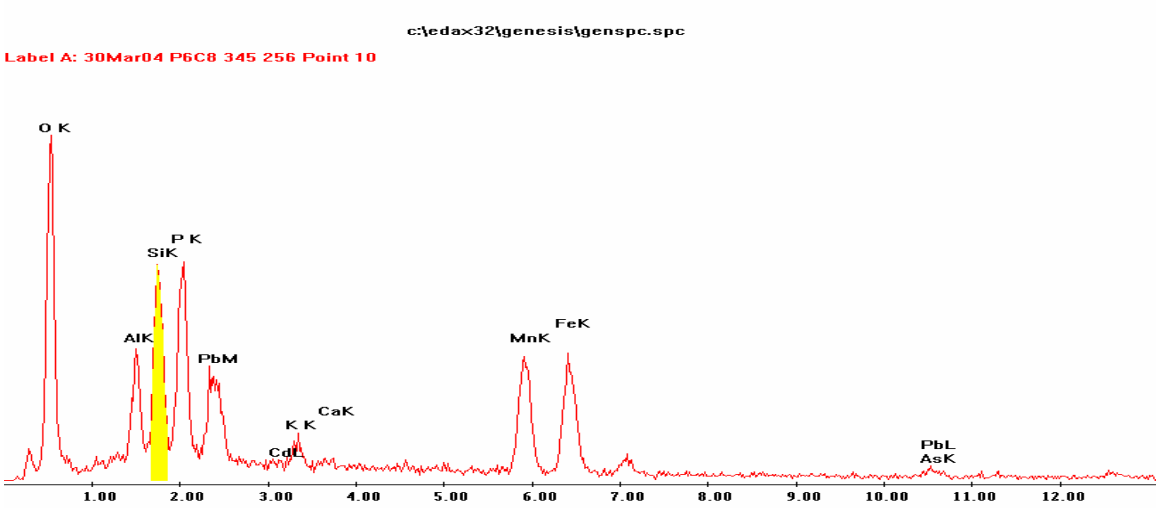

Point 11

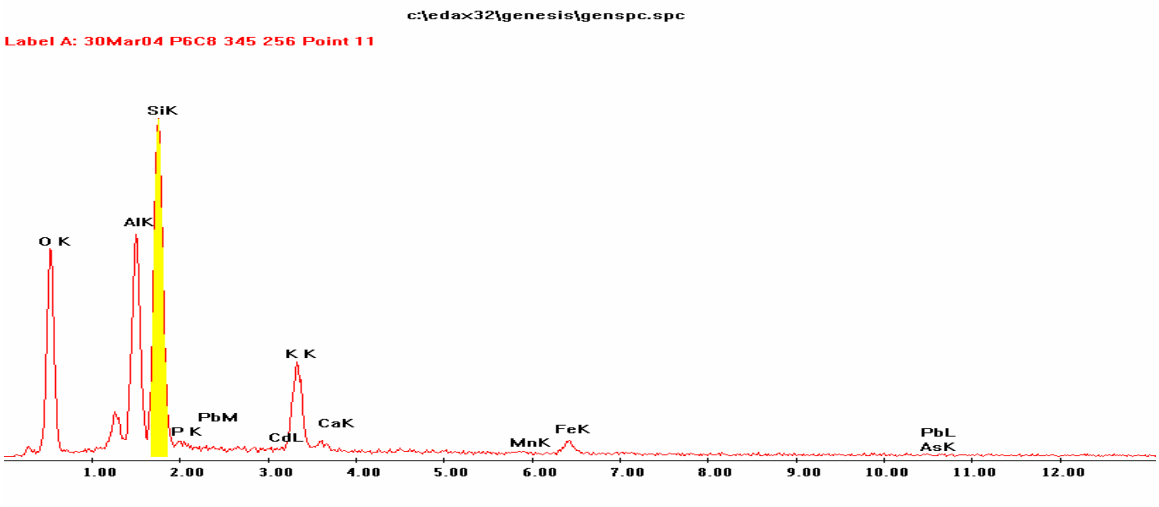

Point 12

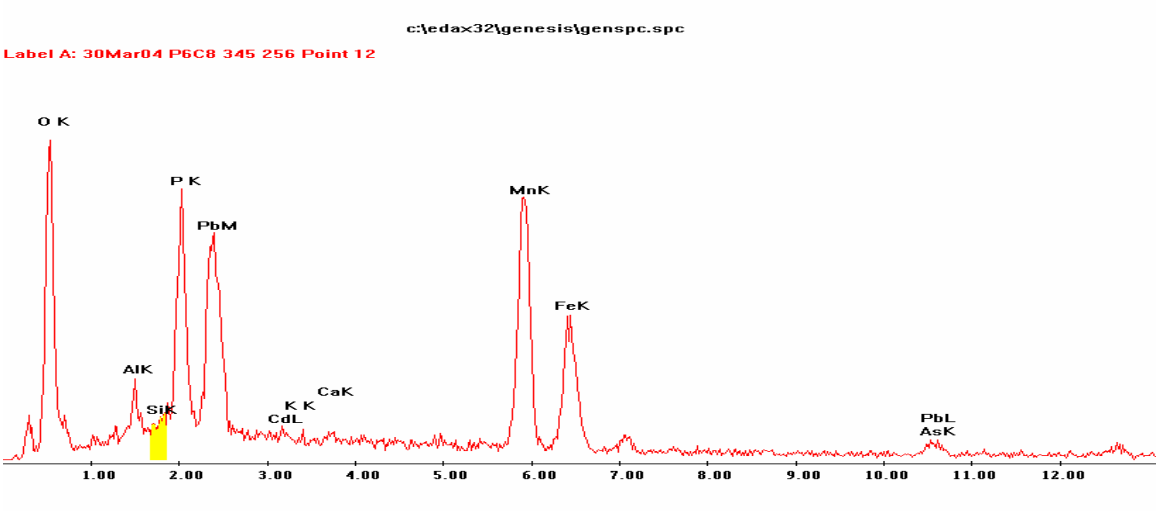

Point 13

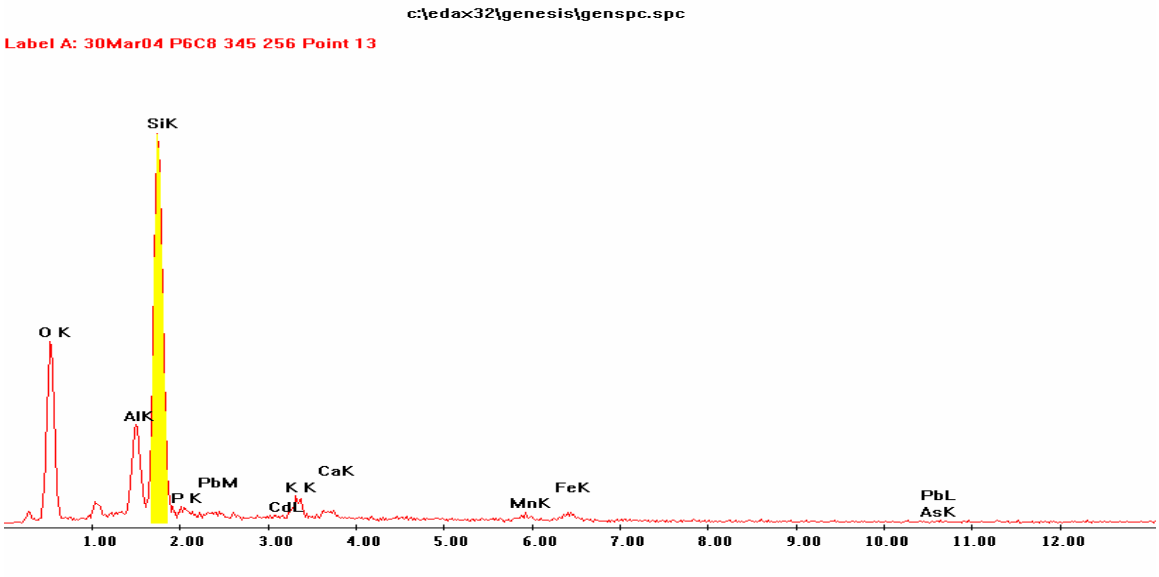

P6C8 – 361, 147

BSE Image

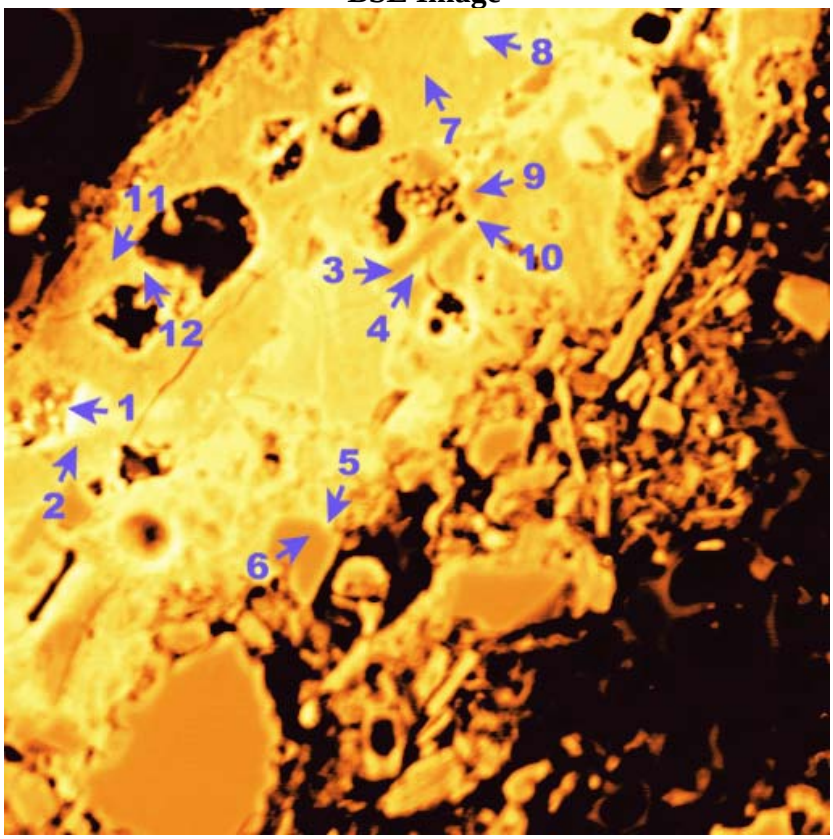

Iron (Fe)

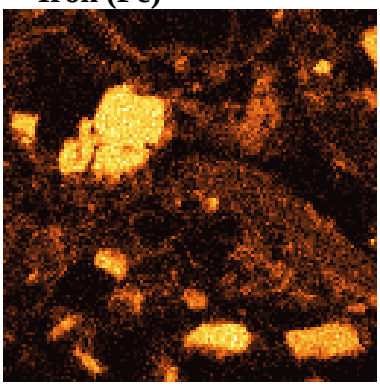

Manganese (Mn)

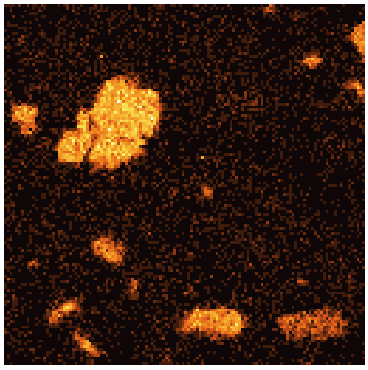

Phosphorous (P)

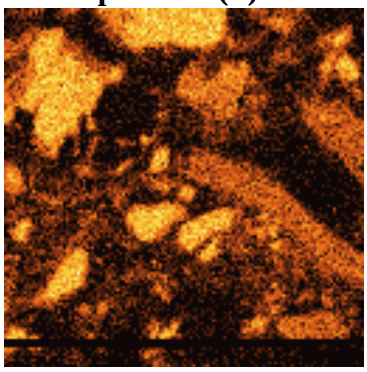

Lead (Pb)

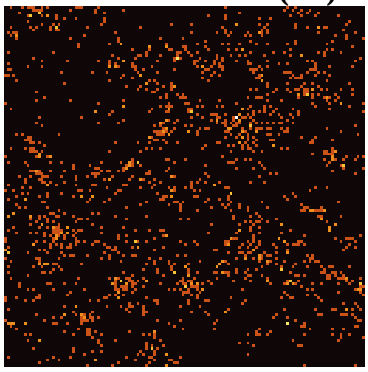

Silicon (Si)

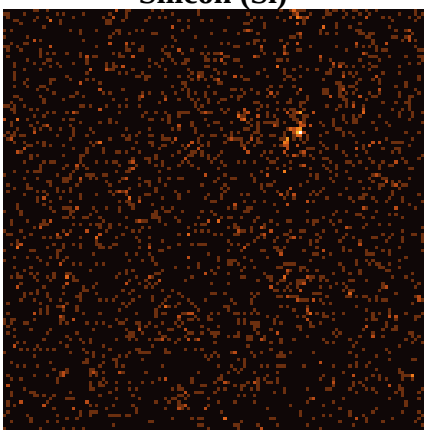

EDS Scan Images by Point

Point 1

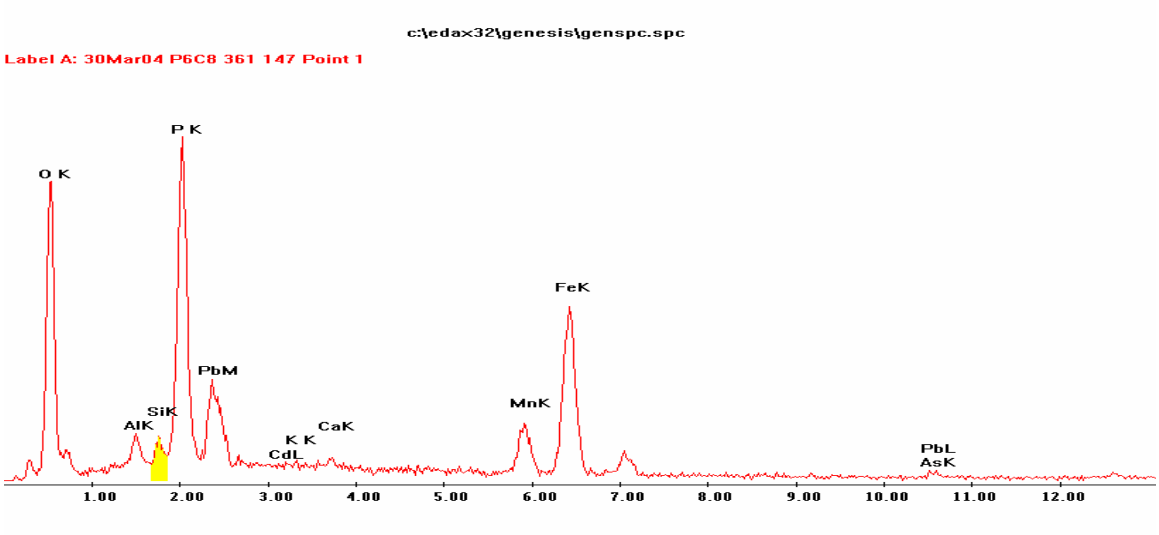

Point 2

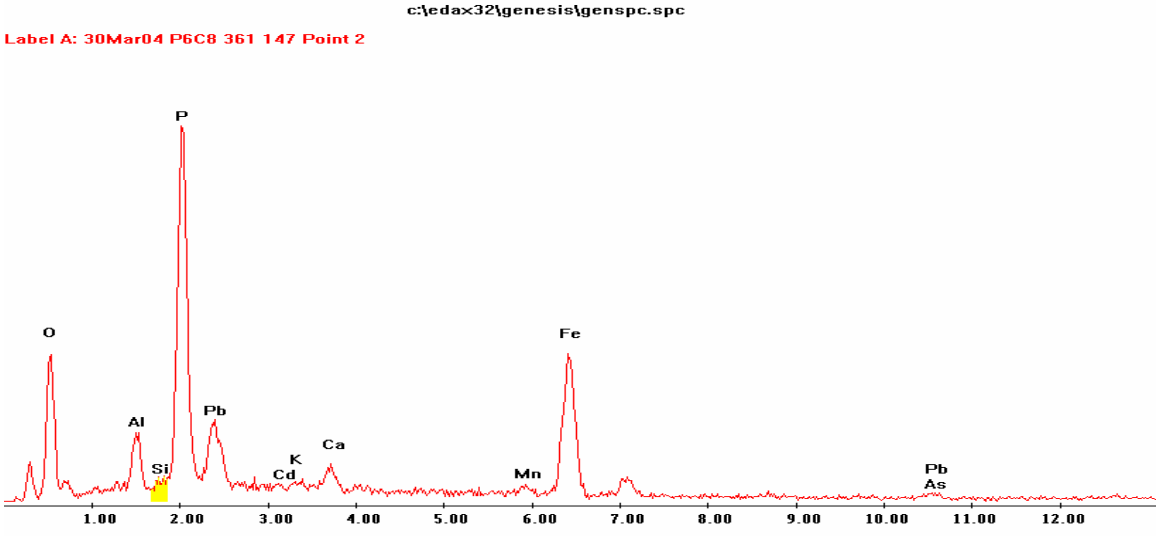

Point 3

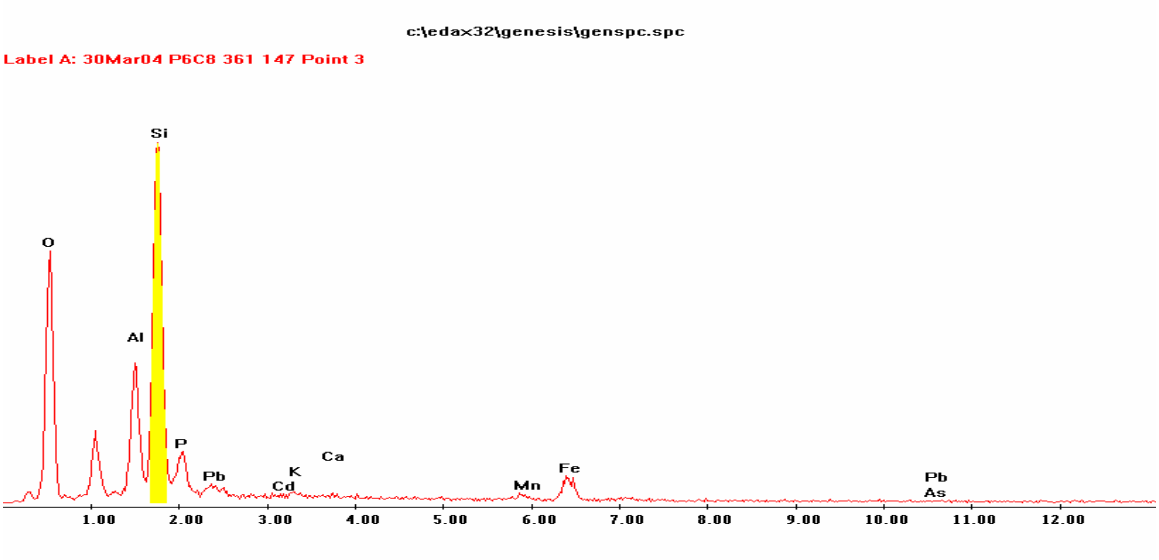

Point 4

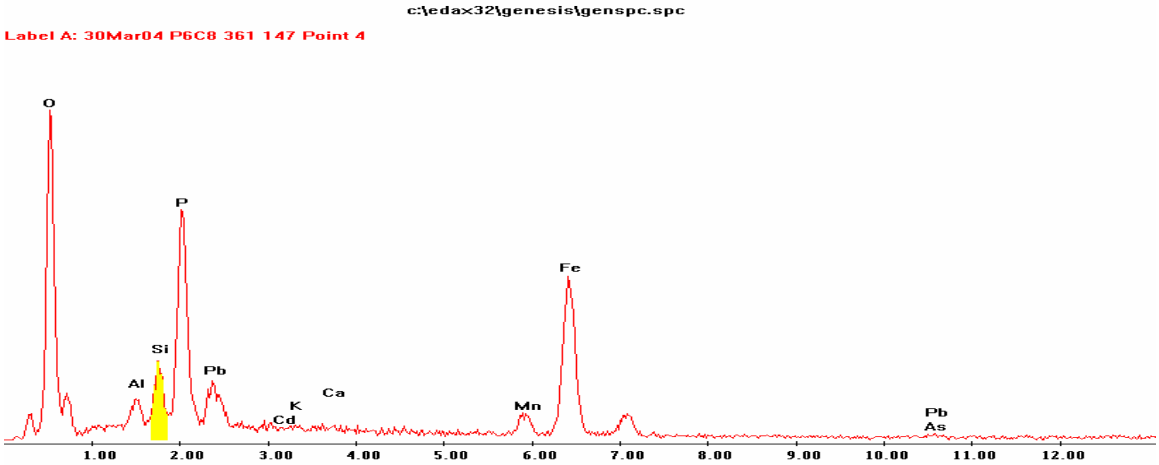

Point 5

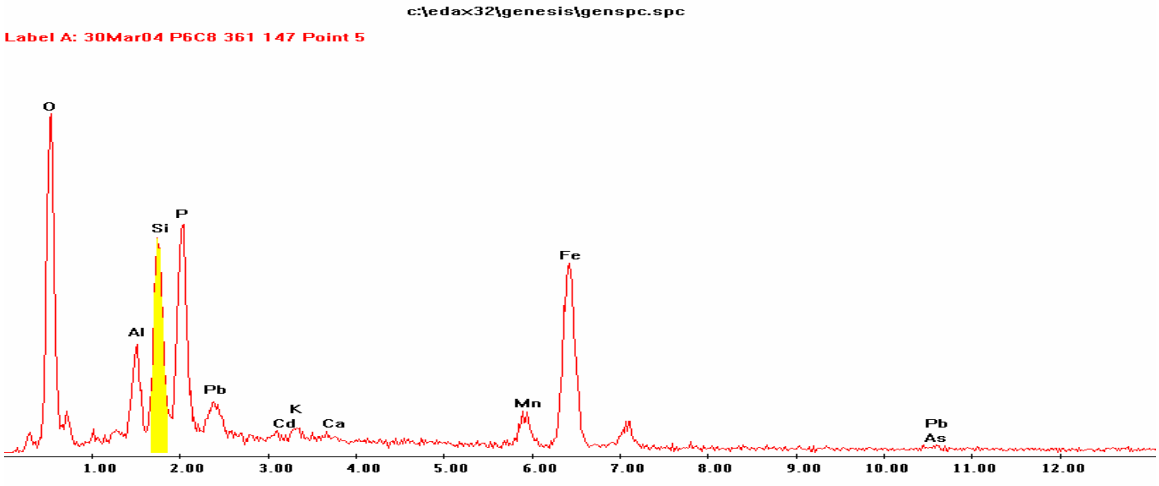

Point 6

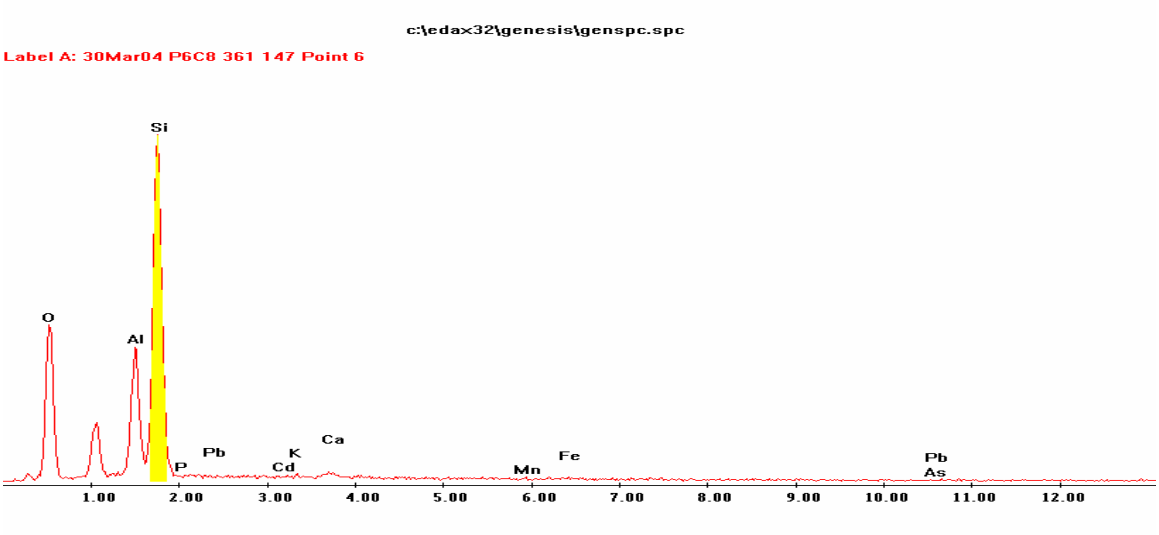

Point 7

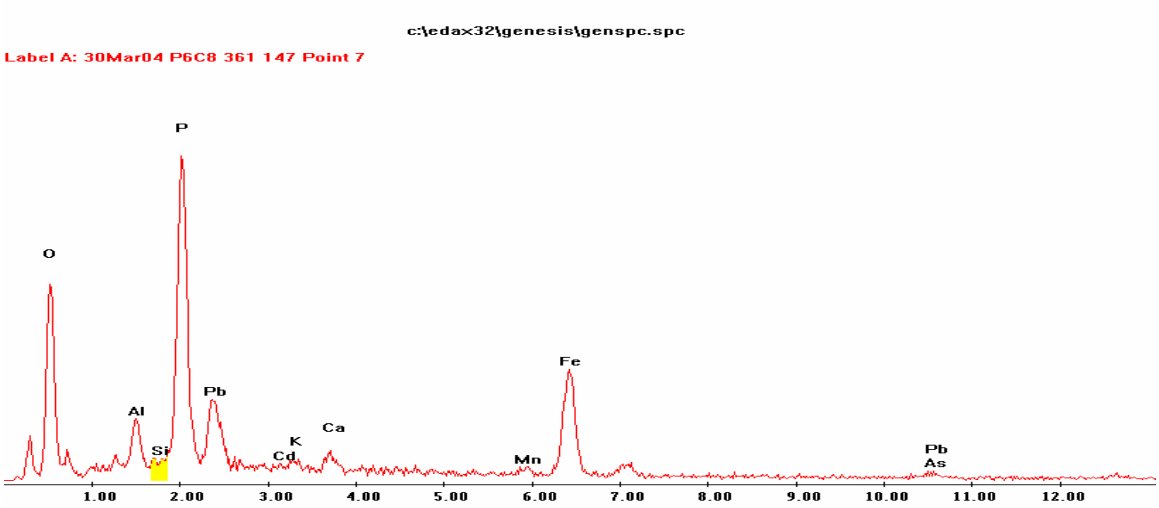

Point 8

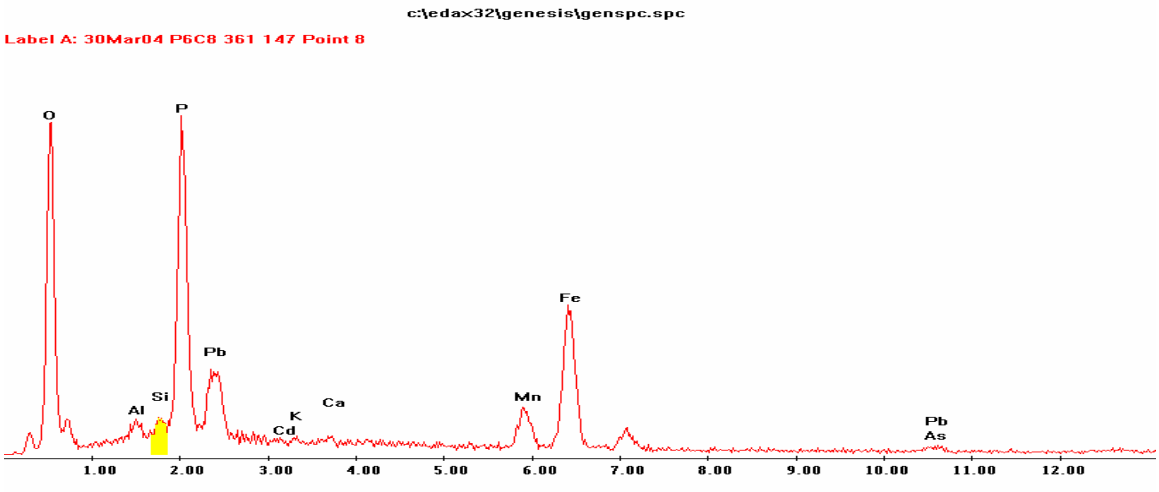

Point 9

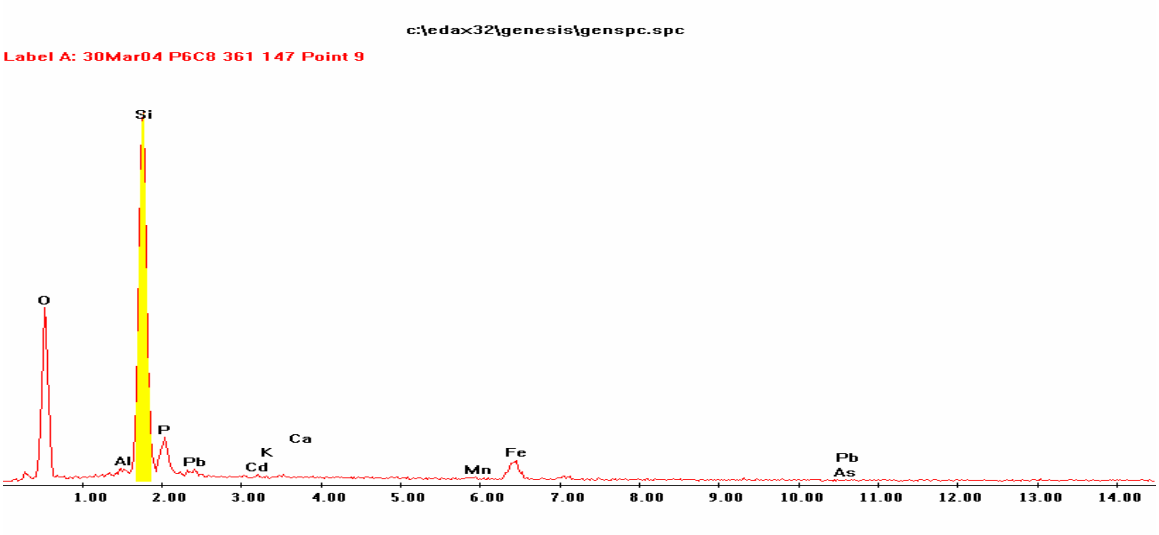

Point 10

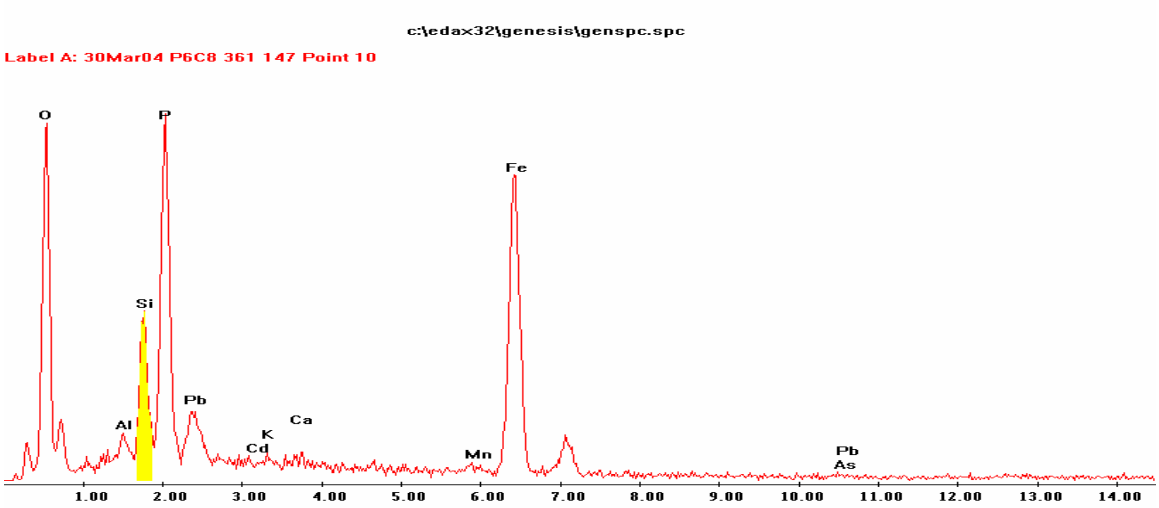

Point 11

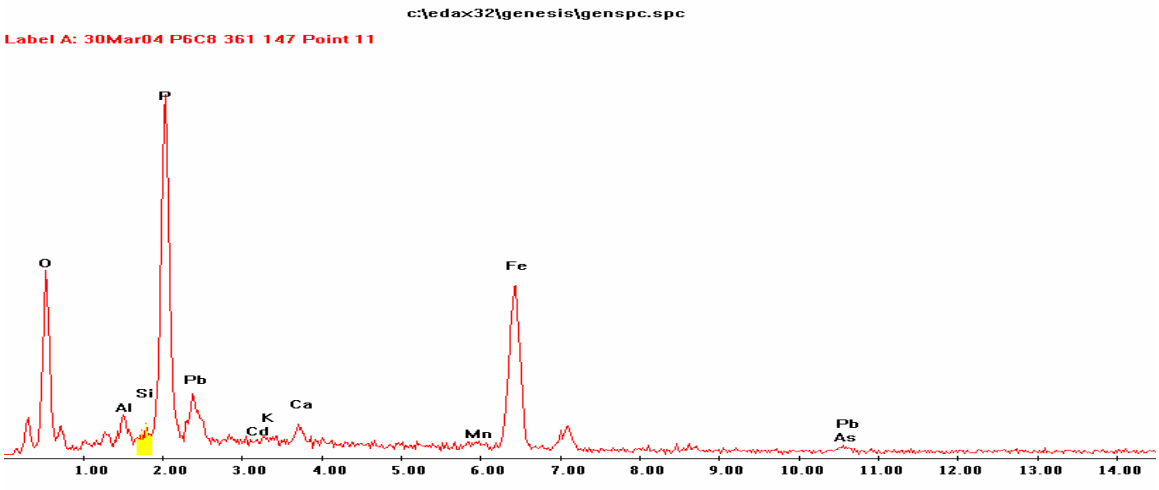

Point 12

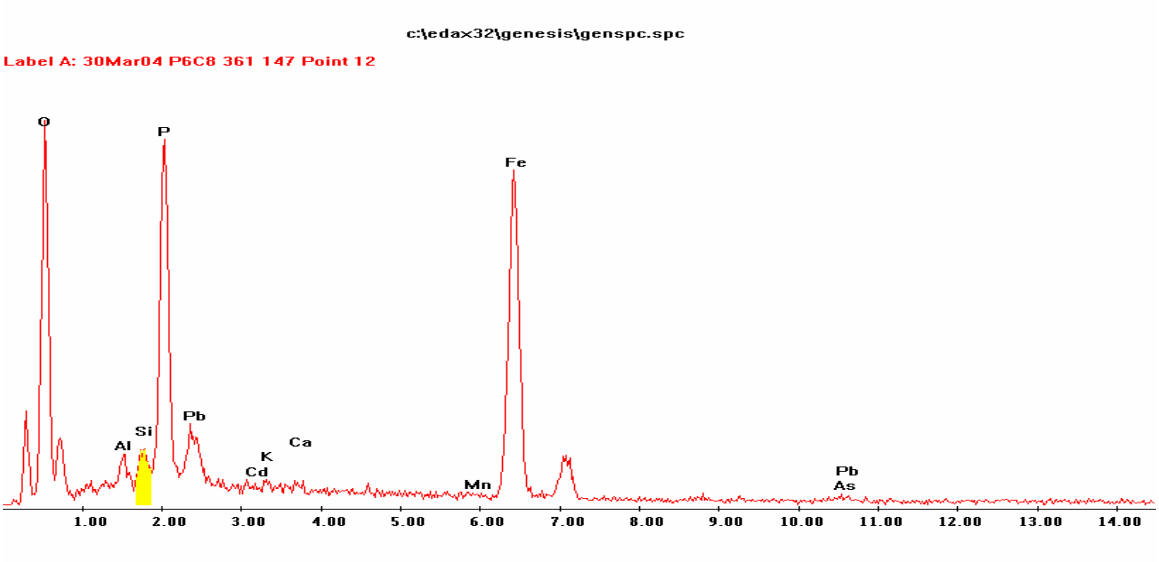
c:\edax32\genesis\genspc.spc
Label A: 30Mar04 P6C8 361 147 Point 12
O
P
Fe
Pb
Si
Al
Ca
K
Cd
Mn
Pb
As
1.00
2.00
3.00
4.00
5.00
6.00
7.00
8.00
9.00
10.00
11.00
12.00
13.00
14.00

P6C8 – 399, 228

BSE Image

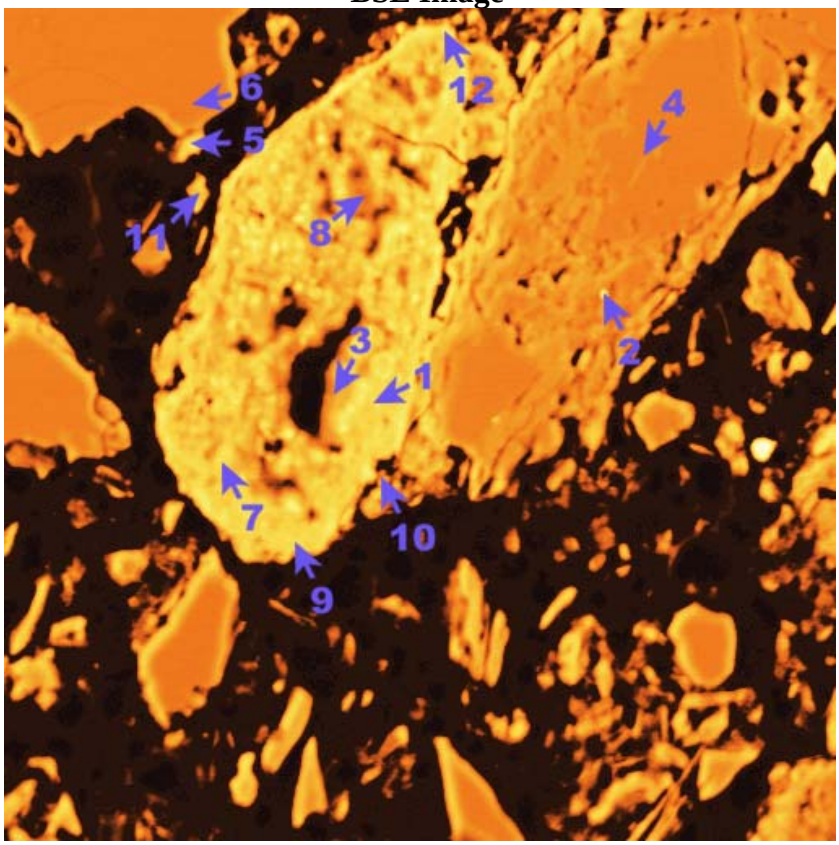

Iron (Fe)

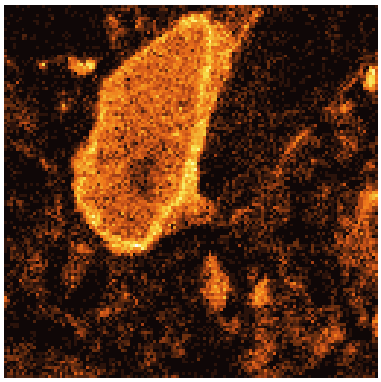

Manganese (Mn)

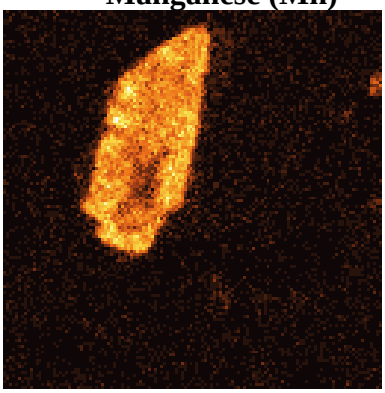

Phosphorous (P)

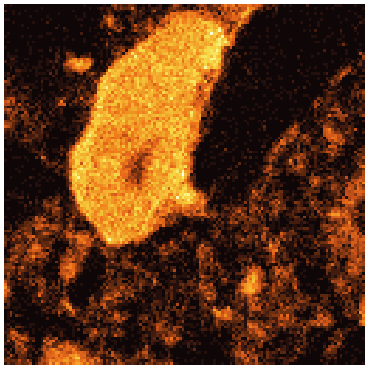

Lead (Pb)

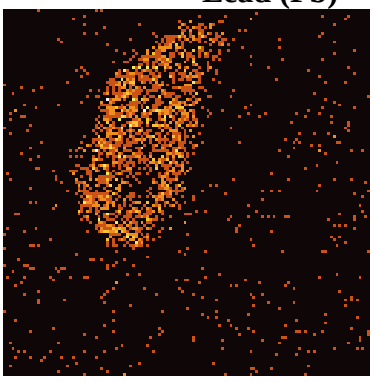

Silicon (Si)

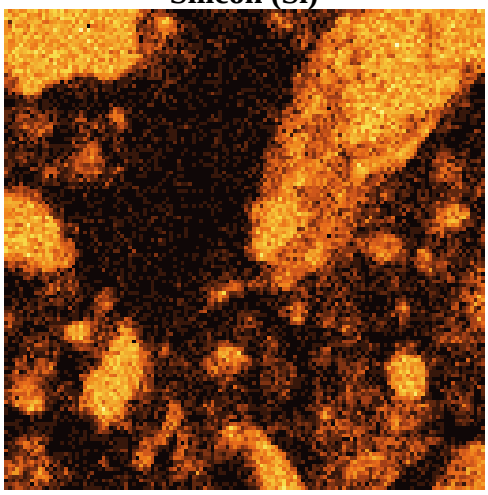

EDS Scan Images by Point

Point 1

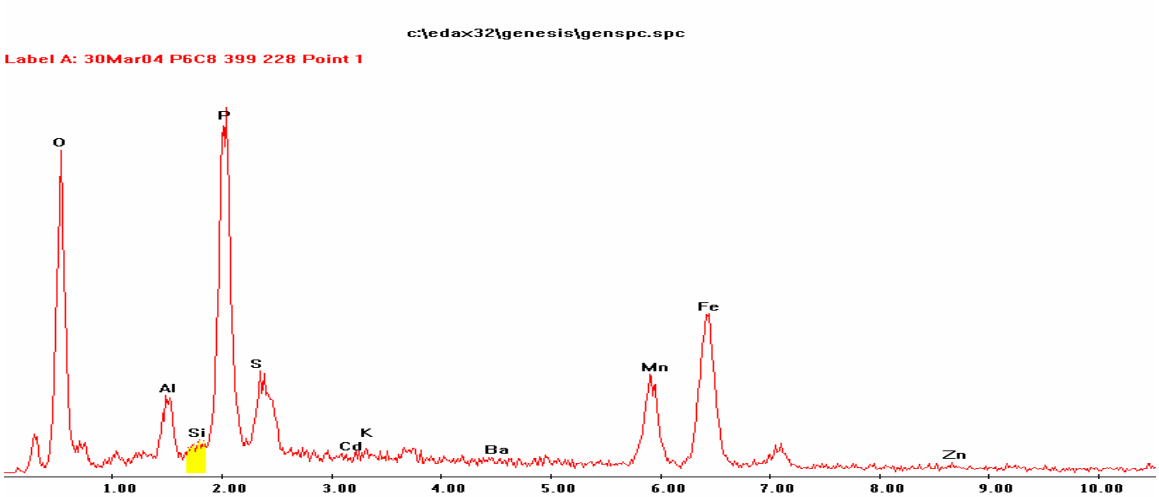

Point 2

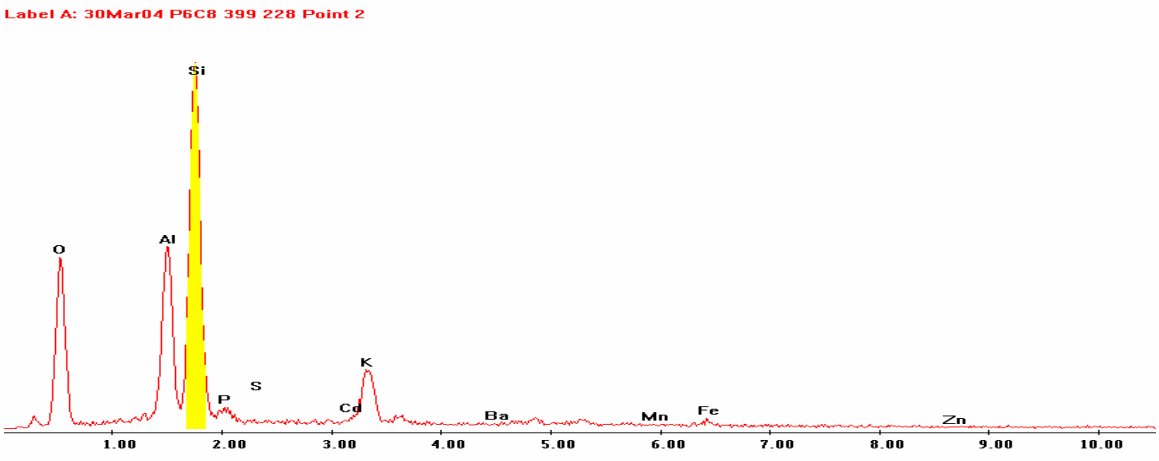

Point 3

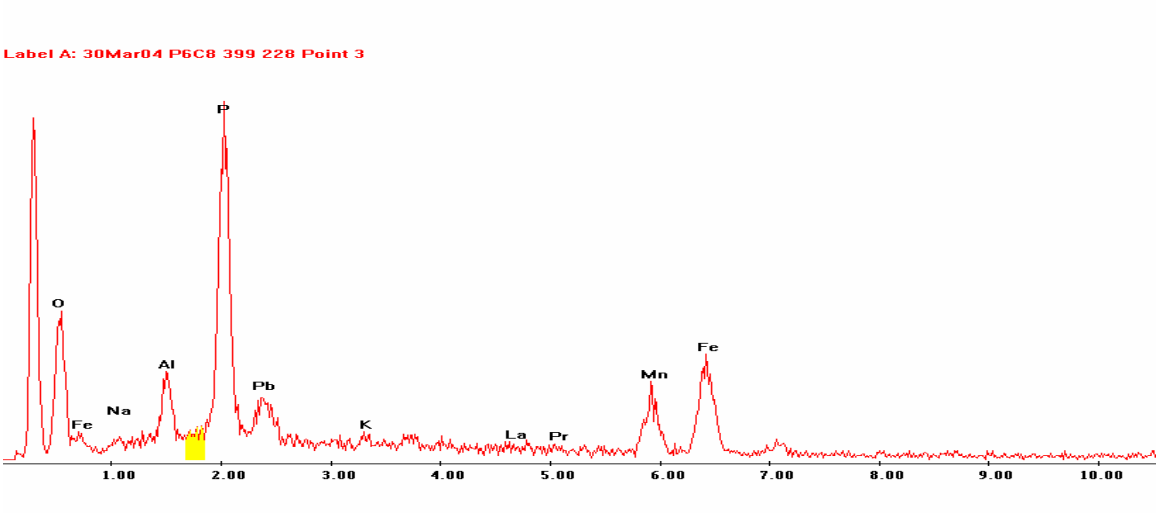

Point 4

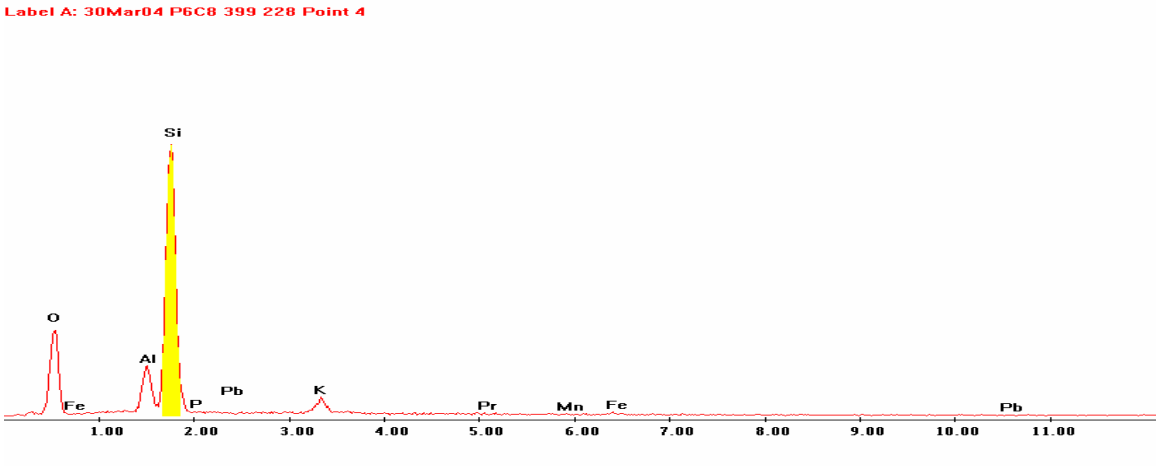

Point 5

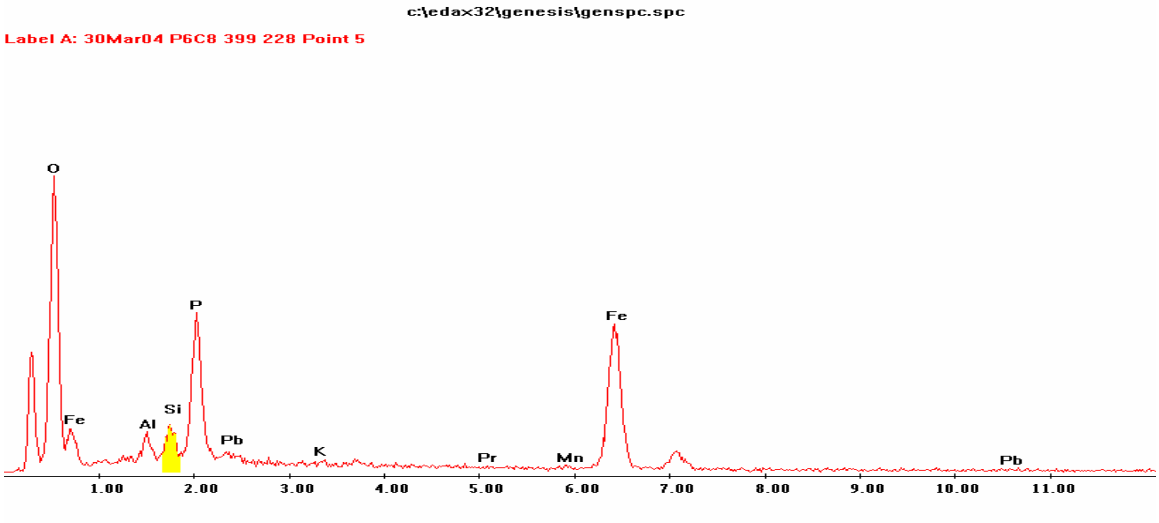

Point 6

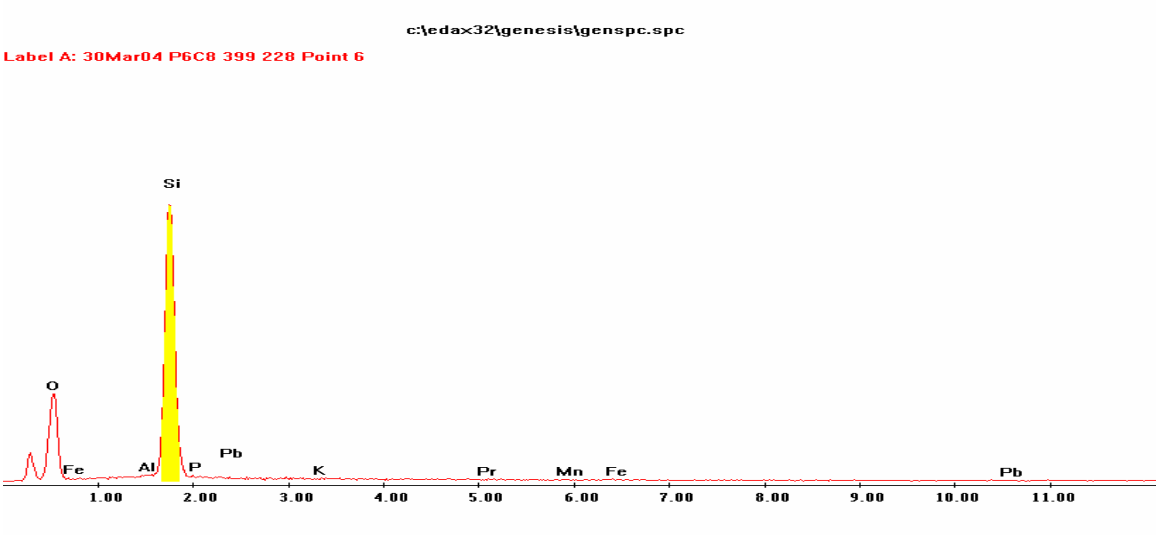

Point 7

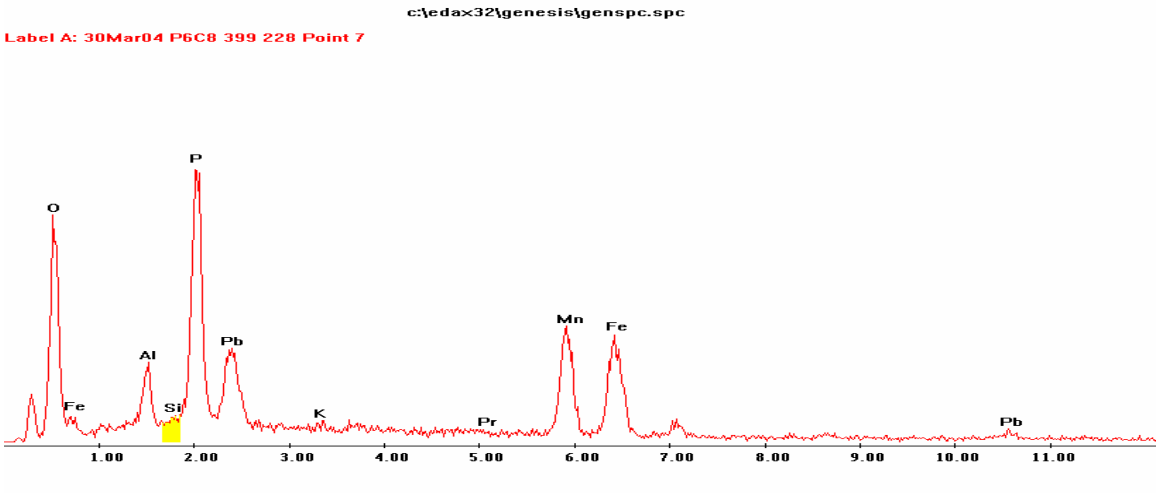

Point 8

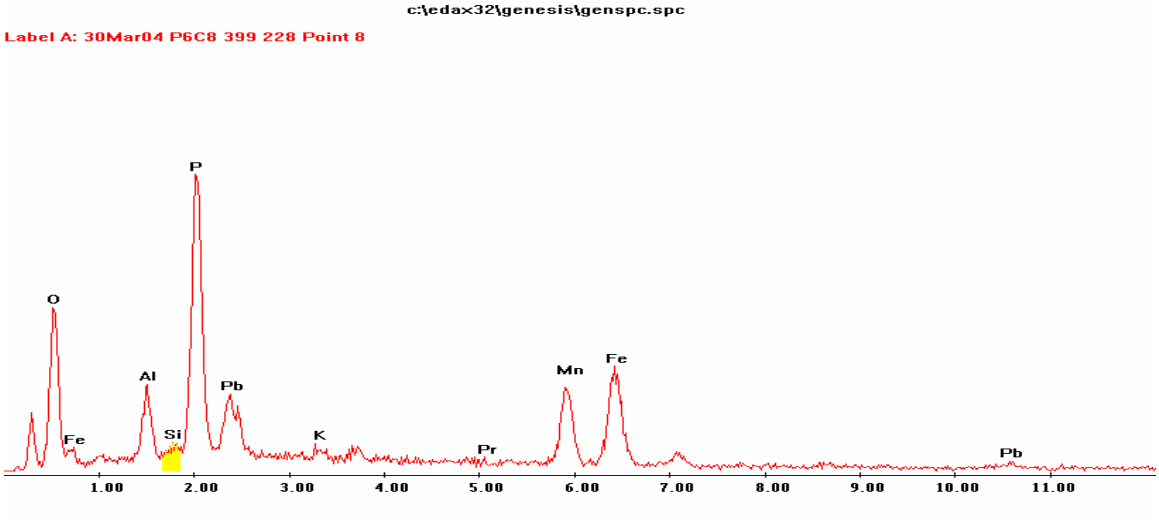

Point 9

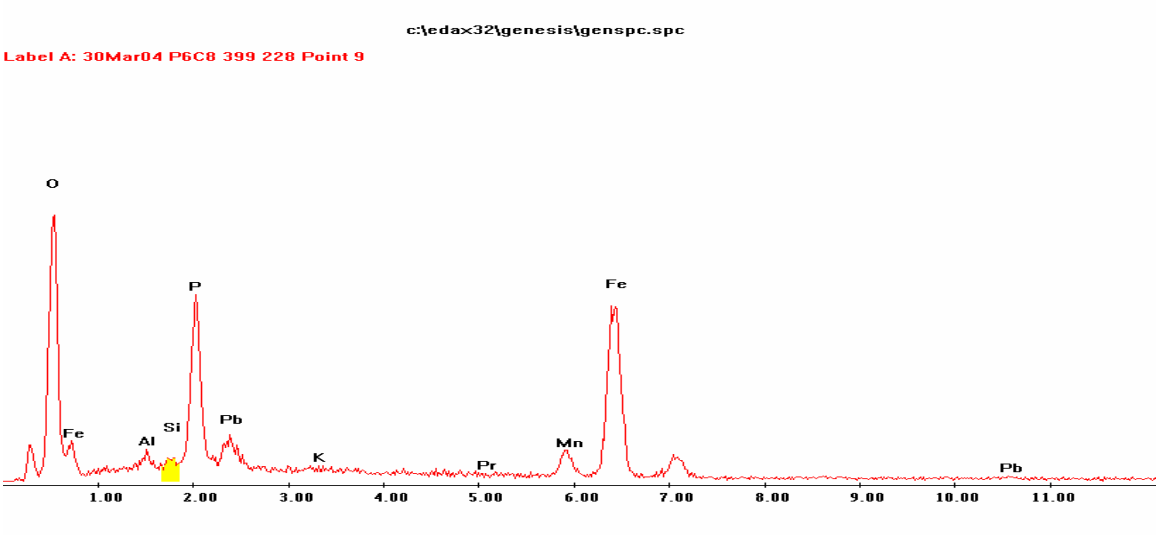

Point 10

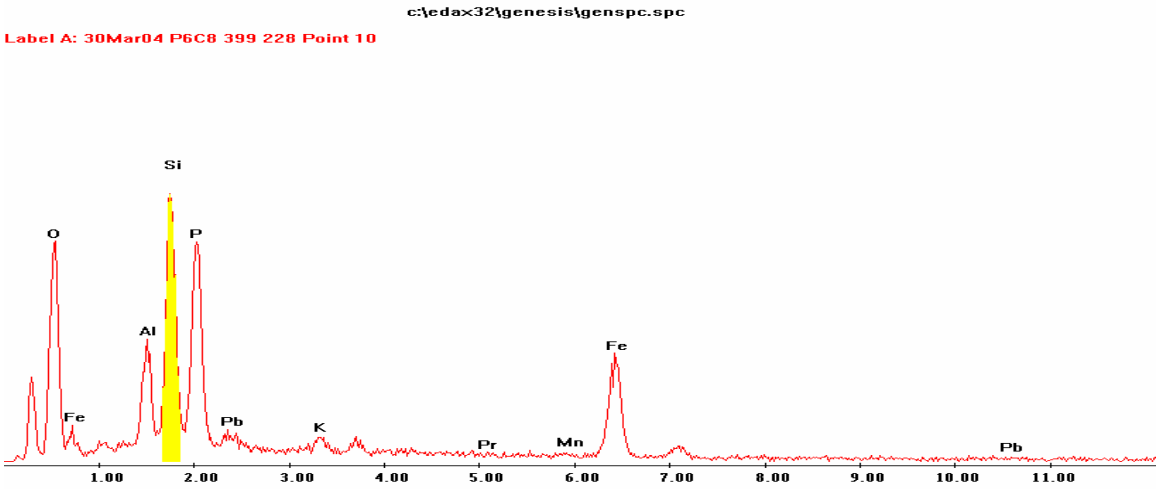

Point 11

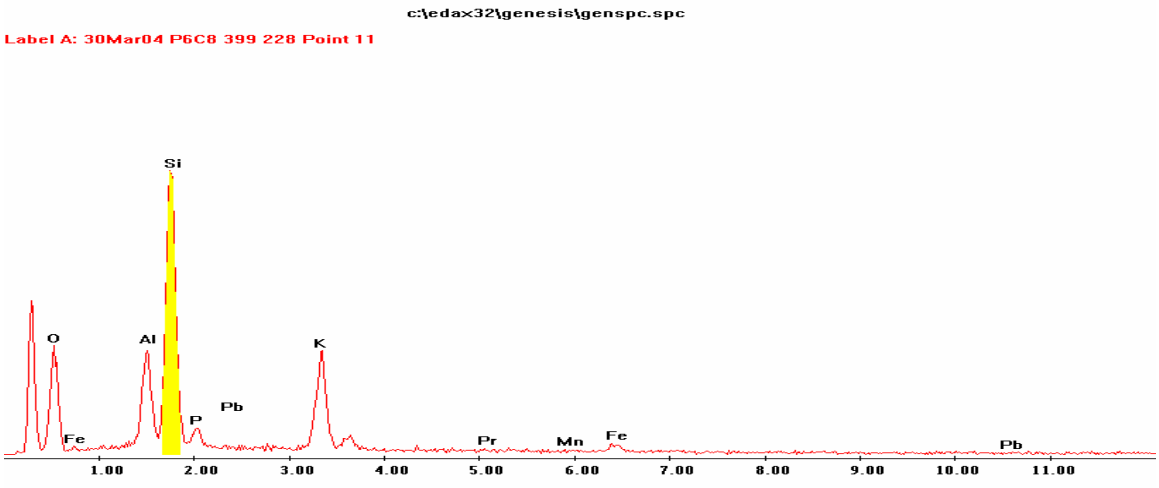

Point 12

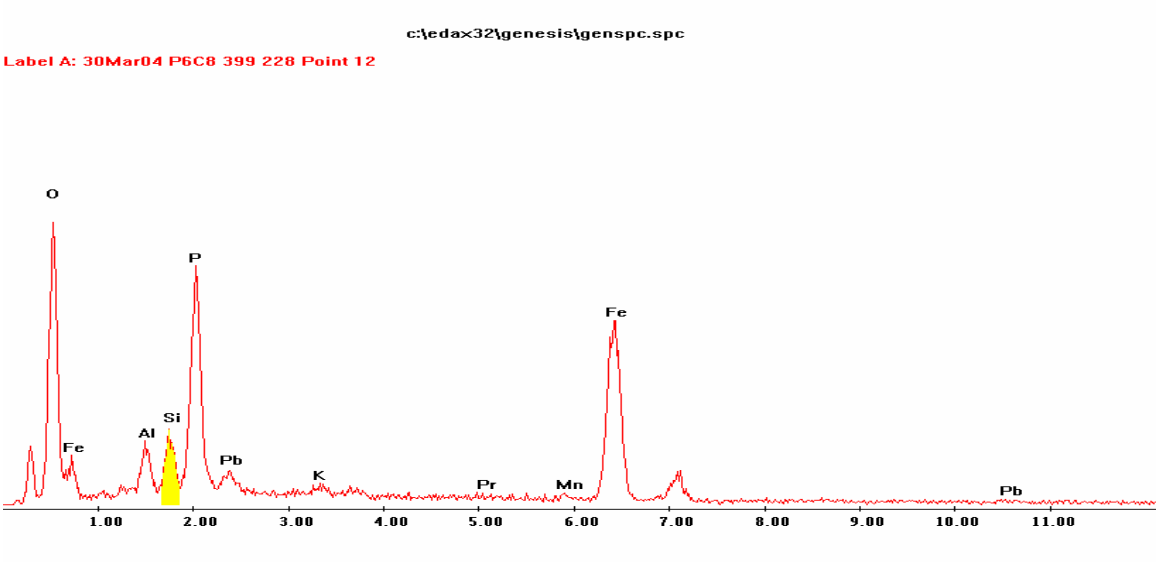
c:\edax32\genesis\genspc.spc
Label A: 30Mar04 P6C8 399 228 Point 12
O
Fe
Al
Si
P
Pb
K
Pr
Mn
Fe
Pb
1.00
2.00
3.00
4.00
5.00
6.00
7.00
8.00
9.00
10.00
11.00

P6C8 – 400, 208

BSE Image

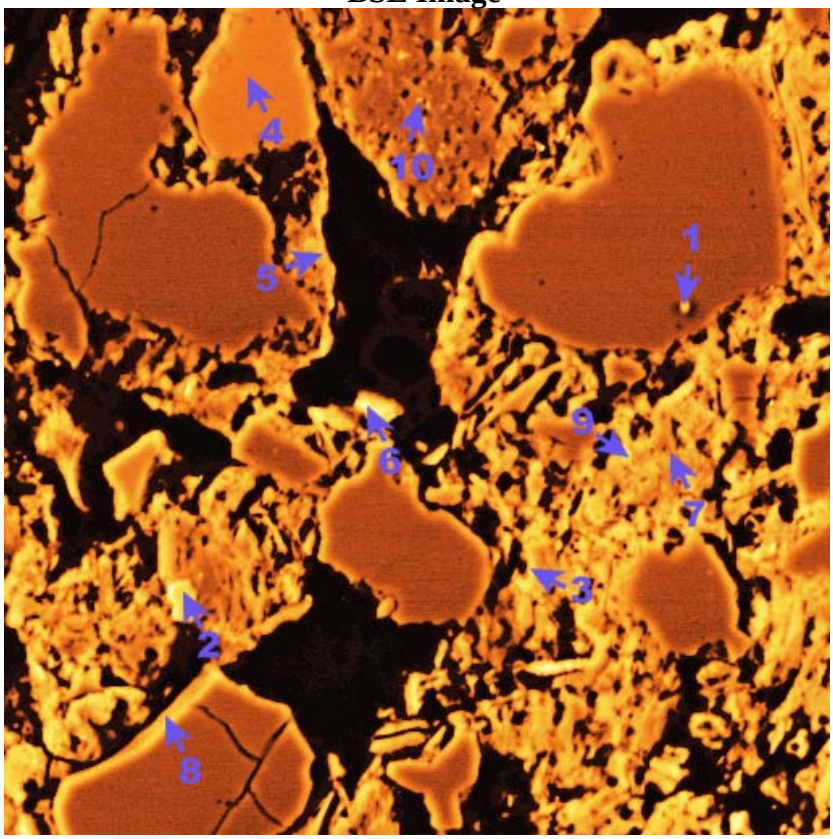

Iron (Fe)

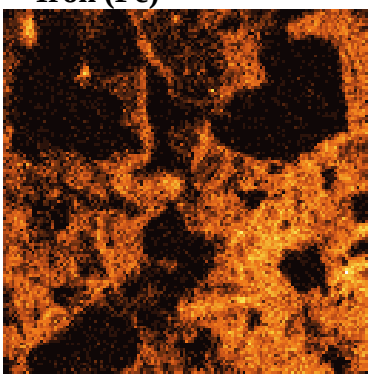

Manganese (Mn)

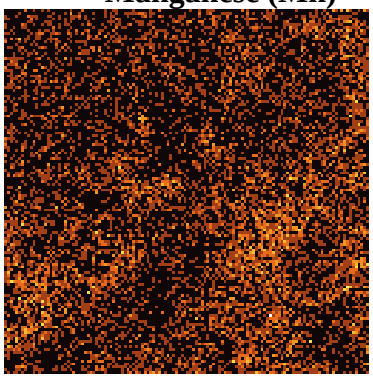

Phosphorous (P)

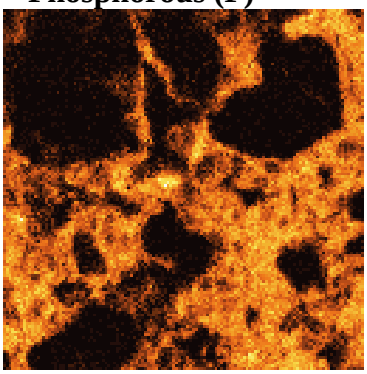

Lead (Pb)

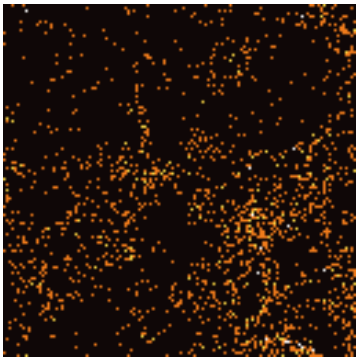

Silicon (Si)

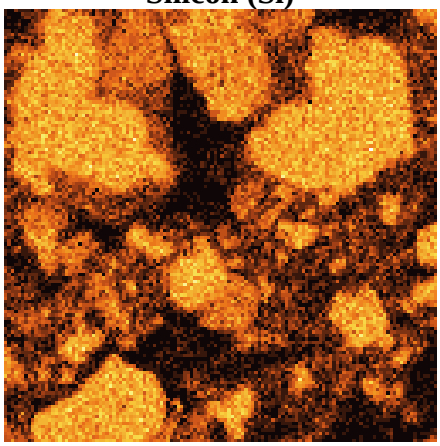

EDS Scan Images by Point

Point 1

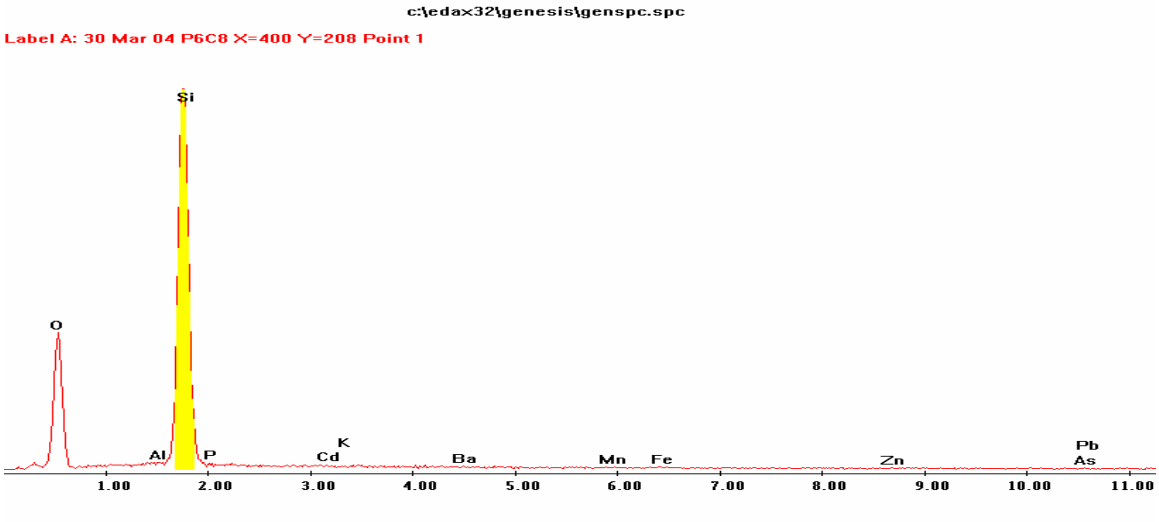

Point 2

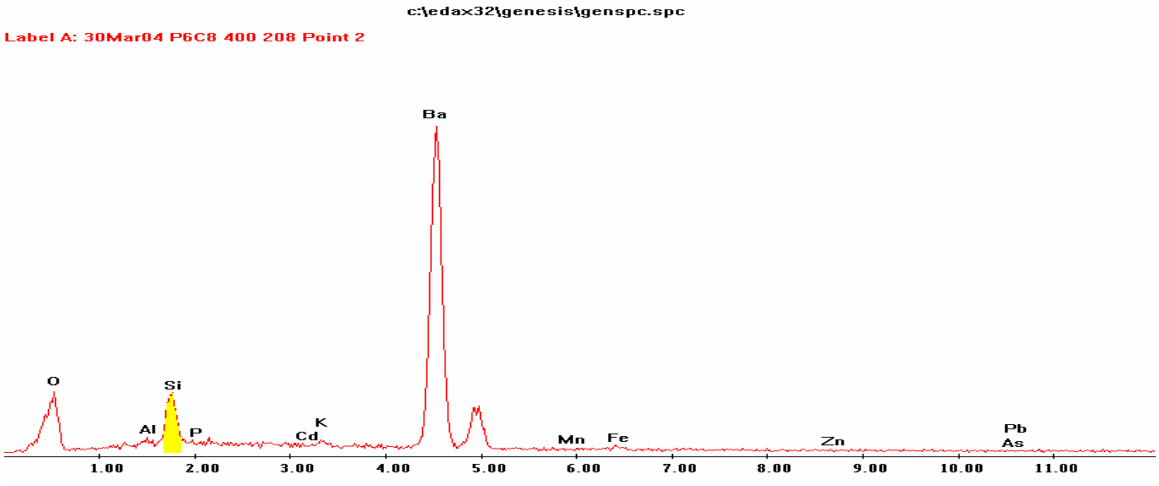

Point 3

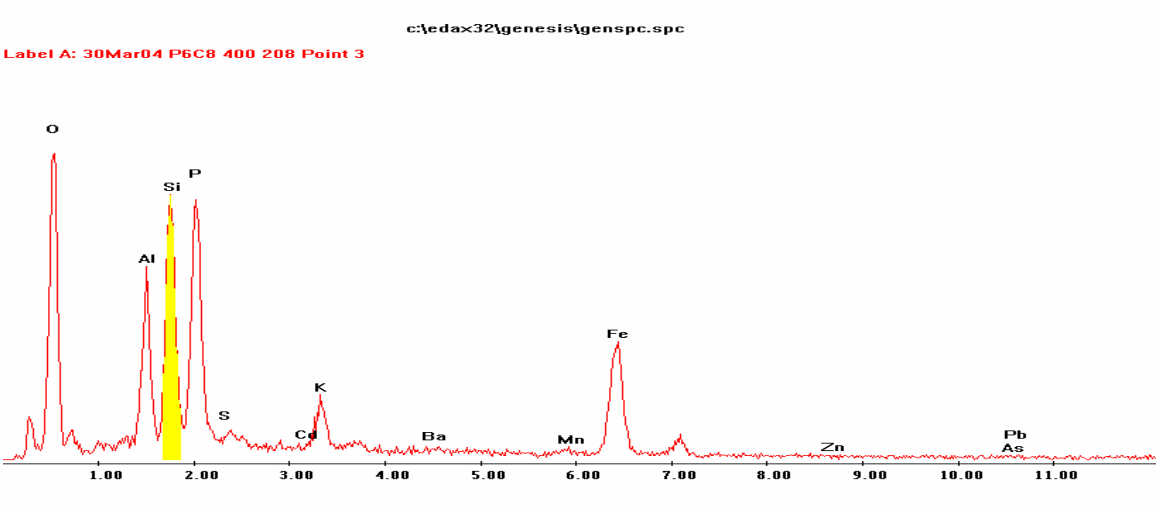

Point 4

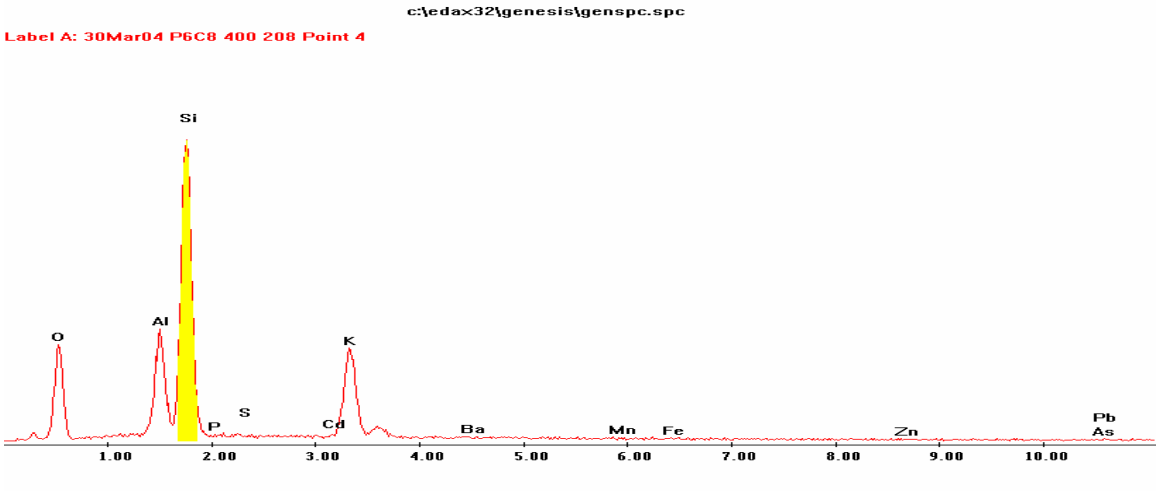

Point 5

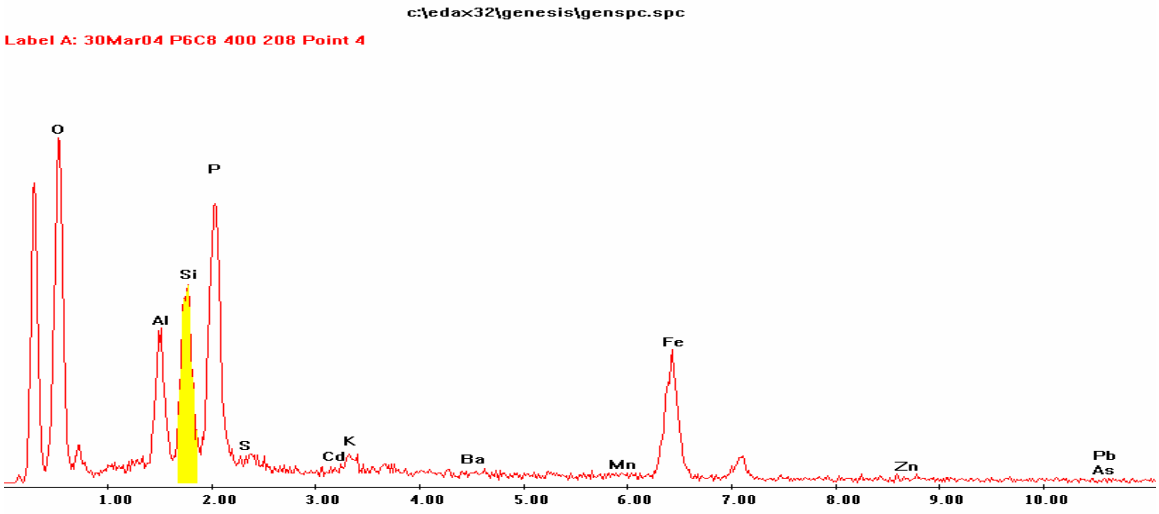

Point 6

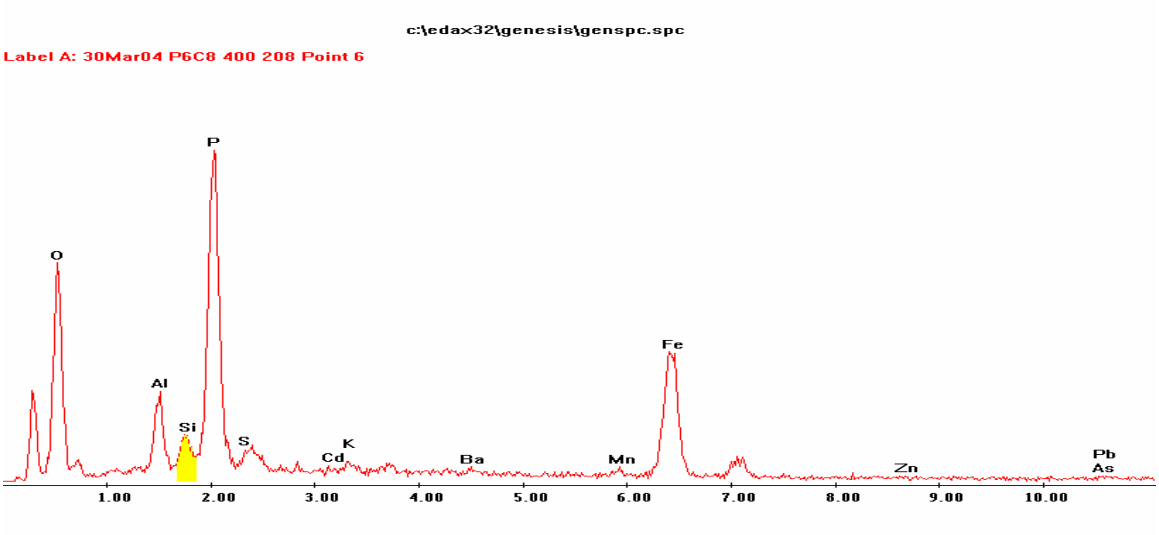

Point 7

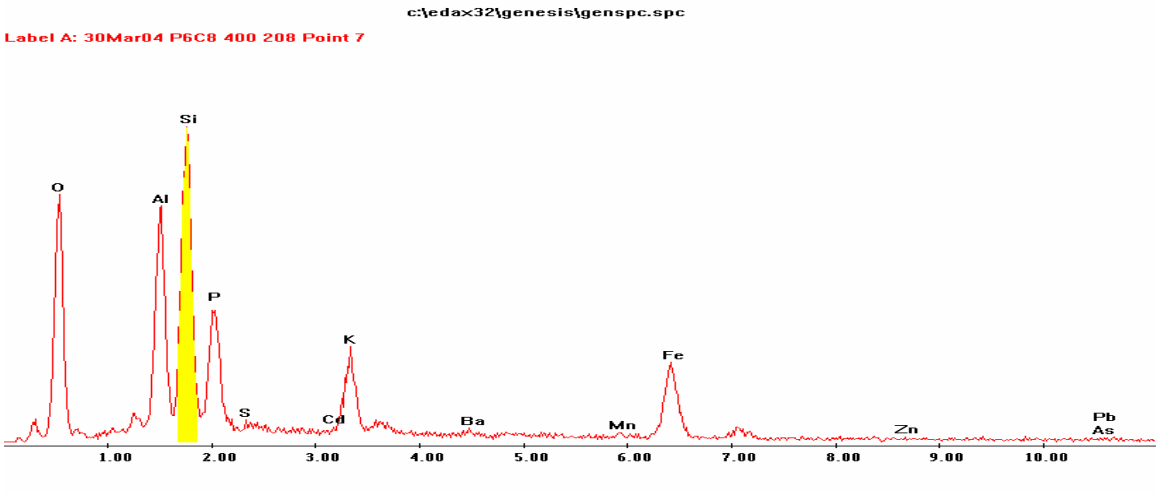

Point 8

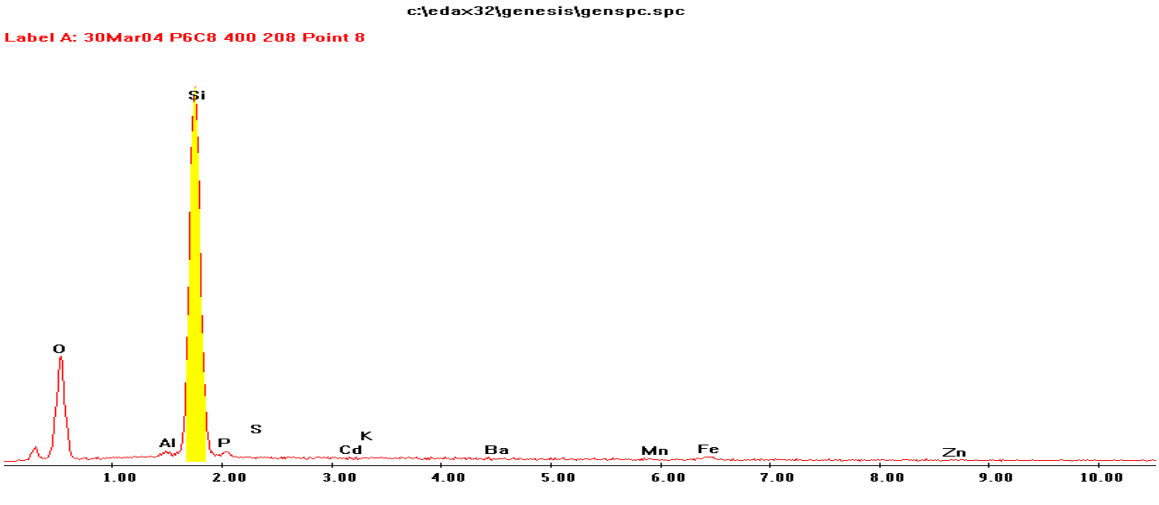

Point 9

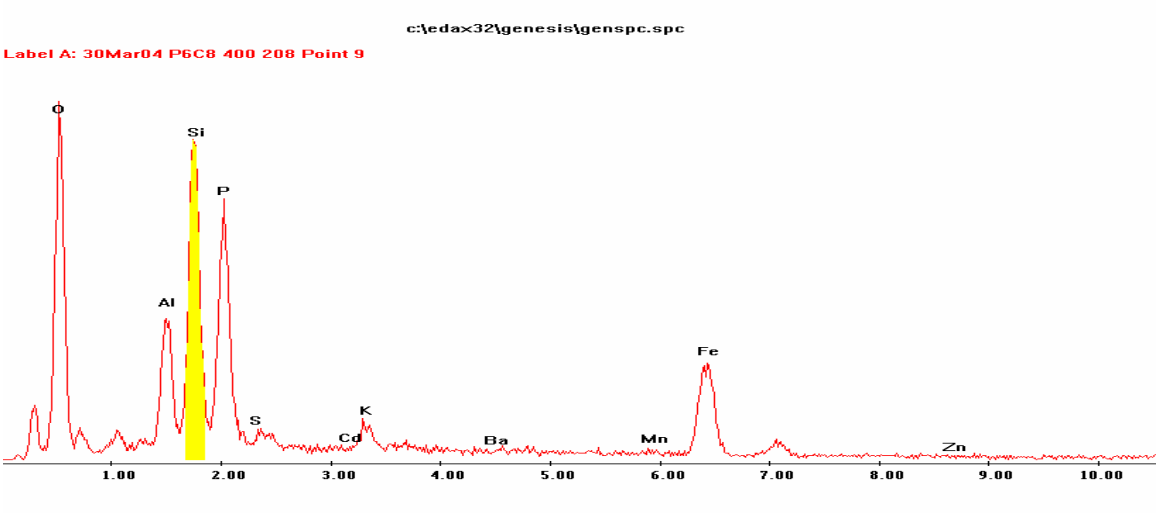

Point 10

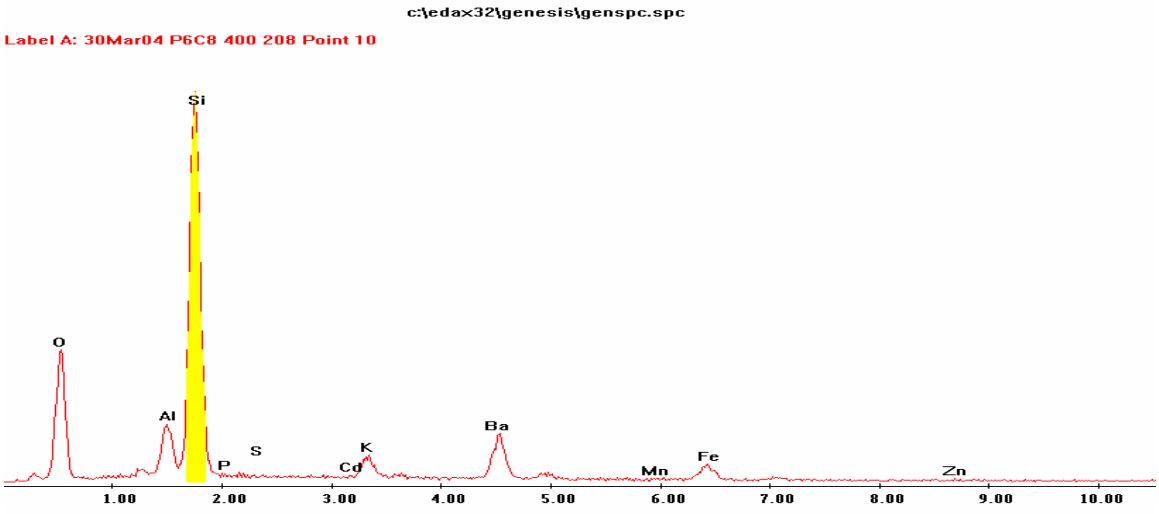

P6C8 – 454, 290

BSE Image

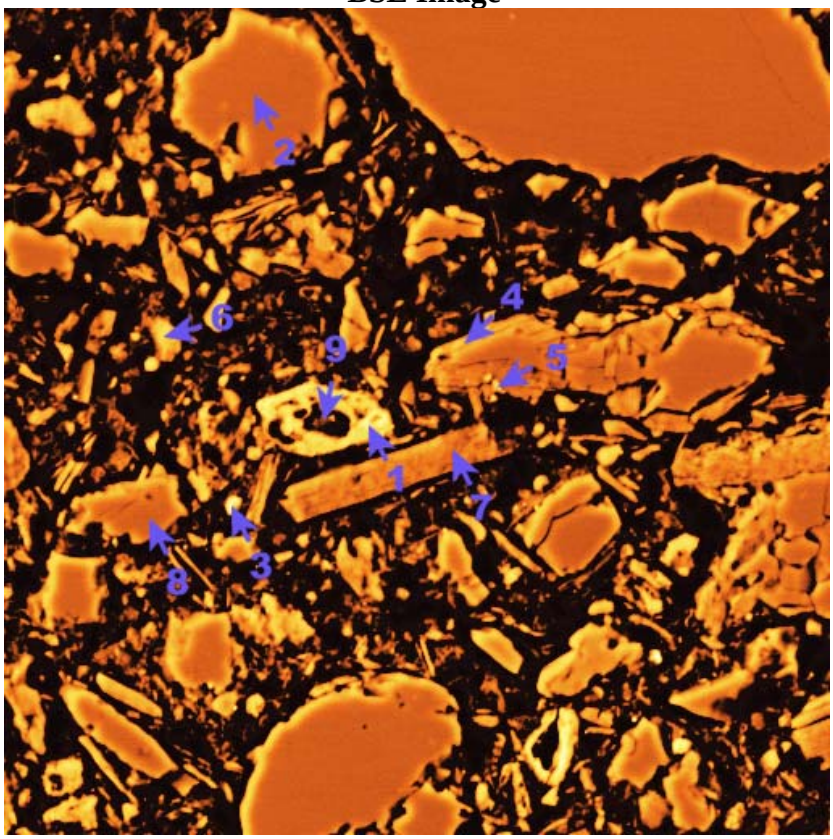

Iron (Fe)

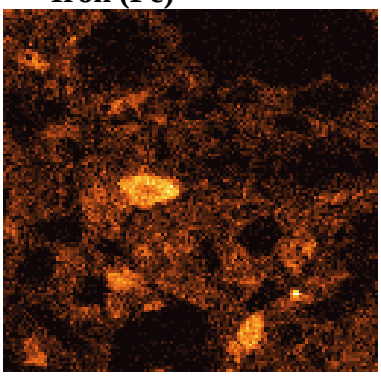

Manganese (Mn)

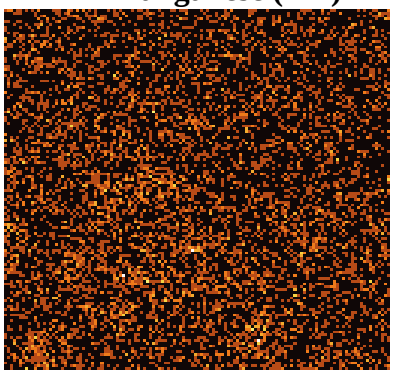

Phosphorous (P)

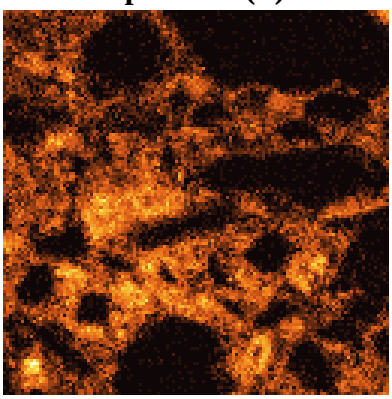

Lead (Pb)

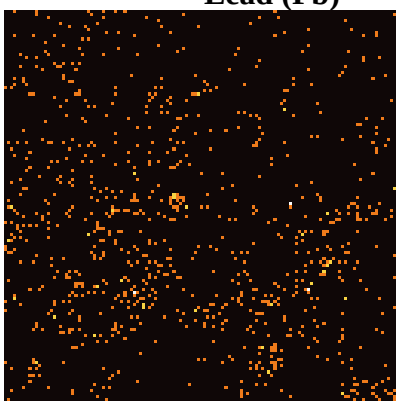

Silicon (Si)

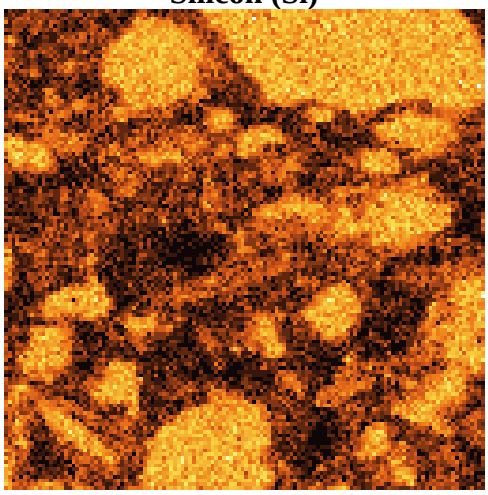

EDS Scan Images by Point

Point 1

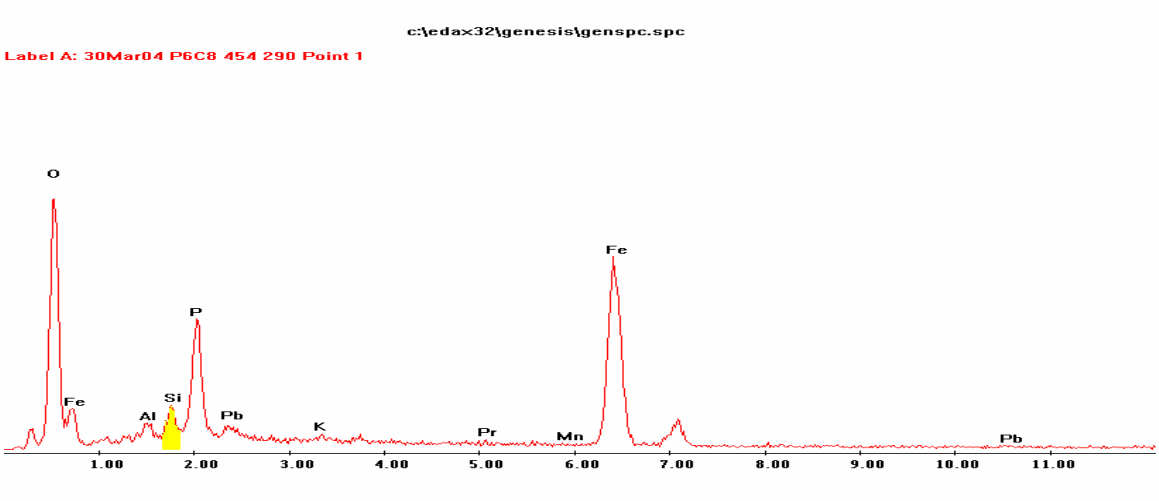

Point 2

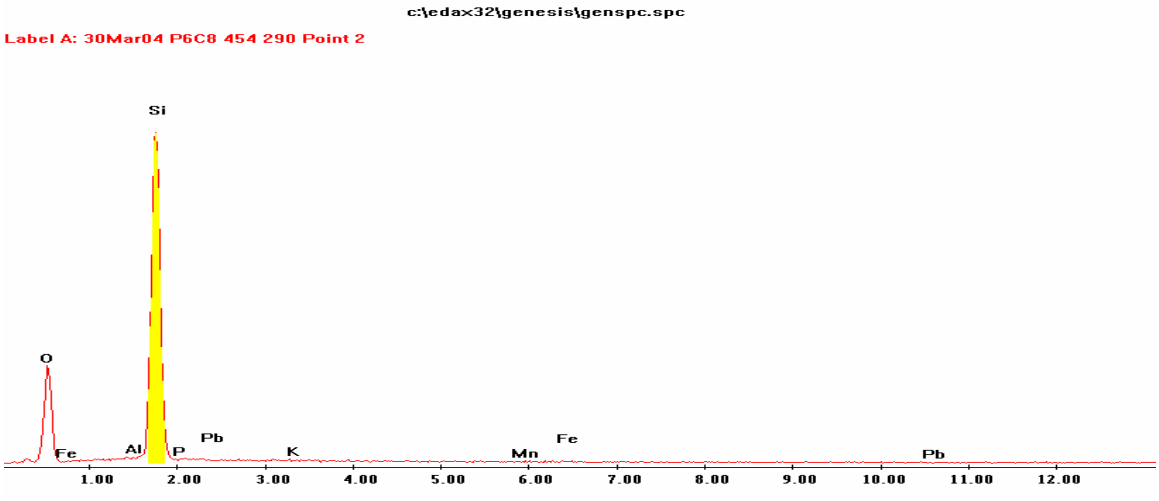

Point 3

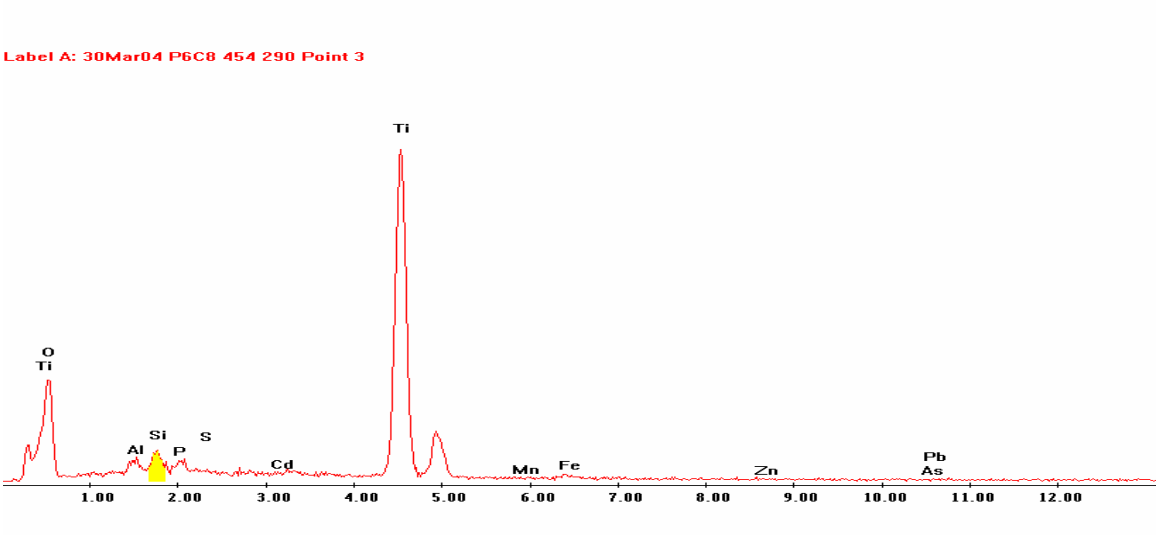

Point 4

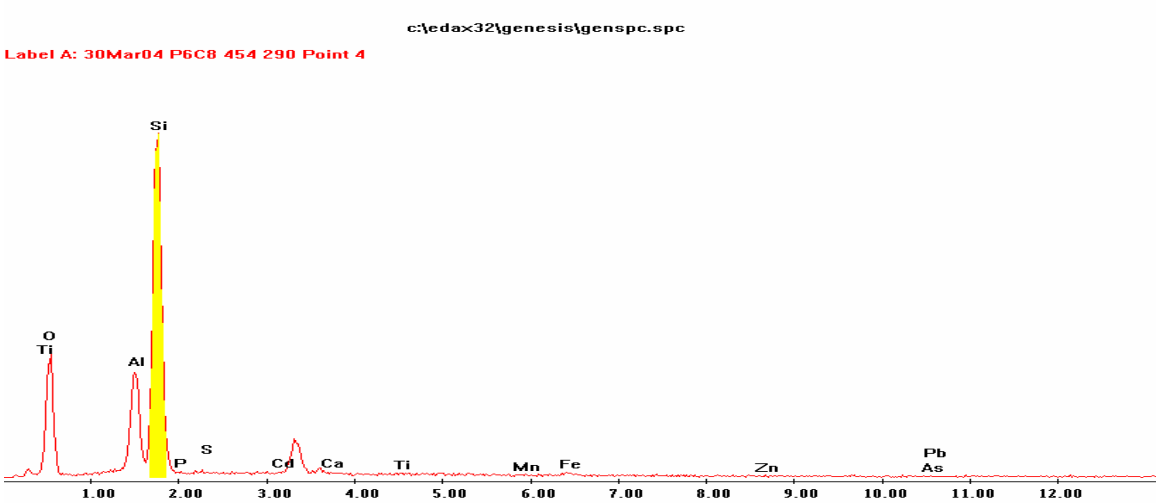

Point 5

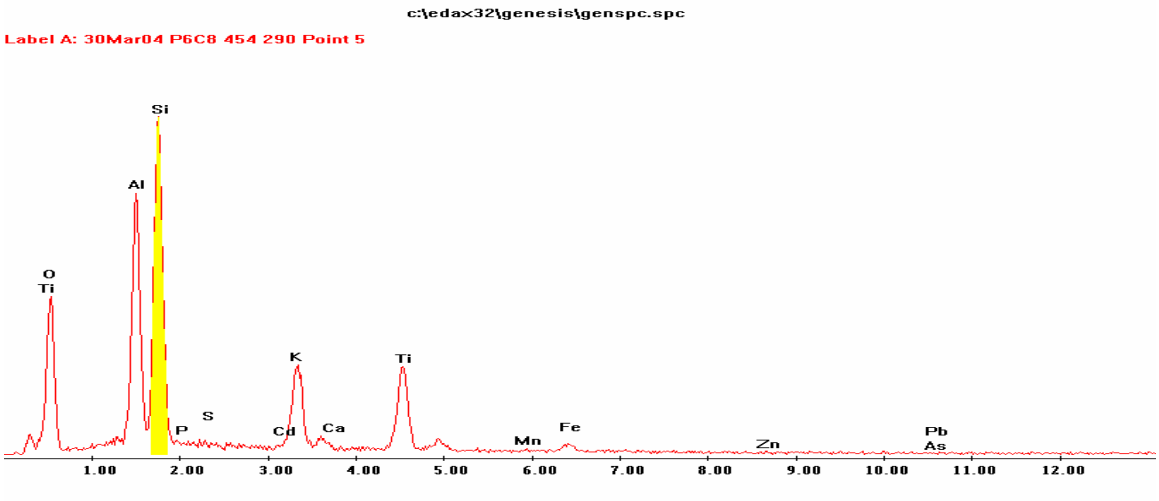

Point 6

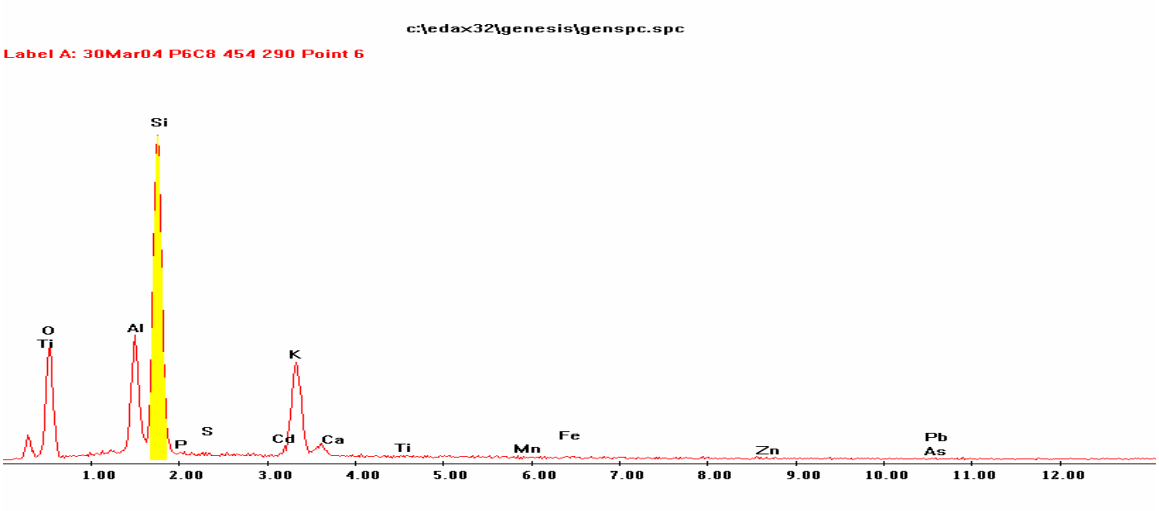

Point 7

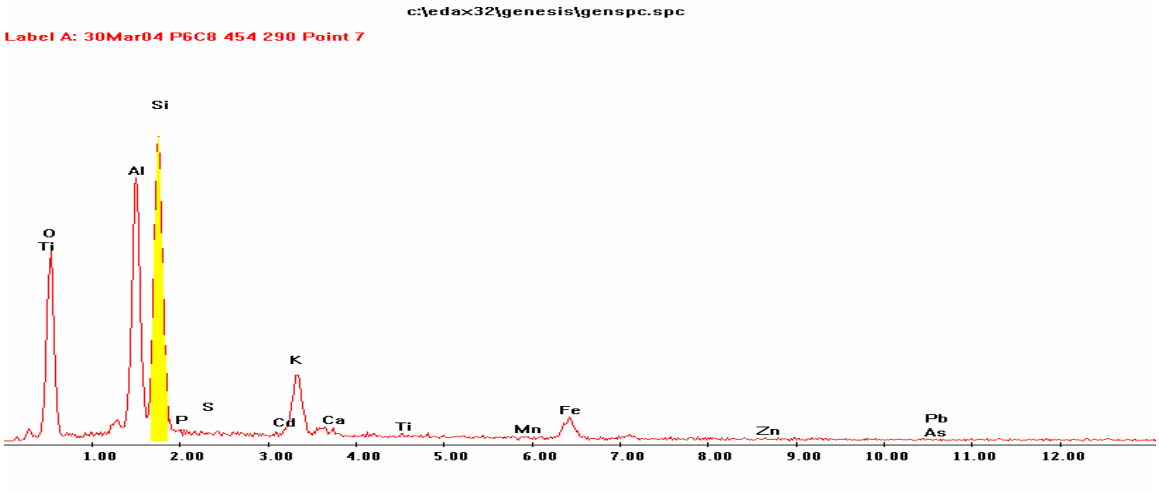

Point 8

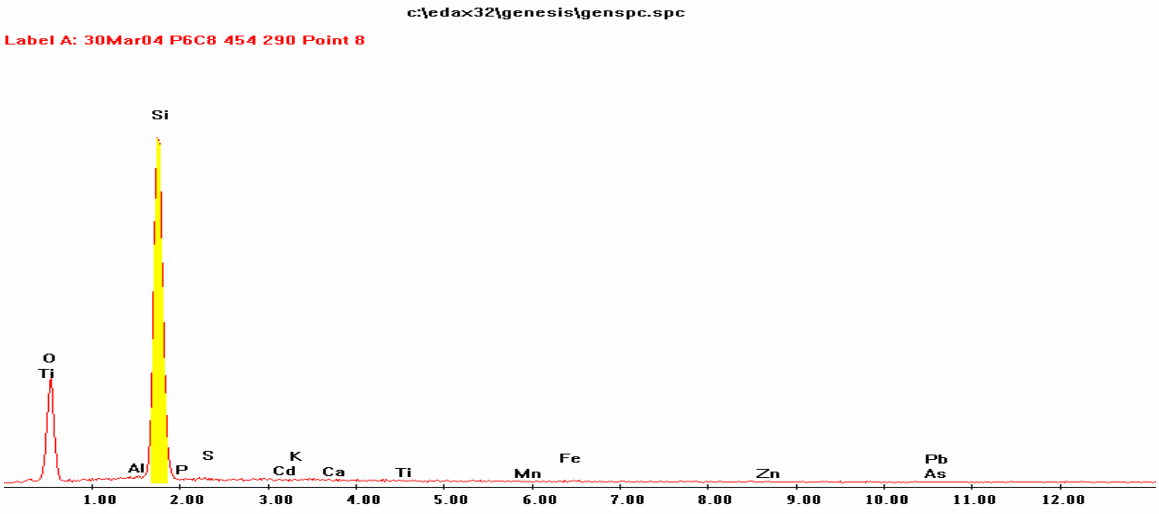

Point 9

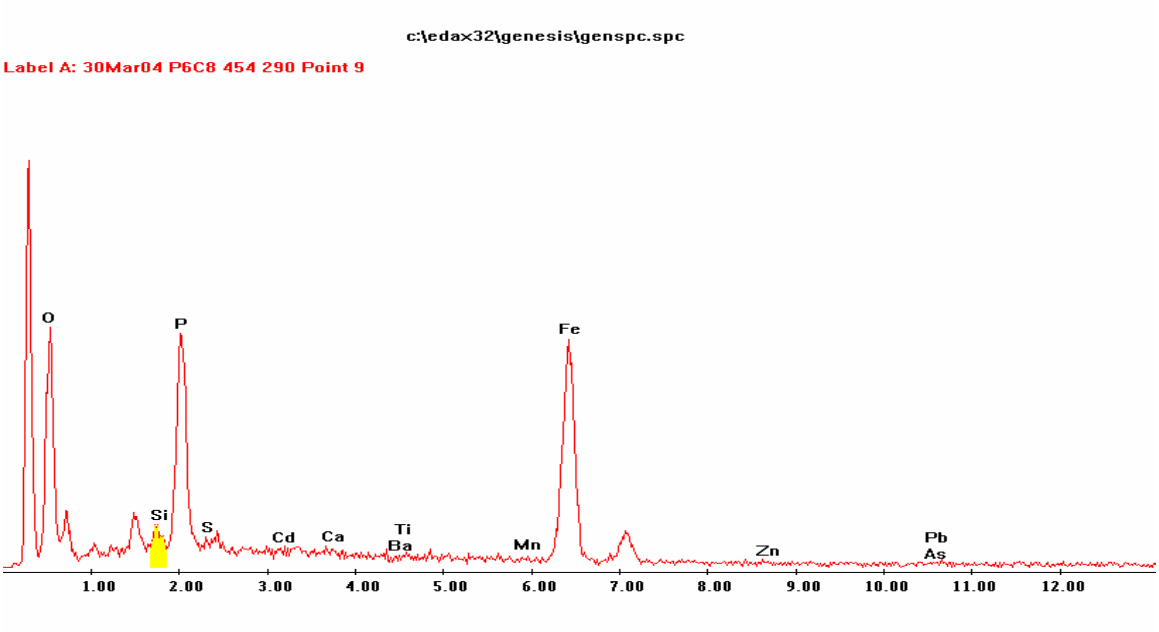
c:\edax32\genesis\genspc.spc
Label A: 30Mar04 P6C8 454 290 Point 9
O
P
Fe
Si
S
Cd
Ca
Ti
Ba
Mn
Zn
Pb
As
1.00
2.00
3.00
4.00
5.00
6.00
7.00
8.00
9.00
10.00
11.00
12.00

P6C9 – 395, 183

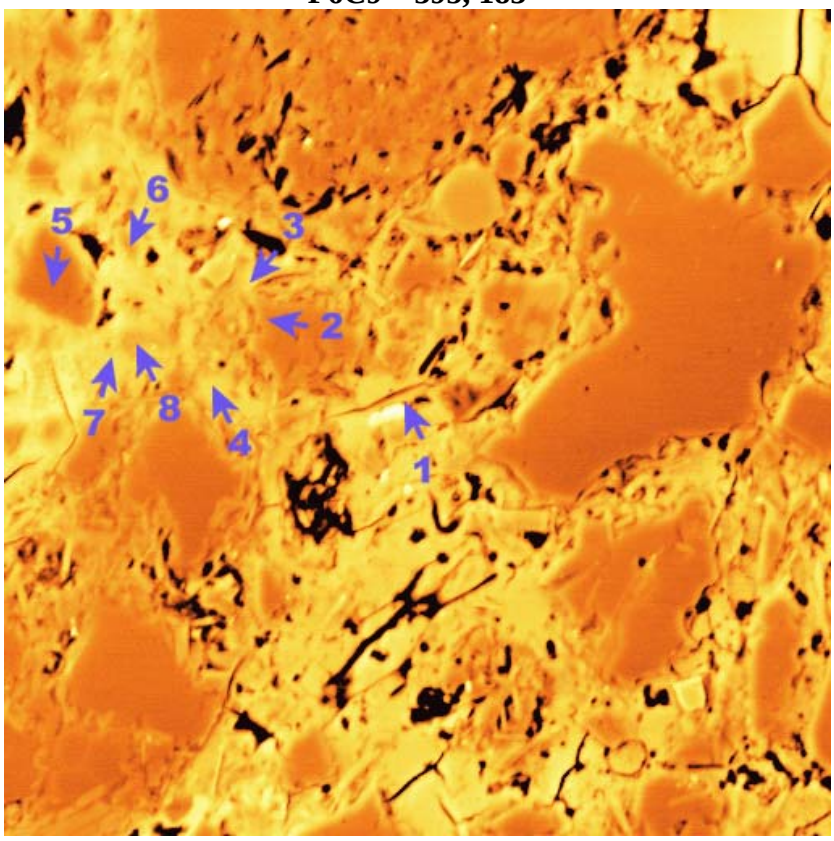

BSE Image

Iron (Fe)

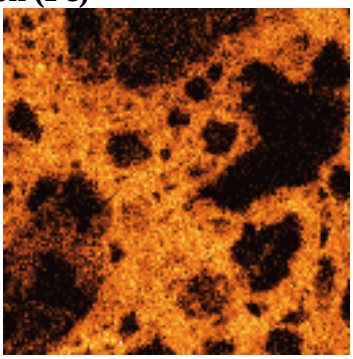

Manganese (Mn)

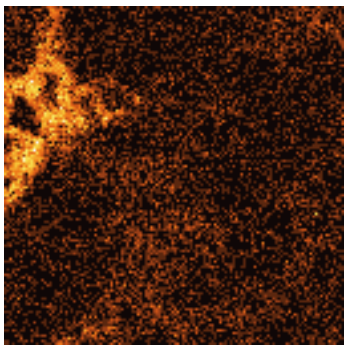

Phosphorous (P)

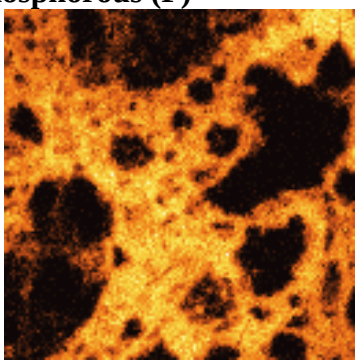

Lead (Pb)

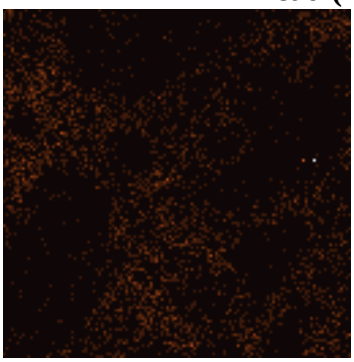

Silicon (Si)

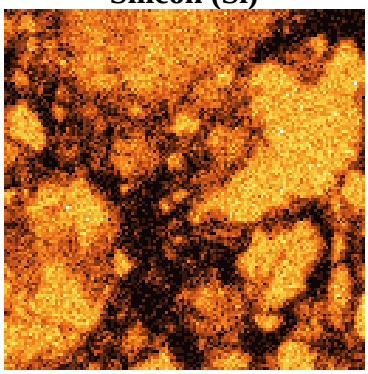

EDS Scan Images by Point

Point 1

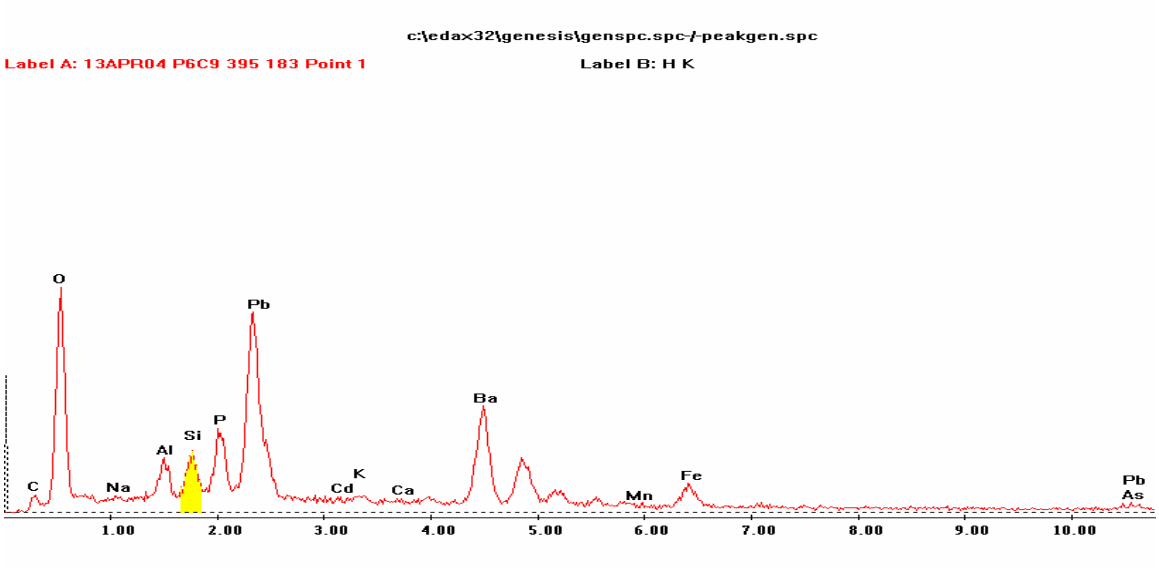

Point 2

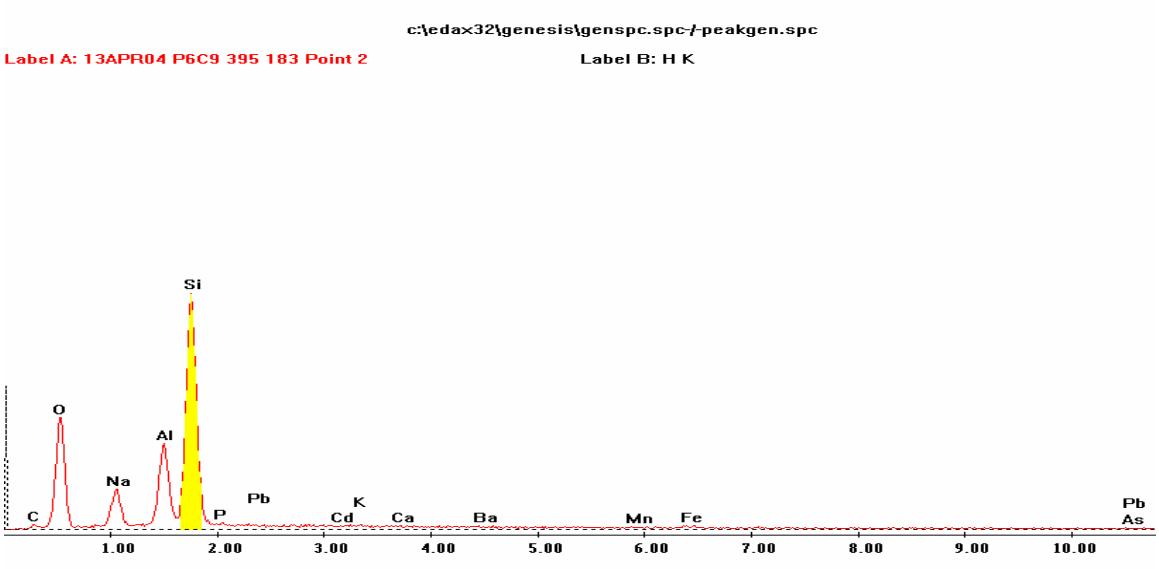

Point 3

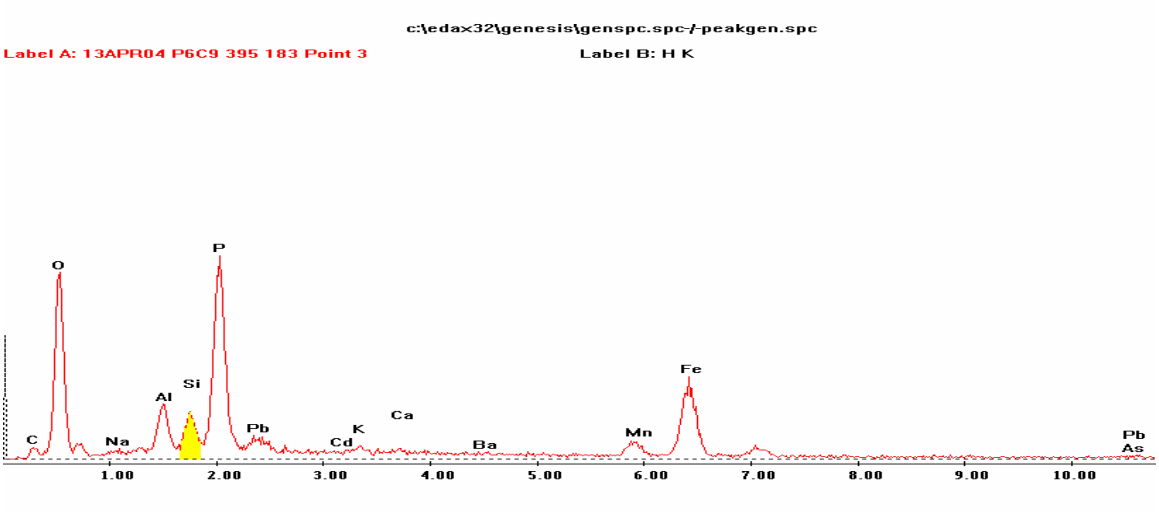

Point 4

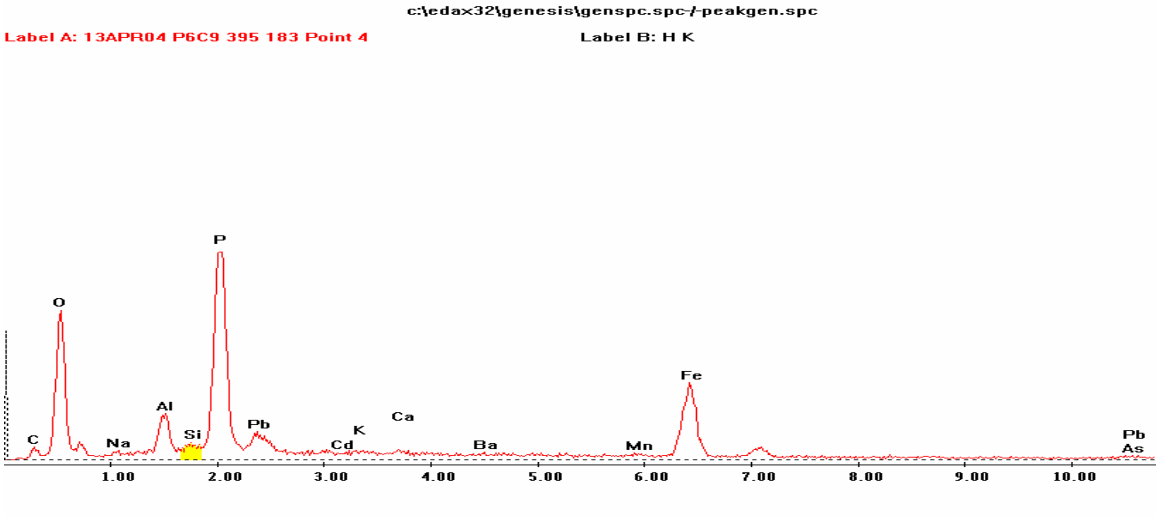

Point 5

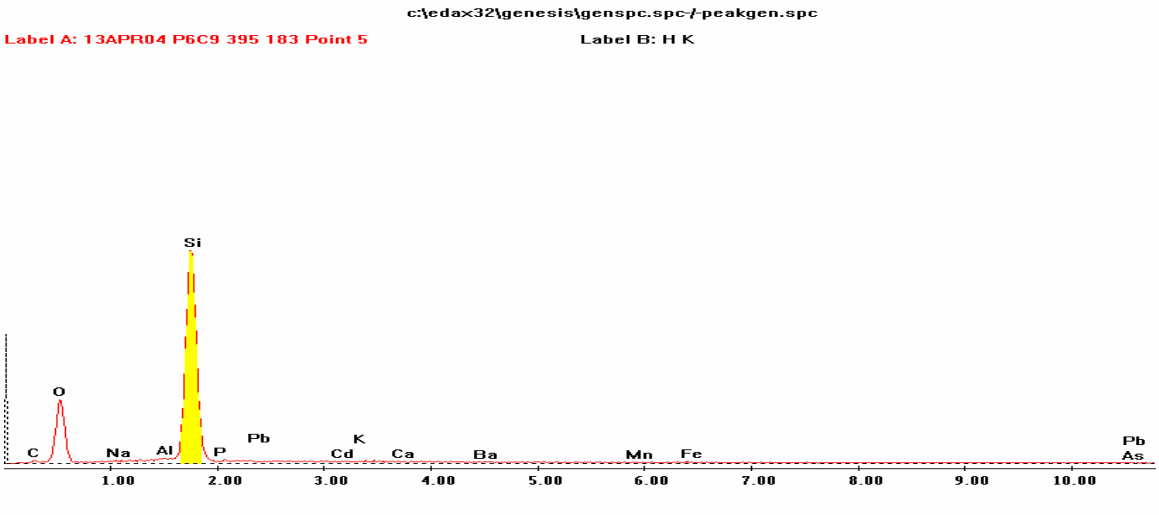

Point 6

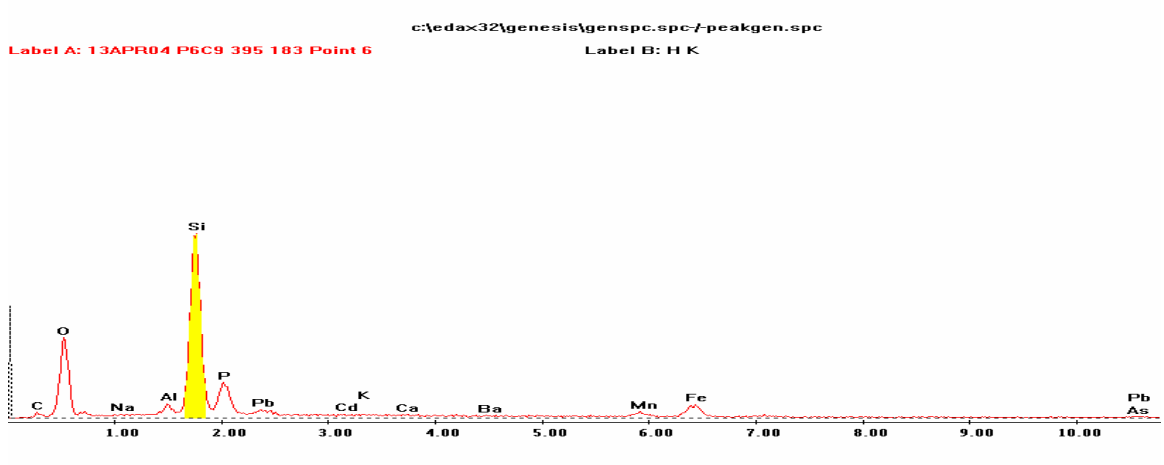

Point 7

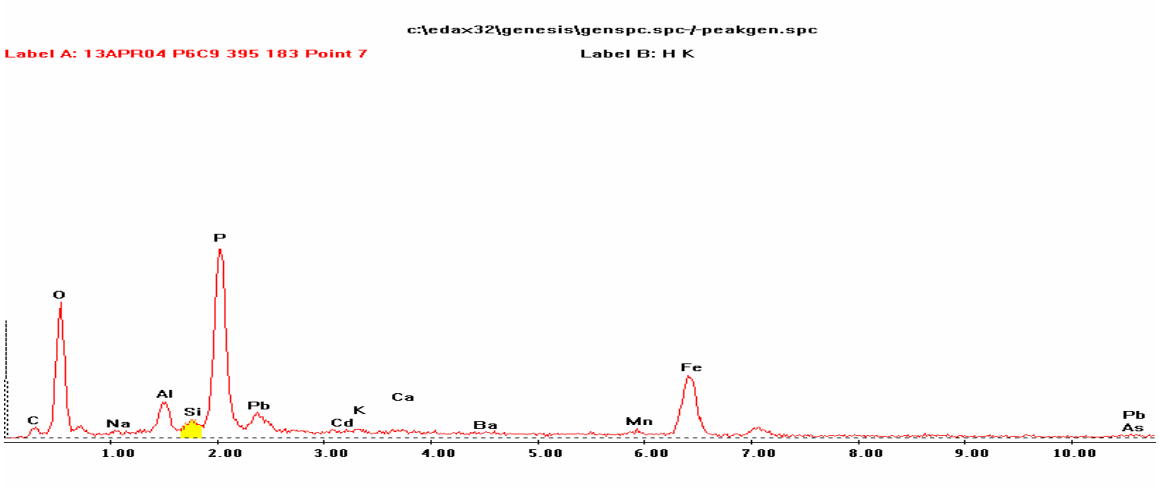

Point 8

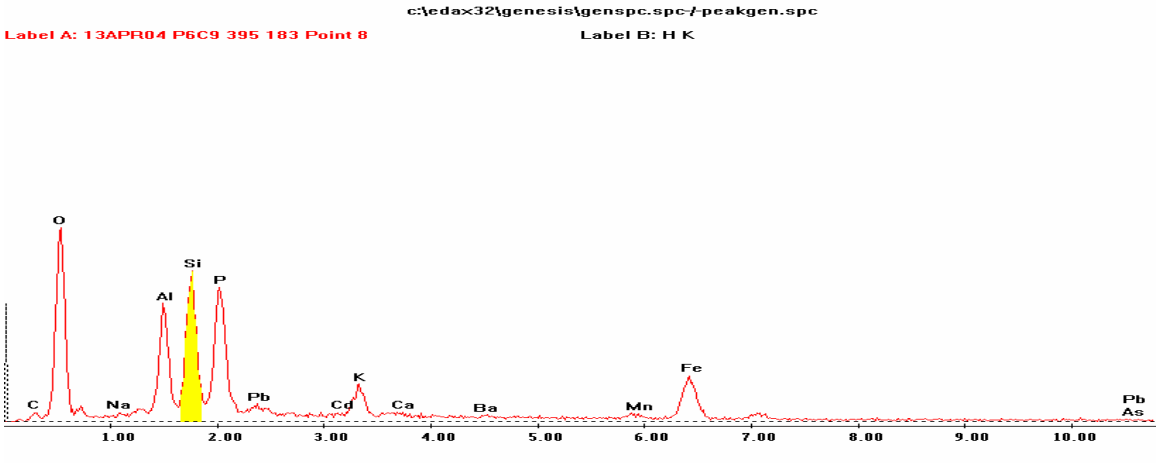

P6C9 – 452, 188

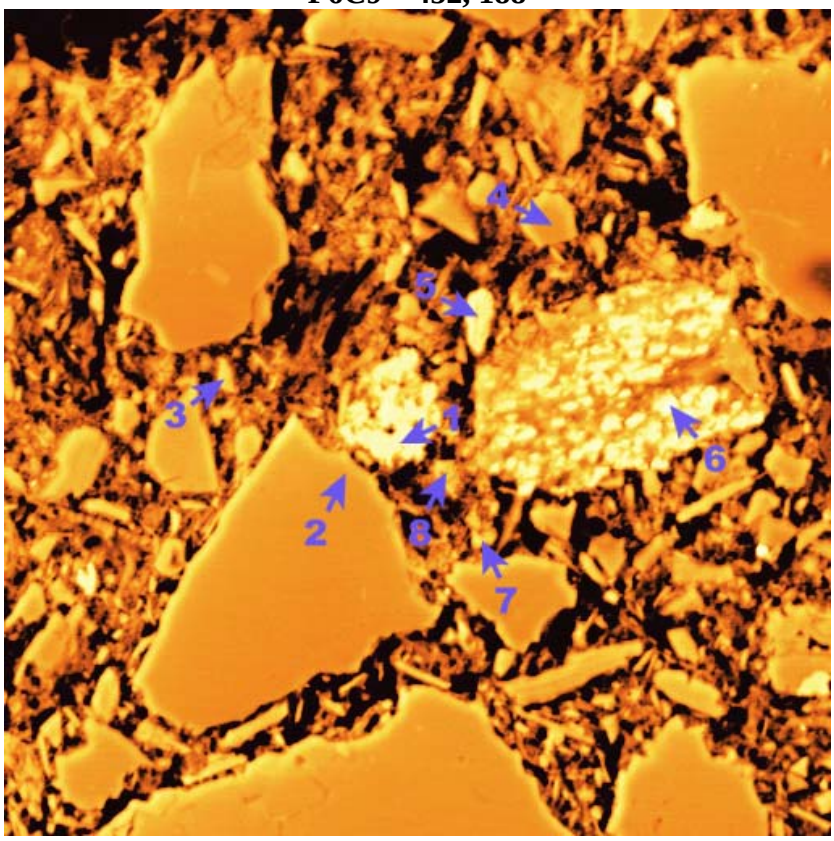

BSE Image

Iron (Fe)

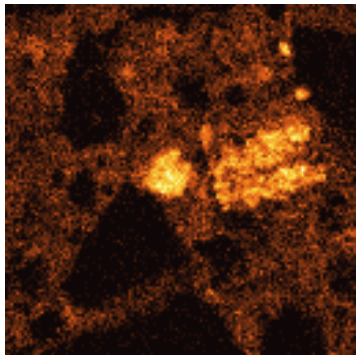

Manganese (Mn)

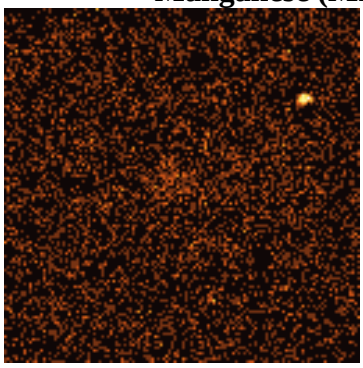

Phosphorous (P)

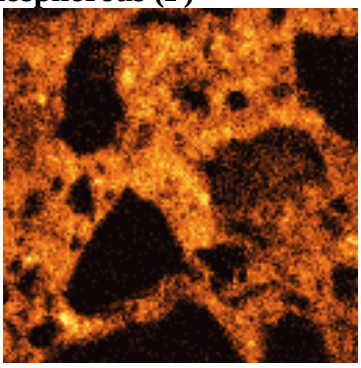

Lead (Pb)

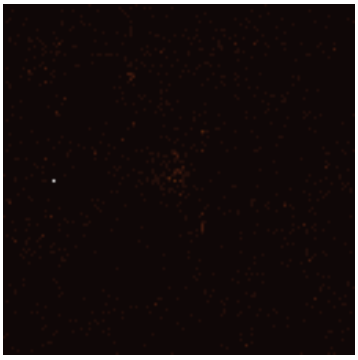

Silicon (Si)

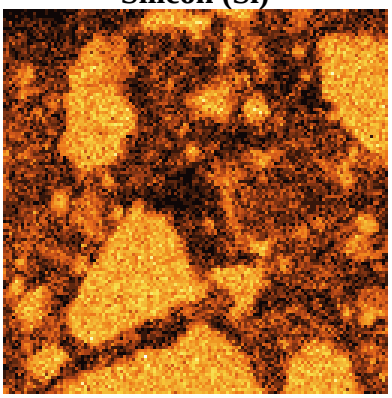

EDS Scan Images by Point

Point 1

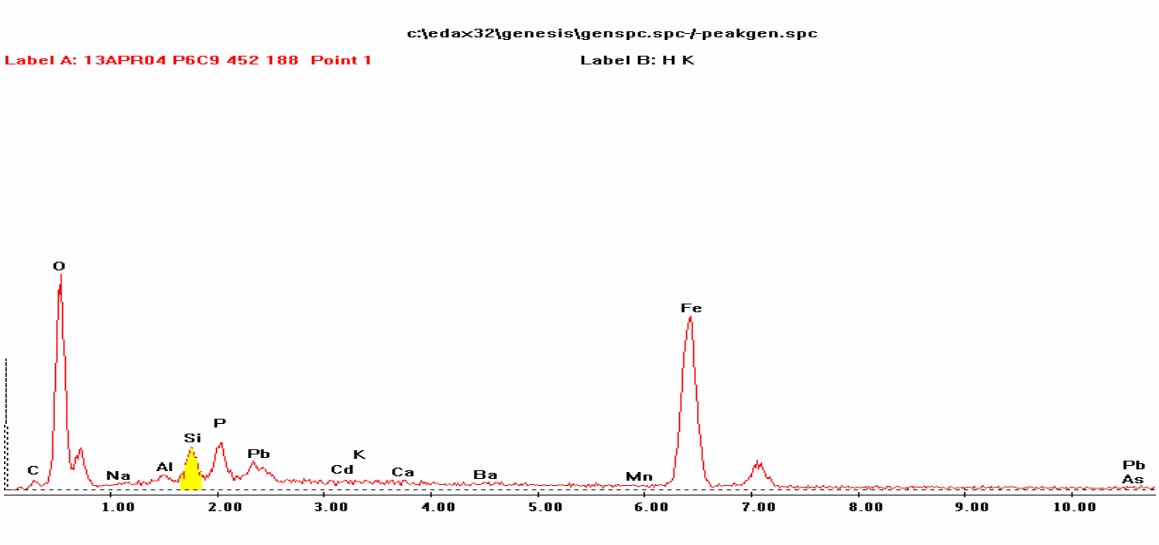

Point 2

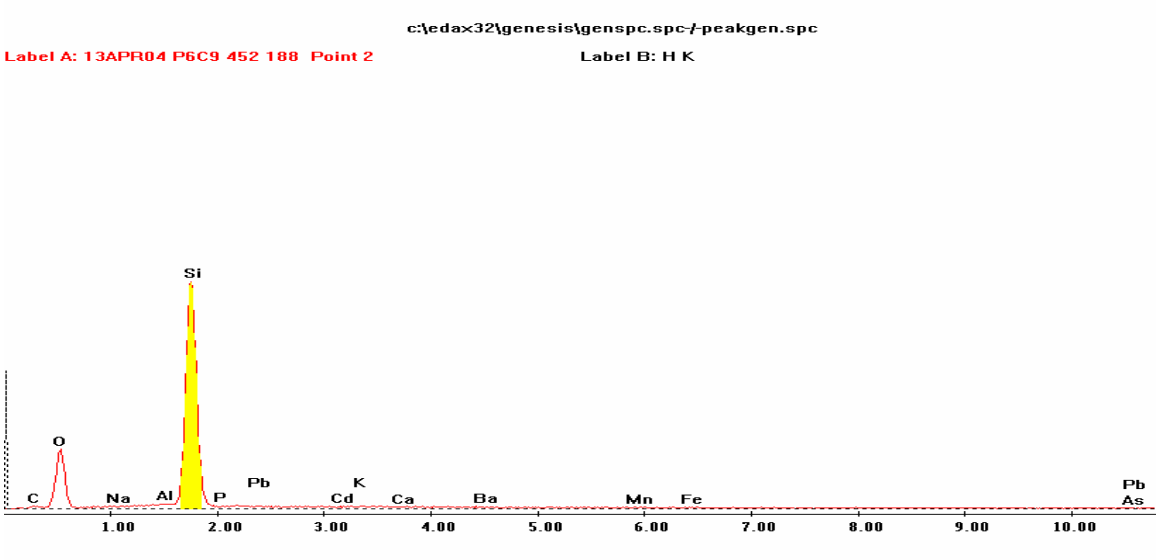

Point 3

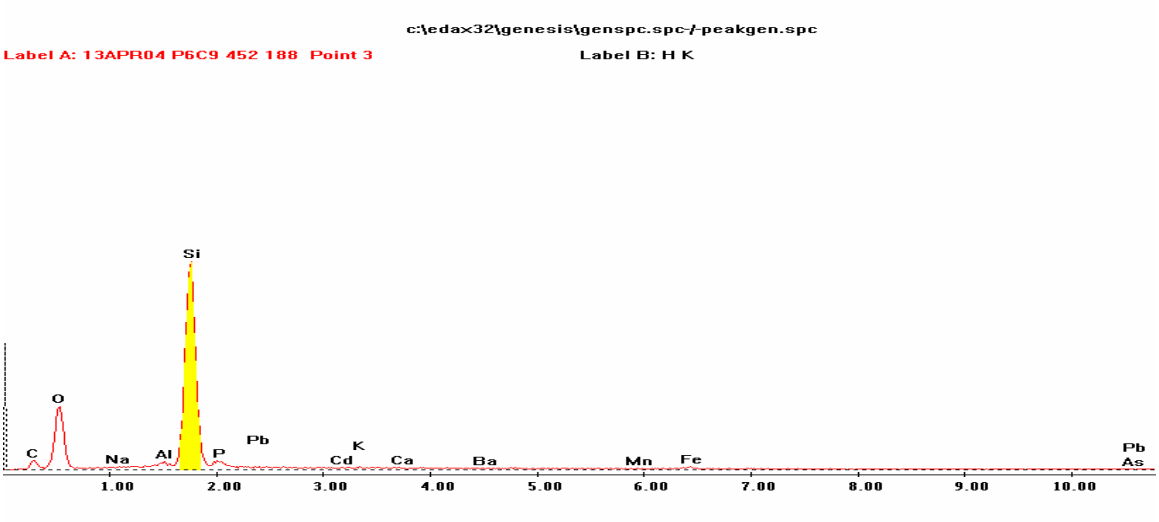

Point 4

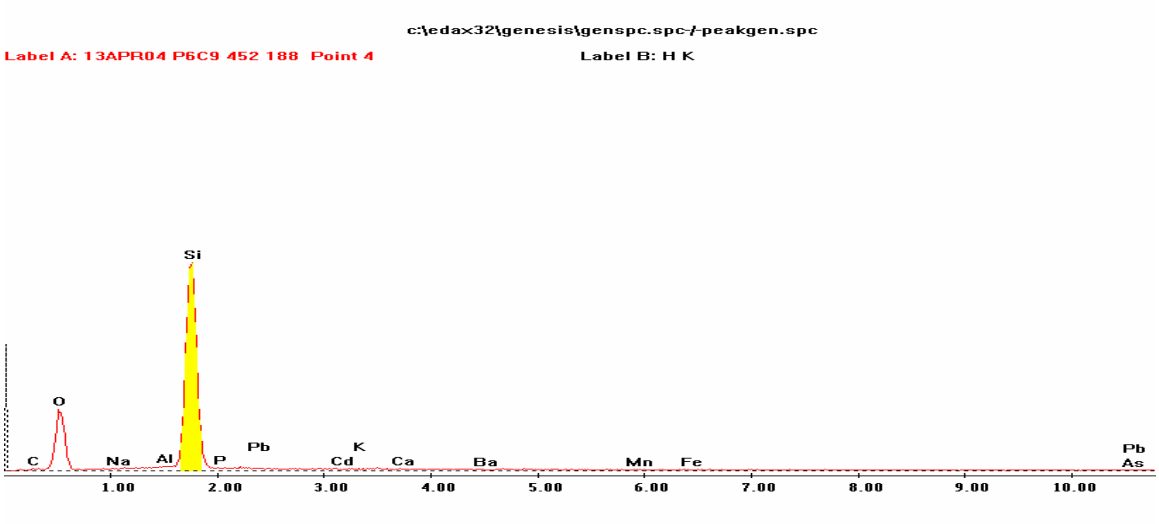

Point 5

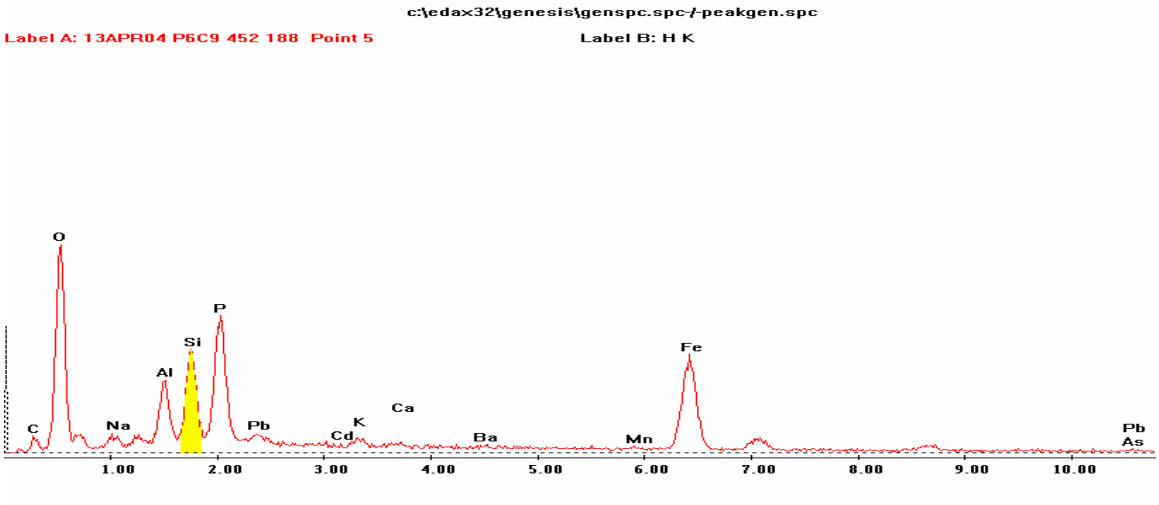

Point 6

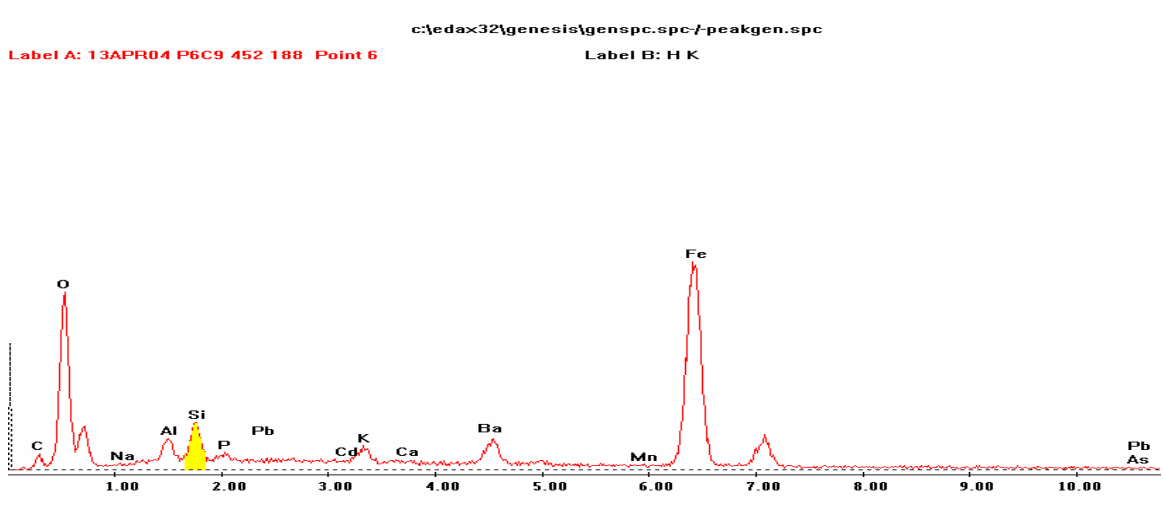

Point 7

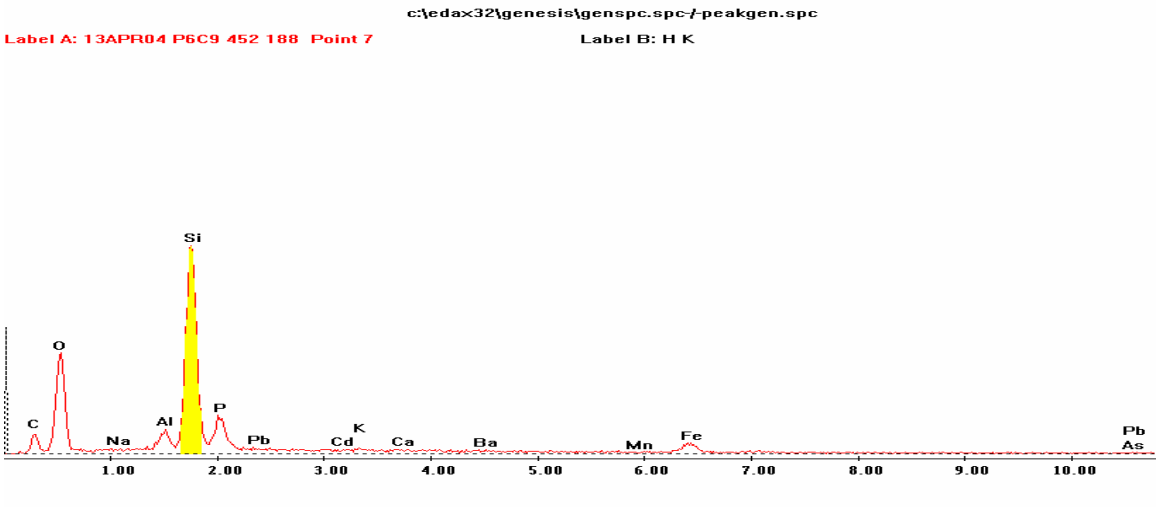

Point 8

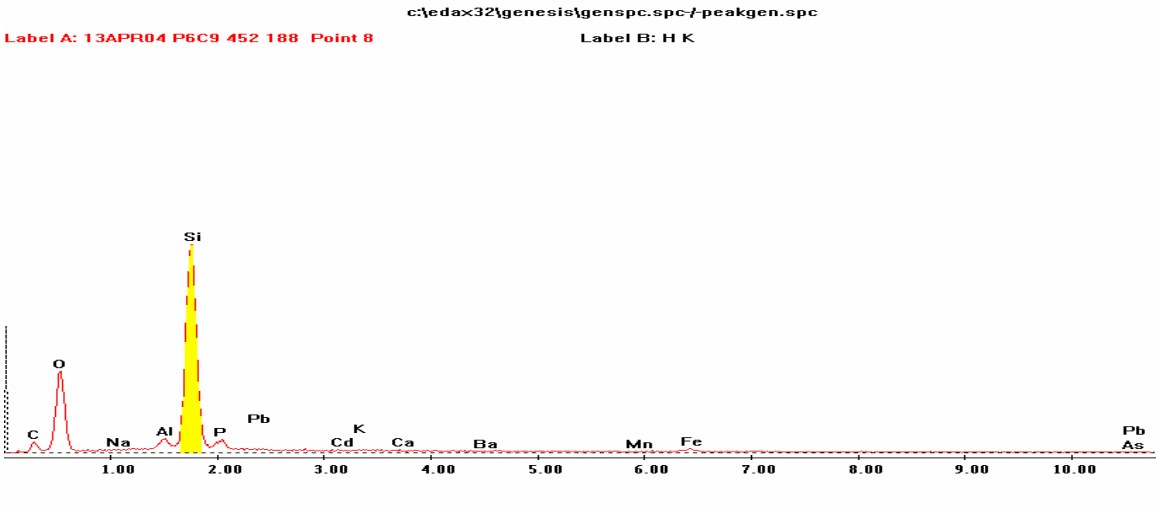

P6C9 – 482, 224

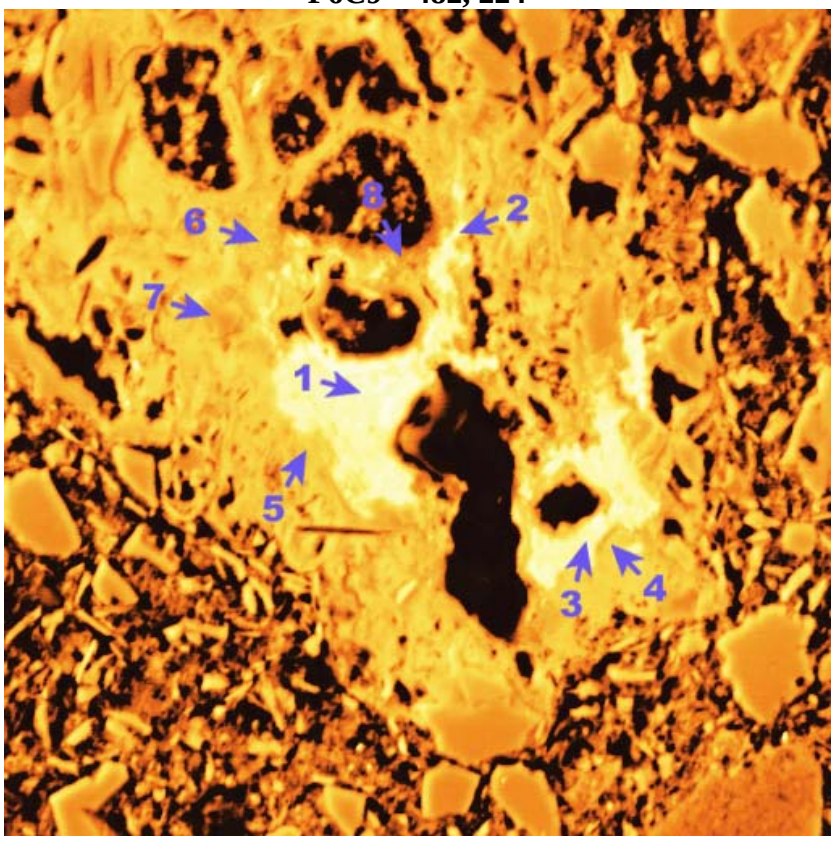

BSE Image

Iron (Fe)

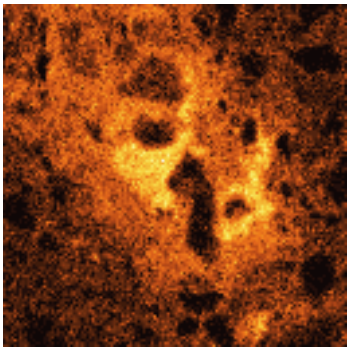

Manganese (Mn)

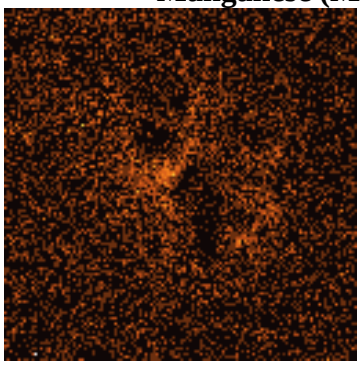

Phosphorous (P)

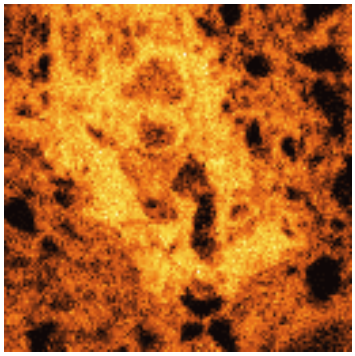

Lead (Pb)

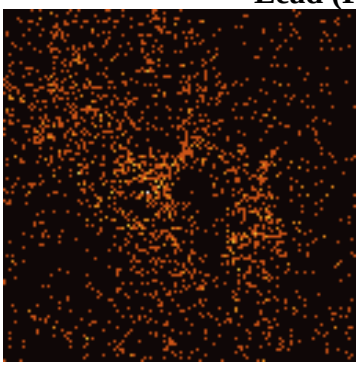

Silicon (Si)

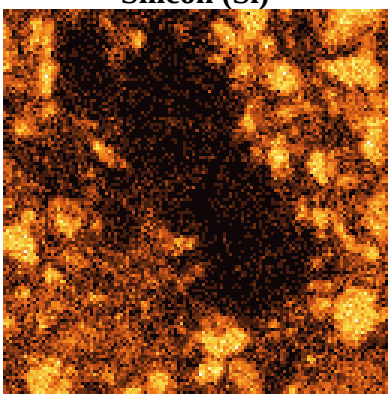

EDS Scan Images by Point

Point 1

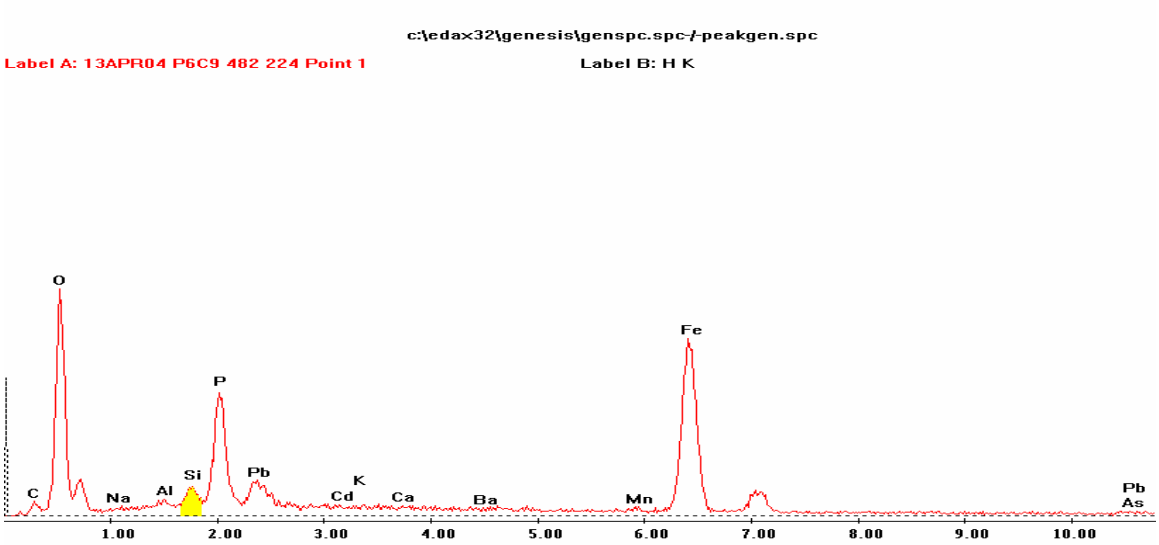

Point 2

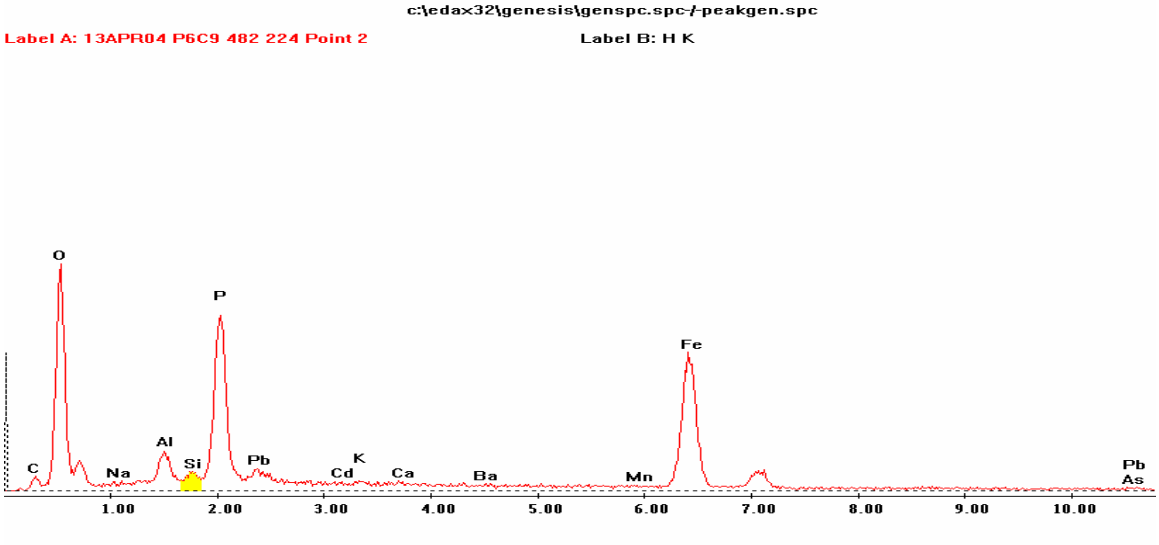

Point 3

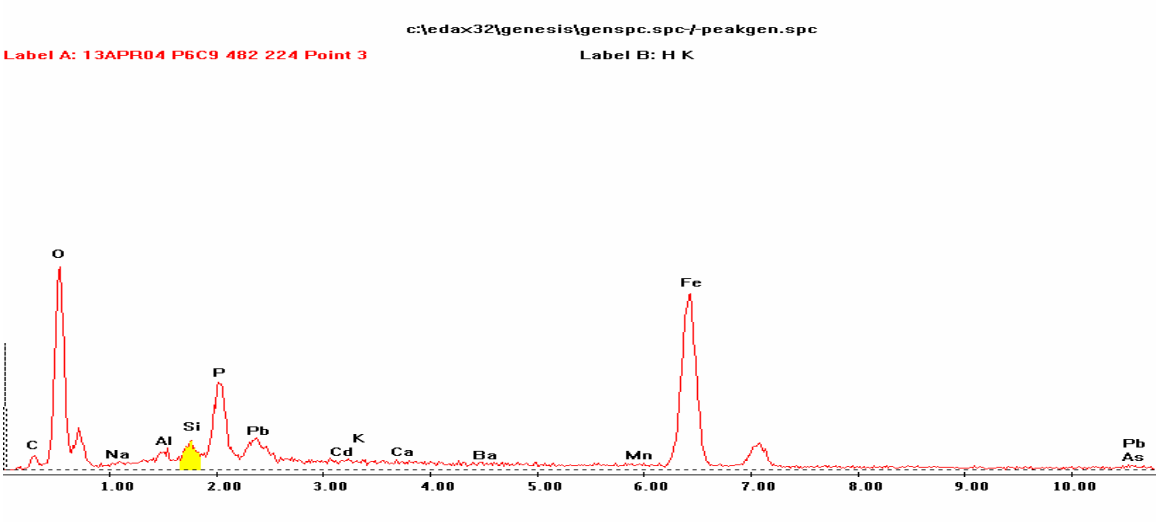

Point 4

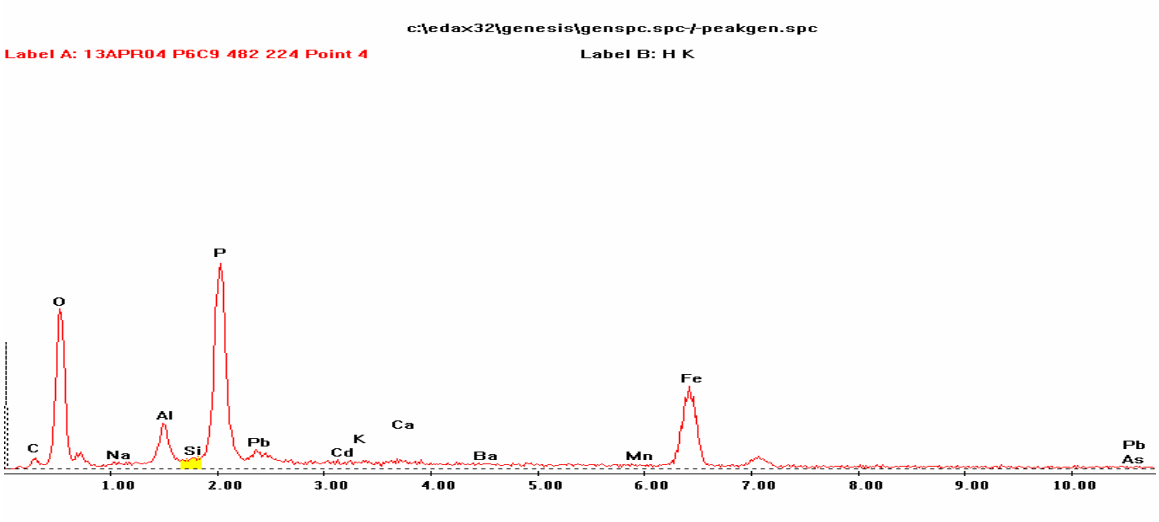

Point 5

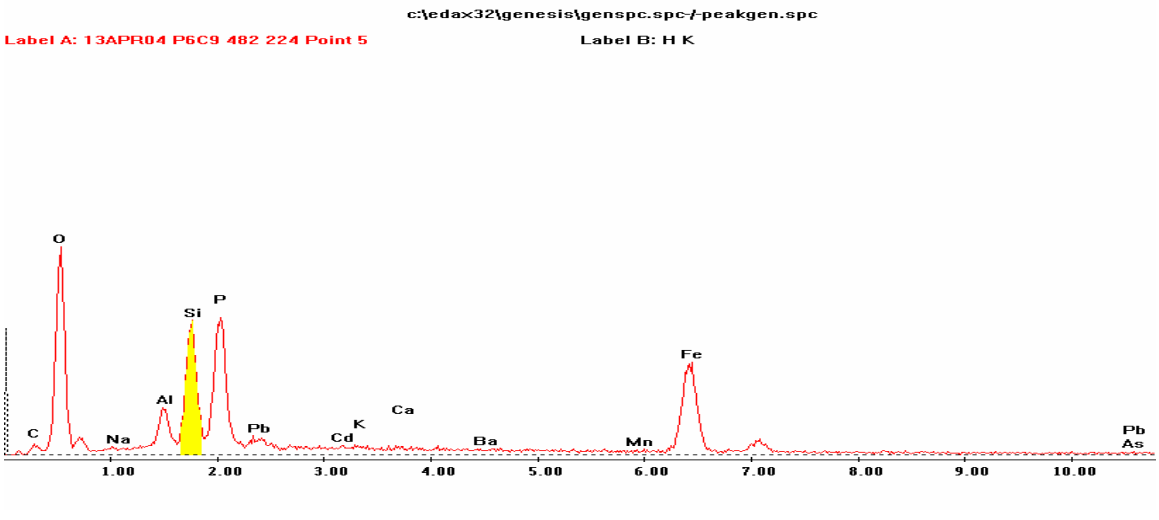

Point 6

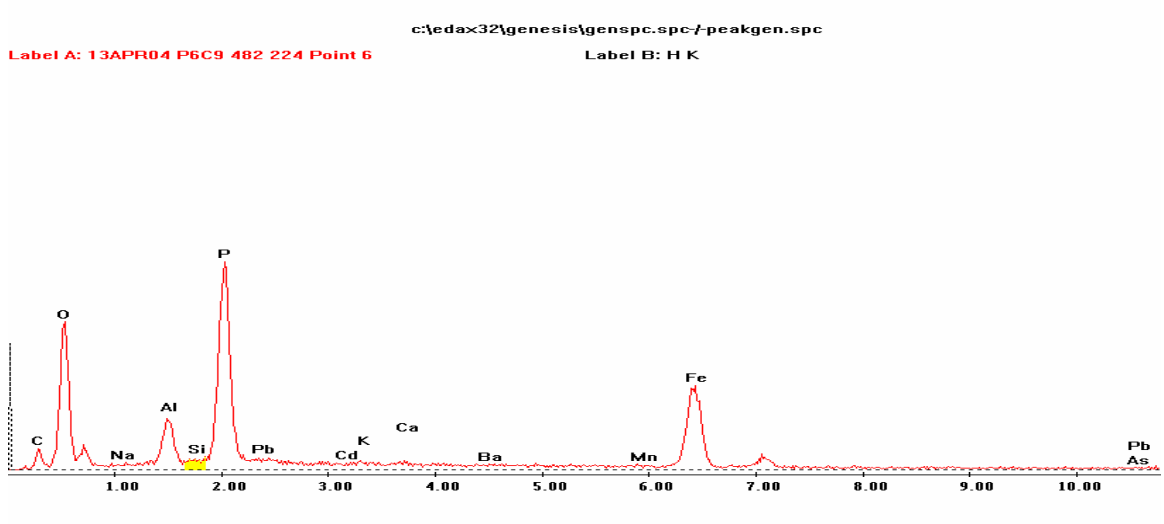

Point 7

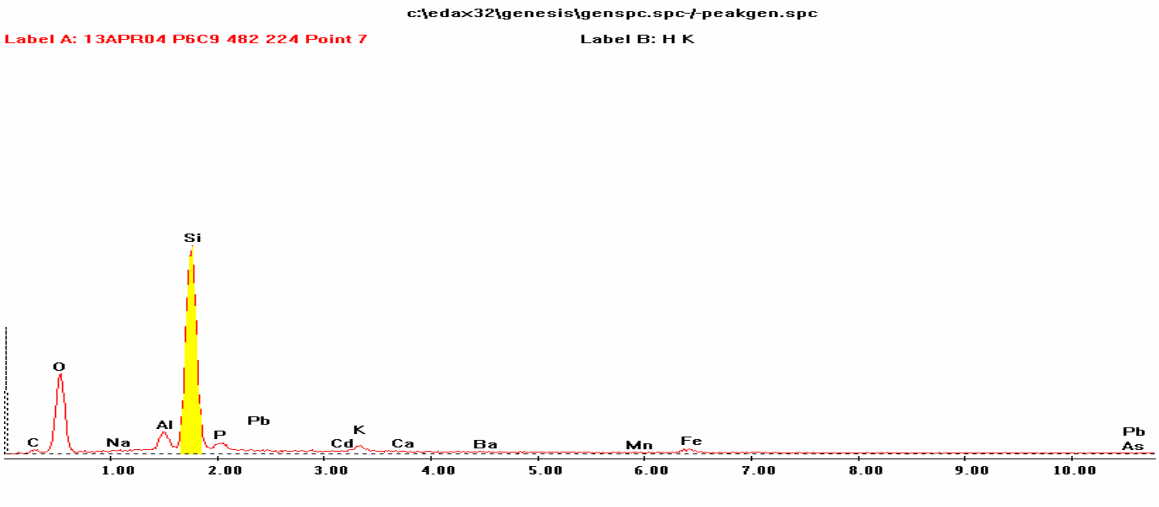

Point 8

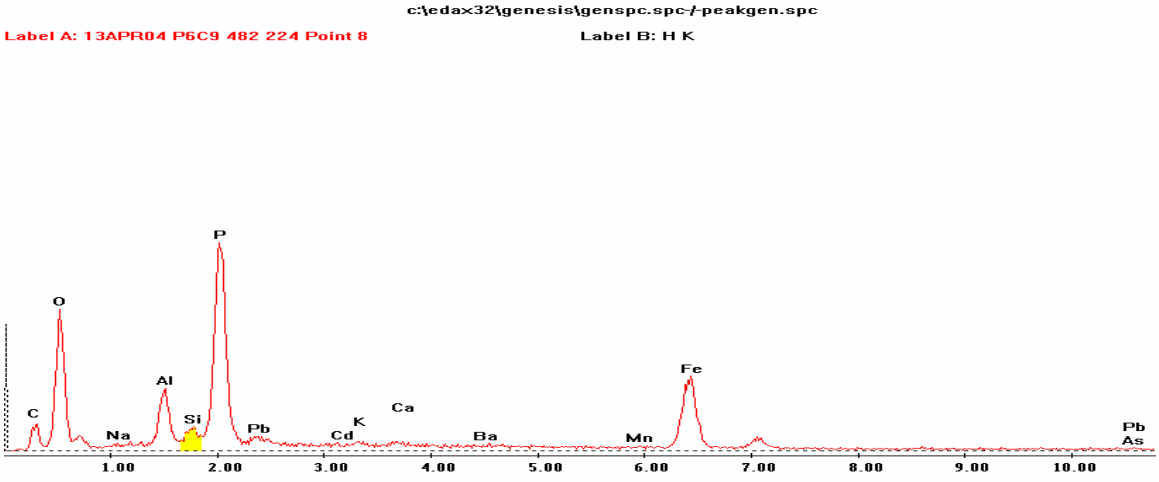

P6C9 – 331, 212

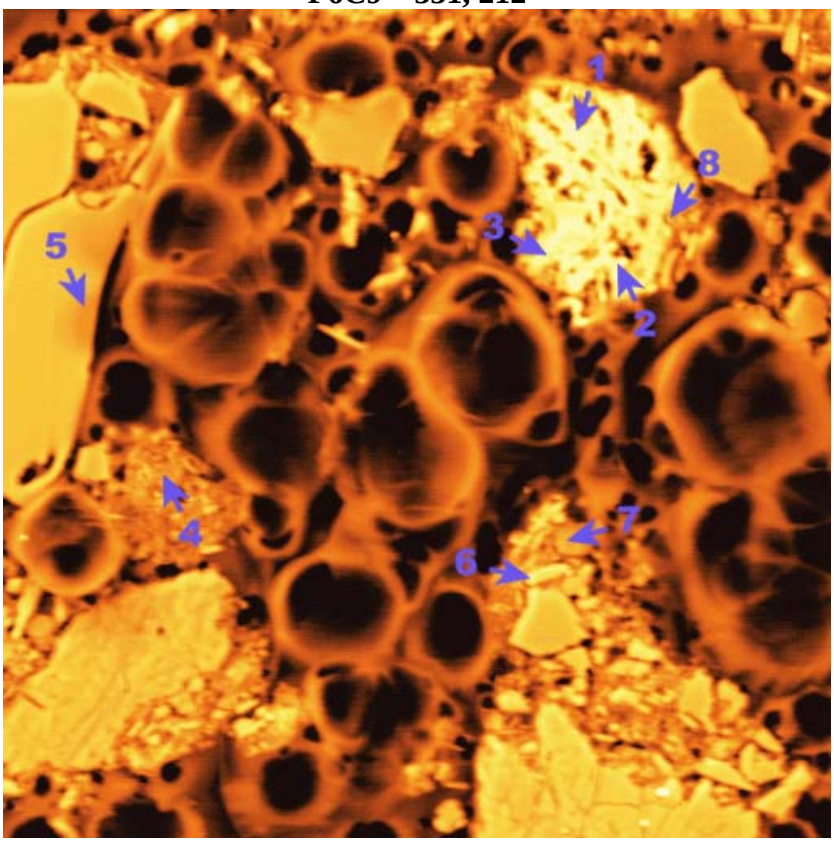

BSE Image

Iron (Fe)

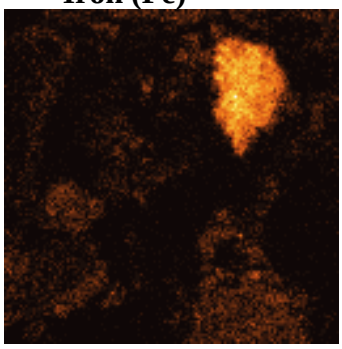

Manganese (Mn)

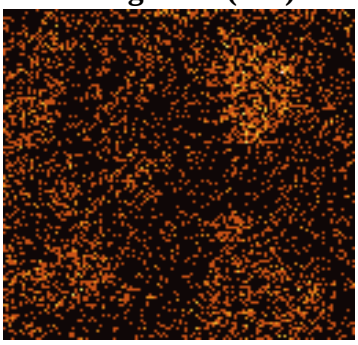

Phosphorous (P)

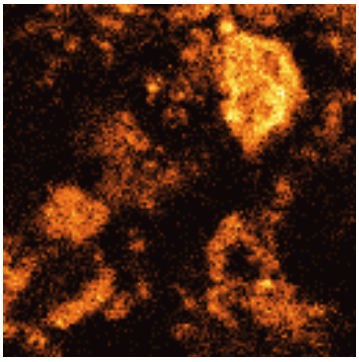

Lead (Pb)

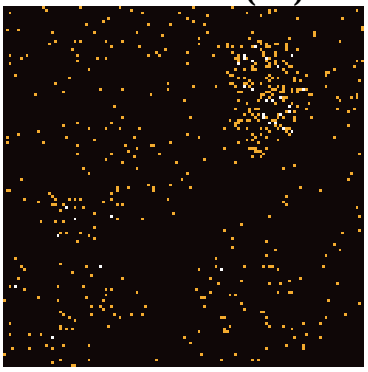

Silicon (Si)

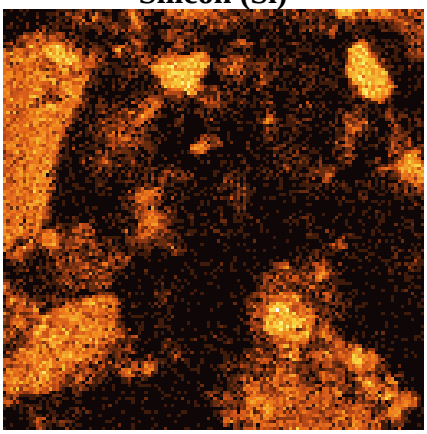

EDS Scan Images by Point

Point 1

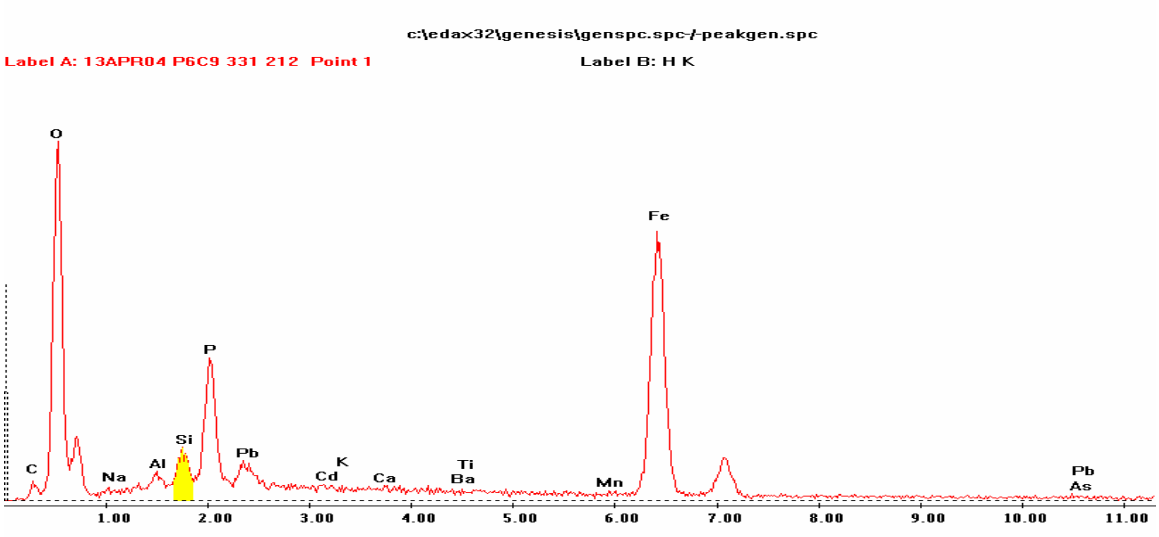

Point 2

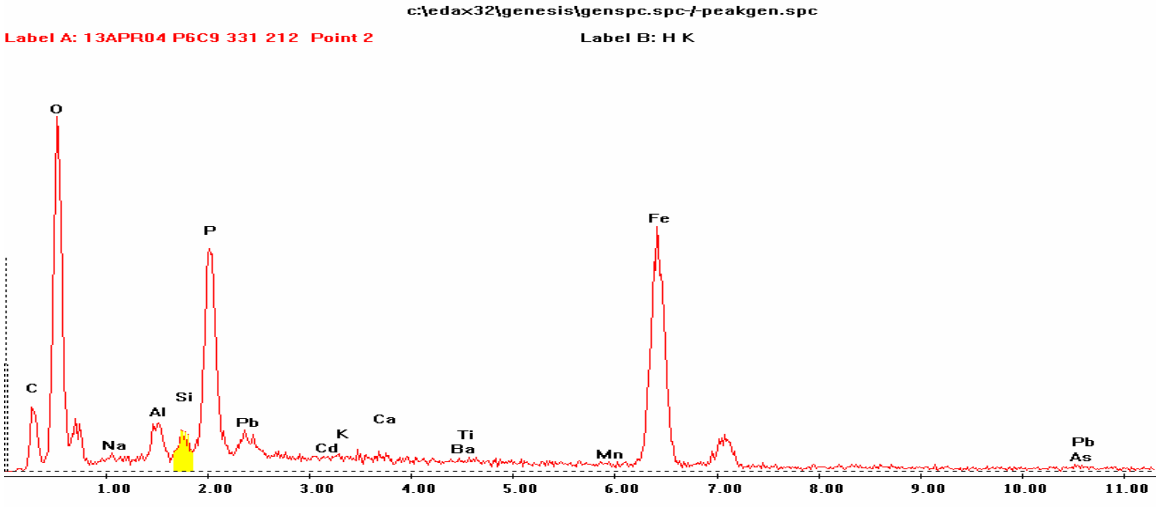

Point 3

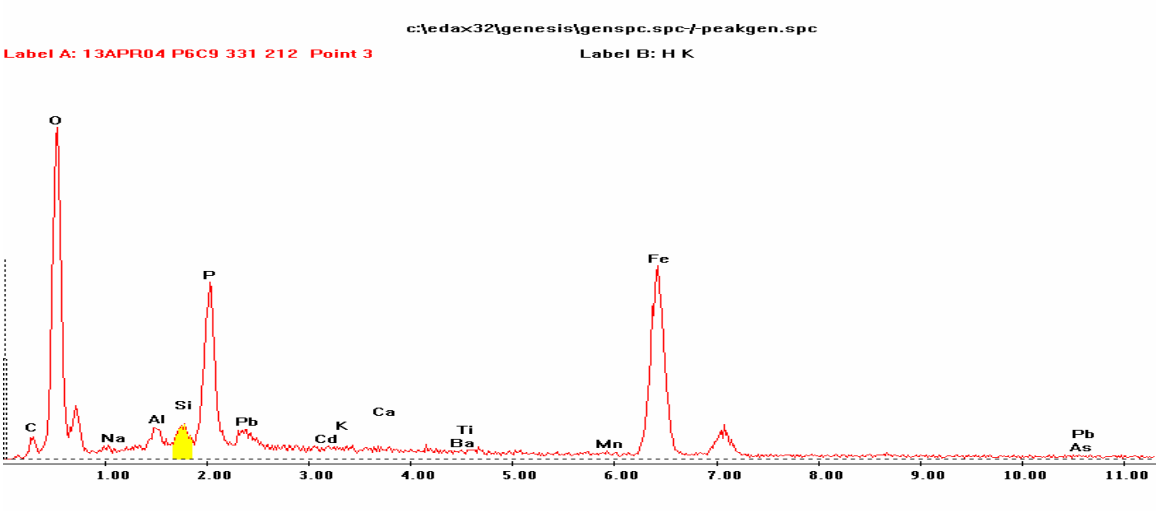

Point 4

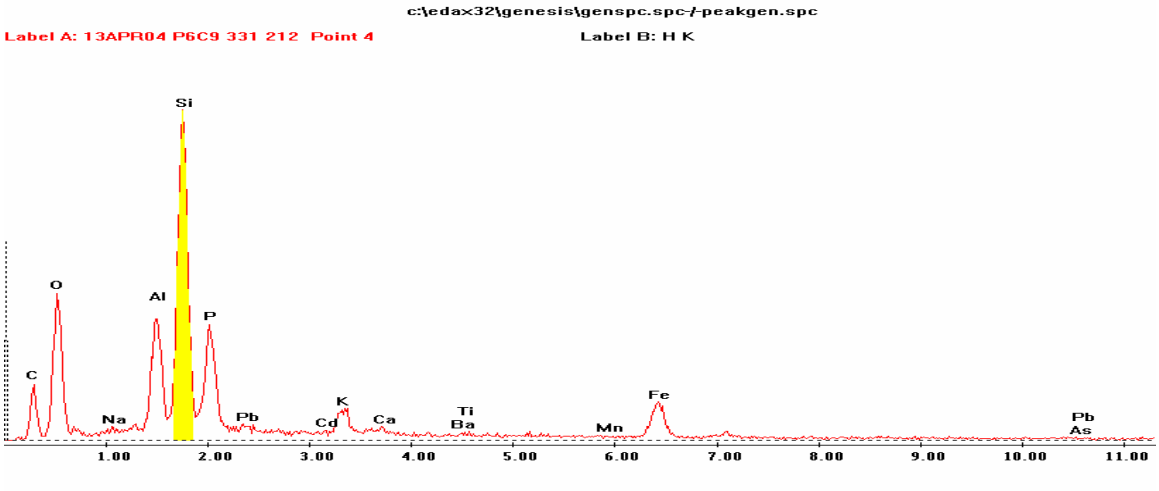

Point 5

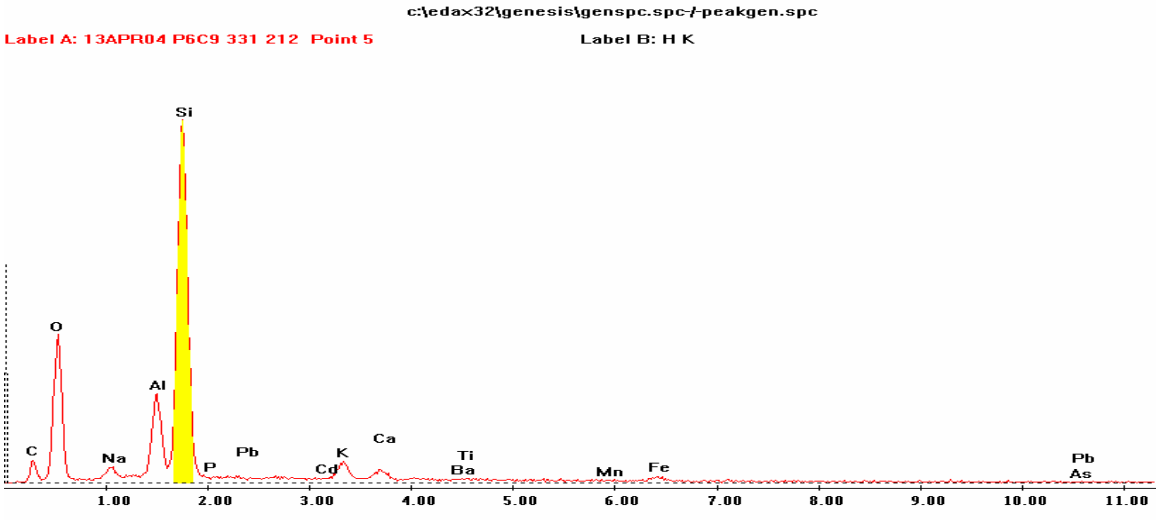

Point 6

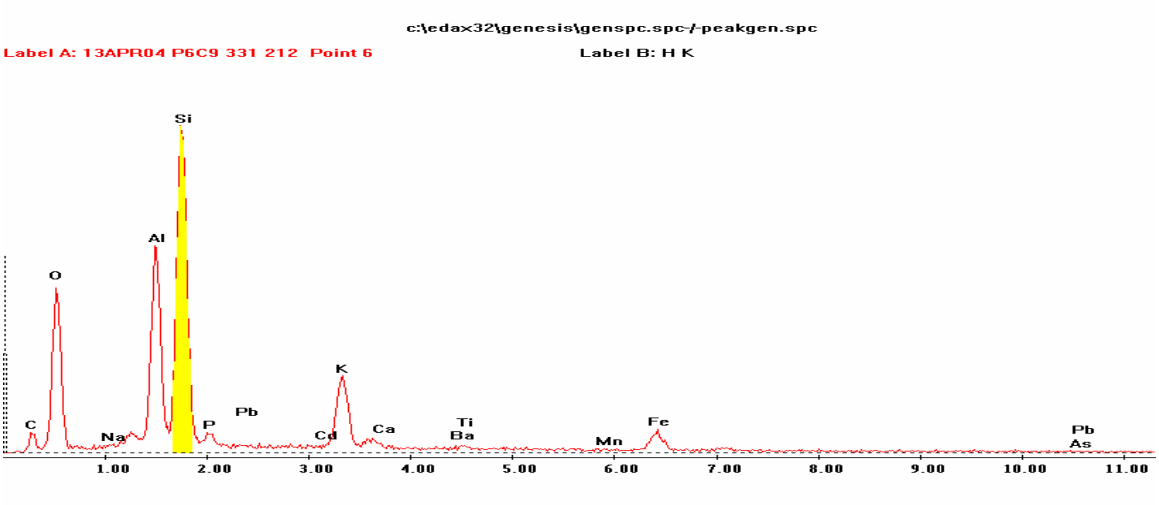

Point 7

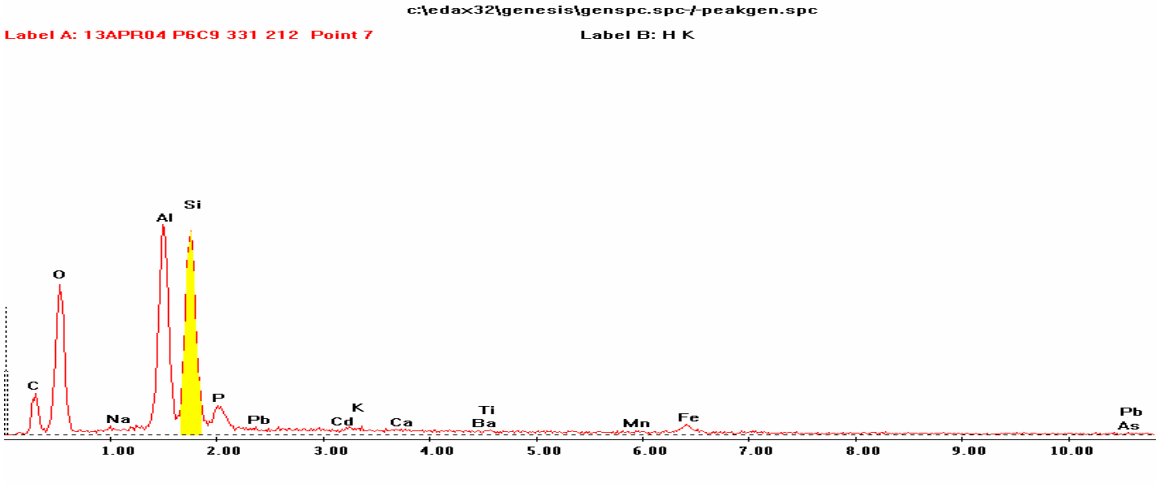

Point 8

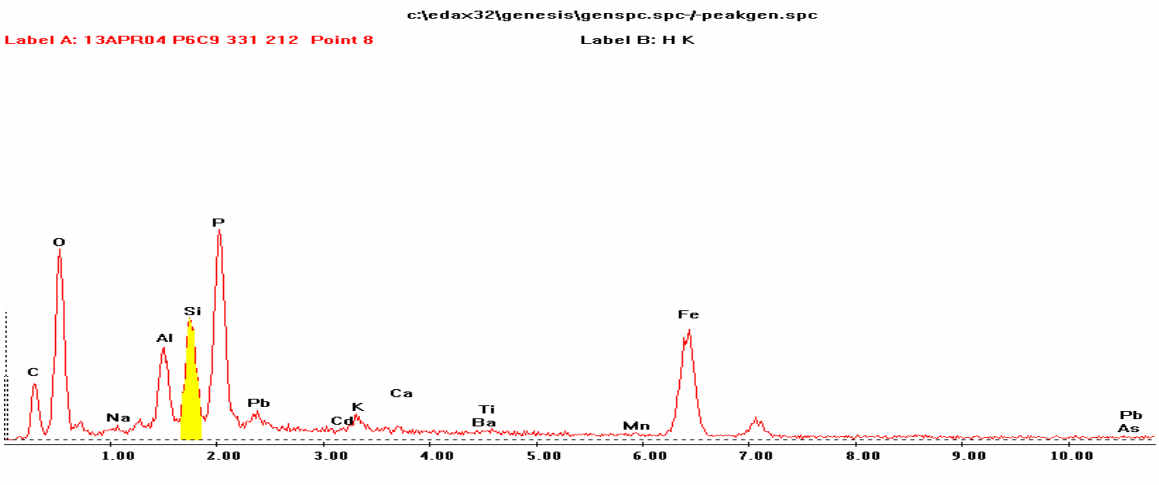

P6C9 – 357, 180

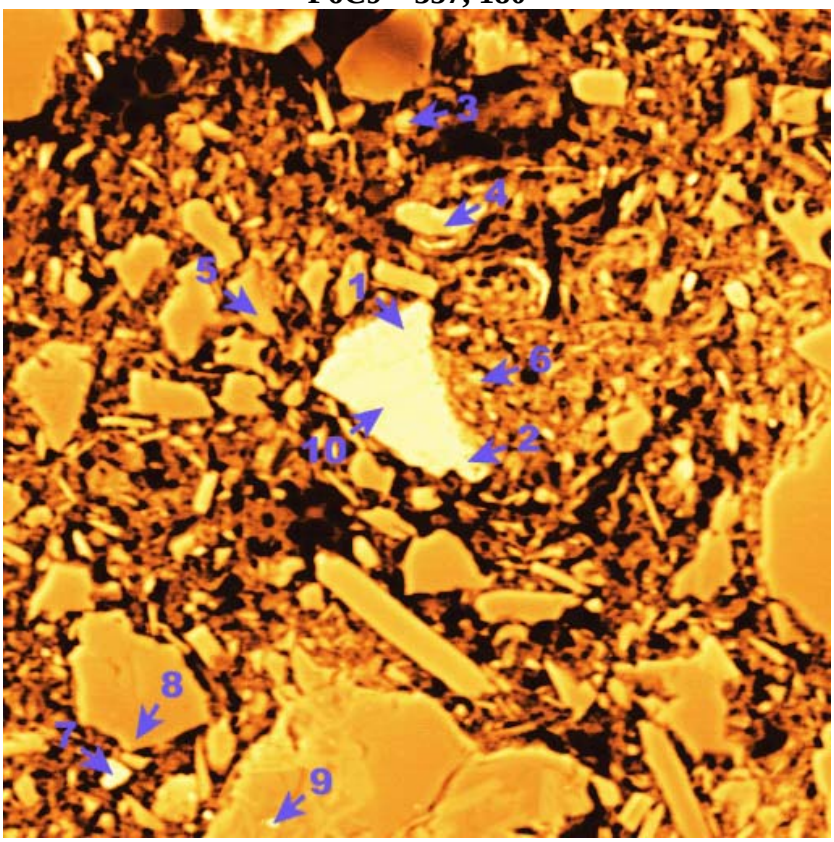

BSE Image

Iron (Fe)

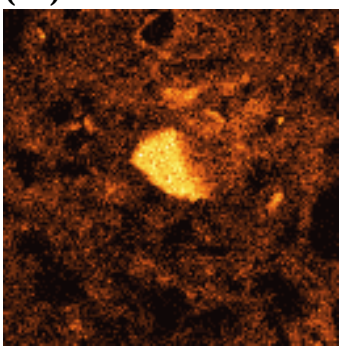

Manganese (Mn)

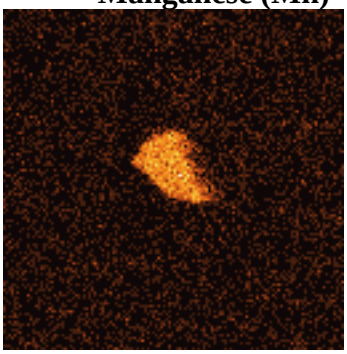

Phosphorous (P)

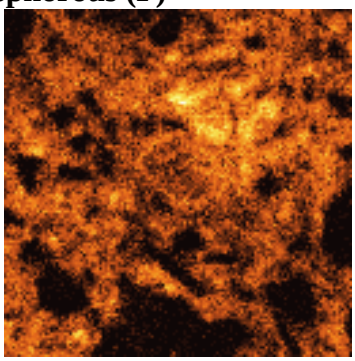

Lead (Pb)

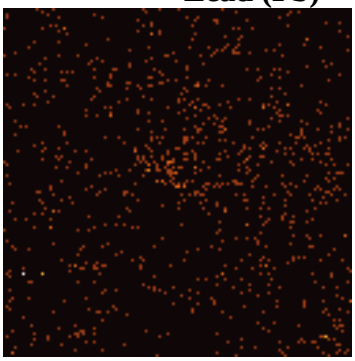

Silicon (Si)

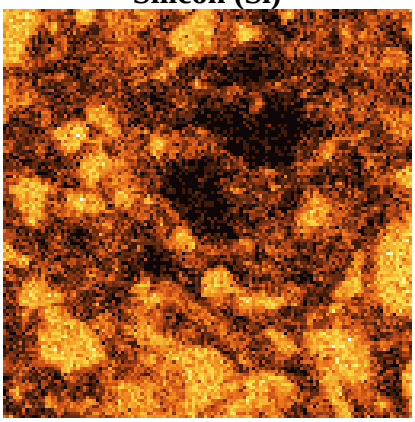

EDS Scan Images by Point

Point 1

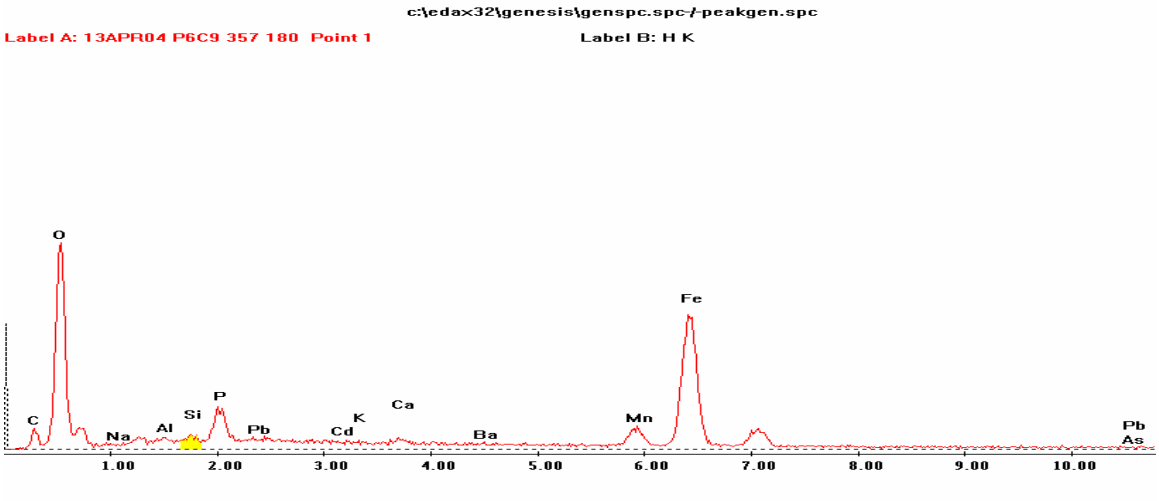

Point 2

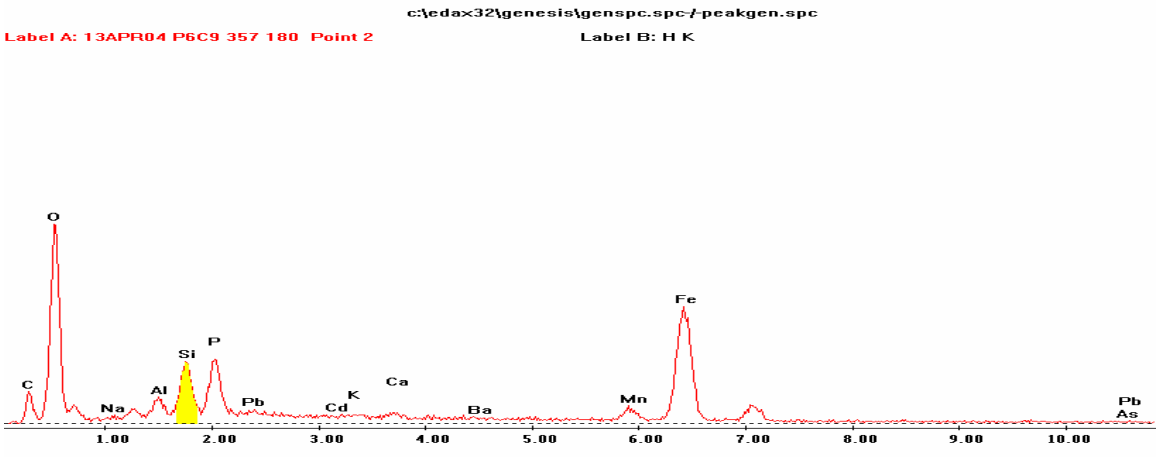

Point 3

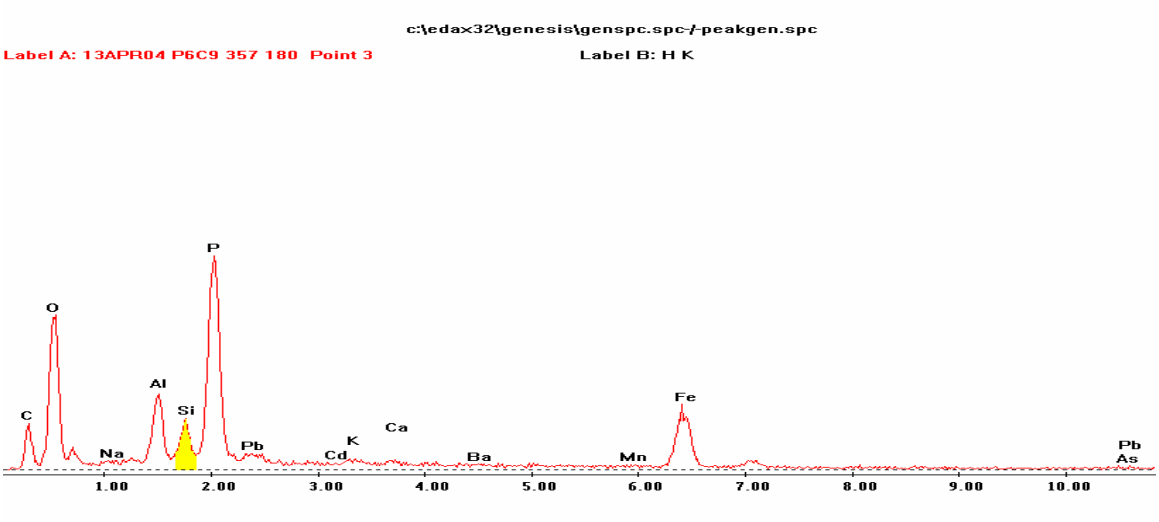

Point 4

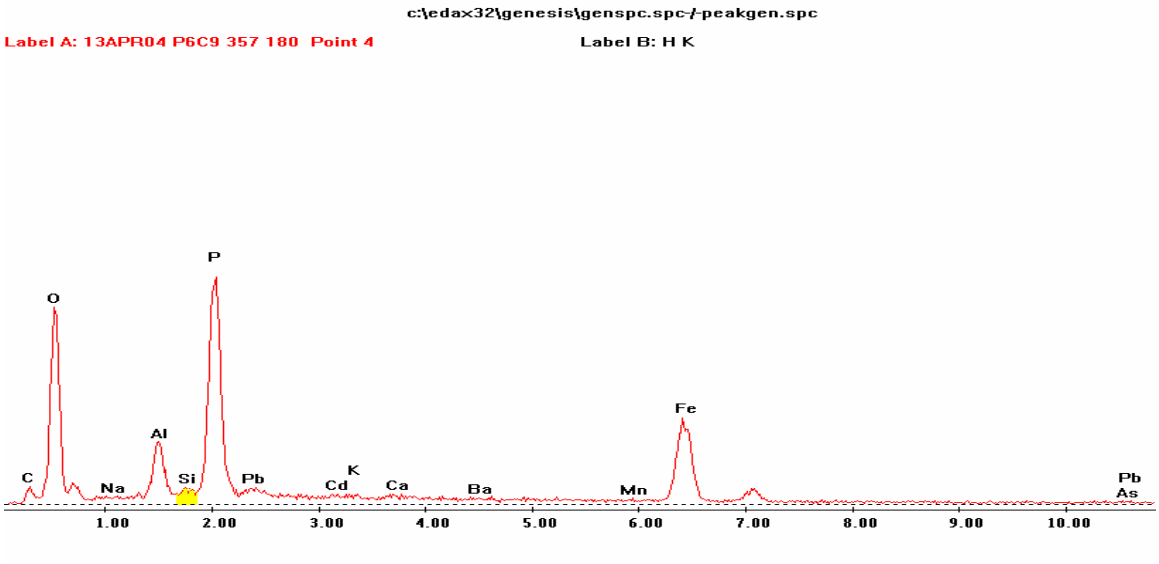

Point 5

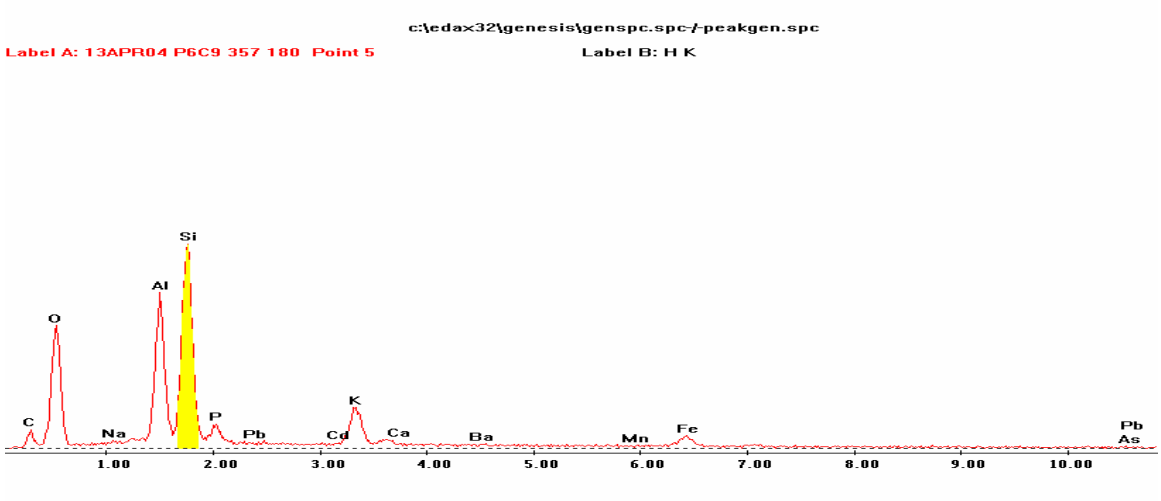

Point 6

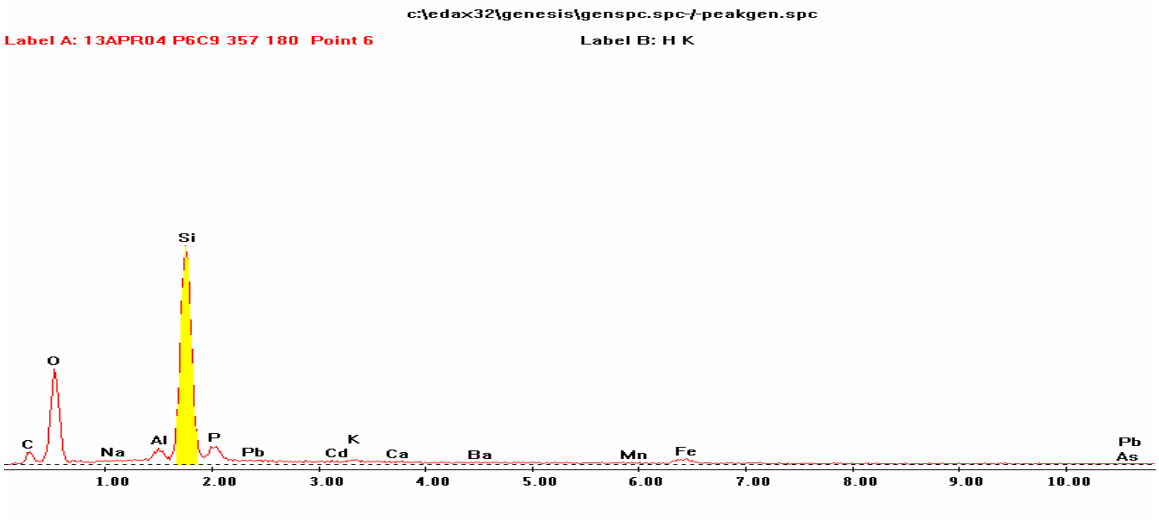

Point 7

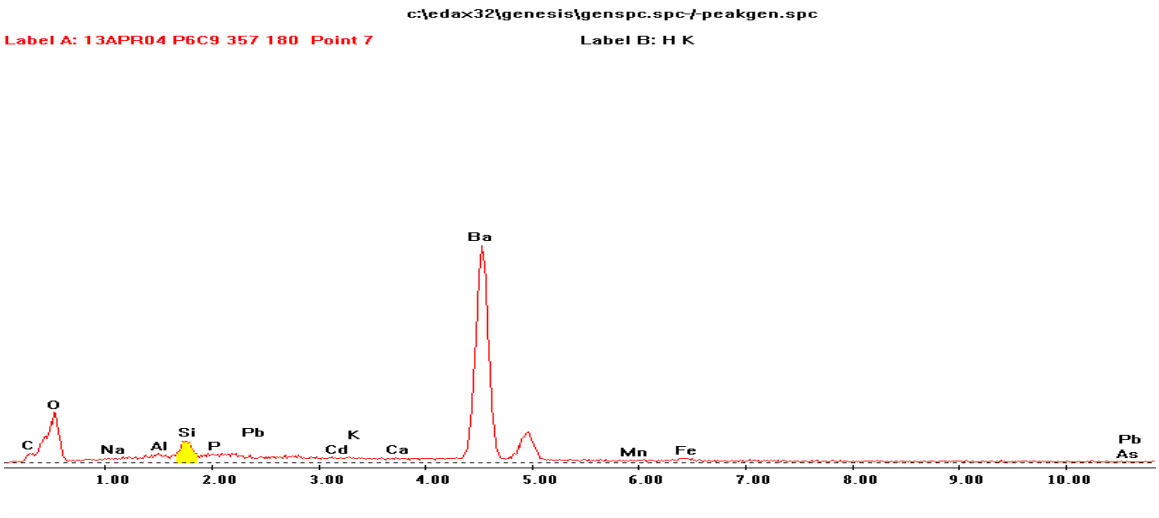

Point 8

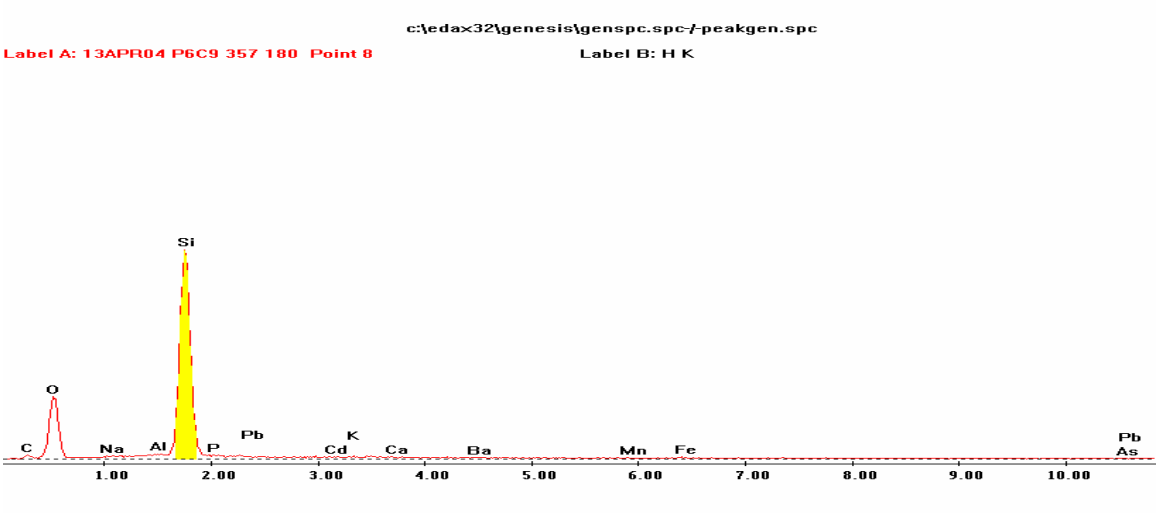

Point 9

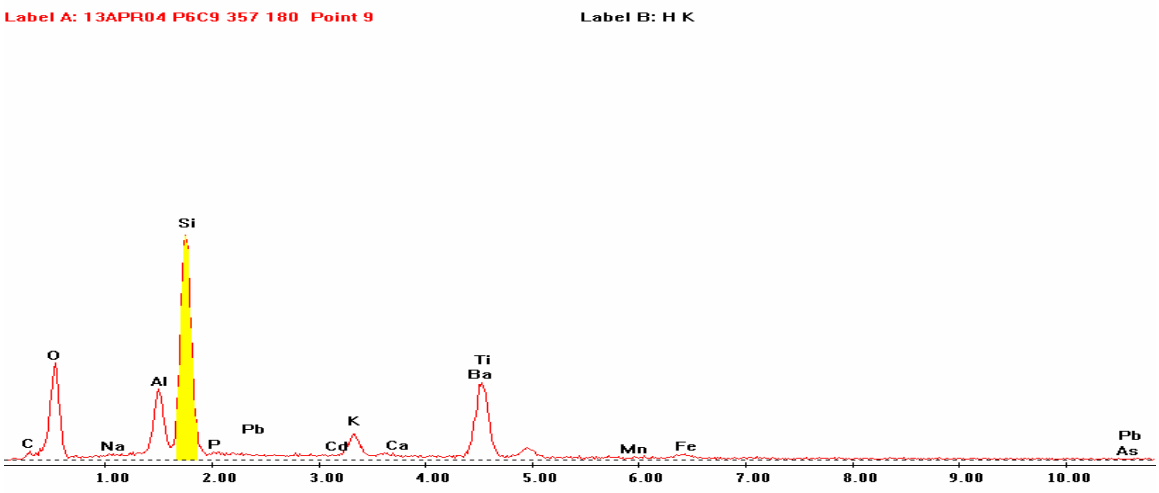

Point 10

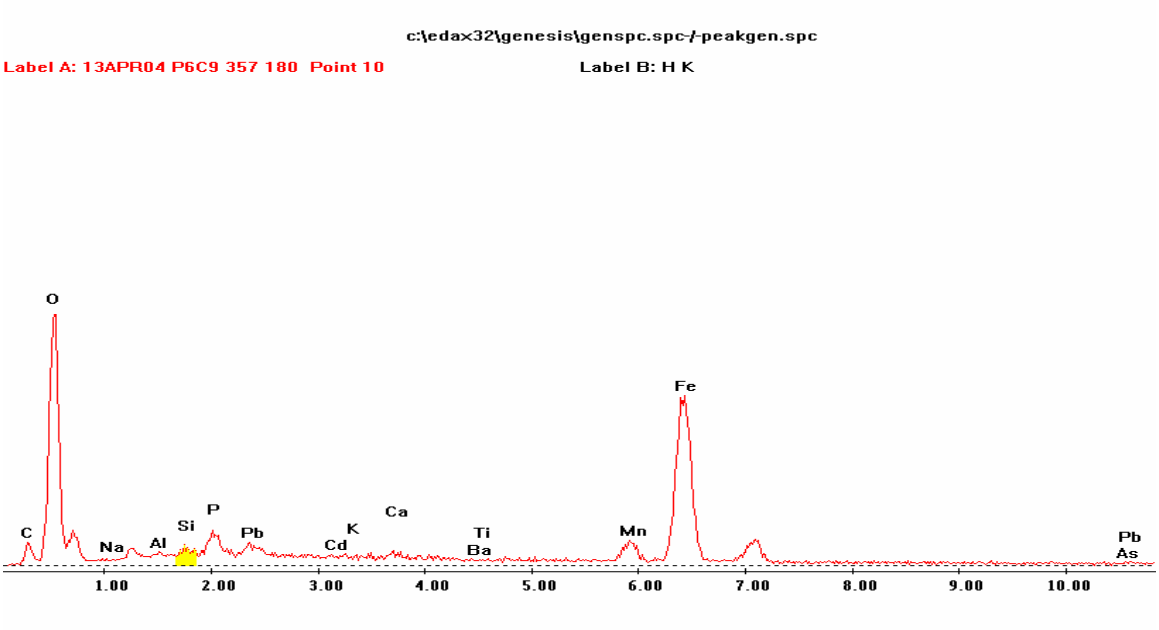

Plot 8

P8C7 – 312, 164

BSE Image

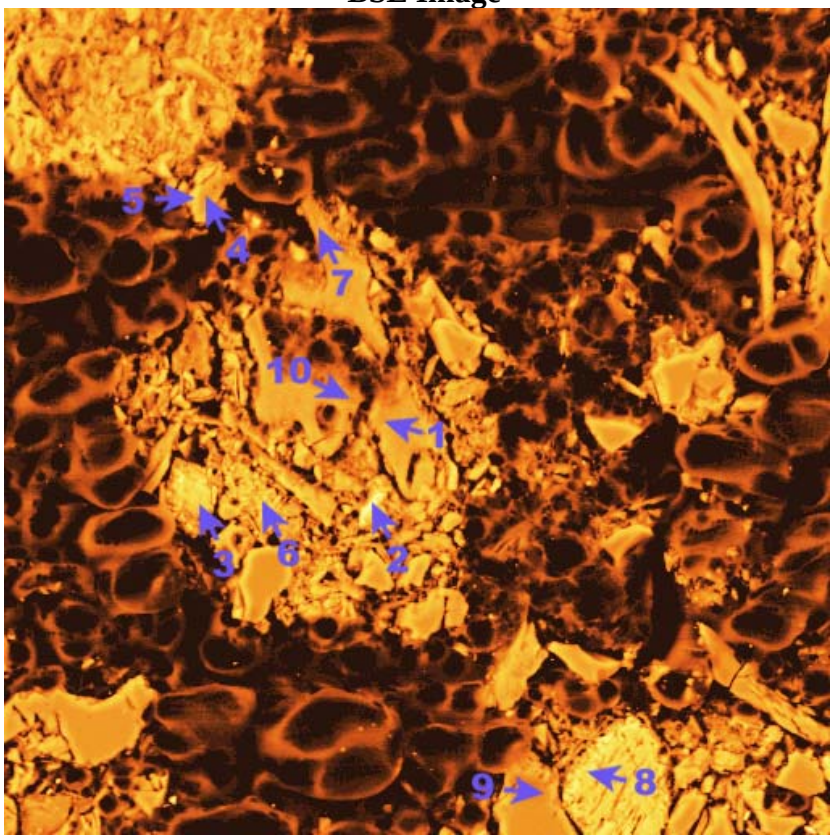

Iron (Fe)

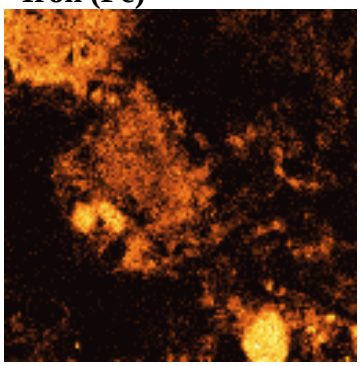

Manganese (Mn)

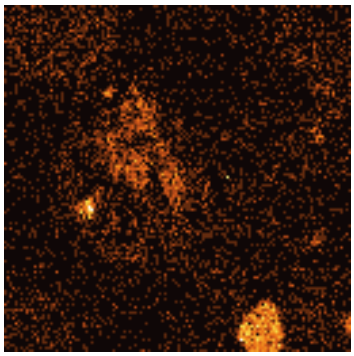

Phosphorous (P)

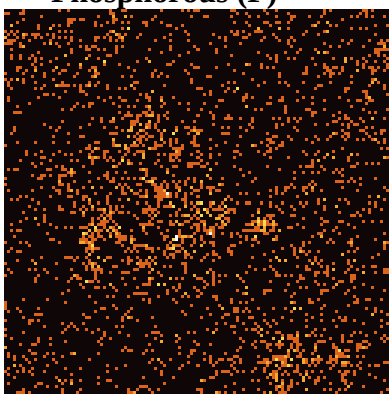

Lead (Pb)

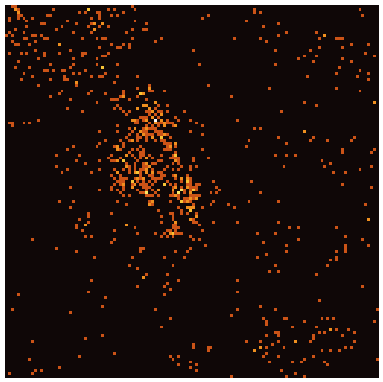

Silicon (Si)

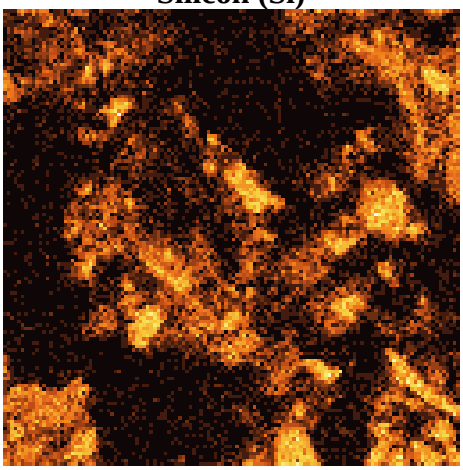

EDS Scan Images by Point

Point 1

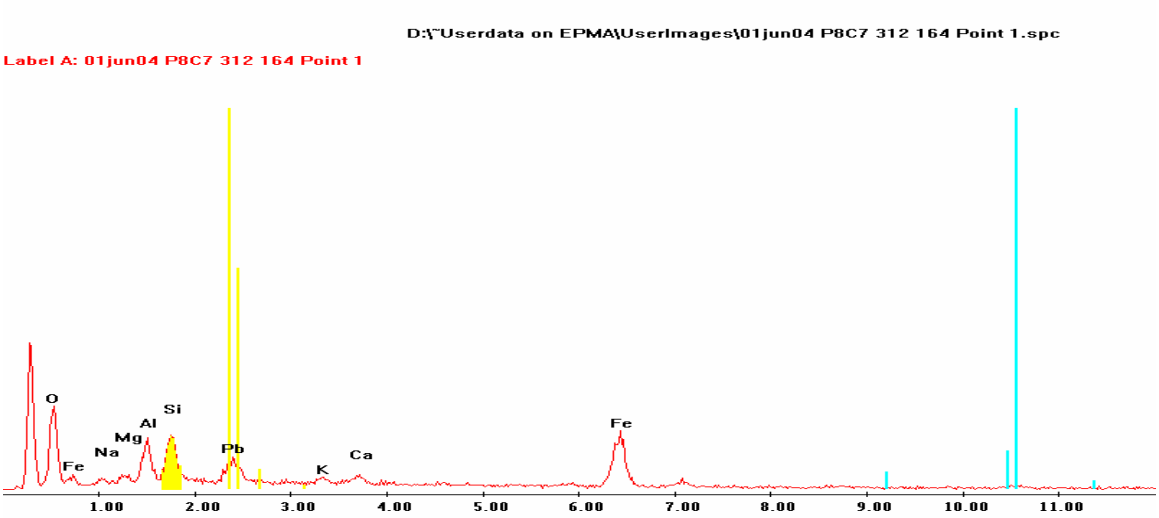

Point 2

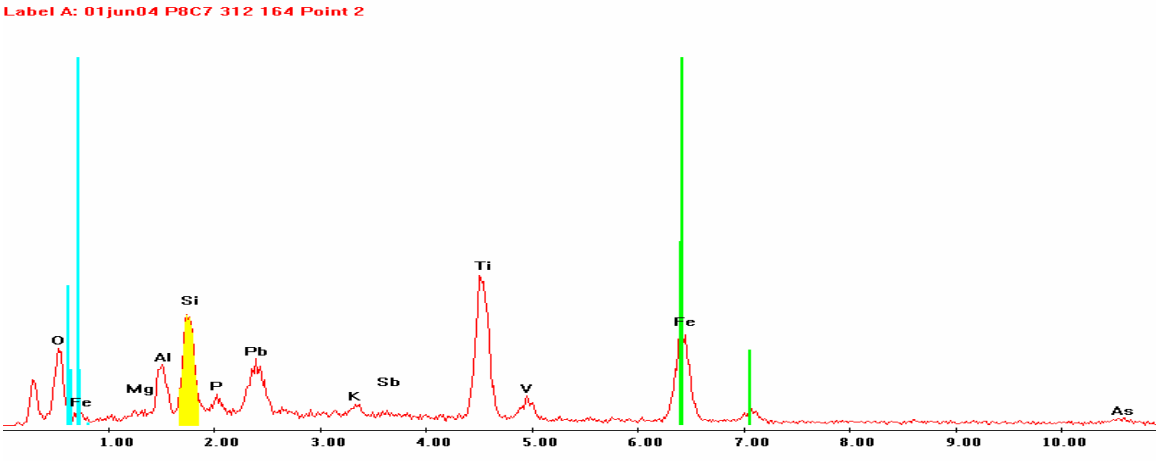

Point 3

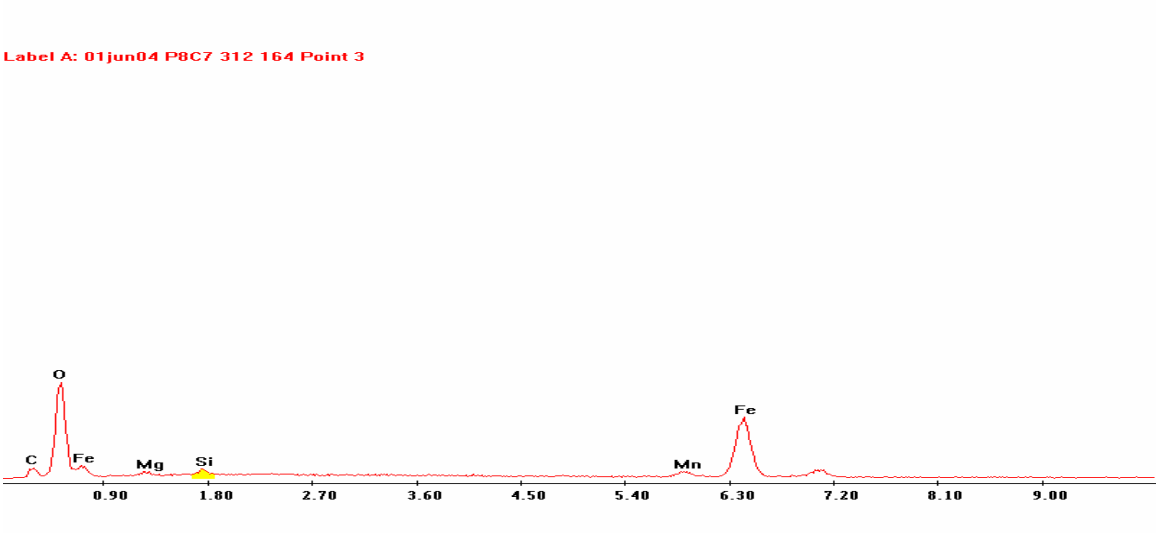

Point 4

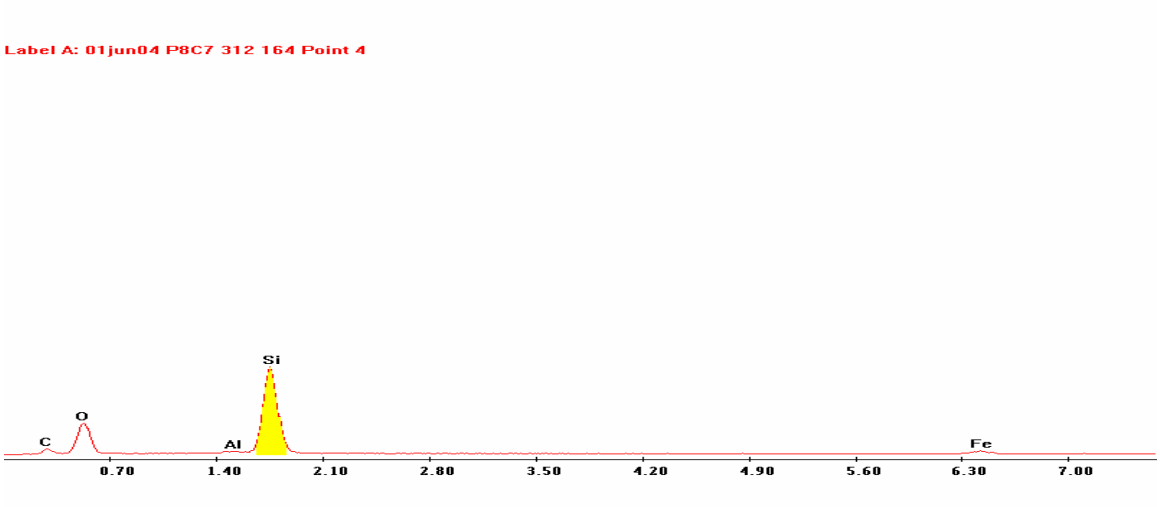

Point 5

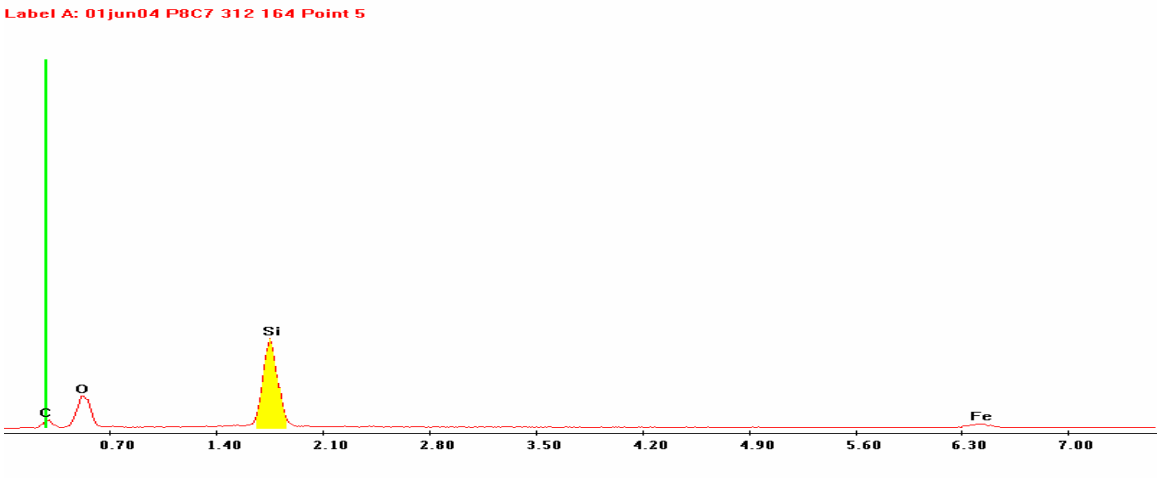

Point 6

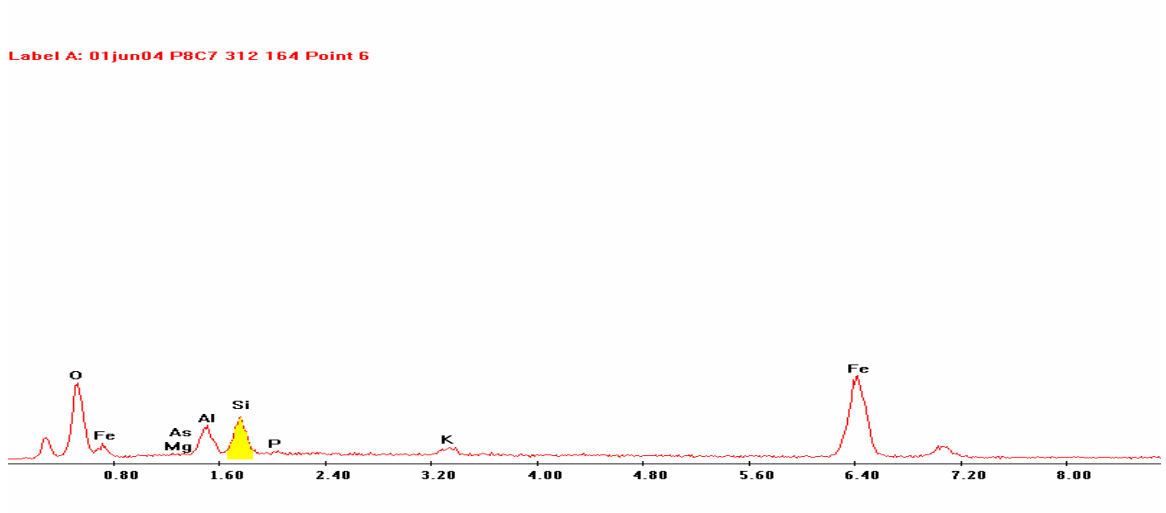

Point 7

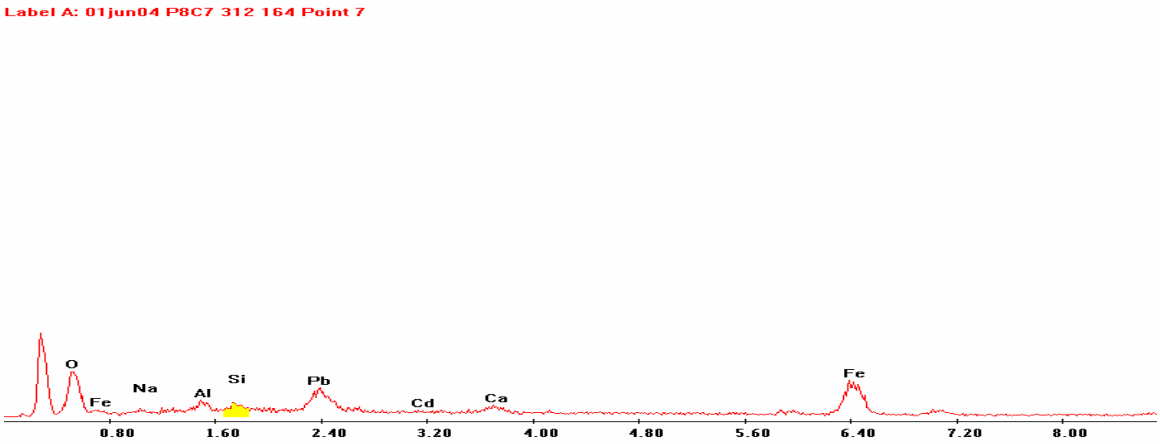

Point 8

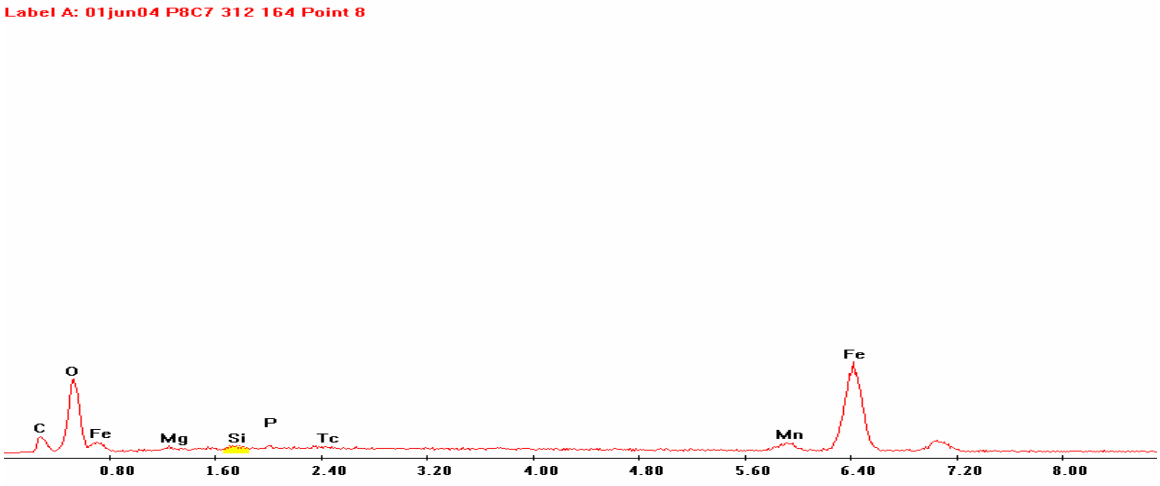

Point 9

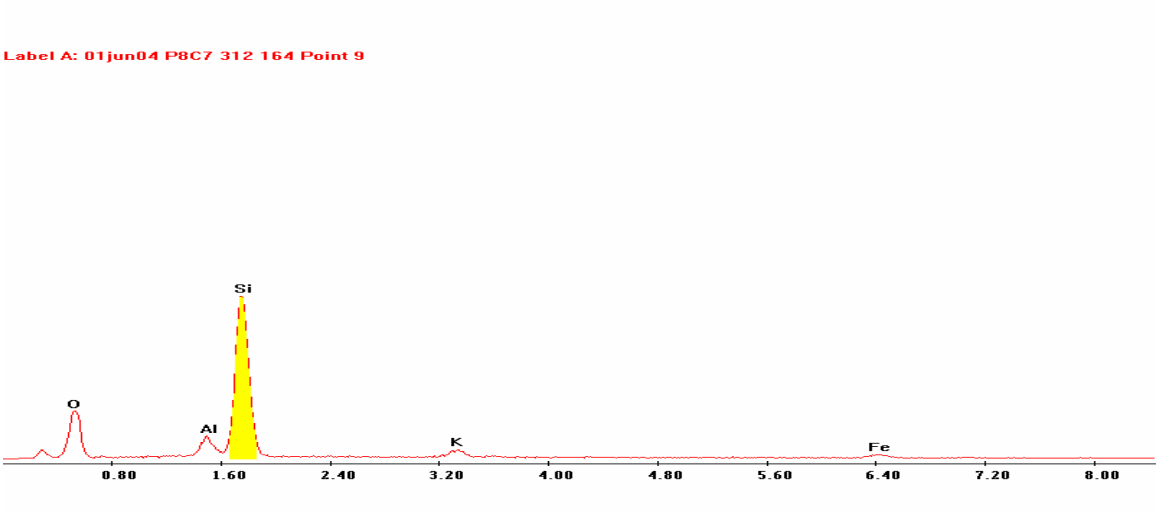

Point 10

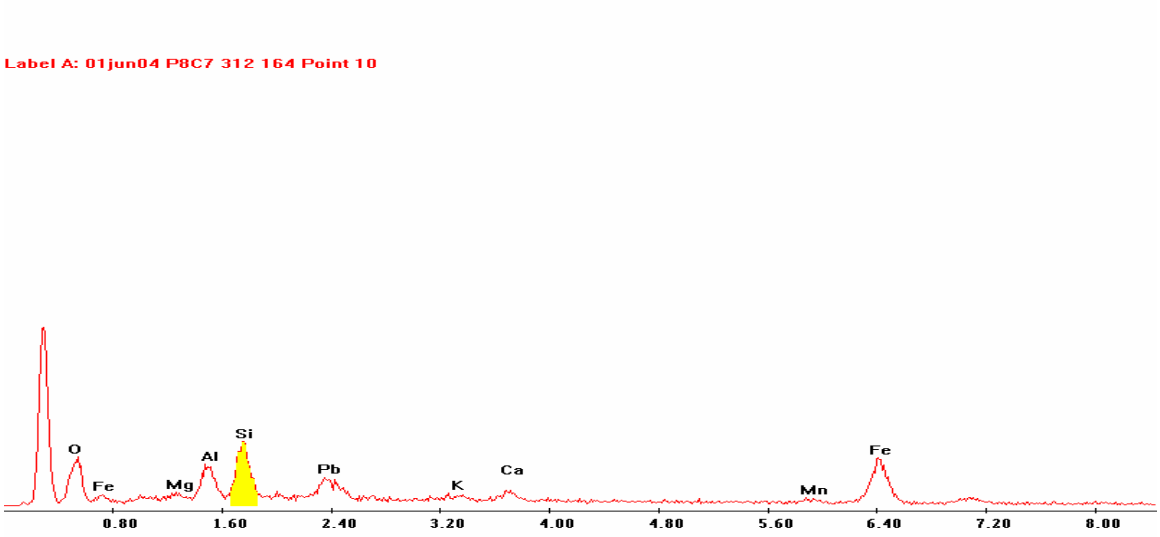

P8C7 – 325, 345

BSE Image

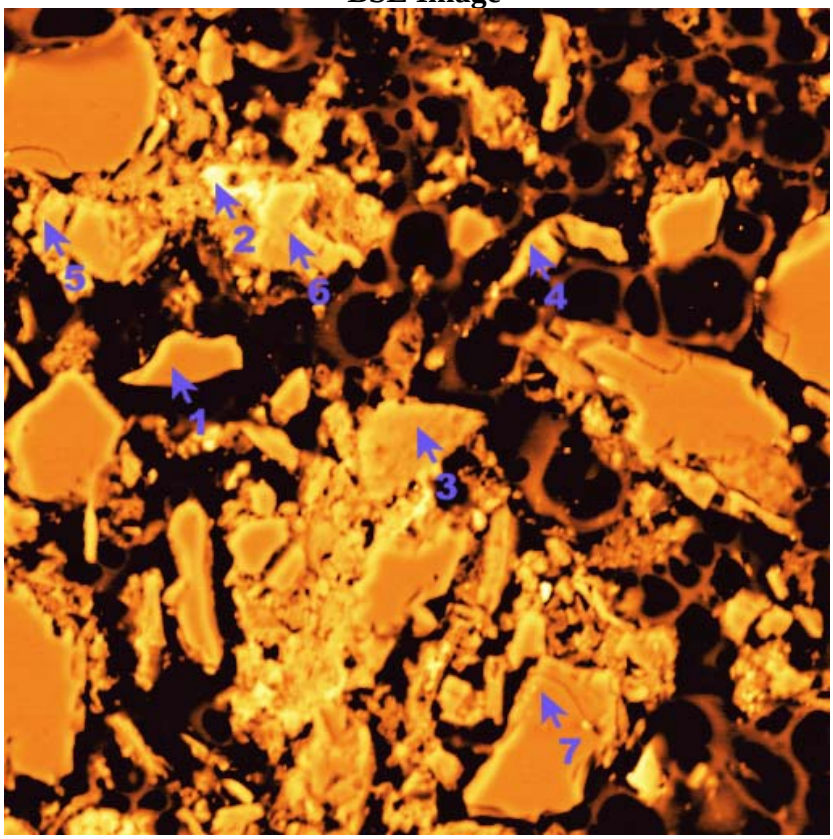

Iron (Fe)

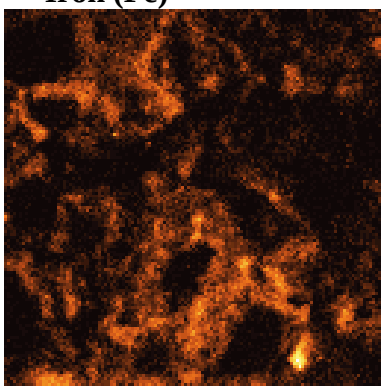

Manganese (Mn)

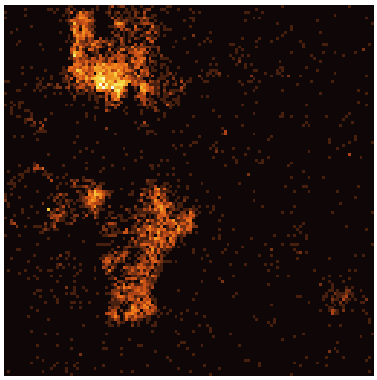

Phosphorous (P)

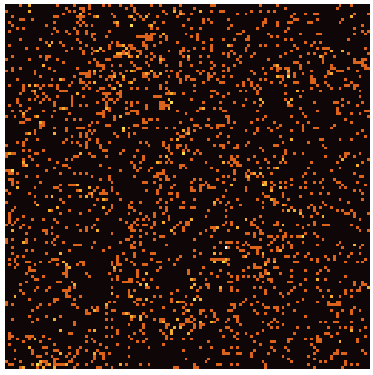

Lead (Pb)

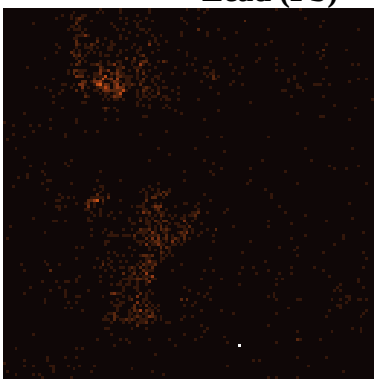

Silicon (Si)

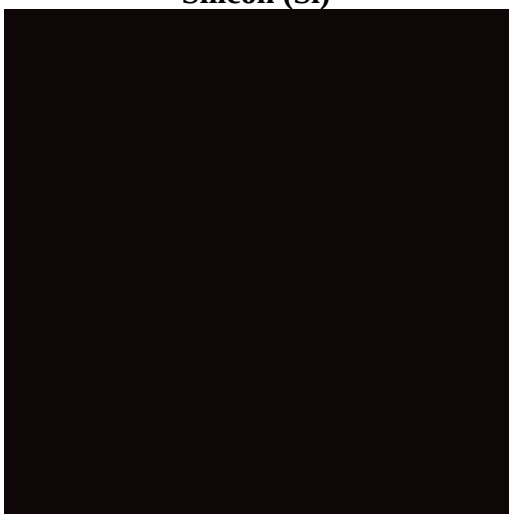

EDS Scan Images by Point

Point 1

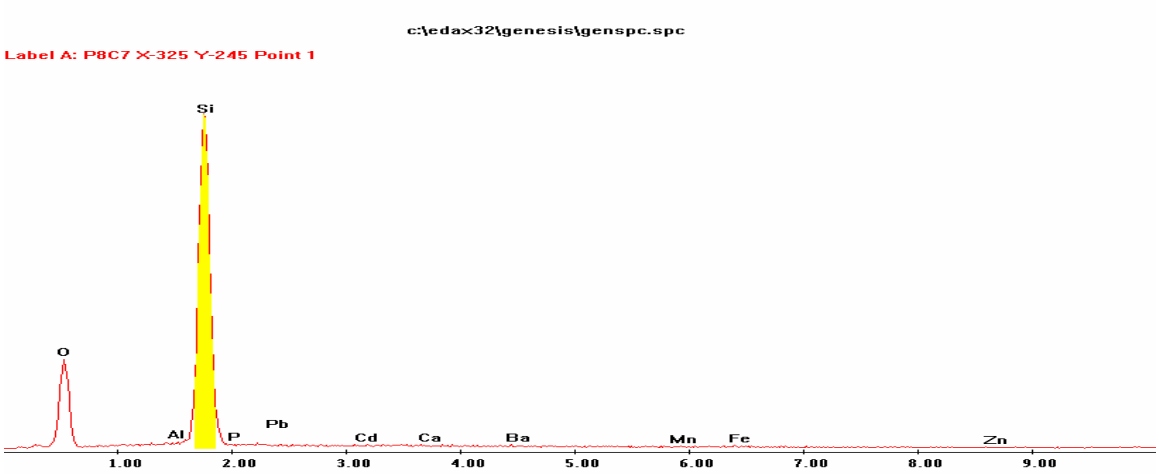

Point 2

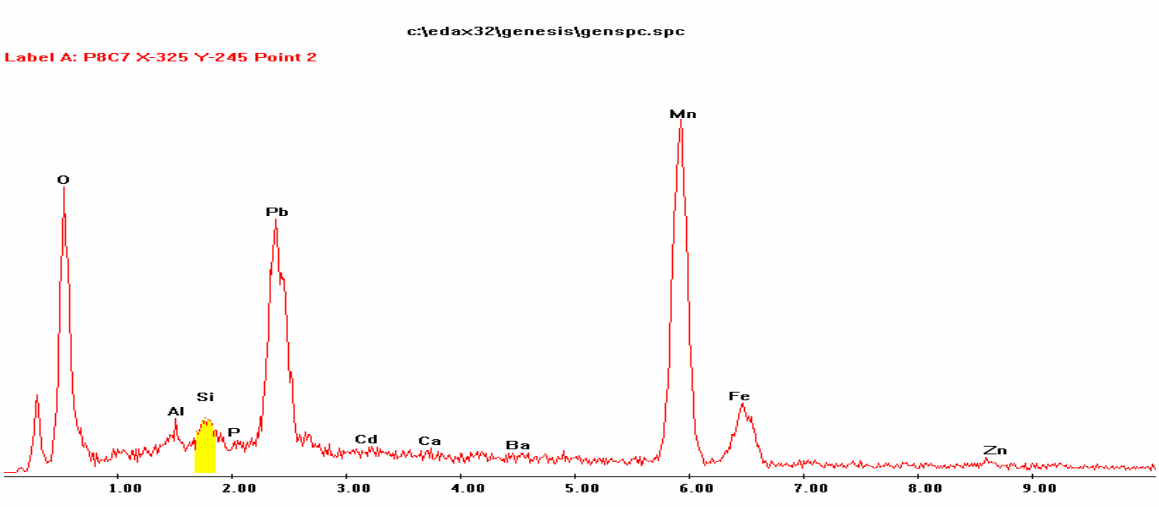

Point 3

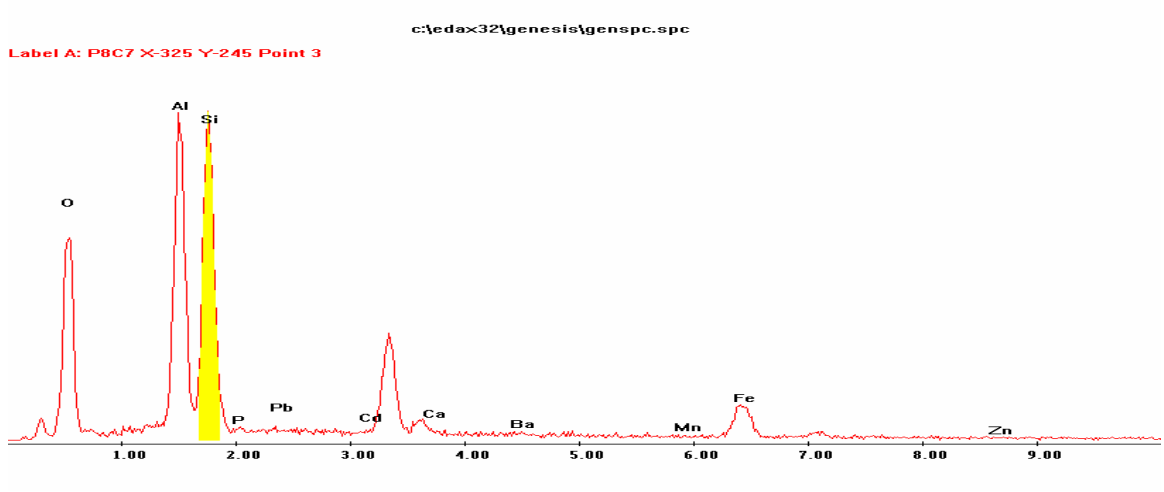

Point 4

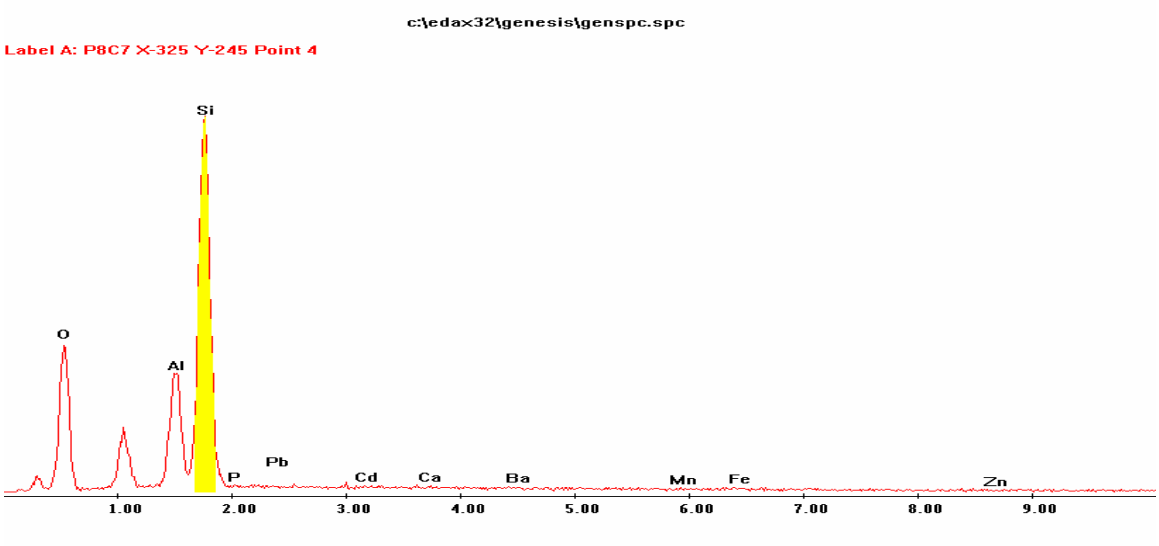

Point 5

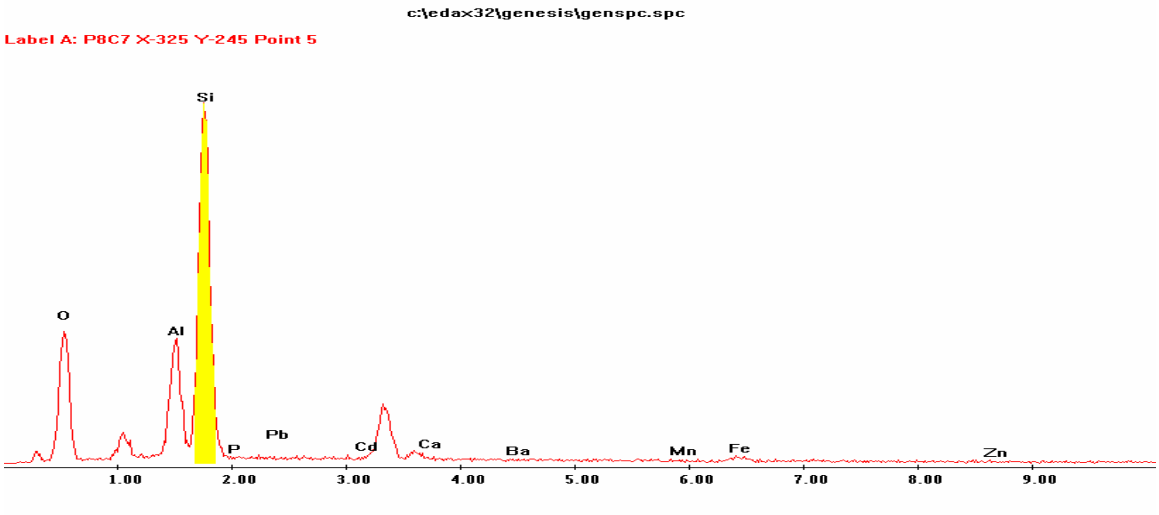

Point 6

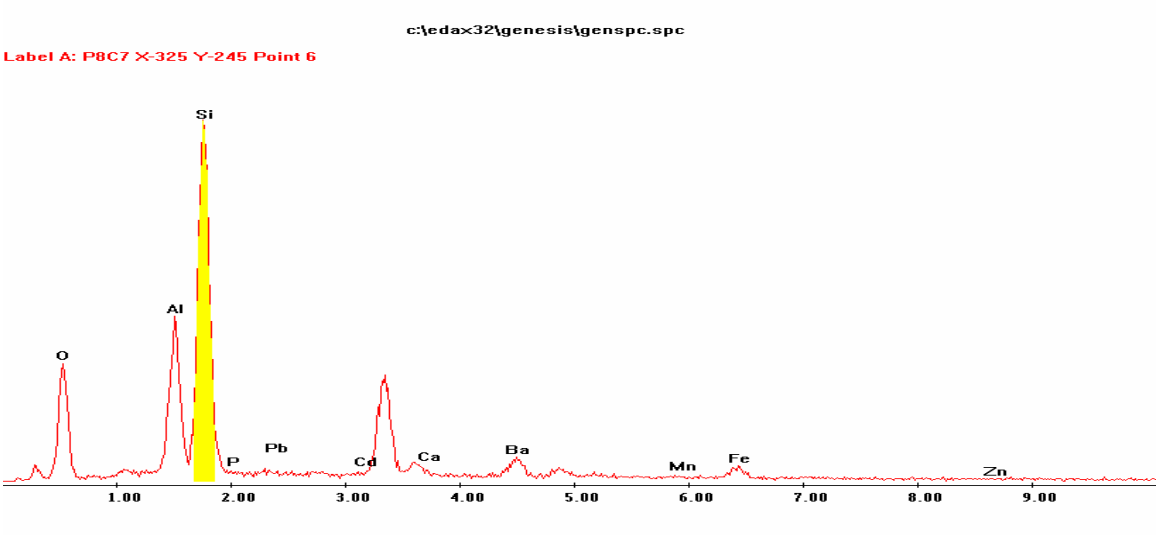

Point 7

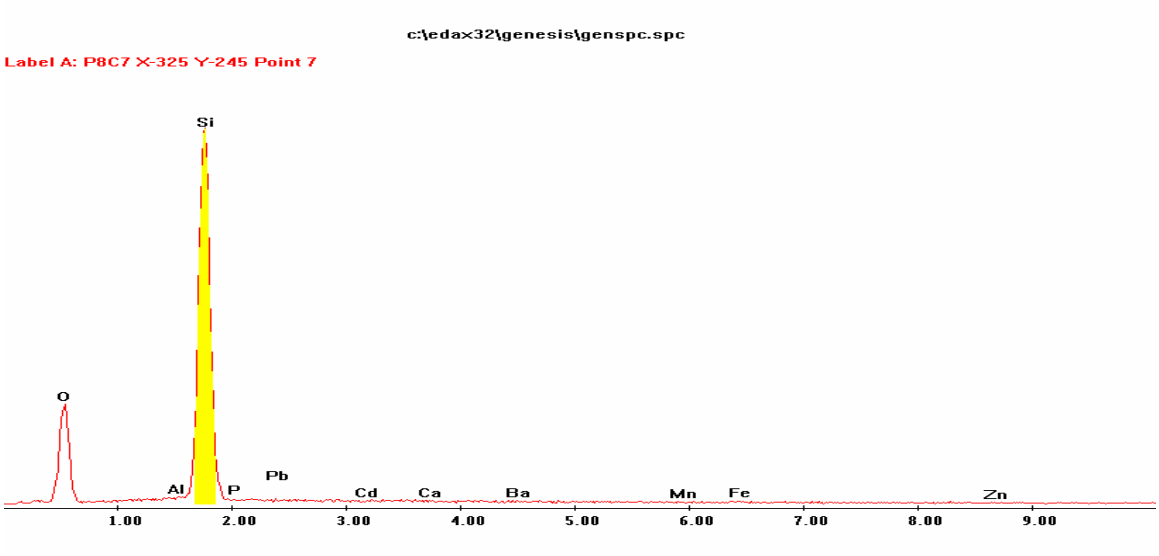

P8C7 – 380, 269

BSE Image

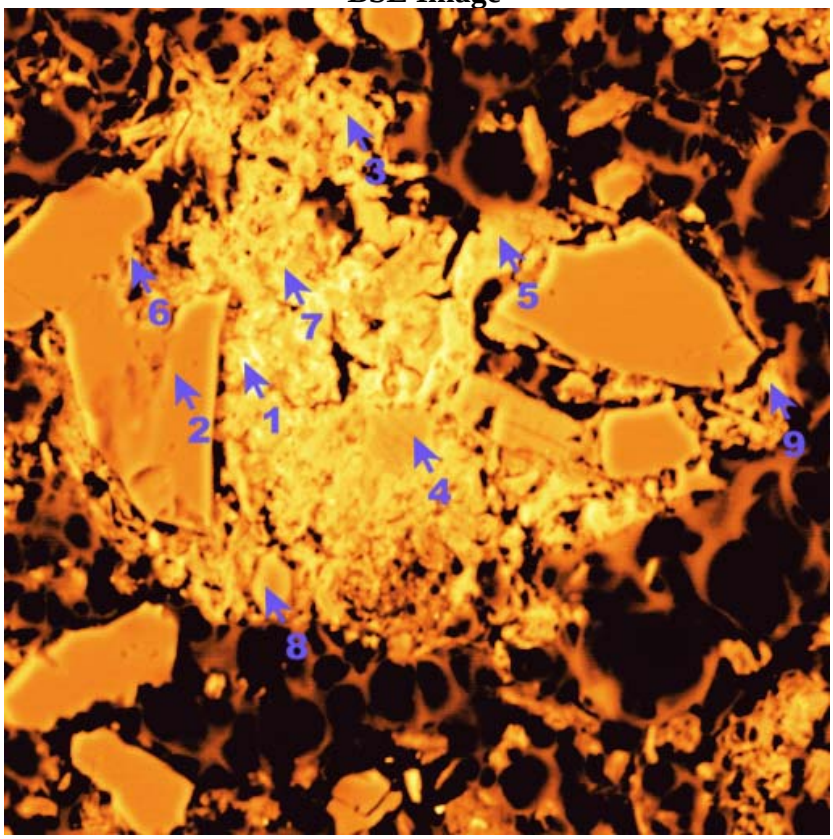

Iron (Fe)

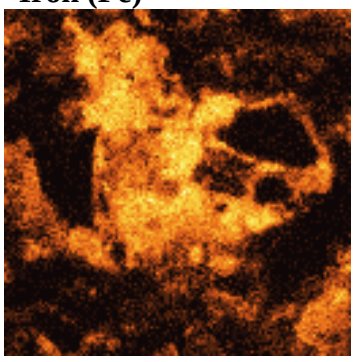

Manganese (Mn)

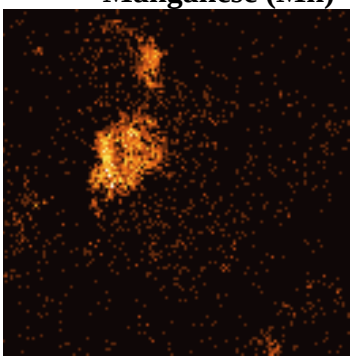

Phosphorous (P)

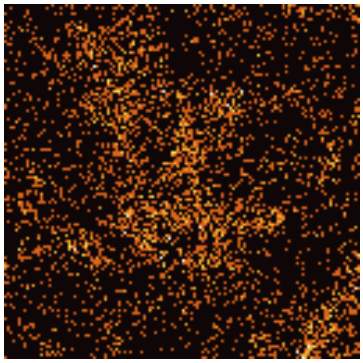

Lead (Pb)

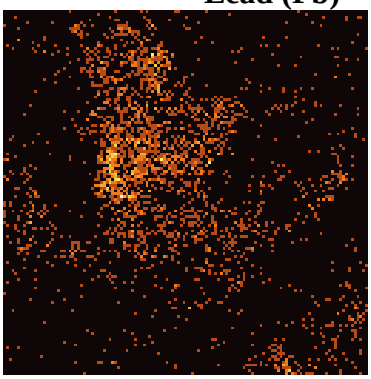

Silicon (Si)

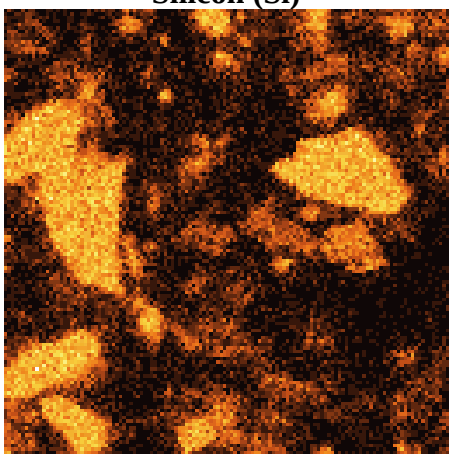

EDS Scan Images by Point

Point 1

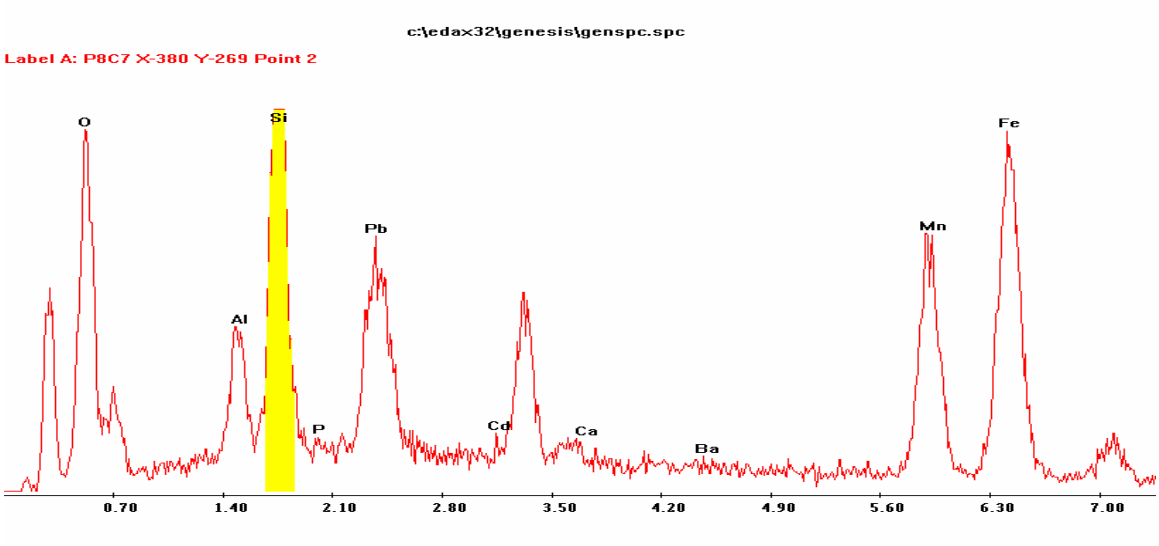

Point 2

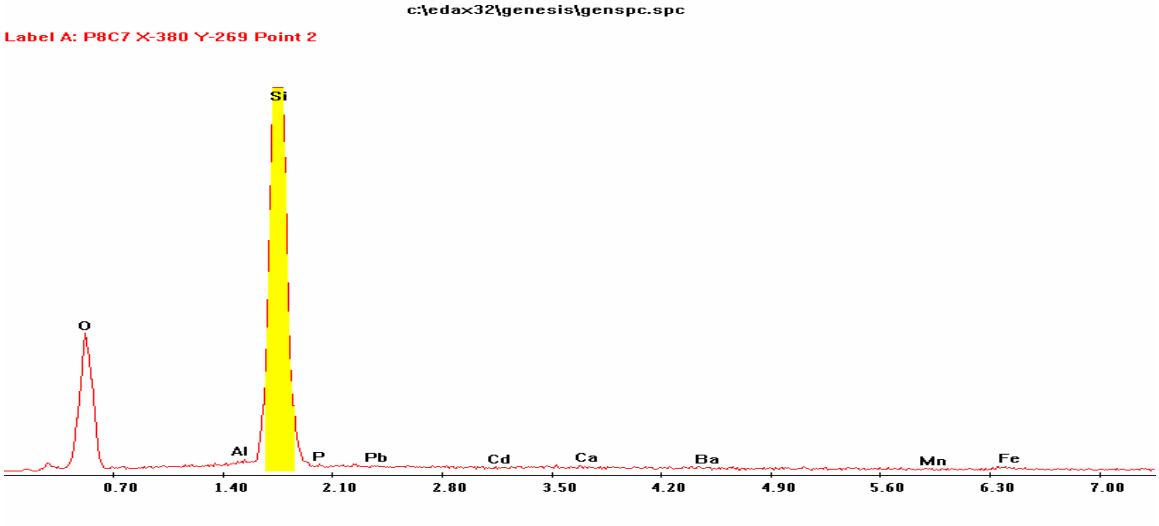

Point 3

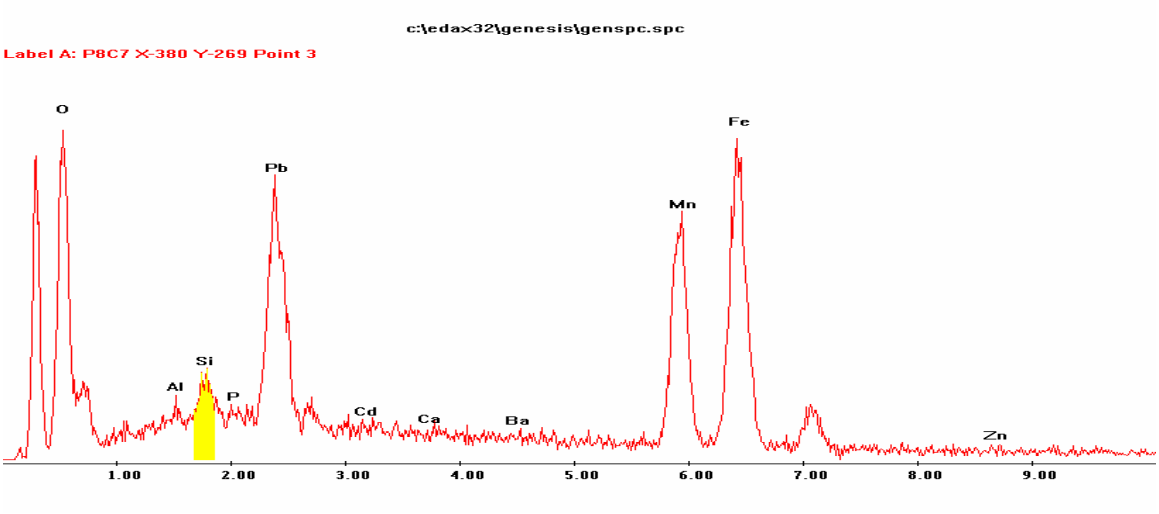

Point 4

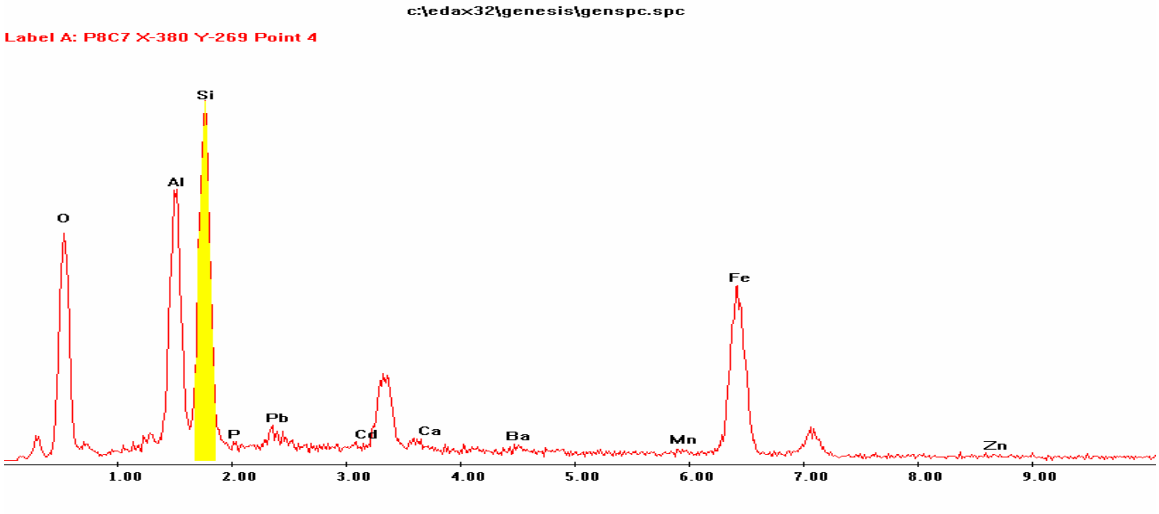

Point 5

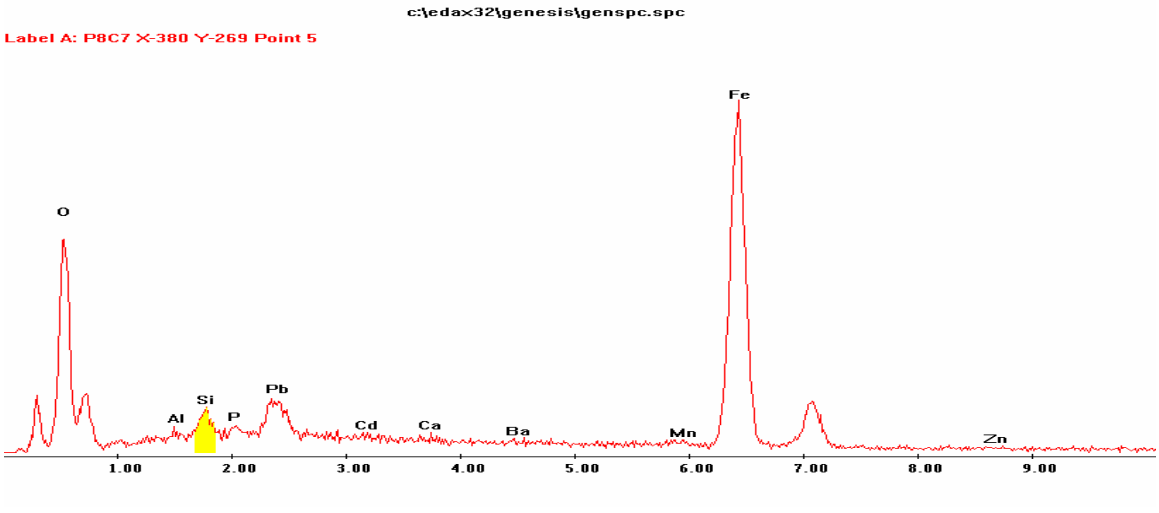

Point 6

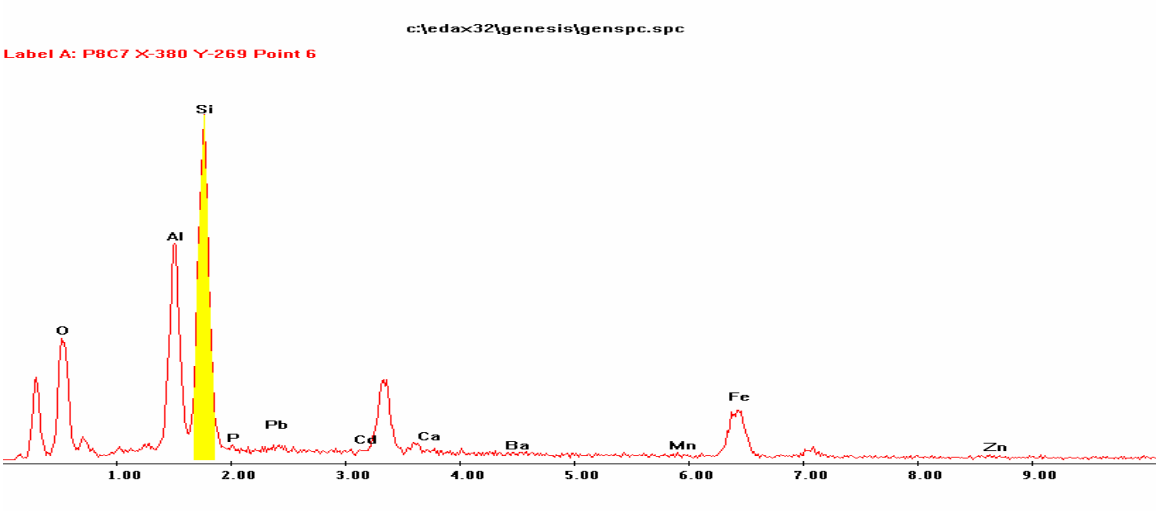

Point 7

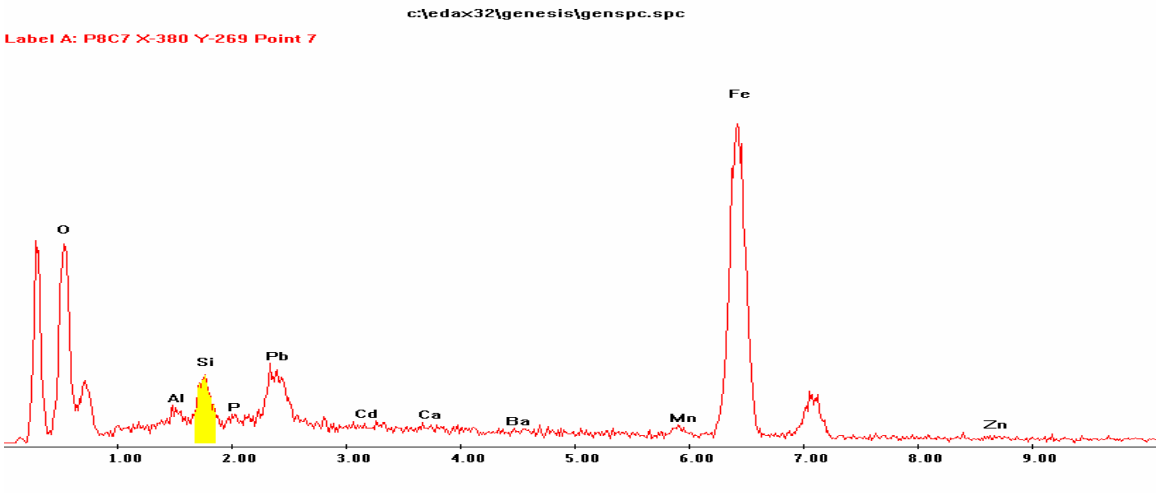

Point 8

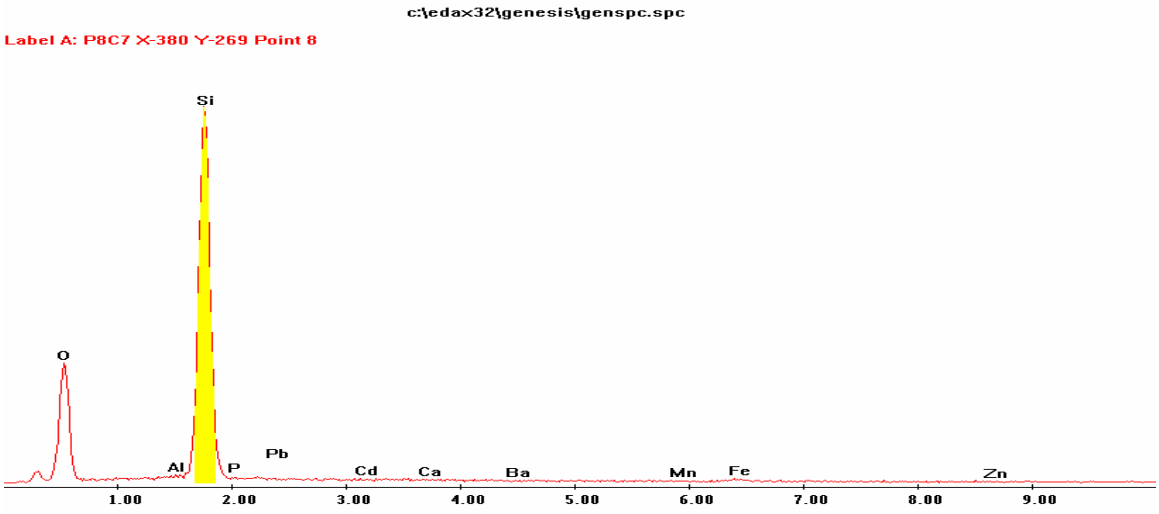

Point 9

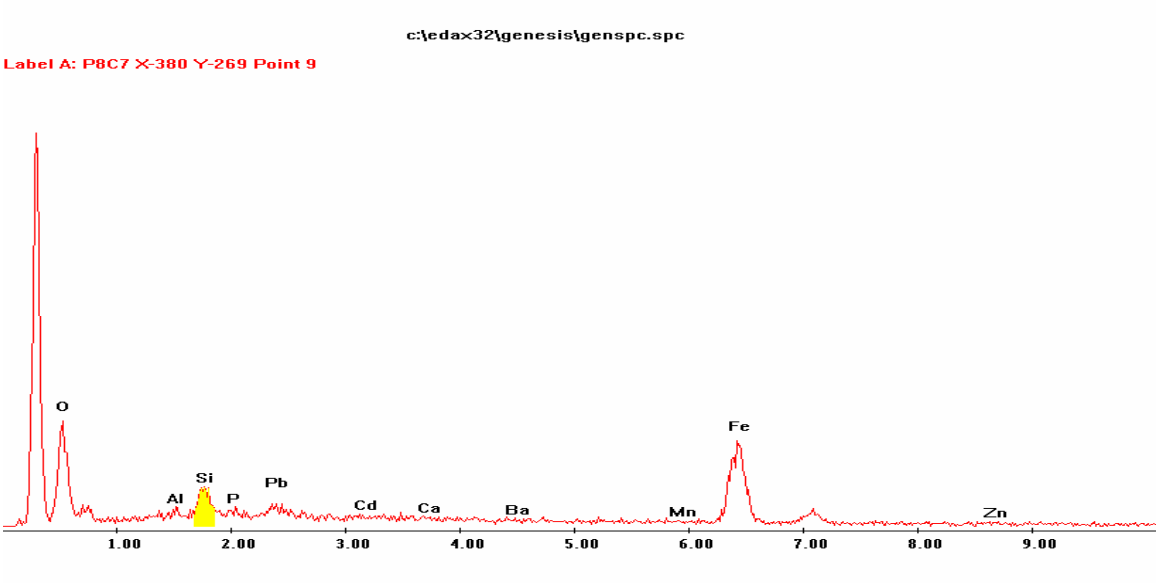
c:\edax32\genesis\genspc.spc
Label A: P8C7 X-380 Y-269 Point 9
O
Al
Si
P
Pb
Cd
Ca
Ba
Mn
Fe
Zn
1.00
2.00
3.00
4.00
5.00
6.00
7.00
8.00
9.00

P8C7 – 398, 323

BSE Image

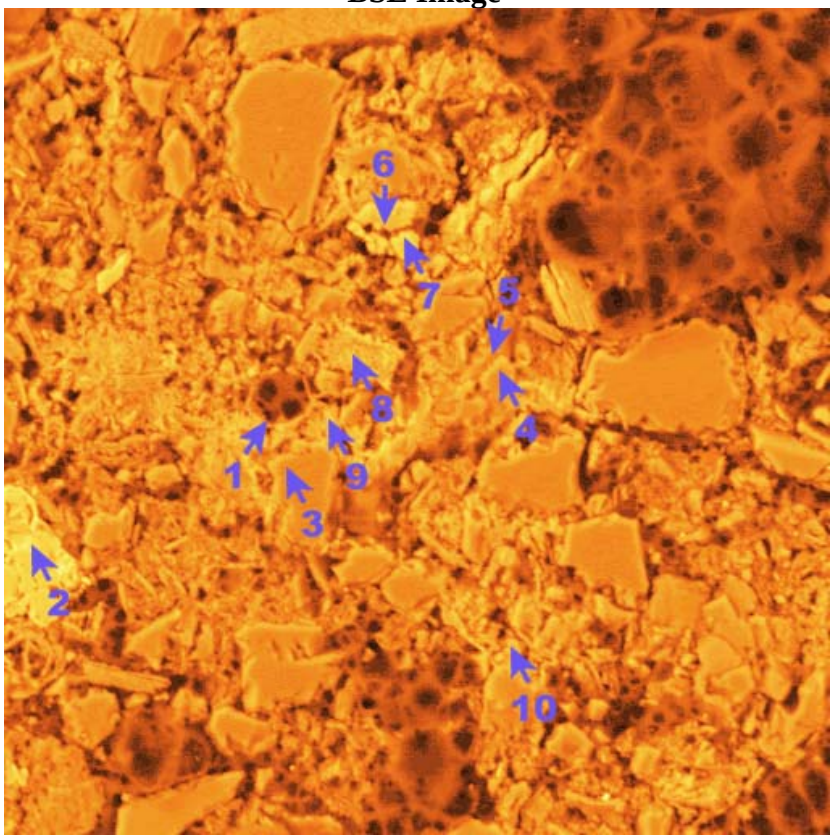

Iron (Fe)

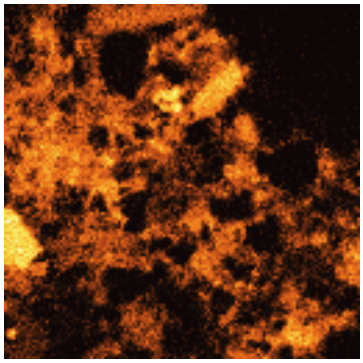

Manganese (Mn)

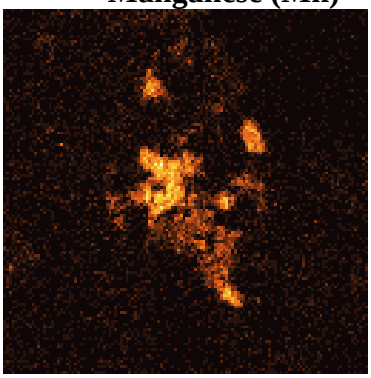

Phosphorous (P)

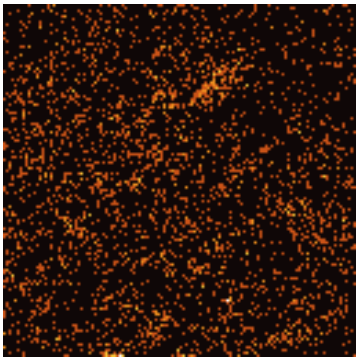

Lead (Pb)

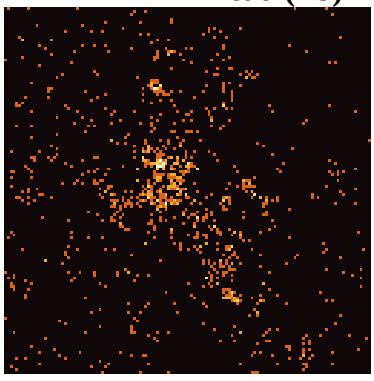

Silicon (Si)

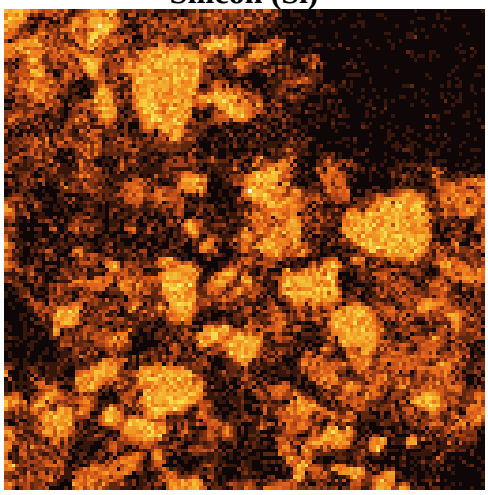

EDS Scan Images by Point

Point 1

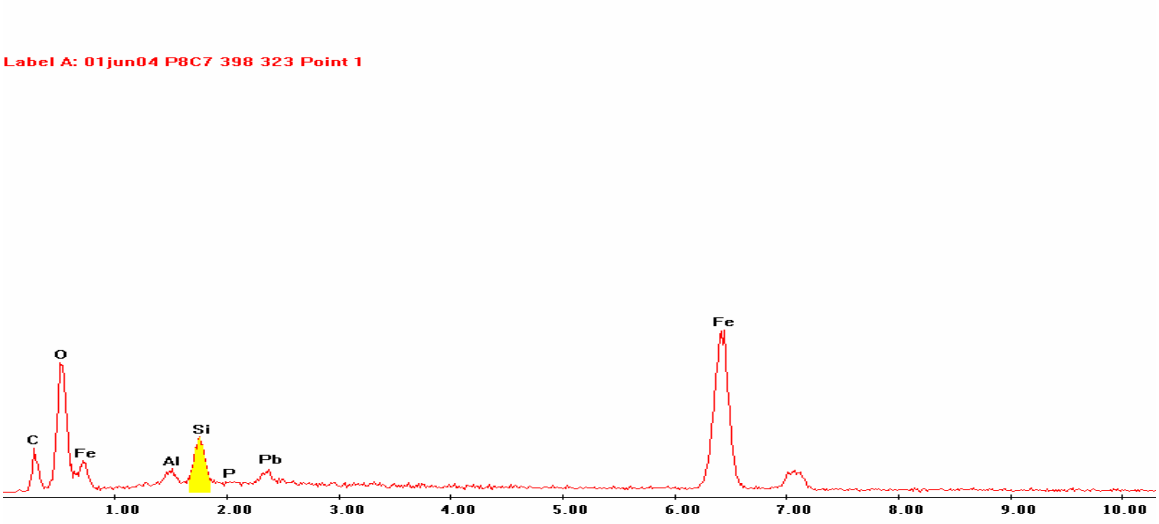

Point 2

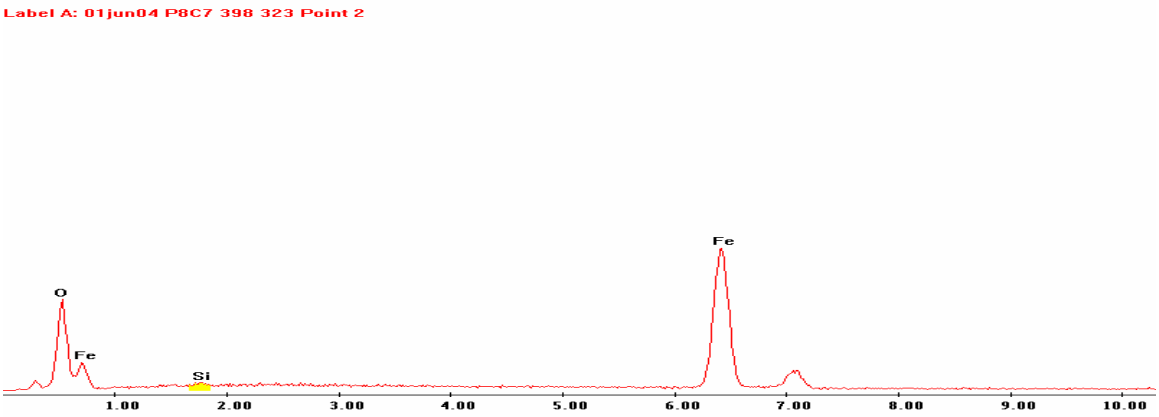

Point 3

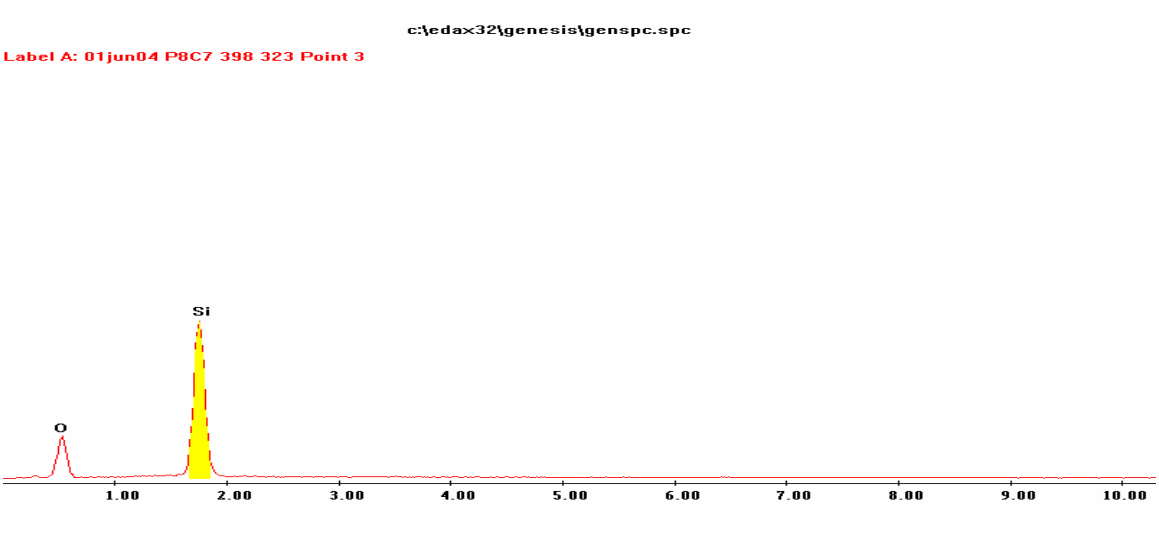

Point 4

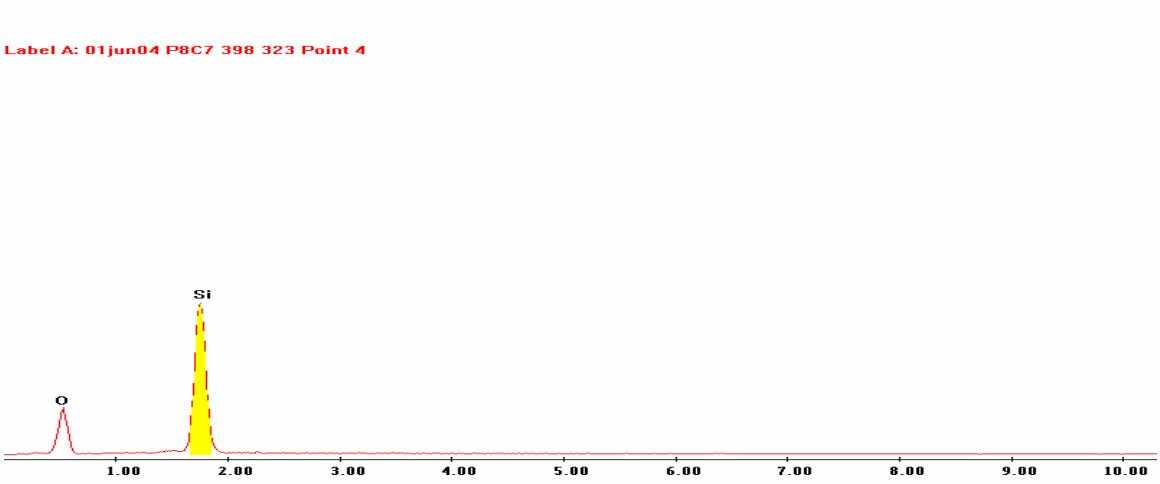

Point 5

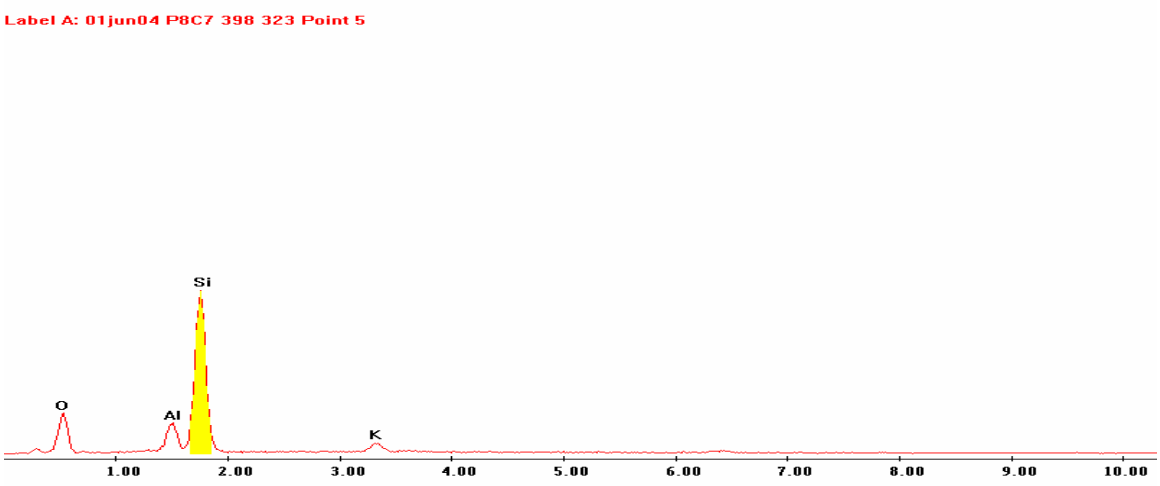

Point 6

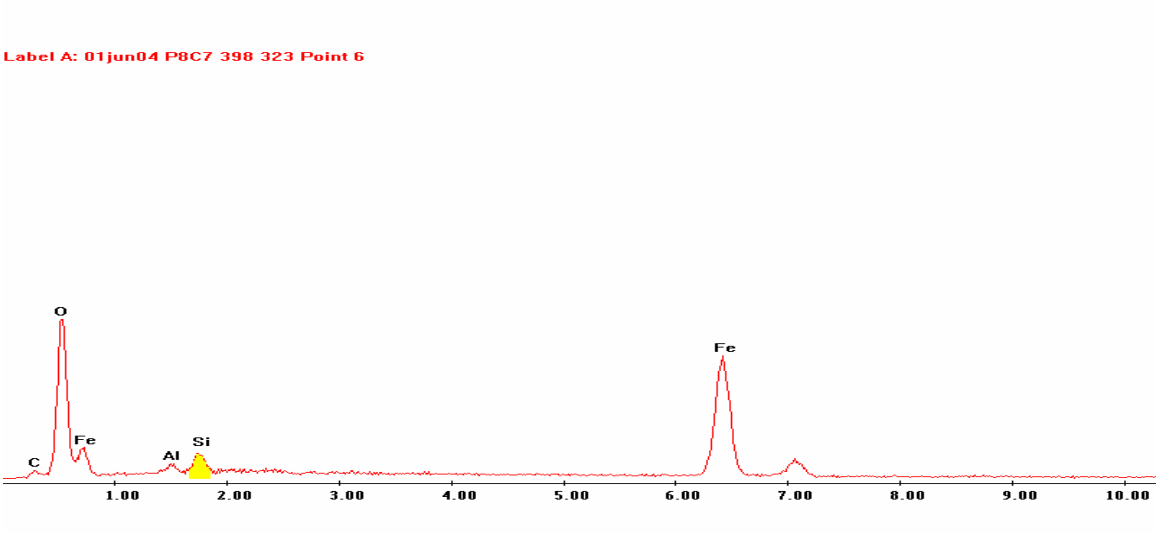

Point 7

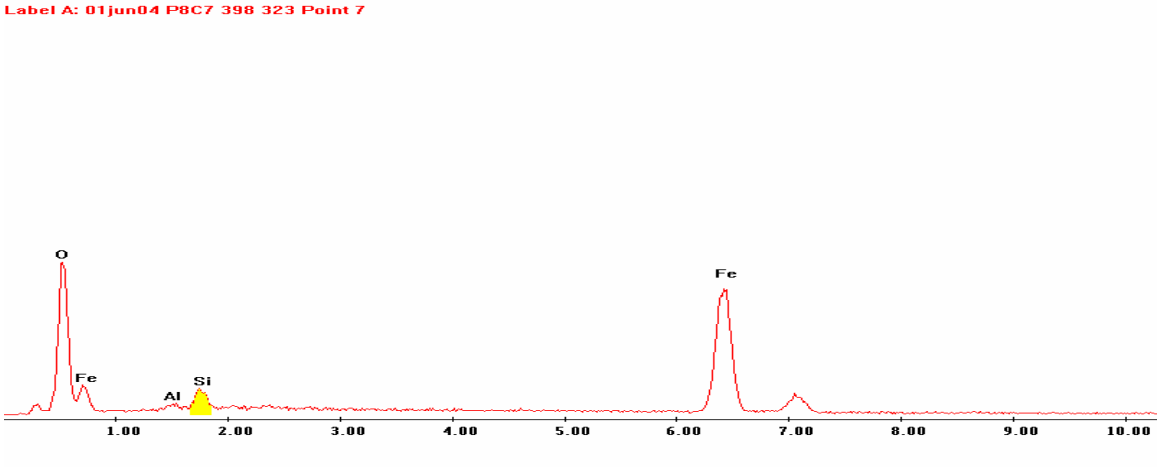

Point 8

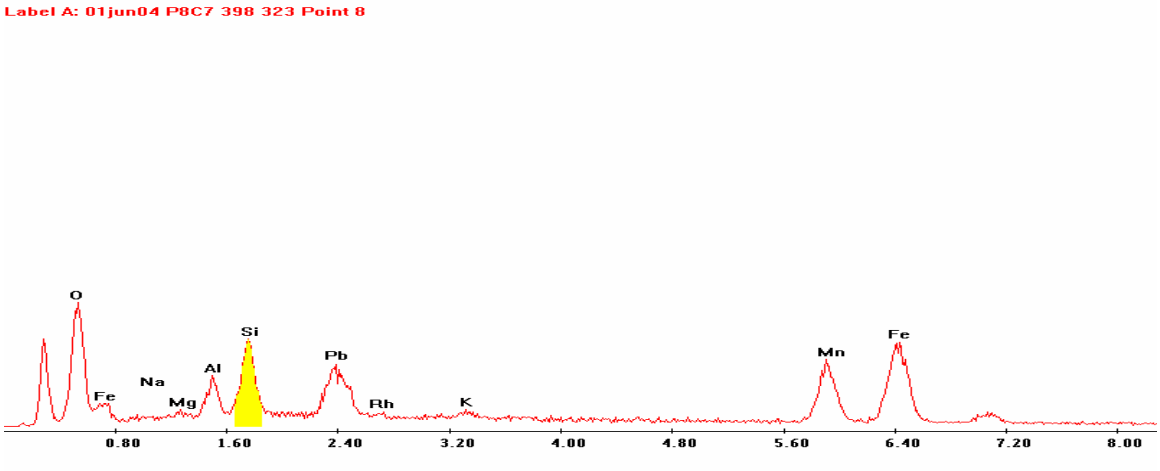

Point 9

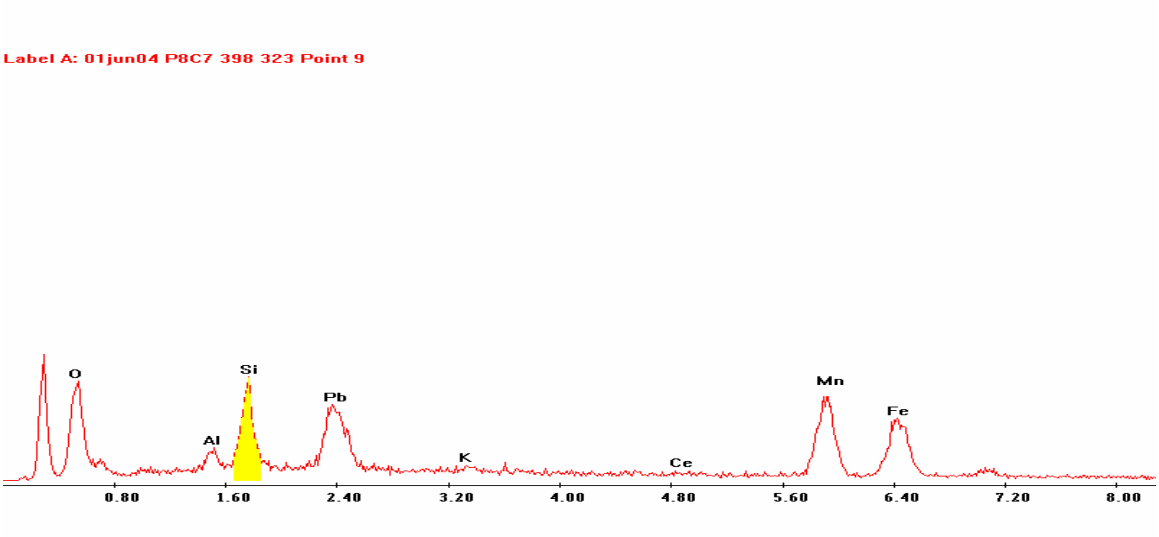

Point 10

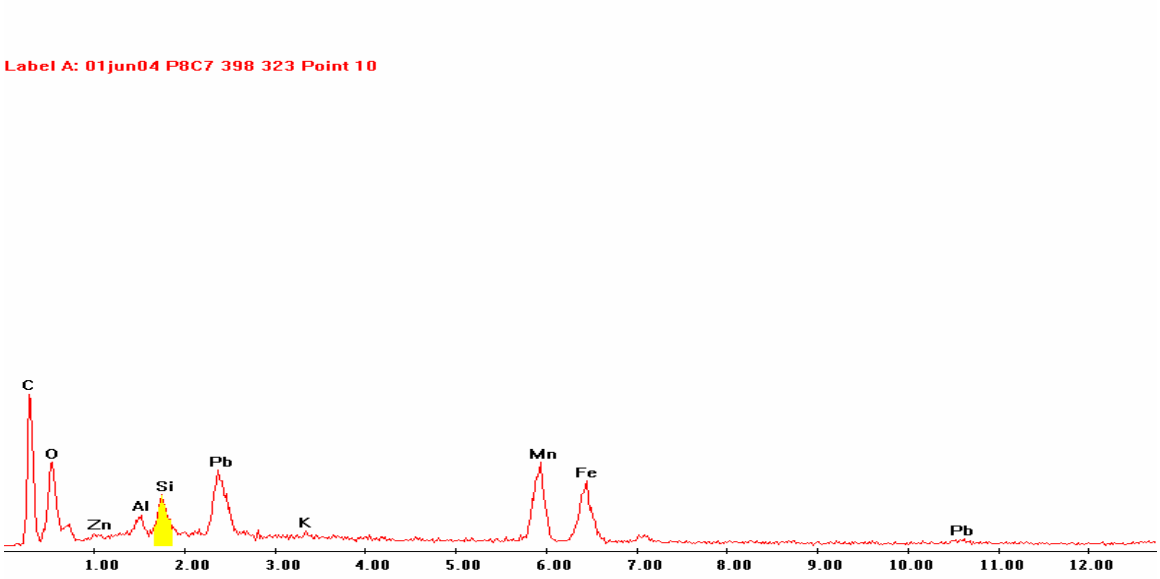

P8C7 – 456, 196

BSE Image

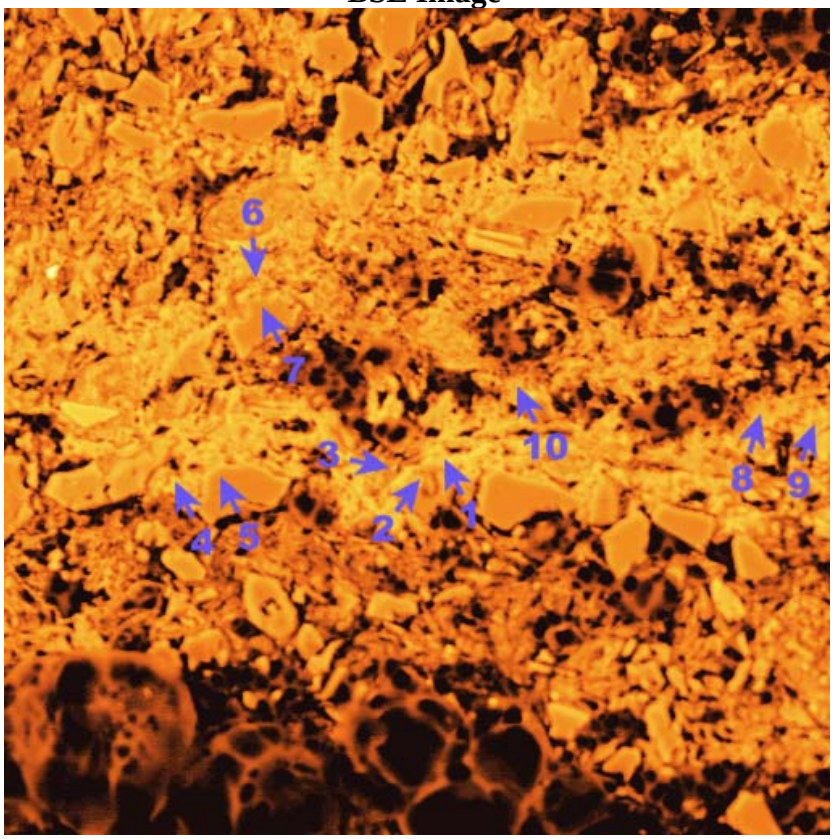

Iron (Fe)

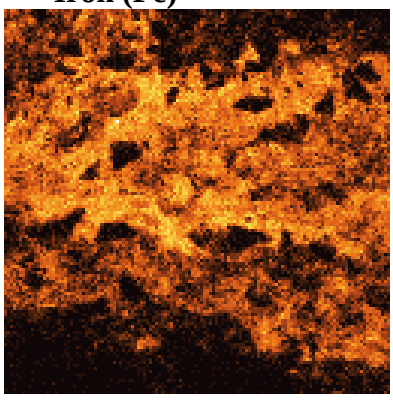

Manganese (Mn)

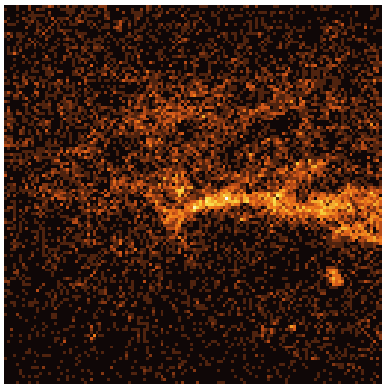

Phosphorous (P)

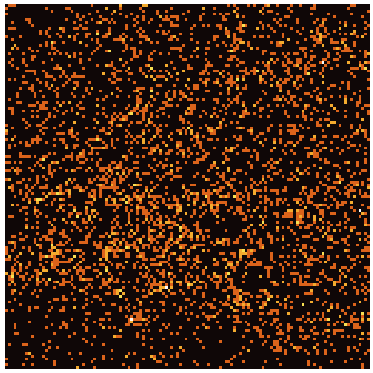

Lead (Pb)

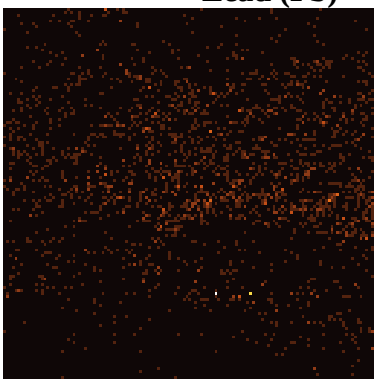

Silicon (Si)

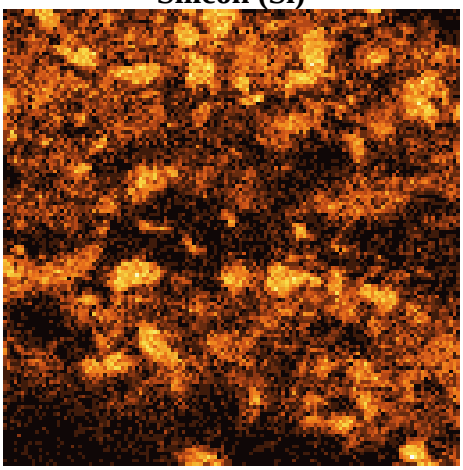

EDS Scan Images by Point

Point 1

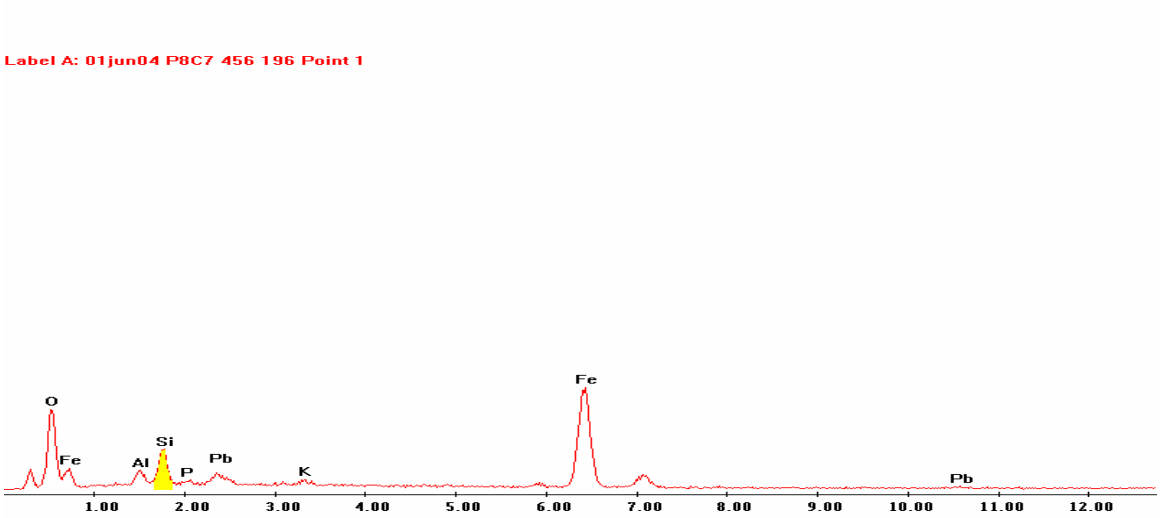

Point 2

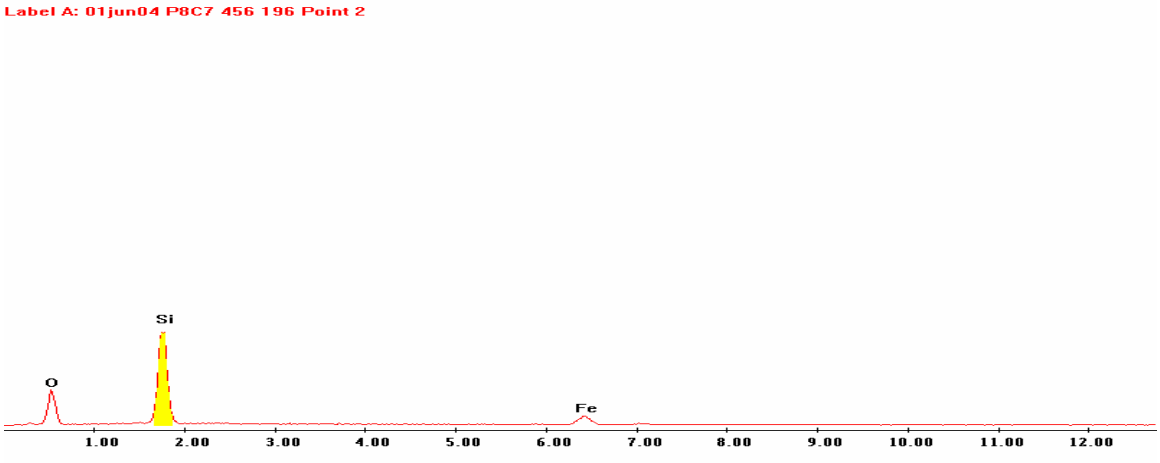

Point 3

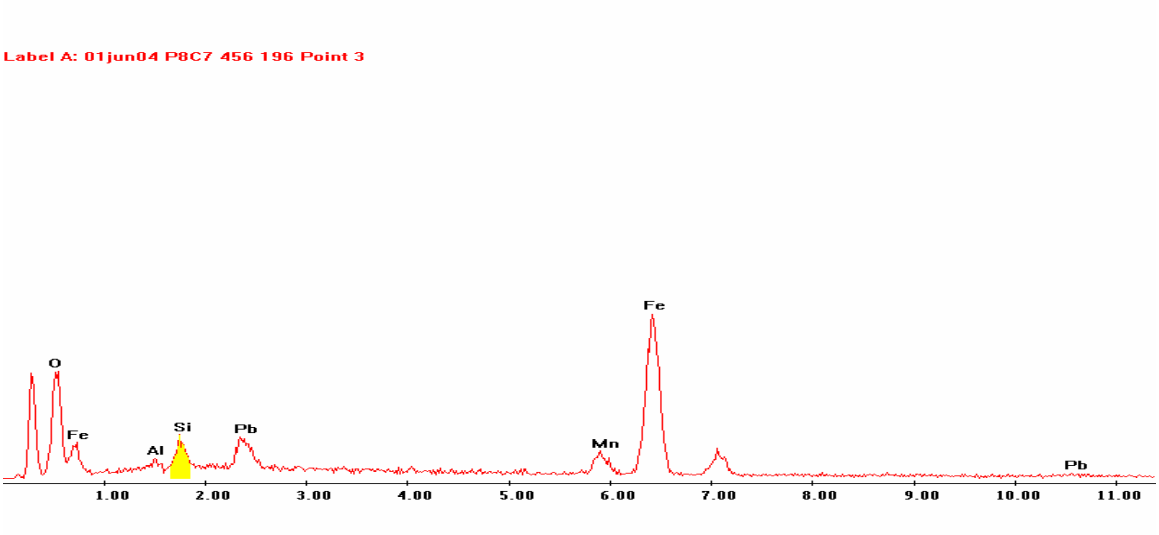

Point 4

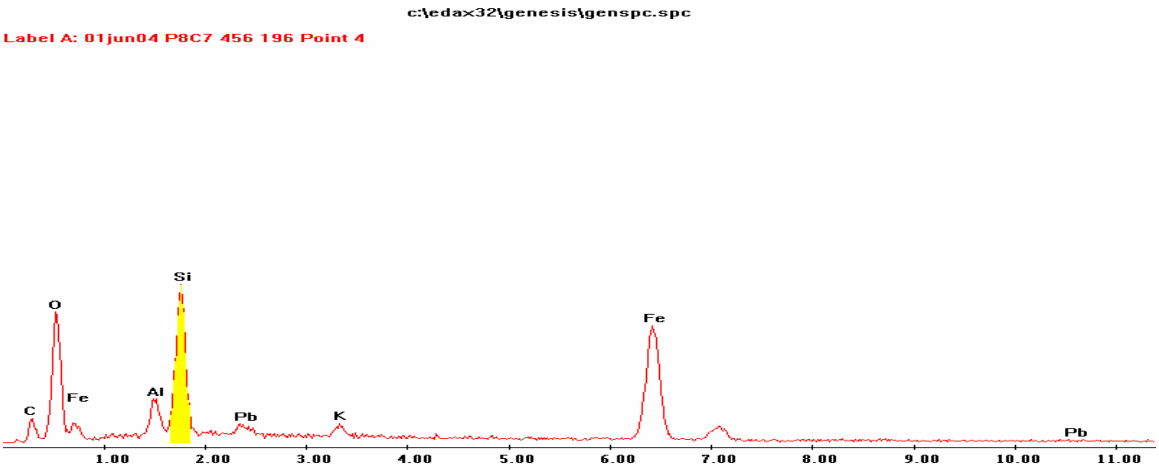

Point 5

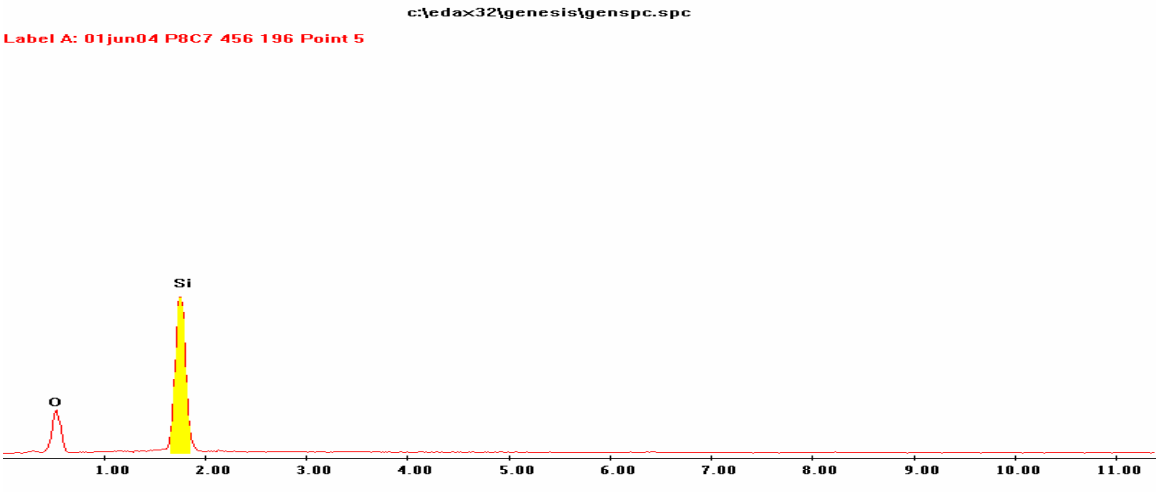

Point 6

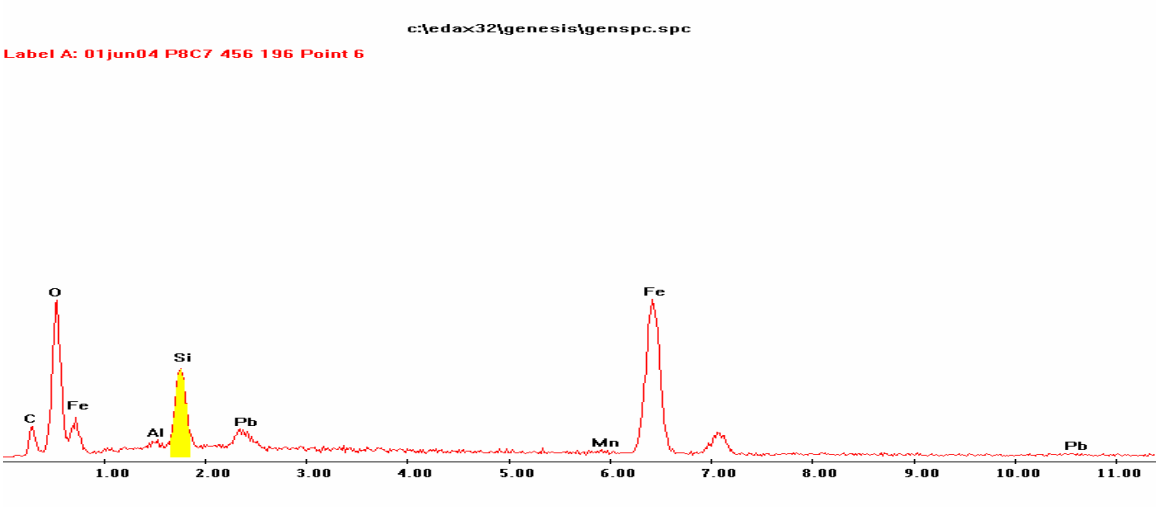

Point 7

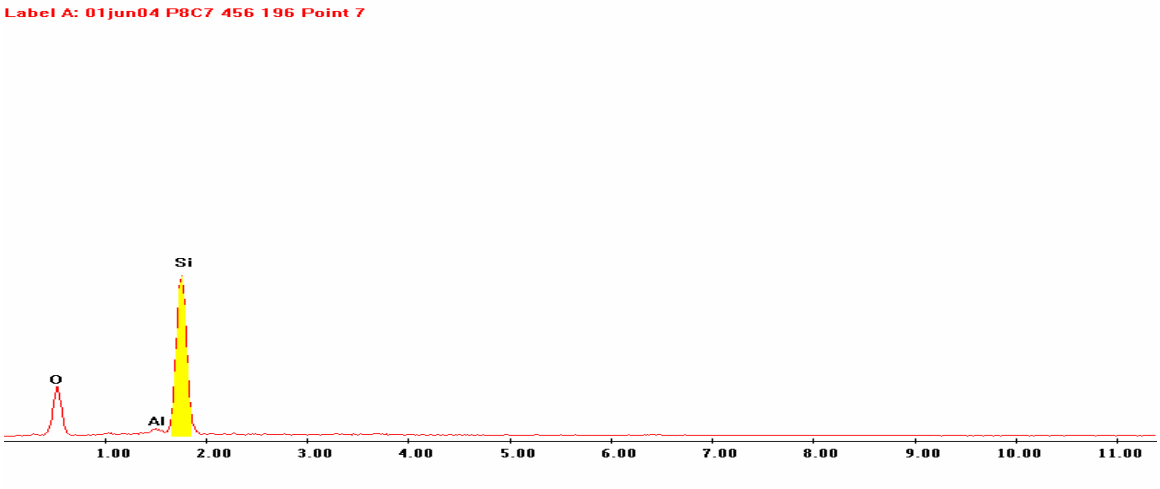

Point 8

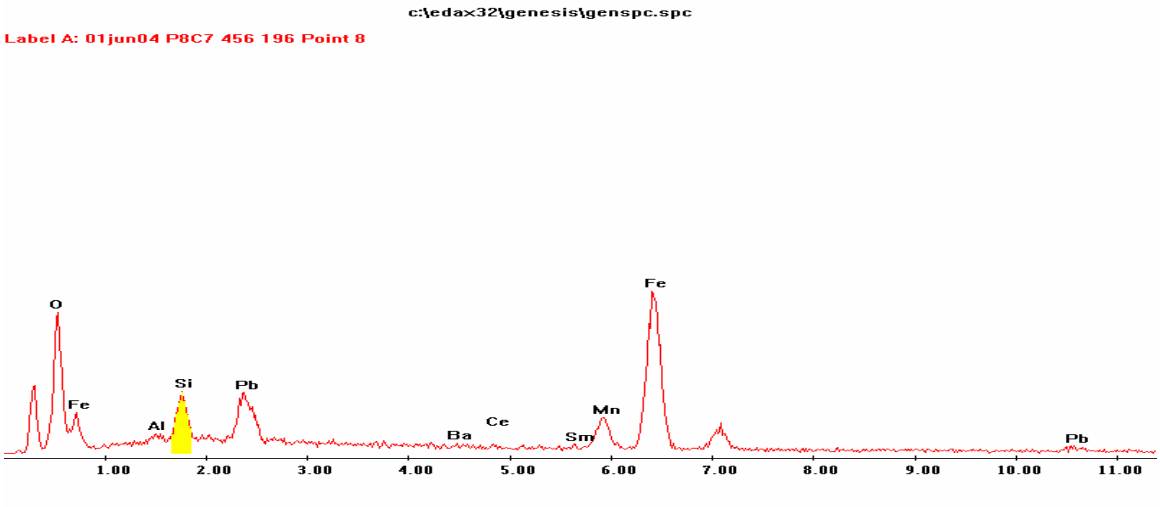

Point 9

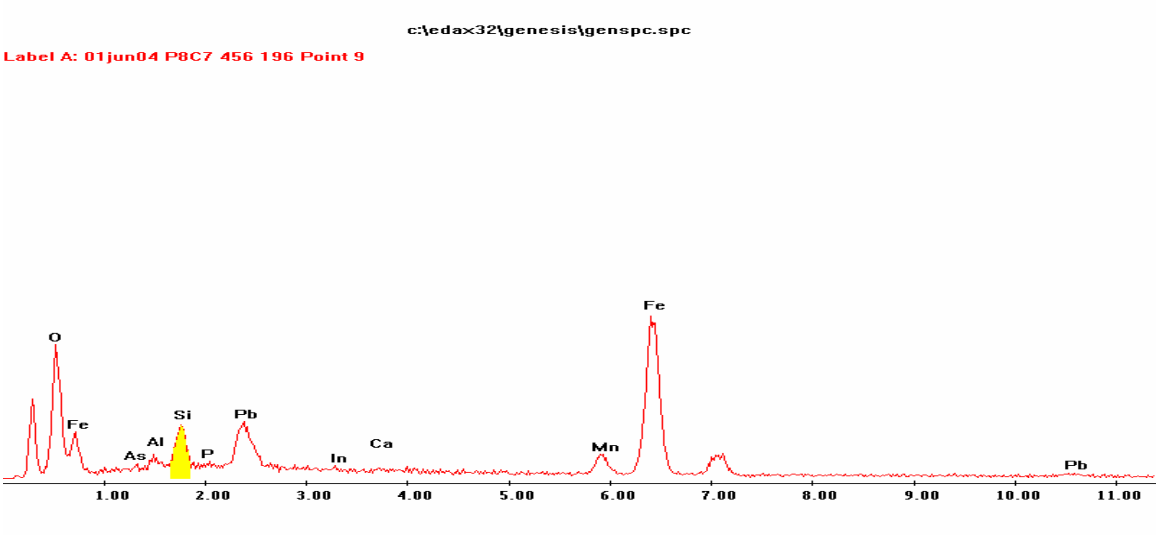

Point 10

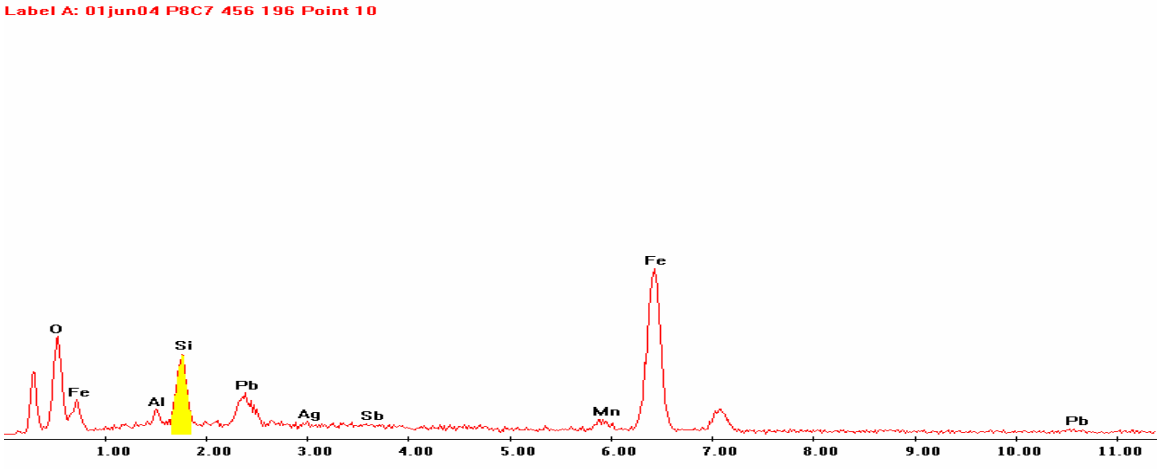

P8C7 – 490, 265

BSE Image

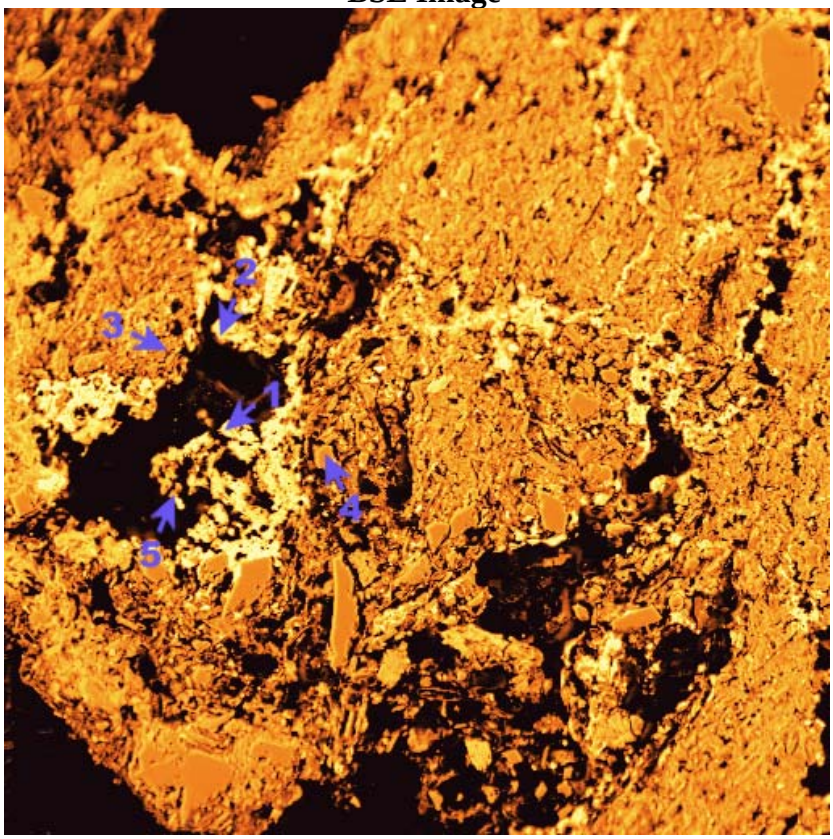

Iron (Fe)

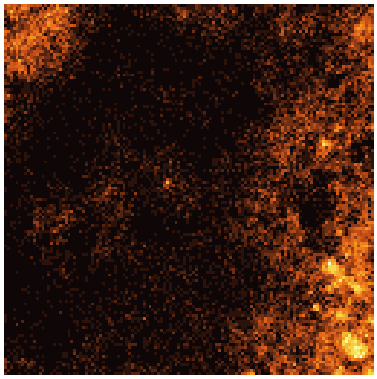

Manganese (Mn)

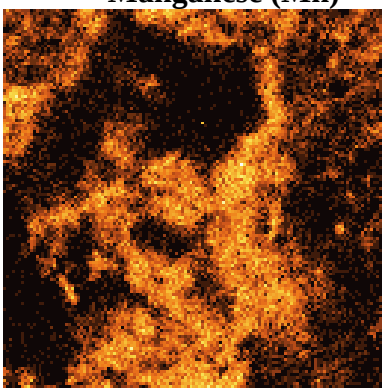

Phosphorous (P)

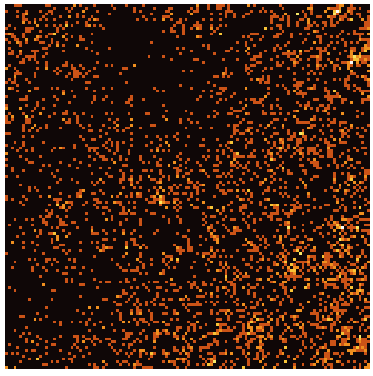

Lead (Pb)

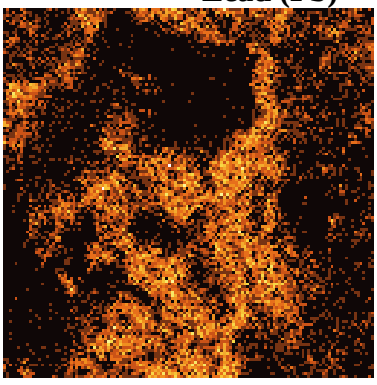

Silicon (Si)

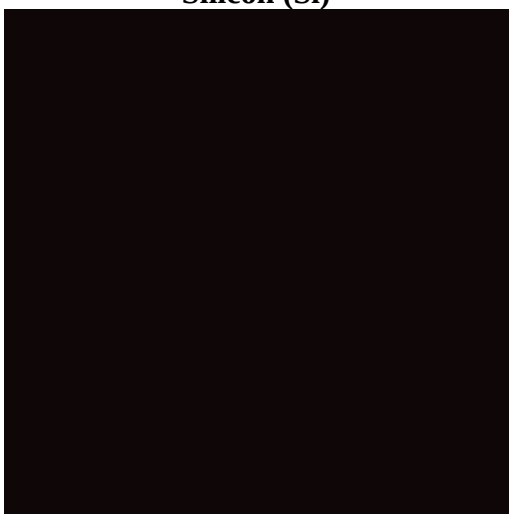

EDS Scan Images by Point

Point 1

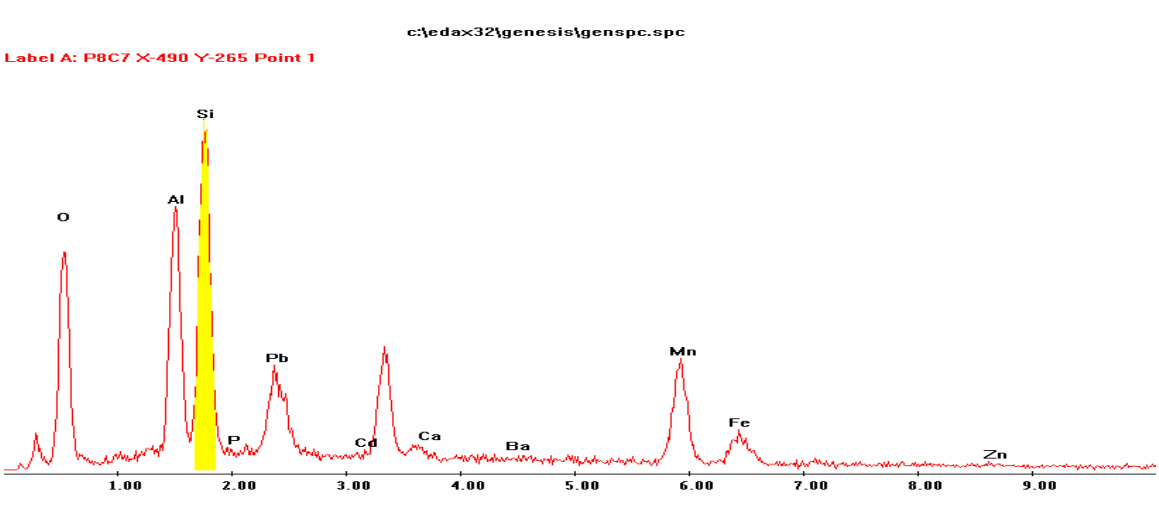

Point 2

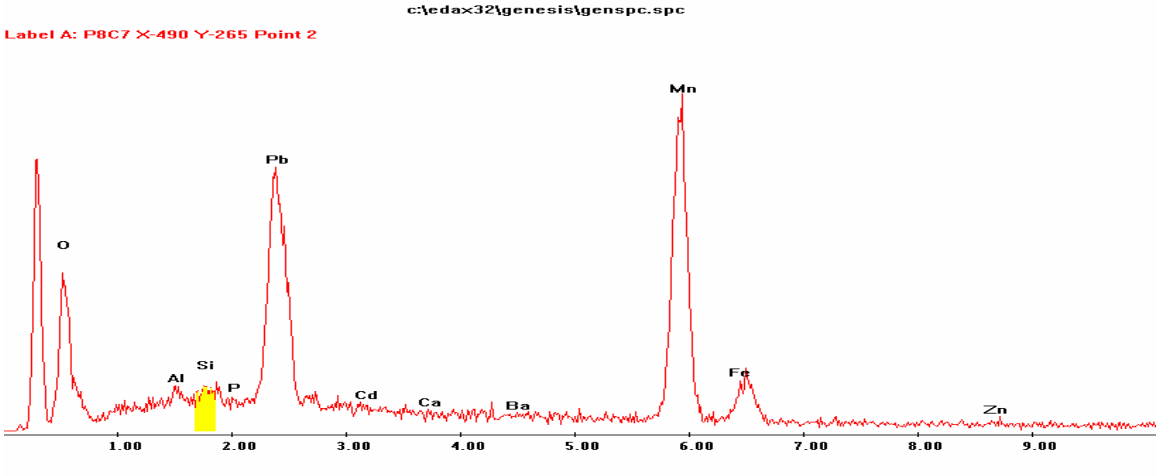

Point 3

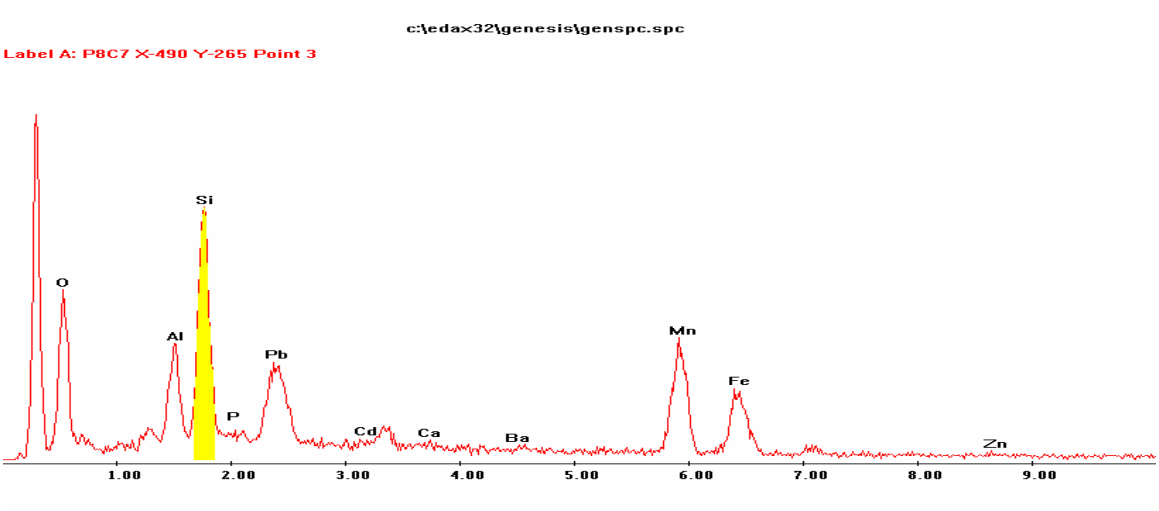

Point 4

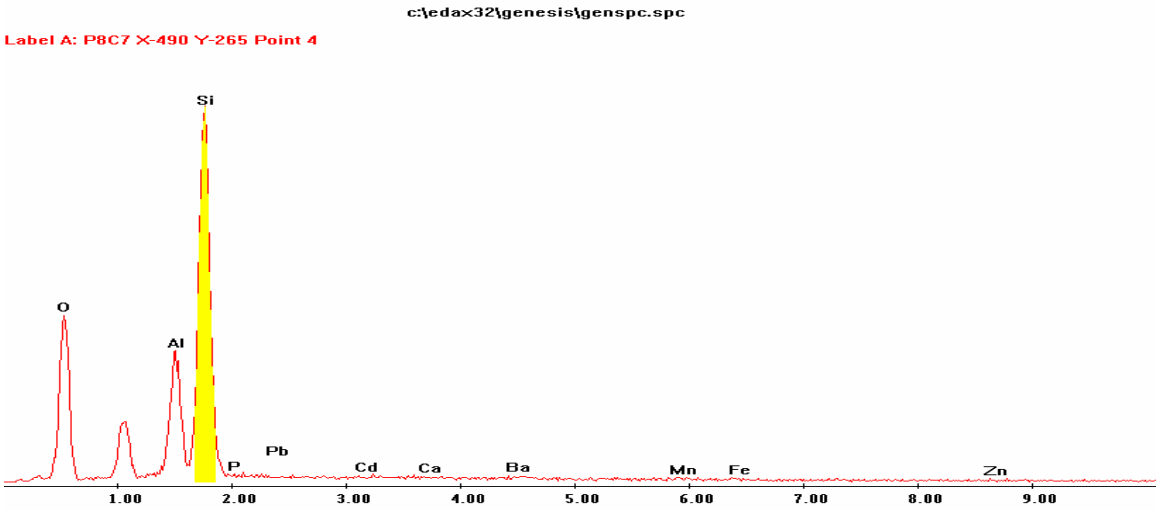

Point 5

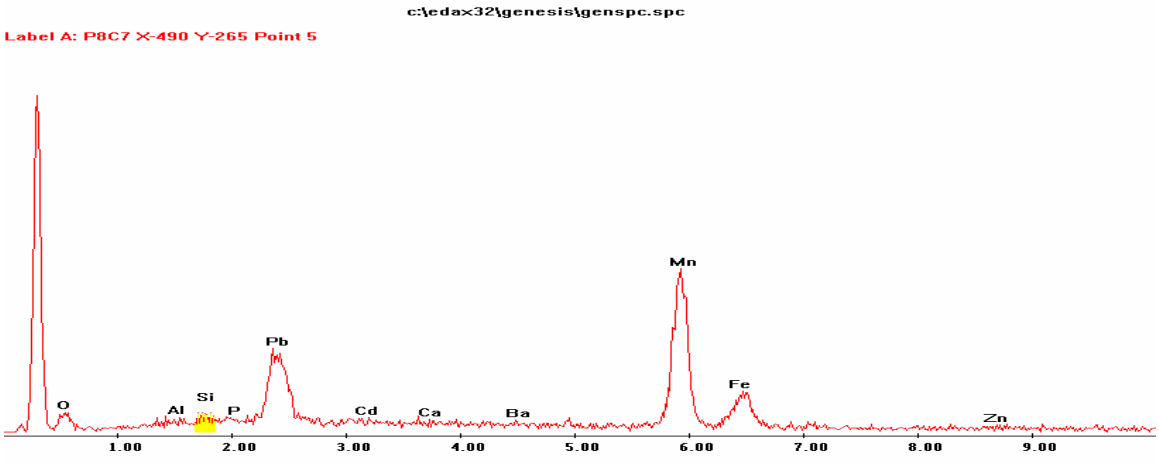

Point 6

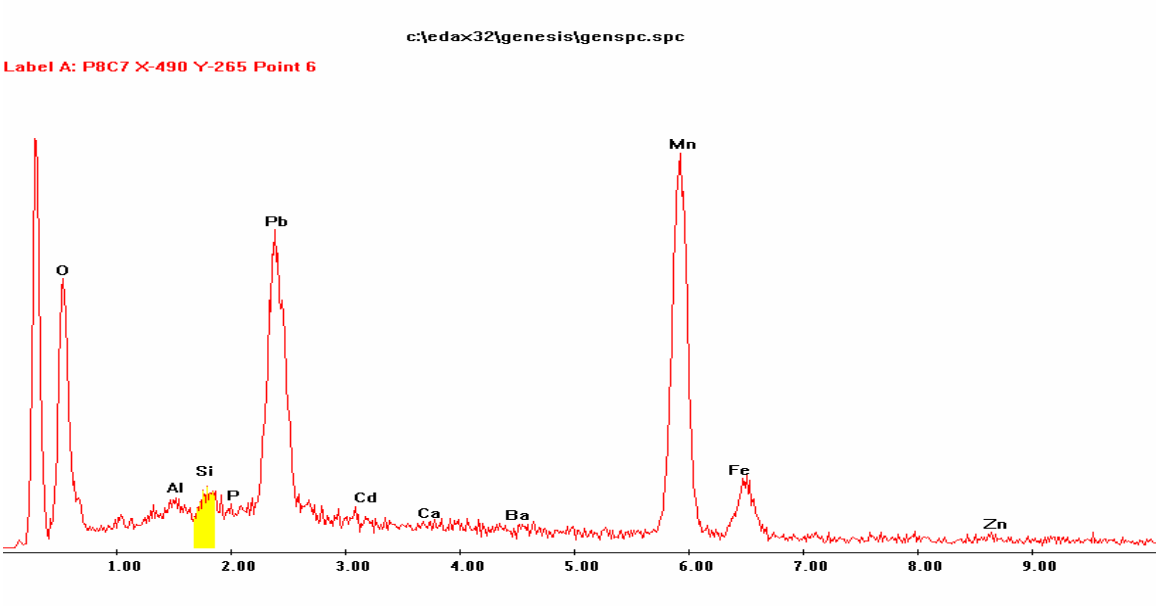
c:\edax32\genesis\genspc.spc
Label A: P8C7 X-490 Y-265 Point 6
O
Al
Si
P
Pb
Cd
Ca
Ba
Mn
Fe
Zn
1.00
2.00
3.00
4.00
5.00
6.00
7.00
8.00
9.00

P8C8 – 302, 323

BSE Image

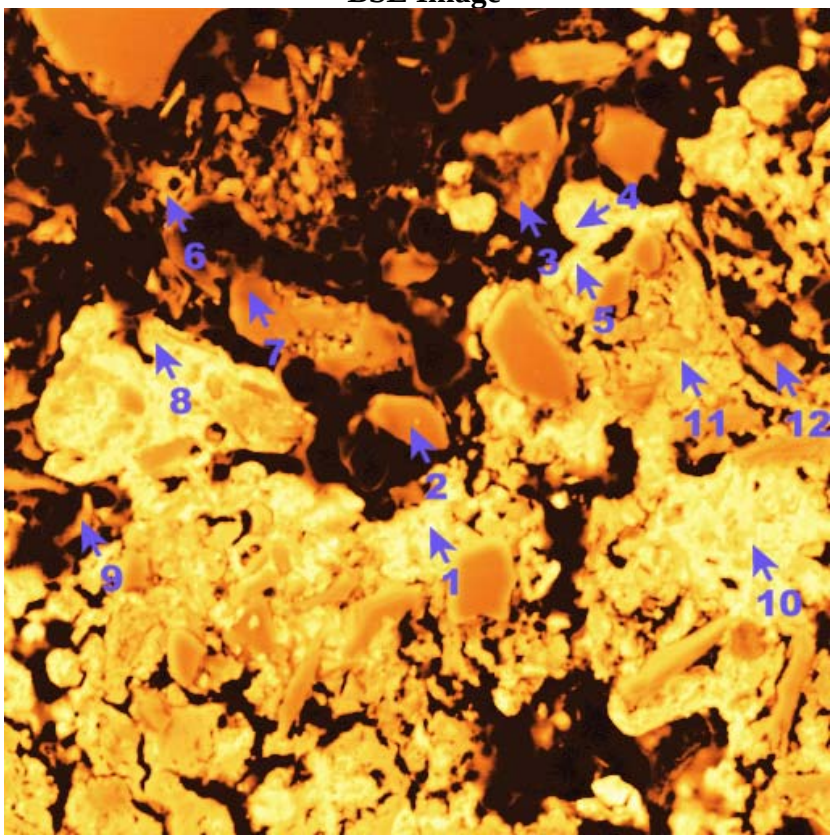

Iron (Fe)

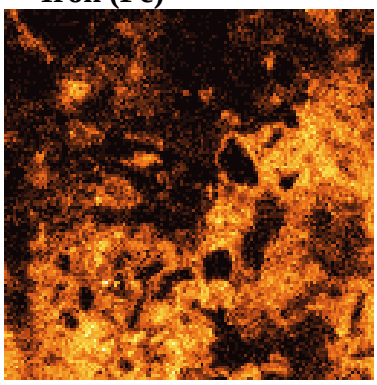

Manganese (Mn)

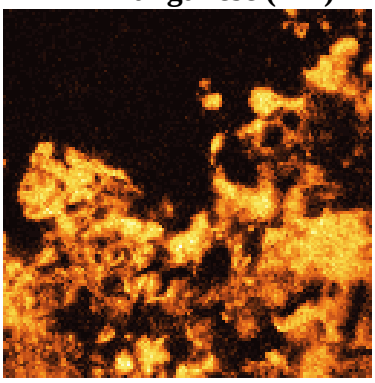

Phosphorous (P)

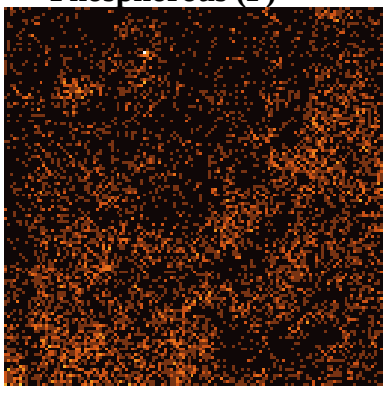

Lead (Pb)

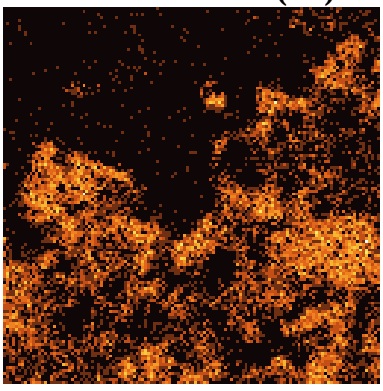

Silicon (Si)

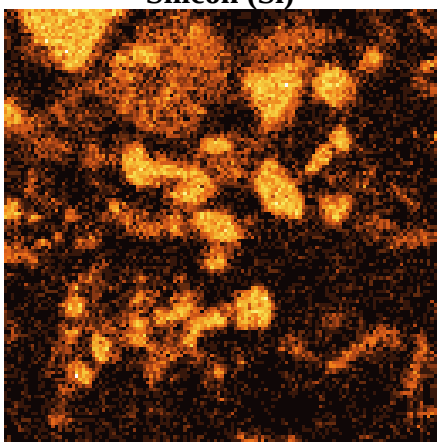

EDS Scan Images by Point

Point 1

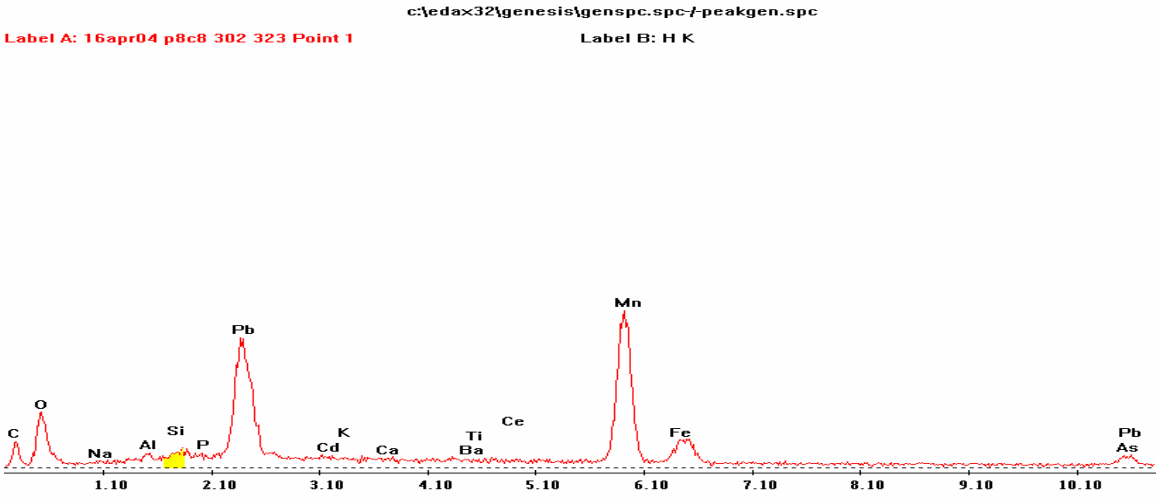

Point 2

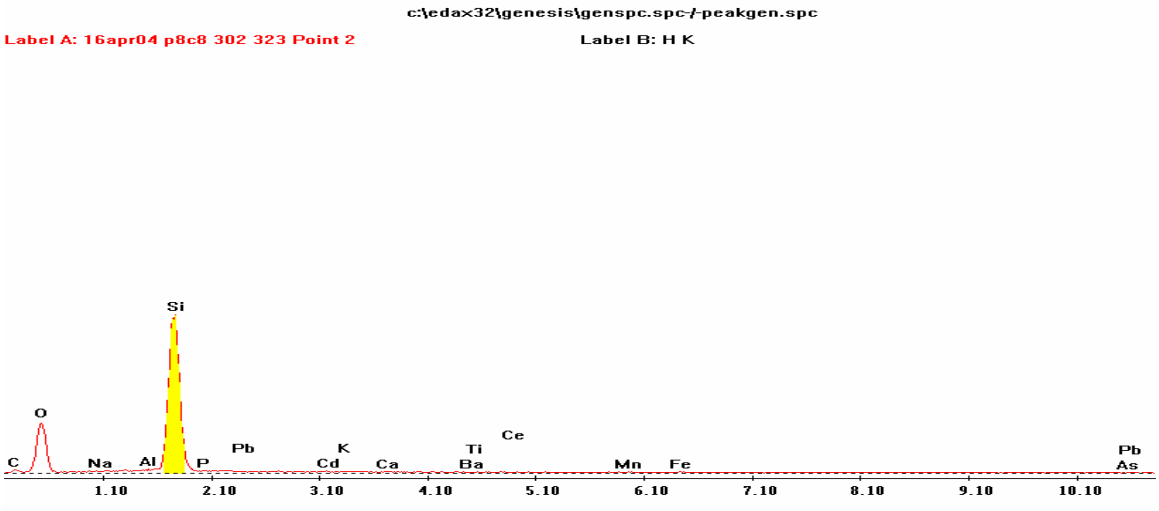

Point 3

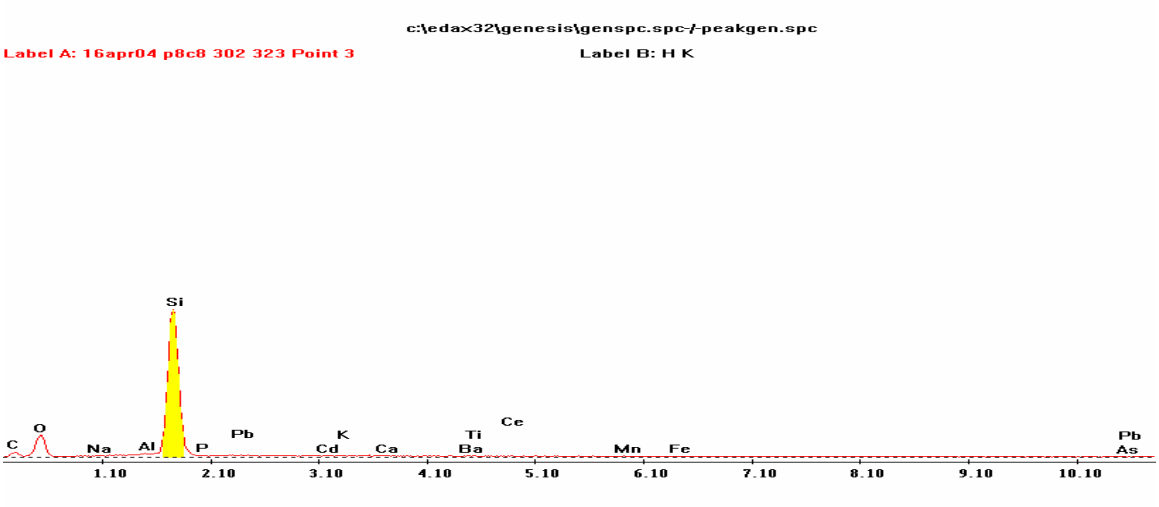

Point 4

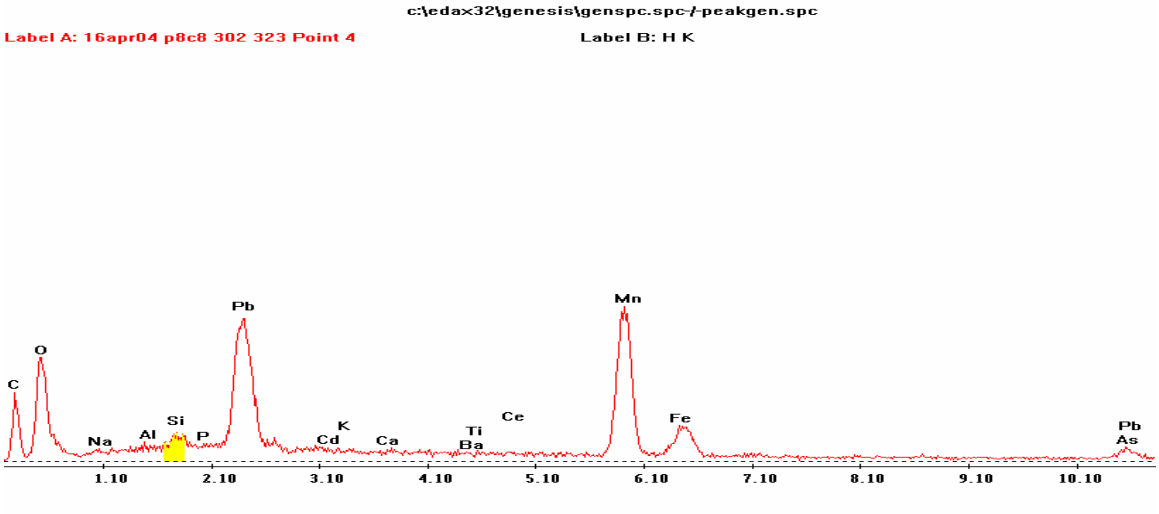

Point 5

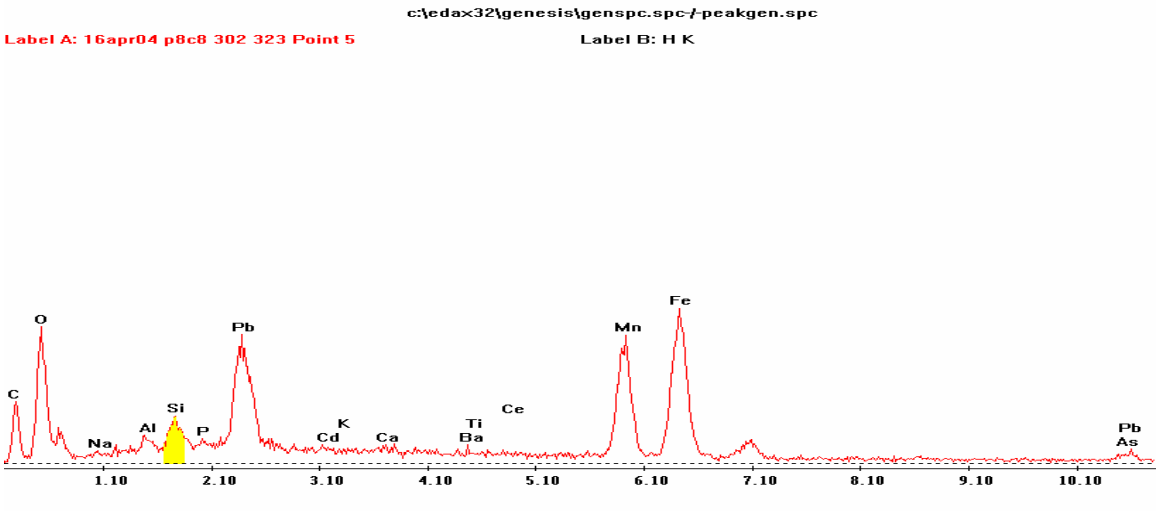

Point 6

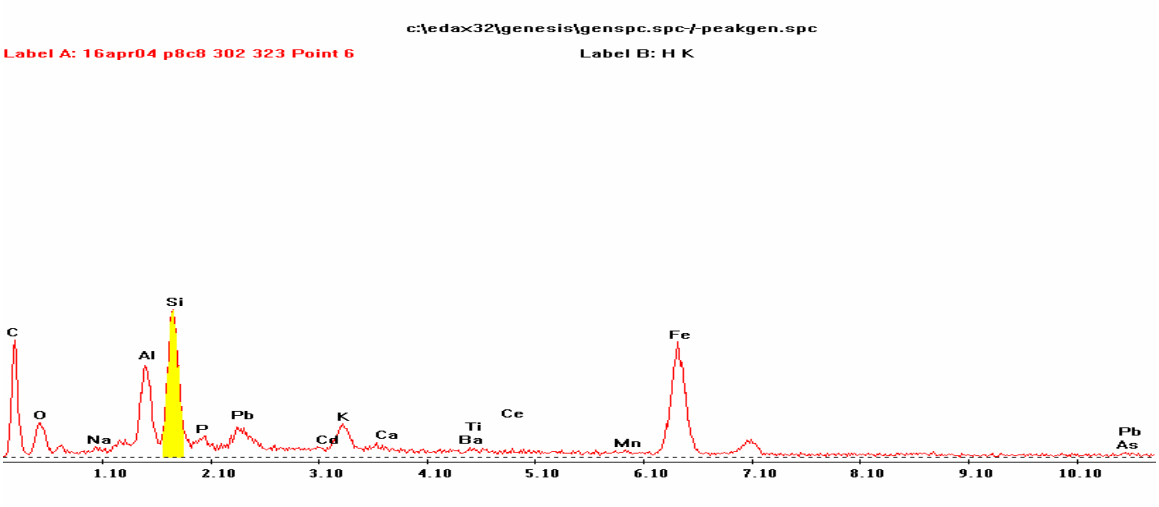

Point 7

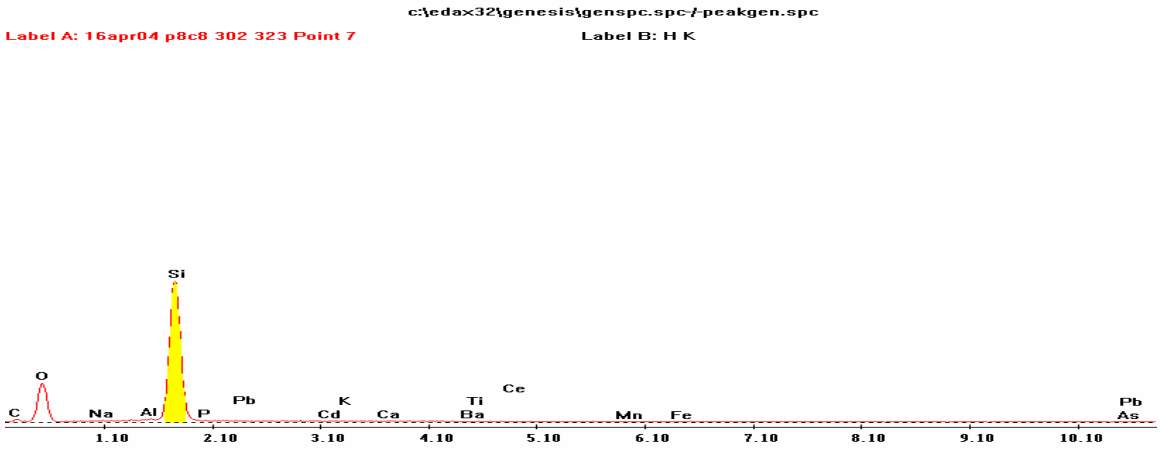

Point 8

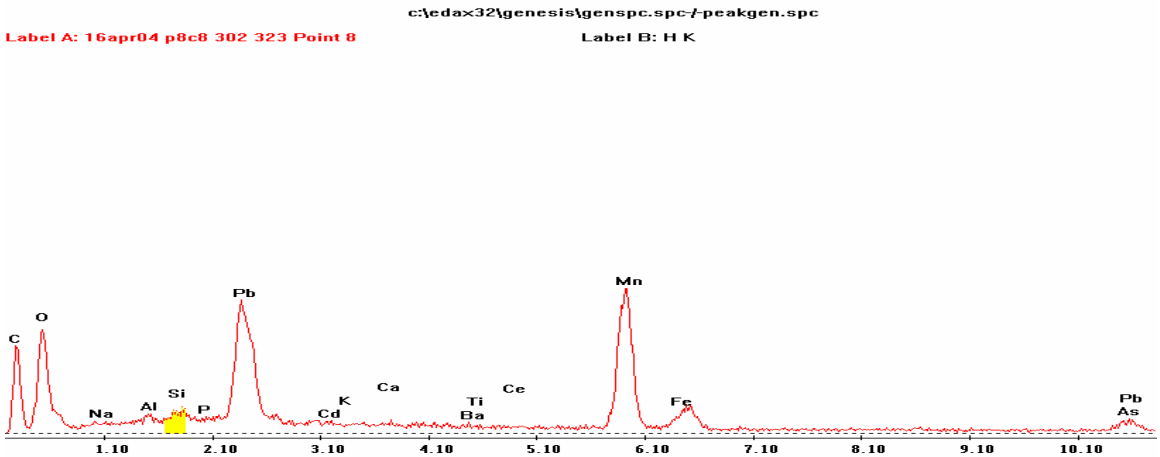

Point 9

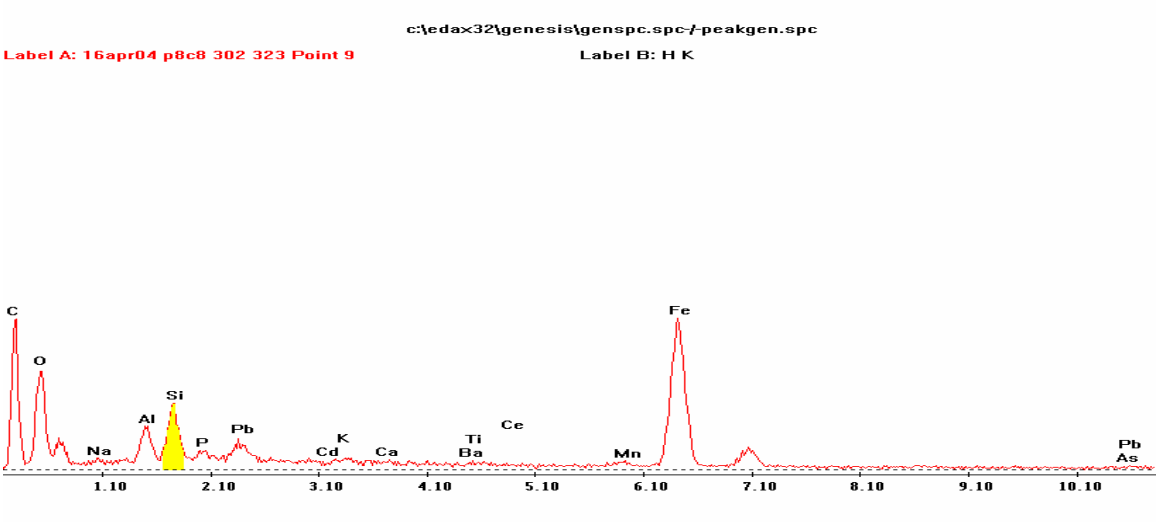

Point 10

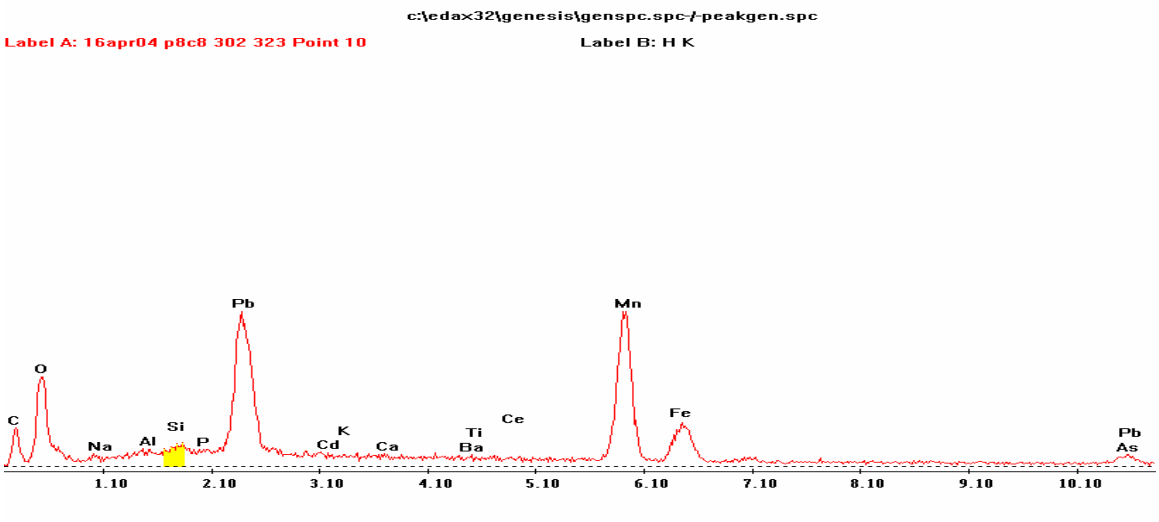

Point 11

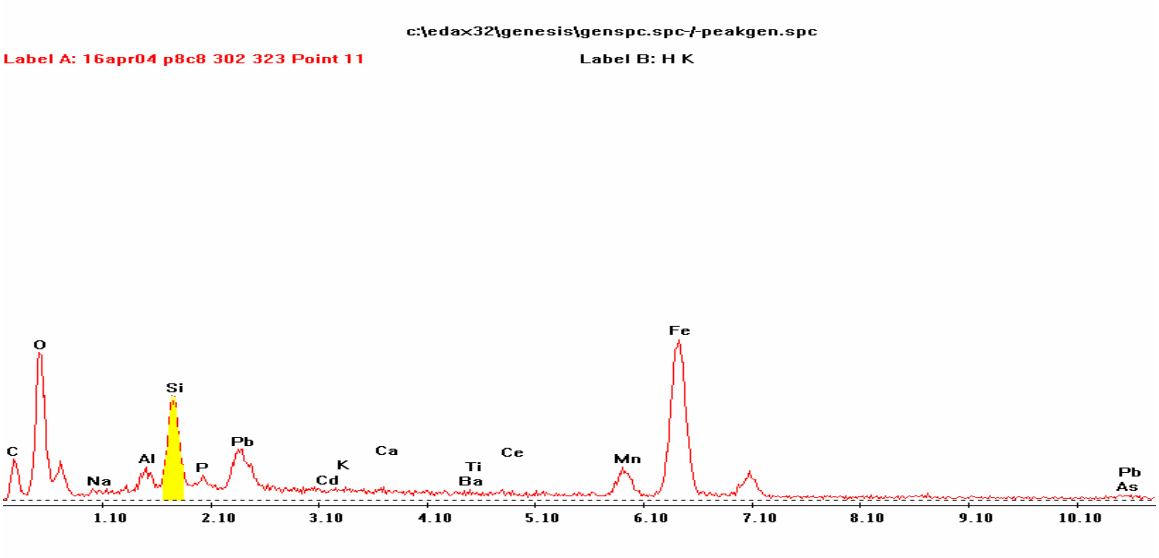

Point 12

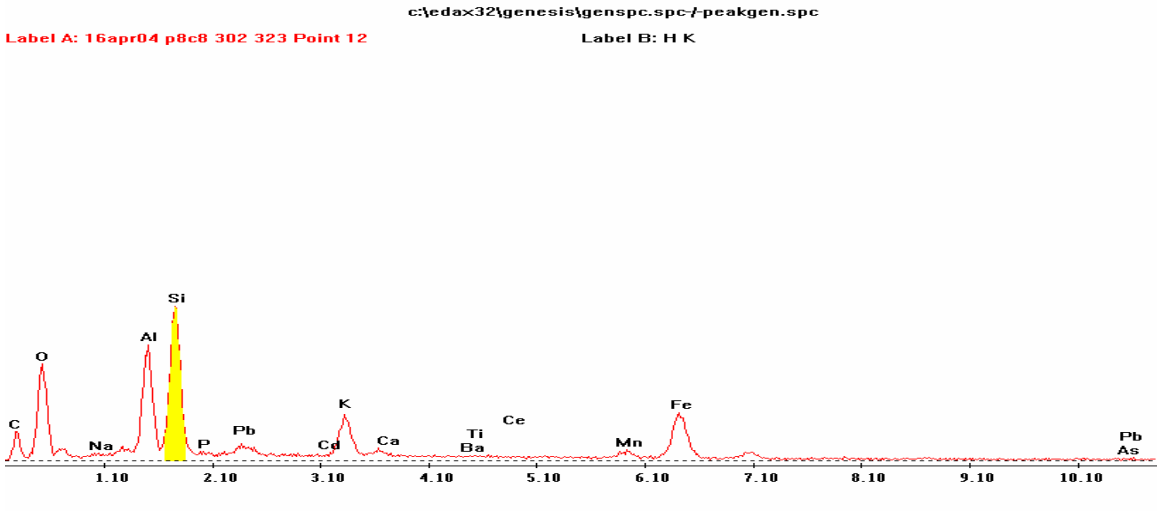

P8C8 – 328, 276

BSE Image

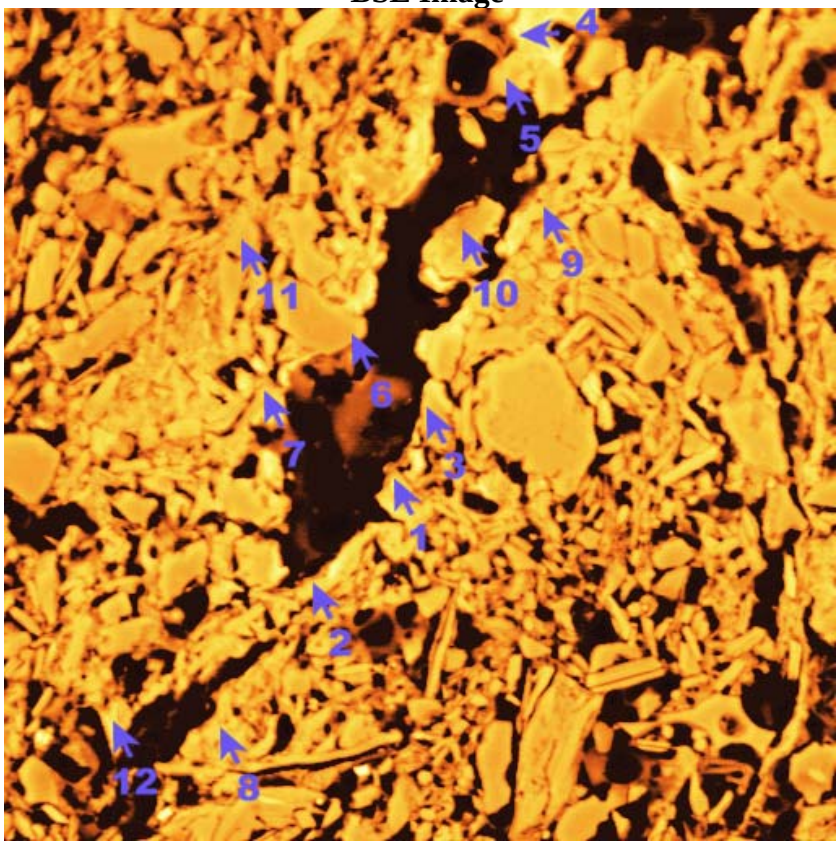

Iron (Fe)

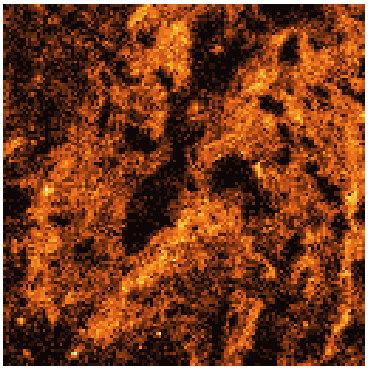

Manganese (Mn)

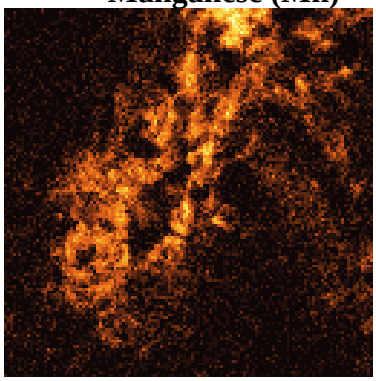

Phosphorous (P)

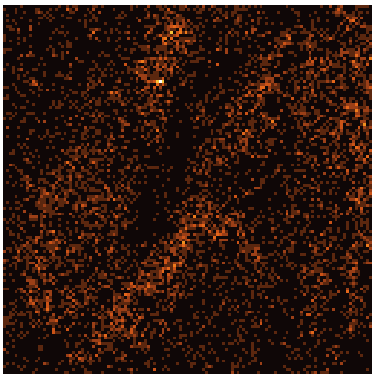

Lead (Pb)

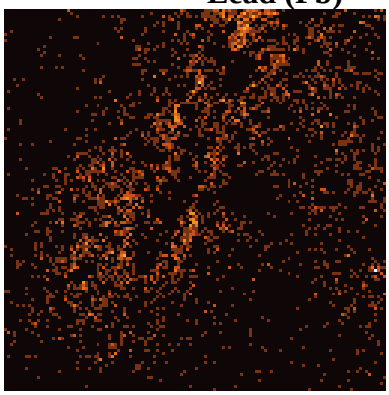

Silicon (Si)

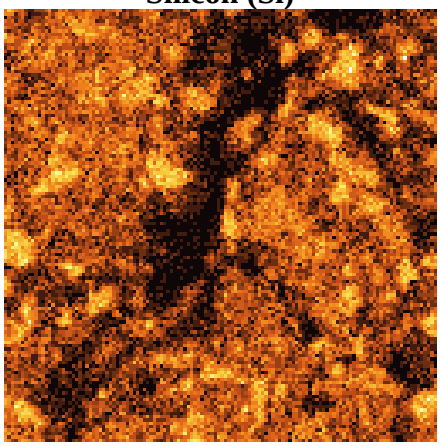

EDS Scan Images by Point

Point 1

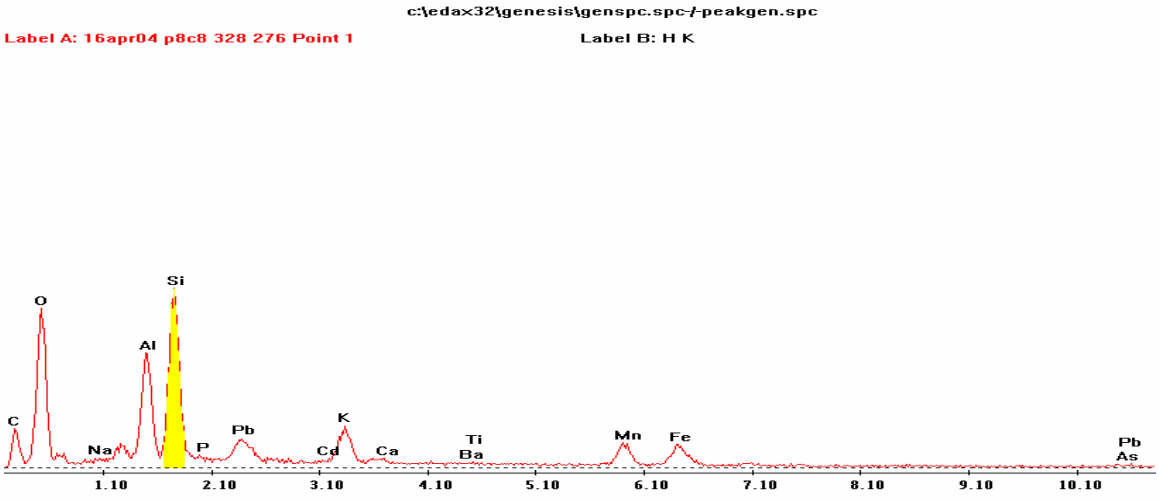

Point 2

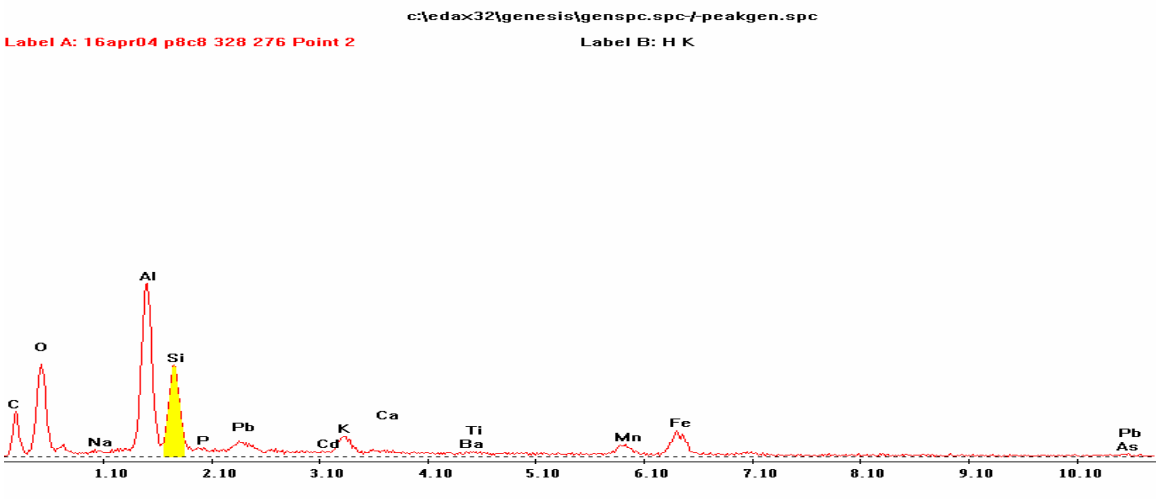

Point 3

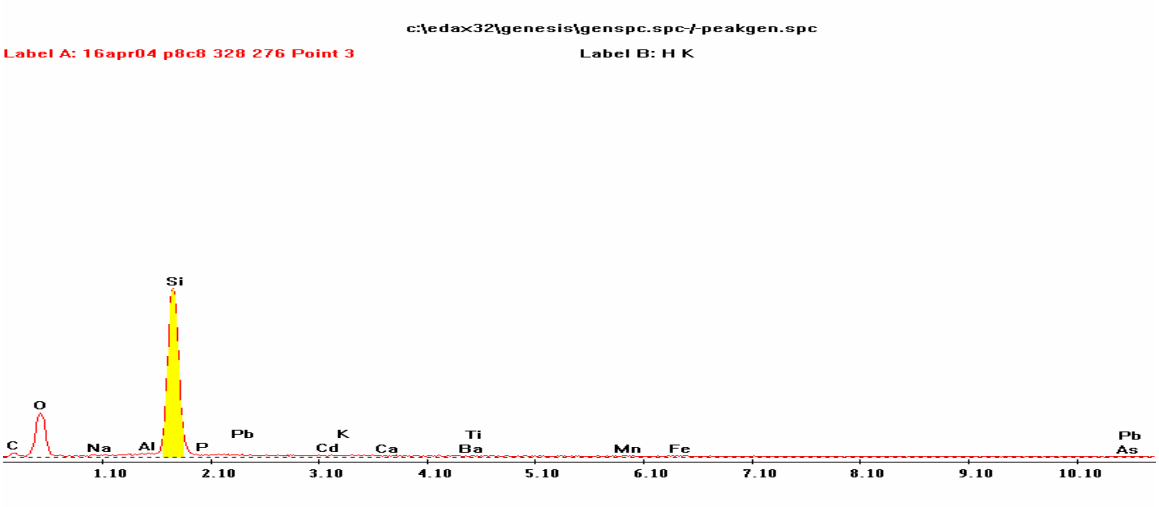

Point 4

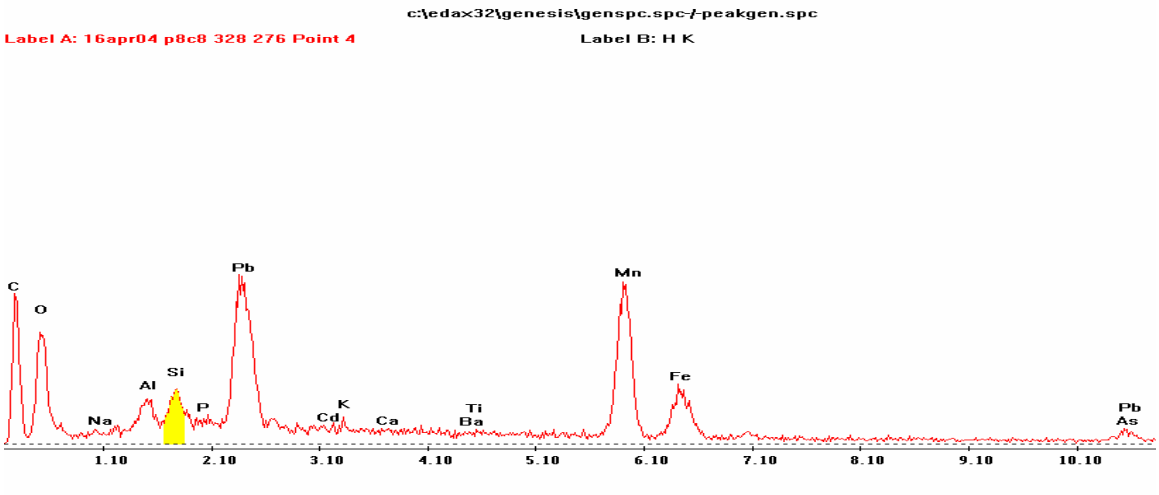

Point 5

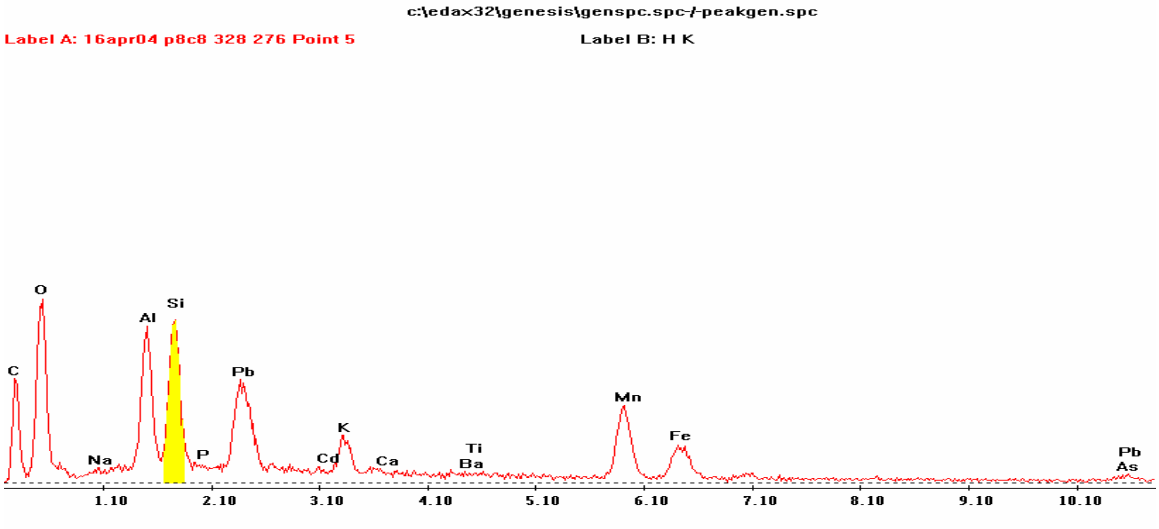

Point 6

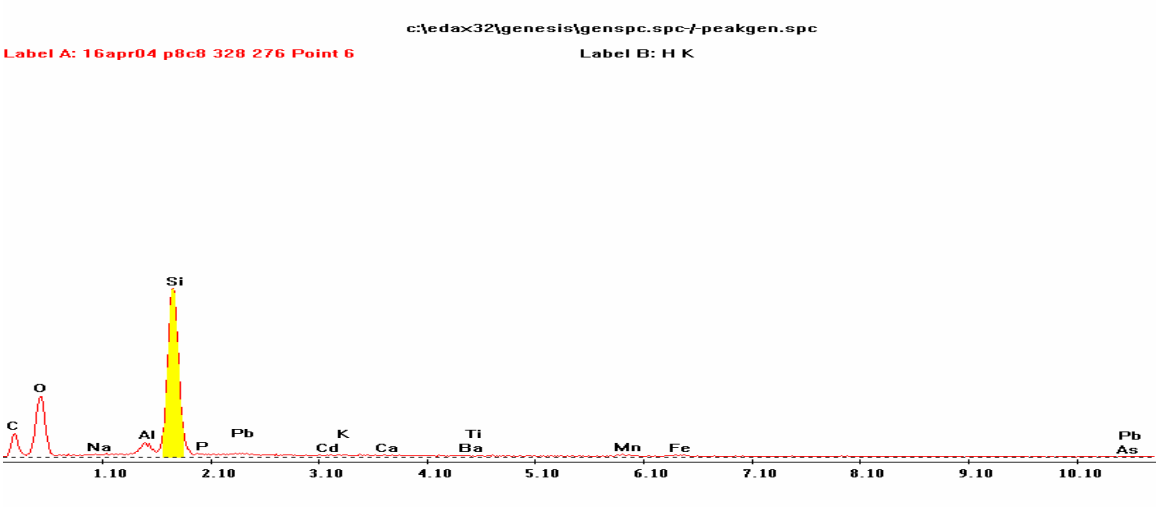

Point 7

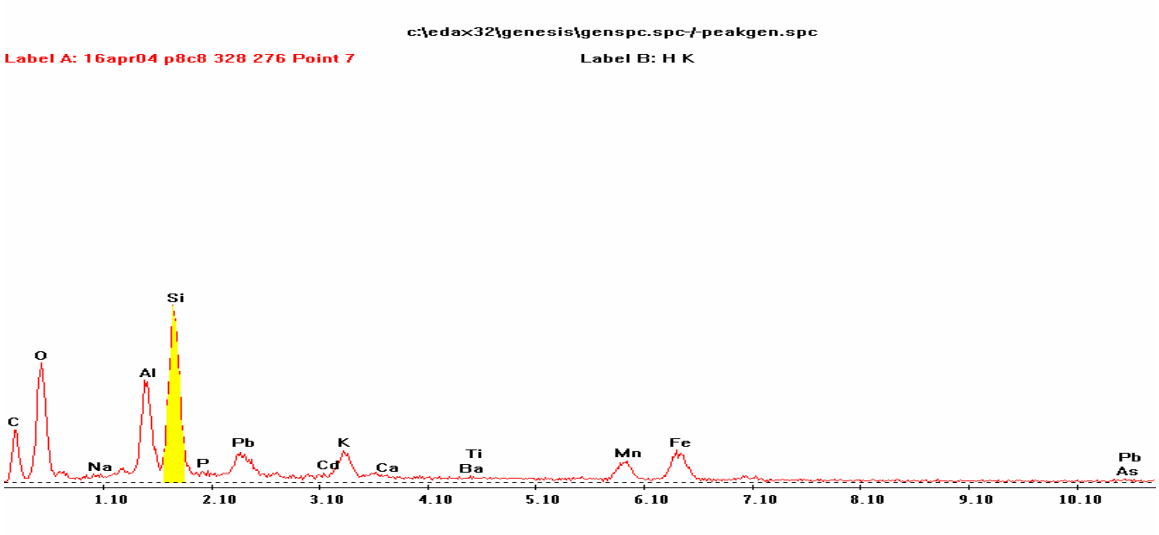

Point 8

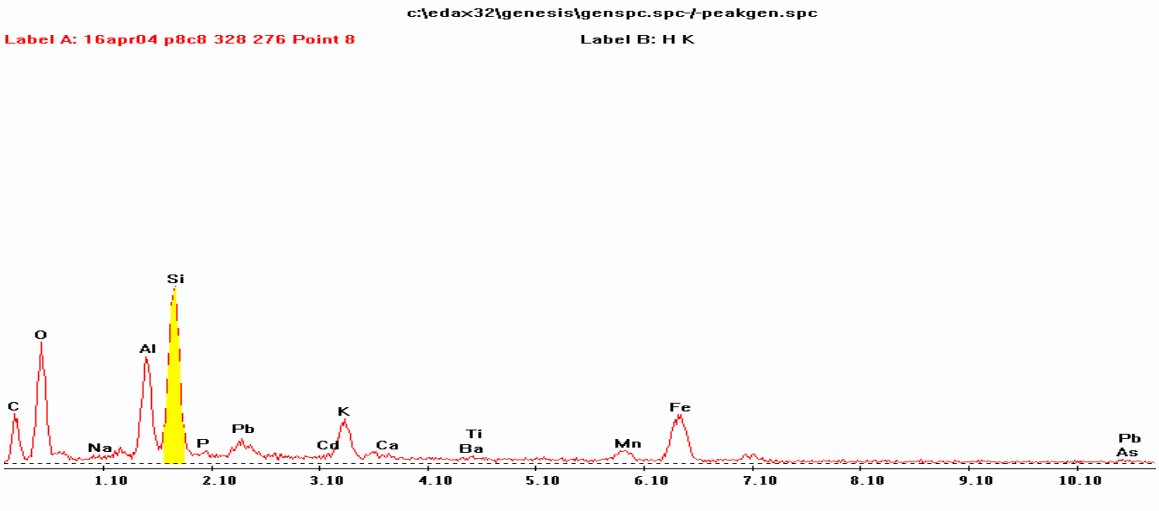

Point 9

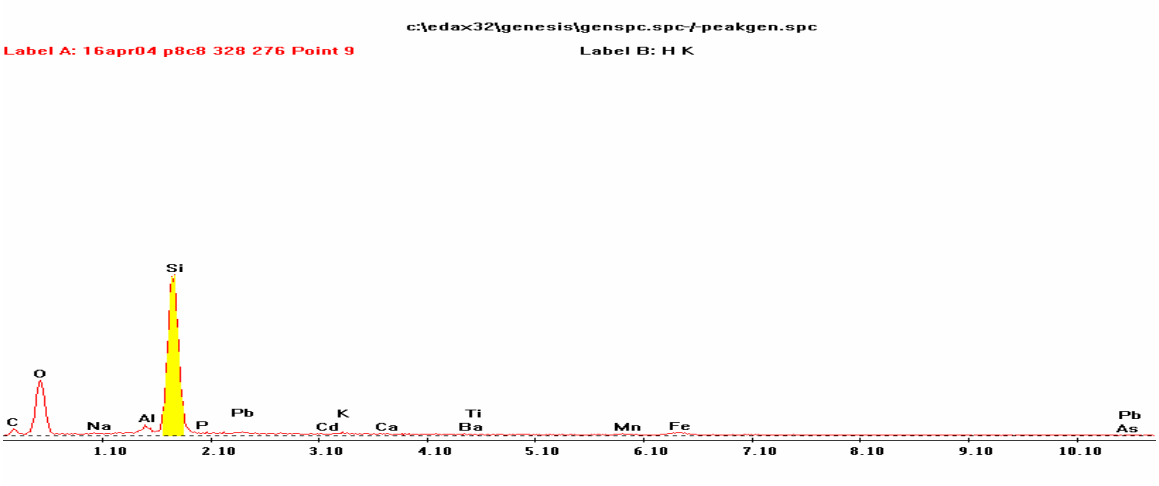

Point 10

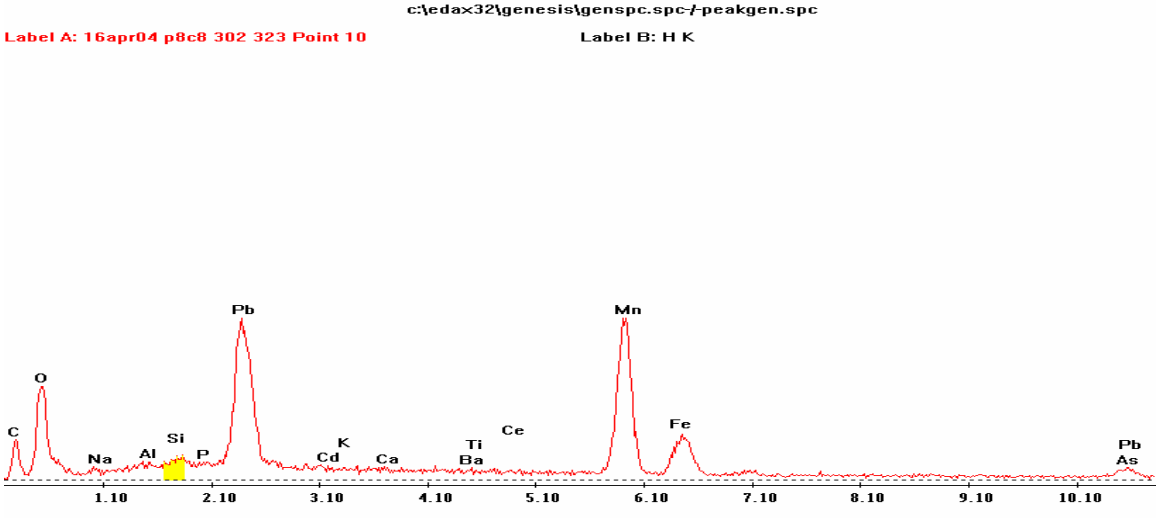

Point 11

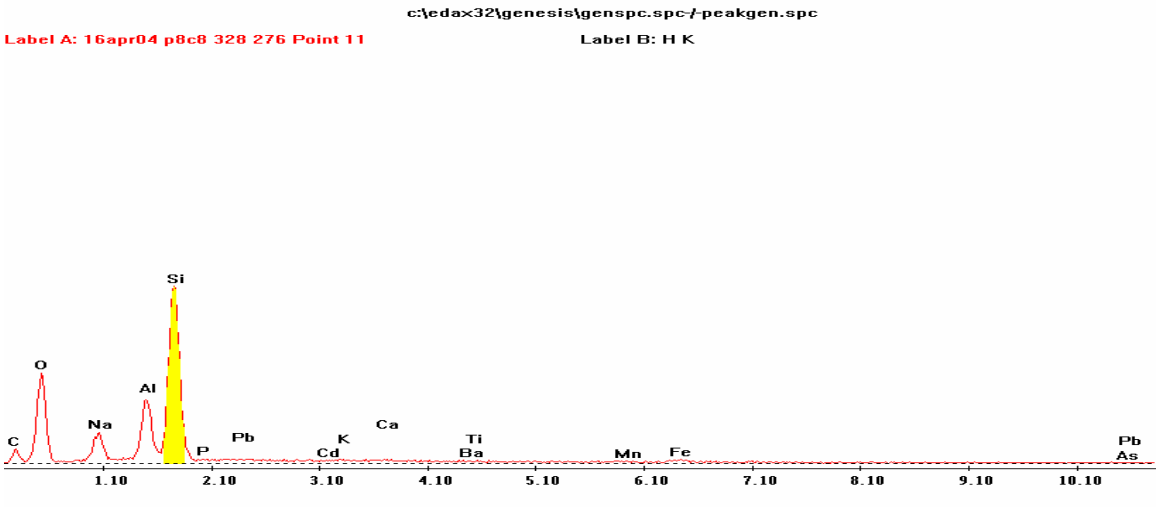

Point 12

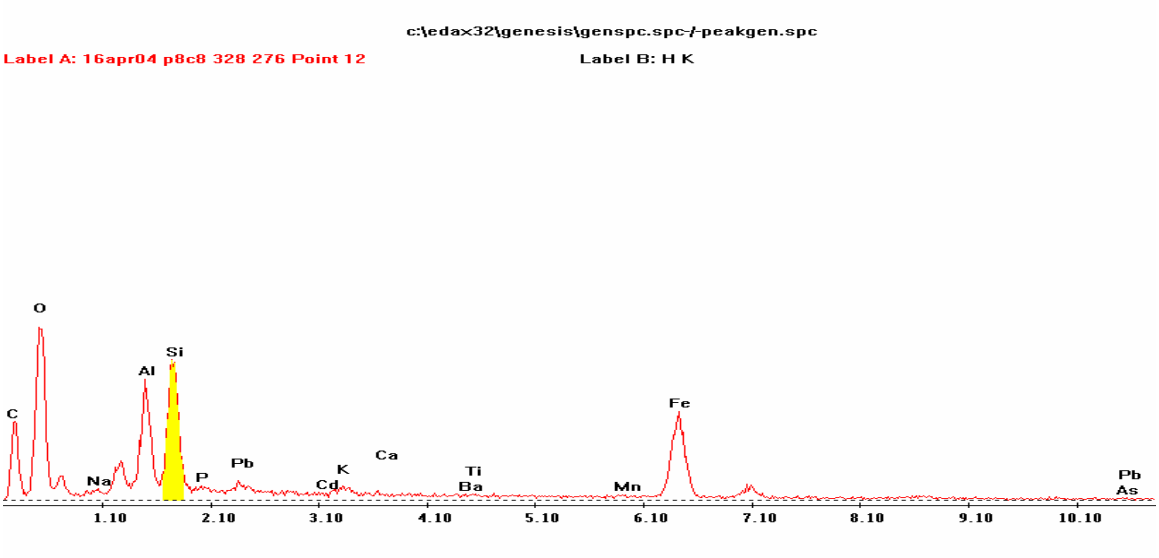
c:\edax32\genesis\genspc.spc-/-peakgen.spc
Label A: 16apr04 p8c8 328 276 Point 12
Label B: H K
O
Si
Al
C
Na
P
Pb
Cd
K
Ca
Ti
Ba
Mn
Fe
Pb
As
1.10
2.10
3.10
4.10
5.10
6.10
7.10
8.10
9.10
10.10

P8C8 – 333, 340

BSE Image

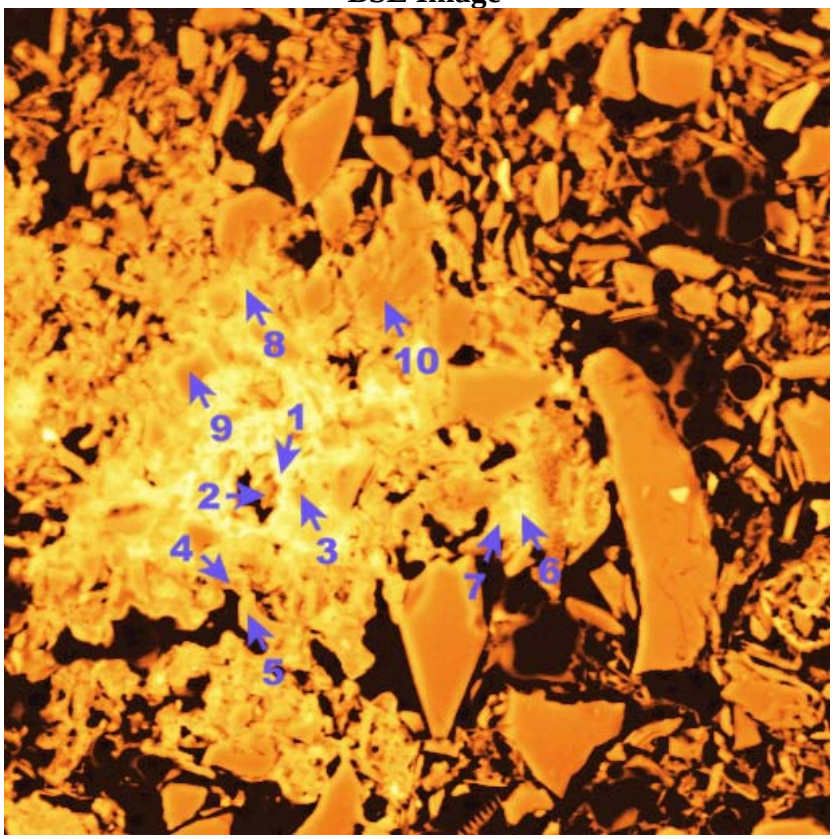

Iron (Fe)

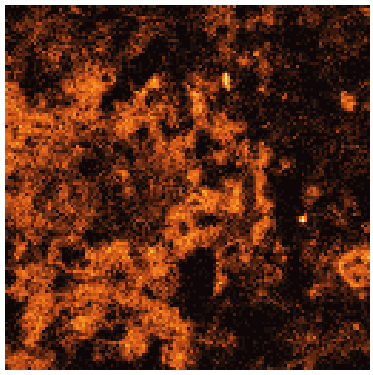

Manganese (Mn)

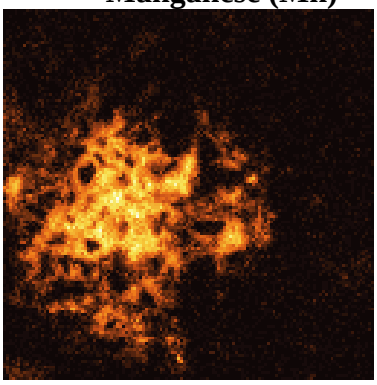

Phosphorous (P)

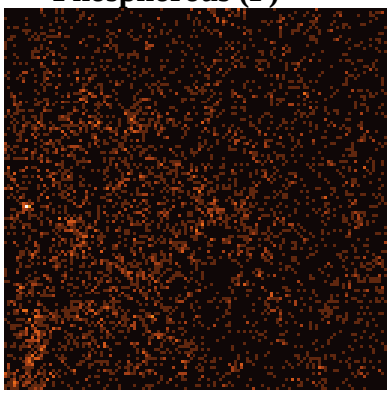

Lead (Pb)

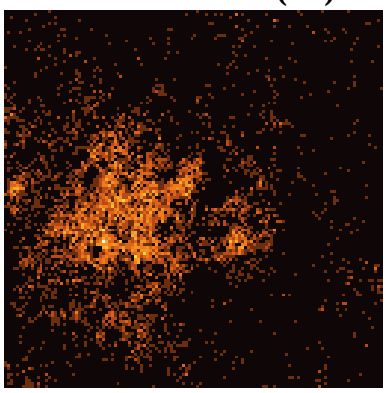

Silicon (Si)

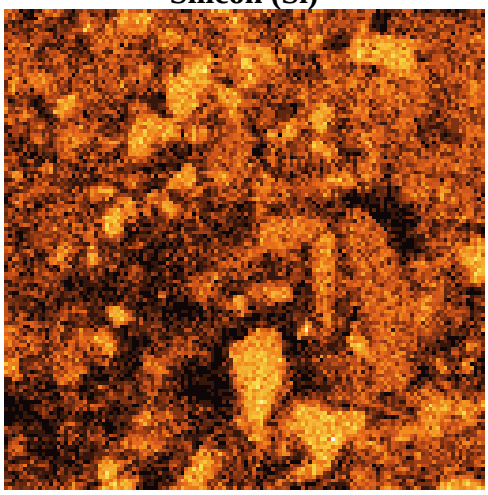

EDS Scan Images by Point

Point 1

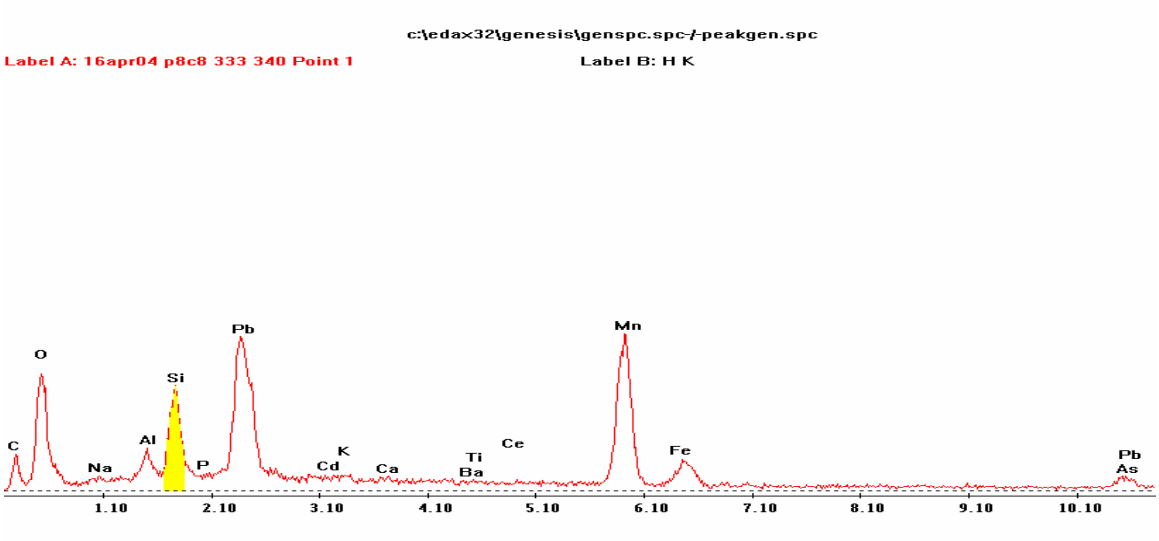

Point 2

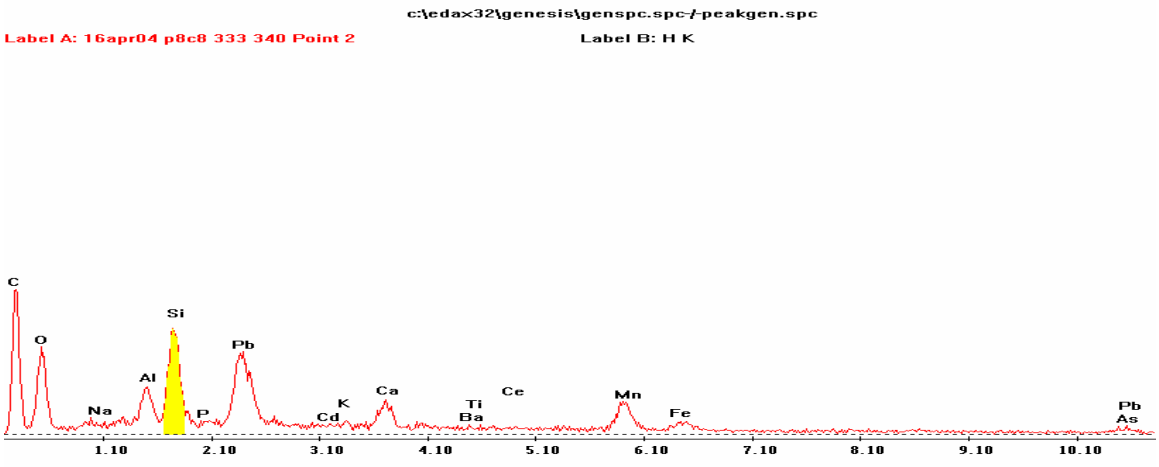

Point 3

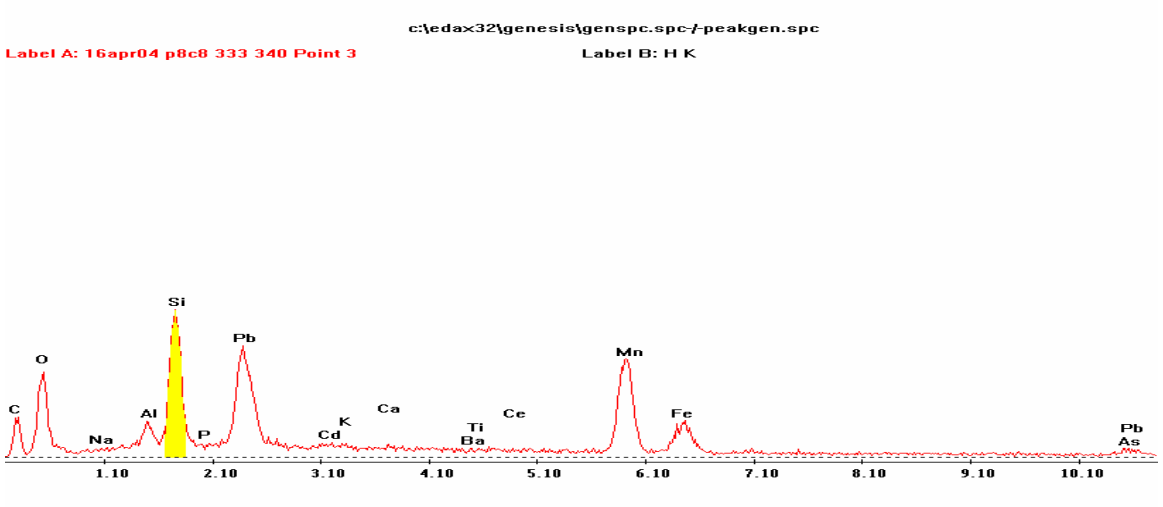

Point 4

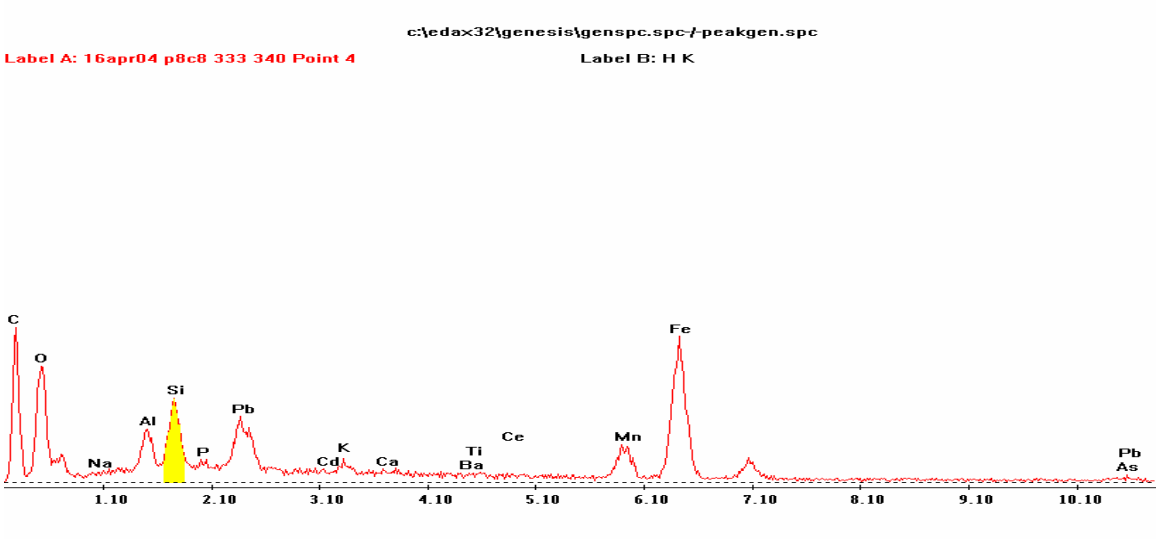

Point 5

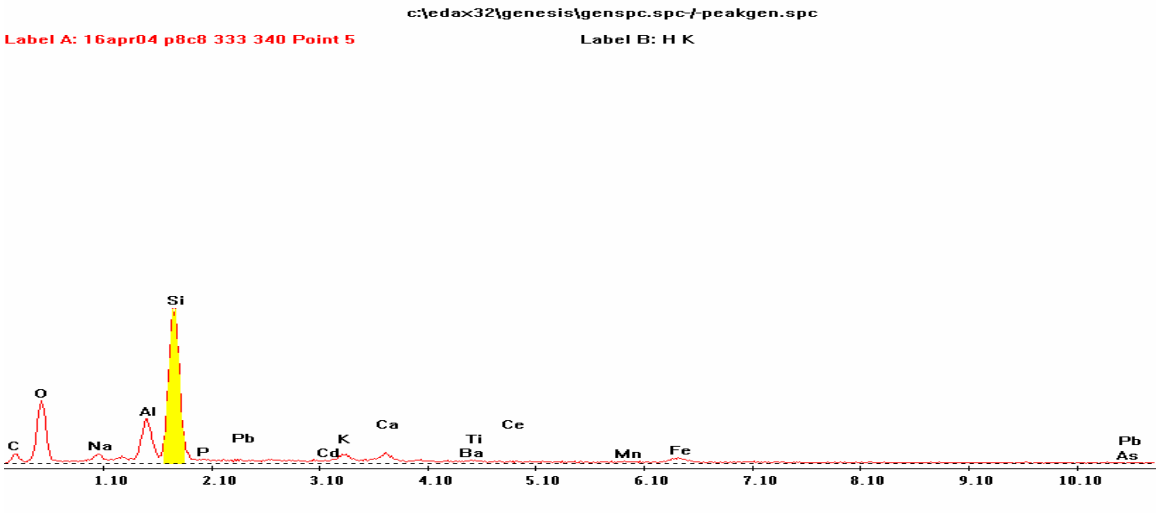

Point 6

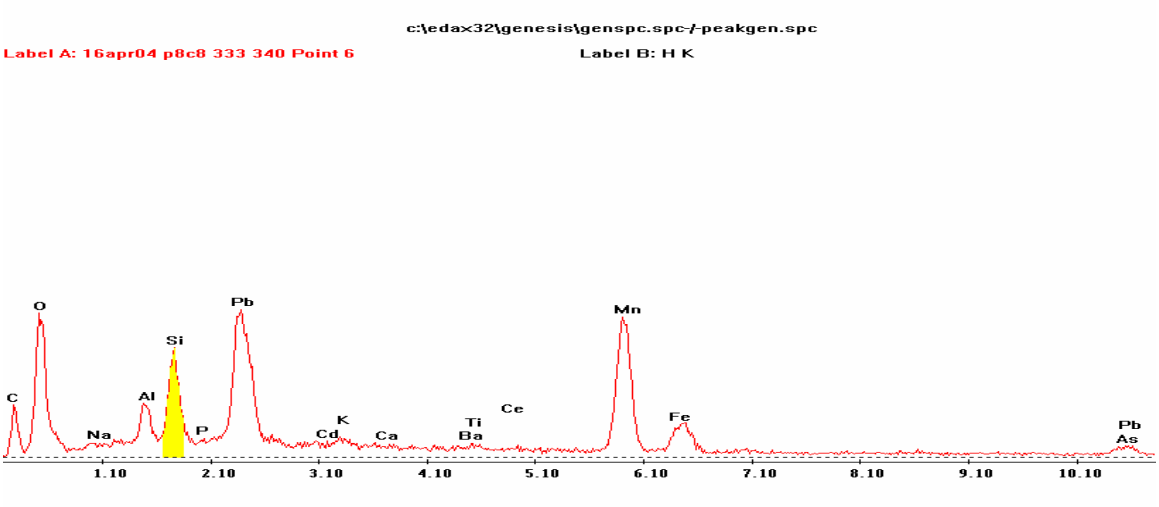

Point 7

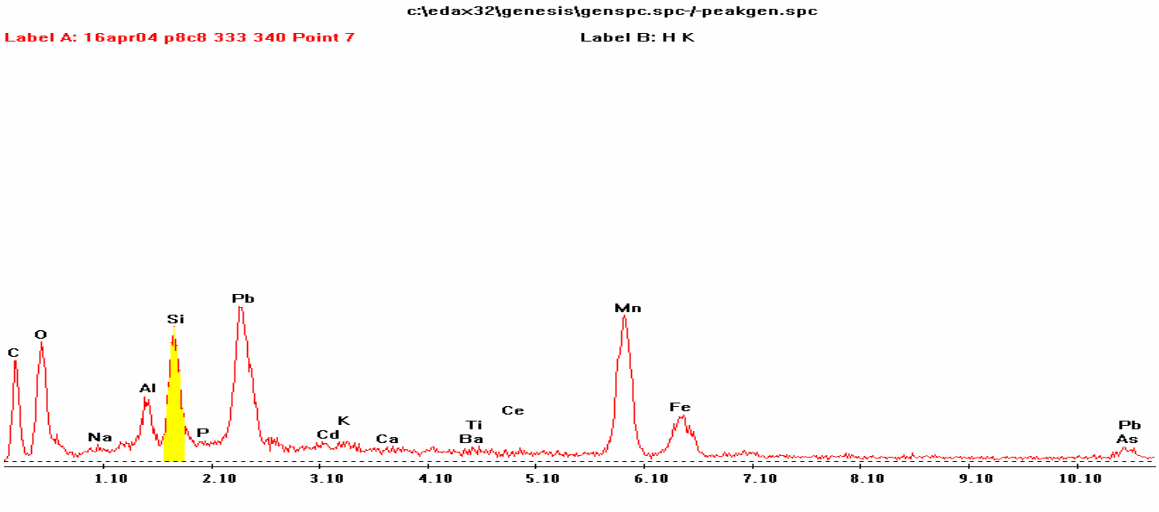

Point 8

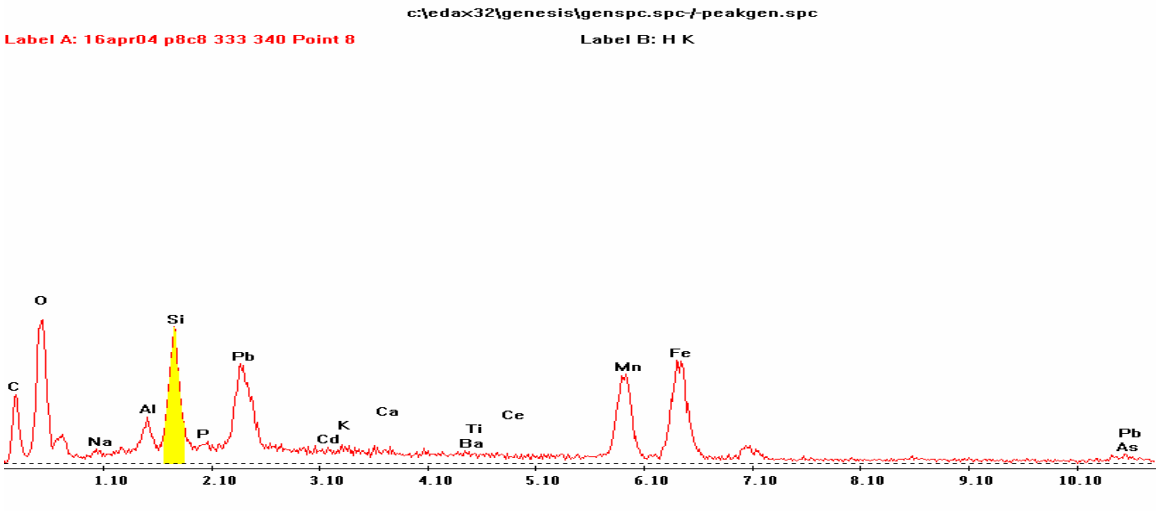

Point 9

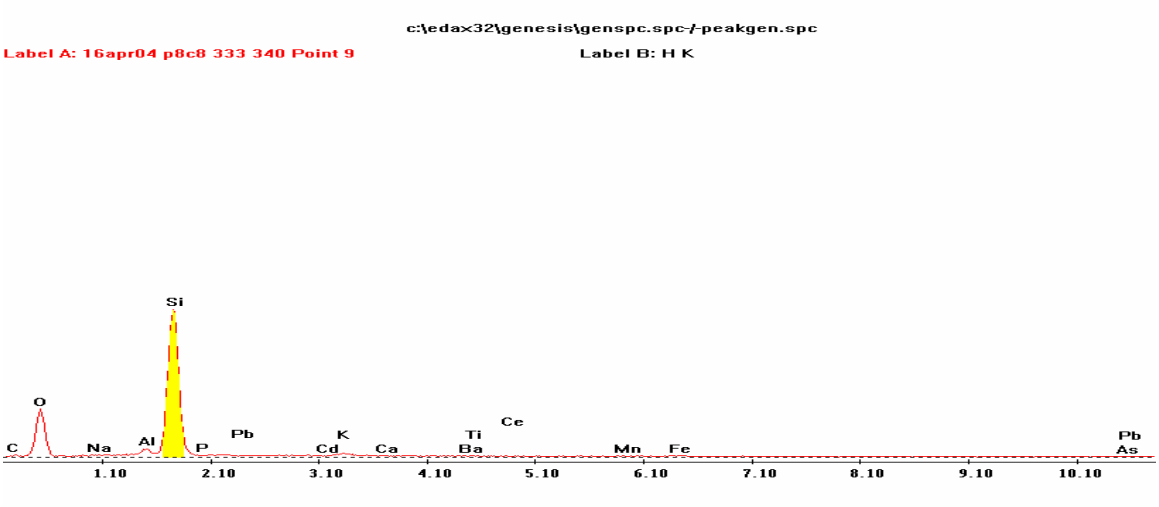

Point 10

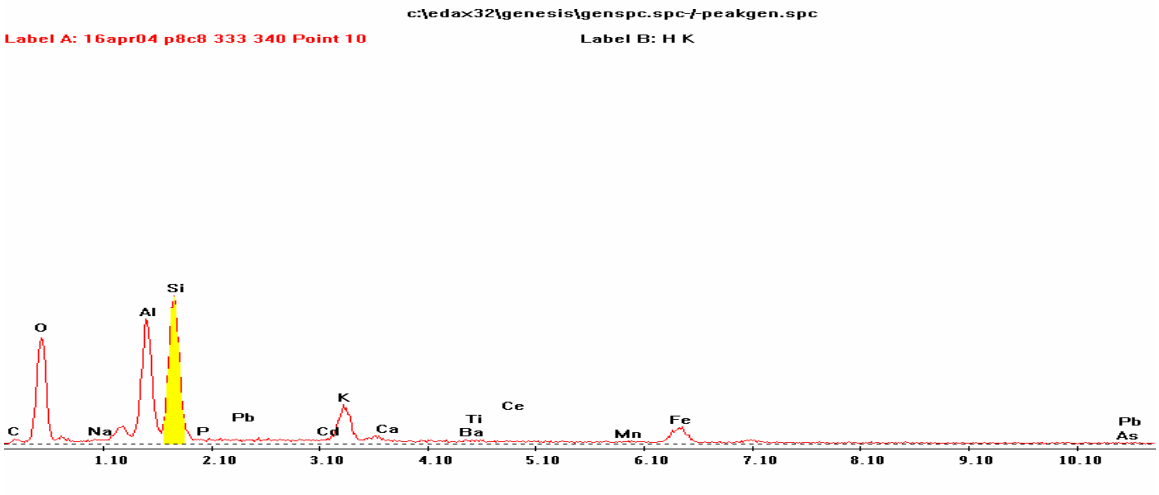

P8C8 – 354, 225

BSE Image

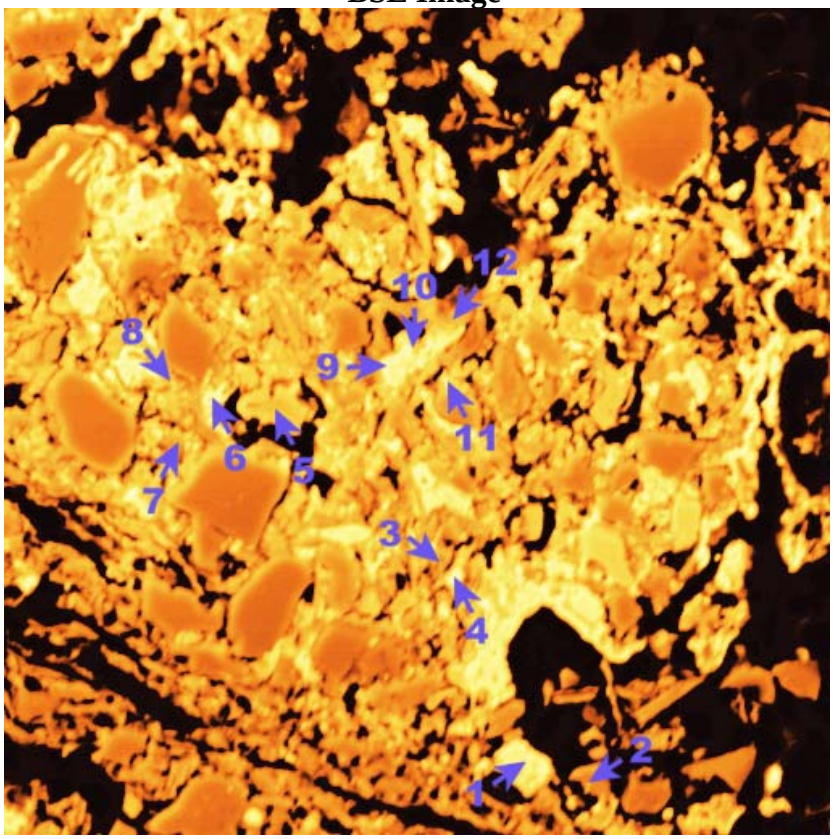

Iron (Fe)

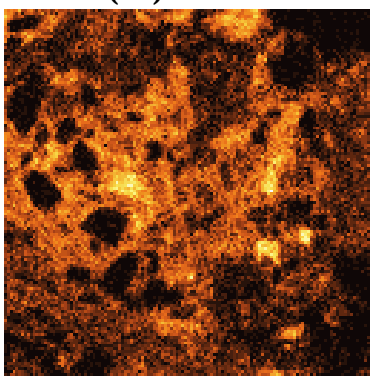

Manganese (Mn)

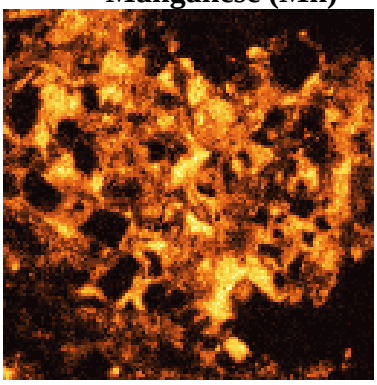

Phosphorous (P)

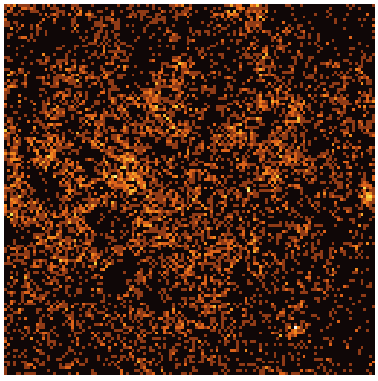

Lead (Pb)

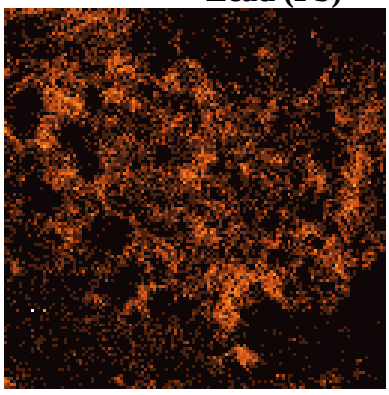

Silicon (Si)

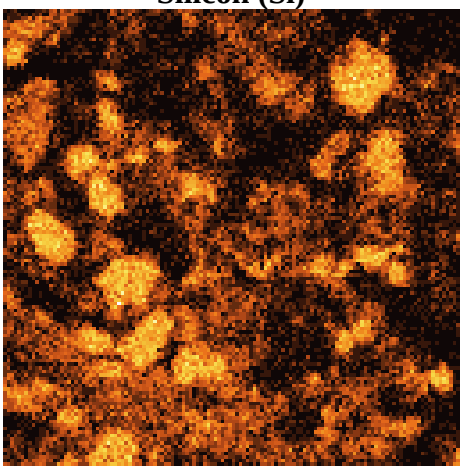

EDS Scan Images by Point

Point 1

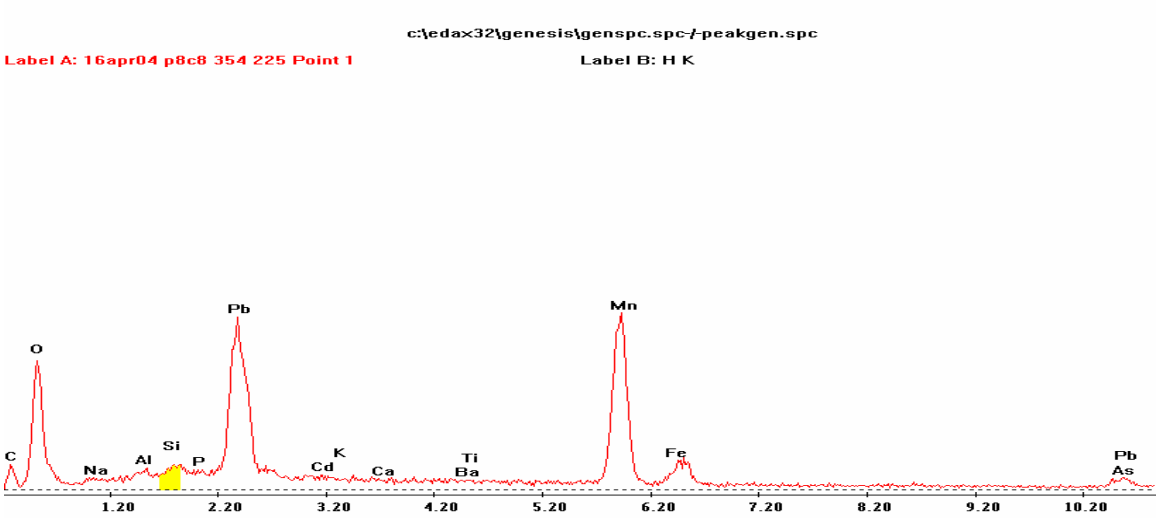

Point 2

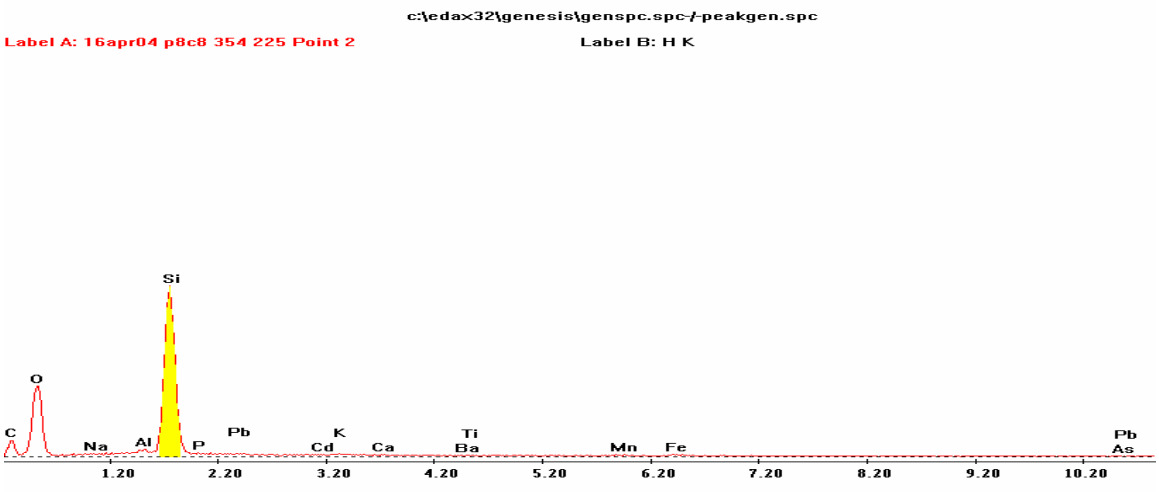

Point 3

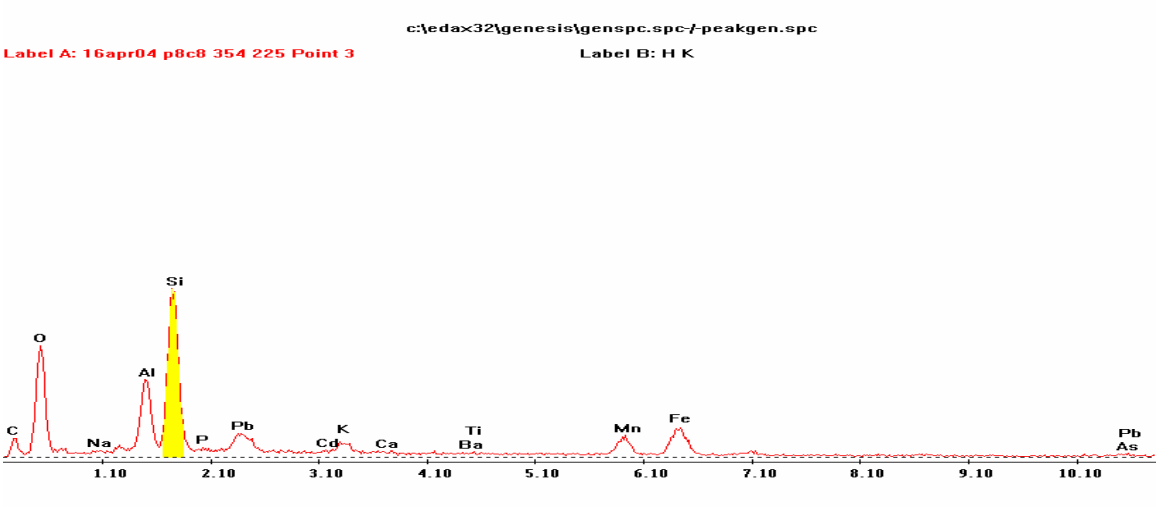

Point 4

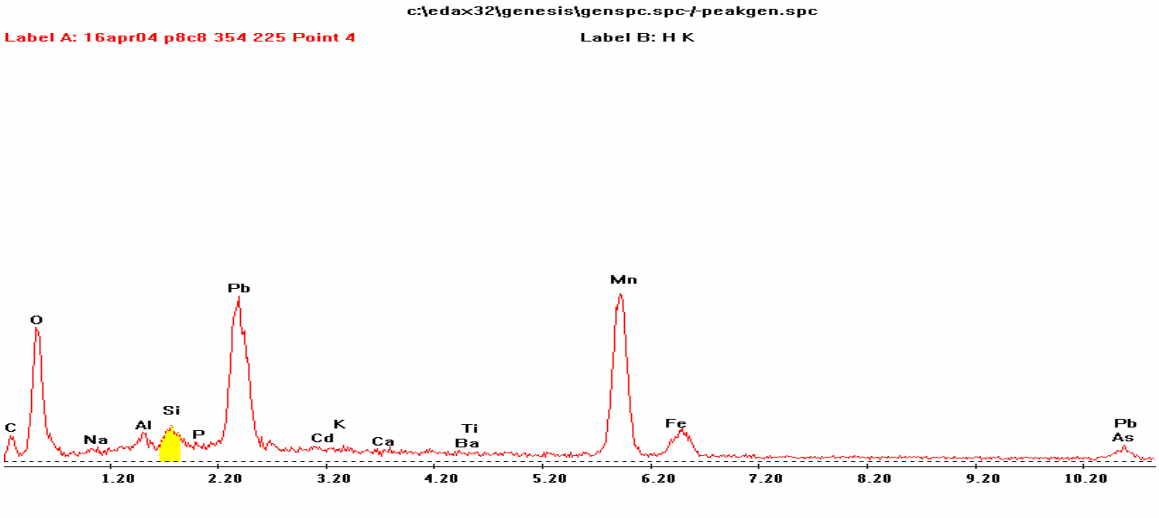

Point 5

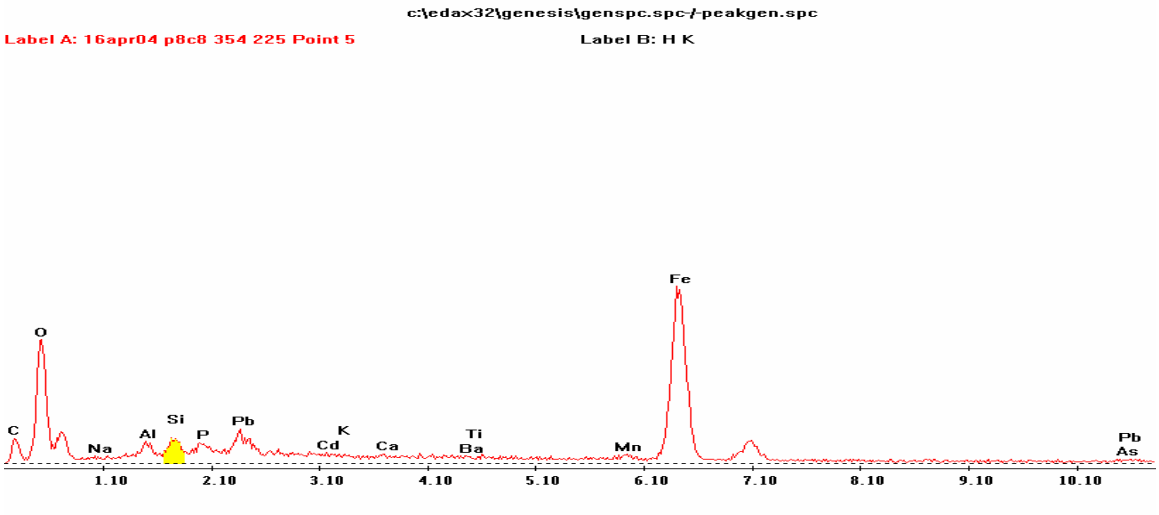

Point 6

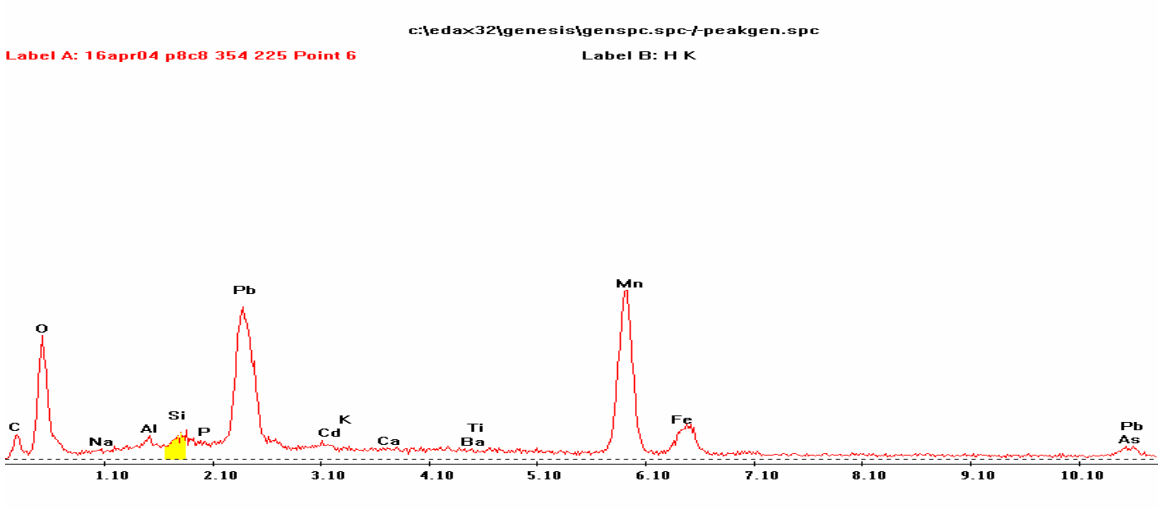

Point 7

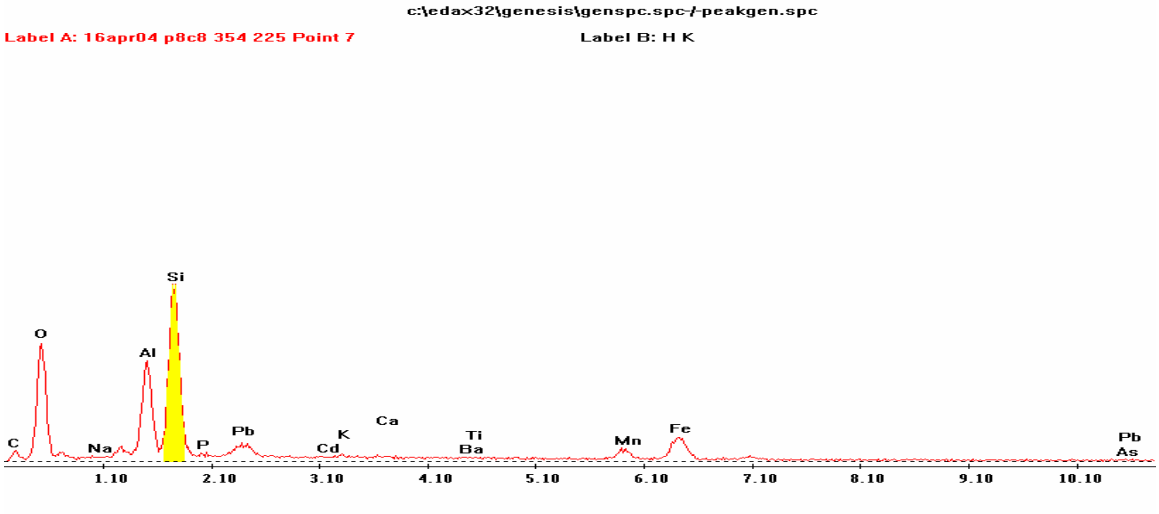

Point 8

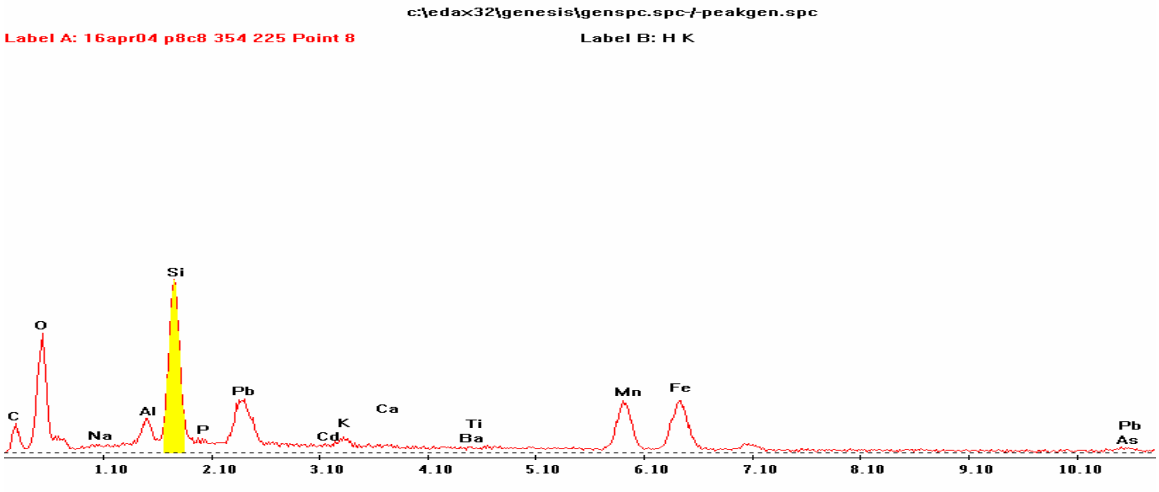

Point 9

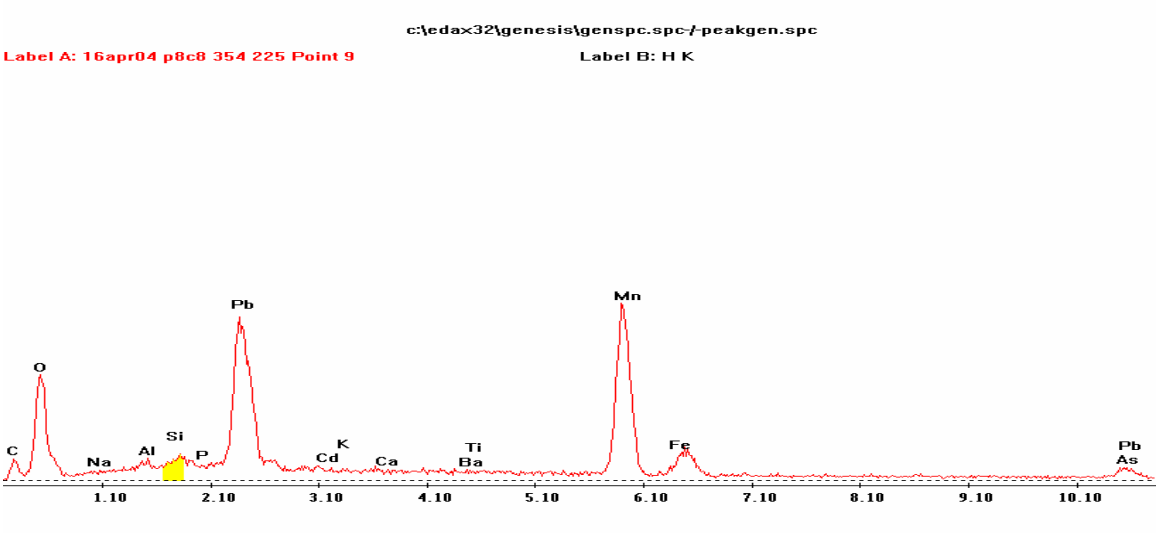

Point 10

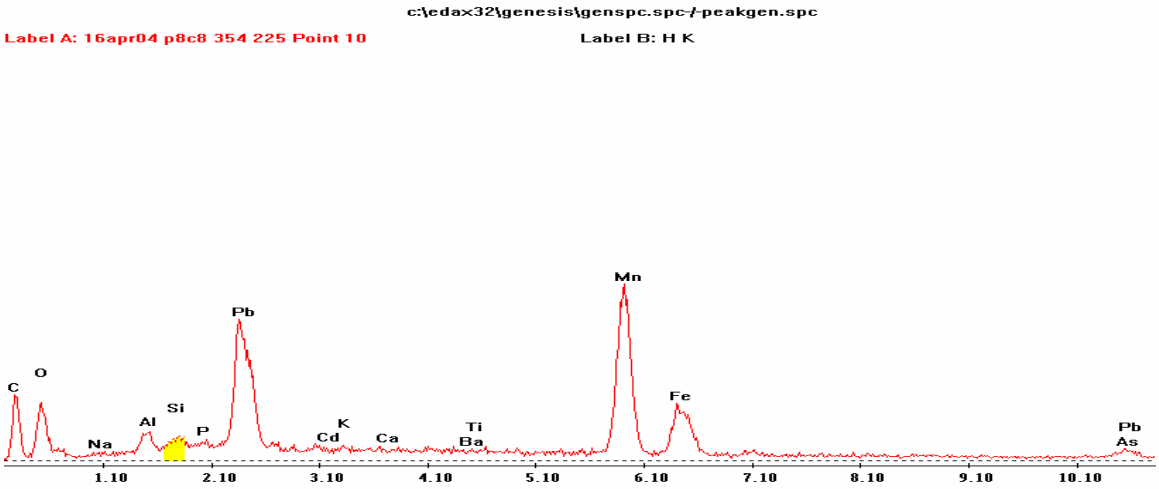

Point 11

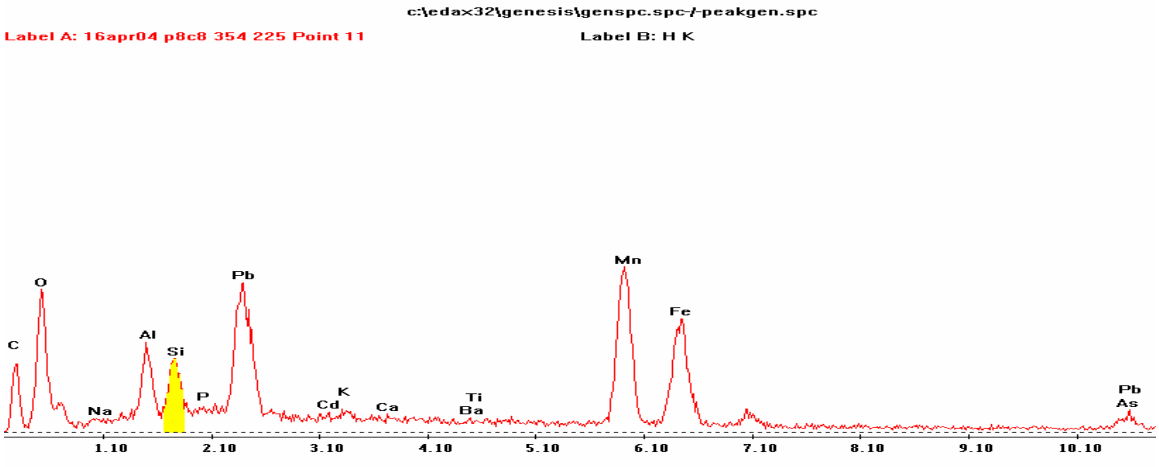

Point 12

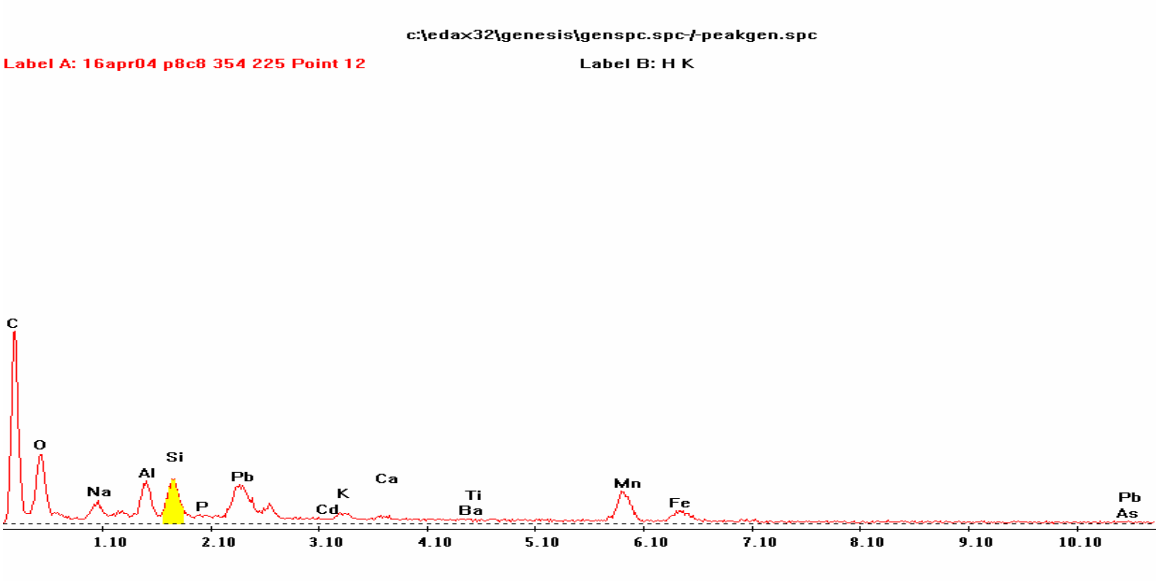
c:\edax32\genesis\genspc.spc-/-peakgen.spc
Label A: 16apr04 p8c8 354 225 Point 12
Label B: H K
C
O
Na
Al
Si
P
Pb
Cd
K
Ca
Ti
Ba
Mn
Fe
Pb
As
1.10
2.10
3.10
4.10
5.10
6.10
7.10
8.10
9.10
10.10

P8C8 – 361, 241

BSE Image

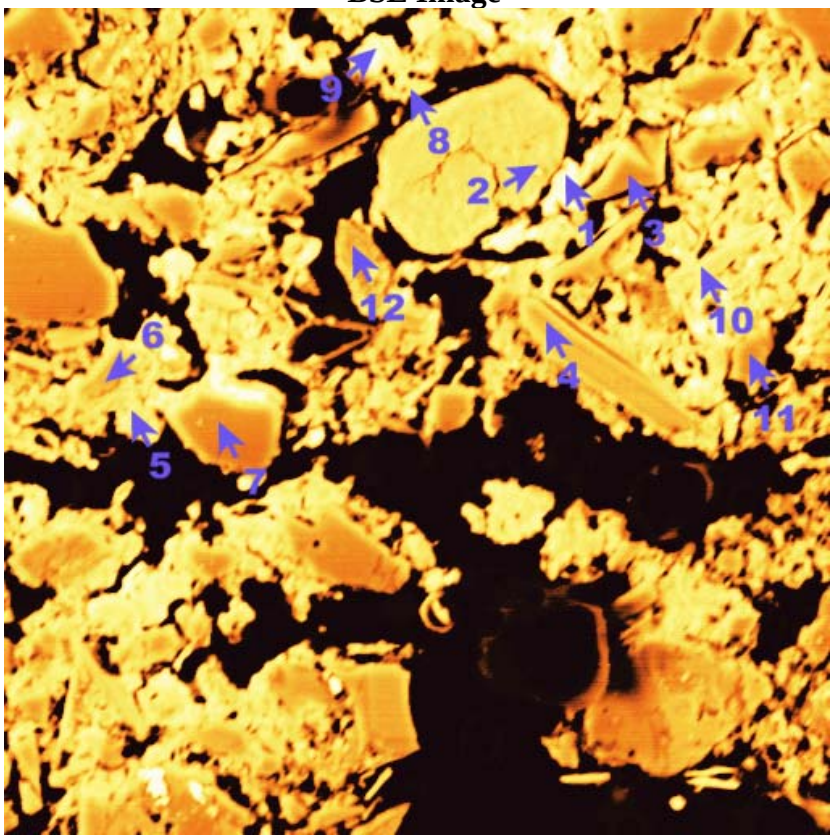

Iron (Fe)

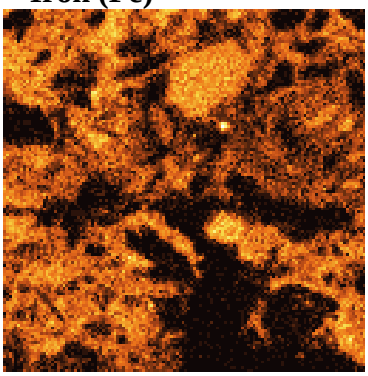

Manganese (Mn)

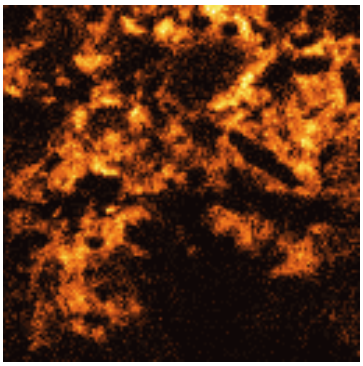

Phosphorous (P)

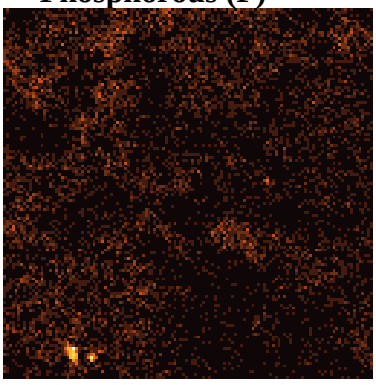

Lead (Pb)

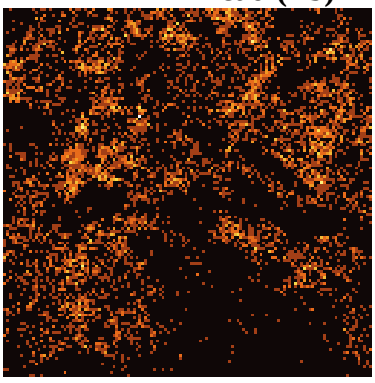

Silicon (Si)

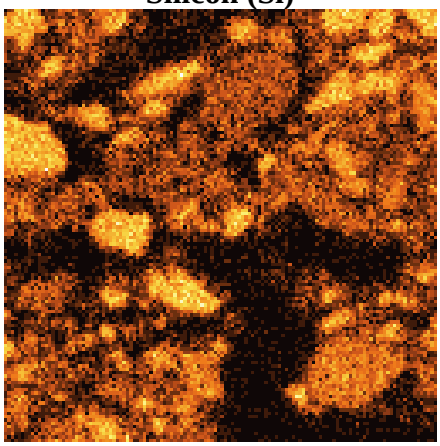

EDS Scan Images by Point

Point 1

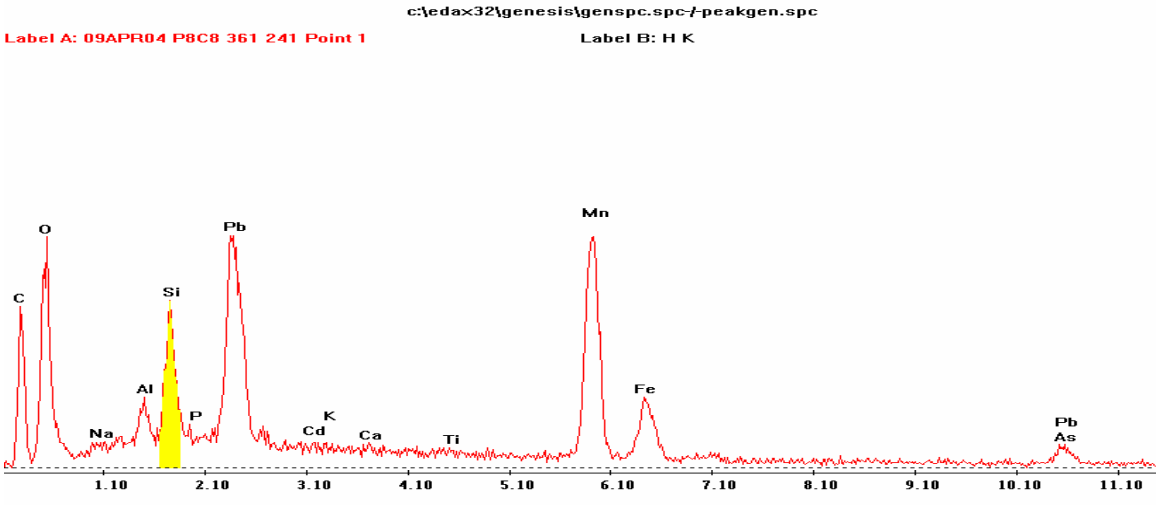

Point 2

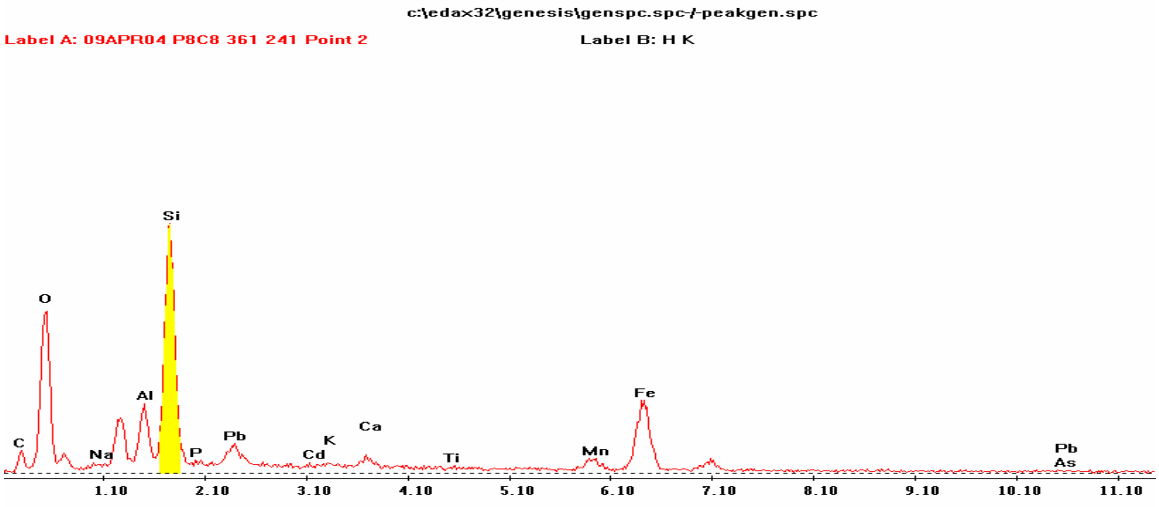

Point 3

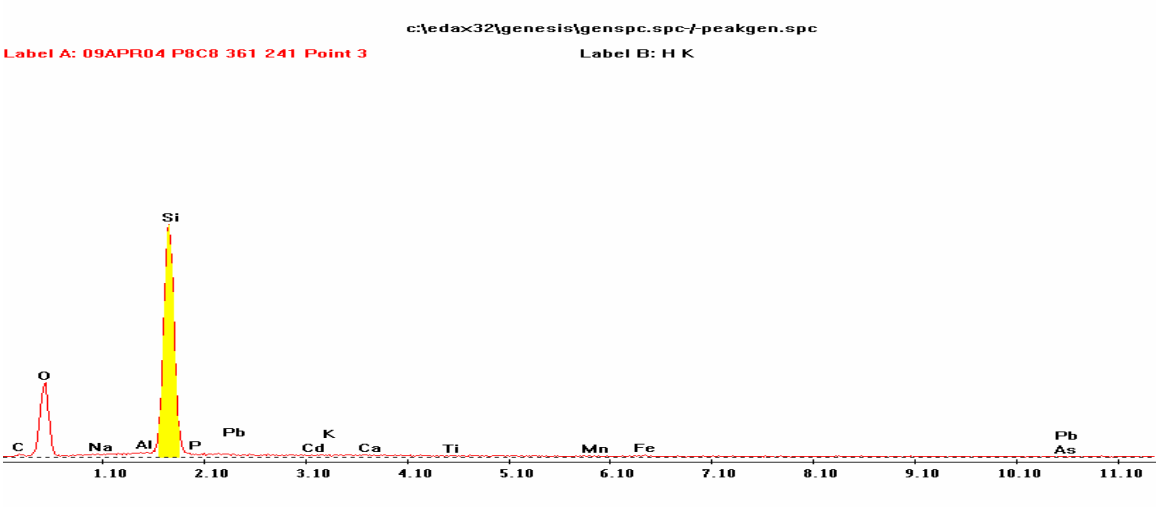

Point 4

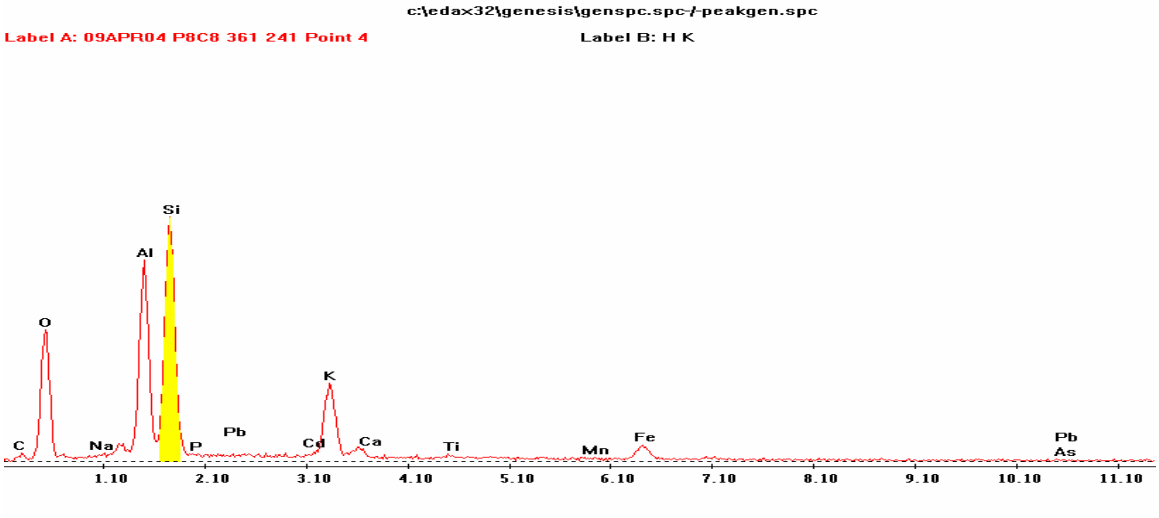

Point 5

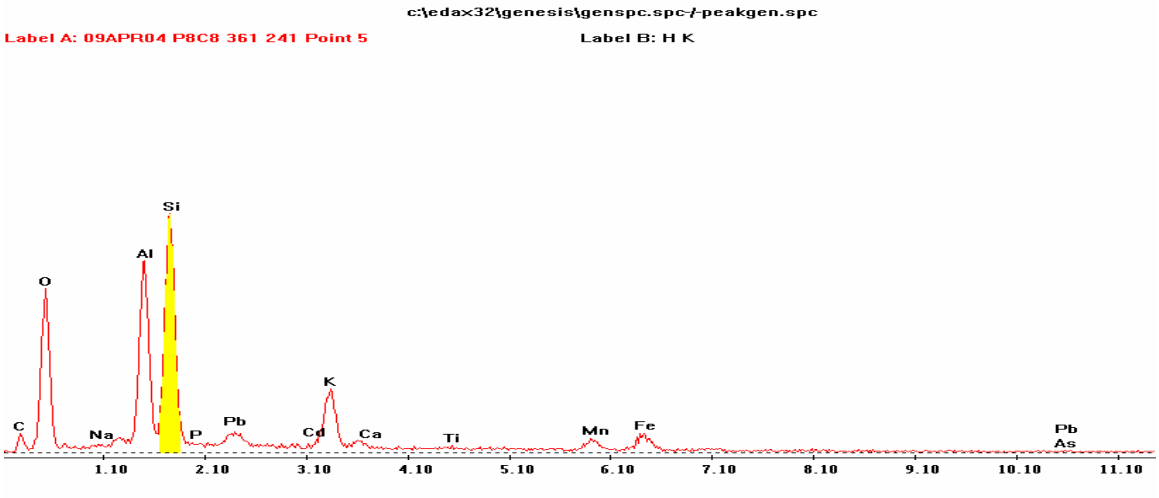

Point 6

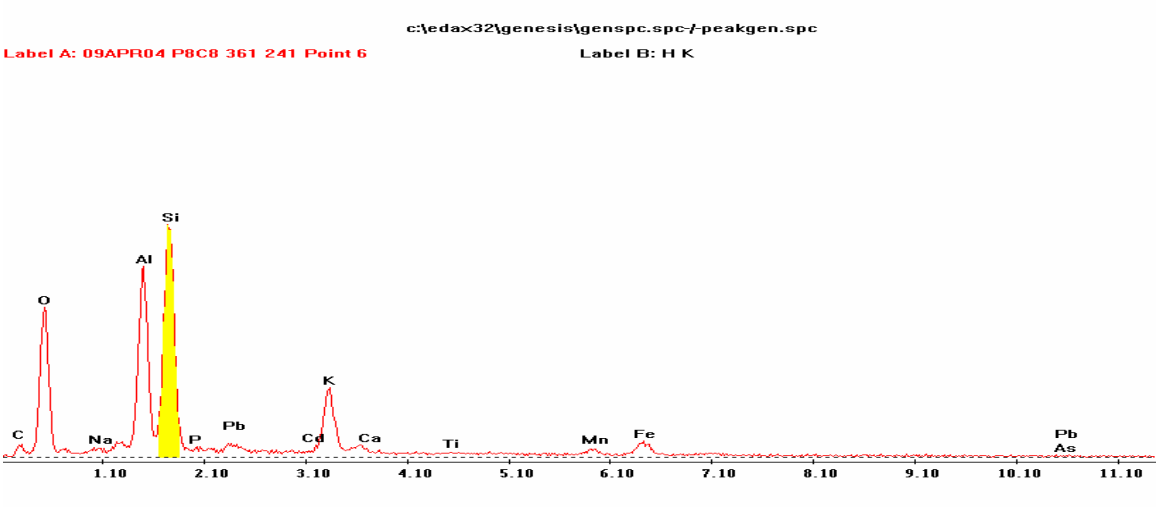

Point 7

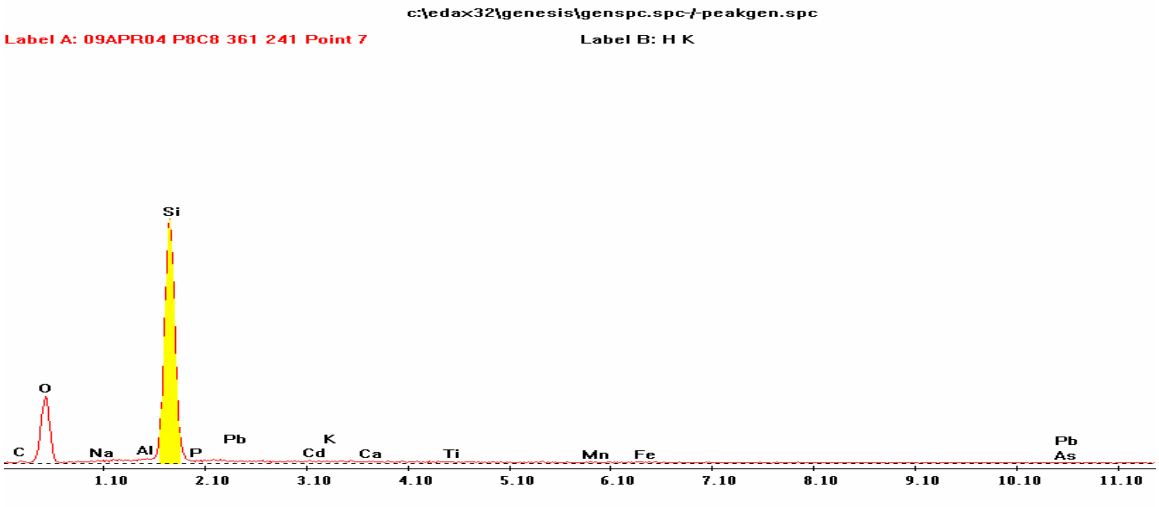

Point 8

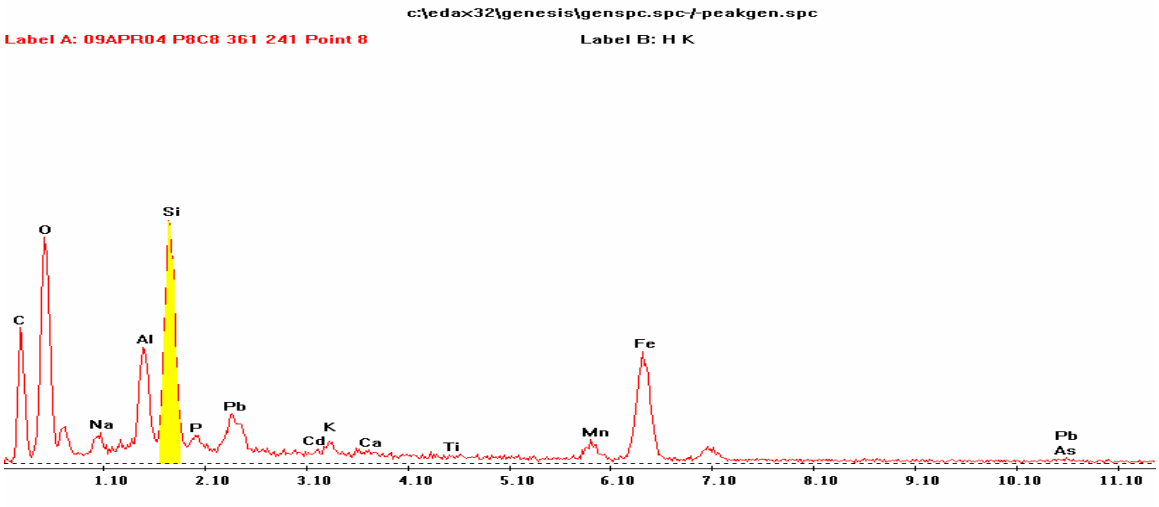

Point 9

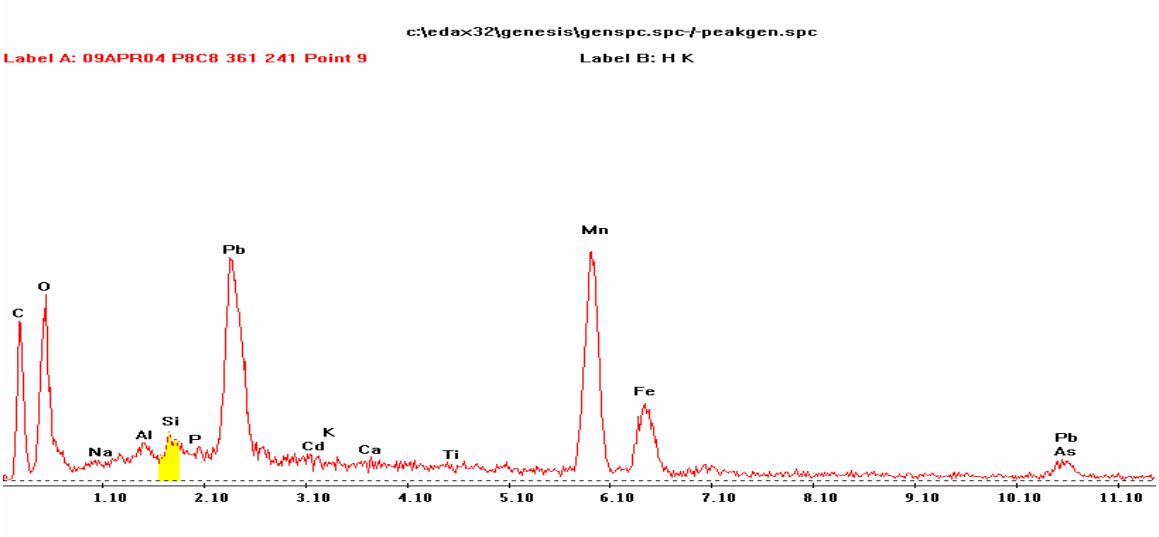

Point 10

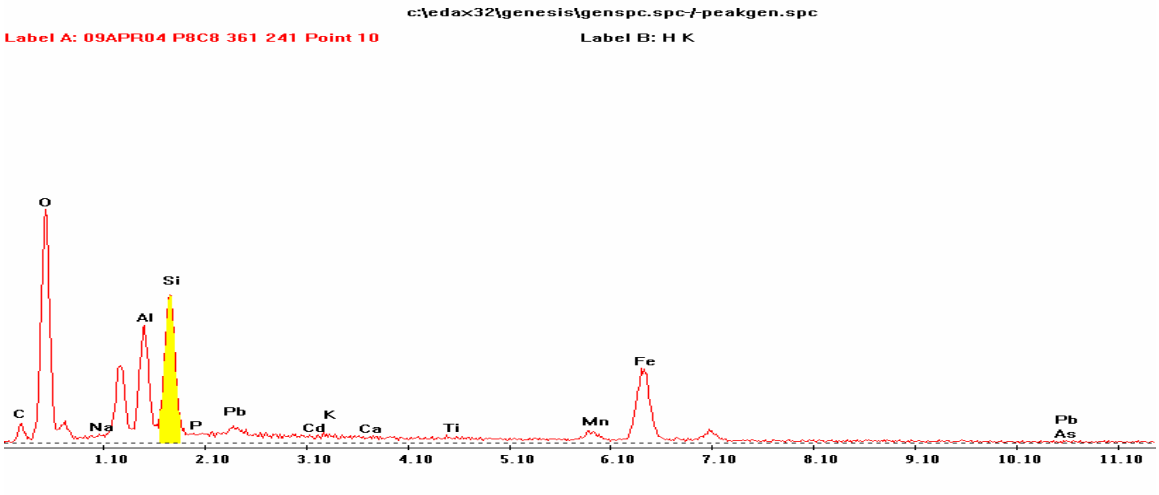

Point 11

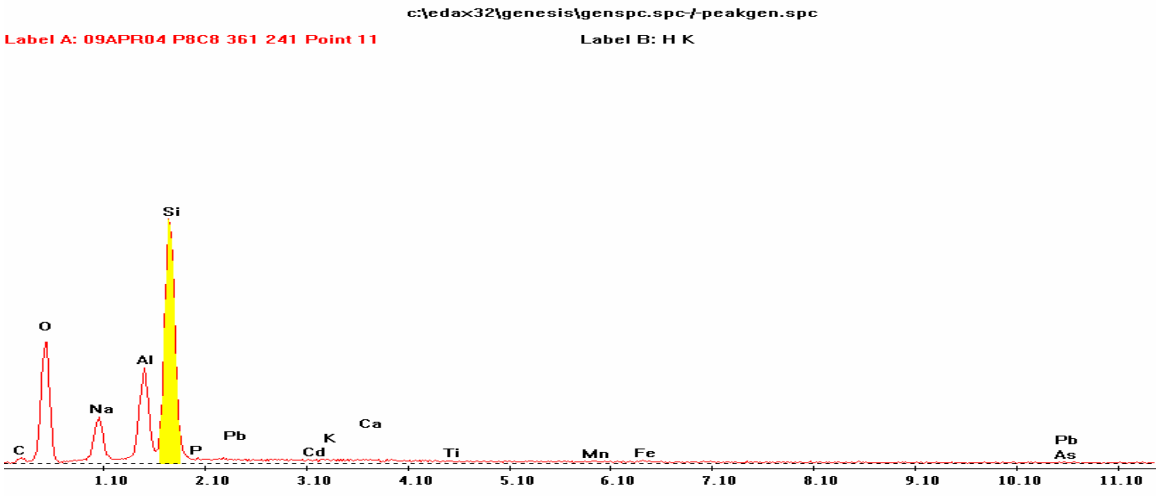

Point 12

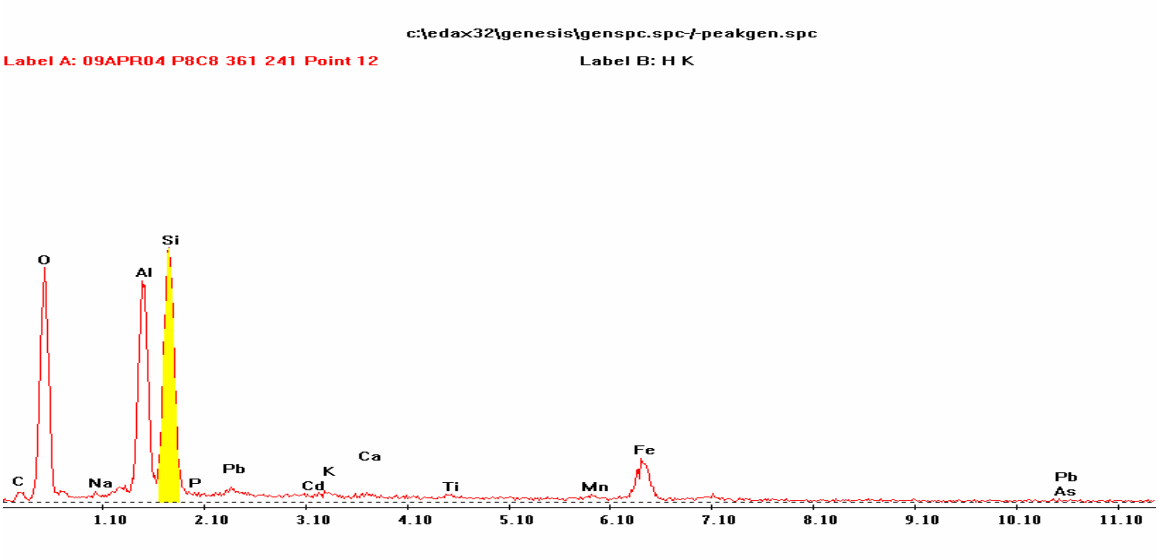
c:\edax32\genesis\genspc.spc-/-peakgen.spc
Label A: 09APR04 P8C8 361 241 Point 12
Label B: H K
O
Al
Si
C
Na
P
Pb
Cd
K
Ca
Ti
Mn
Fe
Pb
As
1.10
2.10
3.10
4.10
5.10
6.10
7.10
8.10
9.10
10.10
11.10

P8C8 – 395, 203

BSE Image

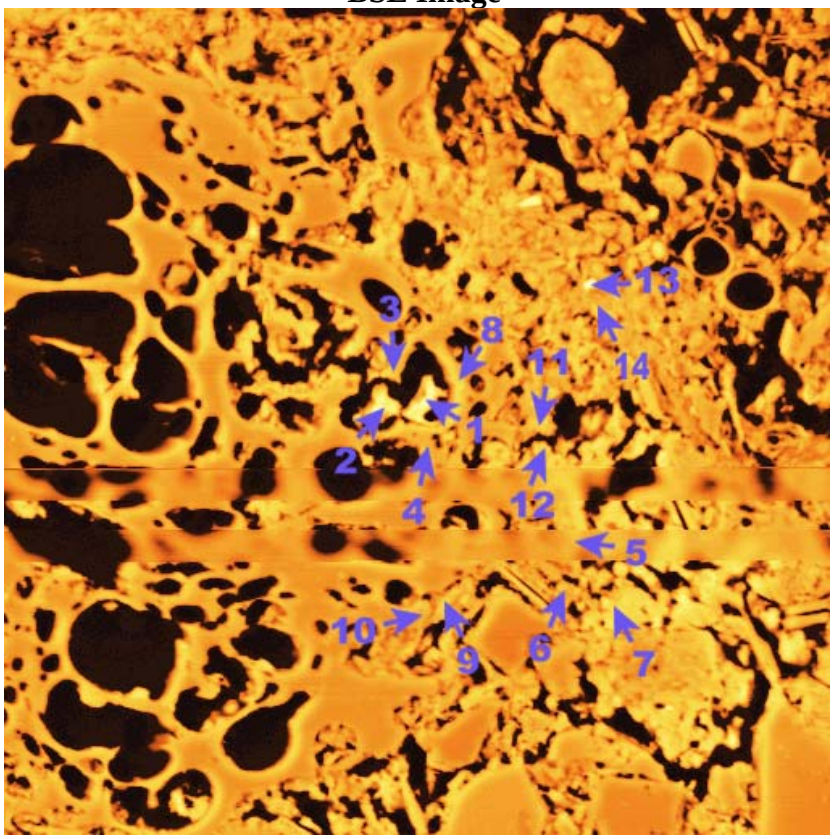

Iron (Fe)

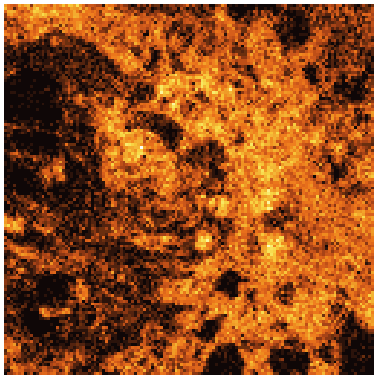

Manganese (Mn)

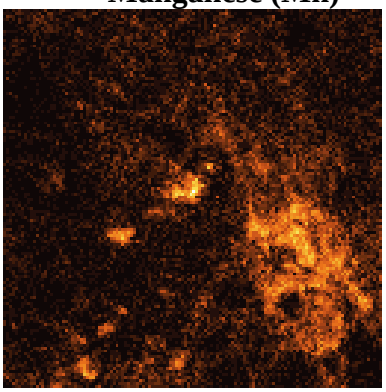

Phosphorous (P)

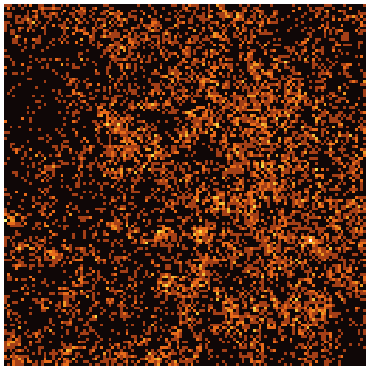

Lead (Pb)

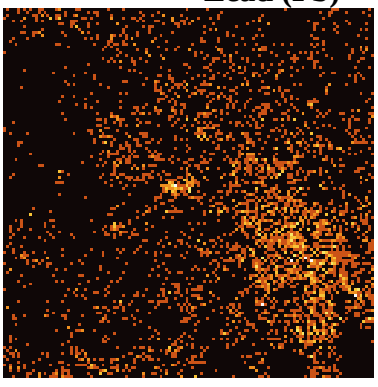

Silicon (Si)

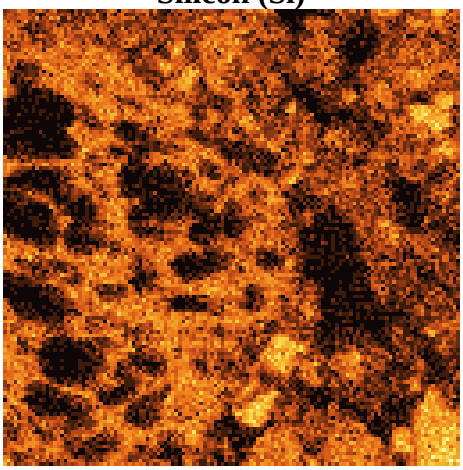

EDS Scan Images by Point

Point 1

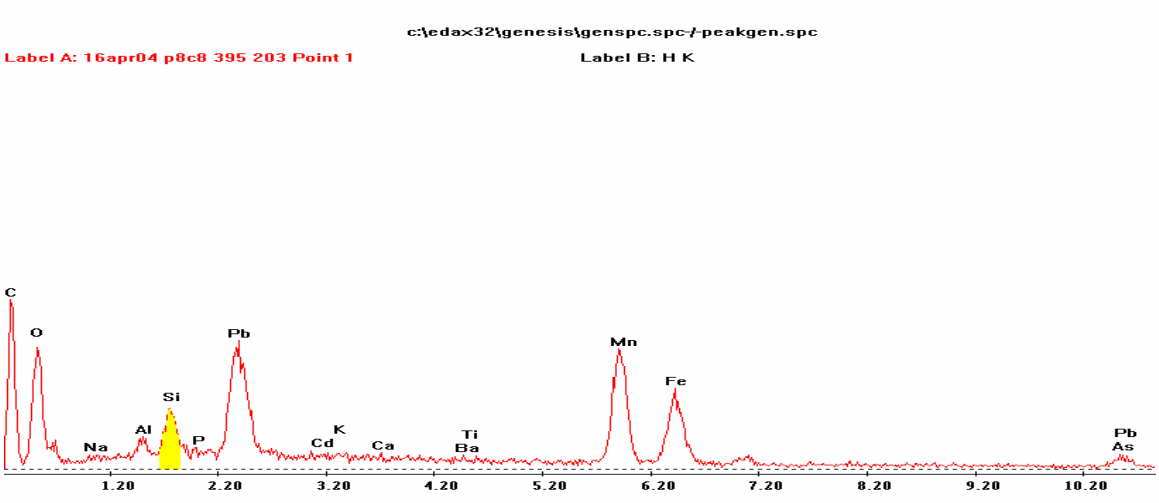

Point 2

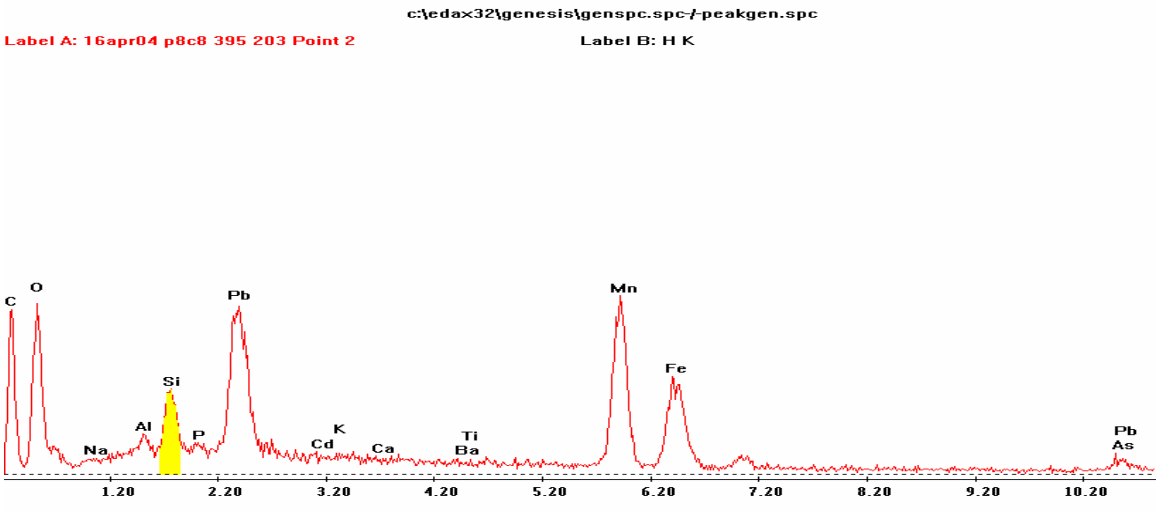

Point 3

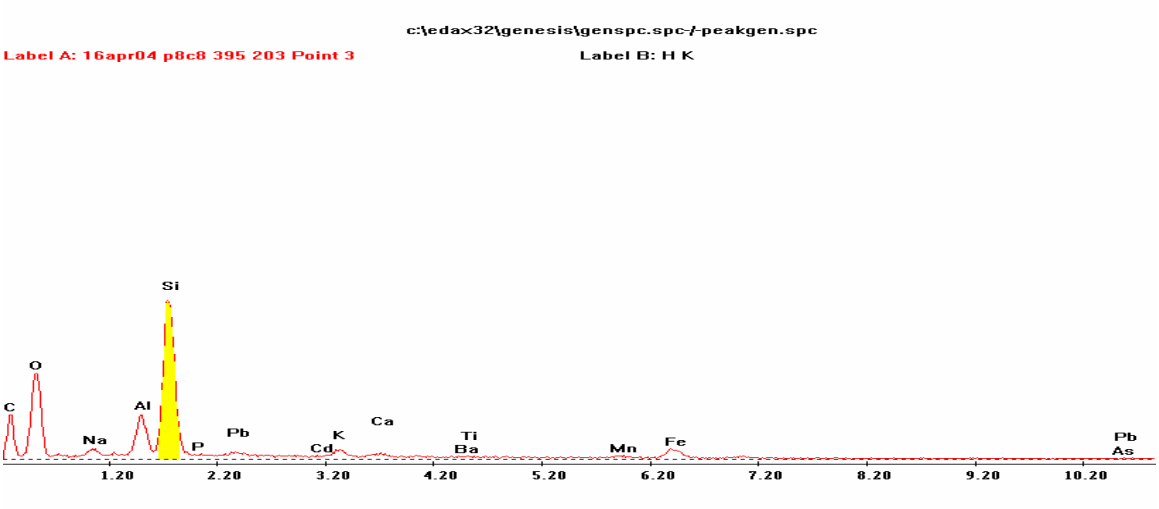

Point 4

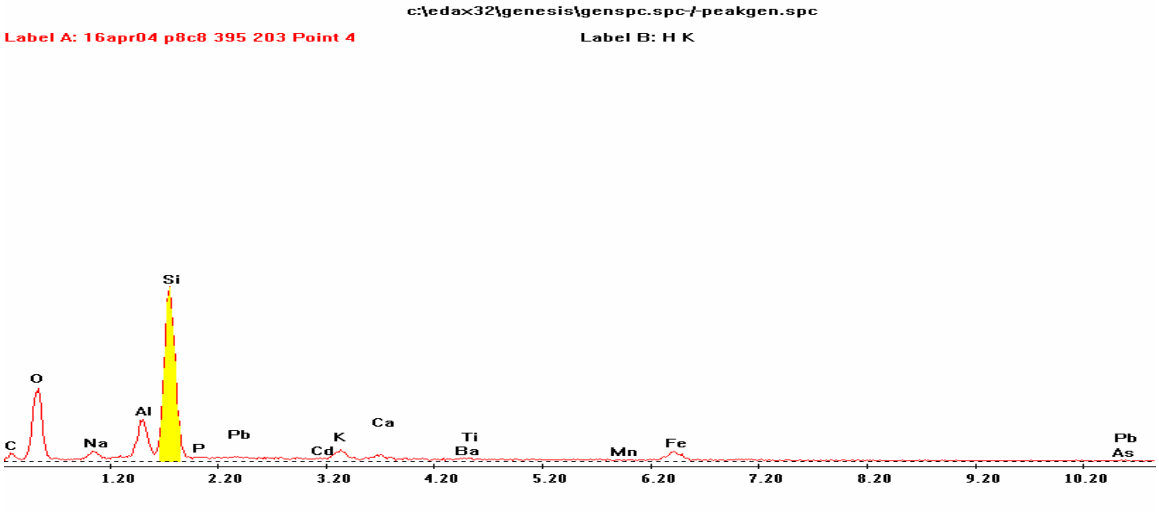

Point 5

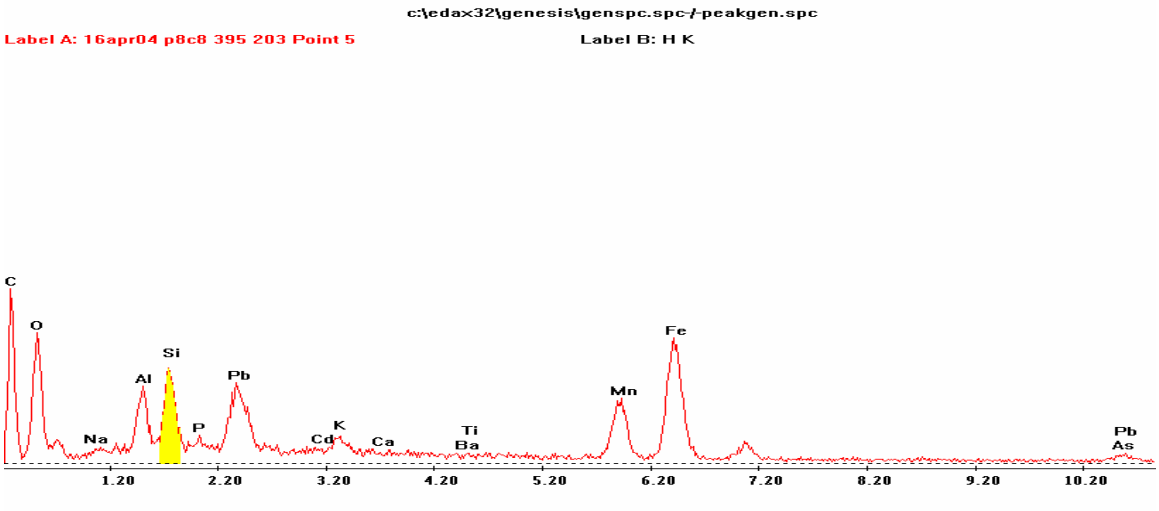

Point 6

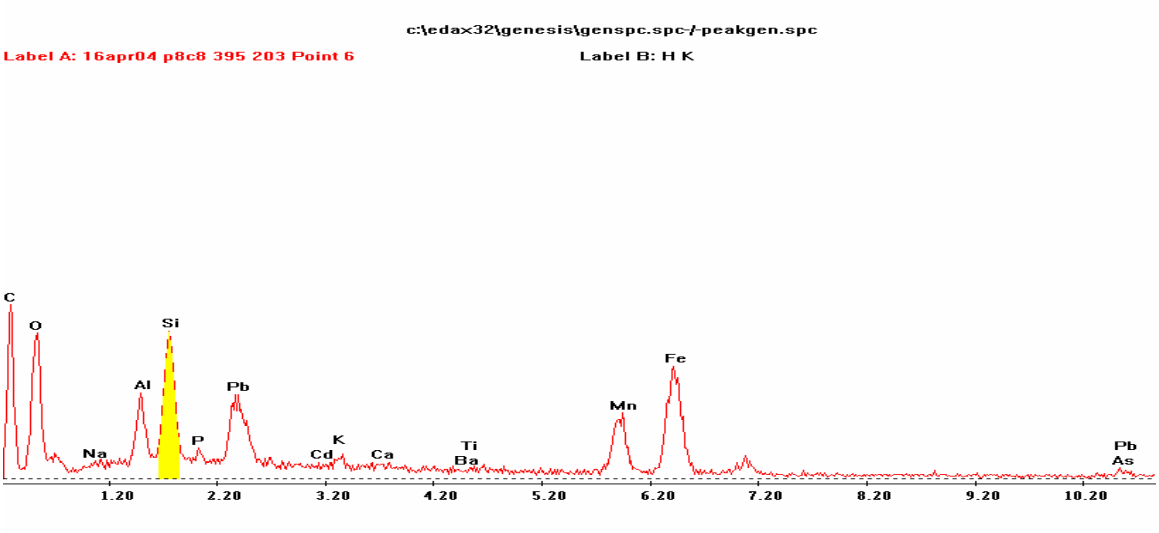

Point 7

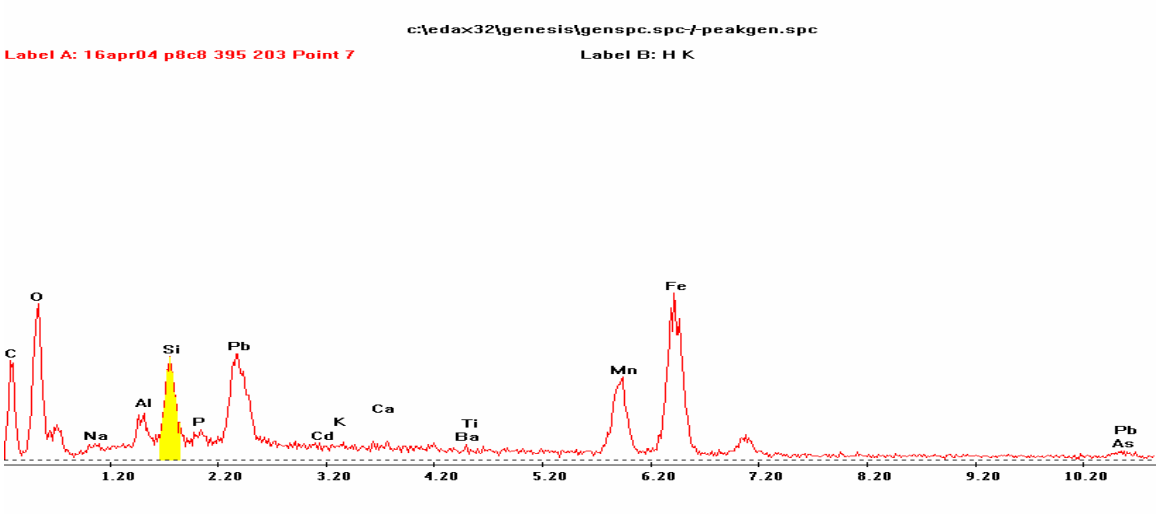

Point 8

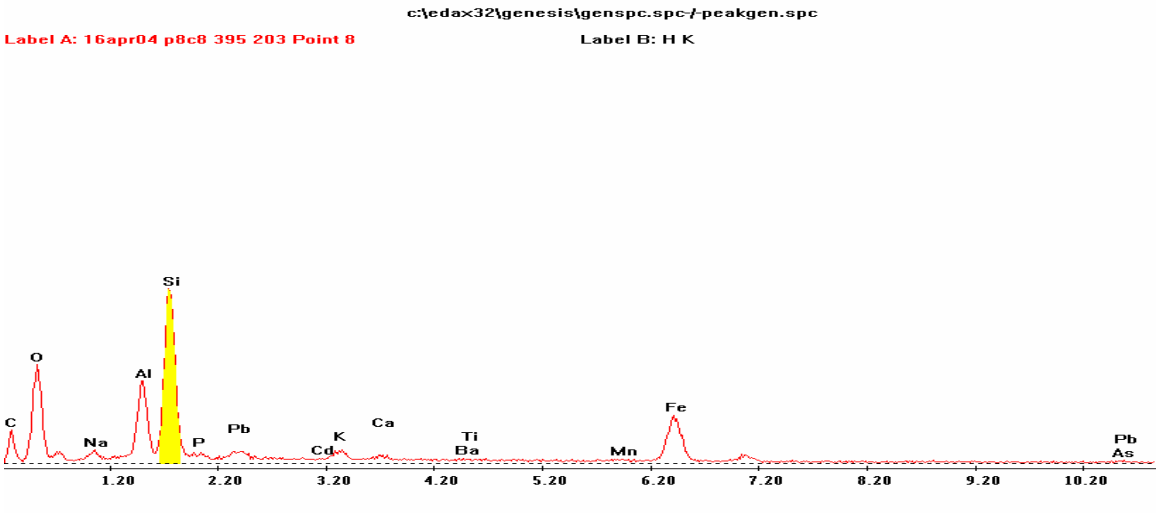

Point 9

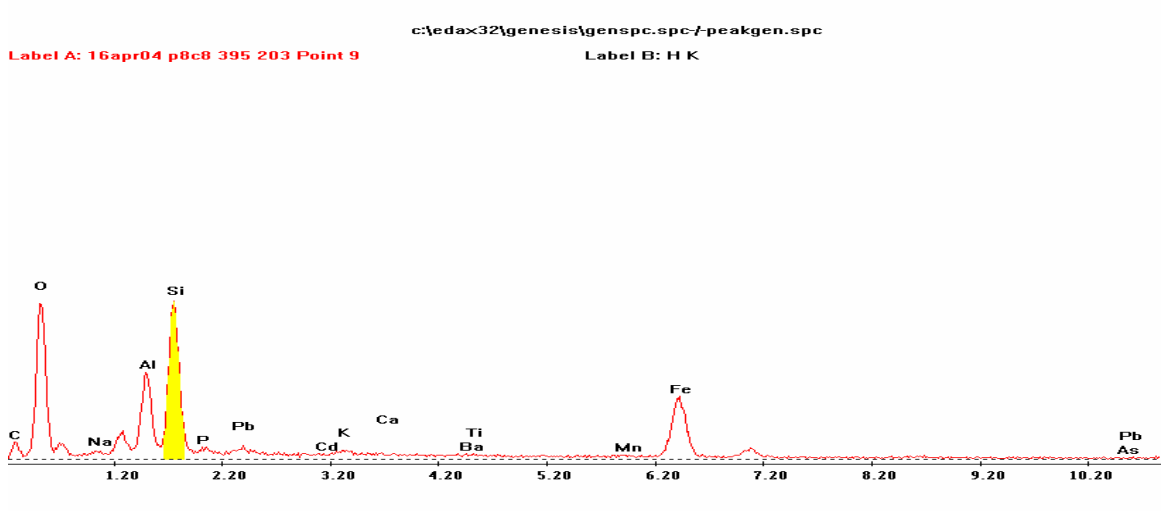

Point 10

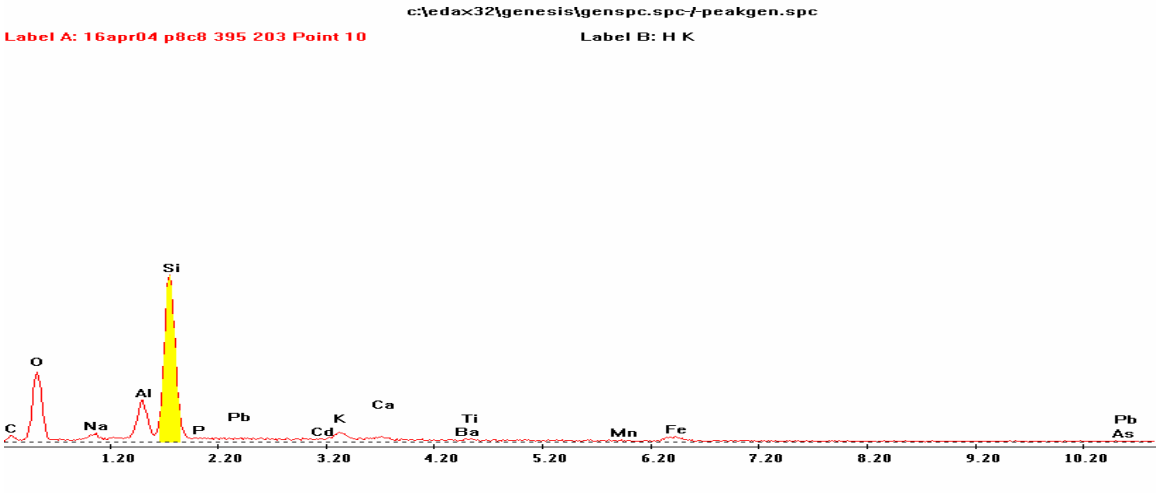

Point 11

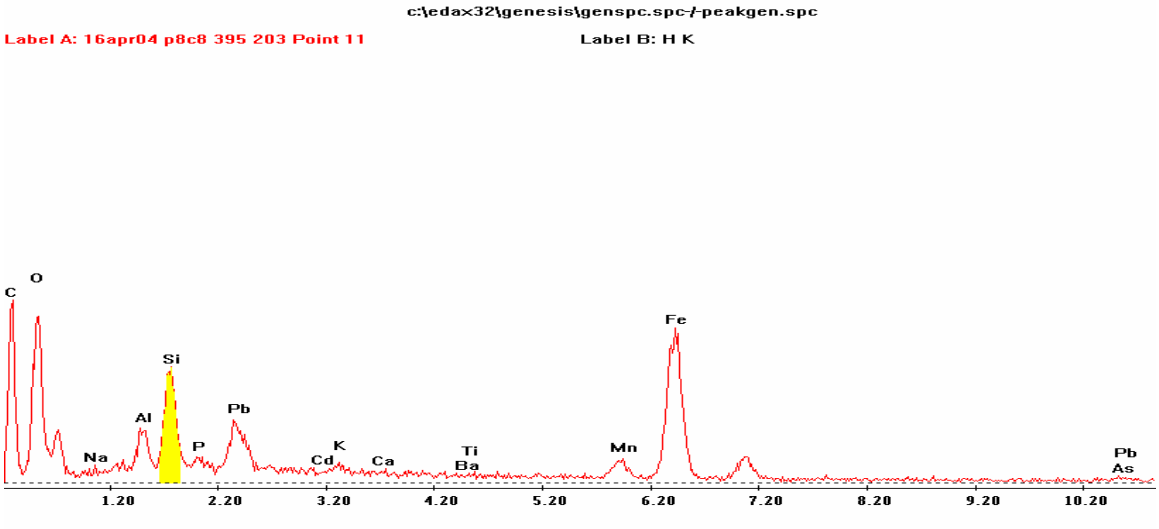

Point 12

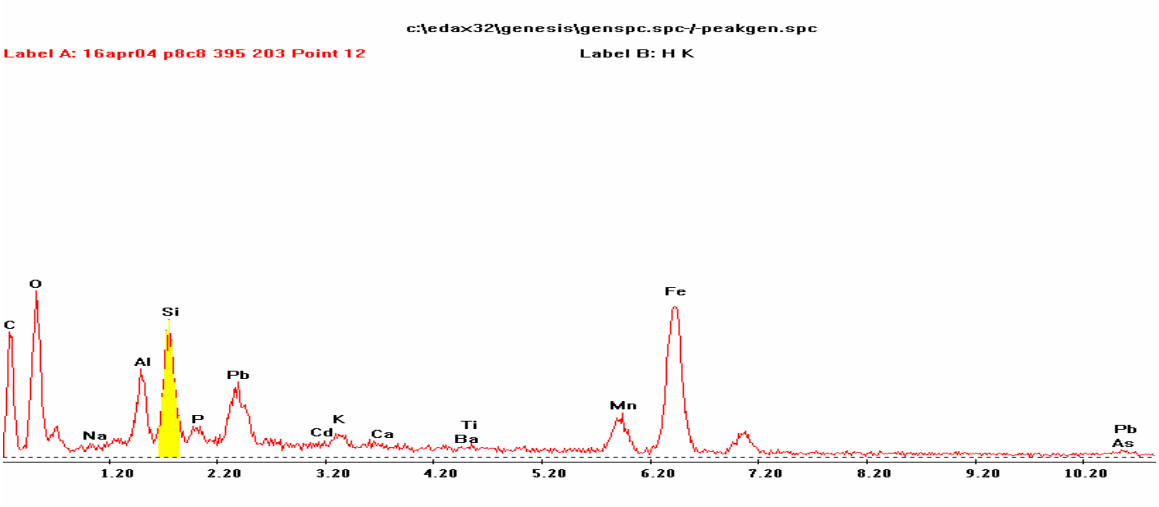

Point 13

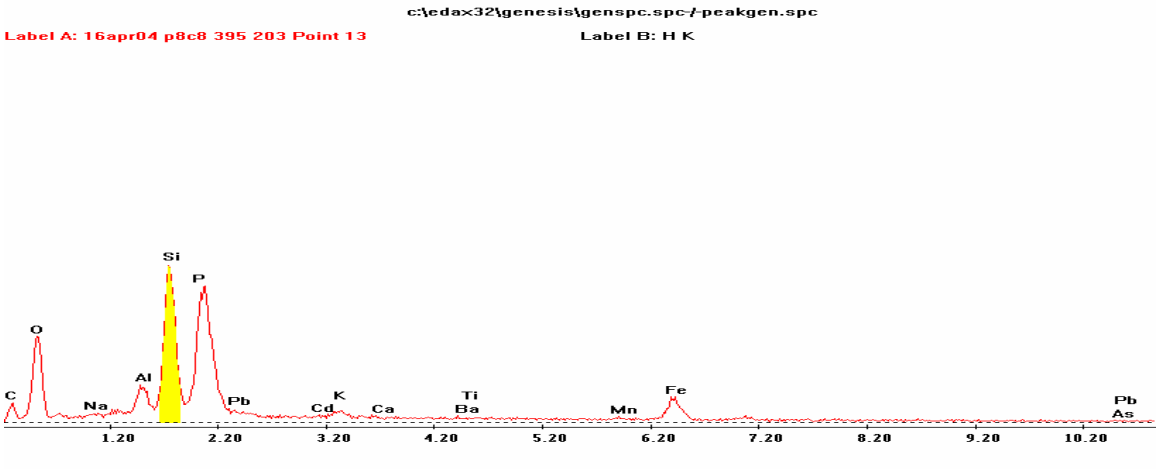

Point 14

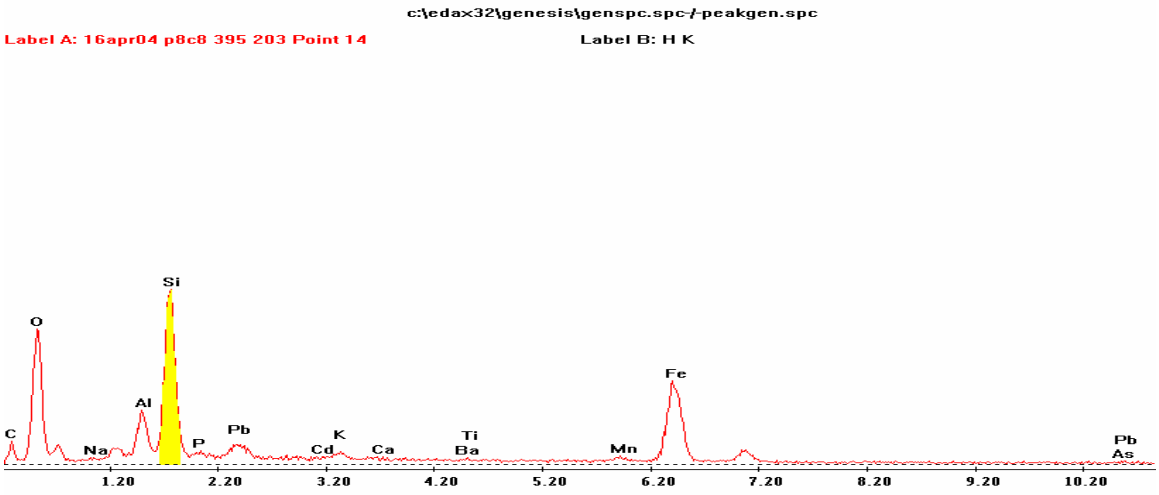

P8C8 – 399, 204

BSE Image

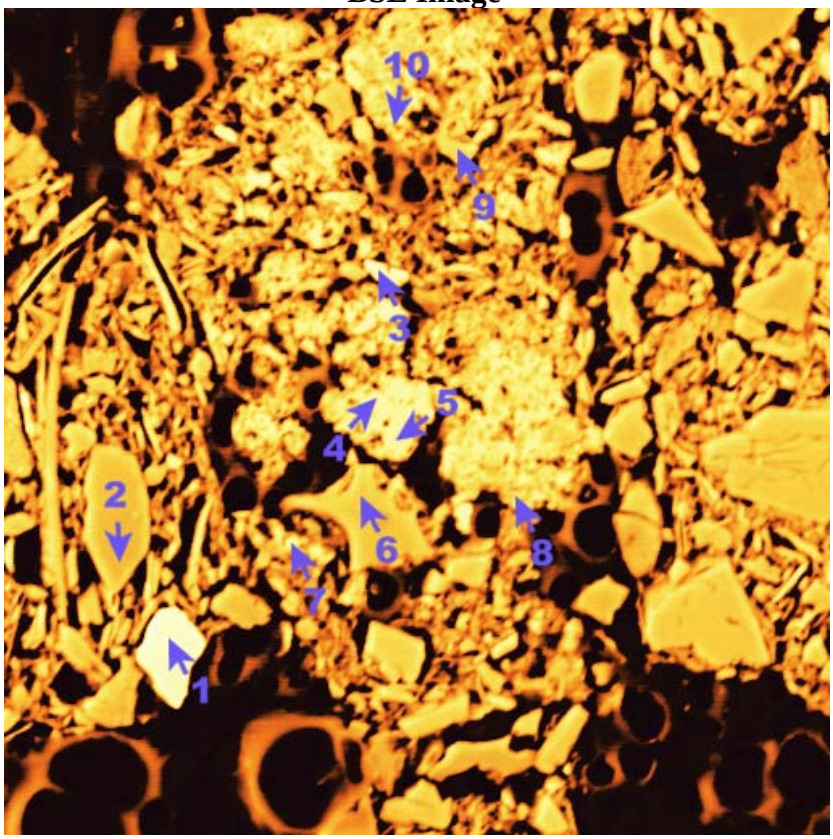

Iron (Fe)

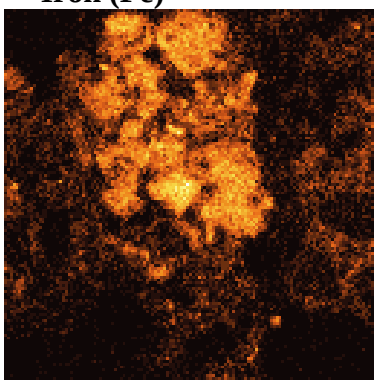

Manganese (Mn)

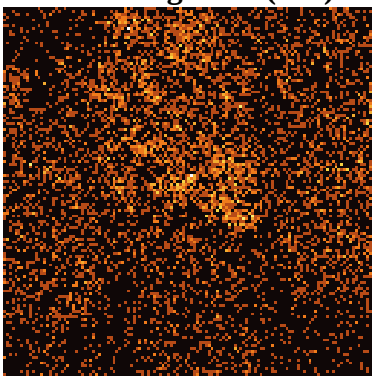

Phosphorous (P)

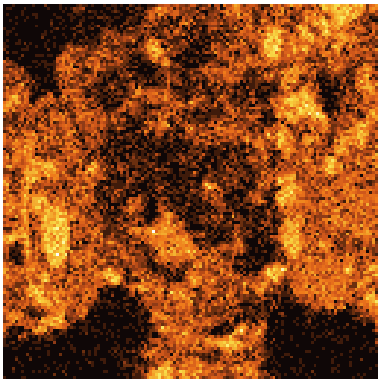

Lead (Pb)

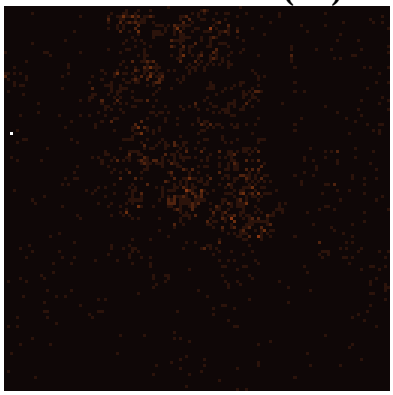

Silicon (Si)

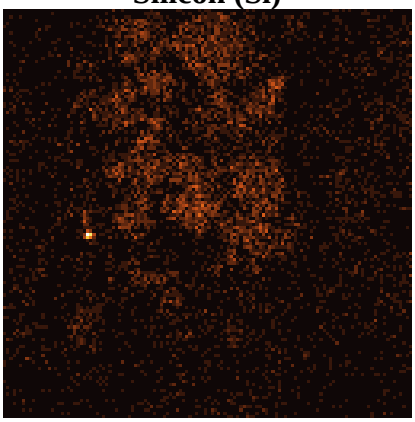

EDS Scan Images by Point

Point 1

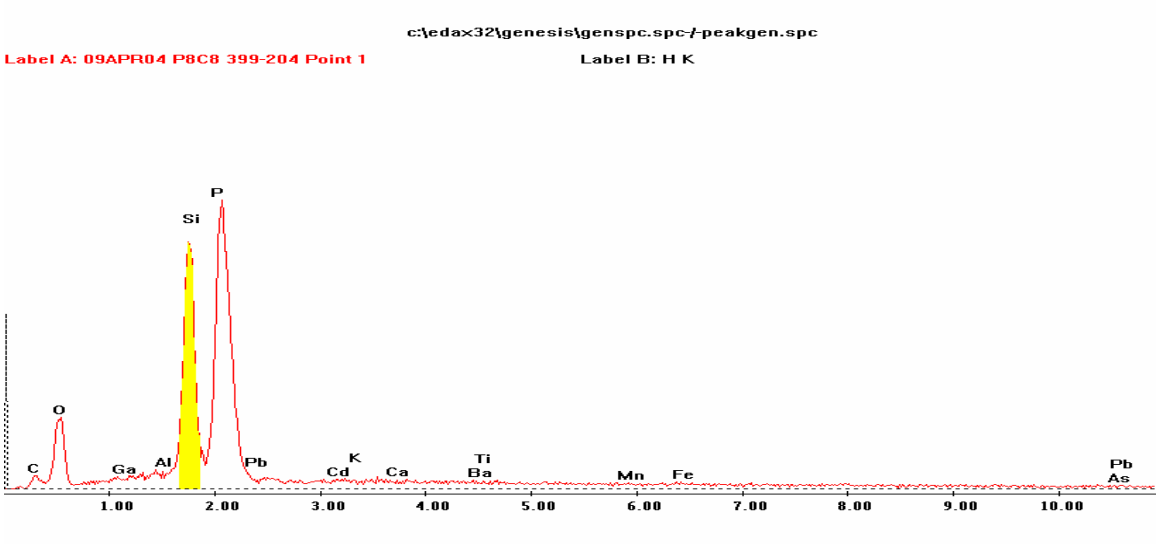

Point 2

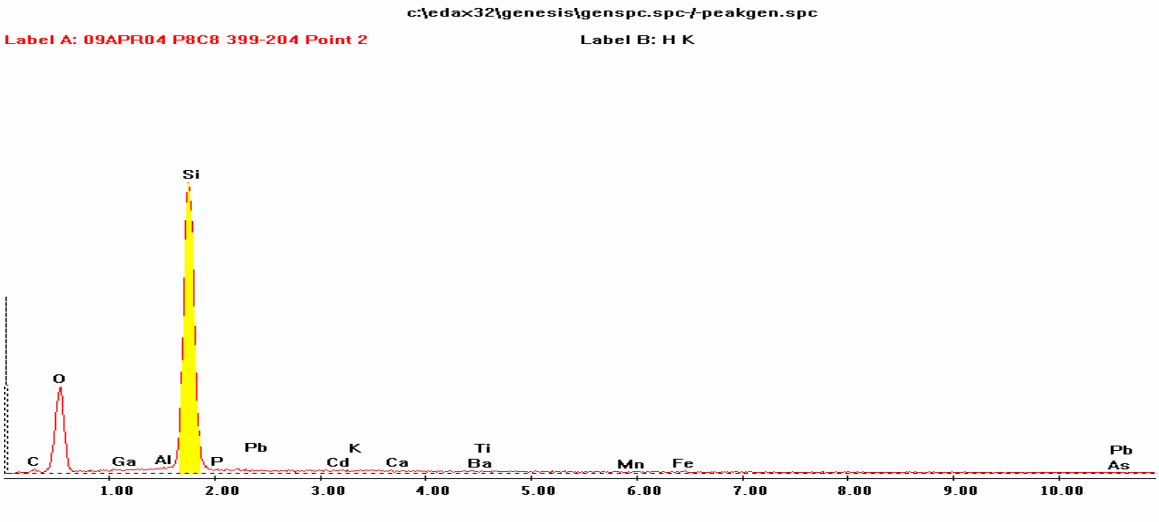

Point 3

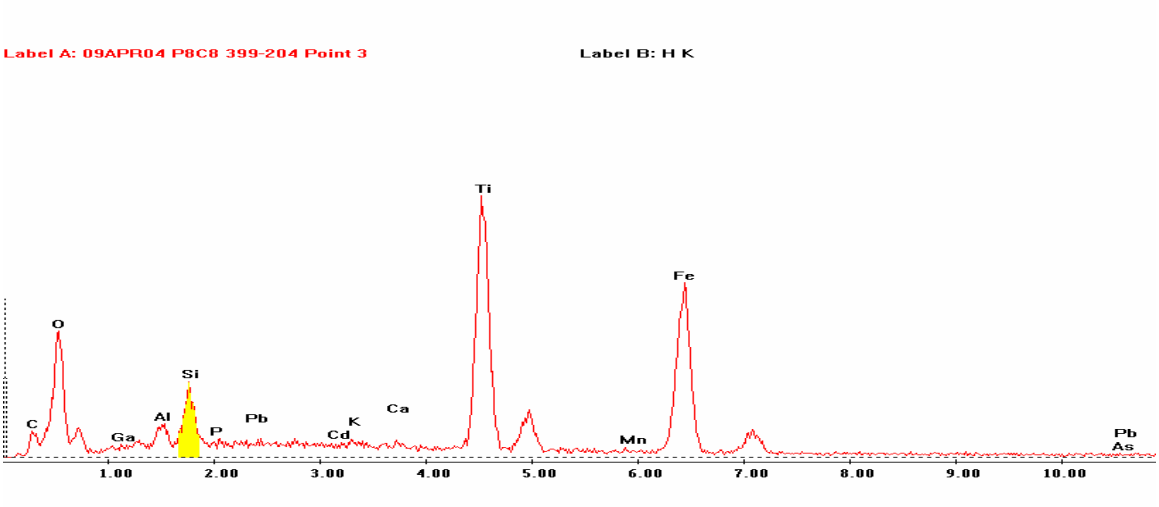

Point 4

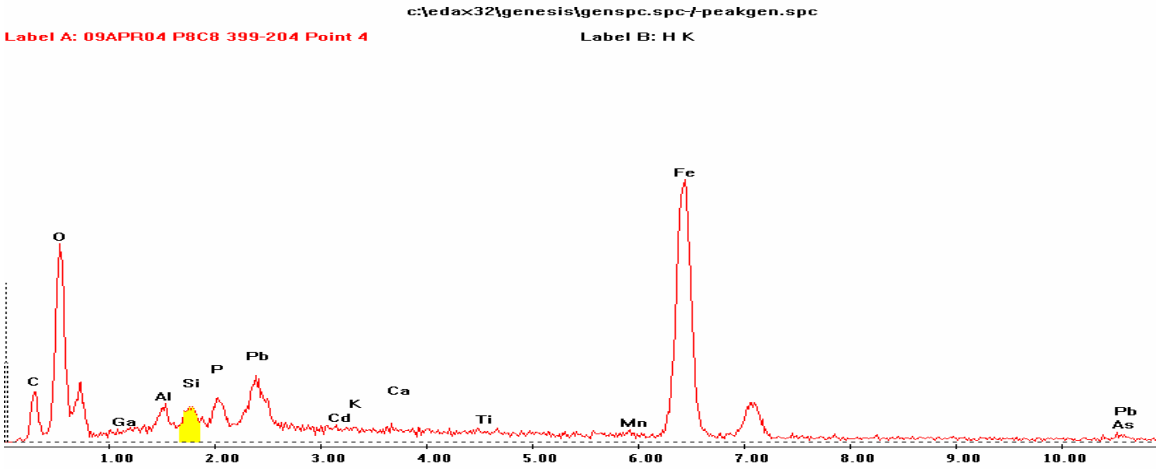

Point 5

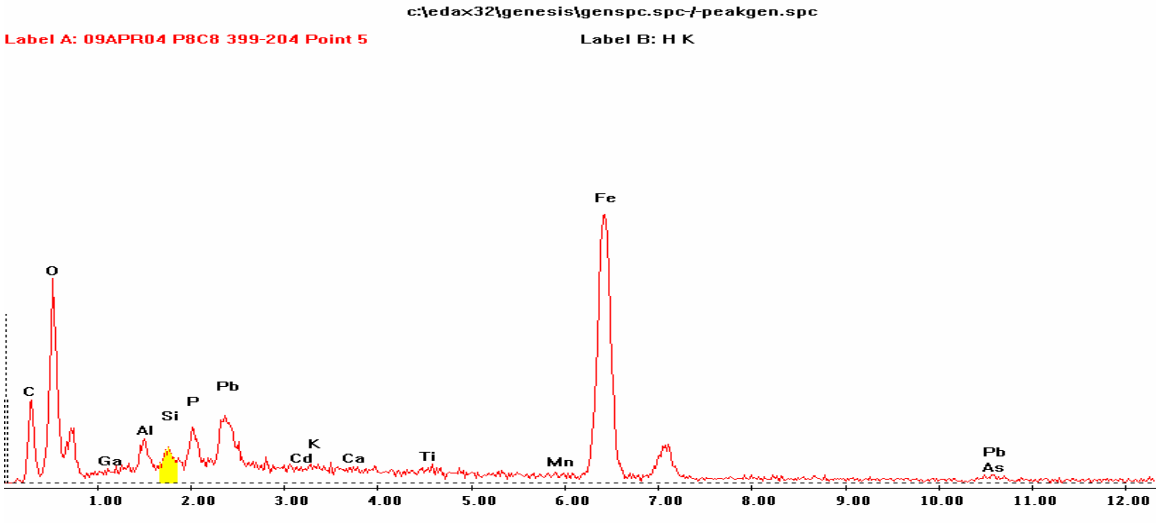

Point 6

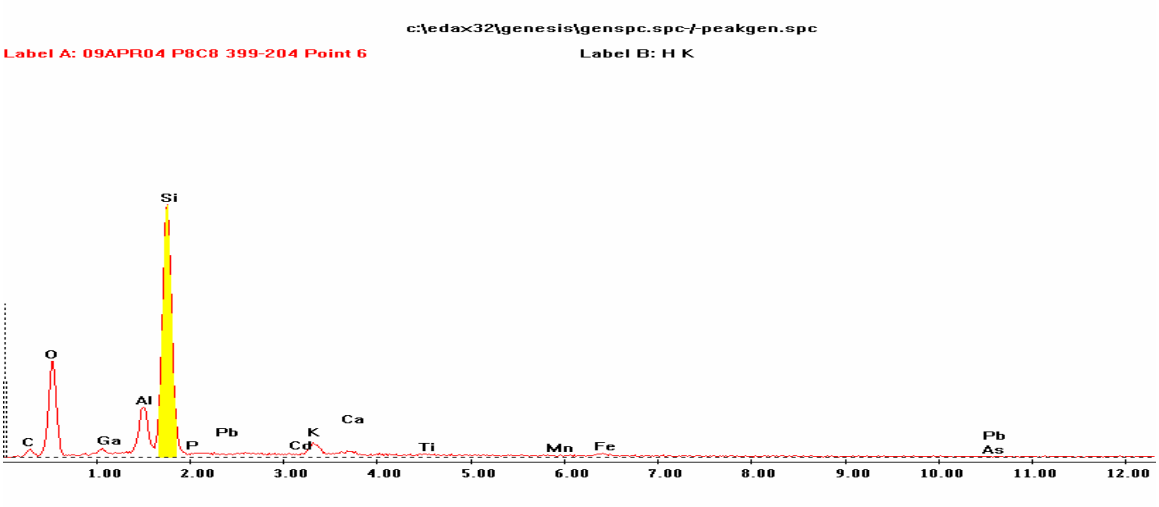

Point 7

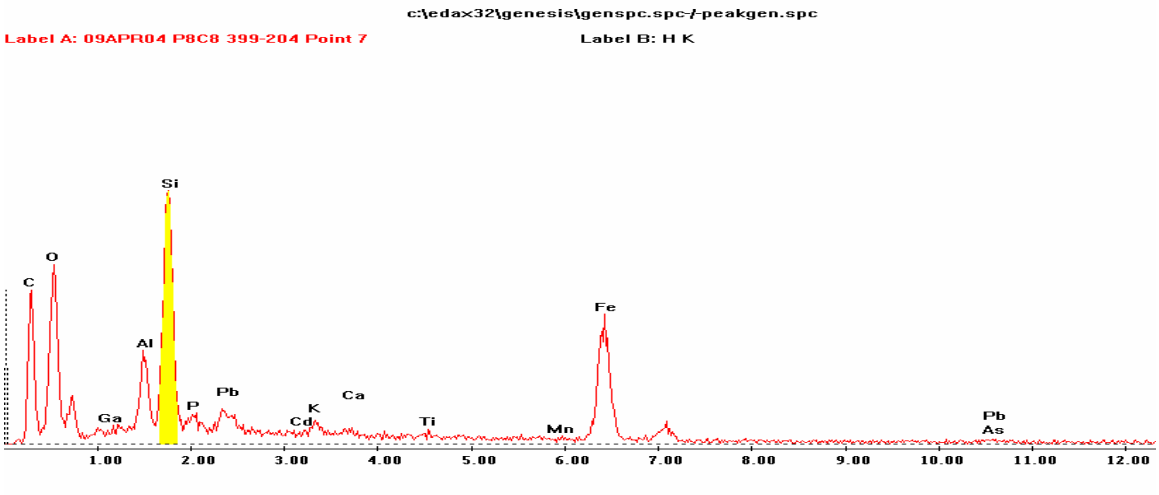

Point 8

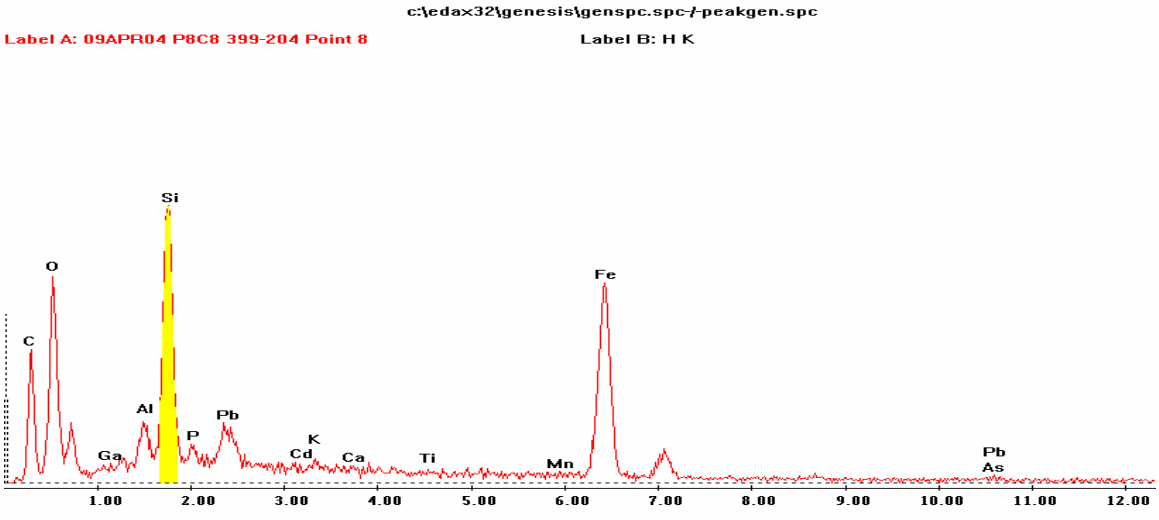

Point 9

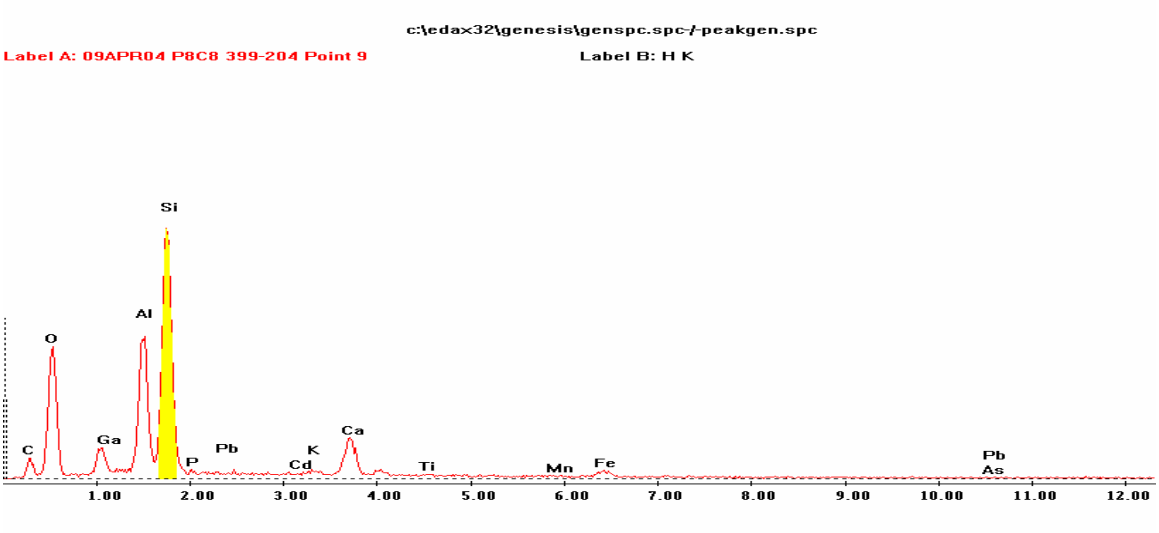

Point 10

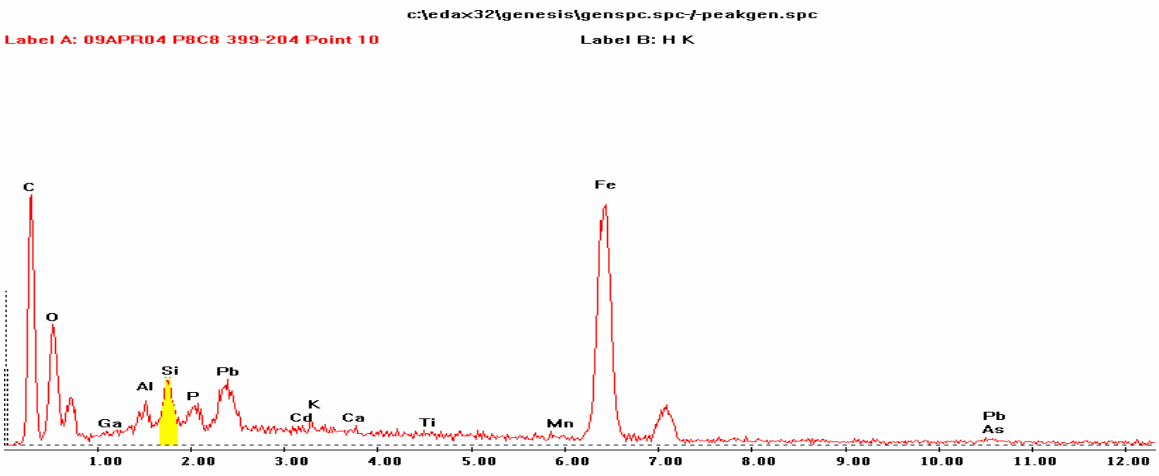

P8C8 – 413, 208

BSE Image

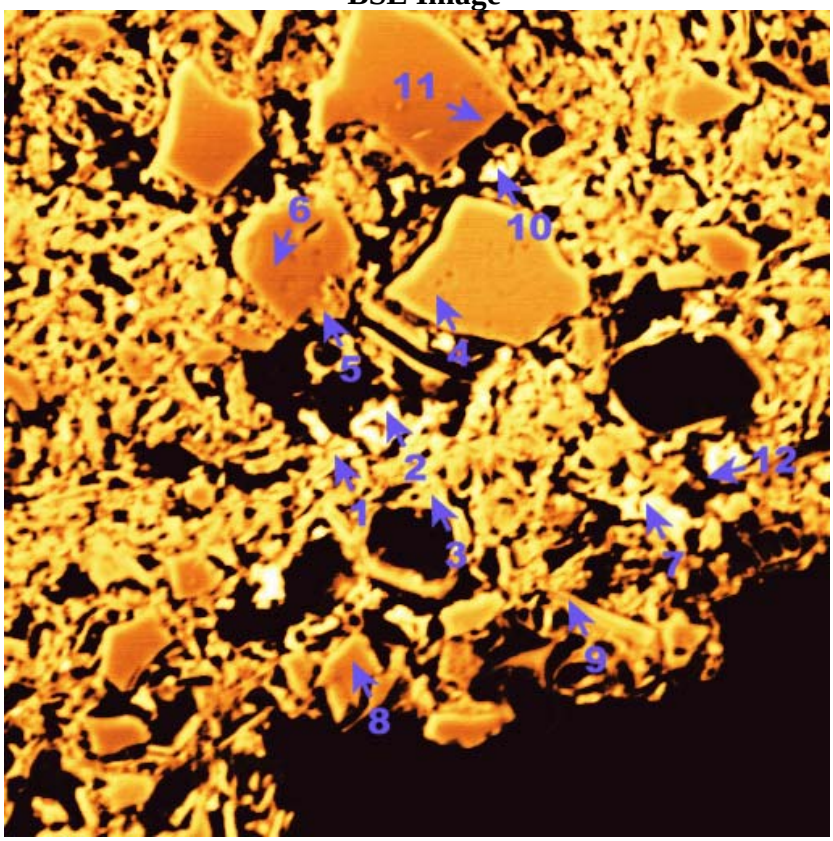

Iron (Fe)

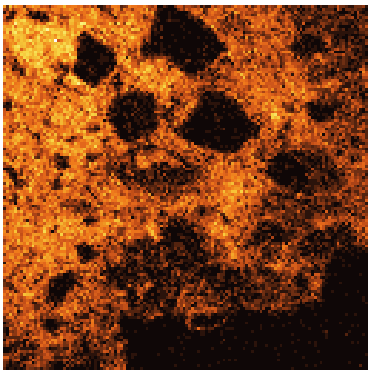

Manganese (Mn)

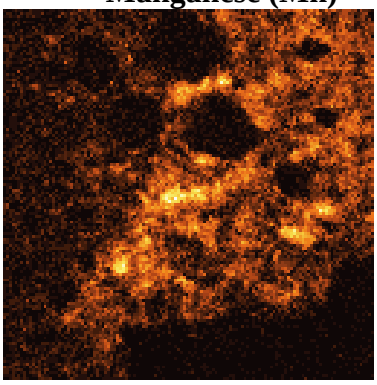

Silicon (Si)

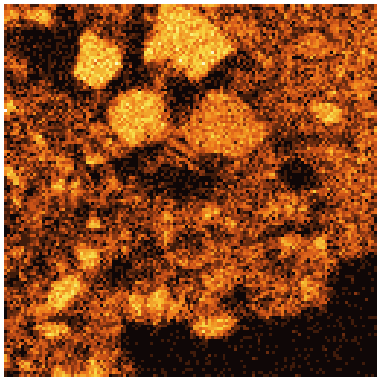

Lead (Pb)

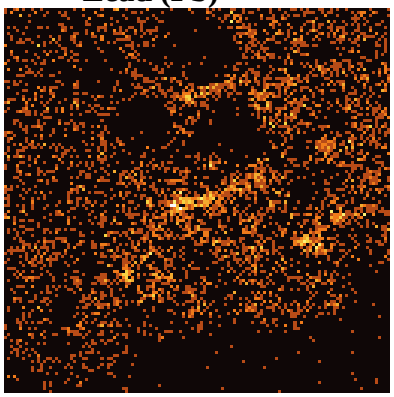

Phosphorus (P)

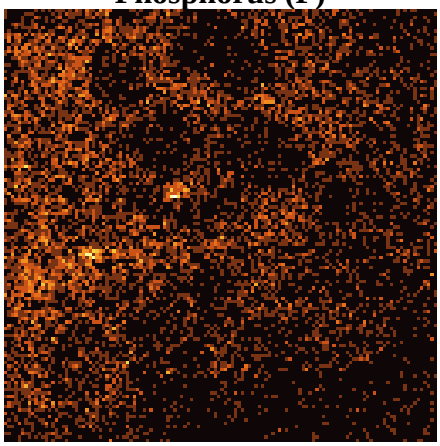

EDS Scan Images by Point

Point 1

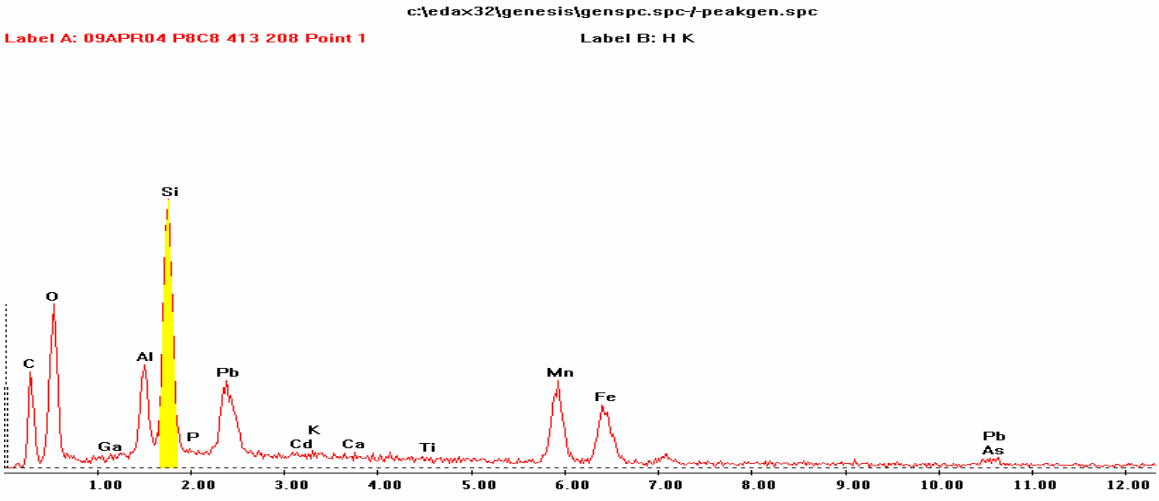

Point 2

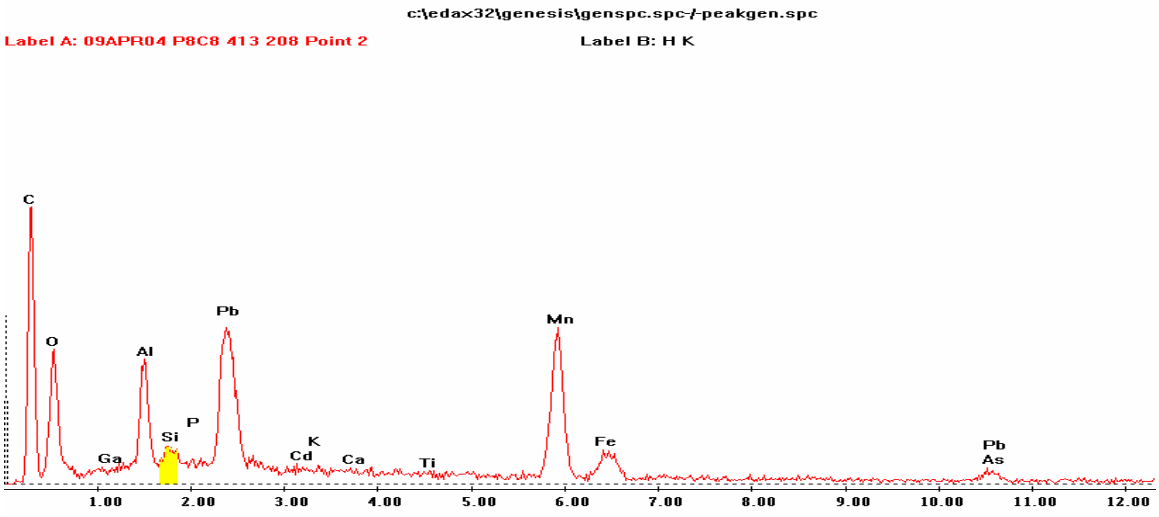

Point 3

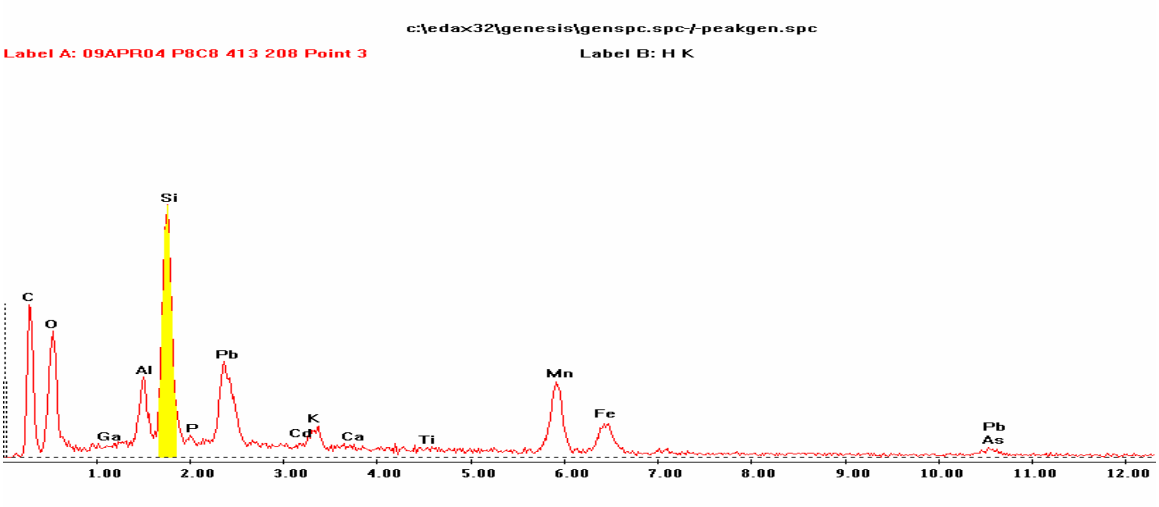

Point 4

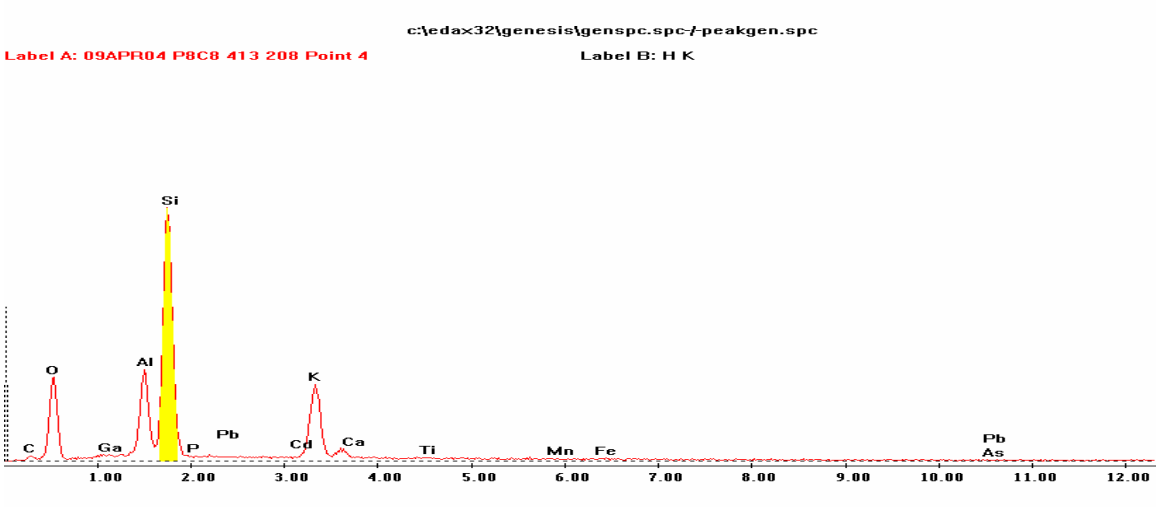

Point 5

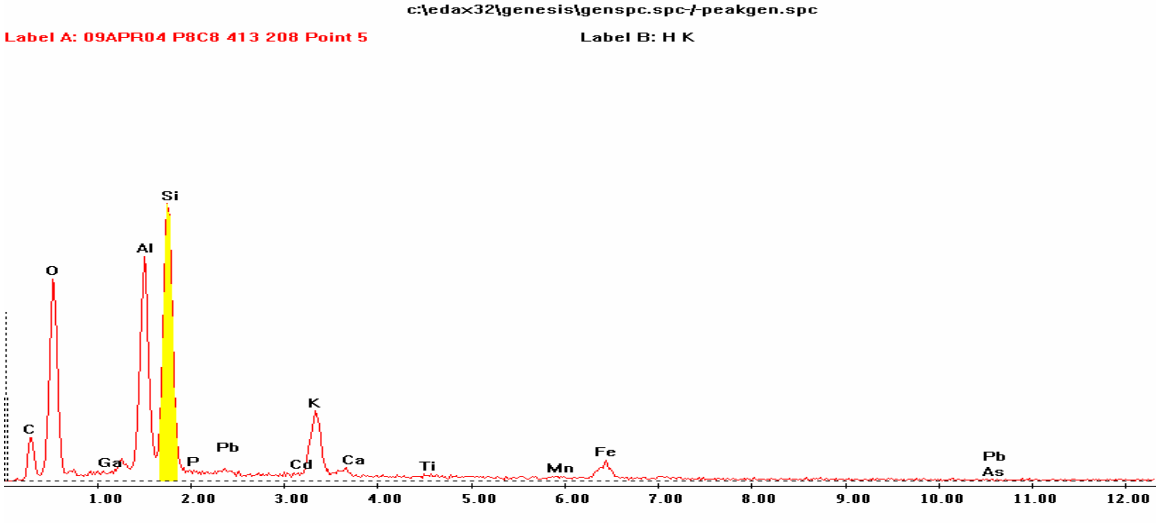

Point 6

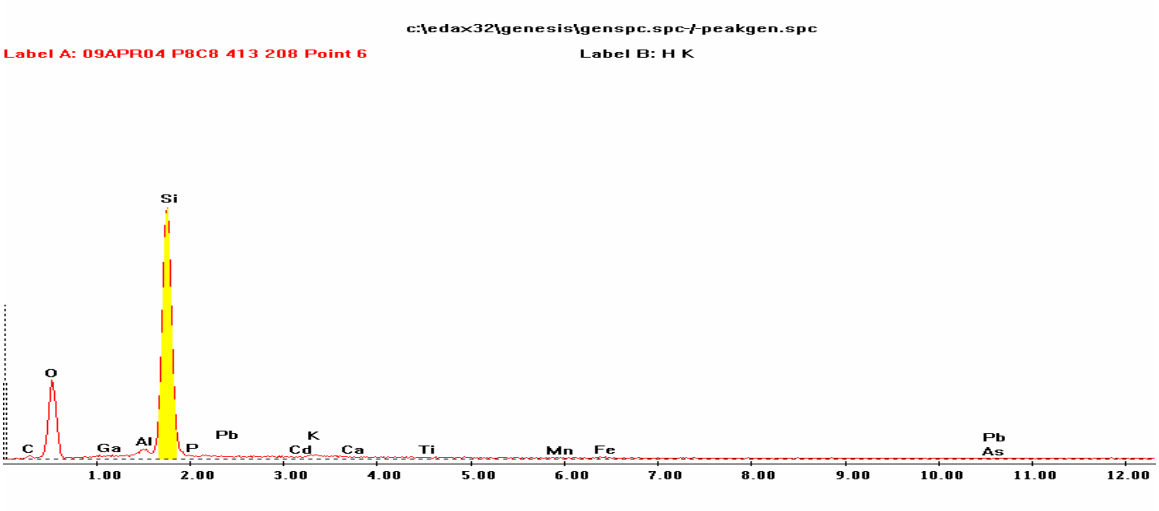

Point 7

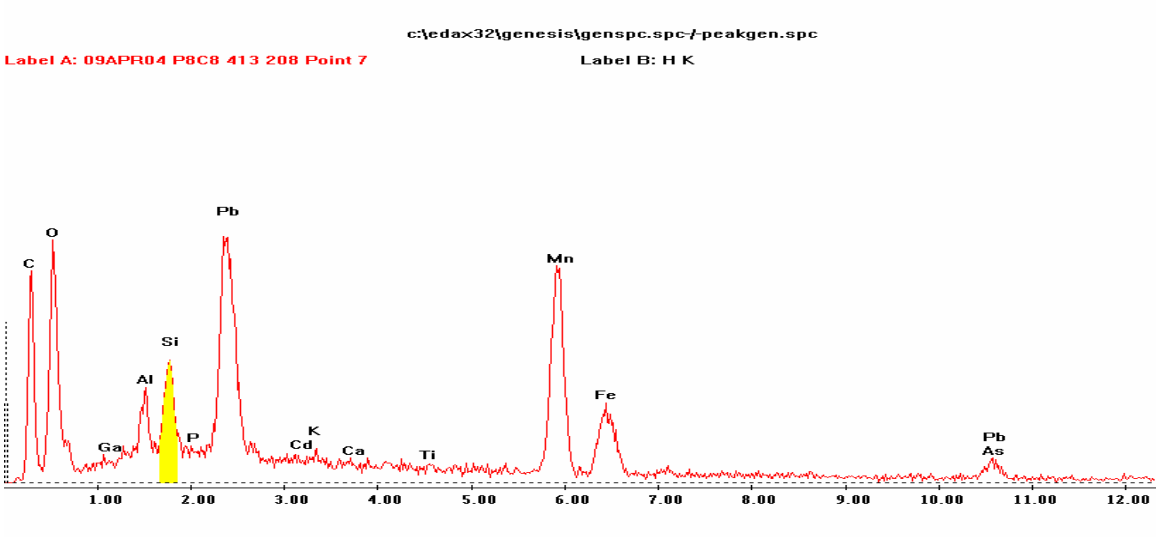

Point 8

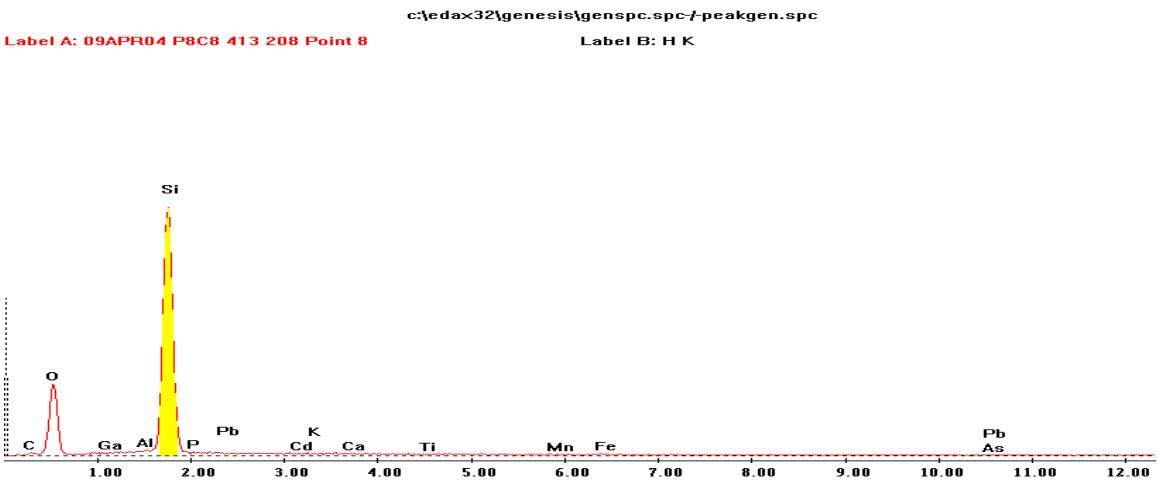

Point 9

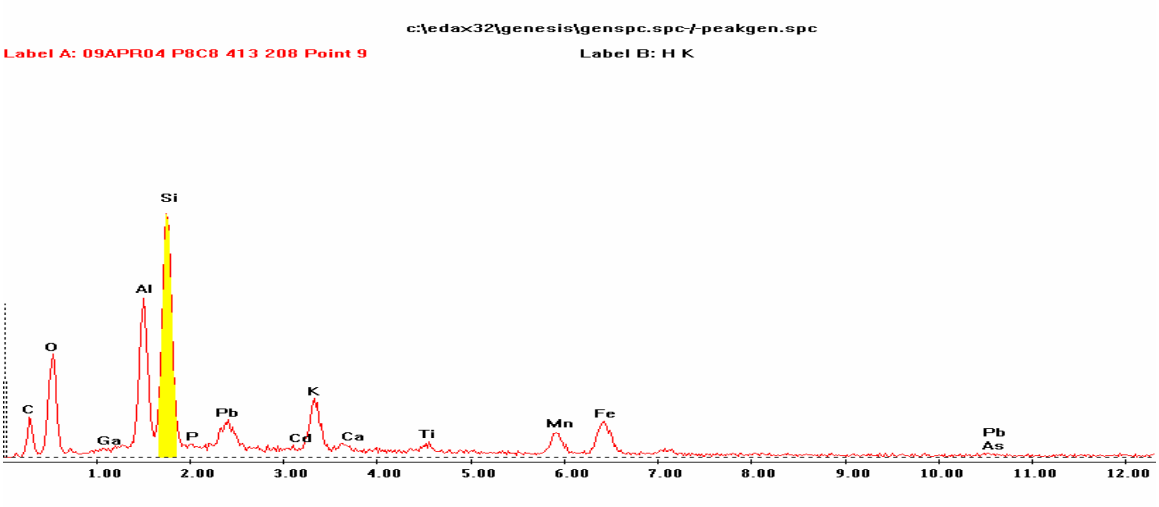

Point 10

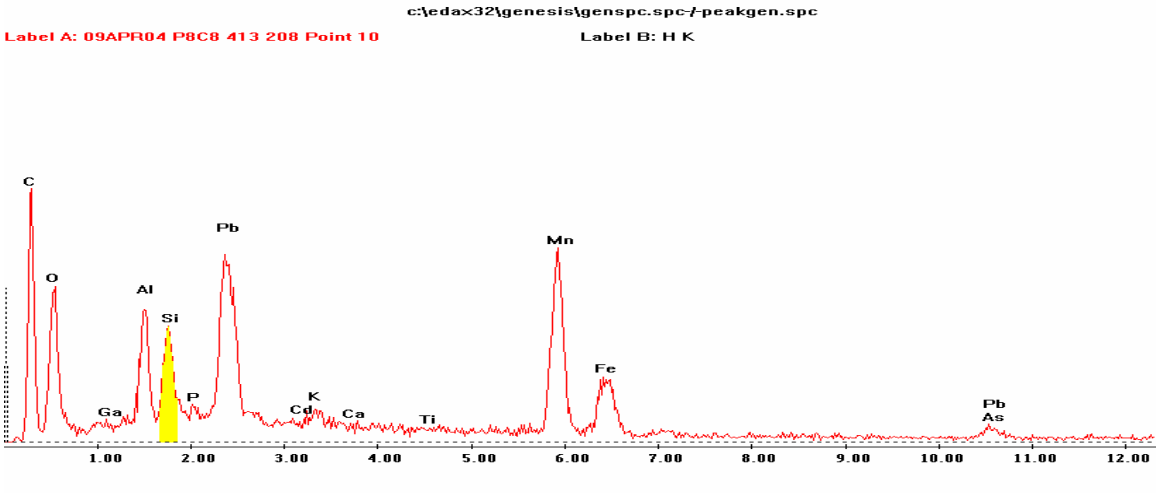

Point 11

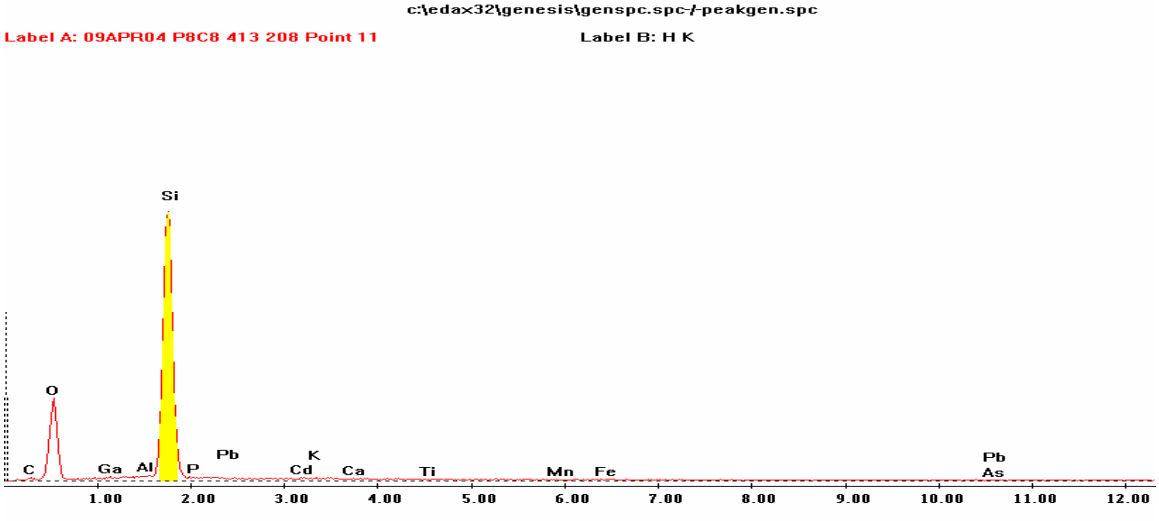

Point 12

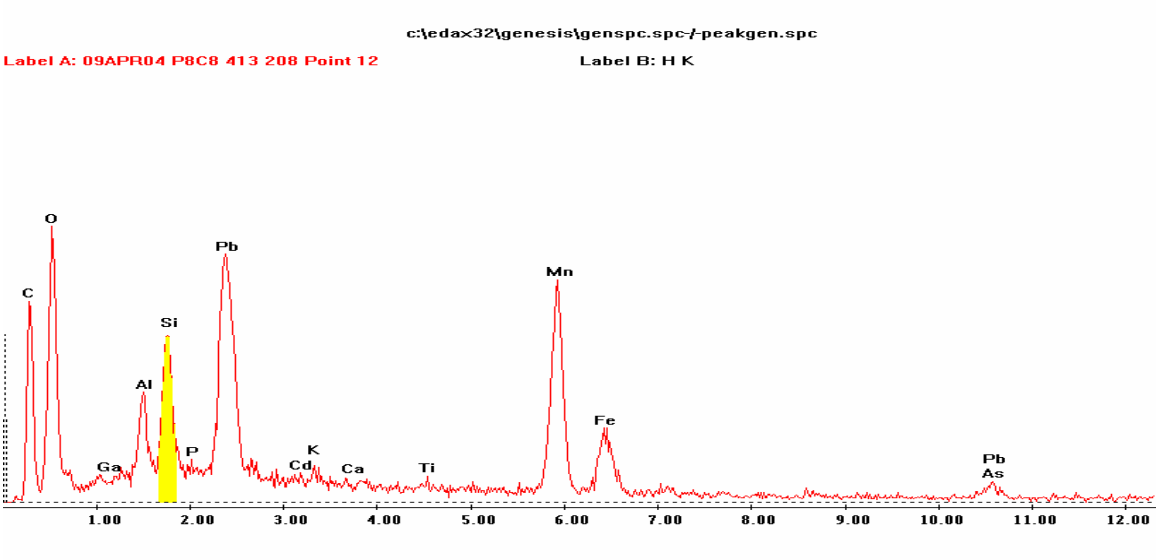
c:\edax32\genesis\genspc.spc-/-peakgen.spc
Label A: 09APR04 P8C8 413 208 Point 12
Label B: H K
O
C
Pb
Mn
Si
Al
Fe
Ga
P
K
Cd
Ca
Ti
Pb
As
1.00
2.00
3.00
4.00
5.00
6.00
7.00
8.00
9.00
10.00
11.00
12.00

P8C8 – 429, 346

BSE Image

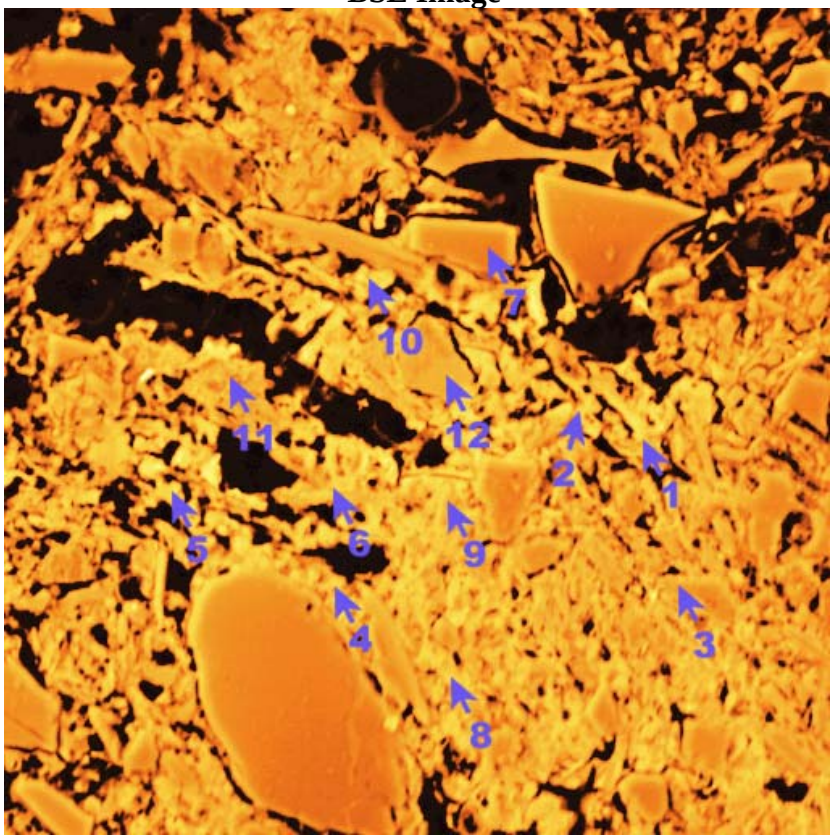

Iron (Fe)

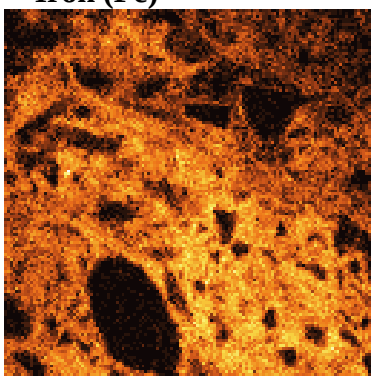

Manganese (Mn)

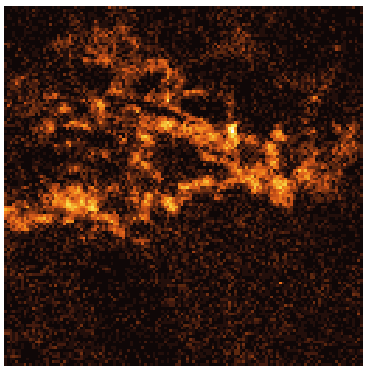

Phosphorous (P)

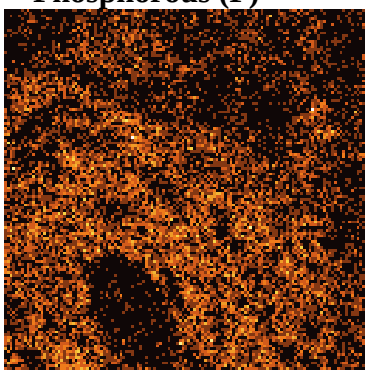

Lead (Pb)

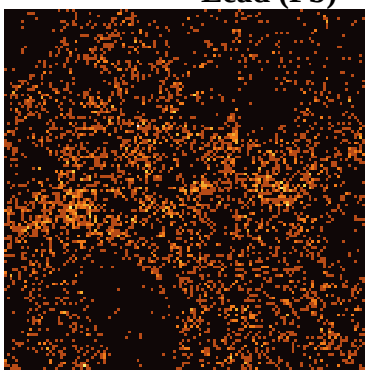

Silicon (Si)

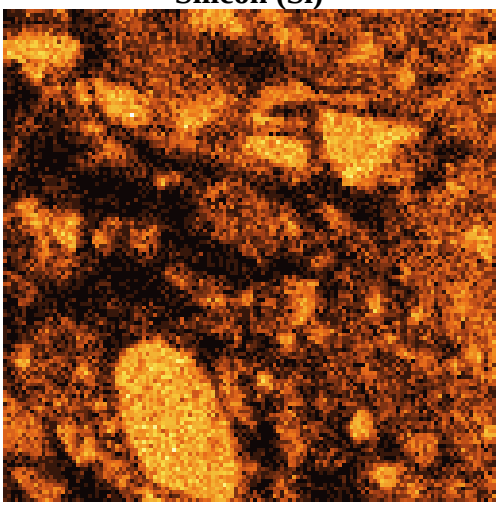

EDS Scan Images by Point

Point 1

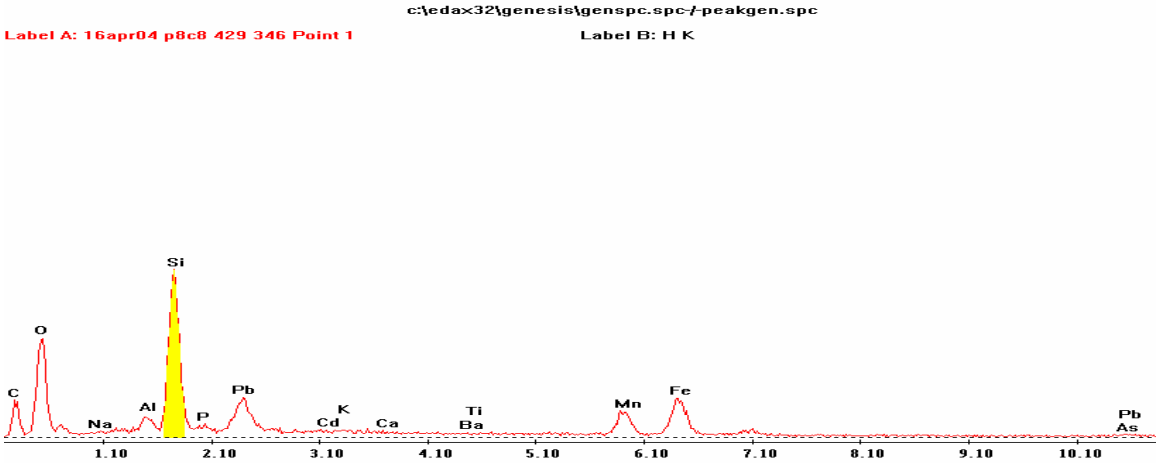

Point 2

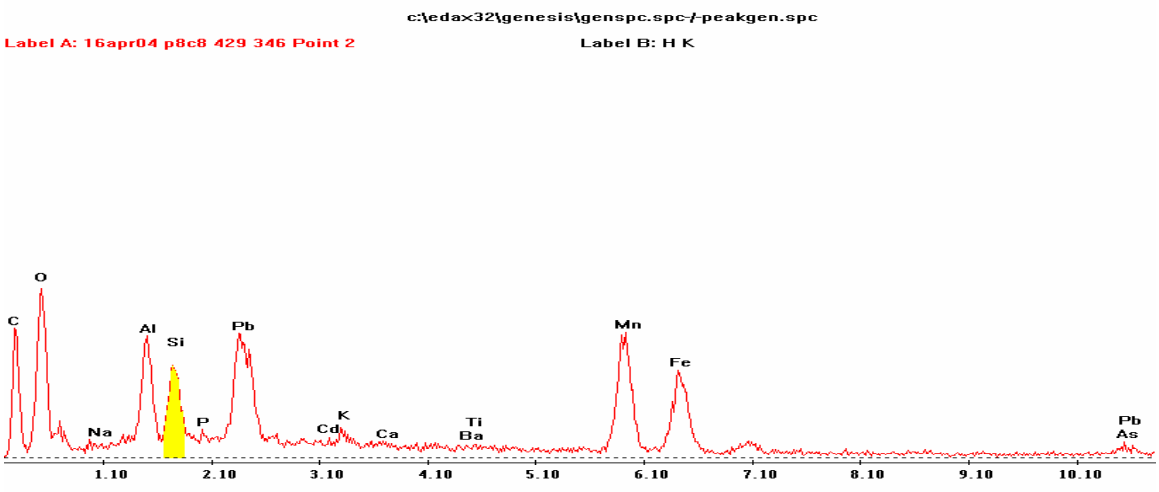

Point 3

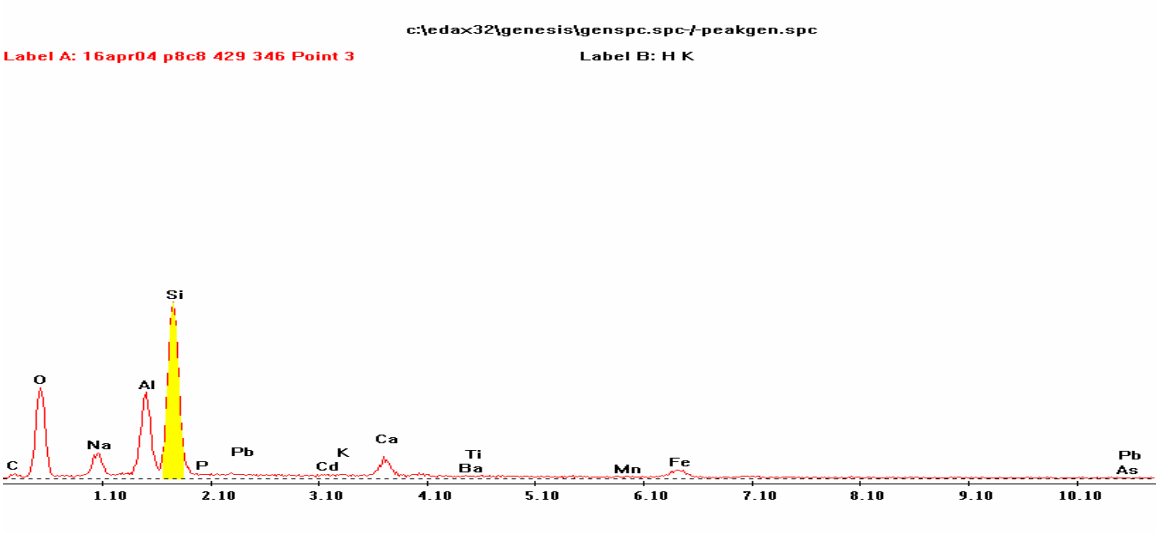

Point 4

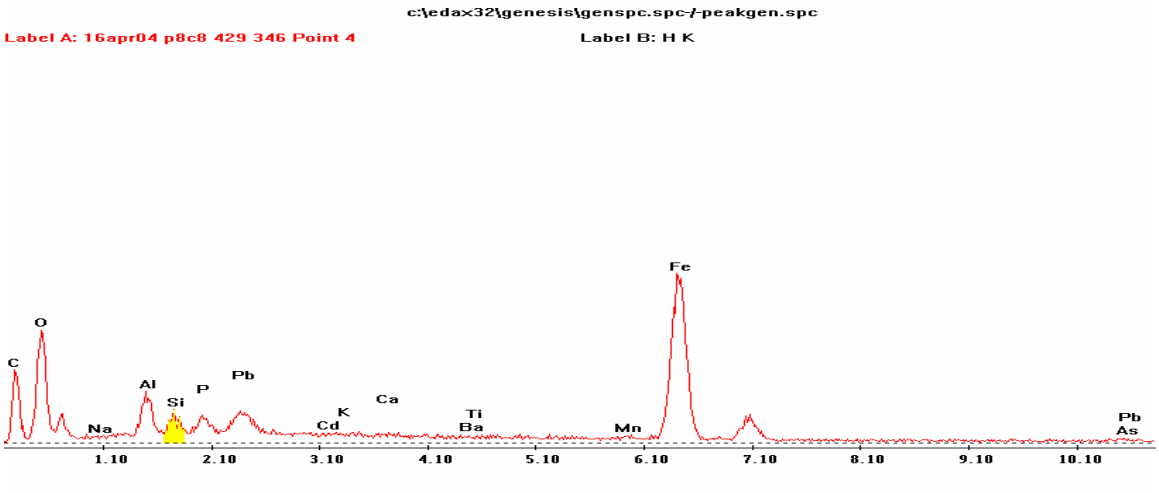

Point 5

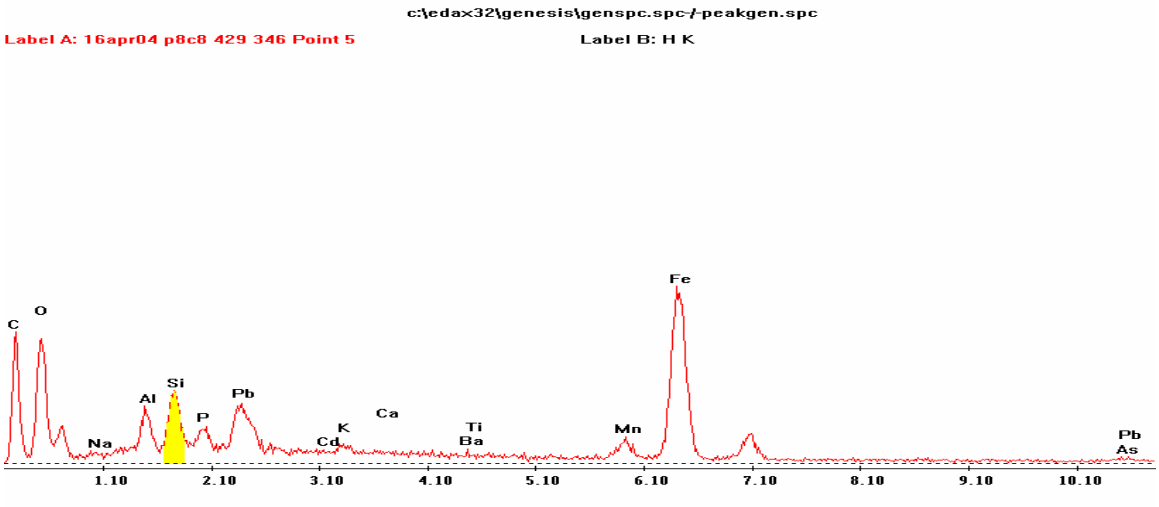

Point 6

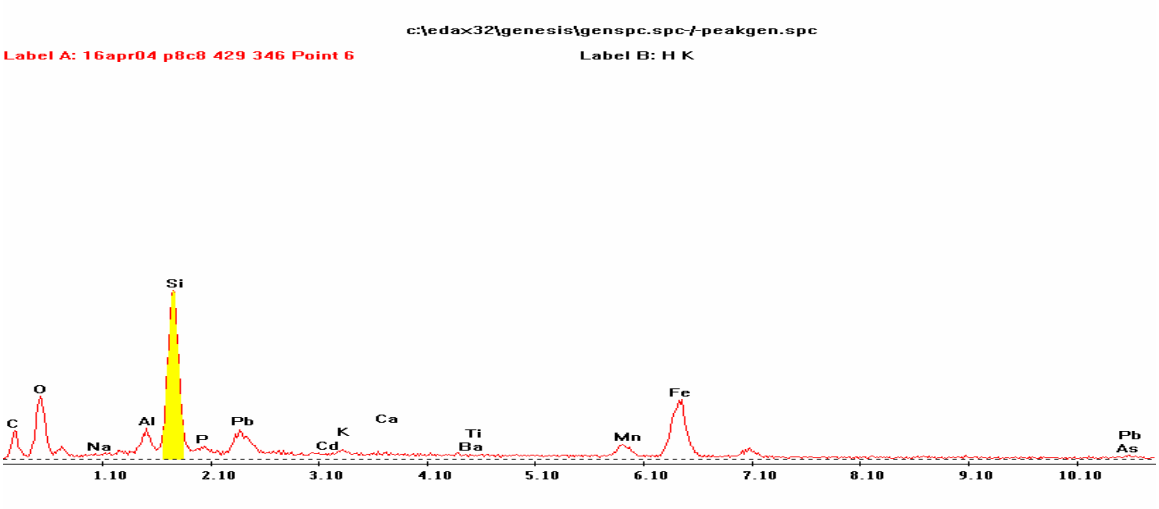

Point 7

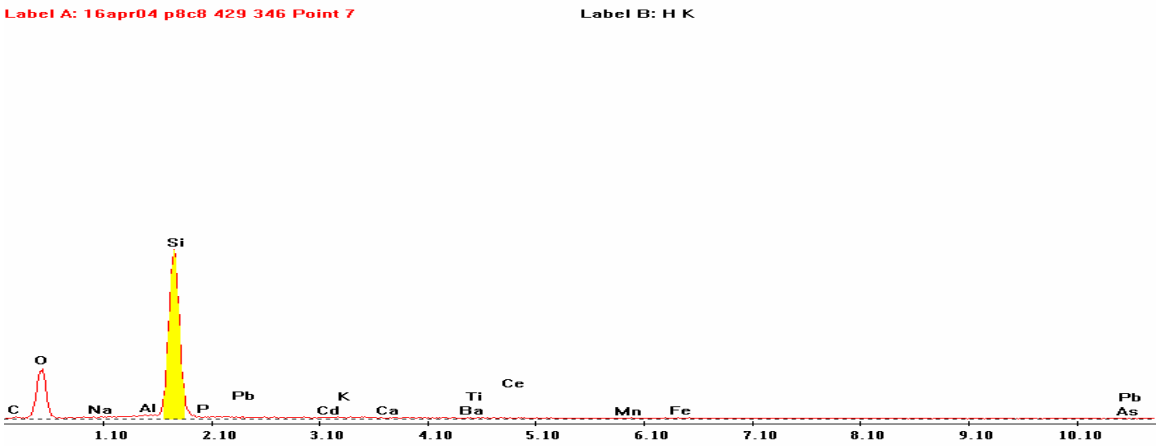

Point 8

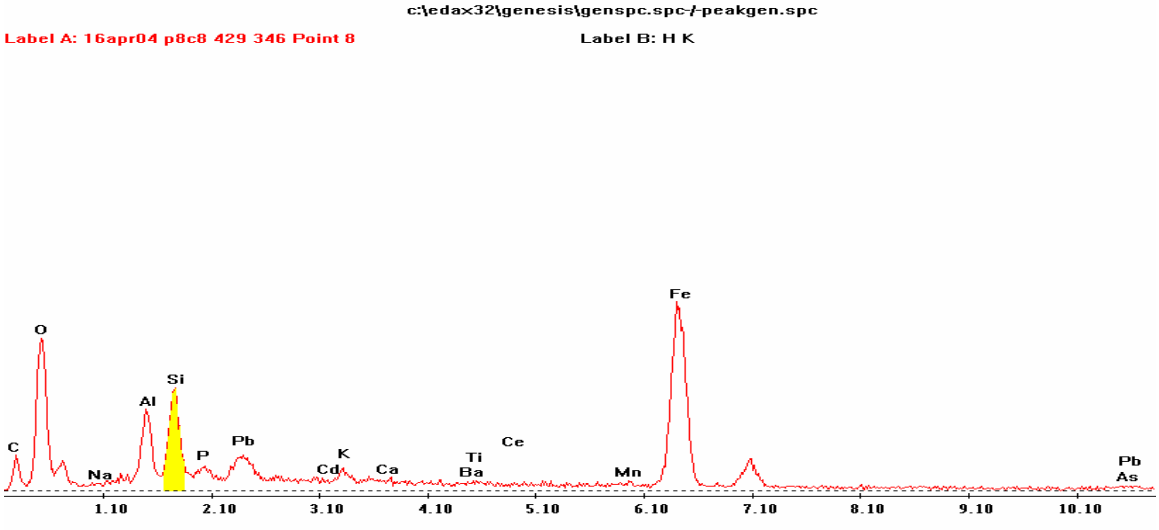

Point 9

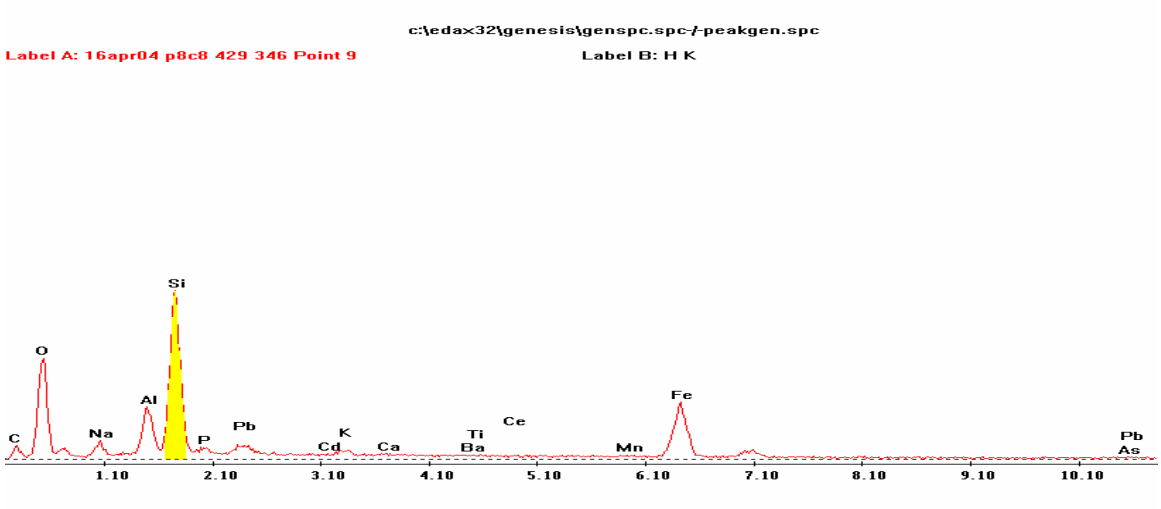

Point 10

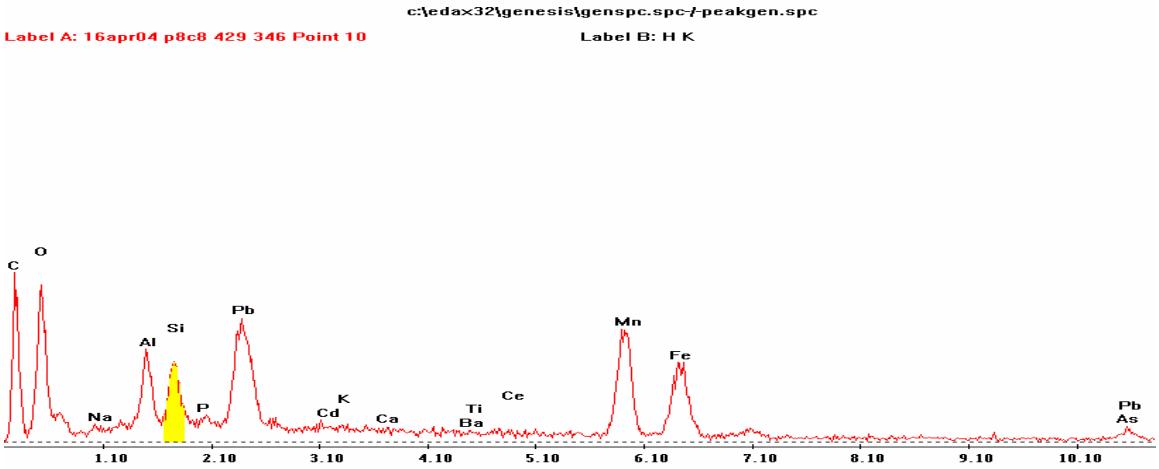

Point 11

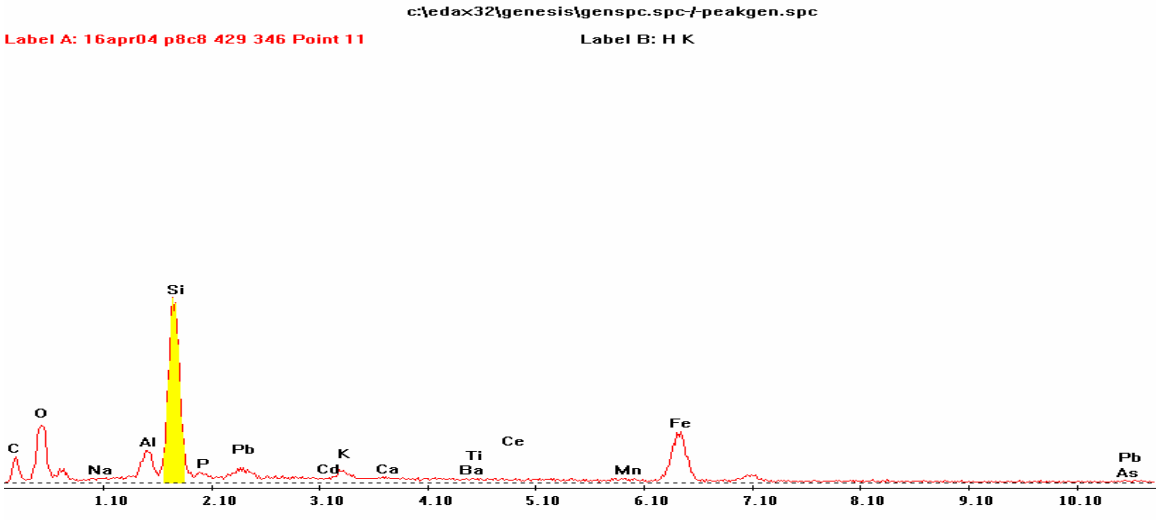

Point 12

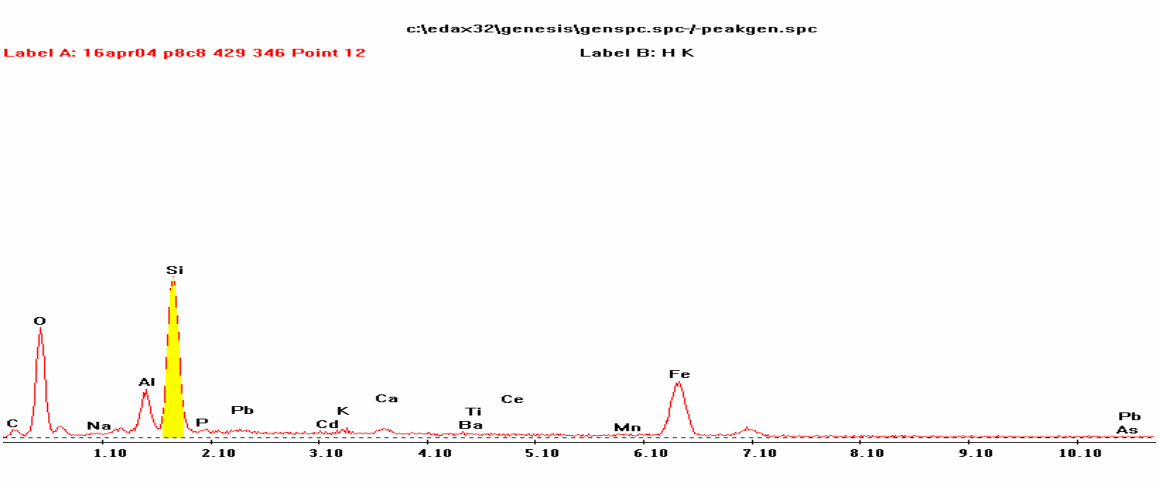
c:\edax32\genesis\genspc.spc-/-peakgen.spc
Label A: 16apr04 p8c8 429 346 Point 12
Label B: H K
C
O
Na
Al
Si
P
Pb
Cd
K
Ca
Ti
Ba
Ce
Mn
Fe
Pb
As
1.10
2.10
3.10
4.10
5.10
6.10
7.10
8.10
9.10
10.10

P8C8 – 442, 252

BSE Image

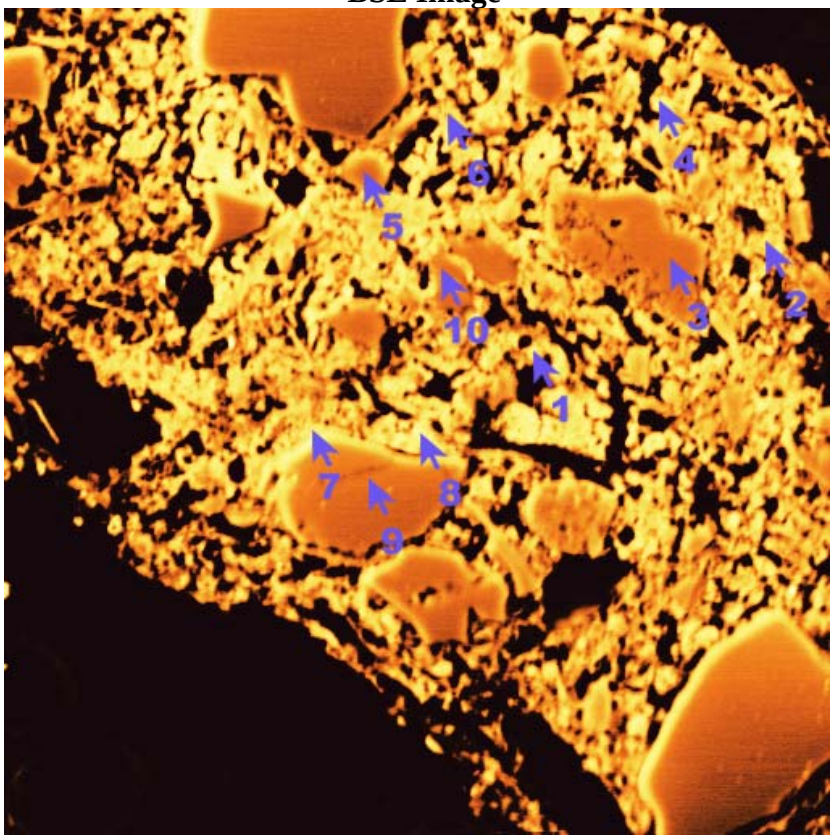

Iron (Fe)

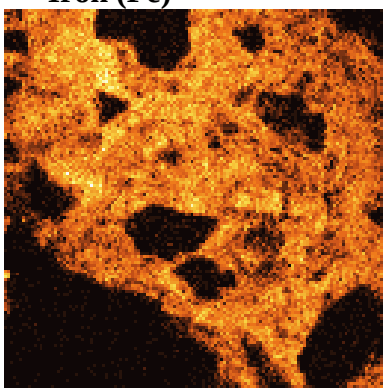

Manganese (Mn)

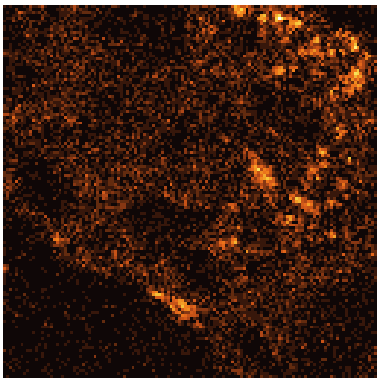

Phosphorous (P)

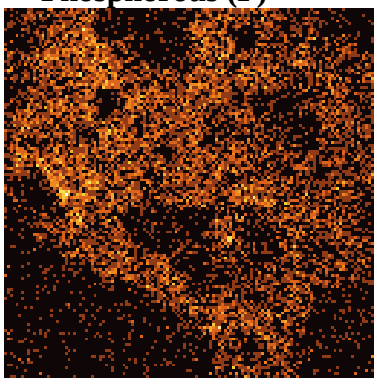

Lead (Pb)

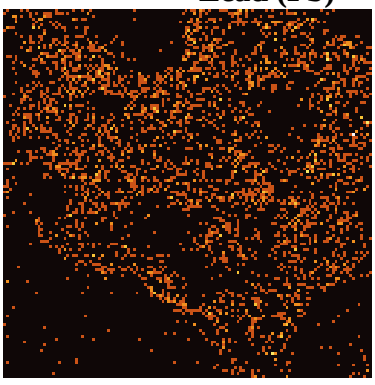

Silicon (Si)

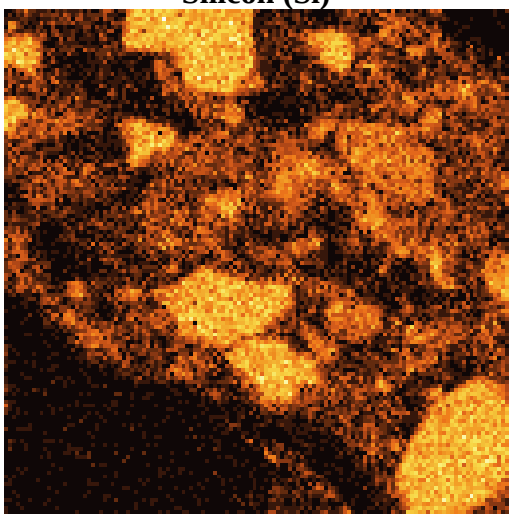

EDS Scan Images by Point

Point 1

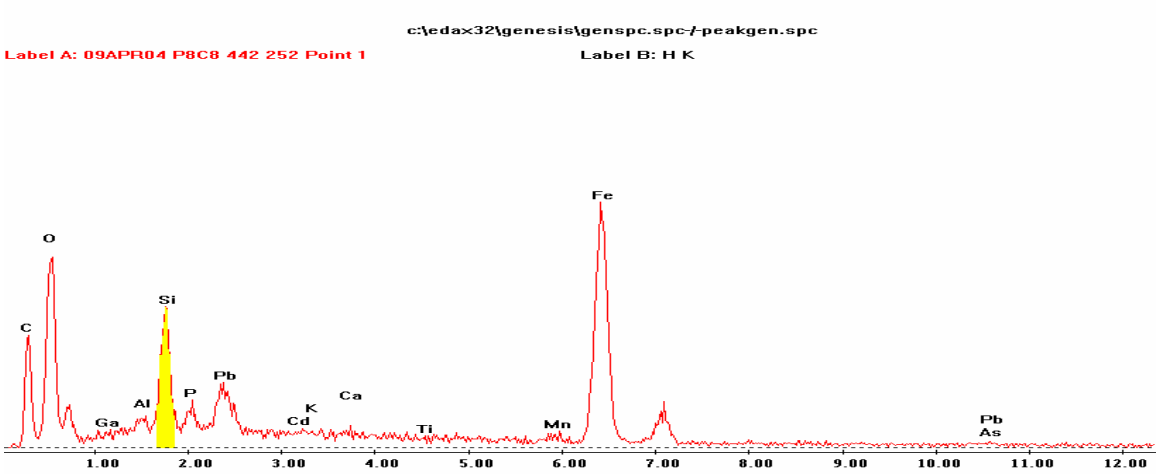

Point 2

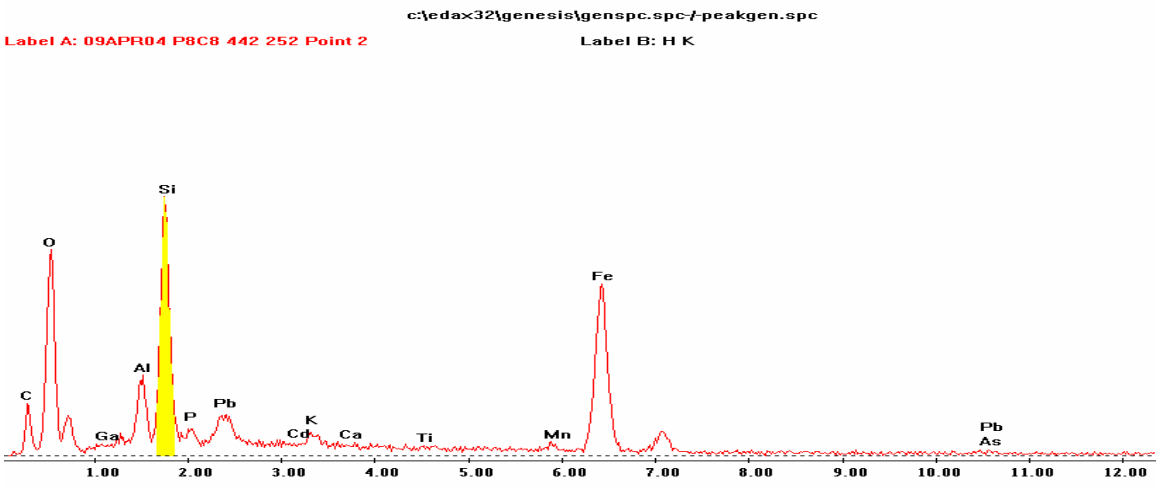

Point 3

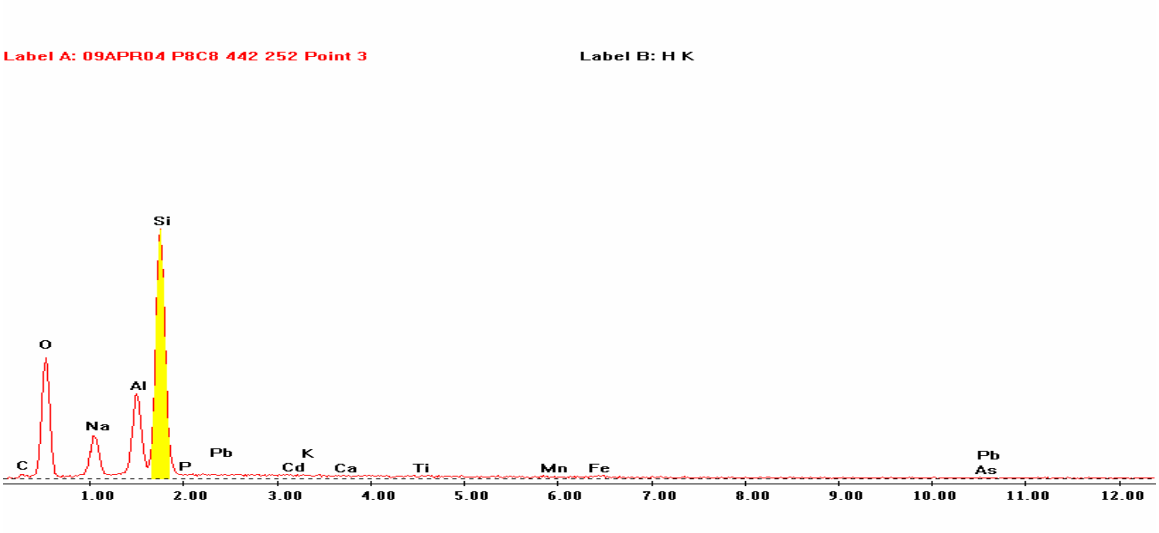

Point 4

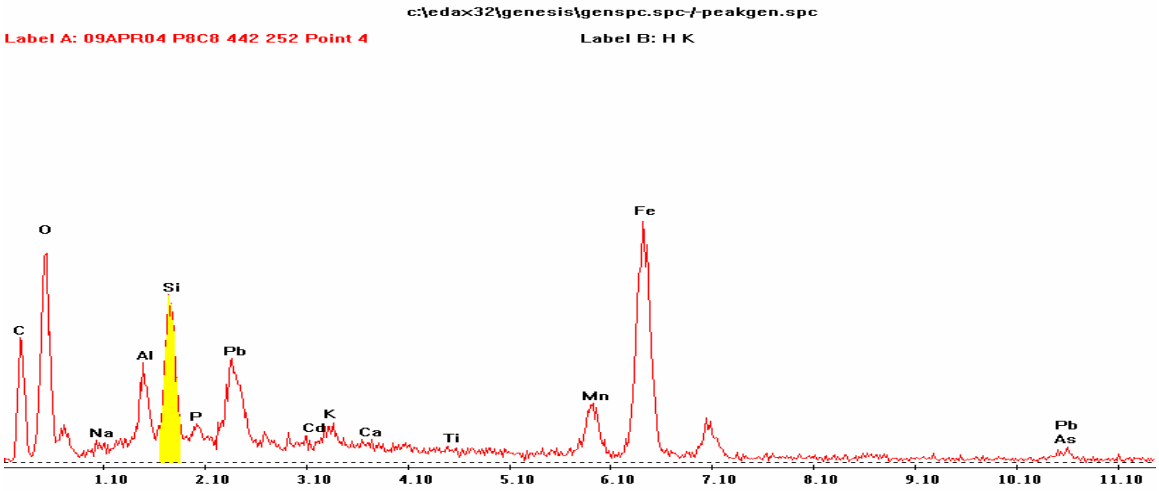

Point 5

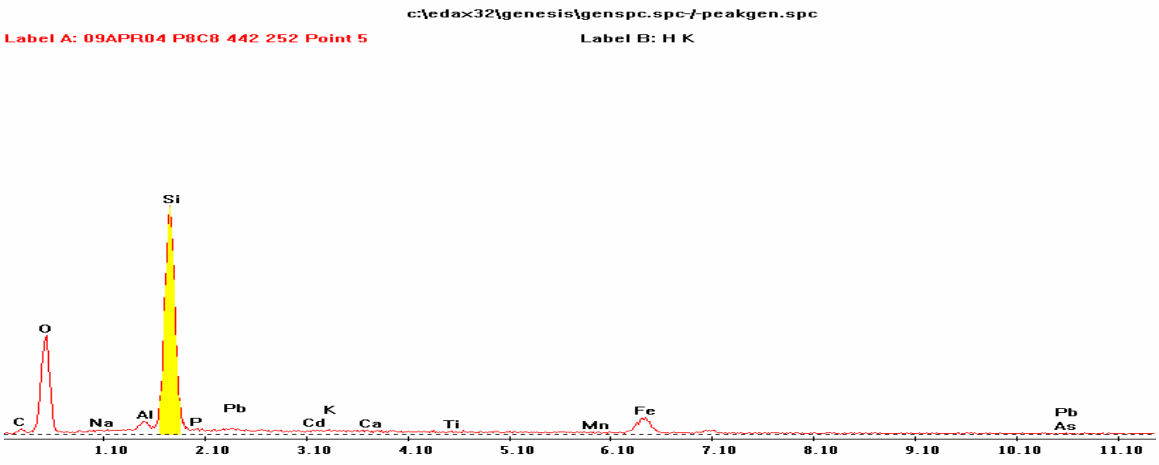

Point 6

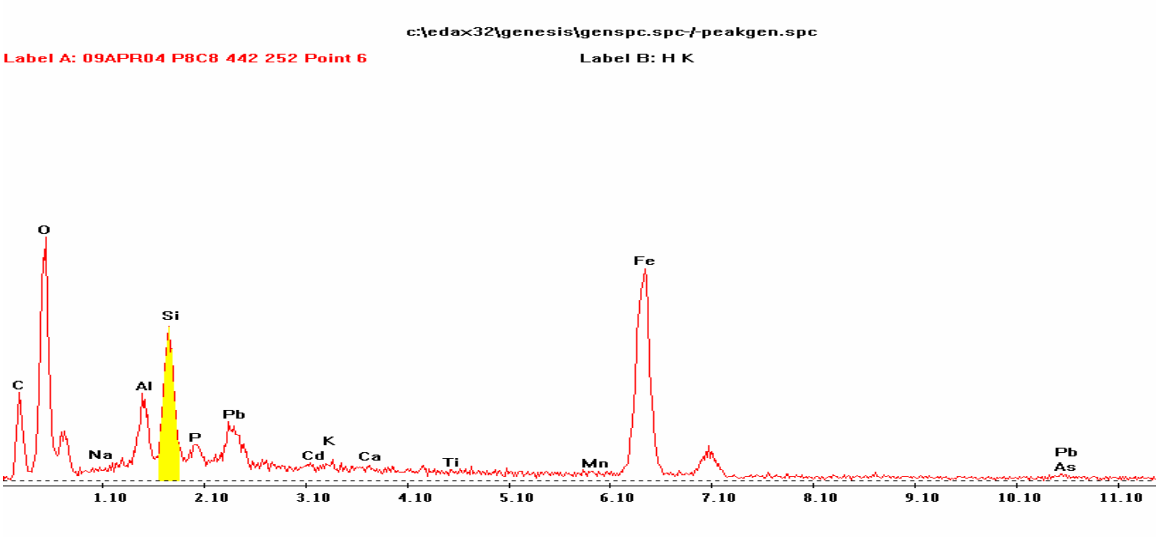

Point 7

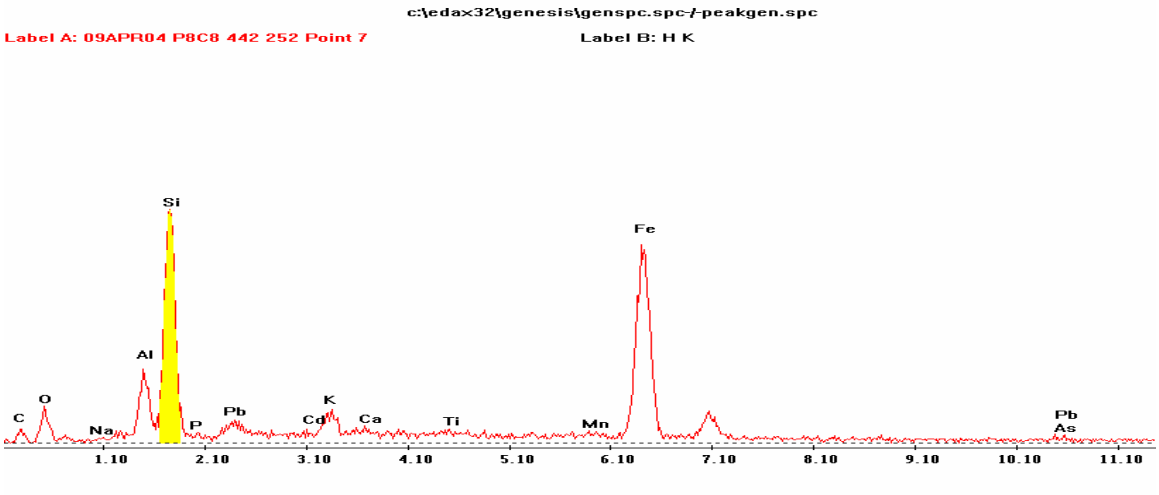

Point 8

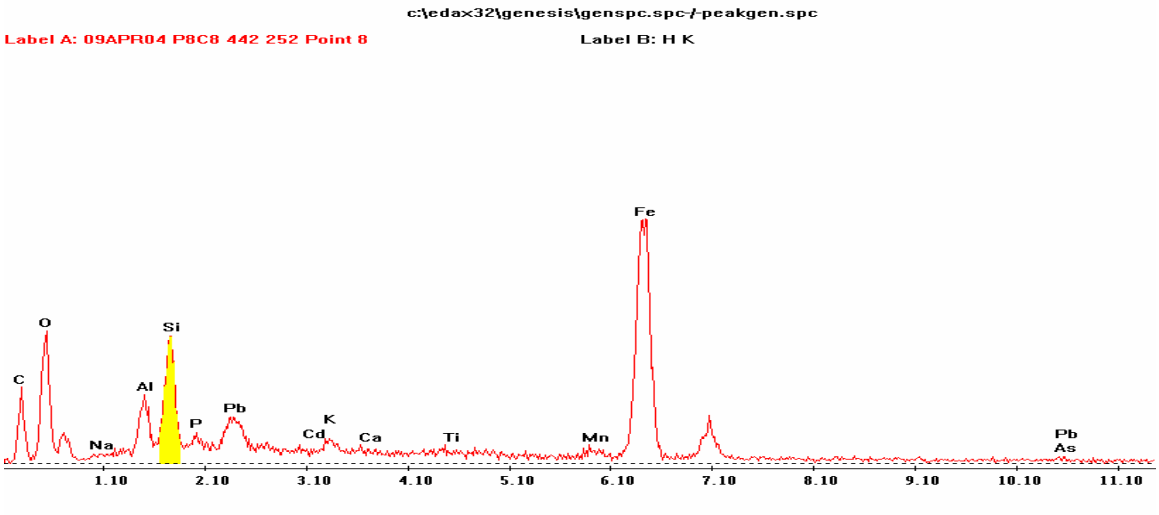

Point 9

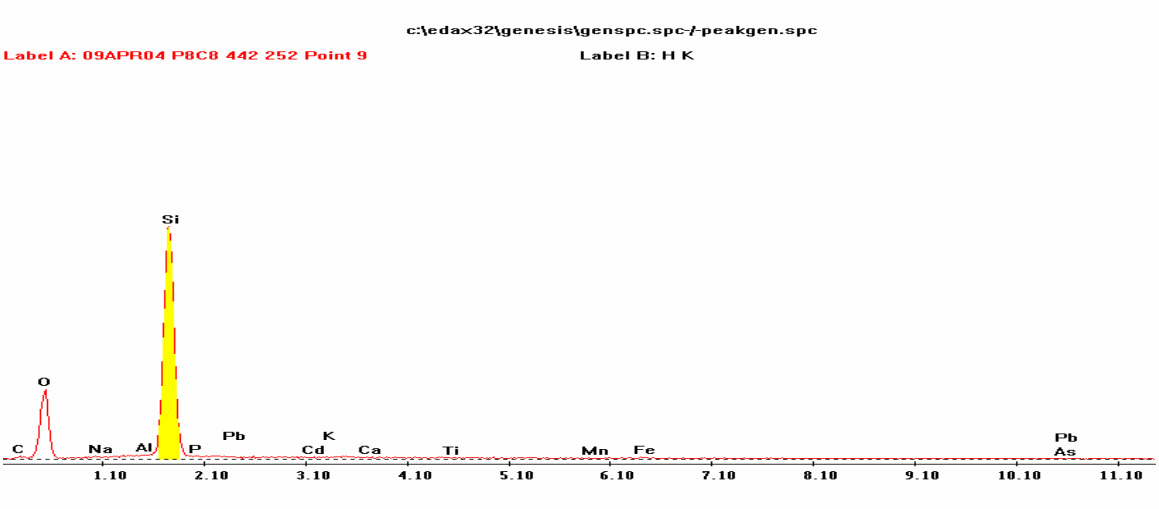

Point 10

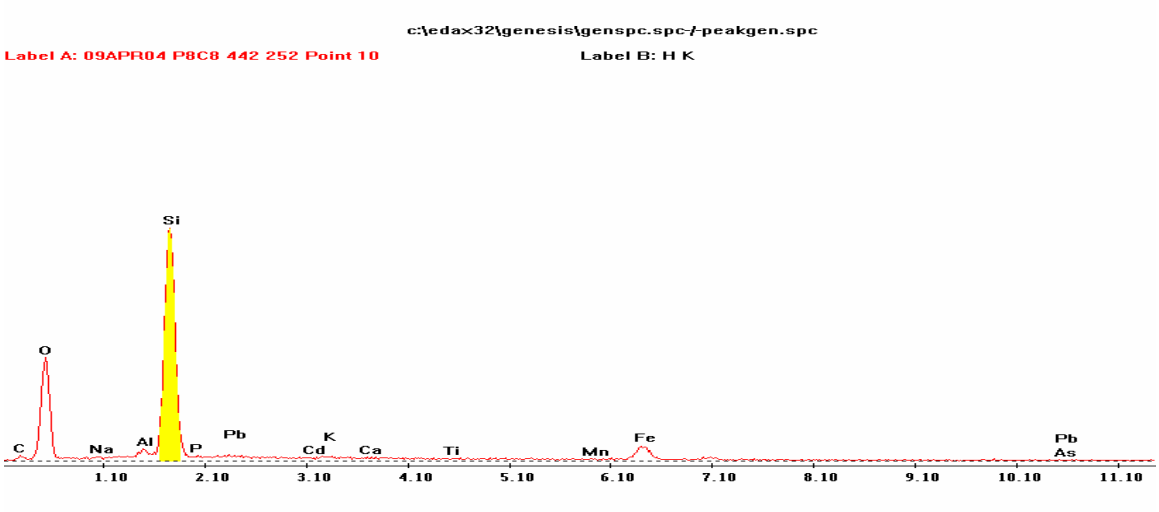

P8C8 – 472, 213

BSE Image

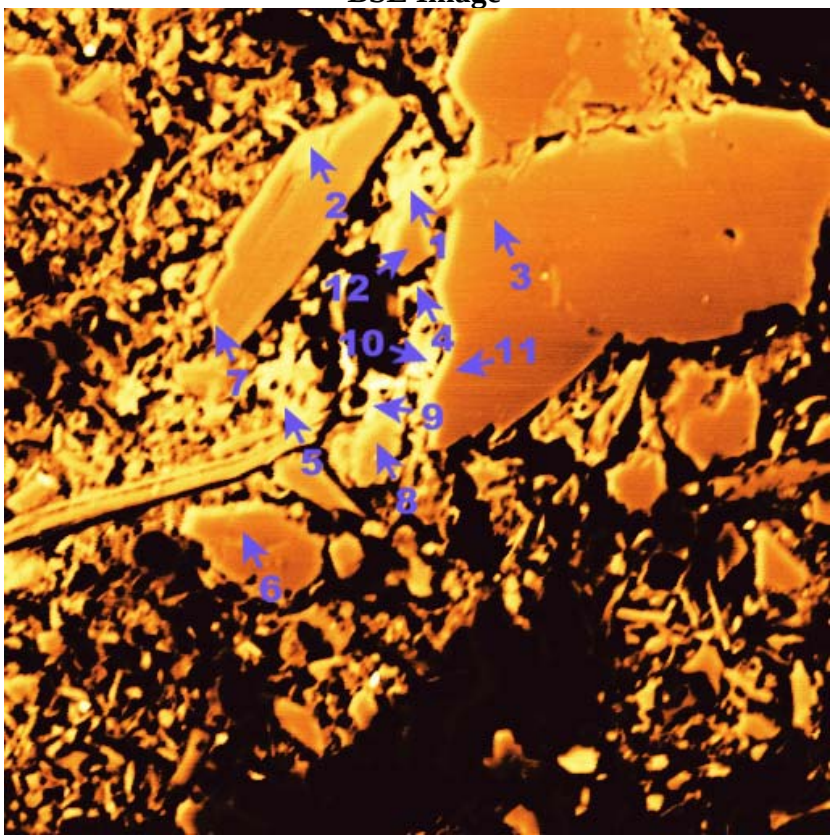

Iron (Fe)

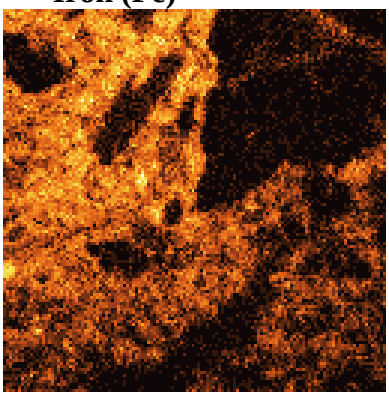

Manganese (Mn)

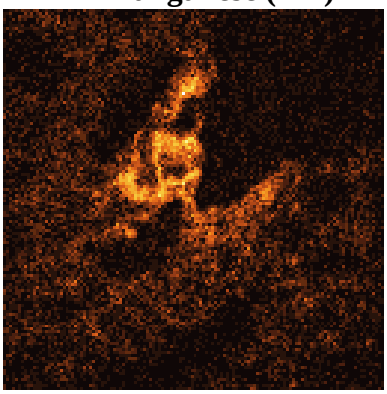

Phosphorous (P)

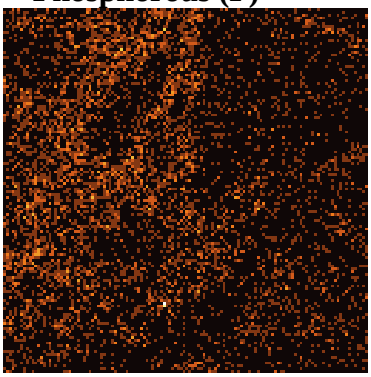

Lead (Pb)

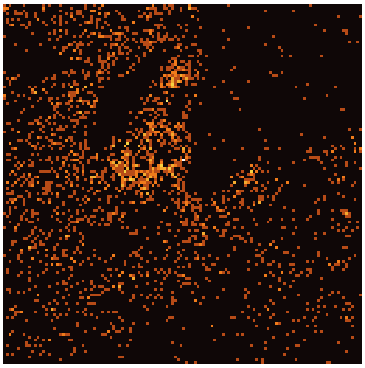

Silicon (Si)

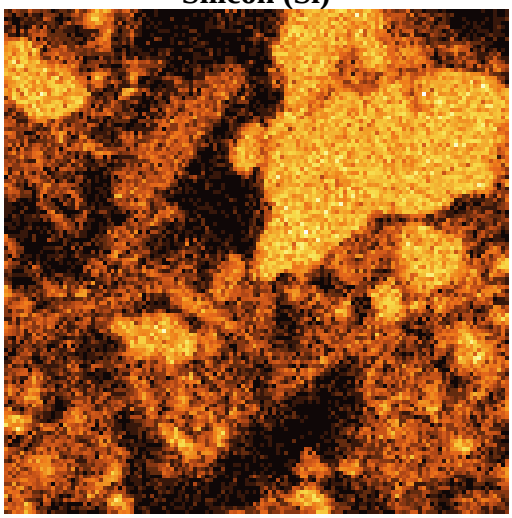

EDS Scan Images by Point

Point 1

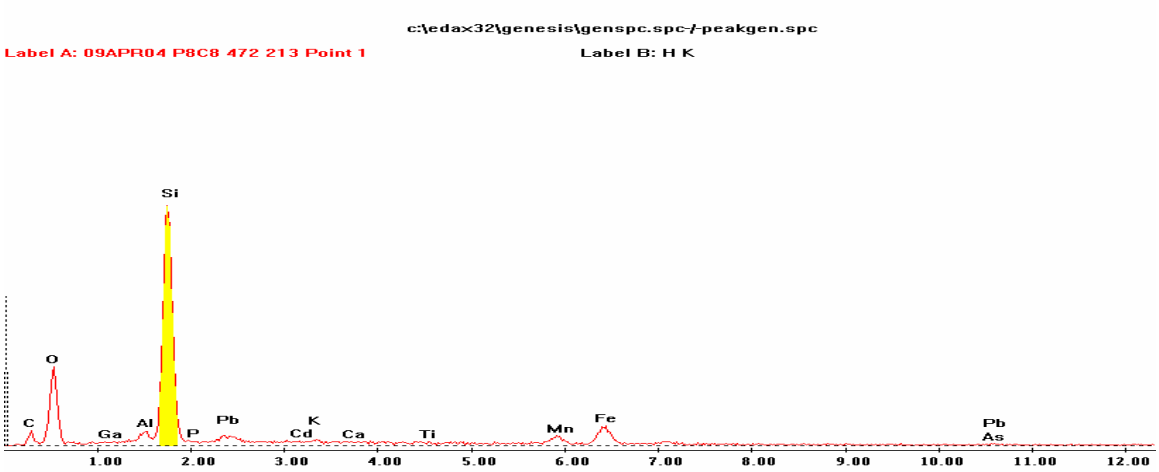

Point 2

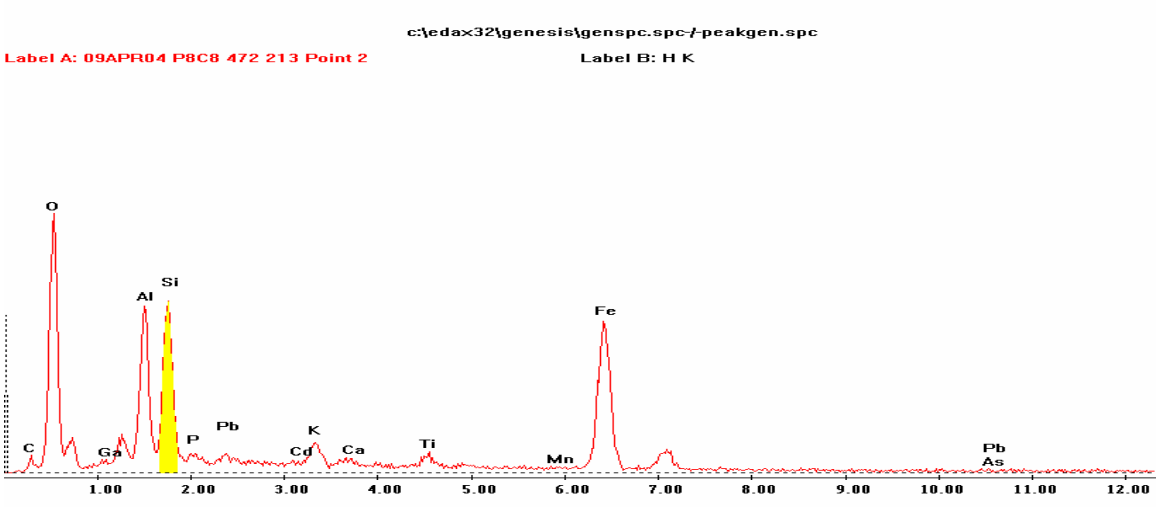

Point 3

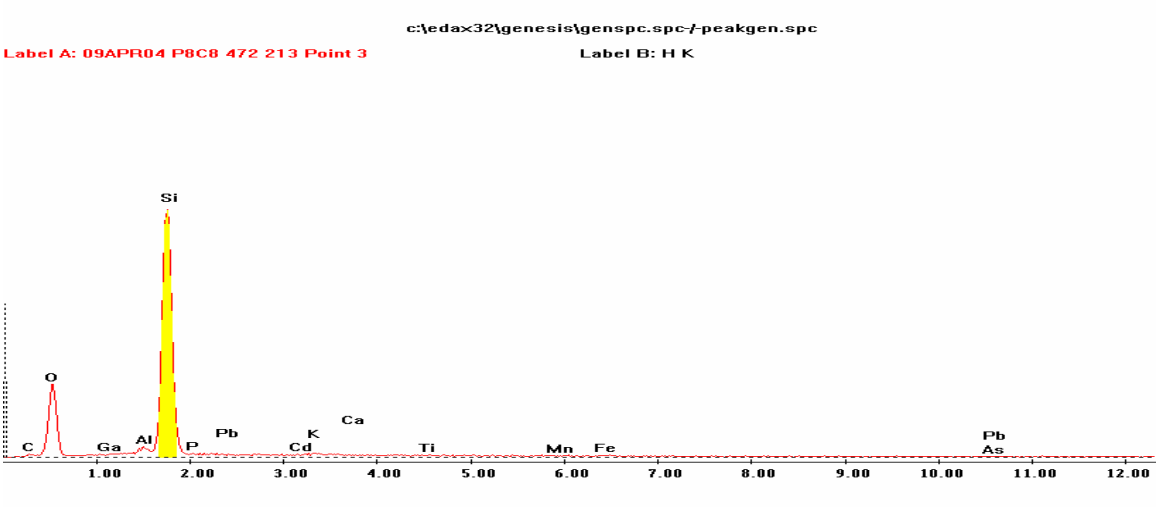

Point 4

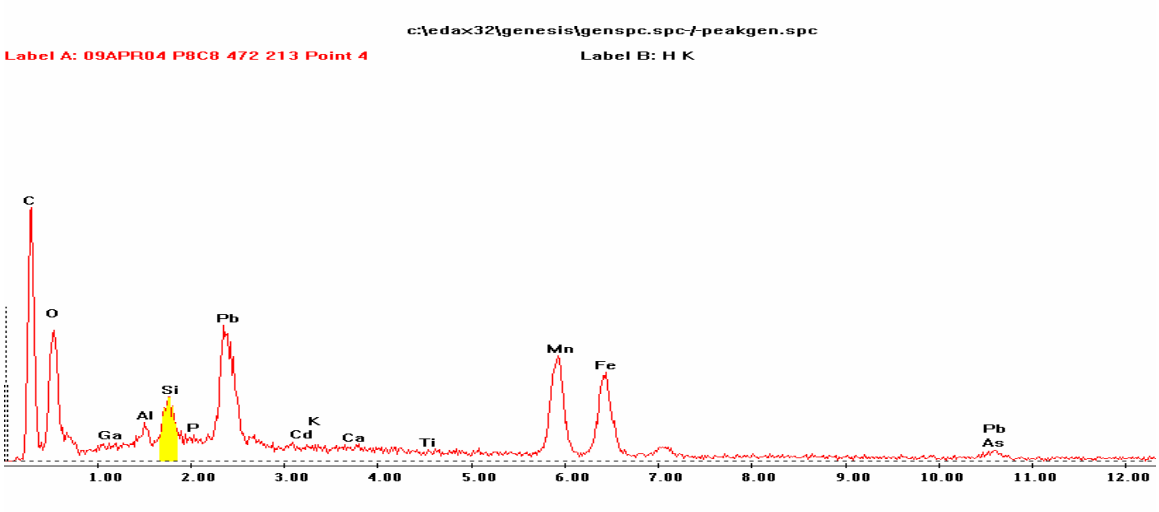

Point 5

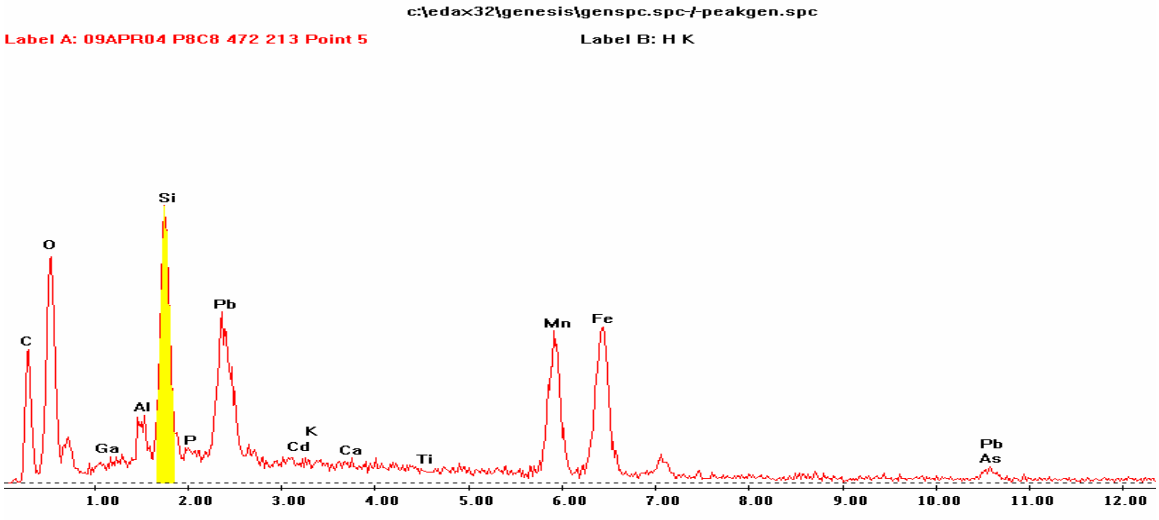

Point 6

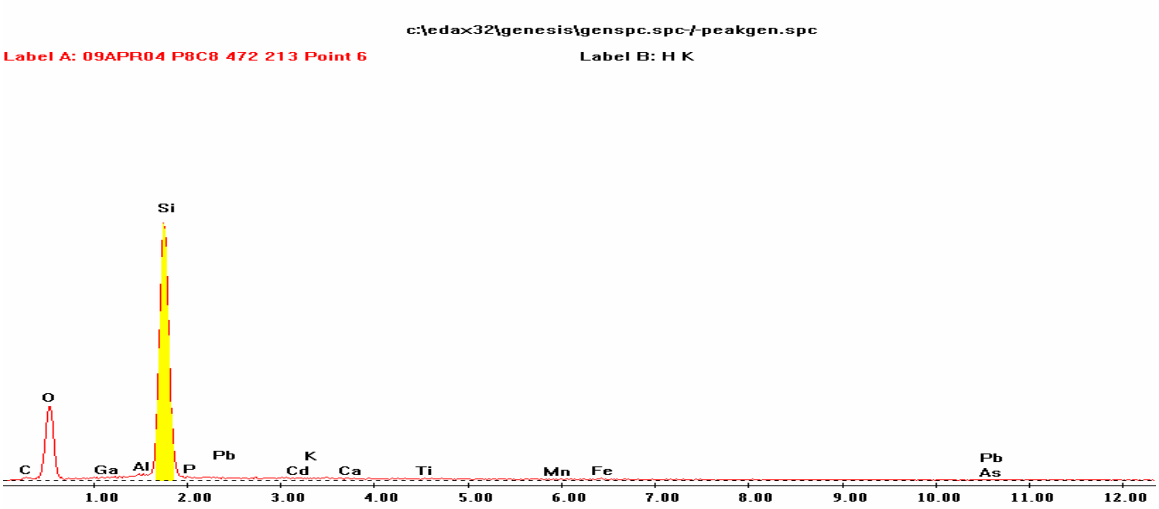

Point 7

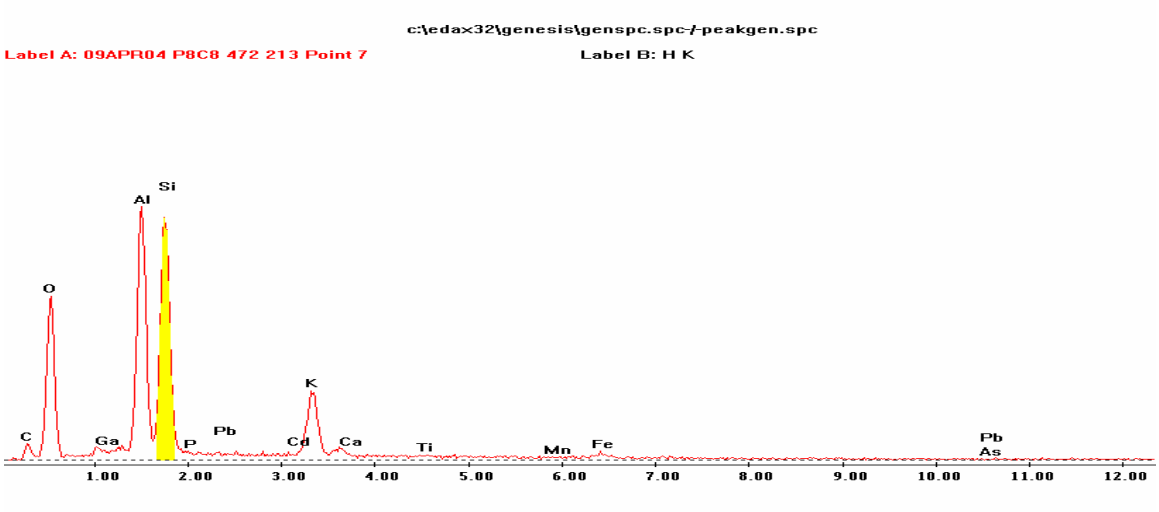

Point 8

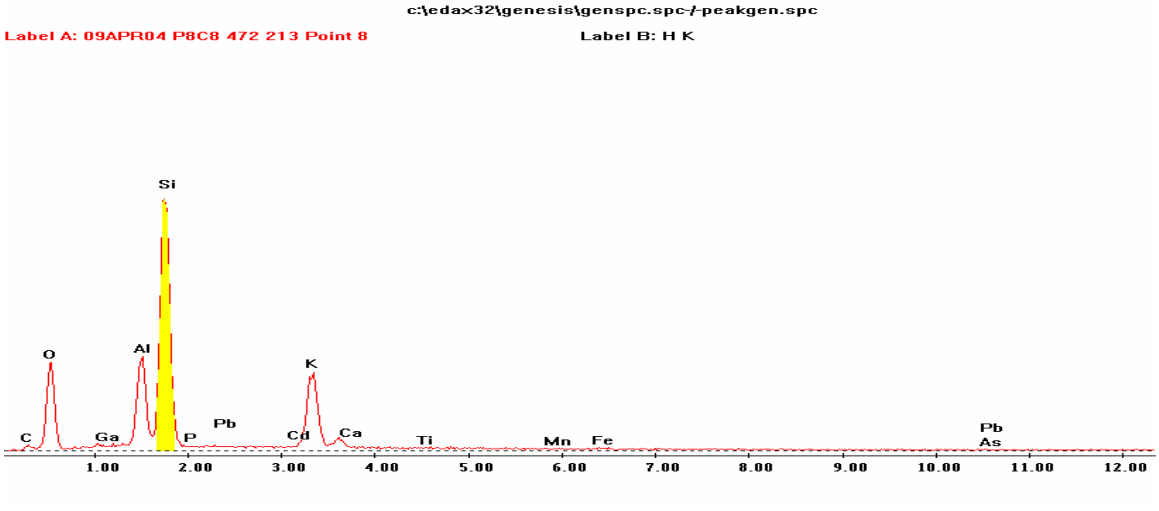

Point 9

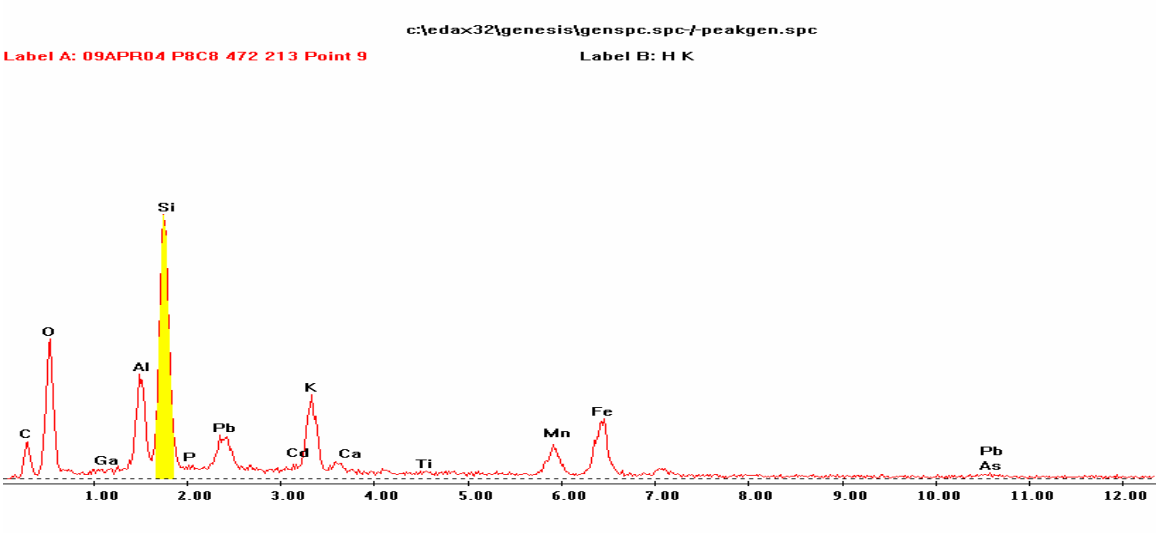

Point 10

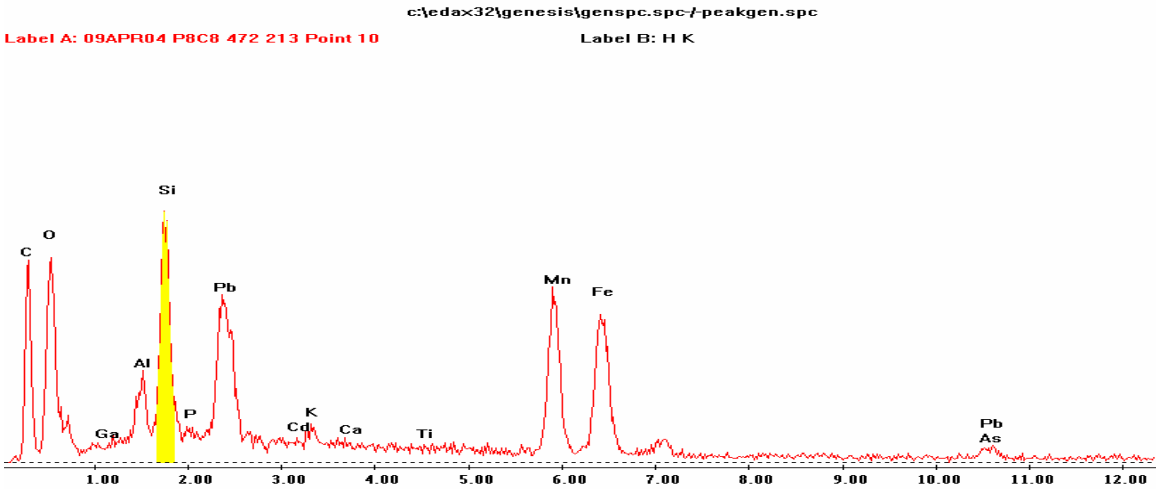

Point 11

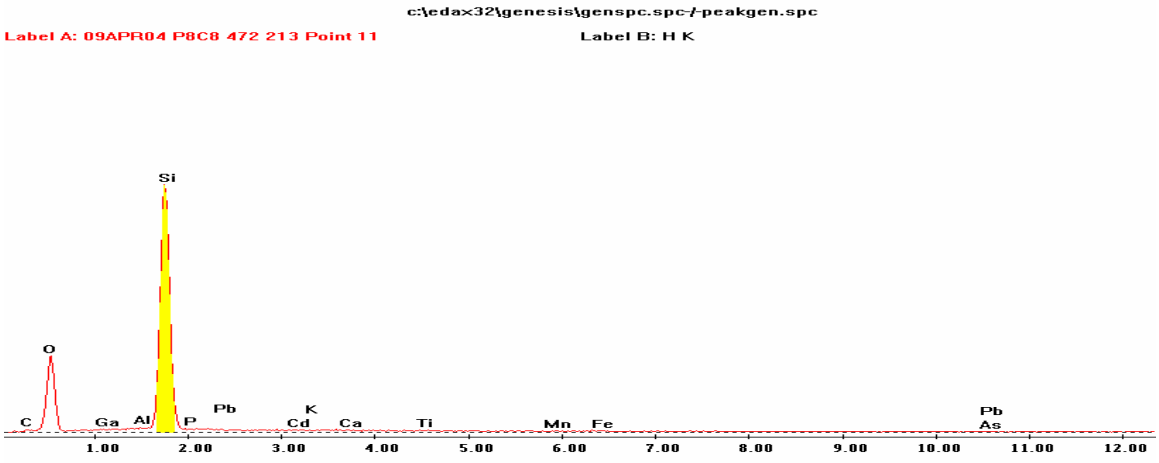

Point 12

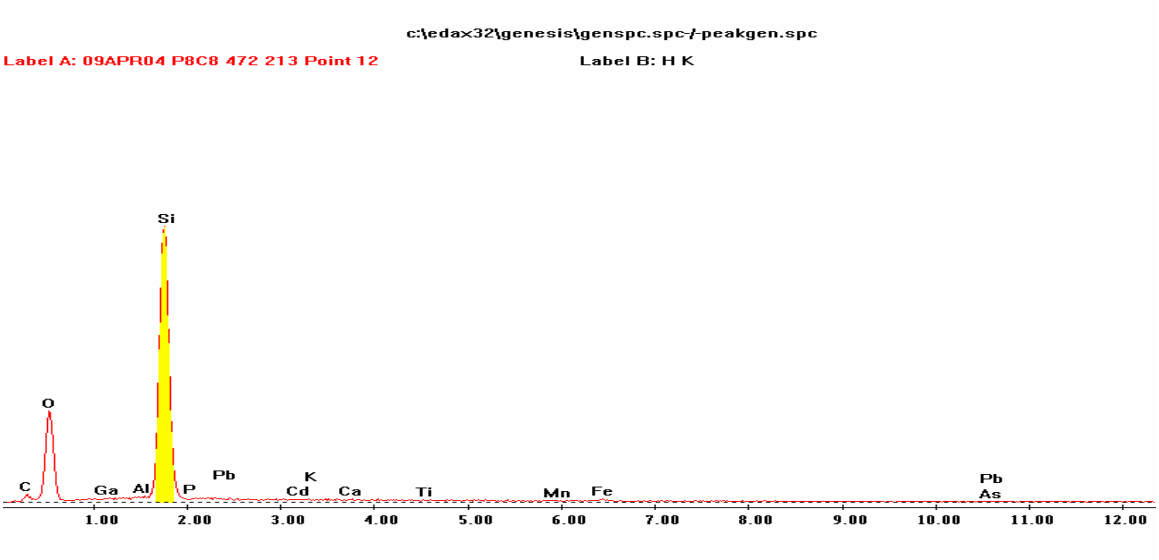
c:\edax32\genesis\genspc.spc-/-peakgen.spc
Label A: 09APR04 P8C8 472 213 Point 12
Label B: H K
Si
O
C
Ga
Al
P
Pb
K
Cd
Ca
Ti
Mn
Fe
Pb
As
1.00
2.00
3.00
4.00
5.00
6.00
7.00
8.00
9.00
10.00
11.00
12.00

P8C9 – 413, 154

BSE Image

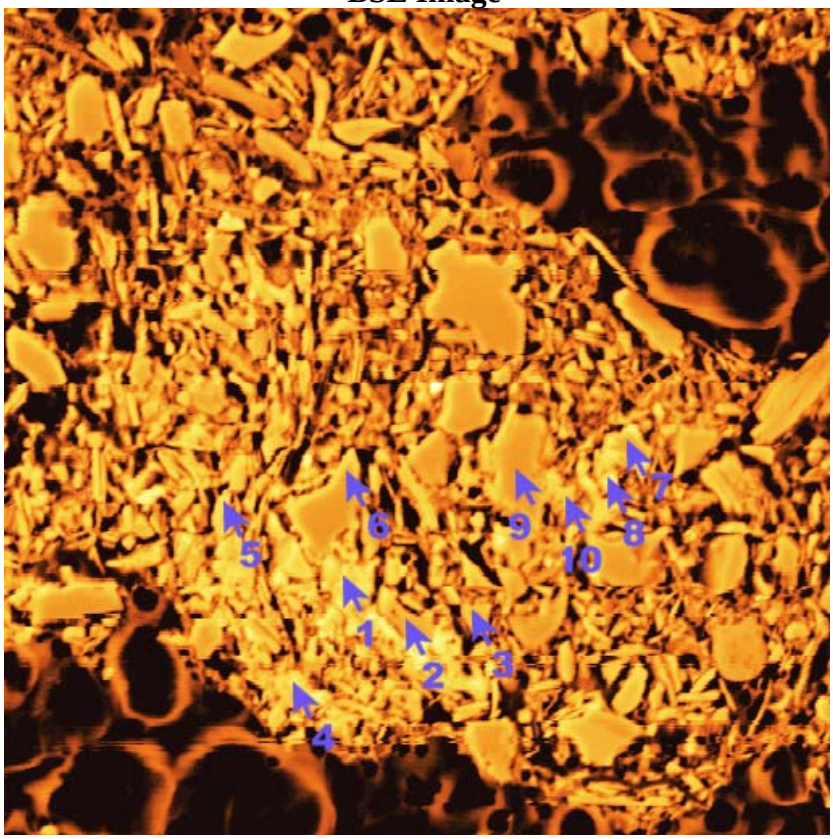

Iron (Fe)

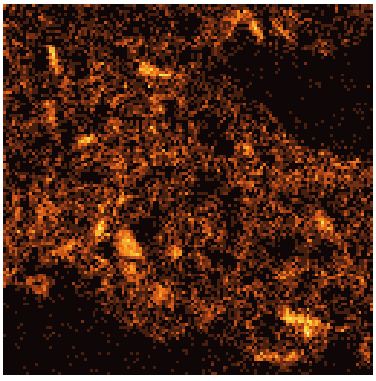

Manganese (Mn)

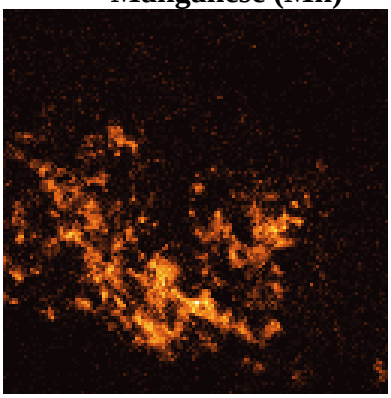

Phosphorous (P)

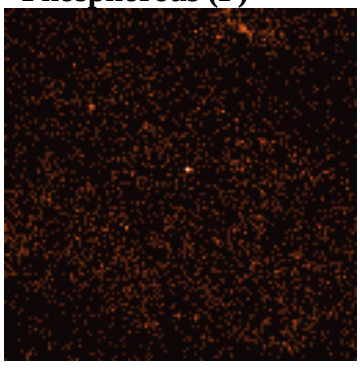

Lead (Pb)

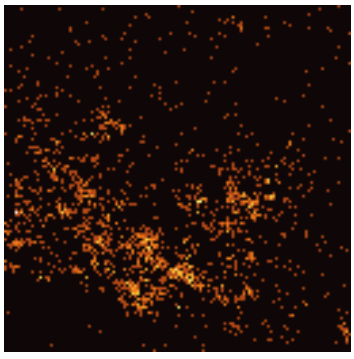

Silicon (Si)

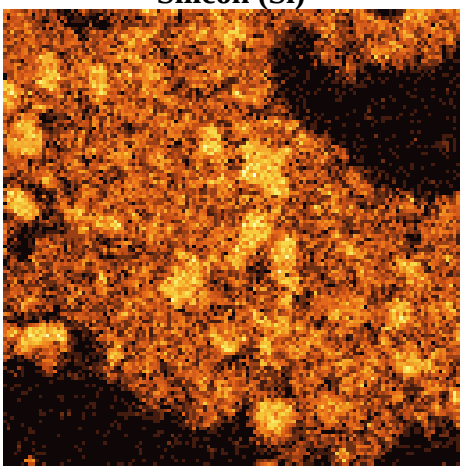

EDS Scan Images by Point

Point 1

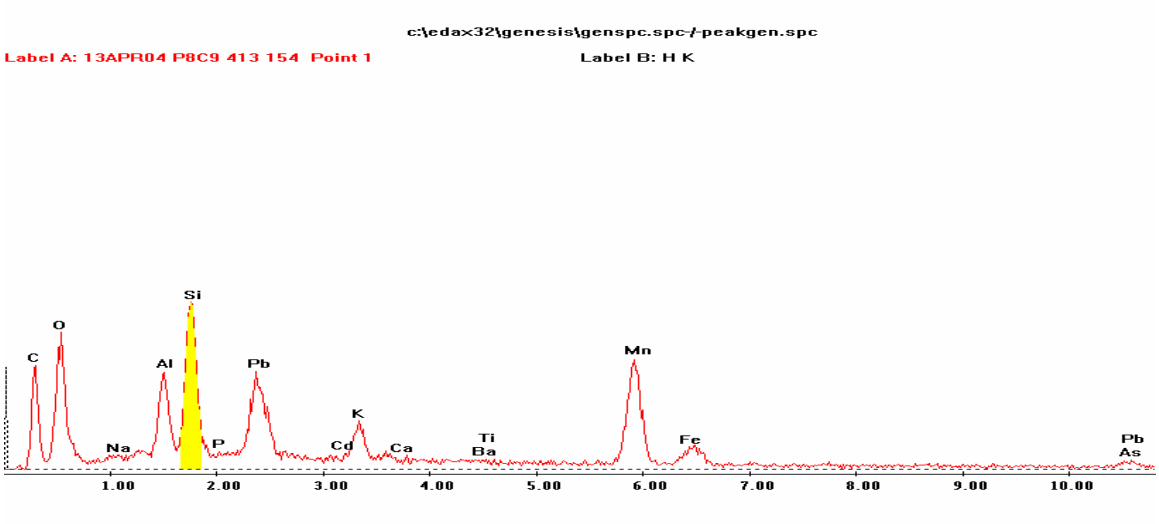

Point 2

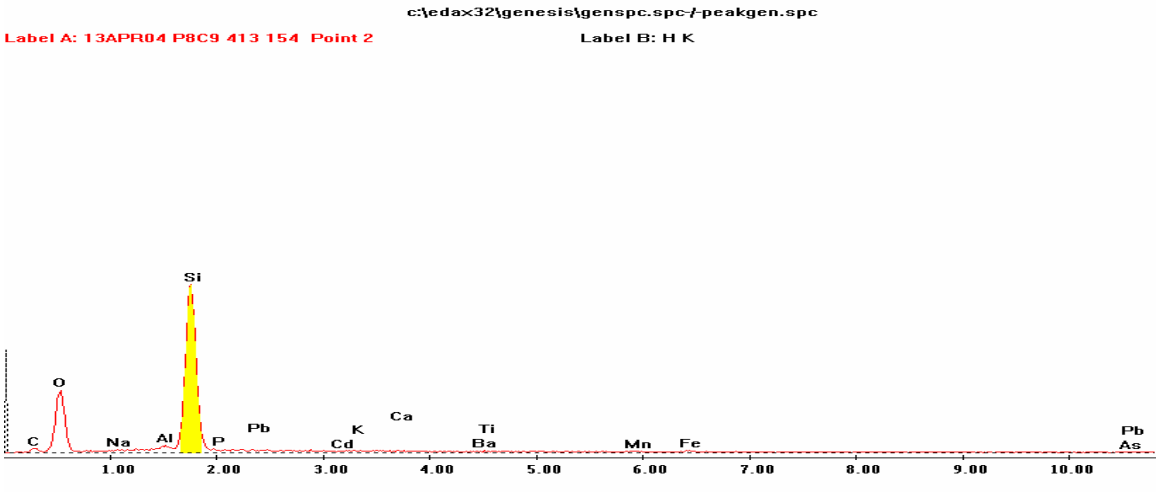

Point 3

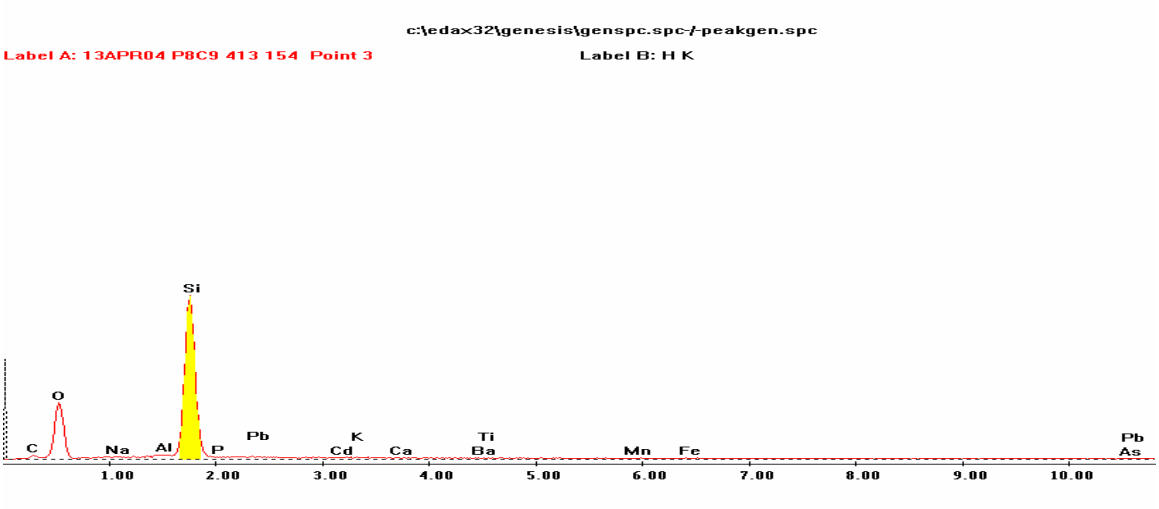

Point 4

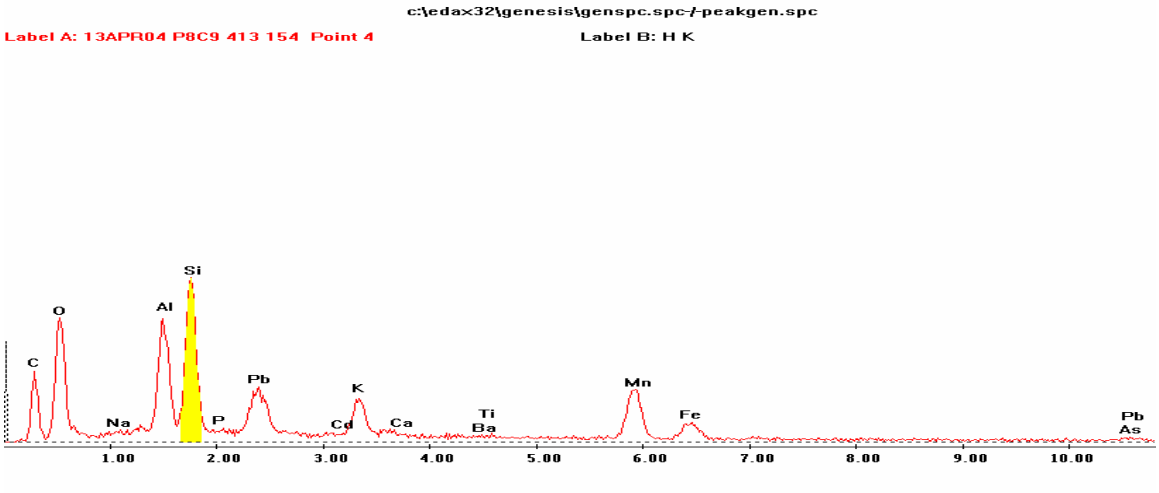

Point 5

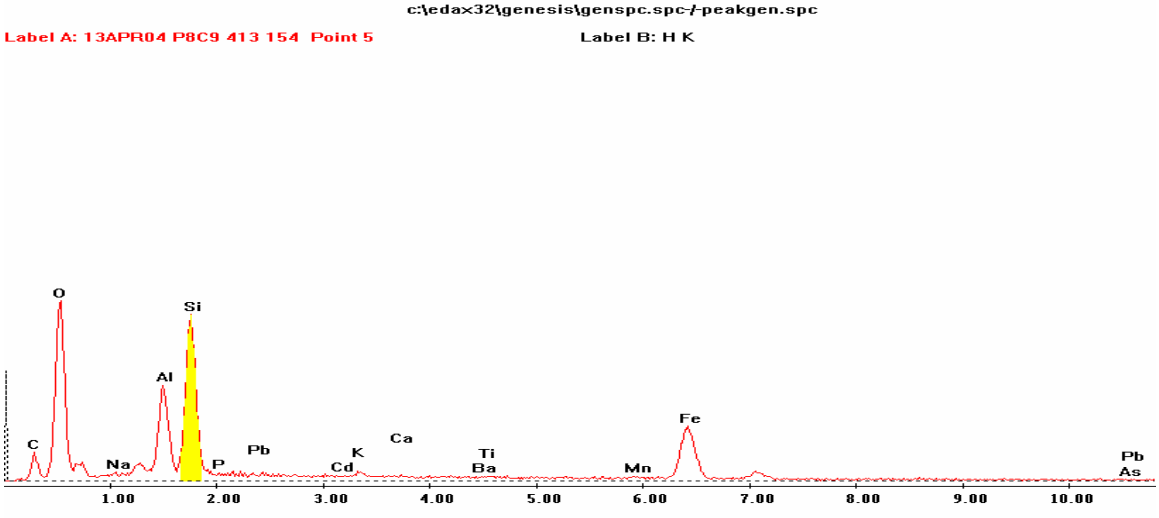

Point 6

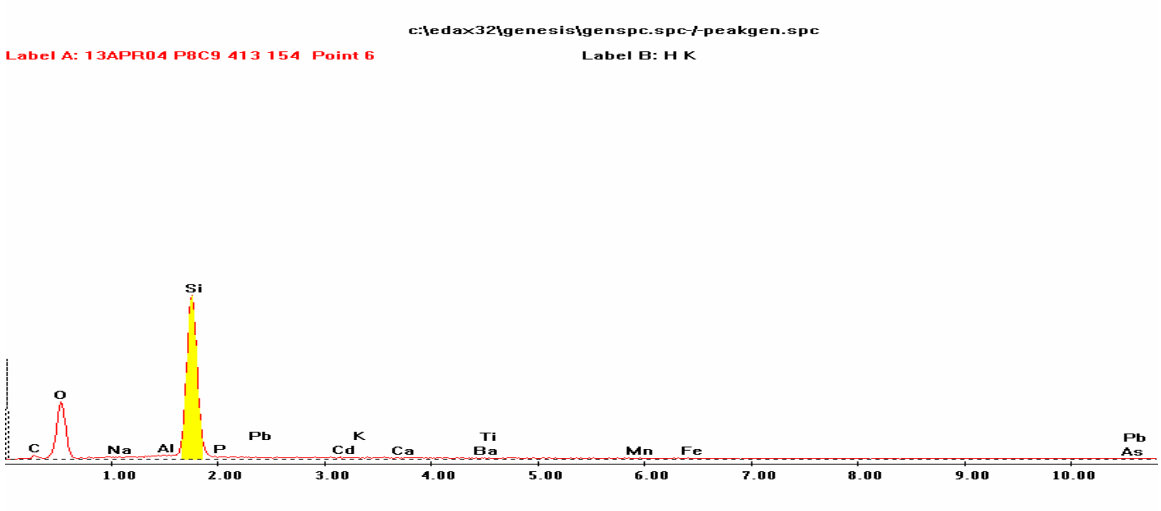

Point 7

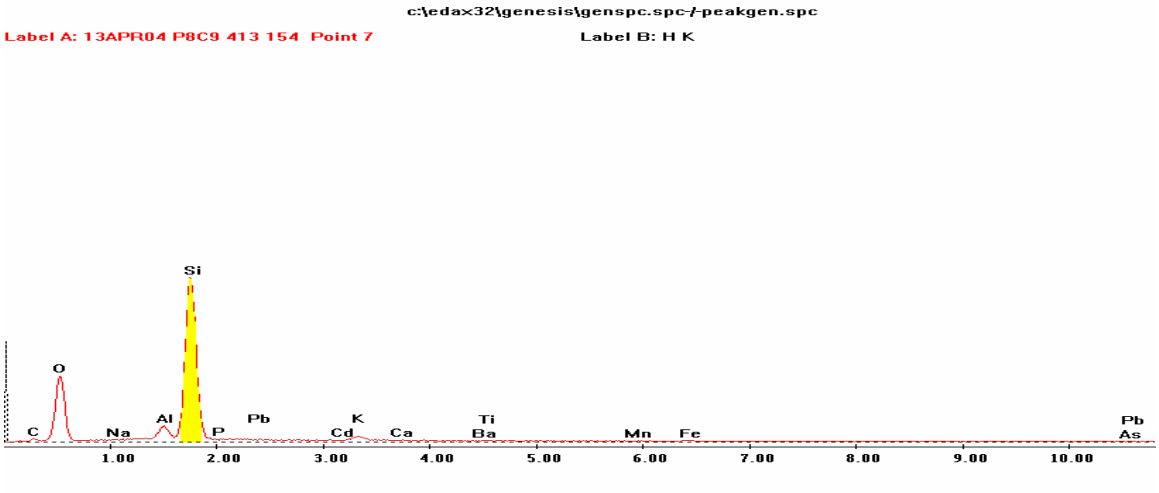

Point 8

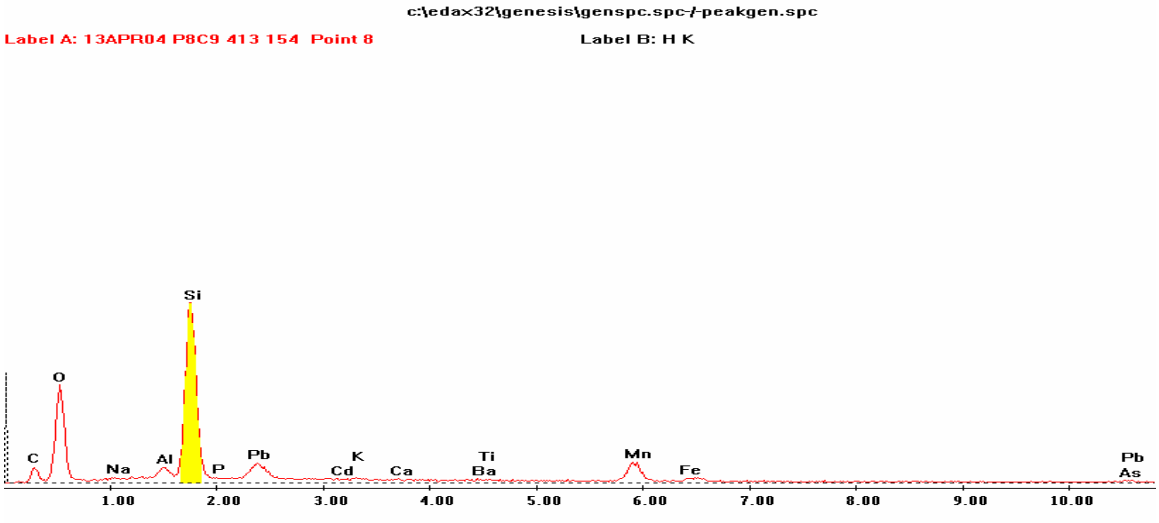

Point 9

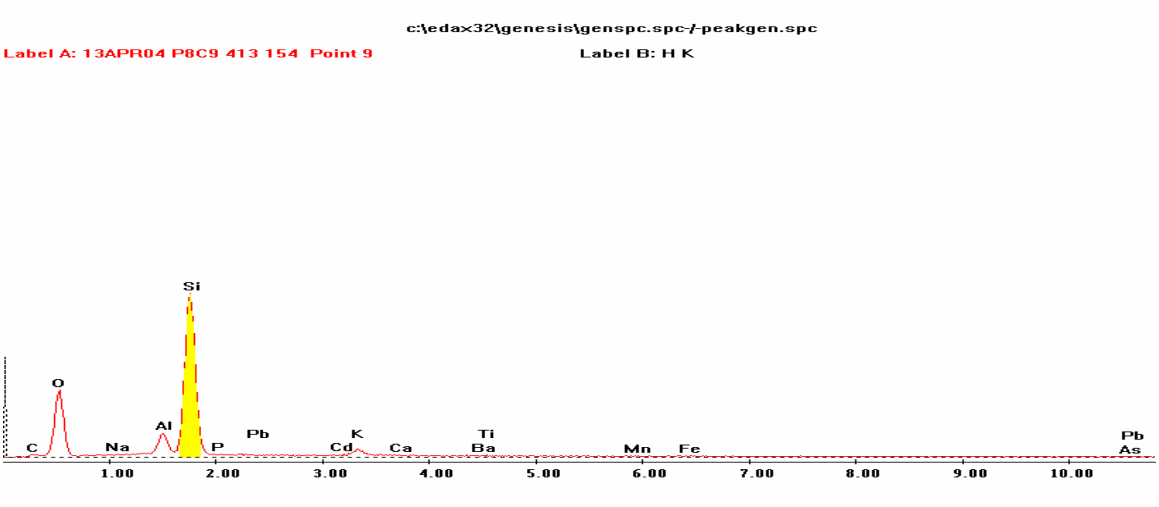

Point 10

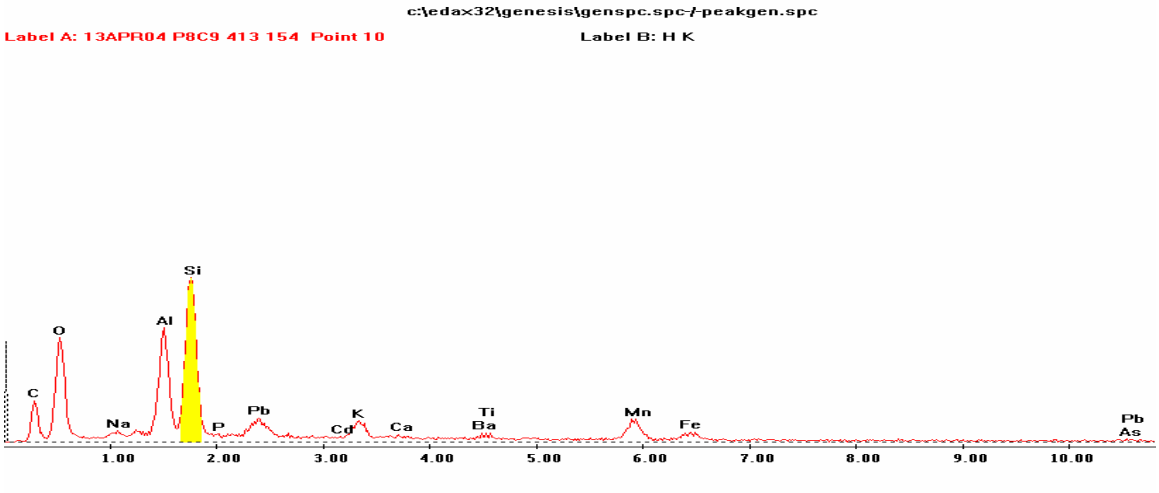

P8C9 – 448, 239

BSE Image

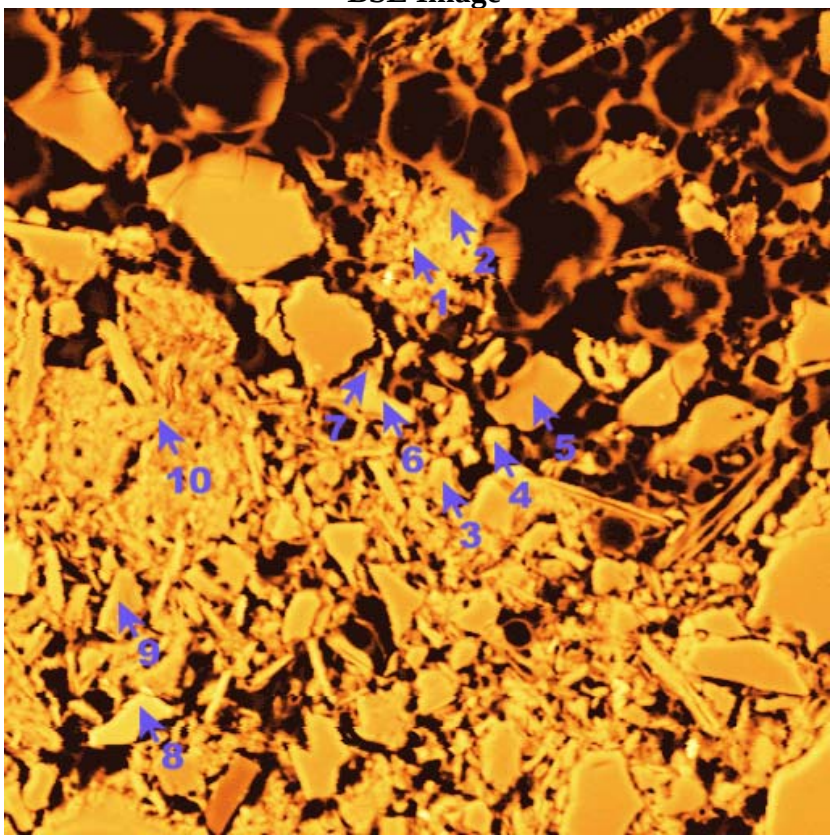

Iron (Fe)

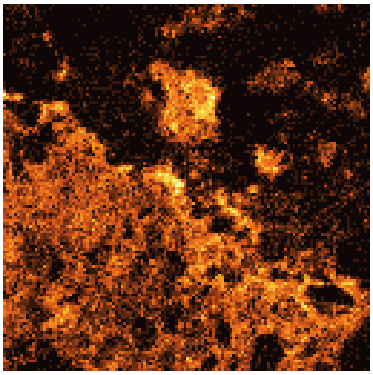

Manganese (Mn)

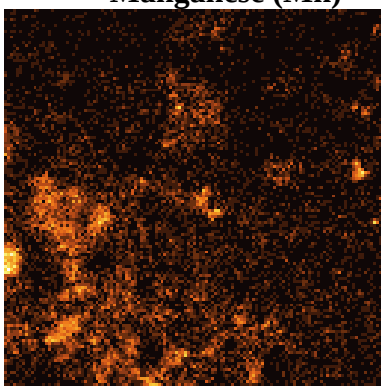

Phosphorous (P)

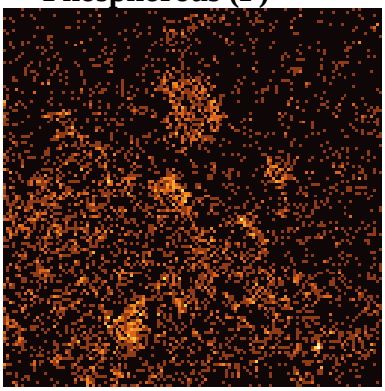

Lead (Pb)

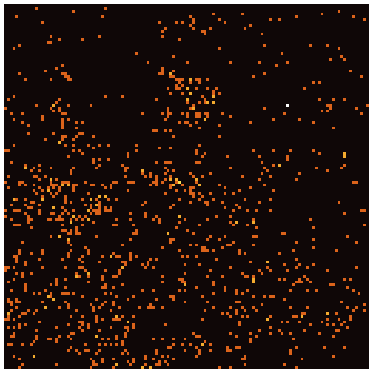

Silicon (Si)

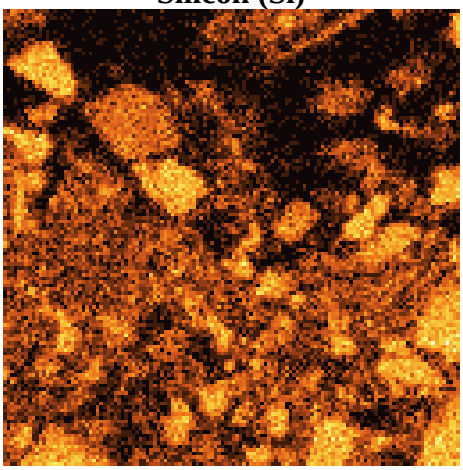

EDS Scan Images by Point

Point 1

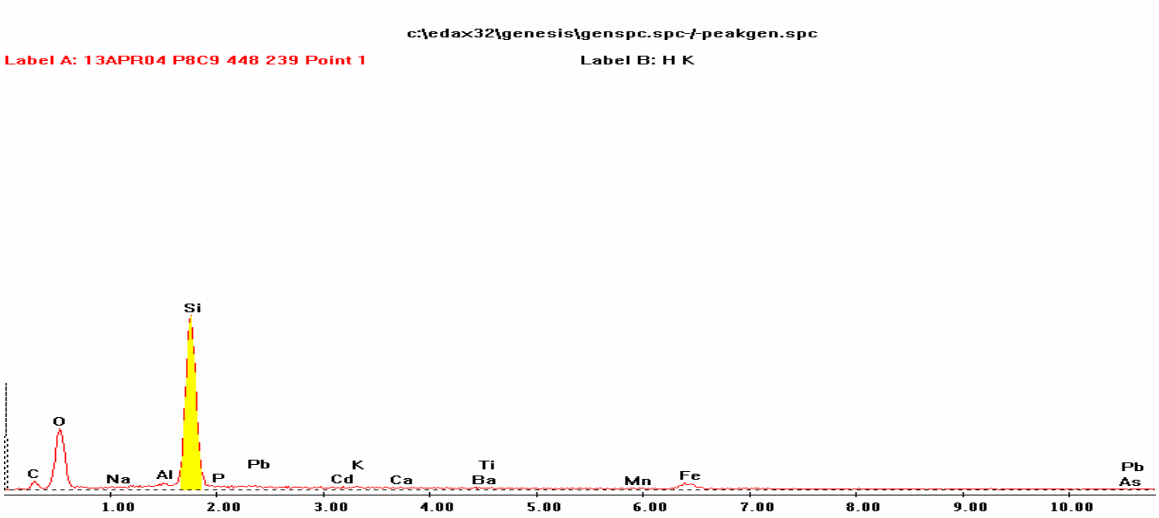

Point 2

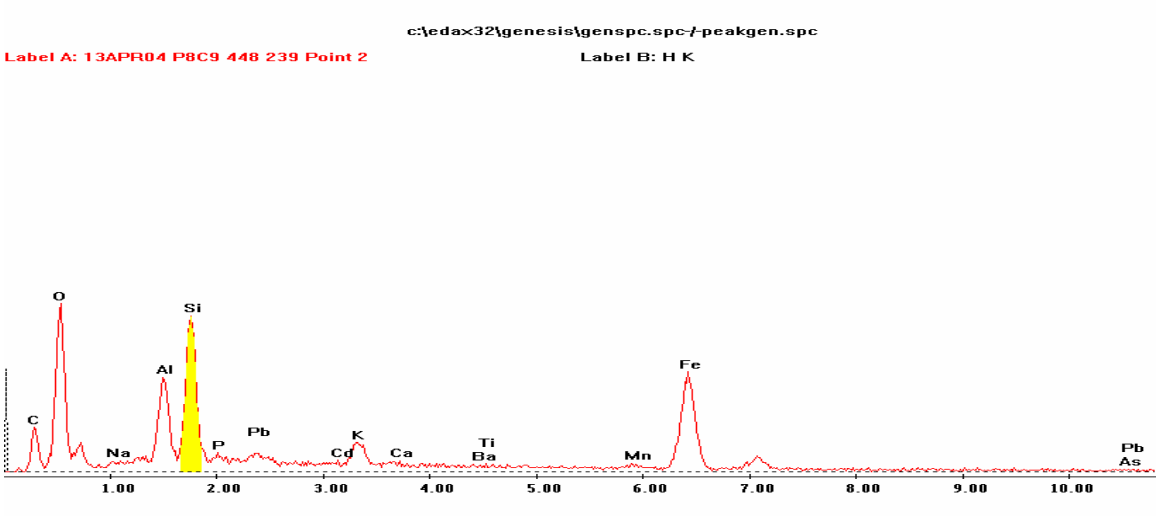

Point 3

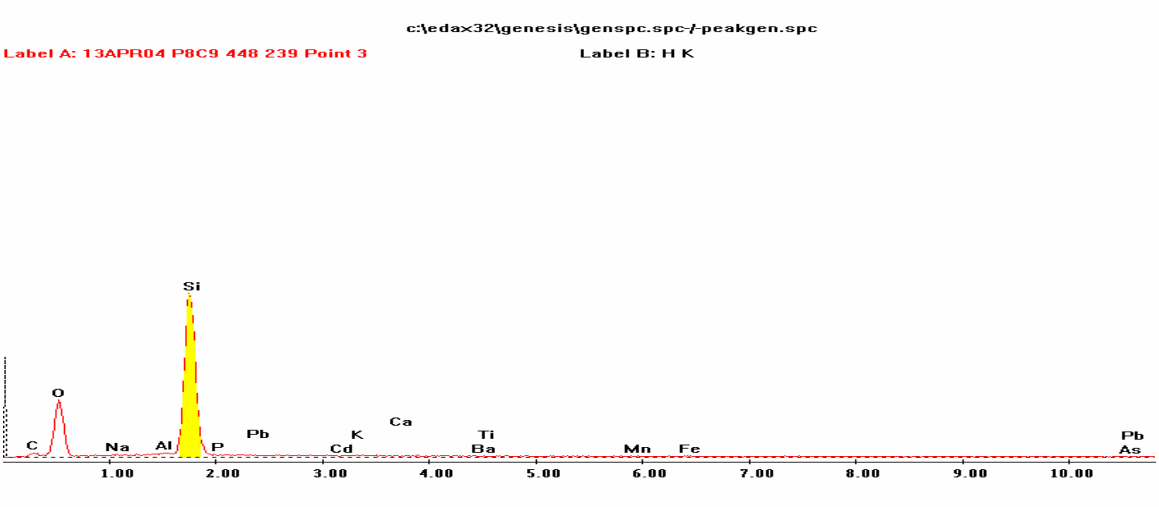

Point 4

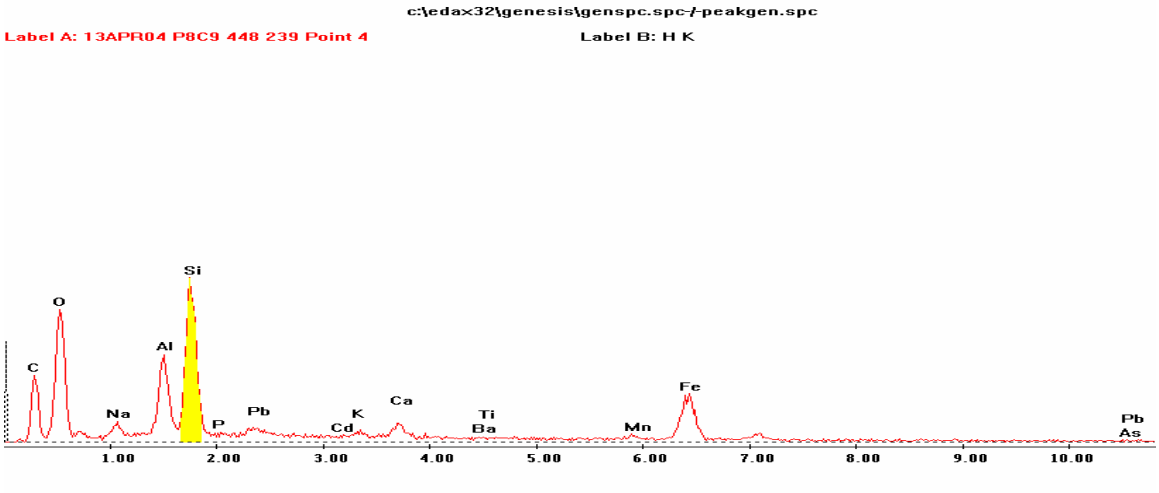

Point 5

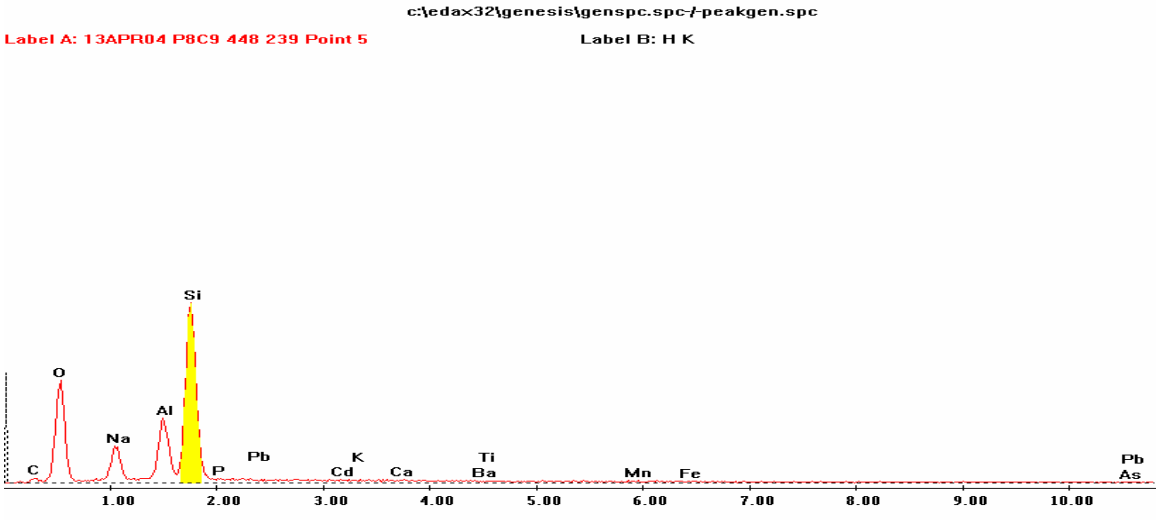

Point 6

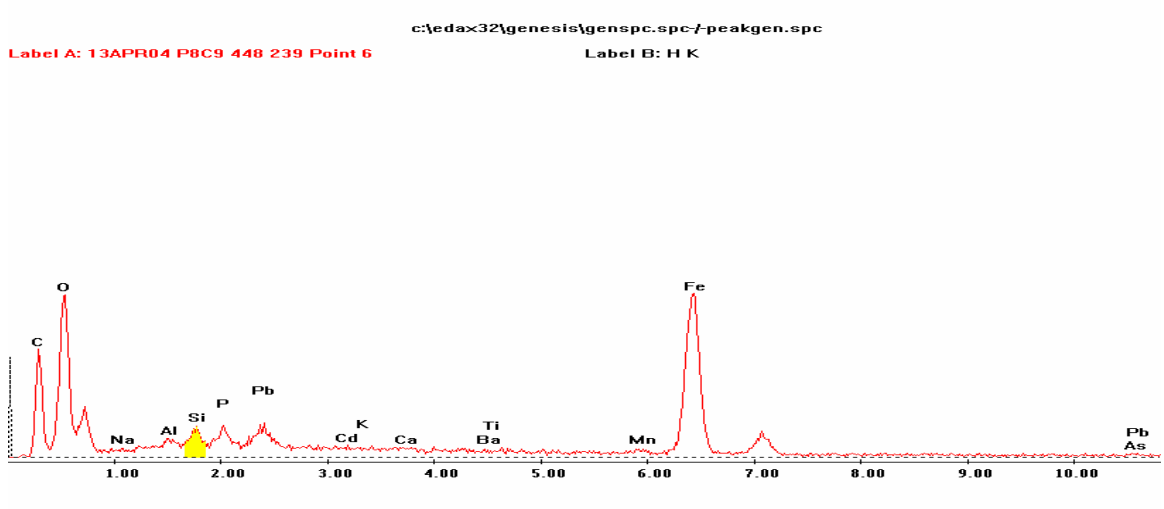

Point 7

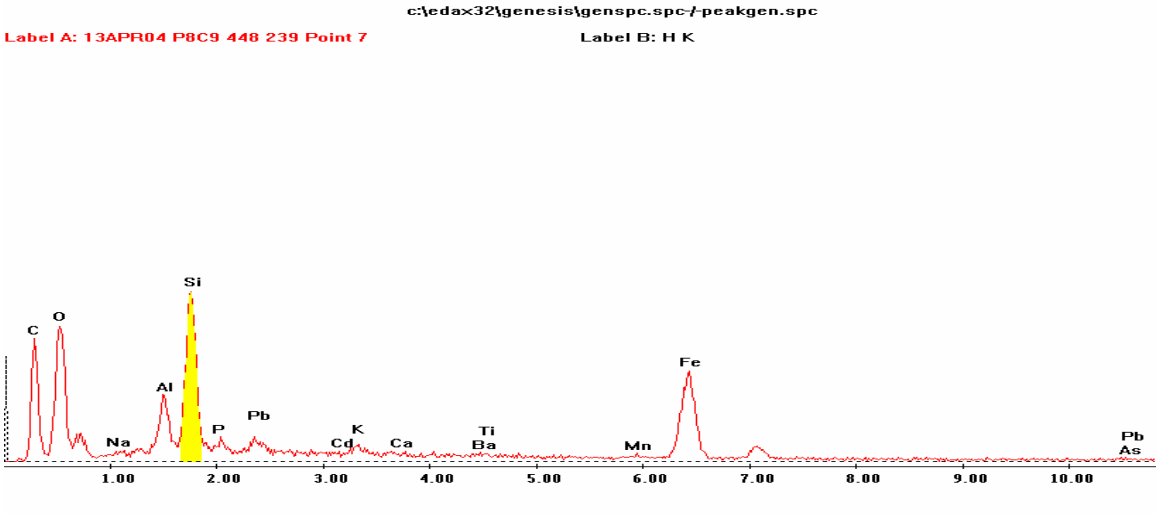

Point 8

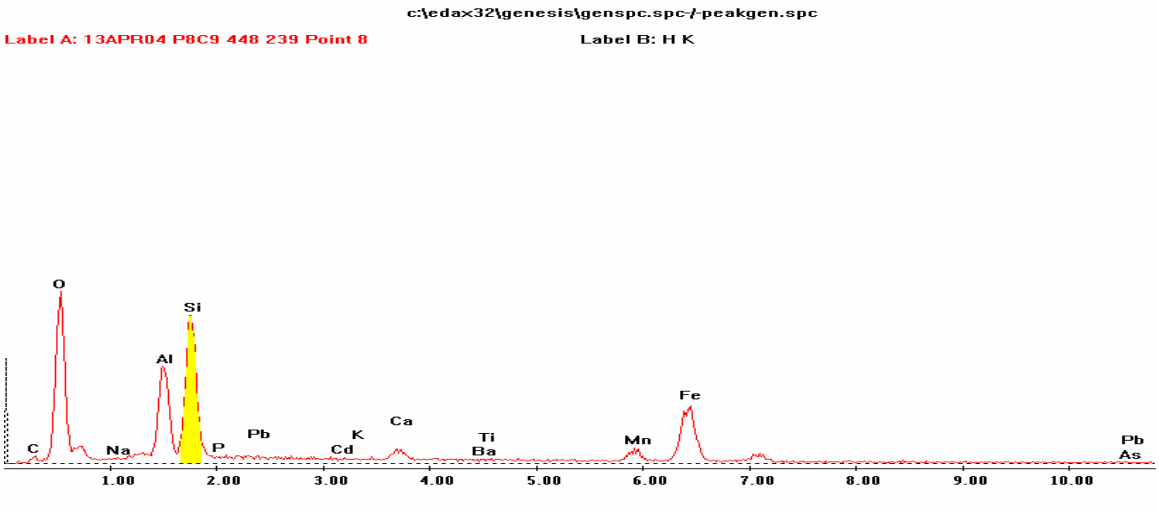

Point 9

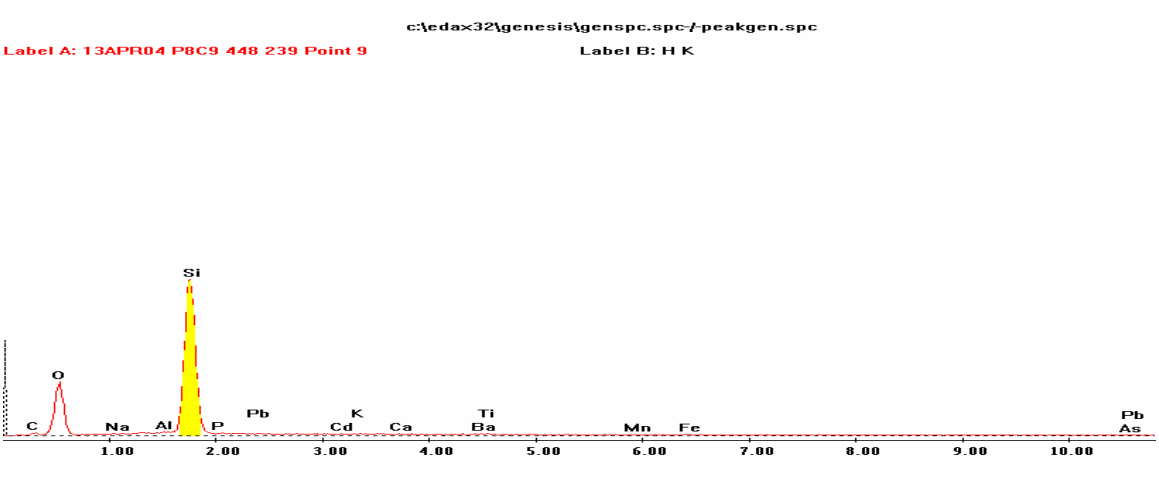

Point 10

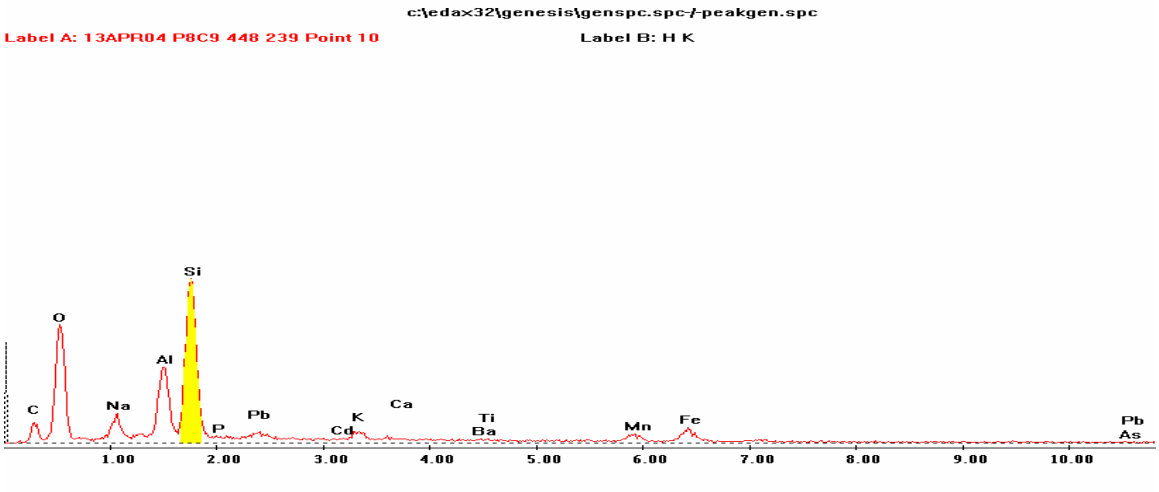

P8C9 – 451, 293

BSE Image

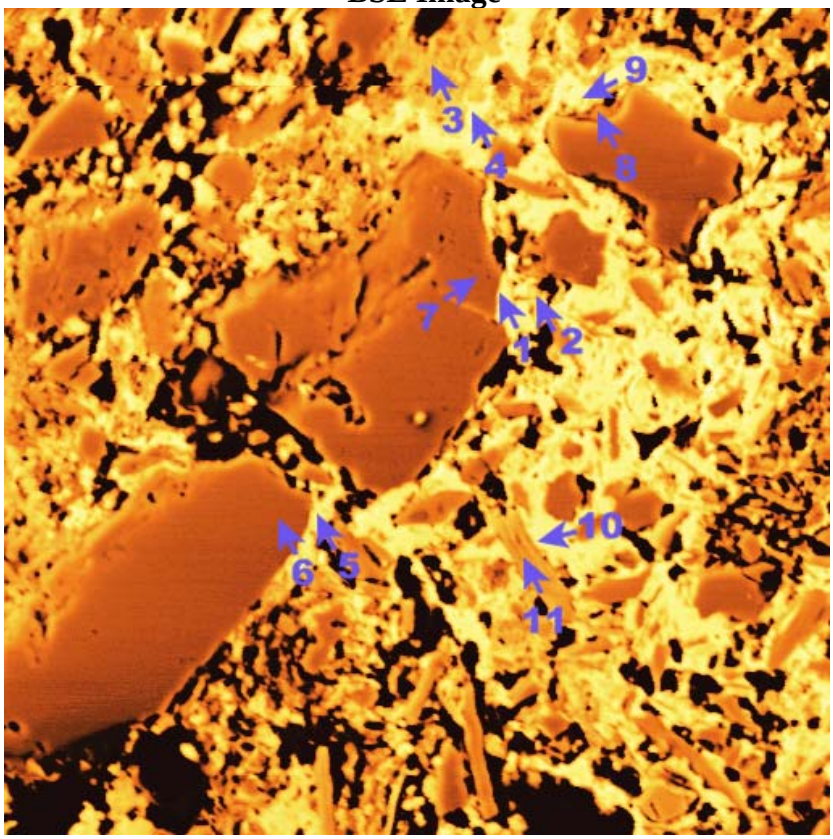

Iron (Fe)

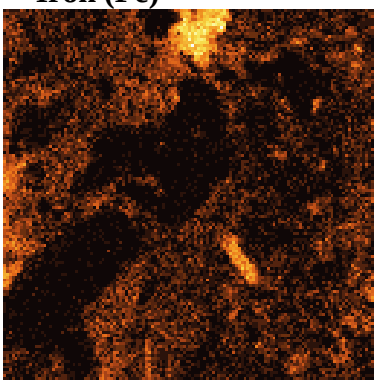

Manganese (Mn)

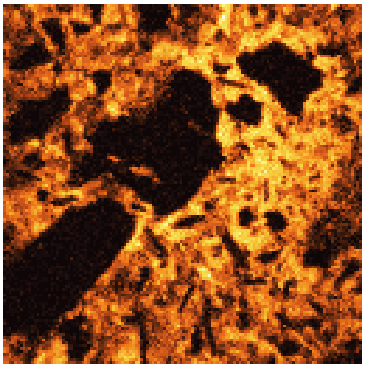

Phosphorous (P)

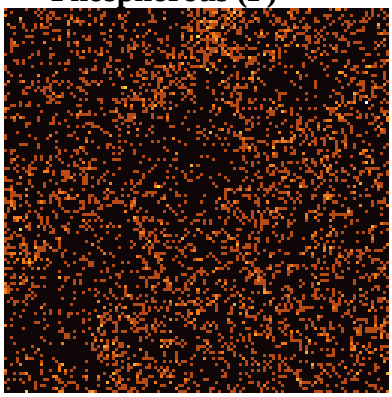

Lead (Pb)

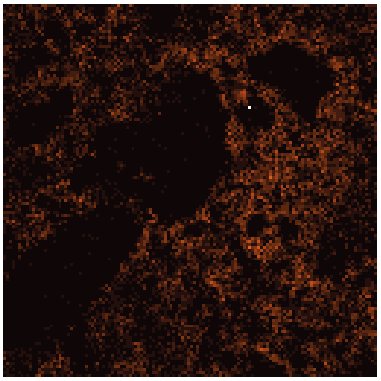

Silicon (Si)

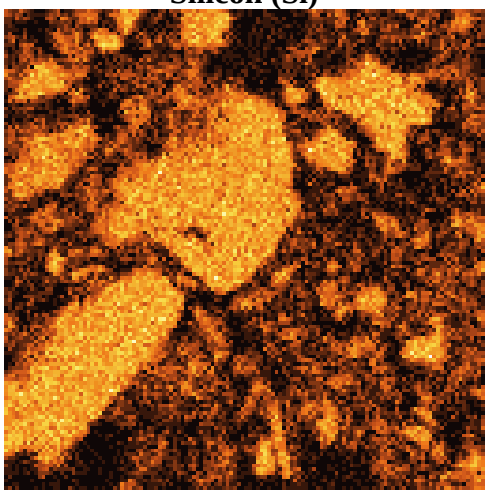

EDS Scan Images by Point

Point 1

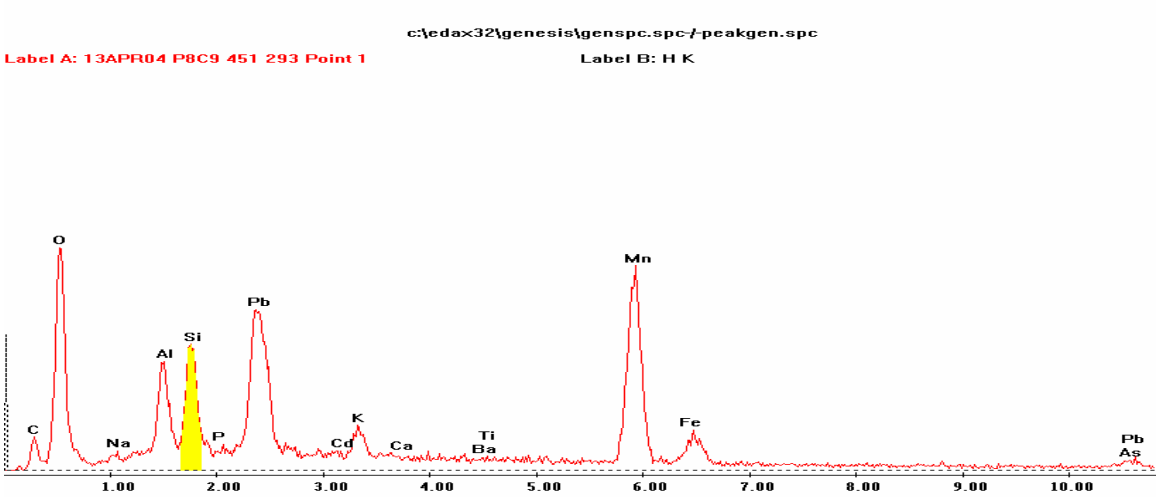

Point 2

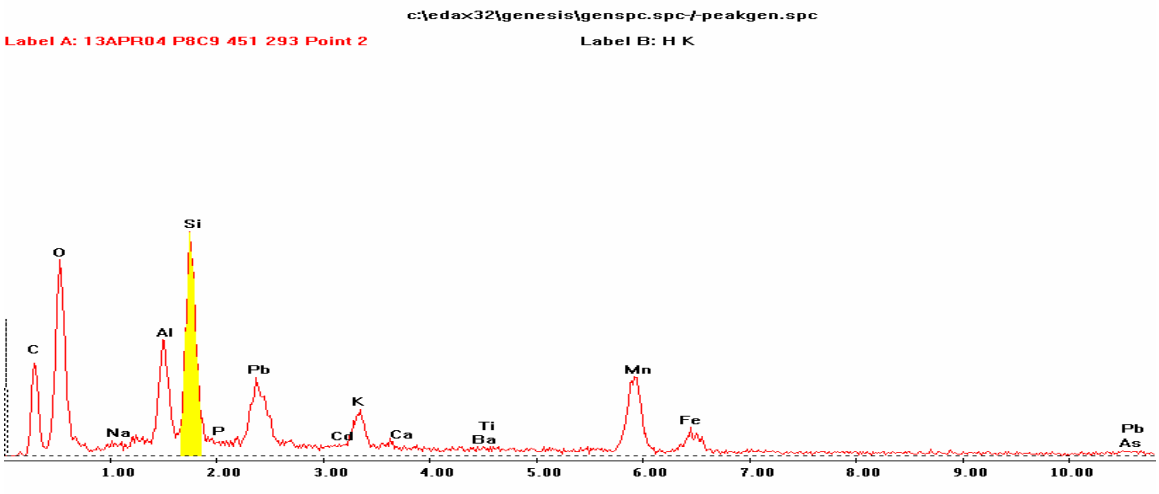

Point 3

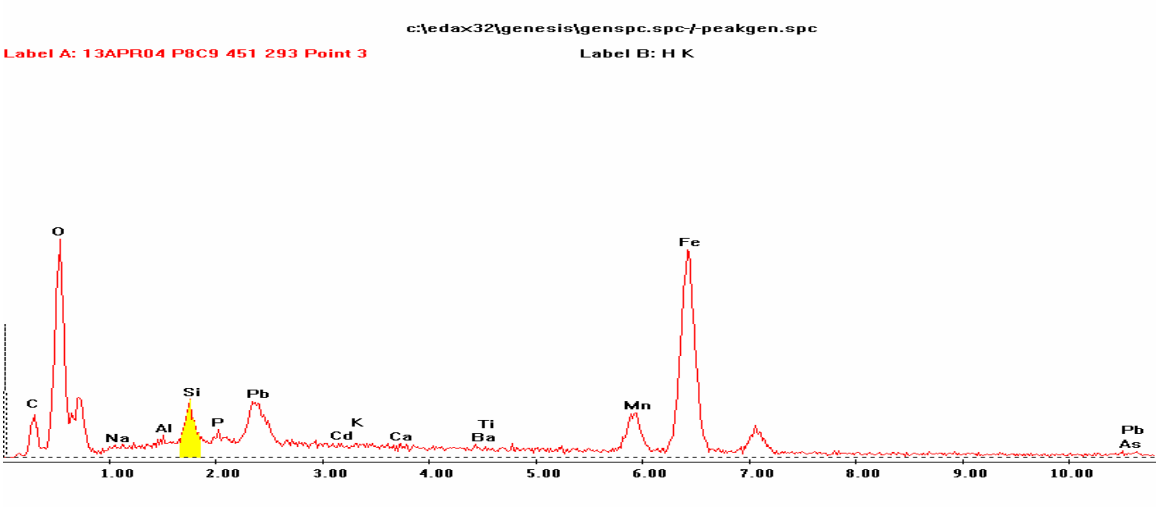

Point 4

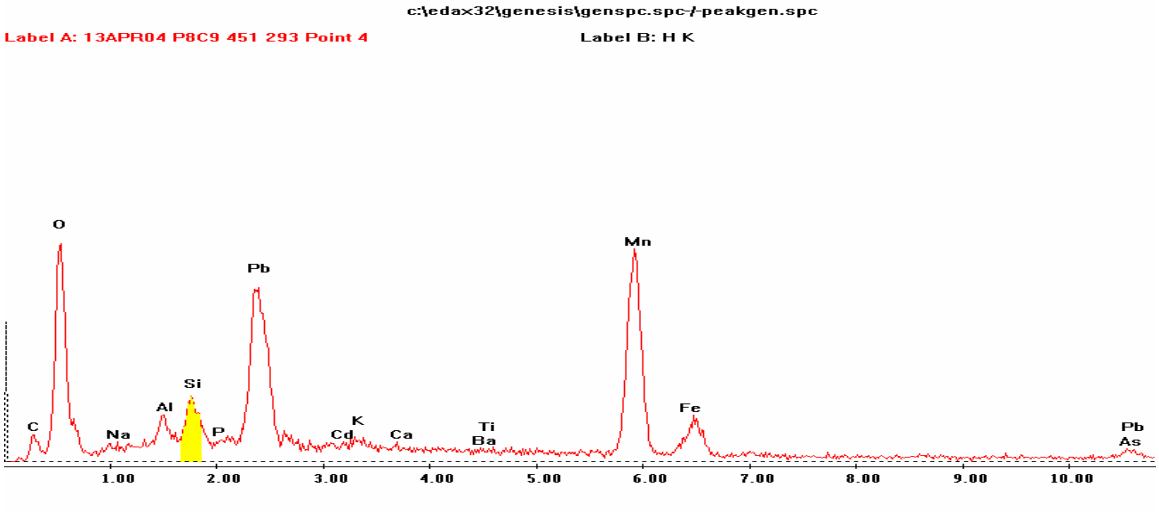

Point 5

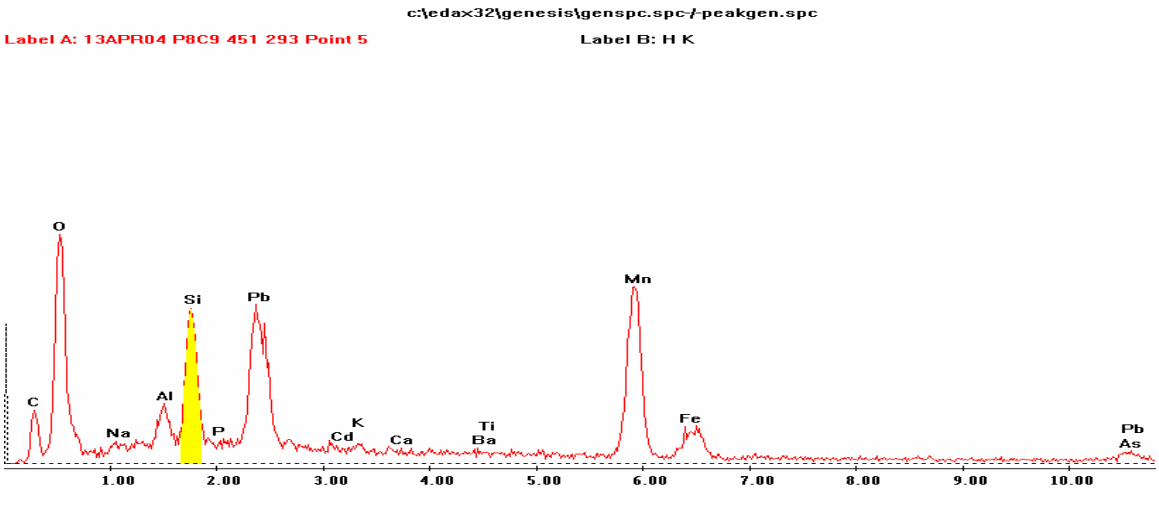

Point 6

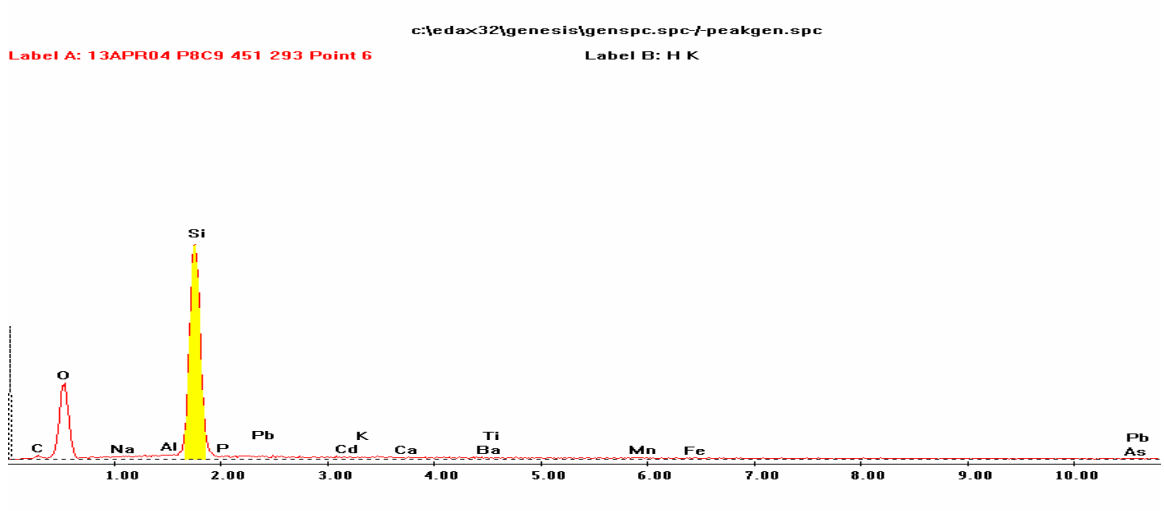

Point 7

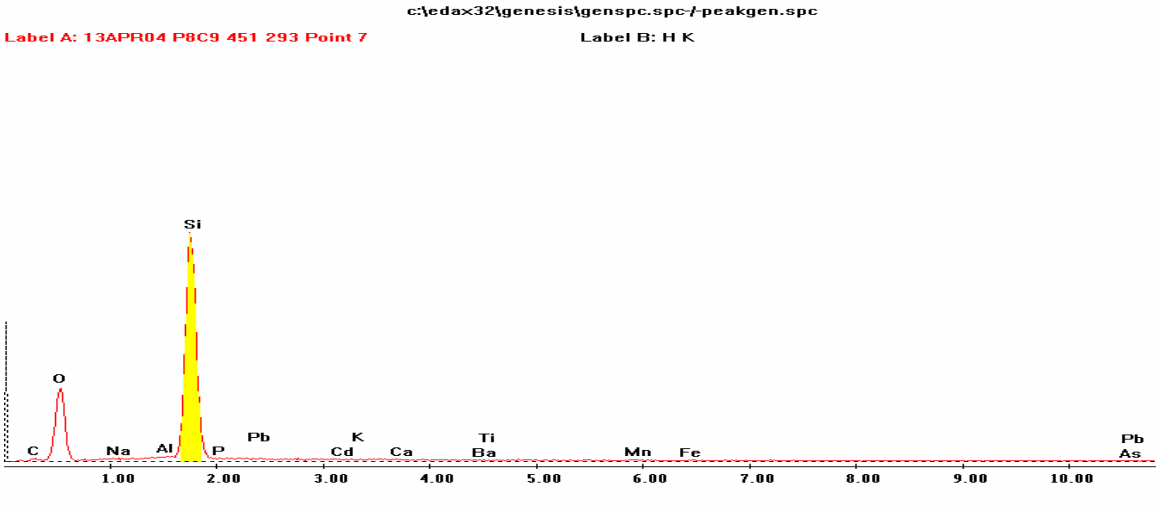

Point 8

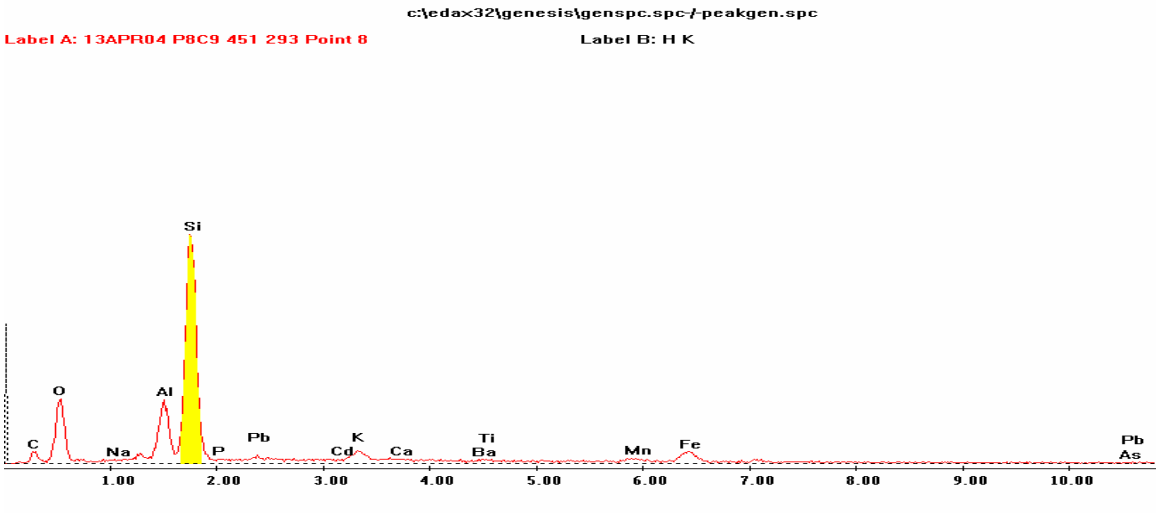

Point 9

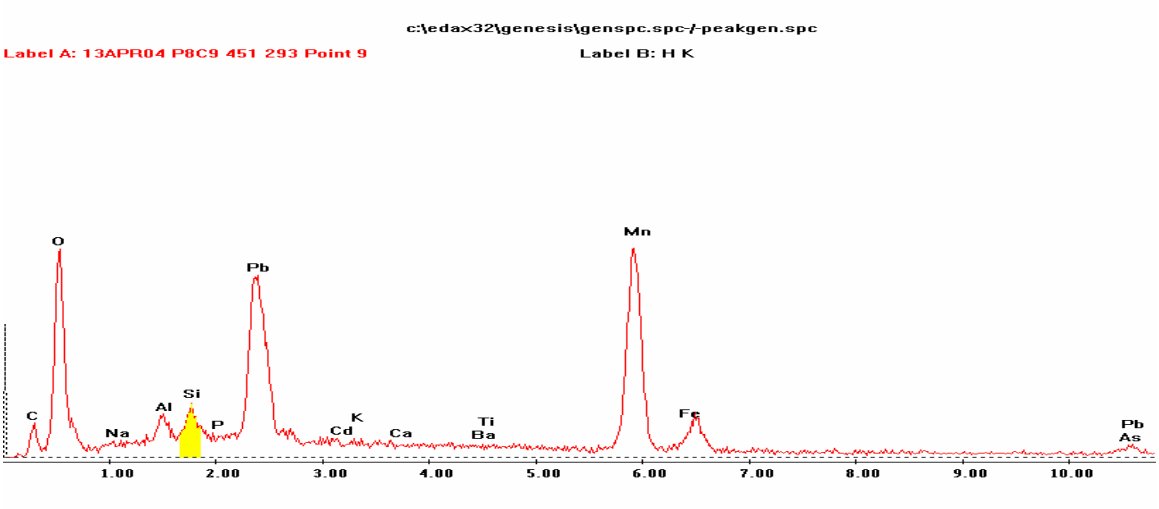

Point 10

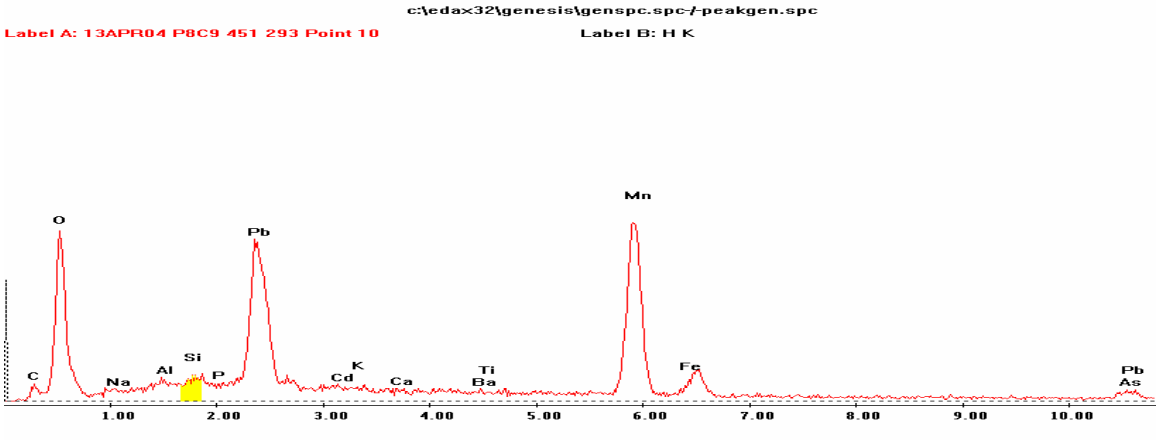

Point 11

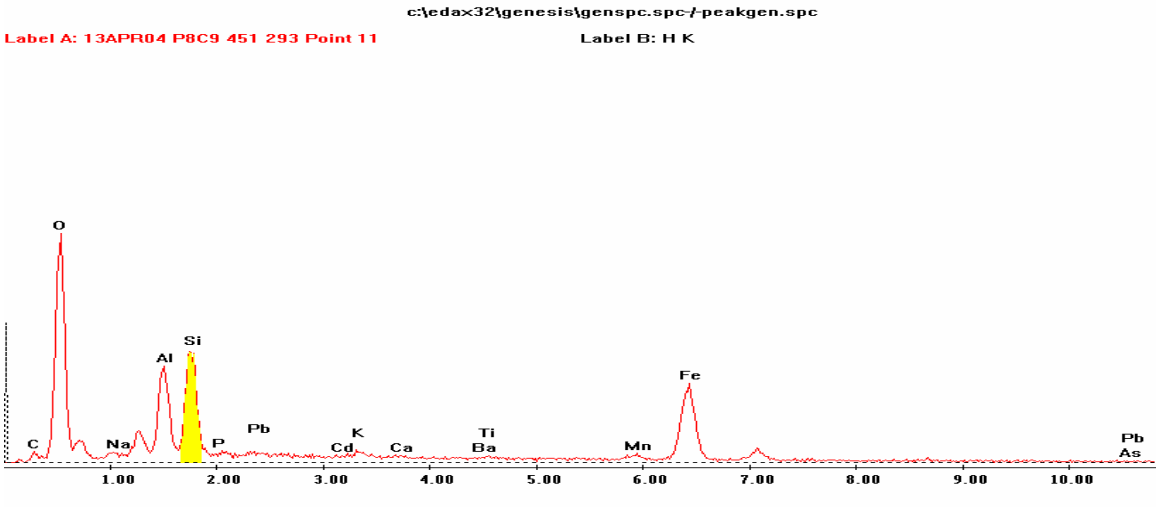

P8C9 – 456, 227

BSE Image

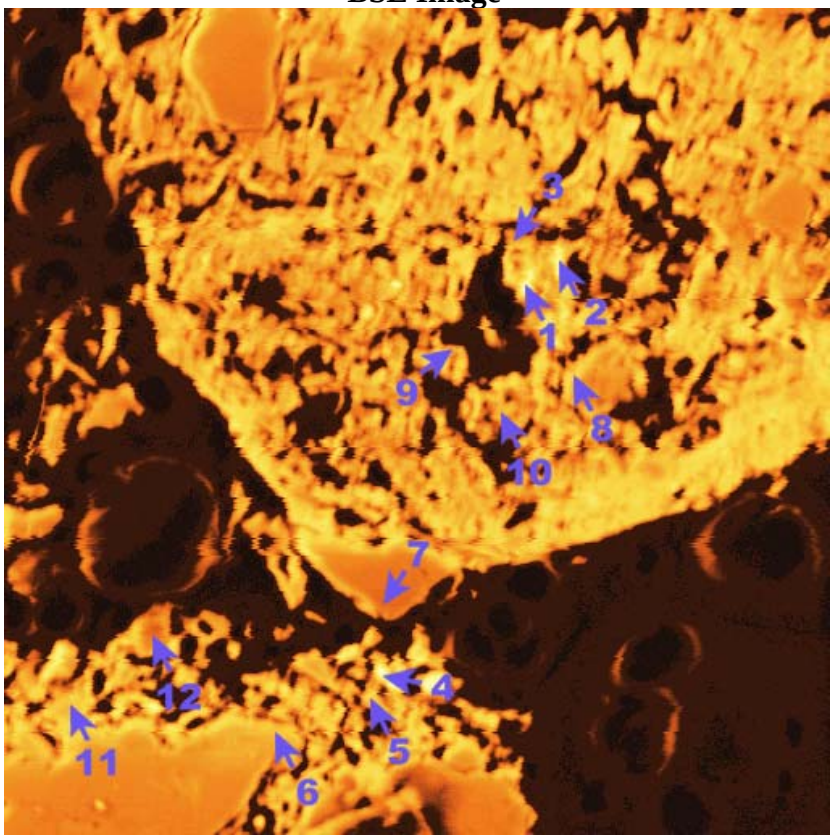

Iron (Fe)

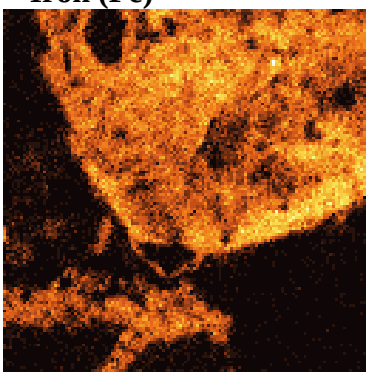

Manganese (Mn)

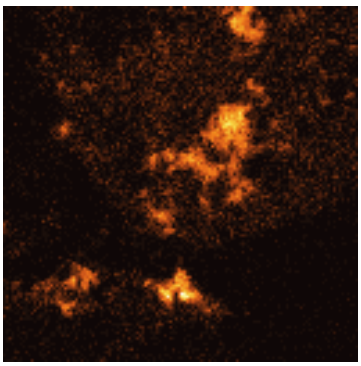

Phosphorous (P)

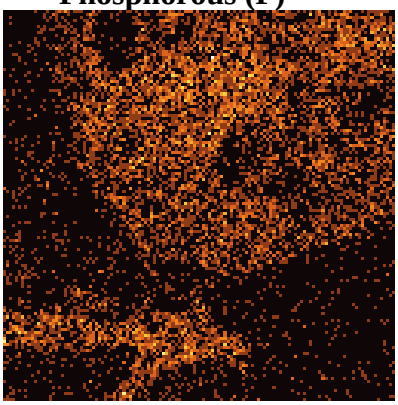

Lead (Pb)

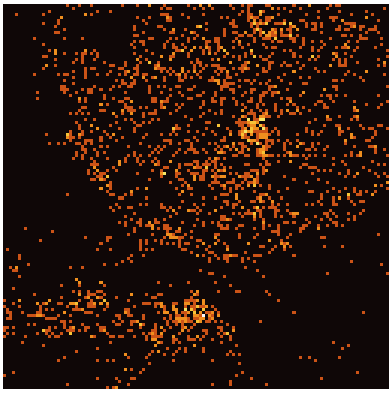

Silicon (Si)

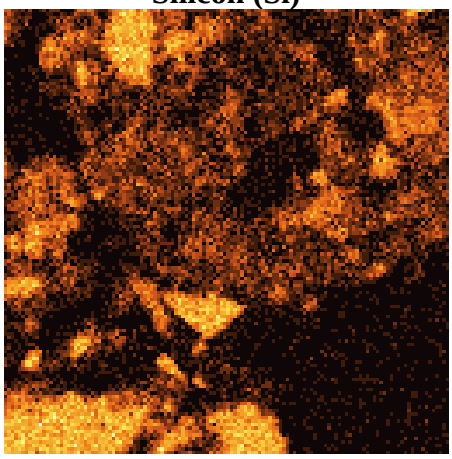

EDS Scan Images by Point

Point 1

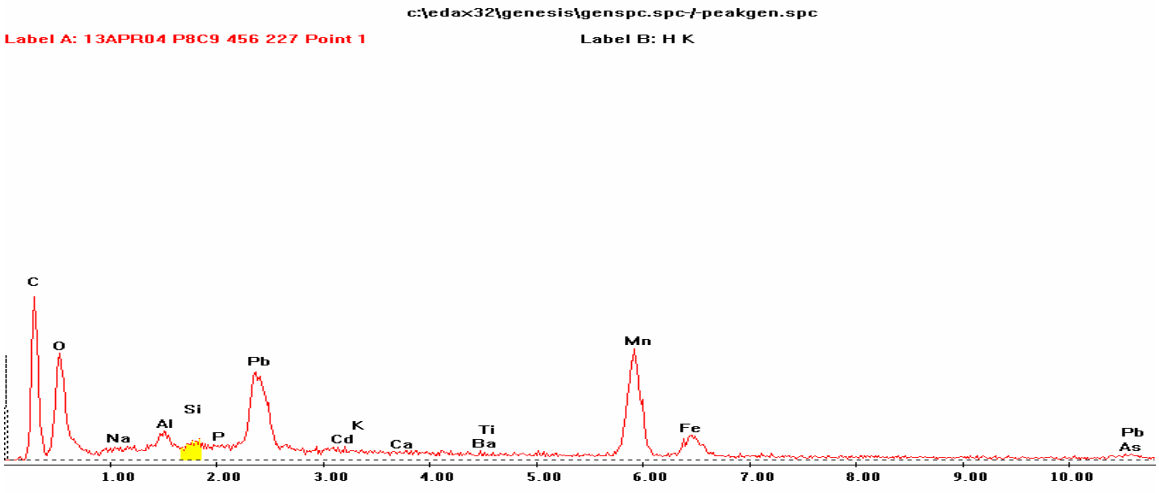

Point 2

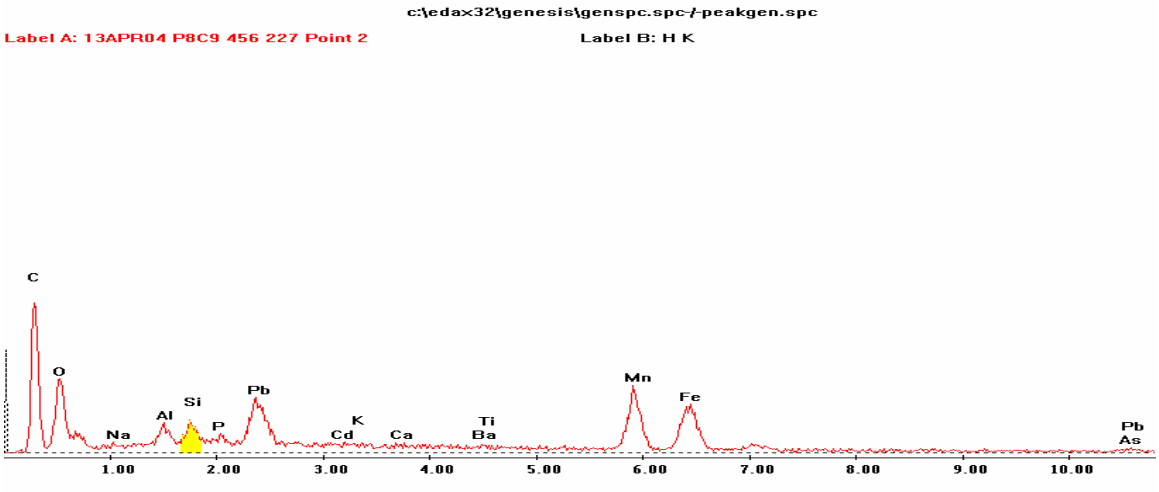

Point 3

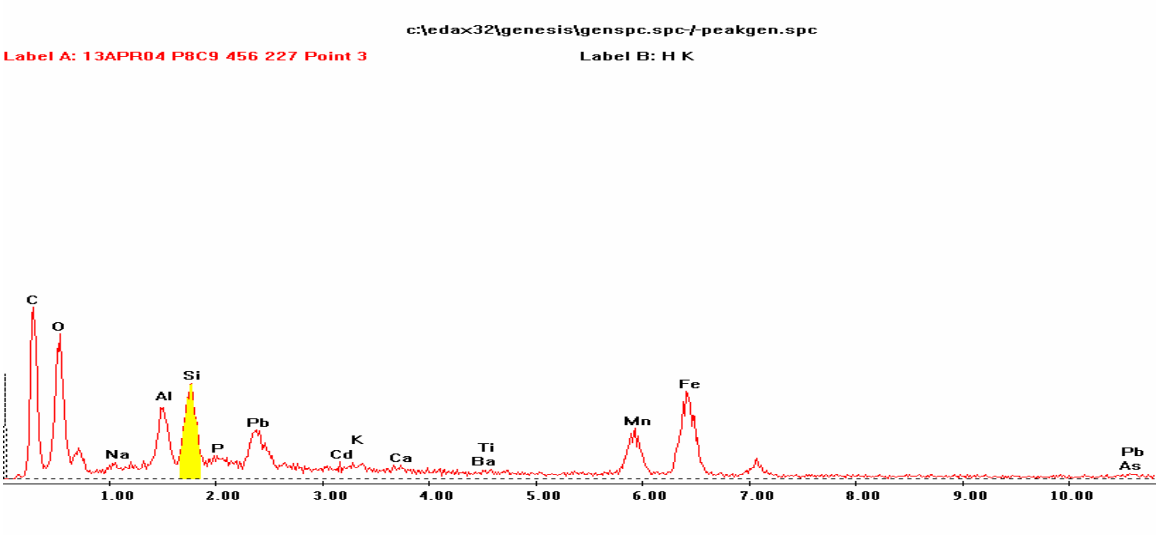

Point 4

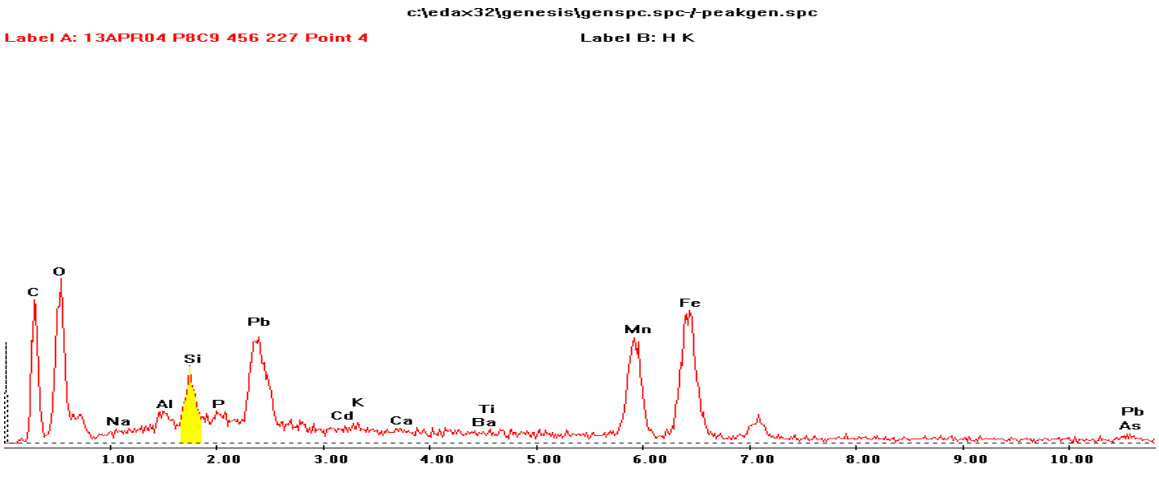

Point 5

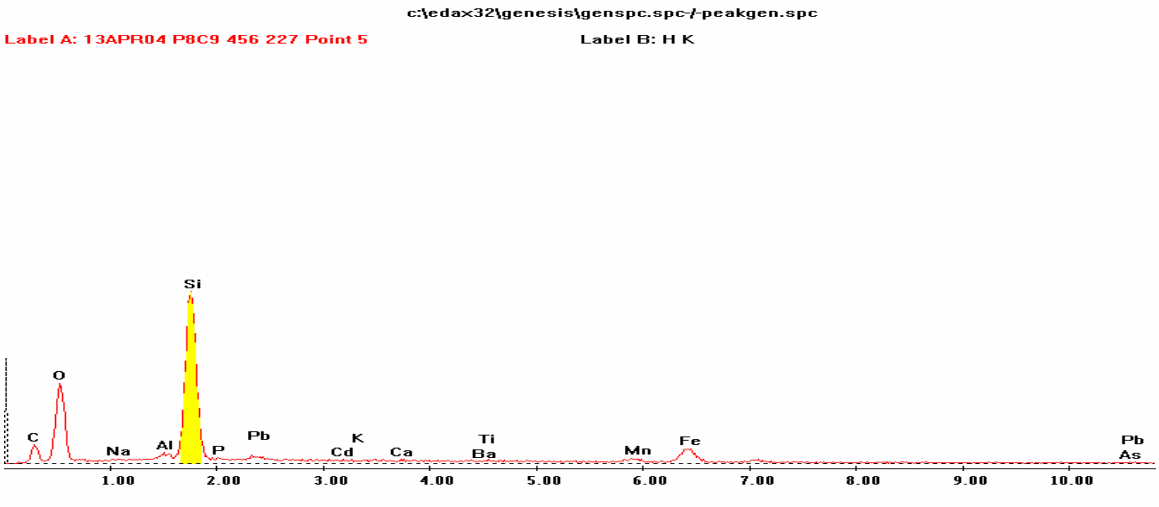

Point 6

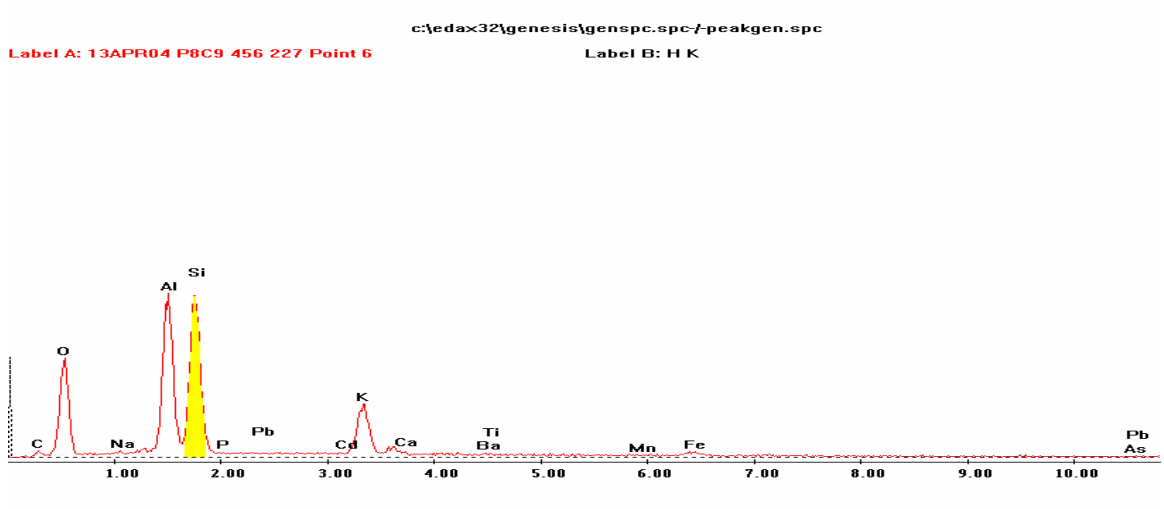

Point 7

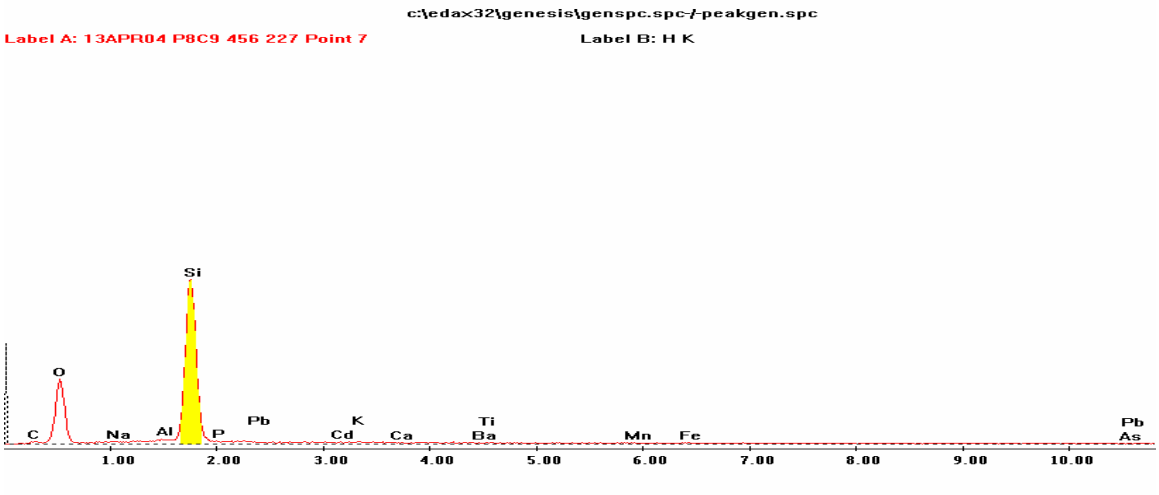

Point 8

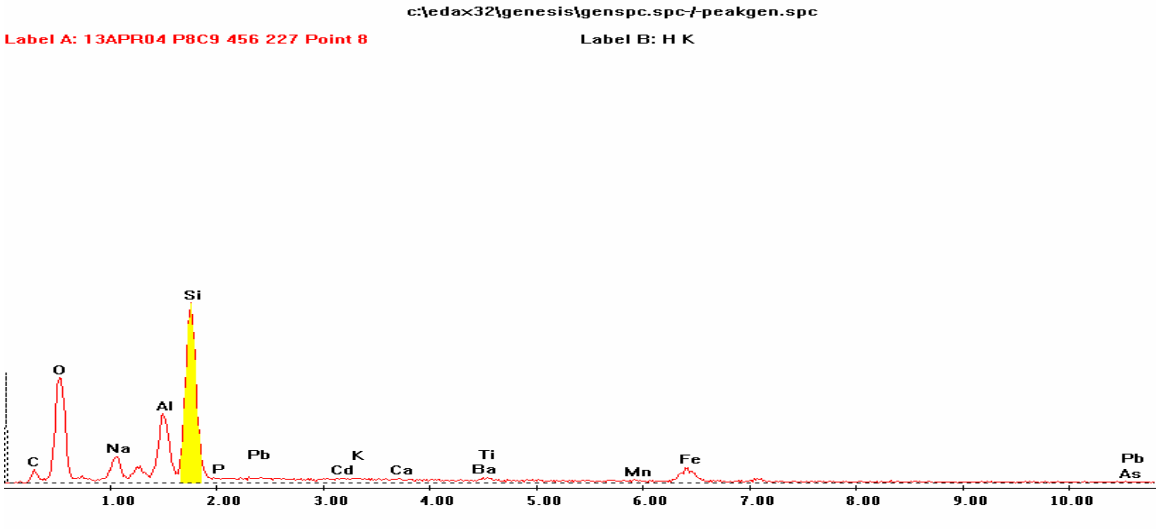

Point 9

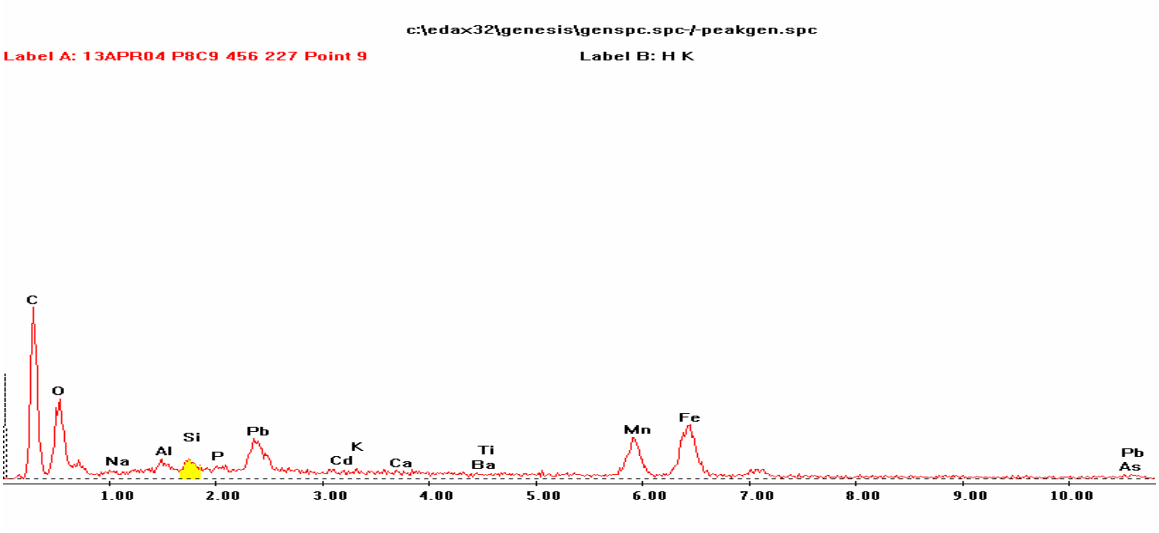

Point 10

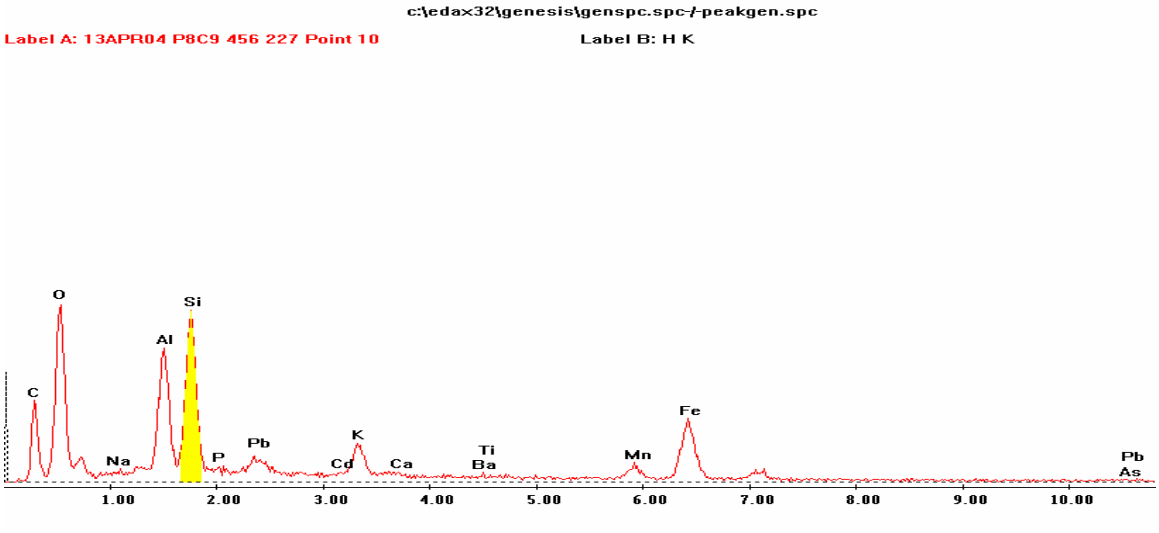

Point 11

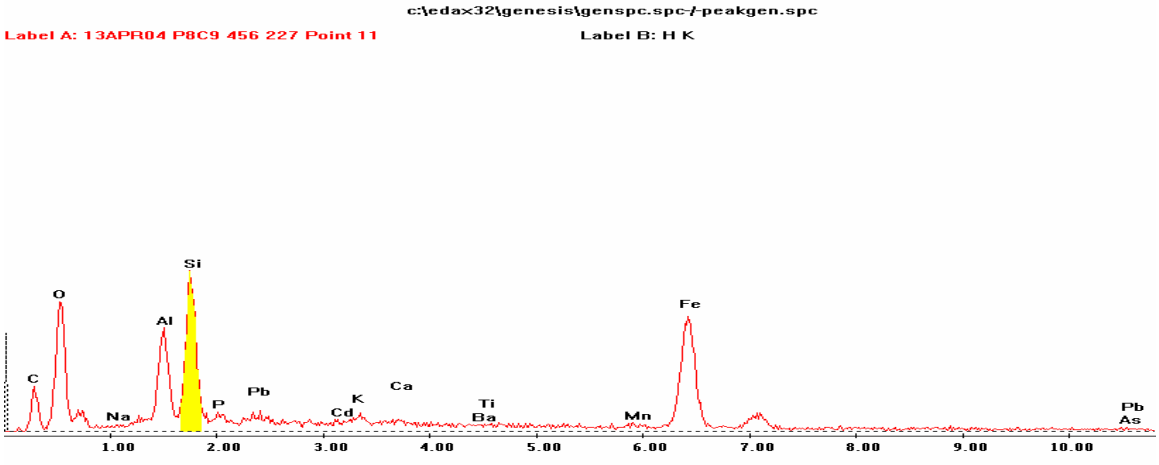

Point 12

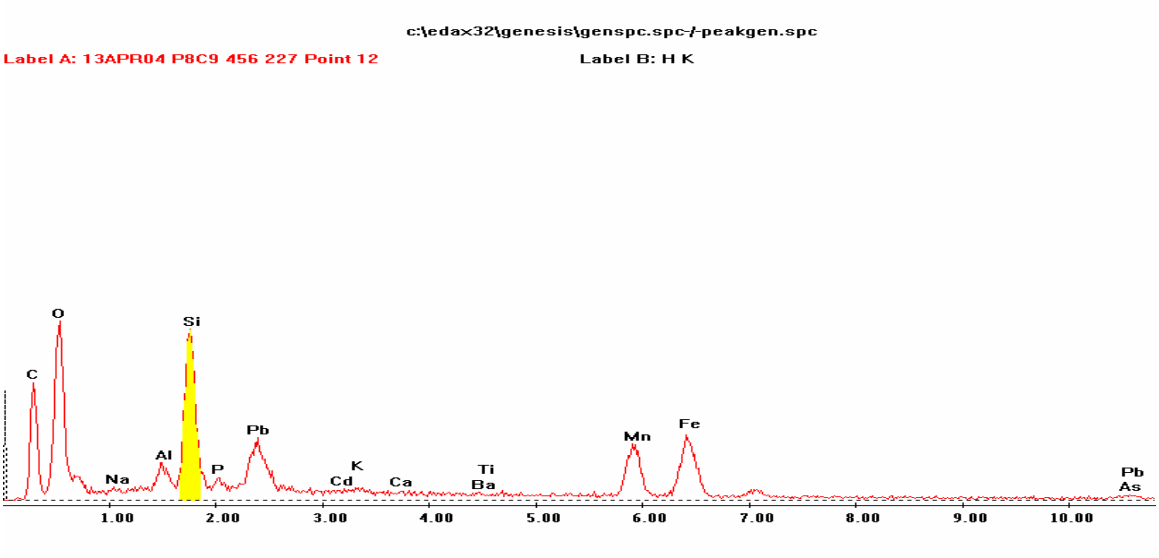
c:\edax32\genesis\genspc.spc-/-peakgen.spc
Label A: 13APR04 P8C9 456 227 Point 12
Label B: H K
O
Si
C
Pb
Mn
Fe
Al
Na
P
K
Cd
Ca
Ti
Ba
Pb
As
1.00
2.00
3.00
4.00
5.00
6.00
7.00
8.00
9.00
10.00

P8C9 – 484, 269

BSE Image

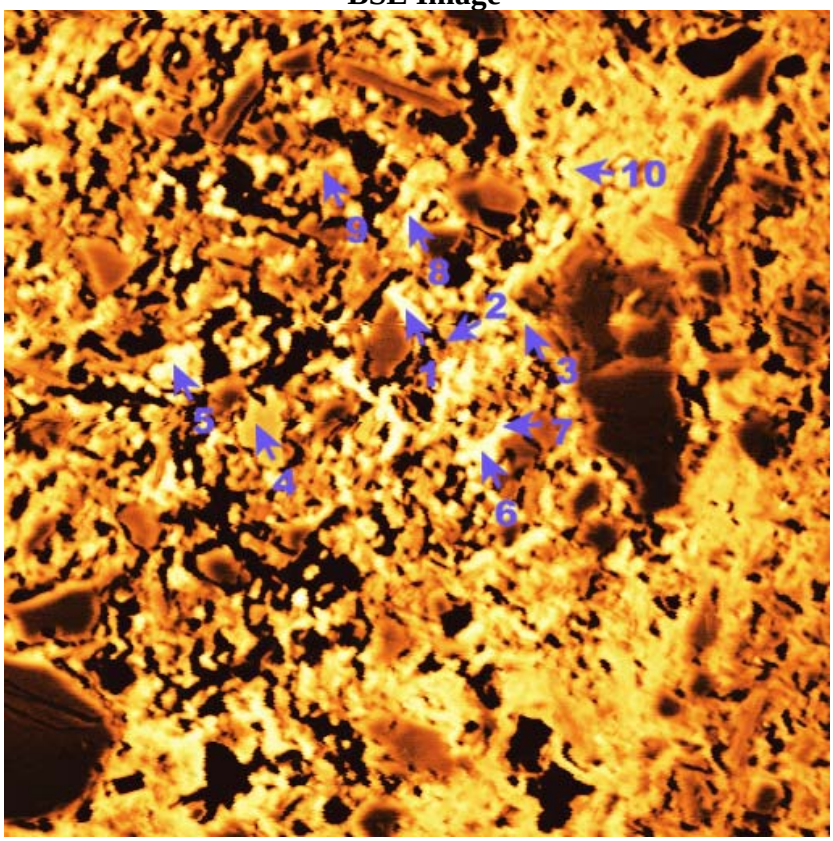

Iron (Fe)

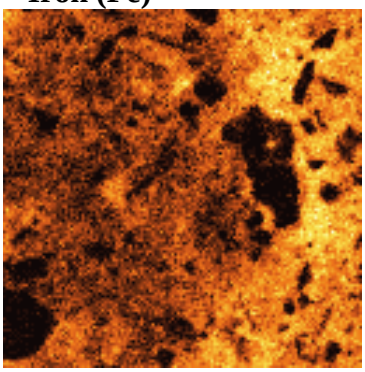

Manganese (Mn)

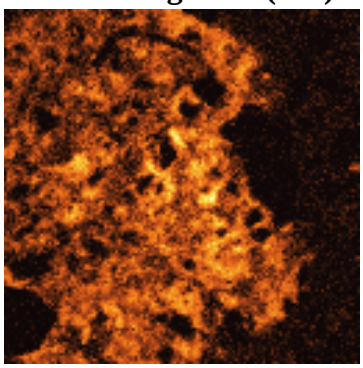

Phosphorous (P)

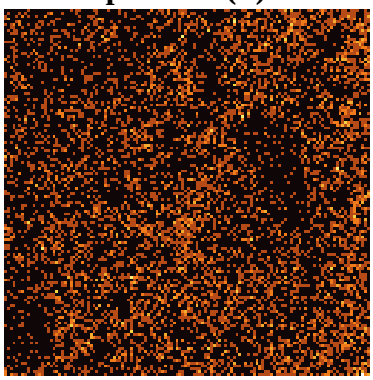

Lead (Pb)

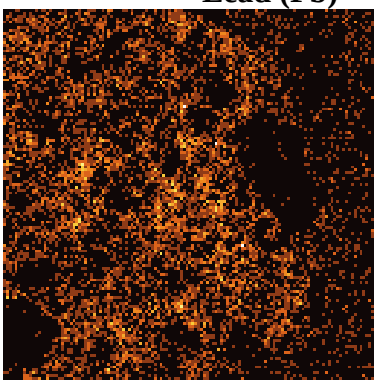

Silicon (Si)

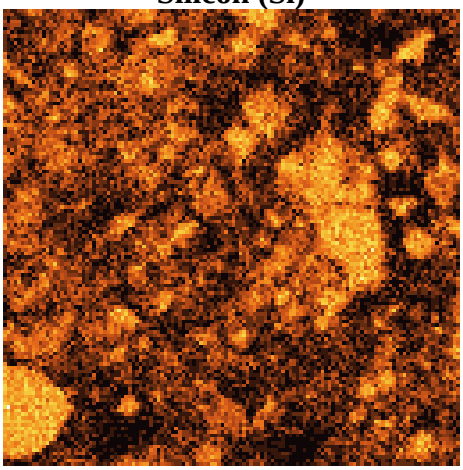

EDS Scan Images by Point

Point 1

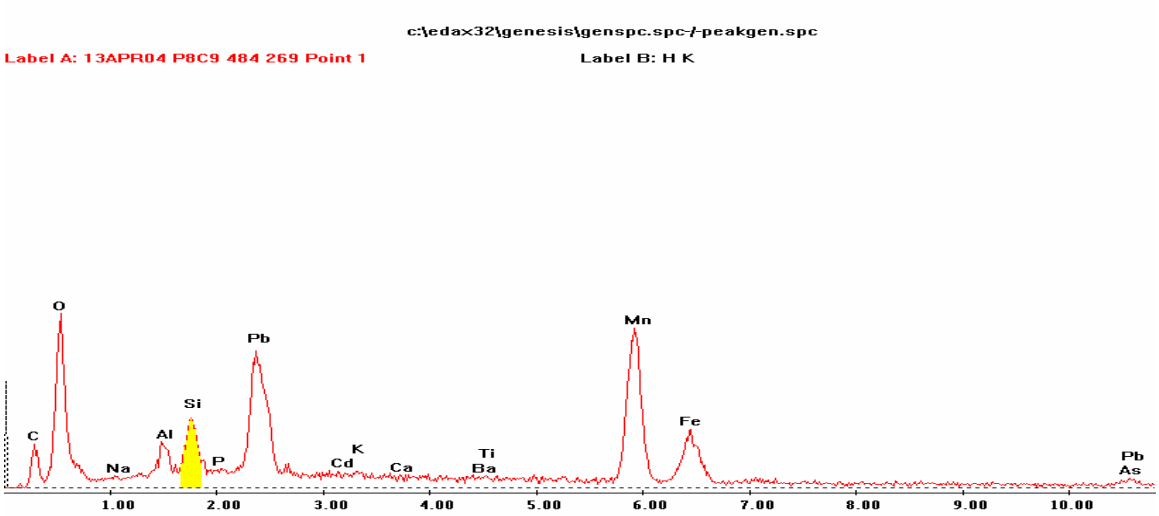

Point 2

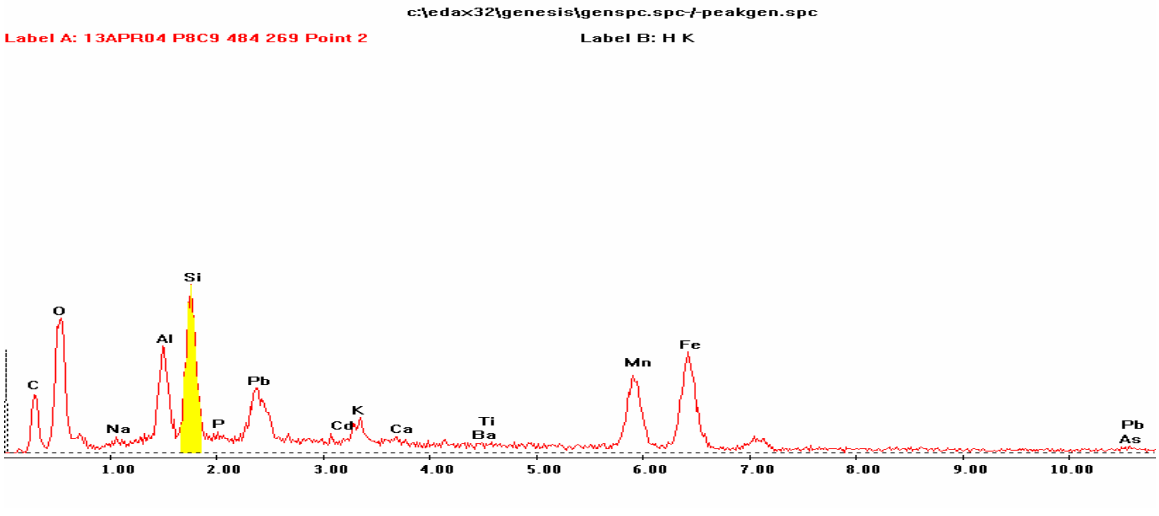

Point 3

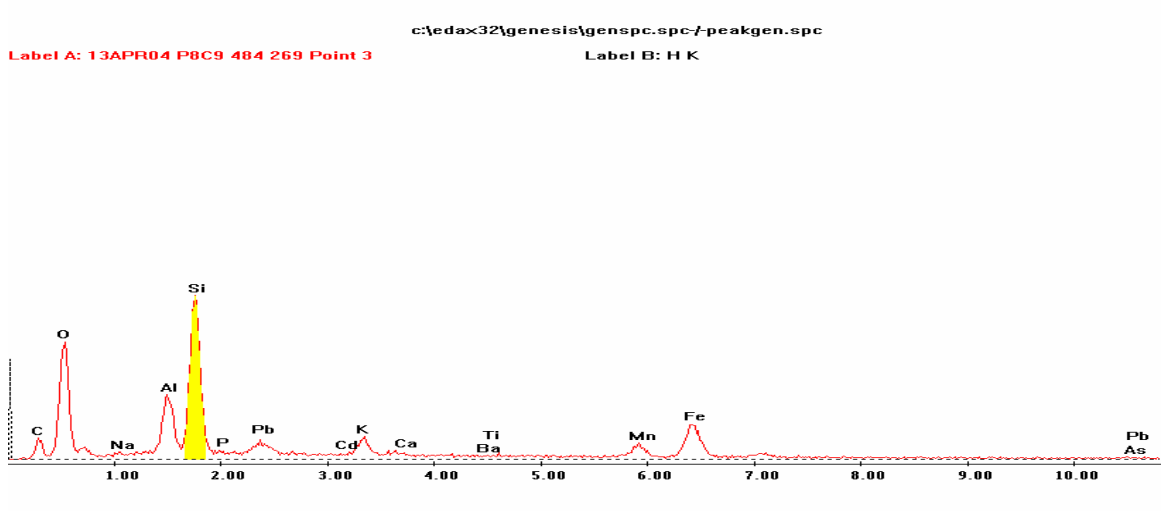

Point 4

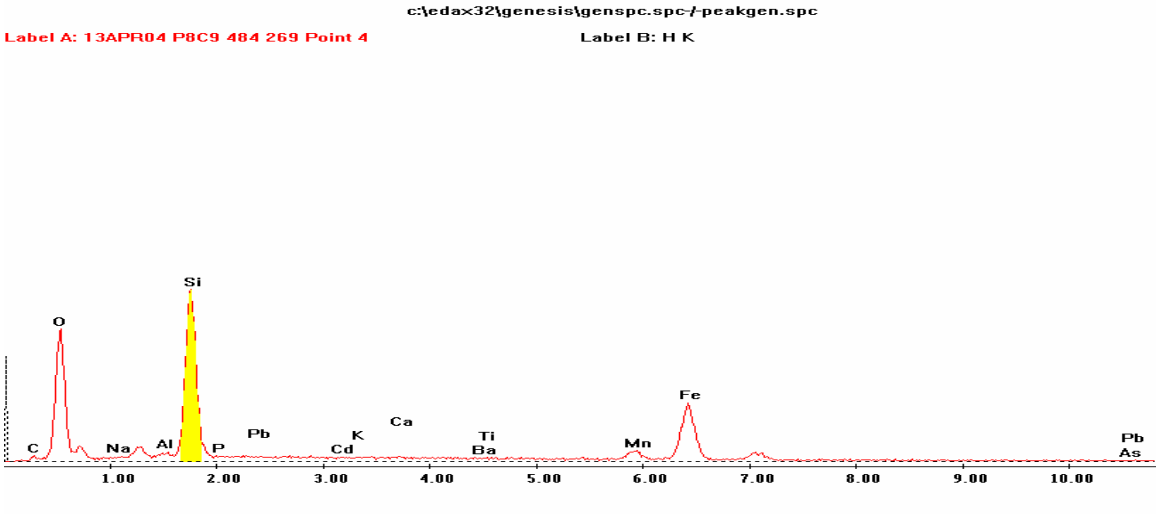

Point 5

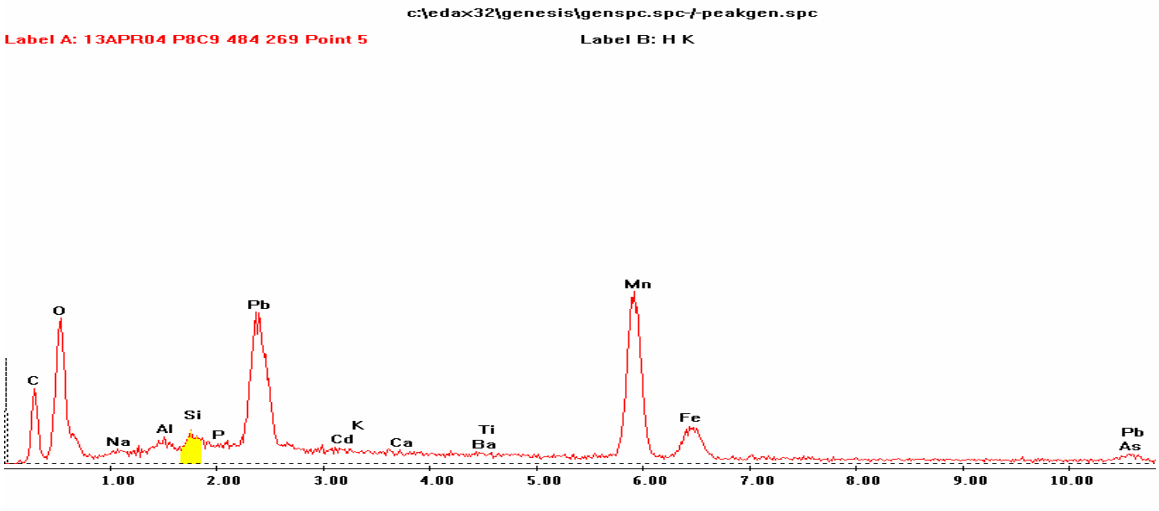

Point 6

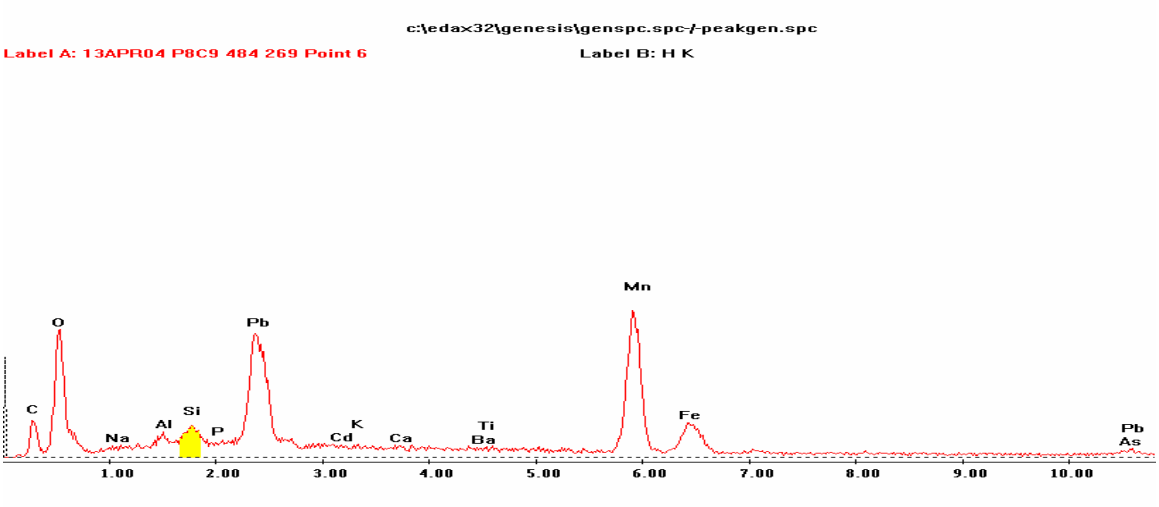

Point 7

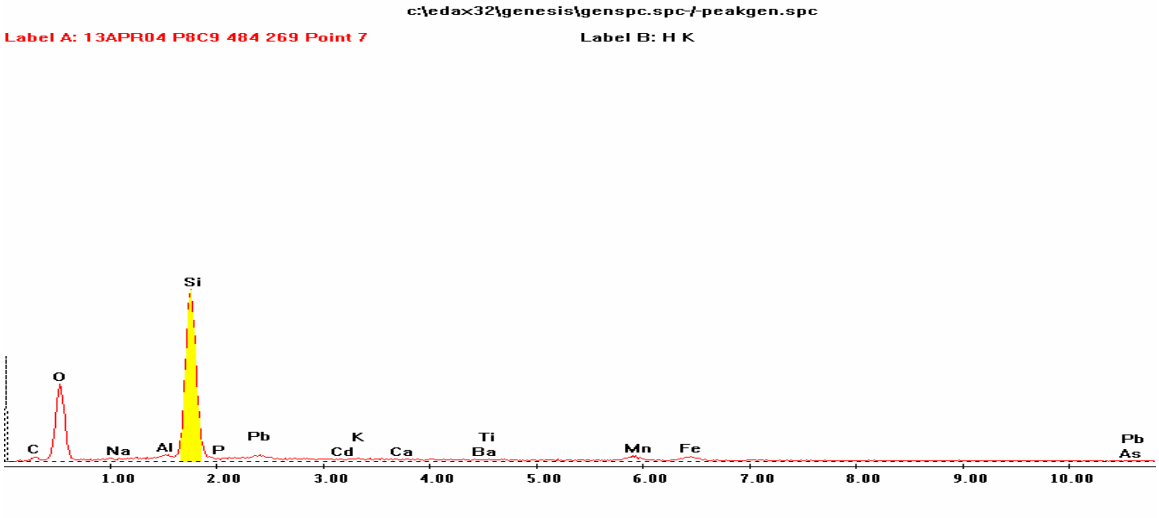

Point 8

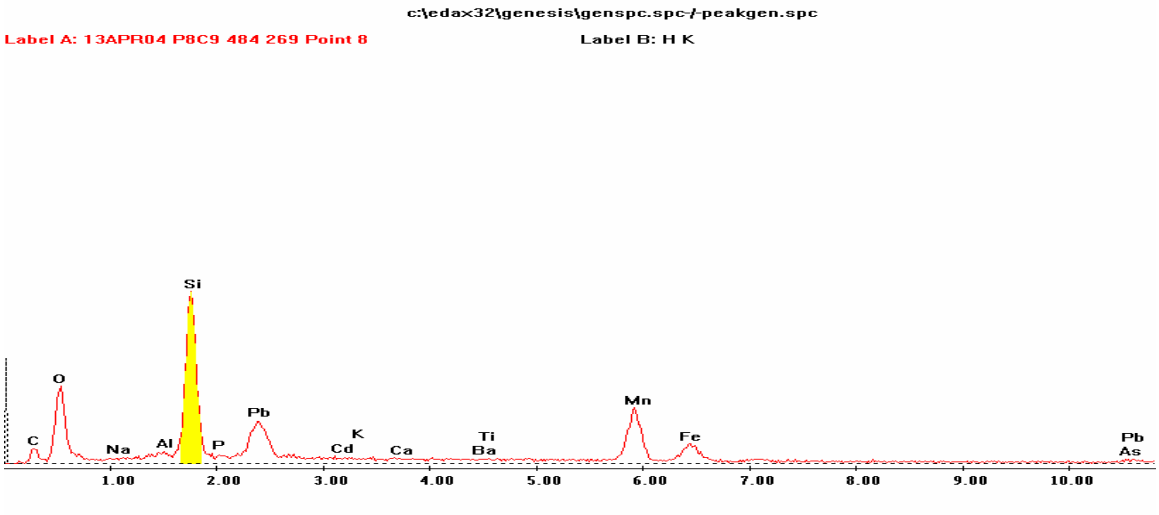

Point 9

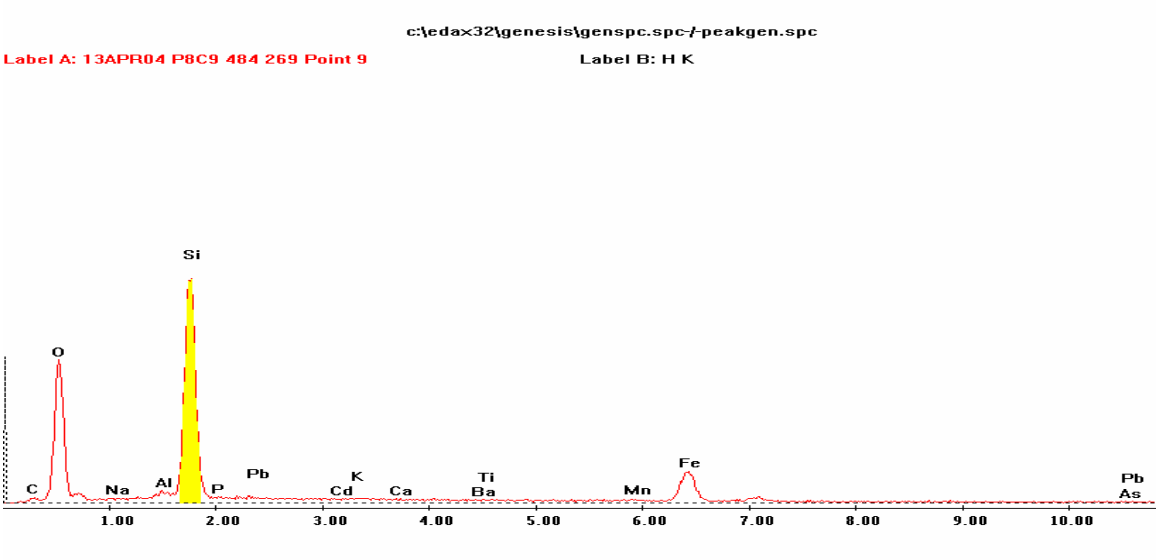

Point 10